Virchows Arch (2004) 444:1–2
DOI 10.1007/s00428-003-0958-0

EDITORS' NOTE

Günter Klöppel

News from the Managing Editors, 2003–2004

Published online: 24 December 2003

Fig. 1 Professor Philipp Heitz

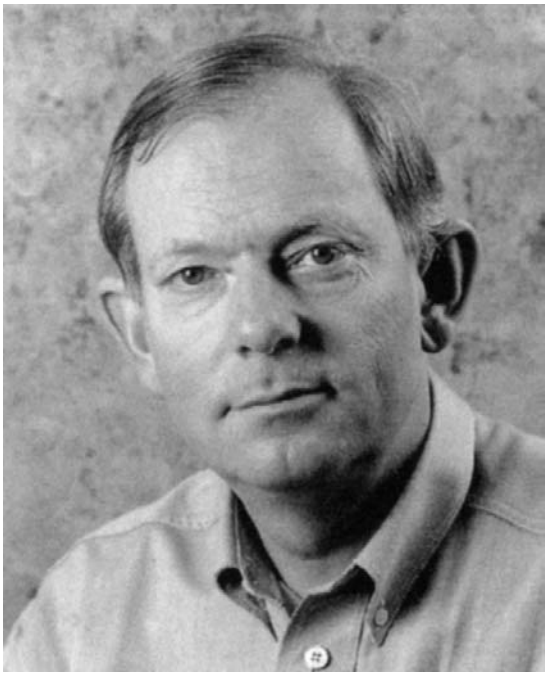

Fig. 2 Professor Fred Bosman

At the end of 2003, Professor Philipp Heitz (Fig. 1) resigned from his position as member of the Board of Managing Editors of the journal. He had been associated with Virchows Archiv as managing editor for 5 years, having been first invited to become a reviewer for Virchows Archiv B in 1994, when Ulrich Pfeifer was the editor of that journal. As managing editor, he was mainly responsible for manuscripts dealing with endocrine pathology. We are deeply indebted to him for his many years of dedicated service to the journal and we are happy that he is going to stay on as member of the editorial board.

Professor Fred Bosman (Fig. 2), head of the Department of Pathology at the University Hospital of Lausanne, and Professor Heinz Höfler (Fig. 3), head of the Department of Pathology of the Technical University of Munich, have joined us as managing editors of Virchows Archiv. Both have been associated with the journal as editors since 1994. Fred Bosman and Heinz Höfler have outstanding reputations as scientists in the fields of gastrointestinal and molecular pathology and are members of a large number of international societies. Fred Bosman also served in the Executive Committee of the European Society of Pathology and is one of the organizers of the EuroCellPath courses. Professor Höfler

G. Klöppel (✉)
Universitätsklinikum Schleswig-Holstein,
Institut für Pathologie,
Michaelisstrasse 11, 24104 Kiel, Germany
e-mail: gkloeppel@path.uni-kiel.de

Fig. 3 Professor Heinz Höfler

is currently chairman of the European Society of Pathology Working Group on Molecular Pathology.

With the appointment of two new managing editors, the total number of managing editors has increased to six. Professor Höfler will run the editorial office, which will remain in Kiel in the capable hands of Mrs. Brütting and be supervised from Munich. This will be possible because we are introducing an online submission and reviewing system based on Manuscript Central. Professor Klöppel, who until now has managed the editorial office from Kiel, will concentrate in future on the recruitment and supervision of review articles.

Finally, we would like to express our gratitude to the editors and all other scientists from various countries who have helped us to make Virchows Archiv a successful journal of the European Society of Pathology.

Virchows Arch (2004) 444:3–12
DOI 10.1007/s00428-003-0943-7

REVIEW ARTICLE

Elie Serge Zafrani

Non-alcoholic fatty liver disease: an emerging pathological spectrum

Received: 7 October 2003 / Accepted: 4 November 2003 / Published online: 18 December 2003

Abstract The spectrum of pathological lesions observed in non-alcoholic fatty liver disease (NAFLD) is wide and strongly resembles that of alcohol-induced liver disease. It ranges from fatty liver to steatohepatitis, progressive fibrosis and cirrhosis. Hepatocellular carcinoma is a possible complication of NAFLD, but whether it is related to frequently associated metabolic disorders (e.g., overweight, diabetes) or to underlying cirrhosis is unclear. This disease is the result of a multi-factorial process in which insulin resistance seems to play a major role in the initial accumulation of fat in the liver, whereas multiple causes of mitochondrial dysfunction and oxidative stress can induce the secondary occurrence of necroinflammatory lesions and fibrosis. Genetic factors might explain why only some patients with simple steatosis will develop steatohepatitis and fibrosis. Due to the increasing prevalence of obesity in Western countries, NAFLD will possibly be a public health problem and the liver disease of the future.

Keywords Non-alcoholic fatty liver disease · Steatohepatitis · Liver fibrosis · Insulin resistance · Mitochondrial dysfunction

Introduction

Non-alcoholic fatty liver disease (NAFLD) has probably become one of the most common causes of chronic liver disease in Western countries and might be, in the future, an important public health problem [4, 20, 53]. This condition, with an uncertain natural history, may be severe and is characterized by a wide spectrum of pathological lesions, ranging from simple steatosis to steatohepatitis, advanced fibrosis, cirrhosis and even hepatocellular carcinoma. These lesions closely resemble those induced by alcohol, but occur in patients who deny excessive alcohol consumption.

This disease raises numerous questions concerning its definition, epidemiology and associated conditions, its clinical presentation, natural history, pathophysiology and management. Addressing some of these questions will be the major purpose of the present review.

E. S. Zafrani (✉)
Département de Pathologie,
Hôpital Henri Mondor,
94010 Créteil cedex, France
e-mail: elie-serge.zafrani@hmn.ap-hop-paris.fr
Tel.: +33-14-9812730
Fax: +33-14-9812733

What is NAFLD?

Association of liver steatosis, inflammation and fibrosis has been known for several decades. It has been documented in non-alcoholic patients following surgical jejunoileal bypass for morbid obesity [57], in obese patients who had not undergone weight-loss surgery [2] and in diabetics [28]. The term non-alcoholic steatohepatitis (NASH) was coined by Ludwig et al. to describe biopsy findings, including steatosis, necrosis, inflammation, Mallory bodies and fibrosis in patients, mainly obese women, who did not drink alcohol [45]. This has brought interest to this entity and promoted further research, but NASH refers to necroinflammatory lesions associated with steatosis (i.e., steatohepatitis) and only corresponds to part of NAFLD, which is now the preferred term to more accurately designate the much wider spectrum, consisting of simple steatosis, steatohepatitis, cirrhosis and hepatocellular carcinoma. Recent conferences have also stressed the need for a consensus regarding classifying, grading and staging NAFLD [53, 65].

Although the value of liver biopsy in routine practice has been debated, essentially due to the risks and cost of this procedure and due to the lack of effective therapy, it is the only accurate diagnostic method, and it is essential for grading and staging the disease and for including patients in clinical trials [63, 65].

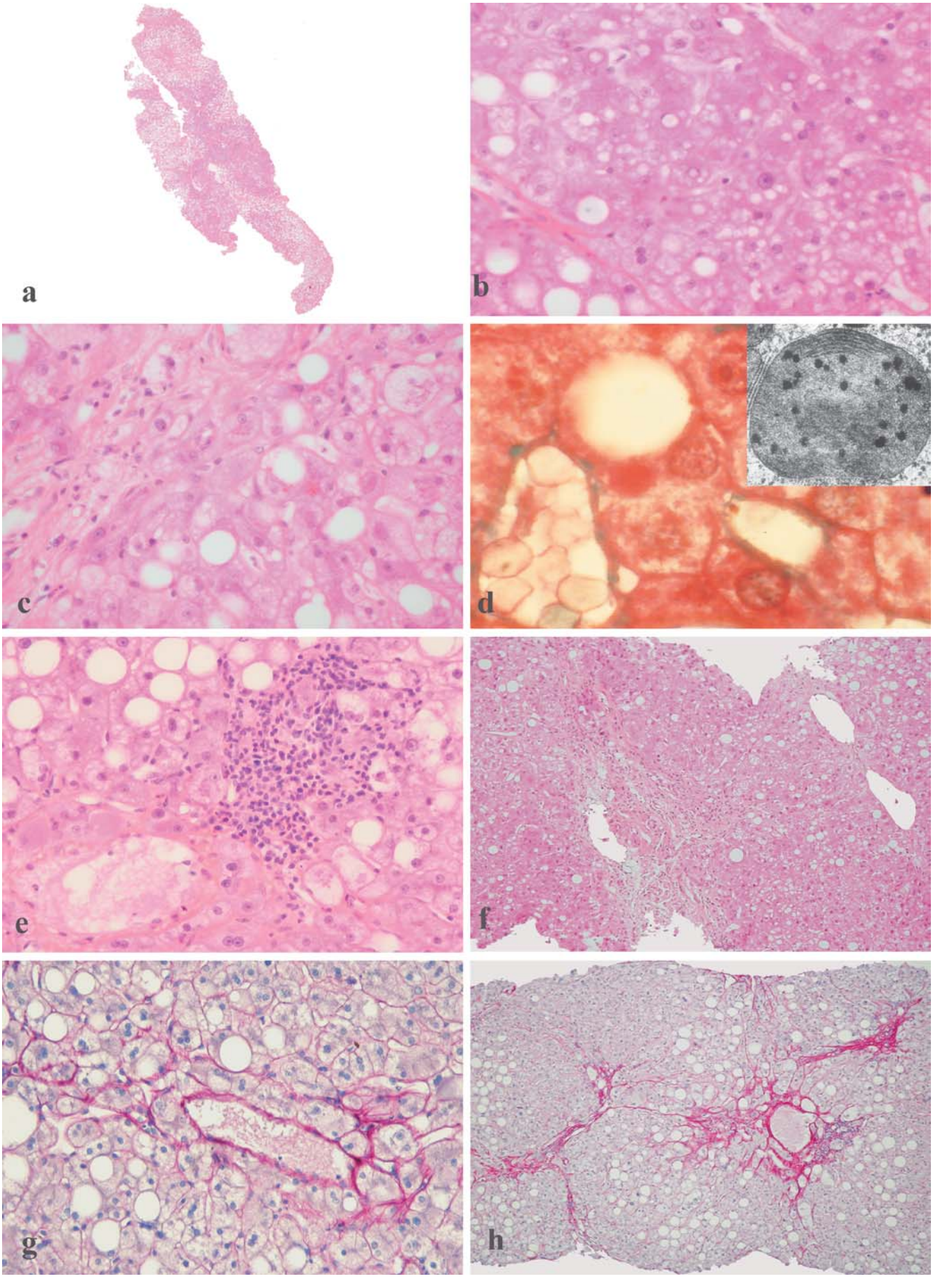
a
b
c
d
e
f
g
h

Histological findings

The spectrum of pathological lesions observed in NAFLD is hardly distinguishable from that of alcohol-induced liver disease (Fig. 1). Differences between the two conditions are essentially based on clinical and biochemical arguments, in addition to evaluation of alcohol intake: patients with alcoholic hepatitis are usually sicker, have higher serum bilirubin levels, have an aspartate aminotransferase to alanine aminotransferase ratio superior to 1 and more frequently have cirrhosis [65]. Histologically, necroinflammatory activity and fibrosis are probably milder, Mallory bodies rarer and glycogen nuclei more prevalent in NAFLD [65].

Steatosis

Hepatocellular steatosis (Fig. 1) is usually macrovesicular, made of large intracytoplasmic droplets displacing the nucleus at the cell periphery. Macrovesicular fatty change is occasionally associated with microvesicular steatosis, consisting of small intracytoplasmic lipid droplets leaving the nucleus at the center of the hepatocytes (Fig. 1b). Steatosis of varied degrees may either be diffuse within the hepatic lobule or predominate in zone 3, around terminal hepatic veins. Glycogen nuclei (Fig. 1b) are seen in at least one-third of the patients [63].

Steatohepatitis

Steatohepatitis is defined by the association of steatosis with other hepatocellular lesions, essentially necroinflammatory changes. Ballooned hepatocytes are enlarged, with a clear cytoplasm, and apoptotic bodies can be noted. Mallory bodies (Fig. 1c), consisting of intracytoplasmic aggregates of cytokeratin intermediate filaments, are not constantly observed, and their presence is not necessary for the diagnosis of steatohepatitis. They may be small, sparse and inconspicuous [63]. Eosinophilic inclusions, corresponding on electron microscopy to abnormal giant mitochondria with loss of cristae (Fig. 1d) and containing paracrystalline formations [15, 66], are occasionally observed in the cytoplasm of the hepatocytes.

Intensity of the inflammatory infiltration varies with the severity of steatohepatitis. Inflammation is usually mixed, made of lymphocytes and neutrophils located in the lobule (Fig. 1e), around altered hepatocytes or in the portal areas (Fig. 1f). The degree of stainable iron, when present, must be indicated.

Fig. 1 Histological findings in non-alcoholic fatty liver disease. **a** Simple steatosis without necroinflammatory lesions or fibrosis (hematoxylin and eosin, ×1.25). **b** Macrovesicular and microvesicular hepatocellular steatosis, with glycogen nuclei (hematoxylin and eosin, ×40). **c** Mallory bodies and mild polymorphous inflammatory infiltrate (hematoxylin and eosin, ×40). **d** A round eosinophilic inclusion can be seen in the cytoplasm of a hepatocyte containing a macrovacuole of fat (Masson's trichrome, ×100); this inclusion corresponds to an ultrastructurally abnormal mitochondrion (*inset*). **e** An intralobular aggregate of inflammatory cells, essentially lymphocytes, is located near a terminal hepatic vein (hematoxylin and eosin, ×20). **f** Moderate portal inflammation with portal and periportal fibrosis (hematoxylin and eosin, ×10). **g** Mild zone 3 perisinusoidal fibrosis, around a terminal hepatic vein (picrosirius red and hematoxylin, ×20). **h** Fibrous bridges between terminal hepatic veins and portal areas (picrosirius red and hematoxylin, ×10)

Fibrosis and cirrhosis

Extent of fibrosis is of prognostic importance. Perisinusoidal fibrosis is initially mild and predominates in zone 3, around terminal hepatic veins (Fig. 1g). It is then associated with portal and periportal fibrosis with progressive formation of fibrous bridges between terminal hepatic veins and portal areas or between adjacent portal tracts (Fig. 1h). Cirrhosis is obtained when hepatocellular nodules are completely surrounded by annular fibrosis. Liver failure, portal hypertension and hepatocellular carcinoma may then complicate the disease [13, 34, 62]. Some degree of fibrosis is found in up to two-thirds of the patients at the time of diagnosis, whereas cirrhosis is noted in up to 16 percent [4, 63]. In cirrhotic patients, histological features suggestive of steatohepatitis (e.g., steatosis, predominance of neutrophils in the inflammatory infiltrate) may have regressed or are no longer present [4, 14, 60]. It is, thus, noteworthy that NAFLD is more frequently considered a major cause of cryptogenic cirrhosis [14, 58, 62, 63].

Grading and staging

Since prognosis of NAFLD depends on the severity of the pathological findings, grading and staging the lesions observed on liver biopsy appears necessary. Grading evaluates the degree of steatosis and necroinflammatory changes, whereas staging estimates the extent of fibrosis.

A system referring to NAFLD correlates certain histological features with long-term prognosis [49]. Type 1 corresponds to simple steatosis, type 2 to steatosis with lobular inflammation, type 3 requires the additional presence of ballooned hepatocytes and type 4 the existence of Mallory bodies or fibrosis [49]. Among 132 patients with a mean follow-up of 9 years, cirrhosis occurred in 3.4 percent of types 1 and 2 patients and in 24.7 percent of types 3 and 4 patients [49].

Another method, which is limited to the classification of NASH, has been proposed [11]. Three grades of necroinflammatory activity, based on an overall impression of the intensity of hepatocellular and inflammatory changes, have been defined [11]: mild (grade 1), moderate (grade 2) and severe (grade 3). Staging reflects the pattern and the extent of fibrosis as well as architectural remodeling [11]: focal or extensive zone 3 perisinusoidal fibrosis is noted in stage 1; stage 2 adds focal or extensive periportal fibrosis; focal or extensive bridging fibrosis is

observed in stage 3; stage 4 corresponds to cirrhosis. Such a grading and staging system is much like what is used for chronic hepatitis C [7, 72], but intra-observer and inter-observer variations in liver biopsy interpretation have not been studied.

Epidemiology and conditions associated with NAFLD

NAFLD is, perhaps, one of the most common liver disorders. It is associated with various conditions (Table 1) and has been reported in all age groups, including children, the highest prevalence being observed in patients 40–49 years old [65]. Although studies published before 1990 emphasized that NASH mostly occurred in women, more recent publications have shown that the disease is equally frequent in men [6, 71]. There is increasing evidence that NAFLD essentially represents the hepatic component of a metabolic syndrome characterized by obesity, hyperinsulinemia, peripheral insulin resistance, diabetes, hypertriglyceridemia and hypertension [46, 47].

Obesity

Obesity, defined by a body mass index superior to 30 kg/m^2, is clearly associated with NASH, but most patients are moderately overweight [53, 65]. The likelihood of developing NASH increases with the degree of obesity, and resolution of a fatty liver may occur following gradual weight loss [65]. It must be noted that obesity is not invariably present in NASH patients, and many patients have a normal body weight [6].

Diabetes

Type 2 diabetes is a component of the metabolic syndrome and is associated with obesity and NAFLD [45, 60]. Both obesity and diabetes are associated with peripheral insulin resistance, hyperinsulinemia, increased free fatty acid levels and hypertriglyceridemia. Recently, the demonstration of peripheral insulin resistance, increased fatty acid β-oxidation and hepatic oxidative stress in patients, with either steatosis alone or NASH, suggests a link between obesity, insulin resistance and NAFLD [66].

Table 1 Conditions associated with non-alcoholic fatty liver disease

1. Insulin resistance
Obesity
Diabetes
2. Disorders of lipid metabolism
Hypertriglyceridemia
Abetalipoproteinemia
Hypobetalipoproteinemia
Lipodystrophy
Weber-Christian syndrome
3. Severe weight loss
Jejunoileal or gastric bypass
Starvation
4. Total parenteral nutrition
5. Latrogenic agents
Drugs: amiodarone, tamoxifen, diltiazem
Toxic exposure: industrial solvents

Miscellaneous disorders

In rare disorders of lipid metabolism (e.g., abetalipoproteinemia) as well as in rare syndromes characterized by severe insulin resistance (e.g., limb lipodystrophy), NAFLD with possible advanced fibrosis and cirrhosis may be observed [53, 59]. Other metabolic, surgical and genetic conditions are also associated with NALFD: jejunoileal bypass [57] or gastroplasty [31, 50] as treatments for morbid obesity, biliopancreatic diversion, extensive small bowel resection and prolonged total parenteral nutrition [24], small intestinal diverticulosis with bacterial overgrowth [63], Wilson's disease [53] and Weber-Christian syndrome [38].

Several drugs (e.g., amiodarone, tamoxifen, antiretroviral nucleoside analogues) and environmental factors (e.g., industrial solvents) may be responsible for hepatic lesions identical to those observed in NAFLD and alcohol-induced liver disease [23, 53, 65]. It is of interest that many of these conditions have in common either abnormal fat metabolism or mitochondrial dysfunction. Since NAFLD does not constantly occur in every patient having one of the above mentioned disorders or being exposed to iatrogenic agents, it is reasonable to postulate that this liver disease results from the conjunction or the potentiation of deleterious effects of several factors.

NAFLD and viral hepatitis C

Although steatosis and fibrosis are two of the histological hallmarks of chronic viral hepatitis C [68], it is generally not admitted that viral C infection should be included in the list of causes of NAFLD. However, it is of interest that, in chronic viral hepatitis C, steatosis seems to be more prevalent in patients infected with the genotype 3a virus [64] and that its degree is related to body mass index and to progressive fibrosis [1]. Steatosis might be due to a direct cytopathogenic effect of hepatitis C virus, since it has been shown in transgenic mice and in cell cultures that structural and non-structural viral proteins modify triglyceride metabolism and induce mitochondrial alterations, increasing oxidative stress [42, 54]. Steatosis might also interfere with response to antiviral therapy in chronic hepatitis C. Absence of steatosis is, indeed, associated with a better response [36], whereas high body mass index is an independent risk factor for non-response [10].

Viral hepatitis C and NAFLD are common causes of liver disease. It is, therefore, not surprising that they can

coexist in the same patients. A recent report has shown that steatohepatitis was observed in 5.5 percent of all cases of chronic viral hepatitis C, and that among 85 patients with histological features of steatohepatitis, 54 also had hepatitis C viral infection without history of alcohol abuse [12].

Clinical presentation, laboratory abnormalities and radiological findings

Most patients with NAFLD are asymptomatic, and the liver disease may be incidentally discovered during evaluation of hypertension, diabetes or morbid obesity [53, 65]. Hepatomegaly is the only physical finding in most patients [4, 6, 45]. Stigmata of signs of chronic liver disease, such as spider nevi, palmar erythema or signs of portal hypertension, should remind that cirrhosis can already be constituted at the time of diagnosis in up to 16 percent of the patients [4, 63] and that NAFLD is probably a major cause of cryptogenic cirrhosis [14, 62, 63].

Mild to moderate elevation of serum aspartate or alanine aminotransferase activities is usually the only laboratory abnormality, and NAFLD is the most usual cause of unexplained persistent elevation of these enzymatic activities, once hepatitis C and other known etiologies of chronic liver disease have been ruled out [65]. The ratio of aspartate aminotransferase to alanine aminotransferase is usually less than 1, but it increases with progression of fibrosis, leading to a loss of diagnostic value in patients with cirrhosis [4, 6]. Serum alkaline phosphatase or γ-glutamyltransferase activities may be mildly elevated. Presence of antinuclear antibodies in the serum, the significance of which is unknown, has been reported in 10 to 25 percent of patients [65]. It is not surprising that 30 to 50 percent of patients with NASH have diabetes or glucose intolerance [26, 40, 45, 75] and that 20 to 80 percent of patients have hypertriglyceridemia [26, 40, 45, 60]. Other abnormalities, including hypoalbuminemia, prolonged prothrombin time and hyperbilirubinemia, may be found in patients with cirrhosis. Changes in blood iron store parameters have been noted in approximately 10 percent of patients [5, 6, 61], but hepatic iron levels are usually within the normal ranges [5, 6, 49, 61]. It has been suggested that iron overload could be associated with increased fibrosis [30]. However, these findings have not been confirmed by other studies [5, 19, 76]. The significance of hemochromatosis gene mutations in the pathogenesis and progression of NAFLD remains controversial [19, 30].

Imaging findings (i.e., increased echogenicity, low density hepatic parenchyma on computed tomography) reflect the presence of steatosis and are useful to detect a space-occupying lesion that could correspond to hepatocellular carcinoma, occurring either on NAFLD-associated cirrhosis or on non-cirrhotic liver.

Natural history of NAFLD: from steatosis to hepatocellular carcinoma?

As already emphasized, NAFLD is characterized by a spectrum of pathological lesions ranging from simple steatosis to cirrhosis and its complications, including hepatocellular carcinoma. It is usually considered that these lesions represent different stages in the natural history of the disorder.

In patients with only fatty liver at the time of diagnosis, progression to steatohepatitis with fibrosis seems rare. In one longitudinal series of 40 patients with only fatty liver, no instance of evolution toward fibrosis or cirrhosis was observed after a median follow-up of 11 years [71]. Other reports also consider NAFLD a low-grade severity disorder [40, 60]. Matteoni et al.'s findings, which stress the importance of histologically grading necroinflammatory activity for predicting progression toward cirrhosis, have already been detailed [49]. As a matter of fact, it must be pointed out that there is no correlation between liver biopsy findings and biochemical abnormalities. It has, indeed, been recently shown that a low normal alanine aminotransferase value is not a guarantee against steatohepatitis with advanced fibrosis, since the entire spectrum of NAFLD could be seen in individuals with normal values, and the histological lesions did not differ whether alanine aminotransferase levels were elevated or not [51].

In patients with NASH, multivariate analyses show that older age, obesity and diabetes are independent predictors of marked liver fibrosis [5]. In severely obese patients, a raised index of insulin resistance, systemic hypertension and elevated serum alanine aminotransferase activity have been demonstrated to be independent predictors of NASH, whereas moderate alcohol consumption seemed to reduce the risk of NAFLD, possibly by reducing insulin resistance [27]. In obese patients with minimal fibrosis, histological improvement may occur following slowly achieved weight loss [65]. If weight loss is rapid, progression of the disease may be accelerated [3].

The precise risk of mortality in patients with NAFLD is not known. Many factors might be implicated, including complications and comorbidities of obesity and diabetes and liver disease, itself. Cirrhosis independently increases mortality [49], probably due to liver failure, portal hypertension and hepatocellular carcinoma. Growing evidence indicates that hepatocellular carcinoma should be considered in the natural history of progressive NAFLD [13, 48, 52, 60], since clinical and biological features suggestive of NASH are more frequently observed in patients with hepatocellular carcinoma arising on cryptogenic cirrhosis than in age- and sex-matched patients with hepatocellular carcinoma arising on viral or alcoholic cirrhosis [13]. Whether tumor development is secondary to the metabolic abnormalities associated with NASH or to underlying cirrhosis is not clear. Interestingly, hepatocellular carcinoma may be observed in the absence of cirrhosis in NASH patients with minimal

portal and periportal fibrosis [8]. In addition, the recently published results of a large prospectively studied cohort of American adults has demonstrated that increased body weight, with possible NAFLD, was associated with increased death rates for all cancers, including liver cancers, especially in men [16].

Pathophysiology

The pathological lesions and the natural history of NAFLD probably reflect a complex multi-factorial process in which the genetic environment is of importance [74], since it has yet to be understood why only steatosis occurs in some patients whereas others develop steatohepatitis, cirrhosis or hepatocellular carcinoma. Insulin resistance, abnormal metabolism of fatty acids, mitochondrial dysfunction and oxidative stress, dysregulation of cytokines and production of various mediators are the main interacting factors implicated in the pathophysiology of NAFLD. A recent study has shown that 4 genes contributing to impaired insulin sensitivity were overexpressed in the livers of patients with NAFLD, whereas 12 genes important for maintaining mitochondrial function were underexpressed [70].

Insulin resistance, fatty acids and steatosis

Hepatocellular steatosis (i.e., cytoplasmic accumulation of lipids, mostly triglycerides) results from fatty acid metabolism disturbance in the liver that is secondary to insulin resistance (Fig. 2). In obese and diabetic patients, there is an increase of plasmatic free fatty acid levels, due to an abnormal release by insulin-resistant adipocytes [69]. This, in conjunction with increased hepatic synthesis of free fatty acids due to high glucose and insulin levels, contributes to an increase of their intrahepatocellular pool, which is in equilibrium with expanded hepatic triglyceride pool. Steatosis, thus, occurs and is further aggravated by: (a) impairment of triglyceride export into the space of Disse, possibly because of apolipoprotein B-100 decreased synthesis [18] and inhibition of microsomal triglyceride transfer protein [44] and (b) insufficient compensation of the expanded free fatty acid pool by increased free fatty acid mitochondrial β-oxidation [66].

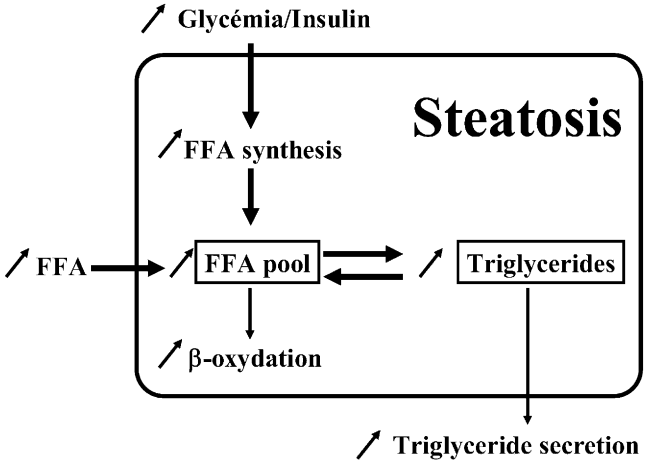

Fig. 2 Pathophysiological mechanism of hepatocellular steatosis in obese and diabetic patients. Increased intracellular free fatty acid (FFA) pool due to increased plasmatic FFA levels, increased FFA synthesis and insufficient FFA β-oxidation, is in equilibrium with an increased triglyceride pool further expanded by impaired triglyceride export

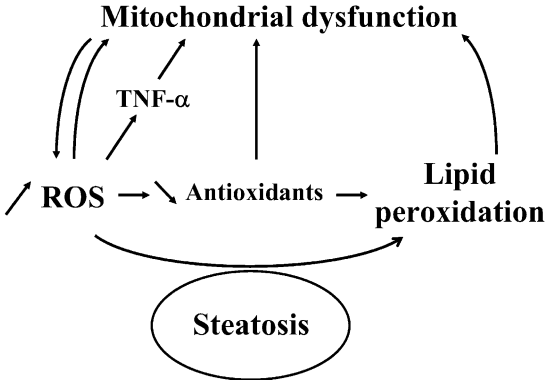

Fig. 3 Reactive oxygen species (ROS) produced in hepatocytes oxidize unsaturated lipids of fat deposits (steatosis) and, thus, induce lipid peroxidation, which causes mitochondrial dysfunction. Reactive oxygen species can also directly damage mitochondrial DNA, trigger synthesis of several cytokines such as tumor necrosis factor α (TNF-α), which may alter mitochondria. They can induce depletion of antioxidants, which enhances lipid peroxidation

Whereas steatosis remains the only liver lesion in many patients with NAFLD, some silently develop necroinflammation and progressive fibrosis. The reasons for the possible deleterious effects of steatosis are not completely understood, but the presence of oxidizable lipids in hepatocytes could trigger lipid peroxidation, mitochondrial dysfunction, oxidative stress and cytokine production [56].

Mitochondrial dysfunction, oxidative stress and cytokine production

Normal hepatocytes produce large amounts of reactive oxygen species (ROS), which are mainly formed in mitochondria and also formed by microsomal cytochrome P_{450} [56]. When there is steatosis, ROS can oxidize the unsaturated lipids of fat deposits (Fig. 3) and, thus, induce lipid peroxidation, which has been demonstrated in animal models as well as in patients with NASH [43, 56, 66].

Lipid peroxidation releases reactive aldehydes that damage mitochondrial DNA, which encodes some of the respiratory chain polypeptides [56]. Lipid peroxidation products also are able to directly inactivate respiratory chain polypeptides [56]. These two inhibitory effects, added to those induced by an increase of production of dicarboxylic acids (formed by microsomal ω-oxidation of

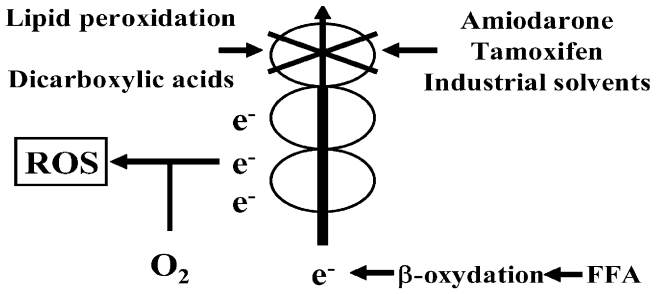

Fig. 4 Impairment of the flow of electrons (e^-) in the respiratory chain, and increased formation of reactive oxygen species (ROS). Role of lipid peroxidation products, dicarboxylic acids and iatrogenic agents such as amiodarone, tamoxifen or industrial solvents

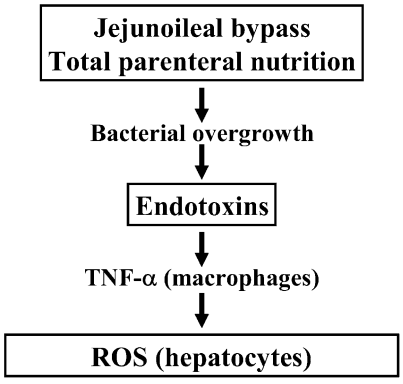

Fig. 5 Mechanism of formation of reactive oxygen species (ROS) in jejunoileal bypass and total parenteral nutrition. *TNF-α* tumor necrosis factor *α*

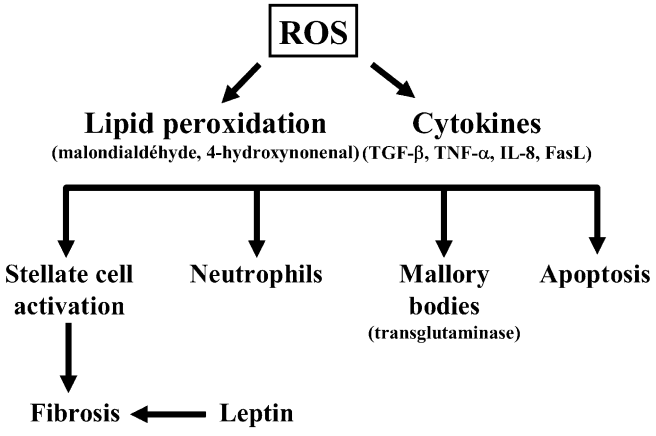

Fig. 6 The effects of reactive oxygen species (ROS) explain many of the histological findings in steatohepatitis and fibrosis. Leptin has also a profibrogenic action. *TGF-β* transforming growth factor-*β*, *TNF-α* tumor necrosis factor *α*, *IL-8* interleukin 8, *FasL* Fas ligand

free fatty acids), result in marked impairment of the flow of electrons (Fig. 4) in the respiratory chain [56] and might explain decreased recovery from hepatic adenosine triphosphate depletion in patients with NASH after fructose infusion [22]. The observation of ultrastructural mitochondrial lesions in patients with NASH (Fig. 1d) could be the morphological counterpart of these metabolic abnormalities [15, 66]. Since free fatty acid mitochondrial *β*-oxidation, which generates electrons that are transferred to the respiratory chain, is increased [66], there is an imbalance between input and outflow of electrons in the respiratory chain, and mitochondrial ROS formation is enhanced [56]. This increased ROS production has additional effects (Fig. 3) that aggravate this vicious circle. Reactive oxygen species further increase lipid peroxidation, can directly damage mitochondrial DNA and trigger synthesis of several cytokines [39, 73], including tumor necrosis factor *α* (TNF-*α*), which may alter mitochondria [56]. They might be implicated in increased Fas-mediated hepatocellular apoptosis in patients with NASH [29]. Finally, they can induce a depletion of antioxidants, such as vitamin E, but the results of vitamin E supplementation in patients with NASH are controversial [32, 39].

In patients receiving drugs known to be responsible for NASH (e.g., amiodarone, tamoxifen), production of ROS could even be greater (Fig. 4), since agents as amiodarone have been shown to directly hamper electron flow in rat hepatocytes [9]. In patients with jejunoileal bypass or under total parenteral nutrition (Fig. 5), bacterial overgrowth in excluded intestine releases endotoxins that stimulate ROS and TNF-*α* synthesis by Kupffer cells [56, 73], which are enlarged and form centrilobular aggregates in patients with NASH [41]. TNF-*α* then acts on hepatocytes to damage mitochondria and increase ROS formation [56]. Such drugs and toxins are examples of a "second hit" necessary to be added to steatosis (i.e., the "first hit") to explain evolution toward steatohepatitis [25].

Do pathophysiological mechanisms explain the histopathological lesions of NAFLD?

In summary, many of the lesions observed in the histopathological spectrum of NAFLD are probably explained by the complex network of pathophysiological mechanisms. Fat accumulated within the liver may remain without associated necroinflammatory damage in many patients over a long period of time [71]. In some patients, additional events, essentially represented by the deleterious effects of ROS (Fig. 6), are responsible for progression to steatohepatitis, fibrosis and cirrhosis.

Indeed, lipid peroxidation releases reactive aldehydes, such as malondialdehyde and 4-hydroxynonenal [56], and ROS increase the expression of numerous cytokines, including TNF-*α*, Fas ligand, transforming growth factor-*β* (TGF-*β*) and interleukin-8 [56, 73]. Both lipid peroxidation products and cytokines seem to be responsible for the histopathological lesions observed in NASH:

- TNF-α and Fas ligand trigger apoptosis by permeabilizing mitochondrial membranes
- TGF-β stimulates transglutaminase, which allows polymerization of cytokeratins to form Mallory bodies
- Interleukin-8 and 4-hydroxynonenal are chemoattractive for neutrophils
- TGF-β activates perisinusoidal stellate cells, and lipid peroxidation products increase their production of collagen, thus, leading to perisinusoidal fibrosis and cirrhosis; in addition, hyperleptinemia, a common finding in obese patients, might promote profibrogenic responses in the liver, in part by upregulating TGF-β [33, 35, 67]

As far as hepatocellular carcinoma is concerned, several clinical studies strongly suggest that it should be considered within the NAFLD spectrum [13, 48, 52, 60], but mechanisms of carcinogenesis in this context have not been studied, and it is, indeed, unclear whether this tumor is related to NASH-related cirrhosis or to metabolic disturbances associated with NAFLD.

Management

Management of NAFLD should take into account the pathophysiological mechanisms that are implicated, the natural history of the disease and the safety and cost of the therapeutic options [53, 65]. Resolution of histological abnormalities, as determined by liver biopsy, should remain the gold standard for treatment outcomes. Until now, there are no published controlled trials of treatment modalities in NAFLD. Management is, therefore, directed toward correction of risk factors, and treatments try to correct putative pathophysiological abnormalities. Exercise and diet are essential, and weight must be controlled. Insulin resistance must be improved by antidiabetic/insulin sensitizing agents, and hyperlipidemia must be treated. Drugs with potential hepatoprotective effects, antioxydants agents and iron reduction therapy may be used [53, 65].

Whether alcohol intake should be prohibited is not clearly established. In the absence of formal data, the pragmatic recommendation is abstinence if significant fibrosis is present [53]. The concomitant use of drugs that may induce steatohepatitis (e.g., amiodarone, tamoxifen) requires weighing of risks and benefits [53]. An interesting unresolved issue is the problem of occupational exposure to industrial solvents and their harmful effects on the liver [23, 53].

Since NAFLD is probably a major cause of cryptogenic cirrhosis, many patients have likely been transplanted for such an indication. Both recurrence and de novo occurrence of NASH have been reported after surgery [21, 37]. Fatty liver constantly recurs within 5 years, but progression to steatohepatitis with fibrosis is very rare, and clinical outcome is similar to that of other groups of patients undergoing transplantation [21]. NAFLD may also develop in patients receiving a graft for indications other than cryptogenic cirrhosis, i.e., alcoholic cirrhosis, primary biliary cirrhosis and primary sclerosing cholangitis [21]. Fatty liver is noted in 25 percent of such patients within 5 years, and there is no instance of progression to fibrosis [21]. The occurrence of NAFLD following transplantation may be related, in part, to weight gain and also to immunosuppression with corticosteroids and cyclosporine [17, 21, 55].

Conclusion

NAFLD is a major cause of liver-related morbidity in Western countries, with possible progression to cirrhosis, liver failure and hepatocellular carcinoma. Liver biopsy remains the best procedure to provide diagnostic and prognostic information. Since insulin resistance and oxidative stress play a major role in its pathogenesis, NAFLD should be searched for in overweight and diabetic patients. Management is usually aimed at reducing weight and treating associated disorders, but the role of specific pharmacological agents remains to be established. Considering the surge of obesity in developed areas of the world, is NAFLD the liver disease of the future?

References

1. Adinolfi LE, Gambardella M, Andreana A, Tripodi MF, Utili R, Ruggiero G (2001) Steatosis accelerates the progression of liver damage of chronic hepatitis C patients and correlates with specific HCV genotype and visceral obesity. Hepatology 33:1358–1364
2. Adler M, Schaffner F (1979) Fatty liver hepatitis and cirrhosis in obese patients. Am J Med 67:811–816
3. Andersen T, Gluud C, Franzmann MB, Christoffersen P (1991) Hepatic effects of dietary weight loss in morbidly obese subjects. J Hepatol 12:224–229
4. Angulo P (2002) Nonalcoholic fatty liver disease. N Engl J Med 346:1221–1231
5. Angulo P, Keach JC, Batts KP, Lindor KD (1999) Independent predictors of liver fibrosis in patients with nonalcoholic steatohepatitis. Hepatology 30:1356–1362
6. Bacon BR, Farahvash MJ, Janney CG, Neuschwander-Tetri BA (1994) Nonalcoholic steatohepatitis: an expanded clinical entity. Gastroenterology 107:1103–1119
7. Bedossa P, Poynard T (1996) An algorithm for the grading of activity in chronic hepatitis C. The METAVIR Cooperative Study Group. Hepatology 24:289–293
8. Bencheqroun R, Duvoux C, Luciani A, Zafrani ES, Dhumeaux D (2003) Carcinome hépatocellulaire en l'absence de cirrhose au cours d'une stéato-hépatite non alcoolique. Gastroenterol Clin Biol (in press)
9. Berson A, De Beco V, Letteron P, Robin MA, Moreau C, El Kahwaji J, Verthier N, Feldmann G, Fromenty B, Pessayre D (1998) Steatohepatitis-inducing drugs cause mitochondrial dysfunction and lipid peroxidation in rat hepatocytes. Gastroenterology 114:764–774
10. Bressler BL, Guindi M, Tomlinson G, Heathcote J (2003) High body mass index is an independent risk factor for nonresponse to antiviral treatment in chronic hepatitis C. Hepatology 38:639–644
11. Brunt EM, Janney CG, Di Bisceglie AM, Neuschwander-Tetri BA, Bacon BR (1999) Nonalcoholic steatohepatitis: a proposal

for grading and staging the histological lesions. Am J Gastroenterol 94:2467–2474
12. Brunt EM, Ramrakhiani S, Cordes BG, Neuschwander-Tetri BA, Janney CG, Bacon BR, Di Bisceglie AM (2003) Concurrence of histologic features of steatohepatitis with other forms of chronic liver disease. Mod Pathol 16:49–56
13. Bugianesi E, Leone N, Vanni E, Marchesini G, Brunello F, Carucci P, Musso A, De Paolis P, Capussotti L, Salizzoni M, Rizzetto M (2002) Expanding the natural history of nonalcoholic steatohepatitis: from cryptogenic cirrhosis to hepatocellular carcinoma. Gastroenterology 123:134–140
14. Caldwell SH, Oelsner DH, Iezzoni JC, Hespenheide EE, Battle EH, Driscoll CJ (1999) Cryptogenic cirrhosis: clinical characterization and risk factors for underlying disease. Hepatology 29:664–669
15. Caldwell SH, Swerdlow RH, Khan EM, Iezzoni JC, Hespenheide EE, Parks JK, Parker WD Jr (1999) Mitochondrial abnormalities in non-alcoholic steatohepatitis. J Hepatol 31:430–434
16. Calle EE, Rodriguez C, Walker-Thurmond K, Thun MJ (2003) Overweight, obesity, and mortality from cancer in a prospectively studied cohort of U.S. adults. N Engl J Med 348:1625–1638
17. Cassarino DS, Swerdlow RH, Parks JK, Parker WD Jr, Bennett JP Jr (1998) Cyclosporin A increases resting mitochondrial membrane potential in SY5Y cells and reverses the depressed mitochondrial membrane potential of Alzheimer's disease cybrids. Biochem Biophys Res Commun 248:168–173
18. Charlton M, Sreekumar R, Rasmussen D, Lindor K, Nair KS (2002) Apolipoprotein synthesis in nonalcoholic steatohepatitis. Hepatology 35:898–904
19. Chitturi S, Weltman M, Farrell GC, McDonald D, Liddle C, Samarasinghe D, Lin R, Abeygunasekera S, George J (2002) HFE mutations, hepatic iron, and fibrosis: ethnic-specific association of NASH with C282Y but not with fibrotic severity. Hepatology 36:142–149
20. Clark JM, Brancati FL, Diehl AM (2002) Nonalcoholic fatty liver disease. Gastroenterology 122:1649–1657
21. Contos MJ, Cales W, Sterling RK, Luketic VA, Shiffman ML, Mills AS, Fisher RA, Ham J, Sanyal AJ (2001) Development of nonalcoholic fatty liver disease after orthotopic liver transplantation for cryptogenic cirrhosis. Liver Transpl 7:363–373
22. Cortez-Pinto H, Chatham J, Chacko VP, Arnold C, Rashid A, Diehl AM (1999) Alterations in liver ATP homeostasis in human nonalcoholic steatohepatitis: a pilot study. JAMA 282:1659–1664
23. Cotrim HP, Andrade ZA, Parana R, Portugal M, Lyra LG, Freitas LA (1999) Nonalcoholic steatohepatitis: a toxic liver disease in industrial workers. Liver 19:299–304
24. Craig R, Neymann T, Jeejeebhoy K, Yokoo H (1980) Severe hepatocellular reaction resembling alcoholic hepatitis with cirrhosis after massive small bowel resection and prolonged total parenteral nutrition. Gastroenterology 79:131–137
25. Day CP, James OF (1998) Steatohepatitis: a tale of two "hits?" Gastroenterology 114:842–845
26. Diehl AM, Goodman Z, Ishak KG (1988) Alcohollike liver disease in nonalcoholics. A clinical and histologic comparison with alcohol-induced liver injury. Gastroenterology 95:1056–1062
27. Dixon JB, Bhathal PS, O'Brien PE (2001) Nonalcoholic fatty liver disease: predictors of nonalcoholic steatohepatitis and liver fibrosis in the severely obese. Gastroenterology 121:91–100
28. Falchuk KR, Fiske SC, Haggitt RC, Federman M, Trey C (1980) Pericentral hepatic fibrosis and intracellular hyalin in diabetes mellitus. Gastroenterology 78:535–541
29. Feldstein AE, Canbay A, Angulo P, Taniai M, Burgart LJ, Lindor KD, Gores GJ (2003) Hepatocyte apoptosis and fas expression are prominent features of human nonalcoholic steatohepatitis. Gastroenterology 125:437–443
30. George DK, Goldwurm S, MacDonald GA, Cowley LL, Walker NI, Ward PJ, Jazwinska EC, Powell LW (1998) Increased hepatic iron concentration in nonalcoholic steatohepatitis is associated with increased fibrosis. Gastroenterology 114:311–318
31. Hamilton D, Vest T, Brown B, Shah A, Menguy R, Chey W (1983) Liver injury with alcoholic-like hyalin after gastroplasty for morbid obesity. Gastroenterology 85:722–726
32. Hasegawa T, Yoneda M, Nakamura K, Makino I, Terano A (2001) Plasma transforming growth factor-beta1 level and efficacy of alpha-tocopherol in patients with non-alcoholic steatohepatitis: a pilot study. Aliment Pharmacol Ther 15:1667–1672
33. Honda H, Ikejima K, Hirose M, Yoshikawa M, Lang T, Enomoto N, Kitamura T, Takei Y, Sato N (2002) Leptin is required for fibrogenic responses induced by thioacetamide in the murine liver. Hepatology 36:12–21
34. Hui JM, Kench JG, Chitturi S, Sud A, Farrell GC, Byth K, Hall P, Khan M, George J (2003) Long-term outcomes of cirrhosis in nonalcoholic steatohepatitis compared with hepatitis C. Hepatology 38:420–427
35. Ikejima K, Takei Y, Honda H, Hirose M, Yoshikawa M, Zhang YJ, Lang T, Fukuda T, Yamashina S, Kitamura T, Sato N (2002) Leptin receptor-mediated signaling regulates hepatic fibrogenesis and remodeling of extracellular matrix in the rat. Gastroenterology 122:1399–1410
36. Kaserer K, Fiedler R, Steindl P, Müller C, Wrba F, Ferenci P (1998) Liver biopsy is a useful predictor of response to interferon therapy in chronic hepatitis C. Histopathology 32:454–461
37. Kim WR, Poterucha JJ, Porayko MK, Dickson ER, Steers JL, Wiesner RH (1996) Recurrence of nonalcoholic steatohepatitis following liver transplantation. Transplantation 62:1802–1805
38. Kimura H, Kako M, Yo K, Oda T (1980) Alcoholic hyalins (Mallory bodies) in a case of Weber-Christian disease: electron microscopic observations of liver involvement. Gastroenterology 78:807–812
39. Kugelmas M, Hill DB, Vivian B, Marsano L, McClain CJ (2003) Cytokines and NASH: a pilot study of the effects of lifestyle modification and vitamin E. Hepatology 38:413–419
40. Lee RG (1989) Nonalcoholic steatohepatitis: a study of 49 patients. Hum Pathol 20:594–598
41. Lefkowitch JH, Haythe JH, Regent N (2002) Kupffer cell aggregation and perivenular distribution in steatohepatitis. Mod Pathol 15:699–704
42. Lerat H, Honda M, Beard MR, Loesch K, Sun J, Yang Y, Okuda M, Gosert R, Xiao SY, Weinman SA, Lemon SM (2002) Steatosis and liver cancer in transgenic mice expressing the structural and nonstructural proteins of hepatitis C virus. Gastroenterology 122:352–365
43. Letteron P, Fromenty B, Terris B, Degott C, Pessayre D (1996) Acute and chronic hepatic steatosis lead to in vivo lipid peroxidation in mice. J Hepatol 24:200–208
44. Letteron P, Sutton A, Mansouri A, Fromenty B, Pessayre D (2003) Inhibition of microsomal triglyceride transfer protein: another mechanism for drug-induced steatosis in mice. Hepatology 38:133–140
45. Ludwig J, Viggiano TR, McGill DB, Oh BJ (1980) Nonalcoholic steatohepatitis: Mayo Clinic experiences with a hitherto unnamed disease. Mayo Clin Proc 55:434–438
46. Marchesini G, Forlani G (2002) NASH: from liver diseases to metabolic disorders and back to clinical hepatology. Hepatology 35:497–499
47. Marchesini G, Bugianesi E, Forlani G, Cerrelli F, Lenzi M, Manini R, Natale S, Vanni E, Villanova N, Melchionda N, Rizzetto M (2003) Nonalcoholic fatty liver, steatohepatitis, and the metabolic syndrome. Hepatology 37:917–923
48. Marrero JA, Fontana RJ, Su GL, Conjeevaram HS, Emick DM, Lok AS (2002) NAFLD may be a common underlying liver disease in patients with hepatocellular carcinoma in the United States. Hepatology 36:1349–1354
49. Matteoni CA, Younossi ZM, Gramlich T, Boparai N, Liu YC, McCullough AJ (1999) Nonalcoholic fatty liver disease: a

spectrum of clinical and pathological severity. Gastroenterology 116:1413–1419
50. Melinek J, Livingston E, Cortina G, Fishbein MC (2002) Autopsy findings following gastric bypass surgery for morbid obesity. Arch Pathol Lab Med 126:1091–1095
51. Mofrad P, Contos MJ, Haque M, Sargeant C, Fisher RA, Luketic VA, Sterling RK, Shiffman ML, Stravitz RT, Sanyal AJ (2003) Clinical and histologic spectrum of nonalcoholic fatty liver disease associated with normal ALT values. Hepatology 37:1286–1292
52. Nair S, Mason A, Eason J, Loss G, Perrillo RP (2002) Is obesity an independent risk factor for hepatocellular carcinoma in cirrhosis? Hepatology 36:150–155
53. Neuschwander-Tetri BA, Caldwell SH (2003) Nonalcoholic steatohepatitis: summary of an AASLD Single Topic Conference. Hepatology 37:1202–1219
54. Okuda M, Li K, Beard MR, Showalter LA, Scholle F, Lemon SM, Weinman SA (2002) Mitochondrial injury, oxidative stress, and antioxidant gene expression are induced by hepatitis C virus core protein. Gastroenterology 122:366–375
55. Palmer M, Schaffner F, Thung SN (1991) Excessive weight gain after liver transplantation. Transplantation 51:797–800
56. Pessayre D, Berson A, Fromenty B, Mansouri A (2001) Mitochondria in steatohepatitis. Semin Liver Dis 21:57–69
57. Peters RL, Gay T, Reynolds TB (1975) Post-jejunoileal-bypass hepatic disease. Its similarity to alcoholic hepatic disease. Am J Clin Pathol 63:318–331
58. Poonawala A, Nair SP, Thuluvath PJ (2000) Prevalence of obesity and diabetes in patients with cryptogenic cirrhosis: a case-control study. Hepatology 32:689–692
59. Powell EE, Searle J, Mortimer R (1989) Steatohepatitis associated with limb lipodystrophy. Gastroenterology 97:1022–1024
60. Powell EE, Cooksley WG, Hanson R, Searle J, Halliday JW, Powell LW (1990) The natural history of nonalcoholic steatohepatitis: a follow-up study of forty-two patients for up to 21 years. Hepatology 11:74–80
61. Ratziu V, Giral P, Charlotte F, Bruckert E, Thibault V, Theodorou I, Khalil L, Turpin G, Opolon P, Poynard T (2000) Liver fibrosis in overweight patients. Gastroenterology 118:1117–1123
62. Ratziu V, Bonyhay L, Di Martino V, Charlotte F, Cavallaro L, Sayegh-Tainturier MH, Giral P, Grimaldi A, Opolon P, Poynard T (2002) Survival, liver failure, and hepatocellular carcinoma in obesity-related cryptogenic cirrhosis. Hepatology 35:1485–1493
63. Reid AE (2001) Nonalcoholic steatohepatitis. Gastroenterology 121:710–723
64. Rubbia-Brandt L, Leandro G, Spahr L, Giostra E, Quadri R, Male PJ, Negro F (2001) Liver steatosis in chronic hepatitis C: a morphological sign suggesting infection with HCV genotype 3. Histopathology 39:119–124
65. Sanyal AJ (2002) AGA technical review on nonalcoholic fatty liver disease. Gastroenterology 123:1705–1725
66. Sanyal AJ, Campbell-Sargent C, Mirshahi F, Rizzo WB, Contos MJ, Sterling RK, Luketic VA, Shiffman ML, Clore JN (2001) Nonalcoholic steatohepatitis: association of insulin resistance and mitochondrial abnormalities. Gastroenterology 120:1183–1192
67. Saxena NK, Ikeda K, Rockey DC, Friedman SL, Anania FA (2002) Leptin in hepatic fibrosis: evidence for increased collagen production in stellate cells and lean littermates of ob/ob mice. Hepatology 35:762–771
68. Scheuer PJ, Ashrafzadeh P, Sherlock S, Brown D, Dusheiko GM (1992) The pathology of hepatitis C. Hepatology 15:567–571
69. Shepherd PR, Kahn BB (1999) Glucose transporters and insulin action—implications for insulin resistance and diabetes mellitus. N Engl J Med 341:248–257
70. Sreekumar R, Rosado B, Rasmussen D, Charlton M (2003) Hepatic gene expression in histologically progressive nonalcoholic steatohepatitis. Hepatology 38:244–251
71. Teli MR, James OF, Burt AD, Bennett MK, Day CP (1995) The natural history of nonalcoholic fatty liver: a follow-up study. Hepatology 22:1714–1719
72. The French METAVIR Cooperative Study Group (1994) Intraobserver and interobserver variations in liver biopsy interpretation in patients with chronic hepatitis C. Hepatology 20:15–20
73. Tilg H, Diehl AM (2000) Cytokines in alcoholic and nonalcoholic steatohepatitis. N Engl J Med 343:1467–1476
74. Valenti L, Fracanzani AL, Dongiovanni P, Santorelli G, Branchi A, Taioli E, Fiorelli G, Fargion S (2002) Tumor necrosis factor [alpha] promoter polymorphisms and insulin resistance in nonalcoholic fatty liver disease. Gastroenterology 122:274–280
75. Wanless IR, Lentz JS (1990) Fatty liver hepatitis (steatohepatitis) and obesity: an autopsy study with analysis of risk factors. Hepatology 12:1106–1110
76. Younossi ZM, Gramlich T, Bacon BR, Matteoni CA, Boparai N, O'Neill R, McCullough AJ (1999) Hepatic iron and nonalcoholic fatty liver disease. Hepatology 30:847–850

Virchows Arch (2004) 444:13–19
DOI 10.1007/s00428-003-0923-y

ORIGINAL ARTICLE

Luca Di Tommaso · Maria P. Foschini · Teresa Ragazzini · Elisabetta Magrini · Adele Fornelli · Ian O. Ellis · Vincenzo Eusebi

Mucoepidermoid carcinoma of the breast

Received: 10 July 2003 / Accepted: 7 October 2003 / Published online: 21 November 2003

Abstract Five cases of mucoepidermoid carcinoma (MEC) of the breast are reported. All patients were women ranging in age from 29 years to 80 years. As histological grading is one of the most important prognostic factors in breast invasive carcinomas, MEC was graded using the Auclair et al. [1] grading system specific for MEC of salivary glands and the Elston and Ellis [4] grading method, a widely employed grading system in breast cancer. It was found that the two different grading systems appear to be interchangeable in assessing the grade of MEC of the breast. Accordingly, three cases were regarded low grade (G. 1), one intermediate (G. 2) and one high grade (G. 3). The cases were studied with immunohistochemistry and were found to have the same keratin pattern shown by their salivary gland counterpart. It was found that there are more similarities than differences between MEC of the breast and of salivary glands.

Keywords Mucoepidermoid carcinoma · Breast · Salivary glands

L. Di Tommaso · M. P. Foschini · T. Ragazzini · E. Magrini · V. Eusebi (✉)
Dipartimento di Scienze Oncologiche,
Sezione di Anatomia Patologica,
Università di Bologna, Ospedale Bellaria,
Via Altura 3, 40139 Bologna, Italy
e-mail: vincenzo.eusebi@ausl.bo.it
Fax: +39-05-16225759

A. Fornelli
Anatomic Pathology,
Ospedale Maggiore,
Bologna, Italy

I. O. Ellis
Department of Histopathology,
City Hospital NHS Trust,
Nottingham, United Kingdom

Introduction

Salivary gland-like tumours of the breast share histological features with their salivary counterpart. Among these, tumours showing pure myoepithelial or combined epi-myoepithelial differentiation, i.e. adenomyoepithelioma, malignant myoepithelioma, pleomorphic adenoma, adenoid cystic carcinoma and syringoid tumours, even if rare, are well-known breast lesions. A second group of salivary gland-like lesions of the breast devoid of myoepithelial differentiation includes mucoepidermoid carcinoma and entities such as acinic cell carcinoma and oncocytic carcinoma [8].

Mucoepidermoid carcinoma (MEC) of the breast is similar to its salivary counterpart, which is composed of basaloid, intermediate, epidermoid and mucinous cells. Since the work of Patchefsky et al. [16], less than 20 cases of breast MEC have been reported, mostly as single case reports [2, 5, 9, 10, 12, 13, 14, 15, 17, 19].

Here five new cases of MEC are described and diagnostic criteria and clinical-pathological correlation are discussed. Immunohistochemical findings were also studied in order to establish similarities or differences with salivary gland MEC.

Materials and methods

Five cases of MEC retrieved from the consultation files of one of us (VE) constitute the basis of the present study. Selected blocks were serially cut in four cases and stained with haematoxylin-eosin and alcian blue (AB) (pH 2.5) and periodic acid-Schiff (PAS) after diastase digestion. The block for case 2 was not obtained and, therefore, no immunoistochemistry was done in this case. For immunohistochemistry, a routine avidin-biotin complex (ABC) method was used [3]. Before immunostaining, sections were steamed in citrate buffer for 25 min and cooled for 5 min to retrieve different epitopes. Cytokeratin 7 antigen retrieval was performed with enzymatic digestion: slides were prewarmed in water bath for 5–10 min in phosphate-buffered saline (PBS) 1× at 37°C followed by a water bath with protease XIV (sigma 0.05%) in PBS 1× for 6 min at 37 C. Source and dilutions of the antisera used are listed in Table 1. The tumours were graded according to Auclair et al. [1], which is a specific grading system for MEC of salivary

Table 1 Antisera employed for immunoistochemistry. *ED* enzymatic digestion, *PC* pressure cooking

Antibody	Source	Dilution and clone	Antigen retrieval
Cytokeratin 7	Dako	1:100 (OV-TL 12/30)	ED
Cytokeratin 14	Biogenex	1:100 (LL002)	PC
Anti-mitochondrial	Biogenex	1:100 (113-1)	/
Smooth muscle actin	Dako	1:100 (1A4)	/
Calponin	Biogenex	1:60 (CALP)	PC
p63	Neomarkers	1:200 (4A4)	/
E-cadherin	Zymed	1:1000 (HECD-1)	PC

Table 2 Clinical features of the present series. *LCQ* lower central quadrant, *UOQ* upper outer quadrant

Case	Sex/age (years)	Clinical presentation	Site	Size (cm)
1	Female/80	Well circumscribed nodule	Unknown, left	0.5
2	Female/29	Nodule	LCQ, left	0.8
3	Female/54	Cystic lesion with nipple discharge	Retroareolar, left	1.5
4	Female/55	Cystic lesion with nipple discharge	Retroareolar, left	0.6
5	Female/36	Suspicious of malignancy	UOQ, left	1.1

Table 3 Pathological features of the present series. *Au* grading according to Auclair et al. [1]. *L* low, *In* intermediate, *H* high, *El-El* grading according to Elston & Ellis [4], *AW* alive and well, *FU* follow-up, *HPF* high-power field

Case	Border	Cysts	Cellular atypia	Mitoses	Necrosis	Nerve invasion	Nuclear grade	Histological grade	FU (months)
1	Circumscribed	50%	No	0/10 HPF	No	No	1	Au: L, El-El: 1	5:AW
2	Circumscribed	10%	No	1/10 HPF	No	No	1	Au: L, El-El: 1	90:AW
3	Circumscribed	50%	No	3/10 HPF	No	No	1	Au: L, El-El: 1	13:AW
4	Circumscribed	10%	Mild	4/10 HPF	No	No	2	Au: In, El-El: 2	3:AW
5	Stellate	No	Severe	7/10 HPF	Yes	Yes	3	Au: H, El-El: 3	18:AW

glands. The Elston and Ellis [4] grading method for breast carcinoma was also used for comparison.

Results

Clinical findings

Clinical data are summarised in Table 2. All patients were female with ages ranging from 29 years to 80 years (mean 51 years). In two cases, the lesion presented as a well-circumscribed nodule (cases 1 and 2). In two cases (cases 3 and 4), the lesion was cystic with nipple discharge, and, in the remaining case (case 5), a malignant lesion was suspected. A quadrantectomy followed by lymph-node dissection was performed in the latter case, while the remaining four patients underwent only surgical excision of the lump. In two cases (cases 3 and 4), the patients were additionally treated with quadrantectomy followed by lymph-node dissection after the diagnosis of breast cancer.

Follow-up information was available in all cases: patients were alive and well without evidence of recurrent disease after a period ranging from 3 months to 90 months (mean 26 months).

Morphological findings

Morphological features are summarised in Table 3. At scanning magnification, all cases presented as nodular lesions. Four cases had lesional pushing margins delimited by a fibrous pseudo-capsule where lymphocytes and plasma cells were often visible (Fig. 1A, B). Case 5, on the contrary, showed stellate margins. The lesions were constituted by neoplastic solid nests and cystic spaces sometimes filled with mucoid material. The cysts constituted more than 50% of the tumour in two cases (cases 1 and 3) (Fig. 2), less than 10% of the tumour in cases 2 and 4, while case 5 was predominantly solid (Fig. 7). In addition, cases 1, 3 and 4 were characterised by the presence of intralesional dilated ducts filled with a neoplastic solid polypoid proliferation that, similarly to the rest of the tumour, contained small cysts (Fig. 4A). Small foci of well-differentiated ductal carcinoma in situ (DCIS) [11] were also present (Fig. 4B).

At high power, the tumours were composed by various proportion of basaloid, intermediate, epidermoid and mucinous cells in different cases, similarly to what is seen in MEC of salivary glands (Fig. 5A). Basaloid cells were small in size and oval in shape; they had oval nuclei with dark, coarse chromatin and appeared mostly numerous at the periphery of neoplastic nests (Fig. 3). Intermediate cells were larger than basaloid cells, had eosinophilic cytoplasm and oval nuclei with small nucleoli (Fig. 5B). Epidermoid cells were twice the size of intermediate cells, had polygonal shape, eosinophilic

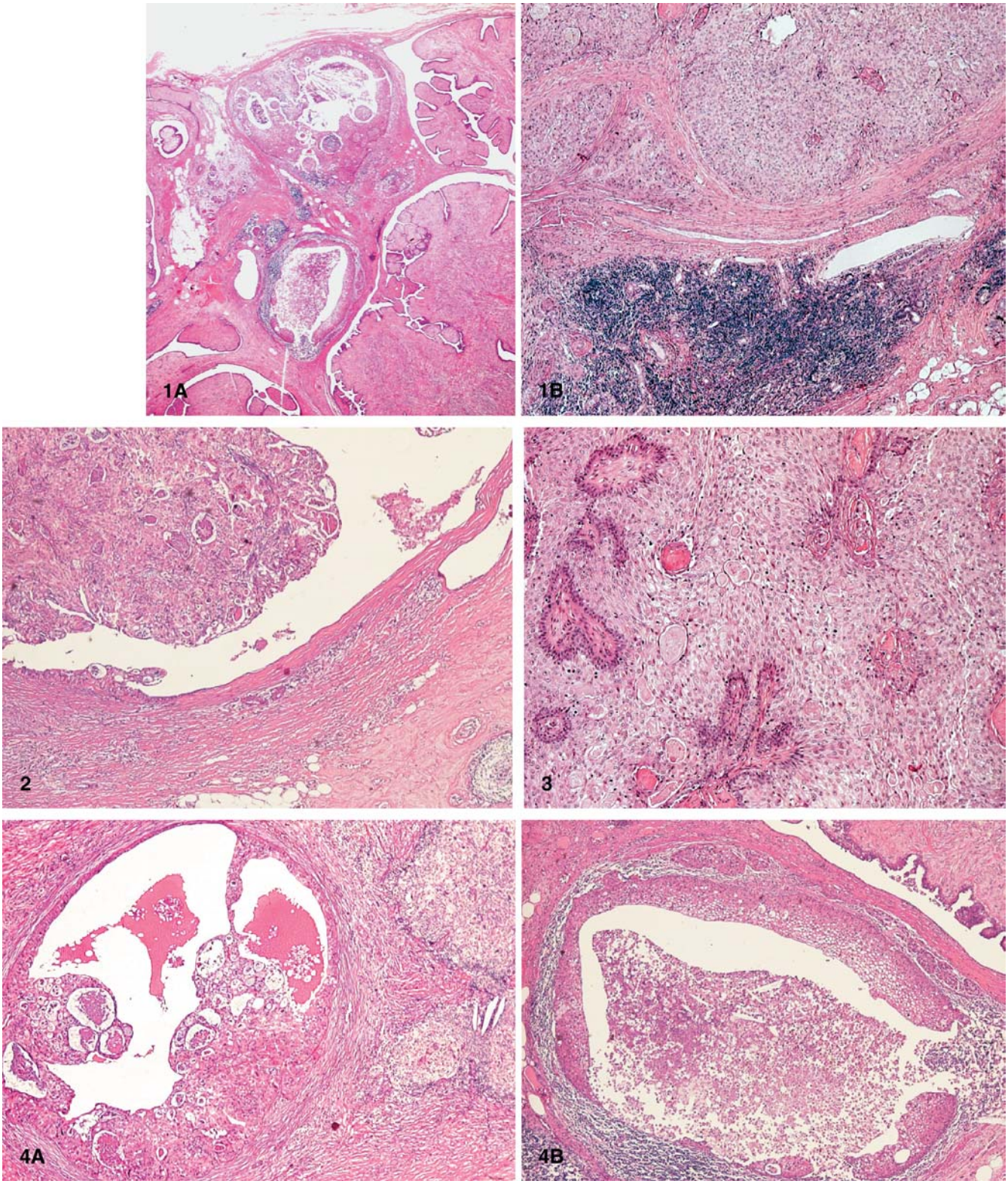

Fig. 1 **A** Case 1: cystic mucoepidermoid carcinoma appears in the contest of a phylloides tumour. **B** Case 3: the tumours are circumscribed by a thick fibrous pseudo capsule and a rim of lymphocytes and plasma cells

Fig. 2 Case 3: large cysts filled with solid proliferation of neoplastic cells

Fig. 3 Case 2: glandular spaces filled with mucoid material. Basaloid cells are small in size and appear located at the periphery of neoplastic sheets

Fig. 4 **A** Case 3: intralesional dilatated ducts filled with neoplastic solid polypoid proliferation. **B** Case 1: the in situ lesion contains necrotic debris and superficially simulates a poorly differentiated ductal carcinoma in situ

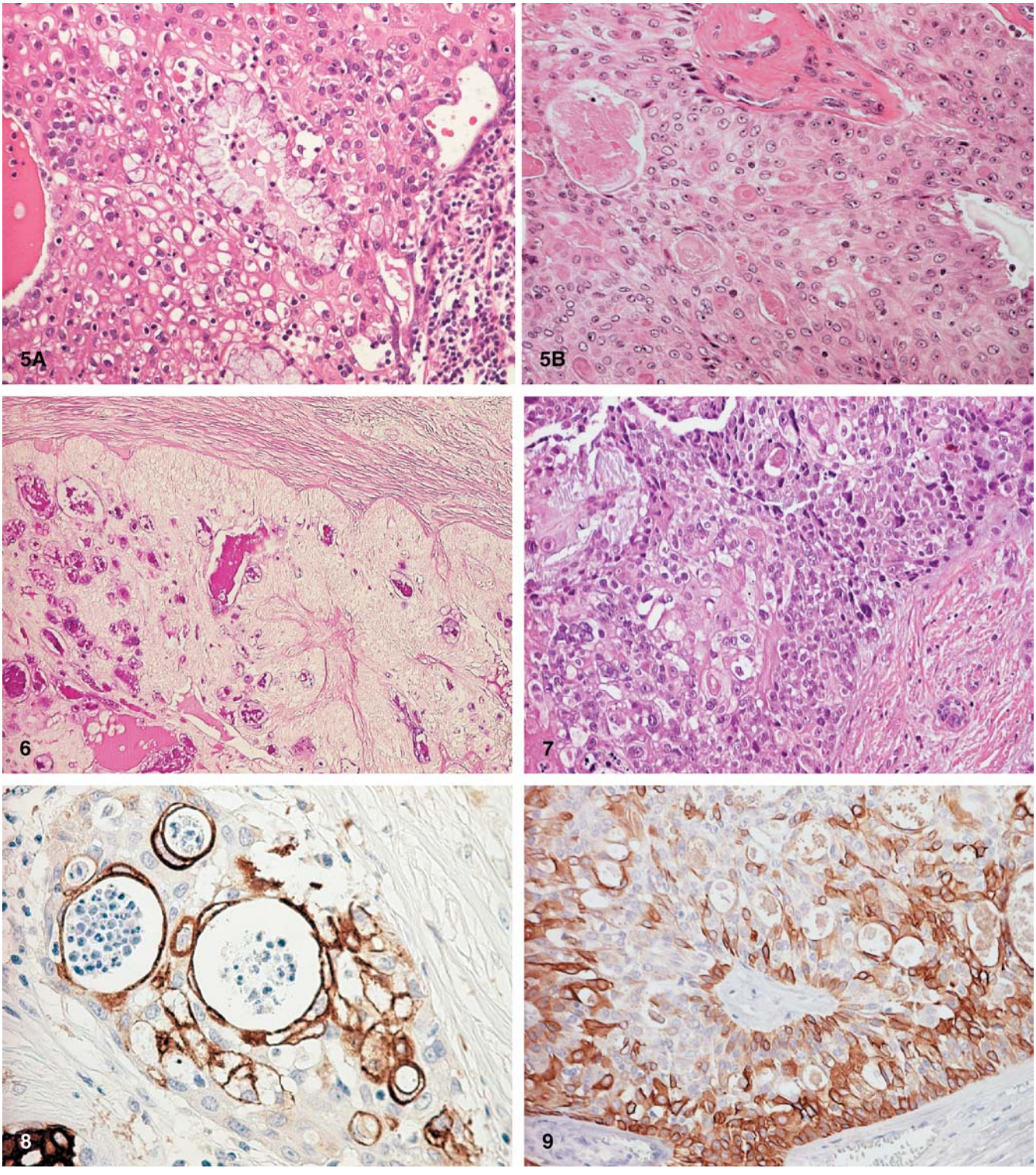

Fig. 5 **A** Case 1: columnar mucinous cells were seen intermingled with intermediate and epidermoid clear cells. **B** Case 3: small cystic spaces filled with mucin are visible in the context of intermediate and epidermoid cells

Fig. 6 Case 3: cysts were mainly filled by periodic acid-Schiff-positive mucoid material

Fig. 7 Case 5: severe nuclear pleomorphism and prominent nucleoli are visible

Fig. 8 Case 1: cytokeratin 7 mainly stains cells bordering glandular spaces; intermediate cells are also decorated

Fig. 9 Case 4: cytokeratin 14 mainly stains basaloid cells and scattered intermediate cells

Table 4 Immunohistochemical profiles of different cell types

Antibody	Basaloid	Intermediate	Epidermoid	Mucinous*
Cytokeratin 7	0/4	3/4	4/4	4/4
Cytokeratin 14	4/4	3/4	0/4	0/4
Mitochondria	2/4	2/4	2/4	0/4
Smooth muscle actin	0/3	0/3	0/3	0/3
Calponin	0/3	0/3	0/3	0/3
p63	3/3	3/3	0/3	0/3
E-cadherin	2/2	2/2	2/2	2/2

* Columnar mucinous cells were observed only in case 1 and were positive for cytokeratin 7

cytoplasm with well-defined cytoplasmic borders and round to oval nucleus. Epidermoid cells constituted the greatest component of the neoplastic nests. Cystic spaces were mainly lined by flat cells. The latter were devoid of cytoplasmic vacuoles, but their cytoplasm stained either with AB or PAS. The mucoid material that filled the cysts was also positive for PAS (Fig. 6), while the glycocalyx of the luminal cells was stained by AB. In case 1, the cystic lumina contained necrotic debris. On the contrary, dilated ducts were devoid of mucin. Rare columnar mucinous elements with basally located nuclei and cytoplasm, reminiscent of intestinal goblet cells, were seen bordering the cysts in one case (case 1) (Fig. 5A).

Mitoses were absent in one case (case 1) and were infrequent in two cases [1/10 high-power field (HPF) case 2 and 3/10 HPF case 3]. Case 4 showed a moderate number of mitoses (4/10 HPF) with mild cytological atypia. Case 5 showed numerous mitoses (7/10 HPF) and severe cytological atypia (Fig. 7). In this same case, confluent areas of necrosis were seen, as well as nerve invasion, while no necrotic areas nor nerve invasion were seen in the other cases.

Each single cell type presented a characteristic cytokeratin (CK) profile (Table 4). CK 7 was mainly observed in the cells composing the central part of the neoplastic nests and in the cells lining glandular and cystic spaces (Fig. 8). On the contrary, CK 14 predominated in cells located in the outer layers of the neoplastic nests where basaloid cells are seen (Fig. 9). In addition, most of the cells were highlighted by anti-mitochondrion antibody in two cases (cases 3 and 4) (Fig. 10). Both basaloid and intermediate cells were positive for p63, while smooth muscle actin (SMA) and calponin (CALP) were negative in all tumour cells. SMA, CALP and p63 were positive in the myoepithelial layer outlining the in situ lesions seen in cases 1, 3 and 4.

Case 1 arose at the periphery of a benign phylloid tumour (Fig. 1A), while, in the remaining cases, the surrounding parenchyma was normal. When the tumours were graded according to Auclair et al. [1], cases 1 to 3 appeared low grade, case 4 intermediate, and case 5 was regarded a high grade. Three cases (cases 1, 2, 3) were grade 1, one (case 4) grade 2 and one (case 5) grade 3, according to Elston and Ellis [4].

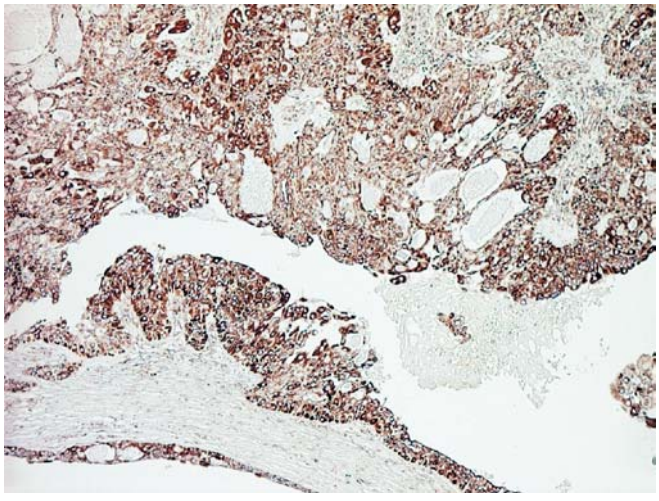

Fig. 10 Case 4: antimitochondrion antibody stains numerous cells

Discussion

MEC of salivary glands as defined by Foote et al. [6] is a malignant epithelial tumour composed of varying proportions of basaloid, intermediate, squamous and mucinous cells at the same time. If the criteria proposed by these authors are applied in a stringent fashion, only rare breast tumours published in the English literature can be accepted as primary MEC of the breast (Table 5, Table 6). Patchefsky et al. [16] reported two cases of well-differentiated MEC of the breast, showing gross and microscopic features similar to their salivary gland analogue. Five additional cases of low-grade MEC of the breast showing cyst formation were reported by Fisher et al. [5]. The case reported by Tjalma et al. [19] recurred as a high-grade MEC after 32 months, but the patient was alive after 12 years. The spectrum of MEC slightly enlarges if high-grade lesions are considered (Table 6). High-grade MEC appears histologically ill-defined, even in salivary glands, as described in the paper by Foote et al. [6]. Malignant MEC were considered those tumours showing rare mucous producing cells and "traits not substantially different from those ordinarily present in epidermoid and squamous carcinomas...basal cell epithelioma...highly cellular transitional cell carcinoma". The lack of specific criteria is probably responsible for the fact that Fisher et al. [5] have not found a single case of high-grade MEC out of their series of 1665 consecutive

Table 5 Review of the literature. *F* female, *LOQ* lower outer quadrant, *UOQ* upper outer quadrant, *UIQ* upper internal quadrant, *NS* not stated, *AW* alive and well, *FU* follow-up

Low-grade mucoepidermoid carcinoma						
Case	Age (years)/sex	Site and size	Lymph-node metastasis	Distant metastasis	Treatment	FU (months)
Patchefsky et al. [16]	66/Female	LOQ, right; 1.3 cm	0/20	0	Radical mastectomy	94:°
Patchefsky et al. [16]	70/Female	UOQ, right; 5 cm	NS	0	Quadrantectomy	10:AW
Fisher et al. [5]	65/Female	Right, 2 cm	NS	0	Lumpectomy	60:AW
Fisher et al. [5]	71/Female	Left; 2 cm	0/19	0	Modified radical mastectomy	48:AW
Fisher et al. [5]	57/Female	Right; 2.5 cm	0/11	0	Modified radical mastectomy	120:AW
Fisher et al. [5]	49/Female	Right; 3.7 cm	0/13	0	Radical mastectomy	108:AW
Fisher et al. [5]	60/Female	Left; 4 cm	NS	0	Simple mastectomy	48:°
Hanna et al. [9]	51/Female	Left; 2 cm	0	0	Modified radical mastectomy	8:AW
Tjalma et al. [19]	58/Female	UOQ, right; 3.5 cm	1/17	0	Radical mastectomy	16: local recurrence; 32: re-recurrence as high grade tumour, 156:AW

° Died for other cause

Table 6 Review of the literature. *F* female, *LOQ* lower outer quadrant, *UOQ* upper outer quadrant, *UIQ* upper internal quadrant, *NS* not stated, *AW* alive and well, *DOD* died of disease, *FU* follow-up

"High-grade" mucoepidermoid carcinoma						
Case	Age (years)/Sex	Site and size	Lymph-node metastasis	Distant metastasis	Treatment	FU (months)
Kovi et al. [12]	46/Female	Retroareolar, left; 9 cm	17/19	NS	Modified radical mastectomy	NS
Hastrup and Sehested [10]	59/Female	Left; 1 cm	0/4	Lung, bone, liver	Modified radical mastectomy	26:DOD
Leong and Williams [13]	57/Female	Left; 3,5 cm	0/20	Bone, lung	Simple mastectomy	6:DOD
Luchtrath and Moll [14]	60/Female	NS; 5 cm	12/18	Bone	Radical mastectomy	30:DOD
Pettinato et al. [17]	72/Female	Right; 7 cm	16/19	Lung	Modified radical mastectomy	10:DOD
Markopoulos et al. [15]	40/Female	UIQ, right; 2 cm	0	0	Wide local excision+lymph node dissection	60:AW
Berry et al. [2]	51/Female	Left ; 3.5 cm mass	0	0	Radical mastectomy	NS
Hanna et al. [9]	31/Female	NS	2/18	0	Modified radical mastectomy	14:AW

invasive breast carcinoma. Tavassoli [18] used interchangeably the terms MEC and adenosquamous carcinoma of the breast. Finally, those occasional cases reported as high-grade MEC of the breast in the literature constitute a very heterogeneous group of tumours. In all these cases, a squamous pleomorphic carcinoma was intermingled with adenocarcinomatous proliferation and mucous-producing cells and probably are invasive tumours with different lineages of differentiation, difficult to locate in the group of MEC.

The cases of MEC here reported, showing cystic to solid features, were composed of various types of cells reminiscent of basaloid, intermediate, squamous and mucinous cells, seen in MEC of salivary glands. In addition, the staining pattern of CK 7 positive cells located in the central part of the neoplastic nests and of CK 14 cells predominantly located in the outer layers of neoplastic nests recapitulate the zoning phenomenon described in MEC of salivary glands by Foschini et al. [7]. This pattern of CK staining is unique and shared by both mammary and salivary gland MEC and is very useful to establish the correct diagnosis of MEC. This is mostly pertinent in high-grade MEC, as in the present case 5. In the absence of this very distinct pattern, the diagnosis of high-grade MEC can be very problematic.

With the Auclair et al. [1] grading system, three cases appeared low grade, one intermediate and one high grade. The Elston and Ellis grading system led to four grade-1, one grade-2 and one grade-3 lesions. Therefore, it appears that, in this respect, both grading systems are equivalent and, therefore, the indication given by Elston and Ellis [4] to grade all invasive carcinomas is very pertinent in MEC.

The breast, the major salivary glands and the skin adnexae are tubulo-acinar structures derived from embryonic ectoderm. The common origin probably explains similar morphological features shared by some of their tumours.

Breast and salivary gland MEC are very similar, but not superimposable, lesions. Associated DCIS that were seen in three of the present cases are not recorded in salivary glands. In addition, mitochondrion-rich neoplastic cells are more numerous in MEC of salivary glands than in breast.

All patients were alive and well without evidence of recurrence or distant metastasis. Admittedly, the follow-up of the present series is short; nevertheless, MEC of the breast do not seem to be aggressive lesions, as none of the cases of well-differentiated MEC in the literature gave birth to metastases or led to the death of the patients. On the contrary, high-grade MEC have led to the death of patients in no fewer than four cases out of six patients for which follow-up is available.

Acknowledgements Drs. S. Fiaccavento, P. Fontana, S. Rahimi, S. Sulfaro and S. Cerasoli must be thanked for having permitted the enclosure of cases 2, 3, 4, and 5. The work was granted by the University of Bologna (60%) and by the "Programma ricerca scientifica di rilevante interesse nazionale 2002" (40%).

References

1. Auclair PL, Goode RK, Ellis GL (1992) Mucoepidermoid carcinoma of intraoral salivary glands. Cancer 69:2021–2030
2. Berry MG, Caldwell C, Carpenter R (1998) Mucoepidermoid carcinoma of the breast: a case report and review of the literature. Eur J Surg Oncol 24:78–80
3. Di Tommaso L, Scarpellini F, Salvi F, Ragazzini T, Foschini MP (2000) Progesterone receptor expression in orbital cavernous hemangiomas. Virchows Arch 436:284–288
4. Elston CW, Ellis IO (1991) Pathological prognostic factors in breast cancer. 1. The value of histological grade in breast cancer: experience from a large study with long-term follow-up. Histopathology 19:403–410
5. Fisher ER, Gregorio RM, Palekar AS, Paulson JD (1983) Mucoepidermoid and squamous cell carcinomas of breast with reference to squamous metaplasia and giant cell tumors. Am J Surg Pathol 7:15–27
6. Foote FW, Becker WF, Stewart FW (1945) Muco-epidermoid tumors of salivary glands. Ann Surg 122:820–844
7. Foschini MP, Marucci G, Eusebi V (2002) Low-grade mucoepidermoid carcinoma of salivary glands: characteristic immunohistochemical profile and evidence of striated duct differentiation. Virchows Arch 440:536–542
8. Foschini MP, Reis-Filho JS, Eusebi V, Lakhani SR (2003) Salivary gland-like tumours of the breast: surgical and molecular pathology. J Clin Pathol 56:497–506
9. Hanna W, Kahn HJ (1985) Ultrastructural and immunohistochemical characteristics of mucoepidermoid carcinoma of the breast. Hum Pathol 16:941–946
10. Hastrup N, Sehested M (1985) High-grade mucoepidermoid carcinoma of the breast. Histopathology 9:887–892
11. Holland R, Peterse JL, Millis RR, et al (1994) Ductal carcinoma in situ: a proposal for a new classification. Semin Diagn Pathol 11:167–180
12. Kovi J, Duong HD, Leffall LD (1981) High grade mucoepidermoid carcinoma of the breast. Arch Pathol Lab Med 105:612–614
13. Leong AS-Y, Williams JAR (1985) Mucoepidermoid carcinoma of the breast: high grade variant. Pathology 17:516–521
14. Luchtrath H, Moll R (1989) Mucoepidermoid mammary carcinoma. Immunohistochemical and biochemical analyses of intermediate filaments. Virchows Arch 416:105–113
15. Markopoulos C, Gogas H, Livaditou A, Floros D (1998) Mucoepidermoid carcinoma of the breast. J Gynecol Oncol 291–293
16. Patchefsky AS, Frauenhoffer CM, Krall RA, Cooper HS (1979) Low grade mucoepidermoid carcinoma of the breast. Arch Pathol Lab Med 103:196–198
17. Pettinato G, Insabato L, De Chiara A, Manco A, Petrella G (1989) High-grade mucoepidermoid carcinoma of the breast. Fine needle aspiration cytology and clinicopathologic study of a case. Acta Cytologica 33:195–200
18. Tavassoli FA (1999) Pathology of the breast. Appleton-Lange, Stamford
19. Tjalma WAA, Verslegers IOJ, De Loecker PAJ, Van Mark EAE (2002) Low and high grade mucoepidermoid carcinomas of the breast. Eur J Gynecol Oncol 23:423–425

Virchows Arch (2004) 444:20–27
DOI 10.1007/s00428-003-0921-0

ORIGINAL ARTICLE

Takahiro Hasebe · Satoshi Sasaki · Shigeru Imoto · Atsushi Ochiai

Prognostic significance of the intra-vessel tumor characteristics of invasive ductal carcinoma of the breast: a prospective study

Received: 12 March 2003 / Accepted: 21 September 2003 / Published online: 18 November 2003

Abstract Invasive ductal carcinomas (IDCs) of the breast are composed of stroma-invasive tumors and tumors in vessels. The purpose of this study was to prospectively investigate whether the histological characteristics of the tumors in vessels were more significantly associated with the outcome of 393 IDC patients than well-known histological parameters. Multivariate analyses showed greater than six apoptotic figures in tumor cells in lymph vessels to be significantly associated with increased hazard rates (HRs) of tumor recurrence and death in IDC patients without nodal metastasis ($P<0.05$). Among IDC patients with nodal metastasis whose tumors were positive for estrogen receptors (ERs) or progesterone receptors (PRs) or both, greater than six apoptotic figures in tumor cells in lymph vessels and greater than four mitotic figures in tumor cells in lymph vessels significantly increased the HR of tumor recurrence and the HR of death, respectively ($P<0.05$). Among IDC patients with nodal metastases whose tumors were negative for ERs and PRs, multivariate analyses showed that greater than two apoptotic figures in the blood vessel tumor emboli significantly increased the HRs of tumor recurrence and death ($P<0.005$). We conclude that apoptotic figures and mitotic figures in tumor cells in vessels are very important prognostic indicators for patients with IDC of the breast.

T. Hasebe · A. Ochiai (✉)
Pathology Division,
The National Cancer Center Research Institute East,
6-5-1 Kashiwanoha, Kashiwa, 277-8577 Chiba, Japan
e-mail: aochiai@east.ncc.go.jp
Tel.: +81-47-1346855
Fax: +81-47-1346865

S. Sasaki
Epidemiology and Biostatistics Division,
The National Cancer Center Research Institute East,
Chiba, Japan

S. Imoto
Department of Breast Surgery,
The National Cancer Center Hospital East,
Chiba, Japan

Keywords Apoptosis · Mitosis · Lymph vessel · Blood vessel · Breast cancer

Introduction

Invasive ductal carcinomas (IDCs) of the breast are composed of primary invasive tumor cells, non-invasive tumor cells, and tumor stroma. Some invasive tumor cells are capable of invading lymph vessels and blood vessels, and they are most likely responsible for the lymph-node metastasis and distant organ metastasis that are the most important prognostic indicators for IDC patients.

Recently, we have clearly demonstrated that number of apoptotic and mitotic figures in tumor cells in lymph and blood vessels are more significantly associated with tumor recurrence or death of IDC patients than the number or quantity of tumor cells in lymph and blood vessels [9, 10]. This strongly suggests that the histological characteristics of tumor cells in blood vessels as well as in lymph vessels play important roles in tumor progression of IDCs.

The purpose of this study was to prospectively investigate the histological characteristics of the tumors in lymph and blood vessels together that were significantly associated with the outcome of IDC patients according to nodal metastasis, estrogen receptor (ER), and progesterone receptor (PR) status, as we had separately evaluated the prognostic significance of the histological characteristics of the tumor cells in lymph vessels and blood vessels in IDCs in previous studies [9, 10]. The results showed that apoptotic and mitotic figures in tumors in lymph and blood vessels had a significant effect on the prognosis of IDC patients independent of nodal status or ER/PR status.

Materials and methods

Consecutive cases (n=393) of IDC of the breast (the same series as in a previous study) [9] surgically treated between July 1992 and November 1998 at the National Cancer Center Hospital East served

as the subject of this study. Clinical information was obtained from the patients' medical records after complete histological examination of all IDCs. All patients were Japanese women, and they ranged in age from 28 years to 78 years old (mean, 51 years). All had a solitary lesion. Of patients, 210 were premenopausal, and 183 were postmenopausal. Partial mastectomy had been performed in 55, modified radical mastectomy in 314, and standard radical mastectomy in 24. Axillary lymph-node dissection consisting of levels I, II, and ±III was carried out in all patients. None of the patients had received radiotherapy or chemotherapy before surgery, but 290 patients had received adjuvant therapy. Of the 188 IDC patients without nodal metastasis, 88 had not received adjuvant therapy, 24 had received tamoxifen, 45 had received cyclophosphamide, methotrexate, and 5-FU, adriamycin and cyclophosphamide, or epirubicin and cyclophosphamide, and 31 had received chemotherapy plus tamoxifen. Of the 205 IDC patients with nodal metastases, 15 had not received adjuvant therapy, 34 had received tamoxifen, 51 had received chemotherapy, and 105 had received chemotherapy plus tamoxifen. There were no cases of inflammatory breast cancer in this series. All tumors were classified according to the pathological TNM (pTNM) classification [16]. ERs and PRs in the cytosol fractions were determined by enzyme immunoassay (Otsuka Assay Laboratory, Tokushima, Japan). The upper cutoff values of the ER and PR assays were 13 fmol/mg protein and 10 fmol/mg protein, respectively.

For pathological examination, the surgically resected specimens were fixed in 10% formalin overnight at 4°C, and multiple histological sections were taken from each tumor in order to measure the maximum tumor diameter and area. The sections were processed routinely and embedded in paraffin.

The following parameters of primary invasive tumor cells were examined, and the following cutoff values were established in previous studies [9, 10] based on univariate analyses using the Cox proportional hazard regression model [2]: (1) invasive tumor size ($\leq$20 mm versus >20 mm), (2) structural features (papillary/cribriform/solid versus strand), (3) nuclear atypia (mild/moderate versus severe), (4) number of mitotic figures ($\leq$6 versus >6), (5) number of apoptotic figures ($\leq$16 versus >16), (6) tumor necrosis (absent versus present) [5], (7) fibrotic focus (FF) dimension (tumor recurrence, absent/$\leq$8 mm versus >8 mm; tumor death, absent/$\leq$17 mm versus >17 mm) [6, 7, 8], (8) maximum distance of adipose tissue invasion from the tumor margin ($\leq$2 mm versus >2 mm), and (9) histological grade [3]. The number of tumor cell mitotic figures at the most advanced edge of the tumor was counted in ten high-power fields by the routinely used method [3], and the highest count in the ten fields was used for comparison with the number of mitotic figures in the tumor cells in the vessels. The mitotic figures in the tumor cells in the vessels were counted in the same manner, and the count field containing the greatest number of tumor cell apoptotic figures was used [11]. We did not use the indices, such as per/1000 tumor cells, for the assessments of mitotic and apoptotic figures, as it is difficult for pathologists to use such indices to evaluate mitotic and apoptotic figures in IDCs in routine examinations.

Based on the criteria used to identify lymph vessels [9, 14], in this study we defined "lymph vessel invasion by tumor cells" as tumor cell nests in vessels lined by endothelium with no supporting smooth muscle or elastica (Fig. 1A), and lymph vessels invaded were observed in 209 of 393 cases in this study. We evaluated lymph vessel invasion at or beyond the border of the stroma-invasive tumor area in order to distinguish lymph vessel invasion from the artifactual spaces that often form around nests of tumor cells. The following parameters of tumor cells in lymph vessels were examined with their cutoff values established in the previous studies [9] on the basis of the univariate analyses using the Cox proportional hazard regression model [2]: (1) number of lymph vessels invaded (absent/$\leq$5 versus >5), (2) maximum dimension of tumor emboli (absent/$\leq$2.25 mm versus >2.25 mm), (3) maximum distance of tumor emboli from the primary-invasive tumor margin (absent/$\leq$3 mm versus >3 mm), (4) structural features (absent/papillary/cribriform/solid versus strand), (5) nuclear atypia (absent/mild/moderate versus severe), (6) number of mitotic figures

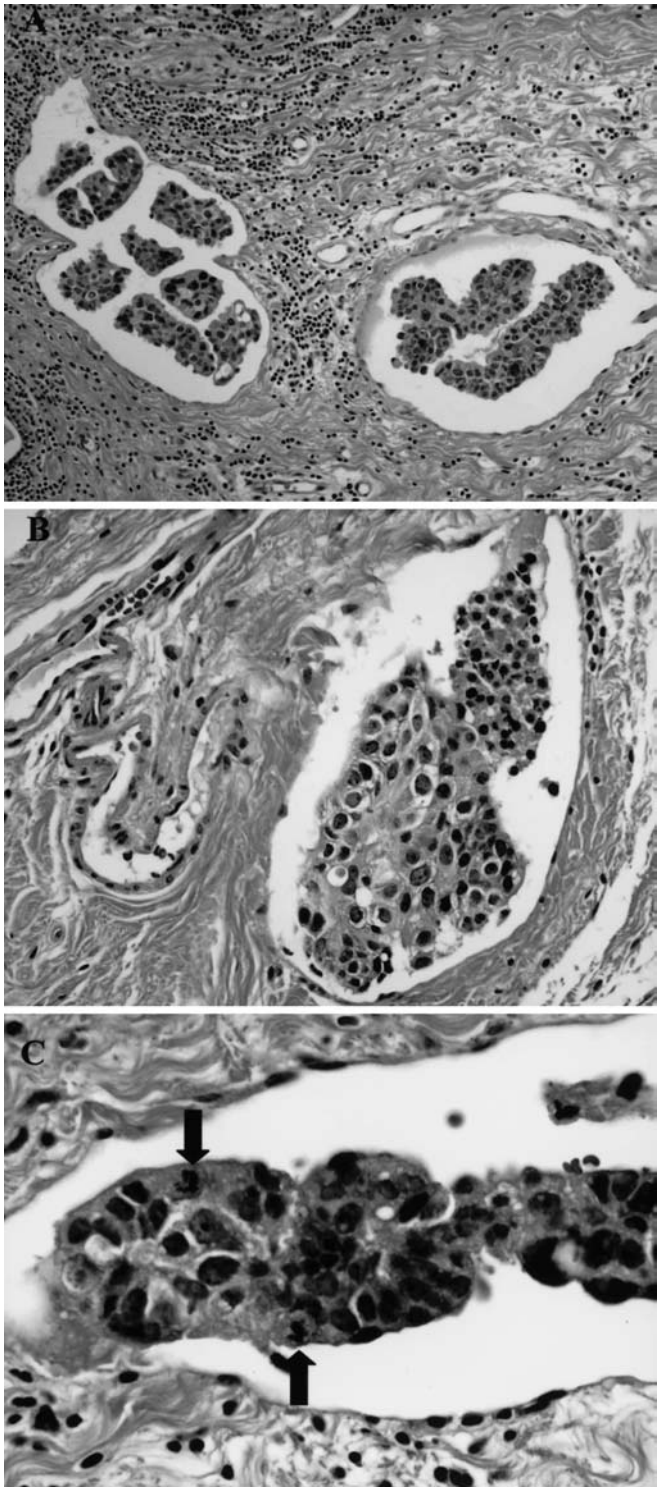

Fig. 1 Lymphatic vessel invasion by invasive ductal carcinoma cells. **A** Ductal carcinoma cells in lymph vessels. The spaces around the clump of tumor cells are lined with endothelium and filled with lymph fluid. **B** Carcinoma cells within lymph vessel exhibiting many apoptotic figures. **C** Carcinoma cells in lymph vessel exhibiting two mitotic figures (*arrows*)

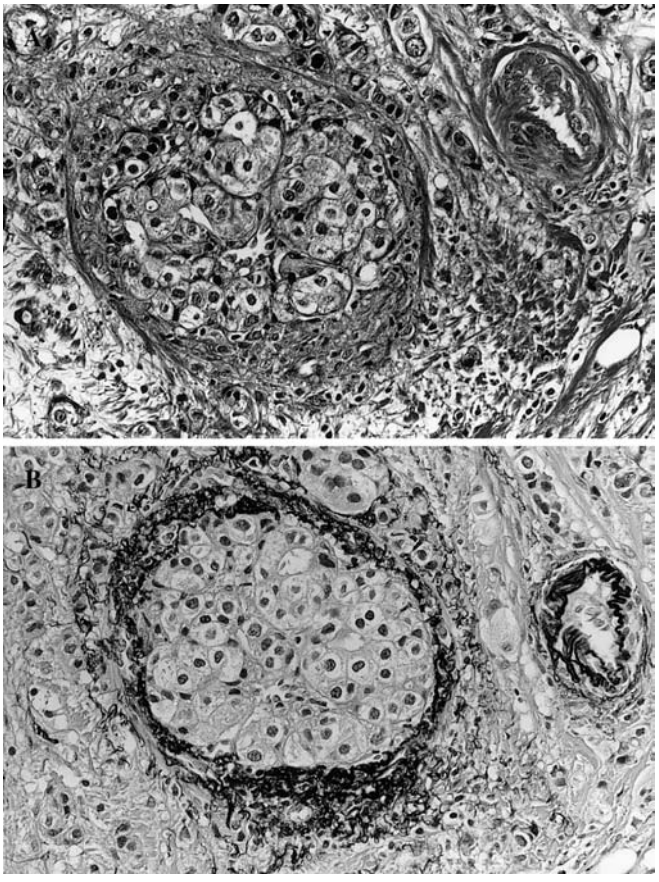

Fig. 2 Blood vessel invasion by invasive ductal carcinoma cells. **A** The round nest can be seen to be accompanied by one artery. **B** The nest surrounded by elastic fibers is recognizable as blood vessels being invaded by tumor cells. There is no zonal space between the outside of the carcinoma nest and the elastic fibers of the blood vessel

(absent/$\leq$4 versus >4) (Fig. 1B), and (7) number of apoptotic figures (absent/$\leq$6 versus >6) (Fig. 1B).

We defined tumor cell nests in vessels lined by endothelium with supporting smooth muscle or elastica as "blood vessel invasion by tumor cells" [10, 14] and examined all tumor areas in order to evaluate the presence of blood vessels invaded by the tumor cells. Blood vessels invaded were observed in 237 of 393 cases in this study. Since intraductal carcinomas within stroma-invasive tumors often have depositions of elastic fibers around their ducts, blood vessel invasion was diagnosed with confidence only when tumors were demonstrated within one or both of a pair of vessels, as demonstrated by the elastic fiber stain (Fig. 2A, B, and Fig. 3A, B). Furthermore, we found that all IDC ducts have a zonal space between the external duct epithelium and duct elastic fibers (Fig. 4A, B) and that zonal spaces still exist between the outer surfaces of intra-ductal carcinoma nests and duct elastic depositions (Fig. 4C, D). Kato et al. [12] and Farahmand and Cowan [4] have already indicated the presence of a zonal space-like space between the external duct epithelium and duct elastic fibers. Blood vessels had no zonal space within their wall, as fine to coarse elastic fibers blending with smooth muscle fibers in their smooth muscle layers were observed. Thus, this finding was very useful for distinguishing intraductal carcinoma nests from blood vessel tumor emboli. However, since it was somewhat difficult to differentiate blood vessel tumor emboli from the following status, we omitted the blood vessel tumor emboli-like foci from the count of blood vessel tumor emboli: (1) when several intraductal carcinoma components were present in the areas surrounding blood vessel tumor emboli-like foci; (2) when blood vessel tumor emboli-like foci surrounded by elastic fibers are present within a fibrotic center in primary-invasive tumors; and (3) when blood vessel tumor emboli-like foci not surrounded by elastic fibers exist within one or both of a pair of vessels.

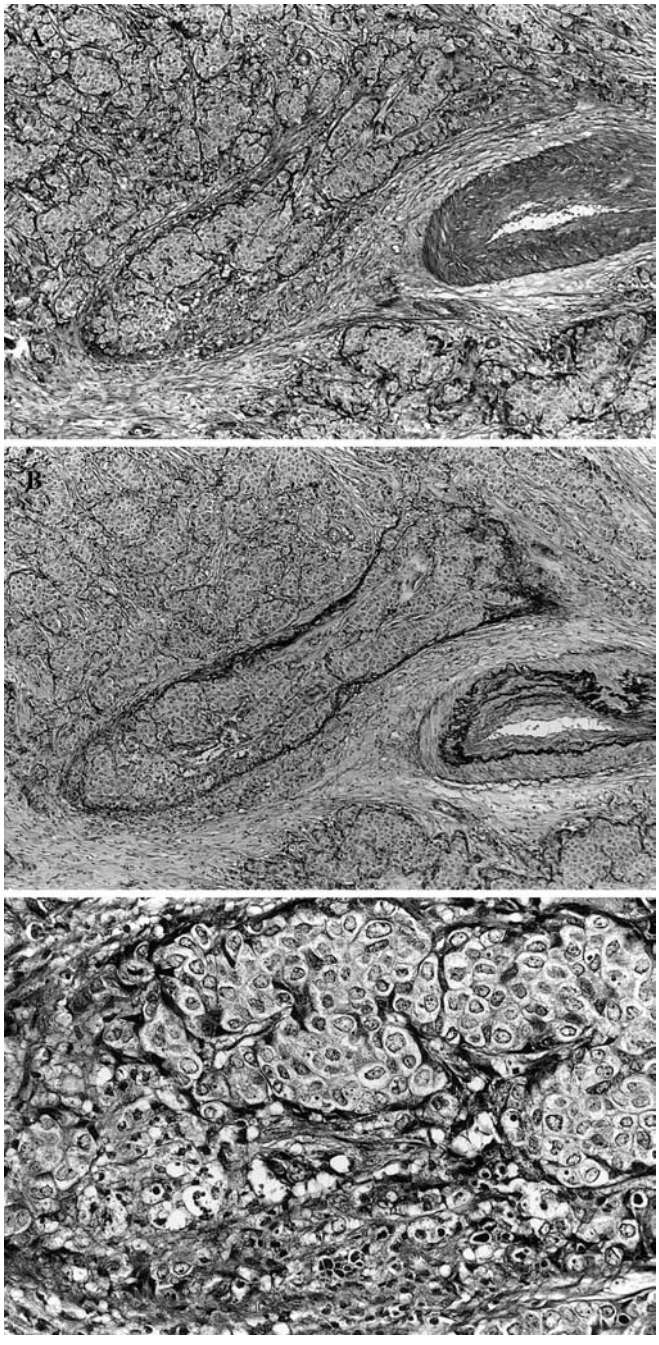

Fig. 3 Blood vessel invasion by invasive ductal carcinoma cells. **A**, **B** The large oval and elongated ductal carcinoma nest is observed next to a large artery. The nest surrounded by elastic fibers is recognizable as blood vessel tumor emboli. There is no zonal space between the outside of the carcinoma nest and the elastic fibers of the blood vessel. **C** Many apoptotic tumor cells are observed within the blood vessel tumor emboli (*lower area*), and two mitotic figures are also observed in the tumor cells (*arrowheads*)

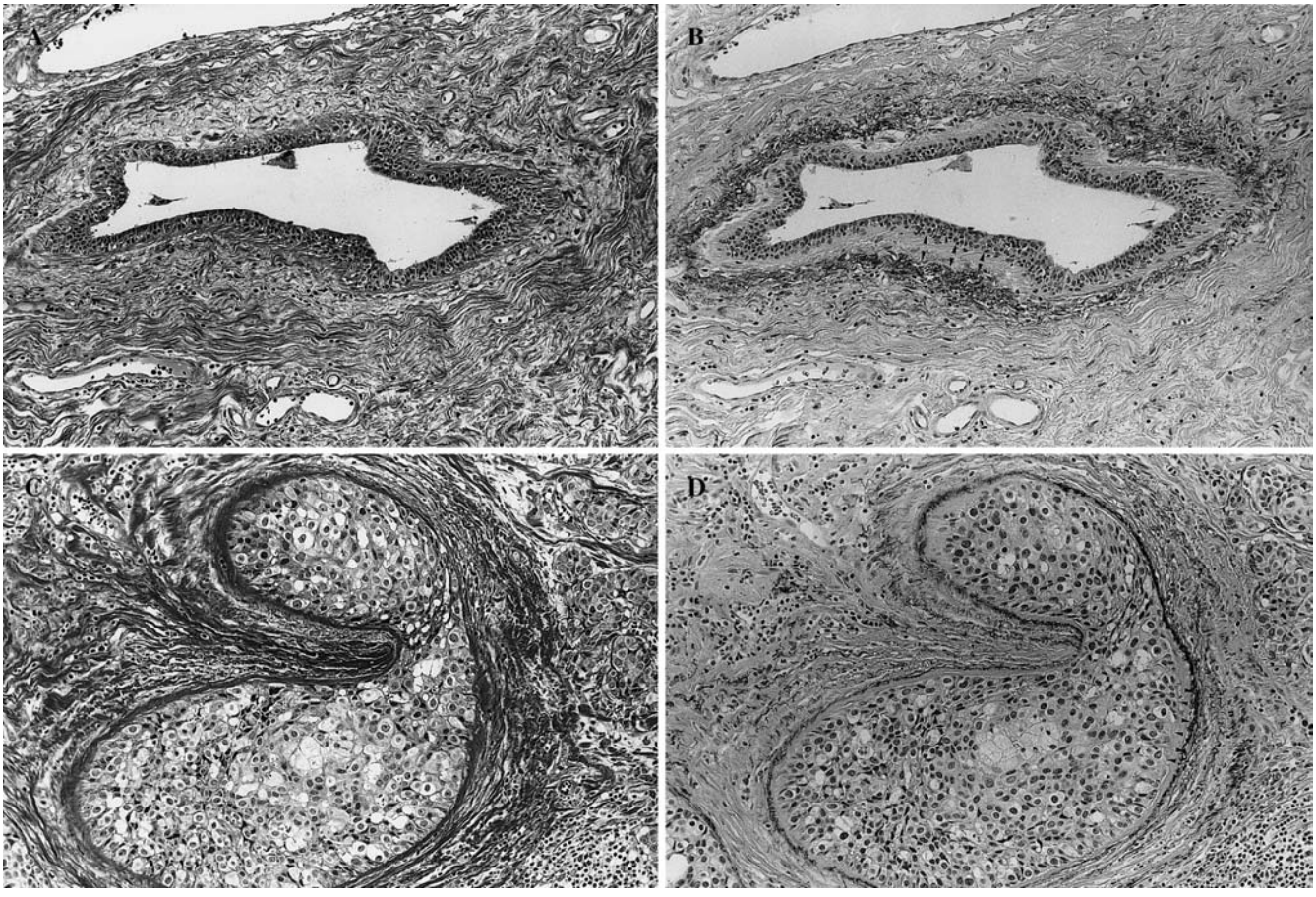

Fig. 4 Duct without carcinoma nest and duct filled with ductal carcinoma. **A**, **B** The duct is surrounded by elastic fibers, and there is a zonal space between the external ductal epithelium and elastic fibers (*arrowheads*). **C**, **D** Duct filled with intraductal carcinoma cells has a zonal space between the outside of the carcinoma nest and the elastic fibers of the duct (*arrowheads*)

The following parameters of tumor cells in blood vessels were examined with the cutoff values established in the previous studies [10]based on the univariate analyses using the Cox proportional hazard regression model [2]: (1) number of blood vessels invaded (absent/$\leq$2 versus >2), (2) maximum dimension of tumor emboli (absent/$\leq$2 mm versus >2 mm), (3) nuclear atypia (mild/moderate versus severe), (4) number of mitotic figures (absent/$\leq$2 versus >2, Fig. 3C), (5) number of apoptotic figures (absent/$\leq$2 versus >2, Fig. 3C), and (6) fibrosis grade in blood vessel tumor emboli (none/mild/moderate versus severe).

The numbers of mitotic and apoptotic figures in tumor cells in vessels were assessed in the vessels within ten high-power fields, and the one high-power field out of the ten high-power fields that shows the vessel tumor emboli that have the highest counts was used for comparison with the number of mitotic and apoptotic figures in the primary invasive tumor cells. In cases with small numbers of tumor emboli, mitotic and apoptotic figures were counted in less than ten high-power fields, and the one high-power field with tumor emboli that have the highest counts within the one high-power field was used for comparison with the number of mitotic and apoptotic figures in the primary invasive tumor cells. Since all tumor cells in blood vessels had formed a solid nest, this structural feature of tumor cells in blood vessels was excluded in the present study. The dimension of the largest tumor embolus in vessels and the distance between lymph vessel tumor emboli and the stroma-invasive tumor margin were measured with a microscope equipped with a ×10 eyepiece counting a graticule.

One author (T.H.) assessed all characteristics of the primary invasive tumors and tumors in vessels, and another author (A.O.) identified the characteristics of IDCs to confirm tumor cell characteristics in the tumor components examined by T.H. Whenever there was a discrepancy, both authors re-examined the slides to reach a consensus.

Patient survival was evaluated by follow-up for a median period of 65 months as of November 2001. Among the patients as a whole, 95 developed tumor recurrence, 64 experienced distant organ metastasis, and 45 had died of their disease. Metastasis or local recurrence was considered evidence of tumor relapse, and only deaths due to breast cancer were considered for the purposes of this study. Distant organ metastasis was detected in bone (30 cases), liver (17 cases), lung (17 cases), and brain (4 cases).

We used Spearman's correlation coefficient test to analyze the correlations between numbers of mitotic figures and apoptotic figures in the same tumor component in primary invasive tumors, tumor cells in lymph vessels, and tumor cells in blood vessels in 147 IDCs with invasion of lymph vessels and blood vessels.

We prospectively analyzed the predictive power of the histological characteristics of the tumor cells in vessels and of primary invasive tumor cells for tumor recurrence and death in the following groups without knowledge of patient outcomes: (1) a lymph-node-negative IDC group, (2) a group with IDC positive for ERs, PRs, or both and with nodal metastasis, and (3) a group of IDCs negative for ERs and PRs both with nodal metastasis by multivariate analysis employing the Cox proportional hazard regression model [2] and the step-down method, until all remaining factors were significant at a P value below 0.05. The multivariate analyses for IDCs without nodal metastasis were adjusted for age ($\leq$39 years versus >39 years), adjuvant therapy (not given versus

given) and ER and PR expression (negative versus either positive/both positive), and the multivariate analyses for IDCs with nodal metastases were adjusted for age, adjuvant therapy and nodal status (≤3 versus >3). All analyses were performed with Statistica/Windows software (StatSoft, Tulsa, Oklahoma).

Results

Mean mitotic and apoptotic figures values

The highest mean numbers of mitotic and apoptotic figures in IDC were observed in the primary invasive tumors (Table 1). There was a significant correlation between the number of tumor cell mitotic figures and the number of tumor cell apoptotic figures in the same tumor components.

Multivariate analyses for parameters significantly associated with tumor recurrence and death in patients with lymph node-negative IDC

IDCs with lymph vessel tumor emboli containing greater than six apoptotic figures significantly increased the HRs of tumor recurrence and death in the multivariate analyses (Table 2). IDCs with a FF greater than 8 mm in dimension significantly increased the HR of tumor recurrence in the multivariate analyses. IDCs with negative ER/PR status significantly increased the HR of tumor death in the multivariate analyses.

Multivariate analyses for parameters significantly associated with tumor recurrence and death in IDCs positive for ERs, PRs, or both with lymph-node metastases

Four or more nodal metastases significantly increased the HRs of tumor recurrence and death on the multivariate analyses (Table 3). Mitotic figures greater than six in primary invasive tumor cells, apoptotic figures greater than six in tumor cells in lymph vessels, and the presence of skin invasion significantly increased the HRs of tumor recurrence. Histological grade 3 and mitotic figures greater than four in tumor cells in lymph vessels were significantly associated with increased HRs of tumor death in the multivariate analyses.

Multivariate analyses for parameters significantly associated with tumor progression in IDCs negative for both ERs and PRs with lymph-node metastases

Apoptotic figures greater than two in tumor cells in blood vessels was the only parameter that significantly increased the HRs of both tumor recurrence and death in the multivariate analyses (Table 4). Six or more lymph vessels invaded significantly increased the HR of tumor recurrence in the multivariate analysis. The presence of tumor necrosis significantly increased the HR of tumor death in the multivariate analyses.

Table 1 Mean values and standard deviations of numbers of mitotic and apoptotic figures in each tumor component of invasive ductal carcinomas with lymph vessels and blood vessels invaded (n=147). The Spearman's correlations between mitotic figures (MF) and apoptotic figures (AF) of tumor cells in the same tumor component

	Number of MFs Mean±SD	Number of AFs Mean±SD	R, P values
Primary invasive tumors	5.0±3.9	14.5±22.7	0.52, <0.001
Lymph-vessel tumor emboli	1.7±2.7	8.4±16.4	0.69, <0.001
Blood vessel tumor emboli	1.8±2.5	7.6±19.4	0.69, <0.001

Table 2 Multivariate analyses for tumor recurrence and death in invasive ductal carcinomas without nodal metastasis (n=188). *TRR* tumor recurrence rate, *MR* mortality rate, *HR* hazard rate, *CI* confidence interval, *Fibrotic focus*− fibrotic focus absent, *ER* estrogen receptor, *PR* progesterone receptor, *ER/PR*+ either or both positive, *ER/PR*− both negative. The multivariate analyses for TRR and MR were performed by employing the Cox proportional hazard regression model. The step-down method was used until all the remaining parameters were significant at a P level below 0.05 in the multivariate analysis

Parameters	Cases	TRR	(%)	HR/95% CI/P value	MR	(%)	HR/95% CI/P value
Number of apoptotic figures in lymph-vessel tumor emboli							
≤6	177	21	(12)	Referent	5	(3)	Referent
>6	11	5	(45)	4.4/1.7–12.0/0.003	4	(36)	11/2.9–41.8/0.018
Fibrotic focus							
−/≤8 mm	146	12	(8)	Referent			
>8 mm	42	14	(33)	4.6/2.1–10.0/<0.001			
ER/PR status							
−	67				8	(12)	Referent
+	121				1	(1)	0.1/0.01–0.7/<0.001

Table 3 Multivariate analyses for tumor recurrence and death in invasive ductal carcinomas positive for estrogen receptors (ERs), progesterone receptors (PRs), or both with lymph-node metastasis (n=130). *TRR* tumor recurrence rate, *MR* mortality rate, *HR* hazard rate, *CI* confidence interval, *ER/PR+* either or both positive, *ER/PR−* both negative. The multivariate analyses for TRR and MR were performed by employing the Cox proportional hazard regression model. The step-down method was used until all the remaining parameters were significant at a *P* level below 0.05 in the multivariate analysis

Parameters	Cases	TRR	(%)	HR/95% CI/*P* value	MR	(%)	HR/95% CI/*P* value
Lymph-node metastasis							
≤3	64	6	(9)	Referent	2	(3)	Referent
>3	66	26	(39)	4.3/1.7–10.7/0.002	10	(15)	7.0/1.4–33.4/0.016
Number of mitotic figures in primary-invasive tumor cells							
≤6	104	18	(17)	Referent			
>6	26	14	(54)	4.8/1.6–10.0/<0.001			
Number of apoptotic figures in lymph-vessel tumor emboli							
≤6	103	19	(18)	Referent			
>6	27	13	(48)	2.9/1.4–5.9/0.005			
Skin invasion							
Absent	100	20	(20)	Referent			
Present	30	12	(40)	2.1/1.0–4.4/0.044			
Histological grade							
1 and 2	86				2	(2)	Referent
3	44				10	(23)	8.7/1.8–41.6/0.007
Number of mitotic figures in lymph-vessel tumor emboli							
≤4	120				8	(7)	Referent
>4	10				4	(40)	4.6/1.3–16.2/0.018

Table 4 Multivariate analyses for tumor recurrence and death in IDCs negative for both estrogen receptors (ERs) and progesterone receptors (PRs) and with lymph-node metastases (n=75). *TRR* tumor recurrence rate, *MR* mortality rate, *HR* hazard rate, *CI* confidence interval, *ER/PR+* either or both positive, *ER/PR−* both negative. The multivariate analyses for TRR and MR were performed by employing the Cox proportional hazard regression model. The step-down method was used until all the remaining parameters were significant at a *P* level below 0.05 in the multivariate analysis

Parameters	Cases	TRR	(%)	HR/95% CI/P-value	MR	(%)	HR/95% CI/P-value
Number of apoptotic figures in blood vessel tumor emboli							
≤2	45	16	(36)	Referent	7	(16)	Referent
>2	35	23	(77)	2.5/1.3–4.9/0.007	17	(57)	6.3/2.6–15.7/<0.001
Number of lymph vessels invaded							
≤5	38	12	(32)	Referent			
>5	37	27	(73)	2.4/1.2–5.0/0.016			
Tumor necrosis							
Absent	53				13	(25)	Referent
Present	22				11	(50)	3.8/1.6–9.0/0.002

Discussion

In the previous studies, the numbers of apoptotic figures and mitotic figures in tumor cells in the lymph and blood vessels were independent prognostic characteristics for IDC patients without nodal metastasis [9, 10]. In this study, the number of apoptotic figures in tumor cells in lymph vessels was the only histological characteristic significantly predicting tumor recurrence and death in IDCs without nodal metastasis in the multivariate analysis. Thus, we conclude that the number of apoptotic figures in tumor cells in the lymph vessels is the best histological characteristic of tumor cells in the vessels to accurately predict tumor recurrence or death of IDC patients without nodal metastasis.

The previous studies clearly showed that the number of mitotic figures of tumor cells in the lymph and blood vessels, the number of apoptotic figures of tumor cells in the lymph and blood vessels, and the number of lymph vessels invaded are significant prognostic histological characteristics for tumor recurrence or death of IDC patients with nodal metastases [9, 10]. Among these characteristics of IDC patients with nodal metastasis, the number of apoptotic figures of tumor cells in blood vessels was the only prognostic characteristic accurately predicting tumor recurrence and death of IDC patients negative for both ER and PR. Thus, we conclude that the number of apoptotic figures of tumor cells in the blood vessels is the best prognostic vessel tumor characteristic for IDC patients with nodal metastasis and negative for

both ERs and PRs. Although no significant prognostic characteristics common to tumor recurrence and death were observed, we were able to accurately predict outcomes in IDC patients with nodal metastasis and positive for ERs, PRs, or both by evaluating the numbers of apoptotic and mitotic figures of tumor cells in the lymph vessels.

Apoptotic and mitotic figures of tumor cells in lymph and blood vessels had better predictive prognostic power than the numbers of lymph vessels or blood vessels showing invasion. This strongly suggests that metastatic IDC nests in other organs seeded via lymph and blood vessels cannot be established solely on the basis of large numbers of lymph and blood vessels being invaded or large quantities of tumor cells being present in the lymph and blood vessels. The numbers of apoptotic and mitotic figures in tumor cells in lymph and blood vessels probably reflects the characteristics of the individual tumor cells. The two counts in tumor cells in lymph and blood vessels were significantly correlated with each other, and, in this study, highly apoptotic or mitotic tumor cells in lymph and blood vessels had greater prognostic predictive power than primary invasive tumors. Based on these findings, tumor cells with a high turnover rate in lymph or blood vessels probably have a greater ability to form metastatic foci in lymph nodes or distant organs than primary invasive tumor cells with a high turnover rate, and they are, therefore, probably responsible for the lethal effect in IDC patients. Méhes et al. frequently observed apoptotic tumor cells in peripheral blood samples of breast cancer patients and stated that determining the extent to which circulating apoptotic tumor cells contribute to the clinical findings of breast cancer patients would be of prognostic value [13]. Since the circulating apoptotic tumor cells in IDCs most likely originate from tumor cells that invaded the blood or lymph vessels within primary invasive tumors, the results of the current study probably provide the information Méhes wished to obtain.

In this study, we assessed lymph vessel tumor emboli and blood vessel tumor emboli only by hematoxylin-eosin (HE) staining and elastica staining, respectively. HE and elastica stainings in combination with immunostaining, e.g., for vascular endothelial growth factor-C [15], vascular endothelial growth factor receptor-3 [17], podoplanin [1], Factor VIII, CD31, CD34, or actin, may enable more accurate identification of the presence of lymph and blood vessel tumor emboli than HE or elastica staining alone. However, Kato et al. clearly demonstrated that the assessment of blood vessel tumor emboli by elastica staining has a power to accurately predict the outcome of IDC patients superior to the combined assessment of elastica staining and immunostaining [12]. In addition, the assessments of lymph and blood vessel tumor emboli by HE and elastica staining in this study clearly demonstrated significant associations with the outcome of IDC patients, and, in routine examinations, these staining methods could not be performed in all IDCs. We, therefore, conclude that the criteria used in this study to assess lymph and blood vessel invasion by HE and elastica staining are very useful as a means of accurately determining whether tumor emboli are present in lymph vessels and blood vessels.

In conclusion, this study clearly demonstrated a significant role of apoptotic and mitotic figures in tumor cells in lymph and blood vessels in the tumor progression of IDCs of the breast. Next, we will attempt to identify unknown factors that accelerate the tumor cell life cycle in lymph and blood vessel tumor emboli as well as the lethal functions of highly proliferative and apoptotic tumor cells in lymph and blood vessels. This information should provide valuable insight into tumor progression via the vessel system.

Acknowledgements This work was supported in part by a Grant-in-Aid for Cancer Research from the Ministry of Health and Welfare (11–12) and by a Grant-in-Aid for the Second Term Comprehensive 10-year Strategy for Cancer Control from the Ministry of Health and Welfare in Japan.

References

1. Birner P, Shindl M, Oberman A, Breitenecker G, Kowalski H, Oberhuber G (2001) Lymphatic microvessel density as a novel prognostic factor in early stage invasive cervical cancer. Int J Cancer 95:29–33
2. Cox DR (1972) Regression models and life-tables. J R Stat Soc 34:87–220
3. Elston CW, Ellis IO (1991) Pathological prognostic factors in breast cancer. I. The value of histological grade in breast cancer: experience from a large study with long-term follow-up. Histopathology 19:403–410
4. Farahmand S and Cowan DF (1991) Elastosis in the normal aging breast. A histopathologic study of 140 cases. Arch Pathol Lab Med 115:1241–1246
5. Gilchrist KW, Gray R, Fowble B, Tormey DC, Taylor SG (1993) Tumor necrosis is a prognostic predictor for early recurrence and death in lymph node-positive breast cancer: a 10-year follow-up study of 728 Eastern Cooperative Oncology Group patients. J Clin Oncol 11:1929–1935
6. Hasebe T, Tsuda H, Hirohashi S, et al (1998) Fibrotic focus in infiltrating ductal carcinoma of the breast: a significant histopathological prognostic parameter for predicting the long-term survival of the patients. Breast Cancer Res Treat 49:195–208
7. Hasebe T, Sasaki S, Imoto S, Ochiai A (2001) Highly proliferative fibroblasts forming fibrotic focus govern metastasis of invasive ductal carcinoma of the breast. Mod Pathol 14:325–337
8. Hasebe T, Sasaki S, Imoto S, Mukai K, Yokose T, Ochiai A (2002) Prognostic significance of fibrotic focus in invasive ductal carcinoma of the breast: a prospective study. Mod Pathol 15:502–516
9. Hasebe T, Sasaki S, Imoto S, Ochiai A (2002) Characteristics of tumors in lymph vessels play an important role in the tumor progression of invasive ductal carcinoma of the breast: a prospective study. Mod Pathol 15:904–913
10. Hasebe T, Sasaki S, Imoto S, Ochiai A (2003) Histological characteristics of tumors in blood vessels play an important role in the tumor progression of invasive ductal carcinoma of the breast. Cancer Science 94:158–165
11. de Jong JS, van Diest PJ, Baak JPA (2000) Number of apoptotic cells as a prognostic marker in invasive breast cancer. Br J Cancer 82:368–373
12. Kato T, Kameoka S, Kimura T, Nishikawa T, Kobayashi M (2002) Blood vessel invasion as a predictor of long-term

survival for Japanese patients with breast cancer. Breast Cancer Res Treat 73:1–12
13. Méhes G, Witt A, Kubista E, Ambros PF (2001) Circulating breast cancer cells are frequently apoptotic (short communication). Am J Pathol 159:17–20
14. Rosen PP (ed) (1996) Breast pathology. Lippincott-Raven, Philadelphia, pp 283–285
15. Skobe M, Hamberg LM, Hawighorst T, et al (2001) Concurrent induction of lymphangiogenesis, angiogenesis and macrophage recruitment by vascular endothelial growth factor-C in melanoma. Am J Pathol 159:893–903
16. Sobin LH, Witteklnd CH (eds) (1997) TNM classification of malignant tumors, 5th edn. Wiley-Liss, New York, pp 123–130
17. Yonemura Y, Fushida S, Bando E, et al (2001) Lymphangiogensis and the vascular endothelial growth factor receptor-3 in gastric cancer. Eur J Cancer 37:918–923

Virchows Arch (2004) 444:28–35
DOI 10.1007/s00428-003-0889-9

ORIGINAL ARTICLE

Koutaro Shinmura · Tsuyoshi Ishida · Takahiro Goto · Masahiko Kuroda · Hiroyuki Hattori · Shuzou Nagai · Tetsuo Imamura · Kiyoshi Mukai · Atsuhiro Imakiire

Expression of cyclooxygenase-2 in chondroblastoma: immunohistochemical analysis with special emphasis on local inflammatory reaction

Received: 7 April 2003 / Accepted: 28 July 2003 / Published online: 9 September 2003

Abstract To investigate the frequency and mechanism of the peritumoral inflammatory reaction in chondroblastoma, we evaluated the relationship between clinicoradiological findings and immunohistochemical expression of cyclooxygenase-2 (COX-2) in excised tumors. Twenty-one cases of chondroblastoma were studied. Imaging analysis was performed with radiographs and T1- and T2-weighted magnetic resonance images in all cases and with computed tomography scan and bone scintigraphy in some cases. Immunohistochemical study for COX-2 was carried out using formalin-fixed paraffin-embedded tissues. Periosteal reaction was observed in 6 cases (29%) and bone marrow edema in 15 cases (71%). Soft-tissue edema, joint effusion, and synovitis were found in 10 cases (48%), in 7 cases (33%), and in 9 cases (43%), respectively. Immunohistochemical expression of COX-2 in chondroblastoma cells was found in 15 of 21 cases (71%). The intensity of COX-2 immunoreactivity was correlated statistically with the presence of periosteal reaction, bone-marrow edema, soft-tissue edema, and synovitis. Our results indicate that activation of eicosanoid synthesis by COX-2 expression in the tumor itself is probably an important factor, inducing peritumoral inflammatory changes in chondroblastomas.

Keywords Chondroblastoma · Cyclooxygenase-2 · Immunohistochemistry · Inflammation · Radiographs · CT · MRI

K. Shinmura · H. Hattori · S. Nagai · A. Imakiire
Department of Orthopedic Surgery,
Tokyo Medical University,
Nishishinjuku 6-7-1, Shinjuku-ku, 160-0013 Tokyo, Japan

T. Ishida · M. Kuroda · K. Mukai
First Department of Pathology,
Tokyo Medical University,
Shinjuku 6-1-1, Shinjuku-ku, 160-8402 Tokyo, Japan

T. Goto
Department of Orthopaedic Surgery,
Faculty of Medicine, The University of Tokyo,
Hongo 7-3-1, Bunkyo-ku, 113-8655 Tokyo, Japan

T. Imamura
Department of Surgical Pathology,
Teikyo University School of Medicine,
Kaga 2-11-1, Itabashi-ku, 173-8605 Tokyo, Japan

T. Ishida (✉)
First Department of Pathology,
Tokyo Medical University,
Shinjuku 6-1-1, Shinjuku-ku, 160-8402 Tokyo, Japan
e-mail: ishida@tokyo-med.ac.jp
Tel.: +81-33-3516141
Fax: +81-33-3526335

Introduction

Chondroblastoma is a relatively rare benign cartilage tumor, representing approximately 1% of all primary bone tumors [7, 21]. It most frequently occurs in the second decade of life and arises in the epiphysis or apophysis of long tubular bone, especially of the proximal and distal femur, proximal tibia, and proximal humerus. Chondroblastoma is typically a well-demarcated lytic lesion with or without calcification on radiographs.

In some chondroblastoma cases, synovitis and inflammatory reactions around the tumor may be found, and these findings are well demonstrated by different imaging modalities, including magnetic resonance imaging (MRI). MRI is a sensitive imaging modality for demonstrating these inflammatory reactions; thus, MRI may lead to overestimation of the aggressiveness and extent of the tumor. Knowledge of the potential pitfalls may help to avoid misplaced reliance on MRI for benign bone tumor diagnosis [12]. Some chondroblastoma tissues contain high levels of prostaglandins (PGs), which are considered to play an important role in the development of a peritumoral inflammatory reaction revealed by imaging studies [25]. PGs are produced from phospholipids via arachidonic acid metabolism by cyclooxygenase-2 (COX-2). Thus, we sought to examine the expression of COX-2

in chondroblastoma tissue and to evaluate the relationship between COX-2 expression and the inflammatory reaction of the peritumoral tissues in chondroblastomas.

Materials and methods

Tumor samples

We retrieved 21 cases of chondroblastoma from the files of Division Surgical Pathology, Tokyo Medical University Hospital; Department of Pathology, Teikyo University School of Medicine; and Department of Pathology, The University of Tokyo Hospital. Treatment was curettage in all but two of these cases, and it was en-block excision in these two cases. The histopathological diagnosis of each tumor was re-confirmed by two of the authors (T. Is. and T. Im.) according to the criteria described in the bone tumor textbooks [7, 21].

Clinical and imaging studies

Clinical symptoms were evaluated for signs and symptoms of local inflammation, including the presence of local pain, swelling, limitation in range of motion in the adjacent joint, and muscle atrophy of affected limb. In all cases, plain radiographs and T1- and T2-weighted MRI were available for review. Tomogram, computed tomography (CT) scan, and bone scintigram were also examined in some cases. MRI was obtained using either a 0.5- or 1.5-T unit prior to surgery. MRI techniques, however, were not tightly controlled because of the different scanners available at the different institutes examined in this study. A range of spin-echo pulse sequences was obtained for T1- and T2-weighted images. Gadolinium-labeled diethylene triamine pentaacetate (Gd-DTPA)-enhanced T1-weighted images were obtained in 15 cases. The presence of a periosteal reaction was evaluated by radiographs, tomograms, and CT scans. Bone-marrow edema, soft-tissue swelling and edema, joint effusion, and synovitis were evaluated on MRI. Bone marrow demonstrating lower signal intensity than normal marrow intensity on T1-weighed images as well as high signal intensity on T2-weighed images was considered positive for intramedullary bone-marrow edema [19, 22]. For joint effusion, accumulation of joint fluid that is clearly demonstrated in the joint space adjacent to the tumor as high signal intensity on T2-weighed images was considered a positive finding. Synovitis and soft-tissue swelling and edema were defined as tissue swelling with high signal intensity on T2-weighted images or on Gd-DTPA-enhanced T1-weighted images [1, 9].

Histological and immunohistochemical studies

Tumor tissues were fixed in 10% formalin and embedded in paraffin. Histological sections were cut at 3 μm thickness and stained with hematoxylin and eosin. Immunohistochemical study was carried out by the labeled streptavidin biotin (LSAB) method using LSAB kit (Dako, Capinteria, CA). Polyclonal antibody for COX-2 (IBL; Fujioka, Japan, dilution 1:50) was used for primary antibody. Deparaffinized sections were incubated in methanol with 0.3% hydrogen peroxide to eliminate endogenous peroxidase activity. Antigen retrieval method was applied with autoclaving at 110°C for 10 min in 10 mM citrate buffer (pH 6.0). Colorectal adenocarcinoma tissue known to express COX-2 was used as a positive control. As the negative control, the primary antibody was replaced with Tris-NaCl buffer. The results of immunoreactivity were divided into four grades according to the number of positive cells, i.e., negative staining (0–9%), 0; weak staining (10–29%), 1+; moderate staining (30–49%), 2+; strong staining (50%>), 3+. In three cases, the synovial tissue adjacent to the tumor was also examined histologically and immunohistochemically. Immunohistochemical evaluation in 20 cases of giant cell tumor (GCT) (14 male and 6 female, age range 20–75 years, mean age 33 years) of bone in the epiphysis of the long bones (location as follows: proximal tibia, 7 cases; distal femur, 6 cases; distal radius, 3 cases; proximal humerus, 2 cases; sacrum and acetabulum, 1 case each) other than two cases was performed in comparison with chondroblastomas.

Statistical analysis

Correlation between the grading of COX-2 expression and inflammatory reactions was tested by the Spearman's correlation coefficient by rank test. Statistical significance was defined as $P<0.05$.

Results

In the 21 cases examined (7 male and 14 female; age range 11–35 years), the location of the tumor was the proximal femur (7 cases), distal femur (3 cases), proximal humerus (7 cases), proximal tibia (2 cases), and acetabulum and calcaneus (1 case each). Although local pain was a common complaint, details of pain relief from NSAIDs were unknown.

Clinical symptoms and radiological features

Clinical data are summarized in Table 1. Symptoms considered indicative of inflammation were observed. Local pain and limitation in range of motion in the affected joint were observed in 20 (95%) and 15 (71%) cases, respectively. Muscle atrophy of affected limb was recognized in 10 cases (48%), which had a substantial impairment of movement caused by pain. In preoperative laboratory data, a slight increase of white blood cells was seen in only one case. C-reactive protein was within normal limits in all cases.

Imaging findings of tumors studied were all well-circumscribed radiolucent lesion with a sclerotic rim (Fig. 1, Fig. 2). Calcification, punctuated or flocculant, was found in 12 cases (57%). Cystic changes demonstrated by MRI were found in 12 cases (57%). Interruption of the cortex was noted on CT scan in 10 cases (48%).

On plain radiograph, a periosteal reaction was observed in 6 cases (29%). The affected anatomical locations of these periosteal reaction-positive cases were all long tubular bone. Specifically, the location of the tumor in 4 of 6 cases was the proximal humerus. The femur and tibia were the site of the lesion in one case each. In 5 cases, a distinctive layered-type periosteal reaction along the diametaphyeal shaft distant from the tumor was recognized. In the remaining 1 case, remarkable periosteal reaction of solid buttressing type was seen along the proximal shaft of the humerus (Fig. 1). Bone-marrow edema was revealed in 15 cases (71%). The extent of edema varied from slight to prominent, and tended to localize to marrow space distant from original tumors (Fig. 1B, C, D, Fig. 2A, B). Soft-tissue edema was revealed, extending to peritumoral muscles in 10 cases (48%) and was seen in 5 of the 7 cases affecting in the

Table 1 Summary of clinical symptoms, imaging findings, and immunohistochemical cyclooxygenase-2 (COX-2) expression. *ROM* range of motion, *GT* greater trochanter, *0* negative staining, *1+* weak staining, *2+* moderate staining, *3+* strong staining

Case no.	Age/sex	Location	Clinical symptoms				Inflammatory reactions in images					COX-2 expression
			Local pain	Swelling	Limitation of ROM	Muscle atrophy	Periosteal reaction	Bone-marrow edema	Soft-tissue edema	Joint effusion	Synovitis	
1	11 years/female	Humerus (proximal)	+	+	+	+	+	+	+	−	+	3+
2	26 years/female	Femur (GT)	+	−	−	−	−	+	−	−	−	1+
3	19 years/female	Acetabulum	+	−	+	+	−	−	−	−	−	0
4	20 years/male	Humerus (proximal)	+	+	+	−	+	+	+	+	+	1+
5	21 years/male	Humerus (proximal)	+	+	+	−	−	−	−	−	−	0
6	11 years/female	Humerus (proximal)	+	+	+	+	−	+	+	−	−	1+
7	16 years/male	Tibia (proximal)	−	+	+	−	+	+	+	−	+	2+
8	16 years/male	Humerus (proximal)	+	+	+	−	+	+	+	−	−	3+
9	35 years/male	Calcaneus	+	−	−	−	−	+	−	−	−	0
10	20 years/female	Femur (head)	+	−	−	−	−	−	−	−	−	0
11	15 years/male	Tibia (proximal)	+	−	−	+	−	−	−	−	−	1+
12	27 years/female	Femur (head)	+	−	+	−	−	+	+	+	+	1+
13	19 years/female	Femur (distal)	+	+	−	−	−	+	+	+	+	1+
14	13 years/male	Humerus (proximal)	+	−	+	+	−	+	+	+	+	2+
15	13 years/female	Femur (distal)	+	+	+	+	+	+	−	−	−	1+
16	11 years/female	Femur (distal)	+	+	+	+	−	+	−	+	+	2+
17	19 years/female	Femur (GT)	+	−	−	−	−	−	−	−	−	0
18	15 years/female	Femur (Head)	+	−	+	+	−	+	+	+	+	3+
19	15 years/female	Humerus (proximal)	+	+	+	+	+	+	−	−	−	3+
20	17 years/female	Femur (head)	+	−	+	−	−	−	−	−	−	0
21	15 years/female	Femur (head)	+	−	+	+	−	+	+	+	+	3+

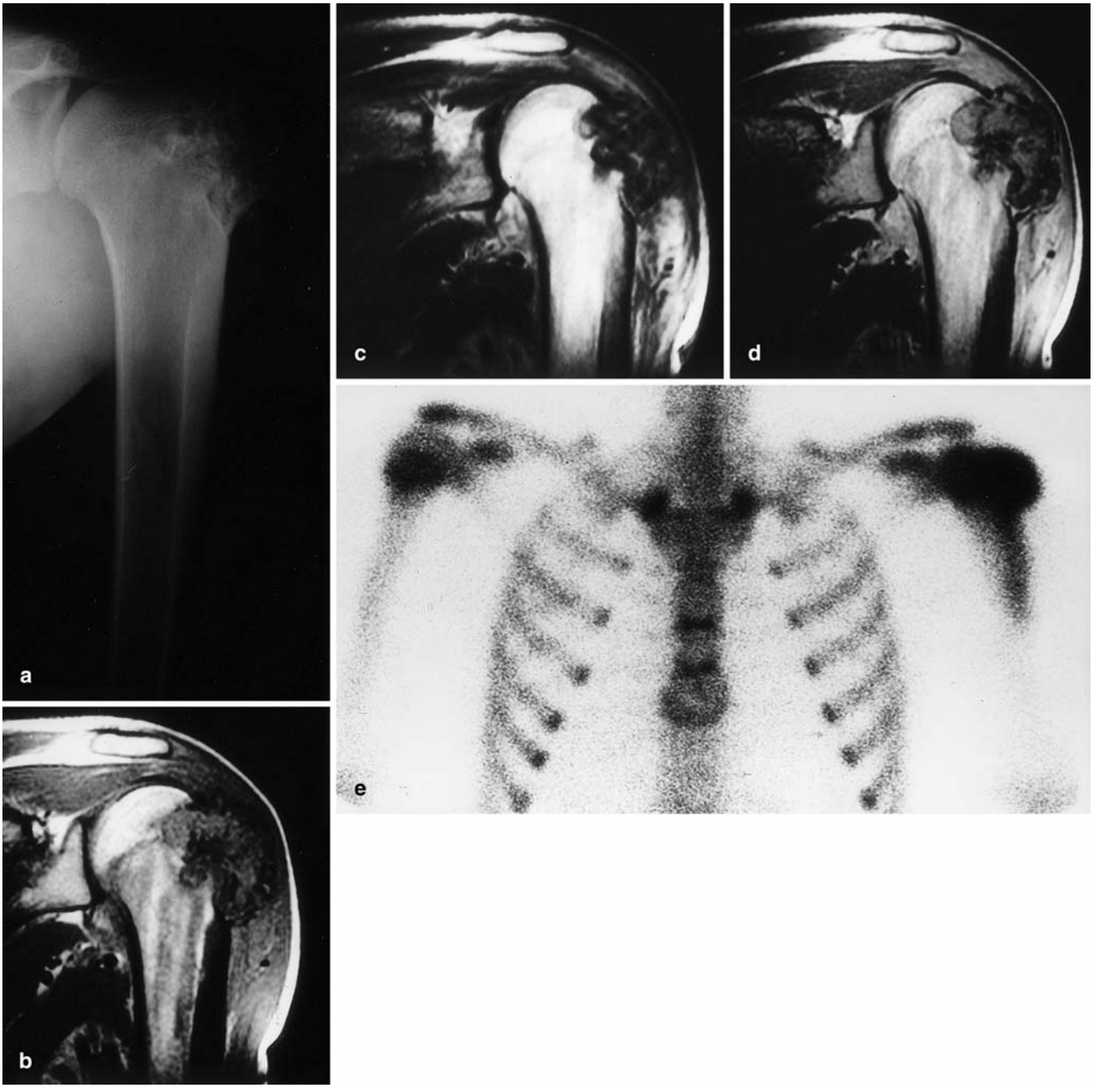

Fig. 1 A A plain radiograph of the humerus shows a well-circumscribed calcified tumor of the epiphysis with conspicuous periosteal reaction of solid buttressing type along the diametaphyseal shaft far from the tumor (case no. 8). **B** Coronal T1-weighted magnetic resonance (MR) image [repetition time (TR)/echo time (TE): 450/25] reveals a protruding tumor showing intermediate to low signal intensity. Bone-marrow edema is also identified as a longitudinal area of low signal intensity descending into the diaphyseal shaft. **C** Coronal T2-weighted MR image (TR/TE: 3000/100) reveals a low signal intensity tumor and bone-marrow edema showing high signal intensity. **D** Gadolinium-labeled diethylene triamine pentaacetate-enhanced T1-weighted image reveals bone-marrow edema as an area of high signal intensity and soft-tissue edema in the rotator cuff and deltoid muscle around the tumor. **E** Bone scintigram shows intense uptake in the proximal humerus and also less intense uptake along the lateral shaft far beyond the tumor itself

proximal humerus. Joint effusion had various patterns from slight to extreme in 7 cases (33%) and was seen in 3 of the 5 cases affecting in the femoral head (Fig. 2A, B). Synovitis was found in only 9 cases (43%) (Fig. 2A, B).

Immunohistochemical study

The histology of the tumors demonstrated findings typical of chondroblastoma, with sheet-like proliferation of round-shaped chondroblasts and foci of chondroid matrix

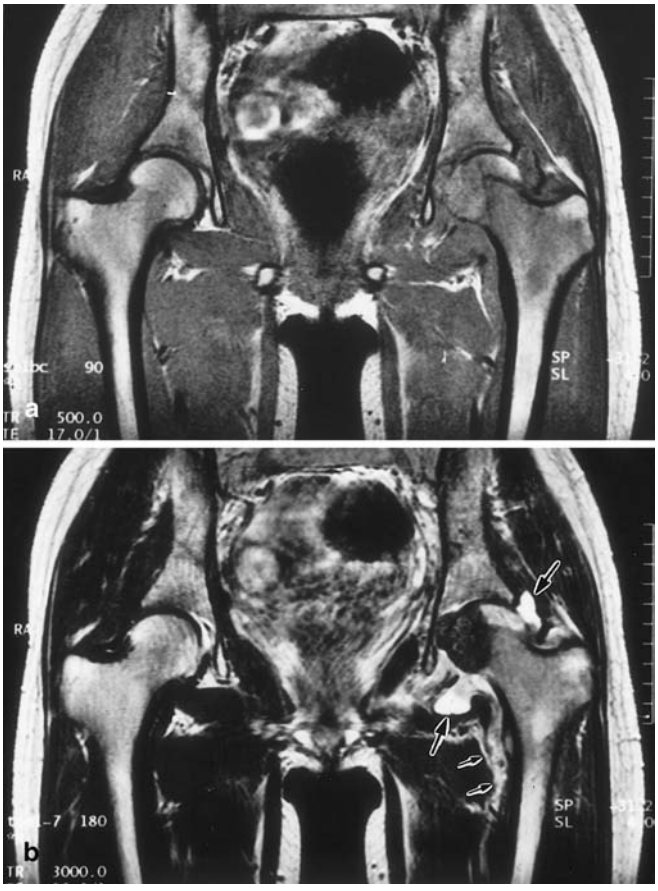

Fig. 2 **A** Coronal T1- weighted image (TR/TE: 500/17) reveals a well-demarcated tumor with isointensity and bone-marrow edema showing low signal intensity in the intertrochanteric area (case no. 18). **B** Coronal T2-weighted image (TR/TE: 3000/96) reveals bone-marrow edema with high signal intensity in the corresponding area of T1-weighted image and obvious joint effusion (*large arrows*) and synovitis (*small arrows*) in affected side. The tumor shows low signal intensity

production associated with occasional chicken-wire calcification and scattered osteoclast-like giant cells (Fig. 3A). These findings were observed in all cases in most areas, or at least within the focal area of tumors studied. Synovial tissue studied in three cases showed reactive synovitis with hyperemia, edema, and lymphoplasmacytic infiltration (Fig. 3B).

The results of immunohistochemical study are summarized in Table 1. Of 21 tumors, 15 (71%) were positive for COX-2 (Fig. 3C, D). The staining intensity was unequivocally positive among all COX-2-positive cases. In contrast, three samples of synovial tissue of the affected joint and all 20 GCT did not express COX-2. In 15 COX-2-positive cases, 7 cases showed only weak staining (1+), but 3 cases showed moderate staining (2+). In the remaining 5 cases, multiple foci of COX-2-positive tumor cells were observed, and they were classified as strong staining (3+). The expression of COX-2 was found in both areas of cellular sheet of tumor cells and tumor cells embedded in the chondroid matrix. There was no change of staining property among chondroblasts and cells within the cartilage matrix. Osteoclast-like giant cells were consistently negative for COX-2. There was no correlation of histological features (mitotic activity, apoptosis, tumor vessel formation, and tumor size) except inflammatory reactions and COX-2 expression.

Statistical analysis

The grading of COX-2 immunoreactivity was correlated with the presence of periosteal reaction (P=0.035), bone-marrow edema (P<0.01), soft-tissue edema (P=0.037), and synovitis (P=0.015).

Discussion

In general, radiological images correspond well with the aggressiveness of bone tumors. Radiographically, non-aggressive tumors showed bland-looking appearances without periosteal reaction, cortical violation, and adjacent tissue inflammation. These entities usually contain benign tumors and tumor-like lesions. However, aggressive lesions, such as malignant bone tumors, some osteomyelitis, and eosinophilic granuloma, induce tissue reactions adjacent to the lesions. These reactions include a periosteal reaction, bone-marrow and soft-tissue edema, synovial fluid accumulation, and soft-tissue swelling. In some benign tumors, however, these prominent tissue reactions, which are normally associated with aggressive or malignant bone lesions, have been described [12]. Osteoid osteoma is a typical example of such a benign tumor [17, 18]. Recent imaging advances, especially MRI, have revealed that other benign tumors, e.g., chondroblastomas, demonstrate tissue reactions around them[3, 12, 16, 23, 25].

In general, chondroblastoma shows a well-circumscribed radiolucent lesion with or without calcification and sclerotic rim. In addition to these findings, inflammatory responses, including periosteal reaction, bone-marrow and soft-tissue edema, and synovitis, have been described in some chondroblastomas by plain film or MRI. A thick-solid or layered-type periosteal reaction distant from the lesion itself has been found in 20–90% of cases of chondroblastoma on radiography or MRI [2, 3, 4, 8, 12, 13, 15, 16, 23, 25]. Bone-marrow edema extending to the circumference of the tumor is observed in 82–92% of cases on MRI, and soft-tissue edema is also found in 58–82% of cases [15, 16, 23]. Approximately 30% of cases are associated with joint effusion as demonstrated by MRI [15, 16, 25]. In our study, the frequency of inflammatory reaction was similar to previously reported data. Periosteal reaction was noted in 29%, bone-marrow edema in 71%, soft-tissue edema in 48%, joint effusion in 33%, and synovitis in 43% of cases examined. Therefore, the frequencies of inflammatory reactions found in chondroblastoma cases appear to be consistent across institutions.

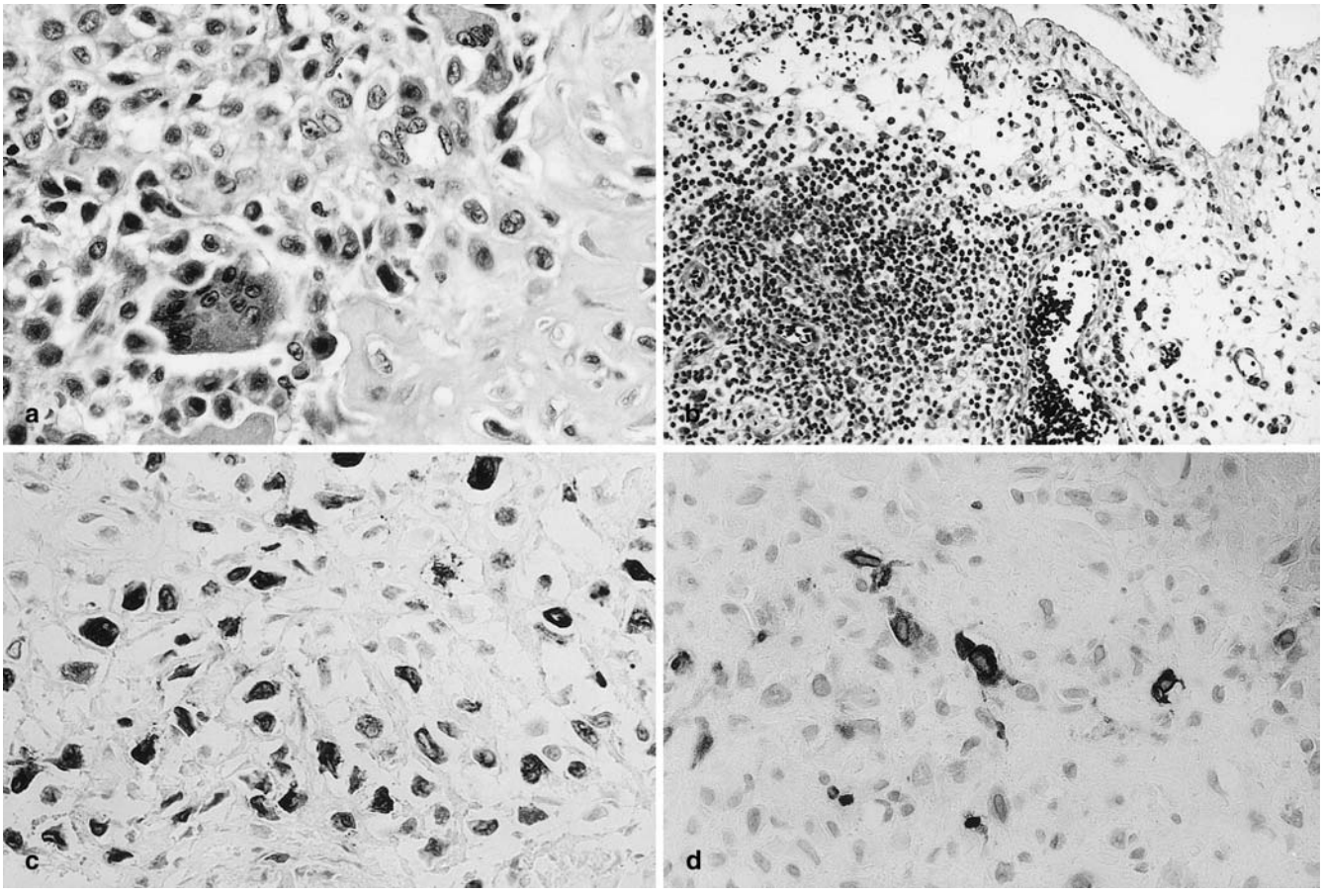

Fig. 3 **A** Histology of the tumor shows sheet-like proliferation of chondroblasts and chondroid matrix production (case no. 18) (hematoxylin and eosin, ×100). **B** Histology of synovium shows reactive synovitis with edema, hyperemia, and lymph follicle (case no. 21) (hematoxylin and eosin, ×50). **C–D** Immunohistochemical staining for cyclooxygenase-2 (COX-2). **C** The tumor cells are diffusely positive for COX-2 in (3+) case (case no. 8) (×100). **D** COX-2 expression is seen in (1+) case (case no. 2) (×100)

The mechanism of inflammatory reactions that are sometimes observed in benign bone tumors remains unclear. Recent studies suggest, however, that high levels of PGs within the lesion, such as osteoid osteoma and chondroblastoma, may play an important role for the development or maintenance of inflammatory reactions [5, 10, 11, 24, 26].

COX is the essential regulatory enzyme of the eicosanoid biosynthetic pathway and catalyzes the conversion of arachidonic acid into PGG2 and PGH2. PGH2 is subsequently converted into various eicosanoids including PGE2, PGF2α, PGI2, and the like. COX has two different isoforms, COX-1 and COX-2, derived from distinct genes, respectively. COX-1 is constitutively expressed and mediates many of the housekeeping functions of COX in nearly all tissues under basal conditions [6]. Conversely, COX-2 is inducible and is considered to be a key mediator of inflammation via the eicosanoid biosynthetic pathway.

In osteoid osteomas, PGs are thought to be responsible for inflammatory reactions around the nidus and for nocturnal pain that is characteristically relieved by nonsteroidal anti-inflammatory drugs (NSAIDs). Osteoblastic tumor cells within the osteoid osteoma nidus have shown diffuse immunoreactivity for COX-2 [17, 18, 20]. Bone-marrow edema around the lesion detected by MRI is greatly reduced or eliminated after surgical removal of the nidus [18]. Taken together, these data suggest that COX-2 expression in osteoid osteoma cells may play a major role in activating the eicosanoid biosynthetic pathway leading to bone-marrow edema and other inflammatory reactions found in osteoid osteoma cases.

In our study, immunohistochemical expression of COX-2 in chondroblastoma cells was found in 15 of 21 cases (71%). Osteoclastic giant cells and synovial tissue and osteoblasts around the lesion were all negative for COX-2. Bone-marrow edema was observed in 14 of 15 COX-2-positive cases; however, only 1 case was observed in which COX-2 staining was negative and bone-marrow edema was present. COX-2 expression is seen in all periosteal reaction-, joint effusion-, synovitis-, and soft-tissue edema-positive cases. No cases were seen with negative COX-2 staining that were positive for periosteal reaction, joint effusion, synovitis, or soft-tissue edema. These observations indicate that COX-2 expression in tumor tissue and inflammatory reactions are closely

related and are statistically significant. In addition, a small COX-2-positive chondroblastoma (case no.13) was also associated with these inflammatory reactions [14]. Conversely, in relatively large, COX-2-negative chondroblastomas, the inflammatory reactions are not found. Thus, it appears that the most important factor for inducing inflammatory reactions in chondroblastoma is COX-2 expression in the lesion itself, most likely via activation of eicosanoid biosynthetic pathway. The study of PG concentration in chondroblastoma is limited; however, Wold et al. demonstrated that one chondroblastoma tumor sample contained increased levels of PGE2 relative to the adjacent bone [24]. Another study reported by Yamamura et al. showed higher levels of PGs in eight cases of chondroblastoma than that of other cartilage tumors and GCT [26].

In osteoid osteoma, diffuse intense immunoreactivity for COX-2 was found in osteoblastic tumor cells [17, 18, 20]. COX-2 immunoreactivity in chondroblastomas was less intense than in typical cases of osteoid osteoma [14]. Among chondroblastoma cases, intensity of COX-2 expression may also correlate with the intensity of peritumoral inflammatory reactions, but does not correlate with tumor size.

Bone-marrow edema is more frequently seen than other peritumoral inflammatory changes. This could be related to the fact that bone marrow is adjacent to the tumor and that MRI is a very sensitive imaging modality. The periosteum, synovium, and joint cavity are not close to the tumor itself; therefore, the concentration of PGs in these tissues is likely lower than within the bone marrow immediately surrounding the lesion. In addition, plain radiography and CT are less sensitive imaging modalities for the detection of periosteal reaction.

GCT is an aggressive tumor that generally occurs in the epiphysis like chondroblastoma. Despite histological similarities, these two entities must be distinguished because of their radically different biological behavior. Although local aggressiveness is frequently observed in giant cell tumor, peritumoral inflammatory changes have not been noted in giant cell tumor. Interestingly, all 20 cases of giant cell tumor studied show neither COX-2 immunoreactivity nor inflammatory reactions. Thus, peritumoral inflammatory reactions are not related to tumor histology, size, location, and aggressiveness, but are related to COX-2 expression in the tumor tissue.

In summary, there is the possibility that increased COX-2 expression is only an associated finding with inflammation; nevertheless, our study suggests that COX-2 expression is likely an important factor for inducing peritumoral inflammatory changes in chondroblastomas. The same mechanism, activation of eicosanoid biosynthetic pathway by COX-2 within the tumor, functions in these secondary inflammatory reactions, such as bone-marrow edema and periosteal reaction both in the chondroblastoma and osteoid osteoma.

References

1. Beltran J, Chandnani V, McGhee RA Jr, Kursunoglu-Brahme S (1991) Gadopentetate dimeglumine-enhanced MR imaging of the musculoskeletal system. Am J Roentgenol 156:457–466
2. Bloem JL, Mulder JD (1985) Chondroblastoma: a clinical and radiological study of 104 cases. Skeletal Radiol 14:1–9
3. Braunstein E, Martel W, Weatherbee L (1979) Periosteal bone apposition in chondroblastoma. Skeletal Radiol 4:34–36
4. Brower AC, Moser RP, Kransdorf MJ (1990) The frequency and diagnostic significance of periostitis in chondrobalstoma. Am J Roentgenol 154:309–314
5. Ciabattoni G, Tramburrelli F, Greco F (1991) Increased prostacyclin biosynthesis in patients with osteoid osteoma. Eicosanoids 4:165–167
6. Crofford LJ (1997) COX-1 and COX-2 tissue expression: implications and predictions. J Rheumatol 24:15–19
7. Dorfman HD, Czerniak B (eds) (1998) Benign cartilage tumors. In: Bone tumors. Mosby, St. Louis, pp 253–352
8. Edel G, Ueda Y, Nakanishi J, Brinker KH, Roessner A, Blasius S, Vestring T, Muller-Miny H, Erlemann R, Wuisman P (1992) Chondroblastoma of bone. Virchows Archiv 421:355–366
9. Erlemann R, Reiser MF, Peters PE, Vasallo P, Nommensen B, Kusnierz-Glaz CR, Ritter J, Roessner A (1989) Musculoskeletal neoplasms: static and dynamic Gd-DTPA-enhanced MR imaging. Radiology 171:767–773
10. Greco F, Tamburrelli F, Ciabattoni G (1991) Prostaglandins in osteoid osteoma. Int Orthopaedics 15:35–37
11. Hasegawa T, Hirose T, Sakamoto R, Seki K, Ikata T, Hizawa K (1993) Mechanism of pain in osteoid osteomas: an immunohistochemical study. Histopathology 22:487–491
12. Hayes CW, Conway WF, Sundaram M (1992) Misleading aggressive MR imaging appearance of some benign musculoskeletal lesions. Radiographics 12:1119–1134
13. Hudson TM, Hawkins IF Jr (1981) Radiological evaluation of chondroblastoma. Radiology 139:1–10
14. Ishida T, Goto T, Motoi N, Mukai K (2002) Intracortical chondroblastoma mimicking intra-articular osteoid osteoma. Skeletal Radiol 31:603–607
15. Jee WH, Park YK, McCauley TR, Choi KH, Ryu KN, Suh JS, Suh KJ, Cho JH, Lee JH, Park JM, Lee YS, Ok IY, Kim JM (1999) Chondroblastoma: MR characteristics with pathologic correlation. J Comput Assist Tomogr 23:721–726
16. Kaim AH, Hugli R, Bonel HM, Jundt G (2002) Chondroblastoma and clear cell chondrosarcoma: radiological and MRI characteristics with histopathological correlation. Skeletal Radiol 31:88–95
17. Kawaguchi Y, Sato C, Hasegawa T, Oka S, Kawahara H, Norimatsu H (2000) Intraarticular osteoid osteoma associated with synovitis: a possible role of cyclooxygenase-2 expression by osteoblasts in the nidus. Mod Pathol 13:1086–1091
18. Kawaguchi Y, Hasegawa T, Oka S, Sato C, Arima N, Norimatsu H (2001) Mechanism of intramedullary high intensity area on T2-weighted magnetic resonance imaging in osteoid osteoma: a possible role of COX-2 expression. Pathol Int 51:933–937
19. Moore SG, Bisset GS 3rd, Siegel MJ, Donaldson JS (1991) Pediatric musculoskeletal MR imaging. Radiology 179:345–360
20. Mungo DV, Zhang X, O'Keefe RJ, Rosier RN, Puzas JE, Schwarz EM (2002) COX-1 and COX-2 expression in osteoid osteomas. J Orthopaedic Res 20:159–162
21. Unni KK (ed) (1996) Benign chondroblastoma. In: Dahlin's bone tumors: general aspects and data on 11,087 cases, 5th edn. Lippincott-Raven, Philadelphia, pp 47–57
22. Vogler JB 3rd, Murphy WA (1988) Bone marrow imaging. Radiology 168:679–693
23. Weatherall PT, Maale GE, Mendelsohn DB, Sherry CS, Erdman WE, Pascoe HR (1994) Chondroblastoma: classic and confusing appearance at MR imaging. Radiology 190:467–474

24. Wold LE, Pritchard DJ, Bergert J, Wilson DM (1988) Prostaglandin synthesis by osteoid osteoma and osteoblastoma. Mod Pathol 1:129–131
25. Yamamura S, Sato K, Sugiura H, Iwata H (1996) Inflammatory reaction in chondroblastoma. Skeletal Radiol 25:371–376
26. Yamamura S, Sato K, Sugiura H, Katagiri H, Ando Y, Futatsu H, Iwata H (1997) Prostaglandin levels of primary bone tumor tissues correlate with peritumoral edema demonstrated by magnetic resonance imaging. Cancer 79:255–261

Virchows Arch (2004) 444:36–42
DOI 10.1007/s00428-003-0898-8

ORIGINAL ARTICLE

Yoshinori Fujimura · Masaharu Takeda · Hidenori Ikai · Ken Haruma · Takeshi Akisada · Tamotsu Harada · Tatsuya Sakai · Masanobu Ohuchi

The role of M cells of human nasopharyngeal lymphoid tissue in influenza virus sampling

Received: 7 March 2003 / Accepted: 6 July 2003 / Published online: 10 October 2003

Abstract Little is known about the role of the M cells of human nasopharyngeal lymphoid tissue in the sampling of viruses that cause respiratory infections. To clarify whether M cells could function as a gateway for influenza virus into human nasopharyngeal lymphoid tissue, excised adenoid tissue was incubated in media containing influenza A virus for 30, 60, and 90 min, respectively. Transmission electron microscopic observation revealed that many influenza viruses adhered to M cell surfaces and were taken up into the cytoplasmic vesicles of M cells after 30 min incubation; the viruses had been transported into enfolded lymphoid cells after 60 min incubation. By staining M cells with *Sambucus nigra* lectin, which specifically recognizes the NeuAcα2,6 Gal linkage of sialoprotein, it was also found that abundant receptors for the human influenza virus are present on the M cell surface. Our findings indicated that M cells of human nasopharyngeal tonsils function as a major port for influenza A virus entry and that the virus could be efficiently transferred to enfolded macrophages and lymphoid cells by M cells. The transport of influenza viruses to lymphoid cells by M cells may promote antigen delivery to the immune system, and these findings may be important for systemic delivery of those influenza viruses that have the capacity to productively infect cells outside of the respiratory tract.

Y. Fujimura (✉) · M. Takeda · H. Ikai · K. Haruma
Division of Gastroenterology, Department of Medicine,
Kawasaki Medical School,
701-0192 Kurashiki, Japan
e-mail: fujimura@med.kawasaki-m.ac.jp
Tel.: +81-86-4621111
Fax: +81-86-4621199

T. Akisada · T. Harada
Department of Otolaryngology,
Kawasaki Medical School,
701-0192 Kurashiki, Japan

T. Sakai · M. Ohuchi
Department of Microbiology,
Kawasaki Medical School,
701-0192 Kurashiki, Japan

Keywords M cell · Influenza A virus · NALT · Lectin · Electron microscopy

Introduction

Human influenza viruses cause highly acute respiratory diseases and are occasionally implicated in worldwide pandemics. The primary site of viral infection is the upper respiratory tract, with secondary involvement of the lungs [18]. Antiviral IgA antibodies appear in the upper respiratory tract after primary infection with the influenza virus [19]. The nasal mucosa is the first site of contact with any inhaled viruses. However, little is known about the role of the M cells of human nasopharyngeal lymphoid tissue (NALT) in the sampling of influenza virus.

In humans, the collection of oropharyngeal tissue and NALT is called a Waldeyer's ring. The palatine tonsils, nasopharyngeal tonsils (adenoids), and lingual tonsils constitute the major part of Waldeyer's ring. The epithelium of NALT consists of a great number of ciliated epithelial cells, columnar cells, a few mucous goblet cells, and M cells. In rodents, a specialized follicle-associated epithelium containing M cells is observed overlying NALT [17]. The rodent M cells of NALT are responsible for sampling and transporting antigens to underlying lymphoid tissue [8, 10]. The experiments with rodents demonstrated that the nasal administration of antigens should be as effective as enteric immunization [16]. In humans, the M cells of NALT are ultrastructurally and functionally similar to those in Peyer's patches and colonic lymphoid follicles [4, 5]. It has been shown that horseradish peroxidase (HRP) can easily be taken up by M cells of human NALT [4]. These observations suggest that microorganisms may also be exclusively sampled through M cells in the nasal cavity.

Although the role of NALT in local immune responses against pathogens in the respiratory tract could be very important, it has not yet been elucidated whether M cells in human NALT interact with viruses during the initial

stages of influenza infection. In the present study, we demonstrated that influenza virus particles are efficiently taken up by M cells of human NALT and then transferred to macrophages and lymphocytes.

Materials and methods

Tissue samples

Tissue samples were obtained from five patients with chronic inflammation (four males and five females; ages, 2–14 years) by adenotomy at the Kawasaki Medical School Hospital. All patients or legal guardians of patients gave informed consent. The tissues obtained were divided into two parts for organ culture with influenza A virus and for lectin staining.

Organ cultures of human nasopharyngeal tonsils and incubation with influenza A viruses

After adenotomy, tissues obtained were immediately placed in a culture media (RPMI 1640; Gibco, NY) and incubated in a humid atmosphere of 95% air and CO_2 at 37°C. After a 20-min incubation of each sample in 5 ml RPMI 1640 medium, the culture was mixed with 3 ml of influenza A virus suspension, which contained approximately 109 virus particles per milliliter. After incubations for 30, 60, or 90 min, the specimens were washed twice with fresh medium and fixed in 2.5% glutaraldehyde at 4°C for 2 h in preparation for transmission electron microscopy. A cultured control group without viruses was also prepared.

Preparation of influenza A viruses

Influenza A virus MRC-11 reassortant, which consists of the hemagglutinin and neuraminidase of Port Chalmers/1/73 (H3N2) strain with other components of PR/8 strain, was grown in the allantoic sac of 11-day-old embryonated chicken eggs and was concentrated as previously described [11].

Processing for transmission electron microscopy

After fixation in 2.5% glutaraldehyde at 4°C for 2 h, samples were fixed in 1% osmium tetroxide for 2 h, dehydrated through an ethanol series, transferred to propylene oxide, and embedded in epoxy resin. Ultrathin sections were made with a Leica Reichert Ultracut S ultramicrotome with diamond knives. These sections were stained with uranyl acetate and lead citrate and examined in a Hitachi H-7100 electron microscope.

For negative staining, the virus was suspended in 0.1 M cacodylate buffer containing 0.6 M KCl and 2% glutaraldehyde (pH 7.2) at 4°C for 15 min, and then washed with the same buffer. One drop of the virus suspension was placed on a coated grid, stained with uranyl acetate, and examined in a Hitachi H-7100 electron microscope.

Detection of sialoglycan on the cell surface with lectin

For detection of influenza virus receptor by lectin staining, a part of the adenoid tissue was rinsed with 0.01 M phosphate-buffered saline (PBS) (pH 7.6), fixed in a periodate-lysine-2% paraformaldehyde solution for 6 h at 4°C, rinsed with a series of PBS-containing graded concentrations of sucrose, and then embedded in Tissue-Tek OCT compound (Sakura Finetek USA, Inc., Torrance, CA, USA). The fixed tissue was sectioned at 7 μm with a cryostat, mounted on poly-L-lysine-coated glass slides (Dako, Kyoto, Japan), and air dried at room temperature for 3 h. Specimens were immersed in 10% normal sheep serum (Vector Laboratories, Burlingame, CA, USA) for 30 min to block any non-specific reaction. The specimens were rinsed with PBS and incubated in an appropriately diluted digoxigenin-labeled *Sambucus nigra bark* (SNA) (Boehringer Mannheim, Germany) overnight at 4°C in a humidified chamber. Endogenous peroxidase activity remaining in the tissue was inactivated by incubation with methanol containing 0.3% hydrogen peroxide for 10 min. After washing with PBS, the specimens were incubated with HRP-labeled anti-digoxigenin antibody (Roche Molecular Biochemicals, Mannheim, Germany) for 6 h in moist chambers at 4°C. The specimens were rinsed with PBS, fixed with 0.5% glutaraldehyde in PBS, and then rinsed carefully with PBS six times for each 5 min. The samples were stained with 0.02% 3,3′-diaminobenzidine tetrahydrochloride (DAB; Organon Teknika Corp., Durham, NC, USA) in 0.05 M Tris buffer (pH 7.6) for 30 min at room temperature and subsequently stained with a 0.02% DAB solution containing 10 mM hydrogen peroxide plus 10 mM sodium azide for 10 min.

For immunoelectron microscopy, specimens were treated as described above, postfixed with 2% osmium tetraoxide (Ted Pella, Inc., Redding, CA, USA) in PBS for 1 h, dehydrated, and then embedded in epoxy resin. Ultrathin sections were stained with lead citrate for 1 min and subjected to electron microscopic observation.

Neuraminidase treatment

Neuraminidase purified from *Clostridium perfringens* (type VIII, Sigma Chemical Co., Louis Mo., USA) was used to confirm the specificity of SNA for sialoglycan. For neuraminidase treatment as previously described [6], the deparaffinized sections were washed with 0.1 M sodium acetate buffer, pH 5.5, and incubated at 37°C for 5 h with neuraminidase at a concentration of 1 U/ml in 0.1 M sodium acetate buffer, pH 5.5, and 0.04 M calcium chloride. Sections were then washed with 0.01 M PBS and lectin staining was carried out as described above.

Results

Electron microscopic observation of influenza A virus by negative staining

To control the quality of the virus preparation and identify the sizes of virus particles, a part of the preparation was negatively stained and subjected to electron microscopy. As shown in Fig. 1, round virus particles with diameters of 100–160 nm were observed. This virus preparation was then used for the following study.

Transmission electron microscopic observation of nasopharyngeal tonsils cultured with influenza A viruses

Transmission electron microscopy showed that the cytoplasm of M cells was attenuated by enfolding lymphoid cells. Their microvilli were irregular, and many small vesicles were recognized in their cytoplasm. After 30 min incubation, many viruses were found on the surfaces of M cells (Fig. 2). After 60 min incubation, the viruses were found on the surfaces and within large vesicles of M cells (Fig. 3 and Fig. 4). Spike-like structures were clearly observed on the surfaces of virus particles (*arrow*, in Fig. 3). After 90 min incubation, the viruses were often

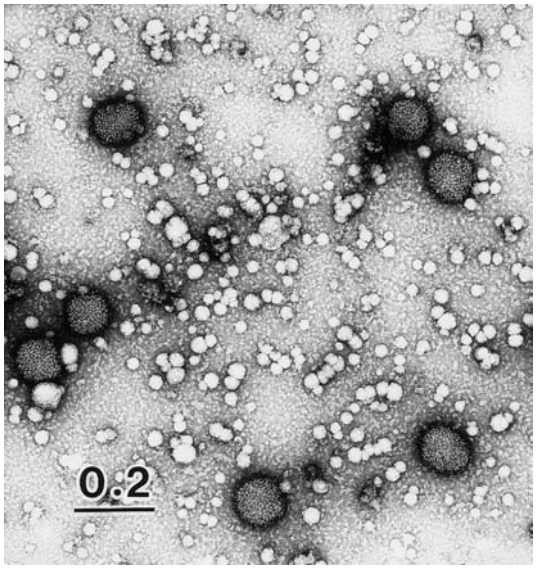

Fig. 1 Negatively stained image of suspension of influenza A viruses. Virus particles sized from 100 nm to 160 nm are seen

found within large vesicles of M cells (Fig. 4 and Fig. 5a). Virus particles were also found within a small vesicle in the cytoplasm of a lymphoid cell enfolded by M cells (Fig. 5b). Few virus particles were observed on the surfaces or insides of other epithelial cells covering the epithelia of lymphoid follicles of nasopharyngeal tonsils (data not shown). No virus-like particles were observed in the control group (data not shown), confirming that the particles observed in this experiment were influenza viruses, not artifacts.

Detection of sialoglycan in nasopharyngeal tonsils

SNA lectin was used to examine the distribution of influenza virus receptors in nasopharyngeal tonsils. SNA recognizes the Neuα2,6Gal linkage of sialoglycoprotein [11, 12], which is thought to be a specific receptor for the human influenza A virus [13]. Tissue was stained with digoxigenin-labeled SNA and HRP-labeled anti-digoxigenin antibody. Figure 6a shows intense SNA staining of the apical surface and surrounding areas of the epithelium of lymphoid follicles. The pretreatment of the specimen with *Cl. Perfringens* neuraminidase clearly reduced SNA lectin staining, demonstrating that this SNA staining was specific for sialoglycan, not any artifact (Fig. 6b). Immunoelectron microscopy of lymphoid follicles stained with SNA lectin revealed that microvilli on the surface of M cells, adjacent columnar cells, and lymphoid cells possessed abundant receptors for the influenza virus (Fig. 7a). Enlargement for observation showed that the receptor sialoglycan was also found on the insides of vesicles in the cytoplasm of M cells (Fig. 7b).

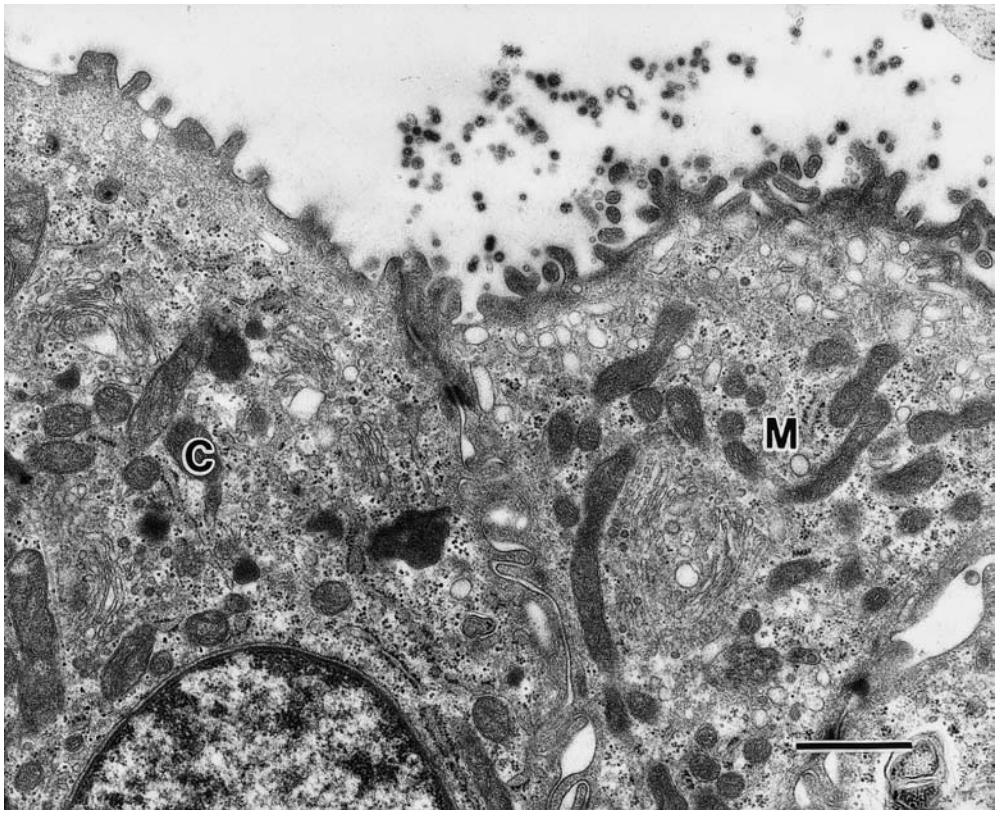

Fig. 2 A transmission electron micrograph shows many virus particles on the surface of M cells that have the irregular and branch-shaped microvilli, and small vesicles in their cytoplasm. *M* M cell, *C* columnar cell. *Bar* 1 μm

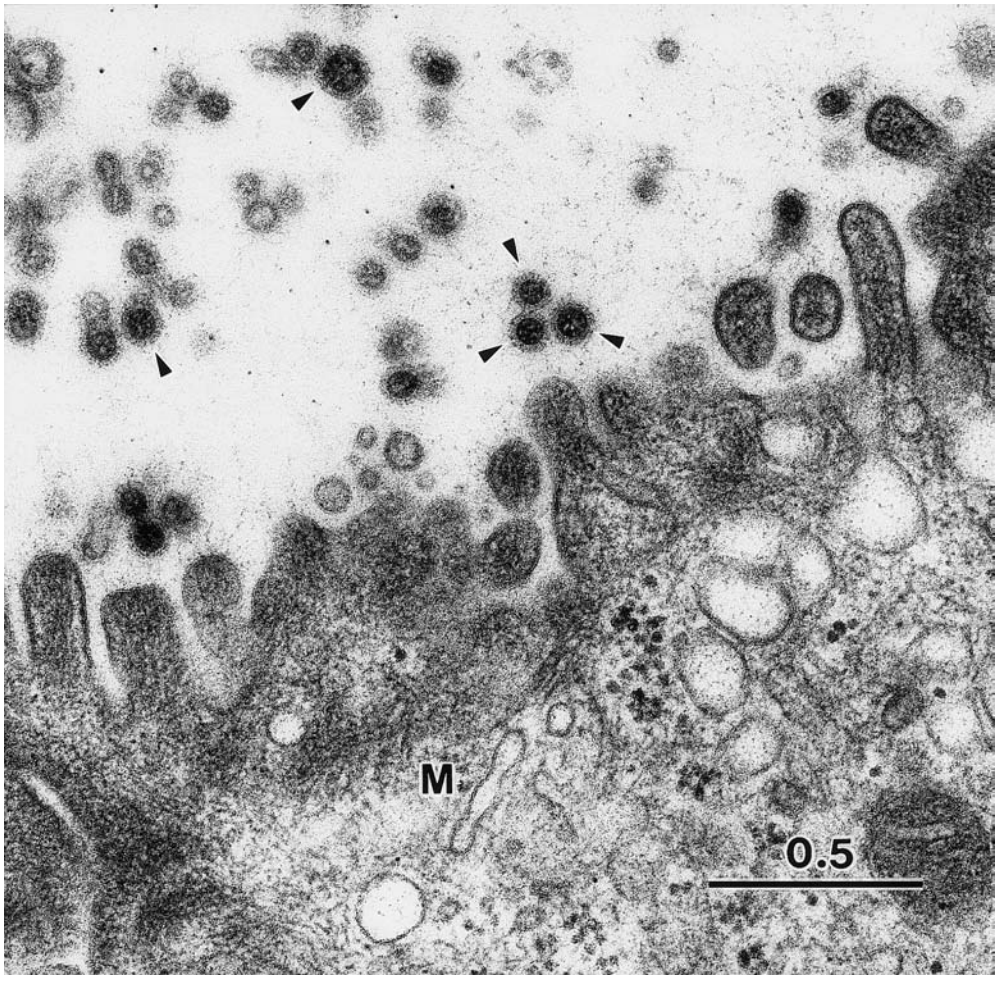

Fig. 3 Enlargement of transmission electron micrograph shows a parallel section of the apex of the same M cell seen in Fig. 2. The glycocalyx links virus particles to M cells. Virus particles have many spikes on their surface (*arrowheads*). *M* M cell

Discussion

Organ cultures of human adenoids have occasionally been used to investigate the pathogenesis of the influenza A virus. It was found that influenza virus infection caused the loss of ciliated and basal epithelial cells in an adenoid organ culture and that inflammatory cells from the lymphoid follicles migrated into the lamina propria [3]. It is thought that human influenza virus binds to ciliated cells, but not to non-ciliated cells, of the tracheal epithelium and that functional receptors are expressed on the surfaces of only ciliated cells [2]. However, there is no information concerning the entry of influenza virus through M cells of human NALT. The present study demonstrated the presence of a viral receptor on the M cell surface and showed that influenza A virus could efficiently bind to the M cells of human adenoid organ culture. Our transmission electron microscopy observations revealed that the influenza A virus could also be efficiently taken up by M cells and transported into enfolded lymphoid cells within 90 min after viral infection. These findings suggested that M cells could be a major port for entry of the influenza A virus. The inductive function of NALT might be crucial for the initiation of an immune response in the upper aerodigestive tract in an influenza viral infection. NeuAcα2,6 Gal linkage of sialoglycan is thought to be an essential part of the receptor for human influenza A virus [7, 9, 15]. The present study has shown an abundant presence of NeuAcα2,6 Gal-containing sialoglycan on the M cell surface, as well as on the adjacent columnar cell surface. This observation indicates that the mechanism of M cell sampling of influenza viruses relates to a receptor-mediated transcytosis. Several viruses, including reoviruses, poliovirus, and HIV, have been observed to be transported efficiently across M cells of Peyer's patches by transcytosis [1, 14, 20]. Although the virological significance of the virus entry into M cells remains to be resolved, the results obtained in the present study imply that an influenza virus could easily pass through M cells and enter lymphoid cells and that the virus could cause a kind of viremia through the infected lymphoid cells. Free infections of an influenza virus have not been detected in blood during influenza. However, infected macrophages or other lymphoid cells could function as vehicles through the bloodstream, which could deliver progeny viruses to blood capillary cells in various organs.

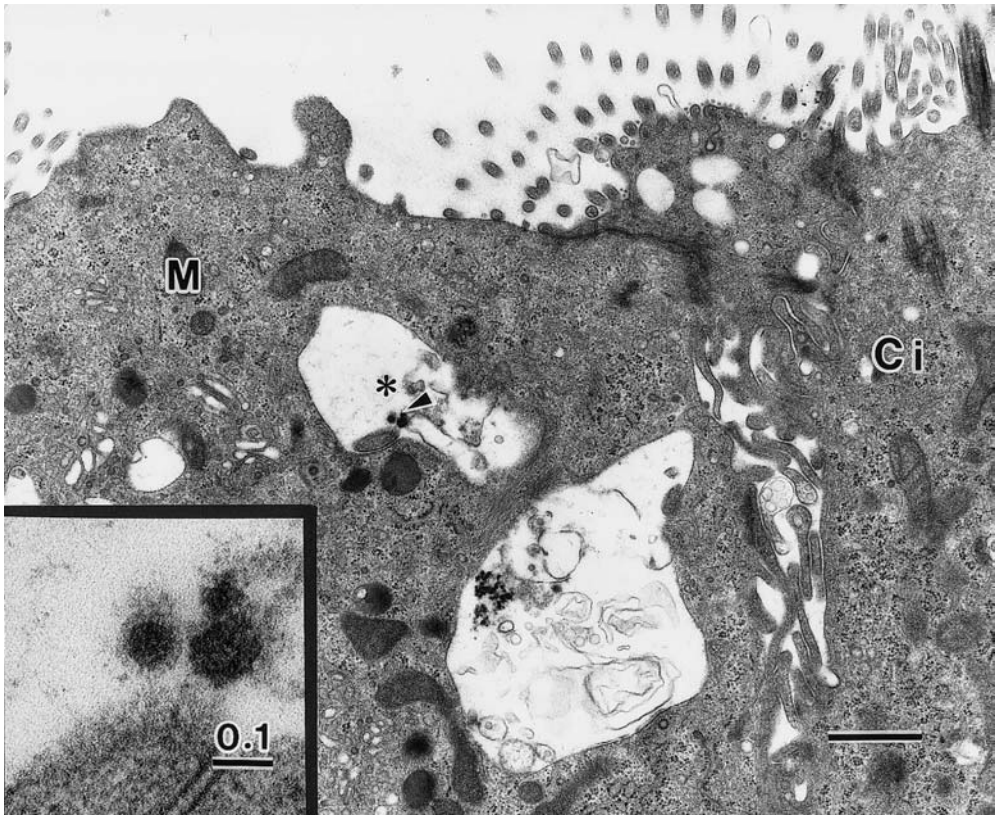

Fig. 4 A transmission electron micrograph shows a virus particle within the large vesicles of an M cell. Cytoplasmic microvilli and large vesicles are seen in the M cell. *Inset* shows enlargement of a virus particle in the large vesicle of the M cell, as indicated by an *asterisk* in the main figure. *M* M cell, *Ci* ciliary cell. *Bar* 1 μm

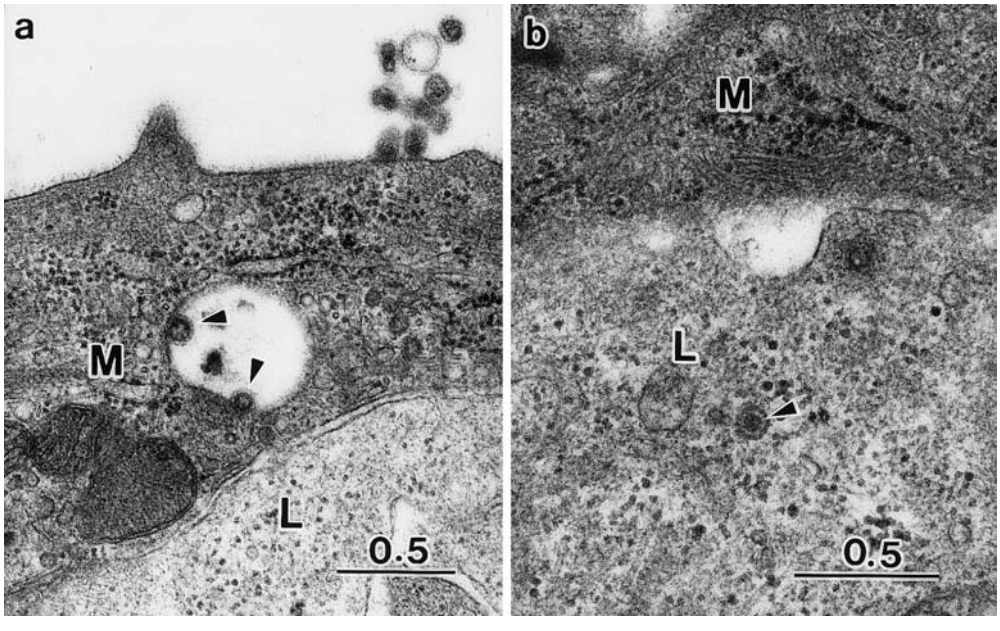

Fig. 5 A transmission electron micrograph shows an M cell that has enfolded a lymphoid cell. **a** Transcytized virus particles (*arrowheads*) are recognized in the vesicle of an M cell near an enfolded lymphoid cell. **b** A transcytized virus particle (*arrowhead*) is recognized in the vesicle of an enfolded lymphoid cell. *M* M cell, *L* lymphoid cell

In Japan, influenza encephalopathy is a severe problem in children during the influenza season. If the influenza virus could infect capillary cells in brain via infected macrophages or lymphoid cells, it might cause the breakdown of the blood–brain barrier, which could lead to an acute influenza encephalopathy. This hypothesis needs to be investigated, but, as of yet, we do not have an appropriate animal model for influenza encephalopathy. The establishment of such a model is timely and urgently needed.

In conclusion, the present study suggested that the transport of influenza viruses to lymphoid cells by M cells may promote antigen delivery to the immune system, and this may be important for systemic delivery of those

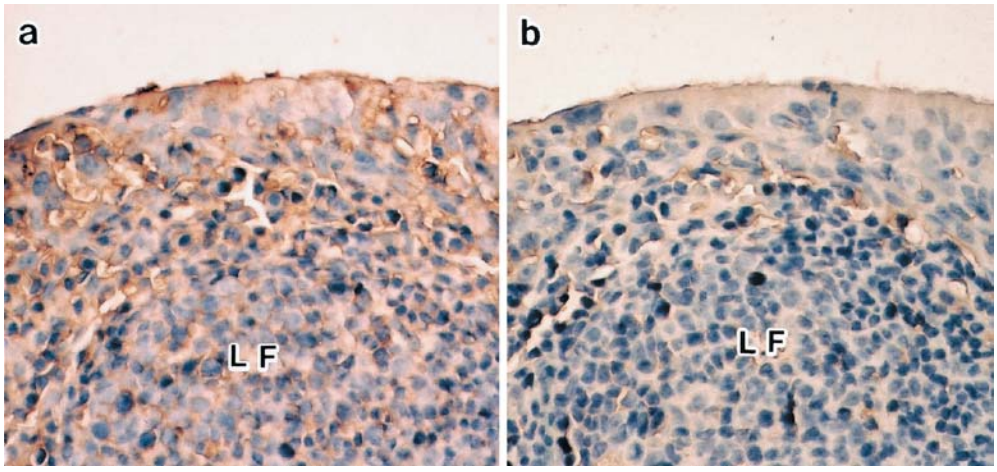

Fig. 6 *Sambucus nigra* (SNA) lectin staining of the surface epithelium of adenoid tissue. **a** The surface and cytoplasmic vesicles of covering epithelium of lymphoid follicles are stained positively by SNA lectin (×370). **b** SNA lectin staining of the parallel section as in **a** after neuraminidase digestion. Staining intensity is reduced (×370). *LF* lymphoid follicle

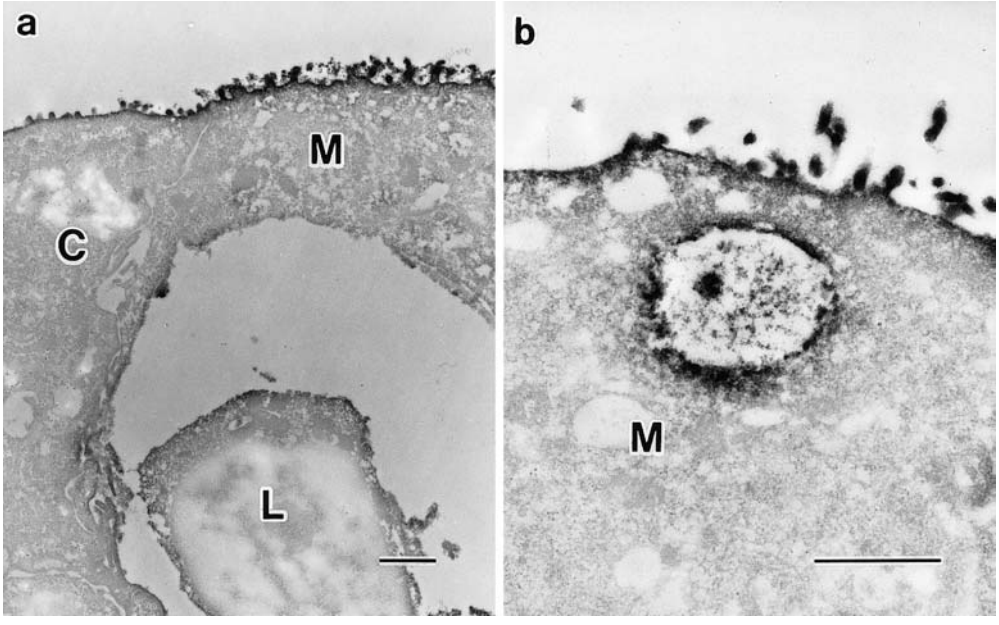

Fig. 7 An immunoelectron micrograph of an M cell stained by *Sambucus nigra* (SNA) lectin. **a** SNA lectin is much more recognized on the surface of the M cell than in adjacent columnar cells. *Bar* 1 μm. **b** Enlargement of cytoplasm of near the surface of an M cell. SNA lectin is also localized inside vesicles in the M cell. *Bar* 1 μm, *M* M cell, *L* lymphoid cell

influenza viruses that have the capacity to productively infect cells outside of the respiratory tract.

Acknowledgements This work was supported by project research grants from the Kawasaki Medical School, a grant-in-aid for scientific research from the Ministry of Education, Science, and Culture (15591072), and a grant-in-aid for scientific research from the Ministry of Health, Labour and Welfare of Japan.

References

1. Amerongen H, Welzin R, Farnet C, Michetti P, Haseltine W, Neutra MR (1991) Transepithelial transport of HIV-1 by intestinal M cells: a mechanism for transmission of AIDS. J Acquir Immune Defic Syndr 4:760–765
2. Couceiro JN, Paulson JC, Baum LG (1993) Influenza virus strains selectively recognize sialyloligosaccharides on human respiratory epithelium: the role of the host cell in selection of hemagglutinin receptor specificity. Virus Res 29:155–165
3. Edwards KM, Snyder PN, Stephens DS, Wright PF (1986) Human adenoid organ culture: a model to study the interaction of influenza A with human nasopharyngeal mucosa. J Infect Dis 153:41–47
4. Fujimura Y (2000) Evidence of cells as portals of entry for antigens in the nasopharyngeal lymphoid tissue of humans. Virchows Arch 436:560–566
5. Fujimura Y, Owen RL (2000) The intestinal epithelial M cell—properties and function. In: Kirsner JB (ed) Inflammatory bowel disease, 5th edn. Saunders, Philadelphia, pp 33–44
6. Iwakawa K, Ueda N, Murao S, Kobayashi N (1996) Altered carbohydrate composition in colorectal adenomas and carcinomas: histochemical characterization of N- acetylgalactosamine, L-fucose, and o-acetylated sialic acid. J Gastroenterol 31:24–32
7. Knossow M, Gaudier M, Douglas A, Barrere B Bizebard T, Barbey C, Gigant B, Skehel JJ (2002) Mechanism of neutralization of influenza virus infectivity by antibodies. Virology 302:294–298
8. Kuper CF, Hameleers DMH, Bruijntjes JP, Van der Ven I, Biewenga J, Sminia T (1990) Lymphoid and non-lymphoid cells in nasal-associated lymphoid tissue (NALT) in the rat. An immuno- and enzyme-histochemical study. Cell Tissue Res 29:371–377

9. Matrosovich M, Klenk HD (2003) Natural and synthetic sialic acid-containing inhibitors of influenza virus receptor binding. Rev Med Viol 13:85–97
10. Neutra MR, Pringault E, Kraehenbuhl JP (1996) Antigen sampling across epithelial barriers and induction of mucosal immune responses. Ann Rev Immunol 14:275–300
11. Ohuchi R, Ohuchi M, Garten W, Klenk HD (1991) Human influenza virus hemagglutinin with high sensitivity to proteolytic activation. J Virol 65:3530–3537
12. Rogers GN, Paulson JC (1983) Receptor determinants of human and animal influenza virus isolates: differences in receptor specificity of H3 hemagglutinin based on species of origin. Virology 127:361–373
13. Shibuya N, Goldstein IJ, Broekhaet WF, Nsimbe-Lubake M, Peeters B, Pneumans WJ (1987) The elderberry (Sambuccus nigra L.) bark lectin recognizes the NeuAc(α2,6) Gal/GalNAc sequence. J Biol Chem 262:1596–1601
14. Sicinski P, Rowinski J, Warchol JB, Jarzabek Z, Gut W, Szczygiel B, Bielecki K, Koch G (1990) Poliovirus type 1 enters the human host through intestinal M cells. Gastroenterology 98:56–58
15. Skehel JJ, Wiley DC (2000) Receptor binding and membrane fusion in virus entry: the influenza hemagglutinin. Ann Rev Biochem 69:531–569
16. Sminia T, Kraal G (1999) Nasal-associated lymphoid tissue. In: Ogra PL Mestecky J, Lamm ME, Strober W, McGhee JR, Bienenstock J (eds) Handbook of mucosal immunology. Academic, San Diego, pp 357–364
17. Spit BJ, Hendriksen EGJ, Bruijntjes JP, Kuper CF (1989) Nasal lymphoid tissue in the rat. Cell Tissue Res 255:193–198
18. Sweet C, Smith H (1980) Pathogenicity of influenza virus. Microbiol Rev 44:303–330
19. Tamura S-I, Iwasaki I, Thompson AH, Asanuma H, Chen Ze, Suzuki Y, Aizawa C, Kurata T (1998) Antibody-forming cells in the nasal-associated lymphoid tissue during primary influenza virus infection. J Gen Virol 79:291–299
20. Wolf JL, Kauffman RS, Finberg R, Dambrauskas R, Fields BN, Trier JS (1983) Determinants of retrovirus interaction with the intestinal M cells and absorptive cells of murine intestine. Gastroenterology 85:291–300

Virchows Arch (2004) 444:43–48
DOI 10.1007/s00428-003-0902-3

ORIGINAL ARTICLE

Lea Pylkkänen · Henrik Wolff · Tuula Stjernvall · Aija Knuuttila · Sisko Anttila · Kirsti Husgafvel-Pursiainen

Reduced Fhit protein expression in human malignant mesothelioma

Received: 4 March 2003 / Accepted: 8 July 2003 / Published online: 16 October 2003

Abstract Human malignant mesothelioma (MM) is an aggressive neoplasm related to occupational exposure to asbestos and characterised by a long latency time. Multiple chromosomal deletions and DNA losses have been revealed in MM by studies performed with karyotypic, comparative genomic hybridisation and loss of heterozygosity (LOH) analyses. Among frequently deleted chromosomal sites, LOH at chromosome 3p has been detected in MM, suggesting the presence of one or several tumour suppressor genes that have an important role in development of the disease. The *FHIT* (fragile histidine triad) tumour suppressor gene, located at 3p14.2, has been proposed to be a target to major human lung carcinogens, such as tobacco smoke and asbestos. Although many studies have indicated decreased Fhit protein expression in a variety of malignancies, there is no report of *FHIT* gene aberrations or Fhit protein abnormalities in MM. We examined expression of the Fhit protein and LOH at the *FHIT* gene in malignant mesothelioma. Altogether, 13 paraffin embedded MM tumours were analysed for Fhit protein expression, and 21 fresh tumours and 10 cell cultures for LOH at the *FHIT* gene with two intragenic microsatellite markers. All tumours showed less intense immunostaining than normal bronchial epithelium or mesothelium. Fhit expression was absent or reduced in 54% (7 of 13) of the tumours, with the weakest staining observed in poorly differentiated areas. Allele loss was seen in 3 of 10 (30%) of the MM cell lines, but only in 1 of the 21 fresh tumours studied, suggesting concealment of LOH by normal cells present in MM tumours. In conclusion, our present data indicate a frequent decrease of Fhit protein expression, thus supporting the significance of *FHIT* inactivation in development of MM.

Keywords Malignant mesothelioma · *FHIT* gene · Fhit protein expression · Loss of heterozygosity · Asbestos exposure

L. Pylkkänen · K. Husgafvel-Pursiainen
Department of Industrial Hygiene and Toxicology,
Finnish Institute of Occupational Health,
Helsinki, Finland

H. Wolff · T. Stjernvall · S. Anttila
Department of Occupational Medicine,
Finnish Institute of Occupational Health,
Helsinki, Finland

A. Knuuttila
Department of Medicine,
Division of Respiratory Diseases Helsinki,
University Central Hospital,
Helsinki, Finland

K. Husgafvel-Pursiainen (✉)
Department of Industrial Hygiene and Toxicology,
Finnish Institute of Occupational Health,
Topeliuksenkatu 41 a A, 00250 Helsinki, Finland
e-mail: kirsti.husgafvel-pursiainen@ttl.fi
Tel.: +358-9-47472212
Fax: +358-9-47472110

Introduction

Human malignant mesotheliomas (MM) are aggressive tumours originating from mesothelial cells lining pleural, peritoneal and pericardial cavities [1]. Although MM is a relatively rare neoplasm, its incidence has been rising during the past decades, mainly due to increased occupational exposure to asbestos, which is the primary causal factor in the aetiology of MM [8]. A long latency between the exposure and onset of the disease is characteristic of MM, suggesting that multiple somatic genetic events are required for malignant transformation of mesothelial cells [19].

Studies performed with cytogenetic and comparative genomic hybridisation as well as loss of heterozygosity (LOH) analyses demonstrate occurrence of several genetic alterations, most commonly losses of chromosomal regions in human MM [11]. Most frequently deleted chromosomal regions are 22q and 9p [18]. Both these regions harbour a tumour suppressor gene, *NF2* (neurofibromatosis type 2) and *p16/CDKN2A*, respectively, which have been shown to be altered in many MMs [3].

Among losses at different chromosomal sites, frequent deletions of the short arm of chromosome 3 in MM have been reported [21, 32, 38]. The *FHIT* (fragile histidine triad) tumour suppressor gene [23], located at 3p14.2, has been suggested to be a target of major human lung carcinogens, such as tobacco smoke and asbestos [9]. The Fhit protein has been reported to be expressed in most non-neoplastic human tissues, and the highest levels of expression have been detected in epithelial cells. The protein is also consistently expressed in benign mesothelium [39]. Although *FHIT* abnormalities, either allele deletions or loss of protein expression, have been investigated extensively in many types of human cancer, including lung cancer [13, 22, 26, 31], there is no report, to our knowledge, of alterations in the *FHIT* gene aberration or Fhit protein expression in MM.

We examined Fhit protein expression and *FHIT* allele loss in MM tumours and cell lines. Most patients had been exposed to asbestos at work. Protein expression was decreased in all tumour samples examined relative to normal bronchus epithelium and mesothelium. Markedly reduced expression was seen in 54% of the tumours, and tumour cells with the poorest differentiation showed the weakest immunostaining. LOH of the *FHIT* gene was detected in three of ten cell lines (30%) and in one (1/21, 5%) fresh tumour sample. Frequent Fhit protein decrease suggests its involvement in the development of MM.

Materials and methods

Study population

Altogether, 26 MM cases were studied. Data for demographic, clinico-pathological and exposure characteristics of the cases are given in Table 1. The diagnosis of malignant mesothelioma was confirmed for each case by the Finnish National Mesothelioma Panel. According to occupational history and/or fibre analysis [34], 19 of 25 (76%) patients had been exposed to asbestos at work (concentration $\geq 1\times10^6$ fibres per gram dry tumour tissue), and 6 cases were non-exposed ($<1\times10^6$ fibres/g); this data was missing from 1 case. Most of the tumours represented a mixed histological type; however, all the tumours analysed for protein expression were of epithelial origin. Cultured MM cells or cell lines (10 cases) from surgically resected tumours [24] and fresh frozen tumour specimens from 21 MM cases were analysed (Table 1). Four of the cell lines had been established previously and were long term (M9 K, M10 K, M33 K and M38 K); whereas six were newly established cell cultures and examined in passages 1–4 (M138 K, M143 K, M144 K, M146 K, M150 K and M153 K). Tumour samples were stored at −70°C prior to DNA extraction. For each specimen, we had access to the corresponding normal tissue (blood or peripheral pleura) of the patient. Immunohistochemical staining for Fhit protein expression was studied in 13 paraffin-embedded tumour samples.

PCR and LOH analysis

DNA was extracted from blood, frozen fresh tumours or cell cultures using proteinase-K digestion and phenol/chloroform purification followed by ethanol precipitation. Special care was taken by the pathologist when dissecting the tumour specimen to avoid contamination by normal tissue. DNA was amplified by polymerase chain reaction (PCR) with two highly polymorphic

Table 1 Malignant mesothelioma cases and samples studies. Fresh tumour samples and cell lines were analysed for loss of heterozygosity (LOH), and paraffin-embedded samples for immunohistochemical staining. + sample analysed, − sample not analysed

Tumor no.	Age (years)	Sex	Asbestos exposure	Histology	Sample analysed for LOH or protein expression		
					Fresh tumour	Cell line	Paraffin-embedded tumour
M13	72	Male	Yes	Mixed	+	−	−
M28	54	Male	Yes	Epithelial	+	−	+
M30	46	Male	Yes	Mixed	+	−	+
M65	63	Male	Yes	Epithelial	+	−	+
M79	61	Male	Yes	Mixed	+	−	+
M91	72	Male	Yes	Epithelial	+	−	−
M92	44	Male	Yes	Mixed	+	−	−
MO3	57	Male	Yes	Mixed	−	−	+
M119	49	Male	Yes	Mixed	+	−	−
M122	51	Male	Yes	Mixed	+	−	−
M127	55	Male	Yes	Not specified	+	−	−
M129	65	Female	Yes	Not specified	+	−	−
M9	52	Male	Yes	Mixed	+	+	−
M10	52	Male	Yes	Epithelial	+	+	+
M33	42	Male	Yes	Mixed	+	+	−
M38	55	Male	Yes	Mixed	+	+	−
M138	57	Male	Yes	Mixed	−	+	−
M144	75	Male	Yes	Mixed	−	+	+
M150	59	Male	Yes	Mixed	+	+	−
M100	39	Male	No	Epithelial	+	−	+
M101	79	Male	No	Epithelial	+	−	−
M143	49	Female	No	Epithelial	+	+	+
M146	58	Male	No	Mixed	−	+	+
M153	60	Male	No	Mixed	+	+	+
M42	57	Female	No	Mixed	+	−	+
M83	No data	No data	No data	Epithelial	−	−	+

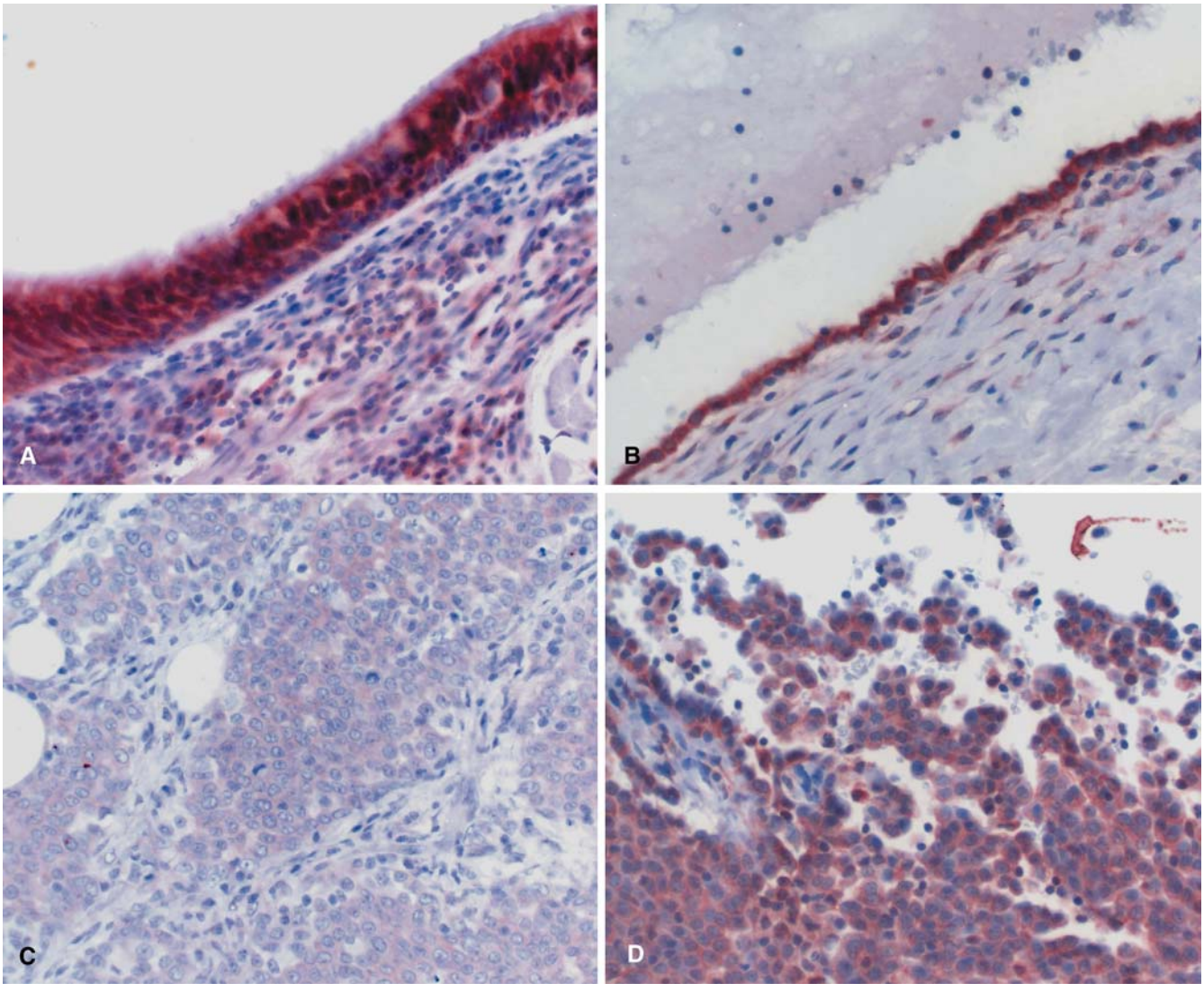

Fig. 1 Positive fragile histidine triad immunostaining in normal bronchial epithelium (**A**) and in mesothelium (**B**). Poorly differentiated papillary mesothelioma (**C**) versus well-differentiated area (**D**) of the same tumour; the former representing approximately 5% of the tumour

intragenic microsatellite markers, D3S1313 and D3S1234. The markers were obtained from Research Genetics (Huntsville, AL).

Genomic DNA (100 ng) was amplified (30 cycles) according to standard protocols in a volume of 10 μl. PCR products were radiolabelled during the amplification reaction and separated by electrophoresis in 6% polyacrylamide gels (7.7 M urea). After electrophoresis, the gels were dried and exposed to X-ray film. Absence or significant decrease of one allele in the tumour compared with the normal reference tissue was considered LOH.

Immunohistochemical studies

Expression of the Fhit protein was examined in a set of paraffin-embedded tumour (PET) specimens (n=13). A rabbit polyclonal antibody raised against glutathione S-transferase-Fhit protein, a generous gift from Dr. Kay Huebner, Kimmel Cancer Center, Philadelphia, Pennsylvania, was used in the immunohistochemical analysis. Sections of 4–5 μm were cut from the PET samples, deparaffinised and microwaved for 4×5 min in 0.01 M Na-citrate buffer (pH 6.0). Immunostaining was performed with the help of a TechMate Horizon (Dako A/S, Glsotrup, Denmark) autostainer (room temperature, 30 min). An automated protocol named MSIP and recommended by the manufacturer was used. All reagents are made by Dako (A/S) for routine use with the stainer. The dilution of the antibody was 1:500. As a control, non-specific rabbit IgG (Santa Cruz Biotechnology Inc., Santa Cruz, CA) at a concentration corresponding to that of the Fhit antibody was used to stain all sections using an identical protocol.

Evaluation of the Fhit positivity (H.W.) was based on the intensity of staining using scoring from 1 to 5 (1=marginal, close to background; 2=weak; 3=moderate; 4=high; 5=overstaining) and the percentage of positively staining cells. Normal columnar epithelium of the bronchus and the mesothelium indicated positive immunostaining with the intensity score 4. The combination of staining intensity and percentage of positive stained cells was classified in the following three groups:

a. Absent or markedly reduced expression: staining intensity $\leq$1 or staining intensity 2 in <30% of cells;
b. Reduced expression: staining intensity 2 or 3 in 30–50% of the cells;

Table 2 Immunostaining of the fragile histidine triad (Fhit), and loss of heterozygosity (LOH) for the *FHIT* gene in malignant mesothelioma tumors and cell lines. The results are compared with those of lung cancers from cases with occupational exposure

Tumour	Fhit staining			LOH at *FHIT* [2]		
	Total number studied	Negative or reduced		Total number studied	LOH detected	
		n	(%)		*n*	(%)
Malignant mesothelioma						
Tumours	13	7	(54)	20	1	(5)
Cell lines	No data	No data	No data	10	3	(30)
Non-small cell lung cancer[1]	19	13	(68)	24	7	(29)
Squamous cell carcinoma	9	8	(89)	11	4	(36)
Adenocarcinoma	9	4	(44)	10	1	(10)
Large-cell carcinoma	1	1	(100)	2	1	(50)
Adeno-squamous cell carcinoma	0	0	(0)	1	1	(100)

[1] Pylkkänen et al. 2002 [26]
[2] The intragenic markers studied were D3S1234 and D3S1313

c. Positive expression: staining intensity 3 or 4 in >50% of the cells.

The scorer was blinded to results obtained from the LOH analysis.

Results

Protein expression

Intensive immunohistochemical staining for the Fhit protein was observed in the normal columnar epithelium of the bronchus and mesothelium. Compared with this positive staining, the protein expression was decreased in all tumours examined. Four cases showed markedly reduced expression (staining intensity 1 in 1–100%, or 2–3 in <30% of the cells), three cases showed considerably reduced expression (2–3 in 30–50% of the cells), and six cases showed a positive expression (intensity 3 in >50% of the cells). Heterogeneous staining with more strongly positive Fhit expression was seen in areas of well-differentiated tumour, and low staining intensity was noted in areas of poor differentiation. Examples of Fhit expression in normal bronchial epithelium and mesothelium as well as in a MM tumour with well-differentiated papillary cells and poorly differentiated area are shown in Fig. 1.

Allele loss

Altogether, 21 MM tumours and ten cell cultures were investigated for the presence of allele deletion at the *FHIT* gene with two intragenic microsatellite markers (D3S1234 and D3S1313). Allele loss was detected in three of ten cell cultures (30%). One of the corresponding fresh tumour samples also showed LOH. The low LOH frequency in fresh tumour samples was most likely caused by an unavoidable presence of normal cells in the tumour specimens, subsequently covering the existence of LOH. Table 2 summarises the results of immunostaining of the Fhit protein and LOH analyses in malignant mesothelioma tumours and cell lines, and in lung cancer cases associated with asbestos exposure.

Discussion

Several recurrent genomic alterations are characteristic to MMs, but no single specific gene has been yet indicated. Deletions or mutations of two known tumour suppressor genes (*NF2* at 22q.12 and *p16/CDKN2A* at 9p21) have been observed in MM [3, 10, 25, 27]. However, MM appears to involve other genes as well, since inactivation of these genes often occurs with low frequency. In a recent study, we detected recurrent allelic deletion in several chromosomal regions in MM cell cultures [26]. In addition to frequent loss at *NF2* and *p16/CDKN2A* gene regions, we also detected frequent deletions at 3p14.2, where the *FHIT* gene resides. The inactivation of the *FHIT* gene is involved in lung cancer [9, 17, 30, 35] and many other cancer types [5, 14, 29, 36, 37]. The *FHIT* gene suppresses growth of cancer cells [28], and, in carcinogen-treated *FHIT*-deficient mice, development of multiple tumours was inhibited by transfection of an intact human *FHIT* gene [12].

The Fhit protein is expressed in most non-neoplastic human tissues, and the highest levels of expression is detected in epithelial cells. Also, mesothelial cells from benign body cavity effusion consistently express strong immunoreactivity for the Fhit protein [39]. In the present study, all MM tumours showed a decrease in the expression of the Fhit protein, compared with the normal mesothelium. Immunohistochemical analysis indicated absent or reduced expression in 7 of 13 (54%) of the cases studied. Interestingly, high intensity of Fhit staining was seen in the areas of well-differentiated tumours, and low intensity of staining was noted in those of poor differentiation. A similar expression pattern was reported in tongue carcinoma, where Fhit expression was higher in the well-differentiated areas than in poorly differentiated areas [20]. A correlation between the absence or reduction of Fhit expression and advanced tumour stage has been observed in bladder and lung cancers [2]. In a recent study, reduction or absence of Fhit protein was shown to

be associated with high proliferation and large tumour size of breast carcinomas [4]. Such observations may suggest that *FHIT* inactivation is a relatively late event in the neoplastic progression in MM as well.

LOH was detected in three of ten (30%) MM cell cultures studied with two highly polymorphic loci intragenic to the *FHIT* gene. The low rate of LOH detected in fresh tumour samples is probably due to the presence of normal cells in tumour samples typical to MM. Another point is that Fhit staining in many tumour types is often heterogeneous, displaying a mixed pattern of both low and high staining intensity [5, 7, 16, 33]. In addition, the *FHIT* gene, as with many other tumour suppressor genes, may be inactivated by alternative mechanisms. Tumour-acquired methylation of the CpG islands of the promoter regions of *FHIT* gene resulting in silencing of transcription has been reported to occur in lung cancer. In a recent study, *FHIT* methylation was detected in 37% of primary non-small cell lung cancers and 65% of lung cancer cell lines, and methylation significantly correlated with loss of Fhit expression [40]. We detected LOH in MM cells in very early passages (1–3) in culture, which may suggest that a relatively large proportion of malignant cells in the original tumours, in fact, carry allele loss at 3p.

Association between asbestos exposure and reduced Fhit expression has been suggested in lung cancer [22, 26]. In this study, malignant mesothelioma cases associated with occupational asbestos exposure showed frequent reduction of Fhit protein expression. These observations further support previous suggestions that the *FHIT* gene alterations may be involved in the development of neoplasms associated with environmental carcinogen exposure [2, 6, 22, 26]. In conclusion, our present data show that absent or markedly reduced Fhit expression was frequent in MM. However, *FHIT* inactivation may, instead, be a late event, as suggested by the pattern of immunostaining of the tumour cells. As in nearly all MM patients, the first manifestation of malignancy is bloody effusion of the pleural cavity [15]. Immunostaining of Fhit protein could perhaps serve as a biomarker for detection of malignant cells in the effusions.

References

1. Attanoos RL, Gibbs AR (1997) Pathology of malignant mesothelioma. Histopathology 30:403–418
2. Baffa R, Gomella LG, Vecchione A, Bassi P, Mimori K, Sedor J, Calviello CM, Gardiman M, Minimo C, Strup SE, McCue PA, Kovatich AJ, Pagano F, Huebner K, Croce CM (2000) Loss of FHIT expression in transitional cell carcinoma of the urinary bladder. Am J Pathol 156:419–424
3. Bianchi AB, Mitsunaga SI, Cheng JQ, Klein WM, Jhanwar SC, Seizinger B, Kley N, Klein-Szanto AJ, Testa JR (1995) High frequency of inactivating mutations in the neurofibromatosis type 2 gene (NF2) in primary malignant mesotheliomas. Proc Natl Acad Sci U S A 92:10854–10858
4. Campiglio M, Pekarsky Y, Menard S, Tagliabue E, Pilotti S, Croce CM (1999) FHIT loss of function in human primary breast cancer correlates with advanced stage of the disease. Cancer Res 59:3866–3869
5. Capuzzi D, Santoro E, Hauck WW, Kovatich AJ, Rosato FE, Baffa R, Huebner K, McCue PA (2000) Fhit expression in gastric adenocarcinoma: correlation with disease stage and survival. Cancer 88:24–34
6. Chizhikov V, Chikina S, Gasparian A, Zborovskaya I, Steshina E, Ungiadze G, Samsonova M, Chernyaev A, Chuchalin A, Tatosyan A (2002) Molecular follow-up of preneoplastic lesions in bronchial epithelium of former Chernobyl clean-up workers. Oncogene 21:2398–2405
7. Connolly DC, Greenspan DL, Wu R, Ren X, Dunn RL, Shah KV, Jones RW, Bosch FX, Munoz N, Cho KR (2000) Loss of fhit expression in invasive cervical carcinomas and intraepithelial lesions associated with invasive disease. Clin Cancer Res 6:3505–3510
8. Craighead JE, Mossman BT (1982) The pathogenesis of asbestos-associated diseases. N Engl J Med 306:1446–1455
9. Croce CM, Sozzi G, Huebner K (1999) Role of FHIT in human cancer. J Clin Oncol 17:1618–1624
10. Deguen B, Goutebroze L, Giovannini M, Boisson C, van der Neut R, Jaurand MC, Thomas G (1998) Heterogeneity of mesothelioma cell lines as defined by altered genomic structure and expression of the NF2 gene. Int J Cancer 77:554–560
11. De Rienzo A, Testa JR (2000) Recent advances in the molecular analysis of human malignant mesothelioma. Clin Ther 151:433–438
12. Fong LY, Fidanza V, Zanesi N, Lock LF, Siracusa LD, Mancini R, Siprashvili Z, Ottey M, Martin SE, Druck T, McCue PA, Croce CM, Huebner K (2000) Muir-Torre-like syndrome in Fhit-deficient mice. Proc Natl Acad Sci U S A 97:4742–4747
13. Geradts J, Fong KM, Zimmerman PV, Minna JD (2000) Loss of Fhit expression in non-small-cell lung cancer: correlation with molecular genetic abnormalities and clinicopathological features. Br J Cancer 82:1191–1197
14. Guo Z,Johansson SL, Rhim JS, Vishwanatha JK (2000) Fragile histidine triad gene expression in primary prostate cancer and in an in vitro model. Prostate 43:101–110
15. Hanselaar AG (2002) Additional techniques in serous effusion. Anal Cell Pathol 24:1–4
16. Hao XP, Willis JE, Pretlow TG, Rao JS, MacLennan GT, Talbot IC, Pretlow TP (2000) Loss of fragile histidine triad expression in colorectal carcinomas and premalignant lesions. Cancer Res 60:18–21
17. Hirao T, Nelson HH, Ashok TD, Wain JC, Mark EJ, Christiani DC, Wiencke JK, Kelsey KT (2001) Tobacco smoke-induced DNA damage and an early age of smoking initiation induce chromosome loss at 3p21 in lung cancer. Cancer Res 61:612–615
18. Kivipensas P, Bjorkqvist AM, Karhu R, Pelin K, Linnainmaa K, Tammilehto L, Mattson K, Kallioniemi OP, Knuutila S (1996) Gains and losses of DNA sequences in malignant mesothelioma by comparative genomic hybridization. Cancer Genet Cytogenet 89:7–13
19. Lee WC, Testa JR (1999) Somatic genetic alterations in human malignant mesothelioma. Int J Oncol 14:181–188
20. Lee JI, Soria JC, Hassan K, Liu D, Tang X, El-Naggar A, Hong WK, Mao L (2001) Loss of Fhit expression is a predictor of poor outcome in tongue cancer. Cancer Res 61:837–841
21. Lu YY, Jhanwar SC, Cheng JQ, Testa JR (1994) Deletion mapping of the short arm of chromosome 3 in human malignant mesothelioma. Genes Chromosomes Cancer 9:76–80
22. Nelson HH, Wiencke JK, Gunn L, Wain JC, Christiani DC, Kelsey KT (1998) Chromosome 3p14 alterations in lung cancer: evidence that FHIT exon deletion is a target of tobacco carcinogens and asbestos. Cancer Res 58:1804–1807
23. Ohta M, Inoue H, Cotticelli MG, Kastury K, Baffa R, Palazzo J, Siprashvili Z, Mori M, McCue P, Druck T, Croce CM, Huebner K (1996) The FHIT gene, spanning the chromosome 3p14.2 fragile site and renal carcinoma-associated t(3;8) breakpoint, is abnormal in digestive tract cancers. Cell 84:587–597
24. Pelin-Enlund K, Husgafvel-Pursiainen K, Tammilehto L, Klockars M, Jantunen K, Gerwin BI, Harris CC, Tuomi T, Vanhala E, Mattson K, Linnainmaa K (1990) Asbestos-related

malignant mesothelioma: growth, cytology, tumorigenicity and consistent chromosome findings in cell lines from five patients. Carcinogenesis 11:673–681
25. Prins JB, Williamson KA, Kamp MM, van Hezik EJ, van der Kwast TH, Hagemeijer A, Versnel MA (1998) The gene for the cyclin-dependent-kinase-4 inhibitor, CDKN2A, is preferentially deleted in malignant mesothelioma. Int J Cancer 75:649–653
26. Pylkkänen L, Wolff H, Stjernvall T, Tuominen P, Sioris T, Karjalainen A, Anttila S, Husgafvel-Pursiainen K (2002) Reduced Fhit protein expression and loss of heterozygosity at FHIT gene in tumours from smoking and asbestos-exposed lung cancer patients. Int J Oncol 20:285–290
27. Sekido Y, Pass HI, Bader S, Mew DJ, Christman MF, Gazdar AF, Minna JD (1995) Neurofibromatosis type 2 (NF2) gene is somatically mutated in mesothelioma but not in lung cancer. Cancer Res 55:1227–1231
28. Siprashvili Z, Sozzi G, Barnes LD, McCue P, Robinson AK, Eryomin V, Sard L, Tagliabue E, Greco A, Fusetti L, Schwartz G, Pierotti MA, Croce CM, Huebner K (1997) Replacement of Fhit in cancer cells suppresses tumorigenicity. Proc Natl Acad Sci U S A 94:13771–13776
29. Sorio C, Baron A, Orlandini S, Zamboni G, Pederzoli P, Huebner K, Scarpa A (1999) The FHIT gene is expressed in pancreatic ductular cells and is altered in pancreatic cancers. Cancer Res 59:1308–1314
30. Sozzi G, Veronese ML, Negrini M, Baffa R, Cotticelli MG, Inoue H, Tornielli S, Pilotti S, De Gregorio L, Pastorino U, Pierotti MA, Ohta M, Huebner K, Croce CM (1996) The FHIT gene 3p14.2 is abnormal in lung cancer. Cell 85:17–26
31. Sozzi G, Pastorino U, Moiraghi L, Tagliabue E, Pezzella F, Ghirelli C, Tornielli S, Sard L, Huebner K, Pierotti MA, Croce CM, Pilotti S (1998) Loss of FHIT function in lung cancer and preinvasive bronchial lesions. Cancer Res 58:5032–5037
32. Taguchi T, Jhanwar SC, Siegfried JM, Keller SM, Testa JR (1993) Recurrent deletions of specific chromosomal sites in 1p, 3p, 6q, and 9p in human malignant mesothelioma. Cancer Res 53:4349–4355
33. Tomizawa Y, Nakajima T, Kohno T, Saito R, Yamaguchi N, Yokota J (1998) Clinicopathological significance of Fhit protein expression in stage I non-small cell lung carcinoma. Cancer Res 58:5478–5483
34. Tuomi T, Huuskonen MS, Tammilehto L, Vanhala E, Virtamo M (1991) Occupational exposure to asbestos as evaluated from work histories and analysis of lung tissues from patients with mesothelioma. Br J Int Med 48:48–52
35. Wistuba II, Behrens C, Virmani AK, Mele G, Milchgrub S, Girard L, Fondon JW 3rd, Garner HR, McKay B, Latif F, Lerman MI, Lam S, Gazdar AF, Minna JD (2000) High resolution chromosome 3p allelotyping of human lung cancer and preneoplastic/preinvasive bronchial epithelium reveals multiple, discontinuous sites of 3p allele loss and three regions of frequent breakpoints. Cancer Res 60:1949–1960
36. Yoshino K, Enomoto T, Nakamura T, Sun H, Ozaki K, Nakashima R, Wada H, Saitoh J, Watanabe Y, Noda K, Murata Y (2000) FHIT alterations in cancerous and non-cancerous cervical epithelium. Int J Cancer 85:6–13
37. Yuan BZ, Keck-Waggoner C, Zimonjic DB, Thorgeirsson SS, Popescu NC (2000) Alterations of the FHIT gene in human hepatocellular carcinoma. Cancer Res 60:1049–1053
38. Zeiger MA, Gnarra JR, Zbar B, Linehan WM, Pass HI (1994) Loss of heterozygosity on the short arm of chromosome 3 in mesothelioma cell lines and solid tumors. Genes Chromosomes Cancer 11:15–20
39. Zimmerman RL (2000) FHIT protein is expressed in benign mesothelium and has no clinical value in detecting carcinoma in body cavity effusions. Appl Immunohistochem Molecul Morphol 8:154–157
40. Zochbauer-Muller S, Fong KM, Maitra A, Lam S, Geradts J, Ashfaq R, Virmani AK, Milchgrub S, Gazdar AF, Minna JD (2001) 5′ CpG island methylation of the FHIT gene is correlated with loss of gene expression in lung and breast cancer. Cancer Res 61:3581–3585

Virchows Arch (2004) 444:49–55
DOI 10.1007/s00428-003-0903-2

ORIGINAL ARTICLE

Yasushi Takagi · Toshio Nikaido · Toshihiko Toki · Naoko Kita · Makoto Kanai · Takashi Ashida · Satoshi Ohira · Ikuo Konishi

Levels of oxidative stress and redox-related molecules in the placenta in preeclampsia and fetal growth restriction

Received: 11 July 2003 / Accepted: 2 September 2003 / Published online: 22 October 2003

Abstract Recent evidence suggests that oxidative stress is involved in the pathophysiology of preeclampsia. Using immunohistochemistry and Western blotting, we investigated the oxidative stress- and redox-related molecules, such as 8-hydroxy-2′-deoxyguanosine (8-OHdG), 4-hydroxynonenal (4-HNE), thioredoxin (TRX) and redox factor-1 (ref-1) in the placenta in preeclampsia, intrauterine growth restriction (IUGR), preeclampsia + IUGR and in normal pregnancy. Using immunohistochemistry, the level of 8-OHdG was significantly higher in IUGR (P=0.012) or preeclampsia + IUGR (P=0.0021) than in normal pregnancy, while TRX expression was significantly higher in preeclampsia (P=0.045), and ref-1 expression was significantly higher in preeclampsia (P=0.017), IUGR (P=0.016) and preeclampsia + IUGR (P=0.0038) than in normal pregnancy. The levels of 4-HNE did not differ significantly between either preeclampsia or IUGR and normal pregnancy. A significant positive correlation was observed between TRX and ref-1 expressions in both normal (ρ=0.52) and complicated (ρ=0.43) pregnancies. Using Western blotting, ref-1 expression tended to be higher in complicated pregnancies than in normal pregnancy (P=0.09). These results suggest that oxidative DNA damage is increased in IUGR and that redox function is enhanced in both preeclampsia and IUGR compared with normal pregnancy.

Y. Takagi · T. Toki · N. Kita · M. Kanai · T. Ashida · S. Ohira · I. Konishi
Department of Obstetrics and Gynecology,
Shinshu University School of Medicine,
Matsumoto, Japan

T. Nikaido (✉)
Department of Organ Transplants, Reconstructive Medicine and Tissue Engineering,
Shinshu University Graduate School of Medicine,
3-1-1 Asahi, 390-8621 Matsumoto, Japan
e-mail: tnikaido@hsp.md.shinshu-u.ac.jp
Tel.: +81-26-3373193
Fax: +81-26-3372573

Keywords Oxidative stress · Intrauterine fetal growth restriction · Redox function · Placenta · Preeclampsia

Introduction

Preeclampsia is a serious complication of pregnancy and continues to be a leading cause of maternal death during pregnancy in developed countries [6]. Although the exact etiology and pathogenesis of preeclampsia are still unknown, there is substantial evidence that maternal endothelial cell dysfunction leads to manifestations of preeclampsia, such as altered vascular reactivity, vasospasms and increased vascular permeability [19, 21]. It has been known for some years that placental ischemia is involved in the development of preeclampsia [13, 32] and that placental ischemia causes fetal hypoxia and acidosis, which lead to intrauterine fetal growth restriction (IUGR) [26]. The frequent occurrence of IUGR in preeclampsia may seem to imply that preeclampsia and IUGR share a common pathogenesis. However, IUGR can occur without any signs of preeclampsia, and not all preeclamptic pregnancies are associated with IUGR [4]. Although placental ischemia/hypoxia is likely to be a common etiological factor for preeclampsia and IUGR, the underlying relationship between preeclampsia and IUGR is not well understood.

There is growing evidence that oxidative stress is involved in normal pregnancies. The serum levels of oxidative stress-related molecules, such as lipid peroxides and malondialdehyde, have been found to be higher in pregnant women than in non-pregnant women [15]. The placenta, which is regarded as a source of such molecules [11], produces 4-hydroxynonenal (4-HNE) and thioredoxin (TRX) in normal pregnancies [1, 3, 14]. Meanwhile, maternal endothelial cell dysfunction has attracted attention as a key event in the development of the diverse clinical manifestations of preeclampsia [21], and the placenta is regarded as a major source of the factors that lead to such dysfunction in preeclampsia [20]. Recent evidence suggests that, in preeclampsia, both placental

and maternal free radical reactions promote a cycle of events that compromise the defensive functioning of the vascular endothelium [7]. In IUGR, as well as in preeclampsia, increased vascular resistance in the placenta is likely to result in reduced utero-placental perfusion and to be the cause of placental hypoxia or ischemia [28]. Several studies have investigated oxidative stress-related molecules in preeclamptic pregnancies. The level of 4-HNE and the level of isoprostane, a marker of oxidative stress that induces vasoconstriction, are both higher in the placenta in preeclamptic pregnancies than in normal pregnancies [14, 30]. The level of malondialdehyde, an indicator of mitochondrial lipid peroxides, is higher in the mitochondrial fraction of preeclamptic placental tissues than in those obtained from normal placentae [31]. The expression of xanthine dehydrogenase/xanthine oxidase, which generates reactive oxygen species, is elevated in the cytotrophoblast from preeclamptic women [12]. The levels of superoxide, protein thiol/disulphide oxidoreductases and 2,3-dioxygenase (a free radical scavenger) are reported to be higher in preeclamptic placentae than in normal placentae [22, 23, 25].

It has recently been reported that oxidative stress causes vascular dysfunction in the placenta in preeclampsia [16] and that antioxidants decrease the risk of preeclampsia [2]. These lines of evidence seem to suggest that oxidative stress may be involved in the development of preeclampsia [7, 29]. However, few studies have investigated the status of oxidative stress and reductive reactions in preeclampsia and IUGR concurrently. The aim of the present study was to elucidate the role of oxidative stress in preeclampsia and IUGR by examining the levels of oxidative stress-related molecules, such as 8-hydroxy-2′-deoxyguanosine (8-OHdG) (a hydroxy product of deoxyguanosine that is generated by the DNA damage caused by oxidative stress), 4-HNE (a product of lipid peroxidation), and redox-regulating molecules, such as TRX (reductive enzyme) and redox factor-1 (ref-1) (repairs DNA damage and acts as a redox-modifying factor) in the placenta in normal pregnancy and in complicated pregnancies (preeclampsia with or without IUGR and IUGR alone).

Materials and methods

Tissue collection

For immunohistochemistry, normal placental tissues were collected from 42 patients (6–40 weeks); 10 were in the first trimester (6–13 weeks), 9 in the second trimester (14–27 weeks) and 23 in the third trimester (28–40 weeks). The cases in the third trimester had normal blood pressure and were uncomplicated (i.e., had no serious maternal or fetal complications, such as preeclampsia or IUGR). Preeclampsia was defined as gestational hypertension accompanied by proteinuria. Hypertension was defined as an increase of 30 mmHg in systolic or of 15 mmHg in diastolic blood pressure (compared with values obtained prior to 20 weeks) or an absolute blood pressure greater than 140/90 mmHg. Proteinuria was defined as greater than 500 mg per 24-h collection period or greater than 2+ in voided random urine specimens [18]. Women who had chronic hypertension and/or proteinuria prior to pregnancy were excluded. All the preeclampsia cases (n=24) had both hypertension and proteinuria; 19 had severe hypertension (absolute blood pressure greater than 160/110 mmHg) + proteinuria and 5 had mild hypertension + proteinuria. IUGR referred to a small for date newborn who had a birth weight less than the 10th percentile for its gestational age (by Japanese standards) [24]. Gestational age was adjusted according to ultrasonographic findings in early gestation in all IUGR cases. No fetal anomalies were present in IUGR cases. Placentae from complicated pregnancies were collected from 41 cases; 13 were complicated by preeclampsia alone (28–39 weeks), 17 by IUGR alone (28–40 weeks) and 11 by preeclampsia + IUGR (28–40 weeks). Histologically, none of the placentae examined were complicated by overt chorioamnionitis. All the tissues were fixed with 10% phosphate-buffered formalin and embedded in paraffin. For Western blotting, placental tissues were collected from eight women with a normal pregnancy (9–39 weeks) and from five with preeclampsia (28–39 weeks), three with IUGR (28–36 weeks) and one with preeclampsia + IUGR (36 weeks). The placental tissues were used with the approval of the Ethics Committee of Shinshu University and with the consent of the patients.

Immunohistochemistry

Immunohistochemical staining was carried out on paraffin sections, with the streptavidin-biotin-peroxidase complex method performed using a Histofine SAB-PO kit (Nichirei, Tokyo, Japan). To evaluate oxidative stress and reductive reactions in the tissues, we selected four markers: 8-OHdG (a hydroxy product of deoxyguanosine that is generated by the DNA damage caused by oxidative stress), 4-HNE (a product of lipid peroxidation), TRX and ref-1. The primary antibodies used were those against 8-OHdG [clone, N45.1; Japan Institution for Aging (JICA), Fukuroi, Japan] [5], 4-HNE (JICA) [27], TRX (kindly provided by Professor Junji Yodoi, Kyoto University, Kyoto, Japan) [17] and ref-1 (Santa Cruz Biotechnology, Santa Cruz, CA, USA). Anti-ref-1 was polyclonal (rabbit), whereas the other three antibodies were monoclonal (mouse). The above antibodies (8-OHdG, 4-HNE, TRX and ref-1) recognize the hydroxy base of 8-OHdG at the 8th position, 4-HNE bound to histidine, human recombinant TRX and a peptide mapping at the carboxy terminus of ref-1 of human origin, respectively. Collected placental tissues were immediately fixed in 10% buffered formalin. Sections were deparaffinized, rehydrated and heated in 0.01 M citrate buffer (pH 6.0) for 15 min in a microwave oven. After endogenous peroxidase activity had been blocked, they were incubated with normal goat or rabbit serum to reduce non-specific binding. They were then incubated with one of the primary antibodies or with normal serum (as a negative control) at 4°C overnight. The sections were incubated with biotinylated anti-rabbit IgG (goat) or anti-mouse IgG (rabbit) and with peroxidase-conjugated streptavidin. The sections were stained with diaminobenzidine and counterstained with hematoxylin.

The degree of immunostaining was evaluated semi-quantitatively on the basis of the percentage of positive cells in the trophoblast: diffusely positive (++) when positive cells accounted for more than 50%, partially positive (+) when positive cells were 5–49% and focally positive (+/−) when positive cells were less than 5%. The percentage of positive cells was calculated in ten randomly selected high power fields that did not contain placental infarction. In accordance with the location of the major trophoblast types positive for the oxidative stress-related markers examined, the degree of immunostaining for 8-OHdG, TRX and ref-1 was evaluated in the cytotrophoblast, and the degree of immunostaining for 4-HNE was evaluated in the syncytiotrophoblast. The results of immunostaining were evaluated without knowledge of the pregnancy diagnosis.

Western blotting

Placental tissues were snap-frozen and stored at −80°C. The tissues were homogenized in a lysis buffer [50 mM Tris-HCl, pH 8.0, 0.25 M NaCl, 0.5% NP-40, 1 mM phenylmethylsulfonyl fluoride (PMSF) (Sigma), 1 μg/ml aprotinin (Boehringer Mannheim), 1 μg/ml leupeptin (Boehringer Mannheim), 20 μg/ml *N*-α-tosyl-L-phenyl-alanyl chloromethyl ketone (TPCK) (Boehringer Mannheim)]. The lysates were centrifuged at 13,000 *g* for 20 min at 4°C and the supernatants were stored at −80°C. Extracts equivalent to 30 μg of total protein were separated by sodium dodecyl sulfate-polyacrylamide gel electrophoresis (10% acrylamide) and then transferred onto nitrocellulose membranes (Hybond TM-C super, Amersham, Buckinghamshire, UK). The membranes were blocked in Tris-buffered saline with Tween-20 (TBST) (0.2 M NaCl, 10 mM Tris, pH 7.4, 0.2% Tween-20) containing 5% non-fat dry milk and 0.02% NaN_3 for 1 h, then incubated with antibodies against 4-HNE (JICA), TRX (provided by Professor Junji Yodoi), ref-1 (Santa Cruz) or β-actin (Biomakor, Rehovot, Israel) in TBST containing 5% non-fat dry milk. Western blotting was not performed for 8-OHdG, since 8-OHdG is a nucleoside, not a protein. The membranes were incubated with sheep anti-rabbit IgG or with anti-mouse IgG (Amersham) in TBST containing 2% non-fat dry milk. Bound antibody was detected by means of an enhanced chemiluminescence system (Amersham). The density of the bands on the filters was quantified by densitometric analysis using a Quantity One Scan System (ATTO, Tokyo, Japan). The levels for 4-HNE-labeled protein, TRX and ref-1 were adjusted with respect to β-actin expression by dividing the density of each band by the corresponding band density for β-actin. Since the number of cases used for Western blotting was small, we compared the expression of these molecules in the third-trimester placenta between normal pregnancies (n=4) and all complicated pregnancies (preeclampsia and/or IUGR, n=9).

Statistical analysis

The Kruskal-Wallis rank test, Scheffe's F-test, Spearman's rank correlation test (for the data of immunohistochemistry) and Mann-Whitney's U-test (for the data of Western blotting) were used for statistical analyses using StatView v.5.0 (Abacus, Berkeley, CA, USA). Normal placental tissues from the third trimester (n=23) were used as a control for the complicated pregnancies. A P value <0.05 or a correlation coefficient (ρ) greater than 0.4 or less than −0.4 (in the case of Spearman's rank correlation) was considered significant.

Results

Immunohistochemistry

Positive immunostaining for 8-OHdG and ref-1 was observed within the nuclei. Positive immunostaining for 4-HNE was observed in the cytoplasm and/or cell membrane. Positive immunostaining for TRX was observed within both the nuclei and the cytoplasm. In the placentae obtained from normal pregnancies, positive staining for 8-OHdG, TRX and ref-1 was mostly observed in the cytotrophoblast throughout gestation, the syncytiotrophoblast being only focally positive for these molecules (Fig. 1). In the early stages of gestation, the trophoblast of the cell column was extensively positive for 8-OHdG, TRX and ref-1. In addition, many different types of cells, including Hofbauer's cells and endothelial cells, were also positive for 8-0HdG. In contrast, positive staining for 4-HNE was mostly observed in the syncytiotrophoblast and only rarely in the cytotrophoblast throughout gestation. Hofbauer cells were mostly positive for 8-OHdG, TRX and ref-1, but negative for 4-HNE. There was no significant correlation between gestational age and the level of 8-OHdG, 4-HNE, TRX or ref-1.

In the placentae from cases with preeclampsia and/or IUGR, the localization of positive immunostaining for 8-OHdG, 4-HNE, TRX and ref-1 was similar to that observed in the normal placentae. The results obtained for the degree of immunostaining of these molecules during the third trimester in normal placentae versus disease are summarized in Table 1. The presence of 8-OHdG was significantly greater in IUGR (P=0.012) or preeclampsia + IUGR (P=0.0021) than in normal pregnancy (Fig. 2), but it did not differ significantly between preeclampsia and normal controls (P=0.14). No significant difference was observed in 4-HNE staining between either type of complicated pregnancy and normal pregnancy. The expression of TRX was significantly greater in preeclampsia (P=0.045) than in normal pregnancy, but it did not differ significantly between IUGR (P=0.15) or preeclampsia + IUGR (P=0.11) and normal controls

Table 1 Degree of immunostaining for oxidative stress-related molecules in placentae obtained during the third trimester in normal and complicated pregnancies. Criteria used to assess the degree of immunostaining are described in the text. *IUGR* intrauterine growth restriction, *8-OHdG* 8-hydroxy-2′-deoxyguanosine, *4-HNE* 4-hydroxynonenal, *TRX* thioredoxin, *ref-1* redox factor-1

	8-OHdG			4-HNE			TRX			ref-1		
	(+/−)	(+)	(++)	(+/−)	(+)	(++)	(+/−)	(+)	(++)	(+/−)	(+)	(++)
Normal (n=23)	14	8	1	22	1	0	19	4	0	20	2	1
Preeclampsia (n=13)	2	9	2	12	1	0	4	9	0	5	3	5*
IUGR (n=17)	3	6	8*	13	3	1	9	6	2	6	5	6*
Preeclampsia+ IUGR (n=11)	1	6	4**	9	2	0	4	6	1	3	2	6**

*P<0.05 versus normal
**P<0.005 versus normal

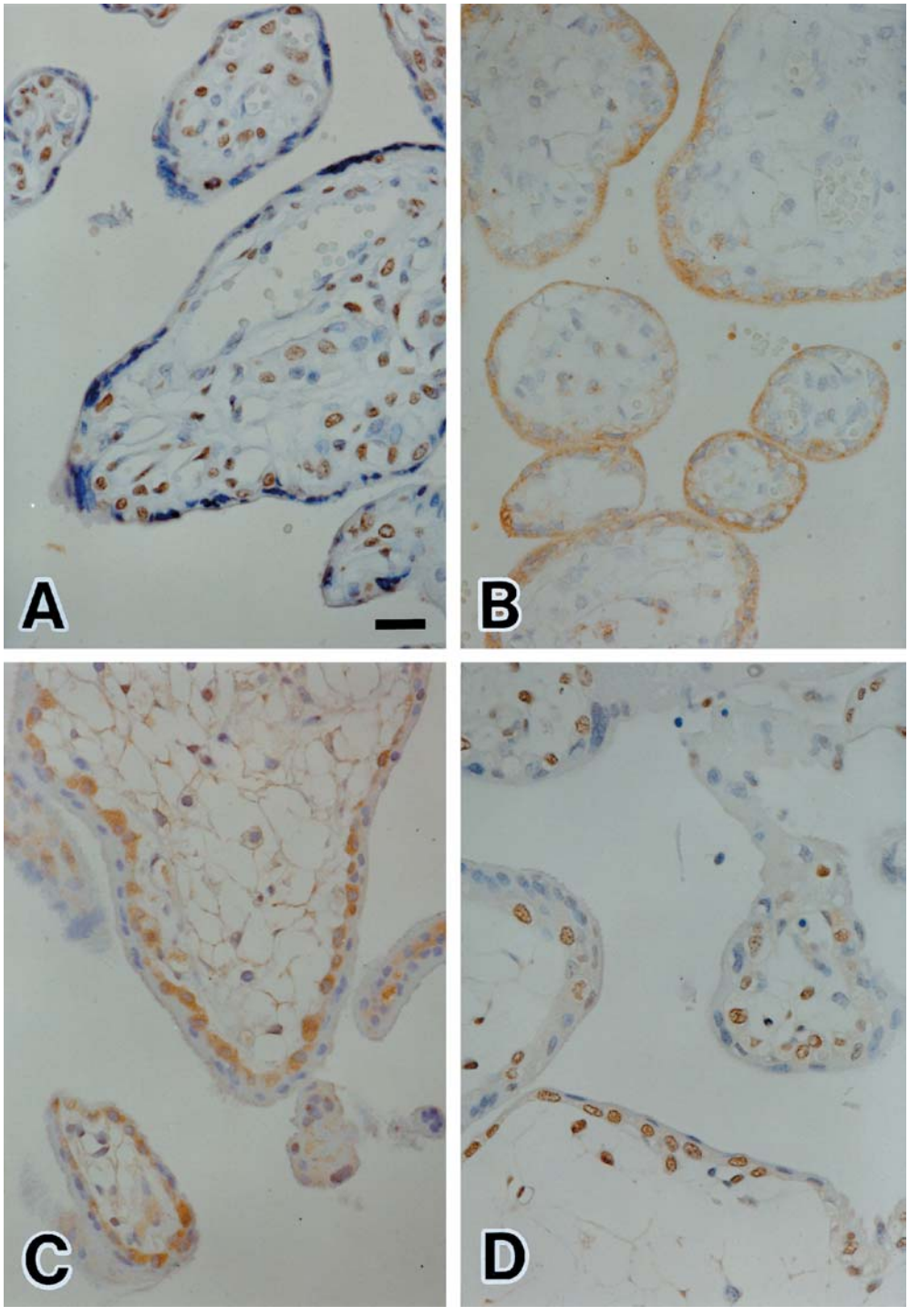

Fig. 1 Immunostaining for oxidative stress-related molecules in the placenta in normal pregnancy. **A** 8-Hydroxy-2′-deoxyguanosine (28 weeks). **B** 4-Hydroxynonenal (19 weeks). **C** Thioredoxin (9 weeks). **D** Redox factor-1 (11 weeks) (×350). *Scale bar*=27 μm (applies to all *panels*)

(Fig. 3). Ref-1 expression was significantly higher in preeclampsia (P=0.017), IUGR (P=0.016) and preeclampsia + IUGR (P=0.0038) than in normal pregnancy (Fig. 4).

The correlations between the expressions of pairs of the four molecules are shown in Table 2 (normal pregnancy) and Table 3 (complicated pregnancies). In normal pregnancy, significant positive correlations were observed between 8-OHdG and TRX (ρ=0.46), and between TRX and ref-1 (ρ=0.52). In the complicated pregnancies, a significant positive correlation was observed only between TRX and ref-1 (ρ=0.43).

Western blotting

In the placentae obtained from normal and complicated pregnancies, specific bands were detected for 4-HNE-

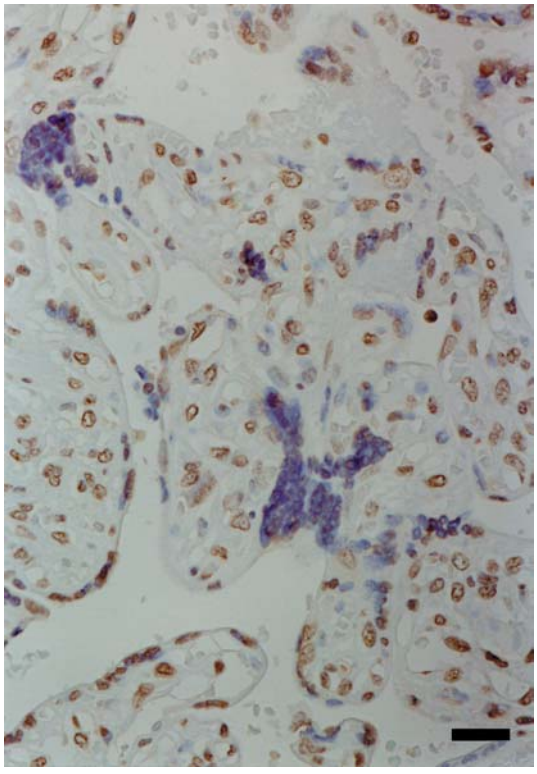

Fig. 2 Immunostaining for 8-hydroxy-2′-deoxyguanosine in the placenta in preeclampsia + intrauterine growth restriction (37 weeks) (×350). *Scale bar*=27 μm

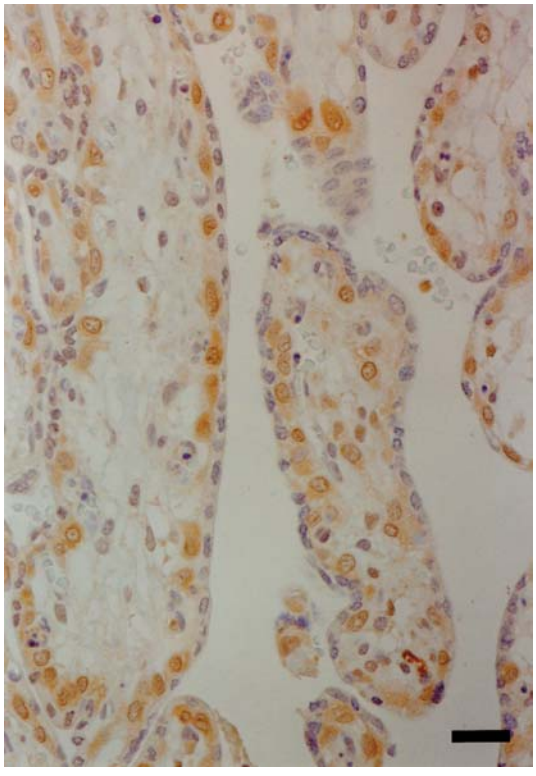

Fig. 3 Immunostaining for thioredoxin in the placenta in intrauterine growth restriction (28 weeks) (×350). *Scale bar*=27 μm

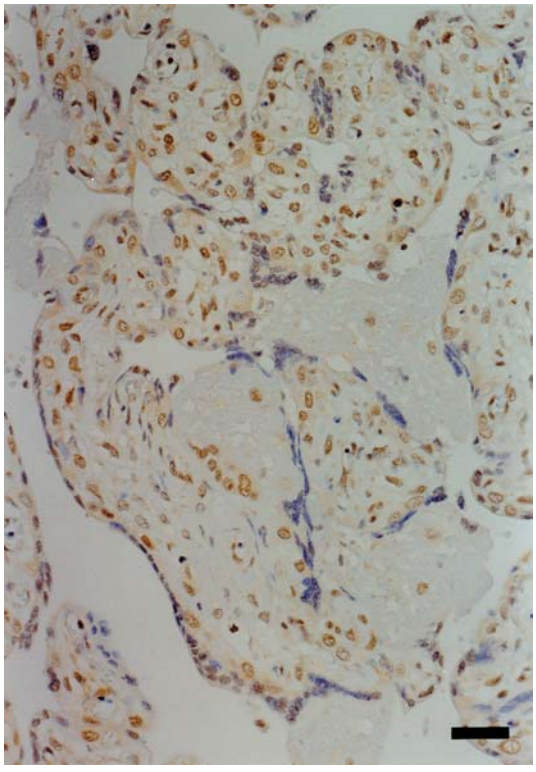

Fig. 4 Immunostaining for ref-1 in the placenta in intrauterine growth restriction (28 weeks) (×270). *Scale bar*=35 μm

Table 2 Correlation between the immunostaining of pairs of oxidative stress-related molecules in normal pregnancy. Data are presented as correlation coefficients. *8-OHdG* 8-hydroxy-2′-deoxyguanosine, *4-HNE* 4-hydroxynonenal, *TRX* thioredoxin, *ref-1* redox factor-1

	ref-1	TRX	4-HNE
8-OHdG	0.22	0.46*	0.22
4-HNE	−0.04	0.14	
TRX	0.52*		

* Correlation coefficient >0.4

Table 3 Correlation between the immunostaining of pairs of oxidative stress-related molecules in complicated pregnancies. Data are presented as correlation coefficients. *8-OHdG* 8-hydroxy-2′-deoxyguanosine, *4-HNE* 4-hydroxynonenal, *TRX* thioredoxin, *ref-1* redox factor-1

	ref-1	TRX	4-HNE
8-OHdG	0.32	0.27	−0.13
4-HNE	0.35	0.01	
TRX	0.45*		

* Correlation coefficient >0.4

labeled protein, TRX and ref-1 (at 70 kDa, 14 kDa and 35 kDa, respectively). β-Actin was expressed at 42 kDa in all the samples. In normal pregnancy, the levels of 4-HNE-labeled protein, TRX and ref-1 did not show significant changes during gestation. Ref-1 expression tended to be greater in complicated pregnancies than in

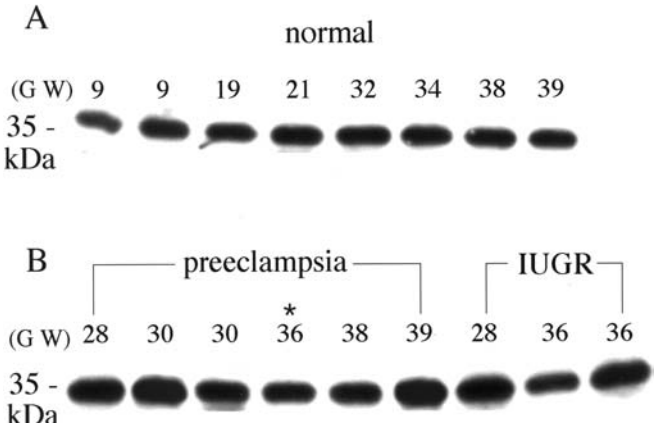

Fig. 5 Expression of redox factor-1 in placentae obtained from normal (**A**) and complicated (**B**) pregnancies (Western blotting). *GW* gestational weeks, *asterisk* case with preeclampsia + intrauterine growth restriction

normal pregnancies, but the difference was not significant (P=0.09) (Fig. 5). No significant difference was found in the level of 4-HNE-labeled protein or TRX between complicated and normal pregnancies.

Discussion

In the present study, the placental 8-OHdG level was significantly greater in IUGR or preeclampsia + IUGR than in normal pregnancy, but it did not differ significantly between preeclampsia and normal pregnancy, suggesting that oxidative DNA damage is increased in preeclampsia with IUGR but not in preeclampsia without IUGR. However, the placental ref-1 expression was significantly greater in preeclampsia, IUGR and preeclampsia + IUGR than in normal pregnancy, suggesting that the redox function is accelerated in both preeclampsia and IUGR. Thus, redox function was elevated in the preeclamptic placentae, irrespective of the presence of IUGR, while oxidative DNA damage was increased only in the preeclamptic placentae associated with IUGR. In other words, there was a discrepancy between the levels of oxidative DNA damage and redox function in the placentae from preeclampsia without IUGR. Although the reason for this is unknown, we can speculate that, in preeclampsia without IUGR, elevated redox function may be compensating for the DNA damage caused by enhanced oxidative stress in preeclampsia. In other words, IUGR associated with preeclampsia may possibly be due to decompensation of placental function against oxidative stress. However, there is a possibility that, with disease conditions, more cells (of different type) may express the molecules, rather than each cell showing an increased concentration of molecules.

Elevation of ref-1 expression in the placenta in preeclampsia and/or IUGR did not reach significance in our Western blotting study. The reason for this may be (1) the number of cases analyzed using Western blotting was smaller than those using immunohistochemistry or (2) contamination by other cells expressing ref-1 (such as Hofbauer cells) within the tissue homogenates. However, the level of oxidative DNA damage would seem to be elevated in IUGR during the third trimester, and, at the same time, the redox system, especially ref-1 (which repairs DNA damage and acts as a redox-modifying factor), is activated in both IUGR and preeclampsia.

The levels of 4-HNE did not differ significantly between either preeclampsia or IUGR and normal pregnancy, suggesting that the lipid hyperoxidation status is not elevated in the placentae from preeclampsia or IUGR. The result is consistent with that reported in a recent paper [22]. To judge from the localization of the molecules studied, oxidative DNA damage appears to occur mainly in rapidly growing cells, such as those of the trophoblast of the cell columns, while lipid hyperoxidation occurs mainly in the superficial cell layers, such as those of the syncytiotrophoblast. These results suggest that oxidative stress may influence the placentae or trophoblastic cells differently between DNA damage and lipid hyperoxidation.

Recently, it has been reported that ischemia–reperfusion injury may be associated with increased levels of oxidative stress in preeclampsia [8]. Placental ischemia can induce IUGR irrespective of the presence of preeclampsia. Since the oxidative DNA damage (as reflected by 8-OHdG) was elevated in the placentae from IUGR or preeclampsia + IUGR (but not in those from preeclampsia with no IUGR), ischemia–reperfusion injury may be also involved in the pathogenesis of IUGR. A recent investigation has emphasized the presence of placental "hyperoxia" rather than hypoxia in IUGR [10]. In fact, hyperoxic status induces an increase in reactive oxygen species (ROSs) and leads to oxidative DNA injury [9]. Thus, oxidative DNA damage due to ischemia–reperfusion injury and/or hyperoxia may be associated with the development of IUGR. Moreover, elevated placental ref-1 expression observed in IUGR indicates that the redox function and DNA repair function may be enhanced so as to compensate for the adverse influence on cells exerted by the increased oxidative DNA damage. However, since the basic role of oxidative stress is not very well understood in preeclampsia or IUGR, nor, indeed, in normal pregnancy, further investigations will clearly be needed.

Acknowledgement The authors thank Professor Junji Yodoi, Kyoto University, for providing the antibody against thioredoxin.

References

1. Casasco A, Calligaro A, Casasco M, Tateo S, Icaro Cornaglia A, Reguzzoni M, Farina A (1997) Immunohistochemical localization of lipoperoxidation products in normal human placenta. Placenta 18:249–253
2. Chappell LC, Seed PT, Briley AL, Kelly FJ, Lee R, Hunt BJ, Parmar K, Bewley S, Shennan AH, Steer PJ, Poston L (1999) Effect of antioxidants on the occurrence of pre-eclampsia in

women at increased risk: a randomised trial. Lancet 354:810–816
3. Ejima K, Nanri H, Toki N, Kashimura M, Ikeda M (1999) Localization of thioredoxin reductase and thioredoxin in normal human placenta and their protective effect against oxidative stress. Placenta 20:95–101
4. Friedman SA, Taylor RN, Roberts JM (1991) Pathophysiology of preeclampsia. Clin Perinatol 18:661–682
5. Hattori Y, Nishigori C, Tanaka T, Uchida K, Nikaido O, Osawa T, Hiai H, Imamura S, Toyokuni S (1996) 8-hydroxy-2′-deoxyguanosine is increased in epidermal cells of hairless mice after chronic ultraviolet B exposure. J Invest Dermatol 107:733–737
6. Hauth JC, Cunningham FG (1999) Preeclampsia-eclampsia. In: Lindheimer MD, Roberts JM, Cunningham FG (eds) Chesley's hypertensive disorders in pregnancy, 2nd edn. Appleton & Lange, Stamford, pp 169–199
7. Hubel CA (1999) Oxidative stress in the pathogenesis of preeclampsia. P Soc Exp Biol Med 222:222–235
8. Hung TH, Skepper JN, Burton GJ (2001) In vitro ischemia-reperfusion injury in term human placenta as a model for oxidative stress in pathological pregnancies. Am J Pathol 159:1031–1043
9. Kasai H (1997) Analysis of a form of oxidative DNA damage, 8-hydroxy-2′-deoxyguanosine, as a marker of cellular oxidative stress during carcinogenesis. Mutat Res 387:147–163
10. Khaliq A, Dunk C, Jiang J, Shams M, Li XF, Acevedo C, Weich H, Whittle M, Ahmed A (1999) Hypoxia down-regulates placenta growth factor, whereas fetal growth restriction up-regulates placenta growth factor expression: molecular evidence for "placental hyperoxia" in intrauterine growth restriction. Lab Invest 79:151–170
11. Little RE, Gladen BC (1999) Levels of lipid peroxides in uncomplicated pregnancy: a review of the literature. Reprod Toxicol 13:347–352
12. Many A, Hubel CA, Fisher SJ, Roberts JM, Zhou Y (2000) Invasive cytotrophoblasts manifest evidence of oxidative stress in preeclampsia. Am J Pathol 156:321–331
13. Mise H, Sagawa N, Matsumoto T, Yura S, Nanno H, Itoh H, Mori T, Masuzaki H, Hosoda K, Ogawa Y, Nakao K (1998) Augmented placental production of leptin in preeclampsia: possible involvement of placental hypoxia. J Clin Endocrinol Metab 83:3225–3229
14. Morikawa S, Kurauchi O, Tanaka M, Yoneda M, Uchida K, Itakura A, Furugori K, Mizutani S, Tomoda Y (1997) Increased mitochondrial damage by lipid peroxidation in trophoblastic cells of preeclamptic placentas. Biochem Mol Biol Int 41:767–775
15. Morris JM, Gopaul NK, Endresen MJR, Knight M, Linton EA, Dhir S, Anggard EE, Redman CWG (1998) Circulating markers of oxidative stress are raised in normal pregnancy and pre-eclampsia. Br J Obstet Gynaecol 105:1195–1199
16. Myatt L, Kossenjans W, Sahay R, Eis A, Brockman D (2000) Oxidative stress causes vascular dysfunction in the placenta. J Matern Fetal Med 9:79–82
17. Nakamura H, Nakamura K, Yodoi J (1997) Redox regulation of cellular activation. Annu Rev Immunol 15:351–369
18. National High Blood Pressure Education Program Working Group (1990) Report on high blood pressure in pregnancy. Am J Obstet Gynecol 163:1689–1712
19. Pascoal IF, Lindheimer MD, Nalbantian-Brandt C, Umans JG (1998) Preeclampsia selectively impairs endothelium-dependent relaxation and leads to oscillatory activity in small omental arteries. J Clin Invest 101:464–470
20. Redman CW (1991) Current topic: preeclampsia and the placenta. Placenta 12:301–308
21. Roberts JM, Taylor RN, Musci TJ, Rodgers GM, Hubel CA, McLaughlin MK (1990) Preeclampsia: an endothelial cell disorder. Am J Obstet Gynecol 163:1365–1366
22. Santoso DI, Rogers P, Wallace EM, Manuelpillai U, Walker D, Subakir SB (2002) Localization of indoleamine 2,3-dioxygenase and 4-hydroxynonenal in normal and pre-eclamptic placentae. Placenta 23:373–379.
23. Shibata E, Ejima K, Nanri H, Toki N, Koyama C, Ikeda M, Kashimura M (2001) Enhanced protein levels of protein thiol/disulphide oxidoreductases in placentae from pre-eclamptic subjects. Placenta 22:566–572
24. Shinozuka N, Masuda H, Kagawa H, Taketani Y (1996) Standard values of ultrasonographic fetal biometry. Jpn J Med Ultrasonics 23:877–888
25. Sikkema JM, van Rijn BB, Franx A, Bruinse HW, de Roos R, Stroes ES, van Faassen EE (2001) Placental superoxide is increased in pre-eclampsia. Placenta 22:304–308
26. Soothill PW, Nicolaides KH, Campbell S (1987) Prenatal asphyxia, hyperlacticaemia, hypoglycaemia and erythroblastosis in growth retarded fetuses. Br Med J 294:1051–1053
27. Toyokuni S, Miyake N, Hiai H, Hagiwara M, Kawakishi S, Osawa T, Uchida K (1995) The monoclonal antibody specific for the 4-hydroxy-2-nonenal histidine adduct. FEBS Lett 359:189–191
28. Trudinger BJ, Giles WB, Cook CM, Bombardieri J, Collins L (1985) Fetal umbilical artery flow velocity waveforms and placental resistance: clinical significance. Br J Obstet Gynaecol 92:23–30.
29. Walsh SW (1998) Maternal-placental interactions of oxidative stress and antioxidants in preeclampsia. Semin Reprod Endocrinol 16:93–104
30. Walsh SW, Vaughan JE, Wang Y, Roberts LJ II (2000) Placental isoprostane is significantly increased in preeclampsia. FASEB J 14:1289–1296
31. Wang Y, Walsh SW (1998) Placental mitochondria as a source of oxidative stress in pre-eclampsia. Placenta 19:581–586
32. Zamudio S, Palmer SK, Regensteiner JG, Moore LG (1995) High altitude and hypertension during pregnancy. Am J Human Biol 7:183–193

Virchows Arch (2004) 444:56–60
DOI 10.1007/s00428-003-0907-y

ORIGINAL ARTICLE

Masae Mikami · Hirotaka Koizumi · Masamitsu Ishii · Hisaya Nakajima

The identification of monoclonality in fibrous dysplasia by methylation-specific polymerase chain reaction for the human androgen receptor gene

Received: 3 June 2003 / Accepted: 28 August 2003 / Published online: 24 October 2003

Abstract The nature of fibrous dysplasia, a well-known and relatively common bone lesion, is controversial. We report here the first polymerase chain reaction (PCR)-based clonality analysis of fibrous dysplasia in which 11 cases obtained from females with a polymorphism at the human androgen receptor gene locus (*HUMARA*) were examined using a methylation-specific PCR procedure. This assay allowed accurate evaluation of the clonality status of this disease by eliminating restriction enzyme digestion that had been used previously in conventional *HUMARA* analysis. Eight samples proved to be informative for the assay, and they all showed non-random X-chromosome inactivation, indicative of a monoclonal pattern. These findings demonstrate a clonal origin for fibrous dysplasia, suggesting that the disease is a neoplastic lesion rather than a "dysplastic" process, as has been generally believed.

Keywords Fibrous dysplasia · Monoclonality · Methylation-specific PCR (MSP) · Human androgen receptor gene (*HUMARA*)

M. Mikami · H. Koizumi (✉)
Department of Pathology,
St. Marianna University School of Medicine,
216-8511 Kawasaki, Japan
e-mail: koizumi@marianna-u.ac.jp
Tel.: +81-44-9778111
Fax: +81-44-9777827

M. Ishii
Department of Surgery,
St. Marianna University School of Medicine,
216-8511 Kawasaki, Japan

H. Nakajima
Department of Orthopedic Surgery,
St. Marianna University School of Medicine,
216-8511 Kawasaki, Japan

Introduction

Fibrous dysplasia is a benign skeletal disorder characterized by replacement of a localized area of bone by a proliferation of fibrous tissue intermixed with foci of immature non-lamellar bone [7]. The disease may involve either a single bone (monostotic form, 85% of cases) or multiple bones (polyostotic form, 15% of cases). Additionally, lesions characteristic of fibrous dysplasia may be clustered into only one or two anatomic regions (monomelic form) or exhibit a widespread involvement of the skeleton (polymelic form) [9]. Some patients can present with endocrine dysfunction (generally precocious puberty) and cutaneous cáfe-au-lait spots, a collection of features referred to as the McCune-Albright syndrome [15].

The nosologic status of fibrous dysplasia remains controversial. In current major textbooks that describe bone pathology, fibrous dysplasia is regarded as a non-neoplastic process [23] and is also defined elsewhere as a dysplastic disorder of bone [7]. Nonetheless, there is specific evidence that favors a neoplastic origin for fibrous dysplasia, including the presence of chromosomal aberrations [4], activating mutations in the *GNAS1* gene [25], overexpression of the c-*fos* proto-oncogene [2] and occasional malignant changes in this disease [20].

One of the defining properties of neoplastic processes is that they are clonal in nature [13]. This feature can be evaluated by analyzing the inactivation pattern of the X-chromosome in lesional tissue from female patients [24]. This is based upon the assumption that a non-neoplastic polyclonal process should show a random inactivation pattern of both paternal and maternal X-chromosomes, whereas a neoplastic lesion should result in a non-random inactivation pattern. In the present study, we used a recently developed methylation-specific polymerase chain reaction (PCR) (MSP)-based approach, which analyzed the DNA methylation status near a trinucleotide repeat polymorphism of the human androgen receptor gene (*HUMARA*) on the X-chromosome [14], to determine the clonality of fibrous dysplasia.

Materials and methods

Sample collections and DNA isolation

We studied surgical specimens from 11 female patients with fibrous dysplasia (aged between 9 years and 45 years). These samples had been processed for conventional histopathological examination at the St. Marianna University Hospital from 1983 to 1999. All specimens were obtained from areas of abnormal bone by curettage, which enabled us to use the sections composed only of lesional tissue in subsequent analysis. The study protocol was approved by the human ethics review committee of the St. Marianna University School of Medicine.

Several 5-μm sections from archival formalin-fixed and paraffin-embedded tissue were directly placed in a microfuge tube, dewaxed in xylene for 15 min and cleared with absolute ethanol for 5 min at room temperature. The samples were centrifuged at 10,000 rpm for 5 min between each reagent change. The samples were air-dried and placed in 50 μl of proteinase K digestion buffer [50 mM Tris-HCl, pH 8.0; 1 mM ethylene diamine tetraacetic acid (EDTA); 0.5% Tween 20]. Digestion was carried out for 5 days at 55°C with daily replacement of proteinase K (250 μg/ml working concentration), followed by boiling for 10 min to inactivate the enzyme [5]. Control DNA from leukocytes of a normal female donor was isolated according to a standard protocol [21].

Bisulfite treatment

The DNA was treated with sodium bisulfite as described previously [10]. Briefly, DNA solution was denatured with sodium hydroxide and then incubated at 55°C overnight with hydroquinone (Wako, Osaka, Japan) and sodium bisulfite (Sigma, St. Louis, MO, USA). The DNA was purified using the Wizard DNA clean-up system (Promega, Madison, WI, USA), and the chemical reaction was completed by sodium hydroxide. After ethanol precipitation, the treated DNA was resuspended in 20 μl of TE (10 mM Tris-HCl, pH 8.0; 1 mM EDTA).

PCR amplification

PCR was carried out using AR-M (MF2/MR3) and AR-U (UF2/UR1) primer sets as described by Kubota et al. [14]. One primer was labeled with the fluorescent dye 6-FAM. The polymerase (HotStar Taq; Qiagen, Hilden, Germany) was activated at 95°C for 15 min. The DNA was amplified in an ATG model EZC-96 thermocycler (Asahi Techno Glass, Chiba, Japan) for 40 cycles at 94°C for 30 s, 58°C for 30 s, and 72°C for 30 s, followed by a final extension at 72°C for 10 min. The PCR products were mixed with size markers (GeneScan 350 TAMRA; Applied Biosystems, CA, USA) and analyzed on an automated sequencer (310 ABI genetic analyzer) using GeneScan version 3.7 software.

Results

Histopathology

Clinical data from each case sample are summarized in Table 1, and each of these was monostotic. On histology, all 11 lesions displayed the typical appearance of fibrous dysplasia: irregular trabeculae of woven bone were embedded in a moderately cellular fibrous matrix. The bony trabeculae had variable and irregular shapes. Osteoblastic rimming of the trabeculae was characteristically inconspicuous and some of the trabeculae seemed to emerge from the surrounding fibrous background (Fig. 1). In none of the cases examined was any associated lesion, such as an aneurysmal bone cyst, detected.

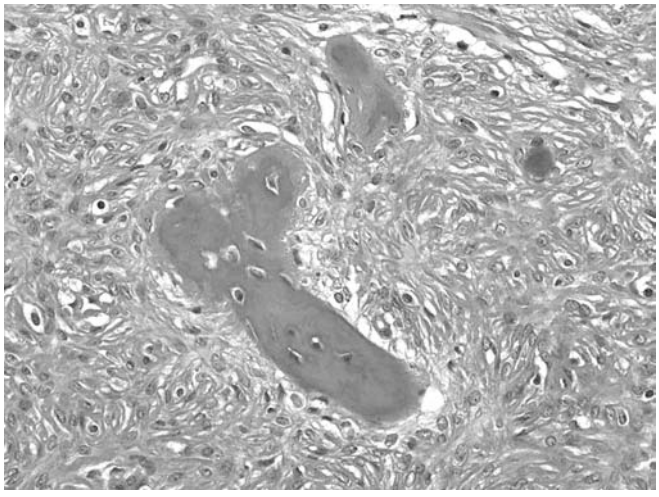

Fig. 1 Histological study of a fibrous dysplasia. Trabeculae of woven bone without an osteoblast rim exist in a moderately cellular fibrous stroma with plump to oval spindle cells. Hematoxylin & eosin, ×200

Table 1 Results of human androgen receptor gene locus-methylation-specific polymerase chain reaction (PCR) (*HUMARA*-MSP) analysis in 11 patients with fibrous dysplasia. *N/A* not applicable (no amplified DNA was detected)

Case no.	Age (years)	Location	*HUMARA*
1	44	Tibia	Monoclonal
2	17	Unknown	Monoclonal
3	13	Hand	Monoclonal
4	45	Unknown	Monoclonal
5	17	Skull	Monoclonal
6	9	Tibia	Monoclonal
7	13	Fibula	Monoclonal
8	33	Skull	Monoclonal
9	20	Skull	Homozygous
10	30	Tibia	Homozygous
11	35	Unknown	N/A

Clonality analysis

Table 1 summarizes the results of the *HUMARA*-MSP analysis. Two patients (cases 9 and 10) showed homozygosity for the *HUMARA* polymorphism and, therefore, further analysis would have been uninformative. No MSP products were amplified from one further patient (case 11), whereas the remaining eight patients all showed non-random X-chromosome inactivation (a monoclonal pattern, Fig. 2a, b), whilst control leukocyte DNA exhibited random inactivation (a polyclonal pattern, Fig. 2c).

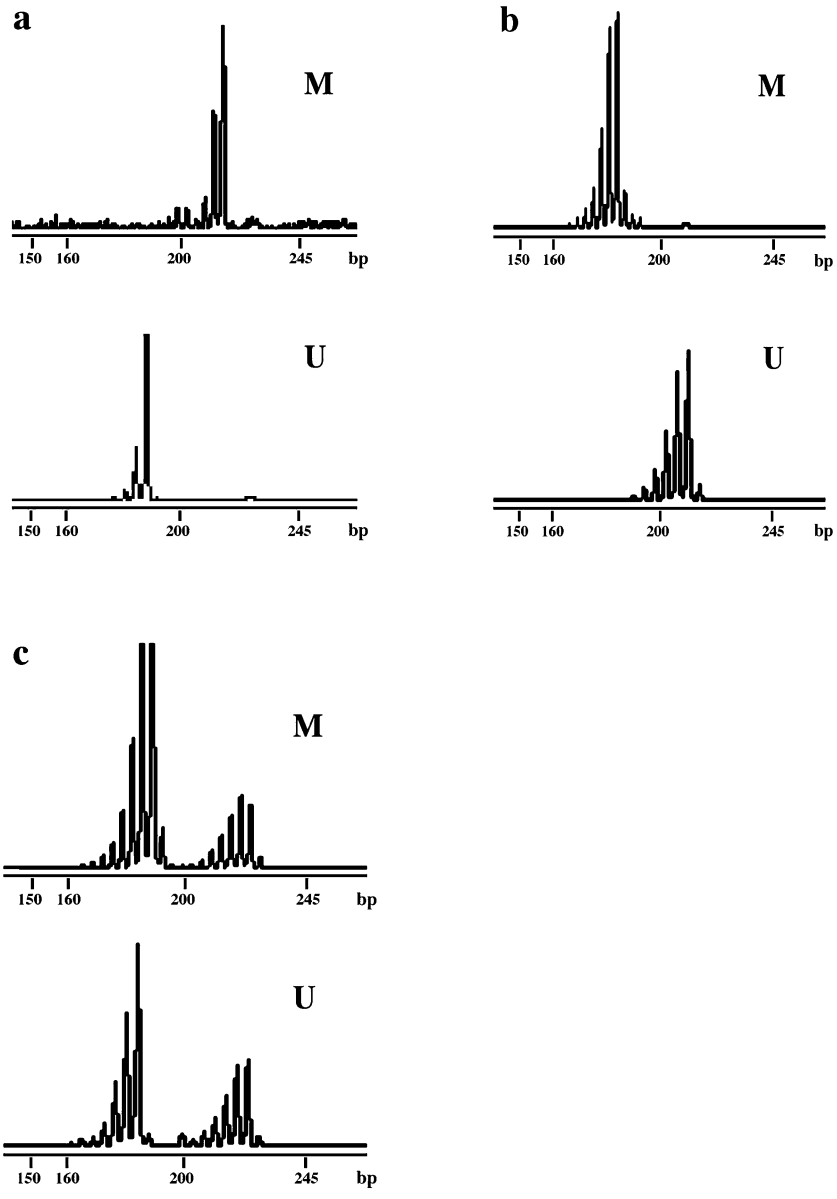

Fig. 2 Examples of clonality analysis using the human androgen receptor gene locus-methylation-specific polymerase chain reaction (PCR) (*HUMARA*-MSP) assay. **a, b** Monoclonal patterns in fibrous dysplasia (**a** case 2; **b** case 6). **c** Polyclonal pattern in a normal female. *M* PCR with methylation-specific primers; *U* PCR with unmethylation-specific primers. Monoclonal and polyclonal patterns consist of two and four distinct peaks, respectively

Discussion

An analysis of clonality in the nodular mass of various organs reveals important information about the origin of these lesions. Recently, a PCR-based method for clonal analysis, which examines the DNA methylation status near the CAG trinucleotide repeat polymorphism of the *HUMARA* locus using restriction enzymes, has been developed [1, 19]. The advantage of this method is not only that the *HUMARA* locus is highly informative, but also that it is PCR based and, therefore, applicable to small quantities of DNA. It has now been used in a number of studies to determine the clonal nature of non-neoplastic and neoplastic lesions [17, 18, 22]. However, several problems have prevented the application of this method in a routine clinical setting. One important constraint was that the methylation-sensitive restriction enzyme digestion often gave ambiguous results, possibly due to partial digestion of template DNA and the presence of several minor labeled bands amongst the PCR products.

Recently, MSP analysis, which consists of chemical conversion of DNA and a subsequent MSP reaction, was developed to detect the promoter methylation of several genes [10]. This method was also reported to be applicable to X-chromosome inactivation analysis [14]. Since the *HUMARA*-MSP assay is based on bisulfite modification and not the use of restriction enzymes [10, 14], the problems associated with incomplete enzyme digestion are avoided. Incomplete bisulfite modification will not affect the results, due to the use of specific primers in the MSP method. It has now been demonstrated that clonality analysis using MSP is more precise and easier to interpret than analyses that use methylation-

sensitive restriction enzymes [12]. We subsequently performed a *HUMARA*-MSP assay to precisely evaluate the clonality status of fibrous dysplasias in this present study.

All cases in which we successfully analyzed fibrous dysplasia have proved to be monoclonal. The demonstration of a clonal process for fibrous dysplasia seems to favor a neoplastic theory rather than a "dysplastic" change. However, it should be remembered that PCR-based clonality analysis occasionally produces a pseudomonoclonal result [6]. The major mechanism for this is the patch-size concept [8, 11] such that if, after cell division, progeny cells remain adjacent to each other, large patches of cells are formed, all of which contain an identical pattern of X-chromosome inactivation. Lesions arising from two, three or more cells within a patch will show the same pattern of X-chromosome inactivation and, thus, appear monoclonal. This concept is a particularly important consideration when using very small tissue samples obtained by microdissection. To avoid this problem, Diaz-Cano et al. [6] have recommended the use of sample sizes larger than 100 cells or 0.25 cm^2. Since we have used a large quantity of samples without performing microdissection in the present study (see Materials and methods), the possibility of pseudomonoclonality resulting from the patch theory was quite low. Hence, we conclude that fibrous dysplasia is monoclonal in nature, which is indicative of a neoplastic process at the origin.

No MSP products were obtained from one patient sample (case 11). This seemed, however, to be the simple result of DNA degradation during storage of the sample, as a standard control PCR of this DNA using β-globin primers also failed (data not shown).

Recent cytogenetic studies using short-term culture have revealed chromosome abnormalities in some fibrous dysplasias. Combined with previously published data, Dal Cin et al. [4] observed various types of clonal karyotypic aberrations, including trisomy 2 and rearrangements involving chromosome 12, in 8 of 11 fibrous dysplasias. Studies on fibrous dysplasia occurring in McCune-Albright syndrome have revealed somatic mutations in the gene encoding the α subunit of Gs protein (*GNAS1*), suggesting that activation of this gene and subsequent c-*fos* overexpression play a central role in the development of these lesions [2, 25]. Recently, similar *GNAS1* mutations have been found to occur in both monostotic and polyostotic fibrous dysplasia [3, 16]. This combination of findings also indicates that fibrous dysplasia is, indeed, truly neoplastic in nature, and the results obtained in our present molecular analysis also provide strong additional supportive evidence of this interpretation.

In summary, we report here the first PCR-based evidence for a monoclonal and possibly neoplastic origin for fibrous dysplasia. Together with several additional lines of evidence [2, 3, 4, 16, 20, 25], our findings strongly suggest that fibrous dysplasia should, in the future, be regarded as a benign tumor of the bone. Additional studies, however, with larger sample sizes will be needed to conclusively prove our hypothesis.

Acknowledgements We thank Dr. Tosihito Shinagawa (St. Marianna University Seibu Hospital) for providing tissue materials. We also thank Shigeko Ohnuma and Kazuyo Hagimura for their excellent technical assistance, and Dr. Toshyuki Uchikoshi and Dr. Mamoru Tadokoro for their constant support and encouragement. This work was supported in part by a Grant-in-Aid for Scientific Research from the Ministry of Education, Culture, Sports, Science and Technology of Japan (no. 14571708).

References

1. Allen RC, Zoghbi HY, Moseley AB, Rosenblatt HM, Belmont JW (1992) Methylation of HpaII and HhaI sites near the polymorphic CAG repeat in the human androgen-receptor gene correlates with X chromosome inactivation. Am J Hum Genet 51:1229–1239
2. Candeliere GA, Glorieux FH, Prud'homme J, St.-Arnaud R (1995) Increased expression of the c-fos proto-oncogene in bone from patients with fibrous dysplasia. N Engl J Med 332:1546–1551
3. Candeliere GA, Roughley PJ, Glorieux FH (1997) Polymerase chain reaction-based technique for the selective enrichment and analysis of mosaic arg201 mutations in G alpha s from patients with fibrous dysplasia of bone. Bone 21:201–206
4. Dal Cin P, Sciot R, Brys P, De Wever I, Dorfman H, Fletcher CD, Jonsson K, Mandahl N, Mertens F, Mitelman F, Rosai J, Rydholm A, Samson I, Tallini G, Van den Berghe H, Vanni R, Willen H (2000) Recurrent chromosome aberrations in fibrous dysplasia of the bone: a report of the CHAMP study group. Chromosomes and morphology. Cancer Genet Cytogenet 122:30–32
5. Diaz-Cano SJ, Brady SP (1997) DNA extraction from formalin-fixed, paraffin-embedded tissues: Protein digestion as a limiting step for retrieval of high-quality DNA. Diagn Mol Pathol 6:342–346
6. Diaz-Cano SJ, Blanes A, Wolfe HJ (2001) PCR techniques for clonality assays. Diagn Mol Pathol 10:24–33
7. Dorfman HD, Czerniak B (1998) Bone tumors. Mosby Publishers, St. Louis, pp 441–481
8. Fialkow PJ (1976) Clonal origin of human tumors. Biochim Biophys Acta 458:283–321
9. Forest M, Tomeno B, Vanel D (1998) Orthopedic surgical pathology: diagnosis of tumors and pseudotumoral lesions of bone and joints. Churchill Livingstone, Edinburgh, pp 595–612
10. Herman JG, Graff JR, Myohanen S, Nelkin BD, Baylin SB (1996) Methylation-specific PCR: a novel PCR assay for methylation status of CpG islands. Proc Natl Acad Sci U S A 93:9821–9826
11. Iannaccone PM, Weinberg WC, Berkwits L (1987) A probabilistic model of mosaicism based on the histological analysis of chimaeric rat liver. Development 99:187–196
12. Kim N-G, Roh JK, Kim J-H, Chung WY, Park CS, Kim H (1999) Clonality analysis using methylation-specific polymerase chain reaction: a novel method for investigating tumor clonality. Lab Invest 79:1727–1729
13. Knudson AG (1985) Hereditary cancer, oncogenes, and antioncogenes. Cancer Res 45:1437–1443
14. Kubota T, Nonoyama S, Tonoki H, Masuno M, Imaizumi K, Kojima M, Wakui K, Shimadzu M, Fukushima Y (1999) A new assay for the analysis of X-chromosome inactivation based on methylation-specific PCR. Hum Genet 104:49–55
15. MacMahon HE (1971) Albright's syndrome—thirty years later (polyostotic fibrous dysplasia). Pathol Ann 6:81–146
16. Marie PJ, de Pollak C, Chanson P, Lomri A (1997) Increased proliferation of osteoblastic cells expressing the activating Gs alpha mutation in monostotic and polyostotic fibrous dysplasia. Am J Pathol 150:1059–1069

17. Middleton SB, Frayling IM, Phillips RK (2000) Desmoids in familial adenomatous polyposis are monoclonal proliferations. Br J Cancer 82:827–832
18. Mutter GL, Boynton KA (1995) X chromosome inactivation in the normal female genital tract: implications for identification of neoplasia. Cancer Res 55:5080–5084
19. Mutter GL, Chaponot ML, Fletcher JA (1995) A polymerase chain reaction assay for non-random X chromosome inactivation identifies monoclonal endometrial cancers and precancers. Am J Pathol 146:501–508
20. Ruggieri P, Sim FH, Bond JR, Unni KK (1994) Malignancies in fibrous dysplasia. Cancer 73:1411–1424
21. Sambrook J, Russell DW (2001) Molecular cloning: A laboratory manual. Cold Spring Harbor Laboratory Press, New York, pp 6.4–6.12
22. Saxena A, Alport EC, Custead S, Skinnider LF (1999) Molecular analysis of clonality of sporadic angiomyolipoma. J Pathol 189:79–84
23. Unni KK (1996) Dahlin's bone tumors. General aspects and data on 11,087 cases. Lippincott-Raven Publishers, Philadelphia, pp 367–376
24. Vogelstein B, Fearon ER, Hamilton SR (1987) Clonal analysis using recombinant DNA probes from the X chromosome. Cancer Res 47:4806–4813
25. Weinstein LS, Shenker A, Gejman PV, Merino MJ, Friedman E, Spiegel AM (1991) Activating mutations of the stimulating G protein in the McCune-Albright syndrome. N Engl J Med 325:1688–1695

Virchows Arch (2004) 444:61–65
DOI 10.1007/s00428-003-0930-z

ORIGINAL ARTICLE

Jessy Lardon · Niki Huyens · Ilse Rooman · Luc Bouwens

Exocrine cell transdifferentiation in dexamethasone-treated rat pancreas

Received: 28 July 2003 / Accepted: 16 October 2003 / Published online: 25 November 2003

Abstract Injured pancreatic tissue, for example, after duct ligation, undergoes remodeling, which involves the replacement of exocrine acini by duct-like structures. This acinoductal metaplasia is probably at least partly due to transdifferentiation of amylase-positive, cytokeratin-20 (CK20)-negative acinar cells into amylase-negative, CK20-positive duct-like cells. Due to the kinetics of these phenotypic changes, however, it has not been possible to demonstrate transitional stages of differentiation, which would express both markers at the same time. We took advantage of the fact that dexamethasone treatment inhibits the loss of amylase from acinar cells to demonstrate transitional cells co-expressing amylase and CK20. This was found both in vivo, where duct-ligation induced metaplasia, and in vitro, after isolation of acini. In addition, we found evidence for an acinar-to-islet conversion under the form of transitional cells co-expressing amylase and insulin. These observations strengthen the notion that fully differentiated cells, such as exocrine pancreatic cells, retain the capacity to undergo important phenotypic switches. This finding could have applications in tissue engineering or cell replacement strategies.

Keywords Pancreas · Islets of Langerhans · Stem cells · Metaplasia · Regeneration

Introduction

Adult pancreatic tissue retains the capacity to regenerate or repair after injury. As in the case of several other epithelial tissues, such as in the airways [10, 15], pancreatic tissue repair proceeds through the dedifferentiation of epithelial cells, followed by proliferation and redifferentiation [3, 14]. The initial pancreatic tissue remodeling that has been observed in different experimental models and in pancreatitis generally includes acinoductal metaplasia, i.e., the replacement of exocrine acini by pseudo-ductal complexes. This involves apoptotic elimination of part of the acinar cells, whereby surviving acinar cells are thought to transdifferentiate into duct cells and, thereby, participate in the formation of ductal complexes [3, 4, 13]. This transition, however, is difficult to prove from in vivo observations. In the in vivo model of duct ligation-induced pancreas remodeling, we found that acini are replaced by ductal complexes within 5 days following ligation, but we failed to demonstrate transitional forms between acinar and ductal cells [25]. In vitro, it has been demonstrated that acinar cells can adopt a ductal phenotype [1, 12]. We studied a model of acinoductal transdifferentiation from purified rat acinar cells [21, 22]. In this culture model, acinar cells adopt a ductal phenotype within 5 days of culture. We found that specific cytokeratins represent good markers for ductal differentiation, especially cytokeratin 20 (CK20) [5, 8, 9]. In vitro, acinar cells lose their expression of amylase and zymogen granules (acinar markers) prior to expressing CK20 protein [21]. Thus, we failed to demonstrate transitional stages of differentiation that would be characterized by the co-expression of amylase and CK20, both in vitro and in vivo. For the present study, we found that the synthetic glucocorticoid dexamethasone inhibits the loss of amylase during acinoductal transdifferentiation. We took advantage of this effect to look for transitional stages of differentiation.

J. Lardon · N. Huyens · I. Rooman · L. Bouwens (✉)
Cell Differentiation Unit, Diabetes Research Center,
Vrije Universiteit Brussel,
Laarbeeklaan 103, 1090 Brussels, Belgium
e-mail: lucbo@expa.vub.ac.be
Tel.: +32-24-774457
Fax: +32-24-774545

Materials and methods

Animals and animal procedures

Male Wistar rats of 250–300 g body weight (12 weeks of age) were used (Janvier, Le Genest-St-Isle, France). Rats were subjected to ligation of the exocrine ducts, draining the splenic half of the pancreas, as described previously [25], and were sacrificed in

groups of three after 5, 7 or 10 days. Head and tail parts, representing respectively unligated and ligated parts, were processed separately. In some of the animals, dexamethasone (Sigma, Bornem, Belgium) was administered by daily subcutaneous injections of 0.5 mg/kg body weight. Experiments were approved by the ethics committee of the Free University of Brussels.

Isolation and culture of exocrine cells

Pancreas tissue from normal rats was enzymatically dissociated; acini were purified by centrifugal elutriation and cultured in suspension, as described [21]. Dexamethasone was added to the culture medium at a final concentration of 1 μM.

Immunohistochemistry of pancreas tissue and cell cultures

For immunohistochemical staining, pancreas tissue was fixed in buffered 4% formaldehyde and embedded in paraffin. Sections of 4-μm thickness were immunostained with the streptavidin-biotin method and reaction product was visualized with diaminobenzidine as described [7, 25].

For double stainings, we used the indirect method with fluorescein isothiocyanate (FITC)- and tetramethyl rhodamine isothiocyanate (TRITC)-labeled secondary antibodies (Jackson Immunoresearch, West Grove, PA). Primary antibodies used in this study were polyclonal anti-insulin (C. Van Schravendijk, VUB, Brussels) [7, 8], monoclonal anti-CK20 (Novocastra, Newcastle-upon-Tyne, UK) [7, 8] and polyclonal anti-alpha-amylase (Sigma, St-Louis, MO). Controls consisted of omitting the primary antibody or of substituting it with irrelevant mouse IgG or diluted serum and resulted in complete absence of staining. For cell cultures, the cells were fixed, pelleted in agarose and processed in the same way as for tissue [21].

Results

In vivo observations

Duct ligation results in a conversion of the original acinar exocrine tissue into ductal complexes within the ligated part of the pancreas [22, 25]. This conversion is complete after 5 days post-ligation. The epithelial cells of the ductal complexes stain negatively for the acinar cell marker amylase and positively for the CK20-marker of duct cells (Fig. 1A, B). However, in dexamethasone-treated animals, amylase immunoreactivity was retained in the ductal complexes (Fig. 1C, D). Furthermore, these amylase-positive cells from the ligated part co-expressed CK20 after dexamethasone treatment (Fig. 2). Original intra- or interlobular ducts that were recognizable by their larger size were amylase negative and CK20 positive (Fig. 2). In the unligated part, co-expression of amylase and CK20 was never observed. There, acini retained their normal amylase immunoreactivity and remained CK20 negative. This phenotype was maintained until the end of the experimental period of 10 days. Dexamethasone treatment did not modify this normal immunostaining pattern in the unligated part of the pancreas. These

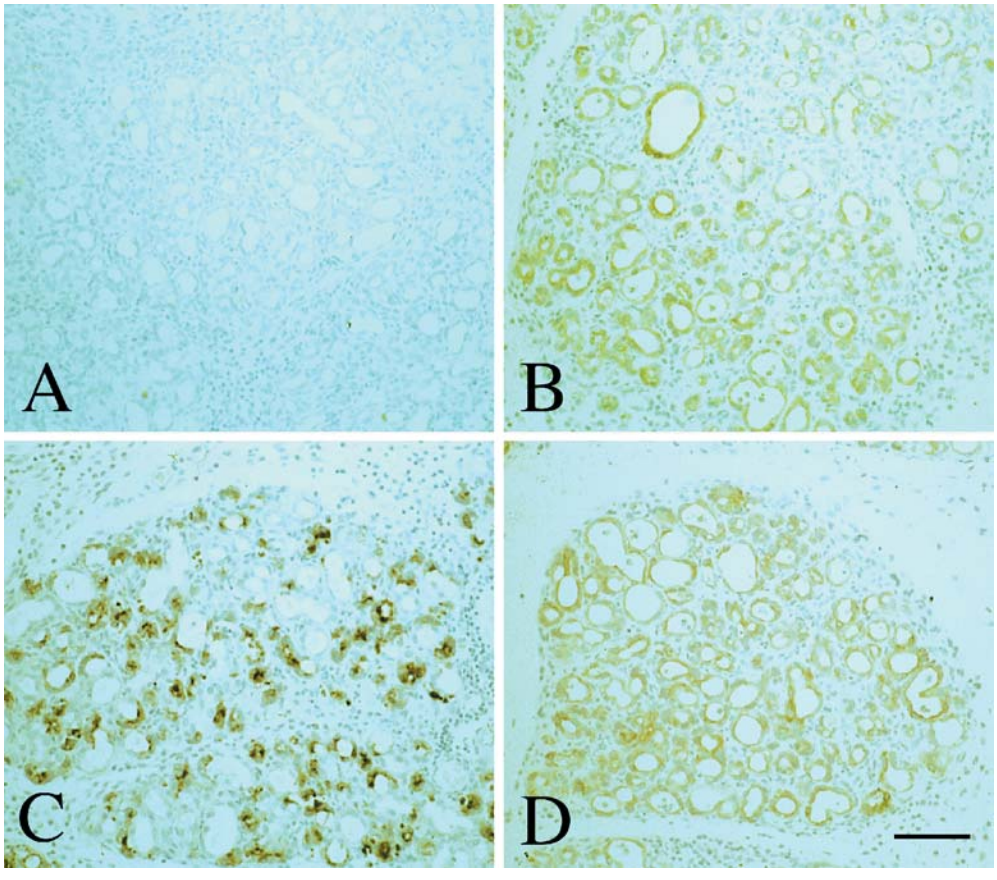

Fig. 1 Immunohistochemical staining for amylase (**A**, **C**) or cytokeratin 20 (**B**, **D**). **A**, **B** Ligated control pancreas (7 days). **C** **D** Ligated, dexamethasone-treated pancreas (7 days; 0.5 mg/kg/day). *Bar* 60 μm

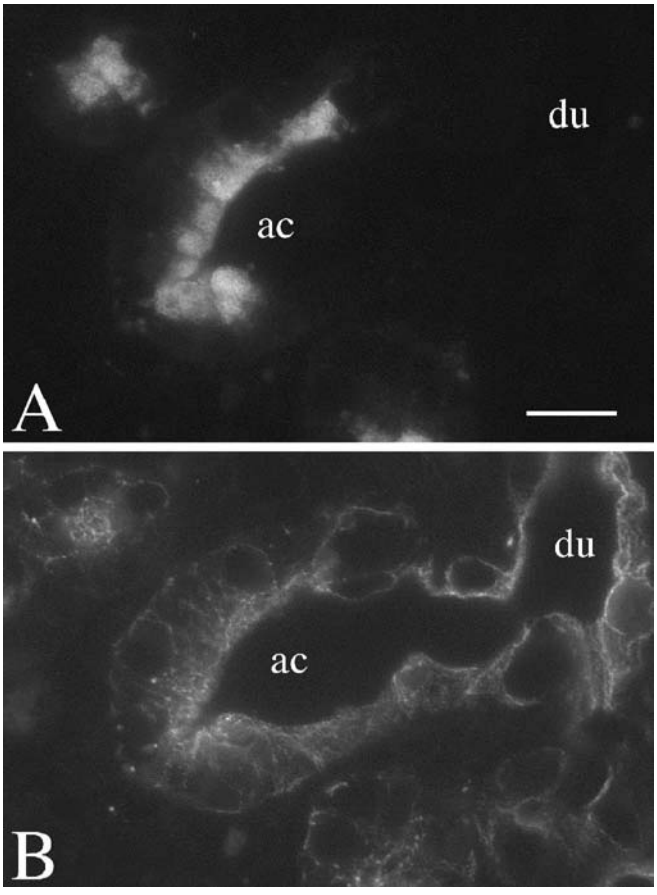

Fig. 2 Double immunofluorescence staining for amylase (**A**) and cytokeratin 20 (**B**) showing double-positive transitional cells (*ac*) and an amylase-negative original duct (*du*). Ligated, dexamethasone-treated pancreas (7 days; 0.5 mg/kg/day). *Bar* 10 μm

observations demonstrate transitional stages of differentiation between acinar and duct-like cells in ligated pancreas.

We also found cells immunoreactive for both amylase and insulin, indicating the occurrence of transitions from acinar to islet cells in the duct-ligated pancreas (Fig. 3). Such transitional cells were not found in untreated animals, nor in the heads of duct-ligated animals that had received dexamethasone, nor in duct-ligated animals that did not receive dexamethasone.

In vitro observations

When cultured in suspension in the absence of dexamethasone in the culture medium, acinar cells had lost amylase immunoreactivity after 4 days of culture (Fig. 4A). However, in the presence of dexamethasone in the medium, the cells remained amylase positive (Fig. 4C). These cells started to co-express the ductal marker CK20 from 5 days of culture (Fig. 4B, D). The cells maintained this phenotype until 10 days, when the cultures were stopped. Most cells co-expressed amylase and CK20 as seen by double immunofluorescence staining (Fig. 5). Thus, also in vitro, dexamethasone partially inhibits the acinoductal transdifferentiation, leading to cells that express markers of both cell types. These cultures contained very few insulin-positive cells and no amylase–insulin double-positives were noticed.

Discussion

In this study, we present immunohistochemical evidence for acinoductal transdifferentiation. Although we demonstrated this event previously in an in vitro model, we failed to provide direct evidence for such a transition from acinar to ductal cells in vivo. This was due to the sequential order in which amylase expression is first lost (by the fourth day of culture), and CK20 expression starts (1 day later) [21]. Amylase is a well-known acinar cell marker, and CK20 has been shown to represent a very good marker of duct cells [5, 8, 9]. Dexamethasone is known to stimulate amylase expression in acinar cells [16, 19, 24]. This explains our observation that dexamethasone interfered with the normal loss of amylase during acinoductal transdifferentiation both in vivo and in vitro. The cells retained amylase immunoreactivity during the formation of ductal complexes in vivo or duct-like aggregates in vitro, due to the effect of dexamethasone. They gained expression of the CK20 ductal marker as a result of partial transdifferentiation induced by the

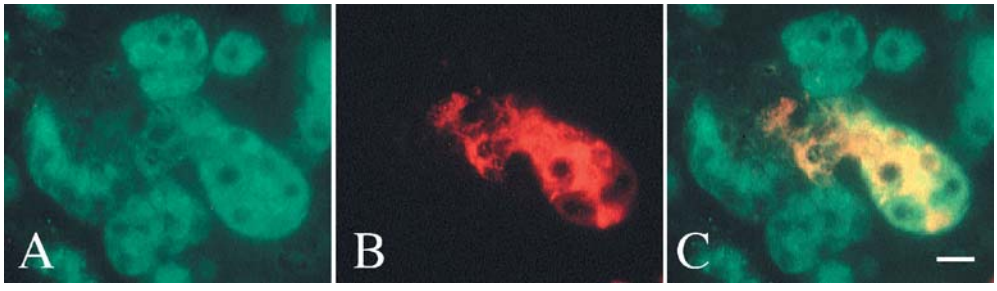

Fig. 3 Double immunofluorescence demonstration of amylase and insulin in an acinoinsular transitional structure of a duct-ligated dexamethasone-treated pancreas (7 days; 0.5 mg/kg per day). **A** Amylase in *green* fluorescence. **B** Insulin in *red* fluorescence. **C** Amylase + insulin in *yellow* (*double*) fluorescence. *Bar* 10 μm

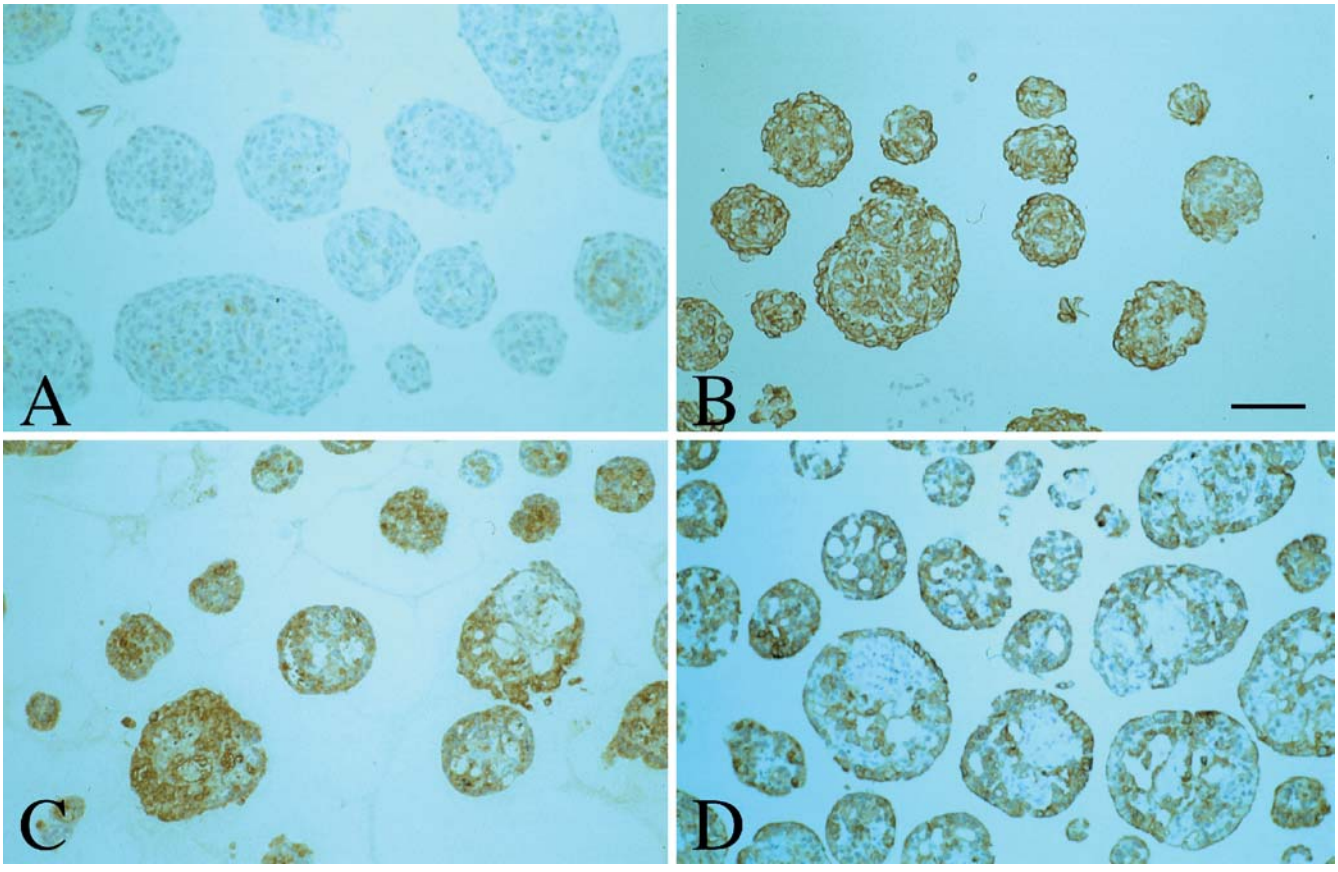

Fig. 4 Immunohistochemical staining for amylase (**A**, **C**) or cytokeratin 20 (**B**, **D**) in isolated exocrine acini after a culture period of approximately 1 week. **A**, **B** Control without dexamethasone. **C**, **D** In the presence of dexamethasone (1 μM). *Bar* 60 μm

ligation or isolation conditions. We can rule out the possibility that dexamethasone induced de novo expression of amylase in duct cells, first, because ducts outside the ductal complexes in the ligated part of the pancreas, as well as in the unligated part, were amylase negative and, second, because in vitro, more than 90% of the cells were acinar cells at the start of the culture, and there was no proliferation of contaminating centroacinar or ductular cells [21].

Interestingly, we also observed cells containing amylase and insulin in dexamethasone-treated duct-ligated rats. We have previously shown that islet neogenesis is induced in duct-ligated pancreas and that transitional cells can be seen that contain CK20 and insulin, but we did not notice amylase–insulin double-positive cells [24]. However, others have reported amylase–insulin co-expressing cells at an early stage after duct ligation, when there is still expression of amylase [2], and in interferon-gamma transgenic mice, where islet neogenesis is also induced from ductal complexes [11]. We showed that cultured acinar cells start to express the beta-cell marker and

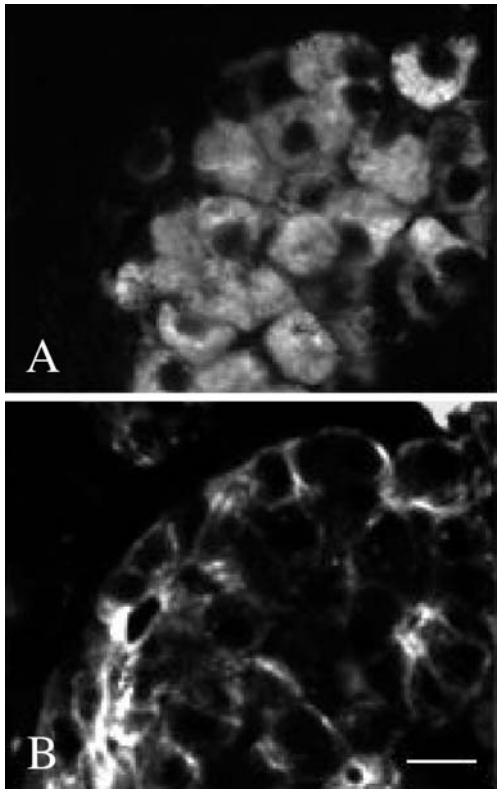

Fig. 5 Double immunofluorescence staining for amylase (**A**) and cytokeratin 20 (**B**) in isolated exocrine acini after a culture period of approximately 1 week in the presence of dexamethasone (1 μM). *Bar* 10 μm

insulin-transactivating transcription factor Pdx-1 and the islet cell marker PGP9.5 [21]. Acinar to beta cell and acinar to ductal cell transdifferentiation was also demonstrated in the rat during prolonged hyperglycemia [18]. Glucocorticoid treatment is known to increase the beta cell mass secondary to insulin resistance [17]. Whether the new beta cells originate from acinar, ductal or beta cells, themselves, is not yet clear.

These observations demonstrate that acinar exocrine cells can transdifferentiate to islet endocrine cells as suggested previously [6, 23] and as demonstrated for an acinar tumor cell [20]. This plasticity of acinar cells indicates that they can be considered as a kind of multipotential progenitor cell.

Acknowledgements This work was supported by a Focused Research Grant from EFSD/JDRF/Novo Nordisk. Additional support was obtained from the Fund for Scientific Research-Flanders (FWO-grant G001502). Ilse Rooman is a post-doctoral research fellow from the Fund of Scientific Research-Flanders. Emmy De Blay is acknowledged for her skilful technical assistance. We are grateful to Dr. Daniël Pipeleers for general and logistic support.

References

1. Arias AE, Bendayan M (1993) Differentiation of pancreatic acinar cells into duct-like cells in vitro. Lab Invest 69:518–530
2. Bertelli E, Bendayan M (1997) Intermediate endocrine-acinar pancreatic cells in duct ligation conditions. Am J Physiol 273:C1641–C1649
3. Bockman DE (1995) Toward understanding pancreatic disease: from architecture to cell signalling. Pancreas 11:324–329
4. Bockman DE, Merlino G (1992) Cytological changes in the pancreas of transgenic mice overexpressing transforming growth factor alpha. Gastroenterology 103:1883–1892
5. Bouwens L (1998) Cytokeratins and cell differentiation in the pancreas (review article). J Pathol 184: 234–239
6. Bouwens L (1998) Transdifferentiation versus stem cell hypothesis for the regeneration of islet beta-cells in the pancreas. Microsc Res Tech 43:332–336
7. Bouwens L, De Blay E (1996) Islet morphogenesis and stem cell markers in rat pancreas J Histochem Cytochem 44:947–951
8. Bouwens L, Wang RN, De Blay E, Pipeleers DG, Klöppel G (1994) Cytokeratins as markers of ductal cell differentiation and islet neogenesis in the neonatal rat pancreas. Diabetes 43:1279–1283
9. Bouwens L, Braet F, Heimberg H (1995) Identification of rat pancreatic duct cells by their expression of cytokeratins 7, 19 and 20 in vivo and after isolation and culture. J Histochem Cytochem 43:245–253
10. Erjefalt JS, Erjefalt I, Sundler F, Persson CG (1995) In vivo restitution of airway epithelium. Cell Tissue Res 281:305–316
11. Gu D, Arnush M, Sarvetnick N (1997) Endocrine/exocrine intermediate cells in streptozotocin-treated Ins-IFN-g transgenic mice. Pancreas 15:246–250
12. Hall PA, Lemoine NR (1992) Rapid acinar to ductal transdifferentiation in cultured human exocrine pancreas. J Pathol 166:97–103
13. Iovanna JL (1996) Redifferentiation and apoptosis of pancreatic cells during acute pancreatitis. Int J Pancreatol 20:77–84
14. Iovanna JL, Lechene de la Porte P, Dagorn JC (1992) Expression of genes associated with dedifferentiation and cell proliferation during pancreatic regeneration following acute pancreatitis. Pancreas 7:712–718
15. Knight D (2001) Epithelium-fibroblast interactions in response to airway inflammation. Immunol Cell Biol 79:160–164
16. Lee PC, Kratz B, Kim O, Moshier J, Lin CH (1990) Expression of the amylase gene in the rat exocrine pancreas during postnatal development: effect of dexamethasone. Biochim Biophys Acta 1049:244–248
17. Lenzen S, Bailey CJ (1984) Thyroid hormones, gonadal and adrenocortical steroids and the function of the islets of Langerhans. Endocr Rev 5:411–434
18. Lipsett M and Finegood DT (2002) Beta-cell neogenesis during prolonged hyperglycemia in rats. Diabetes 51:1834–1841
19. Logsdon CD, Perot KJ, McDonald AR (1987) Mechanism of glucocorticoid-induced increase in pancreatic amylase gene transcription. J Biol Chem 15:15765–15769
20. Mashima H, Ohnishi H, Wakabayashi K, Mine T, Miyagawa J, Hanafusa T, Seno M, Yamada H, Kojima I (1996) Betacellulin and activin A coordinately convert amylase-secreting pancreatic AR42 J cells into insulin-secreting cells. J Clin Invest 97:1647–1654
21. Rooman I, Heremans Y, Heimberg H, Bouwens L (2000) Modulation of rat pancreatic acinoductal transdifferentiation and expression of PDX-1 in vitro. Diabetologia 43:907–914
22. Rooman I, Lardon J, Schuit F, Flamez D, Bouwens L (2001) Mitogenic effect of gastrin and expression of gastrin receptors by duct-like cells of rat pancreas. Gastroenterology 121:940–949
23. Rooman I, Lardon J, Bouwens L (2002) Gastrin stimulates beta-cell neogenesis and increases islet mass from transdifferentiated but not from normal exocrine pancreas tissue. Diabetes 51:686–690
24. Slater EP, Hesse H, Muller JM, Beato M (1993) Glucocorticoid receptor binding site in the mouse alpha-amylase 2 gene mediates response to the hormone. Mol Endocrinol 7:907–914
25. Wang RN, Klöppel G, Bouwens L (1995) Duct to islet cell differentiation and islet growth in the pancreas of duct ligated adult rats. Diabetologia 38:1405–1411

Virchows Arch (2004) 444:66–73
DOI 10.1007/s00428-003-0926-8

ORIGINAL ARTICLE

Toshiharu Hayashi · Aiko Ishii · Satoru Nakai · Keiko Hasegawa

Ultrastructure of goblet-cell metaplasia from Clara cell in the allergic asthmatic airway inflammation in a mouse model of asthma in vivo

Received: 26 May 2003 / Accepted: 6 October 2003 / Published online: 25 November 2003

Abstract Mucus overproduction from goblet cells, a characteristic feature of the allergic asthmatic inflammation induced by ovalbumin (OVA) in mice, was examined morphologically. In OVA-untreated (normal) mice, there were no goblet cells in intrapulmonary bronchus and bronchiole. However, goblet cells with or without hyperplasia in the mucosa of inflamed bronchus–bronchiole were recognized in the allergic asthmatic mice. The nonciliated epithelium containing electron lucent granules (mucus) showed many similarities to Clara cells, which have characteristic secretory granules and many mitochondria, except for the less-developed smooth endoplasmic reticulum seen in normal mice. Ciliated Clara cells with or without mucus were rarely recognized. In addition, mucus was found in neither ciliated nor basal epithelium. The present study suggests that goblet-cell metaplasia in the bronchus and bronchiole of inflamed mucosa may be derived, at least in part, from Clara cells.

Keywords Goblet cell · Clara cell · Metaplasia · Differentiation · Mouse asthma

Introduction

Airway hyperresponsiveness, eosinophil recruitment into peribronchial walls and mucus overproduction in bronchial epithelial cells characterize allergic asthma [3, 5, 6, 10, 11, 18, 21, 25]. Mucus production by goblet cells in local bronchial–bronchiolar lesions causes airway mucus plugging [22]. Differences exist between mouse and human airway epithelia, including stem cell/plasticity capabilities and cellular composition (e.g., goblet cells and Clara cells) [23]. Clara cells represent the most abundant secretory cell type of both proximal and distal airways in the lungs of rodents, whereas Clara cells are the most abundant cells of the distal airway in humans [1, 15, 16]. Thus, goblet cells at distal sites are considered to be metaplasia from Clara cells in human asthma [8]. However, there are no goblet cells in the intrapulmonary bronchus and bronchiole of normal mice [15, 16]. This suggests that goblet-cell metaplasia may occur in the intrapulmonary airway in a mouse model of asthma. Though numerous studies of asthma using a mouse model have been reported [3, 5, 6, 10, 11, 18, 21, 25], an in vivo ultrastructure study has not yet been reported in murine models of allergic asthma. The aim of the present study was to clarify the cell type morphologically responsible for the goblet-cell metaplasia that occurs in the late-phase allergic asthmatic airway inflammation, induced by ovalbumin (OVA), in mice.

T. Hayashi (✉) · A. Ishii · S. Nakai · K. Hasegawa
Laboratory of Veterinary Pathology, Faculty of Agriculture, Yamaguchi University,
1677-1 Yoshida, 753-8515 Yamaguchi, Japan
e-mail: hayashi@agr.yamaguchi-u.ac.jp
Tel.: +81-83-9335890
Fax: +81-83-9335890

Materials and methods

Specific pathogen-free 25-week-old female DBA/1 J mice (Kyudo, Saga, Japan) were used. Animal experiments described in this study were approved by the Animal Research Ethics Board of the Faculty of Agriculture at Yamaguchi University.

Asthma model and sampling

The sensitization and challenge procedure was performed by the simple modification of the method described previously [6]. In brief, the mice (n=10) were sensitized intraperitoneally (i.p.) by the injection of 20 μg OVA (Grade V; Sigma, St. Louis, MO, USA) in 2.0 mg aluminum hydroxide (Alum, SERVA, Heidelberg, Germany) adjuvant (OVA/Alum), which was suspended in 0.1 ml phosphate-buffered saline (PBS; pH 7.2), on day 0 and boosted i.p. with 20 μg OVA/Alum on day 10. On day 14, 4 days after the second sensitization, 200 μg OVA in 50 μl PBS was challenged intranasally under a mixture of ketamine (45 mg/kg BW; Sankyo Co., Tokyo, Japan) and xylazine (8 mg/kg BW; Bayer Co., Tokyo, Japan) anesthesia i.p. On day 18, 4 days after the challenge, the mice were sacrificed and lungs were obtained for histology and electron microscopy. Lungs were also obtained from OVA-untreated normal age-matched female DBA/1 J mice (n=5).

Lungs (asthmatic, n=6; normal, n=3) were fixed in 10% neutral buffered formalin (pH 7.4), and 4-μm-thick sections of the left

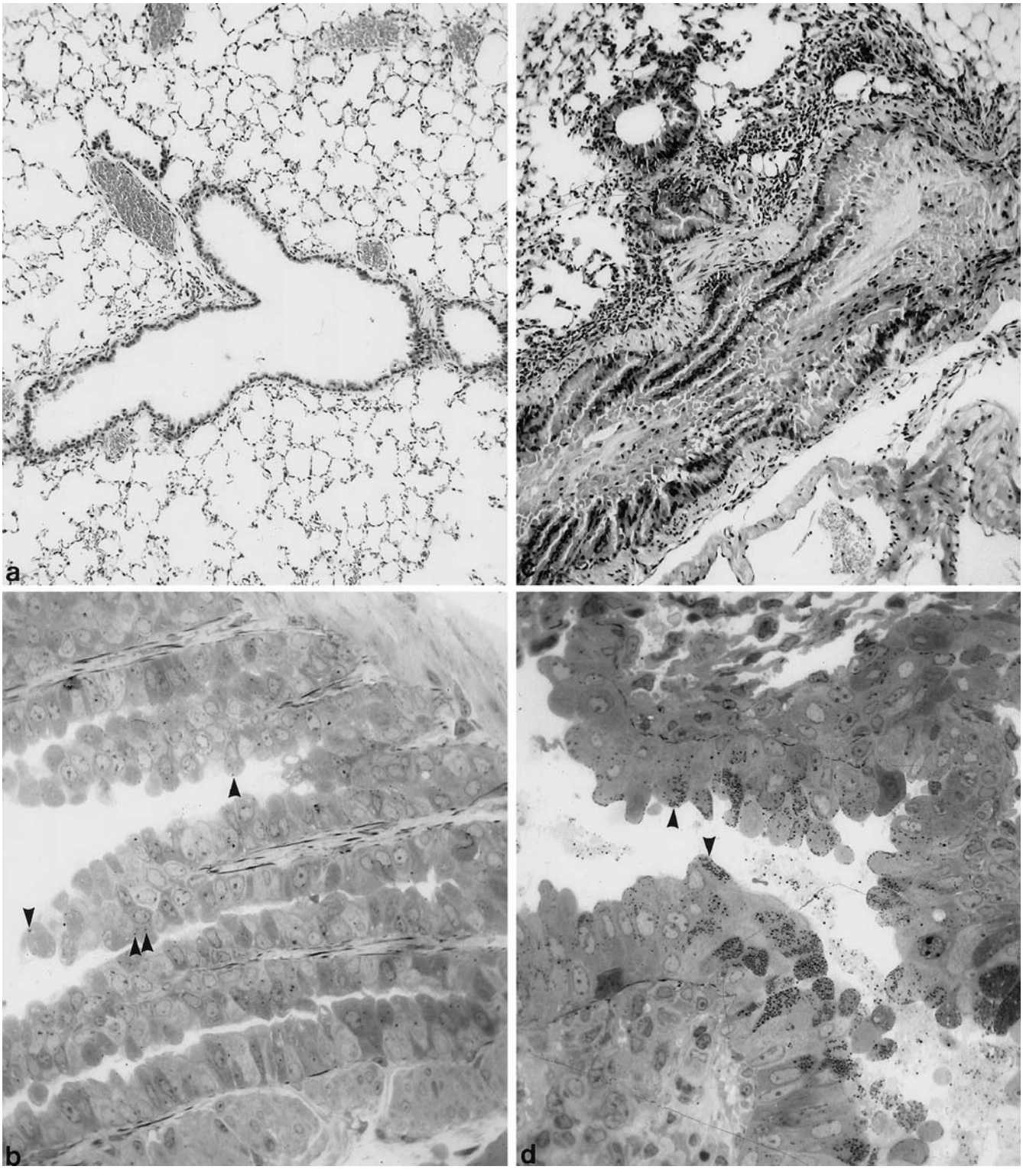

Fig. 1 Normal (**a** and **b**) and allergic (**c** and **d**) asthmatic mice. Normal bronchus shows no goblet cells (**a**), and non-ciliated epithelium contains a few fine granules stained with toluidine blue (TB) (**b**, *arrow heads*). In bronchial lesions, there are desquamated epithelial cells and mucus within bronchial lumen, hyperplastic goblet cells, infiltration of bronchus mucosa with eosinophils and lymphocytes with edema and hypertrophy of smooth muscles (**c**) and increased number and size of granules compared with normal mice in an allergic asthmatic mouse (**d**, *arrowheads*). **a**, **c** Hematoxylin & eosin, ×200. **b**, **d** TB, ×450

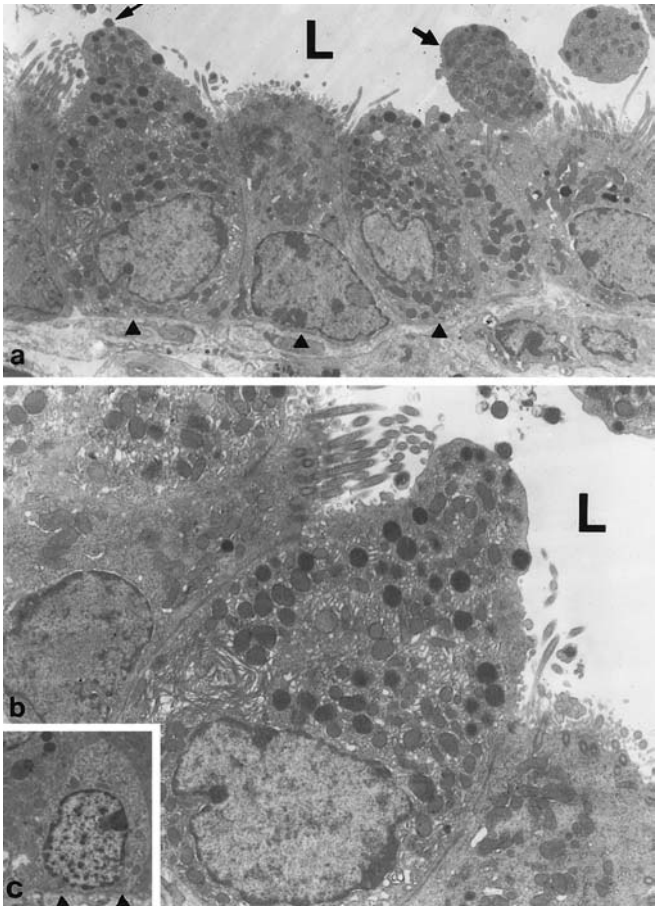

Fig. 2 Ciliated and non-ciliated (Clara) cells can be seen equally in the bronchus of a normal mouse. Merocrine (**a**, *small arrow* and **b**, *enlargement of small arrow of* ***a***) and apocrine secretion (**a**, *big arrow*) of electron-dense secretory granules are also recognized in Clara cells having many mitochondria and developed smooth endoplasmic reticulum. A basal cell (**c**) located adjacent to basement membrane. *Arrowheads BM* basement membrane, *L* lumen. **a** and **c** ×2,500, **b** ×10,000

lungs were prepared from paraffin wax-embedded tissue and stained with hematoxylin and eosin, alcian blue (AB) at pH 2.5 and/or periodic acid-Schiff (PAS). A part of the left lungs (asthmatic, n=4; normal, n=2) was immersed in glutaraldehyde at 4°C for 2 h. The tissues were then post-fixed in 2% osmium at 4°C for 2 h, dehydrated in graded ethanols at 4°C and embedded in araldite. The orientation of the blocks was achieved by examining 1-μm sections stained with toluidine blue (TB). Ultra-thin sections were made and stained with uranyl acetate and lead nitrate, and intrapulmonary bronchus and bronchioles were observed using electron microscopy (JEM-100CX II, Tokyo, Japan).

Results

Light microscopy

In OVA-untreated (normal) mice, the epithelium of the intrapulmonary bronchus–bronchiole consisted of a single columnar epithelial cell layer (Fig. 1a). There were no goblet cells characterized by packed AB/PAS-positive granules (mucus), and they also lacked submucosal glands. A few small PAS-positive and AB-negative granules were observed in the non-ciliated epithelial cytoplasm. A few fine granules, which corresponded with PAS-positive granules, stained with TB in semi-thin sections were observed in the apical site of the non-ciliated epithelium (Clara cells) in normal mice (Fig. 1b).

In most allergic asthmatic mice, there was severe infiltration of eosinophils and lymphocytes with edematous changes in bronchial–bronchiolar mucosa and walls as well as sloughed and destructed hypertrophic epithelial cells mixed with some eosinophils and lymphocytes. Discharged mucus filled in the bronchial–bronchiolar lumens. In general, inflammatory lesions in bronchus (Fig. 1c) were more severe than those in bronchiole. Epithelium with or without hyperplasia contained AB/PAS-positive neutral and acidic mucus. In hyperplastic lesions, non-ciliated cells increased, whereas there was no increase or reduction in the number of ciliated cells. Hypertrophic smooth muscle, thickness and destruction of basement membrane were observed in most cases. There was severe perivascular infiltration of eosinophils and lymphocytes with proliferation of endothelial cells in small arteries, and a few mast cells were detected in the bronchus–bronchiole mucosa using TB staining. An increased number and size of fine granules (Fig. 1d) stained with TB in the apical site or scattered in the cytoplasm of the non-ciliated epithelium were observed.

Electron microscopy

In normal mice, there were mainly three cell types in the epithelium of the intrapulmonary bronchus and bronchiole: ciliated, non-ciliated and basal (Fig. 2). The epithelium was reduced in thickness in the more distal airways. Both the ciliated and non-ciliated (Clara) cells adhering to neighboring cells by desmosomes were seen equally throughout the bronchus and bronchiole (Fig. 2a). Clara cells with or without a few short microvilli, but with no cilia, had a lot of smooth endoplasmic reticulum (s.e.r.) and mitochondria, appearing dark with a few or no cristae. A few round, homogeneous fine electron-dense secretory granules (S.G.) (Fig. 2a, b), which do not have a clear membrane bound, corresponding to fine granules stained with TB (to a varying degree) were also located most regularly in the apical portion of Clara cells. In some Clara cells, S.G. appeared to be in the process of extrusion into the lumen of the airway by merocrine and apocrine secretions (Fig. 2a, b). Compared with other two-cell types of epithelium, basal cells, which are small polyhedral cells on the basement membrane, were few and distributed throughout the bronchus and bronchiole and adhered to neighboring cells by desmosomes. The nucleus occupied a large portion of the cells with tonofilaments having a few organella (Fig. 2c).

In the allergic asthmatic mice (Fig. 3, Fig. 4, Fig. 5, Fig. 6, Fig. 7, Fig. 8, Fig. 9), hypertrophic epithelial cells increased in their size with or without hyperplasia.

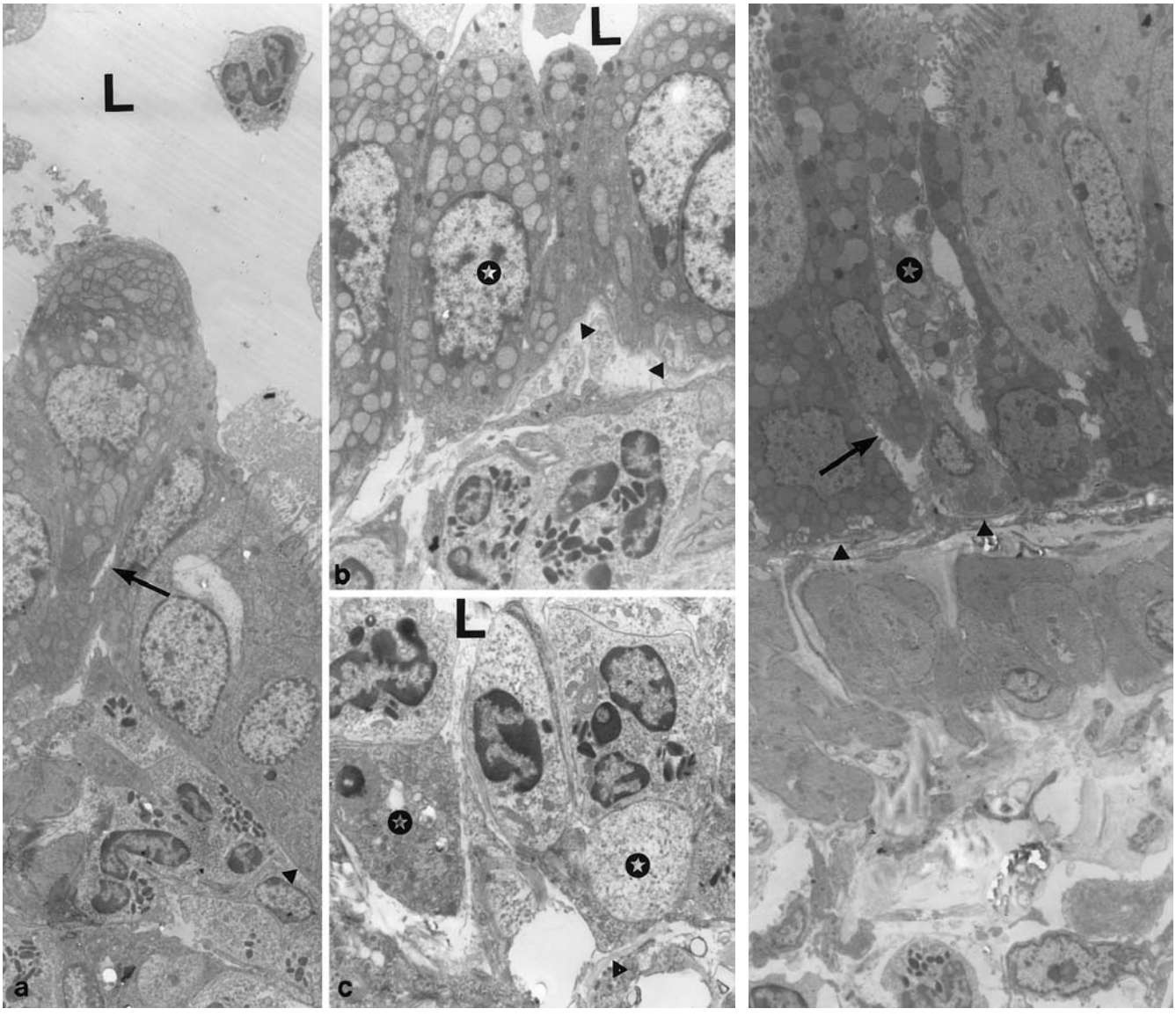

Fig. 3 Partial widening of the intercellular space (**a**, *arrow*), detached epithelium from destructed basement membrane (**b**, *star mark*) and destruction of epithelial cells (**c**, *star mark*) with infiltration of eosinophils are seen. *Arrowheads* basement membrane, *L* lumen. **a** ×1800, **b** ×2900 and **c** ×3600

Fig. 4 Destruction of an epithelial cell (*star mark*) and partial widening of the intercellular space (*arrow*) are seen in an inflamed area of the asthmatic mouse. Hypertrophic smooth muscle cells and edema are also seen in bronchial wall. *Arrowheads* basement membrane. ×2500

Widening of intercellular spaces in epithelium with (Fig. 3) or without (Fig. 4) infiltration of eosinophils was observed. Sometimes degranulation of specific granules of eosinophils was observed. Destructed epithelial cells (Fig. 3c, Fig. 4) and basement membranes were also observed. Hyperplastic Clara cells had varying degrees of typical S.G., many mitochondria and less-developed s.e.r. (Fig. 5a). Clara cells with S.G., but not ciliated cells (Fig. 5b, c), contained electron lucent granules (mucus). In those cells, S.G. were secreted by merocrine (Fig. 5b) and apocrine (Fig. 6a), as seen in normal mice, and mucus was secreted by merocrine (Fig. 6b). In addition, basal cells did not have mucus (Fig. 6c). Though developed s.e.r. is one characteristic feature of Clara cells, in general, Clara cells with S.G. containing mucus had less-developed s.e.r. (Fig. 5, Fig. 6, Fig. 7, Fig. 8, Fig. 9). There was no correlation between number of S.G. and number of mucus granules (Fig. 7). Also, hyperplastic epithelium, which lacks characteristics of ciliated and basal cells, resembling Clara cells with a few or no S.G. (Clara-like cells) was observed in bronchial (Fig. 8) and bronchiolar lesions. In addition, ciliated epithelial cells having S.G. with or without mucus were rarely seen (Fig. 9).

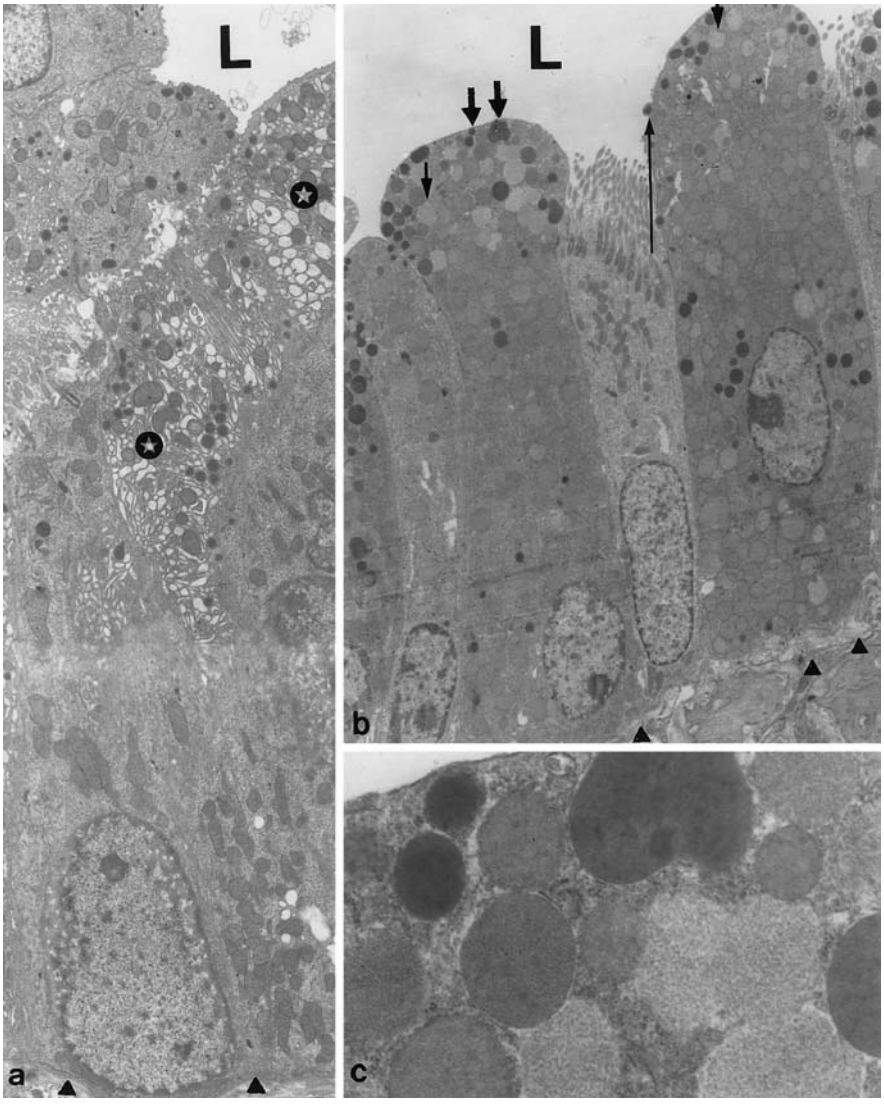

Fig. 5 Hyperplastic non-ciliated epithelial (Clara) cells having secretory granules (S.G.) and developed smooth endoplasmic reticulum (s.e.r.) (*star marks*) without mucus are seen (**a**). Clara cells with S.G. having many mitochondria and less-developed s.e.r. contain electron lucent granules (mucus, *small arrow*), and ciliated cells have no mucus in an allergic mouse (**b**). S.G. (*big arrows*, **b**) and merocrine secretion (*long arrow*, **b**) and enlargement of S.G. are seen (**c**). *Arrowheads* basement membrane, *L* lumen. ×2500

Discussion

Mucus-secreting cells (goblet cells), which do not exist in intrapulmonary bronchus and bronchiole in normal mice [15, 16], developed in the bronchial–bronchiolar lesions with infiltration of lymphocytes and eosinophils in the late allergic asthmatic model of mice [6]. In the allergic asthmatic mice, the mucus containing non-ciliated epithelial cells showed many similarities to Clara cells in normal mice, since they lack cilia and have S.G. secreted by merocrine and apocrine fassion [20] as well as many mitochondria with poorly developed cristae [1, 15, 25]. In addition, mucigen granules, which are stained with AB/PAS corresponding to electron lucent granules, secreted by merocrine fassion [1, 15, 25] were observed in these cells. Moreover, there was no evidence of basal cells and ciliated cells with mucus. It seems likely, as it has been shown from in vitro and in vivo studies, that Clara cells have a capacity to differentiate into goblet cells [2] directly via activation of epidermal growth factor receptor (EGRF-R) cascade in tracheal epithelium in a rat model, suggesting that EGRF-R activation may promote selective cell differentiation (not proliferation), from Clara cells to goblet cells [9, 12]. Therefore, goblet cells may, at least in part, be differentiated from Clara cells directly in this model.

Rarely were Clara cells with cilia observed. First, ciliated epithelium may be differentiated from Clara cells. It is possible, since Clara cells isolated from rabbit lungs differentiated into ciliated cells [7]. In addition, some Clara cells with cilia contained mucus. This suggests that goblet-cell metaplasia may occur after differentiation of Clara cells into ciliated epithelial cells. It is possible, since some Clara cells having cilia without mucus isolated from rabbit lung were shown to differentiate into ciliated cells [7].

Hyperplasia of Clara and Clara-like cells was found. It has been suggested that pulmonary neuroendocrine cells serve as a pluripotent stem cell population, capable of regenerating Clara cell progenitors in injured asthmatic

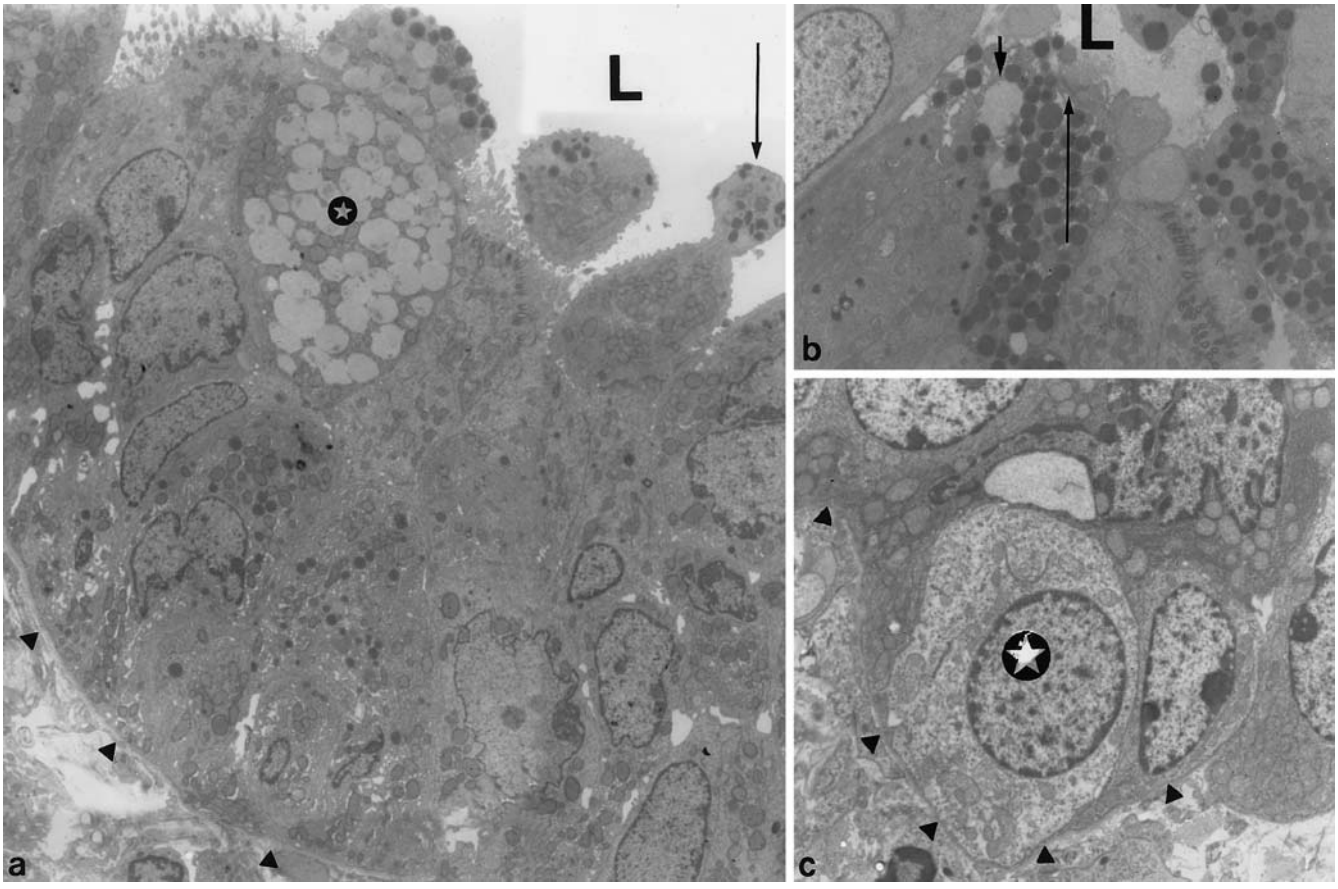

Fig. 6 Hyperplastic epithelia are recognized in an allergic asthmatic mouse. Some Clara cells having secretory granules contain mucus (*star mark*), and apocrine secretions are visible (*long arrow*) (**a**). Merocrine excretion of mucus (*long arrow*) and mucus (*short arrow*) are recognized (**b**). A basal cell (*star mark*) has no mucus. *Arrowheads* basement membrane, *L* lumen. **a** and **c** ×1700, **b** ×4500

lung [13, 14, 17]. In re-population of airway after injury, a morphological derivative of the Clara cell, referred to as a type-A cells, lack the differentiated ultrastructural features, such as s.e.r. and S.G., that are characteristic of mature Clara cells [4]. Thus, Clara-like cells in the present study, which lack a characteristic feature, such as type-A cells, may be immature Clara cells. One possibility is that Clara-like cells are considered to be differentiated from neuroendocrine cells. However, the present study demonstrates that goblet-cell metaplasia was observed in bronchus other than terminal bronchiole, suggesting that the origin of Clara cells may not be neuroendocrine cells, since those cells are only located in terminal bronchioles [13, 14, 17]. Also, it has been suggested that involvement of the neuroepithelial cells is not yet conclusive in the origin of re-population after injury in the airway [14]. Therefore, hyperplastic Clara-like cells may be derived from immature Clara cells at the site of the bronchus and bronchiole, and, thereafter, goblet-cell metaplasia may occur in Clara cells indirectly. It is possible, since proliferative ability of immature Clara cells has been reported [13]. In addition, it has been reported recently that interleukin (IL)-9 in airway injury repair resulted in goblet-cell hyperplasia in murine models of asthma [23], and IL-13 may be responsible for mucus overproduction [25]. Further studies are needed to clarify the origin of goblet cells other than Clara cells and the involvement of cytokines in goblet-cell metaplasia and hyperplasia.

In the allergic asthmatic mice, increased S.G., which are identical to Clara cell secretory (specific) protein (CCSP), were seen [19]. As shown here, Clara cells having increased S.G. (CCSP) with or without mucus suggests no relationship between increased CCSP and formation of mucus granules. The significance of increased CCSP in allergic status may be the result of protection against injurious agents in environmental air [24].

In conclusion, the present ultrastructural study suggests that goblet-cell metaplasia may be differentiated from Clara cells directly or indirectly in the late-phase allergic airway inflammation in a mouse model of asthma in vivo. Also, mucus hyperproduction is an important finding in chronic bronchitis, cystic fibrosis and bronchiectasis in humans [22]. Thus, our findings provide information for analysis of mucin production from goblet cells in an animal model of respiratory diseases.

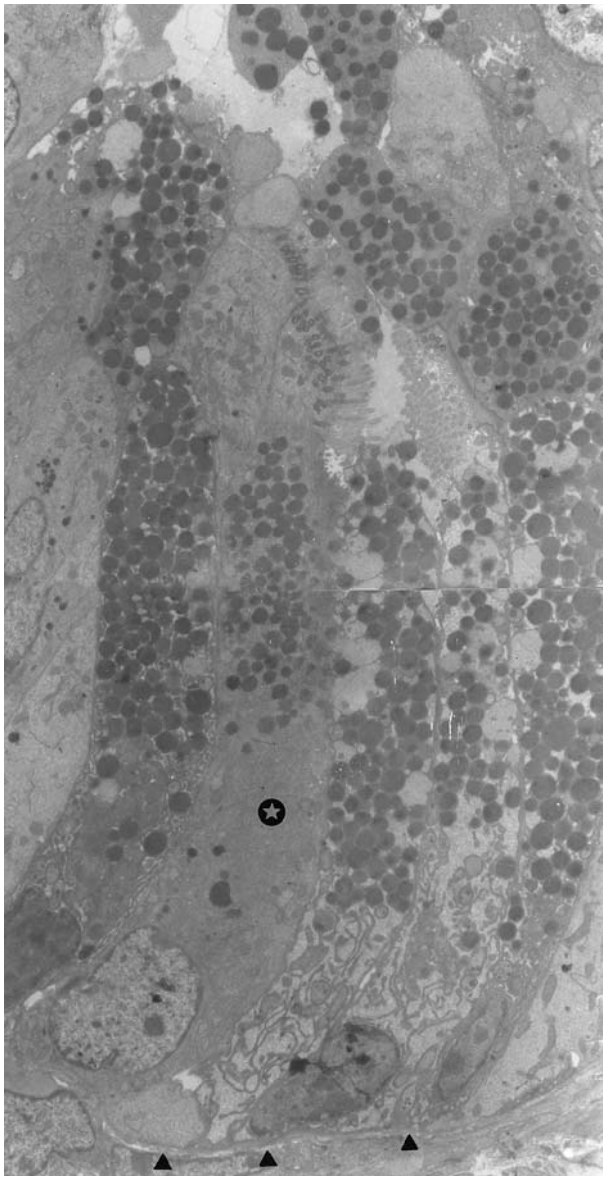

Fig. 7 An epithelial cell with secretory granules and cilia has no mucus (*star mark*). *Arrowheads* basement membrane, *L* lumen. ×4000

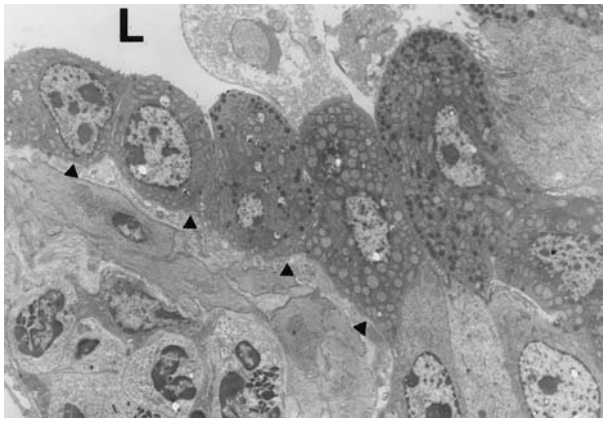

Fig. 8 Epithelial cells with or without secretory granules. *Arrowheads* basement membrane, *L* lumen. ×4000

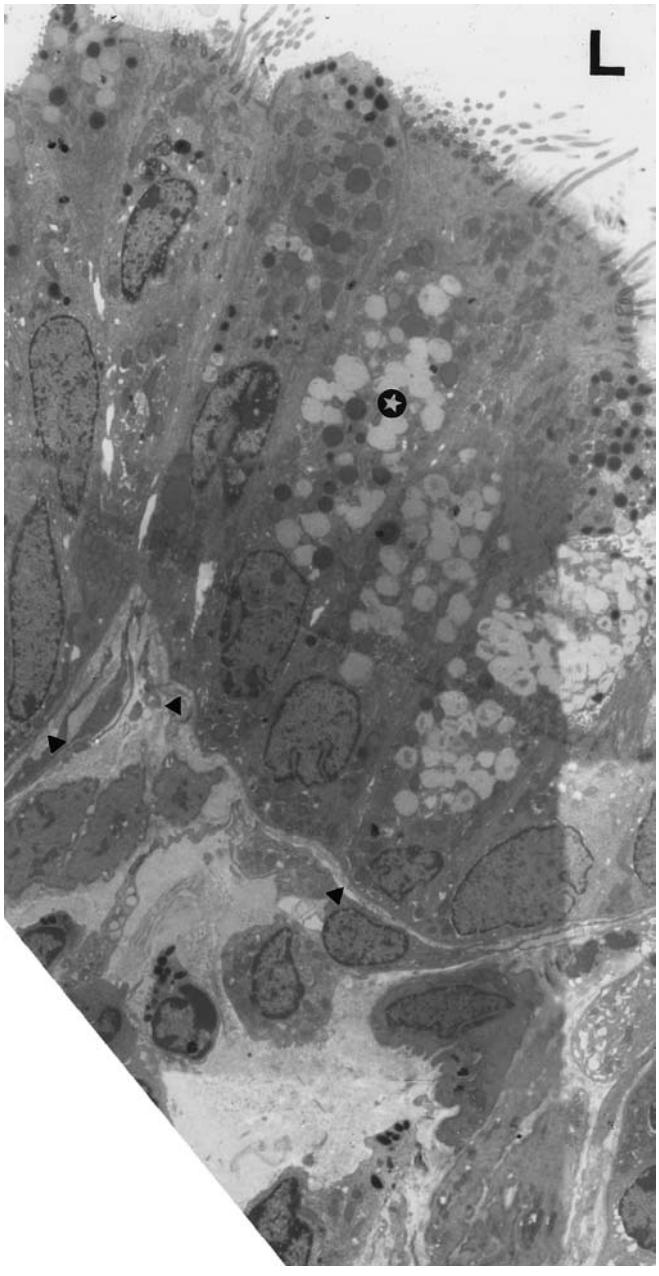

Fig. 9 Most mucus-containing cells are Clara cells in an allergic asthmatic mouse. *Star mark* shows an epithelial cell with secretory granules having mucus and cilia. *Arrowheads* basement membrane, *L* lumen. ×3000

Acknowledgement This study was supported in part by a grant-in-aid of the Ministry of Education, Science, Sports and Culture of Japan (no. 15380210).

References

1. Breeze RG, Wheeldom EB, Pirie HM (1976) Cell structure and function in the mammalian lung: the trachea, bronchi and bronchioles. Vet Bull 46:319–336
2. Brody AR, Hook GE, Cameron GS, Jetten AM, Butterick CJ, Nettesheim P (1987) The differentiation capacity of Clara cells isolated from the lungs of rabbits. Lab Invest 57:219–229

3. Corry DB, Folkesson HG, Warnock ML, Erle DJ, Matthay MA, Wienerkronish JP, Locksley R (1996) Interleukin 4, but not interleukin 5 or eosinophils is required in a murine model for acute airway hyperreactivity. J Exp Med 183:109–117
4. Evance MJ, Cabral-Anderson LJ, Freeman G (1978) Role of the Clara cell in renal of the bronchiolar epithelium. Lab Invest 38:648–653
5. Galli SJ (1997) Complexity and redundancy in the pathogenesis of asthma reassessing the roles of mast cells and T cells. J Exp Med 186:343–347
6. Hayashi T, Maeda K, Hasegawa K, Nakai S, Hamachi T, Iwata H (2002) Systemic administration of interferon-γ-expressing plasmid reduces late allergic bronchitis in a mouse model of asthma. Int J Exp Pathol 83:81–86
7. Hook GE, Brody AR, Cameron GS, Jetten AM, Gilmore LB, Nettesheim P (1987) Repopulation of denuded tracheas by Clara cells isolated from the lungs of rabbit. Exp Lung Res 12:311–329
8. Kilburn KH (1974) Functional morphology of the distal lung. Int Rev Cytol 37:153–270
9. Kim S, Shim JJ, Burgel PR, Ueki IF, Dao-Pic T, Tam DC, Nadel JA (2002) IL-13-induced Clara cell secretory protein expression in airway epithelium: role of EGFR signaling pathway. Am J Physiol Lung Cell Mol Physiol 283:L67–L75
10. Kosgren M, Erjefalt JS, Korsgren O, Sundler F, Persson CG (1997) Allergic eosinophil-rich inflammation develops in lung and airways of B cell-deficient mice. J Exp Med 185:885–892
11. Lei HY, Huang KJ, Shen CK, Huang JL (1989) An antigen-specific hypersensitivity which does not fit into traditional classification of hypersensitivity. J Immunol 143:432–438
12. Nadel JA (2001) Role of epidermal growth factor receptor activation in regulating mucin synthesis. Respir Res 2:85–89
13. Ogawa T, Tsubakihara M, Ichikawa M, Kanisawa M (1993) An autoradiographic study of the renewal of mouse bronchiolar epithelium following bromobenzene exposure. Toxicol Pathol 21:547–553
14. Otto WR (2002) Lung epithelial stem cells. J Pathol 197:527–535
15. Pack RS, Al-Ugaily LH, Morris AG (1981) The cells of the tracheobronchial epithelium of the mouse: a quantitative light and electron microscopy study. J Anatomy 132:75–84
16. Plopper CG, Mariassy AT, Wilson DW, Alley JL, Nishio SJ, Nettesheim P (1983) Comparison of nonciliated tracheal epithelial cells in six mammalian species: ultrastructure and population densities. Exp Lung Res 5:281–294
17. Reynolds SD, Giangreco A, Power JHT, Stripp BR (2000) Neuroepithelial bodies of pulmonary airway serve as a reservoir of progenitor cells capable of epithelial regeneration. Am J Pathol 156:269–278
18. Seminario M-C, Gleich GJ (1994) The role of eosinophils in the pathogenesis of asthma. Curr Opin Immunol 6:860–864
19. Singh G, Katyal SC (1997) Clara cells and the Clara cell 10 KD protein (CC10). Am J Respir Cell Mol Biol 17:141–143
20. Stinson SF, Loosli CG (1978) Ultrastructural evidence concerning the mode of secretion of electron-dense granules by Clara cells. J Anat 127:291–298
21. Takeda K, Hamelmann E, Joetham A, Shultz LD, Larsen GL, Irvin CG, Gelfand EW (1997) Development of eosinophilic airway inflammation and airway hyperresponsiveness in mast cell-deficient mice. J Exp Med 186:449–454
22. Takeyama K, Dabbagh K, Lee H-M, Agusti C, Lausier JA, Ueki IF, Grattan KM, Nadel JA (1999) Epidermal growth factor system regulates mucin production in airways. Pro Natl Acad Sci U S A 96:3081–3086
23. Vermeer PD, Harson R, Einwalter LA, Moninger T, Zabner J (2003) Interleukin-9 induces goblet cell hyperplasia during repair of human airway epithelia. Am J Respir Cell Mol Biol 28:286–295
24. Yu M, Zheng X, Witschi H, Pinkerton KE (2002) The role of interleukin-6 in pulmonary inflammation and injury induced by exposure to environmental air pollutants. Toxicol Sci 68:488–497
25. Zhu Z, Horner RJ, Wang Z, Chen Q, Geba GP, Wang J, Zhang Y, Elias JA (1999) Pulmonary expression of interleukin-13 causes inflammation, mucus hypersecretion, subepithelial fibrosis, physiologic abnormalities, and eotaxin production. J Clin Invest 103:779–788

Virchows Arch (2004) 444:74–81
DOI 10.1007/s00428-003-0891-2

ORIGINAL ARTICLE

Beate Warncke · Monika Valtink · Judith Weichel · Katrin Engelmann · Hansjörg Schäfer

Experimental rat model for therapeutic retinal pigment epithelium transplantation—unequivocal microscopic identification of human donor cells by in situ hybridisation of human-specific Alu sequences

Received: 2 April 2003 / Accepted: 1 August 2003 / Published online: 28 October 2003

Abstract Transplantation of retinal pigment epithelial (RPE) cells is discussed as a possible therapeutic approach for retinal degeneration. Xenogeneic transplantation of human RPE cells in animal models has been studied extensively. Various methods have been used to identify the graft cells, but these methods interfere with cell behaviour so that the monitored physiological post-transplantation course may be influenced. In the present study, we applied a method for an unequivocal identification of the graft cells without interfering cell metabolism or behaviour using in situ hybridisation (ISH) of human specific Alu sequences. Visualisation of the strong extended nuclear signal of Alu sequences was much easier than that of the small nuclear signals of donor-specific sex chromosome probes. With Alu probe, even single graft cells can be identified and their development can be observed in short-term and long-term studies. With this procedure, we could prove that donor cells were injected correctly into the subretinal space by a special injection technique that we developed previously. In combination with immunohistochemistry, donor cells could be clearly discriminated from macrophages, which contained phagocytosed donor cell fragments. Application of these ISH methods for species-specific identification was valuable for follow-up-studies of RPE transplantation.

B. Warncke · H. Schäfer (✉)
Department of Pathology,
University Hospital Hamburg-Eppendorf,
Martinistrasse 52, 20246 Hamburg, Germany
e-mail: schaefer@uke.uni-hamburg.de
Tel.: +49-40-428032858
Fax: +49-40-428036409

M. Valtink · J. Weichel · K. Engelmann
Department of Ophthalmology,
University Hospital Hamburg-Eppendorf,
Martinistrasse 52, 20246 Hamburg, Germany

M. Valtink · K. Engelmann
Department of Ophthalmology,
University Hospital Dresden, Carl Gustav Carus,
Fetscherstrasse 74, 01307 Dresden, Germany

Keywords Retinal pigment epithelium · Xenotransplantation · Alu sequences · Human specific sequences · Microscopical graft cell detection

Introduction

Inherited or acquired abnormalities of retinal pigment epithelium (RPE) are causally related to several types of clinically important retinal dystrophies, e.g. age-related macular degeneration (AMD) [17] or certain forms of retinitis pigmentosa [8]. In the Western world, 20% of the people aged over 65 years are affected; thus, AMD has become the major cause for blindness [26, 30]. Current therapeutic strategies focus on treatment of symptoms and side effects, such as excision of choroidal neovascularisation membranes or laser treatment, but causally acting therapies do not exist thus far. Transplantation of RPE cells may provide a promising therapeutic approach to treat these retinal degenerations. Transplanted cells may be native, cultured or even genetically modified. Experimental cell transplantation in animal models has been studied extensively, and first transplantations in humans have already been performed [22]. While some short-term experiments yielded results that indicate integrity of the transplants and a therapeutic success, i.e. a delay of the recipients' retinal degeneration [21], most of these studies are lacking unequivocal identification of the transplanted RPE cells to provide a solid base for follow-up studies.

In former studies, various methods were used to identify the transplanted RPE cells. Some investigators chose an albinotic animal model and identified the transplanted RPE cells by pigmentation [9, 10, 12, 28]. Other groups used cells that phagocytosed carbon particles before transplantation to enhance pigmentation [5, 6]. Other methods tested were fluorescence dyes [3, 4, 12, 27], labelled nucleotides with ^{3}H-thymidine [14, 27] or 5-bromodesoxyuridine [29, 31] or transfecting graft cells with green fluorescent protein- or LacZ-encoding genes [11, 16]. Table 1 shows these various methods and their disadvantages. None of these methods is practicable for

Table 1 Various methods to identify donor retinal pigment epithelial cells and their disadvantages. *GFP* green fluorescent protein

Former methods of identification	Disadvantages
Pigmentation	Secondary pigmentation of recipient pigmented macrophages after phagocytosis
Phagocytosis of carbon particles before transplantation	Marked macrophages after phagocytosis Marker is not permanently bound to cellular structures
Fluorescence dyes before transplantation	Non-specific staining and time-dependent bleaching Marked macrophages after phagocytosis
3H-thymidine and BrdU	Depends on mitosis Non-specific Radioactivity may influence cell behaviour
Transfection with GFP-/LacZ-encoding genes	Transfection may influence cell behaviour Sensitivity, some cells do not express GFP/LacZ
Sex chromosome in situ hybridisation	Small dot-like signals are sometimes difficult to detect

long-term studies, and most of them had influence on cell behaviour or metabolism.

Besides the disadvantage of influencing cell behaviour using these methods, clear identification of transplanted pigment epithelium is questionable, since host macrophages may resemble graft cells after phagocytosis of transplanted donor cells or cell fragments. This is of relevance, as, in fact, phagocytic infiltration and degeneration of graft cells after allo- or xenogeneic RPE cell transplantation have been demonstrated [2, 23]. The reasons for such inflammatory processes, including rejection phenomena, remain to be clarified.

In summary, the following critical points are a prerequisite for successful graft cell identification: (1) the identification method should be sensitive and detect even single cells, as the number of graft cells may be very low after transplantation; (2) the method should not disturb the physiology of the graft RPE cells; (3) degenerated and phagocytosed graft cell fragments should be distinguishable from well-preserved graft cells. According to former studies, these demands are of major importance.

In the present study, we transplanted human retinal pigment epithelial cells into various rat tissues, including the subretinal space [19]. Two in situ hybridisation (ISH) procedures (on human sex chromosomes and on human-specific Alu sequences) to discriminate grafted human cells from recipient animal cells were compared. Here, we describe the establishment of a method to specifically identify normal non-pretreated transplanted human RPE cells in the rat subretinal space using in situ hybridisation and detection of human Alu DNA sequences. In addition to the above-mentioned methodical points, the aim of this study was to investigate whether the transplanted cells could, indeed, be localised in the appropriate subretinal space using the applied experimental model. With this specific method to detect human donor cells and to discriminate them from recipient macrophages, single cells in the recipients' subretinal space could be identified. Thus, the dimension of donor cell loss and host macrophage invasion after xenogeneic transplantation without immunosuppression could be examined, providing a relevant base for subsequent follow-up studies. In principle, this sensitive and selective staining technique of human donor cells may also be applied to other xenogeneic transplantation models.

Materials and methods

Preparation of human ocular donor tissues

After removal of the corneoscleral disc from three donor eyes for organ culture according to Böhnke [1], one eye was prepared for histological examination according to the method of Naumann [15]. The other two eyes were used for preparation of ciliary body and retinal pigment epithelium. For this purpose, the anterior uveal segment was dissected and iris and lens were removed to leave the fragmented ciliary body for transplantation purposes. Retinal pigment epithelium was isolated using mechanical preparation of the choroid and subsequent incubation of the choroidal sheets in a trypsin solution [trypsin/ethylene diamine tetraacetic acid (EDTA) 0.02%/0.05%; Invitrogen] for 10 min at room temperature. The enzymatic reaction was stopped by adding an equal volume of fetal calf serum (FCS; Seromed). The procedure was repeated two times, the cell suspensions were combined and centrifuged at 100×*g* for 5 min. The supernatant was discarded, the cells were washed once with phosphate-buffered saline (PBS), centrifuged again, and the pelleted cells were instantly used for transplantation. The state of the cells in general was assumed to be appropriate for transplantation, as from past experience we know that cells isolated by this procedure were also able to grow in cell culture, which proves their vitality. Nevertheless, we know that, depending on post mortem time, some of the cells will not be able to integrate.

Animal experiments

Five Royal College of Surgeons (RCS) rats of the congeneic pink-eyed, wild-type rat strain served as experimental animals for transscleral transplantation of RPE cells into the subretinal space and for obtaining rat liver specimens. These rats spontaneously develop a severe retinal dystrophy, rendering them as a model for human retinal dystrophies [13]. The animals were kindly provided by E. El-Hifnawi, Medical University of Lübeck, Germany, and held free from common pathogens. The experiments followed the guidelines of the ARVO (Association of Research in Vision and Ophthalmology) statements of the Use of Animals in Research and the NIH "Principles of laboratory animal care". For each experiment, the animals were anesthetised by intraperitoneal injection of ketamine hydrochloride (80 mg/kg; Parke Davis) and xylazine hydrochloride (10 mg/kg; Bayer) after sedation by ether inhalation (ASID Bonz).

Four RCS rats received subretinal human RPE cell xenografts according to a procedure previously developed by our group [24].

In brief, after anaesthesia of the animals, a canthotomy was performed, and the conjunctiva was dissected. The eyebulb was mechanically fixed at the eye muscles and a scleral incision was made close to the superior limbus. Approximately 10 μl of pelleted RPE cells were aspirated into a subretinal cannula (Visitec No. 5178), which was connected to an oil-hydraulic microinjection pump (Celltram Oil pump; Eppendorf). The cannula was inserted into the scleral wound and gently pushed forward until a slight bleeding indicated the penetration of the choroid. Then the cells were slowly injected into the subretinal space until the ejected fluid created a visible subscleral bleb. The needle was then removed and the subretinal bleb was marked with sterile tissue adhesive (Tissucoll Duo S; Baxter) stained with autoclaved tissue marker (Davidson Marking System green; Bradley Products Inc.). The sclera and the canthotomy wound were closed using a suture (10–0 Ethilon; Ethicon). The eyes were treated with gentamycin eye drops (Ursapharm). As shown in Fig. 2a, most of the injected cells were localised in aggregates at the correct subretinal site. However, in addition, easily visible cell complexes single scattered transplanted cells undetectable by conventional histological methods may be deposed after dilution in a larger three-dimensional area extended around the injection site. The animals were anaesthetised again as described above 1 day, respectively, 1 month after transplantation and killed with an overdose of CO_2 in order to enucleate the eyes. The enucleated eyes were fixed with 4% paraformaldehyde in 0.1 M PBS (pH 7.4) at room temperature for 12 h with the medial and lateral eye poles cut off to allow easy penetration of the fixative.

For comparison and control of the marker procedure, selective staining of transplanted cell suspensions was compared with staining of implanted entire human tissue specimens. For this purpose, the fifth rat was anaesthetised and killed as described above. One eye bulb was enucleated and an incision was made into the eye close to the limbus. A fragment of human ciliary body was transferred into the anterior chamber of the enucleated eye bulb, and the incision was closed with tissue adhesive. Furthermore, a piece of liver (maximal diameter approximately 1 cm) was explanted from this animal. Then, a 0.6-mm^3-sized flap was cut out of the explant, human RPE cell suspension was injected into the gap using an Eppendorf pipette and injected cells were fixed within the tissue with tissue adhesive. Eye and liver tissue were then fixed in 4% paraformaldehyde in 0.1 M PBS (pH 7.4) for 48 h.

Preparation of histological specimens

After fixation, the tissues were embedded in paraffin according to routine procedures. Serial sections of the liver 4-µm thick and the globes were cut through the centre of the grafted area parallel to the inferior-posterior axis and mounted on Superfrost slides. Each tenth section was stained with periodic acid-Schiff (PAS). At each level, subsequent sections were used for in situ hybridisation on X and Y chromosomes or Alu sequences, respectively, or for immunohistochemical procedures. The stained sections were evaluated using light microscopy and photographed.

In situ hybridisation of X and Y chromosome

Deparaffinised sections mounted on Superfrost slides were pretreated with 0.01 M citrate buffer pH 6.0 (2 min microwave), sodium thiocyanate (6.49 g/100 ml A. dest., 10 min at 80°C) and pepsin digestion (1–4 mg/ml, 3–8 min at 37°C). The time of protease digestion has to be tested in advance, particularly as retinal tissue includes different cell types with very different sensitivities to protease treatment. We checked tissue integrity after every minute of ongoing digestion using light microscopy and performed the final assay with 3 mg/ml (180 mg Pepsin, 48 ml A. dest., 12 ml 1 N HCl) for 3 min and 5 min. The DNA strands were denaturated at 80°C for 30 min on a heating plate. A human-specific digoxigenin-labelled X, respectively, Y probe (Qbiogene) was applied for hybridisation (overnight at 37°C) in a humidity box. The probes were incubated under coverslips fixed with rubber cement. After removal of the coverslips, washing [2× sodium saline citrate (SSC) with 50% formamide, 15 min at 40°C] and inhibition of endogenous peroxidase with 3% H_2O_2 (10 min at room temperature), proteins were blocked with normal goat serum (Dako, 45 min at room temperature). Bound probe was detected by the following sequence: mouse-anti-digoxigenin (Boehringer), biotin-labelled goat-anti-mouse serum (Dianova) and streptavidine-peroxidase (Dianova), each for 30 min at 37°C. Peroxidase activity was detected by 3,3′diaminobenzidine (DAB) (Dako, 10 min in the dark). The sections were counterstained with haemalaun and mounted in Eukitt®.

ISH of human Alu sequences

Standard protocol

Sections were deparaffinised in xylene, rehydrated in graded ethanol series and air dried. The tissue was treated with 100 µg/ml proteinase K (Boehringer) in TES pH 7.4 (10 mM Tris, 10 mM NaCl, 1 mM EDTA) for 5 min at room temperature and dried from ethanol. A 20-µl fluorescein-labelled Alu probe (BioGenex) was added, and coverslips were fixed with rubber cement. Sections were denaturated on a heating plate at 95°C for 10 min. For hybridisation, the sections were incubated at 37°C overnight in a humidity box. The rubber cement and the coverslips were removed and the sections were washed in TBS pH 7.6 (50 mM Tris, 150 mM NaCl). After inhibition of the endogenous peroxidase with 3% H_2O_2 and the use of a protein block, signal amplification was achieved using an anti-fluorescein antibody and biotinylated F(ab)2 fragments followed by enzyme-streptavidin label, exactly according to instructions of the manufacturer (BioGenex, Super Sensitive ISH Detection System). Visualisation was performed by 3-amino-9-ethylcarbazole (AEC)- or DAB-chromogen. The sections were counterstained with haemalaun and mounted in glycerin/gelatin or Eukitt®.

Modified protocol

In some cases, we modified this protocol, as the endogenous pigment of the RPE cells could easily be mistaken for DAB-stained dots, and vice versa, particularly in areas with high cellularity. To discriminate endogenous pigment in RPE from the histochemical reaction product, the deparaffinised sections were depigmented by 0.25% $KMnO_4$ for 5–10 min and cleared in 5% oxalic acid before proteinase K treatment. The extension of depigmentation is critical for cell morphology, as complete depigmentation may artificially decrease preservation of the cells. Thus, sometimes compromise between complete depigmentation and acceptable morphology is inevitable. The Alu probe was diluted 1:10 in hybridisation mixture [13 ml formamide, 4 ml dextransulphate, 1 ml salmon sperm DNA, 2 ml 20×SSC (pH 7.0, 150 mM NaCl, 15 mM Na-citrate-dihydrate)]. A stringent washing procedure was performed according to Jensen et al. [7] using SSC with 0.1% sodium dodecyl sulfate (SDS): 2×SSC/0.1% SDS for 2×5 min at room temperature, 0.1×SSC for 10 min at 40°C, 2×SSC/0.1% SDS for 5 min at room temperature.

Immunohistochemical marker reaction on rat macrophages

A mouse-anti-rat monoclonal antibody (mAb clone ED1; Serotec), which was detected by using the standard APAAP (alkaline phosphatase/anti-alkaline phosphatase) method (Dako), was used to identify rat macrophages. This antibody recognises a glycoprotein predominantly expressed on lysosomal membranes. The protocol has been optimised by testing sections of rat spleen. The sections were deparaffinised, rehydrated and treated with proteinase K (100 µg/ml TES, pH 7.4, for 10 min at room temperature). After proteinase K was blocked with absolute ethanol, the slides were

covered with normal pig serum (1:20 with TBS pH 7.6, for 10 min at room temperature). Sections were then incubated with primary antibody [(mouse anti-rat ED1, 1:200 with Tris-buffered saline (TBS)/3% bovine serum albumin] for 30 min at 37°C, followed by incubation with the secondary antibody (rabbit anti-mouse; Dako) for 2×15 min at 37°C and the APAAP-complex (monoclonal mouse; Progen, 1:50 with TBS). After incubation on alkaline phosphatase activity with a new fuchsin coupled substrate for 30 min at room temperature in the dark, the reaction was stopped with 1% HCl. This method yields a pink signal of the labelled areas that is well contrasted with pigmentation due to melanin. The sections were counterstained with haemalaun and mounted in glycerine gelatine.

Results

In order to find a marker method to identify human graft cells after xenogeneic transplantation without previous influence on function of the graft cells, we established an ISH procedure with human-specific Alu probes, which was expected to yield a particularly strong and specific nuclear signal. First, we wanted to make sure that there is, indeed, a strong positive signal in all human cells and no signal in rat cells to ensure identification of small numbers or even single graft cells. Thus, we first embedded human and rat liver tissue together and ran an Alu ISH, following the standard protocol. All human nuclei were strongly stained throughout the nuclear area. None of the rat cells was positive (figure not shown).

Every cell type needs a special ISH pre-treatment. The protease digest, in particular, is a very sensitive step, as retinal cells are difficult to handle. Thus, in the next step, we embedded human RPE cells in rat liver tissue and ran the Alu-ISH. A modified ISH protocol, including depigmentation, dilution of Alu probe and a stringent washing procedure using SDS led to an acceptable result with positive staining of all human nuclei (Fig. 1a, b).

Next, we embedded pigment epithelium and choroid of human eye (Fig. 1c, d) to prove that the modified protocol works with different human ocular cell types. The difficulty was to find a compromise between the aggressive chemical procedure of depigmentation and the sensibility of retinal cell structure. As shown in Fig. 1d, depigmentation was performed carefully enough to preserve cell integrity despite specific nuclear staining. We also tested ISH on human-specific X and Y chromosomes (Fig. 1e) to identify human cells; however, compared with the Alu signal (hu in Fig. 1f), we found these small dot-like signals much less comfortable to assess.

We then implanted a fragment of a human ciliary body in rat eye bulb (Fig. 1f), and even this last preceding methodological test showed very satisfactory results. Almost all human cell nuclei were stained perfectly, but none of the rat nuclei was stained. Background staining was reduced to a minimum. Because of the intense pan-nuclear signal, the staining pattern was already visible in low magnification.

Based on this methodical work, we were now able to have unequivocal identification of human donor RPE cells transplanted to rat bulbs. For this, the modified protocol described in "Materials and methods" was applied. The rat eye bulbs were enucleated 1 day, respectively, 1 month after transplantation. Post-op (1 day) ISH of Alu sequences yielded a strong nuclear signal in the transplanted human RPE cells. As shown in Fig. 2a, most of these cells were located at the transplantation site. After application of the elaborated special injection technique, many of the transplanted cells were situated at the physiological subretinal site, without inappropriate damage of the covering retinal layer (Fig. 2a, b). Alu-ISH showed some cells with a more diffuse cytoplasmic staining 1 month post-operatively, but with negativity of nuclei (Fig. 2e).

Figure 2c, f shows an immunohistochemical staining with mAb ED1, a rat-specific anti-macrophages antibody. Some macrophages were detectable 1 day after transplantation (Fig. 2c).

ED1-positive macrophages could be detected all over the transplantation area 1 month after transplantation (Fig. 2f). Comparing staining pattern and cytological features of rat macrophages to the cytoplasmic Alu-ISH staining (Fig. 2e), we conclude that the macrophages were secondarily pigmented due to phagocytosis of RPE fragments. In PAS-stained sections (Fig. 2a, d), these cells could easily be mixed up with the grafted RPE cells, since both cell types appear pigmented—the graft cells originally and the macrophages after phagocytosis. After Alu-ISH and ED1-staining, it appeared evident that after 1 month, vital human graft cells were no longer detectable in the host tissue.

Discussion

Transplantation of RPE cells is a promising therapeutic option for retinal degeneration that originates in the RPE cell layer. RPE transplantations have extensively been studied in animal models, mostly in the RCS rat model of retinal degeneration, but also in albinotic mice, rats, rabbits or even in primates [22]. However, first transplantations in humans were less successful than transplantations in animal models, and investigators began to re-evaluate RPE cell transplantation in animal models. In our study, we sought to address critical, limiting aspects of RPE cell transplantation, i.e. (1) to unequivocally identify grafted cells in the recipient tissue, (2) to verify anatomically correct localisation of transplanted cells in the subretinal space without iatrogenic damage of recipient tissue, and, based on the first two aspects, (3) to follow up the fate of the grafted cells and host tissue reactions. Special emphasis was put on identification and localisation of grafted cells as well as tissue reactions towards the graft. We demonstrate, by means of our previously described optimised transplantation technique [24], that it is possible to transplant cells into the subretinal space and that the grafted cells can be distinguished from recipient pigmented cells. In addition to tracing subretinally transplanted RPE cells, the established method can also be used to selectively identify

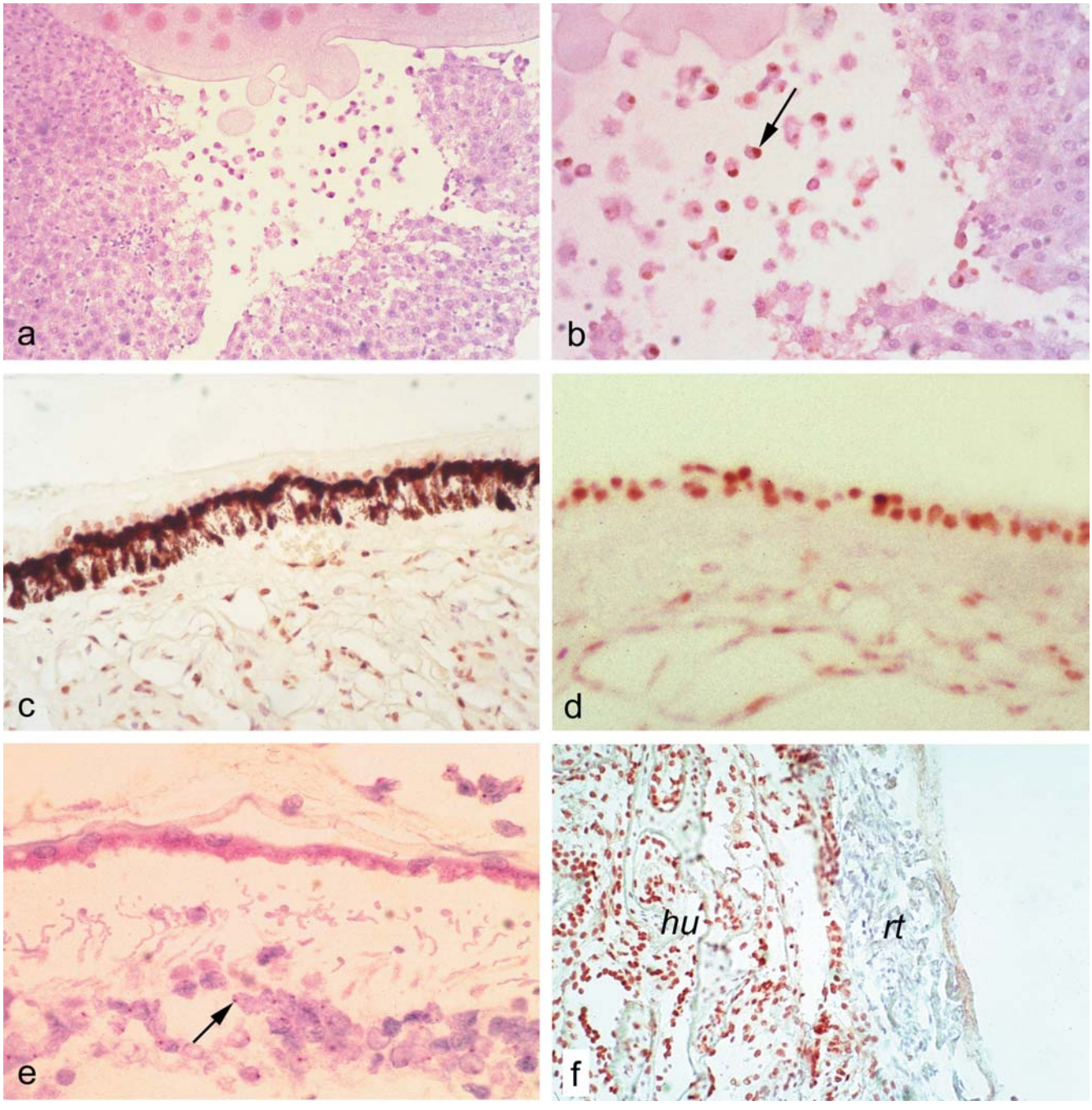

Fig. 1 Survey (**a**) and detail (**b**) of a cell suspension of human retinal pigment epithelium (hRPE) injected into rat liver. After depigmentation, in situ hybridisation (ISH) on Alu sequences presents a dark staining of the entire nucleus exclusively in human cells *(arrow)*. Pigment epithelium and choroid of human eye without depigmentation (**c**) and after depigmentation (**d**). Distinct positivity of Alu sequences in almost every nucleus without difficulties in discrimination of specific nuclear staining from endogenous dark pigment. After depigmentation, clearly visible specific pan-nuclear staining on Alu sequences, even in RPE cells. **e** Demonstration of human specific Y chromosomes in human retina and RPE. This method yields only small dot-like nuclear signals (*arrow*), which, in case of incomplete depigmentation, may sometimes be difficult to discriminate from residual pigment, particularly in the case of irregularly and densely arranged transplanted cells and nuclei. **f** Human ciliary body implanted into rat eye bulb. Distinct nuclear staining of Alu sequences in the human cells (*hu*) contrasting well with negativity in rat tissue (*rt*). ×127 (**a**); ×254 (**b**); ×254 (**c**); ×313 (**d**); ×561 (**e**); ×141 (**f**), all 3,3′diaminobenzidine-stained

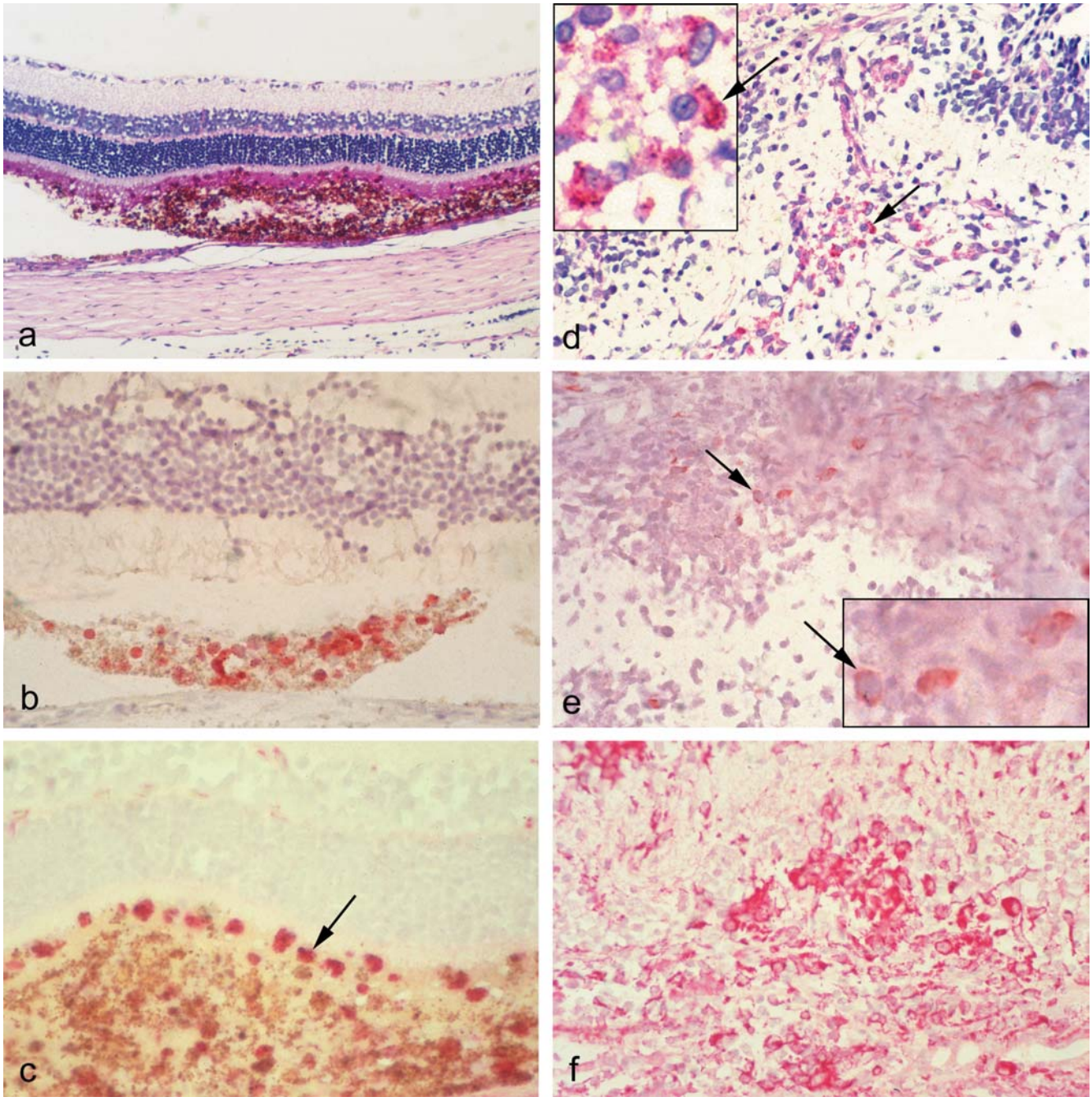

Fig. 2 Royal College of Surgeons rat eye bulbs after transplantation of a suspension of pigmented human retinal pigment epithelium (RPE) cells. Enucleation 1 day (**a**, **b**, **c**), respectively, 1 month (**d**, **e**, **f**) after transplantation. **a** Successful transplantation with adequate subretinal position of transplanted pigmented RPE cells. periodic acid-Schiff, ×127. **b** Easy identification of transplanted human RPE cells by well-contrasting pan-nuclear staining of Alu sequences. Alu probe, 3,3′diaminobenzidine (DAB), ×365. **c** Cytoplasmatic staining of some solitary macrophages (*arrow*) between RPE cells in early phase after transplantation. ED-1 antibody, alkaline phosphatase/anti-alkaline phosphatase, ×365. **d** Intense inflammatory and proliferative tissue reaction at transplantation site 1 month postoperatively. Note pigmented cells (*arrows*) difficult to interpret in standard staining. PAS, ×254; *inset*: ×1016. **e** Alu ISH positivity exclusively in cytoplasm of rare disseminated cells (*arrows*); no nuclear staining. It is concluded that Alu-positive material arises from phagocytosed RPE fragments. Alu probe, DAB, ×254; *inset*: ×1266. **f** Identification of numerous macrophages 1 month post-operatively. ED-1 antibody, amino-9-ethylcarbazole, ×254

Table 2 In situ hybridisation (ISH) with Alu probes to identify human cells and the advantages of this method

Our method of identification	Advantages
Alu-ISH identifies human cell nuclei	Strong staining of entire cell nuclei Almost every single cell nucleus is stained After phagocytosis by host macrophages staining shows cytoplasmatic signals Post-mortem staining does not influence cell behaviour

human cells other than RPE after transplantation in any animal tissue.

With regard to allogeneic transplantations, in most studies, an ISH with X- and Y-chromosome specific probes has been applied. In our experiments, this procedure revealed appropriate results, but the results sometimes were not easy to interpret. There is only one, respectively, two spots in each graft cell nucleus, and these small spots may falsely be interpreted as pigment granules or remainders of pigment after incomplete depigmentation. Although pigment granules are localised in the cytoplasm, there may be a misinterpretation when nuclei are lying close, overlapping and in more than one layer (Fig. 1e) or when cells are not arranged accurately due to injecting a cell suspension. In our kind of experiments, we needed to find even single cells, which are very difficult to detect, by looking for a small dot-like signal.

In view of these difficulties, in this study, we now present histochemical identification of transplanted cells using a method that allows detection even of single human cells in histological specimens of rat eyes using ISH and visualization of repetitive human-specific Alu sequences. The Alu repeats are a family of short interspersed elements that are found in excess of a million copies, which means an estimated 5% of the human genome consists of Alu repeats [18, 20]. These sequences were mainly used to discriminate human from mouse cells via dot-blot [25] or in combination with LacZ reporter genes [7].

With Alu ISH on histological sections, no pre-transplantational manipulation of the RPE cells is necessary. Table 2 shows the advantages of our method. In addition to the advantage of intense pan-nuclear staining, the use of in situ hybridisation with an Alu probe is a post-mortem tracing technique of the cells, so that origin and functional situation of the donor cells can be preserved and uninfluenced follow-up of the donor cells in the recipient eye, even for long-term transplantation, is possible.

Figure 2a, b, c shows sections of the enucleated rat eye bulb 1 day after injection. We were able to localise the applied cells and to prove that our special injection technique was able to transplant donor cells correctly into the subretinal space. Beyond the question of localisation, the Alu-ISH enables us to follow up the fate of the RPE cells for days and weeks after injection.

In former studies, when we used pigmentation for identification of human RPE cells, we presumed the existence of secondary pigmented macrophages that could easily be confused with RPE cells. After transplantation by injecting donor cells through the choroidea, macrophages would be able to reach the subretinal space. These macrophages could have become pigmented after phagocytosis of RPE cell debris as part of the inflammatory reaction against donor cells, and these macrophages could also dispose of the debris left by the insufficient RPE cells. This might lead to an ephemeral improvement after transplantation before the donor cells were disposed as well.

Figure 2d, e, f shows a section of the enucleated rat eye bulb 1 month after injection. The Alu sequences were definitely localised in the cytoplasmic compartment (Fig. 2e). To verify our assumption of macrophage invasion and transplant phagocytosis, we ran an immunohistochemical assay using a macrophage specific antibody (Fig. 2c, d, e, f). Comparing these figures by distribution pattern, cytological features and number of cells, we conclude that the macrophages were secondarily pigmented due to phagocytosis. Figure 2a, b, c shows a section of the enucleated rat eye 1 day after infection. Even at this time, we were able to detect rat macrophages.

In summary, after Alu ISH and ED1-staining, we have now proved that after 1 month postoperatively, the human graft cells do no longer exist in the host tissue. Since our experiments were performed without immunosuppression, whether this is an effect of non-specific resorptive processes or a sign of an immunological reaction has to be clarified in further studies. With the presented application for species-specific identification, it is now possible to study the fate of transplanted cells in xenogeneic models. Follow-up-studies can now be performed in order to answer questions such as: How do donor cells behave during weeks after injection? Does the physiological function of the donor cells depend on their environment? and Do the topographical and immunological conditions allow a long-term survival?

Our established method is a comfortable tool that allows a precise follow-up of human donor cells in animal organism. In contrast to other methods, we get a strong staining even of single human cells and, as a post-mortem method, it does not influence cell metabolism or behaviour. The unequivocal detection of transplanted cells is of significant interest for any xenogeneic transplantation experiment.

Acknowledgements This work was supported by grants from the Waltraut und Sieglinde Hildebrandt-Stiftung im Stifterverband für die Deutsche Wissenschaft, Germany, and the Hamburger Krebsgesellschaft, Germany.

References

1. Böhnke M (1991) Corneal preservation in organ culture. Curr Opin Ophthalmol 2:432–442
2. Crafoord S, Dafgard-Kopp E, Seregard S, Algvere PV (2000) Cellular migration into neural retina following implantation of melanin granules in the subretinal space. Graefes Arch Clin Exp Ophthalmol 238:682–689
3. Del Cerro M, Notter MFD, Wiegand SJ, Jiang LQ, del Cerro C (1988) Intraretinal transplantation of fluorescently labelled retinal cell suspensions. Neurosci Lett 92:21–26
4. Del Priore L, Kaplan H, Silverman M, Valentino T, Mason G, Hornbeck R (1993) Experimental and surgical aspects of retinal pigment epithelial cell transplantation. Eur J Implant Ref Surg 5:128–132
5. El Dirini AA, Wang H, Ogden TE, Ryan SJ (1992) Retinal pigment epithelium implantation in the rabbit: technique and morphology. Graefes Arch Clin Exp Ophthalmol 230:292–300
6. He S, Wang HM, Ogden TE, Ryan SJ (1993) Transplantation of cultured human retinal pigment epithelium into rabbit subretina. Graefes Arch Clin Exp Ophthalmol 231:737–742
7. Jensen UB, Jensen TG, Jensen PKA, Rygaard J, Hansen BS, Fogh J, Kolvraa S, Bolund L (1994) Gene transfer into cultured human epidermis and its transplantation onto immunodeficient mice: an experimental model for somatic gene therapy. J Invest Dermatol 103:391–394
8. Kellner U (1997) Hereditäre Netzhautdystrophien Teil 2: differentialdiagnose. Ophthalmologe 94:450–465
9. Kohen L, Enzmann V, Faude F, Wiedemann P (1997) Mechanisms of graft rejection in the transplantation of retinal pigment epithelial cells. Ophthalmic Res 29:298–304
10. La Vail MM, Li L, Turner JE, Yasumura D (1992) Retinal pigment epithelial cell transplantation in RCS rats: normal metabolism in rescued photoreceptors. Exp Eye Res 55:555–562
11. Lai CC, Gouras P, Doi K, Lu F, Kjeldbye H, Goff SP, Pawliuk R, Leboulch P, Tsang SH (1999) Tracking RPE transplants labeled by retroviral gene transfer with green fluorescent protein. Invest Ophthalmol Vis Sci 40:2141–2146
12. Li L, Turner JE (1988) Transplantation of retinal pigment epithelium cell to immature and adult rat hosts. Short-term and long-term survival characteristics. Exp Eye Res 47:771–785
13. Litchfield TM, Whiteley SJO, Lund RD (1997) Transplantation of retinal pigment epithelial, photoreceptor and other cells as treatment for retinal degeneration. Exp Eye Res 64:655–666
14. Lopez R, Gouras P, Brittis M, Kjeldbye H (1987) Transplantation of cultured rabbit retinal epithelium to rabbit retina using a closed-eye method. Invest Ophthalmol Vis Sci 28:1131–1137
15. Naumann GOH (1980) Pathologie des Auges. Springer-Verlag, Berlin Heidelberg New York
16. Osusky R, Jiang M, Buchi ER, Spee C, Ye J, Ryan Sj (1995) beta-Galactosidase transgene expression in transplanted rabbit retinal pigment epithelial cells in vivo. Graefes Arch Clin Exp Ophthalmol 233:220–225
17. Pauleikhoff D, Holz FG (1996) Die altersabhängige Makuladegeneration. 1. Epidemiologie, Pathogenese und diagnostische Differenzierung. Ophthalmologe 93:299–315
18. Rudin CM, Thompson CB (2001) Transcriptional activation of short interspersed elements by DNA-damaging agents. Genes Chromosomes Cancer 30:64–71
19. Schäfer H, Warncke B, Weichel J, Engelmann K, Zander AR (2001) Microscopical identification of transplanted cells on single-cell level shown on an experimental model of congenital retinal dystrophy and in human liver after transplantation of bone marrow stem cells. Pathol Res Pract 197:364
20. Szmulewicz MN, Novick GE, Herrara RJ (1998) Effects of Alu insertion on gene function. Electrophoresis 19:1260–1264
21. Turner JE, Blair JR, Seiler M, Aramant R, Laedtke TW, Chappell ET, Clarkson L (1988) Retinal transplants and optic nerve bridges: possible strategies for visual recovery as a result of trauma or disease. Int Rev Neurobiol 29:281–308
22. Valtink M, Weichel J, Richard G, Engelmann K (2001) Transplantation of retinal pigment epithelium cells. In: Alberti WE, Richard G, Sagerman RH (eds) Age-related macular degeneration: current treatment concepts. Springer Verlag, Berlin Heidelberg New York, pp 65–76
23. Weichel J, Warncke B, Valtink M, Engelmann K, Schäfer H (2000) Evidence of graft cell loss after xenogenic transplantation of human RPE cells into RCS rats. Ophthalmic Res 32[Suppl 2]:54
24. Weichel J, Valtink M, Engelmann K, Richard G (2002) Use of an oil-hydraulic microinjection pump for subretinal infusions. Ophthalmic Surg Lasers 33:340–342
25. Weisberg TF, Cahill BK, Vary CPH (1996) Non-radioisotopic detection of human xenogeneic DNA in a mouse transplantation model. Mol Cell Probes 10:139–146
26. Williams RA, Brody BL, Thomas RG, Kaplan RM, Brown SI (1998) The psychosocial impact of macular degeneration. Arch Ophthalmol 116:514–520
27. Wongpichedchai S, Weiter JJ, Weber P, Dorey K (1992) Comparison of external and internal approaches for transplantation of autologous retinal pigment epithelium. Invest Ophthalmol Vis Sci 33:3341–3352
28. Yamaguchi K, Yamaguchi K, Young RW, Gaur VP, Greven CM, Slusher MM, Turner JE (1992) Vitreoretinal surgical technique for transplanting retinal pigment epithelium in rabbit retina. Jpn J Ophthalmol 36:142–150
29. Ye J, Wang H, Ogden TE, Ryan SJ (1999) Allotransplantatio of rabbit retinal pigment epithelial cells double-labelled with 5-bromodeoxyuridine (BrdU) and natural pigment. Curr Eye Res 12:629–639
30. Young RW (1987) Pathophysiology of age-related macular degeneration. Surv Ophthalmol 31:291–306
31. Young RW, Gaur VP, Li L, Turner JE (1991) Transplantation of 5-bromodeoxyuridine labeled retinal pigmented epithelial cells on Bruch's membrane in the rabbit. Invest Ophthalmol Vis Sci 32:982

Virchows Arch (2004) 444:82–86
DOI 10.1007/s00428-003-0909-9

CASE REPORT

Elisabetta Magrini · Antonella Pragliola · Anna Farnedi · Christine M. Betts · Roberto Cocchi · Maria P. Foschini

Cytogenetic analysis of myoepithelial cell carcinoma of salivary gland

Received: 18 June 2003 / Accepted: 9 September 2003 / Published online: 24 October 2003

Abstract Myoepithelial cell carcinoma (MCC) of the salivary gland is a rare entity. Here, we describe the karyotype of MCC. The patient was a 53-year-old man, with a rapidly growing lesion of the palate. Despite complete surgical excision, radio- and chemotherapy, the lesion rapidly harboured local and distant metastases leading to the death of the patient, 4 months after the diagnosis. On histological and ultrastructural examination, the primary tumour and the related metastases were composed of oval and spindle cells, with features of myoepithelial cell differentiation reported in the literature. Cytogenetic analysis showed a composite karyotype in the primary tumour: 45~46,XY, +3[cp3]/ 44~45,XY, -17[cp4]/ 46,XY[5]. The lymph-node metastasis was near-triploid and showed a complex karyotype. Our cytogenetic data differ from those described in benign or slowly growing salivary gland tumours showing myoepithelial cell differentiation. It is suggested that highly aggressive tumours might follow a different pathway of malignant transformation.

Keywords Myoepithelial cell carcinoma · Karyotype · Cytogenetic analysis · Salivary gland · Chromosome 17

E. Magrini · A. Farnedi · M. P. Foschini (✉)
Anatomia Patologica, Università di Bologna,
Ospedale Bellaria, Via Altura 3, 40139 Bologna, Italy
e-mail: Mariapia.foschini@ausl.bologna.it
Tel.: +39-051-6225523
Fax: +39-051-6225759

R. Cocchi
Department of Maxillo-Facial Surgery,
Ospedale Bellaria, Bologna, Italy

A. Pragliola
Anatomic Pathology, Ospedale Bufalini, Cesena, Italy

C. M. Betts
Department of Experimental Pathology,
University of Bologna, Italy

Introduction

Myoepithelial cell carcinoma (MCC) is a rare malignant tumour of the salivary glands, composed almost entirely of cells showing myoepithelial cell differentiation. Cytogenetic data present in the English literature are limited to benign myoepitheliomas or to benign and malignant salivary gland tumours showing epithelial and myoepithelial cell differentiation, while no cytogenetic data have been described on pure MCC. We recently had the opportunity to examine the karyotype of a pure MCC of the salivary glands.

Clinical history

The patient was a 53-year-old male with a painless mass of the hard palate. A computed tomography scan showed a wide lesion extending from the palate submucosa and invading the maxillary bone. The lesion was surgically removed. Metastases to laterocervical lymph nodes appeared 45 days after surgery. Radiotherapy was performed. The patient developed lung and skin metastases and died of disease 4 months after the first surgical intervention.

Material and methods

Histology and immunohistochemistry

Fresh biopsy tissue was partly used for cytogenetic studies and partly routinely processed for normal histology. Subsequently, serial sections were cut from selected blocks and stained by a routine immunohistochemical method, employing the following antibodies; calponin (clone CALP, diluted 1:60; Biogenex); caldesmon (clone h-CD, diluted 1:60; Biogenex), cytokeratin 14 (clone LL002, diluted 1:100; Biogenex); cytokeratin 7 (clone OV\TL 12\30, diluted 1:100; Dako); smooth muscle actin (clone 1A4, diluted 1:100; Dako), p53 (diluted 1:50, Dako) and p63 (diluted 1:400, Neomarkers).

For electron microscopy, small blocks were microdissected from paraffin embedded samples. They were then routinely dewaxed by immersion overnight in xylol and rehydrated to phosphate buffer through a graduated diluted alcohol series. Fragments were then re-fixed in buffered glutaraldehyde and post-fixed in OsO4, dehydrated in alcohol and propylene oxide and embedded in Epon 812. Thin sections were stained with uranyl

acetate and Reynold's lead citrate and observed in a Philips CM 10 TEM.

Culturing and cytogenetic analysis

Fresh representative samples of two lesions directly withdrawn from surgical specimens were submitted for cytogenetic investigation. Cell suspensions were obtained after enzymatic digestion with collagenase 400 U/ml (Worthington Biochemical Inc) at 37°C for 16–18 h as described by Limon et al. [7].

Cell suspensions were seeded and cultured for 2 days (for primary and metastasis) in DMEM-F 12 (GIBCO, Milan, Italy) supplemented with 10% fetal bovine serum (Hy-Clone Laboratories, Celbio, Milan, Italy) and antibiotics/fungizone.

Chromosome preparations were made using standard cytogenetic techniques on in situ metaphases isolated from primary short-term cultured cells after overnight incubation with Colcemid (0.03 μg/ml). The cultures were harvested by subjecting the cells to hypotonic treatment with 0.8% of sodium citrate preheated at 37°C at room temperature for 35 min and fixed with a mixture of methanol/glacial acetic acid (3:1) using four changes. The chromosomes were G-banded using HCl and Wright staining, 20 G-banded metaphases were evaluated for each case and three slides observed for elude a clonal growth of the same cell. The karyotypes were described according to the ISCN 1995 Guidelines for Cancer [4].

Results

Histopathological features

Histopathological features of primary and metastatic tumours were similar, so they will be described together. The tumours were composed of sheets of oval to spindle cells, with markedly atypical nuclei and eosinophilic cytoplasm. Mitoses were numerous and atypical. Necrosis was focally present (Fig. 1A). On immunohistochemistry, the neoplastic cells were focally positive with cytokeratins 14 and 7 (Fig. 1B) and diffusely positive with calponin (Fig. 1C). In addition, a strong nuclear positivity was observed for p53 (Fig. 1D) and focal positivity was observed for p63 (Fig. 1E). No features of a pre-existing benign tumour, such as pleomorphic adenoma, were seen.

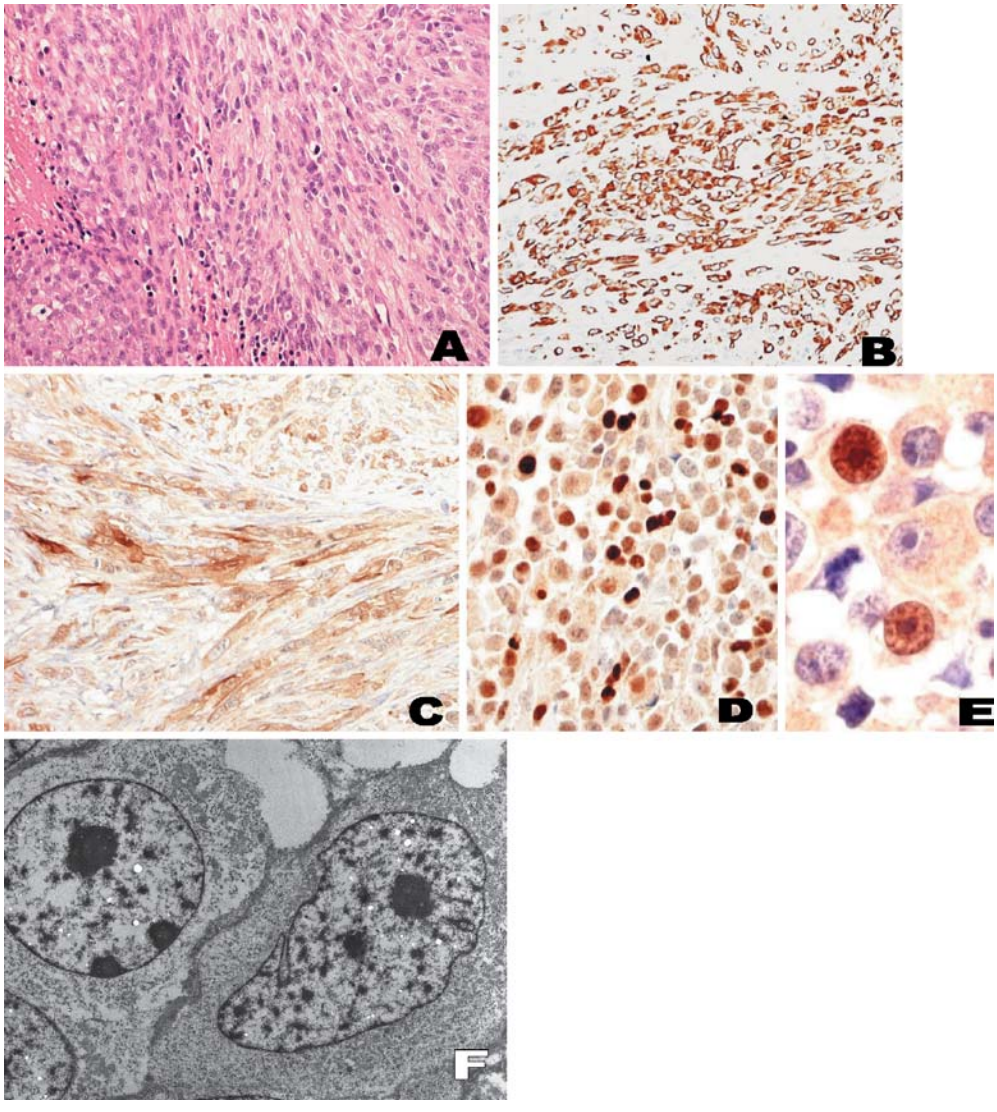

Fig. 1 **A** On hematoxylin & eosin examination, the lesion was composed of spindle and oval atypical cells, with areas of necrosis. The cells were strongly positive with low-weight cytokeratin (**B**) and calponin (**C**). In addition, nuclear positivity was observed for p53 antibody (**D**) and focally for p63 (**E**). At ultrastructure (**F**) the neoplastic cells were focally surrounded by basal membrane and contained intermediate filaments

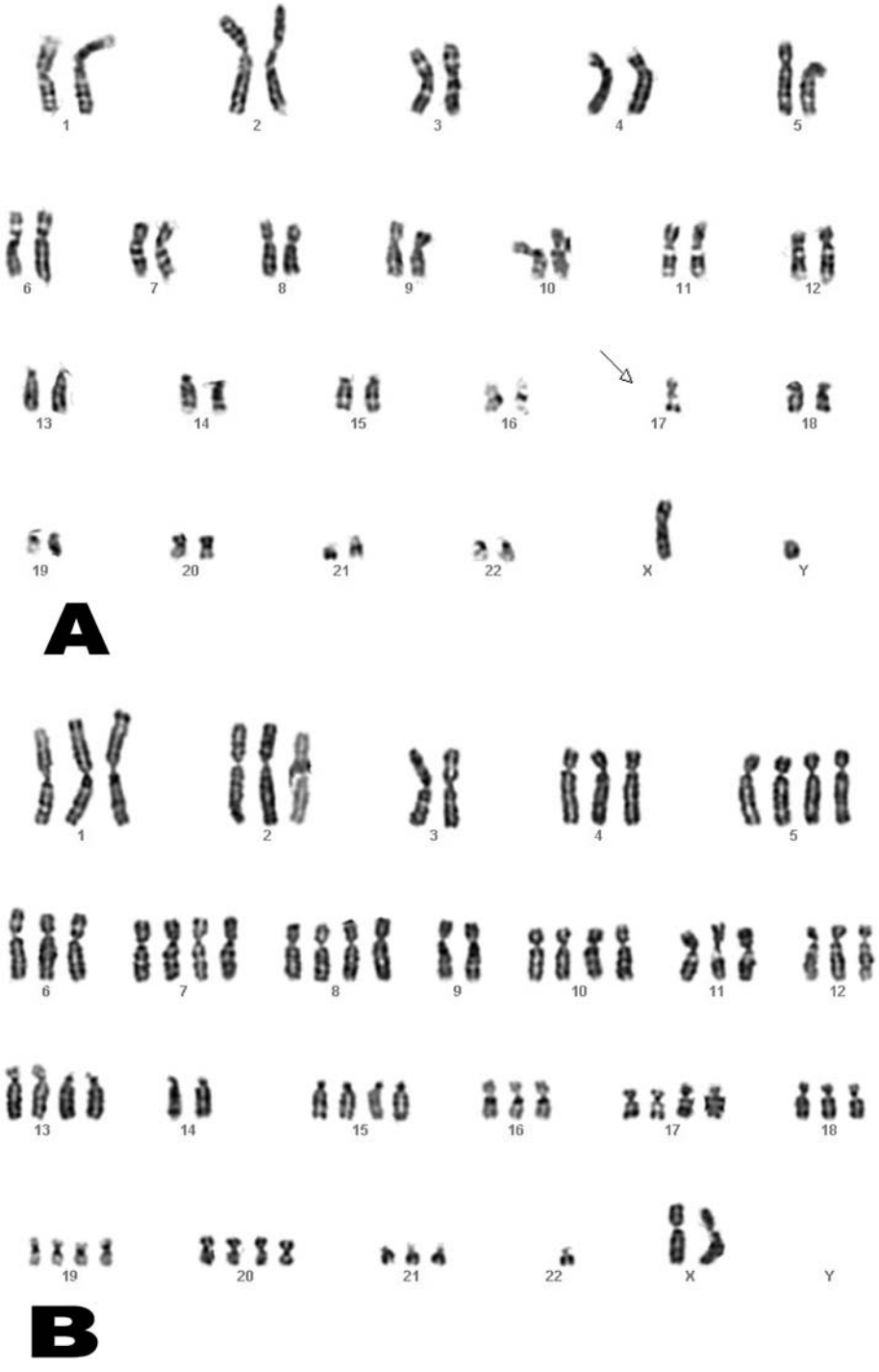

Fig. 2 **A** Representative karyogram in primitive tumour. The *arrow* indicates chromosome 17 monosomy. **B** Representative karyotype of myoepithelial cell carcinoma metastasis, showing a complex picture

Ultrastructural examination confirmed pure myoepithelial cell differentiation (Fig. 1F). The neoplastic cells were generally similar to one another, displaying large, round or irregular shaped nuclei with dispersed chromatin and prominent nucleoli. Low magnification revealed that cells were polygonal, oval or elongated with smooth cytoplasmic contours showing abundant irregularities and specialised junctions. At higher magnification, tumoural cells were attached to each other by small desmosomes or tight junctions, rarely by well-formed desmosomes. Most frequently, the intercellular spaces were widened and filled with granulo-filamentous material. Often, basal membranes were multilayered. Actin-like filaments were haphazardly distributed within the cytoplasm, lacking arrangement in bundles and never showing focal densities. Within a few cells, small fascicles of intermediate filaments were occasionally observed in a paranuclear position.

Cytogenetic analysis

The primary tumour showed the modal number near-diploid (range:44–47 chromosomes). Fifteen metaphases were evaluated, revealing a composite karyotype: 45~46,XY, +3[cp3]/ 44~45,XY, -17[cp4]/ 46,XY[5]; no clonal abnormalites in the other metaphases were observed (Fig. 2A). The metastasis was near-triploid (58–80) with 16 evaluated metaphases, showing a complex karyotype: 69~74,XY, -Y(12), +2(6), -3(12), +5(8), +6(7), +7(9), +8(8)+11(6), +12(6), -13(9), -14(11), +15(6), -15(5), +16(6), +17(11), +18(7)+19(8), +20(13), +21(4), -22(13), +M1(2)(cp16) (Fig. 2B).

Discussion

Benign and malignant salivary gland tumours showing myoepithelial cell differentiation present specific and recurrent chromosomal alterations. The alterations most frequently observed are translocations involving 12q12 and del(9)(q22.1q22.3), associated in some cases with translocations involving 1q and12q [2]. In addition, benign salivary gland tumours, showing epithelial and myoepithelial cell differentiation, such as pleomorphic adenoma, often show 8q12 and 12q13-q15 alterations. A benign myoepithelioma showed a similar karyotype, associated with a translocation between 1q and 12q [2]. Malignant salivary gland epithelial–myoepithelial tumours usually show deletions at the long arm of chromosome 6 [10]. In addition, adenoid cystic carcinoma is characterised by structural alterations in chromosomes 6q and 9p. Polymorphous low-grade adenocarcinoma shares the 12q alteration found in pleomorphic adenoma and the alterations in chromosomes 6 and 9 that characterise adenoid cystic carcinoma [3, 8]. Cytogenetic data reported to date are limited to benign or to slowly growing malignant epithelial–myoepithelial salivary gland tumours.

The case described here was a highly aggressive tumour, harbouring early local and distant metastases and causing the death of the patient. On histology, immunohistochemistry and ultrastructural analysis, it was composed of poorly differentiated cells, showing features of myoepithelial cell differentiation; thus, it was diagnosed as pure MCC. Cytogenetic analysis showed different alterations from those described in benign and low-grade malignancy cases. Specifically, the primary tumour showed alterations in chromosomes 3 and 17.

Losses at 17p have been previously described, by comparative genomic hybridization, in MCC of the breast [5] showing aggressive behaviour. Alterations in chromosome 17 have been rarely documented in salivary gland tumours. In adenoid cystic carcinomas, Martins et al. [8] reported rearrangements in 17p12-p13, while Roijer et al. [11] described a del(17)(p13). Interestingly, the two cases of Martins et al. [8], showing alterations of chromosome 17, gave lung metastases, while in the case of Roijer et al. [11], the patient was alive and well, but after only a 1-year follow-up. Loss of chromosome 17 has been described as an early event in the malignant transformation of pleomorphic adenoma [6]. The tumour suppressor gene TP53 is localised on chromosome 17. Deletions or loss of heterozygosity in 17p might be accompanied by overexpression of the p53 protein detected by immunohistochemistry. In the present case, the p53 antibody strongly stained all the neoplastic nuclei of the primary and metastatic MCC. p53 Protein accumulation has been detected also in pleomorphic adenomas with malignant transformation [6].

Alterations on chromomosome 3 have been rarely described in salivary gland tumours [4]. They might involve the TP63 gene. TP63 is a recently recognised member of the p53 gene family, localised at chromosome 3q27–28. TP63 gives two main isoforms, TAp63/p51 and ΔNp63 /p73L. TAp63/p51, through bindings with p53 gene interaction domains, induces growth suppression and apoptosis, while ΔNp63/p73L favours cell proliferation by inhibiting the transactivating activity of TAp63/p51. The p63 protein is localised in nuclei of basal and myoepithelial cells of salivary glands and breast and is expressed in myoepithelial tumours of the breast [1].

Weber et al. [13] studied TP53 mutations and p63 expression in a series of benign salivary gland tumours. They found a TP53 mutated gene in 4 of 42 pleomorphic adenomas, 3 of 12 myoepitheliomas and 1 of 8 canalicular adenomas. The same types of tumours showed a dominant expression of the ΔNp63 isoform, leading to the hypothesis that these findings might reflect the possible malignant potential of the lesion.

Although MCC can be histologically classified as high- and low-grade malignant tumours, histology is not always predictive of the clinical outcome of the single case [12].

The data previously published in the literature together with the present cytogenetic findings suggest that alterations in chromosomes 3 and 17 could be an important step in the malignant transformation of basal/myoepithelial cells. Subsequent studies on larger series will establish whether they are predictive of poor clinical outcome.

Acknowledgements Prof. Vincenzo Eusebi is thanked for having critically reviewed the paper, Mrs. Luciana Muzzi for technical help. The study has been supported by grants from the University of Bologna.

References

1. Barbareschi M, Pecciarini L, Cangi MG, Macri E, Rizzo A, Viale G, Doglioni C (2001) p63, a p53 homologue, is a selective nuclear marker of myoepithelial cells of the human breast. Am J Surg Pathol 25:1054–1060
2. El-Naggar AK, Lovell M, Callender DL, Ordonez N, Killary M (1999) Cytogenetic analysis of a primary salivary gland myoepithelioma. Cancer Genet Cytogenet 113:49–53
3. El-Naggar AK, Lovell M, Callender DL, Killary AM (1999) Limited non-random chromosomal aberrations in a recurrent

adenoid cystic carcinoma of the parotid gland. Cancer Genet Cytogenet 106:66–69
4. Jin C, Martins C, Jin Y, Wiegant J, Wennerberg J, Dictor M, Gisseksson D, Strombeck B, Fonseca I, Mitelman F, Tanke HJ Hoglund M, Mertens F (2001) Characterization of chromosome aberrations in salivary gland tumors by FISH, including multicolor COBRA-FISH. Genes Chromosomes Cancer 30:161–167
5. Jones C, Foschini MP, Chaggar R, Lu YJ, Wells D, Shipley JM, Eusebi V, Lakhani SR (2000) Comparative genomic hybridization analysis of myoepithelial carcinoma of the breast. Lab Invest 60:831–836
6. Li X, Tsuji T, Wen S, Mimura Y, Sasaki K, Shinozaki F (1997) Detection of numeric abnormalities of chromosome 17 and p53 deletions by fluorescence in situ hybridization in pleomorphic adenomas and carcinomas in pleomorphic adenoma. Correlation with p53 expression. Cancer 79:2314–2319
7. Limon J, Dal Cin P, Sandberg A (1986) Application of long-term collagenase disaggregation for the cytogenetic analysis of human solid tumors. Cancer Genet Cytogenet 23:305–313
8. Martins C, Fonseca I, Roque L, Riberio C, Soares J (2001) Cytogenetic similarities between two types of salivary gland carcinoma: adenoid cystic carcinoma and polymorphous low-grade adenocarcinoma. Cancer Genet Cytogenet 128:130–136
9. Mitelman F (ed) (1995) ISCN, An International system for human cytogenetic nomenclature. Basel, Karger
10. Mitelman F (1998) Catalog of chromosome aberrations in cancer, 6th edn. Wiley-Liss, New York
11. Röijer R, Dahlenfors J, Mark J, Stenman G (1997) Observations by chromosome banding, FISH and immunohistochemistry in an adenoid cystic carcinoma with del (17)(p13) as the sole deviation. Virchows Arch 430:339–342
12. Savera AT, Sloman A, Huvos AG, Klimstra DS (2000) Myoepithelial carcinoma of the salivary glands. A clinicopathologic study of 25 patients. Am J Surg Pathol 24:761–774
13. Weber A, Langhanki L, Schutz A, Gerstner A, Bootz F, Wittekind C, Tannapfel A (2002) Expression profiles of p53, p63, and p73 in benign salivary gland tumors. Virchows Arch 441:428–436

Virchows Arch (2004) 444:87–89
DOI 10.1007/s00428-003-0917-9

CASE REPORT

Annette Zimpfer · Albert Propst · Gregor Mikuz · Wolfgang Vogel · Luigi Terracciano · Sylvia Stadlmann

Ciprofloxacin-induced acute liver injury: case report and review of literature

Received: 18 July 2003 / Accepted: 19 September 2003 / Published online: 8 November 2003

Abstract Ciprofloxacin is a fluorinated quinolone antibiotic with relatively low occurrence of adverse side effects. However, increasing evidence suggests that ciprofloxacin may cause severe liver damage. Until now, 14 cases of ciprofloxacin-associated liver injuries have been reported. We describe a case of a 22-year-old male who developed hepatic failure after intake of ciprofloxacin. The patient had been treated with 2×250 mg ciprofloxacin per day. He presented with symptoms of acute liver failure 14 days later. Liver biopsy revealed extensive hepatocellular necrosis involving zones 3 and 2 of hepatic acini and a mixed inflammatory infiltration containing abundant eosinophils. Symptoms resolved after corticoidsteroid therapy. In the present paper, we report the clinico-pathological characteristics of a case of ciprofloxacin-associated acute hepatic failure and discuss the current literature.

Keywords Quinolone · Ciprofloxacin · Hepatitis · Liver injury

Introduction

Ciprofloxacin is a fluorinated quinolone antibiotic with a broad spectrum of activity. Its indication includes treatment of the urinary tract, bone and joint, lower respiratory tract, and skin infections. However, despite its high effectiveness and relative safety, several cases of ciprofloxacin-associated liver injury have recently been described [1, 2, 3, 4, 5, 6, 7, 8, 9, 10, 11, 13, 14, 17]. In the present paper, we report the clinico-pathological characteristics of a case of ciprofloxacin-associated acute hepatic failure and discuss the current literature.

A. Zimpfer · L. Terracciano
Institute of Pathology, University of Basel,
Schoenbeinstrasse 40, 4003 Basel, Switzerland

A. Propst · W. Vogel
Department of Gastroenterology and Hepatology,
University Hospital Innsbruck,
Anichstrasse 35, 6020 Innsbruck, Austria

G. Mikuz · S. Stadlmann (✉)
Institute of Pathology, University of Innsbruck,
Muellerstrasse 44, 6020 Innsbruck, Austria
e-mail: sylvia.stadlmann@uibk.ac.at
Tel.: +43-512-5073657
Fax: +43-512-582088

Case report

A 22-year-old man had been treated with ciprofloxacin at a daily dose of 2×250 mg for 7 days during a non-specific bacterial infection of the skin. After 14 days of ciprofloxacin intake, the patient was admitted to hospital because of nausea and jaundice. There was no history of liver disease, blood transfusion, alcohol, or other medication. An ultrasound of the abdomen revealed no obstruction of the common bile duct and no hepato- or splenomegaly. Laboratory findings showed the typical pattern of acute liver failure with elevated serum transaminases [aspartate aminotransferase (AST) 907 U/l; alanin aminotransferase (ALT) 890 U/l], and alkaline phosphatase (AP 180 U/l), gamma-glutamyltransferase (γGT 73), reduced prothrombin (PT)-time (40%), and elevated serum bilirubine (16.9 mg/dl). Serology for hepatitis A, B, C, cytomegalovirus (CMV), adenovirus, HIV1, 2, and cocksackievirus were negative. Epstein-Barr virus (EBV), herpes simplex, and varicella anti-IgM were negative with positive anti-IgG titers. Autoimmune hepatitis and autoimmune cholangiopathy as well as metabolic liver diseases were excluded based on normal anti-IgM and negative antinuclear antibody (ANA), antimitochondrial antibody (AMA), and antineutrophil cytoplasmic antibody (ANCA) titers. Blood count showed mild leukocytosis with lymphopenia (10.5%) and elevation of neutrophils (56.5%), but no eosinophilia. Liver biopsy revealed extensive hepatocellular necrosis predominantly involving zones 3 and 2 of hepatic acini and a moderate mixed inflammatory infiltration of portal tracts and necrotic areas with abundant eosinophilic granulocytes (Fig. 1A, B).

A diagnosis of ciprofloxacin-associated hepatitis was rendered, and the patient was put on steroids. The treatment consisted of methylprednisolone at a daily dose of 50 mg for 7 days followed by slow tapering to a maintenance dose of 10 mg daily. Liver function tests and levels of AST and ALT improved rapidly, reaching normal levels within 1 week. The patient could be discharged in a clinically asymptomatic condition 8 days after admission.

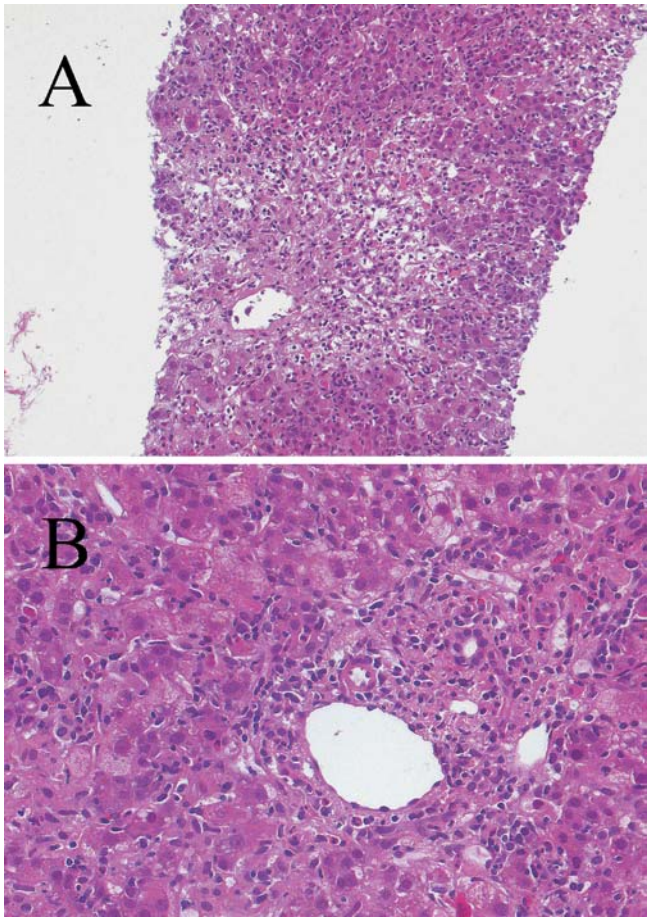

Fig. 1 **A, B** Liver biopsy shows confluent necrosis involving zones 3 and 2 of the acini (hematoxylin & eosin, original magnification ×4, ×10). In the necrotic areas and in the portal tracts, a mixed inflammatory infiltrate with abundant eosinophils can be recognized. Numerous acidophilic bodies are seen in zone 1 of the hepatic acini (hematoxylin & eosin, original magnification ×10, ×20)

Discussion

Ciprofloxacin is a widely used, broad-spectrum antibiotic that is generally associated with mild, reversible elevation of liver enzymes and bilirubin in about 2–3% of patients [15]. However, increasing evidence suggests that ciprofloxacin may also cause severe liver damage. Up to now, 14 cases of ciprofloxacin-associated liver injury have been documented in the literature (Table 1). Eight (57.1%) of the patients were men and six (42.9%) were women. This corresponds to a male to female ratio of 1.3, with an age of 23 years to 92 years at the time of diagnosis (mean 54.9±22.5 years). The time between initiation of ciprofloxacin and acute hepatic injury ranged from 1 day to 21 days (mean 6.3±5.9 days). In addition, one case of chronic cholestatic liver disease, occurring approximately 6.5 months after treatment with ciprofloxacin and ornidazol, has been documented in the literature [3]. In only two cases reported thus far, a direct association of liver injury and ciprofloxacin exposure has been proved [2, 10]. In all other cases, there were other medications involved, which prevented a clear relation between ciprofloxacin and hepatotoxicity. All patients rapidly improved after cessation of ciprofloxacin, except for two cases where ciprofloxacin-intake resulted in fulminant hepatitis and death. Based on the current literature, it seems that ciprofloxacin can cause three characteristic histological patterns of hepatic injury: (a) pure hepatocellular cholestasis, (b) hepatocellular necrosis of zone 3, or (c) a mixed pattern disease (Table 1). In the present report, we describe a case of ciprofloxacin-induced acute hepatitis with extensive hepatocellular necrosis and a mixed inflammatory infiltrate with abundant eosinophils. Similar to the majority of cases reported in the literature, the clinical course of our patient improved rapidly after corticosteroid therapy and cessation of ciprofloxacin. Unfortunately, only two cases of unequivocal ciprofloxacin-related liver injury have been documented thus far (Table 1); whereas, in all other cases,

Table 1 Clinico-pathological findings of reported cases of ciprofloxacin-associated liver injury. *NA* not available

Case no.	Age	Sex	Daily dose (mg)	Previous exposure	Other medications	Time to liver injury (days)	Previous liver injury	Histology	Follow-up	References
1	23	Female	NA	NA	NA	NA	NA	NA	NA	[4]
2	66	Male	1000	NA	Yes	2	No	Centrilobular necrosis	Died	[8]
3	46	Female	NA	NA	Yes	NA	No	NA	Recovered	[11]
4	92	Male	400	NA	Yes	2	No	NA	Died	[6]
5	84	Female	500	Yes	Yes	9	No	NA	Recovered	[13]
6	36	Male	1500	NA	Yes	7	No	NA	Recovered	[1]
7	27	Male	1500	No	No	10	No	NA	Recovered	[2]
8	50	Male	500	NA	NA	5	NA	Centrilobular cholestasis	Recovered	[9]
9	44	Female	500	NA	Yes	21	No	Centrilobular bridging necrosis	Recovered	[14]
10	47	Male	1000	NA	No	2	NA	Cholestasis and spotty necrosis	Recovered	[10]
11	32	Male	1000	NA	Yes	2	No	Periportal and centrilobular necrosis	Recovered	[5]
12	63	Female	500	NA	Yes	200	No	Fibrosing cholestatic hepatitis and spotty necrosis	Recovered	[3]
13	79	Female	500	NA	Yes	2	No	NA	Recovered	[7]
14	80	Male	1000	No	Yes	8	No	NA	Recovered	[17]

patients received additional drugs. Differences in morphological patterns of hepatic injury, therefore, may be due to mixed etiology. However, based on these data, a diagnosis of ciprofloxacin-induced hepatic injury should be favored if (a) the patient has a positive drug history (1–21 days), (b) liver biopsy reveals hepatocellular necrosis and/or cholestasis predominantly in zone 3 with a mixed inflammatory infiltrate containing eosinophils, and (c) serology is negative for viral or autoimmune hepatitis.

The pathomechanisms of ciprofloxacin-related liver injury are still unclear. The drug has been reported to exhibit in vitro cytotoxicity when incubated with rat hepatocytes at concentrations of 200 mg/ml, which corresponds to approximately 20 times the average human serum concentration [12]. Based on the available clinicopathologic observations, it appears likely that predominantly dose-independent idiosyncratic, and, more rarely, dose-dependent toxic reaction, may be involved [1, 2, 3, 4, 5, 6, 7, 8, 9, 10, 11, 13, 14, 17]. This, in fact, is supported by the relatively short delay between the initiation of ciprofloxacin and the development of liver injury in the majority of the reported cases [1, 2, 4, 5, 6, 7, 8, 9, 10, 11, 13, 14, 17]. The acute onset of disease and the lacking correlation between the dose and resulting liver damage suggests this type of drug reaction in our patient. The preferential zone-3 distribution of hepatic damage, in addition, suggests a possible involvement of the cytochrome P_{450} enzyme. The enzyme activity is highest in zone 3, and it has been shown that ciprofloxacin suppresses relevant cytochromes P_{450} at the transcription level [16].

Ciprofloxacin is still advertised as an effective and safe antibiotic. However, although quinolone antibiotic-related hepatic injury occurs infrequently, the consequences can be severe, and a detailed patient and drug history should be obtained in patients receiving ciprofloxacin.

References

1. Aggarwal A, Gurka J (1995) Probable ciprofloxacin induced cholestasis. Aust N Z J Med 25:541–542
2. Alcalde M, Donoso MS, Carcfa-Diaz M, Pascasio JM, Narvaez I (1995) Liver disfunction due to ciprofloxacin. Acta Gastroenterol Belg 58:475–476
3. Bataille L, Rahier J, Geubel A (2002) Delayed and prolonged cholestatic hepatitis with ductopenia after long-term ciprofloxacin therapy for Crohn's disease. J Hepatol 37:696–699
4. Benichou C (1992) Guide pratique de pharmacovigilance. Pradel, Paris, pp 195–196
5. Contreras MA, Luna R, Mulero J, Andreu JL (2001) Severe ciprofloxacin-induced acute hepatitis. Eur J Clin Microbiol Infect Dis 20:434–435
6. Fuchs S, Simon Z, Brezin M (1994) Fatal hepatic failure associated with ciprofloxacin. Lancet 343:738–739
7. Goetz M, Galle PR, Schwarting A (2003) Non-fatal acute liver injury possibly related to high-dose ciprofloxacin. Eur J Microbiol Infect Dis 22:294–296
8. Grassmick BK, Lehr VT, Sundareson AS (1992) Fulminant hepatic failure possibly related to ciprofloxacin. Ann Pharmacother 26:636–639
9. Hautekeete ML, Kockx MM, Naegels S, Holvoet JK, Hubens H, Kloppel G (1995) Cholestatic hepatitis related to quinolones: a report of two cases. J Hepatol 23:759–760
10. Labowitz JK, Silverman WB (1997) Cholestatic jaundice induced by ciprofloxacin. Dig Dis Sci 42:192–194
11. Levinson JR, Kumar A (1993) Ciprofloxacin induced cholestatic jaundice: a case report. Am J Gastroenterol 88:1619
12. Nordann P (1989) Cytotoxicity and uptake of pefloxacin, ciprofloxacin and ofloxacin in primary cultures of rat hepatocytes. J Chemother 24:355–363
13. Sherman O, Beizer JL (1994) Possible ciprofloxacin-induced acute cholestatic jaundice. Ann Pharmacother 28:1162–1164
14. Villeneuve JP, Davies C, Cote J (1995) Suspected ciprofloxacin-induced hepatotoxicity. Ann Pharmacother 29:257–259
15. Wolfson JS, Hooper DC (1991) Overview of fluoroquinolone safety. Am J Med 91:153–161
16. Xie HJ, Broberg U, Griskevicius L, Lundgren S, Carlens S, Meurling PC, Rane A, Hassan M (2003) Alteration of pharmacokinetics of cyclophosphamide and suppression of the cytochrome P450 genes by ciprofloxacin. Bone Marrow Transplant 31:197–203
17. Zaidi SA (2003) Hepatitis associated with amoxicillin/clavulanic acid and/or ciprofloxacin. Am J Med Sci 325:31–33

Virchows Arch (2004) 444:90–91
DOI 10.1007/s00428-003-0924-x

LETTER TO THE EDITOR

Dimas Suarez-Vilela · Francisco Miguel Izquierdo-Garcia · José Luis Olcoz-Goñi

Sinus histiocytosis with massive lymphadenopathy and giant cell hepatitis. An unreported association

Received: 9 July 2003 / Accepted: 8 October 2003 / Published online: 18 November 2003

Sir, We report a case of sinus histiocytosis with massive lymphadenopathy (SHML) associated with giant cell hepatitis, probably of autoimmune origin, in an 18-year-old man. SHML is a rare histiocytic proliferative disorder of unknown origin. This disease is not always limited to lymph nodes, but it could also involve a wide spectrum of extranodal sites [4]. SHML has also been reported in patients with immunodisorders [3, 4, 8]. However, in our review of the literature, we have not found any case of this entity associated with post-infantile giant cell hepatitis (PIGCH). This patient was treated with corticoids, and he had a good clinical response; the serum studies of the hepatic enzymes became normal, and the nodes decreased in size.

Our patient was an 18-year-old white man with a clinical history of asthma, hypersensitivity to pirazolone, and a probable episode of acute hepatitis when he was 8 years old. In February 1993, he was operated on in another hospital for leg varix, and 3 days later he suffered choluria and jaundice, and an increase of serum glutamic oxaloacetic transaminase (SGOT) and serum glutamic pyruvic transaminase (SGPT) above 1000 UI/l was found at that time. The levels of the enzymes decreased progressively, but they were still not normal after 6 months, and the patient was sent to the Department of Internal Medicine of our hospital. On clinical examination, multiple small, peripheral, enlarged lymph nodes, light hepatomegalia, and moderate splenomegalia were found. Serum studies results were: SGOT 42 UI/l, SGPT 91 UI/l, alkaline phosphatase 453 UI/l, total bilirubin 1.91 mg/1 dl. The hemogram and proteins were normal. Tests for A, B, C hepatitis (HAV, HBV, HCV), Epstein-Barr (E. Barr), herpes simplex, parainfluenza, rubella, mumps viruses, human immunodeficiency virus (HIV), and cytomegalovirus (CMV) were negative. Anti-smooth-muscle antibodies were positive at a dilution of 1/80. Other autoantibodies were negative. After the findings of both node and hepatic biopsies, a treatment with 10 mg/day of prednisone was started. The serum levels of the hepatic enzymes became normal, and the nodes decreased in size, but the splenomegalia persisted. The patient was lost for follow-up 1 year later.

The biopsy of a laterocervical lymph node showed expanded sinuses filled by numerous histiocytes with round or oval vesicular nuclei and small nucleoli. The cytoplasm of the majority of the histiocytes was abundant and pale pink, with indistinct margins. Many of them contained in their cytoplasms well-preserved lymphocytes and some isolated plasma cells and neutrophils (Fig. 1). Mitotic figures were infrequent. The cytoplasm of these

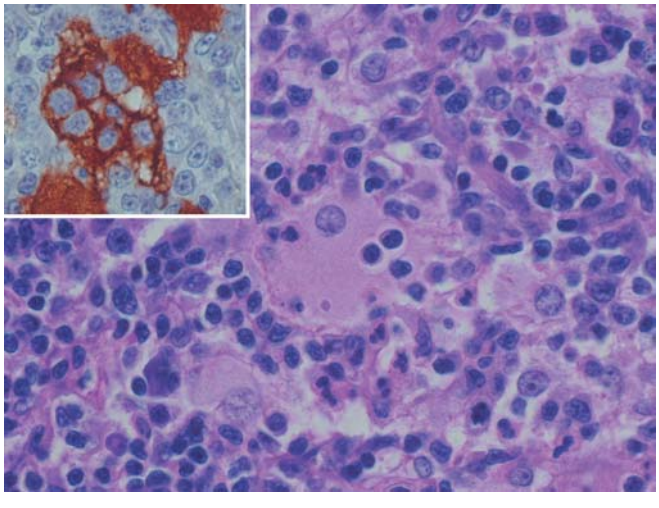

Fig. 1 Histiocytic cells with vesiculous nuclei. Lymphocytes inside vacuoles are found in their cytoplasms. Intense cytoplasmic reactivity of the histiocytes for s-100 protein (*inset*). With this staining, the lymphophagocytosis is more remarkable

D. Suarez-Vilela (✉) · F. M. Izquierdo-Garcia
Servicio de Anatomía Patológica,
Hospital de León,
Altos de la Nava s/n, 24008-León, Spain
e-mail: pacoizq20@hotmail.com
Tel.: +34-98-7237400

J. L. Olcoz-Goñi
Gastroenterology Departament,
Hospital de León,
Altos de la Nava s/n, 24008-León, Spain

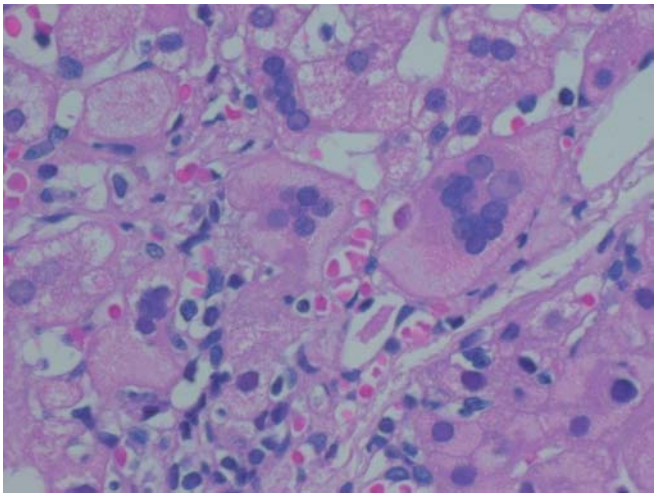

Fig. 2 Giant cell transformation of hepatocytes

cells stained for S-100 protein (Biogenex) (Fig. 1), CD68 (KP1) (Dako), lisozyme (Biogenex), α-1-antitrypsin (Biogenex), α-1-antichymotrypsin (Biogenex), (MAC-387) (Immustain), CD30 (Dako), peaunut lectin (Kem-en-Tec), and concanavalin A lectin (Kem-en-Tec). They were negative for CD1a (Serotec).

On the liver biopsy, the general architecture was preserved, with lymphoid infiltrates in portal areas, but both interface hepatitis and ductal damage were not found. In the plates of hepatocytes, there was extensive giant cell transformation, mainly in the areas III of Rappaport. The syncytial hepatocytes contained between six and ten nuclei, without mitosis (Fig. 2). Hepatocellular necrotic changes were light, with scanty inflammation. Both portal and lobular fibrosis were not found. Canalicular cholestasis was focally present. There was no evidence of histiocytic infiltrates, as those of the lymph node.

The histological findings of the lymph node correspond to SHML and those of the liver to giant cell hepatitis. SHML, or Rosai-Dorfman disease, is a disorder of histiocytic elements that usually affects young patients and is a little more common in males [4]. This disease may be purely nodal, but extranodal involvement may be found in 40% of the cases [4], affecting principally bone, skin, soft tissue, central nervous system, eye, salivary glands, respiratory tract, and the genitourinary system. The digestive system is affected exceptionally, [4, 6] and only five cases have been described in the liver [1, 4, 6]. The histological findings of SHML in liver are typical of the disease with portal, lobular, or nodular infiltrates of histiocytic cells with lymphophagocytosis. In no case of SHML with hepatic involvement have syncytial multinucleated cells, as those found in this case, been described. The etiology of SHML is not clear, and several pathogenetic mechanisms have been proposed, such as herpes virus 6 infection [7], or immune alterations [3, 4, 8]. Related to this latter aspect, it is known that around 10% of the cases of SHML coexist with immune-mediated diseases as autoantibodies-mediated anemia, arthritis, glomerulonephritis, juvenile diabetes, asthma, or repetitive infections [3, 4].

Giant cell hepatitis is a frequent pattern of liver injury in the neonate, but it is rare after infancy. In adult patients, giant cell hepatitis has been attributed to infections by different viruses (HAV, HBV, HCV, CMV, E. Barr, HIV, Paramixovirus), drug reactions or autoimmune disease [2, 5, 9]. Overall evidence of autoimmune disease was found in 40% of the patients [2]. It would appear that PIGCH is best regarded as an unusual reaction pattern that can occur in both acute and chronic hepatitis. In this case, the serum studies for virus was negative, and there was no evidence of therapy with any drugs related to PIGHC. The clinical history of asthma and hypersensitivity, the finding of anti-smooth muscle antibodies, and the good response to corticoids are in favor of an autoimmune etiology for the giant cell hepatitis of this patient.

To our knowledge, the association of SHML and PIGCH has not been previously described. In this case, the simultaneous presentation of these two entities could be not purely coincidental, and it raises the possibility of a common pathogenetic way, probably related to immunologic disorders.

Acknowledgements We thank very sincerely Dr. J. Rosai for studying the case and confirming the diagnosis and Dr. S. Salas-Valién for photographic and informatic assistance.

References

1. Buchino JJ, Byrd RP, Kemtz DR (1982) Disseminated Sinus histiocytosis with massive lymphadenopathy: its pathologic aspects. Arch Pathol Lab Med 106:13–16
2. Devaney K, Goodman ZD, Ishak KG (1992) Postinfantile giant-cell transformation in hepatitis. Hepatology 16:327–333
3. Foucar E, Rosai J, Dorfman RF, Eyman JM (1984) Immunologic abnormalities and their significance in sinus histiocytosis with massive lymphadenopathy. Am J Clin Pathol 82:515–525
4. Foucar E, Rosai J, Dorfman R (1990) Sinus histiocytosis with massive lymphadenopathy (Rosai-Dorfman disease): review of the entity. Semin Diagn Pathol 7:19–73
5. Johnson SJ, Mathew J, MacSween RNM, Bennett MK, Burt AD (1994) Post-infantile giant cell hepatitis: histological and immunhistochemical study. J Clin Pathol 47:1022–1027
6. Lauwers GY, Perez-Atayde A, Dorfman RF, Rosai J (2000) The digestive system manifestations of Rosai-Dorfman disease (Sinus histiocytosis with massive lymphadenopathy): review of 11 cases. Hum Pathol 31:380–385
7. Levine PH, Jahan N, Murari P, Manak M, Jaffe ES (1992) Detection of human herpes virus 6 in tissues involved by sinus histiocytosis with massive lymphadenopathy (Rosai-Dorfman disease). J Infect Dis 166:291–295
8. Maennle DL, Grierson HL, Gnarra DG, Weisenburger DD (1991) Sinus histiocytosis with massive lymphadenopathy: a spectrum of disease associated with immune dysfunction. Pediatr Pathol 11:399–412
9. Philips MJ, Blendis LM, Poucel S, Patterson J, Petric M, Roberts E, Levy GA, Superina RA, Greig PD, Cameron R, Langer B, Purcell RH (1991) Syncytial giant-cell hepatitis. Sporadic hepatitis with distinctive pathological features, a severe clinical course and paramixoviral features. N Engl J Med 324:455–460

Virchows Arch (2004) 444:92–94
DOI 10.1007/s00428-003-0916-x

LETTER TO THE EDITOR

A. Brunner · A. Tzankov · T. Akkad · K. Lhotta · G. Bartsch · G. Mikuz

Wegener's granulomatosis presenting with gross hematuria due to prostatitis

Received: 7 July 2003 / Accepted: 19 September 2003 / Published online: 24 October 2003

Sir, Wegener's granulomatosis (WG) represents a systemic vasculitis usually affecting the upper respiratory tract (74%), lungs (70%) and kidneys (46%) and affecting men and women equally, with a peak occurrence during the fifth and sixth decades of life [4, 5]. The etiology is unknown, but generation of anti-neutrophil cytoplasmic antibodies (c-ANCA) and activation of cellular response probably triggered by a preceding infection are discussed [1]. The diagnosis of WG should be made considering clinical presentation, histological findings in biopsy specimens and measurement of c-ANCA, which are highly specific [4]. Histologically, "dirty" liquefactive and/or coagulative necroses with a large number of eosinophilic granulocytes, scanty lymphocytes, plasma cells and multinucleated giant cells associated with a destructive leukocytoclastic vasculitis of arteries and veins are usually found in the lesions of the upper airways and lungs [5]. Renal disease includes focal necrotizing glomerulonephritis or interstitial nephritis [2, 5]. Clinically, WG presents with symptoms of the upper and lower respiratory tract, including nasal obstruction, discharge, ulcers, sinusitis or otitis, cough, hemoptysis and dyspnea, often associated with a progressive loss of renal function with microhematuria, nephritic urine sediment, moderate proteinuria up to rapidly progressive renal failure and systemic symptoms such as fever, weight loss and sweats [5].

We report the case of a 51-year-old man who was admitted to our hospital in September 1996 with a 3-month history of gross hematuria and mild dysuria. The patient claimed to have increasing weakness, sweats and weight loss as well as subfebrile temperatures. For the previous 3 weeks, the patient had arthralgias in the large joints and suffered from tinnitus accompanied by a hearing loss. The patient's blood pressure was 115/89 mmHg. He had a Horner syndrome on the right eye and chronic seromucinous otitis media. Chest X-ray remained inconspicuous. Magnetic resonance scan revealed increased contrast medium storage in the mastoid bone, the frontal and maxillar sinus on the left side consistent with an inflammatory process. Except for leukocytosis, increased C-reactive protein (10.64 mg/ml) and a serum creatinine of 0.9 mg/dl, laboratory parameters were unremarkable. Urine analysis revealed leukocyturia (75 leukocytes/μl), gross hematuria (250 erythrocytes/μl) but no proteinuria. Urine sediment contained a few hyaline and cellular casts. Urine cultures remained sterile. c-ANCA titer was 1:20. The diagnosis of WG was made and a renal biopsy was performed to determine the extent of renal involvement, revealing just a scarce interstitial chronic inflammatory infiltrate with normal glomeruli. The patient was referred to the urologist for further examination of gross hematuria. On digital rectal examination, the prostate was firm. Cystoscopy showed an inconspicuous bladder, but the prostatic tissue was extensively damaged with ulcers and paracollicular necrosis, suspicious for tuberculosis. Total serum prostate-specific antigen was 0.5 ng/ml. Prostate biopsy was performed, and histological examination revealed multiple granulomas with irregular, stellate and geographic necroses surrounded by histiocytes, lymphocytes, plasma cells and eosinophilic granulocytes (Fig. 1A, C). The center of the granulomas was filled with dirty, amorphous debris. The prostatic acini showed atrophic epithelium with scattered inflammatory infiltrate. A few small blood vessels were cuffed by histiocytes and granulocytes, indicating the presence of vasculitis (Fig. 1B, D). After special stains were performed, there was no evidence of infectious agents; thus, the histological appearance was consistent with the diagnosis of WG. The patient was given cyclophosphamide as well as

A. Brunner · A. Tzankov · G. Mikuz (✉)
Institute of Pathology, University of Innsbruck,
Muellerstrasse 44, 6020 Innsbruck, Austria
e-mail: gregor.mikuz@uibk.ac.at
Tel.: +43-512-5073650
Fax: +43-512-582088

T. Akkad · G. Bartsch
Department of Urology, University of Innsbruck, Austria

K. Lhotta
Department of Internal Medicine, University of Innsbruck, Austria

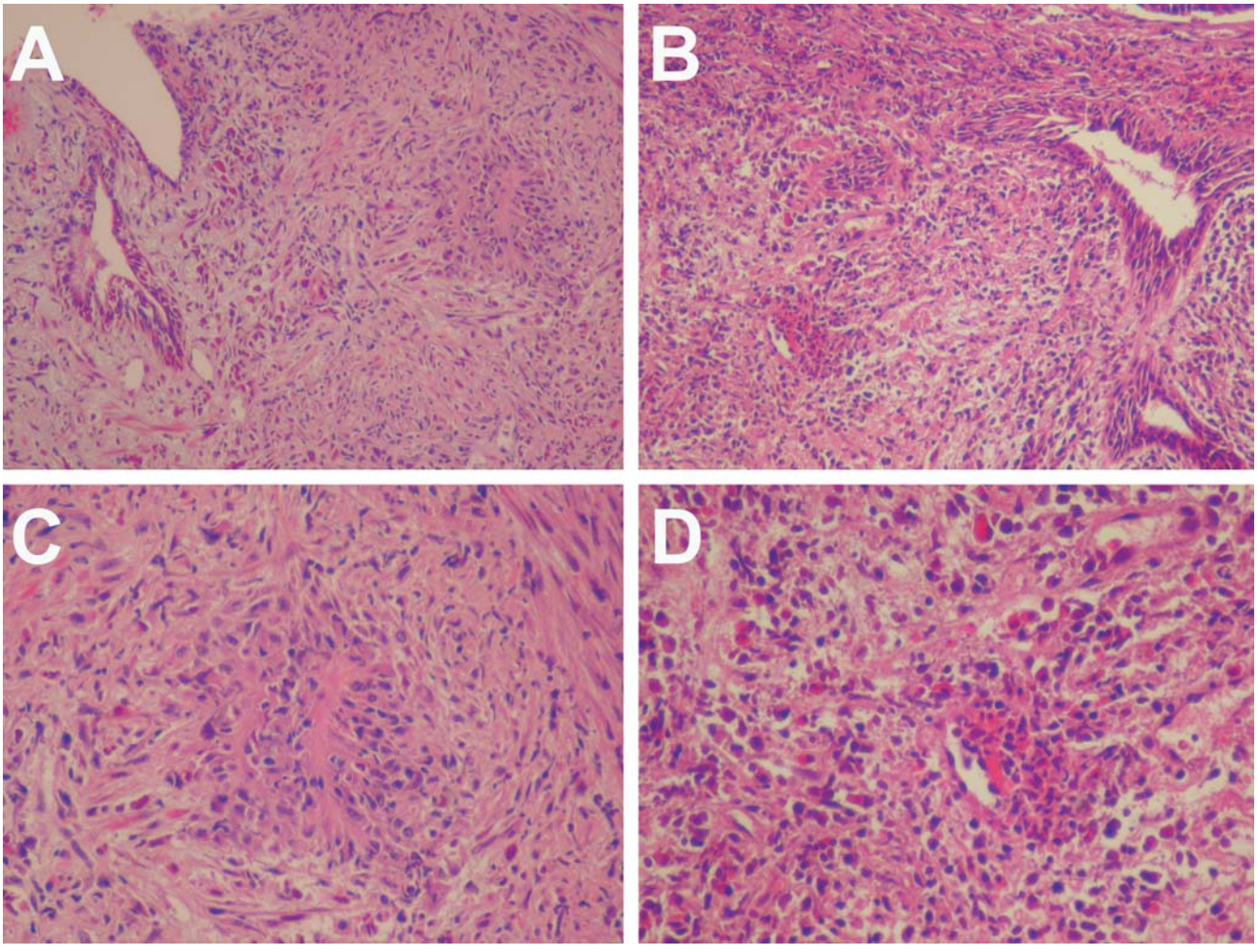

Fig. 1 Prostatic biopsy specimens showing granuloma formation surrounded by histiocytes, lymphocytes, plasma cells and eosinophilic granulocytes (**A** and **C**) as well as small blood vessels cuffed by inflammatory cells indicating vasculitis (**B** and **D**); hematoxylin & eosin stain, 200- and 400-fold magnification

corticosteroids so that symptoms quickly resolved. The patient is still in complete clinical disease remission under therapy with azathioprine 7 years after diagnosis.

WG may occasionally involve the lower urinary tract organs, such as the penis, testes, seminal vesicles and bladder in a decreasing order of frequency [3]. Prostatic involvement in WG is uncommon. In a series of 54 WG patients, Walton and co-authors found prostatic involvement in 7.4% of the cases [5]. Another series from the Mayo clinic reported that 4 of 174 patients (2.3%) with WG had prostatic disease [5]. Only a few cases with symptoms of prostatitis at initial presentation have been reported thus far [3, 4]. However, considering granulomatous prostatitis in a series of 200 cases reported by Stillwell and co-authors, only 4 appeared to be a manifestation of WG [6]. The clinical course of WG of the prostate includes irritating voiding symptoms such as dysuria, urgency and frequency, hematuria and acute urinary retention, but patients mostly remain asymptomatic [5]. On physical examination, the prostate can be firm, enlarged and indurated. Prostatic urethra may appear abnormal on cystoscopy, showing friable and necrotic tissue [5]. Biopsy is necessary to establish the correct diagnosis, as it is difficult to distinguish WG of the prostate from other forms of granulomatous inflammation or prostatic cancer on physical examination [5]. In our case, a patient presented with typical symptoms of WG. Despite gross hematuria for several weeks, renal function was normal. Renal biopsy excluded necrotizing glomerulonephritis as the cause of hematuria. Urological examinations, including cystoscopy, detected a necrotizing prostatitis highly suspicious for tuberculosis. Biopsy specimens revealed a granulomatous process with dirty necroses. Ziehl-Neelsen, Grocott, Warthin-Starry and periodic acid-Schiff stains remained negative, so that a consistency with the primary diagnosis was concluded, and the applied immunosuppressive therapy was continued. This case is remarkable as it demonstrates that the correct classification of a granulomatous disease might be decisive for choosing the correct therapy. For correct

classification of granulomas, infectious agents such as *Mycobacterium tuberculosis*, mycobacteria other than tuberculosis, fungi and spirochetes, *Brucellaceae*, *Schistosomata* and *Echinococci* should be ruled out by special stains [3]. Furthermore, other non-infectious causes of granulomatous prostatitis, including transurethral resection, allergic and simple granulomatous prostatitis as well as sarcoidosis, should also be excluded [3, 6]. An accurate morphological examination enables further subspecification of the granulomas, even in cases where clinical history is unknown. Presence of dirty necrosis, large amount of eosinophilic granulocytes and vasculitis should draw a pathologist's attention to the rare possibility of a WG of the prostate.

References

1. Harper L, Savage CO (2000) Pathogenesis of ANCA associated systemic vasculitis. J Pathol 190:349–359
2. Hoffman GS, Kerr GS, Leavitt RY, Hallahan CW, Lebovics RS, Travis WD, Rottem M, Fauci AS (1992) Wegener's granulomatosis. An analysis of 158 patients. Ann Intern Med 116:488–498
3. Middleton G, Karp D, Lee E, Cush J (1994) Wegener's granulomatosis presenting as lower back pain with prostatitis and ureteral obstruction. J Rheumatology 21:566–556
4. Mundinger A, Pumpe K, Grosser G, Herbst EW, Grotz W, Kropelin T (1989) Primary manifestation of Wegener's granulomatosis of the prostate. Urologe 28:234–236
5. Stillwell TJ, DeRemee RA, McDonald TJ, Weiland LH, Engen DE (1987) Prostatic involvement in Wegener's granulomatosis. J Urol 138:1251–1253
6. Stillwell TJ, Engen DE, Farrow GM (1987) The clinical spectrum of granulomatous prostatitis: a report of 200 cases. J Urol 138:320–323

Virchows Arch (2004) 444:95–97
DOI 10.1007/s00428-003-0920-1

LETTER TO THE EDITOR

Tadashi Terada · Hiroaki Inatsuchi

Small juxtadrenal cellular schwannoma

Received: 3 September 2003 / Accepted: 30 September 2003 / Published online: 21 November 2003

Sir, adrenal and juxtadrenal schwannomas are exceedingly rare; only several case reports have been published in the English literature [1, 3, 4, 5, 6]. We herein report on a case of small juxtadrenal cellular schwannoma.

A 74-year-old Japanese woman presented with lumbago and was admitted to our hospital. Imaging modalities, including computed tomography and magnetic resonance imaging, revealed a right adrenal tumor measuring 20 mm in diameter. Angiography showed that the tumor was supplied by the right adrenal artery. A blood laboratory test, including various adrenal hormones, showed no remarkable abnormalities. Right adrenalectomy was performed under the clinical diagnosis of right adrenal tumor. No findings of von-Recklinghausen's disease were recognized.

Grossly, the resected specimen was a right adrenal gland with surrounding fat tissue. A tumor measuring 25×13×10 mm was present in the periadrenal fat tissue just next to the right adrenal gland (Fig. 1). The tumor was located in the vicinity of the adrenal gland, but not connected by the adrenal gland. The tumor was completely encapsulated, solid, white, and relatively hard in consistency.

Histologically, the tumor was completely encapsulated with fibrous tissue (Fig. 2a). Lymphoid tissue with germinal centers was present in and outside the capsule (Fig. 2a). The tumor was a solid cellular one, composed of spindle cells arranged in a fascicular pattern (Fig. 2b). Neither palisading pattern nor Verocay bodies were noted. Tumor cells showed myxoid appearances in one small area. No necrosis was noted. Cytologically, the tumor cells showed mild hyperchromasia, but mitotic figures were not recognized. Focal areas showed accumulation of foamy macrophages (Fig. 2c). Immunohistochemically, the tumor cells were positive for S-100 protein, vimentin, laminin, and type-IV collagen. They were negative for keratins, epithelial membrane antigen, chromogranin A, synaptophysin, alpha-smooth muscle antigen, and CD34. The Ki-67 labeling of tumor cells using MIB-1 antibody was 2%. The macrophages in the tumor were positive for CD68 (macrophage antigen). The capsule was positive for alpha-smooth muscle actin. The lymphoid tissue in the capsules was positive for CD3 (T cell marker) and CD20 (B cell marker). The pathological diagnosis was cellular schwannoma. The positive reactions of tumor cells for S-100 protein and basal lamina components (laminin and type-IV collagen) supported the schwann cell origin. The right adrenal gland was free of pathological alterations.

Schwannoma occurs largely in hand, neck, and extremities. Schwannoma of retroperitoneal tissue is rare, the incidence being from 0.5% to 1.2% of all benign

Fig. 1 Cut surface of the tumor (*arrow*) and right adrenal gland (*arrowheads*). The tumor is solid, encapsulated, and not connected to the adrenal gland. The adrenal gland is free of pathological alterations

T. Terada (✉)
Department of Pathology,
Shizuoka Municipal Shimizu Hospital,
Shimizu-Miyakami 1231, 424-8636 Shizuoka, Japan
Tel.: +81-54-3361111
Fax: +81-54-3361315

H. Inatsuchi
Department of Urology,
Shizuoka Municipal Shimizu Hospital,
Shizuoka, Japan

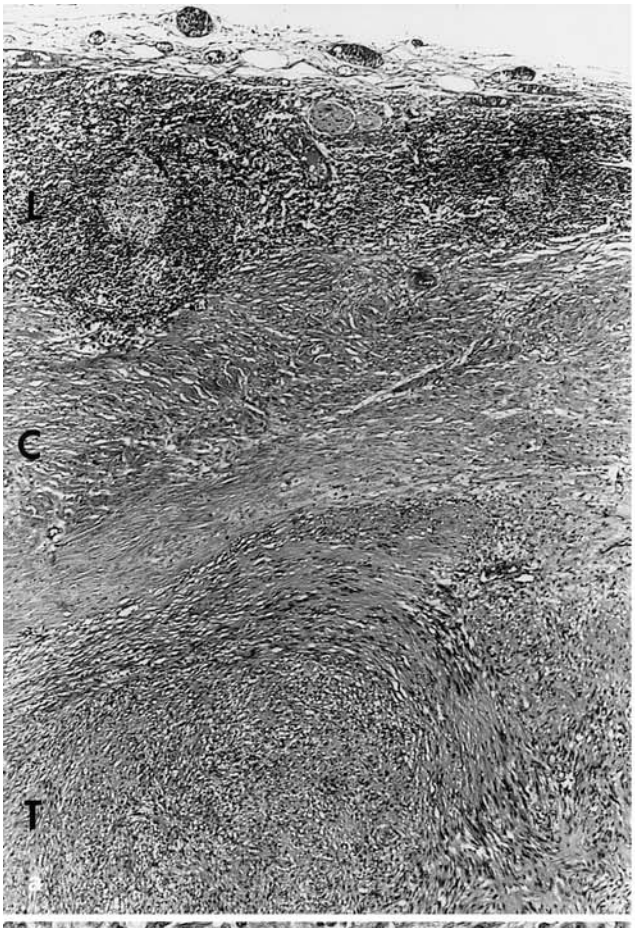
L
C
T

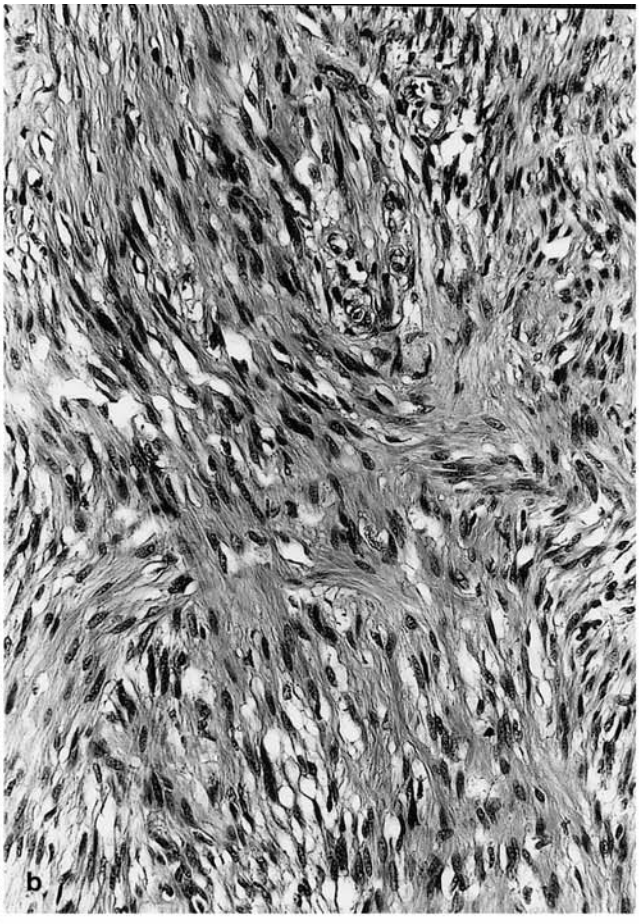
b

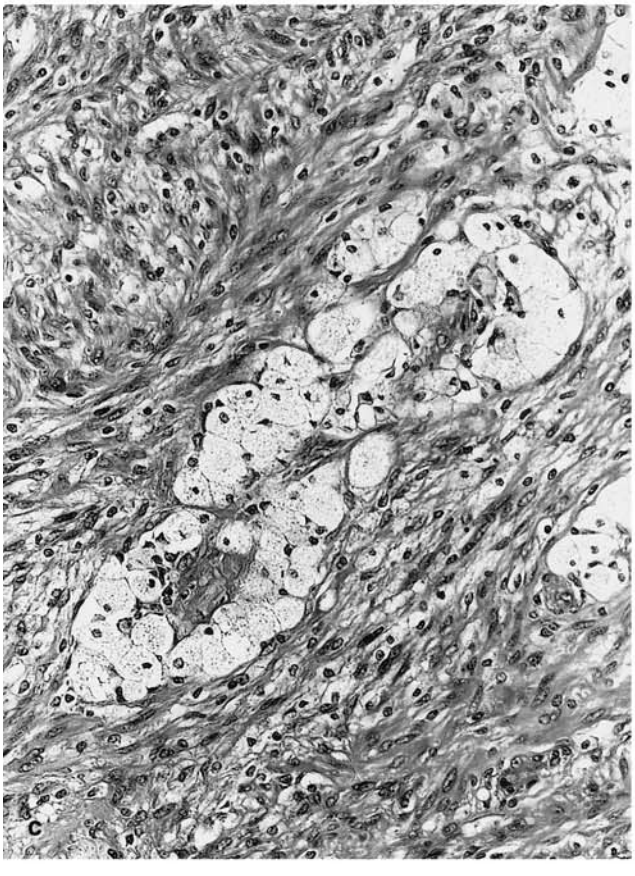
c

Fig. 2 **a** The periphery of the tumor. Lymphoid tissue (*L*) is noted in and outside the capsule (*C*). Tumor tissue (*T*) is seen inside the capsule. Hematoxylin & eosin (HE), ×20. **b** The tumor is mainly composed of spindle cells arranged in a fascicular pattern. Mitotic figures are not seen. HE, ×300. **c** Foamy macrophages in the tumor. HE, ×250

retroperitoneal tumors [3]. In particular, juxtadrenal schwannoma is exceedingly rare; only several cases have been reported in the English literature [1, 3, 4, 5, 6]. Most of them were preoperatively diagnosed as adrenal tumors and were supplied by the adrenal arteries [1, 3, 4, 5, 6], as was the case with the present case. Therefore, juxtadrenal schwannomas tend to be clinically mistaken for adrenal tumors. The present case was relatively small in size compared with previously reported cases [1, 3, 4, 5, 6], suggesting that recent advances in imaging modalities can detect small juxtadrenal schwannoma.

Cellular schwannoma is a variant of schwannoma and is characterized by cellular Antoni A type and rarity of nuclear palisading and Verocay bodies [7]. It is also characterized by the frequent presence of lymphoid tissue in the capsule and foamy macrophages in the tumor cells [7]. The presence of lymphoid tissue and foamy macrophages represents diagnostic criteria of cellular schwannoma [7]. Such features were recognized in the present tumor, confirming that the present tumor is cellular schwannoma. Behrend et al. [1] and Oliver et al. [5] also reported similar tumors of the juxtadrenal region.

Cellular schwannoma is occasionally misdiagnosed as malignant tumors, in particular, malignant peripheral nerve sheath tumors (MPNST) and leiomyosarcoma [2, 7]. MPNST show varied morphologies, such as glandular and epithelioid features, and may resemble cellular schwannoma. Well-differentiated leiomyosarcoma may also resemble cellular schwannoma. The most important differential diagnosis between cellular schwannoma and MPNST and leiomyosarcoma is the number of mitotic figures [2]. Peripheral nerve sheath tumors with mitotic figures greater than 1 per 20 high-power fields may be potentially malignant [2]. Smooth muscle tumors of retroperitoneum with mitotic figures greater than 1 per 10 high-power fields may show malignant potential [2]. Other features suggestive of malignancy are tumor size, necrosis, high cellularity, and nuclear atypia [2]. The present tumor is small and shows no mitotic figures, necrosis, or significant nuclear atypia. The low Ki-67 labeling in the present case also suggests benign nature. Therefore, the present tumor is not malignant.

The tumor capsule in the present case showed immunoreaction for alpha-smooth muscle actin. This phenomenon has not been reported in juxtadrenal schwannoma. This fact suggests that the capsule of the present tumor shows smooth muscle or myofibroblastic phenotypes. In summary, the authors presented a very rare case of small juxtadrenal cellular schwannoma clinically diagnosed as adrenal tumor.

References

1. Behrend M, Kaaden S, Von Wasielewski R, Frericks B (2003) Benign retroperitoneal schwannoma mimicking an adrenal mass. Surg Laparosc Endosc Percutan Tech 13:133–138
2. Brooks JJ (1994) Disorders of soft tissue. In: Sternberg SS (ed) Diagnostic surgical pathology, 2nd edn. Raven Press, New York, pp 147–229
3. Maeshima S, Nakamura H, Nishikawa M, Murakami T, Mitani T, Marukawa T, Hori S, Kozuka T, Irimoto M (1992) Retroperotoneal schwannoma simulating adrenal tumors. Clin Imaging 16:121–124
4. Nazli O, Cal C, Hekimgil M, Tuncyurek M (1998) Juxtadrenal schwannoma. Int Urol Nephrol 30:25–29
5. Oliver WR, Reddick RL, Gillespie GY, Siegal GP (1985) Juxtadrenal schwannoma: verification of the diagnosis by immunohistochemical and ultrastructural studies. J Surg Oncol 30:259–268
6. Pittasch D, Klose S, Schmitt J, Roessner A, Ridwelski K, Lippert H, Lehnert H (2000) Retroperitoneal schwannoma presenting as an adrenal mass. Exp Clin Endocrinol Diabetes 108:318–321
7. White W, Shiu MH, Rosenblum MK, Erlandson RA, Woodruff JM (1990) Cellular schwannoma: a clinicopathologic study of 57 patients and 58 tumors. Cancer 66:1266–1275

Virchows Arch (2004) 444:98
DOI 10.1007/s00428-003-0904-1

BOOK REVIEW

Kerstin Amann

"Renal fibrosis" by M.S. Razzaque

Karger, Basel, 2003 (ISBN 3-8055-7568-8)

Received: 4 August 2003 / Accepted: 26 August 2003 / Published online: 9 October 2003

Dear Sirs, thank you very much for giving me the opportunity to review the recently published book on renal fibrosis, edited by Claude Ronco, in the famous series, Contribution to Nephrology.

Due to recent advances in cell biology and animal pathophysiology, renal fibrosis has emerged as one of the most important and interesting issues in kidney research. Not only has it been shown that the extent of interstitial fibrosis is the most important determinant of kidney function, but we have also learned that various injuries to the kidney may end directly or indirectly in the common pathway of glomerular or interstitial fibrosis. In addition, several clinically important therapeutic agents in renal transplantation, such as cyclosporin A and FK506, are known to induce tubular damage and interstitial fibrosis, which have emerged as major players in long-term graft survival. This specific and clinically most relevant topic is nicely addressed in a separate chapter in the above-mentioned book.

The textbook on renal fibrosis is certainly focused on recent developments in the basic understanding of the pathogenesis of interstitial fibrosis, with a particular focus on causative factors, such as proteinuria, the molecular mechanisms underlying cell injury, the important roles and regulation of TGF-β, chemokines, signaling cascades via NF-kappa B, the role of oxidant stress and the regulation of extracellular matrix metabolism.

What one may possibly miss, however, is a chapter on other non-traditional factors that are known to be important in fibrosis and, in particular, in renal fibrosis, such as endothelin-1, for which excellent experimental and clinical evidence exists. Moreover, potential roles of other profibrogenic factors, such as CTGF or BMP-7 and its downstream signaling cascade, could have been discussed.

Personally, I would prefer to see some of the excellent schematic drawings in color. In addition, as a pathologist, I would like to encourage some of the authors to contact their pathologist to possibly help improve the quality of their photomicrographs.

Certainly, the book is written by leading experts in the field and is most interesting and worthwhile reading, in particular for those who have a deep interest in the pathogenesis of the mechanisms of renal fibrosis in general, but also in some specific disease conditions. As written in the preface, topic selection was performed according to the level of necessary information on the molecular basis of renal fibrosis (and this may explain the lack of more figures to illustrate the findings).

Given the complexity of the topic and the abundance of new information that has emerged in recent years on this particular field, I feel that the book has undertaken an enormous effort to bring together recent experimental in vitro and in vivo data and to clearly define what is important and what is probably only circumstantial. I would, therefore, highly recommend the book to all clinicians and scientists who are interested in a more detailed understanding of renal fibrosis than what is written in the current textbooks of either nephrology or pathology.

K. Amann (✉)
Department of Pathology,
University of Erlangen,
Krankenhausestrasse 8–10, 91054 Erlangen, Germany
e-mail: kerstin.amann@patho.imed.uni-erlangen.de

Virchows Arch (2004) 444:99–100
DOI 10.1007/s00428-003-0954-4

ACKNOWLEDGEMENT TO REFEREES

The Managing Editors are grateful to the following colleagues for generously giving their time in careful evaluation of the manuscripts submitted to *Virchows Archiv* in 2003:

Aguzzi A, Zürich (CH)
Aigner T, Erlangen (D)
Amann K, Erlangen (D)
Arbustini E, Pavia (IT)

Baccarini P, Bologna (IT)
Barbareschi M, Trento (IT)
Barth PJ, Marburg (D)
Berteau P, Paris (F)
Bertoni F, Bologna (IT)
Bisceglie M, S.G. Rotondo (IT)
Bode B, Zürich (CH)
Bohle RM, Gießen (D)
Bordi C, Parma (IT)
Borisch B, Genf (CH)
Bosman FT, Lausanne (CH)
Bostwick DG, Richmond (USA)
Bourgain C, Brüssel (B)
Bouwens L, Brussel (B)
Brambilla E, Grenoble (F)
Briner J, Aarau (CH)
Brinkmann B, Münster (D)
Bruneval P, Paris (F)
Bültmann BD, Tübingen (D)
Büttner R, Bonn (D)
Burg G, Zürich (CH)
Bussolati G, Torino (IT)

Capella C, Varese (IT)
Carcangiu ML, Milano (IT)
Cardesa A, Barcelona (SP)
Carneiro MF, Porto (P)
Cathomas G, Liestal (CH)
Capron F, Paris (F)
Cazals D, Clichy (F)
Chott A, Wien (AU)
Couvelard A, Clichy (F)

Damiani S, Bologna (IT)
Deckert M, Köln (D)
Deimling A v., Berlin (D)
Dei Tos AP, Treviso (IT)
Delling G, Hamburg (D)
Denk H, Graz (AU)
Denkert C, Berlin (D)
Derenzini M, Bologna (IT)
Desmouliere A, Bordeaux (F)
De Wolf-Peeters C, Leuven (B)
Diebold J, München (D)
Doglioni C, Belluno (IT)
Dombrowski F, Magdeburg (D)
Duong T, Paris (F)

Eble JN, Indianapolis (USA)
Ectors N, Leuven (B)
Emile JF, Boulogne (F)

Facchetti F, Brescia (IT)
Falk S, Frankfurt (D)
Faller G, Erlangen (D)
Feller AC, Lübeck (D)
Fend F, München (D)
Ferlicot S, Le Kremlin Bicêtre (F)
Fléjou JF, Paris (F)
Fletcher CDM, Boston (USA)
Foschini MP, Bologna (IT)

Gabbiani G, Genf (CH)
Garbisa S, Padova (IT)
Gerharz CD, Düsseldorf (D)
Goebel HH, Mainz (D)
Graf N, Homburg (D)
Gröne HJ, Heidelberg (D)
Guski H, Berlin (D)

Hailemariam S, Liestal (CH)
Hauptmann S, Halle (D)
Helpap B, Singen (D)
Hengartner H, Zürich (CH)
Höfler H, München (D)
Hofstädter F, Regensburg (D)
Horn LC, Leipzig (D)
Horny HP, Lübeck (D)
Housset C, Paris (F)

In't Veld P, Brüssel (B)

Jochum W, Zürich (CH)
Jundt G, Basel (CH)

Kadar A, Budapest (H)
Kalthoff H, Kiel (D)
Kempf W, Zürich (CH)
Kerjaschki D, Wien (AU)
Kern M, Köln (D)
Kleihues P, Lyon (F)
Klimpfinger M, Wien (AU)
Klimstra D, New York (USA)
Kommoss F, Mannheim (D)
Kos M, Zagreb (CR)
Kreipe H, Hannover (D)
Krenn V, Berlin (D)
Kristiansen G, Berlin (D)
Kurrer M, Zürich (CH)

Lamovec J, Ljubljana (SL)
Lax SF, Graz (AU)
Lazure T, Le Kremlin Bicêtre (F)
Lebail B, Bordeaux (F)
Lebeau A, München (D)
Lehto VP, Helsinki (FIN)
Lenzen S, Hannover (D)
Leoncini L, Siena (IT)
Leone O, Bologna (IT)
Leuschner I, Kiel (D)
Lloyd RV, Rochester (USA)
Löhr JM, Mannheim (D)
Löhrs U, München (D)
Löning T, Hamburg (D)
Longnecker DS, Lebanon (USA)
Lüttges J, Kiel (D)
Lumb, PD, Manchester (UK)

Magrini E, Bologna (IT)
Magro G, Catania (IT)
Matias-Guiu X, Barcelona (E)
McNicol AM, Glasgow (UK)
Mechtersheimer G, Heidelberg (D)
Mentzel T, Friedrichshafen (D)
Michal M, Pilsen (CZ)
Miettinen M, Washington (USA)
Mihatsch M, Basel (CH)
Mihic D, Zürich (CH)
Mikuz G, Innsbruck (AU)
Milde-Langosch K, Hamburg (D)
Millis R, Muldon (UK)
Moch H, Basel (CH)
Möller P, Ulm (D)
Molinie V, Suresnes (F)
Molina T, Paris (F)
Moll R, Marburg (D)
Montironi R, Ancona (IT)
Mori K, Shiga (JP)
Müller JG, Würzburg (D)

Müller KM, Bochum (D)
Müller-Hermelink KM, Würzbug (D)
Müller-Höcker J, München (D)
Mukai K, Tokyo (JP)
Mutter GL, Boston (USA)

Nannini R, Imola (IT)
Nerlich A, München (D)
Nesland JM, Oslo (N)
Nogales F, Granada (E)

Oberhuber G, Überlingen (D)
Odermatt B, Zürich (CH)
Oehmichen M, Kiel (D)
Offerhaus GJA, Amsterdam (NL)
Ott G, Würzburg (D)

Papotti M, Turin (IT)
Paradis V, Clichy (F)
Paraf F, Limoges (F)
Parchi P, Bologna (IT)
Parwaresch MR, Kiel (D)
Paulus W, Münster (D)
Perren A, Zürich (CH)
Pession A, Bologna (IT)
Pfaltz M, Zürich (CH)
Piard F, Dijon (F)
Pietsch T, Bonn (D)
Pileri S, Bologna (IT)
Popper HH, Graz (AU)
Poremba C, Düsseldorf (D)
Pour P, Omaha (USA)
Prat J, Barcelona (SP)

Raup U, Düsseldorf (D)
Reifenberger G, Hamburg (D)
Reiner A, Wien (AU)
Riethdorf L, Hamburg (D)
Röcken C, Magdeburg (D)
Roels H, Ghent (B)
Rosai J, Milano (IT)
Roth J, Zürich (CH)
Royer HD, Berlin (D)
Rudolph P, Kiel (D)
Rüschoff J, Kassel (D)
Ruiter DJ, Nijmegen (NL)

Saeger W, Hamburg (D)
Sapino A, Torino (IT)
Sarbia M, Düsseldorf (D)
Schirmacher P, Köln (D)
Schlüter E, Kiel (D)
Schmid KW, Essen (D)
Schmidt D, Mannheim (D)
Schmitt-Gräff A, Freiburg (D)
Schneider-Stock R, Magdeburg (D)
Schröder S, Hamburg (D)
Schulz A, Giessen (D)
Sciot R, Leuven (B)
Scoazec JY, Lyon (F)
Selves J, Toulouse (F)
Sessa F, Varese (IT)
Simpson R, Exeter (UK)
Sipos B, Kiel (D)
Slootweg PJ, Utrecht (NL)
Sobrinho-Simoes M, Porto (P)
Solcia E, Pavia (IT)
Stallmach T, Zürich (CH)

Stanta G, Triest (IT)
Stoerkel F, Wuppertal (D)
Stolte M, Bayreuth (D)
Sträter J, Ulm (D)
Suster S, Columbus (USA)

Tagliavini F, Milano (IT)
Tallini G, Bologna (IT)
Tannapfel A, Leipzig (D)
Tavassoli FA, New Haven (USA)
Terris B, Paris (F)
Tiene G, Padova (IT)
Tinguely M, Zürich (CH)
Toma V, Zürich (CH)
Tot T, Falun (SW)

van Marck E, Antwerpen (B)
Viale G, Milano (IT)
Vogt P, Zürich (CH)

Wardelmann E, Bonn (D)
Wassef M, Paris (F)
Wendum D, Paris (F)
Werner M, Freiburg (D)
Wernert N, Bonn (D)
Wiestler OD, Bonn (D)
Wittekind C, Leipzig (D)

Yagihashi S, Hirosaki (JP)

Zafrani ES, Créteil (F)
Zamboni G, Verona (IT)
Zimmermann D, Zürich (CH)

Virchows Arch (2004) 444:101–103
DOI 10.1007/s00428-003-0937-5

European Society of Pathology (ESP)

EXTRAORDINARY GENERAL ASSEMBLY

Day: Saturday, February 7, 2004,

Time: 15.30h. In the event of the General Assembly not being quorate a second General Assembly based on simple majority will be called for **16.00h**

Duration: about 2 hours.

Place: Palais des Congrès, Porte Maillot 75016, Paris – France

Agenda:

1. Welcome
2. Approval of agenda
3. Approval of the Minutes of the preceding General Assembly (Ljubljana, September 2003)
4. Report of the President
5. Approval of the adaptation to the Belgian law of the Statutes and By-laws already approved in the General Assembly of Berlin 2001
6. Announcement and consequences of the results of the ballot for election of President-elect (2003-2005)
7. Report of the Chairman of the Organizing Committee of the 20th ESP Congress, Paris 2005
8. Any other business

Antonio Cardesa
President

11–15 February 2004
Conference on "Clinical Oncology 2004/2005"

In cooperation with the National Oncology Societies, the Tumorzentrum Düsseldorf (Director: Prof. Dr. med. R. Haas) will be holding a five-day conference. The results will be published in a symposium volume for the conference. More than 800 experts, mainly from the field of oncology, are expected to attend. The workshop will be held in the MNR Clinic, Lecture Hall 13A. The following general topics have been scheduled:

Wednesday:
Pharynx, larynx, CUP syndrome, parotid gland, nasopharynx, skin tumors
Bier, Dummer, Ganzer, Roth, Ruzicka, Schmitt, Schulte, Stadler, Suter

Thursday:
Esophageal carcinoma, gastric carcinoma, colorectal carcinoma
Gabbert, Häussinger, Knöfel, Ramp, Röher, Röhrborn, Wettstein, Willich, Sauer

Friday:
Seminoma, urinary bladder carcinoma, prostatic carcinoma, renal cell carcinoma
Ackermann, Alberti, Alken, Bamberg, Fornara, Hartmann, Rübben, Vögeli, Wirth

Saturday:
NHL, Hodgkin's disease, ALL, AML, CML, multiple myeloma, bronchial carcinoma, thymona
Bentz, Böhner, Gattermann, Germing, Haas, Kobbe, Stilgenbauer, Schmitt

Sunday:
Mammary carcinoma: biology, new treatment standards
Bender, Dall, Gerber, Harbeck, Kaufmann, Mallmann, von Mickwitz, Nitz, Yarnold

Head of the organization team: Prof. Dr. Stephan Roth, Klinik für Strahlentherapie, Moorenstr. 5, Postfach 101007, 40001 Düsseldorf, Germany

The conference fee will be E30 per day.

The symposium volume published for the conference can be purchased for E20.

For further information, please contact:
Head of the organization team:
Prof. Dr. Stephan Roth
Klinik für Strahlentherapie
Heinrich-Heine-Universität
Moorenstr. 5
40225 Düsseldorf
Germany
Tel.: +49 (0)211 811 8989/7990
Fax: +49 (0)211 811 8051
e-mail: roth@med.uni-duesseldorf.de
www.uni-duessdorf.de/tumorzentrum

1–2 April 2004
Thyroid Pathology for the Practicing Pathologist
15 rue de l'Ecole de Médecine, Paris, France

Join us for a Springtime meeting in Paris!!
A 2-day course will take place in Paris under the auspices of the French Division of the I.A.P. This course will be given in English by Prof. M. Sobrinho-Simoes (Porto) and Prof. R. Heimann (Brussels).
It will consist of lectures alternating with slide reviews and a slide seminar over a multihead microscope. The slide seminar (on CD) will be sent before the meeting. The audience will be limited to 22 participants.
Course fee: 390 euros (320 euros for members of any IAP division). The fee includes registration, hand-out, CD of the slide seminar and coffee breaks.

For further information, please contact:
Mrs. M. Fontanière
Administrative Secretary
French Division of the I.A.P. 32 Cours Albert Thomas
69008, Lyon, France
Fax: 33478754311
E-mail: academie.pathologie@wanadoo.fr

9–12 May 2004
XIV EUROCELLPATH COURSE: The Impact of Proteomics and Genomics in Pathology
Girona, Spain

The Organising Committee of the next EuroCellPath Course invites you to come to the beautiful city of Girona to enjoy an outstanding program on a very timely topic, addressed by leading authorities in the field, in an inspiring setting. The subjects covered in this course will be the following:

- DNA arrays: Methods and Goals
- Tissue Microarrays: A Tool for Rapid, Efficient Translational Research
- Proteomics: From Genes to Functions
- Tissue Procurement and Handling: Laser Capture Microdissection and Other Techniques
- Bioinformatic Tools for Array Data Mining
- Application of Array Genomics and Proteomics in Pathology
- Molecular Pathology of Genes and Proteins: What to Look For and When.

You may also submit your abstracts on these or other related topics, to be presented either as platform or poster during the Course.

For further information, please contact:
Prof. Josep Lloreta-Trull (local organizer)
Department of Pathology
Hospital del Mar-IMAS-IMIM
Universitat Pumpeu Fabra
Passeig Marítim 25–29, 08003-Barcelona, Spain
Tel.: +34 93 248 30 31
Fax: +34 93 248 31 31
E-mail: jlloreta@imas.imim.es or enter the course website
http://www.tilesa.es/eurocellpath04/

10–14 May 2004
Diagnostic Histopathology of Breast Disease
Hammersmith Hospital (Imperial College), London, UK

A week-long course designed for pathologists at Consultant and Senior Trainee level. The course provides a comprehensive coverage of the Histopathology of Breast Disease, with special emphasis on areas that pose diagnostic difficulties. The participants will be given ample time to study histological preparations, followed by illustrated discussion of the cases. There will be special sessions dealing with the interpretation of core biopsies and fine needle aspirations. There will also be several daily talks dealing with specific topics, given by eminent breast pathologists and followed by discussion. The topics will include reporting breast biopsies, immunohistochemistry, receptor and c-erbB-2 assessment, dealing with the gross specimen, prognostic factors, proliferative lesions/carcinoma in situ, problems in breast pathology, mucinous lesions of the breast, a practical approach to the diagnosis of breast lymphomas and molecular pathology including the morphology of breast cancer associated with BRCA1 & 2 mutation. The faculty will include Ian Ellis, Christopher Elston, Andrew Hanby, Kristin Henry, Stephen Humphreys, Sunil Lakhani, Andrew Lee, Naomi Livni, Sarah Pinder and Sami Shousha.

*Further details from***:**
Wolfson Conference Centre
Hammersmith Hospital
Du Cane Road
London W12 ONN, UK
Tel: (44) 20 8383 3117/3227/3245
Fax: (44) 20 8383 2428
E-mail: wcc@ic.ac.uk

4–5 June 2004
15th Ljudevit Jurak International Symposium on Comparative Pathology
(http://www.kbsm.hr/Jurak/symposium.htm), will be held in Multimedial center Sestre milosrdnice University Hospital, Vinogradska 29, Zagreb, Croatia.

The main symposium topic is head and neck pathology (including ophthalmopathology). Symposium includes following sections: Pathological Morphology of the Human and Animal Diseases, Iatrogenic, Environmental and Experimental Pathology, Herman Jurak Round Table on Rheumatological Pathology, Telepathology on-line conference, Clinical Forensic Pathology, Slide Seminars *in Histopathology and Cytopathology*, Quiz on Pathology.

For further information please contact:
Davor Tomas, M.D.
Ljudevit Jurak Clinical Department of Pathology
Sestre milosrdnice University Hospital
Vinogradska 29
10000 Zagreb, Croatia
Phone: 385-1-3787-909
Fax: 385-1-3787-244
e-mail: dtomas@kbsm.hr, juraks@kbsm.hr

1–11 June 2004
International course on Laboratory Animal Science
Utrecht, The Netherlands

A two week intensive course on laboratory animal science will be organized at the Department of Laboratory Animal Science – Utrecht, The Netherlands in June 2004. This course is organized once a year since 1993.

The objective of this course is to present basic facts and principles that are essential for the humane use and care of animals and for the quality of research.

The contents of the course are in line with recommendations of the Federation of European Laboratory Animal Science Associations (FELASA) regarding the training of the young scientist whose research involves the use of vertebrate animals.

The course may also be of interest for those who intend to set up a similar course at their location. For this purpose, during the course the acquisition of teaching materials can be discussed with the course committee.

For information and application forms please contact:
Prof. L.F.M. van Zutphen, PhD or
Mr. Stephan van Meulebrouck, MA
Department of Laboratory Animal Science
Faculty of Veterinary Medicine
P.O. Box 80.166
3508 TD Utrecht
The Netherlands
Tel.: ++31-30-2532033
Fax: ++31-30-2537997
E-mail: pdk@las.vet.uu.nl
Internet: http://las.vet.uu.nl (click on "Education and Training")

11–16 July 2004
ULTRAPATH XII: Conference on Diagnostic Electron Microscopy with Surgical, Clinical, and Molecular Pathology Correlations
Barcelona, Spain

The scientific program will cover diagnostic Electron Microscopy as well as Diagnostic Pathology – with immunohistochemical and molecular correlations – and translational research. Renowned experts in the field from both sides of the Atlantic will present updated comprehensive reviews of significant areas of Pathology. In addition, a new section of the meeting will be devoted to a Pathology Review Course. Platform and Poster presentations will also be an important part of the program.

For further information, please contact:
Josep Lloreta-Trull, M.D., Ph.D. (chairman)
Department of Pathology, Hospital del Mar-IMAS-IMIM
Universitat Pompeu Fabra
Passeig Maritim 25–29, 08003-Barcelona, Spain
Tel.: +34 93 248 30 31
Fax: +34 93 248 31 31
E-mail: jlloreta@imas.imim.es.
The Application form and Abstract form can be found on the meeting website, http://www.tilesa.es/ultrapath04/

27–30 July 2004, London
Practical Pulmonary Pathology

This course is designed to provide histopathology and cytopathology trainees and consultants with an opportunity to study diagnostic lung pathology in a comprehensive manner. It comprises lectures and practical microscopy sessions, the latter making up roughly half the time and consisting of individual study of a unique collection of cases.

For further details and application forms please contact:
Professor B Corrin,
Brompton Hospital
London SW3 6NP
Fax: +44 20 7351 8293.
E-mail: b.corrin@ic.ac.uk

Virchows Arch (2004) 444:105
DOI 10.1007/s00428-004-0978-4

EDITORIAL

Heinz Höfler · Günter Klöppel

New manuscript submission and processing: *Virchows Archiv* goes online!

Published online: 28 January 2004

Beginning in mid-February 2004, Springer-Verlag will introduce an online system for manuscript submission and editorial processing. With ManuscriptCentral (MC), all processing of manuscripts for *Virchows Archiv*, from submittal to acceptance for publication, will be exclusively electronic and online. The author's initial submittal of a manuscript will be online (rather than via mailed paper copy). The Editor-in-Chief, Managing Editors, and reviewers will all retrieve the manuscript online, the author will receive reviewer comments and the publication decision by e-mail and will submit a revised manuscript online, and the final accepted manuscript will be forwarded to the publisher online.

Everyone will have access to the same online system. The new system announced here makes processing of a manuscript, from submittal to publication, completely electronic. These new arrangements should provide several advantages.

The length of time between the manuscript submittal and the publication decision will be shorter because, not only will manuscript transactions be transported nearly instantaneously, but also all transactions will be carefully tracked by the Administrative Center.

Authors need not make and send multiple copies of their manuscripts, but can prepare their initial manuscript in the exact final electronic format required for publication. Mailing and courier costs will be reduced for authors and staff because most transactions will now occur online.

The Administrative Center will prompt all editors and reviewers to keep to promised completion schedules for each review step on each manuscript. Logging into MC for electronic manuscript submission is simple. Online, connect to: http://VirchArch.manuscriptcentral.com. The first time you do this, please check for an existing account. Click the ''check for existing account'' button. If an account exists, you will then receive an automatic e-mail containing your user ID and password. If no account exists, please click "create a new account" and follow the instructions given on the screen, and a new user ID and password will be e-mailed to you. Once you have an account, simply type your user ID and password, and MC will open for you. Complete instructions and help regarding online submittal of a manuscript can be found in MC. After logging in, authors may submit a new manuscript or track a previously submitted manuscript, and reviewers may open and download manuscripts for review. Users' access to information in MC depends on their roles. Authors may only view some information regarding their own manuscripts, reviewers may access the manuscripts and review forms, Managing Editors may additionally access reviewer comments, and the Editor-in-Chief may view all information for all manuscripts. Paper manuscript submittal will only be accepted by *Virchows Archiv* when it is impossible for the author to submit online. If for some reason the authors cannot access ManuscriptCentral, they are asked to send electronic text files and graphics so that all documents may be submitted online by the Administrative Center instead of the author.

Editor-in-Chief
Heinz Höfler

Managing Editor
Günter Klöppel

H. Höfler (✉)
Institut für Pathologie,
Klinikum Rechts der Isar,
Ismaninger Strasse 22, 81675 München, Germany
e-mail: hoefler@lrz.tum.de
Tel.: +49-89-41404160
Fax: +49-89-41404865

G. Klöppel (✉)
Institut für Pathologie,
Universitätsklinikum S-H,
Michaelisstrasse 11, 24105 Kiel, Germany
e-mail: gkloeppel@path.uni-kiel.de
Tel.: +49-431-5973400
Fax: +49-431-5973462

Heinke Brütting
Institut für Pathologie
Universitätsklinikum Schleswig-Holstein
Michaelisstrasse 11
24105 Kiel, Germany
Tel.: +49-431-5973423
Fax: +49-431-5973430
e-mail: virchows.archiv@path.uni-kiel.de

Virchows Arch (2004) 444:106–107
DOI 10.1007/s00428-004-0974-8

SOCIETY NEWS

Antonio Cardesa

Presidential welcome address

Published online: 29 January 2004

Dear members,

Our European Society of Pathology (ESP) is a well-established and flourishing society, founded 40 years ago. At present, we are approximately 1200 members, nearly 90% in good financial standing. Such a large number is unprecedented, due mainly to the high quality of the scientific programmes that the ESP has promoted in recent years. This has attracted a steady increase from new generations of enthusiastic European pathologists. Under the auspices of the ESP, 19 biennial congresses have been organised and well attended. The most recent was held in the delightful and friendly city of Ljubljana in September 2003 and was scientifically very successful and socially most enjoyable. Plans are well advanced for the 20th Congress, to be held in Paris in 2005, and arrangements are also under way for the 21st Congress in Istanbul in 2007.

In addition to the main congresses, the ESP has recently introduced intercongress meetings, which focus particularly on the activities of the working groups. The first was held in 2002 in Baveno, Italy, and was a great success. A second has been scheduled for 2006 in Ioannina, Greece. The other even-numbered year is now occupied by the intercontinental congresses, jointly organised with the Latin American Society of Pathology. The first was held in 2000 on the beautiful island of Madeira, and the second will take place in June 2004 at the spectacular Iguaçu Falls, Brazil. In addition to congresses, the ESP promotes courses at the European School of Pathology (EScoP). These courses are intensive and practically oriented and are very efficiently hosted annually in Turin, Italy, with some being repeated the following year in Krakow, Poland, or in Moscow, Russia. The ESP also sponsors similar courses at the University of Ioannina, aimed particularly at young pathologists in Greece and the Balkans. All of these courses contribute quite decisively to the continuous improvement of the diagnostic standards of pathology throughout Europe and have been attended by several hundred young European pathologists.

The ESP has been eager since its origins to promote basic research in pathology. This crucial aim is being accomplished very effectively through another specific body, the European Course on Cellular Pathology (EUROCELLPATH), which, each year, in a different city of Europe, organises quite selective courses devoted to the more timely topics in molecular and experimental pathology. EUROCELLPATH is a most valuable tool in the hands of the ESP, efficiently enhancing the knowledge of numerous young experimental pathologists throughout our continent.

The working groups are developing as true "European Task Forces of Specialisation in Pathology" and, at the same time, are evolving as crucial links between applied and basic research in each area of speciality. They are an effective way of assembling, by fields of interest, previously disconnected pathologists throughout Europe. As a result, members of the working groups have a forum for discussion and stimulation of new ideas, and several multi-institution studies have resulted.

Virchows Archiv, the official journal of the ESP, celebrated its 100th anniversary in 2003. This journal is not only a legend in the history of European pathology, but, over recent years, it has been updated and restructured to take its rightful place at the forefront of international pathology journals, and, for example, it now accepts papers with colour illustrations at no extra charge. This is a two-way street, as the link with the ESP has very much helped Virchows Archiv's impact factor to rise above 2.0. This increase in scoring will attract even more high-quality papers and, thus, increase the circulation and readership of the journal.

The ESP is regulated in conformity with the provisions of Belgian law and ruled according to its own statutes and bylaws. The General Assembly is the supreme body of the

A. Cardesa (✉)
Universitat Clinica Barcelona,
Depto. Anatomia Patologica,
Calle Villarroel 170, 08036 Barcelona, Spain
e-mail: acardesa@clinic.ub.es
Fax: +34-93-2275717

Society, but among general assemblies, the ESP is directed by an executive committee. It is assisted, in particular, by an advisory council, which has a purely counselling role and helps in planning the programmes of congresses, by a finance committee and by a nomination committee, which advises in nominating officers and committee members. A newly introduced Meeting of Chairpersons of working groups now helps to co-ordinate the activities and structure of these groups. Members are kept informed of the activities of the Society by the bulletin, Europath News, which is periodically inserted in Virchows Archiv, and also by the ESP Website, http://www.europathology.org.

While the scientific structures of the ESP have modernised in recent years, updates to the regulations of the ESP have not kept pace with newer requirements. This is understandable, as most ESP members feel professionally that promotion of science in pathology has a higher priority than legal and administrative issues. Nevertheless, this very reasonable explanation should not be used to justify delays.

Although adaptation to change has led to publication of four new editions of the statutes and bylaws since 1989 (see Members Handbook 2003), further evolution remains necessary, for example, to consider how the impact of the internet and e-mail could help bring together such a geographically widespread society. In particular, I feel that our procedures for the election of officers and members of the executive committee need updating and clarification, especially in light of the recent unexpected difficulties encountered in the election of a President-elect and also in regard to the subsequent resignation of the Secretary. It is, therefore, an urgent need for the ESP to appoint a constitutional committee to look at these regulations to reconsider the electoral regulations currently in force and, if pertinent, to draw up new procedures for the election of officers and members of the executive committee, seeking approval for them at an extraordinary General Assembly. This will ensure that there will be a smooth handover of officers at the European Congress in 2005 and thereafter.

I can report that a new Secretary has been appointed for 2003–2005 by the executive committee; this is a temporary position until the next General Assembly. The postal ballot to confirm or not the position of President-elect will allow the whole membership to express its collective view and should be known by the time this address is published. The next step will be for the executive committee to endorse the result of the ballot and proceed accordingly. It is then envisaged that the extraordinary General Assembly scheduled for 7 February 2004 in Paris (see announcement in Virchows Archiv, November 2003) will finally settle these issues. I believe that it is in the uppermost interest of the ESP to have a duly elected President-elect and Secretary as soon as possible, and that these somewhat complex democratic procedures will result in candidates acceptable to all. I ask all of you to support this procedure and to contribute, at the same time, to restore the traditional harmony and the friendly atmosphere that has always been the basis for the splendid scientific growth of our society.

Last, but not least, I want to express my thanks to you all for your generous support, as well as to my predecessors in office and to the previous and present officers, members of committees and organisers of congresses for their brilliant dedication, tremendous amount of work and invaluable contributions to the success of the ESP. I am confident that despite short-term administrative difficulties, our vibrant ESP will continue to thrive in the future as it has done up to now.

Yours sincerely,
Antonio Cardesa
President
Barcelona, November 2003

Virchows Arch (2004) 444:108–118
DOI 10.1007/s00428-003-0945-5

REVIEW ARTICLE

Gunhild Mechtersheimer · Gerlinde Egerer · Manfred Hensel · Ralf J. Rieker · Martin Libicher · Thomas Lehnert · Roland Penzel

Gastrointestinal stromal tumours and their response to treatment with the tyrosine kinase inhibitor imatinib

Received: 8 September 2003 / Accepted: 4 November 2003 / Published online: 20 January 2004

Abstract Gastrointestinal stromal tumours (GISTs), the most common mesenchymal tumours of the digestive tract, are largely resistant to chemo- and radiotherapy. They are currently defined by their overexpression of the KIT receptor tyrosine kinase (CD117), a member of the family of receptor tyrosine kinases (RTKs), and exhibit *KIT* mutations in more than 85% of cases. Additionally, in more than one-third of *KIT* wild-type GISTs, mutations of platelet-derived growth factor receptor α (PDGF-Rα), which also belongs to the family of RTKs, were recently found. Since these data indicate that uncontrolled RTK signalling may be implicated in the pathogenesis of GISTs, RTKs and the activated downstream signalling cascades are attractive targets in the therapy of these tumours. Imatinib is a small-molecule inhibitor that selectively blocks the activity of the PDGF-R, ABL and KIT receptor tyrosine kinases by competitive binding to the adenosine triphosphate binding site of their catalytic domains. We herein review the molecular pathological, preclinical and clinical data that identify imatinib as a valuable new agent in the treatment of GISTs.

Keywords GIST · KIT · PDGF-Rα · Targeted therapy · RTK inhibitor · Imatinib

Dedicated to Professor Dr. Dr. h.c. H.F. Otto on the occasion of his 65th birthday.

G. Mechtersheimer (✉) · R. J. Rieker · R. Penzel
Institute of Pathology,
University of Heidelberg,
Im Neuenheimer Feld 220, 69120 Heidelberg, Germany
e-mail: gunhild_mechtersheimer@med.uni-heidelberg.de
Tel.: +49-6221-5639909
Fax: +49-6221-565251

G. Egerer · M. Hensel
Department of Internal Medicine V,
University of Heidelberg,
Heidelberg, Germany

M. Libicher
Department of Radiology,
University of Heidelberg,
Heidelberg, Germany

T. Lehnert
Department of Surgery,
University of Heidelberg,
Heidelberg, Germany

Introduction

Gastrointestinal stromal tumours (GISTs) are the most frequent mesenchymal tumours of the gastrointestinal tract. GISTs are now considered to be derived from interstitial cells of Cajal (ICC) or from stem cells with the capacity to differentiate towards ICC [30, 39] and are defined by overexpression of the KIT receptor tyrosine kinase (CD117) in the vast majority of cases [20]. KIT is a transmembrane type-III receptor tyrosine kinase, which, together with platelet-derived growth factor receptor α (PDGF-Rα), PDGF-Rβ, colony-stimulating factor-1R and FLK2/FLT3, belongs to the PDGF subfamily of receptor tyrosine kinases (RTKs) (Fig. 1) [4]. KIT is activated when the extracellular portion binds its ligand, known as stem cell factor (SCF) [70]. KIT is essential for the development of haematopoietic progenitor cells, mast cells, melanocytes, germ cells and ICC [24]. Oncogenic *KIT* mutations have been identified in corresponding neoplasms, such as mastocytosis, acute myeloid leukaemia, chronic myeloproliferative disease, seminoma/dysgerminoma and also GIST [22, 30, 44, 50, 53, 62]. The first report on *KIT* exon 11 mutations in GIST documented not only ligand-independent activation of KIT tyrosine kinase activity, but also the capacity to induce malignant transformation in vitro [30]. Activating *KIT* mutations, affecting mostly exon 11, but also exons 9, 13 and 17, are present in more than 85% of GISTs, small, incidental tumours being included [11, 31, 42, 51, 54, 61, 68]. However, the majority of gastric GISTs with epithelioid phenotype examined were of *KIT* wild type [1, 14, 68]. Interestingly, it was shown that GIST patients with missense *KIT* exon 11 mutations had a significantly higher 5-year recurrence-free survival than GIST patients

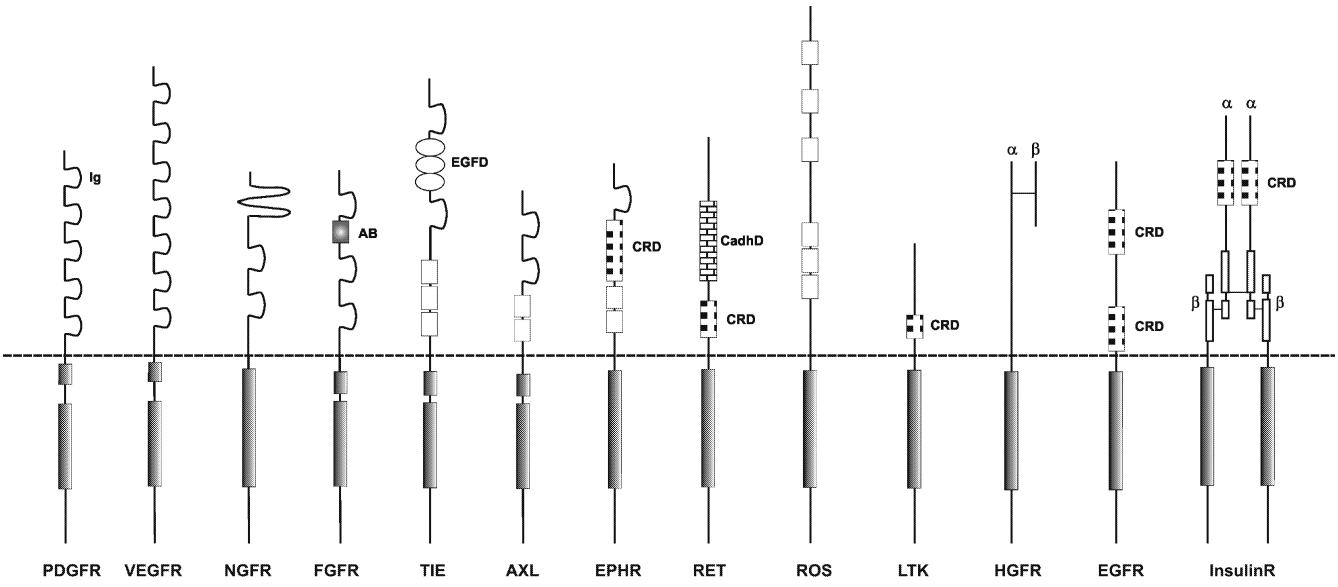

Fig. 1 Receptor tyrosine kinases (RTKs) involved in human malignancies (modified according to Blume-Jensen and Hunter [4]). Each RTK subfamily is represented by a prototypic receptor. The KIT/stem cell factor (SCF)-receptor belongs, together with PDGF-Rα, PDGF-Rβ, colony-stimulating factor-1R and FLK2/FLT3, to the platelet-derived growth factor receptor subfamily (PDGF). Other RTK subfamilies: *VEGFR* vascular endothelial growth factor receptor, *NGFR* nerve growth factor receptor, *FGFR* fibroblast growth factor receptor, *TIE* tyrosine kinase receptor in endothelial cells, *AXL* Tyro3 protein tyrosine kinase, *EPHR* ephrin receptor, *RET* rearranged during transfection, *ROS* RTK expressed in some epithelial cell types, *LTK* leukocyte tyrosine kinase, *HGFR* hepatocyte growth factor receptor, *EGFR* epidermal growth factor receptor, *InsulinR* insulin receptor, *Ig* immunoglobulin-like domain, *AB* acidic box, *EGFD* epidermal growth factor-like domain, *CRD* cystein-rich domain, *CadhD* cadherin-like domain

with other mutation types, and the presence of deletion/insertion *KIT* exon 11 mutations was identified as an independent negative predictor of disease-free survival [58]. Most recently, the type of *KIT* mutation was also found to be of prognostic relevance. Thus, *KIT* exon 11 mutations involving codons 557 and/or 558 were shown to be not only associated with a malignant phenotype, but also with metastatic behaviour of GISTs [69]. Moreover, an association between *KIT* exon 9 mutations and aggressive behaviour and non-gastric primary site of GISTs was reported [1]. These data, together with the presence of germ line mutations of the KIT gene in familial GISTs [32], implicate KIT activation as a central and early event in the pathogenesis of GIST [51]. However, there is a subset of GISTs with *KIT* wild-type being also devoid of high levels of total KIT protein expression. Most recently, activating PDGF-Rα mutations affecting exons 12 and 18 were detected by two independent groups in 14 of 40 and in 5 of 8 *KIT* wild-type GISTs, while being absent in any of 36 and of 10 *KIT* mutant GISTs examined [28, 33]. The biochemical consequences with respect to activating downstream signalling intermediates (Fig. 2), however, were similar in *KIT* mutant and *PDGF-Rα* mutant GISTs, as were the cytogenetic changes associated with tumour progression of the GISTs [28]. These data implicate PDGF-Rα, like KIT a member of the RTK family, in the pathogenesis of GISTs as well.

The development of imatinib mesylate (hereafter imatinib, formerly STI571, Glivec; Novartis, Basel, Switzerland), a selective small molecule inhibitor not only of ABL and PDGF-R, but also of KIT receptor tyrosine kinases [7, 25], has opened a new therapeutic perspective for the treatment of GISTs, which are largely resistant to chemo- and radiotherapy [15].

Receptor tyrosine kinases as targets for anticancer drugs

RTKs, a family of transmembrane cell surface receptors for growth factors and other ligands, are important regulators of cellular tyrosine phosphorylation and mediators of intracellular signalling [36, 56]. At present, 20 different RTK subfamilies are known, of which at least 13 are implicated in human malignancies (Fig. 1) [4]. The RTKs share in common an extracellular, ligand-binding domain, a membrane-spanning region and an intracellular domain containing the kinase enzymatic domain. RTK activation normally occurs through binding of the ligand that induces RTK dimerisation and autophosphorylation of specific tyrosine residues in the kinase domain. The resulting phosphotyrosines carry docking sites for various cell-signalling proteins and induce substrate binding and crossphosphorylation. These steps finally activate complex cell-signalling cascades that control cell growth, proliferation, adhesion, migration, differentiation and apoptosis. The most important downstream signalling cascades activated by RTKs include the Ras-extracellular regulated kinase-mitogen activated (MAP) kinase path-

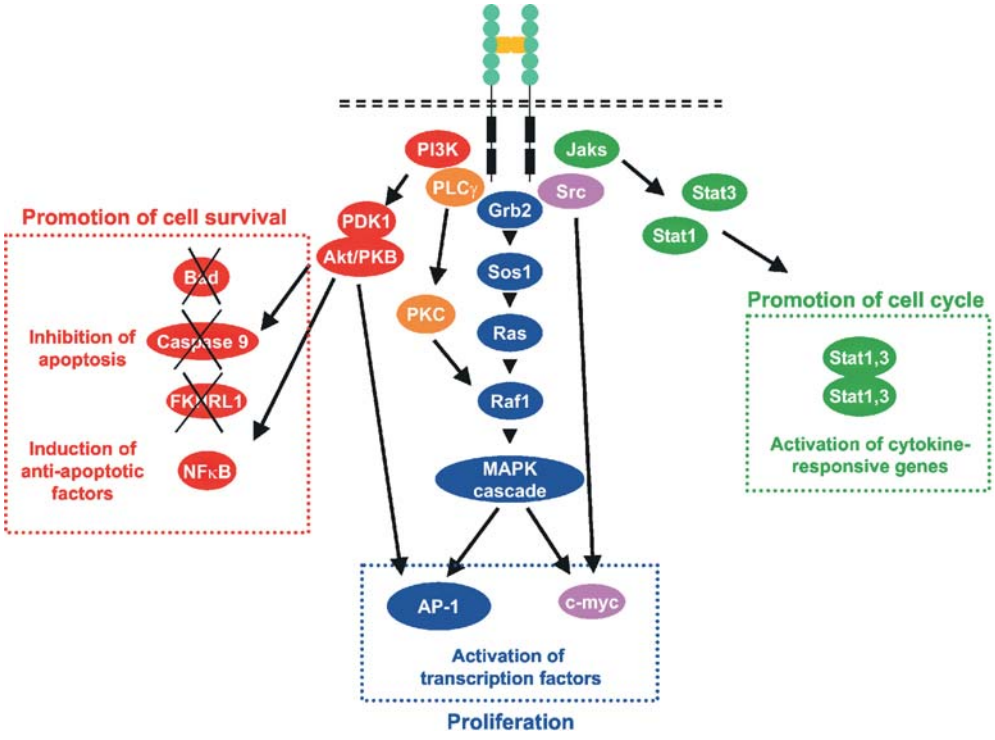

Fig. 2 Schematic illustration of selected signalling pathways activated by RTKs (e.g. KIT, platelet-derived growth factor receptor). The PI3 K (phosphoinositide-3-kinase; orange) pathway leads to the activation of PDK1 (3-phosphoinositide dependent protein kinase-1) and Akt/PKB (protein kinase B). Activated Akt/PKB promotes cell survival via phosphorylation and inactivation of components of the apoptotic pathway, including BAD (BCL2-antagonist of cell death), Caspase 9 and FKHRL1 (forkhead in rhabdomyosarcoma-like 1). Activation of NFκB (nuclear factor kappa B) further opposes apoptosis. The Ras/MAP kinase pathway (*blue*) is initiated by the adapter molecule Grb2 (growth factor receptor-bound protein 2), which forms a complex with Sos1 (son of sevenless homologue 1), a nucleotide exchange factor for Ras (rat sarcoma viral oncogene homologue). Activated Ras interacts directly with Raf1 (murine leukemia viral oncogene homologue 1), the first kinase in the MAPK (mitogen-activated protein kinase) cascade. Stimulation of the MAPK cascade results in cell proliferation mediated by transcription factors such as the AP-1 (activator protein-1) transcription factor complex. Another potent, Ras-independent activator of the MAPK cascade is PKC (protein kinase C), which is activated by PLCγ (phospholipase C gamma 1). The recruitment of the Src tyrosine kinase by direct binding to activated RTKs leads to its activation resulting in various cellular effects, including activation of c-myc (avian myelocytomatosis viral oncogene homologue). Activation of the JAK/STAT pathway (*green*) occurs either by direct phosphorylation of STATs (signal transducer and activator of transcription) or is mediated through receptor-recruited JAKs (Janus kinases). Phosphorylated STATs dimerize and translocate to the nucleus, where they activate the transcription of cytokine-responsive genes

way, the phosphoinositide 3-kinase-Akt and the Janus kinase/signal transducer and activator of transcription pathways (Fig. 2) [56, 71].

In normal cells, the activity of RTKs and their mediated cellular signalling is closely coordinated and controlled. The RTK signalling system can be deregulated either by stimulation through autocrine–paracrine growth factor loops or by gene amplification/overexpression or gene mutation of RTKs. This results, in most instances, in RTKs with constitutive or strongly enhanced signalling capacity, leading to malignant transformation [4].

Since uncontrolled RTK signalling is implicated in the pathogenesis of a variety of tumours, RTKs and the activated signalling cascades are attractive targets in cancer therapy. Strategies for the generation of target-selective anti-cancer drugs include the development of compounds that target the extracellular ligand-binding domain, the intracellular tyrosine kinase domain or the substrate-binding region. Compounds presently being evaluated as inhibitors of signal transduction comprise monoclonal antibodies, which bind to the extracellular domains of RTKs, small-molecule inhibitors, which compete with the adenosine triphosphate (ATP) binding site of the catalytic domain of the enzymes and, as alternative strategies, immunotoxins or antisense oligonucleotides [71]. The clinical value of cancer drugs targeted against specific molecular abnormalities has first been proven by the success of trastuzumab (Herceptin), a monoclonal antibody against the Her-2/neu receptor tyrosine kinase, in the treatment of breast cancer [2, 55]. Meanwhile, imatinib, a small-molecule inhibitor of ABL, KIT receptor and PDGF-R tyrosine kinases, is established in the treatment of chronic myeloid leukaemia and of GISTs [13, 16].

The tyrosine kinase inhibitor imatinib

Development of imatinib and its role in chronic myeloid leukaemia

Imatinib is a small-molecule inhibitor of the 2-phenylaminopyrimidine class that competitively binds to the ATP binding site at the catalytic domain of selected tyrosine kinases, thus inhibiting the tyrosine phosphorylation of their substrates, blocking the downstream signalling and inhibiting cell growth. It was initially identified in a high-throughput screen for compounds that block the activity of the PDGF-R tyrosine kinase [5]. Soon after, imatinib was shown to inhibit ABL and KIT receptor tyrosine kinases as well [6, 7, 25]. In vitro, imatinib blocked the growth of BCR-ABL-expressing cells with little effect on normal cells or cells expressing the related tyrosine kinase Src [18]. Given that chronic myeloid leukaemia (CML) is in approximately 95% of cases characterised by the Philadelphia translocation, t(9;22)(q34;q21), which results in the BCR-ABL chimeric fusion gene, imatinib was evaluated as a molecular targeted therapy in this tumour entity. Since haematological responses to imatinib treatment have been observed in 95% of patients with CML in chronic phase after failure of interferon-α therapy, in 71% of patients with CML in accelerated phase and in 31% of patients with CML in myeloid blast crisis, imatinib treatment proved to be a promising new compound in the treatment of CML patients [13, 34]. Meanwhile, a considerable number of studies have confirmed the clinical value of imatinib in the treatment of CML, either alone or in combination with cytostatic drugs [13].

Role of imatinib in GISTs

Preclinical experience with imatinib in GISTs

In two GIST cell lines, expressing activating *KIT* mutations in exons 11 and 13, respectively, constitutive tyrosine phosphorylation was rapidly and completely abolished in vitro upon administration of imatinib, and effective inhibition of proliferation and apoptosis were observed after prolonged incubation with imatinib [64]. These in vitro data provided a rational basis for the clinical use of imatinib in the treatment of GISTs.

Clinical experience with imatinib in GISTs

The first report of a 50-year-old female patient with a metastatic, *KIT* mutation-positive GIST of the stomach treated with imatinib documented a remarkable response [37]. In a phase-I study performed by the European Organization for Research and Treatment of Cancer (EORTC) Soft Tissue and Bone Sarcoma Group (STBSG), objective responses to treatment with imatinib were seen in 25 of 36 GIST patients at all dose levels applied (400–1000 mg daily) [66]. Of these patients, 19 had confirmed partial responses, and 6 had unconfirmed partial responses or 20–29% regressions; 7 patients were stable, and 4 had progressive disease. Dose-limiting toxic effects included severe nausea, vomiting, edema or rash and were observed in 5 of 8 patients on 500 mg imatinib treatment twice daily. Intratumoural bleeding was seen in 3 patients. In a phase-II multi-centre trial performed in the United States [16], 79 of 147 patients (54%), who were randomly assigned to receive 400 mg or 600 mg of imatinib once daily, had a partial response, and 41 patients (28%) had stable disease. In 20 patients (14%), disease progression was noted. The therapy was generally well tolerated, although mild-to-moderate adverse events, mostly oedema, frequently periorbital, followed by diarrhoea, myalgia and fatigue were common. Serious adverse events occurred in 21% of patients, inter alia gastrointestinal or intra-abdominal haemorrhage, probably related to therapy-induced tumour necrosis, in approximately 5% of patients, who had large, bulky tumours.

In two ongoing phase-III trials, GIST patients are randomly assigned to imatinib 400 mg once daily or 400 mg twice daily. In the Sarcoma Intergroup S0033 study performed in the United States, 746 patients were registered, of which 486 remained on protocol with a median follow-up of 14 months at the presentation of the early results [3]. There was no evidence for a difference in the response rate between the two dose levels of imatinib given, while its effective anti-tumour activity was confirmed: the overall response rate was 43% at 400 mg imatinib and 41% at 800 mg imatinib. The progression-free survival at 6 months was estimated at 80% versus 82% for the 400 mg versus the 800 mg arm, respectively. The overall survival at 6 months was estimated at 91% versus 92% for the two dose levels. In the trial performed by the EORTC STBSG, the Italian Sarcoma Group and the Australian Gastro-Intestinal Tumors Group, 946 patients were registered. At interim analysis, 615 patients with a median follow-up of 8.4 months were able to be evaluated for efficacy of treatment with 400 mg versus 800 mg imatinib [67]. In both the low dose and the high dose arms, 43% of the patients showed objective responses (OR) to imatinib treatment. The 1-year OR estimates were 54% versus 57% for the 400 mg versus the 800 mg arm. The progression-free survival estimates at 6 months and 12 months were 73% versus 78% and 64% versus 69%.

Most recently, imatinib treatment has also been performed in a neoadjuvant setting [8], and adjuvant trials testing the value of imatinib after complete resection in patients with high risk GISTs and with GISTs $\geq$3 cm have been initiated [12].

Radiographic monitoring of imatinib treatment in GISTs

Computed tomography (CT) and magnetic resonance imaging (MRI) are the anatomic imaging techniques most

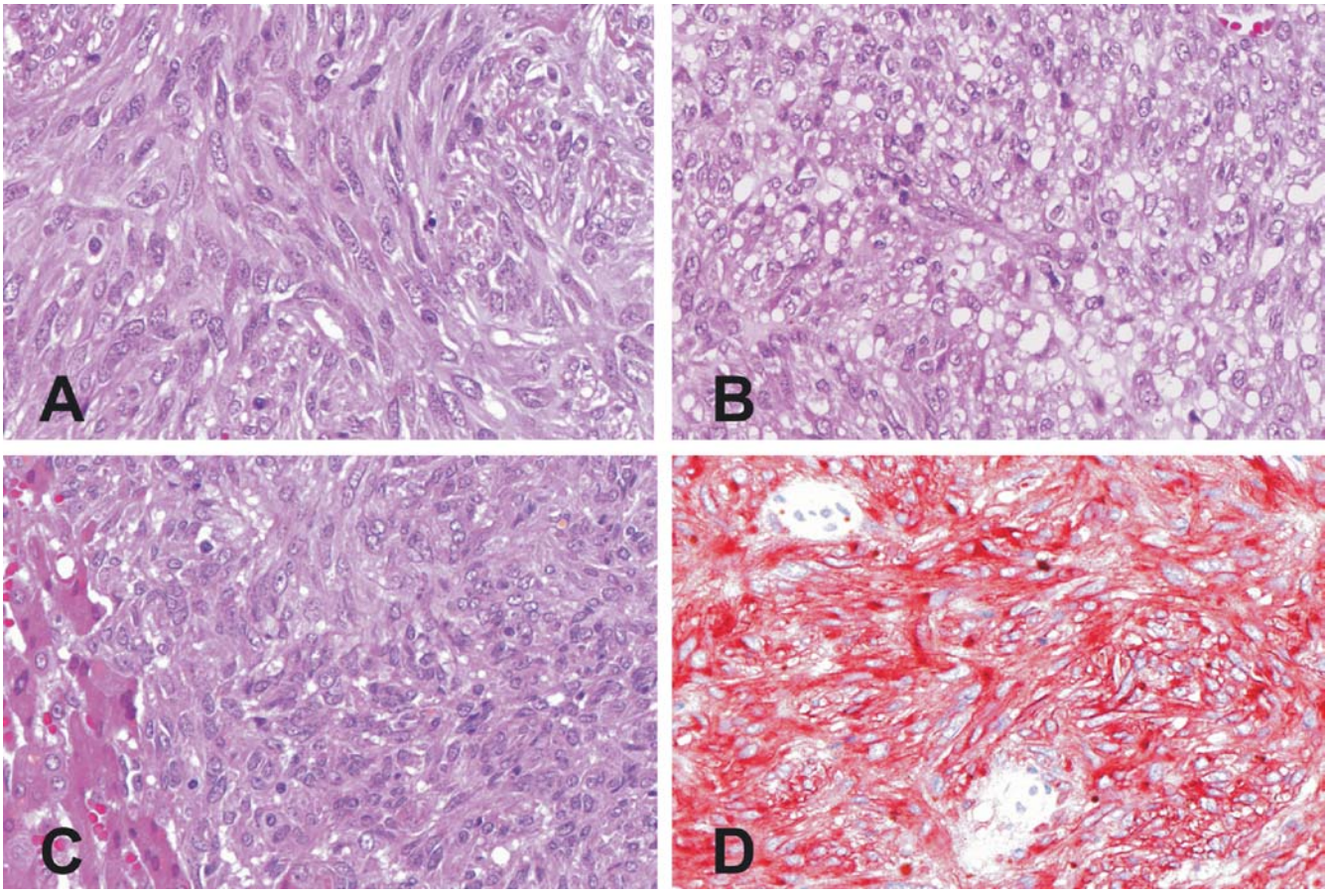

Fig. 3 Gastric primary tumour: **A** plump spindled tumour cells arranged in interwoven fascicles [hematoxylin and eosin (H&E), original magnification ×180], merging imperceptibly with **B** solid sheets of epithelioid tumour cells with vacuolated cytoplasm (H&E, original magnification ×180). **C** Liver metastasis displaying plump, spindled tumour cells sharply demarcated from the adjacent liver tissue (H&E, original magnification ×180). **D** Consistent expression of CD117/KIT in the neoplastic population of the gastric primary tumour (immunoperoxidase, original magnification ×180)

broadly used to assess the response to imatinib treatment. Response is characterised by a cyst-like appearance of the lesions, followed by a reduction in size to complete disappearance of some of the tumour nodules [16, 37]. Using contrast-enhanced CT imaging, it was confirmed that hepatic metastases from GISTs that respond to therapy with imatinib can appear as near-cystic lesions with well-defined borders after 8 weeks of treatment [10].

Standard [^{18}F]fluoro-2-deoxy-D-glucose positron emission tomography (FDG-PET) complements the anatomic imaging techniques. In FDG-PET scans, retention of the [^{18}F]fluoro-2-deoxy-D-glucose tracer correlates with increased metabolic tumour activity relative to normal tissue [65]. FDG-PET was shown to be a rapid and sensitive indicator of response or resistance of GISTs to imatinib [65]. In a phase-II multi-centre trial performed in the United States, the [^{18}F]fluoro-2-deoxy-D-glucose uptake into tumour had decreased markedly from baseline as early as 24 h after a single dose of imatinib in all patients with a response, indicating a strikingly early metabolic response [16]. However, an increase in tumour-related glycolytic activity and/or activity at new sites was observed in all patients with disease progression [12]. Also, FDG-PET results correlated with subsequent evidence of a response or progression on CT and MRI, which have a higher spatial resolution [16, 66]. Therefore, FDG-PET seems to be particularly useful for the early identification of patients whose GISTs will respond to therapy. However, since PET studies are not ubiquitously available and are cost intensive, CT or MRI techniques are more suitable for follow-up studies outside of controlled clinical studies. In addition, not all GISTs have sufficient glucose uptake at baseline evaluation for a positive FDG-PET [66].

Case example

A male Caucasian patient was diagnosed with GIST on ultrasonograph-guided fine-needle biopsy of a large abdominal tumour with sonographically identified synchronous liver metastases at the age of 42 years. Subsequently, total gastrectomy en bloc with omentectomy, splenectomy and resection of liver segments 2/3 was

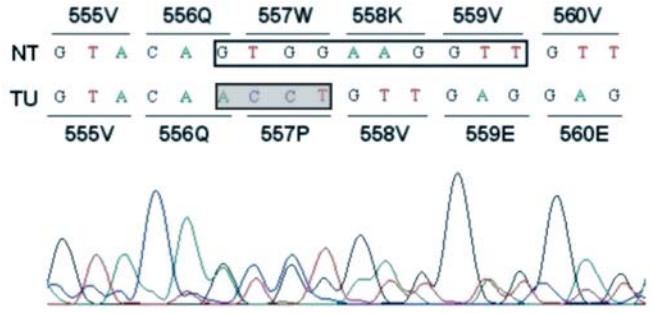

Fig. 4 Partial cDNA sequence corresponding to exon 11 of the KIT gene. The wild type sequence was found in normal tissue samples of the patient's stomach and liver (NT). The deletion (10 bp) identified in the tumour samples of the stomach and the liver is *boxed* in the wild-type sequence. Within the cDNA sequence determined for both tumour samples (TU) the concurrent insertion (4 bp) is *boxed* and *grey shaded*. The codons are indicated *above* (NT) and *below* (TU) the cDNA sequences

performed in the Department of Surgery, University of Heidelberg (Germany). Histological examination of the operation specimen confirmed the diagnosis of a gastric GIST with liver metastases, predominately composed of spindled with foci of epithelioid tumour cells (Fig. 3A, B, C). The tumour cells of both the primary gastric lesion and the liver metastases showed co-expression of CD117 and CD34 in the absence of any detectable muscle-specific actin, desmin and S100 protein (Fig. 3D). Mutational analysis revealed a combined insertion/deletion mutation of *KIT* exon 11 (c.1668_1677 delinsACCT) in both the primary gastric tumour and in one liver metastasis examined, while non-neoplastic tissue showed *KIT* wild-type sequences (Fig. 4). Total body hyperthermia was initiated as an individual "trial of curing" upon the explicit request of the patient 5 months after diagnosis of GIST. Under this treatment, the liver metastases progressed as documented by CT. Oral treatment with imatinib 400 mg daily was started after written informed consent was obtained from the patient and continued with confirmed favourable response 10 months after diagnosis. The drug was well tolerated; transient orbital oedema did not require dose reduction. Follow-up of the liver metastases by MRI (axial Gd-enhanced T1-weighted) showed a considerable reduction in volume and contrast-enhancement with cyst-like appearance under continuous imatinib treatment (Fig. 5A, B, C). The volume reduction

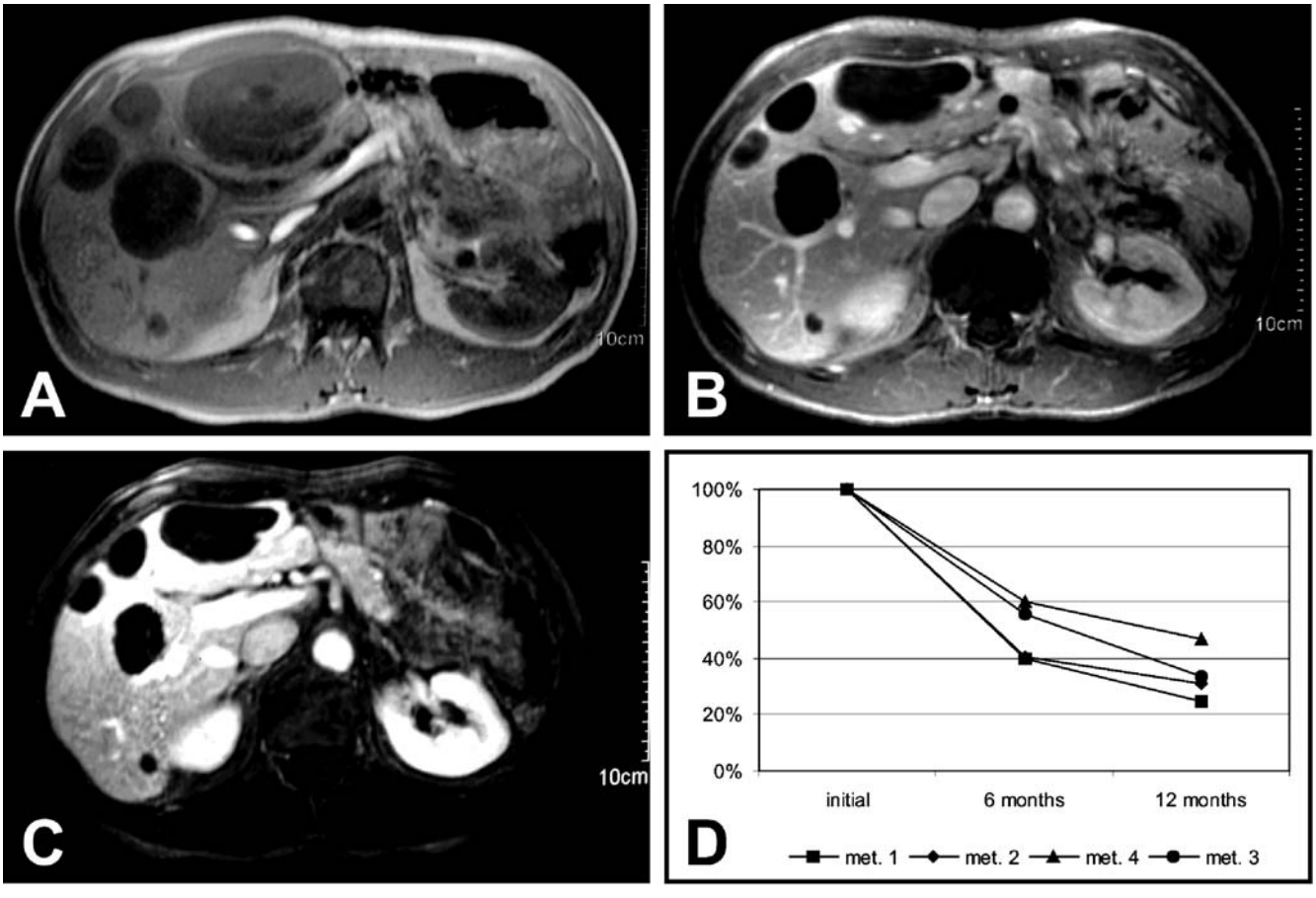

Fig. 5 Magnetic resonance imaging (axial Gd-enhanced T_1-weighted) follow-up studies of the liver metastases during imatinib treatment (**A–C**): compared with initial findings prior to therapy (**A**), the liver metastases showed a considerable reduction in volume after 6 months (**B**), and after 12 months (**C**) of continuous treatment. Initial contrast enhancement with solid hyperintense lesions (**A**) changed to rim-like or hypointense, cystic lesions (**B**, **C**). **D** the volume reduction of the four largest liver metastases (met. 1–met. 4) ranged from 40% to 60% after 6 months and from 53% to 75% after 12 months of continuous treatment

of the four largest metastases ranged from 40% to 60% after 6 months and from 53% to 75% after 12 months of continuous treatment compared with the pretreatment volume (Fig. 5D).

Histopathological monitoring of imatinib treatment in GISTs

Tumour biopsies performed before and after onset of treatment in a subgroup of cases have given insight into the histopathological changes in GISTs responsive to imatinib [8, 16, 37]. Histologically, responsive, cyst-like GIST lesions were characterised by markedly reduced numbers of tumour cells, which were embedded within a myxohyaline stroma, frequently with prominent stromal haemorrhage. The residual tumour cells often showed pyknotic nuclei, which, based on the absence of any detectable expression of the Ki-67 proliferation antigen, were suggested to be not actively dividing.

Influence of the mutational status on treatment response in GISTs

KIT consists of an extracellular domain with five immunoglobulin-like repeats, a transmembrane domain, a juxtamembrane domain and a tyrosine kinase domain with an insert that splits the kinase domain (Fig. 6). Recently, it has been observed that different classes of activating *KIT* mutations respond differentially to KIT inhibitors. Thus, for example, the *KIT* codon 816 mutation found in adult-type human mastocytosis, which causes residue substitution (i.e. D816V) in the activation loop located at the entrance of the enzymatic pocket, is resistant to imatinib [44]. Concerning GISTs, the effectiveness of imatinib in inhibiting the constitutive tyrosine kinase activity has been demonstrated for *KIT* mutations affecting exon 11 (juxtamembrane domain) and exon 13 (kinase domain I) [26, 64]. Recently, it was reported that imatinib also inhibited MAP and Akt phosphorylation of murine lymphoid Ba/F3 cells transfected with mutant *KIT* $^{\text{del559–560}}$ (exon 11) and mutant *KIT* $^{642\text{Glu}}$ (exon 13) [9]. At higher concentrations, KIT, MAP and Akt phosphorylation was also inhibited by imatinib in murine lymphoid Ba/F3 cells transfected with mutant *KIT* $^{820\text{Tyr}}$ (exon 17) [9]. However, the activity of imatinib against *KIT* exon 9 and exon 17 mutations, the latter resulting in substitution of either lysine or histidine for asparagine 822 [51], in GISTs has not been reported thus far. Interestingly, the likelihood of a clinical response to imatinib, as well as the time to treatment failure, correlated with the *KIT* mutational status. Thus, GISTs with a *KIT* exon 11 mutation had a significantly higher partial response rate (72%) than tumours with an exon 9 mutation (31.6%) or no detectable mutation (i.e., *KIT* wild-type GIST) [27]. In addition, the time to treatment failure was significantly longer for patients with *KIT* exon 11 mutation compared with those without *KIT* exon 11 mutation [27]. A multivariate analysis identified the presence of a *KIT* exon 11 mutation as the strongest predictor of clinical response, decreased risk of treatment failure and improved overall survival [29]. In support of these findings, in a series of 17 patients in which imatinib was given in a neo-adjuvant, adjuvant or palliative setting, 8 of 9 patients with partial response to imatinib but none of the 3 patients with progressive or stable disease had *KIT* exon 11 mutations [8]. In addition, a subset of PDGF-Rα mutant isoforms in GISTs were also sensitive to imatinib, both in vitro and clinically [29].

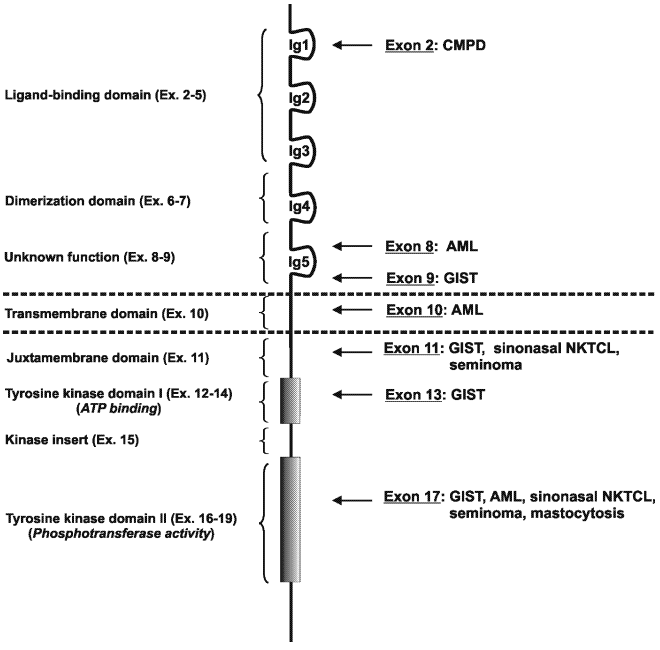

Fig. 6 Scheme of the KIT receptor tyrosine kinase demonstrating the five immunoglobulin-like domains (Ig1–Ig5) in the extracellular ligand-binding region, the transmembrane domain, the juxtamembrane domain, and the two intracellular kinase domains divided by a kinase insert. The reported *KIT* mutations in human tumours in different *KIT* exons are indicated [22, 31, 35, 42, 44, 50, 51, 53, 54, 61, 62, 68]. *CMPD* chronic myeloproliferative disease, *AML* acute myeloid leukaemia, *GIST* gastrointestinal stromal tumour, sinonasal *NKTCL* sinonasal natural killer/T-cell lymphoma

Resistance to imatinib in GISTs

Although most patients with CML in chronic phase achieve durable complete haematological and cytogenetic remissions under treatment with imatinib, primary resistance or relapse occurs, especially in patients with CML in accelerated phase or in blast crisis/advanced stages. The most common mechanisms of resistance to imatinib identified in patients with CML comprise BCR-ABL amplification at the genomic and transcript levels, a variety of point mutations in the ABL tyrosine kinase domain and novel acquired chromosomal aberrations [13, 34].

Primary or late resistance to imatinib has also been observed in GIST patients [16, 66]. Meanwhile, different mechanisms of resistance to imatinib were described in 16 GIST patients with initial (n=3) or late (n=13) resistance [21]. They include (i) acquisition of a new *KIT* or *PDGF-Rα* point mutation in addition to a baseline mutation in the respective gene; (ii) *KIT* genomic amplifications; (iii) activation of an alternate receptor tyrosine kinase protein, accompanied by loss of KIT oncoprotein expression and (iv) *KIT* or *PDGF-Rα* activation, in absence of a secondary genomic mutation and with baseline *KIT* or *PDGF-Rα* mutations outside of the juxtamembrane hot spot regions.

Unresolved questions and future considerations

Clinical trials revealed that monotherapy with imatinib in GISTs is both feasible and effective. Still, many questions about the clinical use of imatinib in GISTs remain unresolved. These include the optimal dosage of imatinib, which is under investigation in randomised clinical trials [3, 67] and the duration of imatinib treatment, which is not yet defined. For the time being, imatinib treatment is continued until tumour progression resistant to dose escalation occurs or severe toxicity takes place. There is also a need for refined clinical and molecular parameters (e.g. the type of *KIT* mutation, see above) to identify patients whose GISTs will respond to imatinib. Last but not least, we have to develop new therapies for GIST patients whose tumours are resistant to imatinib. In this context, it is of interest that 11 of 18 patients (61%) with imatinib-resistant GISTs treated in a phase-I trial with SU11248, a small molecule kinase inhibitor which targets multiple receptor tyrosine kinases, including KIT, PDGF-R, FLT3 and vascular endothelial growth factor receptor-1, had disease regression or stable disease lasting more than 4 months with acceptable tolerability [17]. Additionally, in GIST patients who do not have an optimal response to imatinib monotherapy, combinations with other tyrosine kinase inhibitors or, as already done in CML patients [13], with cytostatic drugs, have to be studied. Finally, adjuvant trials with imatinib after complete surgical excision of high-risk GISTs have been initiated [8, 10].

Potential role of imatinib in other solid tumours

In vitro data suggest that imatinib monotherapy will be effective only against solid tumours whose growth is driven mainly by the uncontrolled activity of the imatinib-sensitive tyrosine kinases, such as KIT and PDGF-R. The mere evidence of KIT or PDGF-R synthesis at the protein level without the demonstration of abnormally upregulated tyrosine kinase activity in tumour cells does not predict efficacy of imatinib treatment [26].

One solid tumour entity that meets the above criteria is the dermatofibrosarcoma protuberans (DFSP) family of tumours. These tumours are characterised by supernumerary ring chromosomes carrying material from 17q22 and 22q13 in proximity to one another or by the translocation t(17;22)(q22;q13). This translocation fuses the collagen type 1α1 (COL1A1) gene to the platelet-derived growth factor β-chain (PDGF B) gene. The variable positions of the COL1A1 breakpoints allow variant fusion genes. The resulting proteins are processed to mature PDGF-BB. This leads to autocrine PDGF-R stimulation in the DFSP family of tumours [59]. In vitro, growth inhibition of human DFSP tumour cell lines was observed with imatinib through induction of apoptosis [60]. More recently, clinical data support the use of imatinib in this tumour family. Four patients with localised DFSP treated with 400 mg imatinib twice daily and one metastatic DFSP treated with 400 mg imatinib once daily showed partial responses, and, in one patient with metastatic DFSP, imatinib 400 mg twice daily led to a complete histological response; however, two patients with metastatic tumours did not respond [46, 47, 52].

The coexpression of PDGF and PDGF-Rs, which is suggestive of autocrine growth stimulation, has been reported in a considerable number of solid tumours, including gliomas, meningiomas, melanomas, neuroendocrine tumours and carcinomas of the prostate, breast, lung, stomach and pancreas [49].

In a subset of high grade gliomas, amplification of PDGF-Rα is observed in addition to co-expression of PDGF-Rα and PDGF A or B chains [19]. In mice, it was shown that intracranial growth of gliomas is sensitive to the treatment with imatinib [38]. These observations have led to the initiation of clinical trials with imatinib in patients with glioblastomas [63].

Autocrine PDGF stimulation is also likely in cancer of the prostate. In both epithelial tumour cells and stromal cells of prostate cancer and of prostatic intraepithelial neoplasia, PDGF-R α and PDGF A chains are coexpressed, while non-neoplastic epithelial and stromal cells of the prostate are devoid of any detectable expression of these molecules [23]. At the time of writing, two phase-II trials of imatinib in hormone-refractory prostate cancer and in newly diagnosed, localised, intermediate- or high-risk prostate cancer are in progress [23].

Desmoid fibromatosis is also known to coexpress PDGF-Rs and PDFG A/B chains [45]. However, in contrast to earlier reports, desmoid fibromatosis does not seem to express KIT [43]. Still, in two patients with uncontrolled local recurrence of extraabdominal desmoid fibromatosis, imatinib treatment resulted in radiographic and clinical responses [45]. This is thought to be due to inhibition of PDGF-R rather than interaction with KIT.

In breast cancer, ovarian cancer, small cell lung cancer (SCLC), melanoma, neuroblastoma and Ewing's sarcoma (ES), coexpression of KIT and of its ligand, SCF, suggests a potential role for imatinib in targeting an autocrine SCF/KIT loop. In most cases, however, the potential role of the SCF/KIT loop in growth stimulation and/or survival of these tumours is unknown [26].

SCLC and ES coexpress KIT and SCF in about 70% and 30% of the cases, respectively. An autocrine growth/stimulation loop has, therefore, been suggested to play a role in tumour development [40, 41]. In vitro, imatinib inhibited SCLC as well as ES growth. However, the concentrations required to kill SCLC and ES cells were much higher than those necessary to kill CML or GIST [40, 48, 57]. This indicates limited therapeutic activity in these tumour types. However, in subsets of SCLC and ES with a high level of KIT expression, the potential activity of imatinib might be exploitable in combination with cytotoxic chemotherapy [57].

Concluding remarks

Therapies targeting deregulated RTKs and downstream signalling pathways are a significant contribution to the treatment of cancers. The unravelling of the role of KIT and PDGF-Rα in the pathogenesis of GISTs has improved their diagnosis and allowed discrimination from other mesenchymal tumours of the gastrointestinal tract. More importantly, it has also led to a new therapeutic option for these radio- and chemotherapy-resistant tumours. Imatinib, a selective small molecule inhibitor of KIT, PDGF-R and ABL tyrosine kinases, is the first effective and generally well-tolerated systemic therapeutic agent for patients with metastatic GISTs. Although imatinib has yielded remarkable therapeutic results, primary and late resistances are documented in a steadily growing number of GIST cases. A better understanding of the mechanisms causing imatinib resistance as well as the identification of the check points leading to activation of the downstream signalling cascades of KIT and PDGF-Rα will aid in the development of additional agents for the molecular-targeted therapy of GISTs and other tumours.

Acknowledgements The technical assistance of Marion Moock and Andrea Müller and the photographic assistance of Ursula Horr and John Moyers are gratefully acknowledged. This study was supported by the Tumorzentrum Heidelberg/Mannheim.

References

1. Antonescu CR, Sommer G, Sarran L, Tschernyavsky SJ, Riedel E, Woodruff JM, Robson M, Maki R, Brennan MF, Ladanyi M, DeMatteo RP, Besmer P (2003) Association of *KIT* exon 9 mutations with nongastric primary site and aggressive behavior: *KIT* mutation analysis and clinical correlates of 120 gastrointestinal stromal tumors. Clin Cancer Res 9:3329–3337
2. Baselga J, Tripathy D, Mendelsohn J, Baughman S, Benz CC, Dantis L, Sklarin NT, Seidman AD, Hudis CA, Moore J, Rosen PP, Twaddell T, Henderson IC, Norton L (1996) Phase II study of weekly intravenous recombinant humanized anti-p185^{HER2} monoclonal antibody in patients with HER2/*neu*-overexpressing breast cancer. J Clin Oncol 14:737–744
3. Benjamin RS, Rankin C, Fletcher C, Blanke C, Von Mehren M, Maki R, Bramwell V, Baker L, Borden E, Demetri GD (2003) Phase III dose-randomized study of imatinib mesylate (STI571) for GIST: intergroup S0033 early results (abstract 3271). Proc Am Soc Clin Oncol 22:814
4. Blume-Jensen P, Hunter T (2001) Oncogenic kinase signalling. Nature 411:355–365
5. Buchdunger E, Zimmermann J, Mett H, Meyer T, Muller M, Druker BJ, Lydon NB (1995) Selective inhibition of the platelet-derived growth factor signal transduction pathway by a protein-tyrosine kinase inhibitor of the 2-phenylaminopyrimidine class. Proc Natl Acad Sci U S A 92:2558–2562
6. Buchdunger E, Zimmermann J, Mett H, Meyer T, Muller M, Druker BJ, Lydon NB (1996) Inhibition of the Abl protein-tyrosine kinase in vitro and in vivo by a 2-phenylamonipyrimidine derivative. Cancer Res 56:100–104
7. Buchdunger E, Cioffi CL, Law N, Stover D, Ohno-Jones S, Druker BJ, Lydon NB (2000) Abl protein-tyrosine kinase inhibitor STI571 inhibits in vitro signal transduction mediated by c-Kit and platelet-derived growth factor receptors. J Pharmacol Exp Ther 295:139–145
8. Bümming P, Andersson J, Meis-Kindblom JM, Klingenstierna H, Engström K, Stierner U, Wängberg B, Jansson S, Ahlman H, Kindblom L-G, Nilsson B (2003) Neoadjuvant, adjuvant and palliative treatment of gastrointestinal stromal tumours (GIST) with imatinib: a centre-based study of 17 patients. Br J Cancer 89:460–464
9. Chen H, Kinoshita K, Ohashi A, Shinomura Y, Matsuzawa Y, Kitamura Y, Hirota S (2003) Imatinib inhibits various types of activating mutant kit found in gastrointestinal stromal tumors. Int J Cancer 105:130–135
10. Chen MYM, Bechtold RE, Savage PD (2002) Cystic changes in hepatic metastases from gastrointestinal stromal tumors (GISTs) treated with Gleevec (imatinib mesylate). AJR 179:1059–1062
11. Corless CL, McGreevey L, Haley A, Town A, Heinrich MC (2002) *KIT* mutations are common in incidental gastrointestinal stromal tumors one centimeter or less in size. Am J Pathol 160:1567–1572
12. Debiec-Rychter M, Lasota J, Sarlomo-Rikala M, Kordek R, Miettinen M (2001) Chromosomal aberrations in malignant gastrointestinal stromal tumors: correlation with c-KIT gene mutation. Cancer Genet Cytogenet 128:24–30
13. Deininger MWN, Druker BJ (2003) Specific targeted therapy of chronic myelogenous leukemia with imatinib. Pharmacol Rev 55:401–423
14. DeMatteo RP (2002) The GIST of targeted cancer therapy: a tumor (gastrointestinal stromal tumor), a mutated gene (*c-kit*), and a molecular inhibitor (STI571). Ann Surg Oncol 9:831–839
15. DeMatteo RP, Heinrich MC, El-Rifai WM, Demetri G (2002) Clinical management of gastrointestinal stromal tumors: before and after STI-571. Hum Pathol 33:466–477
16. Demetri GD, von Mehren M, Blanke CD, van den Abbeele AD, Eisenberg B, Roberts PJ, Heinrich MC, Tuveson DA, Singer S, Janicek M, Fletcher JA, Silverman SG, Silberman SL, Capdeville R, Kiese B, Peng B, Dimitrijevic S, Druker BJ, Corless C, Fletcher CDM, Joensuu H (2002) Efficacy and safety of imatinib mesylate in advanced gastrointestinal stromal tumors. N Engl J Med 347:472–480
17. Demetri GD, George S, Heinrich MC, Fletcher JA, Fletcher CDM, Desai J, Cohen DP, Scigalla P, Cherrington JM, van den Abbeele AD (2003) Clinical activity and tolerability of the multi-targeted tyrosine kinase inhibitor SU11248 in patients (pts) with metastatic gastrointestinal stromal tumor (GIST) refractory to imatinib mesylate (abstract 3273). Proc Am Soc Clin Oncol 22:814
18. Druker BJ, Tamura S, Buchdunger E, Ohno S, Segal GM, Fanning S, Zimmermann J, Lydon NB (1996) Effects of a selective inhibitor of the Abl tyrosine kinase on the growth of Bcr-Abl-positive cells. Nat Med 2:561–566
19. Fleming TP, Saxena A, Clark WC, Robertson JT, Oldfield EH, Aaronson SA, Ali IU (1992) Amplification and/or overexpression of platelet-derived growth factor receptors and epidermal growth factor receptor in human glial tumors. Cancer Res 52:4550–4553
20. Fletcher CDM, Berman JJ, Corless C, Gorstein F, Lasota J, Longley BJ, Miettinen M, O'Leary TJ, Remotti H, Rubin BP,

Shmookler B, Sobin LH, Weiss SW (2002) Diagnosis of gastrointestinal stromal tumors: a consensus approach. Hum Pathol 33:459–465
21. Fletcher JA, Corless CL, Dimitrijevic S, von Mehren M, Eisenberg B, Joensuu H, Fletcher CDM, Blanke C, Demetri GD, Heinrich MC (2003) Mechanisms of resistance to imatinib mesylate (IM) in advanced gastrointestinal stromal tumor (GIST) (abstract 3275). Proc Am Soc Clin Oncol 22:815
22. Gari M, Goodeve A, Wilson G, Winship P, Langabeer S, Linch D, Vandenberghe E, Peake I, Reilly J (1999) c-kit proto-oncogene exon 8 in-frame deletion plus insertion mutations in acute myeloid leukaemia. Br J Haematol 105:894–900
23. George D (2001) Platelet-derived growth factor receptors: a therapeutic target in solid tumors. Semin Oncol 28[Suppl 17]:27–33
24. Gibson PC, Cooper K (2002) CD117 (KIT): a diverse protein with selective applications in surgical pathology. Adv Anat Pathol 9:65–69
25. Heinrich MC, Griffith DJ, Druker BJ, Wait CL, Ott KA, Ziegler AJ (2000) Inhibition of c-kit receptor tyrosine kinase activity by STI571, a selective tyrosine kinase inhibitor. Blood 96:925–932
26. Heinrich MC, Blanke CD, Druker BJ, Corless CL (2002) Inhibition of KIT tyrosine kinase activity: a novel molecular approach to the treatment of KIT-positive malignancies. J Clin Oncol 20:1692–1703
27. Heinrich MC, Corless CL, Blanke C, Demetri GD, Joensuu H, von Mehren M, McGreevey LS, Wait CL, Griffith D, Chen C-J, Haley A, Kiese B, Druker B, Roberts P, Eisenberg B, Singer S, Silberman S, Dimitrijevic S, Fletcher CDM, Fletcher JA (2002) KIT mutational status predicts clinical response to STI571 in patients with metastatic gastrointestinal stromal tumors (GISTs) (abstract 6). Proc Am Soc Clin Oncol 21:2a
28. Heinrich MC, Corless CL, Duensing A, McGreevey L, Chen C-J, Joseph N, Singer S, Griffith DJ, Haley A, Town A, Demetri GD, Fletcher CDM, Fletcher JA (2003) PDGFRA activating mutations in gastrointestinal stromal tumors. Science 299:708–710
29. Heinrich MC, Corless CL, von Mehren M, Joensuu H, Demetri GD, Blanke CD, Dimitrijevic S, Kiese B, Fletcher CDM, Fletcher JA (2003) PDGFRA and KIT mutations correlate with the clinical responses to imatinib mesylate in patients with advanced gastrointestinal stromal tumors (GIST) (abstract 3274). Proc Am Soc Clin Oncol 22:815
30. Hirota S, Isozaki K, Moriyama Y, Hashimoto K, Nishida T, Ishiguro S, Kawano K, Hanada M, Kurata A, Takeda M, Tunio GM, Matsuzawa Y, Kanakura Y, Shinomura Y, Kitamura Y (1998) Gain-of-function mutations of c-kit in human gastrointestinal stromal tumors. Science 279:577–580
31. Hirota S, Nishida T, Isozaki K, Taniguchi M, Nakamura J, Okazaki T, Kitamura Y (2001) Gain-of-function mutation at the extracellular domain of KIT in gastrointestinal stromal tumours. J Pathol 193:505–510
32. Hirota S, Nishida T, Isozaki K, Taniguchi M, Nishikawa K, Ohashi A, Takabayashi A, Obayashi T, Okuno T, Kinoshita K, Chen H, Shinomura Y, Kitamura Y (2002) Familial gastrointestinal stromal tumors associated with dysphagia and novel type germline mutation of KIT gene. Gastroenterology 122:1493–1499
33. Hirota S, Ohashi A, Nishida T, Isozaki K, Kinoshita K, Shinomura Y, Kitamura Y (2003) Gain-of-function mutations of platelet-derived growth factor receptor α gene in gastrointestinal stromal tumors. Gastroenterology 125:660–667
34. Hochhaus A, Kreil S, Corbin AS, La Rosée P, Müller MC, Lahaye T, Hanfstein B, Schoch C, Cross NCP, Berger U, Gschaidmeier H, Druker BJ, Hehlmann R (2002) Molecular and chromosomal mechanisms of resistance to imatinib (STI571) therapy. Leukemia 16:2190–2196
35. Hongyo T, Li T, Syaifudin M, Baskar R, Ikeda H, Kanakura Y, Aozasa K, Nomura T (2000) Specific *c-kit* mutations in sinonasal natural killer/T-cell lymphoma in China and Japan. Cancer Res 60:2345–2347
36. Hubbard SR, Till JH (2000) Protein tyrosine kinase structure and function. Annu Rev Biochem 69:373–398
37. Joensuu H, Roberts PJ, Sarlomo-Rikala M, Andersson LC, Tervahartiala P, Tuveson D, Silberman SL, Capdeville R, Dimitrijevic S, Druker B, Demetri GD (2001) Effect of the tyrosine kinase inhibitor STI571 in a patient with a metastatic gastrointestinal stromal tumor. N Engl J Med 344:1052–1056
38. Kilic T, Alberta JA, Zdunek PR, Acar M, Iannarelli P, O'Reilly T, Buchdunger E, Black PM, Stiles CD (2000) Intracranial inhibition of platelet-derived growth factor-mediated glioblastoma cell growth by an orally active kinase inhibitor of the 2-phenylamino-pyrimidine class. Cancer Res 60:5143–5150
39. Kindblom LG, Remotti HE, Aldenborg F, Meis-Kindblom JM (1998) Gastrointestinal pacemaker cell tumor (GIPACT): gastrointestinal stromal tumors show phenotypic characteristics of the interstitial cells of Cajal. Am J Pathol 152:1259–1269
40. Krystal GW, Honsawek S, Litz J, Buchdunger E (2000) The selective tyrosine kinase inhibitor STI571 inhibits small cell lung cancer growth. Clin Cancer Res 6:3319–3326
41. Landuzzi L, De Giovanni C, Nicoletti G, Rossi I, Ricci C, Astolfi A, Scopece I, Scotlandi K, Serra M, Bagnara GP, Nanni P, Lollini PL (2000) The metastatic ability of Ewing's sarcoma cells is modulated by stem cell factor and by its receptor c-kit. Am J Pathol 157:1–9
42. Lasota J, Wozniak A, Sarlomo-Rikala M, Rys J, Kordek R, Nassar A, Sobin LH, Miettinen M (2000) Mutations in exons 9 and 13 of KIT gene are rare events in gastrointestinal stromal tumors: a study of 200 cases. Am J Pathol 157:1091–1095
43. Lucas DR, Al-Abbadi M, Tabaczka P, Hamre MR, Weaver DW, Mott MJ (2003) c-Kit expression in desmoid fibromatosis. Comparative immunohistochmical evaluation of two commercial antibodies. Am J Clin Pathol 119:339–345
44. Ma Y, Zeng S, Metcalfe DD, Akin C, Dimitrijevic S, Butterfield JH, McMahon G, Longley BJ (2002) The c-*KIT* mutation causing human mastocytosis is resistant to STI571 and other KIT kinase inhibitors; kinases with enzymatic site mutations show different inhibitor sensitivity profiles than wild-type kinases and those with regulatory-type mutations. Blood 99:1741–1744
45. Mace J, Biermann JS, Sondak V, McGinn C, Hayes C, Thomas D, Baker L (2002) Response of extraabdominal desmoid tumors to therapy with imatinib mesylate. Cancer 95:2373–2379
46. Maki RG, Awan RA, Dixon RH, Jhanwar S, Antonescu CR (2002) Differential sensitivity to imatinib of 2 patients with metastatic sarcoma arising from dermatofibrosarcoma protuberans. Int J Cancer 100:623–626
47. McArthur GA, Demetri GD, Heinrich M, van Oosterom A, Fletcher J, Corless C, Fletcher C, Dimitrijevic S, Nikolova Z (2003) Molecular and clinical analysis of response to imatinib for locally advanced dermatofibrosarcoma protuberans (abstract 781). Proc Am Soc Clin Oncol 22:195
48. Merchant MS, Woo C-W, Mackall CL, Thiele CJ (2002) Potential use of imatinib in Ewing's sarcoma: evidence for in vitro and in vivo activity. J Natl Cancer Inst 94:1673–1679
49. Östman A, Heldin C-H (2001) Involvement of platelet-derived growth factor in disease: development of specific antagonists. Adv Cancer Res 80:1–38
50. Reilly JT (2002) Class III receptor tyrosine kinases: role in leukaemogenesis. Br J Haematol 116:744–757
51. Rubin BP, Singer S, Tsao C, Duensing A, Lux ML, Ruiz R, Hibbard MK, Chen C-J, Xiao S, Tuveson DA, Demetri GD, Fletcher CDM, Fletcher JA (2001) KIT activation is a ubiquitous feature of gastrointestinal stromal tumors. Cancer Res 61:8118–8121
52. Rubin BP, Schuetze SM, Eary JF, Norwood TH, Mirza S, Conrad EU, Bruckner JD (2002) Molecular targeting of platelet-derived growth factor B by imatinib mesylate in a patient with metastatic dermatofibrosarcoma protuberans. J Clin Oncol 20:3586–3591
53. Sakuma Y, Sakurai S, Oguni S, Hironaka M, Saito K (2003) Alterations of the *c-kit* gene in testicular germ cell tumors. Cancer Sci 94:486–491

54. Sakurai S, Oguni S, Hironaka M, Fukayama M, Morinaga S, Saito K (2001) Mutations in c-kit gene exons 9 and 13 in gastrointestinal stromal tumors among Japanese. Jpn J Cancer Res 92:494–498
55. Slamon DJ, Leyland-Jones B, Shak S, Fuchs H, Paton V, Bajamonde A, Fleming T, Eiermann W, Wolter J, Pegram M, Baselga J, Norton L (2001) Use of chemotherapy plus a monoclonal antibody against HER2 for metastatic breast cancer that overexpresses HER2. N Engl J Med 344:783–792
56. Schlesinger J (2000) Cell signaling by receptor tyrosine kinases. Cell 103:211–225
57. Scotlandi K, Manara MC, Strammiello R, Landuzzi L, Benini S, Perdichizzi S, Serra M, Astolifi A, Nicoletti G, Lollini P-L, Bertoni F, Nanni P, Picci P (2003) *c-kit* receptor expression in Ewing's sarcoma: lack of prognostic value but therapeutic targeting opportunities in appropriate conditions. J Clin Oncol 21:1952–1960
58. Singer S, Rubin BP, Lux ML, Chen C-J, Demetri GD, Fletcher CDM, Fletcher JA (2002) Prognostic value of *KIT* mutation type, mitotic activity, and histologic subtype in gastrointestinal stromal tumors. J Clin Oncol 20:3898–3905
59. Sirvent N, Maire G, Pedeutour F (2003) Genetics of dermatofibrosarcoma protuberans family of tumors: from ring chromosomes to tyrosine kinase inhibitor treatment. Genes Chromosomes Cancer 37:1–19
60. Sjöblom T, Shimizu A, O'Brian KP, Pietras K, Dal Cin P, Buchdunger E, Dumanski JP, Östman A, Heldin C-H (2001) Growth inhibition of dermatofibrosarcoma protuberans tumors by the platelet-derived growth factor receptor antagonist STI571 through induction of apoptosis. Cancer Res 61:5778–5783
61. Taniguchi M, Nishida T, Hirota S, Isozaki K, Ito T, Nomura T, Matsuda H, Kitamura J (1999) Effect of c-kit mutations on prognosis of gastrointestinal stromal tumors. Cancer Res 59:4297–4300
62. Tian Q, Frierson HF, Krystal GW, Moskaluk CA (1999) Activating c-kit gene mutations in human germ cell tumors. Am J Pathol 154:1643–1647
63. Tremont-Lukats IW, Gilbert MR (2003) Advances in molecular therapies in patients with brain tumors. Cancer Control 10:125–137
64. Tuveson DA, Willis NA, Jacks T, Griffin JD, Singer S, Fletcher CDM, Fletcher JA, Demetri GD (2001) STI571 inactivation of the gastrointestinal stromal tumor c-KIT oncoprotein: biological and clinical implications. Oncogene 20:5054–5058
65. Van den Abbeele AD, Badawi RD (2002) Use of positron emission tomography in oncology and its potential role to assess response to imatinib mesylate therapy in gastrointestinal stromal tumors (GISTs). Eur J Cancer 38[Suppl 5]S60–S65
66. Van Oosterom AT, Judson I, Verwej J, Stroobants S, di Paola ED, Dimitrijevic S, Martens M, Webb A, Sciot R, van Glabbeke M, Siberman S, Nielsen OS (2001) Safety and efficacy of imatinib (STI571) in metastatic gastrointestinal stromal tumours: a phase I study. Lancet 358:1421–1423
67. Verweij J, Casali PG, Zalcberg J, LeCesne A, Reichard P, Blay J-Y, Issels M, van Glabbeke M, Donato Di Paola E, Judson IR (2003) Early efficacy comparison of two doses of imatinib for the treatment of advanced gastro-intestinal stromal tumors (GIST): interim results of a randomized phase III trial from the EORTC-STBSG, ISG and AGITG (abstract 3272). Proc Am Soc Clin Oncol 22:814
68. Wardelmann E, Neidt I, Bierhoff E, Speidel N, Manegold C, Fischer H-P, Pfeifer U, Pietsch T (2002) C-kit mutations in gastrointestinal stromal tumors occur preferentially in the spindle rather than in the epithelioid variant. Mod Pathol 15:125–136
69. Wardelmann E, Losen I, Hans V, Neidt I, Speidel N, Bierhoff E, Heinicke T, Pietsch T, Büttner R, Merkelbach-Bruse S (2003) Deletion of Trp-557 and Lys-558 in the juxtamembrane domain of the *c-kit* protooncogene is associated with metastatic behaviour of gastrointestinal stromal tumors. Int J Cancer 106:887–895
70. Williams DE, Eisenman J, Baird A, Rauch C, Van Ness K, March CJ, Park LS, Martin U, Mochizuki DY, Boswell HS (1990) Identification of a ligand for the c-KIT proto-oncogene. Cell 63:167–174
71. Zwick E, Bange J, Ullrich A (2002) Receptor tyrosine kinases as targets for anticancer drugs. Trends Mol Med 8:17–23

Virchows Arch (2004) 444:119–126
DOI 10.1007/s00428-003-0949-1

ORIGINAL ARTICLE

Irene Esposito · Frank Bergmann · Roland Penzel · Fabio F. di Mola · Shailesh Shrikhande · Markus W. Büchler · Helmut Friess · Herwart F. Otto

Oligoclonal T-cell populations in an inflammatory pseudotumor of the pancreas possibly related to autoimmune pancreatitis: an immunohistochemical and molecular analysis

Received: 4 September 2003 / Accepted: 26 November 2003 / Published online: 14 January 2004

Abstract Inflammatory pseudotumors (IPT), also known as inflammatory myofibroblastic tumors (IMT), are benign inflammatory processes that may have an infectious etiology and are very rare in the pancreatico-biliary region. Recent studies suggest a biological distinction between IPT and IMT, the latter being a true neoplastic process. We describe a case of pancreatic IPT, originally diagnosed as malignancy, which presumably recurred 4 months after the operation. Histologically, the tumor consisted of a smooth muscle actin and CD68-positive spindle cell population and a more abundant mononuclear inflammatory cell population, primarily composed of macrophages and T-lymphocytes. Inflammatory cells were the source of connective tissue growth factor and transforming growth factor-β1 and tended to accumulate around nerves and blood vessels, as well as around residual pancreatic parenchymal elements, where an intense angiogenetic response was detected. Comparative genomic hybridization analysis of the tumor showed no chromosomal imbalances. Polymerase chain reaction-based analysis of T-cell receptor γ gene rearrangement revealed an oligoclonal pattern. These findings suggest that the pathogenesis of aggressive cases of IPT could be related to the development of an intense and self-maintaining immune response, with the emergence of clonal populations of T-lymphocytes. The relation of the pancreatic IPT to autoimmune pancreatitis is emphasized.

Keywords Inflammatory pseudotumor · Pancreas · TCRγ-rearrangement · Autoimmune pancreatitis

I. Esposito (✉) · F. Bergmann · R. Penzel · H. F. Otto
Department of Pathology,
University of Heidelberg,
Im Neuenheimer Feld 220, 69120 Heidelberg, Germany
e-mail: irene_esposito@med.uni-heidelberg.de
Tel.: +49-62-21564351
Fax: +49-62-21565251

F. F. di Mola · S. Shrikhande · M. W. Büchler · H. Friess
Department of General Surgery,
University of Heidelberg,
Germany

S. Shrikhande
Department of Gastrointestinal Surgical Oncology,
Tata Memorial Hospital,
Mumbai, India

Introduction

Inflammatory pseudotumors (IPT), also termed inflammatory myofibroblastic tumors (IMT), are uncommon mass lesions whose origin and pathophysiology are still controversial. They consist of collagen fibers, smooth muscle actin (SMA)-expressing spindle cells (so-called "myofibroblasts") and an intense, mostly lymphoplasmacellular, inflammatory infiltrate [13]. IPT were originally described in the lung and the gastrointestinal tract [7, 29, 33], but they can occur in virtually every anatomical site [12]. The spindle cell component may display atypical features, and it is mandatory to differentiate these lesions from mesenchymal tumors that show histological similarities (e.g., inflammatory fibrosarcoma) [11]. Moreover, recent studies have demonstrated the presence of monoclonality [30], aneuploidy [4] and cytogenetic anomalies [27] in some cases of IMT of various origins. Balanced chromosomal translocations involving the anaplastic lymphoma kinase (ALK) gene have been found in some (but not all) cases of IMT of the lymph node and spleen [27]. Accordingly, the existence of two groups of biologically distinct lesions—namely IMT, which are ALK-positive, and IPT, which are ALK-negative—has been proposed. Nevertheless, the two terms are often used synonymously.

Several investigators have proposed an infectious etiology for IPT/IMT. Members of the herpesvirus family, including Epstein-Barr virus (EBV) [3] and human herpesvirus-8 [18], have been detected by in situ hybridization in the nuclei of the spindle and/or lymphocytic components. DNA fragments with sequence homology to *Pseudomonas veronii* have been isolated from a mesenteric lymph

node of a patient affected by ileo-cecal IPT [9]. Cytokines produced by the microorganisms have been con- sidered responsible for the systemic symptoms of fever, night sweats, fatigue and weight loss frequently reported in IPT.

The two entities of IPT/IMT have been described in the pancreatico-biliary region as single case reports or small series [2, 26, 34, 36, 38], without a clear-cut distinction between them. Here, we report a case of IPT/IMT of the pancreas. We further provide a characterization of its cell population, with particular attention paid to the inflammatory cell component, in view of the fact that the inflammatory cells seem to play a fundamental role in the pathogenesis of the lesion through the production of cytokines and growth factors that, in turn, influence the phenotypic characteristics of the spindle cell and connective tissue elements [23, 28]. We also discuss the potential relationship between IPT and autoimmune pancreatitis.

Clinical history

A 69-year-old male patient presented with a short history of upper abdominal pain and discomfort. Computed tomography scan revealed the presence of a large pancreatic body–tail tumor mass, in close proximity to the superior mesenteric vessels, but without encasement of the vessels themselves (Fig. 1). Fine-needle aspiration cytology and open surgical biopsy of an enlarged left supraclavicular lymph node were performed. The diagnosis was hyperplastic changes and a small lymphangioma, in the absence of malignant cells. At the time of surgery, neither ascitis nor liver or peritoneal metastases were found. A left pancreatectomy with splenectomy and colon splenic flexure resection was performed. An intraoperative frozen section of the tumor mass was interpreted as adenocarcinoma.

The postoperative course was complicated by formation of an intraabdominal abscess and colonic distension. The final histopathological diagnosis was "inflammatory myofibroblastic tumor of the pancreas." The patient was discharged after 1 month of hospitalization. He developed jaundice due to multiple strictures along the extrahepatic bile duct, from the hepatic hilus to the distal choledocus (Fig. 2), 4 months after surgery. He died after 7 months of hospitalization due to sepsis. Serological tests for the detection of EBV, cytomegalovirus (CMV) and human T-cell lymphotropic virus were negative. Laboratory tests revealed serum bilirubin 7 mg/dl, alkaline phosphatase 355 U/l (normal, 40–170 U/l), γ-glutamyl transpeptidase 106 U/l (normal, 3–28 U/l), glutamic pyruvic transaminase 42 U/l (normal, <24 U/l), glutamic oxalacetic transaminase 32 U/l (normal, <18 U/l). Serum total IgG were increased (25.3 g/l, normal 7–16 g/l), but the levels of IgG4 were in the normal range (0.49 g/l, normal 0.052–1.2 g/l).

Fig. 1 Contrast-enhanced computed tomography reveals a diffuse mass in the pancreatic body–tail

Fig. 2 Endoscopic retrograde colangiography showing the presence of multiple strictures along the common bile duct

Materials and methods

Immunohistochemistry

Formalin-fixed, paraffin-embedded or frozen tissue sections cut from the tumor mass were subjected to immunohistochemical analysis using the following primary monoclonal or polyclonal antibodies: pan-cytokeratin (Kl1, Serotec GmbH, Düsseldorf, Germany); cytokeratin 7 (OV-TL12/30, Dako, Carpenteria, CA, USA); vimentin (V9, Dako); SMA (1A4, Dako); CD68 (KP-1, Dako); CD45 (LCA, Dako); CD20 (L26, Dako); CD45RO (UCHL1, Dako); CD3 (Dako); CD4 (OKT-4, Sanquin, Amsterdam, The Netherlands); CD8 (OKT-8, Sanquin); CD43 (DF-T1, Dako); CD56 (Cell Marque, Hot Springs, AR, USA); ALK (Alk1, Dako); CD30 (BER-H2, Dako); CD34 (QBEND-10, Immunotech, Marseille, France); κ and λ chain (A8B5 and N10/2, Dako); tryptase (G3, Chemicon International Inc., Temecula, CA, USA); transforming growth factor beta 1 (TGF-β1) (Santa Cruz Biotechnology, Santa Cruz, CA, USA); connective tissue growth factor (CTGF) (Santa Cruz); Ki-67 (MIB1, Dako); Epstein-Barr virus latent membrane protein (LMP) (CS 1–4, Dako); and CMV early antigen (CCH2, Dako). The streptavidin-biotin-phosphatase method or the peroxidase, biotin-free EnVision+ System (Dako) was used to detect the binding of the primary antibodies.

TCRγ rearrangement

A semi-nested polymerase chain reaction (PCR) analysis of T-cell receptor gamma (TCRγ) gene rearrangement was used to assess

clonality of the lymphocytic population [5]. Briefly, 200 ng of genomic DNA from the tumor and from a peripancreatic hyperplastic lymph node (control) were amplified in two separate reactions, each using the following primers: $V1_{1-8}$ (5′-TGC AGC CAG TCA GAA ATC TTC C-3′) + $JGT_{1/2}$ (5′-AAG TGT TGT TCC ACT GCC AAA-3′) and $V1_{1-8}$ + JGT_3 (5′-AGT TAC TAT GAG C (TC) AGT CCC-3′). The second amplification round was performed with 1 µl of the first PCR product with primer sets $V2_{1-8}$ (5′-ACG GCG TCT TC (AT) GTA CTA TGA C-3′) + $JGT_{1/2}$ and $V2_{1-8}$ + JGT_3. PCR products of the second amplification were separated on a 6% polyacrylamide gel.

Comparative genomic hybridization

To detect possible chromosomal imbalances of the tumor, a comparative genomic hybridization (CGH) analysis was performed as previously described [22]. Briefly, tumor DNA was extracted from paraffin-embedded material. In a nick translation, tumor DNA was biotinylated, and normal human DNA was labeled with digoxigenin. The probes were then hybridized onto metaphase spreads. Avidin-conjugated fluorescein and anti-digoxigenin-rhodamin conjugate were used for signal detection of biotinylated tumor DNA and digoxigenin-labeled reference DNA, respectively. Hybridized metaphases (n=20) were then captured and analyzed using an inverted microscope (Zeiss Axiovert S 100), a charge-coupled device camera and CGH software (MetaSystems, Germany). Chromosomal gains were presumed if the ratio of tumor to normal signals reached or exceeded 1.25. The respective ratio for chromosomal losses was 0.80.

Results

Pathological findings

Macroscopically, a tumor mass without clear-cut demarcation from the surrounding parenchyma was identified in the pancreatic body–tail. The tumor was hard and yellowish gray, and the normal lobular architecture of pancreatic parenchyma was only partially preserved.

Histologically, the tumor consisted of bands of dense collagen tissue that surrounded lobules formed by residual pancreatic parenchyma, mostly represented by islets, degenerating acini and small ducts (Fig. 3A). Some larger ducts were still recognizable. These residual parenchymal elements were embedded in a dense, mostly mononuclear, inflammatory infiltrate, which showed a particular clustering around blood vessels (Fig. 3B, C) and nerves (Fig. 3E). Inflammation of the vessel walls (arteritis and phlebitis) was present (Fig. 3B, C). At the border between the pancreatic mass and the surrounding soft tissue, the connective tissue was more abundant, displaying large hyaline areas and forming a sort of "capsule" around the entire organ. Here, the inflammatory infiltrate was less dense, mostly consisting of lymphoid follicles with germinal centers. The bands of connective tissue contained spindle cells that were sometimes plump, but always cytologically typical. They exhibited vimentin immunoreactivity, indicating their mesenchymal origin, with a large subpopulation of SMA-positive elements (the so-called myofibroblasts) (Fig. 4A, B); some of them were also CD68 positive (Fig. 4C). Moreover, they expressed CTGF and TGFβ-1; CTGF was also extensively expressed in inflamed residual pancreatic ducts and degenerating acini and in the inflammatory infiltrate (Fig. 5A). TGFβ-1 had the same localization of CTGF, with the exception of a diffuse staining in the connective tissue bands, consistent with its secretion into the extracellular space by the fibroblasts (Fig. 5B), and a less frequent expression in inflammatory cells.

The inflammatory infiltrate mostly consisted of CD68-positive mononuclear cells, therefore, identified as macrophages (Fig. 4C). They were particularly abundant in the lobules of residual pancreatic parenchyma, but some of them could also be found in the connective tissue bands.

T-lymphocytes, identified by CD3 and CD45RO immunostaining, were a predominant component of the inflammatory infiltrate. They accumulated around blood vessels, especially small veins (Fig. 3D), and around nerves (Fig. 3F). T-lymphocyte subtyping revealed a slight preponderance of the CD4-positive over the CD8-positive cells. B-lymphocytes (CD20+) and a polyclonal population of plasma cells (κ and λ-chain immunostaining) were also present, although to a lesser extent. CD30 and ALK-expressing lymphocytes were absent, as well as CD56-positive natural killer lymphocytes. At the periphery of the pancreas, lymphocytes were mostly organized in lymphoid follicles with well-developed germinal centers; whereas, in the context of the pancreatic parenchyma, they were part of the diffuse inflammatory infiltrate. Mast cells, identified by specific tryptase immunostaining [17], were mostly found in the lobules of the destroyed pancreatic parenchyma, around degenerating acini and inflamed ducts. Scattered eosinophils were also present.

Angiogenesis, evaluated by means of CD34 immunostaining of endothelial cells, was extremely developed in the degenerating pancreatic parenchyma (Fig. 5C). Immunohistochemical analysis of cell proliferation by identification of the proliferation-associated antigen Ki-67 revealed scattered positivity (proliferating index <5%) in inflammatory cells and regenerating pancreatic ductal cells. The myofibroblast compartment displayed a lower proliferating index (Fig. 5D). Neither EBV-LMP nor CMV-early antigen immunoreactivity was detected.

TCRγ rearrangement

PCR analysis of TCRγ-gene rearrangement revealed three prominent bands in the tumor DNA and a smear in the DNA from the peripancreatic lymph node when the set of primers $V1_{1-8}$ + $JGT_{1/2}$ was used (Fig. 6). This result suggests the existence of an oligoclonal population of T-lymphocytes within the tumor mass and a polyclonal population in the surrounding lymph nodes.

CGH analysis

No chromosomal imbalances were detected by comparative genomic hybridization analysis.

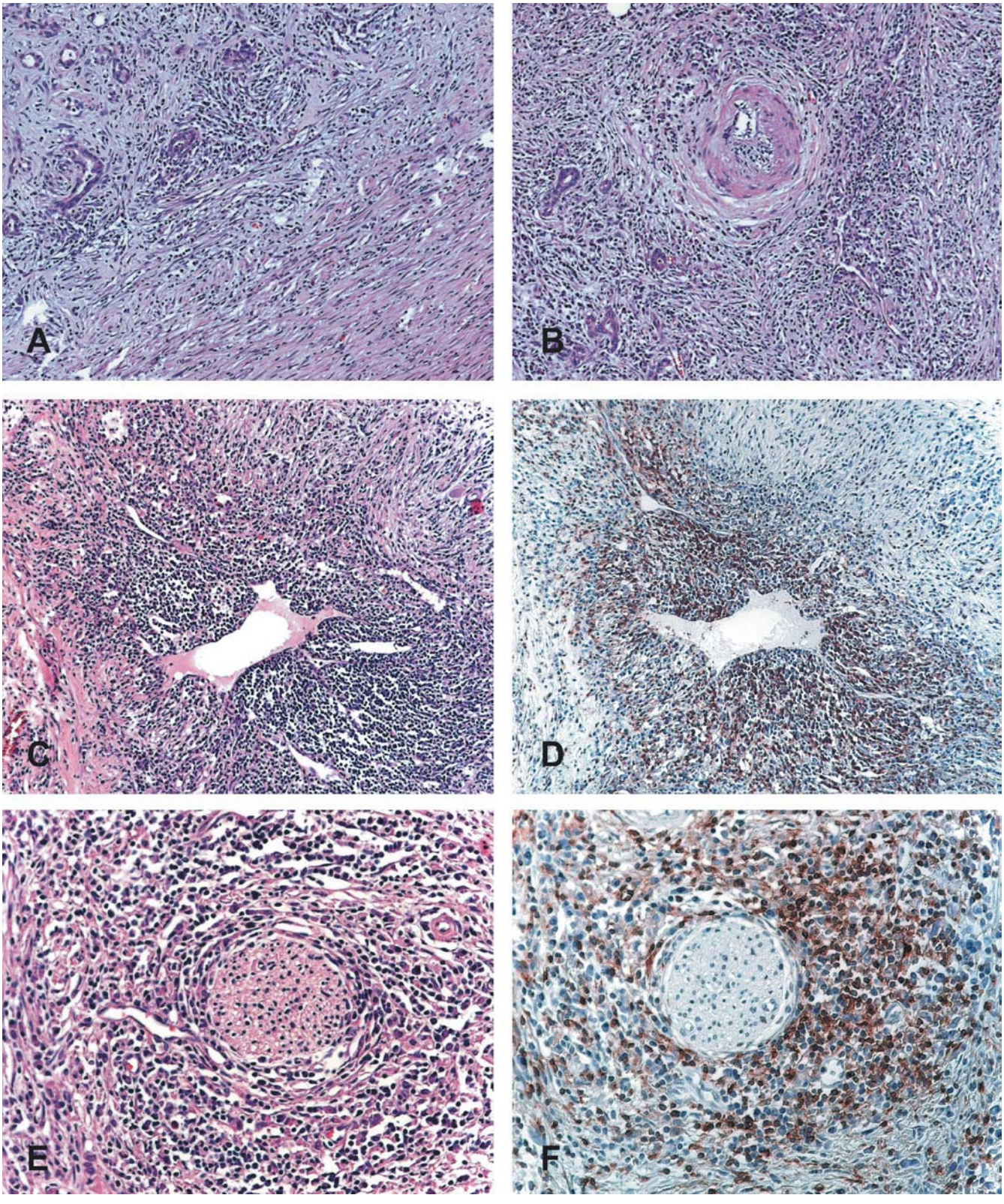

Fig. 3 Inflammatory pseudotumor of the pancreas. **A** The tumor mass consists of two main cell populations: spindle cells, arranged to form large bands of dense collagen (*right*) around and within the pancreatic parenchyma and mononuclear inflammatory cells that surround residual pancreatic ducts (*left*). **B**, **C**, **E** The inflammatory cells accumulate around and in the wall of arteries (**B**), veins (**C**) and around nerves (**E**). **D**, **F** Immunostaining for CD45 RO demonstrates a great preponderance of T-lymphocytes. Original magnifications ×100 (**A**–**D**), ×200 (**E**–**F**)

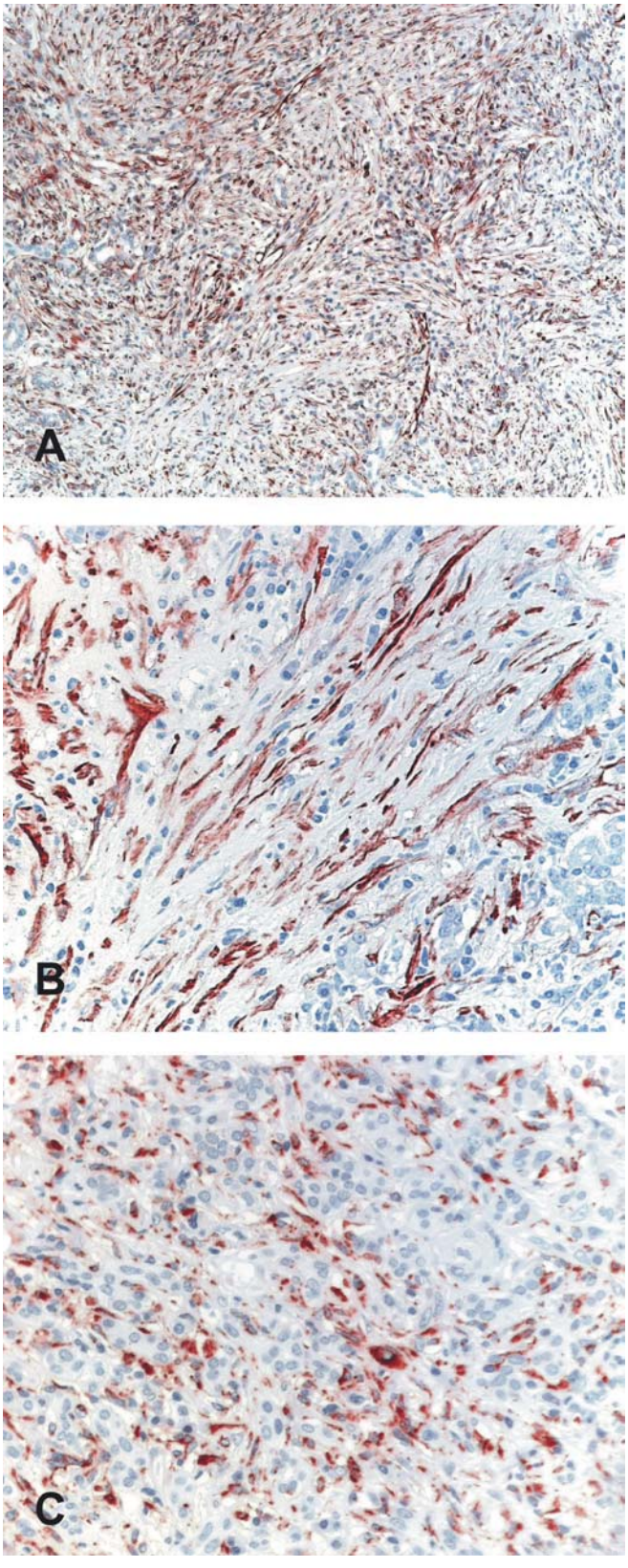

Fig. 4 Immunohistochemical characterization of the cell populations. **A** Immunostaining for vimentin shows a strong positivity in the spindle as well as in the inflammatory cell component. **B** The spindle cells exhibit immunoreactivity for smooth muscle actin. **C** Immunostaining for CD68 reveals that many of the inflammatory cells are macrophages. Original magnifications ×100 (**A**), ×200 (**B**–**C**)

Discussion

This paper describes a case of IPT/IMT arising in the pancreatic body–tail region, which presumably recurred in the pancreatic head–biliary region 4 months after resection. The importance of this pathological lesion, which has been described with increasing frequency in the literature, resides in the fact that it can be preoperatively mistaken for a malignant tumor. Besides this clinical relevance, the biology of IPT/IMT is challenging and not completely clarified. IPT of the pancreas have been described since 1984 [2], but only in recent years have they been better characterized from a biological point of view [26, 34, 36, 38]. This characterization mainly concerns the spindle cell component, consisting of vimentin and SMA-positive myofibroblasts. Table 1 summarizes the more relevant clinical data and immunohistochemical findings of the four studies cited above. Only two of them describe in more detail the inflammatory cell component of IPT/IMT, which mainly consists of macrophages, T-lymphocytes and, to a lesser extent, B-lymphocytes [26, 38]. The relevance of the inflammatory infiltrate in the pathogenesis of pancreatic IPT/IMT is suggested by the findings of the present study: inflammatory cells could play an active fibrogenetic role in IPT/IMT through the production of TGF-β1 and CTGF. These two factors are fundamental mediators of pathological processes characterized by extracellular matrix deposition and fibrosis, such as chronic pancreatitis [15], glomerulosclerosis and tubulo-interstitial fibrosis [8, 20], scleroderma [31] and liver cirrhosis [1]. In chronic pancreatitis, TGF-β1 and CTGF are produced by degenerating acinar cells and metaplastic ducts (tubular complexes), as well as by fibroblasts. In addition, TGF-β1, but not CTGF, is expressed by the inflammatory cell population [15]. In pancreatic IPT/IMT, it is likely that both the residual pancreatic parenchyma and the inflammatory cells induce myofibroblast accumulation through the expression of TGF-β1 and CTGF. A similar phenomenon has been described, for example, in animal models of lung fibrosis [37], where TGF-β1 and CTGF act as the main mediators of the fibrogenic response.

Another interesting and important finding of this study is the identification of clonal populations of T-lymphocytes in the tumor tissue but not in surrounding hyperplastic lymph nodes. Monoclonal T-lymphocytes have been described in inflammatory sclerosing disorders, such as idiopathic retroperitoneal fibrosis [14], which shares some morphological similarities with IPT/IMT. However, they have never been investigated in pancreatic IPT/IMT and have never been found in IPT arising in other anatomical sites [6, 28]. The significance and the origin of the clonal T-lymphocytes in this case of IPT/IMT are currently not known, but it can be speculated that they develop in the context of an intense and destructive, maybe also self-stimulating, inflammatory reaction. The largest number of inflammatory cells was found around residual pancreatic acini and in the walls of blood vessels; in the same areas, the highest proliferative activity of the inflammatory component was detected, as evidenced by Ki-67 immuno-

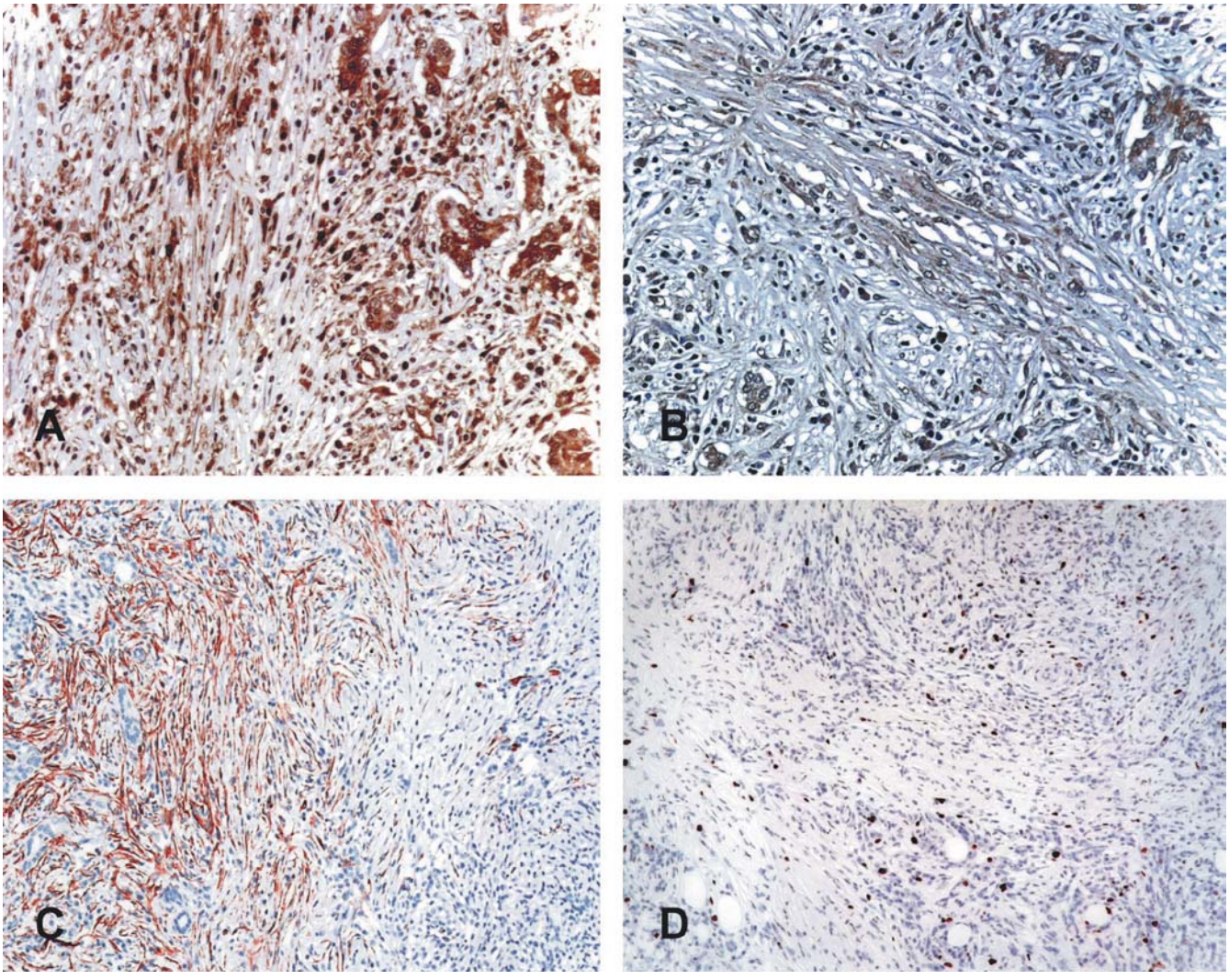

Fig. 5 Connective tissue growth factor (**A**) and transforming growth factor-β (**B**) expression in the proliferating pancreatic ducts, in the inflammatory cells and in the spindle cells. **C** Markedly high angiogenetic activity within the residual pancreatic parenchyma as shown by CD34 immunostaining. **D** The Ki-67 proliferative index is <5% and mostly confined to the inflammatory cells and the residual pancreatic parenchymal elements. Original magnifications ×200 (**A, B**), ×100 (**C**, **D**)

Table 1 Clinical and immunohistochemical characteristics of pancreatic inflammatory pseudotumors/inflammatory myofibroblastic tumors (IPT/IMT)

Author	Sex/age	Immunohistochemistry		Clinical behavior
		Spindle cells	Inflammatory cells	
Zanger P (2002) [38]	F/62	Vimentin+, SMA+	B-lymphocytes*, T-lymphocytes*, CD68 +	No recurrence after 6 months
Wreesman V (2001) [36]	M/62	Actin +, SMA +	Not assessed	No recurrence after 6 years
	M/56	Actin +, SMA +	Not assessed	No recurrence after 5 years
	M/50	Actin +, SMA +	Not assessed	No recurrence after 4 years
	M/45	Actin +, SMA +	Not assessed	No recurrence after 10 years
	F/57	Actin +, SMA +	Not assessed	No recurrence after 3 years
	F/32	Actin +, SMA +	Not assessed	No recurrence after 12 years
Walsh SV (1998) [34]	M/35	Vimentin +, SMA +	CD20 +, OPD4 +, CD8 +	Lung IMT after 6 years
Kroft SH (1995) [26]	F/42	Vimentin +, Actin −	Not assessed	No recurrence after 6 months

SMA: smooth muscle actin
*: no marker specified
OPD4: marker of T-helper/inducer lymphocytes

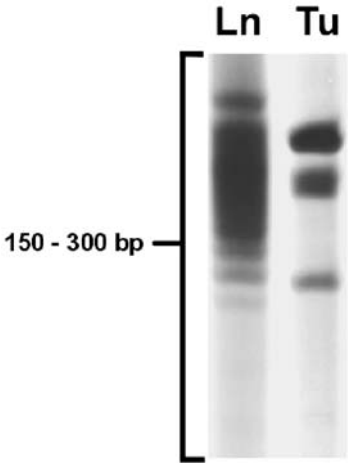

Fig. 6 Analysis of T-cell receptor gamma (TCR-γ) gene rearrangements by polymerase chain reaction and polyacrylamide gel electrophoresis. As detailed in the Materials and Methods section, two sets of primers for the V and J regions of the TCR γ gene were used. Three discrete bands were seen in the tumor DNA (*Tu*), suggesting the existence of oligoclonal populations of T-lymphocytes. Control DNA from a peripancreatic lymph node (*Ln*) gave a smear instead

staining. As a consequence of tissue destruction, new epitopes are exposed, and they trigger an "explosive" immune response that could culminate in the development of clonal populations of lymphocytes. The aggressive course of the disease, with a probable early relapse, could be explained by these considerations. The cause of such an intense immunological response is unknown; some of the main viral pathogens were investigated at the clinical or morphological levels, with negative results.

A recent editorial [12] points to the existence of different subtypes of IPT/IMT: one group arises in a younger population and its main cellular components have the phenotype of myofibroblasts [10], while the second group is represented by the infection-related IPT, and its main cellular components are CD68-positive spindle cells [9]. Accordingly, tumors that fall in the first category are better designated IMT. They can recur and display a sarcomatous progression; they are probably true neoplasms [16]. IMT, with evidence of clonality [30] or of chromosomal translocations involving the ALK receptor tyrosine-kinase locus [19], belong to this category. Therefore, although a histopathological diagnosis of IMT was made, the term IPT would be more appropriate in the case reported here, where the inflammatory component is predominant and the myofibroblastic component has a bland morphological and genetic appearance, as shown by immunostaining (low proliferative activity, no ALK expression) and CGH results. Recently, the relationship between IPT and autoimmune pancreatitis (also known as lymphoplasmacytic sclerosing pancreatitis or duct destructive chronic pancreatitis) has been discussed, and both diseases are considered part of the same disease spectrum. Autoimmune pancreatitis can be associated with the presence of an IPT-resembling tumor-like mass. Histologically, it is characterized by dense periductal lymphoplasmacytic infiltrates, mainly consisting of T-lymphocytes, periphlebitis and interstitial fibrosis [24, 35], features that were also prominent in the case reported here. Moreover, recurrent autoimmune pancreatitis can present with biliary strictures [24] and shows a dramatic response to steroid therapy [21, 32]. Although the diagnostic criteria for autoimmune pancreatitis were not completely fulfilled (e.g., absence of a "ductocentric inflammation," that is, the accumulation of the inflammatory cells around the ducts, with relative sparing of the acinar parenchyma; absence of abnormal IgG4-serum levels) it cannot be excluded that this case of IPT developed in the context of an autoimmune pancreatitis.

A striking aspect of this case of pancreatic IPT is the extraordinary generation of new vessels in the areas of tissue destruction, as revealed by CD34 immunostaining. Angiogenesis develops as a physiological response in the context of wound healing and tissue repair. At the same time, endothelial cells are directly involved in the inflammatory response through the expression of adhesion molecules that play a major role in the recruitment of circulating inflammatory cells [25]. Therefore, the intense angiogenetic response underscores once more the central role of inflammation in the destruction of the pancreatic parenchyma and, consequently, in the pathogenesis of IPT.

In summary, the case reported in this study has the characteristics of the category of IPT described above: the spindle cells are SMA and CD68 positive and do not show any kind of atypia; there are neither chromosomal aberrations nor ALK overexpression. Moreover, the spindle cell component is quantitatively very limited, compared with the number of inflammatory cells (macrophages and T-lymphocytes), and could be interpreted as merely "reactive." The clinical presentation and the morphological aspect strongly suggest an association between pancreatic IPT and autoimmune pancreatitis. These two entities could, therefore, be interpreted as different phases/manifestations of the same disease process. An immune response to an unknown trigger is the main mediator of tissue aggression and destruction and, due to the development of clonal populations of T-lymphocytes, is likely to be capable of self-maintenance. Inasmuch as clonal populations of T-lymphocytes have not previously been reported in IPT, it seems necessary to widen the spectrum of different processes included in the definition of IPT/IMT and to better investigate their relationship with lymphoproliferative disorders.

References

1. Abou-Shady M, Friess H, Zimmermann A, di Mola FF, Guo XZ, Baer HU, Buchler MW (2000) Connective tissue growth factor in human liver cirrhosis. Liver 20:296–304
2. Abrebanel P, Sarfaty S, Gal R, Chaimoff C, Kessler E (1984) Plasma cell granuloma of the pancreas. Arch Pathol Lab Med 108:531–532
3. Arber DA, Kamel OW, van de Rijn M, Davis RE, Medeiros LJ, Jaffe ES, Weiss LM (1995) Frequent presence of the Epstein-

Barr virus in inflammatory pseudotumor. Hum Pathol 26:1093–1098
4. Biselli R, Boldrini R, Ferlini C, Boglino C, Inserra A, Bosman C (1999) Myofibroblastic tumours: neoplasias with divergent behaviour. Ultrastructural and flow cytometric analysis. Pathol Res Pract 195:619–632
5. Bourguin A, Tung R, Galili N, Sklar J (1990) Rapid, nonradioactive detection of clonal T-cell receptor gene rearrangements in lymphoid neoplasms. Proc Natl Acad Sci U S A 87:8536–8540
6. Broughan TA, Fischer WL, Tuthill RJ (1993) Vascular invasion by hepatic inflammatory pseudotumor. A clinicopathologic study. Cancer 71:2934–2940
7. Brunn H (1939) Two interesting benign lung tumours of contradictory histopathology. Remarks in the necessity for maintaining the chest tumour registry. J Thorac Cardiovasc Surg 9:119–131
8. Chen Y, Blom IE, Sa S, Goldschmeding R, Abraham DJ, Leask A (2002) CTGF expression in mesangial cells: involvement of SMADs, MAP kinase, and PKC. Kidney Int 62:1149–1159
9. Cheuk W, Woo PC, Yuen KY, Yu PH, Chan JK (2000) Intestinal inflammatory pseudotumour with regional lymph node involvement: identification of a new bacterium as the aetiological agent. J Pathol 192:289–292
10. Coffin CM, Watterson J, Priest JR, Dehner LP (1995) Extrapulmonary inflammatory myofibroblastic tumor (inflammatory pseudotumor). A clinicopathologic and immunohistochemical study of 84 cases. Am J Surg Pathol 19:859–872
11. Coffin CM, Dehner LP, Meis-Kindblom JM (1998) Inflammatory myofibroblastic tumor, inflammatory fibrosarcoma, and related lesions: an historical review with differential diagnostic considerations. Semin Diagn Pathol 15:102–110
12. Dehner LP (2000) The enigmatic inflammatory pseudotumours: the current state of our understanding, or misunderstanding. J Pathol 192:277–279
13. Dehner LP, Coffin CM (1998) Idiopathic fibrosclerotic disorders and other inflammatory pseudotumors. Semin Diagn Pathol 15:161–173
14. Dent GA, Baird DB, Ross DW (1991) Systemic idiopathic fibrosis with T-cell receptor gene rearrangement. Arch Pathol Lab Med 115:80–83
15. di Mola FF, Friess H, Martignoni ME, Di Sebastiano P, Zimmermann A, Innocenti P, Graber H, Gold LI, Korc M, Buchler MW (1999) Connective tissue growth factor is a regulator for fibrosis in human chronic pancreatitis. Ann Surg 230:63–71
16. Donner LR, Trompler RA, White RR 4th (1996) Progression of inflammatory myofibroblastic tumor (inflammatory pseudotumor) of soft tissue into sarcoma after several recurrences. Hum Pathol 27:1095–1098
17. Esposito I, Friess H, Kappeler A, Shrikhande S, Kleeff J, Ramesh H, Zimmermann A, Buchler M (2001) Mast cell distribution and activation in chronic pancreatitis. Hum Pathol 32:1174–1183
18. Gomez-Roman JJ, Ocejo-Vinyals G, Sanchez-Velasco P, Nieto EH, Leyva-Cobian F, Val-Bernal JF (2000) Presence of human herpesvirus-8 DNA sequences and overexpression of human IL-6 and cyclin D1 in inflammatory myofibroblastic tumor (inflammatory pseudotumor). Lab Invest 80:1121–1126
19. Griffin CA, Hawkins AL, Dvorak C, Henkle C, Ellingham T, Perlman EJ (1999) Recurrent involvement of 2p23 in inflammatory myofibroblastic tumors. Cancer Res 59:2776–2780
20. Gupta S, Clarkson MR, Duggan J, Brady HR (2000) Connective tissue growth factor: potential role in glomerulosclerosis and tubulointerstitial fibrosis. Kidney Int 58:1389–1399
21. Hamano H, Kawa S, Horiuchi A, Unno H, Furuya N, Akamatsu T, Fukushima M, Nikaido T, Nakayama K, Usuda N, Kiyosawa K (2001) High serum IgG4 concentrations in patients with sclerosing pancreatitis. N Engl J Med 344:732–738
22. Isola J, DeVries S, Chu L, Ghazvini S, Waldman F (1994) Analysis of changes in DNA sequence copy number by comparative genomic hybridization in archival paraffin-embedded tumor samples. Am J Pathol 145:1301–1308
23. Kasaragod AB, Lucia MS, Cabirac G, Grotendorst GR, Stenmark KR (2001) Connective tissue growth factor expression in pediatric myofibroblastic tumors. Pediatr Dev Pathol 4:37–45
24. Kloppel G, Luttges J, Lohr M, Zamboni G, Longnecker D (2003) Autoimmune pancreatitis: pathological, clinical, and immunological features. Pancreas 27:14–19
25. Koning GA, Schiffelers RM, Storm G (2002) Endothelial cells at inflammatory sites as target for therapeutic intervention. Endothelium 9:161–171
26. Kroft SH, Stryker SJ, Winter JN, Ergun G, Rao MS (1995) Inflammatory pseudotumor of the pancreas. Int J Pancreatol 18:277–283
27. Kutok JL, Pinkus GS, Dorfman DM, Fletcher CD (2001) Inflammatory pseudotumor of lymph node and spleen: an entity biologically distinct from inflammatory myofibroblastic tumor. Hum Pathol 32:1382–1387
28. Menke DM, Griesser H, Araujo I, Foss HD, Herbst H, Banks PM, Stein H (1996) Inflammatory pseudotumors of lymph node origin show macrophage-derived spindle cells and lymphocyte-derived cytokine transcripts without evidence of T-cell receptor gene rearrangements. Implications for pathogenesis and classification as an idiopathic retroperitoneal fibrosis-like sclerosing immune reaction. Am J Clin Pathol 105:430–439
29. Pettinato G, Manivel JC, De Rosa N, Dehner LP (1990) Inflammatory myofibroblastic tumor (plasma cell granuloma). Clinicopathologic study of 20 cases with immunohistochemical and ultrastructural observations. Am J Clin Pathol 94:538–546
30. Sastre-Garau X, Couturier J, Derre J, Aurias A, Klijanienko J, Lagace R (2002) Inflammatory myofibroblastic tumour (inflammatory pseudotumour) of the breast. Clinicopathological and genetic analysis of a case with evidence for clonality. J Pathol 196:97–102
31. Simms RW, Korn JH (2002) Cytokine directed therapy in scleroderma: rationale, current status, and the future. Curr Opin Rheumatol 14:717–722
32. Stathopoulos G, Nourmand AD, Blackstone M, Andersen D, Baker AL (1995) Rapidly progressive sclerosing cholangitis following surgical treatment of pancreatic pseudotumor. J Clin Gastroenterol 21:143–148
33. Umiker WO, Iverson L (1954) Postinflammatory "tumour" of the lung. Report of four cases simulating xanthoma, fibroma, or plasma cell granuloma. J Thorac Cardiovasc Surg 28:55–63
34. Walsh SV, Evangelista F, Khettry U (1998) Inflammatory myofibroblastic tumor of the pancreaticobiliary region: morphologic and immunocytochemical study of three cases. Am J Surg Pathol 22:412–418
35. Weber SM, Cubukcu-Dimopulo O, Palesty JA, Suriawinata A, Klimstra D, Brennan MF, Conlon K (2003) Lymphoplasmacytic sclerosing pancreatitis. Inflammatory mimic of pancreatic carcinoma. J Gastrointest Surg 7:129–139
36. Wreesmann V, van Eijck CH, Naus DC, van Velthuysen ML, Jeekel J, Mooi WJ (2001) Inflammatory pseudotumour (inflammatory myofibroblastic tumour) of the pancreas: a report of six cases associated with obliterative phlebitis. Histopathology 38:105–110
37. Xing Z, Tremblay GM, Sime PJ, Gauldie J (1997) Overexpression of granulocyte-macrophage colony-stimulating factor induces pulmonary granulation tissue formation and fibrosis by induction of transforming growth factor-beta 1 and myofibroblast accumulation. Am J Pathol 150:59–66
38. Zanger P, Kronsbein U, Merkle P, Bosse A (2002) Inflammatory myofibroblastic tumor of the pancreas with regional lymph node involvement. Pathologe 23:161–166

Virchows Arch (2004) 444:127–134
DOI 10.1007/s00428-003-0948-2

ORIGINAL ARTICLE

Cord Langner · Beate J. Wegscheider · Manfred Ratschek · Luigi Schips · Richard Zigeuner

Keratin immunohistochemistry in renal cell carcinoma subtypes and renal oncocytomas: a systematic analysis of 233 tumors

Received: 26 November 2003 / Accepted: 26 November 2003 / Published online: 16 January 2004

Abstract Keratin immunohistochemistry represents a widely applied differential diagnostic tool in surgical pathology. To investigate the value of keratin subtyping for the diagnosis among histological subtypes of renal cell carcinoma and oncocytomas, we performed a detailed immunohistochemical study, applying 22 different monoclonal keratin antibodies on a large series of 233 renal tumors [125 conventional, 22 chromophobe, and 20 papillary (12 type-1, 8 type-2 tumors) cancers and 66 oncocytomas] using a tissue microarray technique. Immunoreactivity for keratin 7, 8, 18, and 19 was present in all tumor entities, albeit in varying quantities. With antibodies directed against keratins 8 and 18, oncocytomas showed a distinct perinuclear and punctate dot-like pattern, which was not observed in renal cancer specimens. The only tumors showing immunoreactivity for keratin 20 were two type-2 papillary cancers. All other monospecific keratin antibodies yielded consistently negative results. Overall, in contrast to some recent publications, keratin subtyping generally appeared to be of additional value only for the differentiation of renal epithelial tumors. Hence, with respect to differential diagnostic value, Hale's colloidal iron stain and vimentin immunostaining are still the most useful tools in renal tumor pathology.

Keywords Renal cell carcinoma · Oncocytoma · Histological subtype · Keratin · Differential diagnosis

C. Langner (✉) · B. J. Wegscheider · M. Ratschek
Institute of Pathology,
University of Graz, Medical School,
Auenbruggerplatz 25, 8036 Graz, Austria
e-mail: cord.langner@uni-graz.at
Tel.: +43 (0)316 385 83665
Fax: +43 (0)316 384329

L. Schips · R. Zigeuner
Department of Urology,
University of Graz, Medical School,
Auenbruggerplatz 7, 8036 Graz, Austria

Introduction

Renal cell carcinomas (RCCs) account for approximately 2% of annual new cancer cases worldwide, with men having a higher risk than women (male to female ratio = 1.5:1). As for the majority of cancers, tumor stage at presentation and histological tumor grade are the principal prognostic factors [20]. Prognosis is also related to histological subtypes, since patients with conventional RCCs have a poorer cancer-specific survival than patients with papillary or chromophobe tumors [1, 5, 18, 22]. Differential diagnosis among histological RCC subtypes, however, can be difficult in standard hematoxylin and eosin (H&E)-stained sections, especially in poorly differentiated cancers. In these cases, diagnosis is primarily based on the absence of vimentin immunostaining of the chromophobe subtype and its reticular cytoplasmic positivity with Hale's colloidal iron stain [15, 25, 34].

The first comprehensive description of the histopathological features of renal oncocytoma (RO) was presented by Klein and Valensi in 1976 [13]. Today, ROs account for approximately 3–7% of renal cell neoplasms in surgical series [15, 16, 29, 34]. Although a single well-documented case of metastasis to the liver has been reported [27], ROs generally are benign [1, 29]. Therefore, they have to be separated from renal cancer. However, differential diagnosis can, again, be difficult in standard H&E-stained sections, as has just recently been stressed in the review by Perez-Ordonez et al. [27].

In the last few years, keratin typing has been repeatedly applied to facilitate differential diagnosis among RCC histological subtypes [4, 10, 12, 17, 19, 28, 35] and between RCCs and ROs [6, 12, 17, 19, 28, 35, 38]. However, the results reported are, at least as far as the keratin expression profile of ROs is concerned, still limited and partly contradictory. For example, keratin 7 immunoreactivity has been detected in 8–100% [12, 17, 19, 33, 38] and keratin 20 in 0–80% of ROs [12, 33, 38]. Hence, we decided to apply a high throughput tissue microarray technique using 22 different mouse monoclonal antibodies to evaluate the keratin expression profiles

of RCC histological subtypes and ROs in a large series of patients to identify a potential basis for diagnosis and differential diagnosis of these tumor entities.

Materials and methods

Formalin-fixed and paraffin-embedded specimens of 167 RCCs from 167 patients (99 males, 68 females; ratio 1.5:1) and 66 ROs from 63 patients (34 females, 29 males; ratio 1.2:1) operated on between November 1988 and August 2002 were chosen for further analysis. Surgical treatment included either radical nephrectomy (RCC larger than 4 cm) or partial nephrectomy (peripheral tumors smaller than 4 cm and presumed oncocytomas). In the RCC group, mean and median age of patients at operation was 62.3 years and 63.1 years (range 28–85 years), in the RO group, mean and median age was 66.3 years and 69.0 years (range 11–88 years), respectively. All original H&E sections were independently reevaluated by two pathologists (C.L. and M.R.), and discrepancies were resolved by simultaneous reexamination of the slides by both investigators using a double-headed microscope. In selected cases, additional vimentin immunostaining and Hale's colloidal iron stain were applied. In four cases, the original diagnoses of RCC had to be revised and changed into either RO (two cases) or transitional cell carcinoma of the renal pelvis (two cases). Cancer specimens were classified according to the consensus classification of renal cell neoplasia [15, 34]: 125 conventional, 22 chromophobe and 20 papillary (including 12 type-1 and 8 type-2 tumors) RCCs. RO specimens were classified according to the World Health Organization criteria [25] and previously described light microscopic features [16, 27]. After a mean follow-up of 2.2 years, progressive disease was observed in 34 of 167 (20.3%) RCC patients, including 16 patients who died from cancer and 18 patients who currently are alive with metastatic disease. Three patients had died from causes unrelated to RCC. In the RO group, after a mean follow-up of 6.8 years, 57 of 63 patients (90.5%) were alive with no evidence of tumor, while the remaining 6 patients had died of other causes without evidence of tumor recurrence or metastatic disease. All procedures were in accord with the ethical standards established by our institution and approved by the ethics committee.

For immunohistochemical evaluation, a tissue microarray technique was used, which allows staining of a large number of specimens on one slide. Tissue microarrays (TMAs) were prepared using a manual tissue-arraying instrument (Beecher, Silver Spring, MD, USA). The details of this technique have been described previously [14]. At least three cylindrical core biopsies, 0.6 mm in diameter, were taken from different areas of each tumor and arrayed in a recipient paraffin TMA block. Sections from tissue array blocks 4-μm thick were mounted on Superfrost slides for immunohistochemical analysis using automated immunostainers (Dako-Autostainer, Universal Staining System, Dako, Glostrup, Denmark; for pancytokeratin MNF116 VENTANA ES, Ventana, Strasbourg, France). Briefly, TMA sections were deparaffinized, rehydrated in graded alcohols and treated for 5 min with 1% H_2O_2. Thereafter, sections were subjected to antigen retrieval with either microwave treatment (30 min 160 W in 0.01 M sodium citrate buffer pH 7.3), protease digestion (10 min room temperature 0.1% protease type XXIV, Sigma-Aldrich, Steinheim, Germany) or Epitope Retrieval Solution (Dako, code no. K 5205, 40 min 98°C) and subsequently incubated for 30 min with 22 different mouse monoclonal anti-human keratin antibodies. For antibody specificity, dilution, source and positive controls used, see Table 1. Binding of the primary antibody was usually assessed by the Dako LSAB2 System HRP (AEC) Detection kit, for pancytokeratin MNF116, the Ventana Basic DAB Detection Kit was used and for the keratin 14 antibody, both the Dako LSAB2 System HRP (AEC) Detection kit and the Dako EnVision+System (Peroxidase, DAB) were used. Negative controls were performed by substitution of the primary antibody by the Dako ChemMate antibody diluent code no. S 2022. Staining results were assessed in a semi-quantitative fashion independently by two pathologists (C.L. and M.R.). Discrepancies were resolved by simultaneous reexamination of the slides by both investigators using a double-headed microscope. Keratin immunoreactivity was documented in categories as follows: no reactivity; "weak," <10% of cancer cells positive; "moderate," 10–50% of cancer cells positive; "strong," >50% of cancer cells positive. Finally, with the help of the tissue microarray technique, it was ensured that chromophobe RCCs were, in fact, negative for vimentin and positive with Hale's colloidal iron stain, whereas

Table 1 List of antibodies used. *MW* microwave treatment 30 min 160 W in 0.01 M sodium citrate buffer pH 7.3, *P* protease digestion 10 min at room temperature (0.1% protease type XXIV, Sigma-Aldrich, Steinheim, Germany), *ER* epitope retrieval solution (Dako, Glostrup, Denmark, Code No. K 5205) 40 min at 98°C

Antibody specificity	Dilution, antigen retrieval	Positive control	Source
K 1 (Clone 34βB4)	1:10, MW	Skin	Novocastra, Newcastle upon Tyne, UK
K 4 (Clone 6B10)	1:5, MW	Cervix	Monosan, Uden, The Netherlands
K 5/6 (Clone D5/16 B4)	1:50, MW	Breast	Dako, Glostrup, Denmark
K 6 (Clone Ks6.KA12)	Ready to use, MW	Cervix	Progen, Heidelberg, Germany
K 7 (Clone OV-TL 12/30)	1:100, P	Breast	Dako
K 8 (Clone RCK 102)	1:10, P	Breast	ICN, Aurora, USA
K 8/18, LMW (Clone 5D3)	1:50, P	Skin	Novocastra
K 9 (Clones Ks 9.70 and Ks 9.216)	1:20, MW	Palmoplantar Skin	Progen
K 10 (Clone DE-K 10)	1:100 (no retrieval)	Skin	Dako
K 13 (Clone DE-K 13)	1:50, MW	Cervix	Dako
K 14 (Clone LL002)	1:50, MW	Skin	Novocastra
K 15 (Clone LHK 15)	1:50, MW	Skin	NeoMarkers, Fremont, CA, USA
K 16 (Clone LL025)	1:10, MW	Cervix	Novocastra
K 17 (Clone E3)	1:20, MW	Breast	Dako
K 18 (Clone DC 10)	1:10, MW	Breast	Dako
K 19 (Clone RCK 108)	1:100, P	Breast	Dako
K 20 (Clone K_S 20.8)	1:100, P	Colon	Dako
HMW (Clone 34βE12, K 1, 5, 10, 14)	1:50, ER	Prostate	Dako
KL1 (Pan-Keratin)	1:50, ER	Skin	Immunotech, Marseille, France
MNF116 (Pan-Keratin)	1:75, P	Skin	Dako
AE1/AE3 (Pan-Keratin)	1:50, P	Skin	Dako
Lu5 (Pan-Keratin)	1:50, P	Skin	Biocarta, Hamburg, Germany

ROs were negative for vimentin and negative with Hale's colloidal iron stain.

Results

Tumor tissue sufficient for a reliable evaluation of all markers was present in all 167 RCCs and 66 ROs, respectively. The keratin expression profiles of RCC histological subtypes and ROs are summarized in Table 2.

Regarding RCCs, expression of keratins 7, 8, 18, 19, low molecular weight keratin (LMW, 8/18), and the four pankeratin antibodies was noted in all histological subtypes, albeit in varying quantities. For example, keratin 7 was more common in chromophobe (72.7%) and papillary (80.0%) subtypes, but was also found in conventional (13.6%) tumors (Fig. 1a). Regarding only strong keratin 7 expression, the difference was more pronounced, but still 4 of 125 (3.2%) conventional tumors showed keratin 7 immunostaining of more than 50% of cancer cells. With respect to the different types of papillary cancer, keratin 7 immunostaining was seen in all 12 type-1 tumors (always >50% of cancer cells; Fig. 1b), whereas only 4 of 8 (50.0%) type-2 tumors showed keratin 7 immunostaining (always $\leq$50% of cancer cells). Furthermore, 2 of 8 (25%) type-2 papillary cancers were the only tumors in our series showing strong, though heterogeneous, immunoreactivity for keratin 20 (Fig. 1c). With pankeratin antibodies, conventional RCCs showed a predominantly membranous immunoreactivity (Fig. 1d), while cytoplasmic staining was rare and primarily noted in poorly differentiated tumors (Fig. 1e). In contrast, chromophobe tumors showed a characteristic mixture of large cells with circumferential membranous staining (corresponding to the nearly transparent and ballooned cells in H&E-stained sections) and small cells with diffuse cytoplasmic staining, leaving a small perinuclear rim unstained (corresponding to the granular and eosinophilic cells in H&E-stained sections; Fig. 1f).

Regarding ROs, staining with the pankeratin antibodies KL1, MNF116, and Lu5 specifically decorated the great majority of tumor cells and showed three distinct patterns of immunoreactivity (Fig. 2a, b): (i) perinuclear and punctate dot-like, (ii) membranous, and (iii) combination of both (mixed type). Comparable results were obtained with antibodies directed against keratins 8, 18, and 8/18 (LMW); details are given in Table 3. Interestingly, with the pankeratin antibody AE1/AE3, only 32 of 66 (48.5%) ROs were immunoreactive. In all these cases, a strong diffuse granular cytoplasmic staining of single tumor cells and small groups of tumor cells (<10%) was

Table 3 Immunohistochemical staining patterns of renal oncocytomas with antibodies directed against keratin 8 and/or 18

	Immunohistochemical staining patterns		
	Punctate (*n*)	Membranous (*n*)	Mixed (*n*)
KL1	14	32	19
MNF116	10	27	26
Lu5	15	26	21
K 8	16	7	15
K 18	17	34	15
K 8/18 (LMW)	17	14	19

Table 2 Keratin expression profiles (+ overall immunoreactivity; ++ immunostaining of more than 50% of tumor cells) of renal cell carcinomas (RCCs) related to histological subtypes and renal oncocytomas

Antibody specificity	Conventional RCCs (*n*=125)				Chromophobe RCCs (*n*=22)				Papillary RCCs (*n*=20)				Renal oncocytomas (*n*=66)			
	+	%	++	%	+	%	++	%	+	%	++	%	+	%	++	%
K 1	0	0	0	0	0	0	0	0	0	0	0	0	0	0	0	0
K 4	0	0	0	0	0	0	0	0	0	0	0	0	0	0	0	0
K 5/6	0	0	0	0	0	0	0	0	0	0	0	0	0	0	0	0
K 6	0	0	0	0	0	0	0	0	0	0	0	0	0	0	0	0
K 7	17	13.6	4	3.2	16	72.7	13	59.1	16	80.0	12	60.0	42	63.6	1	1.5
K 8	18	14.4	3	2.4	11	50.0	5	22.7	10	50	6	30.0	38	57.6	11	16.7
K 8/18, LMW	35	28.0	8	6.4	13	59.1	6	27.3	17	85.0	10	50.0	50	83.3	19	28.8
K 9	0	0	0	0	0	0	0	0	0	0	0	0	0	0	0	0
K 10	0	0	0	0	0	0	0	0	0	0	0	0	0	0	0	0
K 13	0	0	0	0	0	0	0	0	0	0	0	0	0	0	0	0
K 14	0	0	0	0	0	0	0	0	0	0	0	0	0	0	0	0
K 15	0	0	0	0	0	0	0	0	0	0	0	0	0	0	0	0
K 16	0	0	0	0	0	0	0	0	0	0	0	0	0	0	0	0
K 17	0	0	0	0	0	0	0	0	0	0	0	0	0	0	0	0
K 18	117	93.6	74	59.2	22	100.0	19	86.4	20	100.0	20	100.0	66	100.0	66	100.0
K 19	25	20	4	3.2	5	22.7	0	0	18	90.0	8	40.0	27	40.9	0	0
K 20	0	0	0	0	0	0	0	0	2	10.0	1	5.0	0	0	0	0
HMW	0	0	0	0	0	0	0	0	0	0	0	0	0	0	0	0
KL1	75	60.0	16	12.8	19	86.4	12	54.5	20	100.0	15	75.0	65	98.5	62	93.9
MNF116	98	78.4	62	49.6	22	100.0	18	81.8	20	100.0	19	95.0	63	95.5	61	92.4
AE1/AE3	97	77.6	55	44.0	16	72.7	5	22.7	19	95.0	18	90.0	32	48.5	0	0
Lu5	117	93.6	90	72.0	22	100.0	22	100.0	20	100.0	20	100.0	62	93.9	53	80.3

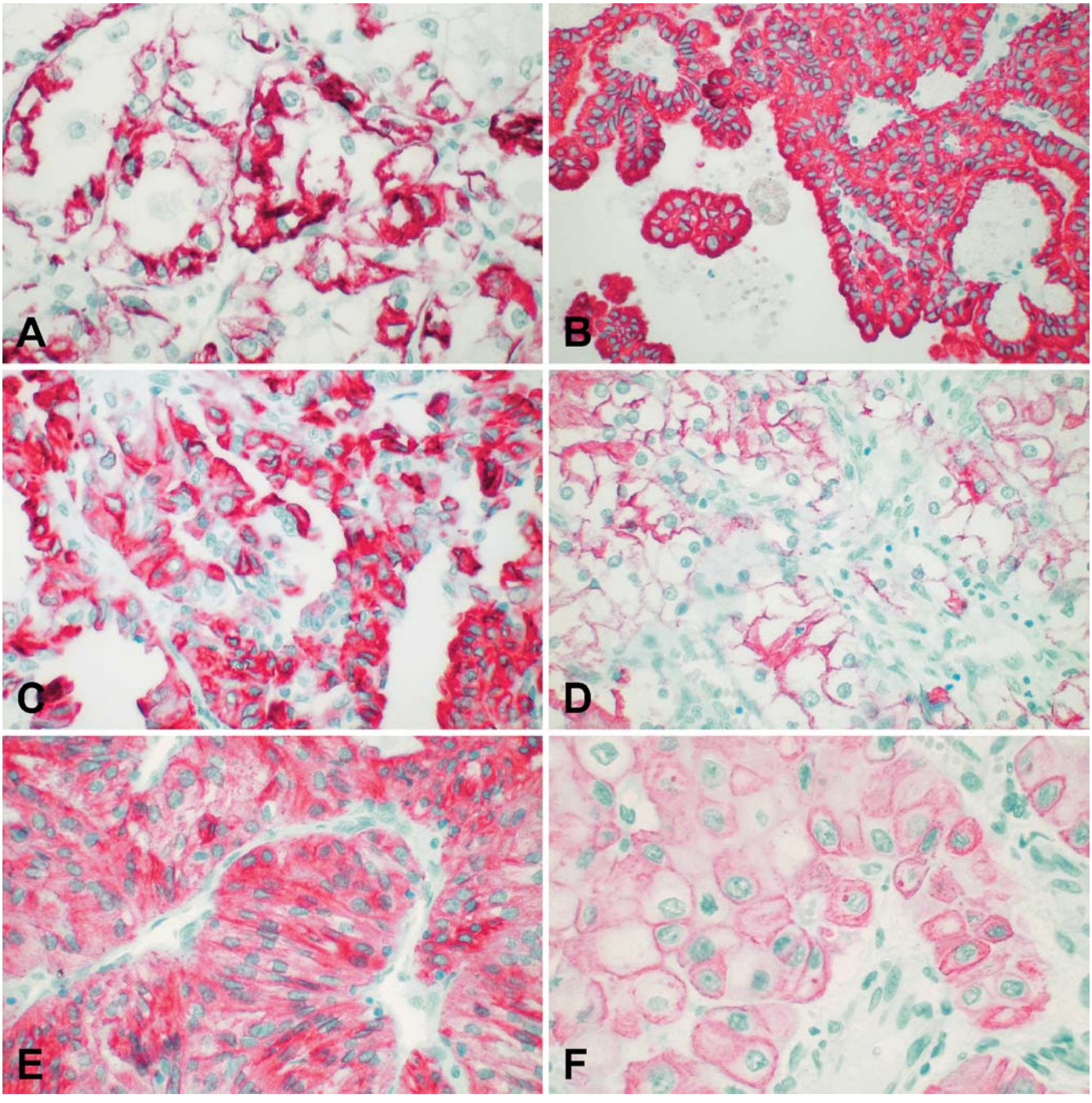

Fig. 1 Keratin immunohistochemistry in renal cell carcinomas (RCCs). Focal keratin 7 immunostaining in conventional (**A**) and strong diffuse staining in type-1 papillary (**B**) RCCs. Distinct keratin 20 immunoreactivity in type-2 papillary RCC (**C**). Strictly membranous immunostaining in a moderately differentiated (**D**) and additional diffuse cytoplasmic reactivity in poorly differentiated (**E**) conventional RCC using pankeratin antibody AE1/AE3. Characteristic heterogeneous immunostaining with a mixture of large cells with membranous staining and small cells with diffuse cytoplasmic staining in chromophobe RCC, using pankeratin antibody AE1/AE3 (**F**)

noted. A similar pattern of reactivity was noted for keratin 7 in 42 of 66 (63.6%) tumors and for keratin 19 in 27 of 66 (40.9%) tumors, respectively (Fig. 2c, d). In general, less than 10% of tumor cells were stained, mostly coexpressing keratins 7 and 19, but differences in immunoreactivity were additionally observed in a minority of cases (Fig. 2e, f). It is worth mentioning that both antibodies, which are known to decorate distal tubule epithelium, frequently disclosed non-neoplastic tubules entrapped, but not destroyed, by the tumor, especially in subcapsular regions. Using the Dako LSAB2 System HRP (AEC) detection kit, the keratin 14 antibody showed a weak diffuse cytoplasmic staining, lacking membranous immunoreactivity in the majority of the cases. By use of

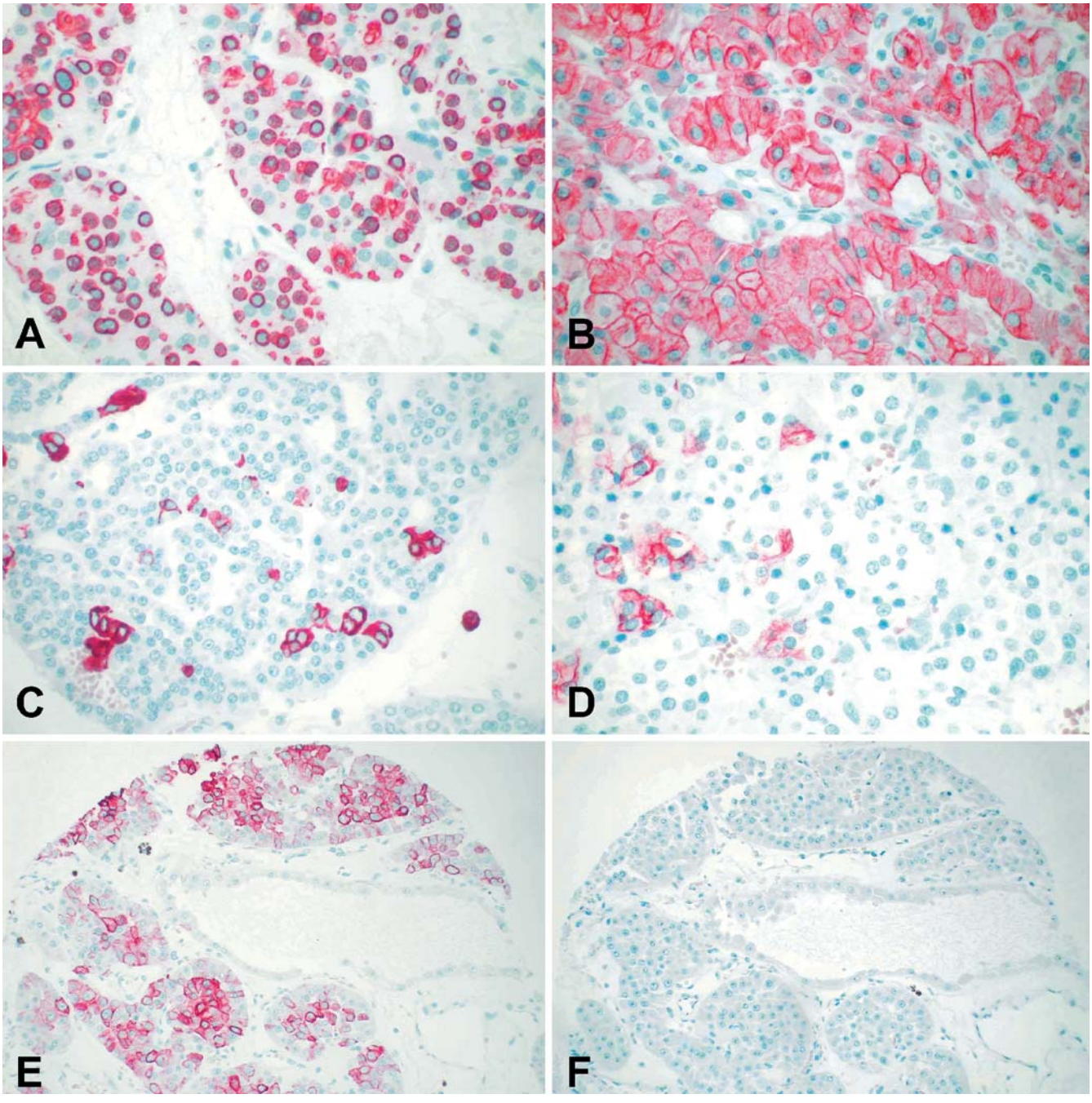

Fig. 2 Immunoreactivity of renal oncocytomas. Staining with pankeratin (KL1) shows a characteristic perinuclear and punctate dot-like (**A**) or membranous (**B**) pattern. Keratin 7 (**C**, **E**) and keratin 19 (**D**, **F**) immunoreactivity reveals a predominantly diffuse cytoplasmic staining in a minority of tumor cells. Mostly, a coexpression of these two keratin subtypes was found, but in few cases a marked difference in staining patterns was observed (**E**, **F**)

the biotin-free EnVision+System, staining for keratin 14 yielded unequivocally negative results. In contrast, a distinct strong immunoreactivity was seen in positive controls with both LSAB2 and EnVision detection systems.

Discussion

Keratins are intermediate filament proteins, which are constituents of the mammalian epithelial cytoskeleton. At least 20 different types have been discriminated in various tissues on the basis of molecular weight and isoelectric pH values. In intermediate filaments, they are present as pairs of type-I (acidic) and type-II (neutral to basic)

proteins. Different subsets of keratins are expressed by different epithelia, and these patterns are largely retained during neoplastic transformation. Hence, epithelia (simple and complex) and epithelial tumors can be classified on the basis of keratin protein expression. Keratin typing has, therefore, been widely applied in surgical pathology as a differential diagnostic tool [7, 23, 24].

With pankeratin antibody cocktails, both RCCs and ROs were stained in the majority of cases. In RO specimens with antibodies recognizing keratins 8 and/or 18 (including the pankeratin reagents KL1, MNF116, and Lu5), distinct patterns of immunoreactivity (membranous or perinuclear/punctate dot-like) were found, thus confirming the results by Bonsib et al. [2, 3], who identified the punctate pattern on the ultrastructural level as paranuclear keratin-containing globular filamentous bodies. It is important to note that with AE1/AE3, a pankeratin antibody preparation without keratin 8 and/or 18 immunoreactivity, only about half of the ROs were stained with less than 10% of tumor cells reacting diffusely without the typical perinuclear/punctate dot-like pattern. Moreover, the characteristic perinuclear/punctate dot-like pattern was absent in all RCCs investigated in our series, thus confirming the results by Bosib et al. [2, 3] and providing a valid basis for differential diagnosis.

Published results on keratin 7 immunostaining in renal epithelial tumors are conflicting. Generally, keratin 7 expression is thought to be infrequent in renal cancer [8, 11, 37]. Keratin 7 is, however, commonly present in the papillary subtype [10, 17, 30]. The strong keratin 7 expression in the relatively benign type 1 compared with the weak expression in the more aggressive type 2 of papillary RCC in our series confirms a previous study by Delahunt and Eble [9], reporting strong or moderate keratin 7 immunoreactivity in 48 of 61 (78.7%) type-1 compared with 3 of 30 (10%) type-2 tumors. Recently, some authors have recommended keratin 7 as a characteristic marker of chromophobe RCCs and ROs, differentiating them from conventional cancers [19]. Others, however, concluded that keratin 7 may be useful in the differential diagnosis of chromophobe RCCs and ROs [12, 17]. In our series, keratin 7 was present in the majority of chromophobe and papillary RCCs, as well as ROs. The low percentage of immunoreactive tumor cells in ROs and their heterogeneous distribution might, however, explain the conflicting results [12, 17, 19, 33, 38]. Although the differential diagnostic value of keratin 7 appears to be limited, it is important to note that, in our series, keratin 7 expression in more than 50% of tumor cells was seen in only 1 of 66 (1.5%) ROs. Therefore, strong keratin 7 immunoreactivity makes the diagnosis of RO very unlikely, whereas it does not exclude conventional cancer, since almost every seventh conventional RCC showed keratin 7 expression in more than 50% of cancer cells. Another feature, that to the best of our knowledge has not been well recognized, is the incorporation of non-neoplastic tubules within ROs, which can easily be detected by their immunoreactivity for keratin 7. In some cases, these tubules can even be traced from the periphery to the center of the tumor by serial sectioning. In two cases, we have also noticed incorporated papillary adenomas at the subcapsular border of the tumors, which were well preserved.

Thus far, keratin 19 immunoreactivity has been systematically investigated only in conventional cancers [4, 12, 26]. The expression in 90% of papillary cancers in our study is in accordance with one recent report by Kim and Kim [12], who noted keratin 19 immunoreactivity in 14 of 20 (70%) papillary RCCs. Keratin 19 immunostaining might, therefore, be of additional value differentiating papillary RCC, especially the solid variant [30], from the eosinophilic variant of chromophobe RCCs [16], since, in our study, chromophobe tumors showed keratin immunostaining in only about 20% of cases. In ROs, keratin 19 immunoreactivity has, thus far, only anecdotally been reported; Pitz et al. [28] analyzed eight ROs and noticed only scattered keratin 19 positive tumor cells in "some cases". Taki et al. [35] found keratin 19 in 1 of 3 ROs, whereas according to Cao and Carsten [4] and Kim and Kim [12], keratin 19 was undetectable in 5 and 12 ROs, respectively. As shown by us, however, keratin 19 can be found in about 40% of RO cases, mostly coexpressed with keratin 7.

Keratin 20 immunoreactivity has been demonstrated only in single cases of renal tubular malignancies [8, 21, 32, 37]. In fact, the general lack of keratin 20 expression was suggested as criterion for differential diagnosis [11]. In our series, the only tumors showing keratin 20 immunoreactivity were two cases of type-2 papillary cancer. Our observation corresponds to a recent study by Kim et al. [12], who reported on 4 of 20 (20%) papillary RCCs showing keratin 20 expression. However, papillary carcinoma subtypes were not mentioned in that study, and additional data are needed to investigate the potential association of keratin 20 with type-2 papillary RCC. Keratin 20 was not detectable in our RO cases, thus confirming the reports obtained from other studies [12, 38]. The results by Stopyra et al. [33], who noticed a punctate dot-like keratin 20 immunoreactivity in as much as 12 of 15 (80%) ROs, could not be confirmed. Whether this discrepancy can be explained by differences in antibody reactivity, selection criteria, or variable thresholds in the interpretation of immunoreactivity, as proposed by Wu et al. [38], remains enigmatic. In any case, the punctate or dot-like pattern of RO produced by pankeratin antibody cocktails could, in our series, clearly be attributed to keratins 8 and 18.

Recently, Chu and Weiss introduced keratin 14 as a marker of RO in the distinction from RCC [6]. In our series, however, keratin 14 antibodies identical to those applied by Chu and Weiss [6] only produced a weak diffuse cytoplasmic staining that spared plasma membranes and lacked the staining intensity seen in positive controls. We regarded this reaction as nonspecific, since we saw a similar, yet somewhat weaker, reaction with other keratin antibodies and with antibodies exclusively recognizing nuclear antigens (p63, steroid hormone receptors; data not shown). This assumption is supported

by the negative staining obtained with the HMW-keratin antibody, which recognizes keratin subtypes 1, 5, 10, and 14. On the ultrastructural level, the cells of all oncocytic tumors are extremely rich in mitochondria [36], and the mitochondrial carboxylases are known to contain biotin as a co-enzyme [31]. Probably, this explains why Chu and Weiss, themselves [6], applying an avidin-biotin-complex method in their study, noticed a correlation between keratin 14 immunoreactivity and the concentration of mitochondria, which they tried to explain by cross-reactivity of the keratin 14 antibody with mitochondrial epitopes. To prove our hypothesis of non-specific staining due to endogenous mitochondrial biotin, we used the biotin-free EnVision+System, and the weak diffuse cytoplasmic staining, seen previously, disappeared.

In conclusion, our results demonstrate that due to lack of consistent differences in immunoreactivity, keratin subtyping only provides additional clues for the classification of renal epithelial tumors. The punctuate/dot-like pattern of ROs with antibodies recognizing keratins 8 and/or 18 appears to be the only useful criterion for differential diagnosis. However, its value is hampered by the fact that only about 50% of ROs show this characteristic morphology. Hence, despite technical and interpretative challenges of Hale's colloidal iron, it is still the most useful stain in differentiating chromophobe RCC from oncocytoma. Moreover, the combination of Hale's colloidal iron with vimentin immunostaining still represents the best way to differentiate chromophobe from conventional renal cancer. The potential value of keratin 20 as a marker for type-2 papillary cancer has to be addressed in future studies. Keratin 14 immunohistochemistry leads to nonspecific staining and cannot be recommended as a diagnostic tool.

Acknowledgements The authors are grateful to Mrs. M. Gogg-Kammerer, Ms. M. Lindbauer, Ms. A. Sommersacher, Mr. M. Al-Effah, and Mr. R. Christof for their excellent technical assistance.

References

1. Amin MB, Amin MB, Tamboli P, Javidan J, Stricker H, De-Peralta Venturina M, Deshpande A, Menon M (2002) Prognostic impact of histologic subtyping of adult renal epithelial neoplasms. An experience of 405 cases. Am J Surg Pathol 26:281–291
2. Bonsib SM, Bray C (1991) Cytokeratin-containing globular filamentous bodies in renal oncocytomas. Ultrastruct Pathol 15:521–529
3. Bonsib SM, Bromley C, Lager DJ (1991) Renal oncocytoma: diagnostic utility of cytokeratin-containing globular filamentous bodies. Mod Pathol 4:16–23
4. Cao Y, Karsten U, Zerban H, Bannasch P (2000) Expression of MUC1, Thomsen-Friedenreich-related antigens, and cytokeratin 19 in human renal cell carcinomas and tubular clear cell lesions. Virchows Arch 436:119–126
5. Cheville JC, Lohse CM, Zincke H, Weaver AL, Blute ML (2003) Comparisons of outcome and prognostic features among histological subtypes of renal cell carcinoma. Am J Surg Pathol 27:612–624
6. Chu PG, Weiss LM (2001) Cytokeratin 14 immunoreactivity distinguishes oncocytic tumour from its renal mimics: an immunohistochemical study of 63 cases. Histopathology 39:455–462
7. Chu PG, Weiss LM (2002) Keratin expression in human tissues and neoplasms. Histopathology 40:403–439
8. Chu PG, Wu E, Weiss LM (2000) Cytokeratin 7 and cytokeratin 20 expression in epithelial neoplasms: a survey of 435 cases. Mod Pathol 13:962–972
9. Delahunt B, Eble JN (1997) Papillary renal cell carcinoma: a clinicopathologic and immunohistochemical study of 105 tumors. Mod Pathol 10:537–544
10. Gatalica Z, Kovatich A, Miettinen M (1995) Consistent expression of keratin 7 in papillary renal-cell carcinoma. J Urol Pathol 3:205–211
11. Han AC, Duszak R Jr (1999) Coexpression of cytokeratins 7 and 20 confirms urothelial carcinoma presenting as an intrarenal tumor. Cancer 86:2327–2330
12. Kim K, Kim S (2002) Immunohistochemical profile of common epithelial neoplasms arising in the kidney. Appl Immunohistochem Mol Morphol 10:332–338
13. Klein MJ, Valensi QJ (1976) Proximal tubular adenomas of the kidney with so-called oncocytic features. A clinicopathologic study of 13 cases of a rarely reported neoplasm. Cancer 38:906–914
14. Kononen J, Bubendorf L, Kallioniemi A, Barlund M, Schraml P, Leighton S, Torhorst J, Mihatsch MJ, Sauter G, Kallioniemi OP (1998) Tissue microarrays for high-throughput molecular profiling of tumor specimens. Nat Med 4:844–847
15. Kovacs G, Akhtar M, Beckwith BJ, Bugert P, Cooper CS, Delahunt B, Eble JN, Fleming S, Ljungberg B, Medeiros LJ, Moch H, Reuter VE, Ritz E, Roos G, Schmidt D, Srigley JR, Storkel S, van den Berg E, Zbar B (1997) The Heidelberg classification of renal cell tumors. J Pathol 183:131–133
16. Kuroda N, Toi M, Hiroi M, Enzan H (2003) Review of chromophobe renal cell carcinomas with focus on clinical and pathobiological aspects. Histol Histopathol 18:165–171
17. Leroy X, Moukassa D, Copin MC, Saint F, Mazeman E, Gosselin B (2000) Utility of cytokeratin 7 for distinguishing chromophobe renal cell carcinoma from renal oncocytoma. Eur Urol 37:484–487
18. Ljungberg B, Alamdari FI, Stenling R, Roos G (1999) Prognostic significance of the Heidelberg classification of renal cell carcinoma. Eur Urol 36:565–569
19. Mathers ME, Pollock AM, Marsh C, O'Donnell M (2002) Cytokeratin 7: a useful adjunct in the diagnosis of chromophobe renal cell carcinoma. Histopathology 40:563–567
20. Méjean A, Oudard S, Thiounn N (2003) Prognostic factors of renal cell carcinoma. J Urol 169:821–827
21. Miettinen M (1995) Keratin 20: immunohistochemical marker for gastrointestinal, urothelial, and Merkel cell carcinomas. Mod Pathol 8:384–388
22. Moch H, Gasser T, Amin MB, Torhorst J, Sauter G, Mihatsch MJ (2000) Prognostic utility of the recently recommended histologic classification and revised TNM staging system of renal cell carcinoma: a Swiss experience with 588 tumors. Cancer 89:604–614
23. Moll R (1994) Cytokeratins in the histological diagnosis of malignant tumors. Int J Biol Markers 9:63–69
24. Moll R (1998) Cytokeratins as markers of differentiation in the diagnosis of epithelial tumors. Subcell Biochem 31:205–262
25. Mostofi FK, Davis CJ (eds) (1998) Histological typing of kidney tumors. International histological classification of tumors, 2nd edn. Springer, Berlin Heidelberg New York
26. O'Hara BJ, Paetau A, Miettinen M (1998) Keratin subsets and monoclonal antibody HBME-1 in chordoma: immunohistochemical differential diagnosis between tumors simulating chordoma. Hum Pathol 29:119–126
27. Perez-Ordonez B, Hamed G, Campbell S, Erlandson RA, Russo P, Gaudin PB, Reuter VE (1997) Renal oncocytoma: a clinicopathologic study of 70 cases. Am J Surg Pathol 21:871–883
28. Pitz S, Moll R, Störkel S, Thoenes W (1987) Expression of intermediate filament proteins in subtypes of renal cell

carcinomas and in renal oncocytomas. Distinction of two classes of renal cell tumors. Lab Invest 56:642–653
29. Renshaw AA (2002) Subclassification of renal cell neoplasms: an update for the practising pathologist. Histopathology 41:283–300
30. Renshaw AA, Zhang H, Corless CL, Fletcher JA, Pins MR (1997) Solid variants of papillary (chromophil) renal cell carcinoma: clinicopathologic and genetic features. Am J Surg Pathol 21:1203–1209
31. Satoh S, Tatsumi H, Suzuki K, Taniguchi N (1992) Distribution of manganese superoxide dismutase in rat stomach: application of triton X-100 and suppression of endogenous streptavidin binding activity. J Histochem Cytochem 40:1157–1163
32. Scarpatetti M, Tsybrovskyy O, Popper HH (2002) Cytokeratin typing as an aid in the differential diagnosis of primary versus metastatic lung carcinomas, and comparison with normal lung. Virchows Arch 440:70–76
33. Stopyra GA, Warhol MJ, Multhaupt HA (2001) Cytokeratin 20 immunoreactivity in renal oncocytomas. J Histochem Cytochem 49:919–920
34. Störkel S, Eble JN, Adlakha K, Amin M, Blute ML, Bostwick DG, Darson M, Delahunt B, Iczkowski K (1997) Classification of renal cell carcinoma. Cancer 80:987–991
35. Taki A, Nakatani Y, Misugi K, Yao M, Nagashima Y (1999) Chromophobe renal cell carcinoma: an immunohistochemical study of 21 Japanese cases. Mod Pathol 12:310–317
36. Tallini G (1998) Oncocytic tumours. Virchows Arch 433:5–12
37. Wang NP, Zee S, Zarbo RJ, Bacchi CE, Gown AM (1995) Coordinate expression of cytokeratins 7 and 20 defines unique subsets of carcinomas. Appl Immunohistochem 3:99–107
38. Wu SL, Kothari P, Wheeler TM, Reese T, Connelly JH (2002) Cytokeratins 7 and 20 immunoreactivity in chromophobe renal cell carcinomas and renal oncocytomas. Mod Pathol 15:712–717

Virchows Arch (2004) 444:135–141
DOI 10.1007/s00428-003-0922-z

ORIGINAL ARTICLE

Britta Halvarsson · Annika Lindblom · Eva Rambech · Kristina Lagerstedt · Mef Nilbert

Microsatellite instability analysis and/or immunostaining for the diagnosis of hereditary nonpolyposis colorectal cancer?

Received: 14 April 2003 / Accepted: 7 October 2003 / Published online: 2 December 2003

Abstract Hereditary nonpolyposis colorectal cancer (HNPCC) represents 2–4% of colorectal cancers and is caused by a constitutional defect in a mismatch repair (MMR) gene, most commonly affecting the genes *MLH1*, *MSH2*, and *MSH6*. The MMR defect results in an increased cancer risk with the greatest lifetime risks for colorectal cancer and endometrial cancer. The HNPCC-associated tumor phenotype is generally characterized by microsatellite instability (MSI) and immunohistochemical loss of expression of the affected MMR protein. We have evaluated the information obtained from MSI analysis and immunostaining for MLH1, MSH2, and MSH6 in a series of 128 tumors from patients suspected of having HNPCC. A MSI-high pattern was present in 59 of 128 (46%) tumors. Loss of immunohistochemical expression for at least one of these MMR proteins was found in 54 of 59 (92%) evaluable MSI tumors. This loss affected MLH1 in 28, MSH2 in 22, and MSH6 in 21 tumors (with MSH6 as the only loss in 4 tumors). Five (8%) MSI-high tumors showed normal MMR protein expression. All 69 microsatellite stable or MSI-low tumors showed normal immunostaining for all three proteins. In 28 patients, all with MSI-H tumors, germ-line mutations of *MLH1, MSH2*, or *MSH6* had been identified, and a corresponding immunohistochemical loss of MMR protein expression was identified in all these cases. In summary, immunostaining for the MMR proteins MLH1, MSH2, and MSH6 had a sensitivity of 92% and a specificity of 100% for detecting MMR-deficient tumors. MMR protein immunostaining facilitates mutation analysis in suspected HNPCC patients, since it pinpoints the mutated gene, but until the genetic background to the MSI tumors with retained MMR protein expression has been clarified, we suggest that MSI and MMR protein immunostaining should optimally be combined in clinical HNPCC analysis.

Keywords Hereditary nonpolyposis colorectal cancer · Microsatellite instability · Immunohistochemistry

B. Halvarsson (✉)
Department of Pathology, The Jubileum Institution,
Lund University Hospital, 221 85 Lund, Sweden
e-mail: Britta.Halvarsson@helsingborgslasarett.se
Tel.: +46-42-101990
Fax: +46-42-101999

B. Halvarsson
Department of Pathology,
Helsingborg Hospital, 251 87 Helsingborg, Sweden

A. Lindblom · K. Lagerstedt
Department of Clinical Genetics,
Karolinska Hospital, 171 76 Stockholm, Sweden

E. Rambech · M. Nilbert
Department of Oncology, The Jubileum Institution,
Lund University Hospital, 221 85 Lund, Sweden

Introduction

Hereditary nonpolyposis colorectal cancer (HNPCC), also referred to as Lynch syndrome, is the most common type of hereditary colorectal cancer syndrome hitherto identified and is estimated to cause 2–4% of colorectal cancers [1, 15]. Patients with HNPCC have an increased risk of several tumor types, with the highest lifetime risks for colorectal cancer (70–90%) and endometrial cancer (40–60%); but, increased risks apply also for other tumor types, such as cancers of the urothelium, the small bowel, and the ovaries [2, 22]. HNPCC patients develop tumors at a young age (mean 44 years) and have a tendency for synchronous or metachronous tumors (a second primary cancer develops in about one-third of the patients) [2]. International and clinically useful diagnostic criteria (the Amsterdam criteria) for HNPCC have been established and serve to provide a uniform clinical diagnosis [20]. However, all HNPCC families do not fulfill the Amsterdam criteria, usually because of a small family size, a weak family history of cancer, or a high age at onset. Although no macroscopic or microscopic features are exclusively associated with HNPCC, several diagnostically useful features exist and include tumors with a predilection for the proximal colon, mucinous carcino-

mas, poor differentiation, an expanding margin, presence of tumor-infiltrating lymphocytes (TIL) and a Crohn's-like lymphocytic reaction [7, 12]. Mutations in mismatch-repair (MMR) genes, most commonly affecting the genes *MLH1*, *MSH2*, and *MSH6* have been identified as the cause of HNPCC (see the ICG-HNPCC database at http://www.nfdht.nl) [10]. Identification of HNPCC families enables inclusion of high-risk individuals into screening programs in order to detect early-stage adenomas or endometrial hyperplasias and, thereby, prevents cancer development, decreases morbidity, and prolongs survival in these patients [10, 19].

The defective MMR that causes HNPCC is in the tumor tissue expressed as microsatellite instability (MSI), a phenomenon that represents a variable length of repeated sequences distributed throughout the genome [3, 12]. MSI is found in more than 95% of HNPCC-associated tumors, but also in about 15% of sporadic colorectal cancers. According to international guidelines, a panel of five microsatellite markers (including the mononucleotide repeat markers BAT25 and BAT26 and the dinucleotide repeat markers D5S346, D2S123, and D17S20) should be used for the classification of MSI. Instability in more than 40% of the markers analyzed is defined as MSI-high (MSI-H), instability in less than 40% of the markers corresponds to MSI-low (MSI-L), and tumors without instability are classified as microsatellite stable (MSS) [3]. Immunohistochemistry (IHC) for the MMR proteins, using commercially available monoclonal antibodies toward MLH1, MSH2, and MSH6, has been introduced as a rapid and cheap complement to the somewhat labor-intensive MSI analysis [4, 5, 6, 8, 9, 11, 14, 16, 17, 18, 20, 21]. The use of IHC analysis using monoclonal antibodies against MLH1 and MSH2 was first reported in 1996 [11]. Subsequent studies evaluating this technique have been performed, and, whereas some investigators advocate the use of IHC as a pre-screening method for mutation analysis, others conclude that IHC cannot replace MSI analysis. The different conclusions reached probably depend on a number of factors, such as selection of the tumor material, the histological types of tumors studied, the antibodies and staining techniques used, and the frequency of the different types of gene alterations in the patient materials. We have correlated the MSI status with the results of immunostaining for MLH1, MSH2, and MSH6 in a retrospective series of patients referred for oncogenetic counseling due to suspected HNPCC.

Materials and methods

The study included 128 patients, 57 men and 71 women, with a mean age of 50 years (range 20–84 years) at the first diagnosis of cancer. All patients were referred to the oncogenetic clinics at the University Hospital in Lund and at the Karolinska Hospital in Stockholm due to suspected hereditary colorectal cancer. The patients were included according to the recommendations from the ethical committees at the Lund University Hospital and the Karolinska Hospital. Of these patients, 52 fulfilled the Amsterdam II criteria for the classification of HNPCC [20], and 48 patients were classified as familial colorectal cancer (Fig. 1). The latter group was defined as patients with at least two first-degree relatives with colorectal cancer at any age, but the families did not fulfill the Amsterdam criteria. An additional 21 patients were included because of colorectal cancer at young age (mean 38 years, range 23–53 years) and 7 patients due to development of metachronous HNPCC-associated cancers (cancers of the colorectum and the endometrium). Whenever possible, a colorectal cancer from the family was selected for MSI and IHC analysis, but in families where no such tumor was available for analysis, other tumor types were analyzed. The study, thus, included 79 colon cancers, 44 rectal cancers, 3 endometrial cancers, 1 gastric cancer, and 1 adenocarcinoma of the cervix. For the MSI and the IHC analyses, tumor blocks with sufficient quantity (approximately at least 30%) viable tumor tissue were selected.

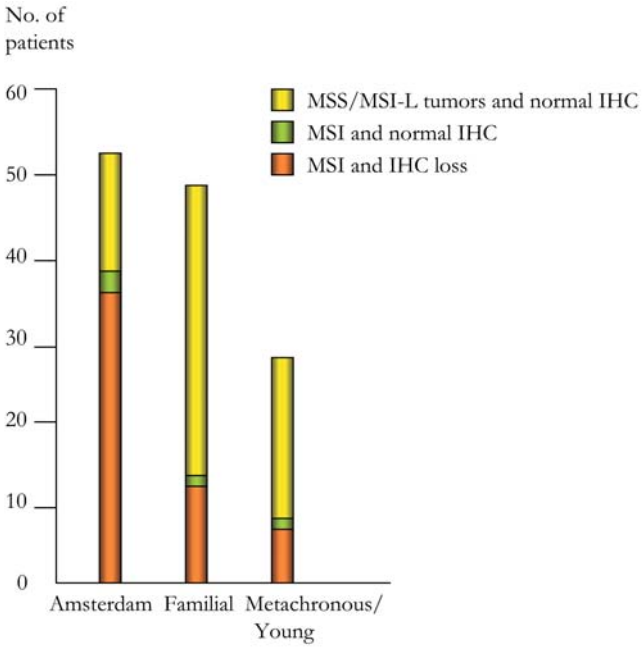

Fig. 1 Distribution of microsatellite instability (MSI) and immunohistochemical (IHC) loss in relation to the clinical group of tumors (patients fulfilling the Amsterdam criteria, patients with familial colorectal cancer, and patients with metachronous cancer or young age at diagnosis). The highest number of tumors with MSI and IHC loss (*orange*) is, as expected, found among patients who fulfill the Amsterdam criteria; whereas, the majority of patients with familial cancer and metachronous tumors/young age have mismatch-repair proficient tumors and retained IHC expression (*yellow*). The "unexplained" cases (*green*) with MSI but retained IHC expression occur in all three groups

Microsatellite analysis

DNA was extracted from fresh frozen tumor tissue and from blood using the Wizard DNA extraction kit (Promega, Madison, WI, USA) according to the manufacturer's recommendations. For DNA extraction from formalin-fixed tissue, 3×10-μm tissue sections were incubated in ethylene diamine tetraacetic acid (EDTA)-Tris-buffer with proteinase K at 65°C for at least 2 h, followed by boiling, centrifugation, and removal of the aqueous phase, which was used for the polymerase chain reaction (PCR) reactions. The MSI status of the majority of the tumors was established using the mononucleotide markers BAT25, BAT26, BAT40, the dinucleotide markers D2S123, D5S346, D17S250, and BAT34C4 (for primer

Table 1 Polymerase chain reaction primer sequences for microsatellite instability analysis

Marker	Primer sequence
BAT25	5′-TCGCCTCCAAGAATGTAAGT-3′ (forward) 5′-TCTGCATTTTAACTATGGCTC-3′ (reverse)
BAT26	5′-TGACTACTTTTGACTTCAGCC-3′ (forward) 5′-AACCATTCAACATTTTTAACCC-3′ (reverse)
BAT34C4	5′-ACCCTGGAGGATTTCATCTC-3′ (forward) 5′-AACAAAGCGAGACCCAGTCT-3′ (reverse)
BAT40	5′-ACAACCCTGCTTTTGTTCCT-3′ (forward) 5′-GTAGAGCAAGACCACCTTG-3′ (reverse)
D5S346	5′-ACTCACTCTAGTGATAAATCG-3′ (forward) 5′-AGCAGATAAGACAGTATTACTAGTT-3′ (reverse)
D2S123	5′-AAACAGGATGCCTGCCTTTA-3′ (forward) 5′-GGACTTTCCACCTATGGGAC-3′ (reverse)

sequences, see Table 1). The MSI-markers used herein are all among those recommended in the NCI reference panel for MSI analysis and have been shown to assess MSI with high accuracy [3]. The PCR amplification reactions were performed using AmpliTaq Gold DNA polymerase (Applied Biosystems-Roche, Foster City, CA, USA). The PCR program consisted of initial denaturation at 94°C for 7 min, followed by 10 cycles of denaturation at 94°C for 15 s, annealing at 45–50°C for 15 s and extension at 72°C for 15 s, followed by 23 cycles of denaturation at 89°C for 15 s, annealing at 45–50°C for 15 s and extension at 72°C for 15 s, followed by a final elongation step at 72°C for 7 min. The MSI analyses were either performed using radioactively labeled PCR products, which were electrophoretically size separated in 6% acrylamide gels or (for the majority of the tumors) using fluorescently labeled primers and size separation of the PCR products on an ABI PRISM 310 Genetic Analyzer (Applied Biosystems). For the latter method, the PCR products were mixed with 12 μl deionized formamide (Hi-Di formamide, Applied Biosystems) and 0.5 μl TAMRA 500 size standard (Applied Biosystems), denatured at 95°C for 2 min, chilled on ice, and separated in Performance Optimized Polymer-4 (POP-4). In the 25 tumors from Stockholm, the MSI status was determined using the "MSI Multiplex Prototype kit" (Promega), which includes the markers BAT25, BAT26, BAT40, MONO27, D3S2432, D7S808, D7S3046, D7S3070, and D10S426. Also for these cases, ampliTaq Gold was used for the PCR amplification and size separation was performed on an ABI PRISM 310 Genetic Analyzer (Applied Biosystems). The classification of MSI-L, MSI-H, and MSS was according to the NIH guidelines [3].

Immunohistochemistry

Immunostaining was performed using 4-μm sections of formalin-fixed, paraffin-embedded tissue, which were mounted on Dako ChemMate Capillary Gap microscope slides (Dako A/S BioTek Solutions, USA) and dried at room temperature overnight followed by incubation at 60°C for 1–2 h. The tissue sections were deparaffinized in xylol and rehydrated through descending concentrations of ethanol. Antigen retrieval was achieved by microwave-treatment in 1 mM EDTA, pH 9.0, at 800 W for 8 min followed by 15 min at 300 W. The slides were then allowed to cool for at least 20 min in the EDTA solution. IHC staining was performed in an automated immunostainer (TechMate 500 Plus, Dako), according to the manufacturer's instructions. The main steps were as follows: mouse monoclonal IgG antibodies to MLH1 (clone G168–15, dilution 1:100; PharMingen, San Diego, CA, USA), MSH2 (clone FE-11, dilution 1:100; Oncogene research products, Boston, MA, USA), or MSH6 (clone 44, dilution 1:1000; BD Transduction Laboratories) were applied and the sections were incubated at room temperature for 25 min. Thereafter, the slides were incubated with biotinylated anti-mouse antibody (Dako) for 25 min (for MLH1 and MSH2) or with rabbit anti-mouse immunoglobulins (Dako, dilution 1:400) for 20 min (for MSH6). Endogenous peroxidase activity was blocked in peroxidase-blocking solution (Dako) for 3×2.5 min. This was followed by incubation with streptavidin-horseradish peroxidase (HRP) for 25 min for MLH1 and MSH2, whereas EnVision/HRP rabbit/mouse (Dako) incubation for 25 min was used for MSH6. Finally, the tissue sections were treated with diaminobenzidine for 3 times 5 min, counterstained with hematoxylin for 1 min, rinsed in running tap water for 10 min, dehydrated in ascending concentrations of alcohol and mounted. After each step, the sections were rinsed in Tris-buffered saline, pH 7.4, and Tween-20. In order to block nonspecific protein binding, bovine serum albumin was added to the buffer before the antibody incubation steps in the MLH1 and MSH2 stainings. A detailed protocol is available from the authors upon request. Two of the authors (B.H. and M.N.) who were blinded regarding the MSI status independently evaluated all stained sections. A positive staining was defined as an unequivocal nuclear staining in the neoplastic cells, and nuclear staining was required in the stromal components of the tumor. Tumor cells without nuclear staining in the presence of staining in normal epithelial, stromal, or inflammatory cells or within infiltrating lymphoid cells were classified as having lost the expression (Fig. 1). In five tumors, a reduced staining intensity for the nuclear staining, in the presence of retained nuclear staining in the stromal cells, was found, and the expression pattern in these tumors was classified as weak (Fig. 2). If nuclear staining was not obtained in the internal control tissue (see above), the sections were classified as non-evaluable.

Results

The MSI analysis of the 128 tumors revealed a MSI-H pattern in 59 tumors, a MSI-L pattern in 4 tumors, and a MSS pattern 65 tumors. The MSI status in relation to clinical characteristics showed MSI-H tumors in 39 of 52 (75%) patients in the Amsterdam-positive group, in 13 of 48 (27%) tumors from patients with familial colorectal cancer, in 7 of 28 (25%) tumors from patients with metachronous tumors or young age at diagnosis (Fig. 1). All 65 MSS and 4 MSI-L tumors showed normal expression of MLH1, MSH2, and MSH6. Loss of expression for at least one of the MMR proteins occurred in 54 of 59 (92%) evaluable tumors and affected MLH1 in 28 tumors, MSH2 in 22 tumors, and MSH6 in 21 tumors (Fig. 2, Table 2). Non-evaluable staining patterns, due to lack of positive staining in the tumor stroma, were seen for MSH6 in three tumors. Weak and heterogeneous staining patterns occurred in five tumors and affected MSH2 in one tumor (which carried a germ-line MSH6 mutation) and MSH6 in four tumors (three of which carried germ-line MSH2 mutations) (Table 2). Among the 22 tumors with MSH2 loss, 17 showed a concomitant loss

Table 2 Summary of the immunohistochemistry (IHC) staining patterns in the 59 microsatellite instability-high (MSI-H) tumors

Staining pattern	Retained	Weak	Loss	NE
Antibody				
MLH1	31	0	28	0
MSH2	36	1	22	0
MSH6	31	4	21	3

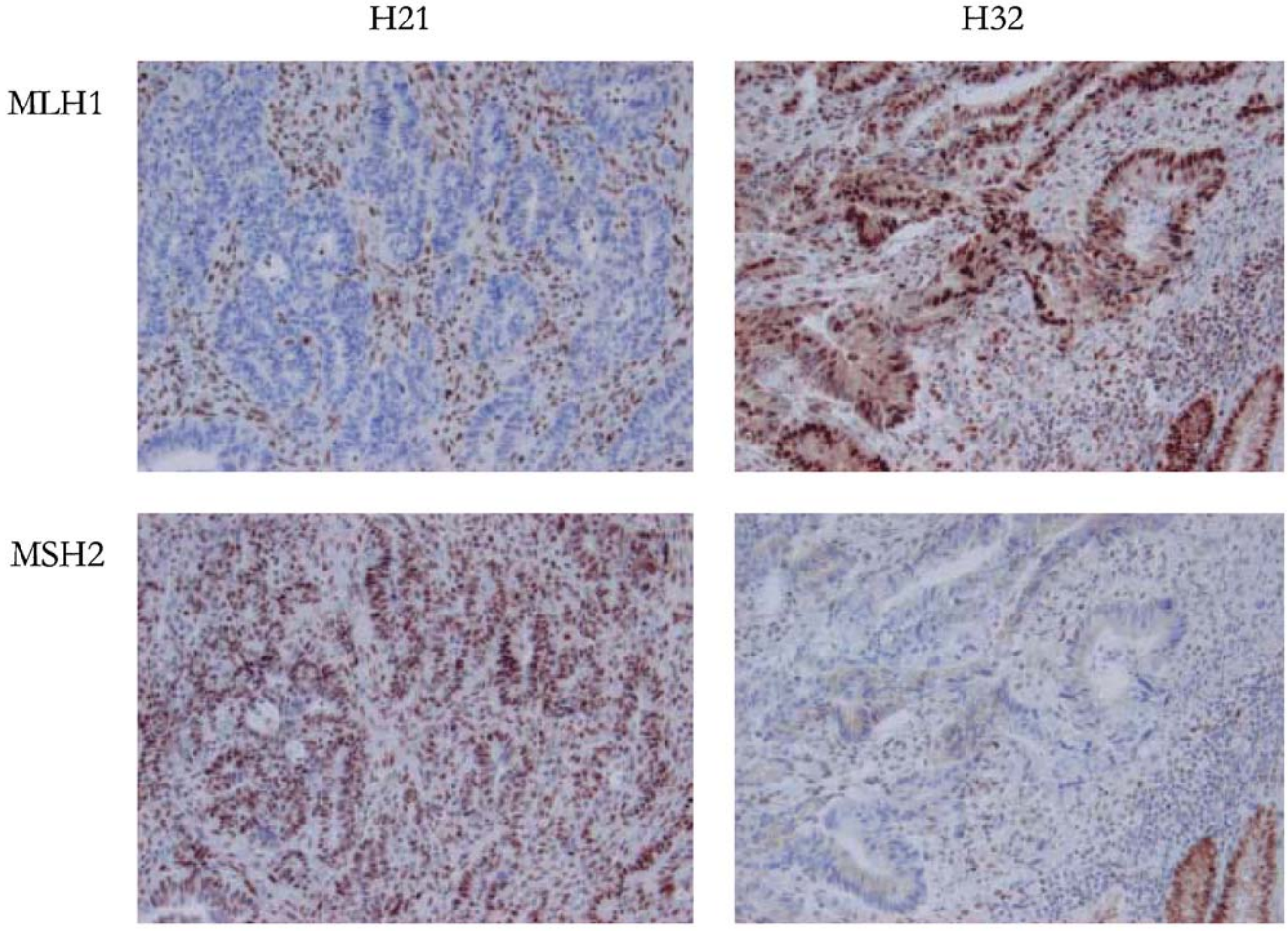

Fig. 2 Immunostaining for the mismatch-repair proteins MLH1 and MSH2. Tumor H21 showing loss of staining for MLH1 and retained staining for MSH2. Tumor H32 with normal staining for MLH1, but loss of staining for MSH2

Table 3 Clinical data on microsatellite instability (MSI) tumors with retained immunohistochemistry (IHC) staining. *NI* no mutation identified in MLH1 and MSH2

Family number	Tumor type	Family history	MSI status	MMR-protein IHC	Mutation
H13	C	Am	MSI-H	MLH1+/MSH2+	NI
H19	E	Fam	MSI-H	MLH1+/MSH2+	NI
H67	C	Am	MSI-H	MLH1+/MSH2+	NI
H102	C	Meta	MSI-H	MLH1+/MSH2+	NI
H117	C	Am	MSI-H	MLH1+/MSH2+	NI

of MSH6 staining, 3 tumors showed a weak staining for MSH6, 1 tumor showed retained staining for MSH6, and, in the remaining tumor, the MSH6 staining was non-evaluable. Four tumors showed loss of MSH6 only. Of the 59 MSI-H tumors, 5 (8%) (4 colorectal cancers and 1 endometrial cancer) showed a normal, retained expression of all three MMR proteins (Table 3).

Discussion

The aim of our study was to assess how MSI analysis and IHC of the MMR proteins MLH1, MSH2, and MSH6 correlated and contributed to the detection of defective MMR in a series of tumors from patients with suspected HNPCC. IHC analysis of tumor tissue from HNPCC patients provides a useful and time-preserving complement to the MSI analysis and is estimated to cost one-quarter the amount of a MSI analysis [6]. MSI analysis requires DNA extraction, PCR amplification, and fragment size analysis; whereas, IHC staining is performed on sections from the paraffin-embedded tumor tissue. Insufficient amounts of DNA may also limit the detection of MSI in small and fragmented tumor biopsies, such as those obtained from needle biopsies or colonoscopic biopsies, IHC does, in most such cases, yield evaluable

results. The option for an IHC analysis on biopsy material is clinically valuable, since a pre-operative diagnosis of HNPCC may influence the type of surgery performed (colectomy is considered because of the high risk of a second primary colorectal cancer). When performing HNPCC diagnosis, loss of IHC staining will also facilitate a subsequent mutation analysis, since it can pinpoint the gene affected and, thereby, direct the mutation analysis. Both methods may give inconclusive results due to poor quality of the tumor material, such as necrotic or irradiated tissue and use of extensive formalin fixation (at high concentration or during long time). Tumor samples older than about 30 years frequently cause problems in these analyses, but failure to obtain good PCR products is, in our experience, approximately as common as poor IHC staining in these cases. We have successfully analyzed samples diagnosed as early as in the 1950s for MSI as well as immunostaining (unpublished observations). Similar findings, with a somewhat higher success rate for the IHC analysis than the MSI analysis in archival samples, have been reported by Lindor et al. [9].

Studies on the correlation between MSI and IHC for the MMR proteins have revealed a high degree of correlation between these methods. The sensitivity for an abnormal MMR protein IHC staining to detect a MSI tumor has, in the larger studies, generally been reported to be between 80% and 95%, and the specificity has reached 100% in most studies [6, 8, 9, 11, 14, 16, 17, 18, 21, 23]. Our finding of loss of expression for the MMR proteins MLH1, MSH2, and/or MSH6 in 54 of 59 (92%) MSI tumors and retained expression in all MSS/MSI-L tumors support these observations. The IHC loss affected MLH1 in 28, MSH2 in 22, and MSH6 in 21 tumors. Although *MLH1* promoter methylation was not excluded, the equal contribution of losses of these MMR proteins suggests that most cases in the study do, indeed, represent HNPCC-associated tumors. The overall correlation between MSI and IHC is probably higher in sporadic MSI cancers than in HNPCC-associated tumors, since the MMR defect in most sporadic tumors is caused by hypermethylation of the *MLH1* promoter; whereas, many different structural gene alterations cause the MMR defect in HNPCC. Although all MSS or MSI-L tumors included in our study showed retained IHC expression of the MMR proteins, loss of IHC staining has been described by other investigators in occasional MSS tumors, although several authors mention heterogeneous staining patterns and suboptimal tissue in these cases [6, 9, 14, 18, 21].

Presence of MSI and retained MMR protein expression was, in our series, found in 5 of 59 (8%) tumors, all of which were MSI-H tumors and occurred in patients within the different clinical groups (Fig. 1, Table 3). This observation is in line with other investigators who have found normal expression in about 1 of 10 MSI-H tumors [5, 9, 18, 21]. Retained IHC expression has been demonstrated in a small number of tumors from patients known to carry germline MMR gene mutations. Indeed, the sensitivity for an IHC loss differs among the different MMR proteins; whereas, virtually all *MSH2* mutant tumors and most *MSH6* mutant tumors loose IHC expression, *MLH1* mutations may more often be accompanied by a normal immunostaining. This is probably due to a higher number of pathogenetic missense mutations, as well as other types of mutations that allow production of a stable and immunoreactive, albeit non-functional, protein in *MLH1* than in the other genes. Furthermore, the MLH1 IHC results seem to be technically more capricious [13]. The finding of MSI in tumor tissue reflects defective MMR caused by two hits to this system. Thus, mutations—germ-line as well as somatic—affecting other genes in this system may be the underlying cause of MSI in some of these cases. Several studies (including ours) show a low number of germ-line mutations in MSI-H tumors with retained expression of MMR protein immunostaining [5, 24]. Utilizing DNA sequencing and quantitative multiplex PCR for the detection of large deletions, we could not identify any germ-line mutations in *MLH1* or *MSH2* in the 5 MSI-H tumors with retained MMR protein expression in our study (unpublished observations). These tumors may carry mutations affecting other genes involved in DNA-repair, such as *PMS2* or *MLH3*. Hence, characterization of the genetic, clinical, and technical background to the discrepant cases is important in order correctly interpret these tumors and will probably influence future recommendations of how MSI and immunostaining should optimally be utilized in HNPCC diagnosis.

Germline HNPCC-causing mutations had been identified in 28 patients in our study. These mutations affected *MLH1* in 10, *MSH2* in 14 and *MSH6* in 4 patients (data not shown). All tumors derived from these patients were MSI-H and showed complete loss of staining for MLH1, MSH2, and/or MSH6, respectively. The MMR proteins MSH2 and MSH6 functionally interact. Tumors with loss of staining for MSH2 have been demonstrated to lose MSH6 in about 80% of the tumors, which suggests that MSH6 is degraded in the absence of its binding partner [16, 23]. Of the 22 tumors with MSH2 loss in our study, 17 (77%) displayed loss of MSH6; whereas, the remaining tumors either showed a retained staining, a weak staining, or were non-evaluable for the MSH6 staining. Thus, our results regarding the concomitant loss of MSH2 and MSH6 are in agreement with previous observations. Three of the patients included in our study carried an identical nonsense mutation in *MSH6*. Although these individuals are not known to be related, the families came from the same geographical region in southern Sweden. All three tumors showed loss of MSH6 staining in the tumor tissue with retained staining in the stromal cells. However, the MSH2 staining varied among these three tumors; one tumor showed loss of MSH2 staining, one showed a weak, poor-quality staining, and the third tumor showed a normal nuclear staining for MSH2 (Fig. 3). This finding demonstrates a variability of the MSH2 staining patterns for a structurally identical nonsense mutation in *MSH6* and implicates that weak or otherwise aberrant staining patterns should lead to mutation analysis in order not to disregard mutant cases.

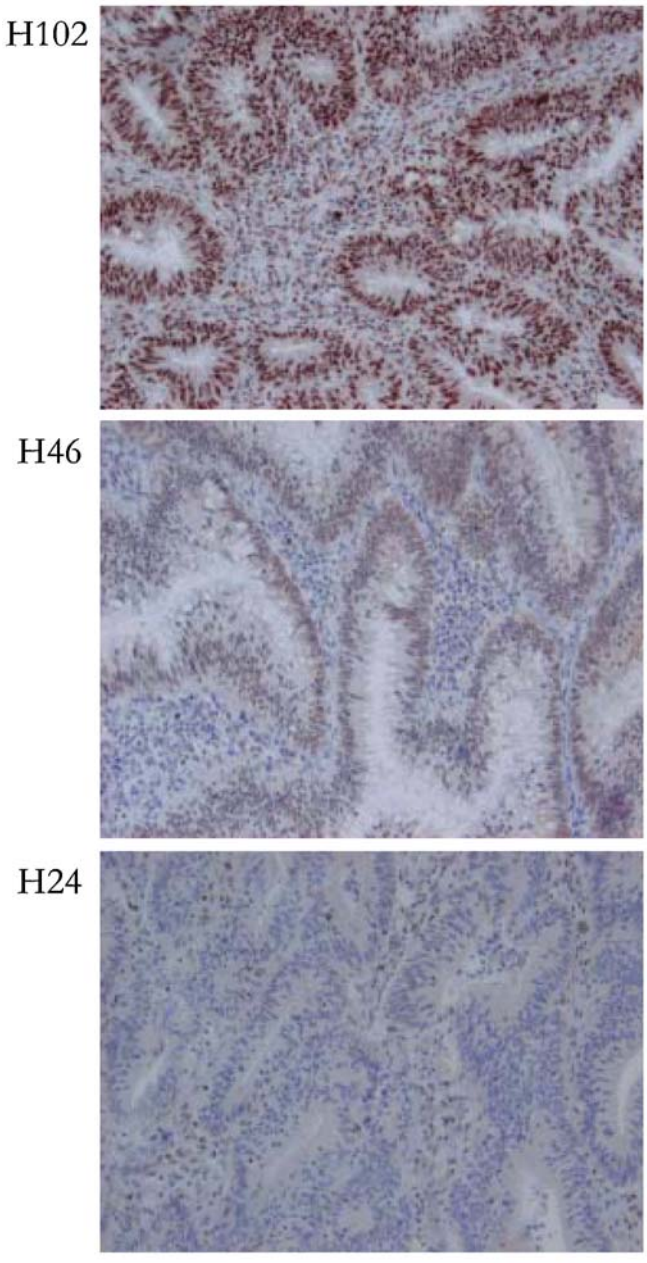

Fig. 3 Immunostaining for MSH2 from three tumors with an identical HNPCC-associated mutation in *MSH6* (CGA→TGA, codon 1035). Whereas all three tumors showed loss of MSH6 staining, the MSH2 staining patterns vary. Tumor H102 shows retained expression for MSH2, tumor H46 shows a weak staining, and tumor H24 shows loss of MSH2 staining in the tumor tissue

We conclude that MMR protein IHC provides a rapid method with a sensitivity around 90% and a specificity of 100% in most studies (including the present one) for detecting tumors with defective MMR. IHC is a useful complement to the MSI analysis and facilitates the mutations analysis in HNPCC patients, since it can, in most cases, pinpoint the mutated gene. However, MSI and IHC are complementary; MSI analysis can identify MMR-deficient tumors in which the defect in not caused by silencing of *MLH1*, *MSH2*, or *MSH6*. IHC, on the other hand, can identify MMR defects in small amounts of tumor tissue (with insufficient DNA to allow MSI analysis). Since about 10% of the MSI-H tumors have a normal MMR protein expression and until the genetic background to these tumors has been clarified, we believe MSI analysis and MMR protein immunostaining should optimally be combined in HNPCC diagnosis in order to maximize the detection of MMR deficient tumors.

Acknowledgements We would like to thank Cecilia Österman for technical assistance and all the co-workers at the oncogenetic clinics, Lund University Hospital, and the Karolinska Hospital in Stockholm for the collaboration around the HNPCC patients. Wolfram Müller, Department of Pathology, Heinrich-Heine University, Düsseldorf, Germany and Sören Nielsen, University Hospital, Ålborg, Denmark are acknowledged for valuable help establishing the immunostaining technique. Financial support was granted from the Swedish Cancer Society, the king Gustaf V's Jubilee Foundation, the Stockholm Cancer Association, the G. A. & E. Nilsson Cancer Fund, the Mrs. B. Kamprad Cancer Fund, the Å. Wiberg Cancer Fund, and the Lund University Hospital Cancer Fund.

References

1. Aaltonen LA, Salovaara R, Kristo P, Canzian F, Hemminki A, Peltomäki P, Chadwick RB, Kääriänen H, Eskelinen M, Järvinen H, Mecklin J-P, de la Chapelle A (1998) Incidence of hereditary nonpolyposis colorectal cancer and the feasibility of molecular screening for the disease. N Engl J Med 338:1481–1487
2. Aarnio M, Sankila R, Pukkala E, Salovaara R, Aaltonen LA, de la Chapelle A, Peltomäki P, Mecklin J-P, Järvinen HJ (1999) Cancer risk in mutation carriers of DNA mismatch-repair genes. Int J Cancer 81:214–218
3. Boland CR, Thibodeau SN, Hamilton SR, Sidransky D, Eshleman JR, Burt RW, Meltzer SJ, Rodriguez-Bigas MA, Fodde R, Ranzani GN, Srivastava S (1998) A national cancer institute workshop on microsatellite instability for cancer detection and familial predisposition: development of international criteria for the determination of microsatellite instability in colorectal cancer. Cancer Res 58:5248–5257
4. Chapusot C, Martin L, Bouvier AM, Bonithon-Kopp C, Ecarnot-Laubriet A, Rageot D, Ponnelle T, Laurent-Puig P, Faivre J, Piard F (2002) Microsatellite instability and intratumoural heterogeneity in 100 right-sided sporadic colon carcinomas. Br J Cancer 87:400–404
5. Christensen M, Katballe M, Wikman F, Primdahl H, Sorensen FB, Laurberg S, Orntoft TF (2002) Antibody-based screening for hereditary nonpolyposis colorectal carcinoma compared with microsatellite instability analysis and sequencing. Cancer 95:2422–2430
6. Debniak T, Kurzawski G, Gorski B, Kladny J, Domagaia W, Lubinski J (2000) Value of pedigree/clinical data, immunohistochemistry and microsatellite instability analyses in reducing the cost of determining hMLH1 and hMSH2 gene mutations in patients with colorectal cancer. Eur J Cancer 36:49–54
7. Jass JR (2000) Familial colorectal cancer: pathology and molecular characteristics. Lancet Oncol 1:220–226
8. Lanza G, Gafa R, Maestri I, Santini A, Matteuzzi M, Cavazzini L (2002) Immunohistochemical pattern of MLH1/MSH2 expression is related to clinical and pathological features in colorectal adenocarcinomas with microsatellite instability. Mod Pathol 15:741–749
9. Lindor NM, Burgart LJ, Leontovich O, Goldberg RM, Cunningham JM, Sargent DJ, Walsh-Vockley C, Petersen G, Walsh MD, Leggett BA, Young JP, Barker MA; Jass JR,

Hopper J, Gallinger S, Bapat B, Redston M, Thibodeau SN (2002) Immunohistochemistry versus microsatellite instability testing in phenotyping colorectal tumors. J Clin Oncol 20:1043–1048
10. Mitchell RJ, Farrington SM, Dunlop MG, Campbell H (2002) Mismatch repair genes hMLH1 and hMSH2 in colorectal cancer: a huge review. Am J Epidemiol 156:885–902
11. Moslein G, Tetsre DJ, Lindor NM, Honchel R, Cunningham JM, French AJ, Halling KC, Schwab M, Goretzki P, Thibodeau SN (1996) Microsatellite instability and mutation analysis of hMSH2 and hMLH1 in patients with sporadic, familial and hereditary colorectal cancer. Hum Mol Genet 5:1245–1252
12. Muc R and Naidoo R (2002) Microsatellite instability in diagnostic pathology. Curr Diagn Pathol 8:318–327
13. Muller W, Burgart LJ, Krause-Paulus R, Thibodeau SN, Almeida M, Bocker Edmonston T, Boland CR, Sutter C, Jass JR, Lindblom A, Lubinsky J, Mac Dermott K, Sanders DSA, Morreau H, Muller A, Oliani C, Orntoft T, Ponz de Leon M, Rosty C, Rodriguez-Bigas M, Ruschoff J, Ruszkiewicz A, Sabourin J, Salovaara R, Möslein G and the ICG-HNPCC (2001) The reliability of Immunohistochemistry as a prescreening method for the diagnosis of hereditary nonpolyposis colorectal cancer (HNPCC)—results of an international collaborative study. Familial Cancer 1:87–93
14. Paraf F, Gilquin M, Longy M, Gilbert B, Gorry P, Petit B, Labrousse F (2001) MLH1 and MSH2 protein immunohistochemistry is useful for detection of hereditary non-polyposis colorectal cancer in young patients. Histopathology 39:250–258
15. Peel DJ, Ziogas A, Fox EA, Gildea M, Laham B, Clements E, Kolodner RD, Anton-Cluver H (2000) Characterization of hereditary nonpolyposis colorectal cancer families from a population-based series of cases. J Natl Cancer Inst 92:1517–1522
16. Plaschke J, Kruger S, Pistorius S, Theissig F, Saeger HD, Schackert HK (2002) Involvement of hMSH6 in the development of hereditary and sporadic colorectal cancer revealed by immunostaining is based on germline mutations, but rarely on somatic inactivation. Int J Cancer 97:643–648
17. Rigau V, Sebbagh N, Olschwang S, Paraf F, Mourra N, Pacr Y, Flejou JF (2003) Microsatellite instability in colorectal carcinoma: the comparison of immunohistochemistry and molecular biology suggests a role for hMSH6 immunostaining. Arch Pathol Lab Med 127:694–700
18. Ruszkiewicz A, Bennett G, Moore J, Manavis J, Rudzki B, Shen L, Suthers G (2002) Correlation of mismatch repair genes immunohistochemistry and microsatellite instability status in HNPCC-associated tumours. Pathology 34:541–547
19. Vasen HF, van Ballegooijen M, Buskens E, Kleibeuker JK, Taal BG, Griffionen G, Nagengast FM, Menko FH, Meera Kahn P (1998) A cost-effectiveness analysis of colorectal screening of hereditary nonpolyposis colorectal carcinoma gene carriers. Cancer 82:1632–1697
20. Vasen HF, Watson P, Mecklin J-P, Lynch HT and the ICG-HNPCC (1999) New clinical criteria for hereditary nonpolyposis colorectal cancer (HNPCC, Lynch syndrome) proposed by the International Collaborative Group on HNPCC. Gastroenterology 116:1453–1456
21. Ward R, Meagher A, Tomlinson I, O'Connor T, Norrie M, Wu R, Hawkins N (2001) Microsatellite instability and the clinicopathological features of sporadic colorectal cancer. Gut 48:821–829
22. Watson P, Lynch HT (2001) Cancer risk in mismatch repair gene mutation carriers. Fam Cancer 1:57–60
23. Young J, Simms LA, Biden KG, Wynter C, Whitehall V, Karamatic R, George J, Goldblatt J, Walpole I, Robin S-A, Borten MM, Stitz R, Searle J, McKeone D, Fraser L, Purdie DR, Podger K, Price R, Buttenshaw R, Walsh MD, Barker M, Leggett BA, Jass JR (2001) Features of colorectal cancers with high-level microsatellite instability occurring in familial and sporadic setting. Am J Pathol 159:2107–2116
24. Yuen ST, Chan TL, Ho JWC, Chan ASY, Chung LP, Lam PWY, Wah Tse C, Wyllie AH, Leung SY (2002) Germline, somatic and epigenetic events underlying mismatch repair deficiency in colorectal and HNPCC-related cancers. Oncogene 21:7585–7592

Virchows Arch (2004) 444:142–148
DOI 10.1007/s00428-003-0931-y

ORIGINAL ARTICLE

Lill-Tove R. Busund · Kim T. Ow · Pamela Russell · Philip J. Crowe · Jia-Lin Yang

Expression of insulin-like growth factor mitogenic signals in adult soft-tissue sarcomas: significant correlation with malignant potential

Received: 28 April 2003 / Accepted: 1 September 2003 / Published online: 12 December 2003

Abstract The insulin-like growth factor (IGF) signal transduction system involves receptors, ligands and binding proteins (IGFBPs) that have been shown to have mitogenic and distinct anti-apoptotic effects on malignant cell lines of both epithelial and mesenchymal origin. Expression of the IGF signal system might be a mechanism by which human soft-tissue sarcomas (STS) obtain a proliferative advantage over normal adjacent tissues. IGFBP2, one of at least six different binding proteins identified to date, is secreted by most sarcoma cell lines and appears to be involved in cell proliferation and transformation. Circulating levels of this protein are markedly increased in malignancy. We have assessed 46 adult STS specimens of low, intermediate and high pathological grade of malignancy for the immunohistochemical expression of IGFBP2, IGF1, IGF2, IGF1 receptor-α and -β (IGF1Rα/β). The protein expression was measured by quantitative color video image analysis and semi-quantitative evaluation, and the measurements correlated well (Spearman, $P<0.001$). Using both methods, significant differences in expression of IGFBP2 among each of the three grades, expression of IGF2 between intermediate and high grade, and expression of IGF1Rβ between low-intermediate and low-high grade were observed (Dunnett test, $P<0.05$). Multiple regression analysis for both quantitative and semi-quantitative data confirmed the significance of the relationship and independence of the proteins, except IGF2. We concluded that IGFBP2 and IGF1Rβ are independent predictors of the malignant potential of adult STS.

Keywords IGF1 · IGF2 · IGF1 receptor α/β · IGFBP2 · Sarcomas

L.-T. R. Busund
Department of Pathology,
University Hospital of North Norway,
9038 Tromsø, Norway

K. T. Ow · P. Russell · J.-L. Yang (✉)
Oncology Research Centre,
Level 2, Clinical Sciences Building, Prince of Wales Hospital,
Barker Street, NSW 2031 Randwick, Australia
e-mail: j.yang@unsw.edu.au
Tel.: +61-29-3822624
Fax: +61-29-3822629

K. T. Ow · P. Russell · J.-L. Yang
Department of Medicine,
University of New South Wales,
NSW 2052, Australia

P. J. Crowe · J.-L. Yang
Department of Surgery,
Prince of Wales Hospital, University of New South Wales,
High Street, New South Wales 2031 Randwick, Australia

Introduction

Soft-tissue sarcomas (STS) are relatively rare tumors representing approximately 1% of human cancers. They occur at different sites of the body and vary greatly in their aggressive abilities. Although several prognostic factors are associated with the metastatic potential of these tumors (tumor size, site, depth and histological type), tumor grade remains the single most reliable prognostic indicator [8]. Despite current management protocols, about 50% of patients with STS eventually will succumb to their disease [18].

There is ample evidence that some human sarcomas depend on specific growth factors, receptors and binding proteins for optimal tumor growth [33]. The insulin-like growth factor (IGF) mitogenic signal transduction system involves ligands, receptors and binding proteins (IGFBPs), which have been shown to have mitogenic and distinct anti-apoptotic effects on malignant cell lines of both epithelial and mesenchymal origin [9, 13, 27]. The IGF1 receptor and its ligands protect cells from apoptosis through manipulation of members of the Bcl-2 family as well as through direct prevention of caspase activation [30]. The crucial role of the IGF system in transformation and apoptosis is further established by the observation that it is a target for tumor suppressors such as p53 [34]. In contrast to the inhibitory effects of wild-type p53 on IGF1 receptor signaling, mutant forms of p53 have been

shown to act as positive regulators of the IGF system [35]. In tumorigenesis, where inactivating mutations in the p53 gene are common, p53-mediated regulation of IGF signal expression may account for the increased levels of these factors in malignant cells that harbor p53 mutations, conferring tumor cells with both a proliferative and survival advantage.

The IGF1 receptor is a transmembrane heterotetramer that mediates the cellular effects of IGFs after binding of the ligand to the extracellular domains of the receptor. IGFs are small peptides that have been shown to mediate the effects of growth hormone on skeletal growth and to have a variety of anabolic effects on cells of connective tissue origin [26]. Although the liver has been identified as the primary endocrine source of serum IGFs in mammals [17], other sources are available for IGF-responsive tissues via autocrine or paracrine pathways [24]. In biological fluids, IGF1 and IGF2 are non-covalently bound to high-affinity IGFBPs, at least six species of which have been identified to date, but with poorly defined functions. IGFBP2 is secreted by many cell lines and appears to be involved in cell proliferation and transformation [2, 23]. Moreover, circulating levels of this protein are markedly increased in malignancy [16, 22]. IGFBP2 is not glycosylated and contains an integrin receptor recognition sequence, suggesting cell association properties [6, 11].

Although previous in vitro investigations have demonstrated expression of IGF1 receptors [9, 13, 27] and IGF1 and 2 ligands [5, 31] in cell lines derived from normal mesenchymal and epithelial tissues as well as cancers, investigation of IGF receptors, ligands and binding proteins in primary sarcoma specimens has been limited. Expression of some members of the IGF family has been demonstrated in some sarcomas using reverse-transcription polymerase chain reaction (RT-PCR) [12]. The objectives of the current investigations were to evaluate expression of IGF1 receptor-α (IGF1Rα) and -β (IGF1Rβ), IGF1 and 2 and one of their binding proteins, IGFBP2, in a variety of human sarcomas using immunohistochemistry and to correlate this expression with the malignant potential of the tumors.

Materials and methods

Patients and samples

Specimens from 46 patients with previously untreated STS referred to the Prince of Wales Hospital, Sydney, Australia, were entered into the study. Primary histological diagnostic confirmation was by 'Trucut' or open excision biopsy, according to the classification of Einzinger and Weiss [12]. Tumors were assigned independently by two pathologists into high, intermediate or low grade according to a scoring system based on the scheme from the French Federation of Cancer Centers Sarcoma Group (FNCLCC) [7, 20, 25], using standard histopathological parameters, including degree of differentiation, mitotic count and microscopically assessed necrosis. The gastrointestinal stromal tumors were graded according to the National Institutes of Health Consensus Conference [15], using tumor size and mitotic count. Depths were classified as superficial or deep to fascia [1].

Immunohistochemistry

For every procedure, samples were randomly chosen from each of the groups. The 5-μm sections of phosphate-buffered saline (PBS) formalin-fixed and paraffin-embedded specimens were routinely dewaxed in Histochoice (Amresco, Ohio), rehydrated in graded series of ethanol and washed in distilled water. Antigen retrieval was performed by placing the specimens in 0.01 M citrate buffer at pH 6.0 and exposing them to microwave heating at intervals of 5 min at 50% maximum power and 10 min at 20% power in a 1200 W microwave oven. The buffer was replenished after each interval to account for evaporation. The sections were cooled at room temperature for 15 min, washed in sterile water for 5 min and PBS, pH 7.6, for 5 min. Endogenous peroxidase activities were quenched in 0.3% H_2O_2/H_2O (Sigma, St. Louis, MO) for 30 min, washed in PBS and followed by blocking of nonspecific antibody binding in 10% goat or rabbit sera for 30 min at room temperature. Tissue sections were incubated overnight at 4°C in a humidifier with primary rabbit polyclonal antibodies diluted in 1% bovine serum albumin (BSA), which recognized IGF1Rα (dilution 1:150), IGF1Rβ (dilution 1:150), IGF1 (dilution 1:150) and with primary goat polyclonal antibodies, which recognized IGF2 (dilution 1:150) and IGFBP2 (dilution 1:150), respectively (Santa Cruz Biotechnology, Santa Cruz, Ca). Negative tissue controls of normal connective tissue were included in each section. As negative staining controls, the primary antibodies were replaced with either 1% BSA/PBS to rule out the effect of endogenous peroxidase or with isotype-matched irrelevant rabbit or goat immunoglobulin, where appropriate, to test for specificity. As secondary antibodies, biotinylated $F(ab')_2$ fragments were used (swine anti-rabbit in dilution 1:300 and rabbit anti-goat in dilution 1:400) (Dako, Carpinteria, CA). Specific cellular immunoreactivity was detected by incubating with avidin-biotin/horseradish peroxidase conjugate for 30 min at room temperature followed by two 5-min washings in PBS. The brown color development was performed using diaminobenzidine tetrahydrochloride (DAB) as chromogen at a dilution of 1:50 (Dako). The sections were lightly counterstained in hematoxylin, dehydrated in a graded series of ethanol, cleared in three changes of xylene and cover-slipped in Eukitt mounting medium.

Semi-quantitative analysis

The degree of expression of IGFBP2, IGF1, IGF2, IGF1Rα and IGF1Rβ was estimated by semi-quantitative analysis and classified into one of four grades: 0 = no staining; 1 = weak staining; 2 = strong staining of 25% or moderate staining of <80%; 3 = strong staining of 25–50% or moderate staining of >80%; 4 = strong staining of >50% tumor cells. Slides were examined and scored independently by two of the authors blinded to any other pathological information. In 75% of cases, the data were similar, and the other 25% were reviewed until final agreement was achieved.

Color video image analysis

The immunostained sections were examined using a Leica (Leitz Laborlux S; Leica, Wetzlar, Germany) microscope (×400) coupled to a video camera (Sony Hyper HAD, color CCD-IRIS/RGB, model DXC-151AP), connected to a computer-aided color video image analysis (VIA) system (Multi-Sync 3 V, model JC-1535VMR; NEC Corporation). After being captured and digitalized onto the video screen, microscopic images were analyzed using an image analysis software program (Leica Q500MC, Microsoft Windows hosted image analysis system, Leica Australia P/L). The images stored in the software were composed of up to 512×512 pixels separated into 8-bit brightness. The transmitted light intensity was standardized by using a fixed rheostat setting at the microscope light source. The stability of the light output was frequently checked during all procedures.

Due to the high cellularity of some samples, sequential fields were systematically examined using a ×40 objective and a ×10 eyepiece within a fixed frame of 45,000×450 pixels (0.2025 mm^2) to increase the number of cells per field. Color values for each of the red, green and blue components were calculated for each pixel from 1 to 255. After counterstaining with Harris's hematoxylin, which allowed excellent separation from DAB staining, a threshold of 170 (range 0–255) was determined for the blue color component as a cut-off range. With this setting, false or weakly positive staining could not be recorded. Ten slides (two of each group) were originally analyzed for this purpose.

Due to heterogeneity of the tumor samples, it was necessary to examine ten fields per slide. This number was determined using a progressive mean graph to achieve a meaningful result in statistical terms. Each slide was initially examined at ×10 magnification for an overall view of the lesion and counter-stain intensity. This practice allowed an area to be chosen that was the most representative, with no tissue folding or overlapping and minimal background staining. The fields were then randomly selected within this area. The degree of staining intensity was estimated as the mean DAB area stained from a minimum of 900 cells in ten microscopic fields at ×400 magnification. Evaluation of the staining reaction, which is usually cytoplasmic, was performed using the cumulative immunoreactivity (IR) score, which is equal to the sum of staining intensity in pixels multiplied by the percentage area stained and divided by ten.

Data from the VIA were divided into five distinct IR groups similar to the semi-quantitative evaluation of staining. Cut-off points defining these groups were determined prior to any analysis to ensure roughly equal numbers per group. The IR scale was as follows: IR 0 = [0–0.1), IR 1 = [0.1–1), IR 2 = [1–5), IR 3 = [5–10), IR 4 = [10, ∞).

Ethics clearance

This study was approved by the research ethics committee of the South Eastern Sydney Area Health Service (REES, Ref.: 00/253).

Statistical analysis

Semi-quantitative data are presented as median ± standard error of the mean (SEM); quantitative data are presented as mean ± SEM. Associations between the semi-quantitative and quantitative estimations of the expression of IGFBP2, IGF1, IGF2, IGF1Rα and IGF1Rβ were tested using Spearman's correlation coefficient. The differences in expression across the three pathological groups (low, intermediate and high grade) were determined by analysis of variance and/or Kruskal-Wallis test where appropriate after assessing homogeneity of variance by Levene's test. The differences between the individual groups were analyzed using the Dunnett T3 method. Multiple regression analysis was used to confirm the significance of the relationship and independence of the factors. All reported P values are two sided. For all these statistical analyses, a P value of less than 0.05 was considered significant. Statistical analysis was performed using SPSS/Win 10.0 statistical package (SPSS, Inc., Chicago, IL).

Results

The ages of the patients included in this study ranged from 16 years to 90 years, with a mean of 55.7 years, and 50% were from each gender. Table 1 provides the clinical details of the sample population. Malignant fibrous histiocytoma, leiomyosarcoma and gastrointestinal stromal tumors were the most common tumor types. Of the tumors, 10 were low grade, 9 were intermediate grade, and 27 were high grade; 30 were 5 cm or more in maximum diameter and 23 were deep to fascia.

Table 1 Clinical characteristics of 46 adult patients with soft-tissue sarcomas. *MFH* malignant fibrous histocytoma, *GIST* gastrointestinal stromal tumor

Characteristics		Number	%
	Mean age	55.7 years (range 16–90 years)	
Gender	Female	23	50.0
	Male	23	50.0
Site	Head/neck	5	10.9
	Upper extremity	5	10.9
	Back/abdominal wall	3	6.5
	Intraperitoneal	8	17.4
	Retroperitoneal	10	21.7
	Pelvis	2	4.3
	Lower extremity	13	28.3
Histological type	Liposarcoma	5	10.9
	Leiomyosarcoma	9	19.6
	Angiosarcoma	4	8.7
	MFH	9	19.6
	GIST	7	15.1
	Synovial sarcoma	3	6.5
	Others	9	19.6
Grade	Low grade	10	21.7
	Intermediate grade	9	19.6
	High grade	27	58.7
Mean tumor size (n=44)*	7.5 cm (range 0.8–27 cm)		
	≥5 cm	30	68.2
	<5 cm	14	31.8
Depth (n=30)	Superficial	7	23.3
	Deep	23	76.7

*Available number (<46) is mentioned

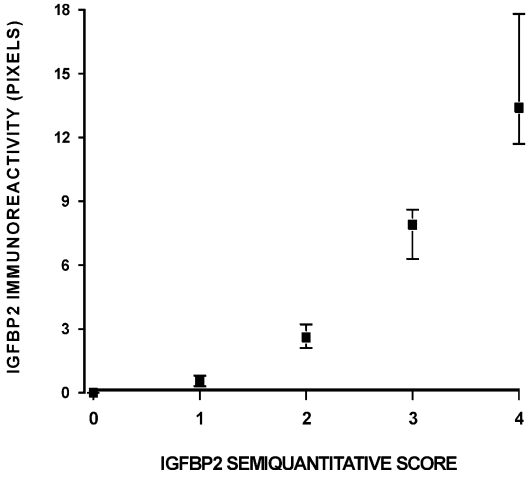

Fig. 1 Insulin-like growth factor binding protein 2 immunoreactivity for video image analysis compared with semi-quantitative scores (median, upper and lower quartiles indicated)

The two procedures, quantitative color VIA and semi-quantitative evaluation, correlated well for all the proteins (Spearman's correlation coefficient, r>0.928, P<0.001), as illustrated for IGFBP2 and IGF1Rβ in Fig. 1 and Fig. 2, respectively.

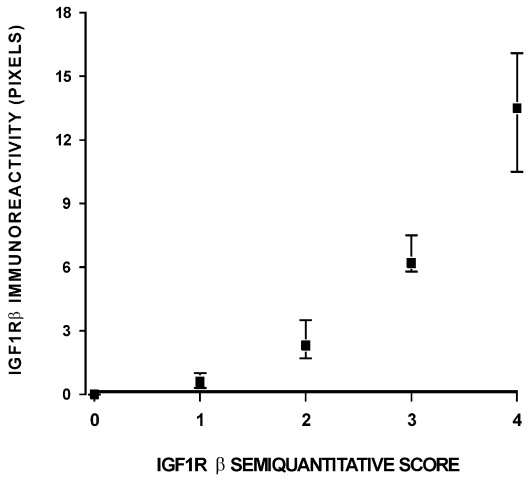

Fig. 2 Insulin like growth factor receptor β immunoreactivity for video image analysis compared with semi-quantitative scores (median, upper and lower quartiles indicated)

The semi-quantitative evaluations of the specimens of each clinical group are presented in Table 2. Significant differences of the immunohistochemical expression of IGFBP2 among the three clinical groups were observed (P<0.001). Significant differences of the expression of IGF2 were observed between intermediate and high grade (P=0.032) and of IGF1Rβ between low-intermediate and low-high grade (P=0.003 and P<0.001, respectively). Multiple regression analysis confirmed the significance of the relationship and independence of the three proteins (P<0.001 for IGFBP2, P=0.035 for IGF2 and P=0.06 for IGF1Rβ).

Heterogeneity of staining, which was mostly intracellular, was noted within individual tumor samples showing either variation in intensity or patchiness of DAB staining (Fig. 3). Data generated by color VIA were used to calculate the mean immunoreactivity (pixels) for each clinical group (quantitative analysis), as shown in Table 3. Corresponding to the semi-quantitative evaluation, the quantitative analysis revealed significant differences in the immunohistochemical expression of IGFBP2 among the three clinical groups ($P\leq$0.030).

Significant differences in the expression of IGF2 were observed between intermediate and high grade (P=0.021) and in IGF1Rβ, between low-intermediate and low-high grade ($P\leq$0.047). Significance was confirmed by multiple regression analysis of the relationship and independence of IGFBP2 (P=0.001) and IGF1Rβ (P=0.004), but not for IGF2.

Discussion

Expression of growth factors and their receptors may be a significant mechanism by which some sarcomas develop abnormal growth. In vitro studies using established cell lines have suggested that tumors expressing IGF1 receptors may be responding, not only to circulating serum levels of IGFs produced by the liver, but also to IGFs

Table 2 Semi-quantitative analysis of the relationship between expression of proteins of the insulin-like growth factor (IGF) family and grade of soft-tissue sarcomas (STS). Expression of signals in IGF-axis are given as median ± SEM. *NS* not significant, *IGFBP* insulin-like growth-factor binding protein, *IGF1R*α insulin-like growth-factor receptor-α, *IGF1R* β insulin-like growth-factor receptor β

	IGFBP2	IGF1	IGF2	IGF1Rα	IGF1Rβ
Low grade	1±0.15	1±0.28	1±0.39	0.5±0.3	1±0.28
Intermediate grade	2±0.17	1±0.26	1±0.24	1±0.29	2±0.29
High grade	3±0.16	2±0.19	2±0.19	1±0.17	3±0.15
Kruskal-Wallis test	H=23.649	H=8.837	H=3.843	H=4.464	H=19.758
Significance	P<0.001	NS	P=0.012	NS	P<0.001
Dunnett test					
Low versus intermediate	P<0.001	NS	NS	NS	P=0.003
Low versus high	P<0.001	NS	NS	NS	P<0.001
Intermediate versus high	P<0.001	NS	P=0.032	NS	NS
Levene test	P<0.001	NS	P=0.035	NS	P=0.006

Table 3 Quantitative analysis by video image analysis of the relationship between expression of proteins of the insulin-like growth factor (IGF) family and grade of soft-tissue sarcomas (STS). Expression of signals in IGF-axis are given as mean ± SEM. *NS* not significant. *IGFBP* insulin-like growth factor binding protein, *IGF1R*α insulin-like growth factor receptor-α, *IGF1R* β insulin-like growth factor receptor-β

	IGFBP2	IGF1	IGF2	IGF1Rα	IGF1Rβ
Low grade	0.8±0.2	0.93±0.6	1.6±0.9	0.6±0.5	1.2±0.5
Intermediate grade	3.9±0.9	1.3±0.6	1.3±0.4	0.6±0.2	5.0±1.2
High grade	7.8±0.9	2.6±1.2	3.6±0.7	1.4±0.3	8.3±0.9
Kruskal-Wallis test	H=22.561	H=1.665	H=6.781	H=8.237	H=20.464
Significance [b]	P<0.001	NS	P=0.034	P=0.016	P<0.001
ANOVA	F=11.68	F=0.495	F=2.714	F=1.616	F=10.028
Significance	P<0.001	NS	NS	NS	P<0.001
Dunnett test					
Low versus intermediate	P=0.030	NS	NS	NS	P=0.047
Low versus high	P<0.001	NS	NS	NS	P<0.001
Intermediate versus high	P=0.025	NS	P=0.021	NS	NS
Levene test	P=0.001	NS	NS	NS	P=0.004

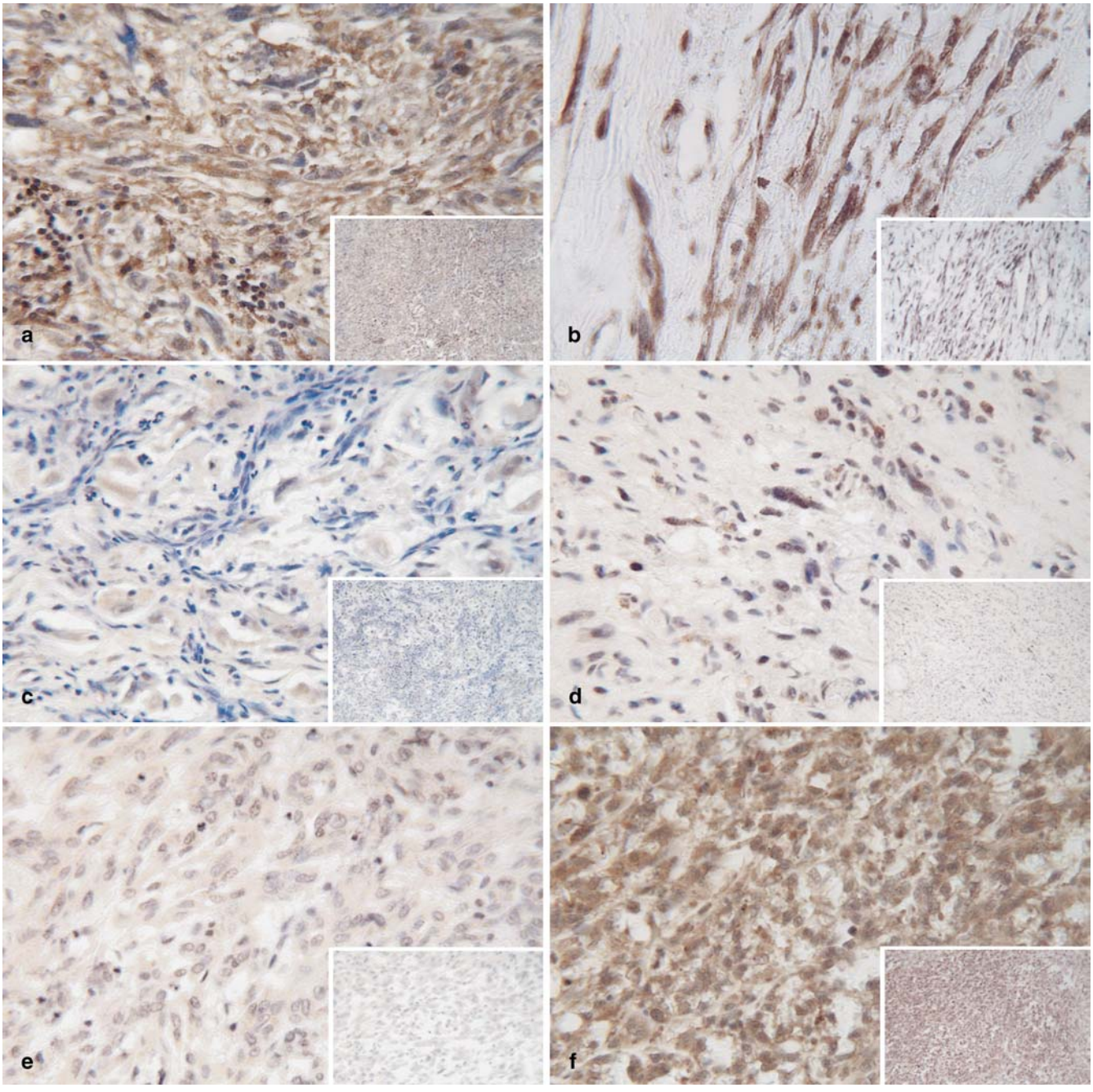

Fig. 3 Immunohistochemical staining of proteins of the insulin-like growth factor (IGF) family in different sarcomas (×400). Inserted pictures (×100). **a** Insulin-like growth factor binding protein (IGFBP2) staining in spindle cell sarcoma. **b** IGFBP2 staining in leiomyosarcoma. **c** IGF2 staining in pleomorphic sarcoma. **d** IGF1 staining in malignant fibrous histiocytoma. **e** Insulin-like growth factor 1 receptor α staining in gastrointestinal stromal tumor. **f** Insulin-like growth factor 1 receptor β staining in angiosarcoma

produced by the tumor itself in an autocrine and/or paracrine manner [10, 13]. Growth and metastasis of murine sarcomas have been shown to be altered by changing serum levels of IGFs [28, 32]. These murine experiments suggested that novel therapeutic approaches based on manipulation of serum IGF might be feasible in IGF-responsive human sarcomas. To date, few studies have attempted either to investigate the expression of IGF receptors, IGF ligands and their binding proteins in sarcomas obtained at surgery or to determine any clinical implications of IGF dependency in vivo.

In this study, we have determined the expression of IGF signals for a cohort of 46 adult patients with STS scored into low, intermediate and high grade of malignancy. Histological grade has been shown to be the most important prognostic factor in adult sarcomas with regard to metastasis development and tumor mortality, although tumor size and tumor location (superficial versus deep)

are also important parameters to consider [7, 19]. The goal of a grading system is primarily to separate tumors of poor prognosis (high grade) from those of good prognosis (low grade) [21]. That is, in a three-grade system, the number of patients in the intermediate grade category, which corresponds to tumors of intermediate malignancy, must be as small as possible. In this respect, the FNCLCC system appears to be more discriminating and efficient than other scoring systems in the selection of patients with tumors of high malignant potential who could benefit from adjuvant therapy [4, 29].

The microcomputer-based color VIA technique for assessing immunohistochemistry staining provides an objective quantitative measurement of tissue features with high sensitivity and specificity. To our knowledge, expression of IGF mitogenic signals has not been evaluated in STS using such a quantitative method. There was good correlation between the color VIA and semi-quantitative analysis despite expected variations due to the degree of subjectivity involved when attempting to incorporate frequency and intensity of staining into a scoring system. Using both methods, all tumors demonstrated some expression of IGF1 receptor. This ubiquitous expression is not surprising, as the normal tissues from which these tumors are derived also express the receptor [17]. The increased expression of IGF2 in high-grade sarcomas suggests that these tumors are capable of IGF-receptor-mediated proliferation by mechanisms of autocrine/paracrine stimulation that are independent of hepatic sources of ligand. However, a more accurate determination of the bioavailability or bioactivity of specific IGF1 and IGF2 ligands in sarcomas will require evaluation of expression of the IGF binding proteins levels, as well as the protein levels of the IGF ligands [3, 14].

Both semi-quantitative and color VIA revealed significant differences in the immunohistochemical expression of IGFBP2, IGF2 and IGF1Rβ between clinical groups. Multiple regression analysis confirmed the significance of the relationship and independence of the three proteins in the semi-quantitative assessment. In the color VIA analysis, the significance of the relationship and independence of IGFBP2 and IGF1Rβ was confirmed, but there was no significance for IGF2 expression. This divergence might be explained by the differences between the two methods. The independent value of IGF2 requires further evaluation, using a larger sample size.

These data suggest that IGF mitogenic signals of autocrine/paracrine regulatory mechanisms might be responsible for the growth of human sarcomas and that IGFBP2 and IGF1Rβ are independent predictors of their malignant potential.

As the IGF signals are directly involved in the perturbation of proliferative and apoptotic pathways of malignant growth, further examination of the relationship between the IGF axis and tumorigenic processes will not only provide new insights into the intracellular mechanisms of cellular growth control, but raise the possibility of targeting components of the IGF system in cancer therapy.

Acknowledgements This work was supported by The Norwegian Cancer Society and Research Fund of the University of New South Wales, Australia. We thank Dr. Peter Bulpitt and Dr. Claire Cooke-Yarborough for excellent assistance and Prof. Christer Busch for helpful discussions.

References

1. American Joint Committee on Cancer (1997) Manual for staging of cancer, 5th edn. Lippincott-Raven, Philadelphia
2. Babajko S, Leneuve P, Loret C, Binoux M (1997) IGF-binding protein-6 is involved in growth inhibition in SH-SY5Y human neuroblastoma cells: its production is both IGF- and cell density-dependent. J Endocrinol 152:221–227
3. Baxter RC, Martin JL (1989) Binding proteins for the insulin-like growth factors: structure, regulation and function. Prog Growth Factor Res 1:49–68
4. Benjamin RS (1995) Adjuvant chemotherapy of soft tissue sarcomas in North America. Recent Results Cancer Res 138:139–145
5. Blatt J, White C, Dienes S, Friedman H, Foley TP Jr (1984) Production of an insulin-like growth factor by osteosarcoma. Biochem Biophys Res Commun 123:373–376
6. Bourner MJ, Busby WH Jr, Siegel NR, Krivi GG, McCusker RH, Clemmons DR (1992) Cloning and sequence determination of bovine insulin-like growth factor binding protein-2 (IGFBP-2): comparison of its structural and functional properties with IGFBP-1. J Cell Biochem 48:215–226
7. Coindre JM, Terrier P, Bui NB, Bonichon F, Collin F, Le Doussal V, Mandard AM, Vilain MO, Jacquemier J, Duplay H, Sastre X, Barlier C, Henry-Amar M, Mace-Lesech J, Contesso G (1996) Prognostic factors in adult patients with locally controlled soft tissue sarcoma. A study of 546 patients from the French Federation of Cancer Centers Sarcoma Group. J Clin Oncol 14:869–877
8. Coindre JM, Terrier P, Guillou L, Le Doussal V, Collin F, Ranchere D, Sastre X, Vilain MO, Bonichon F, N'Guyen Bui B (2001) Predictive value of grade for metastasis development in the main histologic types of adult soft tissue sarcomas: a study of 1240 patients from the French Federation of Cancer Centers Sarcoma Group. Cancer 91:1914–1926
9. Cullen KJ, Yee D, Sly WS, Perdue J, Hampton B, Lippman ME, Rosen N (1990) Insulin-like growth factor receptor expression and function in human breast cancer. Cancer Res 50:48–53
10. Daughaday W (1990) The possible autocrine/paracrine and endocrine roles of insulin growth factors of human tumors. Endocrinology 127:1–4
11. Delhanty PJ, Han VK (1992) The characterization and expression of ovine insulin-like growth factor-binding protein-2. J Mol Endocrinol 9:31–38
12. Einzinger L, Weiss SW (1995) Soft tissue tumors, 3rd edn. Mosby, St. Louis
13. El-Badry OM, Minniti C, Kohn EC, Houghton PJ, Daughaday WH, Helman LJ (1990) Insulin-like growth factor II acts as an autocrine growth and motility factor in human rhabdomyosarcoma tumors. Cell Growth Differ 1:325–331
14. Elgin RG, Busby WH Jr, Clemmons DR (1987) An insulin-like growth factor (IGF) binding protein enhances the biologic response to IGF-I. Proc Natl Acad Sci U S A 84:3254–3258
15. Fletcher CD, Berman JJ, Corless C, Gorstein F, Lasota J, Longley BJ, Miettinen M, O'Leary TJ, Remotti H, Rubin BP, Shmookler B, Sobin LH, Weiss SW (2002) Diagnosis of gastrointestinal stromal tumors: a consensus approach. Hum Pathol 33:459–465
16. Flyvbjerg A, Mogensen O, Mogensen B, Nielsen OS (1997) Elevated serum insulin-like growth factor-binding protein 2

(IGFBP-2) and decreased IGFBP-3 in epithelial ovarian cancer: correlation with cancer antigen 125 and tumor-associated trypsin inhibitor. J Clin Endocrinol Metab 82:2308–2313
17. Froesch ER, Schmid C, Schwander J, Zapf J (1985) Actions of insulin-like growth factors. Annu Rev Physiol 47:443–467
18. Frustaci S, Gherlinzoni F, De Paoli A, Bonetti M, Azzarelli A, Comandone A, Olmi P, Buonadonna A, Pignatti G, Barbieri E, Apicezmerly H, Serraino D, Picci P (2001) Adjuvant chemotherapy for adult soft tissue sarcomas of the extremities and girdles: results of the Italian randomized cooperative trial. J Clin Oncol 19:1238–1247
19. Gaynor JJ, Tan CC, Casper ES, Collin CF, Friedrich C, Shiu M, Hajdu SI, Brennan MF (1992) Refinement of clinicopathological staging for localized soft tissue sarcoma of the extremity: a study of 423 adults. J Clin Oncol 10:1317–1329
20. Guillou L, Coindre JM, Bonichon F, Nguyen BB, Terrier P, Collin F, Vilain MO, Mandard AM, Le Doussal V, Leroux A, Jacquemier J, Duplay H, Sastre-Garau X, Costa J (1997) Comparative study of the National Cancer Institute and French Federation of Cancer Centers Sarcoma Group grading systems in a population of 410 adult patients with soft tissue sarcoma. J Clin Oncol 15:350–362
21. Hajdu SI (1979) History and classification of soft tissue tumors. In: Hajdu SI (ed) Pathology of soft tissue tumors. Lea & Febiger, Philadelphia, pp 1–55
22. Ho PJ, Baxter RC (1997) Insulin-like growth factor-binding protein-2 in patients with prostate carcinoma and benign prostatic hyperplasia. Clin Endocrinol 46:333–342
23. Hoeflich A, Yang Y, Huber S, Rascher W, Koepf G, Blum WF, Heinz-Erian P, Kolb HJ, Kiess W (1996) Expression of IGFBP-2, -3, and -4 mRNA during differentiation of Caco-2 colon epithelial cells. Am J Physiol 271:922–931
24. Isaksson OG, Eden S, Jansson JO (1985) Mode of action of pituitary growth hormone on target cells. Annu Rev Physiol 47:483–499
25. Kandel RA, Bell RS, Wunder JS, O'Sullivan B, Catton CN, White LM, Davis AM (1999) Comparison between a 2- and 3-grade system in predicting metastatic-free survival in extremity soft-tissue sarcoma. J Surg Oncol 72:77–82
26. Mathews LS, Norstedt G, Palmiter RD (1986) Regulation of insulin-like growth factor I gene expression by growth hormone. Proc Natl Acad Sci U S A 83:9343–9347
27. Pollak M, Richard M (1990) Suramin blockade of insulin-like growth factor I-stimulated proliferation of human osteosarcoma cells. J Natl Cancer Inst 82:1349–1352
28. Pollak M, Sem AW, Richard M, Tetenes E, Bell R (1992) Inhibition of metastatic behavior of murine osteosarcoma by hypophysectomy. J Natl Cancer Inst 84:966–971
29. Ravaud A, Bui NB Coindre JM, Lagarde P, Tramond P, Bonichon F, Stockle E, Kantor G, Trojani M, Chauvergne J (1992) Prognostic variables for the selection of patients with operable soft tissue sarcomas to be considered in adjuvant chemotherapy trials. Br J Cancer 66:961–969
30. Resnicoff M, Burgaud JL, Rotman HL, Abraham D, Baserga R (1995) Correlation between apoptosis, tumorigenesis, and levels of insulin-like growth factor I receptors. Cancer Res 55:3739–3741
31. Roholl PJ, Skottner A, Prinsen I, Lips CJ, Den Otter W, Van Unnik JA (1990) Expression of insulin-like growth factor 1 in sarcomas. Histopathology 16:455–460
32. Sekyi-Otu A, Bell R, Andrulis I, Pollak M (1994) Metastatic behavior of the RIF-1 murine fibrosarcoma: inhibited by hypophysectomy and partially restored by growth hormone replacement. J Natl Cancer Inst 86:628–632
33. Sekyi-Otu A, Bell RS, Ohashi C, Pollak M, Andrulis IL (1995) Insulin-like growth factor 1 (IGF-1) receptors, IGF-1, and IGF-2 are expressed in primary human sarcomas. Cancer Res 55:129–134
34. Werner H, Karnieli E, Rauscher FJ, LeRoith D (1996) Wild-type and mutant p53 differentially regulate transcription of the insulin-like growth factor I receptor gene. Proc Natl Acad Sci U S A 93:8318–8323
35. Zhang L, Kashanchi F, Zhan Q, Zhan S, Brady JN, Fornace AJ, Seth P, Helman LJ (1996) Regulation of insulin-like growth factor II P3 promoter by p53: a potential mechanism for tumorigenesis. Cancer Res 56:1367–1373

Virchows Arch (2004) 444:149–152
DOI 10.1007/s00428-003-0935-7

ORIGINAL ARTICLE

Ana-Maria Bamberger · Antonis Makrigiannakis · Martina Schröder · Christoph M. Bamberger · Constantine Relakis · Birgit Gellersen · Karin Milde-Langosch · Thomas Löning

Expression pattern of the CCAAT/enhancer-binding proteins C/EBP-α, C/EBP-β and C/EBP-δ in the human placenta

Received: 22 July 2003 / Accepted: 30 October 2003 / Published online: 23 December 2003

Abstract The human trophoblast has the capacity to invade maternal tissue in a controlled fashion and to produce a wide range of hormones. The transcription factors belonging to the CCAAT/enhancer-binding protein (C/EBP) family are regulators of intracellular processes and mediators of hormone action. C/EBP binding sites have been described in the promoters of several placenta-expressed target genes. In the present study, we used immunohistochemistry and Western-blot analysis to investigate the expression pattern of the three most important members of this family, C/EBP-α, -β, and -δ, in the normal human placenta as well as in isolated trophoblast cell populations. We found C/EBP-α and C/EBP-β expression in the villous syncytiotrophophoblast (ST) and the extravillous (intermediate) trophoblast (EVT), but it was absent from the villous cytotrophoblast (CT). Interestingly, expression of C/EBP-β continued to be very strong up to the third trimester of pregnancy, especially in the ST. C/EBP-δ showed overall lower expression levels, stronger only in the EVT, while CT/ST showed very low/negative expression. These data show for the first time the expression pattern and tissue localization of C/EBP factors in the human placenta, indicating that these factors (especially C/EBP-β) may play important roles in the regulation of placenta-specific genes and processes.

Keywords CCAAT/enhancer-binding proteins · Trophoblast · Extravillous trophoblast · Placenta · Maternal–fetal interface

A.-M. Bamberger (✉) · M. Schröder · K. Milde-Langosch · T. Löning
Department of Gynecopathology, Institute of Pathology, University Hospital Hamburg-Eppendorf, Martinistrasse 52, 20246 Hamburg, Germany
e-mail: abamberger@uke.uni-hamburg.de
Tel.: +49-40-428033162
Fax: +49-40-428032556

C. M. Bamberger
Department of Gynecopathology, Department of Medicine, University Hospital Hamburg-Eppendorf, Martinistrasse 52, 20246 Hamburg, Germany

B. Gellersen
Endokrinologikum Hamburg, Germany

A. Makrigiannakis · C. Relakis
Department of Obstetrics and Gynecology Medical School, University of Crete, 71110 Iraklion, Greece

Introduction

The trophoblast is the first cell type to differentiate in the mammalian conceptus, and its normal development and specific properties are crucial for both implantation and further survival of the embryo. Furthermore, the trophoblast is unique in its ability to proliferate and invade another tissue in a controlled fashion and is, thus, a very interesting model for the study of molecular mechanisms involved in these processes and for differentiating them from those implicated in tumor progression [2].

The CCAAT/enhancer-binding proteins (C/EBP) are a family of transcription factors acting as basic region/leucine zipper DNA-binding proteins [9]. So far, six members of the C/EBP family of transcription factors have been described: C/EBP-α, -β, -δ, -ε, -γ and -ζ [10]. C/EBP-α, -β, -δ and -ζ are found in liver, adipose tissue, intestine, lung, reproductive tissues and cells of the inflammatory system, while C/EBP-ε is mostly restricted to myeloid lineages [6, 8, 10, 11, 12].

The transcription factors belonging to the C/EBP family are important regulators of intracellular processes and mediators of hormone action, and binding sites for these factors have been described in the promoters of several placenta-expressed target genes. However, their specific expression pattern in the human placenta has not been studied thus far. In the present study, we, therefore, used immunohistochemistry, employing isoform-specific antibodies, to investigate the expression pattern of the three most important members of this family, i.e., C/EBP-α, -β and -δ, in cellular populations of the normal human

placenta throughout gestation. Furthermore, Western-blot analysis was performed to analyze their expression in isolated populations of trophoblast cells in primary culture.

Materials and methods

Tissue collection

The tissue material was selected following histological review from the files of the Department of Gynecopathology, University Hospital Hamburg-Eppendorf. For immunohistochemistry, specimens that had been routinely fixed in 4% buffered formalin and embedded in paraffin were used. A total of 45 samples were analyzed, including 22 first trimester, 12 second trimester and 11 third trimester placentas.

Immunohistochemistry

Serial sections of 4–6 μm were cut from paraffin blocks and mounted on 3-aminopropyltriethoxysilane-coated slides, deparaffinized in xylene and rehydrated in graded alcohol to TBS (50 mM Tris, 150 mM NaCl, pH 7.4). The slides were microwaved for 4×5 min in 10 mM citrate, pH 6.0. After cooling down for 20 min, the slides were washed in TBS, blocked for 30 min at room temperature with normal serum (rabbit IgG, ABC Kit, Vector Laboratories), diluted 1:20 in TBS and then incubated overnight at 4°C with specific C/EBP antibodies (C/EBP-α 1:400, C/EBP-β and -δ 1:200; all antibodies from Santa Cruz). For immunohistochemical characterization of intermediate trophoblast, slides were additionally incubated, when necessary, with anti-cytokeratin monoclonal antibody (Dako) diluted 1:50 in TBS. Slides were then reacted with biotin-labeled anti-mouse or anti-rabbit immunoglobulin, incubated with preformed avidin-biotin complex (Vectastain, Vector Laboratories, Burlingame, CA) and detected with 3,3'diaminobenzidine-substrate kit (Vectastain). The slides were counterstained with hemalaun and mounted with glycerine/gelatine.

Isolation of invasive and non-invasive trophoblast populations

Cultures of first trimester invasive and non-invasive trophoblast populations were established and characterized as previously described by Aboagye-Mathiesen [1]. Briefly, eight to ten placentae (5–12 weeks) obtained after legal termination of pregnancy were washed in sterile phosphate buffered saline (s-PBS), and areas rich in chorionic villi were selected, minced between scalpel blades and subjected to three sequential 10 min treatments with 0.125% trypsin and 0.2 mg/ml DNAse I (Boehringer Mannheim, Germany) in s-PBS containing 5 mM $MgCl_2$. Cells released from each 10-min step were pooled and filtered through two layers of muslin, resuspended in 70% percoll (Pharmacia, Uppsala, Sweden) at a density of 2×10^5 cells/ml and put under 20 ml of 25% percoll. Ten milliliters of s-PBS were put on top of the 25%-percoll, and a gradient was established by centrifugation for 20 min at 800×*g*. Cells from the middle band (density 1.048–1.062 g/ml) of the gradient were pooled, washed in s-PBS and seeded at a density of 1×10^6 cells/ml of keratinocyte growth medium (KGM) supplemented with 10% fetal calf serum. Cells were identified as trophoblast using immunocytochemical staining with monoclonal antibodies to cytokeratin (Dako-CK, MNF 116 and 35BH11, 1:100). Their functional ability to produce hormones and the 92- and 72-kDa gelatinases has been described [1]. Cytotrophoblast (CT) was discriminated from syncytiotrophoblast (ST) by morphological criteria (multiple nuclei), with almost complete syncytialization after 72 h in culture. The invasive characteristics of the extravillous trophoblast (EVT) cells were determined using an in vitro matrigel invasion assay as described [1, 7], using transwells with a polycarbonate filter of 2.5 cm diameter and 8-μm pore size. The upper surface of the filter was coated with Matrigel (Collaborative Research, Bedford, MA; dilution 1:20 with KGM). The bottom chamber was filled with 3 ml of KGM containing 10% fetal calf serum. After 72 h of incubation, the cells from the lower wells were harvested and used for Western-blot analysis.

Western-blot analysis

Extraction of proteins from villous and EVT cells was carried out in PBS in the presence of 1 % NP40 and protease inhibitors as previously described [3]. Sodium dodecyl sulfate-polyacrylamide gel electrophoresis was performed in a 7.5% polyacrylamide gel under reducing conditions, applying 50 μg of each sample of the concentrated protein extract. After electrophoretic transfer to nitrocellulose and blocking in TBS containing 5% bovine serum albumin for 2 h, C/EBP specific antibodies (same as used for immunohistochemistry) were added (dilution 1:1000) and incubated overnight at 4 C. Detection was carried out with peroxidase.

Results

C/EBP-α

As shown in Fig. 1, C/EBP-α is expressed in the ST (A) and EVT (B), but not the CT. This is confirmed by Western-blot analysis on isolated primary trophoblast cells (Fig. 2A), showing bands for C/EBP-α in ST and EVT, but not CT. Two isoforms are present, the full-length 42 kDa and the truncated 30-kDa protein.

C/EBP-β

Of all three investigated factors, C/EBP-β showed the highest expression levels. As shown in Fig. 1, C/EBP-β is strongly expressed in villous ST and negative in CT (C). It is also strongly expressed in EVT (D, E). As shown in panel F, strong expression of C/EBP-β can be observed in samples of third trimester placenta (this was not the case with C/EBP-α and -δ, which were negative in third trimester). Western-blot analysis of isolated trophoblast cell populations confirmed the very strong expression levels in the EVT (two different samples shown) and ST, while CT cells were negative (two different samples shown). In both EVT and ST, two isoforms were present, a larger band (approximately 36 kDa) corresponding to the activating molecule liver-enriched activatory protein (LAP) and a smaller band (approximately 20 kDa) corresponding to the dominant inhibitory truncated liver-enriched inhibitory protein (LIP) (Fig. 2B).

C/EBP-δ

As shown in Fig. 1, panels G and H, C/EBP-δ had low expression levels and was barely detectable in villous CT/ST. Somewhat stronger expression could only be ob-

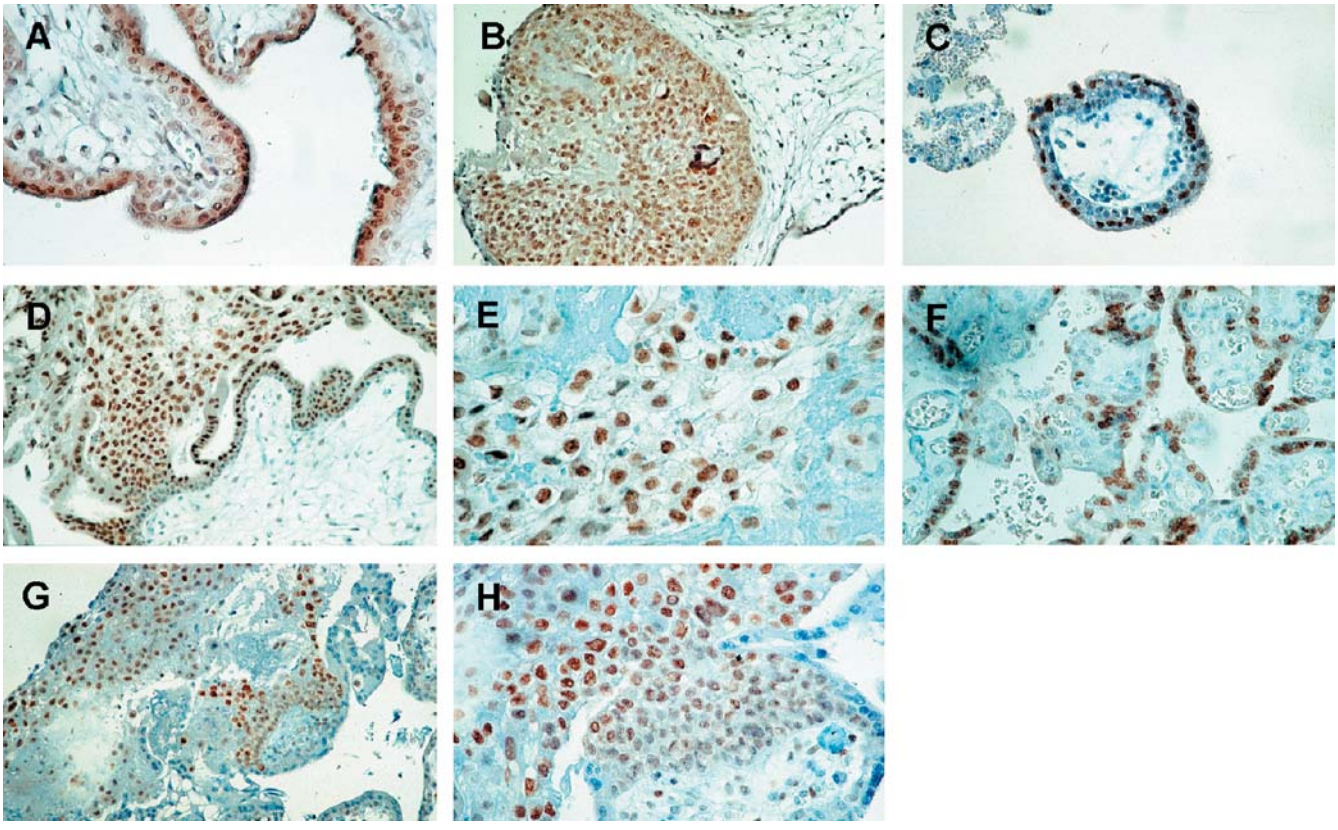

Fig. 1 Immunohistochemical localization of CCAAT/enhancer-binding proteins (C/EBPs) in the human placenta. **A**, **B** C/EBP-α. **C**, **D**, **E**, **F** C/EBP-β. **G**, **H** C/EBP-δ

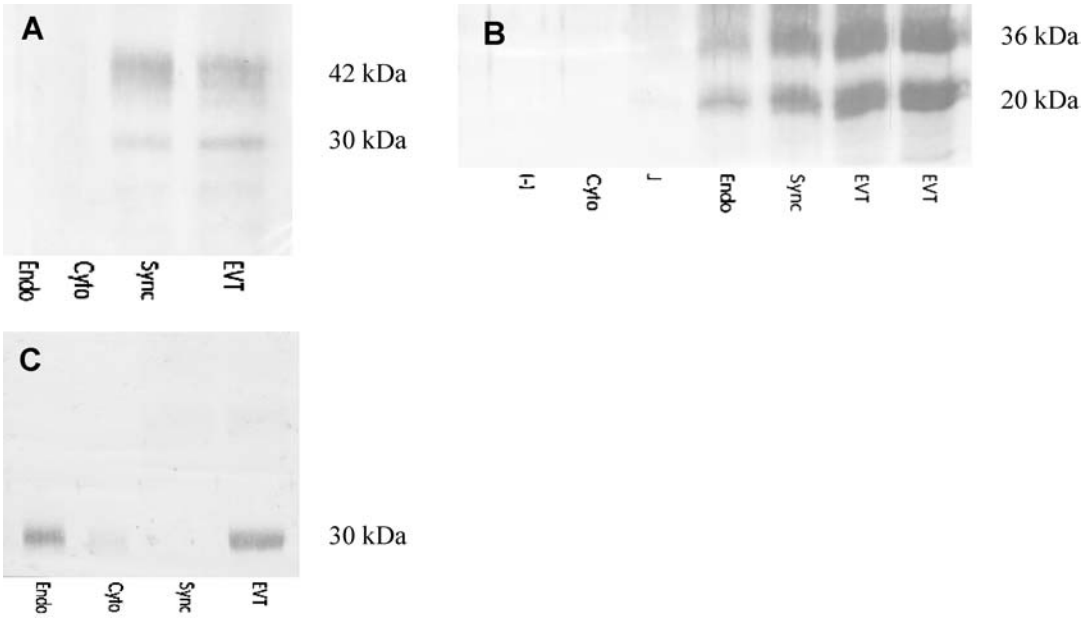

Fig. 2 Western-blot analysis of CCAAT/enhancer-binding protein (C/EBP) expression in isolated trophoblast cell populations. **A** C/EBP-α. **B** C/EBP-β. **C** C/EBP-δ. *EVT* extravillous trophoblast, *SYNC* syncytiotrophoblast, *CYTO* cytotrophoblast, *ENDO* endometrium, *J* JEG-3 trophoblast cell line

served in EVT. This result was confirmed by the Western-blot analysis performed on isolated cells (Fig. 2C).

Discussion

In this study, we investigated for the first time the exact cellular expression pattern of the three most important members of the C/EBP family, i.e., C/EBP-α, -β and –δ, in the different cell types of the human placenta, both in vivo and in vitro, using immunohistochemistry on paraffin sections and Western-blot analysis of isolated trophoblast cell populations in primary culture, respectively. We demonstrated that all three factors are expressed in the EVT, which has the capacity to proliferate and invade the maternal tissue in a tightly controlled manner. Thus, C/EBP factors, most importantly C/EBP-β, which had the highest expression levels, are probably implicated in regulating these processes. In addition, C/EBP-α and -β are expressed in the villous ST, which is an important source of placental hormones.

C/EBP proteins harbor an activation domain, a DNA-binding basic region and a leucine-rich dimerization domain. The dimerization domain is termed "leucine zipper" and contains a heptad of leucine repeats that intercalate with repeats of the dimer partner [10]. C/EBP proteins can dimerize with other C/EBP family members as well as with transcription factors of the NF-kB and Fos/Jun families, and dimerization is a prerequisite to DNA binding [10]. Furthermore, at least two isoforms have been described for both C/EBP-α and C/EBP-β. For C/EBP-α, the full-length protein has 42 kDa and contains three transactivation domains; the shorter 30-kDa protein (starting 351 nucleotides downstream of the first AUG) retains the dimerization and DNA-binding domains, but possesses an altered transactivation potential [10]. C/EBP-β has two isoforms as well, a full-length protein termed LAP (32 kDa) and a truncated form, LIP (20 kDa), which lacks the transactivation domain and can act as a dominant inhibitor [10]. Thus, specificity of gene control by C/EBP transcription factors depends both on the homo- or heterodimerization partner, as well as the specific cellular expression pattern of each factor and its isoforms.

One of the potential target genes for C/EBP factors in the human placenta is the human aromatase cytochrome P_{450} gene (CYP19), for which binding of C/EBP-β (LAP) has been described [13]. Furthermore, C/EBP factors (and especially C/EBP-β) have been shown to stimulate promoter activity of pregnancy-specific glycoproteins, proteins primarily expressed in the placenta, which become the major glycoproteins at term [4]. This stimulation was later shown by Notch to be enhanced [5].

Thus, the C/EBP factors, and especially C/EBPβ, are expressed in the human placenta and participate in the regulation of placental-specific genes.

Acknowledgements We are grateful to Bianca Kelp for excellent technical assistance and to Solveigh Aupers for her help with the immunohistochemistry experiments.

References

1. Aboagye-Mathiesen G, Zdravkovic M, Toth FD, Ebbesen P (1997) Effects of human trophoblast-induced interferons on the expression of c-fms/CSF-1R, EGF-R and c-erbB2 in invasive and non-invasive trophoblast. Placenta 18:155–161
2. Bamberger A-M, Bamberger CM (2002) Placenta. In: Livolsi VA, Asa SL (eds) Endocrine pathology. Churchill Livingstone, New York, pp 351–360
3. Bamberger AM, Riethdorf L, Nollau P, Naumann M, Erdmann I, Götze J, Brümmer J, Schulte HM, Wagener C, Löning T (1998) Dysregulated expression of CD66a (BGP, C-CAM), an adhesion molecule of the CEA family, in endometrial cancer. Am J Pathol 152:1401–1406
4. Chen H, Lin B, Chen CL, Johnson PF, Chou JY (1995) Role of the transcription factor C/EBP beta in expression of a rat pregnancy-specific glycoprotein gene. DNA Cell Biol 14:681–688
5. Chen H, Chong Y, Liu CL (2000) Active intracellular domain of Notch enhances transcriptional activation of CCAAT/enhancer binding protein beta on a rat pregnancy-specific glycoprotein gene. Biochemistry 39:1675–1682
6. Chumakov AM, Grillier I, Chumakova E, Chih D, Slater J, Koeffler HP (1997) Cloning of the novel human myeloid-cell-specific C/EBP-epsilon transcription factor. Mol Cell Biol 17:1375–1386
7. Graham CH, Hawley TS, Hawley RG, MacDougall JR, Kerbel RS, Khoo N, Lala PK (1993) Establishment and characterization of first trimester human trophoblast cells with extended life-span. Exp Cell Res 206:204–211
8. Gronning LM, Dahle MK, Tasken KA, Enerback S, Hedin L, Tasken K, Knutsen HK (1999) Isoform-specific regulation of the CCAAT/enhancer-binding protein family of transcription factors by 3′,5′-cyclic adenosine monophosphate in Sertoli cells. Endocrinology 140:835–843
9. Landschulz WH, Johnson PF, McKnight SL (1988) The leucine zipper: a hypothetical structure common to a new class of DNA binding proteins. Science 240:1759–1764
10. Lekstrom-Himes J, Xanthopoulos KG (1998) Biological role of CCAAT/enhancer-binding protein family of transcription factors. J Biol Chem 273:28545–28548
11. Pall M, Hellberg P, Brannstrom M, Mikuni M, Peterson CM, Sundfeldt K, Norden B, Hedin L, Enerback S (1997) The transcription factor C/EBP-beta and its role in ovarian function; evidence for direct involvement in the ovulatory process. EMBO J 16:5273–5279
12. Sirois J, Richards JS (1993) Transcriptional regulation of the rat prostaglandin endoperoxide synthase 2 gene in granulosa cells. Evidence for the role of a cis-acting C/EBP beta promoter element. J Biol Chem 268:21931–21938
13. Toda K, Nomoto S, Shzuta Y (1996) Identification and characterization of transcriptional regulatory elements of the human aromatase cytochrome P_{450} gene (CYP19). J Steroid Biochem Mol Biol 56:151–159

Virchows Arch (2004) 444:153–157
DOI 10.1007/s00428-003-0950-8

ORIGINAL ARTICLE

Yuri Akishima · Kinji Ito · Lijun Zhang · Yukio Ishikawa · Hideki Orikasa · Hideko Kiguchi · Yoshikiyo Akasaka · Kazuo Komiyama · Toshiharu Ishii

Immunohistochemical detection of human small lymphatic vessels under normal and pathological conditions using the LYVE-1 antibody

Received: 30 June 2003 / Accepted: 10 November 2003 / Published online: 14 January 2004

Abstract The spread of tumor cells via lymphatic vessels to the lymph nodes is an important indicator of malignancy. However, previous markers used to identify lymphatic endothelium gave ambiguous results in immunohistochemical analyses with paraffin-embedded tissues. In this study, we attempted to prepare a polyclonal antibody against human lymphatic vessel endothelial hyaluronan receptor-1 (LYVE-1) for detecting lymphatic vessels using immunohistochemistry. The antibody was raised against a region near the transmembrane anchor of LYVE-1 in New Zealand white rabbits. Immunostainings with anti-LYVE-1 and von Willebrand factor antibodies were performed in various normal and pathological tissues. LYVE-1 expression was confined to the endothelial surface of lymphatic vessels but was not found in the endothelium of blood vessels, which were positive for von Willebrand factor. Our LYVE-1 polyclonal antibody was useful for the identification of small lymphatic vessels in normal human tissues. In addition, the immunostaining enabled us to distinguish lymphatic invasion by malignant tumor cells from blood vessel invasion using paraffin-embedded sections. In conclusion, our polyclonal antibody against the transmembrane anchor of the peptide can be used to detect human lymphatic vessels under various conditions.

Keywords LYVE-1 · von Willebrand factor · Lymphatic endothelial cell · Hyaluronan receptor · Immunohistochemistry

Y. Akishima (✉) · K. Ito · L. Zhang · Y. Ishikawa · Y. Akasaka · T. Ishii
Department of Pathology,
Toho University, School of Medicine,
5-21-16 Omori-Nishi, Otaku, Tokyo, Japan
e-mail: akiyuri@med.toho-u.ac.jp
Tel.: +81-33-7624151
Fax: +81-35-4935414

H. Orikasa
Department of Pathology,
Saiseikai Central Hospital,
Tokyo, Japan

H. Kiguchi
Department of Pathology,
Saiseikai Kanagawaken Hospital,
Yokohama, Japan

K. Komiyama
Department of Pathology,
Nihon University School of Dentistry,
Tokyo, Japan

Introduction

The lymphatics are a significant element of the immune system, which form a network of specialized depots (lymph nodes) and are an important conduit for tumor cells. Indeed, the invasion of peritumor lymphatics is considered an indication of a poor prognosis in patients with malignant tumors [10]. However, it is difficult to identify small lymphatics invaded by malignant cells using immunohistochemistry due to a lack of histological, ultrastructural, or immunohistochemical markers for the accurate differentiation of vascular endothelial cells from lymphatic endothelial cells [1, 3, 9, 16, 18]. In 1998, it was reported that human vascular endothelial growth factor receptor-3 (VEGFR-3) was specifically expressed at the surface of lymphatic endothelial cells [11], though subsequent studies have found that VEGFR-3 also reacted with the endothelial cells of vascular capillaries [15, 20, 23]. In recent reports, other specific proteins of lymphatic endothelial cells have been identified, including lymphatic vessel endothelial hyaluronan receptor-1 (LYVE-1) [1], podoplanin [2], prox-1 [21], desmoplakin [5], D6 [14], the mannose receptor [7], and D2–40 [12]. Immunohistochemical detection of the lymphatic vessels using antibodies against these peptides was possible in some tissues, but difficult in most of the normal or pathological tissues.

Of these specific proteins existing in the lymphatic endothelial cells, we noted that LYVE-1 is a powerful marker of lymphatic structure and function. LYVE-1 is a 322-amino acid type-I integral membrane glycoprotein,

which has 41% similarity to the CD44 hyaluronan receptor [1]. The lymphatics play a vital role in hyaluronan homeostasis; thus, LYVE-1 is specifically expressed in the lymphatic capillaries and small lymphatic vessels in various tissues [8]. LYVE-1 is also present in the sinusoidal endothelium of liver and spleen and in the other cells where hyaluronan is incorporated and degraded; however, it has not been detected in blood vascular endothelium [8]. In this study, we attempted to prepare a polyclonal antibody (pAb) against part of the LYVE-1 peptide to immunohistochemically detect lymphatic vessels and applied it to the identification of small lymphatic vessels in various normal tissues as well as lymphatic invasion by malignant tumors using immunohistochemistry.

Materials and methods

Preparation of affinity purified anti-LYVE-1 antibody

Using New Zealand White rabbits, antisera were raised against the 13-mer peptide (SKKTDKNPEESKC) corresponding to amino acids 297–308 of the LYVE-1 sequence, the area of which has a cytoplasmic tail, near the transmembrane anchor, and a hydrophilic area [1]. The peptide was then coupled with a combination of keyhole limpet hemocyanin and *m*-maleimidobenzoyl-N-hydroxysuccinimide ester. For the production of polyclonal antisera, the peptide conjugate (0.5 mg) was mixed with an equal volume of Freund's complete adjuvant and injected into two rabbits at several subcutaneous sites, with three subsequent boosts in incomplete adjuvant at intervals of 2 weeks. Sera were then tested for reactivity with dot-blotting methods.

Antibodies reactive with the human IgG portion of the immunizing antigen were depleted by preabsorption on an affinity column. For affinity purification of the antibody, the peptide was coupled to Affi-Gel 10 (BioRad, Hercules, CA, USA) following the manufacturer's instructions with a slight modification. The antibody was eluted with 0.1 M glycine/HCl, pH 1.7.

The specificity of the anti-LYVE-1 antibody was ascertained as follows. Full-length LYVE-1 cDNA was prepared using reverse-transcription polymerase chain reaction (RT-PCR). Conventional PCR was performed using the cDNA of normal spleen tissue together with the PCR mix and the following primers: LYVE-1f (sense: GGATCCTGGGTAGGCACGATGGCCAGGTGCTTCAGCCTGGTG; codon 79–111) and LYVE-1r (anti-sense: GCGGCCGCCTAAACTTCAGCTTCCAGGCATCG; codon 1037–1059). A 50-cycle reaction was carried out as follows: 94°C for 30 s; 58°C for 30 s; 72°C for 30 s. The amplified PCR product was cloned into pGEM-T vector (Promega, Madison, WI). The identity of the cDNA fragment was confirmed by sequencing. cDNA of LYVE-1 was subcloned into the expression vector pDON-AI DNA (Takara, Kyoto, Japan). The pDON-AI-LYVE-1 construct and wild-type vector were transiently transfected with COS 7 cells using Lipofectamin 2000 reagent (Invitrogen, Groningen, Netherlands). After 24 h of transfection, the cells were lysed in sodium dodecyl sulfate (SDS)-sample buffer. The lysates were separated by SDS-polyacrylamide gel electrophoresis and transferred to a polyvinyl difluoride filter. Western blotting was used to check the specificity. Furthermore, an inhibition experiment was conducted in which 2 μg of rabbit antibody was added to 10 μg of 13-mer LYVE-1 polypeptide. The transfer filter was incubated with antibodies and visualized with horseradish peroxidase-linked anti-rabbit immunoglobulins using a chemiluminescence system (Amersham Bioscience UK, Little Chalfont, UK).

Immunohistochemistry

For immunohistochemistry, normal and pathological human tissues were obtained from autopsy and surgical cases at Omori Hospital, School of Medicine, Toho University, Tokyo. Written informed consent to use the tissues was provided by the patients' relatives. The tissues were fixed with 10% neutral-buffered formalin (pH 7.2). The fixed tissues were embedded in paraffin, and serial sections were made to compare the localization of LYVE-1 expression with that of von Willebrand factor (vWF) expression.

Sections were dewaxed, dehydrated, and pretreated with Target Retrieval Solution (Dako) at 95°C for 20 min. After a wash in Tris-buffered saline (TBS), they were treated with 3% H_2O_2 for 10 min and then 3% non-fat dry milk in TBS with Tween20 for 30 min. They were incubated with LYVE-1pAb (diluted; 1:200) for 60 min at room temperature. The methods of immunostaining for vWF were the same as above.

For the conventional formalin-fixed paraffin-embedded tissue, prior to the immunostaining procedures, we treated the dehydrated slides with 40 μg/ml of proteinase K (Dako, CA, USA) per milliliters for 5 min at room temperature and a 10 mM citrate buffer solution (pH 6.0) for 10 min at 95°C. After a wash in TBS, they were treated with 3% H_2O_2 and then 3% non-fat dry milk and incubated with LYVE-1pAb (1:400) for one night at 4°C.

For all slides, a wash in TBS was followed by treatment with peroxidase-labeled polymer conjugated to goat anti-rabbit or anti-mouse immunoglobulins (Envision+ kit; Dako) for 30 min at room temperature. The immunostaining was visualized with diaminobenzidine tetrahydrochloride and then counterstained with hematoxylin.

Results

Western blotting for LYVE-1was performed using the protein extracted from full-length LYVE-1-transfected COS 7 cells as the respective antigen. An approximate 45 kDa band was detected, which was absent from mock-transfected cells. Absorption tests showed that LYVE-1 was recognized by the antiserum, and the reaction was completely abolished by preabsorption procedures (Fig. 1). These results demonstrated the strict specificity of our anti-LYVE-1 rabbit pAb for LYVE-1 protein.

To confirm the identification of the LYVE-1 molecule, COS 7 cells were transfected with full-length LYVE-1

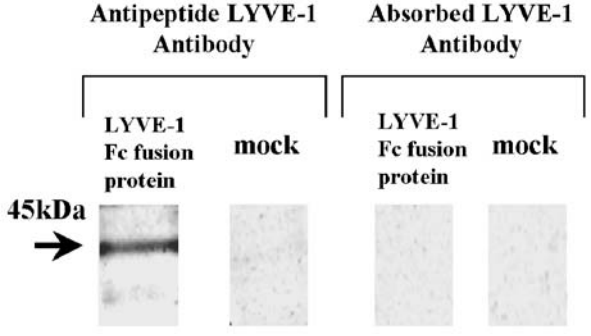

Fig. 1 Full-length lymphatic vessel endothelial hyaluronan receptor-1 (LYVE-1)-transfected COS 7 cells and mock-transfected cells were electrophoresed and Western blotted with antipeptide LYVE-1 polyclonal antibody. An approximate 45-kDa band was detected in LYVE-1-transfected cells, but not mock-transfected cells. It was absent in absorption tests

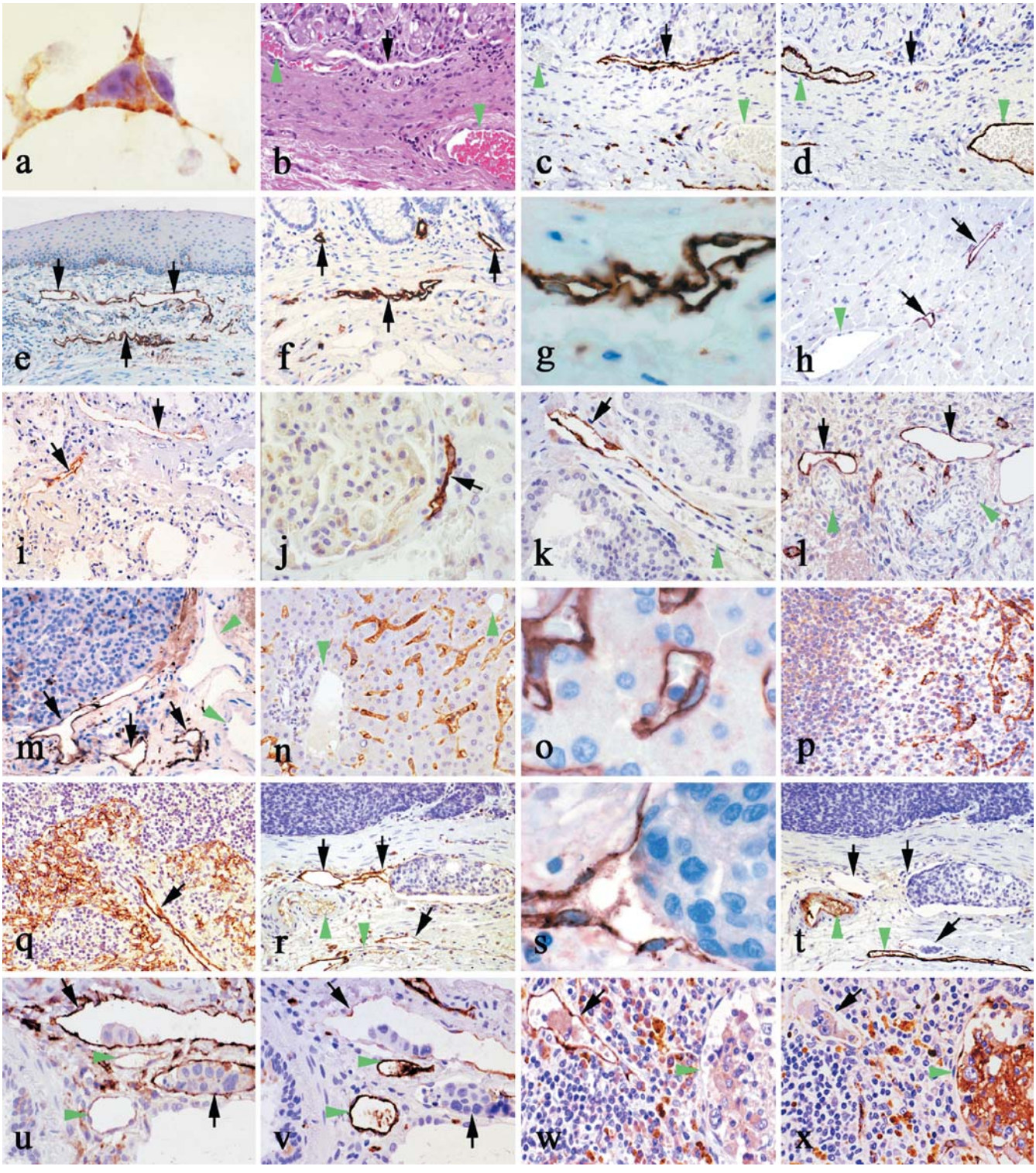

Fig. 2 Immunohistochemistry of lymphatic vessel endothelial hyaluronan receptor-1 (LYVE-1) polyclonal antibody (pAb). *Black arrows* indicate the lymphatic vessels positive for LYVE-1 and *green arrowheads* the blood vessels positive for von Willebrand factor (vWF). LYVE-1 is expressed extensively at the surface and mildly in the cytoplasm of full-length LYVE-1-transfected COS 7 cell (**a**). **b**–**d** Serial sections of gastric tissue (**b** hematoxylin and eosin stain, **c** LYVE-1, **d** vWf). A lymphatic vessel is positive for LYVE-1 (**c**), and blood vessels are positive for vWF (**d**). In the esophagus (**e**), colon (**f**, **g**), heart (**h**), lung (**i**), kidney (**j**), prostate (**k**), ovary (**l**), and pancreas (**m**), lymphatic endothelial cells are positive for LYVE-1. LYVE-1 is also found at the endothelial surface of the hepatic sinusoid (**n**, **o**), splenic sinusoid (**p**) and lymphatic sinus as well as in reticular cells (**q**). In serial sections of the esophageal lymphatic invaded by squamous cell carcinoma (**r**–**t**) and lung invaded by adenocarcinoma (**u**, **v**), the tumor is recognized in a LYVE-1-positive vessel (**r**, **s**, **u** LYVE-1, **t**, **v** vWF). In serial sections of cardiac angiosarcoma, immunostaining for LYVE-1 and vWF demonstrates the invasion by vWF-positive tumor cells of the LYVE-1-positive vessels (**w**) and vWF-positive vessels (**x**), respectively. Brown granules in the stroma are hemosiderin deposits degraded by tumor hemorrhage (**w**, **x**). Magnification: **a** ×550; **g**, **s** ×350; **o** ×300; **j**, **u**, **v** ×250; **w**, **x** ×225; **k**, **p** ×185; **b**–**d**, **f**, **l**, **m**, **q** ×130; **h**, **i**, **n**, **r**, **t** ×110, **e** ×50

cDNA and immunostained with polyclonal LYVE-1 antibody. LYVE-1 was expressed intensely on the cell surface and mildly in the cytoplasm (Fig. 2a).

The results of immunohistochemistry using our LYVE-1 pAb in normal human tissues are shown in Fig. 2b, c, d, e, f, g, h, i, j, k, l, m, n , o, p, q). In the gastrointestinal walls, esophagus, and colon, LYVE-1 was detected at the endothelial surface of the small vessels (Fig. 2b, c, d, e, f, g). The small vessels constituted with LYVE-1-positive endothelial cells were of irregular shape without a thick walled structure and had no red blood cells in their lumens. These vessels were distributed in all layers of the gastrointestinal and esophageal walls. From the morphological characteristics and the distribution patterns of the LYVE-1-positive vessels, our LYVE-1 pAb consistently marked the endothelial cells of the lymphatic vessels. Vessels with LYVE-1-positive endothelium were also detected in the stroma of the heart (Fig. 2h), lung (Fig. 2i), kidney (Fig. 2j), prostate (Fig. 2k), testis, ovary (Fig. 2l), skin, tongue, urinary bladder, thyroid gland, and pancreas (Fig. 2m). In these organs, LYVE-1-positive vessels were abundant in the connective tissues around the arteries, arterioles, veins, and veinlets. In contrast, vWF immunostaining was positive in the endothelium of the vessels having a distinct and thick walled structure, which were morphologically consistent with small arteries or veins. However, vWF was only sporadically or weakly positive in the endothelium of LYVE-1-positive vessels, indicating lymphatic vessels. In the liver, spleen, and adrenal gland, LYVE-1 was expressed on the endothelial surface of the hepatic sinusoid (Fig. 2n, o), splenic sinus (Fig. 2p), and intraglandular capillaries of the adrenal gland, and the stromal area also had LYVE-1-positive vessels. In the lymph nodes, LYVE-1 was found on the endothelial cells of the lymphatic sinus and in reticular cells (Fig. 2q). In all organs examined, LYVE-1 was not seen in endothelial cells of the vessels having a distinct and thick walled structure.

LYVE-1 expression patterns in carcinoma of the esophagus and lung and cardiac angiosarcoma are shown in Fig. 2r, s, t, u, v, w, x. There were only a few LYVE-1-positive endothelial cells in the malignant tissues, but many in the interstitium around the tumors. Vessels encircled by a LYVE-1-positive-endothelium containing tumor emboli in their lumens were observed around the tumor, but the intensity of LYVE-1 expression was weak compared with that in the endothelium without tumor invasion. In the cardiac angiosarcoma, vWF-positive tumor cells invaded the LYVE-1-positive vessels.

As for the conventional formalin-fixed paraffin-embedded tissue, staining results for LYVE-1 in all the organs examined were similar to those in tissue fixed in 10% neutral-buffered formalin. The specificity of the staining was enhanced, and the non-specific reaction was much suppressed by the pretreatment with Pronase K and citrate buffer solution.

Discussion

It has, thus far, been difficult to distinguish between small lymphatic vessels and blood capillaries using light microscopy, as there has been no useful marker specifically identifying the lymphatic vessels in various organs using immunohistochemistry [1, 3, 9, 16, 18]. Therefore, the identification of lymphatic vessels has depended exclusively on two morphological findings; no or little basement membrane and a lack of erythrocytes in lumens. In 1999, Banerji et al. identified the human LYVE-1 molecule as a major receptor of hyaluronan at the surface of the lymphatic endothelium [1]. In the present study, we prepared a pAb against part of the cytoplasmic tail of the LYVE-1 peptide [1]. Immunohistochemistry showed that affinity-purified antipeptide LYVE-1 pAb is a useful antibody for the immunohistochemical identification of the lymphatic endothelium in normal and pathological human tissues. Lymphatic capillaries consist of thin endothelial cells, the nuclei of which bulge into the lumen, and have a partial external basal lamina. In our study, the LYVE-1 molecule was identified as an integral membrane glycoprotein, thus, the expression of LYVE-1 pAb is intense at the endothelial surface in lymphatic capillaries and small lymphatic vessels.

VWF was intensely expressed in the endothelial cells of small arteries and veins. However, in serial sections, LYVE-1 was not detected at the endothelial surface of these vWF-positive vessels. vWF is present in Weibel-Palade bodies, which are abundant in the endothelial cells of blood vessels and may be present in the endothelial cells of lymphatic capillaries [17, 18]. Our immunohistochemical results indicate that antipeptide LYVE-1 pAb does not react with the endothelial cells of small blood vessels. In addition, the distribution of LYVE-1-positive capillaries was consistently different from that of vWF-positive capillaries in human organs, except for the liver, spleen, and adrenal gland, as previously reported for the liver and spleen [6, 13]. These findings suggest that the LYVE-1 pAb specifically reacts only with endothelial cells of the lymphatic vessels in human tissues other than organs with a sinus or sinusoidal structure. LYVE-1 is expressed in the sinusoidal endothelium at the sites where high molecular weight hyaluronan is incorporated and degraded [8, 13].

The cells immunopositive for our LYVE-1 antiserum were partly different from those positive for the polyclonal antiserum against human full-length LYVE-1 Fc fusion protein reported by Banerji et al. [1]. They described that zona reticularis cells in the adrenal gland, exocrine cells/islets of Langerhans in the pancreas, and tubular cuboidal epithelium in the kidney were positive for the full-length LYVE-1 antiserum. In addition, their LYVE-1 antiserum did not react with the stromal vessels, including lymphatic vessels in the prostate, ovary, testis, lung, and heart. In contrast, our LYVE-1 pAb could identify the stromal lymphatic vessels in the heart and urogenital tissues, but did not react with the parenchymal cells of the adrenal gland, pancreas, and kidney. It is

considered that our affinity-purified pAb against the hydrophilic area in the cytoplasmic tail of LYVE-1 has a higher specificity for lymphatic endothelial cells than the LYVE-1 pAb against full-length LYVE-1 Fc fusion protein.

In the malignant tissues examined, the intensity of LYVE-1 expression was partly weaker in the lymphatic vessels invaded by the malignant cells than those not invaded. It is suggested that the LYVE-1 expression at the endothelial surface of the lymphatic vessels is disturbed by the contact with malignant cells. Recently, lymphatic invasion and lymphangiogenesis were demonstrated in malignant tissues by immunostaining for full-length-LYVE-1 antiserum [4, 19, 22]. However, the LYVE-1 pAb raised in the present study consistently gave much better staining results for identifying human small lymphatic vessels under various conditions.

Acknowledgements We are grateful to Dr. Yutaka Hatanaka, Dako Cytomation Corporation for critical assessment of LYVE-1 antibody staining procedures. We also appreciate Ms. Harumi Tamura and Tsukiko Sato, Department of Pathology, Toho University School of Medicine, for excellent technical assistance throughout this study. This study was supported in part by a Saiseikai Research Fund and Project Study at Toho University, School of Medicine.

References

1. Banerji S, Ni J, Wang SX, Clasper S, Su J, Tammi R, Jones M, Jackson DG (1999) LYVE-1, a new homologue of the CD44 glycoprotein, is a lymph-specific receptor for hyaluronan. J Cell Biol 22:789–801
2. Breiteneder-Geleff S, Soleiman A, Kowalski H, Horvat R, Amann G, Kriehuber E, Diem K, Weninger W, Tschachler E, Alitalo K, Kerjaschki D (1999) Angiosarcomas express mixed endothelial phenotypes of blood and lymphatic capillaries: podoplanin as a specific marker for lymphatic endothelium. Am J Pathol 154:385–394
3. Clarijs R, Ruiter DJ, de Waal RM (2001) Lymphangiogenesis in malignant tumours: does it occur? J Pathol 193:143–146
4. Dadras SS, Paul T, Bertoncini J, Brown LF, Muzikansky A, Jackson DG, Ellwanger U, Garbe C, Mihm MC, Detmar M (2003) Tumor lymphangiogenesis: a novel prognostic indicator for cutaneous melanoma metastasis and survival. Am J Pathol 162:1951–1960
5. Ebata N, Nodasaka Y, Sawa Y, Yamaoka Y, Makino S, Totsuka Y, Yoshida S (2001) Desmoplakin as a specific marker of lymphatic vessels. Microvasc Res 61:40–48
6. Grant AJ, Goddard S, Ahmed-Choudhury J, Reynolds G, Jackson DG, Briskin M, Wu L, Hubscher SG, Adams DH (2002) Hepatic expression of secondary lymphoid chemokine (CCL21) promotes the development of portal-associated lymphoid tissue in chronic inflammatory liver disease. Am J Pathol 160:1445–1455
7. Irjala H, Johansson EL, Grenman R, Alanen K, Salmi M, Jalkanen S (2001) Mannose receptor is a novel ligand for L-selectin and mediates lymphocyte binding to lymphatic endothelium. J Exp Med 194:1033–1042
8. Jackson DG (2003) The lymphatics revisited. New perspectives from the hyaluronan receptor LYVE-1. Trends Cardiovasc Med 13:1–7
9. Jackson DG, Prevo R, Clasper S, Banerji S (2001) LYVE-1, the lymphatic system and tumor lymphangiogenesis. Trends Immunol 22:317–321
10. Jain RK, Fenton BT (2002) Intratumoral lymphatic vessels: a case of mistaken identity or malfunction? J Natl Cancer Inst 94:417–421
11. Jussila L, Valtola R, Partanen TA, Salven P, Heikkila P, Matikainen MT, Renkonen R, Kaipainen A, Detmar M, Tschachler E, Alitalo R, Alitalo K (1998) Lymphatic endothelium and Kaposi's sarcoma spindle cells detected by antibodies against the vascular endothelial growth factor receptor-3. Cancer Res 58:1599–1604
12. Kahn HJ, Bailey D, Marks A (2002) Monoclonal antibody D2–40, a new marker of lymphatic endothelium, reacts with Kaposi's sarcoma and a subset of angiosarcomas. Mod Pathol 5:434–440
13. Mouta Carreira C, Nasser SM, di Tomaso E, Padera TP, Boucher Y, Tomarev SI, Jain RK (2001) LYVE-1 is not restricted to the lymph vessels: expression in normal liver blood sinusoids and down-regulation in human liver cancer and cirrhosis. Cancer Res 15:8079–8084
14. Nibbs RJ, Kriehuber E, Ponath PD, Parent D, Qin S, Campbell JD, Henderson A, Kerjaschki D, Maurer D, Graham GJ, Rot A (2001) The beta-chemokine receptor D6 is expressed by lymphatic endothelium and a subset of vascular tumors. Am J Pathol 158:867–877
15. Paavonen K, Puolakkainen P, Jussila L, Jahkola T, Alitalo K (2000) Vascular endothelial growth factor receptor-3 in lymphangiogenesis in wound healing. Am J Pathol 156:1499–1504
16. Pepper MS (2001) Lymphangiogenesis and tumor metastasis: myth or reality? Clin Cancer Res 7:462–468
17. Rand JH, Gordon RE, Sussman II, Chu SV, Solomon V (1982) Electron microscopic localization of factor-VIII-related antigen in adult human blood vessels. Blood 60:627–634
18. Sleeman JP, Krishnan J, Kirkin V, Baumann P (2001) Markers for the lymphatic endothelium: in search of the holy grail? Microsc Res Tech 15:61–69
19. Straume O, Jackson DG, Akslen LA (2003) Independent prognostic impact of lymphatic vessel density and presence of low-grade lymphangiogenesis in cutaneous melanoma. Clin Cancer Res 9:250–256
20. Valtola R, Salven P, Heikkila P, Taipale J, Joensuu H, Rehn M, Pihlajaniemi T, Weich H, de Waal R, Alitalo K (1999) VEGFR-3 and its ligand VEGF-C are associated with angiogenesis in breast cancer. Am J Pathol 154:1381–1390
21. Wigle JT, Oliver G (1999) Prox1 function is required for the development of the murine lymphatic system. Cell 17:769–778
22. Williams CS, Leek RD, Robson AM, Banerji S, Prevo R, Harris AL, Jackson DG (2003) Absence of lymphangiogenesis and intratumoural lymph vessels in human metastatic breast cancer. J Pathol 200:195–206
23. Witmer AN, van Blijswijk BC, Dai J, Hofman P, Partanen TA, Vrensen GF, Schlingemann RO (2001) VEGFR-3 in adult angiogenesis. J Pathol 195: 490–497

Virchows Arch (2004) 444:158–163
DOI 10.1007/s00428-003-0939-3

ORIGINAL ARTICLE

M. Hiroi · N. Kuroda · M. Toi · Y. Hayashi · E. Miyazaki · K. Naruse · H. Enzan

Fascin-positive dendritic cells and fibroblastic reticulum cells build a framework of T-cell areas in lymph nodes

Received: 10 December 2002 / Accepted: 21 October 2003 / Published online: 23 December 2003

Abstract Fascin, a 55-kDa actin-bundling protein, and α-smooth muscle actin (ASMA) were immunohistochemically examined in murine normal and stimulated lymph nodes. In specific pathogen-free young female mice, a few fascin-positive cells (FPCs) were located in the sinus and surrounding tissues, but ASMA-positive cells were undetectable. Following a subcutaneous injection of sheep red blood cells, the numbers of FPCs and their dendrites increased in the paracortex, with the accumulation of activated lymphocytes. Fibroblastic reticulum cells (FRCs), endothelial cells, histiocytic cells and lymphocytes in various stages of maturation were all fascin negative. These results indicated that fascin could be a reliable marker of paracortical dendritic cells in murine lymph nodes. However, FRCs became ASMA positive. Immunoelectron microscopy showed that the FPCs were interdigitating cells and that they closely contacted with FRCs. These two types of cells and reticular fiber formed a network in the paracortex and contacted with each other. In active paracortical response, both FPCs and FRCs are also stimulated and might play a significant role in the maturation of the lymphocytes.

Keywords Dendritic cells · Fascin · Fibroblastic reticulum cells · α-Smooth muscle actin · Murine lymph node

M. Hiroi (✉) · N. Kuroda · M. Toi · Y. Hayashi · E. Miyazaki · H. Enzan
The First Department of Pathology,
Kochi Medical School,
Kohasu, Okoh-Cho, 783-8505 Nankoku City, Kochi, Japan
e-mail: hiroim@kochi-ms.ac.jp
Tel.: +81-88-8802330
Fax: +81-88-8802332

K. Naruse
Department of Clinical Laboratory,
National Kochi Hospital,
Asakura, 780-8507 Kochi, Japan

Introduction

Interdigitating cells (IDCs) are one of typical elements of paracortex and a subset of dendritic cells (DCs). DCs are professional antigen-presenting cells that are involved in initiating primary immunoresponses [21]. They are heterogeneous with regard to their origin and maturation states and are variously termed according to the organ, surface markers and morphology. Consensus states that DCs originate from a hematopoietic progenitor and have myeloid and lymphoid pathways of differentiation [3]. DCs distributed throughout the body (except for the brain) are also called Langerhans cells, dermal dendritic cells, interstitial dendritic cells and veiled cells. Lymphoid organs contain interdigitating cells, germinal center dendritic cells and follicular dendritic cells (FDCs) [5, 9]. However, FDCs differ from ordinary DCs, as they can trap antigen, their origin is controversial, they lack the leukocyte marker CD45, and a unique set of molecules is displayed at their surface [12]. Peripheral tissue DCs capture and process antigens and display antigen peptides with major histocompatibility complex (MHC)-peptide complexes and co-stimulatory molecules at their surface [6, 10]. They simultaneously migrate to regional lymph nodes, where they contact and activate antigen-specific T cells [4, 11, 16]. Although IDCs are so described from the results of electron microscopy and remain unclear, all mature DCs in the T-cell area of lymph nodes are thought to be interdigitating cells [5].

Fascin, a novel marker of DCs [2], is a 55-kDa, actin-bundling protein that regulates the rearrangement of cytoskeletal elements, as well as the interaction between the cytoskeleton and the cell membrane in response to extra- or intracellular signals [22, 27]. The expression of fascin might be associated with dendrite formation [26]. Furthermore, the paracortex has other structural elements, namely post-capillary venules and reticular framework. Fibroblastic reticulum cells (FRCs) produce reticular fibers and build a reticular framework in the lymph nodes. The activity of FRCs, producing these extracellular matrices, was revealed by immunoreactivity for α-smooth

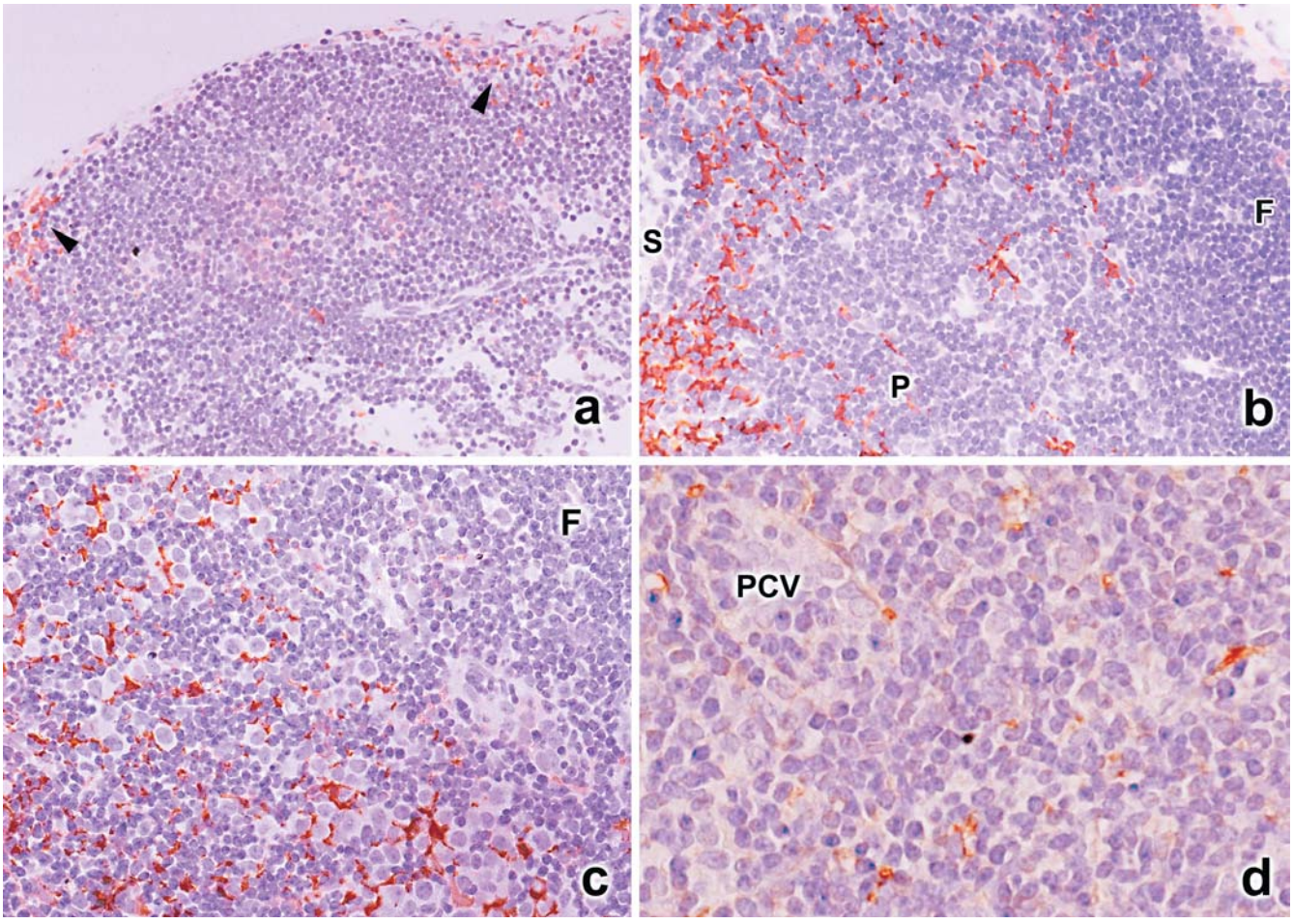

Fig. 1 Immunohistochemical staining for fascin (**a**, **b** and **c**) and α-smooth muscle actin (ASMA) (**d**). **a** Non-stimulated lymph node has incomplete structure. A few fascin-positive cells (FPCs) are located in peripheral sinus (*arrowhead*). **b** Lymphoid follicle (*F*) and paracortex (*P*) are differentiated 1 day after injection. Number of FPCs has increased, and they are distributed mainly adjacent to the sinus (*S*). **c** FPCs are distributed throughout the paracortex 2 days after injection. Large lymphocytes are seen between FPCs and their dendrites. **d** ASMA-positive stains, indicating myofibroblastic-transformed fibroblastic reticulum cells, are scattered in paracortex 5 days after injection. *PCV* post capillary venule

muscle actin (ASMA) [25]. We investigated changes in fascin- and ASMA-positive cells in murine lymph nodes stimulated by an injection of sheep red blood cells.

Materials and methods

Mice

Specific pathogen-free BALB/c female mice (4–5 weeks old) (Japan SLC, Hamamatsu, Japan) were separately housed with free access to food and water in an atmosphere of high-efficiency particulate air-filtered air. All experiments proceeded according to the ethics guidelines of our institution.

Stimulation

Sheep red blood cells (0.1 ml) were injected into the subcutaneous tissue of the upper part of the front paw, and, then, regional axillary lymph nodes were resected 1, 2, 3, 5 and 7 days later.

Light microscopy

Formalin-fixed paraffin-embedded lymph node tissue sections, 4 μm in thickness, were stained with hematoxylin and eosin for immunohistochemistry. Fascin was immunohistochemically stained using the streptavidin-biotin peroxidase complex (Histofine SAB-PO kit, Nichirei Inc., Tokyo, Japan). A monoclonal antibody to fascin (Clone 55K-2 Dako, Glostrup, Denmark) diluted 1:50 was the primary antibody. Antigen was retrieved from the sections by microwave heating in citrate buffer (pH 6.0). We immunohistochemically stained ASMA using enhanced polymer one-step ASMA (clone 1A4, Dako, Glostrup, Denmark).

We double stained frozen sections of stimulated lymph nodes for MHC class II/fascin. We analyzed MHC class-II expression using an unlabeled anti-MHC II antibody (clone IBL-5/22, Neomarkers, Westinghouse, USA), anti-rat IgG antibody labeled with biotin (Dako, Glostrup, Denmark) and Texas red streptavidin (Vector Lab Inc., Burlingame, USA). Anti-fascin antibody was labeled with Alexa fluor 488 using Zenon antibody labeling kit (Molecular probe, Eugene, OR, USA), following the instructions.

Electron microscopy

Tissues were fixed in 2.5% glutaraldehyde, post-fixed in 1% osmium tetroxide and embedded in epoxy resin for electron microscopy. We examined enlarged regional lymph nodes using immunoelectron microscopy 7 days after injection. Primary antibodies for fascin and ASMA were the same as those described above and applied as described [8]. Briefly, microslices fixed with periodate-lysine-paraformaldehyde were incubated with antibodies for fascin and ASMA and then stained using avidin-biotin-peroxidase complex and visualized using 3,3′-diaminobenzidine tetrahydrochloride. Ultrathin sections were examined using an electron microscope (JEOL 100S and 1200EX, JEOL Ltd., Japan).

Results

Light microscopy

Small axillary lymph nodes of control mice contained only primary follicles, immature paracortical areas and sinuses. Germinal centers were absent and the reticular framework was indistinct. A few fascin-positive cells (FPCs) populated the peripheral sinus and interfollicular areas (Fig. 1a). The paracortex became evident and some FPCs with dendritic processes appeared around the sinuses 1 day after injection (Fig. 1b). FPCs became scattered in a gradually expanded paracortex, and fascin-positive cell processes extended between lymphocytes. The numbers of large lymphocytes increased between FPCs and their dendrites (Fig. 1c). Germinal centers containing no FPCs were formed after 5 days, although the number of FPCs and their fascin-positive dendrites increased throughout the paracortex. After 7 days, lymph nodes were more enlarged, but were not significantly larger than those after 5 days. Lymphocytes, histiocytes and endothelial cells were negative for fascin. Fibroblastic cells, including FRCs, are difficult to differentiate from DCs using light microscopy. Follicular dendritic cells and tingible body macrophages were also negative for fascin.

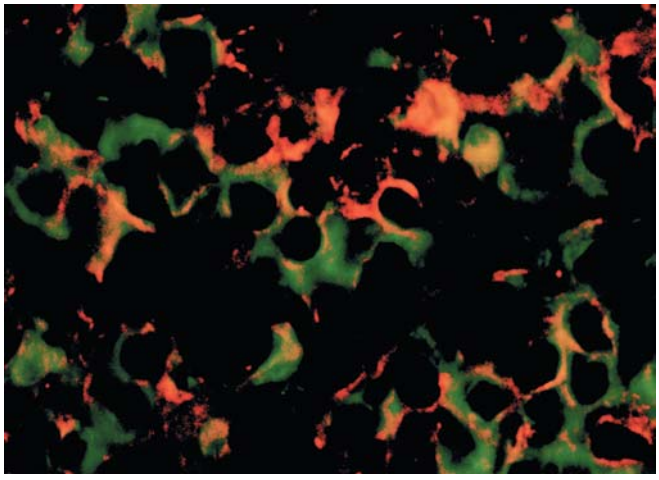

Fig. 2 Fluorescence micrograph of paracortex of lymph node. Major histocompatibility complex II-positive (*red fluorescence*) cells are also stained for fascin (*green fluorescence*) 5 days after injection

Cells were ASMA-positive only in the subcapsular and perivascular areas of control lymph nodes, but not identified in the lymphoid tissue. However, a few ASMA-positive spindle cells appeared in the paracortex and medulla 2 days after injection, and they gradually increased in number (Fig. 1d).

Fluorescence microscopy showed that MHC II-positive cells had numerous dendrites, most of which were also positive for fascin. However, some dendrites were positive only for fascin or MHC II (Fig. 2).

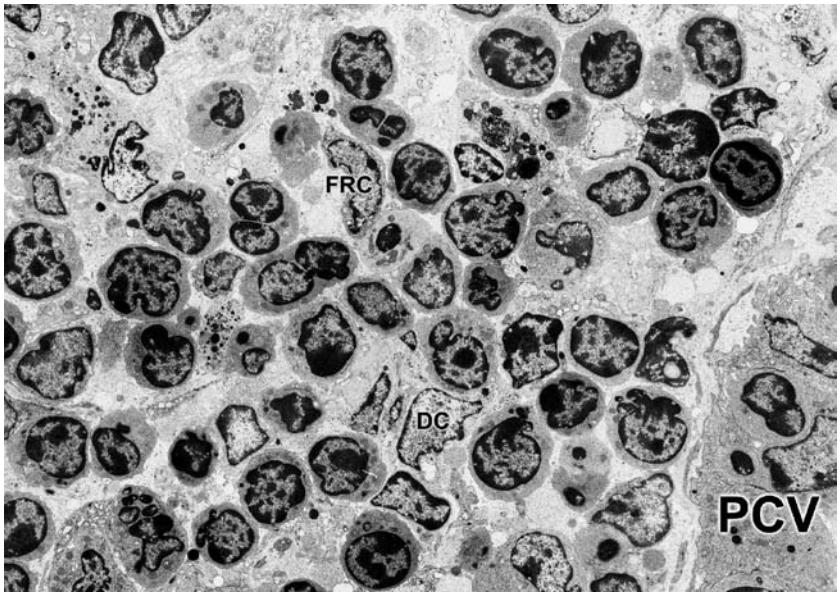

Fig. 3 Electron micrograph of non-stimulated lymph nodes. Indistinct framework of fibroblastic cells and reticular fibers. *DC* dendritic cell, *FRC* fibroblastic reticulum cell, *PCV* post-capillary venule (×2000)

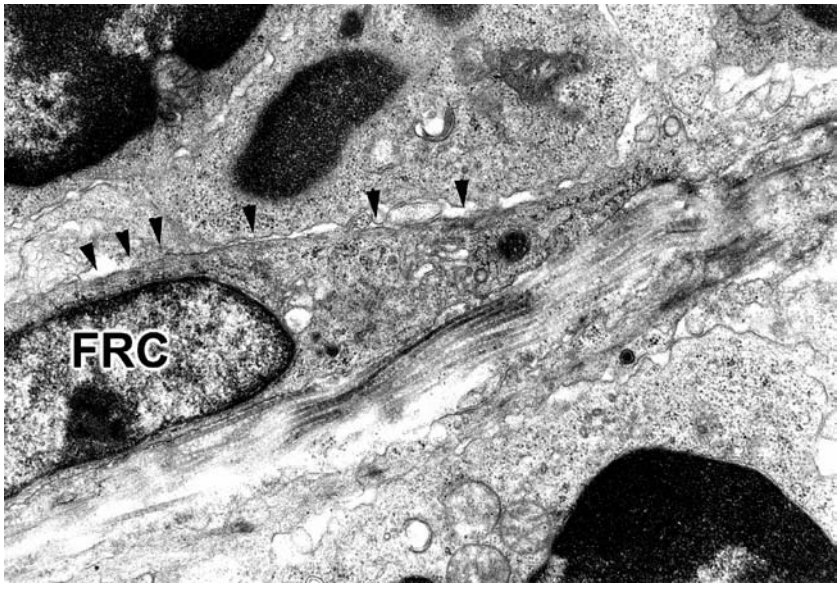

Fig. 4 Electron micrograph of lymph node of 5 days after injection. Fibroblastic reticulum cells are spindle shaped and, in the periphery of cytoplasm, contain bundled filamentswith dense bodies (*arrowhead*) associated with collagen fibers. *FRC* fibroblastic reticulum cell (×15,000)

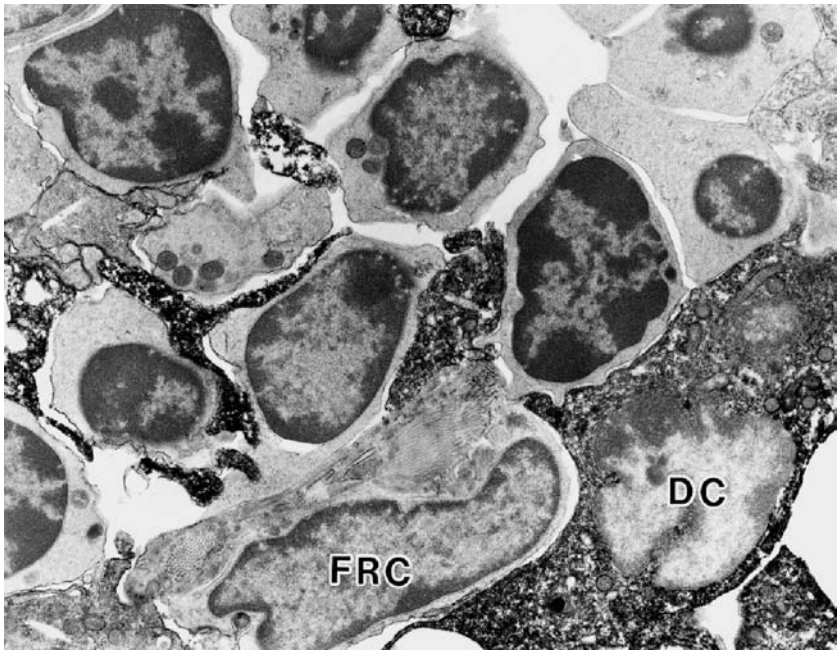

Fig. 5 Immunoelectron microphotograph for fascin of lymph node of 7 days after injection. Obvious electron-dense structures are fascin-positive cells (FPCs) and dendrites with slightly convoluted nuclei. Lymphocytes and fibroblastic reticulum cells (FRCs) are negative for fascin. FPCs and FRCs are in contact and some lymphocytes have protruded into FPCs (×6000)

Electron microscopy

The paracortex was recognized with the post-capillary venules. The DCs had irregularly shaped nuclei. The chromatin pattern was delicate, and nucleoli were inconspicuous. The cytoplasm had few organelles and indistinct dendrites. The FRCs of control mice were short and spindle shaped. Their nuclei were oval or spindle shaped, and nuclear contour was comparatively smooth. Although the cytoplasm contained rough endoplasmic reticulum and microfilaments, they were not distinct. The framework of the collagen fibers was obscure (Fig. 3). After stimulation, the reticular framework of collagen fibers increased, and FRCs became spindle shaped or stellate. Some FRCs had parallel microfilaments with a dense body, indicating that they had undergone myofibroblastic transformation (Fig. 4). DCs also became prominent, frequently with irregular dendrites.

Immunoelectron microscopy identified fascin-positive cells and their dendrites located between lymphocytes. Because FPCs had large irregular-shaped nuclei and dendrites, they morphologically resembled interdigitating cells. Some lymphocytes were in close contact with the FPCs. Spindle-shaped FRCs were negative for fascin and associated with collagen fibers, although FPCs and FRCs were frequently in contact. Lymphocytes, histiocytes and endothelial cells were negative for fascin (Fig. 5).

Discussion

In this study, axillary lymph nodes in untreated young mice had an incomplete reticular network and contained few FPCs. After stimulation by a subcutaneous injection of sheep red blood cells, numbers of FPCs and their dendrites increased. In human tissue, fascin is expressed not only in dendritic cells, but also in various types of cells, such as fibroblasts, neurons, glial cells, endothelial cells and Epstein-Barr virus-transfected B cells and Hodgkin's cells [14, 15, 18, 19]. The present study of murine lymph nodes found that follicular dendritic cells, endothelial cells and lymphocytes were negative for fascin. The morphology and distribution pattern of FPCs suggested that FPCs are interdigitating cells. Double immunofluorescence staining for MHC II and fascin revealed that almost all MHC II-positive cells were also fascin positive, but some dendritic structures were positive only for fascin or MHC II. Fascin is related to dendritic process and exists in various cells as described above. In frozen sections, because the antigenicity is well retained, the other cells, such as fibroblastic cells and endothelial cells, might be positive for fascin. MHC II is also expressed in monocytes/macrophages and B lymphocytes. Immunoelectron microscopy confirmed that FRCs and endothelial cells were negative for fascin and that fascin positivity was restricted to cells with dendritic shape and dendrites, namely dendritic cells in the paracortex. Because the staining procedures were not the same, the findings of some cells might be quite different. Considering all the variables, these results suggested that the presence of paracortical FPCs, which appeared to be classified as IDCs, and fascin is a useful immunohistochemical marker of DCs of formalin-fixed and paraffin-embedded murine lymph nodes. Matured DCs in culture have already undergone morphological changes, including the formation of numerous dendrites [13, 24] and the upregulation of fascin expression [2, 17]. In this study, after the stimulation, FPCs and their fascin-positive cell processes gradually increased in the paracortex. The migration and maturation of DCs were demonstrated using immunohistochemistry with a monoclonal antibody against fascin. At the same time, FRCs became ASMA positive. The phenotypes of fibroblastic stromal cells in various organs transform into myofibroblasts or myofibroblast-like cells and produce various components of extracellular matrices. Cytokines, such as transforming growth factor-beta and granulocyte-macrophage colony-stimulating factor, are involved in this transformation, and the stromal cells became positive or more intensely positive for AMSA. These cytokines are involved in DC maturation. In addition, FRCs that are positive for ASMA seem to produce various extracellular matrices, including adhesion molecules [20]. The expression of fascin is regulated by various extracellular matrices [1, 7, 23]. These two types of cells and reticular fiber build a network in the paracortex, where they are all in contact. In active paracortical response, both FPCs and FRCs are also stimulated and might play a significant role in the maturation of the lymphocytes.

References

1. Adams JC, Clelland JD, Collett GD, Matsumura F, Yamashiro S, Zhang L (1999) Cell-matrix adhesions differentially regulate fascin phosphorylation. Mol Biol Cell 10:4177–4190
2. Al-Alwan MM, Rowden G, Lee TDG, West A (2001) Fascin is involved in the antigen presentation activity of mature dendritic cells. J Immunol 166:338–345
3. Ardavín G, Martínez del Hoyo G, Martín P, Anjuère F, Arias CF, Marín AR, Ruiz S, Parrillas V, Hernández H (2001) Origin and differentiation of dendritic cells. Trends Immunol 22:691–700
4. Austyn JM (1996) New insights into the mobilization and phagocytic activity of dendritic cells. J Exp Med 183:1287
5. Branchereau J, Steinmann RM (1998) Dendritic cells and the control of immunity. Nature 392:245–252
6. Buelens C, Verhasselt V, De Groote D, Thielemans K, Goldman M, Willems F (1997) Human dendritic cell responses to lipopolysaccharide and CD40 ligation are differentially regulated by interleukin-10. Eur J Immunol 27:1848
7. Dieu MC, Vanbervliet B, Vicari A, Bridon JM, Oldham E, Ait Yahia S (1998) Selective recruitment of immature and mature dendritic cells by distinct chemokines expressed in different anatomic sites. J Exp Med 188:373–386
8. Enzan H, Hiroi M, Saibara T, Onishi S, Yamamoto Y, Yamamoto H, Hara H (1991) Immunoelectron microscopic identification of asialo GM1-positive cells in adult rat liver. Virchows Arch 60:389–398
9. Grouard G, Durand I, Filgueira L, Banchereau J, Liu YJ (1996) Dendritic cells capable of stimulating T cells in germinal centers. Nature 384:364–367
10. Hart DN (1997) Dendritic cells: unique leukocyte populations which control the primary immune response. Blood 90:3245
11. Inaba K, Pack M, Inaba M, Sakuta H, Isdell F, Steinman RM (1997) High levels of a major histocompatibility complex II-self peptide complex on dendritic cells from the T cell areas of lymph nodes. J Exp Med 186:665–672
12. Kapasi Z, Qin D, Kerr W, Kosco-Vilbois M, Shultz L, Tew J, Szakal A (1998) Follicullar dendritic cell (FDC) precursors in primary lymphoid tissues. J Immunol 160:1078–1084
13. Larsen CP, Ritchie SC, Pearson TC, Linsley PS, Lowry RP (1992) Functional expression of the costimulatory molecule, B7/BB1, on murine dendritic cell populations. J Exp Med 176:1215–1220
14. Mosialos G, Yamashiro S, Baughman RW, Matsudaira P, Vara L, Matsumura F, Kieff E, Birkenbach M (1994) Epstein-Barr virus infection induces expression in B lymphocytes of a novel gene encoding an evolutionarily conserved 55-kilodalton actin-bundling protein. J Virol 68:7320–7328
15. Pinkus GS, Pinkus JL, Langhoff E, Matsumura F, Yamashiro S, Mosialos G, Said JW (1997) Fascin, a sensitive new marker for Reed Sternberg cells of Hodgkin's disease. Evidence for a dendritic or B cell derivation? Am J Pathol 150:543–562
16. Roake JA, Rao AS, Morris PJ, Larsen CP, Hankins DF, Austyn JM (1995) Dendritic cell loss from nonlymphoid tissues after systemic administration of lipopolysaccharide, tumor necrosis factor, and interleukin 1. J Exp Med 191:2237
17. Ross R, Ross XL, Schwing J, Langin T, Reske KA (1998) The actin-bundling protein fascin is involved in the formation of dendritic processes in maturing epidermal Langerhans cells. J Immunol 160:3776–3782
18. Said JW, Pinkus JL, Yamashita J, Mishalani S, Matsumura F, Yamashiro S, Pinkus GS (1997) The role of follicular and interdigitating dendritic cells in HIV-related lymphoid hyperplasia: localization of fascin. Mod Pathol 10:421–427
19. Said JW, Pinkus JL, Shintaku IP, deVos S, Matsumura F, Yamashiro S, Pinkus GS (1998) Alterations in fascin-express-

ing germinal center dendritic cells in neoplastic follicles of B-cell lymphomas. Mod Pathol 11:1–5
20. Schürch W, Seemayer T, Gabbiani, G (1997) Myofibroblasts. In: Sternberg, S (ed) Histology for pathologists. Ravens Press, New York, pp 129–165
21. Steinmann RM (1991) The dendritic cell system and its role in immunogenicity. Annu Rev Immunol 9:271
22. Stossel TP (1993) On the crawling of animal cells. Science 260:1086–1094
23. Termeer CC, Hennies J, Voith U, Ahrens T, Weiss JM, Prehm P, Simon JC (2000) Oligosaccharides of hyaluronan are potent activators of dendritic cells. J Immunol 165:1863–1870
24. Teunissen MB, Wormmeester J, Krieg SR, Peters PJ, Vogels IM, Kapsenberg ML, Bos JD (1990) Human epidermal Langerhans cells undergo profound morphologic and phenotypical changes during in vitro culture. J Invest Dermatol 94:476
25. Toccanier-Pelte M, Skall O, Kapanci Y, Gabbiani G (1987) Characterization of stromal cells with myoid features in lymph nodes and spleen in normal and pathologic condition. Am J Pathol 129:109–118
26. Yamashiro S, Yamakita Y, Ono S, Matsumura F (1998) Fascin, an actin-bundling protein, induces membrane protrusions and increases cell motility of epithelial cells. Mol Biol Cell 9:993–1006
27. Yamashiro-Matsushita S, Matsumura F (1985) Purification and characterization of an F-actin-bundling protein 55-kilodalton protein from HeLa cells. J Biol Chem 260:5087–5097

Virchows Arch (2004) 444:164–170
DOI 10.1007/s00428-003-0941-9

ORIGINAL ARTICLE

Hiroyuki Kumamoto · Kiyoshi Ooya

Expression of survivin and X chromosome-linked inhibitor of apoptosis protein in ameloblastomas

Received: 9 October 2003 / Accepted: 4 November 2003 / Published online: 9 January 2004

Abstract To clarify the role of apoptosis in oncogenesis and cytodifferentiation of odontogenic epithelium, expression of survivin and X chromosome-linked inhibitor of apoptosis protein (XIAP), inhibitor of apoptosis protein (IAP) family proteins, was examined in tooth germs and in benign and malignant ameloblastomas by means of immunohistochemistry and reverse-transcription polymerase chain reaction. Immunoreactivity for survivin and XIAP was detected in developing and neoplastic odontogenic epithelium. In tooth germs, survivin expression was evident in inner enamel epithelium. Follicular, plexiform and metastasizing ameloblastomas showed survivin reactivity chiefly in neoplastic cells neighboring the basement membrane, and most neoplastic cells in basal cell and desmoplastic ameloblastomas and ameloblastic carcinomas were positive for survivin. Survivin mRNA levels were slightly higher in ameloblastomas than in tooth germs, suggesting that elevation of survivin expression might be involved in oncogenesis of odontogenic epithelium. Immunoreactivity for XIAP was detected in most odontogenic epithelial cells in tooth germs and in benign and malignant ameloblastomas, and XIAP mRNA levels were significantly higher in follicular ameloblastomas than in plexiform ameloblastomas. The expression of survivin and XIAP in odontogenic tissues suggests that these IAP family proteins contribute to the biological properties of ameloblastomas, such as cell survival, proliferation, differentiation and tissue structuring, as well as to cellular regulation during tooth development.

Keywords Ameloblastoma · Apoptosis · IAP · Survivin · XIAP

H. Kumamoto (✉) · K. Ooya
Division of Oral Pathology,
Department of Oral Medicine and Surgery,
Tohoku University Graduate School of Dentistry,
4-1 Seiryo-machi, Aoba-ku, 980-8575 Sendai, Japan
e-mail: kumamoto@mail.tains.tohoku.ac.jp
Tel.: +81-22-7178303
Fax: +81-22-7178304

Introduction

Tumors arising from epithelium of the odontogenic apparatus or from its derivatives or remnants exhibit considerable histological variation and are classified into several benign and malignant entities [6, 16, 26, 30]. Ameloblastoma is the most frequently encountered tumor arising from odontogenic epithelium and is characterized by a benign but locally invasive behavior, with a high risk of recurrence [16, 26, 30]. Histologically, ameloblastoma shows considerable variation, including follicular, plexiform, acanthomatous, granular cell, basal cell and desmoplastic types [16]. Malignant ameloblastoma is defined as a neoplasm in which the pattern of an ameloblastoma and cytological features of malignancy are shown by the primary growth in the jaws and/or by any metastatic growth [16]. Recently, malignant ameloblastoma has been subclassified into metastasizing ameloblastoma and ameloblastic carcinoma on the basis of metastatic spread and cytological malignant features [6]. Several recent studies have detected genetic and cytogenetic alterations in these epithelial odontogenic tumors [9, 12]; however, the detailed mechanisms of oncogenesis, cytodifferentiation and tumor progression remain unknown.

Apoptosis, also known as programmed or physiological cell death, plays diverse roles in embryogenesis and normal homeostasis, as well as in oncogenesis [14, 32, 35]. Apoptotic processes are modulated by various factors, which have inhibitory or stimulatory effects [27, 32, 35]. The inhibitor of apoptosis protein (IAP) family proteins, first described as a baculovirus gene product, are characterized by a novel domain of approximately 70 amino acids, termed the baculovural IAP repeat (BIR), and this domain is capable of inhibiting caspases and, thus, suppressing apoptosis [2, 3, 33]. Proteins containing BIR domains have been recognized in a wide range of eukaryotic species, and eight IAP relatives have been identified in humans [3]. Survivin is an IAP member, whose gene is located on chromosome 17q25, and is a unique bifunctional protein which suppresses apoptosis by

inhibiting caspase-3 and -7 and regulates the G2/M phase of the cell cycle by associating with mitotic spindle microtubules [38]. Expression of survivin is largely absent from normal adult tissues, but is highly identified in developing fetal tissues and many common types of neoplasms [1, 11, 13]. X chromosome-linked IAP (XIAP) is another IAP family protein, whose gene is assigned to chromosomal location Xq25, and strongly suppresses apoptosis by binding distinct caspases, namely caspases-3, -7 and -9 [4, 5, 24]. Expression of XIAP mRNA has been observed in most fetal and adult tissues [24] and is associated with a poor prognosis in some malignancies [7, 34].

Our previous studies confirmed apoptotic cells and several apoptosis-related factors, such as the bcl-2 family proteins, p53, Fas, Fas ligand and heat shock proteins, in tooth germs and ameloblastomas, suggesting that apoptotic cell death has an important role in oncogenesis or cytodifferentiation of odontogenic epithelium [17, 18, 19, 21, 23]. In the present study, expression of survivin and XIAP in benign and malignant ameloblastomas as well as in tooth germs was examined using immunohistochemistry and reverse-transcription polymerase chain reaction (RT-PCR) to clarify the possible role of these IAP family proteins in epithelial odontogenic tumors.

Materials and methods

Tissue preparation

Specimens were surgically removed from 52 patients with epithelial odontogenic tumors at the Department of Oral and Maxillofacial Surgery, Tohoku University Dental Hospital, and affiliated hospitals. The specimens were fixed in 10% buffered formalin for one to several days and were embedded in paraffin. The tissue blocks were sliced into 3-μm-thick sections for routine histological and subsequent immunohistochemical examinations. Tissue sections were stained with hematoxylin and eosin for histological diagnosis according to the World Health Organization histological typing of odontogenic tumors [16]. The tumors comprised 46 ameloblastomas and 6 malignant ameloblastomas. Ameloblastomas were divided into 30 follicular and 16 plexiform types, including 15 acanthomatous, 5 granular cell, 3 basal cell and 4 desmoplastic subtypes. Malignant ameloblastomas were classified into 2 metastasizing ameloblastomas and 4 ameloblastic carcinomas, according to the criteria of Eversole [6]. For semi-quantitative RT-PCR analysis, tumor tissues were immediately frozen on dry ice and stored at −80°C. Specimens of 11 tooth germs of the mandibular third molars, enucleated for orthodontic reasons at the initial stage of crown mineralization, were similarly prepared and compared with the epithelial odontogenic tumors.

Immunohistochemistry

The tissue sections were deparaffinized, immersed in methanol with 0.3% hydrogen peroxide and heated in 0.01 M citrate buffer (pH 6.0) for 10 min by autoclave (121°C, 2 atm). After treatment with normal serum for 30 min, the sections were incubated with primary antibodies at 4°C overnight. The applied antibodies were rabbit anti-survivin polyclonal antibody (Nobus Biologicals, Littleton, CO, USA; diluted at 1:200) and goat anti-XIAP polyclonal antibody (Santa Cruz Biotechnology, Santa Cruz, CA, USA; diluted at 1:50). The standard streptavidin-biotin-peroxidase complex method was performed to bind the primary antibodies with the use of Histofine SAB-PO Kits (Nichirei, Tokyo, Japan). Reaction products were visualized by immersing the sections in 0.03% diaminobenzidine solution containing 2 mM hydrogen peroxide for 1–3 min. Nuclei were lightly counterstained with methylgreen. For control studies of the antibodies, the serial sections were treated with phosphate-buffered saline, normal rabbit IgG and normal goat IgG instead of the primary antibodies and were confirmed to be unstained. Immunohistochemical reactivity for survivin and XIAP was evaluated and classified into three groups: (+) weak, (++) moderate and (+++) strong.

Semi-quantitative RT-PCR analysis

Total RNA was extracted from frozen tissue samples of 8 tooth germs, 32 ameloblastomas and 1 malignant ameloblastoma using an RNeasy Mini Kit (Qiagen, Hilden, Germany), according to the manufacturer's protocol. First-stranded complementary DNA (cDNA) was synthesized from 1 μg of RNA using an Omniscript RT Kit (Qiagen) with oligo-(dT)15 primer (Roche Diagnostics, Mannheim, Germany), as outlined by the manufacturer. The cDNA samples were amplified using a HotstarTaq Master Mix Kit (Qiagen) with specific primers in a DNA thermal cycler (Eppendorf, Hamburg, Germany). Primers used in this study were as follows: 5′-AGCCCTTTCTCAAGGACCAC-3′ (forward) and 5′-GCACTTTCTTCGCAGTTTCC-3′ (reverse) for survivin, yielding a 363-bp product, and 5′-GAAGACCCTTGGGAACAACA-3′ (forward) and 5′-CGCCTTAGCTGCTCTTCAGT-3′ (reverse) for XIAP, yielding a 389-bp product. A housekeeping gene, glyceraldehyde-3-phosphate dehydrogenase (GAPDH), was used as an internal control for the examination of human gene expression, and the primer sequences were 5′-GGAGTCAACGGATTTGGT-3′ (forward) and 5′-GTGATGGGATTTCCATTGAT-3′ (reverse), yielding a 206-bp product. PCR was performed in a total volume of 50 μl, containing 0.5 μg of template cDNA and 0.5 μM of each specific primer set. The procedure for amplification included 35 cycles of denaturation at 94°C for 45 s, annealing at 55°C for 45 s and elongation at 72°C for 60 s with heat starting at 95°C for 15 min and final elongation at 72°C for 10 min. The PCR products were electrophoresed on 2% agarose gel at 100 V for 30 min and visualized with ethidium bromide.

Densitometric values of the PCR products were determined using the software package Scion Image (Scion Corporation, Frederick, MD, USA), and relative mRNA levels (GAPDH-normalized mRNA levels) were obtained by dividing the densitometric values of the PCR products by those of GAPDH.

Statistical analysis

The statistical significance of differences in the percentages of cases with different immunohistochemical reactivity levels and in mean relative mRNA levels was analyzed by means of the Mann-Whitney U test for differences between two groups or the Kruskal-Wallis test for differences among three or more groups. *P* values of less than 0.05 were considered to indicate statistical significance.

Results

Immunohistochemical reactivity for survivin and XIAP

Immunohistochemical reactivity for survivin and XIAP was detected in the cytoplasm of normal and neoplastic odontogenic epithelial cells (Fig. 1, Fig. 2, Table 1). In tooth germs, expression of survivin was more evident in inner enamel epithelium than in outer enamel epithelium and dental lamina (Fig. 1A). Ameloblastomas showed

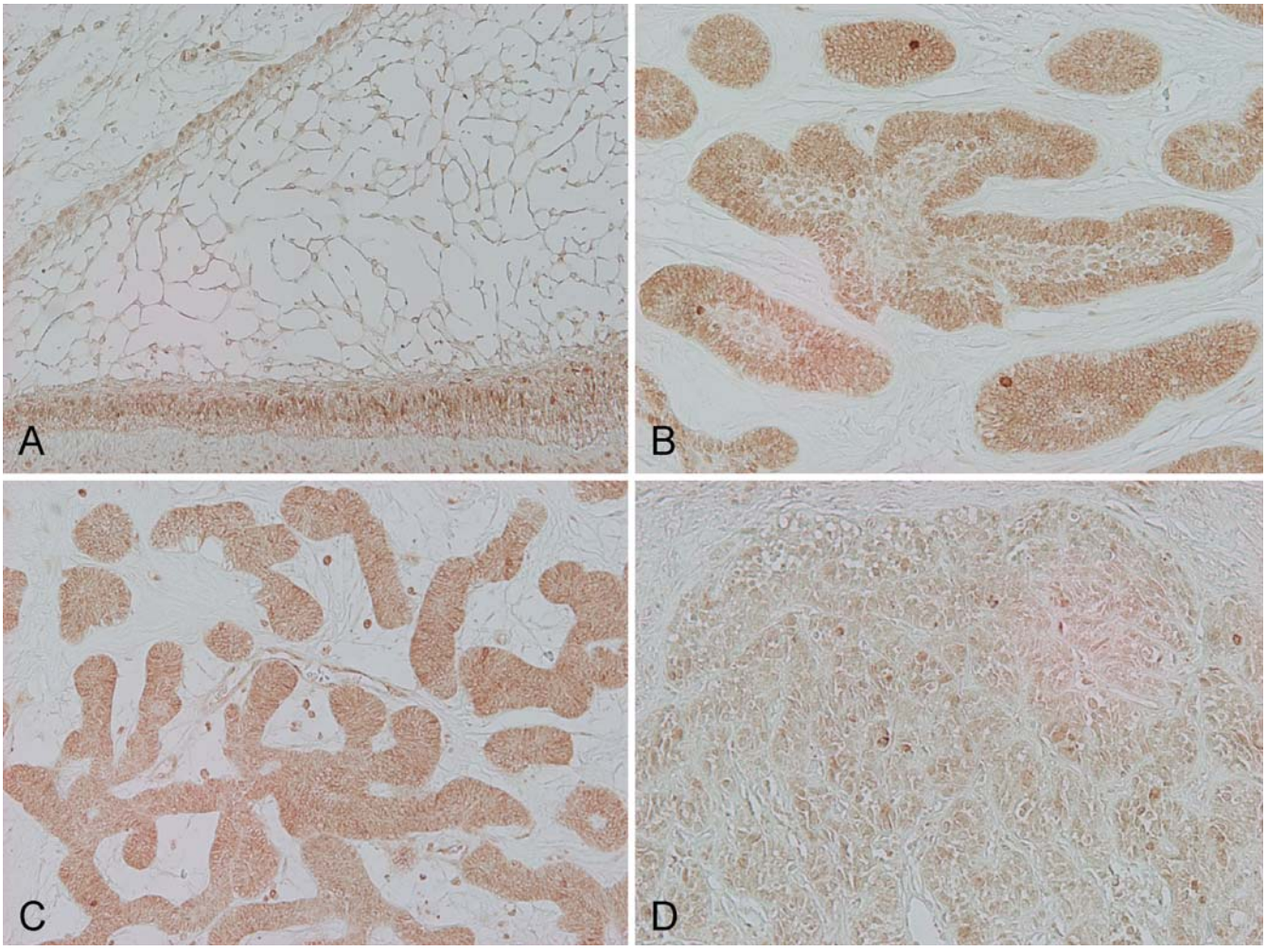

Fig. 1 Immunohistochemical reactivity for survivin. **A** Tooth germ showing strong reactivity in inner enamel epithelium and weak reactivity in outer enamel epithelium ×125. **B** Follicular ameloblastoma showing reactivity in many peripheral columnar cells and some central polyhedral cells ×115. **C** Basal cell ameloblastoma showing strong reactivity in most neoplastic cells ×100. **D** Ameloblastic carcinoma showing reactivity in most neoplastic cells ×125

survivin reactivity in many peripheral columnar or cuboidal cells and some central polyhedral cells (Fig. 1B). Keratinizing cells and granular cells showed no reactivity for survivin in acanthomatous and granular cell ameloblastomas. Basal cell ameloblastomas and desmoplastic ameloblastomas showed survivin reactivity in most neoplastic cells (Fig. 1C). Metastasizing ameloblastomas showed a survivin expression pattern similar to that of the benign ameloblastomas, while ameloblastic carcinomas demonstrated weak to moderate survivin reactivity in most neoplastic cells (Fig. 1D).

Expression of XIAP was detected in most epithelial cells in tooth germs, and some samples showed slightly stronger reactivity in inner enamel epithelium than that in other epithelial components (Fig. 2A). Benign and malignant ameloblastomas showed XIAP reactivity in most neoplastic cells (Fig. 2B, D). In some benign ameloblastomas, peripheral columnar or cuboidal cells exhibited slightly stronger reactivity for XIAP than central polyhedral cells. Keratinizing cells and granular cells in acanthomatous and granular cell ameloblastomas demonstrated markedly decreased reactivity for XIAP (Fig. 2C). Differences in the immunohistochemical detection of survivin and XIAP did not reach statistical significance.

Semi-quantitative RT-PCR profiles of survivin and XIAP mRNA expression

RT-PCR analysis identified expression of mRNA transcripts for survivin and XIAP in all 32 ameloblastomas and the 1 malignant ameloblastoma as well as in the 8 tooth germ tissues, and the PCR products of survivin and XIAP were 363 bp and 389 bp, respectively (Fig. 3). Relative (GAPDH-normalized) mRNA levels of survivin and XIAP expression were quantified as the survivin/GAPDH and XIAP/GAPDH ratios (Table 1). Some ameloblastomas showed higher survivin expression than tooth germ samples, and the mean level of survivin

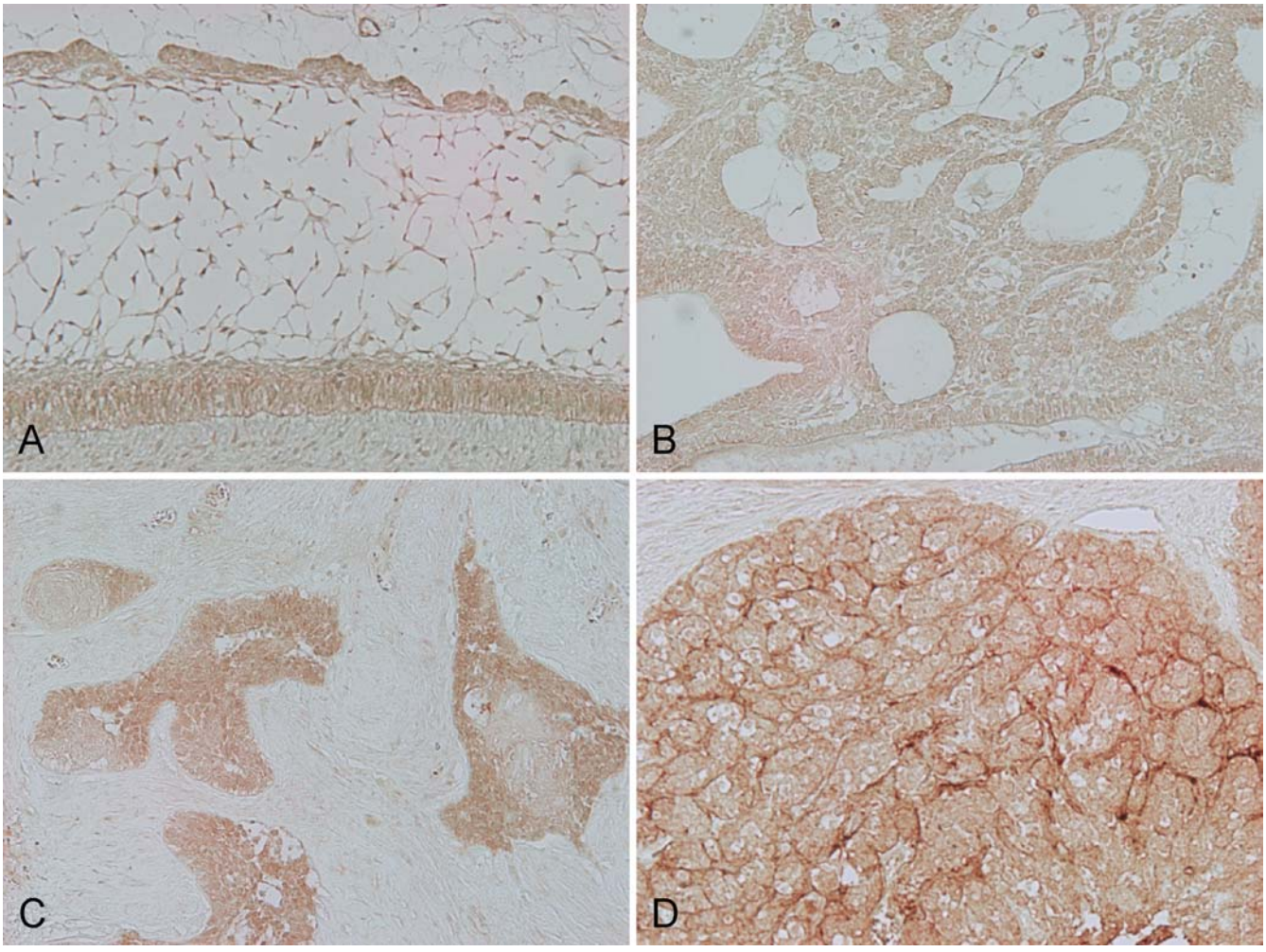

Fig. 2 Immunohistochemical reactivity for X chromosome-linked inhibitor of apoptosis protein. **A** Tooth germ showing reactivity in epithelial components ×120. **B** Plexiform ameloblastoma showing reactivity in most neoplastic cells ×125. **C** Acanthomatous ameloblastoma showing decreased reactivity in keratinizing cells ×95. **D** Ameloblastic carcinoma showing reactivity in most neoplastic cells ×105

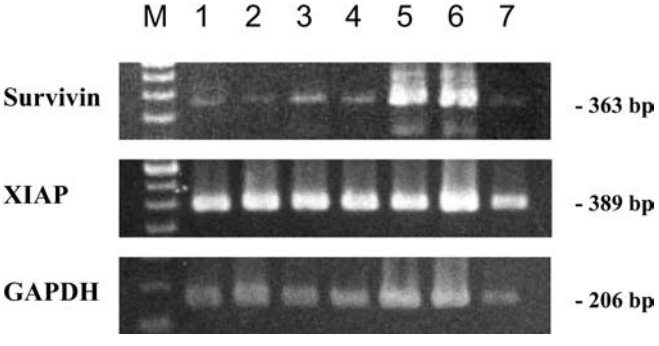

Fig. 3 Reverse-transcription polymerase chain reaction (RT-PCR) analysis of survivin and X chromosome-linked inhibitor of apoptosis protein (XIAP) mRNA expression in tooth germs and ameloblastomas (*M* molecular-weight standard, *1, 2* tooth germs, *3–6* ameloblastomas, *7* malignant ameloblastoma). Survivin and XIAP mRNA expression was seen in all samples. Glyceraldehyde-3-phosphate dehydrogenase (GAPDH) was run as a control to ascertain the integrity of mRNA/cDNA. The sizes of survivin, XIAP and GAPDH PCR products were 363, 389 and 206 bp, respectively

expression in ameloblastomas tended to be higher than that in tooth germs (P=0.0502). Follicular ameloblastomas showed significantly higher levels of XIAP expression than did plexiform ameloblastomas (P<0.05).

Discussion

The IAP family consists of evolutionarily conserved proteins that function to regulate apoptotic cell death [3]. Survivin is highly expressed during embryonic and fetal development, but is not detected in terminally differentiated adult tissues, except for placenta and thymus [1]. Homozygous survivin mutant mice have failed to survive beyond 4.5 days post-coitum [36]. XIAP mRNA is detected in all fetal and adult tissues except for peripheral blood lymphocytes [24]. Mice deficient in XIAP have shown upregulation of other IAP members [8]. These features suggest that expression of survivin and XIAP during embryonic and fetal development may contribute

Table 1 Expression of survivin and XIAP in tooth germs and ameloblastomas. Immunohistochemical reactivity: (+) weak, (++) moderate and (+++) strong. *RT-PCR* reverse-transcription polymerase chain reaction, *GAPDH* glyceraldehyde-3-phosphate dehydrogenase, *XIAP* X chromosome-linked inhibitor of apoptosis protein

	Immunohistochemical reactivity							RT-PCR profile (relative (GAPDH-normalized) mRNA level)		
	n	Survivin			XIAP			*n*	Survivin	XIAP
		(+)	(++)	(+++)	(+)	(++)	(+++)			
Tooth germ	11							8	0.21±0.10	0.97±0.17
Enamel organ	6	4 (36%)	4 (36%)	3 (27%)	1 (9%)	7 (64%)	3 (27%)			
Dental lamina	6	2 (33%)	2 (33%)	2 (33%)	1 (17%)	3 (50%)	2 (33%)			
Ameloblastoma	46	14 (30%)	17 (37%)	15 (33%)	8 (17%)	21 (46%)	17 (37%)	32	0.39±0.22	1.08±0.27
Follocular type	30	10 (33%)	8 (27%)	12 (40%)	6 (20%)	13 (43%)	11 (37%)	20	0.40±0.22	1.17±0.22*
Plexiform type	16	4 (25%)	9 (56%)	3 (19%)	2 (13)	8 (50%)	6 (37%)	12	0.38±0.23	0.93±0.30*
Acanthomatous subtype	15	7 (47%)	4 (27%)	4 (27%)	4 (27%)	7 (47%)	4 (27%)	12	0.43±0.24	1.05±0.27
Granular subtype	5	1 (20%)	2 (40%)	2 (40%)	1 (20%)	2 (40%)	2 (40%)	3	0.25±0.16	1.29±0.19
Basal cell subtype	3	0 (0%)	1 (33%)	2 (67%)	0 (0%)	2 (67%)	1 (33%)	1	0.33	0.81
Desmoplastic subtype	4	1 (25%)	1 (25%)	2 (50%)	0 (0%)	2 (50%)	2 (50%)	1	0.46	1.21
Malignant ameloblastoma	6	3 (50%)	3 (50%)	0 (0%)	2 (33%)	3 (50%)	1 (17%)	1	0.20	0.97
Metastasizing ameloblastoma	2	1 (50%)	1 (50%)	0 (0%)	1 (50%)	1 (50%)	0 (0%)	1	0.20	0.97
Ameloblastic carcinoma	4	2 (50%)	2 (50%)	0 (0%)	1 (25%)	2 (50%)	1 (25%)	0	–	–

*$P<0.05$

to tissue homeostasis and differentiation. Apoptotic cell death is known to play an important role in tooth development [15, 37], and some apoptosis-related factors, such as bcl-2 family proteins and Fas/Fas ligand system, have been identified in tooth germ tissues [18, 21, 31]. In the present study, expression of survivin and XIAP was detected at both protein and mRNA levels in tooth germs at the initial stage of crown mineralization, suggesting that these IAP family proteins play a role in cell survival and differentiation during tooth development.

Survivin functions as a suppressor of apoptotic cell death and is also involved in regulation of cell division [38]. Although expression of survivin is very restricted in normal adult tissues, high expression of survivin is found in many common human malignancies, including pulmonary, colorectal, prostate and breast carcinomas, malignant lymphoma, neuroblastoma and glioblastoma [1, 11, 13]. Increased survivin expression is considered an important indicator of a poor prognosis in some malignancies, such as neuroblastoma and glioblastoma [11, 13]. In the present study, ameloblastomas expressed survivin protein chiefly in neoplastic cells neighboring the basement membrane, and most neoplastic cells in basal cell and desmoplastic ameloblastomas reacted with anti-survivin antibody. Our previous studies detected proliferating cells neighboring the basement membrane and apoptotic cells detached from the basement membrane in ameloblastomas [17, 21]. These features suggest that survivin expression is associated with cell proliferation and differentiation of ameloblastoma cells. Basal cell and desmoplastic ameloblastomas are considered to possess a high potential for cell survival. The expression pattern of survivin was similar to those of the apoptosis inhibitory proteins bcl-2 and bcl-x in ameloblastomas [18, 28], and these apoptosis suppressor proteins of the bcl-2 and IAP families are considered to affect the biological profiles of ameloblastomas. Expression levels of survivin mRNA were slightly higher in ameloblastomas than in tooth germs, suggesting that elevated survivin expression might be involved in oncogenesis of odontogenic epithelium. Survivin expression in malignant ameloblastomas did not distinctively differ from that in tooth germs or benign ameloblastomas.

XIAP binds to and inhibits caspases-3, -7 and -9 but not caspases-1, -6, -8 and -10, and the specificity of caspase inhibition may have therapeutic potential [4, 5]. Expression of XIAP has been observed in human neoplasms, including acute myelogenous leukemia and pulmonary, oral and ovarian carcinomas, as well as in fetal developing and normal adult tissues, and the direct role of XIAP in the resistance of cancer cells to radiation and chemotherapeutic intervention has been demonstrated in these tumors [10, 25, 29, 34]. In the present study, expression of XIAP protein was detected in most neoplastic cells of benign and malignant ameloblastomas, as well as in epithelial cells of tooth germs. Our previous study confirmed caspase-3 expression in tooth germs and ameloblastomas [21]. Based on these features, XIAP was considered to specifically and strongly block caspase-3 activity, thereby allowing normal developing and neoplastic odontogenic epithelial cells to avoid apoptotic cell death. Expression levels of XIAP mRNA did not differ distinctively between normal and neoplastic odontogenic tissues. This finding did not clearly support a specific role of XIAP in oncogenesis of odontogenic epithelium. In our previous studies, increased apoptotic cell death was found

in keratinizing cells and granular cells in acanthomatous and granular cell ameloblastomas [17, 19, 21]. The present study showed markedly decreased expression of XIAP and survivin in keratinizing cells and granular cells in the ameloblastoma subtypes. These features suggest that these IAP family proteins might have a role in terminal differentiation of these neoplastic cells in ameloblastoma variants. We reported that some osteolytic cytokines and stromal microvessel densities clearly differed between follicular and plexiform patterns of ameloblastomas [20, 22]. In the present study, XIAP mRNA levels were significantly greater in follicular ameloblastomas than in plexiform ameloblastomas, and expression of survivin protein tended to be higher in follicular ameloblastomas than in plexiform ameloblastomas. These results suggest that these IAP members may be involved in tissue structuring of ameloblastomas.

In conclusion, expression of survivin and XIAP in tooth germ and benign and malignant ameloblastomas suggests that these IAP family proteins contribute to biological properties of epithelial odontogenic tumors as well as to cellular regulation during tooth development. In addition, the specific expression of survivin suggests that this protein is a potential therapeutic target for epithelial odontogenic tumors.

References

1. Ambrosini G, Adida C, Altieri DC (1997) A novel anti-apoptosis gene, survivin, expressed in cancer and lymphoma. Nat Med 3:917–921
2. Clem RJ, Fechheimer M, Miller LK (1991) Prevention of apoptosis vy a baculovirus gene during infection of insect cells. Science 254:1388–1390
3. Deveraux QL, Reed JC (1999) IAP family proteins: suppressors of apoptosis. Genes Dev 13:239–252
4. Deveraux QL, Takahashi R, Salvesen GS, Reed JC (1997) X-linked IAP is a direct inhibitor of cell-death proteases. Nature 388:300–304
5. Deveraux QL, Roy N, Stennicke HR, Van Arsdale T, Zhou Q, Srinivasula SM, Alnemri ES, Salvesen GS, Reed JC (1998) IAPs block apoptotic events induced by caspase-8 and cytochrome c by direct inhibition of distinct caspases. EMBO J 17:2215–2223
6. Eversole LR (1999) Malignant epithelial odontogenic tumors. Semin Diagn Pathol 16:317–324
7. Ferreira CG, van der Valk P, Span SW, Ludwig I, Smit EF, Kruyt FA, Pinedo HM, van Tinteren H, Giaccone G (2001) Expression of X-linked inhibitor of apoptosis as a novel prognostic marker in radically resected non-small cell lung cancer patients. Clin Cancer Res 7:2468–2474
8. Harlin H, Reffey SB, Duckett CS, Lindsten T, Thompson CB (2001) Characterization of XIAP-deficient mice. Mol Cell Biol 21:3604–3608
9. Heikinheimo K, Jee KJ, Niini T, Aalto Y, Happonen RP, Leico I, Knuutila S (2002) Gene expression profiling of ameloblastoma and human tooth germ by means of a cDNA microarray. J Dent Res 81:525–530
10. Holcik M, Yeh C, Korneluk RG, Chow T (2000) Translational upregulation of X-linked inhibitor of apoptosis (XIAP) increases resistance to radiation induced cell death. Oncogene 19:4174–4177
11. Islam A, Kageyama H, Takada N, Kawamoto T, Takayasu H, Isogai E, Ohira M, Hashizume K, Kobayashi H, Kaneko Y, Nakagawara A (2000) High expression of survivin, mapped to 17q25, is significantly associated with poor prognostic factors and promotes cell survival in human neuroblastoma. Oncogene 19:617–623
12. Jaakelainen K, Jee KJ, Leivo I, Saloniemi I, Knuutila S, Heikinheimo K (2002) Cell proliferation and chromosomal changes in human ameloblastoma. Cancer Genet Cytogenet 136:31–37
13. Kajiwara Y, Yamasaki F, Hama S, Yahara K, Yoshioka H, Sugiyama K, Arita K, Kurisu K (2003) Expression of survivin in astrocytic tumors: correlation with malignant grade and prognosis. Cancer 97:1077–1083
14. Kerr JF, Wyllie AH, Currie AR (1972) Apoptosis: a basic biological phenomenon with wide-ranging implications in tissue kinetics. Br J Cancer 26:239–257
15. Kindaichi K (1980) An electron microscopic study of cell death in molar tooth germ epithelia of mouse embryos. Arch Histol Jpn 43:289–304
16. Kramer IRH, Pindborg JJ, Shear M (1992) WHO histological typing of odontogenic tumours, 2nd edn. Springer, Berlin Heidelberg New York, pp 11–27
17. Kumamoto H (1997) Detection of apoptosis-related factors and apoptotic cells in ameloblastomas: analysis by immunohistochemistry and an in situ DNA nick end-labelling method. J Oral Pathol Med 26:419–425
18. Kumamoto H, Ooya K (1999) Immunohistochemical analysis of bcl-2 family proteins in benign and malignant ameloblastomas. J Oral Pathol Med 28:343–349
19. Kumamoto H, Ooya K (2001) Immunohistochemical and ultrastructural investigation of apoptotic cell death in granular cell ameloblastoma. J Oral Pathol Med 30:245–250
20. Kumamoto H, Ooya K (2004) Expression of parathyroid hormone-related protein (PTHrP), osteoclast differentiation factor (ODF)/receptor activator of nuclear factor-κB ligand (RANKL) and osteoclastogenesis inhibitory factor (OCIF)/osteoprotegerin (OPG) in ameloblastomas. J Oral Pathol Med 33:46–52
21. Kumamoto H, Kimi K, Ooya K (2001) Immunohistochemical analysis of apoptosis-related factors (Fas, Fas ligand, caspase-3 and single-stranded DNA) in ameloblastomas. J Oral Pathol Med 30:596–602
22. Kumamoto H, Ohki K, Ooya K (2002) Association between vascular endothelial growth factor (VEGF) expression and tumor angiogenesis in ameloblastomas. J Oral Pathol Med 31:28–34
23. Kumamoto H, Suzuki T, Ooya K (2002) Immunohistochemical analysis of inducible nitric oxide synthase (iNOS) and heat shock proteins (HSPs) in ameloblastomas. J Oral Pathol Med 31:605–611
24. Liston P, Roy N, Tamai K, Lefebvre C, Baird S, Cherton-Horvat G, Farahani R, McLean M, Ikeda JE, MacKenzie A, Korneluk RG (1996) Suppression of apoptosis in mammalian cells by NAIP and a related family of IAP genes. Nature 379:349–353
25. Matsumiya T, Imaizumi T, Yoshida H, Kimura H, Satoh K (2001) Cisplatin inhibits the expression of X-chromosome-linked inhibitor of apoptosis protein in an oral carcinoma cell line. Oral Oncol 37:296–300
26. Melrose RJ (1999) Benign epithelial odontogenic tumors. Semin Diagn Pathol 16:271–287
27. Reed JC (2000) Mechanisms of apoptosis. Am J Pathol 157:1415–1430
28. Sandra F, Nakamura N, Mitsuyasu T, Shiratsuchi Y, Ohishi M (2001) Two relatively distinct patterns of ameloblastoma: an anti-apoptotic proliferating site in the outer layer (periphery) and a pro-apoptotic differentiating site in the inner layer (centre). Histopathology 39:93–98
29. Sasaki H, Sheng Y, Kotsuji F, Tsang BK (2000) Down-regulation of X-linked inhibitor of apoptosis protein induces apoptosis in chemoresistant human ovarian cancer cells. Cancer Res 60:5659–5666

30. Sciubba JJ, Fantasia JE, Kahn LB (2001) Tumors and cysts of the jaw. Atlas of tumor pathology, 3rd series, Fascicle 29. Armed Forces Institute of Pathology, Washington, DC, pp 71–99
31. Slootweg PJ, de Weger RA (1991) Immunohistochemical demonstration of bcl-2 protein in human tooth germs. Arch Oral Biol 39:545–550
32. Soini Y, Paakko P, Lehto V-P (1998) Histopathological evaluation of apoptosis in cancer. Am J Pathol 153:1041–1053
33. Takahashi R, Deveraux Q, Tamm I, Welsh K, Assa-Munt N, Salvesen GS, Reed JC (1998) A single BIR domain of XIAP sufficient for inhibiting caspases. J Biol Chem 273:7787–7790
34. Tamm I, Kornblau SM, Segall H, Krajewski S, Welsh K, Kitada S, Scudiero DA, Tudor G, Qui YH, Monks A, Andreeff M, Reed JC (2000) Expression and prognostic significance of IAP-family genes in human cancers and myeloid leukemias. Clin Cancer Res 6:1796–1803
35. Thompson CB (1995) Apoptosis in the pathogenesis and treatment of disease. Science 267:1456–1462
36. Uren AG, Wong L, Pakusch M, Fowler KJ, Burrows FJ, Vaux DL, Choo KH (2000) Survivin and the inner centromere protein INCENP show similar cell-cycle localization and gene knock-out phenotype. Curr Biol 10:1319–1328
37. Vaahtokari A, Aberg T, Thesleff I (1996) Apoptosis in the developing tooth: association with an embryonic signaling center and suppression by EGF and FGF-4. Development 122:121–129
38. Yamamoto T, Tanigawa N (2001) The role of survivin as a new target of diagnosis and treatment in human cancer. Med Electron Microsc 34:207–212

Virchows Arch (2004) 444:171–174
DOI 10.1007/s00428-003-0952-6

ORIGINAL ARTICLE

Karel Smetana · Otakar Měřička · Sem Saeland · Jiří Homolka · Jiří Brabec · Hans-Joachim Gabius

Diagnostic relevance of Langerin detection in cells from bronchoalveolar lavage of patients with pulmonary Langerhans cell histiocytosis, sarcoidosis and idiopathic pulmonary fibrosis

Received: 3 June 2003 / Accepted: 26 November 2003 / Published online: 13 January 2004

Abstract The diagnosis of pulmonary Langerhans cell histiocytosis might be refined by demonstrating reliability of a new cell marker, i.e., Langerin (CD207), used on bronchoalveolar lavage fluid. For this purpose, we collected material from patients with this disease and also with sarcoidosis and idiopathic pulmonary fibrosis as controls. In addition to the immunocytochemical detection of Langerin, we examined the expression profiles of CD1a and the macrophage tandem-repeat mannose receptor (CD206). To test accessibility of Langerin, a C-type lectin, for mannosides, we employed reverse lectin histochemistry using mannose-containing neoglycoproteins. The analysis revealed a significantly increased percentage of CD1a- and Langerin-positive cells in pulmonary Langerhans cell histiocytosis in comparison with both other studied diseases. No expression of the 175-kDa mannose-binding lectin (CD206) in Langerhans cells was observed. Evidently, binding sites on the cells were not accessible for the mannose-containing neoglycoligand. These results provide evidence for the usefulness of Langerin-directed immuno- and glycohistochemical monitoring of bronchoalveolar lavage fluid in the diagnosis of pulmonary Langerhans cell histiocytosis.

Keywords Fibrosis · Histiocytosis · Immunohistochemistry · Langerin (CD207) · Lectin · Neoglycoprotein · Sarcoidosis

K. Smetana Jr (✉) · J. Brabec
Institute of Anatomy,
Charles University, 1st Faculty of Medicine,
Unemocnice 3, 128 00 Prague 2, Czech Republic
e-mail: ksmet@lf1.cuni.cz
Tel.: +42-02-24965756
Fax: +42-02-24965770

K. Smetana Jr
Center of Cell Therapy and Tissue Repair,
Charles University, 2nd Faculty of Medicine,
Prague, Czech Republic

O. Měřička · J. Homolka
1st Department of Tuberculosis and Respiratory Diseases,
Charles University, 1st Faculty of Medicine,
Prague, Czech Republic

S. Saeland
Schering-Plough Laboratory for Immunological Research,
Dardilly, France

H.-J. Gabius
Faculty of Veterinary Medicine, Ludwig-Maximilians-University,
Institute of Physiological Chemistry, Munich, Germany

Introduction

The definition of new cell markers by the development of monoclonal antibodies provides a means to refine current diagnostic procedures. Following this first step on the way to proving diagnostic usefulness, the tool under study should next be tested with clinical material. In this study, we have focused on pulmonary Langerhans cell histiocytosis (PLCH). This disease belongs to the Langerhans cell histiocytosis family. The patient ratio between males and females is approximately equal [8, 18]. The etiology of the disease is not fully known, but it is notable that the majority of patients have a tobacco smoking history [2, 3, 12]. The clonal character of Langerhans cells (LC) in PLCH suggests a manifestation of the disease with tumorous character [8]. However, a reactive nature of PLCH is also documented [8, 18]. No characteristic clinical symptoms are attributed to the disease, and its diagnosis is, thus, based on the combination of clinical, radiological and laboratory investigations [18]. Among them, the cytological analysis of bronchoalveolar lavage (BAL) is recommended, with the percentage of Langerhans cells higher than 5% being an important factor for PLCH detection [1, 13]. At present, the apparent quantity of reports employing immunocytochemical monitoring of cells in BAL underscores that it is warranted to develop a reliable screening for this purpose. In this study, we introduce a recently described cell marker for this purpose and validate the application of the procedure by demonstrating marked differences in LC presence in PLCH,

sarcoidosis and idiopathic pulmonary fibrosis (IPF). In addition to monitoring CD1a detection, an antibody against Langerin (CD207), a protein specific for LC in skin and in epithelia, such as lung bronchiolae, with properties of a mannose-reactive C-type lectin, was tested in this study [16, 17]. To address the further question whether the carbohydrate recognition domain of Langerin is accessible for ligand, we selected an α-mannoside-presenting neoglycoprotein as a probe. By concomitantly monitoring the presence of the 175-kDa macrophage mannose receptor (MR; CD206), an internal quality control of cell-type specificity was established.

Materials and methods

Three groups of patients with PLCH (three females, five males, mean age 36±17 years), sarcoidosis (five females, three males, mean age 42±10 years) and IPF (four females, six males, mean age 49±17 years) were included in this study. All patients with PLCH were characterized with tobacco smoking history. The percentage of cell types in BAL fluid collected from patients was evaluated after conventional cytological staining [mean±SD (%), macrophages: 71±10, neutrophils: 4±3, eosinophils: 2±2, lymphocytes: 24±12] to prove usual interstitial pneumonia pattern in combination with clinical criteria of the American Thoracic and European Respiration Societies (2000). The diagnosis was verified histopathologically from biopsy in all cases. BAL was performed according to a standard procedure. Cytospin specimens were prepared, and the cells were fixed with paraformaldehyde. Any antigen-independent binding of antibody, for example, via Fc fragments, was blocked using non-immune swine serum (Dako, Brno, Czech Republic). CD1a was detected using the monoclonal antibody obtained from Immunotech (Prague, Czech Republic) and Langerin using the DCGM4 monoclonal antibody [16]. MR was detected using a goat polyclonal antibody (TNO-PG, Leiden, The Netherlands). Swine anti-mouse antiserum labeled with fluorescein isothiocyanate (ALSEVA, Prague, Czech Republic) and tetramethylrhodamine isothiocyanate (TRITC)-labeled donkey anti-goat antiserum (Santa Cruz, Santa Cruz, CA, USA) were used as second-step antibodies. Accessibility of the carbohydrate-binding site for exogenous ligands was probed using biotinylated neoglycoprotein with covalently attached α-D-mannopyranoside derivatives [5, 6]. TRITC-labeled ExtrAvidin (Sigma-Aldrich, Prague, Czech Republic) was used as the second-step reagent. Non-immune goat serum and mice monoclonal antibodies of the same isotype without reactivity for LC were used as controls of the specificity of the immunohistochemical reaction. Competitive inhibition of neoglycoprotein binding by D-mannose (Sigma-Aldrich, Prague, Czech Republic) was used to ascertain the specificity of the reverse lectin histochemical reaction. The double-labeling reaction at the single-cell level was performed in several specimens according to an optimized protocol [4]. Several specimens were also subject to counterstaining with 4′-6′-diamidino-2-phenylindole (DAPI) (Sigma-Aldrich, Prague, Czech Republic).

A fluorescence microscope Optiphot-2 (Nikon, Prague, Czech Republic) equipped with suitable filterblocks, CCD camera and computer-assisted image analysis system (LUCIA, Laboratory Imaging, Prague, Czech Republic) were used for data collection, storage and analysis. The individual data sets (minimally 500 cells/patient) were statistically analyzed. In detail, with respect to the number of cases, the Shapiro-Wilk's test was used for testing of distribution. Where a derivation from a monitored distribution was detected, the Mann-Whitney test was used for comparison. For calculating of the correlation between two variables, the Spearman correlation coefficient (r), which determines the extent to which values of two variables are "proportional" to each other, was instrumental.

Results and discussion

When performing the immunocytochemical protocol, any antigen-independent staining reaction, for example, using kit reagents, was first excluded. Under these conditions, Langerin (CD207) detection was consistent, reliable and reproducible (Fig. 1). Likewise, CD1a expression was visible. To address the question on the diagnostic value of this procedure, we monitored cell populations originating from patients with PLCH, sarcoidosis and IPF. BAL of patients suffering with PLCH contained a significantly higher number of CD1a- and Langerin-positive cells than BAL of patients with sarcoidosis and IPF (Fig. 2). No apparent differences between the number of CD1a- and Langerin-positive cells in patients with sarcoidosis or IPF were observed. As shown in detail in Fig. 2, Langerin detection improved the P value to 0.000533 for distinguishing between PLCH and sarcoidosis. Interestingly, the numbers of CD1a- and Langerin-positive cells in all tested cases were almost identical ($P<0.0001$, r=0.976), as shown in Fig. 3. This result indicates the high specificity of Langerin detection. Regarding diagnostic assessment, literature data defined a level of more than 5% of LC in BAL as borderline for the diagnosis of PLCH [1, 13]. Two PLCH patients of our group had a percentage of LC of 4%. The clearly increased LC level warrants extending

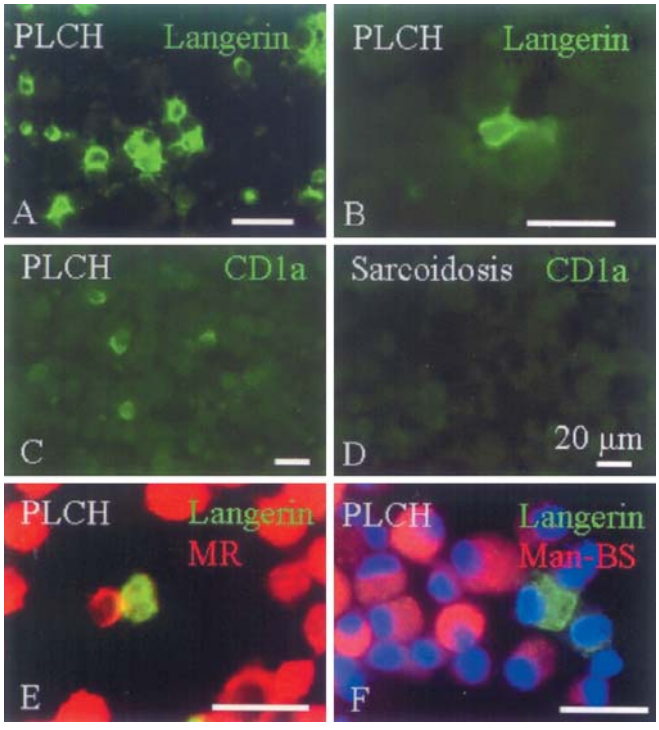

Fig. 1 Representative figures illustrating detection of Langerin (CD207) (*green*, **A**, **B**, **E**, **F**), CD1a (*green*, **C**, **D**), the 175-kDa tandem-repeat C-type mannose receptor (CD206) (*red*, MR, **E**) and mannose-binding sites (*red*, Man-BS, **F**) in cells of bronchoalveolar lavage (BAL) obtained from patients with pulmonary Langerhans cell histiocytosis (PLCH) (**A**, **B**, **E**, **F**) and sarcoidosis (**C**, **D**). Nuclei in **F** are counterstained with 4′-6′-diamidino-2-phenylindole; *bar* is 20 μm

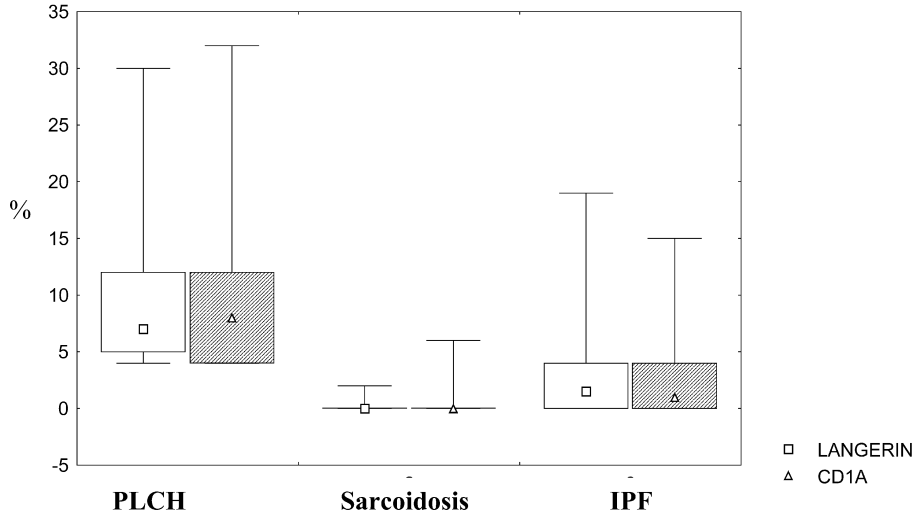

Fig. 2 Difference of the percentage of the number of Langerin- or CD1a-positive Langerhans cells in patients suffering from pulmonary Langerhans cell histiocytosis (PLCH), sarcoidosis and idiopathic pulmonary fibrosis (IPF). The data are statistically evaluated using the Mann-Whitney test. Each value gives the median. Minimal and maximal values are shown by *bars* and 75% of the data lie within the boundaries of the box. In the case of Langerin expression, the difference between pulmonary Langerhans cell histiocytosis and sarcoidosis is significant at the level of P=0.000533 and between pulmonary Langerhans cell histiocytosis and idiopathic pulmonary fibrosis at the level of P=0.016. In the case of CD1a expression, the difference between pulmonary Langerhans cell histiocytosis and sarcoidosis is significant at the level of P=0.002145 and between pulmonary Langerhans cell histiocytosis and idiopathic pulmonary fibrosis at the level of P=0.0147. No significant differences between sarcoidosis and idiopathic pulmonary fibrosis were detected

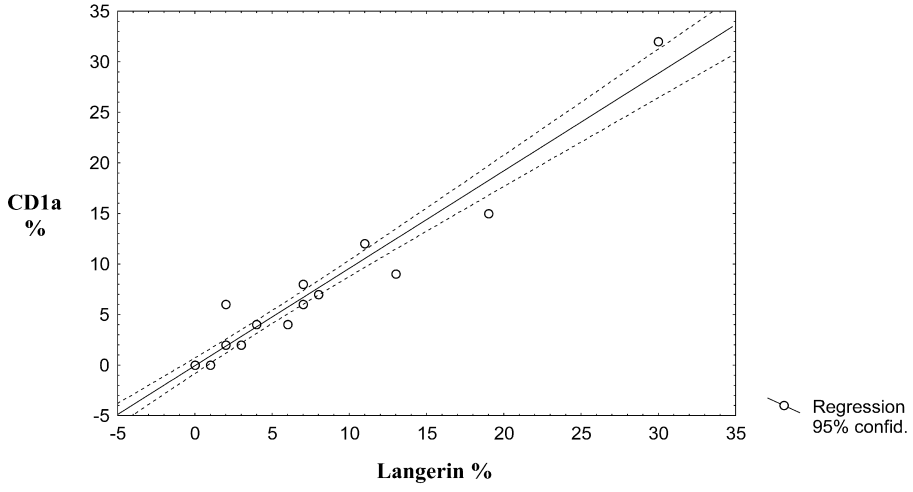

Fig. 3 The percentage of CD1a- and Langerin-positive cells in pulmonary Langerhans cell histiocytosis were almost identical, as was shown by regression analysis using the two data sets yielding a linear relationship at P=0.0001. Since values obtained from two patients were the same, the number of individual observations shown here is 14

diagnostic procedures to clarify clinical manifestations. As required for a valid control, no cells expressing CD1a and Langerin were positive for the presence of the MR. This observation is in complete accord with the fact that, in contrast to macrophages and dendritic cells of the non-Langerhans type, Langerhans cells do not express this lectin [10, 14]. Similar to Langerin, a protein that controls formation of Birbeck granules and is assumed to be important for antigen uptake and presentation, this molecule has lectin properties for mannosides [11, 16, 17]. Using a synthetic class of probe (neoglycoprotein), we, thus, examined whether the CD207-positive cells harbored accessible receptor sites (that is, sites not blocked by endogenous ligands). As a positive control, Langerin- and CD1a-negative cells (predominantly macrophages) specifically bond this glycohistochemical marker, whereas no reactivity was observed for the Langerin- and CD1a-positive cell population (Fig. 1). In this context, it is interesting to refer to previous data that LC infiltrating malignant tumors also expressed Langerin and did not bind the mannose-containing neoglycoprotein in contrast to LC present in normal epithelia, which were reactive with the marker [11]. LC expressing Langerin in Langerhans cell histiocytosis lesions from sites other than the lung are described as having properties of immature LC [7], being able to recognize antigen in contrast to the

PLCH LC that were characterized as mature [15], and, therefore, the uptake of antigen by these cells could be limited. Changes related to the maturation of LC [9], thus, can be relevant for explaining this difference in binding-site accessibility. In conclusion, the immunocytochemical monitoring of BAL focusing on Langerin as new LC marker has proven its usefulness for the diagnosis of patients suffering from PLCH.

Acknowledgements This study was supported by the Ministry of Education, Youth and Sport of the Czech Republic, project no. MSM111100005. The authors are grateful to Mrs. Eva Vancová for excellent technical assistance.

References

1. Auerswald U, Barth J, Magnussen H (1991) Value of CD1-positive cells in bronchoalveolar lavage fluid for the diagnosis of pulmonary histiocytosis X. Lung 169:305–309
2. Colby TV, Lombard C (1993) Histiocytosis X in the lung. Hum Pathol 14:847–856
3. Friedman PJ, Liebow AA, Sokoloff J (1981) Eosinophilic granuloma of lung: clinical aspects of primary histiocytosis in the adult. Medicine (Baltimore) 60:385–396
4. Froňková V, Holíková Z, Liu F-T, Homolka J, Rijken DC, André S, Bovin NV, Smetana K Jr, Gabius H-J (1999) Simultaneous detection of endogenous lectins and their binding capacity at the single cell level—a technical note. Folia Biol (Praha) 45:157–162
5. Gabius H-J (2001) Glycohistochemistry: the why and how of detection and localization of endogenous lectins. Anat Histol Embryol 30:3–31
6. Gabius H-J, Bodanowitz S, Schauer A (1988) Endogenous sugar-binding proteins in human breast tissue and benign and malignant breast lesions. Cancer 61:1125–1131
7. Geissmann F, Lepelletier Y, Fraitag S, Valladeau J, Bodemer C, Debré M, Leborgne M, Saeland S, Brousse N (2001) Differentiation of Langerhans cells in Langerhans cell histiocytosis. Blood 97:1241–1248
8. Harari S, Comel A (2001) Pulmonary Langerhans cell histiocytosis. Sarcoidosis Vasc Diff 18:253–262
9. McDermott R, Ziylan U, Spehner D, Bausinger H, Lipsker D, Mommaas M, Cazenave J-P, Raposo G, Goud B, de la Salle H, Salamero J, Hanau D (2002) Birbeck granules are subdomains of endosomal recycling compartment in human epidermal Langerhans cells, which form where Langerin accumulates. Mol Biol Cell 13:317–335
10. Noorman F, Braat EAM, Barrett-Bergshoeff M, Barbé E, van Leeuwen A, Lindeman J, Rijken DG (1997) Monoclonal antibodies against human mannose receptor as a specific marker in flow cytometry and immunohistochemistry for macrophages. J Leukocyte Biol 61:63–72
11. Plzák J, Holíková Z, Smetana K Jr, Betka J, Hercogová J, Saeland S, Bovin NV, Gabius H-J (2002) Analysis of binding of mannosides in relation to Langerin (CD207) in Langerhans cells of normal and transformed epithelia. Histochem J 34:247–253
12. Schonfeld N, Frank W, Wenig S, Uhrmeister P, Allica F, Preussler H, Grassot A, Loddenkerper R (1993) Clinical and radiologic features, lung function and therapeutic results in pulmonary histiocytosis X. Respiration 60:38–44
13. Sledziewska J, Roginska E, Oblakowski P, Slodowska J, Hawrylkiewicz I, Kus J, Pawlicka L, Pirozynski M, Rowinska-Zakrzewska E (1999) Usefulness of CD1 expression on surface of cells in bronchoalveolar fluid for diagnosis of histiocytosis X—our experience. Pneumol Allergol Pol (in Polish) 67:311–317
14. Smetana K Jr, Holíková Z, Klubal R, Bovin NV, Dvořánková B, Bartůňková J, Liu F-T, Gabius H-J (1999) Coexpression of binding sites for A(B) histo-blood group trisaccharides with galectin-3 and Lag antigen in human Langerhans cells. J Leukocyte Biol 66:644–649
15. Tazi A, Moreau J, Bergeron A, Dominique S, Hance AJ, Soler P (1999) Evidence that Langerhans cells in adult pulmonary Langerhans cell histiocytosis are matured dendritic cells: importance of the cytokine microenvironment. J Immunol 163:3511–3515
16. Valladeau J, Duvert-Frances V, Pinn J-J, Dezutter-Dambuyant C, Vincent C, Massacrier C, Vincent J, Yoneda K, Banchereau J, Caux C, Davoust J, Saeland S (1999) The monoclonal antibody DCGM4 recognizes Langerin, a protein specific for Langerhans cells, and is rapidly internalized from the cell surface. Eur J Immunol 29:2695–2704
17. Valladeau J, Ravel O, Dezutter-Dambuyant C, Moore K, Kleijmeer M, Liu Y, Duvert-Frances V, Vincent C, Schmitt D, Davoust J, Caux C, Lebecque S, Saeland S (2000) Langerin, a novel C-type lectin specific to Langerhans cells, is an endocytic receptor that induces the formation of Birbeck granules. Immunity 12:71–81
18. Vassallo R, Ryu JH, Colby TV, Hartman T, Limper AH (2000) Pulmonary Langerhans cell histiocytosis. N Engl J Med 342:1969–1978

Virchows Arch (2004) 444:175–182
DOI 10.1007/s00428-003-0929-5

ORIGINAL ARTICLE

Edson Mantovani Barbosa · Sueli Nonogaki · Maria Lucia Hirata Katayama · Maria Aparecida Azevedo Koike Folgueira · Venâncio Ferreira Avancini Alves · Maria Mitzi Brentani

Vitamin D3 modulation of plasminogen activator inhibitor type-1 in human breast carcinomas under organ culture

Received: 21 May 2003 / Accepted: 21 September 2003 / Published online: 2 December 2003

Abstract Urokinase plasminogen activator (uPA), its cell-bound receptor (uPAR) and its main inhibitor plasminogen activator type 1 (PAI-1) are present primarily in stromal cells in invasive breast carcinoma. The purpose of this study was to investigate the regulation by 1,25 dihydroxyvitamin-D3 (VD3) of these invasion-associated markers expressed in breast cancer tumors under organ culture, which preserves the interacting network of tumor and stromal cells. Breast carcinoma slices (30 cases), obtained using the Krumdieck tissue slicer, cultured for 48 h in the presence or absence of 100 nM vitamin D3, were embedded in formalin-fixed paraffin. uPA, uPAR, PAI-1 and VD3 receptor (VDR) were analyzed by immunohistochemistry, and their expression, detected in tumor cells and fibroblasts of the specimens, was not statistically changed by culture conditions. The proportion of cases expressing uPA, uPAR and PAI-1 was not affected by VD3 in epithelial cells, but the fraction of cases displaying strong PAI-1 reactivity in fibroblasts was reduced (P=0.016) compared with control slices. Fibroblasts isolated from invasive ductal carcinomas and from normal breast tissues expressed higher VDR mRNA levels than epithelial cells. In cultured tumor fibroblasts, PAI-1 immunostaining and mRNA levels were reduced by VD3-limiting fibroblast contribution to invasion.

Keywords Breast cancer · Calcitriol · Fibroblasts · PAI-1 · Organ culture

E. M. Barbosa
Instituto Brasileiro do Controle do Cancer,
Avenida Alcântara Machado 2576,
CEP 03102-002 São Paulo, SP, Brasil

S. Nonogaki · V. F. A. Alves
Divisão de Patologia, Laboratório de Imunohistoquímica,
Instituto Adolpho Lutz,
Av. Dr. Arnaldo 355, 7º sandar,
CEP 01246-902 São PauloSP, Brasil

M. L. H. Katayama · M. A. A. K. Folgueira · M. M. Brentani (✉)
Departamento de Radiologia, Faculdade de Medicina da USP,
Disciplina de Oncologia,
Av. Dr. Arnaldo 455, 4º andar, Sala 4112,
CEP 01246-903 São Paulo, Brasil
e-mail: mbrentani@lim24.fm.usp.br
Tel.: +55-11-30826580
Fax: +55-11-30826580

Introduction

The physiologically active form of vitamin D3, 1 alpha,25 dihydroxyvitamin D3 (VD3), not only plays a central role in bone and calcium metabolism, but also has potent antiproliferative effects on several malignant cells, including breast carcinoma cells [27]. VD3 exerts its effects via binding to an intracellular receptor (VDR) present in target tissues. There is accumulating evidence that neoplastic as well as normal breast cells in culture and biopsy specimens express the VDR [15, 17]. The prognosis of breast and other cancers is ultimately determined by the tumor ability to invade and metastasize. Although the modulatory effects of VD3 or its analogous on the invasive process have been shown in a variety of human cancer cell types, relatively little is known regarding the molecular basis for the anti-invasive activity of VD3 in breast carcinomas [21, 29, 32, 37, 41, 46].

Degradation of extracellular matrix barriers is a key step in tumor cell invasion. The plasminogen activator system (PA) plays a key role in cancer progression, presumably via mediating extracellular matrix degradation and tumor cell migration. Urokinase-type plasminogen activator (uPA), a serine protease that catalyzes the conversion of plasminogen to plasmin, which in turn catalyzes the degradation of major extracellular matrix components, is of particular importance. uPA, initially secreted as an enzymatically inactive proenzyme, exerts its proteolytic function after binding to a specific high-affinity cell surface receptor (uPAr). The complexed uPA can be inactivated by the plasminogen activator inhibitor

(PAI-1) [2]. However, there is evidence that PAI-1 promotes tumor invasion by potentiating tumor cell detachment from the matrix [12]. High levels of uPA, uPAr and PAI-1, mostly determined by enzyme-linked immunosorbent assay methods, have been found to be informative markers of poor prognosis in breast cancer [34]. The components of the uPA system are present mainly in stromal cells in invasive breast carcinomas [7, 8, 11, 28, 39, 45], and recent results suggest that strong expression of uPA, uPAr and PAI-1 in fibroblasts, as determined using immunohistochemistry, have the most impact on the clinical behavior of breast cancer [13].

The effects of VD3 on the uPA system have been reported in keratinocytes, osteoblasts, leukemic and breast tumor cells in culture [20, 29, 30, 32]. Our approach to examine a possible regulation of the PA system by VD3 in fibroblasts and epithelial cells of the same tumor was to use organ culture, which preserves the interacting network of tumor cells, stromal fibroblasts, endothelial cells and extracellular matrix, representing, therefore, a good model for this evaluation. It has been shown that surgically obtained human breast cancer tissue can be maintained in culture as intact tissue slices, and previous reports attested to the feasibility of this model for the evaluation of retinoids and estradiol effects in pre-clinical tests [26, 35]. Using immunohistochemistry, we described in the present communication the distribution of VD3 receptor, uPA, PAI-1 and uPAr protein expression in breast tumor slices cultured for 48 h in the presence or absence of VD3.

Materials and methods

Patients

Samples from 33 primary breast cancers were sequentially obtained from Instituto Brasileiro do Controle do Câncer (IBCC), São Paulo, Brasil. Of the tumors, 30 (90.9%) were histologically infiltrating ductal carcinomas, and the remaining, lobular or medullar carcinomas, were excluded from this study. In addition to conventional gross and histological analyses of the surgical specimen, another fragment from each tumor was immediately dissected to remove residual normal tissue and divided into two pieces. One was immersed in RPMI medium, brought to the laboratory for organ culture and immediately processed. The other sample was frozen and stored in liquid nitrogen until required. The ethics committee of IBCC approved the study proposal.

Northern analysis

Total RNA was extracted and analyzed by Northern blot technique as previously described [40]. The PAI-1 cDNA fragment [1] was provided by Dr. R. Mira y Lopes of Mount Sinai School of Medicine (New York, NY). The VDR probe was a 2.1-kb pGEM, provided by Dr J. Shine, California Biotechnology Inc., Mountain View, CA [16]. The ribosomic RNA 18S probe [3] was obtained from Dr N. Arnhein, Biochemistry Department, State University of New York, Stony Brook, NY.

Organ culture

All procedures were carried out as previously described [26]. Once in the laboratory, a small piece from each specimen, immersed in RPMI medium, was fixed in 10% buffered formalin and used for confirmation of histopathological diagnosis of invasive breast ductal carcinoma. The remaining tissue was cut in consecutive 0.5-mm-thick slices using the Krumdieck tissue slicer (Alabama Research and Development Corporation, Birmingham, AL). Sequential slices were then cultured or fixed in buffered formalin (the pre-culture samples). Slices to be cultured were transferred to siliconized lens paper squares, which were floated on 5 ml organ culture medium in 35-mm dishes. The medium was RPMI supplemented with 10% bovine fetal serum, 100 U/ml penicillin, 100 μg/ml streptomycin and 5 μg/ml insulin. Cultures were maintained at 37°C in a humidified atmosphere of 95% air/5% CO_2, in the presence or absence of 100 nM 1,25(OH)2D3. Normally, three or four slices were included per group. After 48 h of culture, the slices were fixed in buffered formalin for 18 h. After fixation, both pre-culture and post-culture slices were processed in a histoprocessor Autotechnicon Model 2A and embedded in paraffin. Sequential sections of 3 μm were placed in slides previously treated with 3-aminopropyltriethoxy-silane (Sigma, A3648, USA) and submitted to immunohistochemistry.

Immunohistochemical staining

After deparaffinization in xylene and rehydration in alcohol, antigen retrieval was performed with 10 mM citric acid pH 6.0 in a pressure cooker. Endogenous peroxidase activity was blocked with 6% H_2O_2 followed by incubation with the following monoclonal antibodies in 1% bovine serum albumin in phosphate-buffered saline (PBS) pH 7.4, overnight at 5°C: anti-uPA (ref 3689) and PAI-1 (ref 3785) from American Diagnostic, USA and anti-VDR, clone MA1–710 (ref MA1–710) from Affinity Bioreagents, Golden, CO, USA. Anti uPAR (mAbR2) was kindly provided by Dr. Keld Dano (Finsen Institute, Copenhagen, Denmark).

The slides were then incubated for 30 min at 37°C with biotinylated goat anti-mouse/rabbit Ig, followed by incubation for 30 min at 37°C with the streptavidin-biotin peroxidase (Duet, Dako, k0492, USA). Sections were developed by 3,3′ diaminobenzidine tetrahydrochloride (Sigma, D5637, USA), 6% H_2O_2 and dimethyl sulphoxide. Positive and negative controls were included in each run. The samples were observed at light microscope by two observers (SN and VAFA). Each one of the slides was first semi-quantified for the presence of viable cells, and then, the neoplastic epithelial cells and stromal cells were independently semi-quantified for immunohistochemical expression of each antigen as follows: score 0 (negative), less than 10% of reactive cells; score 1, 1–50% of reactive cells; score 2, more than 50% of reactive cells.

Fibroblast short-term culture

Specimens from normal or neoplastic breast tissues freed of adipose tissue were collected in PBS and finely minced. The micro-fragments were suspended in Dulbecco's Modified Eagle medium with 20% of fetal bovine serum and supplemented with ampicillin and streptomycin (100 μg/ml). Fibroblasts spread out from virtually every tissue fragment, and, after confluency, cells were subcultured using trypsin/ethylene diamine tetraacetic acid. Homogeneous cell cultures were obtained after the third replating. Fibroblasts were characterized using standard immunocytochemical procedures with the following antibodies: pan-cytokeratin (AE1/AE3, MxH), α-smooth muscle actin (HHF35, MxHx) both from Dako Corporation, Denmark, USA and anti-vimentin (clone LN-6) from Sigma-Aldrich Corporation, Saint Louis, MO.

Cell culture

Normal breast luminal cells (HB4a) were donated by Dr. M.J. O'Hare (Ludwig Institute for Cancer Research, London UCL Branch, London W1 W 7BS, United Kingdom) [44]. Breast cancer cell lines (MCF-7 and MDA-MB-231) were purchased from American Type Culture Collection. Cells were grown and maintained in RPMI medium plus 10% fetal bovine serum.

Statistical analysis

To probe for statistically significant associations between variables, chi-square analysis was performed, and a P value of less than 0.05 was considered statistically significant.

Results

Specimens of breast cancer and non-neoplastic tissue samples from 30 patients were analyzed for the expression of VDR mRNA by Northern blotting. Representative Northern signals from paired tumors and the adjacent normal breast tissues are displayed in Fig. 1. The VDR mRNA (4.6 kb) was detected in all tissue samples, albeit with a wide spectrum of relative levels. Quantification of Northern signals after normalization with 18S revealed that VDR mRNA expression levels ranged from 0.3 to 3.6, median 2.3. Normal adjacent tissues expressed VDR within similar ranges (median 1.39). Tissue slices, obtained from pre-culture samples or from organ culture as described in the Materials and Methods section, were fixed in 10% buffered formalin and evaluated using immunohistochemistry. VDR, uPA, uPAr and PAI-1 were assessed in the malignant epithelial cells and in tumor-associated fibroblasts within each section.

Results are summarized in Table 1, Table 2 and Table 3 and are presented as proportion of cases of breast cancer explants in each category of reactivity/total numbers of cases. The difference in the number of cases for each of the antibodies resulted from the absence of "viable cells" present in a particular slide, and all the cases where "viable cells" were not spotted were excluded from this study.

Figure 2A illustrates the expression of VDR in one of the control tumor slices subjected to culture. Staining was seen in the cell nuclei and cytoplasm. VDR immunoreactivity was present in the tumor cells in 70% of cases and in fibroblasts in 66% of cases. Slices maintained in culture for 48 h did not show a decline in scores of VDR staining. Treatment with VD3 slightly increased the

Table 1 Immunohistochemical evaluation of vitamin D3 (VD3) receptor (VDR) in epithelial cells and fibroblast (cases in each category/total cases). Breast cancer slices treated or not with VD3 were immunostained with specific antibody against VDR as described in Materials and methods. Results were graded as: 0 (<10% of stained cells), 1 (10–50% of stained cells) and 2 (>50% of stained cells). *n.s.* not significant

Staining score	Preculture	48 h	48 h plus VD3	P (x^2)
Epithelial cells (n=27)				
0	8 (30%)	6 (22%)	4 (15%)	n.s.
1	7 (26%)	8 (30%)	8 (30%)	
2	12 (44%)	13 (48%)	15 (55%)	
Fibroblasts (n=29)				
0	10 (34.5%)	6 (21%)	4 (14%)	n.s.
1	12 (41.5%)	12 (41.5%)	10 (34%)	
2	7 (24%)	11 (37.5%)	15 (52%)	

Table 2 Proportion of tumor cells staining for urokinase plasminogen activator (uPA), its cell-bound receptor (uPAR) and its main inhibitor plasminogen activator type 1 (PAI-1) (cases in each category/total cases). Breast cancer slices treated or not with vitamin D3 (VD3) were immunostained with specific antibodies against uPA, uPAr and PAI-1 as described in Materials and methods. Results were graded as: 0 (<10% of stained cells), 1 (10–50% of stained cells) and 2 (>50% of stained cells). *n.s.* not significant

Staining score	Preculture	48 h	48 h plus VD3	P (x^2)
uPA (n=25)				
0	1 (4%)	1 (4%)	2 (8%)	n.s.
1	12 (48%)	14 (56%)	13 (52%)	
2	12 (48%)	10 (40%)	10 (40%)	
uPAr (n=27)				
0	3 (11%)	2 (7%)	2 (7%)	n.s.
1	17 (63%)	15 (56%)	17 (63%)	
2	7 (26%)	10 (37%)	8 (30%)	
PAI-1 (n=28)				
0	0 (0%)	0 (0%)	0 (0%)	n.s.
1	0 (0%)	2 (7%)	2 (7%)	
2	28 (100%)	26 (93%)	26 (93%)	

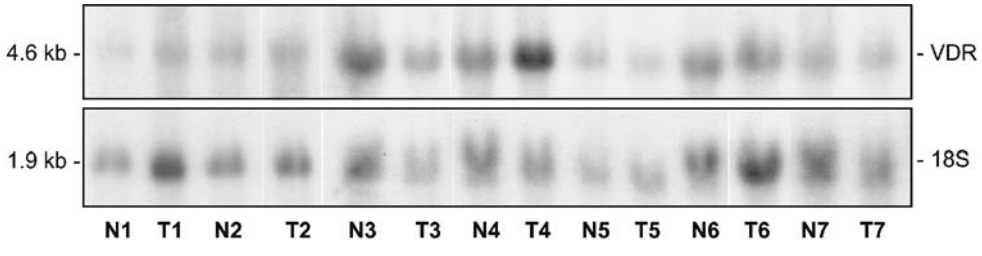

Fig. 1 Expression of vitamin D3 receptor mRNA in breast carcinoma (*T*) and its adjacent normal breast tissue (*N*). Northern blot was performed as described in methods

Table 3 Proportion of fibroblasts staining for urokinase plasminogen activator (uPA), its cell-bound receptor (uPAR) and its main inhibitor plasminogen activator type 1 (PAI-1) (cases in each category/total cases). Breast cancer slices treated or not with vitamin D3 (VD3) were immunostained with specific antibodies against uPA, uPAr and PAI-1 as described in Materials and methods. Results were graded as: 0 (<10% of stained cells), 1 (10–50% of stained cells) and 2 (>50% of stained cells). *n.s.* not significant

Staining score	Hours	48 h	48 h plus VD3	P (x^2)
uPA				
(*n*=25)				
0	0 (0%)	1 (4%)	3 (12%)	n.s.
1	12 (48%)	13 (52%)	11 (44%)	
2	13 (52%)	11 (44%)	11 (44%)	
uPAr				
(*n*=27)				
1	3 (11%)	4 (15%)	3 (11%)	n.s
2	4 (15%)	7 (25%)	7 (25%)	
3	20 (74%)	16 (59%)	17 (63%)	
PAI-1				
(*n*=28)				
0	1 (4%)	3 (11%)	14 (50%)	0.016
1	5 (18%)	8 (29%)	8 (29%)	
2	22 (78%)	17 (60%)	6 (21%)	

number of tumor cells and fibroblasts classified as presenting a highly positive VDR score (Table 1).

Figure 2B shows that uPA is localized in the cancer cells and, in general, a predominantly cytoplasmic staining was found, sometimes localized in the nucleus. uPA is also evident in fibroblasts (Fig. 2C). Of the cases, 96% had expression of uPA in their tumor cells, and, in 100% of cases, it was present in fibroblasts. After a 48-h culture period, in the absence or presence of VD3, no significant differences were seen in the distribution of positivity in either stromal or epithelial cancer cells. Of the cases, 89% revealed immunoreactivity for uPAr in fibroblasts and in epithelial cells. In these cells, a cytoplasm-associated immunostaining was observed (Fig. 2D). VD3 treatment did not affect uPAr expression, independently of cell type (Table 2 and Table 3).

PAI-1 expression was present in cancer cells in cytoplasm and eventually in nuclei in 100% of the specimens (Fig. 3A), and this proportion remained constant throughout the 48-h culture period or after VD treatment. Positive staining was found in the fibroblasts of 96% of the specimens (Fig. 3B). Significantly fewer samples expressed strongly stained PAI-1 (i.e., score 2) in fibroblasts upon VD3 treatment (60% versus 21%, P=0.016) compared with control slices after 48 h in culture (Table 3).

PAI-1 mRNA expression was studied in control slices in culture. PAI-1 mRNA (3.3 kb and 2.4 kb) expression was detected in all cases analyzed (Fig. 4).

As Northern blot analysis does not distinguish among functionally different cell types of the tumor, in a final set of studies, fibroblasts isolated from one area near an invasive ductal breast carcinoma (T) and from normal breast tissue (N) were treated with VD3. Both fibroblast populations were characterized as myofibroblasts and expressed higher VDR mRNA levels (approximately twofold more than the values expressed by the breast epithelial cells analyzed concomitantly: a normal human

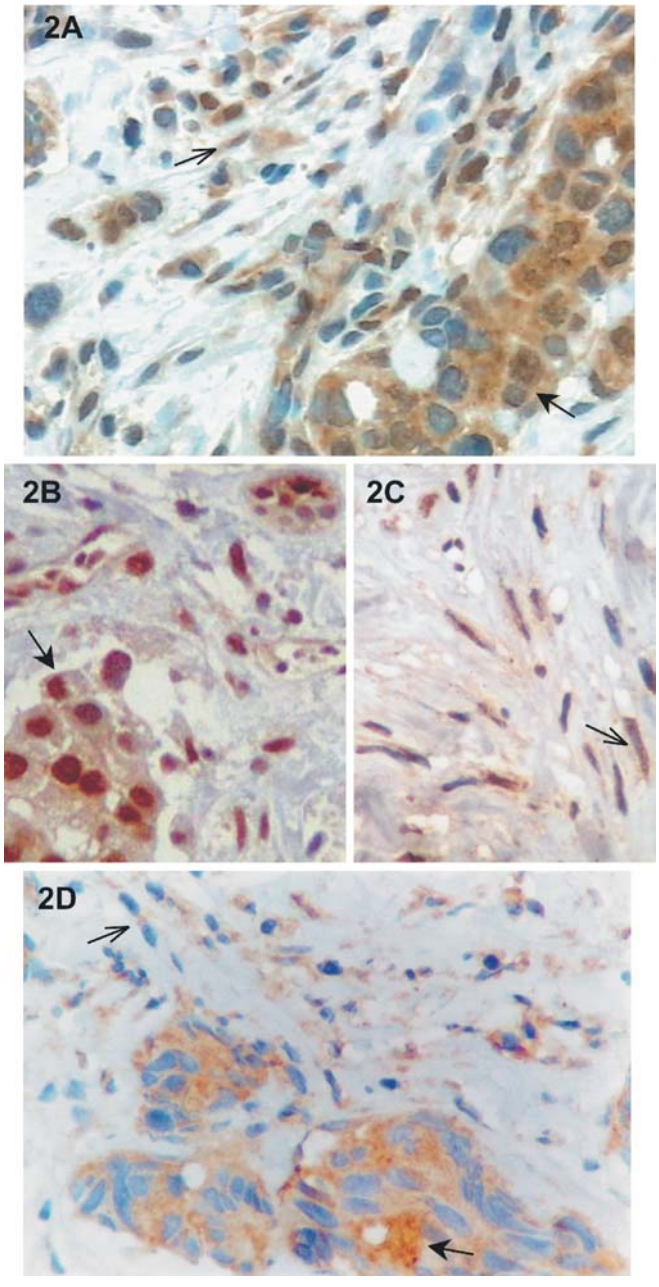

Fig. 2 A Nuclear and cytoplasmic vitamin D receptor immunoexpression indicated by *arrows* in breast tumor cells and fibroblasts. Original magnification ×400. **B** Urokinase plasminogen activator (uPA) immunoexpression located in neoplastic cells (*arrow*). Original magnification ×400. **C** uPA immunoexpression in fibroblasts (*arrow*). Original magnification ×600. **D** The cytoplasmic immunoexpression of the cell-bound receptor of urokinase plasminogen activator (uPAR) was seen in breast tumor cells (*arrow*) and fibroblasts (*arrow*). Original magnification ×600

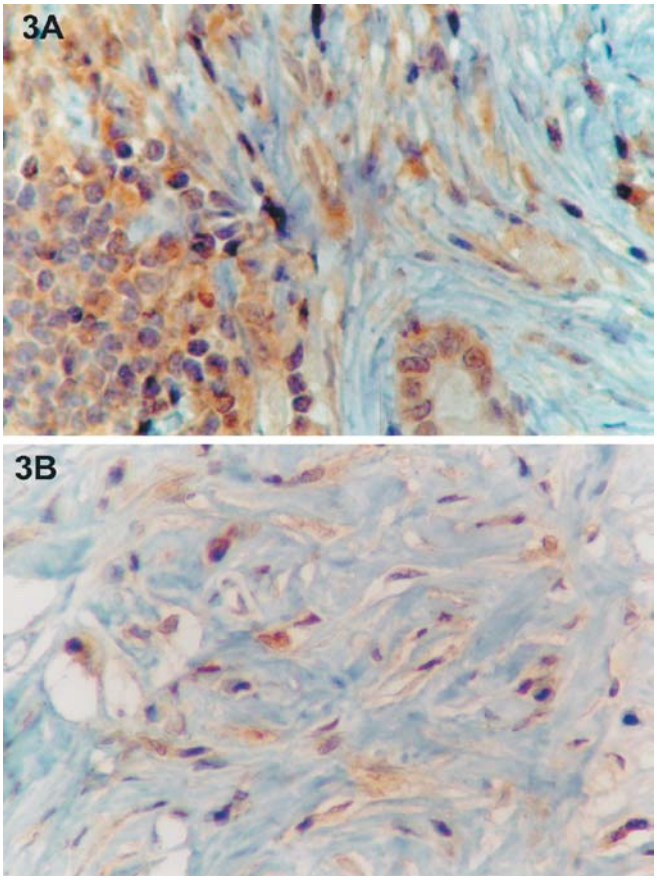

Fig. 3 Plasminogen activator type-1 immunoexpression. Strong immunostaining is depicted in breast carcinoma cells (**A**) and in fibroblasts (**B**). Original magnification ×600

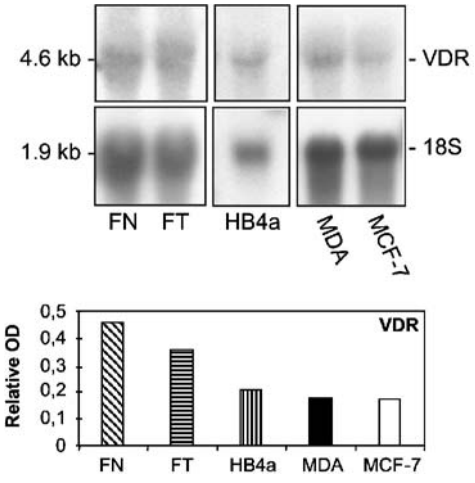

Fig. 5 Expression of vitamin D3 receptor mRNA in human mammary fibroblasts obtained from normal breast tissue (*FN*); tumor-associated fibroblasts (*FT*), normal human mammary luminal (*HB4a*) and breast carcinoma cell lines (*MDA-MB-231* and *MCF-7*). RNA total were extracted, and submitted to Northern blot as described in methods. Band intensities in autoradiograms were quantified by densitometric scanning and data expressed as the ratio of the specific mRNA to 18S ribosomal RNA

epithelial cell (HB4a) and two breast cancer cell lines (MDA-MB-231 and MCF-7) (Fig. 5). Peritumoral fibroblasts in culture responded to the addition of VD3 to the medium, showing a 34% reduction in PAI-1 mRNA expression measured after 48 h of treatment (Fig. 6). In normal fibroblasts, a decrease of 15% was observed. In contrast, in normal human mammary luminal cells and breast cancer cells, PAI-1 mRNA levels were not modified by VD3. All of the tumor fibroblasts in culture were reactive to the anti-PAI-1 antibody. After VD3 treatment, fibroblasts were stained less intensively, showing decreased PAI-1 expression as compared with control tumor fibroblasts (Fig. 7).

Discussion

Our results showed that organ culture of human carcinoma tissues maintained for 48 h preserved the expression profile of VDR, PAI-1, uPA and uPAr similar to that existing in vivo, thus, suggesting cell viability. Each component of the PA system was found both in fibroblasts and epithelial cells, in keeping with several

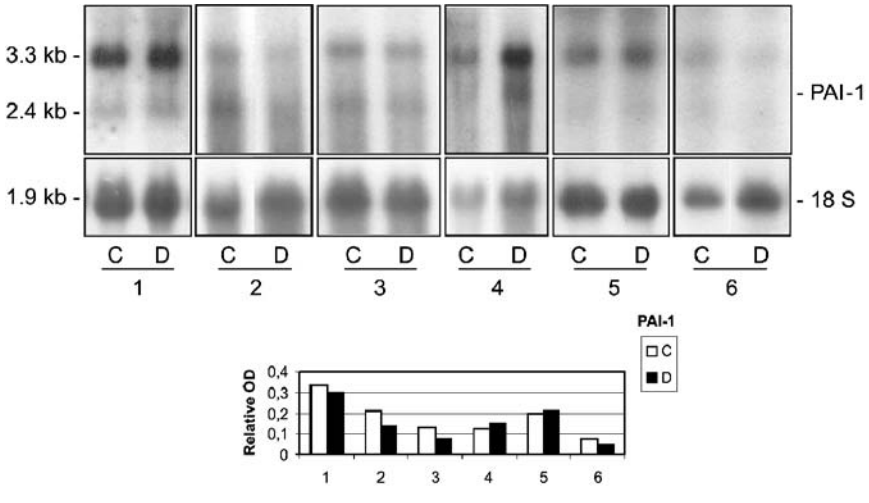

Fig. 4 Expression of plasminogen activator type-1 mRNA in breast carcinoma slices in culture. Total RNA was extracted and submitted to Northern blot as described in methods. Band intensities in autoradiograms were quantified by densitometric scanning and correspondent data expressed as the ratio of the specific mRNA to 18S ribosomal RNA. **C** Control, **D** Vitamin D3 treated

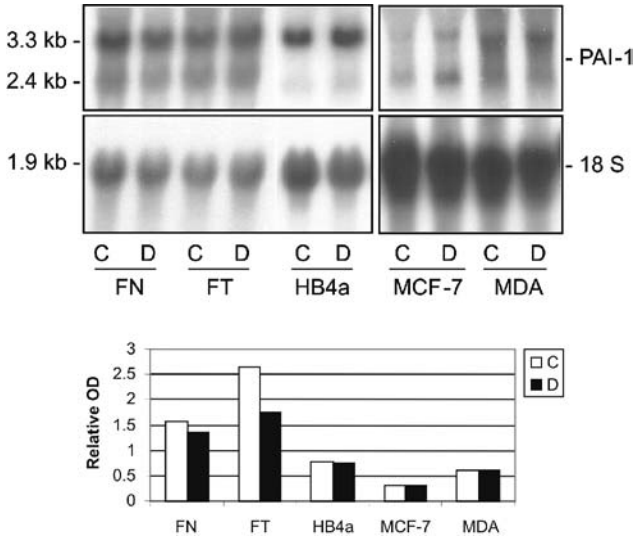

Fig. 6 Expression of plasminogen activator type-1 mRNA in human mammary fibroblasts obtained from normal breast tissue (*FN*); tumor-associated fibroblasts (*FT*) and normal human mammary luminal (*HB4a*), mammary carcinoma cell lines (*MDA MB-231* and *MCF-7*). Cells lines were exposed or not to vitamin D3 (VD3) and total RNA was extracted, and submitted to Northern blot analysis as described in Materials and methods (two independent assays were performed and mean values were presented). Band intensities in autoradiograms were quantified by densitometric scanning and data expressed as the ratio of the specific mRNA to 18S ribosomal RNA. **C** Control. **D** VD3 treated

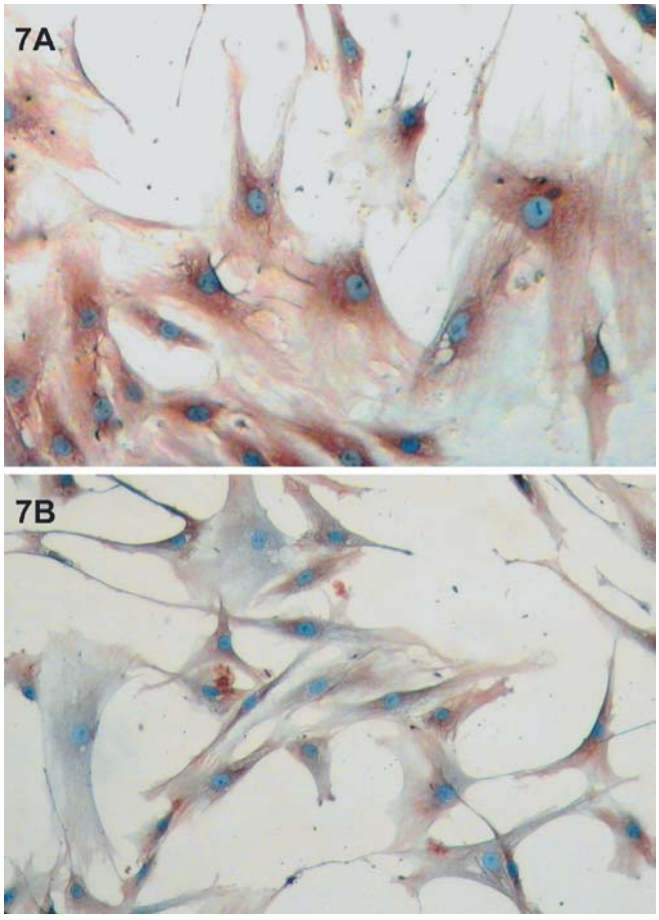

Fig. 7 Cytoplasmic plasminogen activator type-1 immunoexpression in human mammary fibroblasts obtained from tumor-associated fibroblasts. Cultures were maintained at 37°C in a humidified atmosphere of 95% air 5% CO_2, in absence (**A**) or in presence of 100 nM vitamin D (**B**) for 48 h, and then the cells were formalin fixed for 18 h. The immunocytochemical procedure was performed as described in Materials and methods

published studies [7, 8, 11, 28, 39, 45]. Although uPA and PAI-1 have been described as localized in the cytoplasm of cancer cells, we found immunostaining of uPA and PAI-1 to also be present in the nucleus in some samples, as previously published by Jankun et al. [24], using the same antibodies. Those authors suggested that rapid removal of uPA/uPAR/PAI-1 complexes by endocytosis exposes protein to acid proteases of lysosomes, producing different protein fragments, which are able to move to the nucleus. We examined other tissues for uPA so as to ascertain if the tissue preparation caused the unexpected localization of uPA and PAI-1 proteins, but normal tissues never displayed a nuclear localization, thus, suggesting that the nuclear staining of uPA was not due to faulty specimen preparation.

uPAR is attached to the cell membrane by a glycosylphosphatidylinositol anchor, and its expression should be found at the cellular membrane. As demonstrated in our results, some studies also reported a cytoplasmic staining [7, 11, 13]. One possible reason is that the antibody uPAR2 recognizes the cytoplasmic domain or uPAR present in the cytosol. Other possibilities already suggested by Dublin et al. [13] included either inhibition of antibody binding by uPAR binding to its ligand or that the epitope recognized by the antibody at the membrane was hidden by conformational changes in the uPAR molecule [23, 36, 42].

According to Friedrich et al. [18], no visible differences in the expression of VDR at the mRNA level were found compared with normal breast tissue. VDR nuclear staining localization was previously demonstrated in breast cancer [6, 17, 18, 19]. Treatment of slices with vitamin D induced a slight increase in VDR protein expression, due, perhaps, to the fact that VDR half-life was prolonged by vitamin D [33]. Upregulation of VDR immunoreactivity in fibroblasts was previously reported [9].

Vitamin D3 treatment reduced uPA activity in MDA-MB-231 breast carcinoma cells in cultured keratinocytes and in fibroblasts [30, 31]. We did not detect a similar decrease in abundance of uPA protein in our slices in culture. It is possible that uPA protein levels determined using immunohistochemistry might not have been equivalent to PA activity.

In the present study, we have demonstrated a decreased PAI-1 protein content in fibroblasts in either tumor slices or in primary cultured fibroblasts obtained from breast tumors when exposed to VD3. In accordance with our results, it has been previously demonstrated that

VD3 decreases PAI-1 mRNA in osteoblasts [20], and, in cultured keratinocytes, PAI-1 secretion and deposition was similarly inhibited [30]. However, we have not observed PAI-1 modulation in epithelial breast cancer cells, suggesting that VD3 displays divergent effects, which might be cell specific. It is possible to speculate that the differential responsiveness of the epithelial and stromal cells to $1,25(OH)_2D_3$ observed in the present work may reflect the VDR content of each cell or take place at a post-receptor site. A VDR was not demonstrated in the promoter of PAI-1 gene, suggesting that VD3 may not directly affect PAI-1 transcription, but may instead act through alternative pathways, which counteract induction effects by growth factors already described in breast tumor fibroblasts [43].

Our observation of PAI-1 reduction by VD3 treatment is of potential therapeutic interest, given the relevant role proposed for PAI-1 in fibroblasts in promoting cell invasion [4, 13]. Studies in rodent models reported the importance of vitamin D to prevent breast cancer metastasis in vivo and promising results of treatment with vitamin D of metastatic androgen-independent prostate cancer patients were published [5, 14, 22]. The possibility that vitamin D may have attenuated the contribution of breast tumor associated-fibroblasts to invasion adds to the body of evidence described in recent reviews that vitamin D analogues, exerting few calcemic side effects, may be effective in the treatment of breast cancer [10, 25, 38].

Acknowledgements We thank those who appear in section of Materials and methods for providing us with plasmids and antibodies. We are indebted to Dr. C. Krumdieck (University of Alabama, Birmingham, AL) for the kind donation to our institution of a Krumdieck tissue slicer. We also thank Dr. Rafael Mira-y-Lopes for valuable suggestions. Supported by FAPESP and CNPq.

References

1. Andreasen PA, Riccio A, Welinder KG, Douglas R, Sartorio R, Nielsen LS, Oppenheimer C, Blasi F, Dano K (1986) Plasminogen activator inhibitor type-I: reactive center and amino-terminal heterogeneity determined by protein and cDNA sequencing. FEBS Lett 209:213–218
2. Andreasen PA, Kjøller L, Christensen L, Duffy MJ (1997) The urokinase-type plasminogen activator system in cancer metastasis: a review. Int J Cancer 72:1–22
3. Arnheim N (1979) Characterization of mouse ribosomal gene fragments purified by molecular cloning. Gene 7:83–96
4. Bajou K, Noël A, Gerard RD, Masson V, Brunner N, Holst-Hansen C, Skobe M, Fusenig NE, Carmeliet P, Collen D, Foidart JM (1998) Absence of host plasminogen activator inhibitor 1 prevents cancer invasion and vascularization. Nat Med 14:923–928
5. Beer TM, Eilers KM, Garzotto M, Egorin MJ, Lowe BA, Henner WD, Hsieh JT (2003) Weekly high-dose calcitriol and docetaxel in metastatic androgen-independent prostate cancer. Urol Oncol 21:314–315
6. Berger U, McClelland RA, Wilson P, Greene GL, Haussler MR, Pike JW, Colston K, Easton D, Coombes RC (1991) Immunocytochemical determination of estrogen receptor, progesterone receptor, and 1,25-dihydroxyvitamin D3 receptor in breast cancer and relationship to prognosis. Cancer Res 51:239–244
7. Bianchi E, Cohen RL, Dai A, Thor AT, Shuman MA, Smith HS (1995) Immunohistochemical localization of the plasminogen activator inhibitor-1 in breast cancer. Int J Cancer 60:597–603
8. Christensen L, Simonsen ACW, Heegaard CW, Moestrup SK, Andersen JA, Andreasen PA (1996) Immunohistochemical localization of urokinase-type plasminogen activator, type-1 plasminogen-activator inhibitor, urokinase receptor and α2-macroglobulin receptor in human breast carcinomas. Int J Cancer 66:441–452
9. Clemens TL, Garrett KP, Zhou X-Y, Pike JW, Haussler MR, Dempster DW (1988) Immunocytochemical localization of the 1,25-dihydroxyvitamin D3 receptor in target cells. Endocrinology 122:1224–1230
10. Colston KW, Hansen CM (2002) Mechanisms implicated in the growth regulatory effects of vitamin D in breast cancer. Endocr Relat Cancer 9:45–59
11. Constantini V, Sidoni A, Deveglia R, Cazzato OA, Bellezza G, Ferri I, Bucciarelli E, Nenci GG (1996) Combined overexpression of urokinase, urokinase receptor, and plasminogen activator inhibitor-1 is associated with breast cancer progression. Cancer 77:1079–1088
12. Deng G, Curriden SA, Wang S, Rosenberg S, Loskutoff DJ (1996) Is plasminogen activator inhibitor-1 the molecular switch that governs urokinase receptor-mediated cell adhesion and release? J Cell Biol 134:1563–1571
13. Dublin E, Hanby A, Patel NK, Liebman R, Barnes D (2000) Immunohistochemical expression of uPA, uPAR, and PAI-1 in breast carcinoma. Am J Pathol 157:1219–1227
14. El Abdaimi K, Dion N, Papavasiliou V, Cardinal PE, Binderup L, Goltzman D, Ste-Marie LG, Kremer R (2000) The vitamin D analogue EB 1089 prevents skeletal metastasis and prolongs survival time in nude mice transplanted with human breast cancer cells. Cancer Res 60:4412–4418
15. Escaleira MTF, Brentani MM (1999) Vitamin D3 receptor (VDR) expression in HC-11 mammary cells: regulation by growth-modulatory agents, differentiation, and Ha-ras transformation. Breast Cancer Res Treat 54:123–133
16. Faraco JH, Morrison NA, Baker A, Shine J, Frossard PM (1989) ApaI dimorphism at the human vitamin D receptor gene locus. Nucleic Acids Res 17:2150
17. Friedrich M, Rafi L, Tilgen W, Schmidt W, Reichrath J. Expression of 1,25-dihydroxy vitamin D3 receptor in breast carcinoma (1998) J Histochem Cytochem 46:1335–1337
18. Friedrich M, Axt-Fliedner R, Villena-Heinsen C, Tilgen W (2002) Analysis of vitamin D-receptor (VDR) and retinoic X-receptor α in breast cancer. Histochem J 34:35–40
19. Friedrich M, Villena-Heinsen C, Tilgen W, Schmitd W, Reichrath J, Axt-Fliedner R (2002) Vitamin D receptor (VDR) expression is not a prognostic factor in breast cancer. Anticancer Res 22:1919–1924
20. Fukumoto S, Allan EH, Martin TJ (1994) Regulation of plasminogen activator inhibitor-1 (PAI-1) expression by 1,25-dihydroxyvitamin D-3 in normal and malignant rat osteoblasts. Biochem Biophys Acta 1201:223–228
21. González-Sancho JM, Alvarez-Dolado M, Muñoz A (1998) 1,25-Dihydroxyvitamin D3 inhibits tenascin-C expresión in mammary epithelial cells. FEBS Lett 426:225–228
22. Gross C, Stamey T, Hancock S, Feldman D (1998) Treatment of early recurrent prostate cancer with 1,25-dihydroxyvitamin D3 (calcitriol). J Urol 159:2035–2040
23. Hildenbrand R, Glienke W, Magdolen V, Graeff H, Stutte HJ, Schmitt M (1991) Urokinase receptor localization in breast cancer and benign lesions assessed by in situ hybridization and immunohistochemistry. Histochem Cell Biol 110:27–32
24. Jankun J, Merrick HW, Goldblatt PJ (1993) Expression and localization of elements of the plasminogen activation system in benign breast disease and breast cancers. J Cell Biochem 53:135–144
25. Jensen SS, Madsen MW, Lukas J, Binderup L, Bartek J (2001) Inhibitory effects of 1alpha,25-dihydroxyvitamin D(3) on the

G(1)-S phase-controlling machinery. Mol Endocrinol 15:1370–1380
26. Jing Y, Xu XC, Lotan R, Waxman S, Mira-y-Lopes R (1996) Human breast carcinoma slice cultures retain retinoic acid sensitivity. Braz J Med Biol Res 29:1105–1108
27. Katayama MLH, Pasini FS, Folgueira MAAK, Snitcovsky IML, Brentani MM (2003) Molecular targets of 1,25(OH)2D3 in Hc11 normal mouse mammary cell line. J Steroid Biochem Mol Biol 84:57–69
28. Kennedy S, Duffy MJ, Duggan C, Bernes C, Rafferty R, Kramer MD (1998) Semi-quantification of urokinase plasminogen activator and its receptor in breast carcinomas by immunocytochemistry. Brit J Cancer 77:1638–1641
29. Kole KL, Gyetko MR, Simpson RU, Sitrin RG (1991) Calcitriol-mediated modulation of urokinase-type plasminogen activator and plasminogen activator inhibitor-2. Biochem Pharmacol 41:585–591
30. Koli K, Keski-Oja J (1993) Vitamin D3 and calcipotriol decrease extra cellular plasminogen activator activity in cultured keratinocytes. J Invest Dermatol 101:706–712
31. Koli K, Keski-Oja J (1996) Vitamin D3 regulation of transforming growth factor-beta system in epithelial and fibroblast cells relationships to plasminogen activation. J Invest Dermatol Symp Proc 1:33–38
32. Koli K, Keski-Oja J (2000) 1α,25-dihydroxyvitamin D3 and its analogues down-regulate cell invasion associated proteases in cultured malignant cells. Cell Growth Differ 11:221–229
33. Li XY, Boudjelal M, Xiao JH, Peng ZH, Asuru A, Kang S, Fisher J, Voorhees JJ (1999) 1,25-dihydroxyvitamin D3 increases nuclear vitamin D3 receptor by blocking ubiquitin/proteasome mediated degradation in human skin. Mol Endocrinol 13:1986–1994
34. Look MP, van Putten WLJ, Duffy MJ, Harbeck N, Christensen IJ, Thomssen C, Kates R, Spyratos F, Fernö M, Eppenberger-Castori S, Fred Sweep CGJ, Ulm K, Peyrat J-P, Martin P-M, Magdelenat H, Brünner N, Duggan C, Lisboa BW, Bendahl P-O, Quillien V, Daver A, Ricolleau G, Meijer-van Gelder E, Manders P, Fiets WE, Blankenstein MA, Broët P, Romain S, Daxenbihler G, Windbichler G, Cufer T, Borstnar S, Kueng W, Beex LVAM, Klijn JGM, O'Higgins N, Eppenberger U, Jänicke F, Schmitt M, Foekens JA (2002) Pooled analysis of prognostic impact of urokinase-type plasminogen activator and its inhibitor PAI-1 in 8377 breast cancer patients. J Nat Cancer Inst 94:116–128
35. Mira-y-Lopes R, Osborne MP, Depalo AJ, Ossowski L (1991) Estradiol modulation of plasminogen activator production in organ cultures of human breast carcinomas: correlation with clinical outcome of anti-estrogen therapy. Int J Cancer 47:827–832
36. Mondino A, Resnati M, Blasi F (1999) Structure and function of the urokinase receptor. Thromb Haemost 82:19–22
37. Mork-Hansen C, Frandsen TL, Brunner N, Binderup L (1994) 1α,25-dihydroxyvitamin D3 inhibits the invasive potential of human breast cancer cells in vitro. Clin Exp Metastasis 12:195–202
38. Narvaez CJ, Zinser G, Welsh J (2001) Functions of 1alpha,25-dihydroxyvitamin D(3) in mammary gland: from normal development to breast cancer. Steroids 66:301–308
39. Nielsen BS, Sehested M, Timshel S, Pyke C, Danø K (1996) Messenger RNA for urokinase plasminogen activator is expressed in myofibroblasts adjacent to cancer cells in human breast cancer. Lab Invest 74:168–177
40. Ree AH, Pacheco MM; Tvermyr M, Fodstad O, Brentani MM (2000) Expression of a novel factor, com1, in early tumor progression of breast cancer. Clin Cancer Res 6:1778–1783
41. Schwartz GG, Wang MH, Zang M, Singh RK, Siegal GP (1997) 1 alpha,25-dihydroxyvitamin D (calcitriol) inhibits the invasiveness of human prostate cancer cells. Cancer Epidemiol Biomarkers Prev 6:727–732
42. Sidenius N, Blasi F (2003) The urokinase plasminogen activator system in cancer: recent advances and implication for prognosis and therapy. Cancer Metastasis Rev 22:205–222
43. Sieuwerts AM, Martens JW, Dorssers LC, Klijn JG, Foekens JA (2002) Differential effects of fibroblast growth factors on expression of genes of the plasminogen activator and insulin-like growth factor systems by human breast fibroblasts. Thromb Haemost 87:674–683
44. Stamps AC, Davies SC, Burman J, O'Hare MJ (1994) Analysis of proviral integration in human mammary epithelial cell lines immortalized by retroviral infection with a temperature-sensitive SV40 T-antigen construct. Int J Cancer 57:865–874
45. Uemeda T, Eguchi Y, Okino K, Kodama M, Hattori T (1997) Cellular localization of urokinase-type plasminogen activator, its inhibitors, and their mRNAs in breast cancer tissues. J Pathol 183:388–397
46. Yudoh K, Matsui H, Tsuji H (1997) Effects of 1,25-dihydroxyvitamin D3 on tumor cell invasion to the extracellular matrix in human fibrosarcoma HT1080 cells and its correlation with laminin. Tumor Biol 18:69–79

Virchows Arch (2004) 444:183–189
DOI 10.1007/s00428-003-0956-2

ORIGINAL ARTICLE

Anne Jörns · Birgit Kubat · Markus Tiedge · Dirk Wedekind · Hans-Jürgen Hedrich · Günter Klöppel · Sigurd Lenzen

Pathology of the pancreas and other organs in the diabetic LEW.1AR1/Ztm-*iddm* rat, a new model of spontaneous insulin-dependent diabetes mellitus

Received: 17 October 2003 / Accepted: 1 December 2003 / Published online: 20 January 2004

Abstract We studied the histo- and immunopathology of the endocrine and exocrine pancreas and a number of other organs in a new insulin-dependent diabetes mellitus (IDDM) rat model (LEW.1AR1/Ztm-*iddm* rat). The pancreas of the acutely diabetic animals showed an inflammatory infiltrate, involving all islets and ducts. The islet infiltrate was composed mainly of ED1-positive macrophages and T lymphocytes, comprising a large number of $CD8^+$ lymphocytes and a few $CD4^+$ lymphocytes. In addition, the islets displayed apoptotic cells, characterized by condensation and fragmentation of nuclear chromatin. These cells were identified as beta cells by insulin immunostaining. Other endocrine and exocrine glands, including adrenals and thyroid, as well as salivary and submandibular glands, were unaffected. Organs from the digestive tract or systemic circulatory system, including small intestine, liver, heart, and lung also showed no involvement. The kidney was intact in acutely diabetic rats. However, 6 months after diabetes manifestation, pathological changes compatible with a diabetic nephropathy had developed, affecting both the glomerula and the proximal tubular segments. It was concluded that the autoimmune process in this new IDDM rat model is restricted to the endocrine pancreas and leads to apoptotic beta cell destruction.

Keywords Type-1 diabetes mellitus · Animal model · Rat · Autoimmune disease · Beta cell apoptosis · Renal damage

A. Jörns (✉)
Centre of Anatomy,
Hannover Medical School,
30623 Hannover, Germany

B. Kubat
Department of Cell Biology,
Hannover Medical School,
Hannover, Germany

G. Klöppel
Department of Pathology,
University of Kiel,
Kiel, Germany

D. Wedekind · H.-J. Hedrich
Institute for Laboratory Animal Science,
Hannover Medical School,
Hannover, Germany

M. Tiedge · S. Lenzen
Institute of Clinical Biochemistry,
Hannover Medical School,
Hannover, Germany

Introduction

Animal models of type-1 diabetes mellitus (T1DM) play an important role in the elucidation of the autoimmune mechanisms leading to beta cell death [6, 18].The Bio-Breeding (BB) rat and the non-obese diabetic (NOD) mouse, as the most popular rodent models, typically differ from human T1DM with respect to inherited defects of the immune system and a sex preference of diabetes manifestation [6, 18]. The LEW.1AR1/Ztm-*iddm* rat is a new animal model of T1DM, which developed through a spontaneous mutation within an Mhc-congenic LEW.1AR1 colony [19]. The LEW.1AR1/Ztm-*iddm* rat closely resembles the diabetic syndrome in humans, as the animals show a fully developed cellular immune system and no sex bias in the diabetes incidence [19]. Furthermore, this recently described T1DM animal model has a well-characterized genetic background. It may, therefore, be useful for the elucidation of the mechanisms underlying immune-mediated pancreatic beta cell death.

We already reported the main islet changes that occur during the development of diabetes in the LEW.1AR1/Ztm-*iddm* rat. In this study, we focused on the detailed histopathology and immunopathology of the endocrine and exocrine pancreas and a number of other organs, such as the thyroid and the adrenals, which may potentially be involved in the autoimmune process. This systematic investigation allows a comparison with other animal

models of human T1DM, such as the diabetes of the BB rat and the NOD mouse [3, 18] and may help to clarify the specificity of the immune-mediated attack on the beta cells.

Materials and methods

Animals

The LEW.1AR1/Ztm-*iddm* rat is a new model of insulin-dependent diabetes mellitus, which originated in 1997 from the coisogenic LEW.1AR1 strain with a defined Mhc recombinant haplotype (*RT1*^{r2}: *RT1* A^a *B*/*D*^{u} C^u), kept in the Institute for Laboratory Animal Science of Hannover Medical School, as described previously [19]. Briefly, the animals were maintained in a separated minimal barrier sustained facility at 21°C under a 12-h/12-h light/dark cycle and a complete diet for rats (Ssniff V 1324–727, Germany). The animals (fed) used in the present study are from a breeding colony, which is maintained through mating of phenotypically inapparent healthy female and diabetic male LEW.1AR1/Ztm-*iddm* rats [19]. Seven animals, which showed a fulminant development of hyperglycemia (>20 mmol/l blood glucose) at 2 months of age, were sacrificed 1 week after diabetes manifestation. In addition, four animals with moderate hyperglycemia (8–15 mmol/l) were examined for renal changes 6 months after the onset of diabetes. Non-diabetic LEW.1AR1/Ztm-*iddm* rats of 2 months (n=6) and 6 months of age (n=6) were used as controls. On the day of sacrifice, tissue samples were collected for morphological examination of the pancreas and other organs. The different analyses were always performed on the same set of animals. The glucose concentration was determined in blood from the tail vein with the glucose oxidase method using the Glucometer Elite (Bayer, Leverkusen, Germany).

Tissue processing and examination

For light microscopy, tissue specimens of the pancreas and other organs were fixed in 4% paraformaldehyde in 0.15 M phosphate buffered saline (PBS), pH 7.3, or rapidly frozen in liquid nitrogen. The extrapancreatic organs included the thyroid, parathyroid, adrenal, and salivary glands, stomach, heart, lung, liver, small intestine, and kidney, as well as regional pancreatic lymph nodes. Fixed tissue was embedded in paraffin, and frozen tissue was stored at −70°C for cryostat histology. The serial paraffin sections of all organs were conventionally stained with hematoxylin and eosin. Additionally, small pancreatic tissue and renal specimens were fixed in 2% paraformaldehyde and 2% glutaraldehyde in 0.1 M cacodylate buffer, pH 7.3, postfixed in 1% OsO_4, and, finally, embedded in Epon. Semi-thin sections of the pancreatic and renal tissue were stained with toluidine blue [14, 19].

For immunohistochemistry, serial paraffin and cryostat sections were stained by the avidin-biotin-complex method [10]. After overnight incubation with the first antibody, biotinylated goat anti-rabbit IgG (1:100, 30 min) or biotinylated rabbit anti-mouse IgG (1:100, 30 min) (both obtained from Santa Cruz Biotechnology, Santa Cruz, CA, USA) was used as the second antibody and a mixture of streptavidin (1:100) and biotin-peroxidase (1:1000) (Jackson Immuno Research, West Grove, IL, USA) as the third antibody. The peroxidase reaction was visualized using 0.7 mM diaminobenzidine and 0.002% hydrogen peroxidase in PBS, pH 7.3. The following primary antibodies were used: polyclonal antibodies against insulin (A565, Dako, Hamburg, Germany), diluted 1:500, and against rat GLUT2 glucose transporter (WAK Chemie, Homburg, Germany), diluted 1:2000, were used on paraffin sections. The monoclonal antibodies (Serotec, Oxford, England) against macrophages (ED1), B lymphocytes (IgD) and pan-T lymphocytes (R 73), $CD4^+$ T lymphocytes, $CD8^+$ T lymphocytes (β-chain) and NK cells (3.2.3), all diluted 1:500, were used on cryostat sections. All antibodies were tested for method specificity and showed specific immunostaining in control and infiltrated islets in the LEW.1AR1/Ztm-*iddm* rat.

Analysis of sections

Apoptotic cells in the specific parenchyma of the analyzed organs were identified light microscopically by the typical signs, such as cell rounding and nuclear fragmentation, and quantified after TdT-mediated dUTP-biotin nick end labelling (TUNEL) staining [21]. In addition, the features of apoptosis were confirmed by electron microscopy [15]. Immunohistochemically, the remaining pancreatic beta cells in the pancreas sections of all diabetic animals were identified by two specific markers, the GLUT2 glucose transporter in the plasma membrane and insulin in the cytoplasm [7, 13, 14]. The cellular composition of the different subsets of infiltrating immune cells was analyzed with specific antibodies on cryostat sections. In these studies, 15–20 islets were analyzed in each pancreas. The immunostained sections were viewed using bright field illumination with a Zeiss Photomicroscope II (Zeiss, Oberkochen, Germany).

Results

Pancreas

The development of diabetes (blood glucose >20 mmol/l) was accompanied by an inflammatory infiltration of all islets of the pancreas. The islets were surrounded and completely infiltrated by mononuclear immune cells and had lost the majority (>90%) of their beta cells (Fig. 1A). Between the immune cells, there were a few isolated apoptotic pancreatic beta cells with condensation and fragmentation of nuclear chromatin. These cells had lost their contact to the other endocrine cell types that accounted for the residual endocrine cell mass of the islets (Fig. 1B). A quantitative TUNEL analysis in the pancreatic islets of pancreases from seven acutely diabetic rats revealed a rate of 3.9±0.4% apoptotic cells compared with 0.2±0.1% in non-diabetic controls. The still surviving beta cells showed faint insulin immunoreactivity in the cytoplasm and dense GLUT2 immunostaining at the plasma membrane. The residual endocrine cells were mainly glucagon cells and some somatostatin cells. These cells did not show any signs of apoptosis (Fig. 1B).

The pancreatic ducts with epithelium of more than eight to ten cells were surrounded by mononuclear immune cells, which occasionally also infiltrated the epithelial layer (Fig. 2A). In contrast to the beta cells of the pancreatic islets, the duct cells showed no signs of apoptosis (Fig. 2B). Signs of neogenesis were also not observed. The acinar tissue between islets and duct cells remained unaffected, without any signs of infiltration or degenerative lesions. Pancreases of normoglycemic control LEW.1AR1/Ztm rats (blood glucose <5 mmol/l) of the same age always showed well-preserved islets without any infiltration by immune cells.

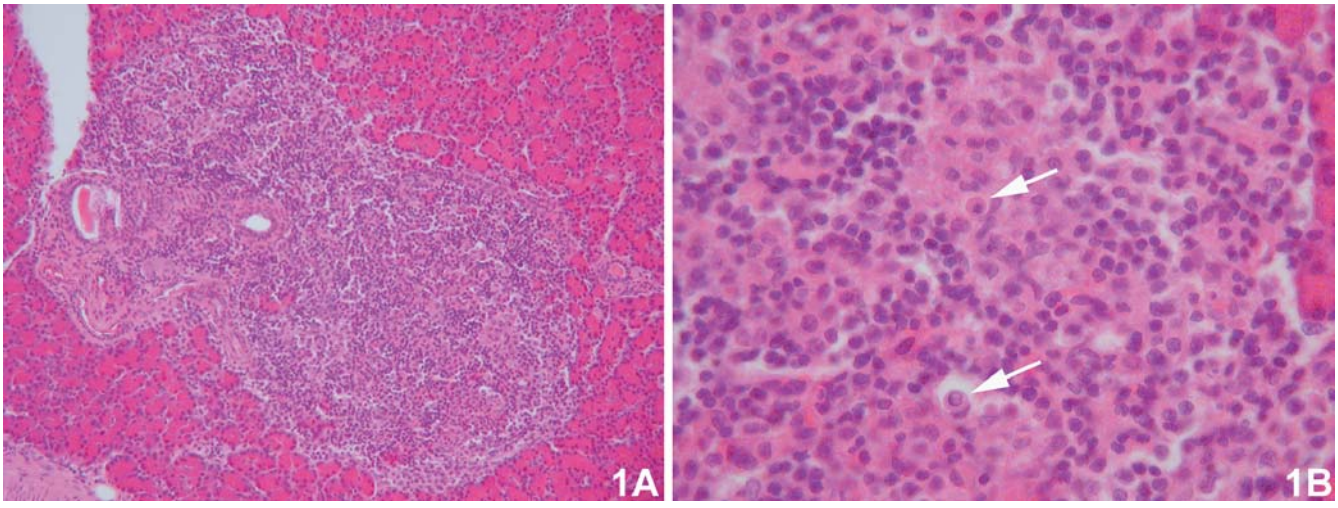

Fig. 1 Infiltration of the islets of Langerhans in the pancreas parenchyma in a severely diabetic (blood glucose >20 mmol/l) LEW.1AR1/Ztm-*iddm* rat. The islet of Langerhans is markedly infiltrated by mononuclear immune cells (**A**). Apoptotic beta cells with a chromatin condensation and fragmentation in the nucleus (*arrows*) lose the contact to the other endocrine cells (**B**). Hematoxylin/eosin ×300 (**A**) ×700 (**B**)

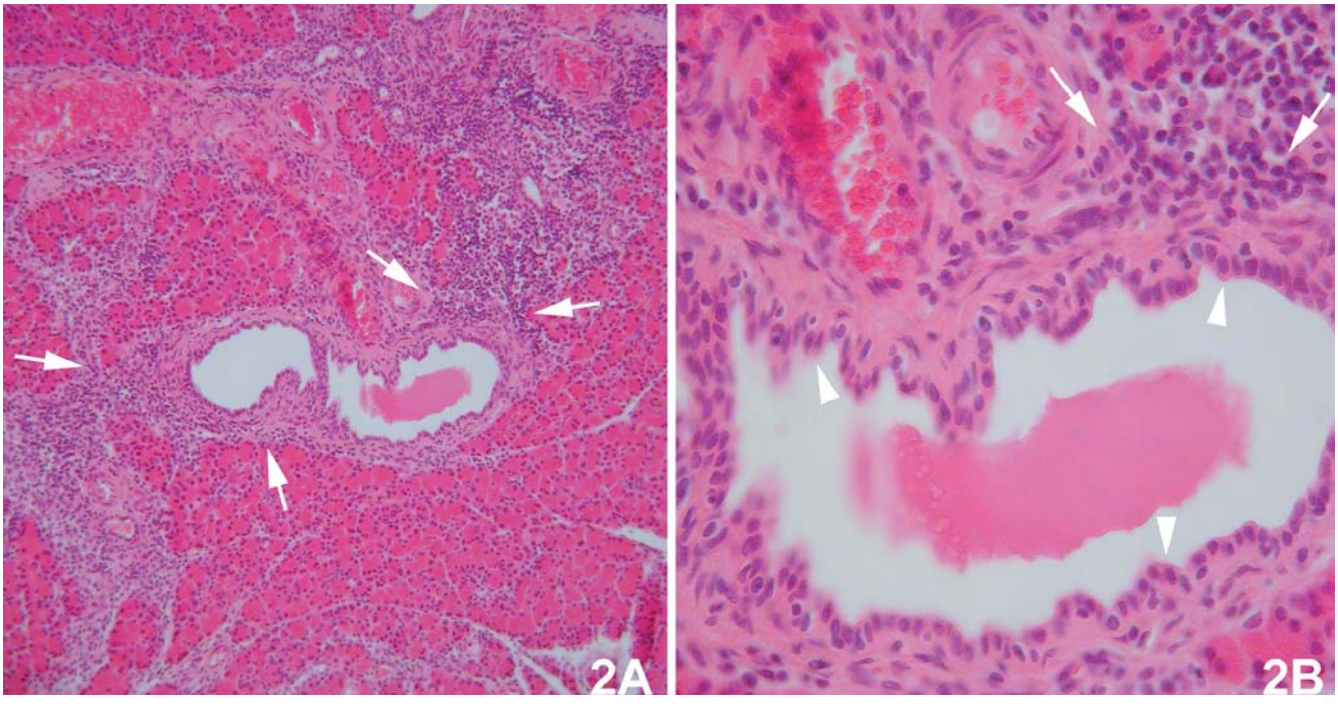

Fig. 2 Infiltration of the ducts of the exocrine pancreas parenchyma in a severely diabetic (blood glucose >20 mmol/l) LEW.1AR1/Ztm-*iddm* rat. The ducts are markedly surrounded and moderately infiltrated by mononuclear immune cells (*arrows*) (**A**). The duct cells show no signs of apoptosis (*arrowheads*) (**B**). Hematoxylin/eosin ×300 (**A**), ×700 (**B**)

Immune cell composition of the islet infiltrates

The islet infiltrates in the diabetic LEW.1AR1/Ztm-*iddm* rats were composed mainly of ED1-positive macrophages (34±3%; *n*=6) (Fig. 3A) and T lymphocytes (Fig. 3B), comprising a small number of $CD4^+$ lymphocytes (4±1%; *n*=6) (Fig. 3C) and a large number of $CD8^+$ lymphocytes (62±5%; *n*=6) (Fig. 3D). B-lymphocytes and natural killer (NK) cells accounted for less than 1% of the immune cells in infiltrated islets with maximally five cells per islet section.

In diabetic rats, ED1-positive macrophages, as well as many T-lymphocytes and some B-lymphocytes and NK cells, were also present in lymph nodes draining the pancreas (not shown). At variance from the situation in the diabetic animals, mesenteric lymph nodes from non-

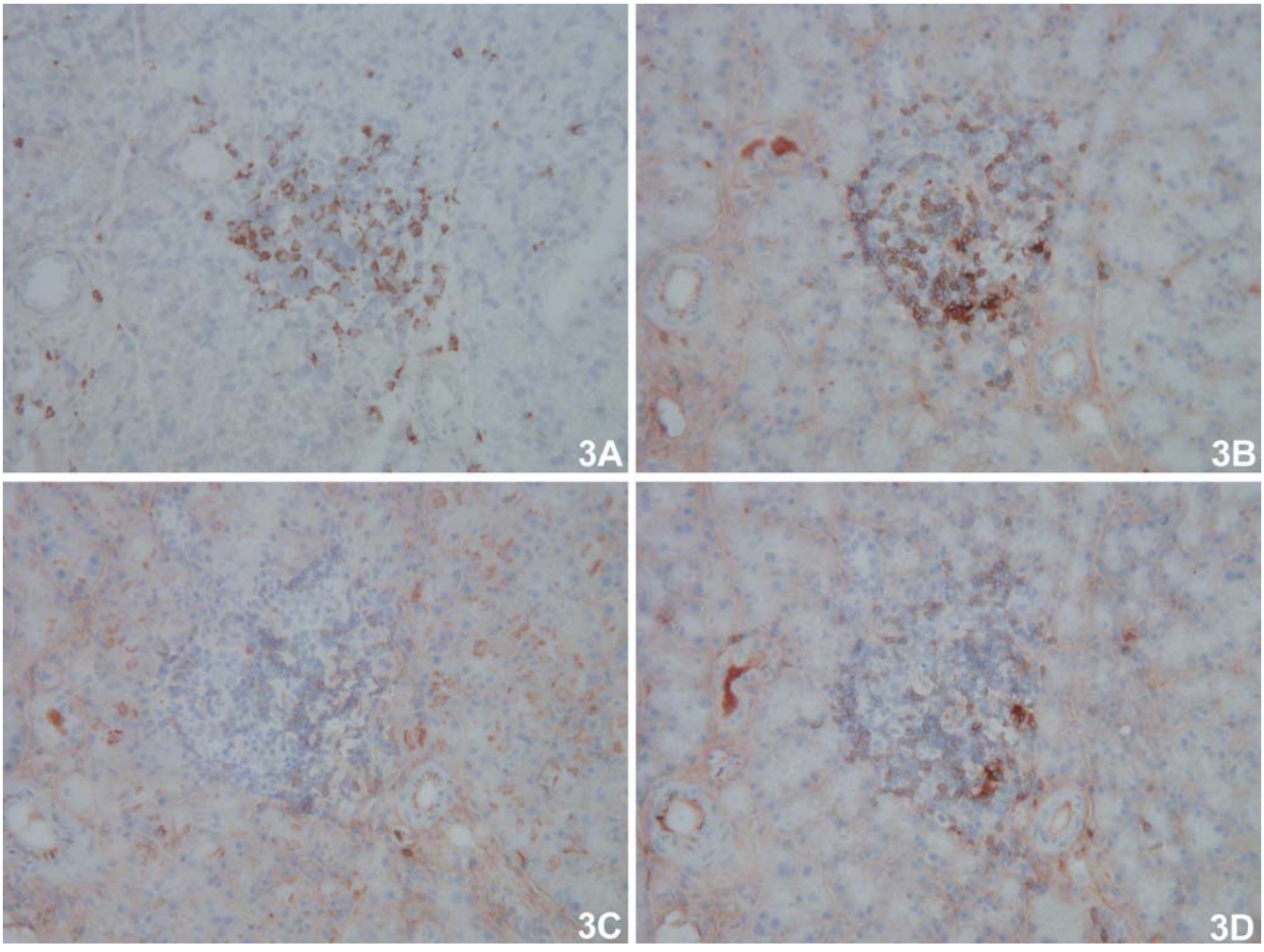

Fig. 3 Immunohistochemical staining of the immune cells in an infiltrated islet of a severely diabetic (blood glucose >20 mmol/l) LEW.1AR1/Ztm-*iddm* rat. Infiltrating macrophages as well as T lymphocytes (RTCα, β T-cells) are the main immune cell subpopulations (**A**, **B**). The T lymphocytes are composed by both $CD4^+$ and $CD8^+$ lymphocytes (**C**, **D**). Immunostaining for ED1 (infiltrating macrophages) (**A**), TCR alpha, beta (pan T lymphocytes) (**B**), $CD4^+$ alpha ($CD4^+$ T lymphocytes) (**C**), and $CD8^+$ beta ($CD8^+$ T lymphocytes) (**D**) ×400

diabetic rats contained two to three times less macrophages and T-lymphocytes (not shown).

Involvement of other organs

To investigate whether other organs besides the pancreas were also affected by the autoimmune process, endocrine glands [such as thyroid (Fig. 4A), parathyroid, and adrenals], exocrine glands [such as submandibular (Fig. 4B), lacrimal, and salivary glands], organs of the digestive tract (such as stomach, small intestine, and liver), and organs of the systemic circulatory system (such as heart and lung) were examined. None of the listed organs revealed any signs of immune cell infiltration.

Morphological alterations in renal tissue from acutely and chronically diabetic rats

The cortical and medullary regions of the kidney of severely diabetic LEW.1AR1/Ztm-*iddm* rats in the acute stage (less than 7 days after diabetes manifestation) were free of any signs of immune cell infiltration. Occasionally, neutrophil granulocytes were observed in loops of glomerular capillaries. Apoptotic events were not detected in the specific cells forming the glomerula or the different tubular segments. Only isolated cells in the proximal tubular segment expressed a large amount of dense bodies, representing intracellular protein aggregates within the cytoplasm (Fig. 5B), in comparison with those of the non-diabetic control LEW.1AR1/Ztm-*iddm* rats (Fig. 5A).

The different regions of the kidney also revealed no signs of infiltration or apoptosis 6 months after manifestation of the diabetic state (Fig. 5C). However, the

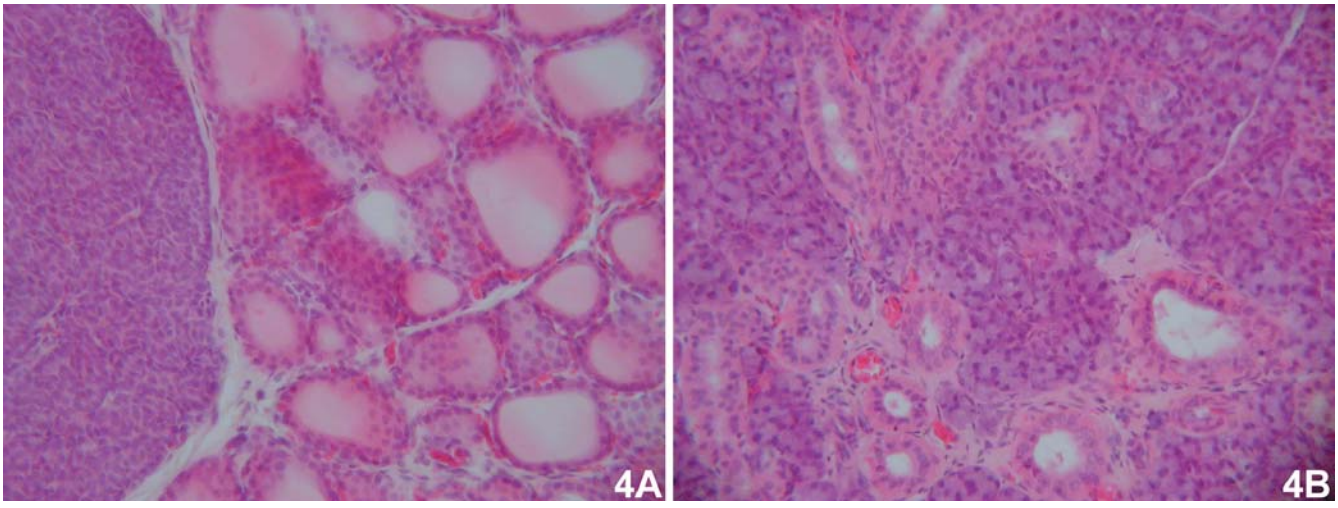

Fig. 4 Involvement of thyroid and salivary glands in the autoimmune process in a severely diabetic (blood glucose >20 mmol/l) LEW.1AR1/Ztm-*iddm* rat. Thyroid and parathyroid gland (**A**) as well as the salivary gland (**B**) show no signs of immune cell infiltration in the parenchyma. Hematoxylin/eosin ×300 (**A**, **B**)

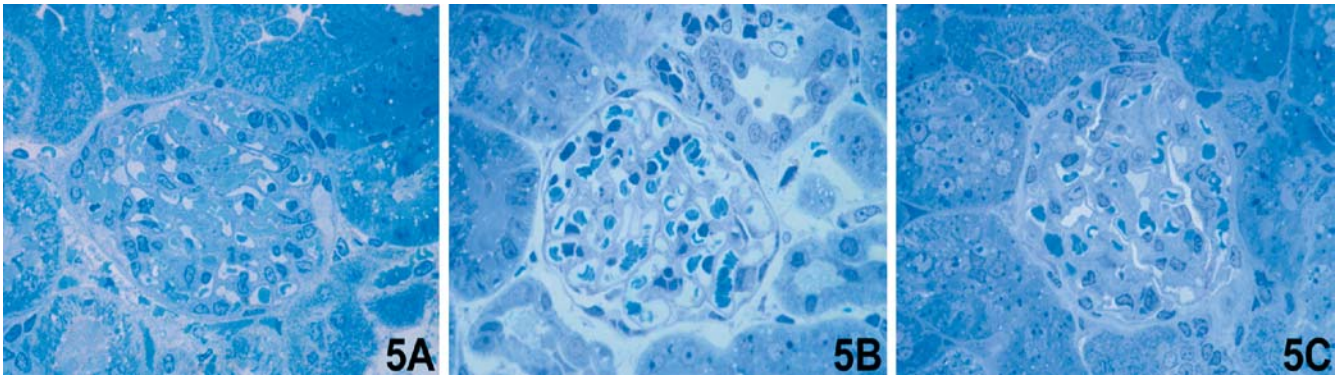

Fig. 5 Alterations in renal tissue of a severely diabetic (blood glucose >20 mmol/l) LEW.1AR1/Ztm-*iddm* rat in the acute and chronic phase. A higher amount of dense bodies in the cells of the proximal tubular segments is visible in the renal tissue of chronically (**C**) than of acutely (**B**) diabetic LEW.1AR1/Ztm-*iddm* rats. In comparison with the renal tissue of a normoglycemic control LEW.1AR1/Ztm-*iddm* rat (**A**), the mesangial cells in the glomerula are increased in the chronically diabetic phase (**C**). Toluidine blue staining ×400 (**A**–**C**)

glomerula showed morphological lesions due to mesangium expansion, resulting from proliferation and hypertrophy of the mesangial cells in the chronically diabetic LEW.1AR1/Ztm-*iddm* rats. The cells of the proximal tubular segment showed a larger amount of dense bodies (Fig. 5C) than those of the acutely diabetic animals (Fig. 5B).

Discussion

In the present investigation, we studied the morphology of the endocrine and exocrine pancreas and of a number of other organs, with respect to a potential involvement in the autoimmune process, which causes the diabetic syndrome in this new T1DM animal model [19]. We found that all islets in the pancreas of the acutely diabetic LEW.1AR1/Ztm-*iddm* rat revealed two significant changes, an immune cell infiltration of the islets of Langerhans, i.e., insulitis, and numerous apoptotic beta cells. In contrast to the situation in BB rats and NOD mice [9], an infiltration of the pancreas was never observed in any of the non-diabetic control animals.

An additional observation was the involvement of the pancreatic ducts in the immune process. This is in agreement with comparable observations in diabetic BB rats and NOD mice [9]. The periductular infiltration by lymphocytes raises the question whether this might be an indication for the presence of a common antigen shared by beta cells and duct cells. This assumption is supported by the finding that duct cells obviously comprise endocrine cells and, in particular, beta cell progenitor cells [23]. However, the fact that the lymphocytic periductal infiltration is not accompanied by any duct cell apoptosis might be interpreted as an indication that the infiltrate is unspecific rather than a specific immune cell response.

The immune cell composition in infiltrated islets in the LEW.1AR1/Ztm-*iddm* rat was comparable with that observed in the diabetic BB rat and the NOD mouse [9, 12, 20, 22]. Macrophages and T lymphocytes were the predominant immune cell types in the islet infiltrate, while other immune cells were rarely found. Qualitatively, this composition also corresponded to the infiltrate that has been described in the pancreas of patients with human T1DM [11, 16].

The most significant observation in this new T1DM animal model was the high frequency of apoptotic beta cells in the infiltrated islets [19]. Due to the fulminant development of diabetes, the maximal rates of beta-cell apoptosis observed were higher than in the BB rat and NOD mouse models [19]. In contrast to the situation in the diabetic BB rat and the diabetic NOD mouse [1, 17, 18], there was no increased rate of immune cell apoptosis in the islet infiltrate. Beta cell apoptosis was always recognized in the vicinity of immune cells, such as T-lymphocytes.

Other organs of the LEW.1AR1/Ztm-*iddm* rat, including the thyroid and adrenal glands, as well as exocrine glands and organs of the intestinal tract and the circulatory system, were not affected by the autoimmune process and showed neither immune cell infiltration nor an increase of apoptotic events. In the diabetic BB rat, infiltration of the endocrine pancreas is typically accompanied by immune cell thyroiditis [2]. In the diabetic NOD mouse, a focal mononuclear infiltration of the thyroid gland was also observed in up to 20% of the animals [4]. Exocrine glands are apparently unaffected in the diabetic BB rat [2]. In contrast, concomitant infiltration of the mandibular, parotid, and lacrimal glands has been observed frequently in diabetic NOD mice [8]. Actually, an infiltration rate of more than 80% has been reported for the salivary gland in this diabetes mouse model [4]. From this comparison, it can be concluded that the immune process in our new T1DM animal model is restricted to the endocrine pancreas and does not involve extrapancreatic tissues as well.

The kidney in acutely diabetic LEW.1AR1/Ztm-*iddm* rats showed no pathological alterations, neither an immune cell infiltration nor an increased rate of apoptosis. This observation is at variance with the situation in the diabetic NOD mouse, where such findings have been reported [22]. Pathological changes compatible with a diabetic nephropathy, such as an increase of mesangial cells in the glomerula or the high number of dense bodies as resorption vacuoles in the tubular segments, developed only in the chronic phase of diabetes in LEW.1AR1/Ztm *iddm* rats several months after manifestation of the disease. Comparable glomerular and tubular changes as typical signs of a diabetic nephropathy have been registered during the chronic phase of the disease also in the kidney of BB rats and NOD mice [5]. Thus, the chronically diabetic LEW.1AR1/Ztm-*iddm* rat may represent an interesting model for the study of late secondary diabetic lesions.

To summarize, the results of this morphological study show that the autoimmune process in the diabetic LEW.1AR1/Ztm-*iddm* rat affects only the beta cells of the islets of Langerhans and, in addition, the ducts in the pancreatic parenchyma. Signs of infiltration as the correlate of an autoimmune process could be detected in none of the other organs of this insulin-dependent diabetes mellitus rat.

Acknowledgements This work has been supported by a grant from the Deutsche Forschungsgemeinschaft (Jo-395 1–1) to A.J. and by the NIH grant 1R21AI55464–01 to S.L. and H.J.H. The technical assistance of M. Böger and U. Sommerfeld is gratefully acknowledged.

References

1. Augstein P, Stephens LA, Allison J, Elefanty AG, Ekberg M, Kay TW, Harrison LC (1998) Beta-cell apoptosis in an accelerated model of autoimmune diabetes. Mol Med 4:495–501
2. Awata T, Guberski DL, Like AA (1995) Genetics of the BB rat: association of autoimmune disorders (diabetes, insulitis, and thyroiditis) with lymphopenia and major histocompatibility complex class II. Endocrinology 136:5731–5735
3. Bieg S, Lernmark A (1999) Animal models for insulin-dependent diabetes mellitus. In: Volpe R (ed) Contemporary endocrinology: autoimmune endocrinopathies. Humana Press, Totowa, pp 113–139
4. Christianson SW, Shultz LD, Leiter EH (1993) Adoptive transfer of diabetes into immunodeficient NOD-scid/scid mice. Relative contributions of CD4+ and CD8+ T-cells from diabetic versus prediabetic NOD.NON-Thy-1a donors. Diabetes 42:44–55
5. Cohen AJ, McGill PD, Rossetti RG, Guberski DL, Like AA (1987) Glomerulopathy in spontaneously diabetic rat. Impact of glycemic control. Diabetes 36:944–951
6. Eisenbarth GS (2003) Type I diabetes. Molecular, cellular and clinical immunology. Oxford University Press, New York, Oxford
7. Elsner M, Tiedge M, Guldbakke B, Munday R, Lenzen S (2002) Importance of the GLUT2 glucose transporter for pancreatic beta cell toxicity of alloxan. Diabetologia 45:1542–1549
8. Hadano H, Suzuki S, Tanigawa K, Ago A (1988) Cell infiltration in various organ and dilatation of the urinary tubule in NON mice. Jikken Dobutsu 37:479–483
9. Homo-Delarche F (1997) Beta-cell behaviour during the prediabetic stage. Part II. Non-insulin- dependent and insulin-dependent diabetes mellitus. Diabetes Metab 23:473–505
10. Hsu SM, Raine L, Fanger H (1981) Use of avidin-biotin-peroxidase complex (ABC) in immunoperoxidase techniques: a comparison between ABC and unlabeled antibody (PAP) procedures. J Histochem Cytochem 29:577–580
11. Imagawa A, Hanafusa T, Itoh N, Miyagawa J, Nakajima H, Namba M, Kuwajima M, Tamura S, Kawata S, Matsuzawa Y, Harlan DM (1996) Islet-infiltrating t lymphocytes in insulin-dependent diabetic patients express CD80 (B7-1) and CD86 (B7-2). J Autoimmun 9:391–396
12. Jansen A, Homo-Delarche F, Hooijkaas H, Leenen PJ, Dardenne M, Drexhage HA (1994) Immunohistochemical characterization of monocytes-macrophages and dendritic cells involved in the initiation of the insulitis and beta-cell destruction in NOD mice. Diabetes 43:667–675
13. Jörns A, Tiedge M, Lenzen S (1999) Nutrient-dependent distribution of insulin and glucokinase immunoreactivities in rat pancreatic β cells. Virchows Arch 434:75–82

14. Jörns A, Tiedge M, Ziv E, Shafrir E, Lenzen S (2002) Gradual loss of pancreatic beta-cell insulin, glucokinase and GLUT2 glucose transporter immunoreactivities during the time course of nutritionally induced type-2 diabetes in Psammomys obesus (sand rat). Virchows Arch 440:63–69
15. Jörns A, Tiedge M, Lenzen S (2002) Thyroxine induces pancreatic beta cell apoptosis. Diabetologia 45:851–855
16. Klöppel G, Clemens A (1996) Insulin-dependent diabetes mellitus. Current aspects of morphology, etiology and pathogenesis. Pathologe 17:269–275
17. Kurrer MO, Pakala SV, Hanson HL, Katz JD (1997) Beta cell apoptosis in T cell-mediated autoimmune diabetes. Proc Natl Acad Sci U S A 94:213–218
18. Lally FJ, Bone AJ (2002) Animal models of type 1 diabetes. In: Pickup JC, Williams G (eds) Textbook of diabetes, Blackwell Scientific Publications, Oxford, pp 19.1–19.17
19. Lenzen S, Tiedge M, Elsner M, Lortz S, Weiss H, Jörns A, Klöppel G, Wedekind D, Prokop CM, Hedrich HJ (2001) The LEW.1AR1/Ztm-iddm rat: a new model of spontaneous insulin-dependent diabetes mellitus. Diabetologia 44:1189–1196
20. Nagata M, Santamaria P, Kawamura T, Utsugi T, Yoon JW (1994) Evidence for the role of CD8+ cytotoxic T cells in the destruction of pancreatic beta-cells in nonobese diabetic mice. J Immunol 152:2042–2050
21. Sgonc R, Wick G (1994) Methods for the detection of apoptosis. Int Arch Allergy Immunol 105:327–332
22. Voorbij HA, Jeucken PH, Kabel PJ, De Haan M, Drexhage HA (1989) Dendritic cells and scavenger macrophages in pancreatic islets of prediabetic BB rats. Diabetes 38:1623–1629
23. Wang RN, Bouwens L, Klöppel G (1996) Beta-cell growth in adolescent and adult rats treated with streptozotocin during the neonatal period. Diabetologia 39:548–557

Virchows Arch (2004) 444:190–193
DOI 10.1007/s00428-003-0940-x

CASE REPORT

Frank Bergmann · Thilo Hackert · Gunhild Mechtersheimer · Roland Penzel · Hendrik Bläker · Irina Berger · Irene Esposito · Markus W. Büchler · Herwart F. Otto

Differential diagnosis of non-epithelial tumors of the pancreas: malignant non-epithelial pancreatic tumor with focal pigmentation

Received: 11 June 2003 / Accepted: 5 November 2003 / Published online: 14 January 2004

Abstract Non-epithelial tumors only rarely affect the pancreas. In this report, we describe a malignant non-epithelial tumor with combined characteristics of malignant peripheral nerve sheath tumor (MPNST) and malignant melanoma. To more closely define the differential diagnosis of MPNST with focal pigmentation versus metastatic melanoma resembling MPNST, the tumor was investigated using histomorphology, immunohistochemistry, electron microscopy, and comparative genomic hybridization. As a result, from these analyses and from clinical findings, the diagnosis of a pancreatic MPNST with focal pigmentation was favored. However, the diagnosis of a malignant melanoma or a composite tumor could not be definitely ruled out, due to the considerable morphological and genotypical overlap between both entities, which can be explained by the close histogenetic relationship between both tumor entities.

Keywords Pancreas · Malignant peripheral nerve sheath tumor · Malignant melanoma

Introduction

Malignant non-epithelial tumors only rarely affect the pancreas, occurring with a relative frequency of approximately 0.6% [9]. Recurrently reported tumors include, among few other entities, malignant peripheral nerve sheath tumors (MPNST) [7, 8, 9, 10, 14, 19]. In general, MPNST may arise either sporadically or in association with hereditary neurofibromatosis (types 1 and 2). Originating from cells of the peripheral nerve sheath, MPNST display varying degrees of Schwann cell differentiation. Furthermore, melanin pigmentation has been reported in a number of extrapancreatic MPNST [5, 12], reflecting the close histogenetic relationship to malignant melanomas. In addition, malignant melanomas may, as well, resemble MPNST histomorphologically [6], making the distinction between both entities difficult in some cases. Although, to date, there are no reports of malignant melanomas primarily arising within the pancreas, metastatic spread into this organ is commonly observed [15]. We report the rare case of a malignant non-epithelial pancreatic tumor with focal melanin pigmentation and discuss the differential diagnosis.

F. Bergmann · G. Mechtersheimer · R. Penzel · H. Bläker · I. Berger · I. Esposito · H. F. Otto
Institute of Pathology,
University of Heidelberg, Germany

T. Hackert · M. W. Büchler
Department of Surgery,
University of Heidelberg, Germany

F. Bergmann (✉)
Pathologisches Institut,
Im Neuenheimer Feld 220/221, 69120 Heidelberg, Germany
e-mail: frank_bergmann@med.uni-heidelberg.de
Tel.: +49-62-21562600
Fax: +49-62-21565251

Clinical history

The 46-year-old male patient was referred to our hospital for re-evaluation of a pancreatic tumor identified at another institution 6 months prior to admission. There, explorative laparotomy with biopsy of the pancreatic mass had led to the diagnosis of an irresectable neurogenic or melanotic tumor. Consecutively, the patient had undergone chemotherapeutic treatment with adriamycin and ifosfamid, which was interrupted after four cycles due to lack of response. The patient did not suffer from any other relevant diseases and did not present any features of hereditary neurofibromatosis. Upon referral to our hospital, computed tomography and magnetic resonance imaging confirmed the pancreatic tumor, depicted as a well-circumscribed mass located in the head of the pancreas without affection of large blood vessels. No primary malignant melanoma or other extrapancreatic manifestations of the tumor were found. Thus, the mass was resected during radical duodeno-pancreatectomy. The patient, again, underwent surgery for a solitary brain metastasis 4 months after being discharged. In the postoperative course, the patient did not recover from bad general condition and died.

Materials and methods

The surgical specimen was fixed in 8% buffered formaldehyde and embedded in paraffin. For histological evaluation, sections were stained with hematoxylin and eosin, as well as with Prussian blue for iron. Immunohistochemical analyses were performed with primary antibodies against vimentin, (1:1000, Dako), S100 (undiluted, Dako), HMB-45 (undiluted, Enzo Diagnostics), CD34 (1:25, Dako), desmin (1:2, Histoprime), chromogranin (undiluted, Dako), and cytokeratins (AE1+3; 1:5, Histoprime and KL1; 1:20, Immunotech), using the avidin-biotin-complex-method.

Small tissue samples were fixed in 3% glutaraldehyde and processed for ultrastructural investigation. Semi-thin sections were stained with toluidine blue. Ultra-thin sections were contrasted with lead and examined using a Zeiss electron microscope.

For cytogenetic analysis, comparative genomic hybridization (CGH) was performed, as described elsewhere [4]. Briefly, tumor DNA was extracted from paraffin-embedded material. In a nick translation, tumor DNA was biotinylated, and normal human DNA was labeled with digoxigenin. Hybridization of the labeled probes onto metaphase spreads was followed by several washing steps. Detection of the probes was performed using avidin conjugated fluorescein for biotinylated tumor DNA and anti-digoxigenin-rhodamin conjugate for digoxigenin-labeled reference DNA. Hybridized metaphases (n=20) were then captured and analyzed using an inverted microscope (Zeiss Axiovert S 100), a charge-coupled device camera and CGH software (MetaSystems, Germany). As CGH frequently yielded false-positive results in the centromeric and telomeric regions as well as for the entire chromosome 19, these chromosomal areas were excluded from the investigation. Chromosomal gains were presumed if the ratio of tumor to normal signals reached or exceeded 1.25. The respective ratio for chromosomal losses was 0.80.

Results

Grossly, the pancreatic tumor presented as a sharply demarcated mass, measuring 7.5 cm in largest diameter. On cut surface, the lobulated, glassy tumor was of white and brownish color, containing areas of microcystic degeneration (Fig. 1).

The tumor consisted of spindle-shaped cells, plump, polygonal cells with epithelioid appearance, and multinucleated giant cells, presenting a rather heterogeneous picture microscopically. In some areas, the cells were arranged in fascicles or whorls; in others, they showed nodular patterns, no recognizable growth pattern, or were of myxoid–cystic appearance. Focally, the tumor showed melanin pigmentation, staining negative with Prussian blue for iron (Fig. 2).

The expansively growing tumor was surrounded by a pseudocapsule, which was only focally infiltrated toward the pancreatic tissue. Intravascular neoplastic emboli were not observed. There were no regional lymph-node metastases.

Immunohistochemical analyses revealed a diffuse positive staining for vimentin and focal positive staining for S100. Expression of HMB-45 was observed within pigmented areas of the tumor. The tumor cells showed no reactivity toward desmin, cytokeratins, chromogranin, and CD34.

Ultrastructural findings comprised cells with large, multi-segmented nuclei, relatively broad and sometimes intertwining cell processes, as well as rudimentary cell junctions. Within pigmented areas of the tumor, the cytoplasm contained melanosomes (Fig. 2D).

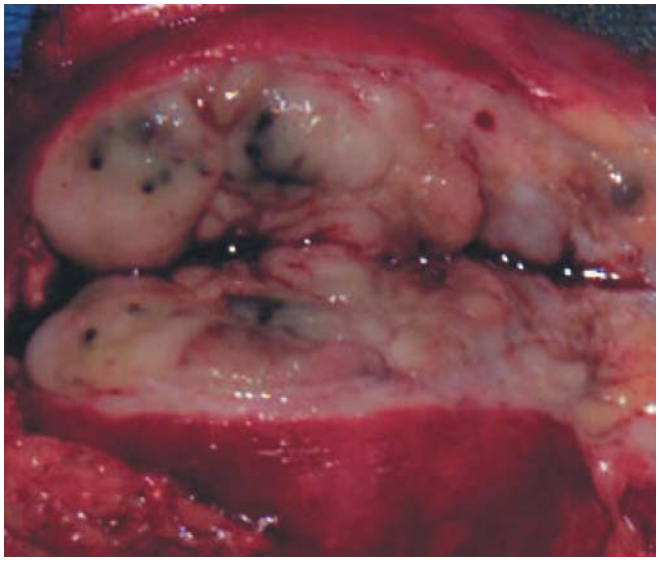

Fig. 1 Grossly, the pancreatic tumor presented as a sharply demarcated mass with lobulated, glassy, white and brownish cut surface, containing areas of microcystic degeneration

Chromosomal imbalances obtained by comparative genomic hybridization included gains of the chromosomal regions 1q, 6p, 13q, and the whole chromosome 8, as well as chromosomal losses of 6q (Fig. 3).

For differential diagnosis of the pancreatic tumor, a malignant peripheral nerve sheath tumor with focal pigmentation and a malignant melanoma were considered. As the brownish cerebral mass displayed histomorphological and immunohistochemical features comparable with the pancreatic tumor, it was classified as a metastasis.

Discussion

In the present study, we describe the rare case of a malignant non-epithelial tumor of the pancreas, showing focal pigmentation and combined morphological features of MPNST and malignant melanoma.

MPNST are most commonly located in the proximal portions of the upper and lower extremities and the trunk, as well as in the head and neck regions [20]. Visceral locations are very rare. Within the pancreas, however, MPNST represent the second most frequent non-epithelial malignant neoplasms, following leiomyosarcomas [9, 10].

To our knowledge, there have been no reports of malignant melanomas primarily arising in the pancreas. However, the pancreas is commonly affected by metastatic spread of melanoma, as demonstrated by autopsy series in up to 37% of cases [15]. Metastatic melanoma in the pancreas usually occurs as part of disseminated metastatic disease. Less frequently, singularly pancreatic metastases were observed as well, with occult primary tumors in some cases [2]. This latter phenomenon has been

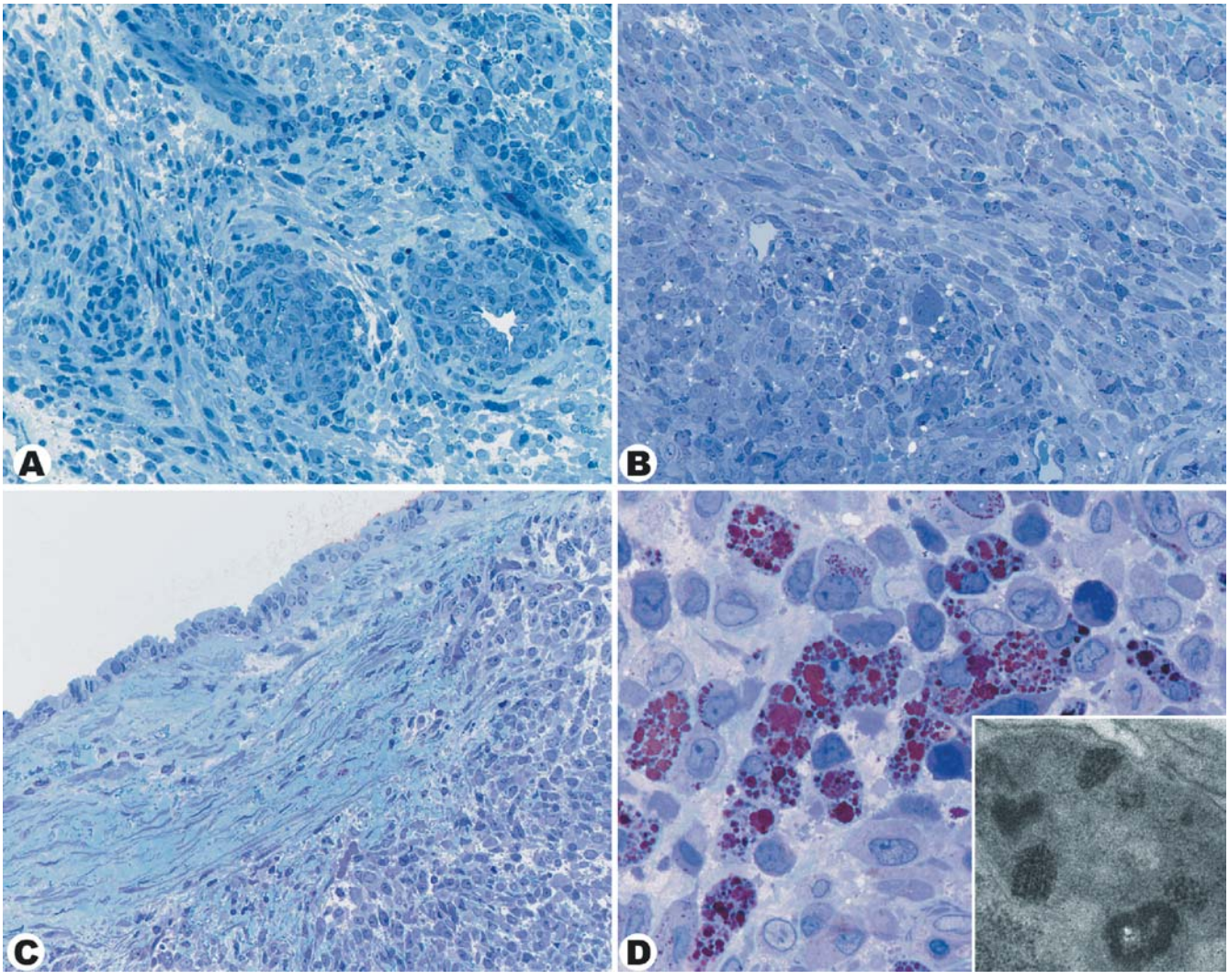

Fig. 2 As demonstrated on semi-thin sections, the pancreatic tumor presented a histomorphologically heterogeneous picture, including spindle-shaped cells and plump polygonal cells with epitheloid appearance (**A**, **B**, **C**, ×200; **D**, ×630), as well as multinucleated giant cells (**B**). Focally, the tumor cells displayed intracytoplasmatic pigmentation (**D**), ultrastructurally corresponding to melanosomes (**D**, *inset*, ×16,000)

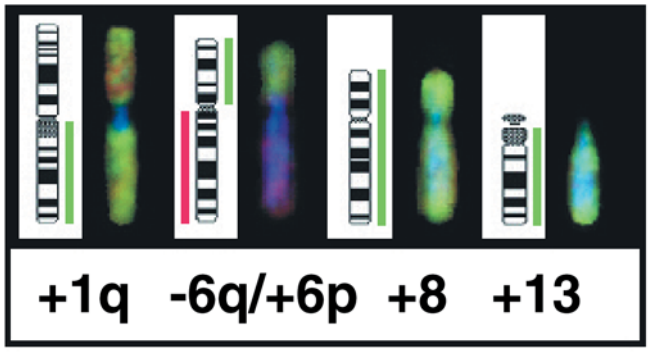

Fig. 3 Comparative genomic hybridization revealed gains of chromosomal regions 1q, 6p, 13q, and the whole chromosome 8, as well as chromosomal losses of 6q

explained by spontaneous regression of the primary tumor and is commonly observed in malignant melanomas [1].

Both MPNST and malignant melanomas originate from neural crest-derived cells [6, 18, 20]. This close histogenetic relationship is reflected by a considerable histomorphological overlap between both entities. Thus, some cases of MPNST (formerly also known as "malignant schwannomas") have been found to show melanin pigmentation, especially when originating from spinal or autonomic nerves near the midline [5, 12, 20]. However, malignant melanomas may display the morphological features of MPNST. This has primarily been observed in melanoma metastases, with primary tumors displaying either the classical morphological features of malignant melanoma or remaining occult [6]. However, primary malignant melanomas resembling MPNST were reported as well [3].

Considerable overlap between features characteristic of MPNST and malignant melanoma was also observed

for the pigmented pancreatic tumor of the present study. Thus, despite extensive histomorphological, immunohistochemical, and ultrastructural examinations, the diagnosis of either MPNST or malignant melanoma could not be definitely clarified.

Beyond morphologically based diagnostic criteria, chromosomal analyses have been frequently recommended as additional tools for the establishment of the diagnosis in soft tissue tumors [16]. In the present study, comparative genomic hybridization was used to detect chromosomal imbalances. These included chromosomal gains on 1q, 6p, 8, and 13q and chromosomal losses on 6q. However, none of the observed chromosomal abnormalities was confined to either only MPNST or malignant melanoma, as considerable overlap between both entities also seems to exist on the chromosomal level [11, 17, 18].

Criteria recommended for the differential diagnosis between MPNST and malignant melanoma [6] were applied to the present study, with the following features favoring the diagnosis of a MPNST: the tumor was located within the nerve-rich pancreas and, therefore, in close anatomic relationship with major nerves. A direct relationship to a nerve was not detected in the present case; however, microscopically, numerous smaller nerves were found to intersperse the tumor. Immunohistochemically, the tumor showed only focal expression of S100 as opposed to diffuse staining, the latter characteristic for malignant melanoma. Positive staining with the melanotic marker HMB-45 was only found in pigmented areas of the tumor, whereas the vast majority of tumor cells did not express HMB-45. Finally, clinical examination failed to detect previous or concomitant primary malignant melanoma.

However, solitary metastatic spread of a pancreatic MPNST into the brain seems rather unusual. Therefore, the diagnosis of an occult malignant melanoma with metastatic spread into the pancreas and the brain should not be definitively ruled out. Beyond this, the diagnosis of a composite tumor consisting of MPNST and malignant melanoma should be considered as well. Comparable cases have been described for angiosarcomas arising within MPNST [13].

In summary, extensive histomorphological, immunohistochemical, ultrastructural, and chromosomal analyses were not sufficient to clearly define the diagnosis of either MPNST with focal pigmentation or malignant melanoma resembling MPNST, due to their close histogenetic relationship. Considering subtle morphological differences between both entities and recognizing a rather unusual pattern of metastatic spread, we favor the diagnosis of a pancreatic MPNST with focal melanin pigmentation.

Acknowledgements We kindly thank Professor G. Klöppel for his expert advice. Furthermore, we thank Mrs. Antoni and Mr. Rieger for their support in performing the electron microscopic analyses, Mrs. Horr and Mr. Moyers for pictorial work, and our technical assistants, especially Mrs. Sturm and Mrs. Appel, for excellent technical assistance.

References

1. Avril MF, Charpentier P, Margulis A, Guillaume JC (1992) Regression of primary malignant melanoma with metastases. Cancer 69:1377–1381
2. Bianca A, Carboni N, Di Carlo V, Falleni M, Ferrero S, Liverani C, Staudacher C, Turra G, Vergani D, Zerbi A (1992) Pancreatic malignant melanoma with occult primary lesion. A case report. Pathologica 84:531–537
3. Diaz-Cascajo C, Hoos A (2000) Histopathologic features of malignant peripheral nerve sheath tumor are not restricted to metastatic malignant melanoma and can be found in primary malignant melanoma also. Am J Surg Pathol 24:1438–1439
4. Isola J, DeVries S, Chu L, Ghazvini S, Waldman F (1994) Analysis of changes in DNA sequence copy number by comparative genomic hybridization in archival paraffin-embedded tumor samples. Am J Pathol 145:1301–1308
5. Jones H, Theaker JM, Kelly PMA, Woods CG, Greenall MJ (1990) Melanocytic schwannomas arising within localized pigmented neurofibromatosis of the sympathetic chain. Histopathology 17:567–569
6. King R, Busam K, Rosai J (1999) Metastatic malignant melanoma resembling malignant peripheral nerve sheath tumor. Am J Surg Pathol 23:1499–1505
7. Komoda H, Nishida T, Yumiba T, Nishikawa K, Kitagawa T, Hirota S, Ito T, Matsuda H (2002) Primary leiomyosarcoma of the pancreas—a case report and case review. Virchows Arch 440:334–337
8. Lee JS, Kim HS, Jung JJ, Han SW, Kim YB (2001) Ancient schwannoma of the pancreas mimicking a cystic tumor. Virchows Arch 439:697–699
9. Lüttges J, Pierré E, Zamboni G, Weh G, Lietz H, Kußmann J, Klöppel G (1997) Maligne nichtepitheliale Tumoren des Pankreas. Pathologe 18:233–237
10. Lüttges J, Mentzel T, Hübner G, Klöppel G (1999) Solitary fibrous tumor of the pancreas: a new member of the small group of mesenchymal pancreatic tumours. Virchows Arch 435:37–42
11. Mechtersheimer G, Otano-Joos M, Ohl S, Benner A, Lehnert T, Willeke F, Möller P, Otto HF, Lichter P, Joos S (1999) Analysis of chromosomal imbalances in sporadic and NF1-associated peripheral nerve sheath tumors by comparative genomic hybridisation. Gen Chromosom Cancer 25:362–369
12. Mennemeyer RP, Hallmann KO, Hammar SP, Raisis JE, Tyrus JS, Bockus D (1979) Melanotic schwannoma. Clinical and ultrastructural studies of three cases with evidence of intracellular melanin synthesis. Am J Surg Pathol 3:3–10
13. Mentzel T, Katenkamp D (1999) Intraneural angiosarcoma and angiosarcoma arising in benign and malignant peripheral nerve sheath tumors: clinicopathological and immunohistochemical analysis of four cases. Histopathology 35:114–120
14. Morita S, Okuda J, Sumiyoshi K, Taketani M, Moriguchi A, Katsu K, Tanigawa N (1999) Pancreatic schwannoma: report of a case. Surg Today 29:1093–1097
15. Patel JK, Didolkar MS, Pickren JW, Moore RH (1978) Metastatic pattern of malignant melanoma: a study of 215 autopsy cases. Am J Surg Pathol 135:807–810
16. Sandberg AA, Bridge JA (eds) (1995) The cytogenetics of bone and soft tissue tumors. Springer, Berlin Heidelberg New York
17. Schmidt H, Würl P, Taubert H, Meye A, Bache M, Holzhausen HJ, Hinze R (1999) Genomic imbalances of 7p and 17q in malignant peripheral nerve sheath tumors are clinically relevant. Gen Chromosom Cancer 25:205–211
18. Slominski A, Wortsman J, Carlson AJ, Matsuoka LY, Balch CM, Mihm MC (2001) Malignant melanoma. Arch Pathol Lab Med 125:1295–1306
19. Solcia E, Capella C, Klöppel G (1997) Tumors of the Pancreas. In: Rosai J, Sobin LH (eds) Atlas of Tumor Pathology, 3rd Series, Fascicle 20. Armed Forces Institute of Pathology, Washington, DC
20. Weiss SW, Goldblum JR (eds) (2001) Enzinger's and Weiss's soft tissue tumors, 4th edn. Mosby, St. Louis

Virchows Arch (2004) 444:194–197
DOI 10.1007/s00428-003-0953-5

CASE REPORT

Ji Shin Lee · Young Bog Kim · Kyung Whan Min

Metaplastic mammary carcinoma with osteoclast-like giant cells: identical point mutation of p53 gene only identified in both the intraductal and sarcomatous components

Received: 9 July 2003 / Accepted: 12 October 2003 / Published online: 8 January 2004

Abstract Metaplastic mammary carcinoma with osteoclast-like giant cells is a rare neoplasm, and the histogenesis of this tumor remains controversial. A case of metaplastic mammary carcinoma with osteoclast-like giant cells in a 72-year-old woman is reported with p53 mutational analysis. Microscopically, the tumor was composed of a dominant sarcomatous stromal component containing osteoclast-like giant cells and a minor component of intraductal carcinoma. Immunostaining for p53 revealed strong positivity in both intraductal and sarcomatous components, but not in osteoclast-like giant cells. Mutational analysis of the p53 gene disclosed an identical point mutation in both intraductal and sarcomatous components, but not in osteoclast-like giant cells, indicating that both components share the same progenitor cells, and osteoclast-like giant cells represent a reactive infiltrate.

Keywords Breast neoplasm · Metaplastic carcinoma · Osteoclast-like giant cells · p53 mutation

Introduction

Metaplastic mammary carcinoma with osteoclast-like giant cells is a rare tumor [4, 12]. This tumor is characterized by an admixture of intraductal or infiltrating carcinoma with areas of bland spindle cell or sarcomatous stroma containing osteoclast-like giant cells.

The histogenesis of this tumor remains controversial and centers around the possibilities of the same progenitor cells giving rise to three different cell lines or each deriving from different progenitor cells. If three histological components of metaplastic carcinoma with osteoclast-like giant cells originated from the same progenitor cells, they are more likely to have identical genetic alterations [1]. Mutation of p53 gene is most commonly observed in various human neoplasms, including breast carcinoma [3, 5].

We report a case of metaplastic carcinoma with osteoclast-like giant cells in which a mutational analysis of p53 gene was carried out in three different components, using microdissection techniques to determine histogenesis.

J. S. Lee (✉)
Department of Pathology,
Seonam University, College of Medicine,
720 Kwangchi-Dong, Namwon, 590-711 Chollabuk-Do, Korea
e-mail: jshinlee@hanmail.net
Tel.: +82-63-6200352
Fax: +82-63-6200355

Y. B. Kim
Department of Surgery,
Seonam University, College of Medicine,
Namwon, Korea

K. W. Min
Department of Pathology,
Deaconess Hospital,
Oklahoma, USA

Clinical history

A 72-year-old woman was admitted to the hospital for diagnosis and treatment of a palpable mass in the upper outer quadrant of the right breast. The mass was hard but focally soft. She had no past or family history of breast disease. An excisional biopsy of the right breast revealed a metaplastic carcinoma with osteoclast-like giant cells. Modified radical mastectomy with axillary lymph-node dissection was performed. The 18 lymph nodes sampled showed no evidence of metastatic disease. After 25 months of follow-up, the patient remains free of disease.

Materials and methods

Immunohistochemistry

Immunohistochemical staining of formalin-fixed, paraffin-embedded sections was performed using the avidin-biotin immunoperoxidase method. The antibodies used are listed in Table 1. The pattern of intensity of cellular immunoreactivity was graded as positive (>30%), intermediate (10–30%), focal (a single focus or multiple discrete foci), or negative.

Table 1 Description of antibodies and immunohistochemical findings. *OGC* osteoclast-like giant cells, *EMA* epithelial membrane antigen

Antibodies			Components		
Name	Source	Pretreatment	Intraductal	Sarcomatous	OGC
Cytokeratin (AE1/AE3)	Dako	Pepsin	Positive	Negative	Negative
EMA	Dako	None	Positive	Negative	Negative
Vimetin	Dako	None	Focal	Positive	Intermediate
Actin	Dako	None	Negative	Focal	Negative
Desmin	Zymed	None	Negative	Negative	Negative
α-1-Antitrypsin	Dako	None	Negative	Negative	Intermediate
CD68	Dako	Microwave	Negative	Negative	Positive
c-erbB-2	Dako	Microwave	Negative	Negative	Negative
Estrogen receptor	Dako	Microwave	Negative	Negative	Negative
Progesterone receptor	Dako	Microwave	Negative	Negative	Negative
p53	Dako	Microwave	Positive	Positive	Negative

Microdissection and p53 mutation analysis

Several 7-μm-thick sections were stained with hematoxylin and eosin and dried for 20 min at room temperature. Intraductal carcinoma, sarcomatous component, osteoclast-like giant cells, and normal breast tissues were respectively microdissected, using a PixCell II Laser Capture Microdissection System (Arcturus Engineering, Mountain View, California, USA). Dissected tissues were placed in a 30-μl lytic solution (0.5% Tween 20, 1 mM ethylenediaminetetraacetate, pH 8.0, and 50 mM Tris-HCl, pH 8.5), proteinase K (2 mg/ml of lytic solution) was added, and the mixture was incubated for 48 h at 37°C. Exons 5 to 8 of the p53 gene were amplified by the polymerase chain reaction. The primers for exons 5 to 8 and the cycle conditions were described previously [2]. The amplified DNA was confirmed by electrophoresis on 2% agarose. DNA was subjected to direct sequencing using an ABI Prism BigDye Terminator Cycle Sequencing Ready Reaction Kit (Perkin-Elmer, Norwalk, Connecticut, USA).

Results

Pathological findings

Gross pathological examination of the excisional specimen revealed an ill-defined, nodular mass of 5.3× 4×3.5 cm in dimension. It appeared firm and solid with foci of visible hemorrhage. Microscopically, the majority of the tumor consisted of sheets of large, round, and polygonal cells with markedly pleomorphic nuclei and numerous abnormal mitoses (Fig. 1A). A deeply eosinophilic osteoid-like substance was present, frequently surrounding individual tumor cells. Multinucleated osteoclast-like giant cells were observed scattered among the pleomorphic tumor cells. The resulting appearance was typical of osteogenic sarcoma. The osteoclast-like giant cells had deeply eosinophilic finely vacuolated cytoplasms and multiple round to oval nuclei aggregating centrally within the cytoplasm. Occasional mononuclear and binuclear forms were also noted. In addition, the tumor presented a minor component composed of intraductal carcinoma exhibiting micropapillary or cribriform growth pattern. Tumor cells in the intraductal component were typical of moderately to poorly differentiated ductal carcinoma. The areas of intraductal carcinoma were admixed or contiguous with the sarcomatous component (Fig. 1B). Osteoclast-like giant cells were not found in the area of intraductal locations. There were also areas of prominent hemorrhage and focal myxoid change.

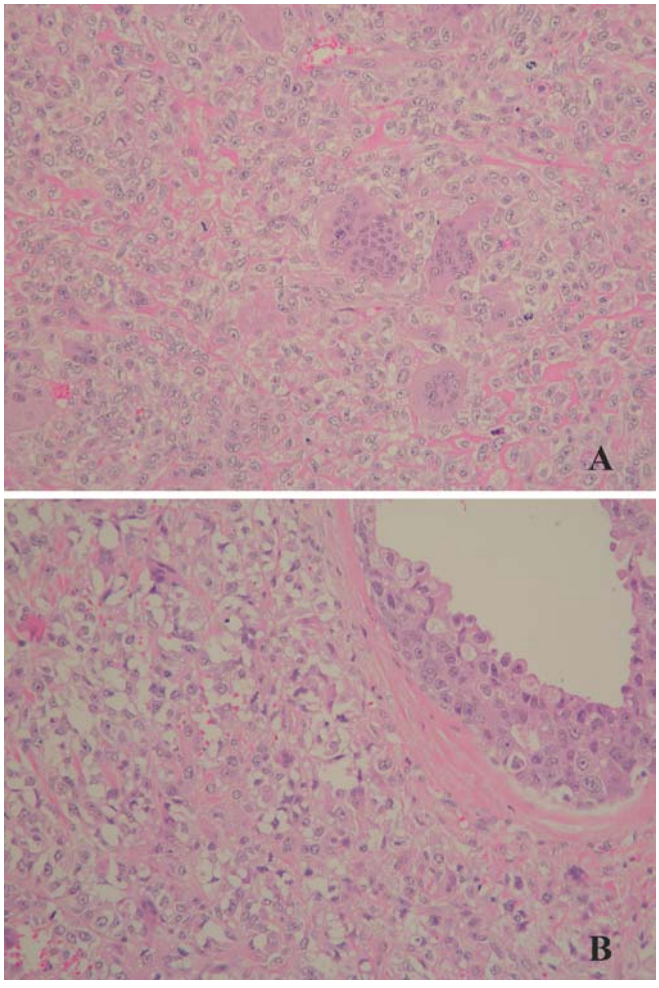

Fig. 1 A The predominant microscopic pattern shows osteoclast-like giant cells scattered in a background of variably pleomorphic cells (hematoxylin-eosin, original magnification ×200). **B** The intraductal carcinoma is contiguous with sarcomatous component (hematoxylin-eosin, original magnification ×200)

Immunohistochemistry

The immunohistochemical results are shown on Table 1. The intraductal component showed positive reactivity for cytokeratin, epithelial membrane antigen (EMA), and focally for vimentin. The tumor cells in the sarcomatous

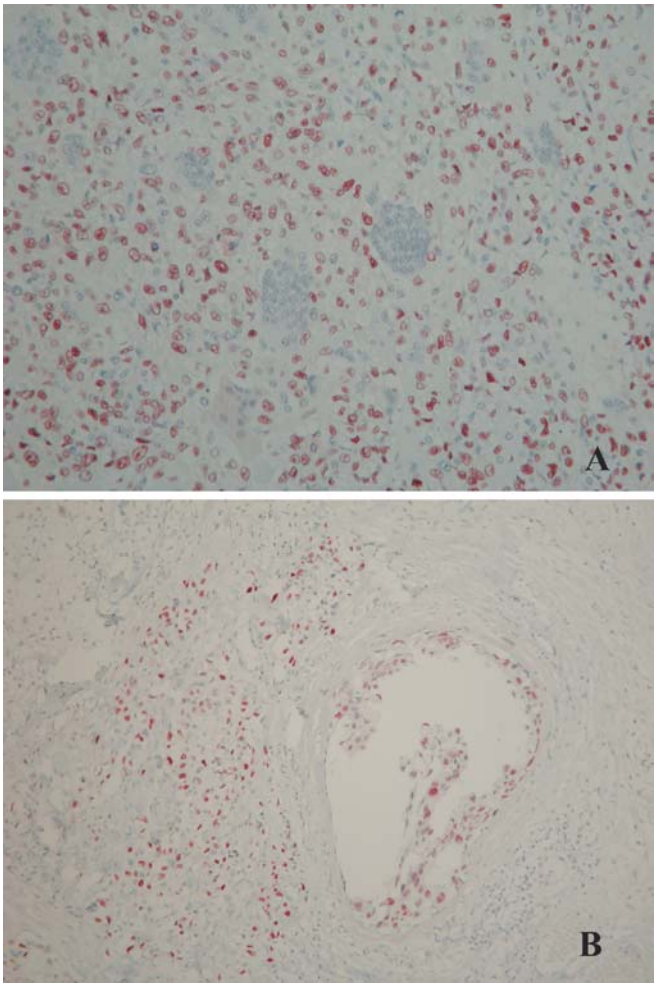

Fig. 2 Immunohistochemical staining of p53. **A** Sarcomatous component displays strong nuclear immunoreactivity with p53, but osteoclast-like giant cells are completely non-immunoreactive (original magnification ×200). **B** Intraductal component shows strong p53 staining (original magnification ×100)

component were positive for vimentin and actin and were negative for cytokeratin and EMA. The osteoclast-like giant cells were only positive for vimentin, α-1-antitrypsin, and CD68. Stains for estrogen receptor, progesterone receptor, and c-erb-B2 were negative in all three components. Immunoreactivity of p53 was detected in both intraductal and sarcomatous components, but not in osteoclast-like giant cells (Fig. 2A, B).

p53 Mutation analysis

In the PCR and sequencing analyses, the same point mutation was identified at codon 185 of exon 5 (transition G→A) in both intraductal and sarcomatous components (Fig. 3). The same point mutation was not observed in the samples from osteoclast-like giant cells and normal breast tissues.

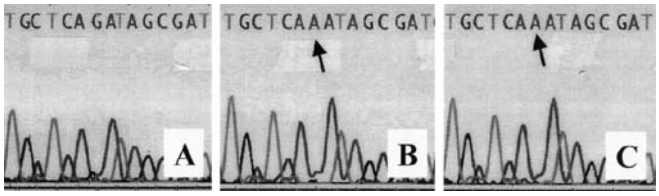

Fig. 3 p53 sequence data of exon 5. G→A transposition mutations are detected in both intraductal and sarcomatous components. *Arrows* indicate site of mutation (**A** Osteoclast-like giant cells. **B** Intraductal component. **C** Sarcomatous component)

Discussion

Metaplastic carcinomas of the breast are uncommon and have been classified morphologically into five distinct subtypes: matrix-producing carcinoma, spindle-cell carcinoma, carcinosarcoma, pure squamous cell carcinoma of ductal origin, and metaplastic carcinoma with osteoclast-like giant cells [11, 12]. Metaplastic carcinoma with osteoclast-like giant cells is distinguished from carcinosarcoma by the presence of osteoclast-like giant cells within cellular stroma [12]. Osteoclast-like giant cells have also been observed in other breast carcinomas [8]. When the osteoclast-like giant cells are present in carcinomas, they are usually found abutting nests of epithelial tumor cells, and are also identified within lumens formed by the cancer cells. However, the osteoclast-like giant cells in metaplastic carcinoma are found within cellular stroma between tumor cells of the sarcomatous component, but are not admixed with tumor cells in carcinomatous areas. In the present case, osteoclast-like giant cells were present in the areas showing characteristic osteosarcomatous differentiation.

To elucidate the histogenetic relationship between epithelial and heterologous elements in metaplastic carcinoma, many investigators applied immunohistochemical analysis, and reported results have been inconsistent. Studies by some authors found coexpression of epithelial and mesenchymal markers in the stromal component of metaplastic carcinomas with osteoclast-like giant cells [12], while other studies failed to find coexpression of vimentin in both elements of metaplastic carcinoma [6, 7]. Cytokeratin expression was only found in the carcinomatous component [6, 7]. In the present case, immunoreactivity for epithelial markers, such as cytokeratin and EMA, was not detected in the sarcomatous component, while vimentin was positive in both sarcomatous and intraductal components. The findings in these reports suggest that tumor cells in metaplastic carcinoma with osteoclast-like giant cells undergo divergent differentiation. Similar findings have also been reported [4].

Recent investigators utilized molecular techniques to characterize clonality of the epithelial and stromal components of these tumors. These investigators took advantage of the fact that p53 gene is one of the most frequent sites of mutation in breast and mutations involving p53 gene are considered to be a relatively late

event in the pathway of malignant transformation cancers [3, 5]. If the three components of metaplastic carcinoma with osteoclast-like giant cells are derived from entirely separate clones, then disparities in p53 mutational change in the three components should be present. However, if the three components of metaplastic carcinoma with osteoclast-like giant cells are derived from the same progenitor cells, the disparities would not be expected. Our immunohistochemical studies demonstrated a strong p53 expression among the intraductal as well as sarcomatous components, whereas the osteoclast-like giant cells were negative for p53. We have employed a microdissection technique to ensure the purity of each component of the tumor. The result of p53 mutation analysis showed the same point mutation in the intraductal and sarcomatous components, whereas the normal tissue and osteoclast-like giant cells were negative for p53 mutation. The results support the concept that the same progenitor cells produce the intraductal and sarcomatous components, although they expressed divergent histological phenotypes. They also indicate that osteoclast-like giant cells are not derived from the same progenitor cells and are most likely a reactive infiltrate. Osteoclast-like giant cells in our case were only immunoreactive for vimentin, α-1-antitrypsin, and CD68, indicating that they belong to the monocyte–histiocyte–macrophage system.

Identical single point mutation of p53 gene in both intraductal and sarcomatous components in our patient and in patients reported by previous investigators render strong support for the concept that the same progenitor cell gives rise to both components [9, 10]. To the best of our knowledge, no previous series included a case of metaplastic carcinoma with osteoclast-like giant cells containing osteogenic sarcoma. We believe that the present case represents the first such example.

In conclusion, the intraductal and sarcomatous components of metaplastic carcinoma with osteoclast-like giant cells might originate from the same progenitor cells, and osteoclast-like giant cells represent a reactive infiltrate.

References

1. Chhieng C, Cranor M, Lesser ME, Rosen PP (1998) Metaplastic carcinoma of the breast with osteocartilaginous heterologous elements. Am J Surg Pathol 22:188–194
2. Dalbagni G, Ren ZP, Herr H, Cordon-Cardo C, Reuter V (2001) Genetic alterations in TP 53 in recurrent urothelial cancer: a longitudinal study. Clin Cancer Res 7:2797–2801
3. Harris AL (1990) Mutant p53: the commonest genetic abnormality human cancer? J Pathol 162:5–6
4. Herrington CS, Tarin D, Buley I, Athanasou N (1994) Osteosarcomatous differentiation in carcinoma of the breast: a case of "metaplastic" carcinoma with osteoclasts and osteoclast-like giant cells. Histopathology 24:282–285
5. Marks JR, Humphrey PA, Wu K, Berry D, Bandarenko N, Kerns BJ, Iglehart JD (1994) Overexpression of p53 and HER-2/neu proteins as prognostic markers in early stage breast cancer. Ann Surg 219:332–341
6. Meis JM, Ordonez NG, Gallager HS (1987) Sarcomatoid carcinoma of the breast: an immunohistochemical study of six cases. Virchows Arch 410:415–421
7. Oberman HA (1987) Metaplastic carcinoma of the breast. A clinicopathologic study of 29 patients. Am J Surg Pathol 11:918–929
8. Tavassoli FA, Norris HJ (1986) Breast carcinoma with osteoclastlike giant cells. Arch Pathol Lab Med 110:636–639
9. Wada H, Enomoto T, Tsujimoto M, Nomura T, Murata Y, Shroyer KR (1998) Carcinosarcoma of the breast: molecular-biological study for analysis of histogenesis. Hum Pathol 29:1324–1328
10. Wang X, Mori I, Tang W, Yang Q, Nakamura M, Nakamura Y, Sato M, Sakurai T, Kennichi K (2001) Metaplastic carcinoma of the breast: p53 analysis identified the same point mutation in the three histologic components. Mod Pathol 14:1183–1186
11. Wargotz ES, Norris HJ (1989) Metaplastic carcinoma of the breast: III. Carcinosarcoma. Cancer 64:1490–1499
12. Wargotz ES, Norris HJ (1990) Metaplastic carcinomas of the breast: V. Metaplastic carcinoma with osteoclastic giant cells. Hum Pathol 21:1142–1150

Virchows Arch (2004) 444:198–201
DOI 10.1007/s00428-003-0919-7

CASE REPORT

Markus Tiemann · Steffi Häring · Marcus Heidemann · Jan Reichelt · Alexander Claviez

Mucosa-associated lymphoid tissue lymphoma in the conjunctiva of a child

Received: 15 July 2003 / Accepted: 23 September 2003 / Published online: 6 December 2003

Abstract Marginal zone lymphoma of the mucosa-associated lymphoid tissue (MALT) occurring in the conjunctiva has yet not been described in pediatric patients. We present a case of a 10-year-old girl with a MALT lymphoma involving the conjunctiva. The tumor consisted of plasma cells and marginal zone cells with discrete epitheliotropism. Immunohistochemical studies revealed positivity for CD20 and cytoplasmic immunoglobulin λ light chain restriction. Polymerase chain reaction-based molecular analysis of the infiltrate showed a monoclonal rearrangement for the hypervariable complimentary determining region III immunoglobulin region; whereas, a polyclonal pattern was seen for the T-cell receptor γ chain. Extensive further examination, including molecular techniques, revealed that the lymphoma was restricted to the conjunctiva (stage IA) and was not associated with any specific infection. The patient was treated with surgery and additional local cryotherapy. After 15 months of follow-up, the patient remains in complete remission.

Keywords MALT lymphoma · Conjunctiva · Child

M. Tiemann (✉)
Department of Hematopathology,
University of Kiel,
Niemannsweg 11, 24105 Kiel, Germany
e-mail: mtiemann@path.uni-kiel.de
Tel.: +49-43-15973427
Fax: +49-43-15973486

M. Heidemann · A. Claviez
Department of Pediatrics,
University of Kiel,
Schwanenweg 20, 24105 Kiel, Germany

S. Häring · J. Reichelt
Department Ophthalmology,
University of Kiel,
Hegewischstraße 2, 24105 Kiel, Germany

Introduction

Marginal zone B cell lymphoma has become a well-defined entity since the concept of non-Hodgkin's lymphoma (NHL) arising from the mucosa-associated lymphatic tissue (MALT) was established by Isaacson et al. [5]. More recently, the new World Health Organization (WHO) classification of malignant lymphomas included marginal zone lymphoma of the MALT and listed several extranodal as well as nodal variants with a unique immunophenotype [6]. There is a growing body of evidence that MALT lymphomas are characterized by specific chromosomal aberrations, such as trisomy 3 and translocations involving the *MALT1* gene [3, 10, 13, 19]. In the last decade, it has been shown that this tumor may occur in various extraintestinal localizations, sometimes even in a region without a preexisting mucosa. MALT lymphomas mainly occur in the sixth and seventh decades of life. In the pediatric age group, this lymphoma is very rare and has been associated with human immunodeficiency virus, but has been also described in immunocompetent children [1]. Here, to the best of our knowledge, we describe for the first time a conjunctival MALT lymphoma in a child.

Clinical history

A 10-year-old girl presented with a painless swelling of the left nasal conjunctiva of a 4-week duration. Symptomatic therapy with corticosteroid eye drops was unsuccessful. Therefore, an excisional conjunctival biopsy was performed under local anesthesia. Unexpectedly, a MALT lymphoma was diagnosed, and a thorough clinical staging was performed. Normal values were obtained for blood and complete serum chemistry. On serum electrophoresis, no paraprotein was detectable. Ultrasonography of peripheral lymph nodes, thyroid gland and abdomen, as well as chest radiography, were normal. Magnetic resonance tomography revealed no cervical, thoracic or cerebral lymphoma manifestations. Esophagogastroduodenoscopy was normal; *H. pylori* was not detectable. Serologically, there was no evidence of any specific viral infection. No lymphoma cells were found in the bone marrow or cerebrospinal fluid. Control examination of both eyes under general anesthesia ruled out residual and contralateral tumor. Therefore, the diagnosis

of a conjunctival MALT lymphoma without systemic involvement (stage I_EA) was made, and no cytostatic drugs or radiotherapy were given. To enhance the effect of local surgical treatment and to avoid late effects from percutaneous radiotherapy, the patient was treated with additional cryotherapy [4]. The girl remains in complete remission 15 months after diagnosis.

Materials and methods

Sections from the formalin-fixed, paraffin-embedded conjunctival biopsy specimen were stained with hematoxylin & eosin (H&E), Giemsa and periodic acid-Schiff (PAS). The immunohistochemical staining employed the alkaline phosphatase-anti-alkaline phosphatase (APAAP) method for monoclonal antibodies and the streptavidin-biotin-complex method for the polyclonal antibodies. The monoclonal antibodies applied included L26 (CD20), anti-CD5 (CD5), Ki-B3 (pan B-cell antigen) and DBA44 (B-cell antigen). The polyclonal antibodies used were anti-CD3 (CD3), anti-μ (IgM), anti-κ (immunoglobulin light chain) and anti-λ (immunoglobulin light chain). Rearrangement analyses of the hypervariable complimentary determining region (CDR) III region of the immunoglobulin heavy chain (IgH) and γ chain of the T-cell receptor (TCR γ) were performed on the conjunctival specimen, bone marrow aspirate and peripheral blood. T-cell receptor rearrangement was demonstrated using a standard multiplex polymerase chain reaction (PCR) system according to Trainor et al. [16]. IgH rearrangement was analyzed using a semi-nested PCR system according to Wan et al. [17]. PCR products were subjected to capillary electrophoresis with an automated analyzer (ABI 310).

Results

Histology of the conjunctival specimen revealed sheets of lymphoid cells with slightly indented nuclei and a sparse cytoplasm, reflecting the typical morphology of marginal zone cells. In addition, there were a considerable number of tumor cells with plasmacytic differentiation. The infiltrate showed discrete epitheliotropism caused by marginal zone cells, resulting in lymphoepithelial lesions of the conjunctival epithelium. The marginal zone cells stained for CD5−, CD20+, Ki-B3− and DBA44−. Plasma cells and marginal zone cells showed immunoglobulin restriction for μ and κ (Fig. 1A, B, C, D). Molecular analysis by PCR revealed an immunoglobulin rearrangement of the hypervariable CDR III region with a predominant clone of 77 base pair length and a polyclonal rearrangement pattern for TCR γ chain (Fig. 2A, B). Molecular analyses of the bone marrow and peripheral blood showed polyclonal rearrangement patterns.

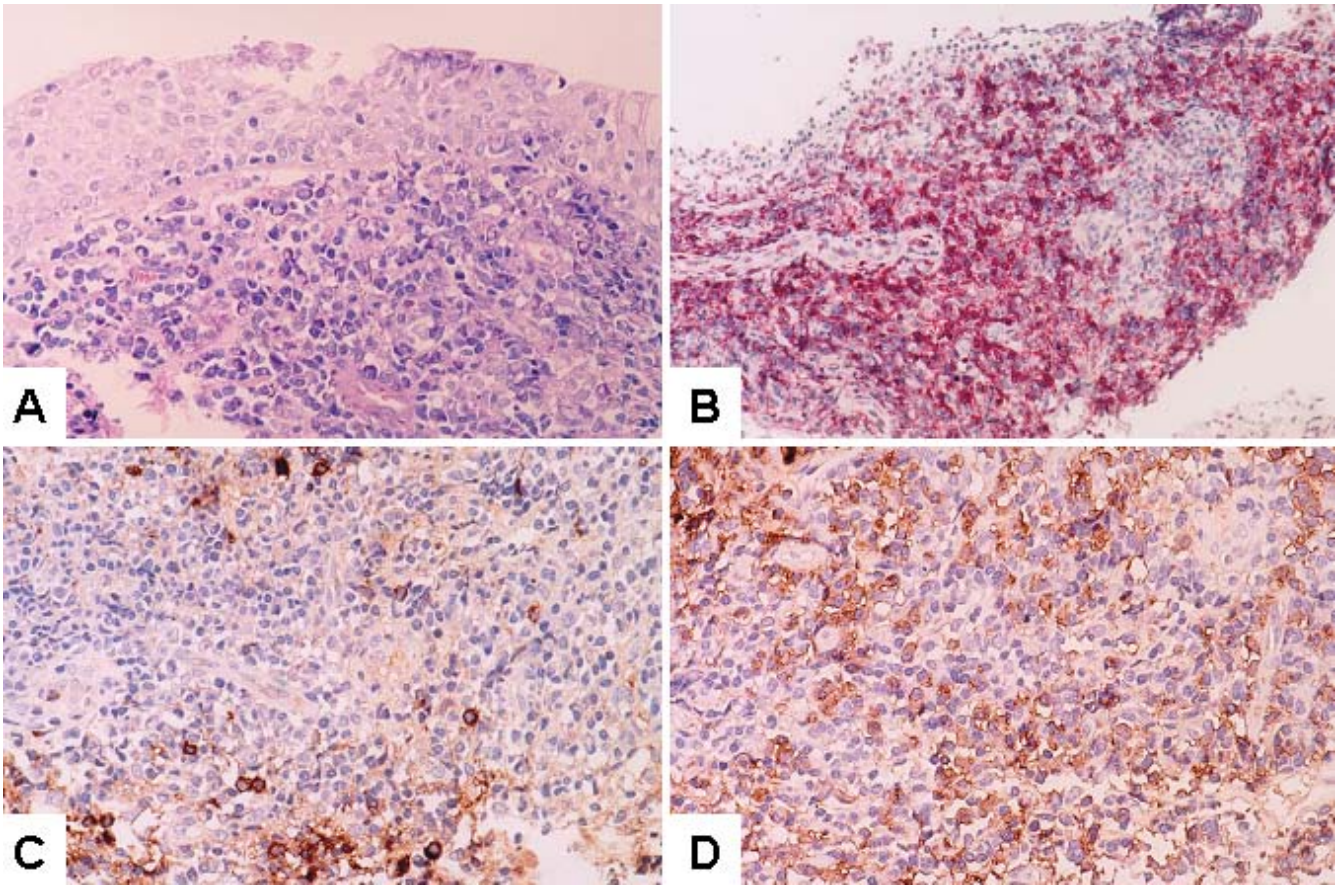

Fig. 1 **A** Conjunctival tumor cell infiltrate showing discrete epitheliotropism. Giemsa, ×100. **B** Immunohistochemical CD20 expression of tumor cells. Partial CD20 antigen loss of plasma cells. Alkaline phosphatase-anti-alkaline phosphatase, ×100. **C** Immunostaining for κ light chain revealing only few reactive plasma cells. Streptavidin-biotin complex, ×200. **D** Immunostaining for λ light chain restricted to tumor plasma cells. Streptavidin-biotin complex, ×200

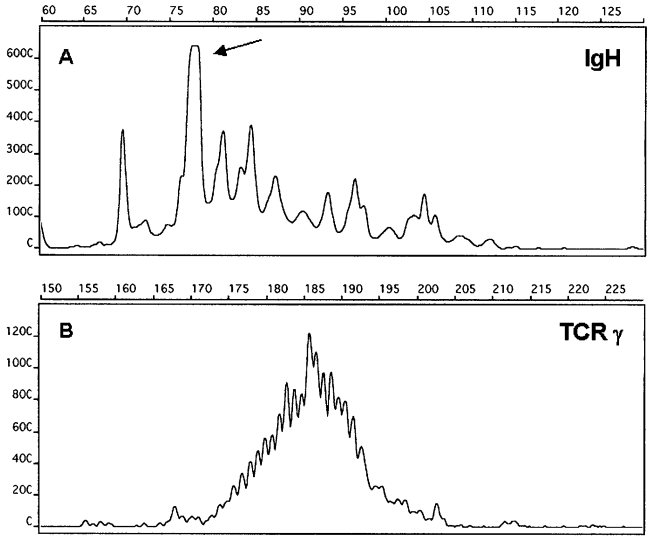

Fig. 2 A Gene scan analysis of the hypervariable complimentary determining region III region of the immunoglobulin heavy chain. Strong clonal peak at 77 bp. The top of the peak is cut due to the large amount of tumor clone polymerase chain reaction. **B** Gene scan analysis of the γ chain of the T-cell receptor showing a polyclonal pattern

Discussion

Primary extranodal B-cell lymphoma is a distinct entity, arising in preformed lymphoid tissues (e.g., in Peyer's plaques) or in newly formed lymphoid compartments. The latter may be acquired during inflammatory processes, such as *H. pylori* gastritis or autoimmune diseases, e.g., Hashimoto's thyroiditis or myoepithelial sialadenitis, associated with Sjögren's syndrome. In adults, Sjögren's syndrome has been observed as a prodromal stage of conjunctival or lacrimal MALT lymphoma. No association with infectious agents (*H. pylori, Borrelia burgdorferi*) has been observed in conjunctival lymphoma thus far.

Eye involvement in NHL is estimated to occur with a frequency of less than 1%. Among these NHL, MALT lymphomas that usually occur in the gastrointestinal tract account for half of the cases and originate from the conjunctiva and lacrimal glands. Recently, a series of 48 children, adolescents and young adults suffering from marginal zone lymphoma has been published [14]. One-third of their patients had extranodal lymphomas. In this subgroup, only one child with a MALT lymphoma involving the lacrimal gland, but with inconclusive immunohistochemistry, was included.

A review of the literature revealed that all patients with a MALT lymphoma in the conjunctiva reported thus far were adults. This appears, therefore, to be the first report of a conjunctival MALT lymphoma occurring in a child.

Medeiros and Harris described several distinct histological subtypes in a large series of orbital and conjunctival lymphomas. Only a subset of the tumors displayed the typical histological features of marginal zone lymphomas: small lymphocytic lymphoma with plasmacytoid differentiation, dense infiltrates of centrocytoid cells, and benign-appearing lymphoid follicles with reactive germinal centers and a variable interfollicular mixture of lymphocytes, plasma cells and histiocytes [8]. However, the infiltrate in our patient consisted of small lymphoid cells and monotypic plasma cells. As with other MALT lymphomas, the tumor showed a distinct epitheliotropism. The classification of conjunctival lymphoma, however, remains problematic using morphology alone or only pan-B cell or pan-T cell immunohistochemical markers. An exact immunophenotyping of B cell subpopulations (CD5–, CD10–, CD20+, CD21–, CD23–, Ki-B3–) is, therefore, mandatory to classify the tumor according to the WHO criteria [18]. Therefore, it is likely that even in large published series on conjunctival tumors, MALT lymphomas comprise only a smaller portion [7, 8]. In addition, monoclonality of tumor cells was demonstrated immunohistochemically and by using molecular methods.

Systemic disease at presentation or during the course can be found in up to one-third of patients with MALT lymphoma [9, 11, 15]. In a large retrospective single-center analysis on a variety of conjunctival benign and malignant lymphoid tumors, 11 of 64 patients with unilateral tumors developed systemic lymphoma, in contrast with 25 of 53 with bilateral involvement [11]. In the multicenter analysis of the International Extranodal Lymphoma Study Group, 124 of 188 (73%) patients with extra-gastric MALT lymphoma presented with localized disease [21]. That series revealed a favorable prognosis for patients with MALT lymphomas with high rates for overall (90%) and cause-specific survival (94%). None of the 18 patients with conjunctival involvement in this survey progressed [21]. Knowles and colleagues found a lower incidence of systemic lymphoma in patients with conjunctival infiltration than those with tumors of the orbit and eyelid region [7]. Although different types of therapy have been employed for patients with MALT lymphoma, surgery is accepted as treatment of choice in patients with isolated conjunctival MALT lymphoma. Combined radiotherapy and chemotherapy has been applied, as these tumors bear the potential to relapse locally and, rarely, also in a systemic pattern [2, 20]. Late complications are, however, seen with radiotherapy doses exceeding 35 Gy [12].

In conclusion, MALT lymphomas may also occur in children. Long-term follow-up is extremely important in this age group, considering the good prognosis in the context of the potential long-term side effects of multimodality treatment.

References

1. Berrebi D, Lescoeur B, Faye A, Faure C, Vilmer E, Peuchmaur M (1998) MALT lymphoma of labial minor salivary gland in an immunocompetent child with a gastric Helicobacter pylori infection. J Pediatr 133:290–292

2. Cahill M, Barnes C, Moriarty P, Daly P, Kennedy S (1999) Ocular adnexal lymphoma-comparison of MALT lymphoma with other histological types. Br J Ophthalmol 83:742–747
3. Dierlamm J, Baens M, Wlodarska I, Stefanova-Ouzounova M, Hernandez JM, Hossfeld DK, Wolf-Peeters C, Hagemeijer A, Van den Berghe H, Marynen P (1999) The apoptosis inhibitor gene API2 and a novel 18q gene, MLT, are recurrently rearranged in the t(11;18)(q21;q21) associated with mucosa-associated lymphoid tissue lymphomas. Blood 93:3601–3609
4. Eichler MD, Fraunfelder FT (1994) Cryotherapy for conjunctival lymphoid tumors. Am J Ophthalmol 118:463–467
5. Isaacson P, Wright DH (1984) Extranodal malignant lymphoma arising from mucosa-associated lymphoid tissue. Cancer 53:2515–2524
6. Isaacson PG, Müller-Hermelink HK, Piris M, Berger F, Nathwani BN, Swerdlow SH, Harris NL (2001) Extranodal marginal zone B-cell lymphoma of mucosa-associated lymphoid tissue (MALT lymphoma). In: Jaffe ES, Harris NL, Stein H, Vardiman JW (eds) World Health Organization classification of tumors. Tumours of haematopoietic and lymphoid tissues. IARC press, Lyon, pp 157–160
7. Knowles DM, Jakobiec FA, McNally L, Burke JS (1990) Lymphoid hyperplasia and malignant lymphoma occurring in the ocular adnexa (orbit, conjunctiva, and eyelids): a prospective multiparametric analysis of 108 cases during 1977 to 1987. Hum Pathol 21:959–973
8. Medeiros LJ, Harris NL (1989) Lymphoid infiltrates of the orbit and conjunctiva. A morphologic and immunophenotypic study of 99 cases. Am J Surg Pathol 13:459–471
9. Nutting CM, Jenkins CD, Norton AJ, Cree I, Rose GE, Plowman PN (2002) Primary orbital lymphoma. Hematol J 3:14–16
10. Ott G, Kalla J, Steinhoff A, Rosenwald A, Katzenberger T, Roblick U, Ott MM, Müller-Hermelink HK (1998) Trisomy 3 is not a common feature in malignant lymphomas of mucosa-associated lymphoid tissue type. Am J Pathol 153:689–694
11. Shields CL, Shields JA, Carvalho C, Rundle P, Smith AF (2001) Conjunctival lymphoid tumors: clinical analysis of 117 cases and relationship to systemic lymphoma. Ophthalmology 108:979–984
12. Stafford SL, Kozelsky TF, Garrity JA, Kurtin PJ, Leavitt JA, Martenson JA, Habermann TM (2001) Orbital lymphoma: radiotherapy outcome and complications. Radiother Oncol 59:139–144
13. Streubel B, Lamprecht A, Dierlamm J, Cerroni L, Stolte M, Ott G, Raderer M, Chott A (2003) T(14;18)(q32;q21) involving IGH and MALT1 is a frequent chromosomal aberration in MALT lymphoma. Blood 101:2335–2339
14. Taddesse-Heath L, Pittaluga S, Sorbara L, Bussey M, Raffeld M, Jaffe ES (2003) Marginal zone B-cell lymphoma in children and young adults. Am J Surg Pathol 27:522–531
15. Thieblemont C, Berger F, Dumontet C, Moullet I, Bouafia F, Felman P, Salles G, Coiffier B (2000) Mucosa-associated lymphoid tissue lymphoma is a disseminated disease in one third of 158 patients analyzed. Blood 95:802–806
16. Trainor KJ, Brisco MJ, Story CJ, Morley AA (1990) Monoclonality in B-lymphoproliferative disorders detected at the DNA level. Blood 75:2220–2222
17. Wan JH, Trainor KJ, Brisco MJ, Morley AA (1990) Monoclonality in B cell lymphoma detected in paraffin wax embedded sections using the polymerase chain reaction. J Clin Pathol 43:888–890
18. Wotherspoon AC, Diss TC, Pan LX, Schmid C, Kerr-Muir MG, Lea SH, Isaacson PG (1993) Primary low-grade B-cell lymphoma of the conjunctiva: a mucosa-associated lymphoid tissue type lymphoma. Histopathology 23:417–424
19. Wotherspoon AC, Finn TM, Isaacson PG (1995) Trisomy 3 in low-grade B-cell lymphomas of mucosa-associated lymphoid tissue. Blood 85:2000–2004
20. Zinzani PL, Magagnoli M, Galieni P, Martelli M, Poletti V, Zaja F, Molica S, Zaccaria A, Cantonetti AM, Gentilini P, Guardigni L, Gherlinzoni F, Ribersani M, Bendandi M, Albertini P, Tura S (1999) Nongastrointestinal low-grade mucosa-associated lymphoid tissue lymphoma: analysis of 75 patients. J Clin Oncol 17:1254–1258
21. Zucca E, Conconi A, Pedrinis E, Cortelazzo S, Motta T, Gospodarowicz MK, Patterson BJ, Ferreri AJ, Ponzoni M, Devizzi L, Giardini R, Pinotti G, Capella C, Zinzani PL, Pileri S, Lopez-Guillermo A, Campo E, Ambrosetti A, Baldini L, Cavalli F (2003) Non-gastric marginal zone B-cell lymphoma of mucosa-associated lymphoid tissue. Blood 101:2489–2495

Virchows Arch (2004) 444:202–203
DOI 10.1007/s00428-003-0928-6

LETTER TO THE EDITOR

Jakob Matschke · Andreas Erbersdobler

Extensive cerebral metastases from neuroendocrine carcinoma of the prostate

Received: 16 September 2003 / Accepted: 10 October 2003 / Published online: 2 December 2003

Sir,
a 78-year-old man was admitted for evaluation of acute confusional state. He had a history of inoperable prostatic carcinoma with orchiectomy 6 years prior to admission and had received chemotherapy with cisplatin for hepatic metastases the year before (results of histological studies were not available). A computed tomography scan did not reveal any relevant pathological findings; notably, no metastases could be seen. Clinically, the man was somnolent and could neither give date, time nor location correctly. There were no pareses or apparent sensory disturbances. Brainstem reflexes were all normal. The plantar response on both sides was flexor. The man's confusion was attributed to hypovolemia, and the clinical status gradually improved after administration of fluid and electrolytes. After 5 days, the man was released to home. He was admitted again 10 days later, and this time he was stuporous, and both plantar responses were extensor. Despite admission of fluids and electrolytes, the man's condition rapidly deteriorated, and he died 5 days after the second admission.

An autopsy was performed, which disclosed extensive carcinoma of the prostate with capsular penetration and infiltration of surrounding tissues, including the bladder neck (pT4). Haematogenous metastases were found in the liver, the vertebral bones and the pleura. There were signs of former transurethral resection procedures and bilateral orchiectomy.

Histological examination of the tumor revealed small cells without glandular differentiation (Fig. 1). Immunohistochemistry demonstrated an expression of pan-cytokeratin, synaptophysin (Fig. 2) and chromogranin A, whereas the reaction against prostate-specific antigen (PSA), prostate-specific acid phosphatase (PSAP), and neuron-specific enolase (NSE) was negative. A diagnosis of small-cell neuroendocrine carcinoma of the prostate was made.

The evaluation of the brain revealed innumerable well-demarcated nodules, mostly located at the junction of gray and white matter in cerebrum and cerebellum as well as in the brainstem. Diameters varied from a few millimeters up to about 1 centimeter (Fig. 3). Each of the nodules was surrounded by moderate peritumoral edema, and there were only slight signs of global brain swelling and herniation phenomena. Histological analysis showed solid sheets of atypical epithelial cells that were similar to the prostatic cancer cells with respect to conventional morphology as well as immunohistochemistry.

Neuroendocrine (NEC) or small-cell carcinoma of the prostate is fairly uncommon, accounting for less than 1%

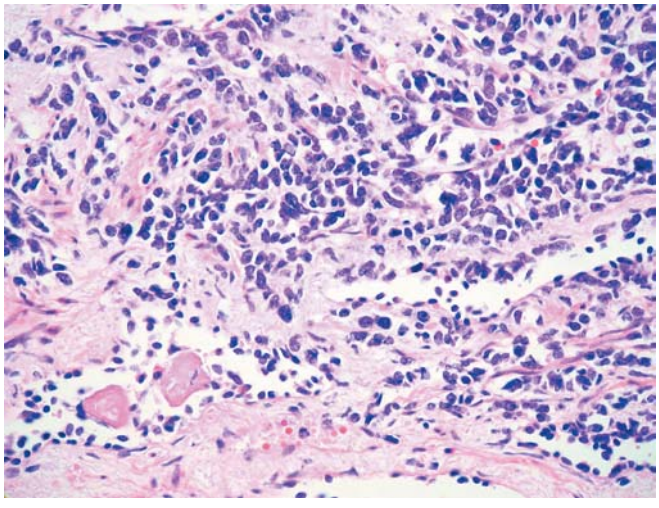

Fig. 1 Small-cell neuroendocrine carcinoma of the prostate. *Lower left* normal prostatic gland. (Haematoxylin & eosin; original magnification ×250)

J. Matschke (✉)
Institute of Neuropathology and Institute of Legal Medicine,
University-Hospital Eppendorf,
Martinistrasse 52, 20246 Hamburg, Germany
e-mail: matschke@uke.uni-hamburg.de
Tel.: +49-40-428033268
Fax: +49-40-428034929

A. Erbersdobler
Institute of Pathology,
University-Hospital Eppendorf,
Martinistrasse 52, 20246 Hamburg, Germany

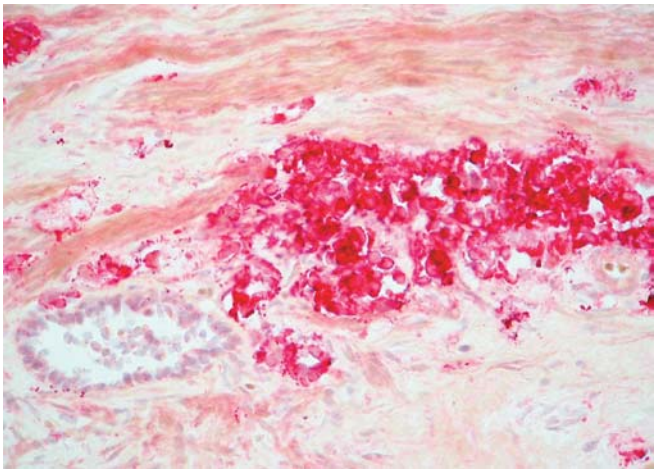

Fig. 2 Small-cell neuroendocrine carcinoma of the prostate. Immunohistochemical reaction against synaptophysin. *Lower left* normal prostatic gland. (Alkaline phosphatase-anti-alkaline phosphatase method; original magnification ×250)

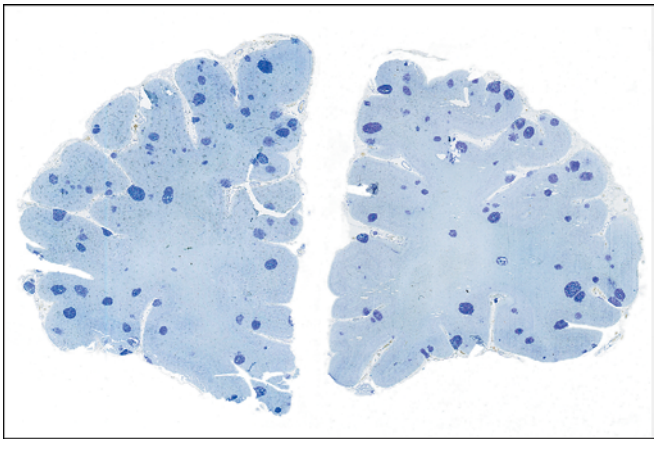

Fig. 3 Extensive cerebral metastases from small-cell carcinoma of the prostate with innumerable nodules mostly in the junction of gray and white matter. Rostral frontal lobes, Nissl's stain

of all prostatic neoplasms [3, 4, 6]. Contrary to the common prostatic adenocarcinomas, NECs have a clear propensity for widespread metastases early in the course of the disease; thus, clinically resembling small-cell carcinomas at other locations. Also, NECs are said to be generally resistant to hormone ablation therapy but are sensitive to chemotherapeutics used with bronchial small-cell carcinoma [3, 4, 6]. Given the similarity of prostatic NECs to small-cell carcinomas at other locations, one would expect a similar propensity for cerebral metastases with prostatic NECs. Nevertheless, to the authors' best knowledge, there are only four published cases, with one case showing "multiple metastases" [5], while in the remaining three cases, two [1] or only one metastasis each could be detected, respectively [2, 7].

Unfortunately, in our case, the diagnosis of prostatic NEC was not done during lifetime. Obviously, the rapid deterioration of the man's medical and neuropsychiatric status was due to the rapid development of the multiple cerebral metastases (the computed tomography scan on the first admission did not reveal any metastases). Without relevant signs of brain swelling, death can be attributed to the numerous metastases lying directly in or in the vicinity to vital centers of the brainstem (not shown here). Even with widespread disease, prostatic NEC shows dramatic responses to combined radiotherapeutic and chemotherapeutic regimens; after appropriate treatment, the patient of Nutting et al. [5] showed "resolution of brain metastases" and "did strikingly well". The patient presented here did not receive any radio- or chemotherapy designed for NEC, probably because a neuroendocrine dedifferentiation of his prostatic carcinoma was not expected. In conclusion, this case dramatically underlines the necessity for clearly distinguishing NECs from typical prostatic adenocarcinoma.

References

1. Blunt DM, Sansom HE, King DM (1996) Imaging of small cell carcinoma of the male urogenital tract. Clin Radiol 51:724–727
2. Freedy RM, Miller KD (1990) Small-cell carcinoma of the prostate: metastases to the brain as shown by CT and MR with pathologic correlation. AJNR 11:947–948
3. Helpap B (2002) Morphology and therapeutic strategies for neuroendocrine tumors of the genitourinary tract. Cancer 95:1415–1420
4. Helpap B, Kloppel G (2002) Neuroendocrine carcinomas of the prostate and urinary bladder: a diagnostic and therapeutic challenge. Virchows Arch 440:241–248
5. Nutting C, Horwich A, Fisher C, Parsons C, Dearnaley DP (1997) Small-cell carcinoma of the prostate. J R Soc Med 90:340–341
6. Solcia E, Kloppel G, Sobin LH (2000) Histological typing of neuroendocrine tumors. International histological classification of tumors. World Health Organization. Springer, Berlin Heidelberg New York
7. Zachariah B, Casey L, Zachariah SB, Baekey P, Greenberg HM (1994) Case report: brain metastasis from primary small cell carcinoma of the prostate. Am J Med Sci 308:177–179

Virchows Arch (2004) 444:204–205
DOI 10.1007/s00428-003-0942-8

LETTER TO THE EDITOR

J. Briese · D. Hatton · F. Stellmacher · H.-P. Horny

Giant metastatic liver in a patient with small-cell neuroendocrine carcinoma of the lung

Received: 17 October 2003 / Accepted: 4 November 2003 / Published online: 12 December 2003

Sir,
The liver is a very common site for metastases, carcinomas of the gut, lung, and breast being among the most frequent primary tumours. We report the unique case of a small-cell neuroendocrine carcinoma of the lung producing multiple metastases in the liver, which led to a gigantic hepatomegaly with a weight of nearly 20 kg. To the best of the authors' knowledge, such an extreme degree of hepatomegaly has never been reported before, neither in inflammatory nor in neoplastic disease. The patient, a 53-year-old male, presented with a 3-month history of abdominal pain, weight loss of about 10 kg and generalised jaundice. A computed tomography of the abdomen revealed multiple disseminated lesions in the liver, which were interpreted as metastatic disease. A biopsy specimen was obtained from the liver. Histology revealed diffuse infiltrates of small pleomorphic tumour cells coexpressing cytokeratin 7, synaptophysin, chromogranin alpha and TTF1 (Fig. 1). The diagnosis of a small-cell neuroendocrine carcinoma, probably of lung origin, was made. The patient, therefore, underwent only palliative treatment. He finally died, with signs of liver failure, due to progressive neoplastic disease. Autopsy revealed a greyish-white tumour measuring 2 cm in largest diameter within the upper lobe of the left lung. There was an unusually huge hepatomegaly with a liver size of 50×40×18 cm (compared with normal values of 25×18×10 cm). More than 90% of the hepatic tissue was replaced by disseminated, sometimes merging, tumour metastases, with a maximum diameter of about 10 cm (Fig. 2). The metastases were relatively sharply demarcated from the surrounding hepatic tissue and showed focal haemorrhage and necroses. Altogether, the total mass of the metastatic tumour within the liver was estimated to be around 17–18 kg, i.e. about 15% of the total body weight of 136 kg.

J. Briese · D. Hatton · F. Stellmacher · H.-P. Horny (✉)
Department of Pathology,
University Clinic of Schleswig-Holstein, Campus Lübeck,
Lübeck, Germany
e-mail: Horny@patho.mu-luebeck.de
Fax: +49-45-15003328

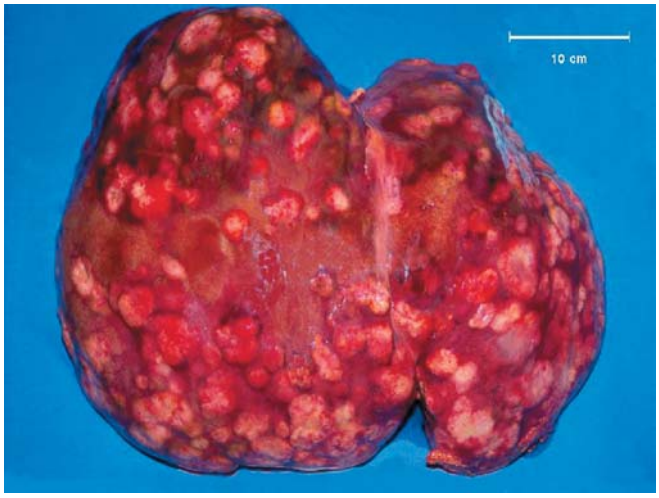

Fig. 1 Gross appearance of a giant metastatic liver with disseminated infiltrates of a small-cell neuroendocrine lung carcinoma. More than 70% of the tissue is neoplastic

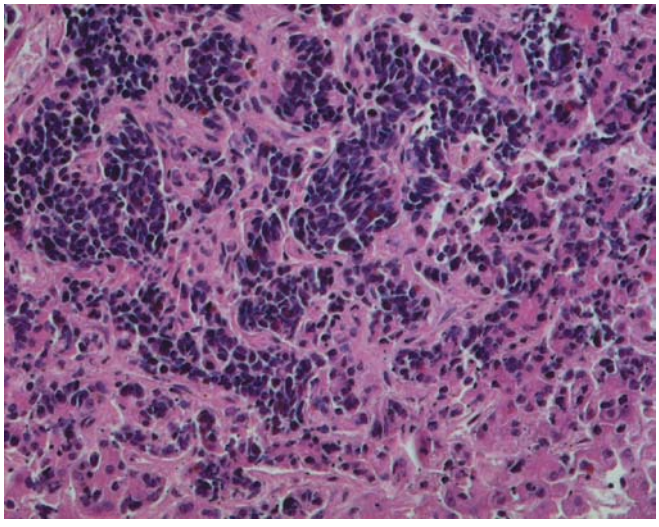

Fig. 2 Histologically, the tumour consists of closely packed small pleomorphic cells with hyperchromatic nuclei and scanty cytoplasm

To summarise, we here present the case of a 53-year-old man who died of metastasising neuroendocrine small-cell carcinoma of the lung. The most impressive feature was a giant hepatomegaly of nearly 20 kg, more than 90% of the tissue being neoplastic. This extreme liver weight seems to be unique, since we found data on liver weights of "only" up to about 7 kg in the following reported cases:

Hepatocellular carcinoma	(6500 g)	[1]
MALT lymphoma	(6100 g)	[3]
Myeloblastic leukaemia	(3000 g)	[2]
Cirrhosis	(4700 g)	[4]

References

1. Horie Y, Maeda N, Kawasaki H, Suyama A (1997) Characteristic differences of hepatocellular carcinoma in Japan, with special reference to liver weight at autopsy. Hepato-Gastroenterology 44:1407–1412
2. Okuda K, Peters RL, Simson I (1984) Gross anatomical features of hepatocellular carcinoma from three disparate geographic areas—proposal of new classification. Cancer 54:2165–2173
3. Okuda K, Nakashima T, Kojiro M, Kondo Y (1986) Hepatocellular carcinoma without cirrhosis in Japanese patients. Gastroenterology 97:140–146
4. Walk L (1983) Liver size and its post-mortem change. Radiologe 23:189–191

Virchows Arch (2004) 444:206–207
DOI 10.1007/s00428-003-0944-6

LETTER TO THE EDITOR

Katsuhito Kamimura · Hiroshi Hojo · Masafumi Abe

Immunohistochemical staining of protein kinase C isozymes (βII and δ) is helpful to distinguish reactive follicles from follicular colonization of MALT lymphoma

Received: 19 May 2003 / Accepted: 23 October 2003 / Published online: 23 December 2003

Sir,

Protein kinase C (PKC) enzymes play a major role in signal transduction and contribute to the regulation of cellular differentiation and proliferation [2]. However, subtype-specific intracellular expression and distribution of PKC are not investigated well in human reactive lymphoid tissues [1]. We tested many antibodies against 11 PKC isozymes (α, βI, βII, γ, δ, ε, ζ, η, ι, θ and μ), and only four antibodies against PKC isozymes (α, βII, γ and δ) were available for immunostaining with formalin-fixed paraffin-embedded sections. We investigated the expression of these four PKC isozymes in five human reactive lymphoid tissues (two chronic tonsillitis and three reactive lymphadenitis). PKC βII-positive B-cells were found in the mantle zones and marginal zones, but hardly in the germinal centers (Fig. 1). PKC δ was expressed on centroblasts and centrocytes in the germinal centers, with strong positive reaction against PKC δ, but on almost no cells in the mantle zones, marginal zones and interfollicular areas. A small number of cells in interfollicular areas were positive for PKC α, and almost all cells in the germinal centers and mantle zones were negative. PKC γ-positive cells were not found in these lymphoid tissues. Based on the data, we analyzed 17 cases with extranodal marginal zone B-cell lymphoma of mucosa-associated lymphoid tissue (MALT lymphoma) to distinguish follicular colonization of MALT lymphoma from reactive lymphoid follicles. The sites of the obtained specimens were stomach (14 cases), rectum (1), lung (1) and thyroid gland (1). Follicular colonization was seen in 13 cases. In non-neoplastic follicles of MALT lymphoma, PKC βII-positive cells were found mainly in the mantle zones, and PKC δ-positive cells were found in the centroblasts and centrocytes in the germinal centers. Neoplastic centro-

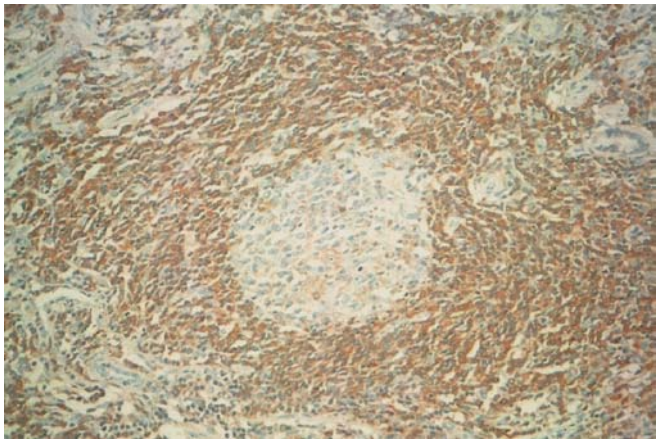

Fig. 1 Immunohistochemistry of protein kinase C (PKC) βII in the reactive follicle. PKC βII-positive B-cells are seen in the mantle zone and marginal zone. Original magnification, ×100

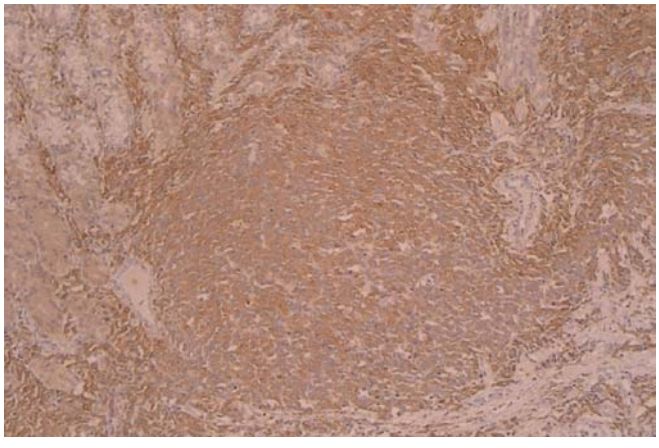

Fig. 2 Immunohistochemistry of protein kinase C (PKC) βII in the follicular colonization of MALT lymphoma. Neoplastic cells showing follicular colonization are positive for PKC βII. Original magnification, ×50

K. Kamimura (✉) · H. Hojo · M. Abe
1st Department of Pathology,
Fukushima Medical University School of Medicine,
1 Hikariga-oka, 960-1295 Fukushima, Japan
e-mail: kami@fmu.ac.jp
Tel.: +81-24-5471165
Fax: +81-24-5484488

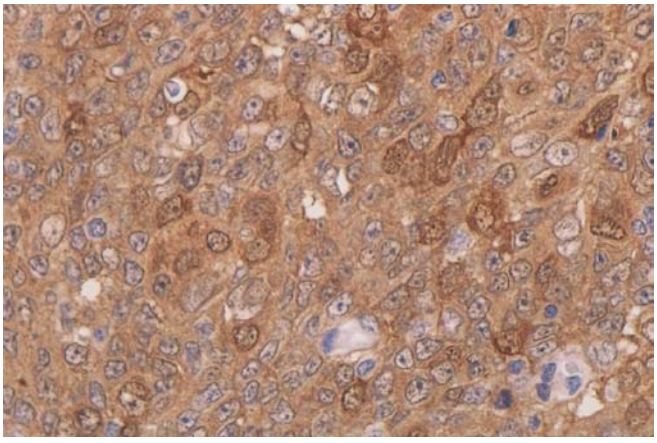

Fig. 3 Immunohistochemistry of protein kinase C (PKC) δ in the follicular colonization of MALT lymphoma. PKC δ expression is stronger in residual germinal center cells than in neoplastic cells. Original magnification, ×400

cyte-like cells, which colonize germinal centers of reactive lymphoid follicles (i.e., follicular colonization) in MALT lymphoma, were strongly positive for PKC βII (Fig. 2) and showed weaker reaction to PKC δ than residual germinal center cells (Fig. 3). The weak expression of PKC δ and strong expression of PKC βII were considered to be characteristic of colonized neoplastic cells. CD21 reacted with fragmented meshworks of follicular dendritic cells in colonized follicles, and centrocyte-like cells were negative for bcl-2 and CD10. These results indicate that immunostaining for PKC δ and PKC βII, combined with CD21, bcl-2 and CD10, is helpful to distinguish follicular colonization of MALT lymphoma from reactive lymphoid follicles.

References

1. Hojo H, Morimura Y, Abe M, Wakasa H (1996) Expression of classical protein kinase C subspecies in non-neoplastic lymphocytes and non-Hodgkin's lymphomas: an immunohistochemical study. Pathol Int 46:148–154
2. Nishizuka Y (1992) Intracellular signaling by hydrolysis of phospholipids and activation of protein kinase C. Science 258:607–614

Virchows Arch (2004) 444:208–210
DOI 10.1007/s00428-003-0946-4

LETTER TO THE EDITOR

Florence Ballaux · Maria Debiec-Rychter · Ivo De Wever · Raf Sciot

Chondroid lipoma is characterized by t(11;16)(q13;p12–13)

Received: 8 July 2003 / Accepted: 25 November 2003 / Published online: 14 January 2004

Sir,
Chondroid lipoma is a rare benign tumor of adipose tissue origin that may mimic myxoid chondrosarcoma and liposarcoma. Karyotypes from two chondroid lipomas have been reported so far, both with a t(11;16)(q13;p12–13) [2, 7]. We report a chondroid lipoma with the same translocation, including ring chromosomes in a small fraction of metaphases.

A 72-year-old female presented with diarrhea. Abdominal computed tomography (CT) revealed no intra-abdominal abnormalities. A left paravertebral intramuscular, non-mineralized mass was found. Additional magnetic resonance imaging (MRI) was performed. The sagittal TIR sequence showed a hypo-intense nodule with a hyper-intense rim, and the T1-weighted images after gadolinium administration demonstrated a strong homogeneous enhancement pattern of the nodule. A tumorectomy was performed. The mass was well defined, lobulated and yellow, with gelatinous areas, and it measured 5.0×3.1×2.5 cm. Microscopically, the tumor was lobulated and surrounded by a thin, fibrous capsule. One nodule was located outside the capsule. The tumor cells were arranged in nests and cords. A major part consisted of small- to medium-sized, slightly eosinophilic, multi-vacuolated cells (Fig. 1a). Some cells presented with an oval-shaped nucleus, while others showed a centrally or peripherally located hyperchromatic, scalloped nucleus (lipoblast-like) (Fig. 1b). Nucleoli were inconspicuous. The cytoplasmic vacuoles contained lipid droplets, confirmed by a positive oil-red-O stain. Mature

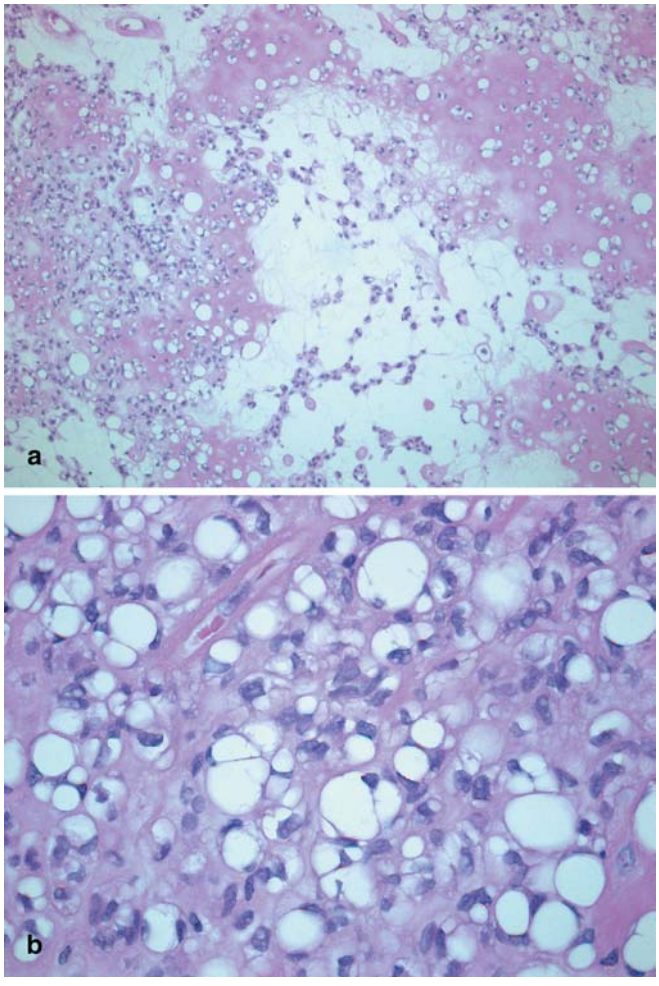

Fig. 1 Hematoxylin and eosin stain, depicting the myxoid to chondroid matrix (**a**) and the vacuolated, lipoblast-like appearance of the tumor cells (**b**)

F. Ballaux · R. Sciot (✉)
Department of Pathology, University Hospital St. Rafaël,
Catholic University Leuven,
Minderbroedersstraat 12, 3000 Leuven, Belgium
e-mail: raf.sciot@uz.kuleuven.ac.be
Tel.: +32-16-336593
Fax: +32-16-336548

M. Debiec-Rychter
Department of Human Genetics,
University Hospitals, Catholic University Leuven,
Leuven, Belgium

I. De Wever
Department of Surgical Oncology,
University Hospitals, Catholic University Leuven,
Leuven, Belgium

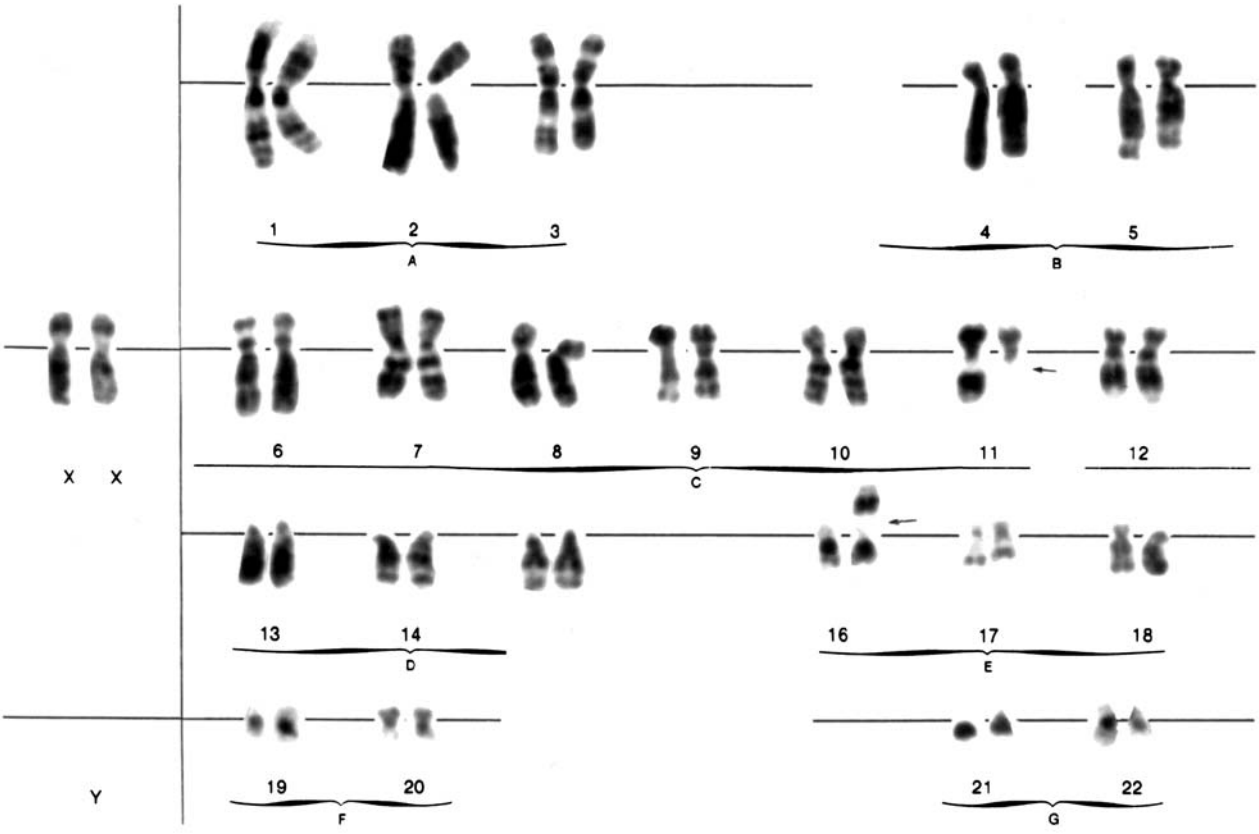

Fig. 2 Gold thioglucose-banded karyotype of chondroid lipoma, showing t(11;16)(q13;p13) as a sole abnormality. *Arrows* indicate chromosome breakpoints

adipocytes were present in fewer numbers. Mitoses were not present. The extracellular matrix was partly composed of a homogeneous, eosinophilic (chondroid) matrix (Fig. 1a). Some cells seemed to reside in lacunar spaces. Myxoid areas were seen as well. Vessels were relatively frequent, some of which were surrounded by a hyalinized cuff. Chicken-wire capillaries were absent. Immunohistochemically, the tumor cells showed focal expression of S-100 protein. No convincing staining for MDM2 was present. The cells were negative for epithelial markers (cytokeratin, epithelial membrane antigen).

Metaphases (n=22) were analyzed and showed an abnormal karyotype: 46,XX,t(11;16)(q13;p13)[20]/47–48, idem,+2–3 r [cp2] (Fig. 2). Using the combination of probes specific for *MDM2* and *CDK4* genes, the partially overlapping red and green signals were visualized over normal chromosomes 12. The ring chromosomes were not labeled.

The histological hallmarks of chondroid lipomas are nests and cords of uni- and multi-vacuolated adipocytes within a prominent myxohyaline to chondroid matrix, resulting in sharply defined cytoplasmic borders [4]. Chondroid lipoma has to be differentiated from myxoid liposarcoma, due to the presence of myxoid areas and (pseudo)lipoblasts. However, myxoid liposarcomas have a delicate plexiform vasculature, do not show a chondroid matrix and have a typical t(12;16)(q13;p11) translocation, absent in this case [4, 8]. Other differential diagnostic possibilities include a mixed/myoepithelial tumor of soft tissue, extraskeletal myxoid chondrosarcoma and epithelioid schwannoma. A mixed/myoepithelial tumor of soft tissue should express epithelial markers and shows a different karyotype [4, 5]. The large number of multivacuolated cells is not characteristic for extraskeletal myxoid chondrosarcoma [4]. From a cytogenetic point of view, t(9;22)(q22;q12) and t(9;17)(q22;q11) have been described in extraskeletal myxoid chondrosarcoma [6]. The tumoral nodule, located outside the capsule, the pseudolipoblasts and the presence of only focal expression of S-100 protein exclude an epithelioid schwannoma [3].

To our knowledge, this is the third case of chondroid lipoma with reported cytogenetic findings. Our data confirm the translocations described in the two other cases. Additional ring chromosomes were seen in a small fraction of metaphases, a feature that is characteristic for atypical lipomatous tumors. This could suggest a link between the presented case and atypical lipomatous tumors. However, fluorescent in situ hybridization analysis did not reveal the presence of *MDM2* or *CDK4* gene sequences within the rings, the amplification of these genes being a constant finding in atypical lipomatous

tumors with ring chromosomes [1]. This was corroborated by the absence of convincing MDM2 staining on immunohistochemistry. In conclusion, the consistent presence of a t(12;16)(q13;p13) represents a diagnostic tool for chondroid lipoma and may, thus, pave the way in search of the genes involved in the pathogenesis of this rare tumor.

References

1. Dei Tos AP, Doglioni C, Piccinin S, Sciot R, Furlanetto A, Boiocchi M, Dal Cin P, Maestro R, Fletcher CD, Tallini G (2000) Coordinated expression and amplification of the MDM2, CDK4, and HMGI-C genes in atypical lipomatous tumours. J Pathol 190:531–536
2. Gisselsson D, Domanski HA, Hoglund M (1999) Unique cytological features and chromosome aberrations in chondroid lipoma. Am J Surg Pathol 23:1300–1304
3. Kindblom LG, Meis-Kindblom JM, Havel G, Busch C (1998) Benign epithelioid schwannoma. Am J Surg Pathol 22:762–770
4. Meis JM, Enzinger FM (1993) Chondroid lipoma. A unique tumor simulating liposarcoma and myxoid chondrosarcoma Am J Surg Pathol 17:1103–1112
5. Pauwels P, Dal Cin P, Roumen R, van den Berghe H, Sciot R (1999) Intramuscular mixed tumour with clonal chromosomal changes. Virchows Arch 434:167–171
6. Sciot R, Dal Cin P, Fletcher C, Samson I, Smith M, De Vos R, Van Damme B, Van den Berghe H (1995) t(9;22)(q22–31;q11–12) is a consistent marker of extraskeletal myxoid chondrosarcoma: evaluation of three cases. Mod Pathol 8:765–768
7. Thomson TA, Horsman D, Bainbridge TC (1999) Cytogenetic and cytologic features of chondroid lipoma of soft tissue. Mod Pathol 12:88–91
8. Turc Carel C, Limon J, Dal Cin P, Rao U, Karakousis C, Sandberg AA (1986) Cytogenetic studies of adipose tissue tumors. II. Recurrent reciprocal translocation t(12;16)(q13;p11) in myxoid liposarcomas. Cancer Genet Cytogenet 23:291–299

Virchows Arch (2004) 444:211–212
DOI 10.1007/s00428-004-0979-3

ANNOUNCEMENTS

1–2 April 2004
Thyroid Pathology for the Practicing Pathologist
15 rue de l'Ecole de Médecine, Paris, France

Join us for a Springtime meeting in Paris!!
A 2-day course will take place in Paris under the auspices of the French Division of the I.A.P. This course will be given in English by Prof. M. Sobrinho-Simoes (Porto) and Prof. R. Heimann (Brussels).
It will consist of lectures alternating with slide reviews and a slide seminar over a multihead microscope. The slide seminar (on CD) will be sent before the meeting. The audience will be limited to 22 participants.
Course fee: 390 euros (320 euros for members of any IAP division). The fee includes registration, hand-out, CD of the slide seminar and coffee breaks.

For further information, please contact:
Mrs. M. Fontanière
Administrative Secretary
French Division of the I.A.P. 32 Cours Albert Thomas
69008, Lyon, France
Fax: 33478754311
E-mail: academie.pathologie@wanadoo.fr

9–12 May 2004
XIV EUROCELLPATH COURSE: The Impact of Proteomics and Genomics in Pathology
Girona, Spain

The Organising Committee of the next EuroCellPath Course invites you to come to the beautiful city of Girona to enjoy an outstanding program on a very timely topic, addressed by leading authorities in the field, in an inspiring setting. The subjects covered in this course will be the following:

- DNA arrays: Methods and Goals
- Tissue Microarrays: A Tool for Rapid, Efficient Translational Research
- Proteomics: From Genes to Functions
- Tissue Procurement and Handling: Laser Capture Microdissection and Other Techniques
- Bioinformatic Tools for Array Data Mining
- Application of Array Genomics and Proteomics in Pathology
- Molecular Pathology of Genes and Proteins: What to Look For and When.

You may also submit your abstracts on these or other related topics, to be presented either as platform or poster during the Course.

For further information, please contact:
Prof. Josep Lloreta-Trull (local organizer)
Department of Pathology
Hospital del Mar-IMAS-IMIM
Universitat Pumpeu Fabra
Passeig Marítim 25–29, 08003-Barcelona, Spain
Tel.: +34 93 248 30 31
Fax: +34 93 248 31 31
E-mail: jlloreta@imas.imim.es or enter the course website
http://www.tilesa.es/eurocellpath04/

10–14 May 2004
Diagnostic Histopathology of Breast Disease
Hammersmith Hospital (Imperial College), London, UK

A week-long course designed for pathologists at Consultant and Senior Trainee level. The course provides a comprehensive coverage of the Histopathology of Breast Disease, with special emphasis on areas that pose diagnostic difficulties. The participants will be given ample time to study histological preparations, followed by illustrated discussion of the cases. There will be special sessions dealing with the interpretation of core biopsies and fine needle aspirations. There will also be several daily talks dealing with specific topics, given by eminent breast pathologists and followed by discussion. The topics will include reporting breast biopsies, immunohistochemistry, receptor and c-erbB-2 assessment, dealing with the gross specimen, prognostic factors, proliferative lesions/carcinoma in situ, problems in breast pathology, mucinous lesions of the breast, a practical approach to the diagnosis of breast lymphomas and molecular pathology including the morphology of breast cancer associated with BRCA1 & 2 mutation. The faculty will include Ian Ellis, Christopher Elston, Andrew Hanby, Kristin Henry, Stephen Humphreys, Sunil Lakhani, Andrew Lee, Naomi Livni, Sarah Pinder and Sami Shousha.

*Further details from***:**
Wolfson Conference Centre
Hammersmith Hospital
Du Cane Road
London W12 ONN, UK
Tel: (44) 20 8383 3117/3227/3245
Fax: (44) 20 8383 2428
E-mail: wcc@ic.ac.uk

4–5 June 2004
15th Ljudevit Jurak International Symposium on Comparative Pathology
(http://www.kbsm.hr/Jurak/symposium.htm), will be held in Multimedial center Sestre milosrdnice University Hospital, Vinogradska 29, Zagreb, Croatia.

The main symposium topic is head and neck pathology (including ophthalmopathology). Symposium includes following sections: Pathological Morphology of the Human and Animal Diseases, Iatrogenic, Environmental and Experimental Pathology, Herman Jurak Round Table on Rheumatological Pathology, Telepathology on-line conference, Clinical Forensic Pathology, Slide Seminars *in Histopathology and Cytopathology*, Quiz on Pathology.

For further information please contact:
Davor Tomas, M.D.
Ljudevit Jurak Clinical Department of Pathology
Sestre milosrdnice University Hospital
Vinogradska 29
10000 Zagreb, Croatia
Phone: 385-1-3787-909
Fax: 385-1-3787-244
e-mail: dtomas@kbsm.hr, juraks@kbsm.hr

1–11 June 2004
International course on Laboratory Animal Science
Utrecht, The Netherlands

A two week intensive course on laboratory animal science will be organized at the Department of Laboratory Animal Science – Utrecht, The Netherlands in June 2004. This course is organized once a year since 1993.

The objective of this course is to present basic facts and principles that are essential for the humane use and care of animals and for the quality of research.

The contents of the course are in line with recommendations of the Federation of European Laboratory Animal Science Associations (FELASA) regarding the training of the young scientist whose research involves the use of vertebrate animals.

The course may also be of interest for those who intend to set up a similar course at their location. For this purpose, during the course the acquisition of teaching materials can be discussed with the course committee.

For information and application forms please contact:
Prof. L.F.M. van Zutphen, PhD or
Mr. Stephan van Meulebrouck, MA
Department of Laboratory Animal Science
Faculty of Veterinary Medicine
P.O. Box 80.166
3508 TD Utrecht
The Netherlands
Tel.: ++31-30-2532033
Fax: ++31-30-2537997
E-mail: pdk@las.vet.uu.nl
Internet: http://las.vet.uu.nl (click on "Education and Training")

11–16 July 2004
ULTRAPATH XII: Conference on Diagnostic Electron Microscopy with Surgical, Clinical, and Molecular Pathology Correlations
Barcelona, Spain

The scientific program will cover diagnostic Electron Microscopy as well as Diagnostic Pathology – with immunohistochemical and molecular correlations – and translational research. Renowned experts in the field from both sides of the Atlantic will present updated comprehensive reviews of significant areas of Pathology. In addition, a new section of the meeting will be devoted to a Pathology Review Course. Platform and Poster presentations will also be an important part of the program.

For further information, please contact:
Josep Lloreta-Trull, M.D., Ph.D. (chairman)
Department of Pathology, Hospital del Mar-IMAS-IMIM
Universitat Pompeu Fabra
Passeig Maritim 25–29, 08003-Barcelona, Spain
Tel.: +34 93 248 30 31
Fax: +34 93 248 31 31
E-mail: jlloreta@imas.imim.es.
The Application form and Abstract form can be found on the meeting website, http://www.tilesa.es/ultrapath04/

27–30 July 2004, London
Practical Pulmonary Pathology

This course is designed to provide histopathology and cytopathology trainees and consultants with an opportunity to study diagnostic lung pathology in a comprehensive manner. It comprises lectures and practical microscopy sessions, the latter making up roughly half the time and consisting of individual study of a unique collection of cases.

For further details and application forms please contact:
Professor B Corrin,
Brompton Hospital
London SW3 6NP
Fax: +44 20 7351 8293.
E-mail: b.corrin@ic.ac.uk

Virchows Arch (2004) 444:213–223
DOI 10.1007/s00428-003-0947-3

REVIEW ARTICLE

Sigurd F. Lax

Molecular genetic pathways in various types of endometrial carcinoma: from a phenotypical to a molecular-based classification

Received: 9 October 2003 / Accepted: 23 November 2003 / Published online: 28 January 2004

Abstract Two types of endometrial carcinoma are distinguished with respect to biology and clinical course. Type-I carcinoma is related to hyperestrogenism by association with endometrial hyperplasia, frequent expression of estrogen and progesterone receptors and younger age, whereas type-II carcinoma is unrelated to estrogen, associated with atrophic endometrium, frequent lack of estrogen and progesterone receptors and older age. Histologically, endometrioid and mucinous carcinomas are considered type I, serous and clear cell carcinomas type II. Molecular data from multiple studies support the hypothesis of different genetic pathways in the development of endometrioid and serous carcinoma. The most frequent genetic alteration in endometrioid carcinoma is PTEN inactivation by mutation, followed by microsatellite instability (MIN) and mutations of K-ras and β-catenin. PTEN and K-ras mutations and MIN are considered early events, occurring in a subset of atypical endometrial hyperplasia, whereas p53 mutation is considered a late event, during progression of about 10–20% of endometrioid carcinomas. In serous carcinoma, p53 mutation is the most frequent genetic alteration, followed by inactivation of p16 and e-cadherin and amplification of her2/neu. p53 mutation occurs in endometrial intraepithelial carcinoma, the putative precursor of serous carcinoma. Considering these genetic pathways, the current histological classification of endometrial carcinoma is molecular based.

Keywords Endometrial carcinoma · Endometrial cancer · Type-I and type-II carcinomas · Molecular pathways · Tumorigenesis · Molecular analysis

S. F. Lax (✉)
Department of Pathology,
General Hospital Graz West,
Goestingerstrasse 22, 8020 Graz, Austria
e-mail: sigurd.lax@meduni-graz.at
Tel.: +43-316-54664652
Fax: +43-316-546674652

Introduction

The tumors of the female genital tract show a broad spectrum of phenotypes, reflecting the variable cellular differentiation in the mullerian system. The differentiation may be either endometrioid, serous, mucinous, urothelial or squamous. Endometrioid differentiation resembles the proliferative or secretory endometrium, whereas serous differentiation reflects the cell types that are present in the mucosa of the Fallopian tube and on the surface of the ovary. Mucin-producing cells are typically present in the endocervix, and squamous epithelium is found in the ectocervix and the vagina. A urothelial differentiation is related to the proximity to the urinary tract. It is yet unclear where clear cell tumors derive from. Clear cells are present in tumors of the kidney and the suprarenal gland, and, thus, clear cell neoplasms of the female genital tract were, in the past, called "mesonephric." However, clear cells with a hobnail appearance also occur in hypersecretory changes of the endometrium and may give rise to tumors.

All these phenotypes may occur in endometrial carcinoma [99]. In the endometrium, the most frequent tumor type is endometrioid adenocarcinoma, whose histological variants may show squamous differentiation, a villoglandular pattern or secretory changes or may be composed of ciliated cells. Serous carcinoma is infrequent compared with endometrioid carcinoma, but clinically important due to its poor clinical outcome [16]. Clear cell and mucinous carcinomas are rare. Of all other tumor types, such as squamous cell carcinoma, transitional cell carcinoma and small cell carcinoma, only single cases or small case studies have been reported. Malignant mixed mullerian tumor (MMMT) may be considered a carcinoma with cellular dedifferentiation (sarcomatoid carcinoma) rather than a neoplasm with true biphasic differentiation [102].

A dualistic model of endometrial tumorigenesis

Currently, two different pathways are distinguished for tumorigenesis of sporadic endometrial carcinoma, one estrogen related and another unrelated to estrogen [41, 84]. These pathways lead to tumor types with a distinctive phenotype and biological behavior. Tumorigenesis of hereditary endometrial carcinoma will be discussed briefly at the end of this article. The majority of sporadic endometrial carcinomas (at least approximately 70–80%), designated as type-I carcinomas, follow the estrogen-related pathway. They seem to arise in the background of unopposed estrogenic stimulation [64], since they are associated with endometrial hyperplasia, express estrogen (ER) and progesterone receptors (PR) [42] and are associated with elevated levels of serum estradiol [85]. Histologically, most tumors show an endometrioid differentiation and are of low grade. In addition, the rare mucinous adenocarcinomas are also considered type-I carcinomas, since they usually express ER and/or PR and are of low histopathological grade. Clinically, type-I carcinomas are overall characterized by a favorable behavior. The major cause of hyperestrogenism is endogenous overproduction of estrogens due to obesity [20] and anovulatory cycles during perimenopause and menopause. In addition, estrogens are unopposed, due to the lack of progestin by decreased ovarian production. Furthermore, hyperestrogenism may be caused by hormone replacement therapy with only estrogen [104] and less frequently by polycystic ovary syndrome or estrogen-producing neoplasm, such as granulosa cell tumor.

About 10–20% of endometrial carcinomas, designated as type-II carcinomas, follow the estrogen-unrelated pathway and arise in the background of atrophic endometrium [84]. These tumors usually occur at a higher age, approximately 5–10 years later than type-I tumors. They are typically high-grade carcinomas of non-endometrioid differentiation, most frequently serous, less frequently clear cell. ER and PR expression is usually negative or weakly positive [42], and serum levels of estradiol are not elevated. Serous carcinoma, the prototype of type-II carcinoma, is frequently associated with endometrial intraepithelial carcinoma (EIC), which is considered the putative precursor [5]. EIC may also be found in proximity to clear cell carcinoma, the other type-II carcinoma [42]. For both serous and clear cell carcinoma, an aggressive clinical course and poor prognosis are well known [3, 16]. In particular, serous carcinoma may show poor prognosis and extensive extrauterine spread at low uterine stage [89, 105]. Small cell, undifferentiated and squamous cell carcinomas may also be encountered among type-II carcinomas, but little is known about their tumorigenesis.

There remain open questions, since not all tumors fit into this dualistic model. It is in debate whether a subset of endometrioid carcinoma, in particular of high grade, may be encountered in type-II carcinoma. The fact that most high-grade endometrioid carcinomas show at least a weak ER and/or PR expression and often contain well-differentiated carcinoma foci favors progression along an estrogen-driven pathway [42, 43]. A subset of low-grade endometrioid carcinoma with ER and PR expression, clearly type-I carcinoma, occurs unrelated to estrogen in the background of atrophic endometrium. Thus, like in any model, there is evidence for exceptions.

This dualistic model of endometrial tumorigenesis is based on a hypothesis by Jan Bokhman [8] in 1982, based solely on clinical observations and clinico-pathological correlations. It was postulated and subsequently broadened by the inclusion of molecular aspects, first on the basis of p53 immunohistochemistry by Drs. Sherman and Kurman [84], approximately a decade later. During the recent years, the dualistic model was supported by molecular genetic analyses performed by different groups [14, 44, 51].

A molecular basis of a dualistic model for sporadic endometrial carcinoma

A molecular basis for the development of malignant tumors was introduced by Vogelstein and coworkers based on the progression of colorectal adenoma to carcinoma [23]. According to this progression model, malignant tumors develop through a series of precursor lesions with cellular atypia and architectural abnormalities, among which the terms dysplasia, carcinoma in situ, intraepithelial neoplasia and atypical hyperplasia are encountered, depending on the particular sites. This process of tumor development is accompanied by a step-wise acquisition of various genetic alterations, in particular, mutations of oncogenes and tumor suppressor genes, and increase in genetic instability. During the recent years, two distinctive types of genetic alterations have been postulated, chromosomal instability (CIN) and microsatellite instability (MIN) [37]. CIN is characterized by major genetic alterations, in particular, gains and losses of chromosome arms and whole chromosomes, respectively [46]. The mechanisms leading to genetic instability seem to be very complex [4]. It is most likely that CIN evolves in small steps and is characterized by an increase of aberrant chromosomal formations from pre-malignant to invasive malignant lesions. In advanced cancer, the spectrum of chromosomal aberrations seems to remain stable for the individual tumor cell, although a marked cell-to-cell variability occurs. This may be, in particular, explained by the fact that advanced tumors have acquired a genotype that is optimal for proliferation, growth and spread [4]. These major genetic alterations are frequently accompanied by inactivation of important regulatory proteins, such as p53, by gene mutations. However, MIN is characterized by minor genetic alterations, in particular, frame-shift mutations in repetitive sequences of the genome, the so-called micro- and minisatellites [63]. Multiple gross chromosomal imbalances are characteristic for CIN, but usually do not occur in MIN+ tumors [88]. Recently, a minor degree of CIN

Table 1 Comparison of major genetic alterations between type-I and type-II endometrial carcinomas as analyzed on endometrioid and serous carcinomas, respectively. For references see text

Genetic alteration	Type-I carcinomas	Type-II carcinomas
Microsatellite instability	20–40%	0–5%
K-ras mutations	15–30%	0–5%
p53 mutations	10–20%	90%
PTEN inactivation	35–50%	10%
β-catenin mutations	25–40%	0–5%
P16 inactivation	10%	40%
E-cadherin alteration	10–20%	80–90%

associated with distinctive chromosomal changes has been found in MIN+ colorectal carcinomas [48].

With respect to the number of altered microsatellites per tumor, tumors with a high number of alterations (>20%=MIN-high) are distinguished from tumors with a low number of alterations (20% and less=MIN-low) [9]. MIN-high was found in about 30% of unselected, consecutive endometrial carcinomas, whereas MIN-low was found only in about 3% of tumors of the same series [25]. Usually, mutations within the repetitive sequences are repaired by a system (the mismatch repair system) of various proteins that are able to cut out the mismatching DNA strain and to replace the incorrect bases [69]. These proteins, of which MLH1, MSH2 and MSH6 are best known, can be inactivated by various mechanisms, particularly, promoter methylation and mutations. In a recent study, about 70% of the MIN-high cases were associated with methylation of MLH1, whereas the remaining 30% of cases revealed unmethylated MLH1 [25]. Of these tumors with unmethylated MLH1, about 15% showed MSH2 mutations, but 60% showed MSH6 mutations, of which almost half were germline mutations. Thus, MSH6 mutations seem to be a frequent cause of MIN [25]. MIN can also affect repetitive coding sequences within important genes, e.g., for apoptosis, DNA reparation and cell growth, such as BAX, transforming growth factor-β II, insulin-like growth factor-receptor II, etc., which are subsequently inactivated [15, 26]. Therefore, inactivation of similar genes may occur as in CIN, but by a different mechanism. It is further worth mentioning that during tumor progression, the number of altered microsatellites increases within MIN-high tumors. Recently, a third type of genetic instability has been postulated, which is characterized by diploidy and minor genetic alterations, in particular, loss of heterozygosity (LOH), but lacks CIN and MIN [4].

Endometrioid and serous carcinoma, which represent the major phenotypes of type-I and type-II endometrial carcinomas, respectively, are characterized by distinctive types of genetic instability and molecular alterations (Table 1). For the other infrequent histological types of endometrial carcinoma, such as mucinous, transitional cell, small cell and clear cell carcinomas, no larger studies have been performed, thus far. Unfortunately, no comprehensive study on the various types of endometrial carcinoma has been performed, including immunohistochemistry for various proteins, ploidy analysis, gene mutation and microsatellite analysis and chromosomal analysis using comparative genomic hybridization (CGH). Thus, the present review remains a collage of data drawn from various studies on different sets of tumors.

Molecular genetic alterations in endometrioid carcinoma

Endometrioid carcinoma is characterized by a variety of genetic alterations, in particular, those affecting proteins bound to the cell membrane and responsible for cell adhesion and signaling transduction. Currently, the most frequently altered gene in endometrioid carcinoma is PTEN, which is located on chromosome 10 and codes for a protein with tyrosine kinase function [56]. Up to 83% of endometrioid carcinomas reveal altered PTEN, characterized by loss of expression [58] (Fig. 1A). The underlying genetic alteration in cases with lost PTEN expression and function is mostly mutation and, less frequently, LOH without mutation [58]. In a subset of about 20% of tumors with altered PTEN, most of which were high stage and MIN+, promoter methylation was found [79]. Some authors found PTEN mutations associated with MIN+ endometrioid carcinomas [96].

MIN is an important genetic alteration in endometrioid carcinoma and its variants [11, 13, 68], occurring in about 20–45% of tumors [50]. Inactivation of MLH1 by methylation of the promoter seems to be the most frequent cause of MIN in sporadic endometrioid carcinomas [21, 26, 78, 87], followed by loss of expression of MSH2 and MSH6 [90, 91]. The mechanism for inactivation of MSH2 is still not clear, since promoter methylation and mutations are rare [21, 33, 40]. MSH6 inactivation seems to be almost always caused by mutation [25].

One of the first genetic alterations described in endometrial carcinoma, which are present in about 20–30% of endometrioid carcinomas, are constitutively activating mutations of the K-ras protooncogene [12, 19]. They are predominantly found in exon 1 (codons 12 and 13) and rarely in exon 2 (codon 61) [82]. K-ras in different exons, as well as K-ras and PTEN mutations, do not seem to concur within the same tumor [29].

β-Catenin mutation is present in about 20% of endometrioid carcinomas [74]. β-Catenin, together with e-cadherin, forms a protein complex, which is associated with the cell membrane and responsible for cell–cell adhesion. In addition, β-catenin is important for the signal transduction pathway in association with the T-cell factor family. The β-catenin pathway can be activated by activating β-catenin mutations or by inactivating e-cadherin mutations. β-Catenin mutations lead to nuclear protein overexpression. β-Catenin mutations and a nuclear expression pattern, respectively, were frequently found in MIN+ and low-grade endometrioid carcinomas [61]. Other investigators detected β-catenin mutation in about 50% of high-grade endometrioid carcinomas [80] and did

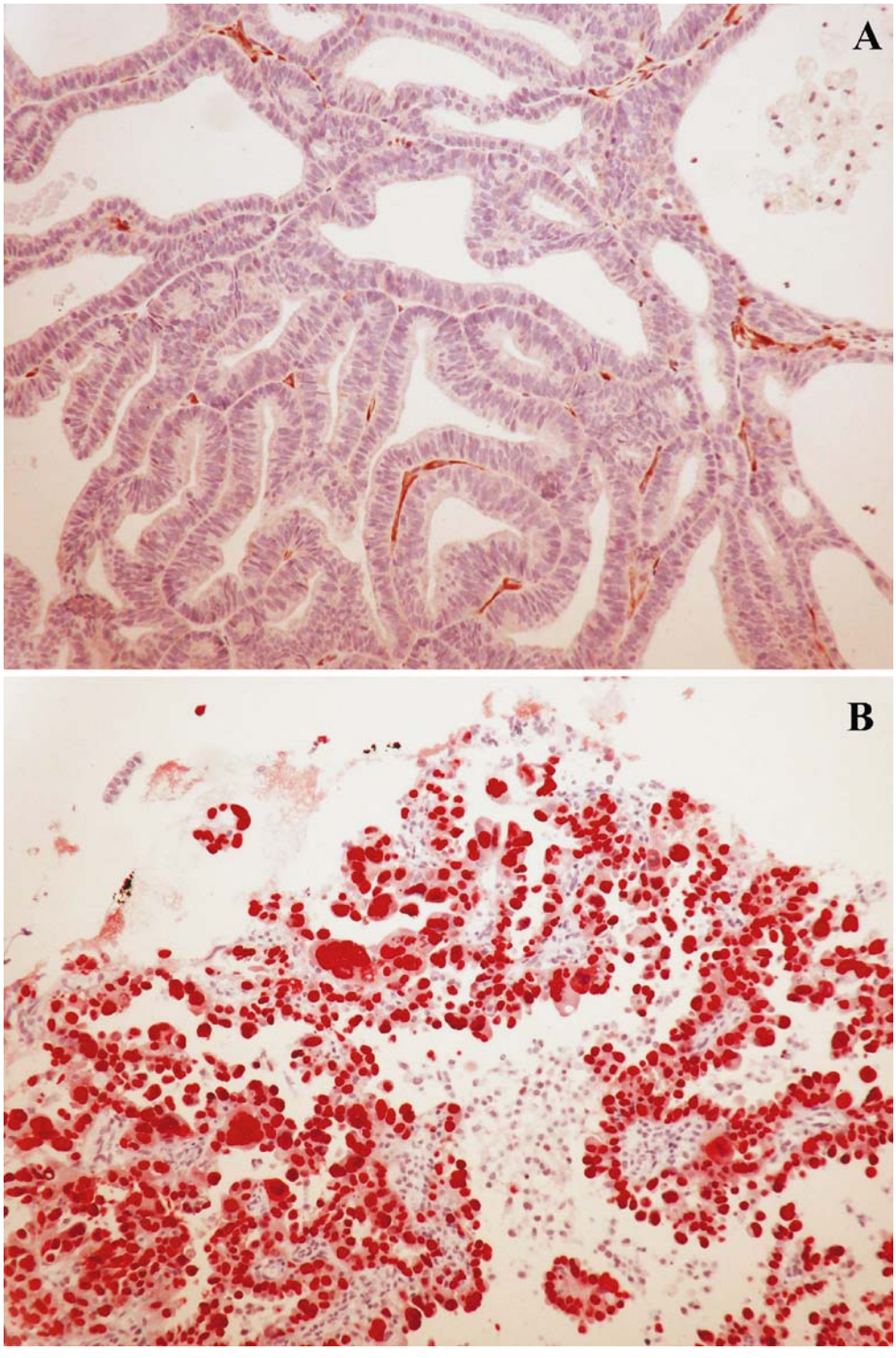

Fig. 1 The major genetic alterations in type-I (**A**) and type-II (**B**) endometrial carcinomas. **A** Loss of PTEN expression in a well-differentiated endometrioid adenocarcinoma due to a point mutation in exon 5 (not shown). Note the positive immunoreactivity in the stroma of the neoplastic papillae. Peroxidase-antiperoxidase (PAP), ×150. **B** Overexpression of p53 represented by a strong diffuse immunoreactivity in a serous carcinoma of the endometrium. PAP, ×150

not find association with MIN [38], respectively. Reduced membranous staining and heterogeneous staining, respectively, for e-cadherin, which is associated either with mutation or methylation, is found in about 5–50% of endometrioid carcinomas [28].

p53 mutations were found in a subset of approximately 10–20% of endometrioid carcinomas, which were mostly grade 3 [44, 66, 67]. Grade 1 carcinomas and atypical hyperplasia seem to lack mutant p53, and, in grade 2 carcinomas, p53 mutations seem to occur rarely [44]. p53 mutations are almost always associated with aneuploidy and do not seem to concur with PTEN mutations in the same tumor [39].

Table 2 Comparison of p53 and K-ras mutations and microsatellite instability (MIN) between endometrioid carcinoma and endometrioid carcinoma with various types of cellular differentiation [42]. *NS* not significant

Genetic alteration	Endometrioid grade 1, 2 (*n*=31)	Low-grade squamous and mucinous (*n*=12)	Endometrioid grade 3 (*n*=10)	High-grade squamous (*n*=4)	*P* value
p53 mutation	3%	0	40%	50%	0.0086
K-ras mutation	23%	42%	20%	25%	NS
Microsatellite instability	26%	25%	30%	50%	NS

Table 3 Comparison of p53 and K-ras mutations and microsatellite instability (MIN) among endometrioid carcinoma with various types of cellular differentiation [42] *NS* not significant

Genetic alteration	Low-grade squamous (*n*=7)	High-grade squamous (*n*=4)	Mucinous (*n*=5)	*P* value
p53 mutation	0	50%	0	0.0024
K-ras mutation	57%	25%	20%	NS
Microsatellite instability	14%	50%	40%	NS

The importance of the cell cycle regulator p16 is controversial, since its alteration varies dramatically in several studies, perhaps due to the applied techniques and interpretation of staining [53, 59, 77, 86]. In a large population-based study, loss of p16 expression was found in less than 10% of endometrioid carcinoma [77]. The underlying mechanism of altered p16 expression is not clear, since neither methylation nor deletion or mutation is frequently found [53, 59, 100].

Her2/neu overexpression seems to play a role in 10–30% of predominantly FIGO [Fédération Internationale de Gynécologie et Obstétrique] grade 2 and 3 endometrioid adenocarcinoma [30, 65, 107]. Amplification was more frequently found than overexpression [72]. Altered expression of the retinoblastoma protein associated with LOH is found about 20% of endometrioid carcinomas [83]. In contrast to colorectal carcinoma, DCC alterations were not found in endometrioid carcinoma [73].

Endometrioid carcinomas with various types of cellular differentiation

Only a few studies have included small numbers of endometrioid carcinomas with various types of cellular differentiation [14, 44, 77]. The available data, thus, have to be interpreted with caution. The data presented in Table 2 and Table 3 are drawn from our own previous analysis [44]. There is evidence that these tumors are genetically related to usual endometrioid carcinoma, since the frequencies of molecular alterations are similar if compared by histological grade. Most data are available for endometrioid adenocarcinoma with squamous differentiation, which harbors MIN and K-ras and p53 similar to usual endometrioid carcinoma. p16 inactivation was found more frequently in endometrioid adenocarcinoma with squamous differentiation than in usual endometrioid carcinoma, but the tumors were not analyzed by grade [77]. Endometrioid carcinoma with mucinous features and secretory variants of endometrioid carcinoma seem to reveal frequent MIN [14, 45].

Serous carcinoma

CIN with extensive disorder of the genome and aneuploidy is typical for serous carcinoma [60, 88]. The most striking genetic alteration, present in about 90% of serous carcinoma, is p53 mutation [97], which is mostly associated with protein overexpression (Fig. 1B). It is still unresolved as to which carcinogenic influence causes these frequent p53 mutations. In contrast to endometrioid carcinoma, MIN is extremely rare among serous carcinoma, as is K-ras and PTEN mutation [44, 96, 98]. Thus far, MIN has only been detected in mixed endometrioid and serous carcinoma, but not in pure serous carcinomas of the endometrium [14]. The differences between serous and endometrioid carcinoma, with respect to MIN and mutations of p53, K-ras and PTEN, are statistically significant [44]. Other genetic alterations that seem to occur more frequently in serous than in endometrioid carcinoma are inactivation of p16 and overexpression of her2/neu. Unfortunately, serous and clear-cell carcinomas were not analyzed separately by most investigators. In one study, p16 inactivation was found in about 45% of serous carcinomas, including some clear cell carcinomas. her2/neu overexpression and gene amplification were found in about 45% [27, 72] and 70% [72] of serous carcinomas, respectively. Furthermore, negative and reduced e-cadherin expression, which is often associated with LOH, occurred in 62% and 87%, respectively, of serous carcinomas (including some clear cell carcinomas) [28, 54]. However, alteration and overexpression of β-catenin is rare in serous carcinoma [61, 80].

Clear cell carcinoma

Thus far, no molecular study on endometrial carcinoma that included a sufficient number of clear cell carcinoma has been published. In various studies, a small number of clear cell carcinomas were analyzed, together with serous carcinomas. Thus, it has been speculated that clear cell carcinoma is similar to serous carcinoma on the molecular

level, particularly, since there are overlaps in biology, clinical behavior and histology. Based on immunohistochemical results, there was evidence that p53 alterations play a minor role compared with serous carcinoma [42]. This seems to be confirmed by mutation analysis [45]. In contrast to serous carcinoma, MIN and PTEN inactivation seem to be rarely found in clear cell carcinoma. As in serous carcinoma, K-ras mutation seems to be absent. EGF-R was frequently overexpressed in a small number of clear cell carcinomas [34].

A progression model for endometrioid carcinoma

There is evidence that the development of endometrioid carcinoma resembles the Vogelstein progression model for colorectal carcinoma (Fig. 2). This hypothesis is supported by the facts that (1) some of the genetic alterations that are found in endometrioid carcinoma are already present in atypical hyperplasia, its immediate precursor lesion; (2) an increase of genetic alterations is found in well-differentiated endometrioid carcinoma compared with atypical hyperplasia; (3) the number of genetic alterations increases according to higher histopathological grade; and (4) a higher number of chromosomal aberrations is found in endometrial carcinoma compared with atypical hyperplasia, using CGH.

Thus far, a progression from simple to complex hyperplasia and, subsequently, to atypical hyperplasia and carcinoma is assumed. Most simple hyperplasias and a subset of complex hyperplasias are polyclonal and, thus, considered reactive processes due to hyperestrogenism, which may regress through progestin treatment [57]. In contrast, most atypical hyperplasias are monoclonal and, thus, considered intraepithelial neoplasias [57]. It is likely that a subset of complex hyperplasia without atypia is neoplastic, too, since it is monoclonal. In addition, the number of chromosomal imbalances in complex hyperplasia is significantly higher than simple hyperplasia and close to the number found in atypical hyperplasia [35]. Since only a part of simple hyperplasias progresses to carcinoma, it is likely that a subset of atypical hyperplasia and endometrioid carcinoma, respectively, arises de novo.

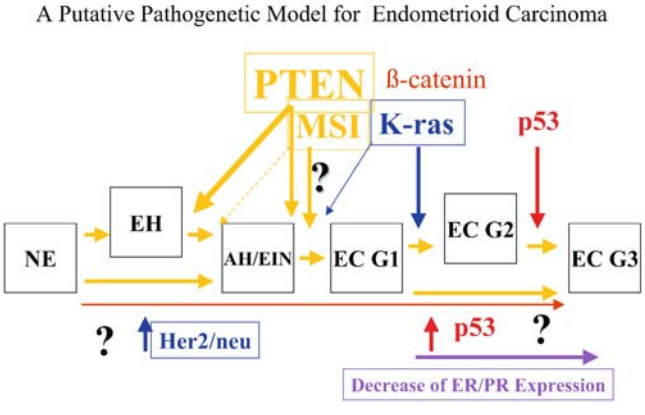

Fig. 2 A putative progression model for endometrioid adenocarcinoma developing through atypical endometrial hyperplasia. Tumor initiation and progression are characterized by acquisition of various molecular alterations of which the most frequent is inactivation of PTEN by mutation. An alternative pathway may directly lead to a high-grade tumor type by p53 mutation and her2/neu amplification, respectively. *NE* normal endometrium, *EH* endometrial hyperplasia without atypia, *AH* atypical endometrial hyperplasia, *EIN* endometrial intraepithelial neoplasia, *EC* endometrioid carcinoma (grade 1–3)

Most of the genetic alterations found in endometrioid carcinoma seem to occur very early in endometrioid tumorigenesis, although it is not clear which are associated with the earliest changes of malignant transformation and progression to neoplasia. In atypical hyperplasia alterations of PTEN, β-catenin, K-ras and MIN are present, of which PTEN inactivation occurs in about 50% of the cases [57]. K-ras mutations [18] and MIN [22, 47] were found in atypical hyperplasia adjacent to endometrioid carcinoma. However, PTEN and K-ras mutations seem to occur earlier, since they were found in simple hyperplasia, partially in association with monoclonality [95]. PTEN inactivation was reported in normally appearing endometrial glands, but the significance of this finding has not yet been determined [58]. Recently, methylation of MLH1 promoter was found in adjacent non-neoplastic endometrium of MIN+ endometrioid carcinomas [32]. E-cadherin expression is normal in endometrial hyperplasia without atypia [76], but altered in 40% of atypical hyperplasia, without showing promoter methylation [54]. It is likely that mutation and methylation of e-cadherin predominantly occurs during the step from atypical hyperplasia to endometrioid carcinoma.

The inactivation of the e-cadherin gene by methylation also seems to play a role during progression of endometrioid carcinoma, since it is most frequently found in grade 3 and least frequently in grade 1 tumors. In addition, p53 mutations [44], amplification and overexpression of her2/neu [72] and p16 inactivation are considered late events during progression and dedifferentiation of endometrioid carcinoma, since they are predominantly found in grade 3 tumors, rarely in grade 1 tumors and are absent in atypical endometrial hyperplasia [30]. Hypothetically, p53 mutations and her2/neu amplification might also be early events in de novo occurring poorly differentiated endometrioid carcinomas, detouring atypical hyperplasia and low-grade carcinoma on an alternative pathway (Fig. 2).

A progression model for serous carcinoma

Mutations of p53 were found in about 80% of endometrial intraepithelial carcinoma (EIC), the putative precursor of serous carcinoma [97], but in contrast to most serous carcinoma without LOH at the locus TP53 (Fig. 3). Thus, it was hypothesized that p53 mutation of one allele occurs early during the development of serous carcinoma's precursor, whereas loss of the normal second allele accompanies progression into serous carcinoma [97].

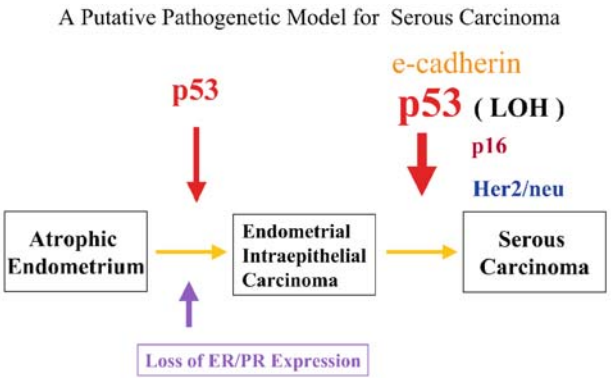

Fig. 3 A putative progression model for serous carcinoma arising from endometrial intraepithelial carcinoma in the background of atrophic endometrium. The major genetic alterations are p53 and e-cadherin mutations

Another group hypothesized that serous carcinoma may develop from endometrioid carcinoma through p53 mutation based on findings in mixed endometrioid and serous carcinomas [51]. It is not clear whether other genetic alterations that are present in serous carcinoma occur early during tumorigenesis, since no analyses on EIC exist.

Prognostic and diagnostic relevance of molecular changes in endometrial carcinoma

p53 and PTEN alterations and her2/neu overexpression showed prognostic significance in several studies, but not independent from histological type and grade [24, 36, 49, 52, 70, 75]. Compared with molecular alterations, histological type and surgical stage are still the strongest prognosticators. Some alterations concur with the histological type. p53 mutation and her2/neu overexpression are associated with poor prognosis and non-endometrioid type. MIN+ seems to be associated with favorable prognosis, but occurs almost exclusively in type-I tumors [14, 52]. With respect to PTEN, the literature is controversial. Loss of PTEN is associated with favorable prognosis and low-grade endometrioid type [70]; however, promoter methylation of PTEN seems to be associated with advanced stage disease [79]. The prognostic value of K-ras mutations seems to depend on age [31]. Among endometrioid carcinoma, the number of genomic aberrations and particular chromosomal changes as determined by CGH seem to have prognostic influence [93]. Due to the lower costs, immunohistochemical analyses of the protein expression are currently preferred to genetic analyses.

Immunohistochemical expression of oncoproteins may also be of diagnostic value. In particular, p53 immunohistochemistry is valuable for diagnosis of serous carcinoma, since an intensive mostly diffuse immunoreactivity is found in about 85–90% of tumors [42]. This might be helpful for the differential diagnosis of papillary endometrial tumors, i.e., papillary endometrioid and serous carcinoma. In addition, most serous carcinomas are negative or only weakly positive for estrogen and progesterone receptors and show a high Ki-67 staining index (40–50% of nuclei) [42]. However, it has to be taken into account that a negative p53 staining does not exclude p53 mutations. Frameshift mutations and stop codons lead to a truncated protein, which is not detected by antibodies and leads to flat negative immunohistochemistry [44, 97]. However, any kind of p53 immunoreactivity does not necessarily predict the presence of p53 mutation [92].

Endometrial carcinoma associated with hereditary syndromes

Compared with sporadic tumors, less is known about the genetic background of hereditary endometrial carcinoma. Most data are drawn from studies on the hereditary nonpolyposis colorectal cancer (HNPCC) syndrome [94, 101, 103]. Some investigators report that, in HNPCC patients, endometrial carcinoma occurs in approximately the same frequency as colorectal carcinoma and may precede its onset [1, 2]. Others state that colorectal carcinoma occurs about ten times more frequently [10]. HNPCC is usually associated with germline mutations of the mismatch repair proteins MLH1, MSH2 and MSH6 [106]. In endometrial compared with colorectal carcinoma, the molecular mechanisms seem to be different with respect to the altered protein. In endometrial carcinomas, inactivation of the MSH2/MSH6 complex seems to play a central role in tumorigenesis [81], even in MLH1 carriers. The endometrial carcinomas arising in HNPCC are related to type-I tumors, since they occur at young age and are histologically of mucinous or endometrioid type [62], but their pathway is driven by germline mutations and is, thus, distinctive. In MSH2 mutation carriers, unlike in MLH1 carriers, a MSI-H status was already present in endometrial hyperplasia without atypia [17]. However, loss of protein expression seems to occur frequently for both MLH1 and MSH2 in endometrial hyperplasia and is considered an early event during tumor development [7]. PTEN inactivation by mutation seems to be also involved in tumorigenesis, since it occurs in about 90% of carcinomas [108].

Future aspects

The development of new technologies provides new perspectives and better tools to comprehensively study cancer than have been possible, thus far [6]. In particular, the cDNA microarray technology allows one to analyze the regulation of thousands of genes within the same tumor. In combination with matrix CGH and tissue arrays, a comprehensive analysis of endometrial carcinomas of various histological and biological types with known clinical behavior will be possible. Two recent compara-

tive analyses between endometrioid and serous carcinomas using cDNA microarrays showed significant differences with respect to up- and downregulated genes [55, 71]. Nevertheless, an enormous amount of work remains to be done to clearly understand the biological processes behind the development of endometrial carcinomas. A major goal for the future might be a further stratification of endometrial carcinoma subtypes according to their genetic alterations, particularly, those with prognostic impact. Thus, future histological classifications will become more molecular based as is the current, but this should not lead to waiver of a solid histological basis.

Acknowledgements The author is dedicating this article to his distinguished teachers in gynecological pathology and molecular pathology, Drs. Robert J. Kurman and Lora H. Ellenson.

References

1. Aarnio M, Mecklin JP, Aaltonen LA, Nystrom Lahti M, Jarvinen HJ (1995) Life-time risk of different cancers in hereditary non-polyposis colorectal cancer (HNPCC) syndrome. Int J Cancer 64:430–433
2. Aarnio M, Sankila R, Pukkala E, Salovaara R, Aaltonen LA, de la Chapelle A, Peltomaki P, Mecklin JP, Jarvinen HJ (1999) Cancer risk in mutation carriers of DNA-mismatch-repair genes. Int J Cancer 81:214–218
3. Abeler VM, Vergote IB, Kjorstad KE, Trope CG (1996) Clear cell carcinoma of the endometrium. Prognosis and metastatic pattern. Cancer 78:1740–1747
4. Albertson DG, Collins C, McCormick F, Gray JW (2003) Chromosome aberrations in solid tumors. Nat Genet 34:369–376
5. Ambros RA, Sherman ME, Zahn CM, Bitterman P, Kurman RJ (1995) Endometrial intraepithelial carcinoma: a distinctive lesion specifically associated with tumors displaying serous differentiation. Hum Pathol 26:1260–1267
6. Baak JP, Path FR, Hermsen MA, Meijer G, Schmidt J, Janssen EA (2003) Genomics and proteomics in cancer. Eur J Cancer 39:1199–1215
7. Berends MJ, Hollema H, Wu Y, van Der Sluis T, Mensink RG, ten Hoor KA, Sijmons RH, de Vries EG, Pras E, Mourits MJ, Hofstra RM, Buys CH, Kleibeuker JH, and van Der Zee AG (2001) MLH1 and MSH2 protein expression as a prescreening marker in hereditary and non-hereditary endometrial hyperplasia and cancer. Int J Cancer 92:398–403
8. Bokhman JV (1983) Two pathogenetic types of endometrial carcinoma. Gynecol Oncol 15:10–17
9. Boland CR, Thibodeau SN, Hamilton SR, Sidransky D, Eshleman JR, Burt RW, Meltzer SJ, Rodriguez-Bigas MA, Fodde R, Ranzani GN, Srivastava S (1998) A National Cancer Institute Workshop on Microsatellite Instability for cancer detection and familial predisposition: development of international criteria for the determination of microsatellite instability in colorectal cancer. Cancer Res 58:5248–5257
10. Brown GJ, St John DJ, Macrae FA, Aittomaki K (2001) Cancer risk in young women at risk of hereditary nonpolyposis colorectal cancer: implications for gynecologic surveillance. Gynecol Oncol 80:346–349
11. Burks RT, Kessis TD, Cho KR, Hedrick L (1994) Microsatellite instability in endometrial carcinoma. Oncogene 9:1163–1166
12. Caduff RF, Johnston CM, Frank TS (1995) Mutations of the Ki-ras oncogene in carcinoma of the endometrium. Am J Pathol 146:182–188
13. Caduff RF, Johnston CM, Svoboda Newman SM, Poy EL, Merajver SD, Frank TS (1996) Clinical and pathological significance of microsatellite instability in sporadic endometrial carcinoma. Am J Pathol 148:1671–1678
14. Catasus L, Machin P, Matias Guiu X, Prat J (1998) Microsatellite instability in endometrial carcinomas: clinicopathologic correlations in a series of 42 cases. Hum Pathol 29:1160–1164
15. Catasus L, Matias-Guiu X, Machin P, Munoz J, Prat J (1998) BAX somatic frameshift mutations in endometrioid adenocarcinomas of the endometrium: evidence for a tumor progression role in endometrial carcinomas with microsatellite instability. Lab Invest 78:1439–1444
16. Cirisano FD Jr, Robboy SJ, Dodge RK, Bentley RC, Krigman HR, Synan IS, Soper JT, Clarke-Pearson DL (2000) The outcome of stage I-II clinically and surgically staged papillary serous and clear cell endometrial cancers when compared with endometrioid carcinoma. Gynecol Oncol 77:55–65
17. de Leeuw WJ, Dierssen J, Vasen HF, Wijnen JT, Kenter GG, Meijers-Heijboer H, Brocker-Vriends A, Stormorken A, Moller P, Menko F, Cornelisse CJ, Morreau H (2000) Prediction of a mismatch repair gene defect by microsatellite instability and immunohistochemical analysis in endometrial tumours from HNPCC patients. J Pathol 192:328–335
18. Duggan BD, Felix JC, Muderspach LI, Tsao JL, Shibata DK (1994) Early mutational activation of the c-Ki-ras oncogene in endometrial carcinoma. Cancer Res 54:1604–1607
19. Enomoto T, Inoue M, Perantoni AO, Terakawa N, Tanizawa O, Rice JM (1990) K-ras activation in neoplasms of the human female reproductive tract. Cancer Res 50:6139–6145
20. Enriori CL, Reforzo-Membrives J (1984) Peripheral aromatization as a risk factor for breast and endometrial cancer in postmenopausal women: a review. Gynecol Oncol 17:1–21
21. Esteller M, Levine R, Baylin SB, Ellenson LH, Herman JG (1998) MLH1 promoter hypermethylation is associated with the microsatellite instability phenotype in sporadic endometrial carcinomas. Oncogene 17:2413–2417
22. Esteller M, Catasus L, Matias Guiu X, Mutter GL, Prat J, Baylin SB, Herman JG (1999) hMLH1 promoter hypermethylation is an early event in human endometrial tumorigenesis. Am J Pathol 155:1767–1772
23. Fearon ER, Vogelstein B (1990) A genetic model for colorectal tumorigenesis. Cell 61:759–767
24. Geisler JP, Geisler HE, Wiemann MC, Zhou Z, Miller GA, Crabtree W (1999) p53 expression as a prognostic indicator of 5-year survival in endometrial cancer. Gynecol Oncol 74:468–471
25. Goodfellow PJ, Buttin BM, Herzog TJ, Rader JS, Gibb RK, Swisher E, Look K, Walls KC, Fan MY, Mutch DG (2003) Prevalence of defective DNA mismatch repair and MSH6 mutation in an unselected series of endometrial cancers. Proc Natl Acad Sci U S A 100:5908–5913
26. Gurin CC, Federici MG, Kang L, Boyd J (1999) Causes and consequences of microsatellite instability in endometrial carcinoma. Cancer Res 59:462–466
27. Halperin R, Zehavi S, Habler L, Hadas E, Bukovsky I, Schneider D (2001) Comparative immunohistochemical study of endometrioid and serous papillary carcinoma of endometrium. Eur J Gynaecol Oncol 22:122–126
28. Holcomb K, Delatorre R, Pedemonte B, McLeod C, Anderson L, Chambers J (2002) E-cadherin expression in endometrioid, papillary serous, and clear cell carcinoma of the endometrium. Obstet Gynecol 100:1290–1295
29. Ikeda T, Yoshinaga K, Suzuki A, Sakurada A, Ohmori H, Horii A (2000) Anticorresponding mutations of the KRAS and PTEN genes in human endometrial cancer. Oncol Res 7:567–570
30. Ioffe OB, Papadimitriou JC, Drachenberg CB (1998) Correlation of proliferation indices, apoptosis, and related oncogene expression (bcl-2 and c-erbB-2) and p53 in proliferative, hyperplastic, and malignant endometrium. Hum Pathol 29:1150–1159
31. Ito K, Watanabe K, Nasim S, Sasano H, Sato S, Yajima A, Silverberg SG, Garrett CT (1996) K-ras point mutations in

endometrial carcinoma: effect on outcome is dependent on age of patient. Gynecol Oncol 63:238–246
32. Kanaya T, Kyo S, Maida Y, Yatabe N, Tanaka M, Nakamura M, Inoue M (2003) Frequent hypermethylation of MLH1 promoter in normal endometrium of patients with endometrial cancers. Oncogene 22:2352–2360
33. Katabuchi H, van Rees B, Lambers AR, Ronnett BM, Blazes MS, Leach FS, Cho KR, Hedrick L (1995) Mutations in DNA mismatch repair genes are not responsible for microsatellite instability in most sporadic endometrial carcinomas. Cancer Res 55:5556–5560
34. Khalifa MA, Mannel RS, Haraway SD, Walker J, Min KW (1994) Expression of EGFR, HER-2/neu, P53, and PCNA in endometrioid, serous papillary, and clear cell endometrial adenocarcinomas. Gynecol Oncol 53:84–92
35. Kiechle M, Hinrichs M, Jacobsen A, Luttges J, Pfisterer J, Kommoss F, Arnold N (2000) Genetic imbalances in precursor lesions of endometrial cancer detected by comparative genomic hybridization. Am J Pathol 156:1827–1833
36. Kihana T, Hamada K, Inoue Y, Yano N, Iketani H, Murao S, Ukita M, Matsuura S (1995) Mutation and allelic loss of the p53 gene in endometrial carcinoma. Incidence and outcome in 92 surgical patients. Cancer 76:72–78
37. Kinzler KW, Vogelstein B (1996) Lessons from hereditary colorectal cancer. Cell 87:159–170
38. Kobayashi K, Sagae S, Nishioka Y, Tokino T, Kudo R (1999) Mutations of the beta-catenin gene in endometrial carcinomas. Jpn J Cancer Res 90:55–59
39. Koul A, Willen R, Bendahl PO, Nilbert M, Borg A (2002) Distinct sets of gene alterations in endometrial carcinoma implicate alternate modes of tumorigenesis. Cancer 94:2369–2379
40. Kowalski LD, Mutch DG, Herzog TJ, Rader JS, Goodfellow PJ (1997) Mutational analysis of MLH1 and MSH2 in 25 prospectively-acquired RER+ endometrial cancers. Genes Chromosomes Cancer 18:219–227
41. Lax SF, Kurman RJ (1997) A dualistic model for endometrial carcinogenesis based on immunohistochemical and molecular genetic analyses. Verh Dtsch Ges Pathol 81228–81232
42. Lax SF, Pizer ES, Ronnett BM, Kurman RJ (1998) Clear cell carcinoma of the endometrium is characterized by a distinctive profile of p53, Ki-67, estrogen, and progesterone receptor expression. Hum Pathol 29:551–558
43. Lax SF, Pizer ES, Ronnett BM, Kurman RJ (1998) Comparison of estrogen and progesterone receptor, Ki-67, and p53 immunoreactivity in uterine endometrioid carcinoma and endometrioid carcinoma with squamous, mucinous, secretory, and ciliated cell differentiation. Hum Pathol 29:924–931
44. Lax SF, Kendall B, Tashiro H, Slebos RJ, Hedrick L (2000) The frequency of p53, K-ras mutations, and microsatellite instability differs in uterine endometrioid and serous carcinoma: evidence of distinct molecular genetic pathways. Cancer 88:814–824
45. Lax SF, Abeler VM, Regitnig P (2001) Molecular genetic analysis of endometrial carcinoma: evidence for 2 genetically distinctive entities. Virchows Arch 439:247
46. Lengauer C, Kinzler KW, Vogelstein B (1997) Genetic instability in colorectal cancers. Nature 386:623–627
47. Levine RL, Cargile CB, Blazes MS, van Rees B, Kurman RJ, Ellenson LH (1998) PTEN mutations and microsatellite instability in complex atypical hyperplasia, a precursor lesion to uterine endometrioid carcinoma. Cancer Res 58:3254–3258
48. Li LS, Kim NG, Kim SH, Park C, Kim H, Kang HJ, Koh KH, Kim SN, Kim WH, Kim NK (2003) Chromosomal imbalances in the colorectal carcinomas with microsatellite instability. Am J Pathol 163:1429–1436
49. Lukes AS, Kohler MF, Pieper CF, Kerns BJ, Bentley R, Rodriguez GC, Soper JT, Clarke-Pearson DL, Bast RC Jr, Berchuck A (1994) Multivariable analysis of DNA ploidy, p53, and HER-2/neu as prognostic factors in endometrial cancer. Cancer 73:2380–2385
50. MacDonald ND, Salvesen HB, Ryan A, Iversen OE, Akslen LA, Jacobs IJ (2000) Frequency and prognostic impact of microsatellite instability in a large population-based study of endometrial carcinomas. Cancer Res 60:1750–1752
51. Matias-Guiu X, Catasus L, Bussaglia E, Lagarda H, Garcia A, Pons C, Munoz J, Arguelles R, Machin P, Prat J (2001) Molecular pathology of endometrial hyperplasia and carcinoma. Hum Pathol 32:569–577
52. Maxwell GL, Risinger JI, Alvarez AA, Barrett JC, Berchuck A (2001) Favorable survival associated with microsatellite instability in endometrioid endometrial cancers. Obstet Gynecol 97:417–422
53. Milde-Langosch K, Riethdorf L, Bamberger AM, Loning T (1999) P16/MTS1 and pRB expression in endometrial carcinomas. Virchows Arch 434:23–28
54. Moreno-Bueno G, Hardisson D, Sarrio D, Sanchez C, Cassia R, Prat J, Herman JG, Esteller M, Matias-Guiu X, Palacios J (2003) Abnormalities of E- and P-cadherin and catenin (beta-, gamma-catenin, and p120ctn) expression in endometrial cancer and endometrial atypical hyperplasia. J Pathol 199:471–478
55. Moreno-Bueno G, Sanchez-Estevez C, Cassia R, Rodriguez-Perales S, Diaz-Uriarte R, Dominguez O, Hardisson D, Andujar M, Prat J, Matias-Guiu X, Cigudosa JC, Palacios J (2003) Differential gene expression profile in endometrioid and nonendometrioid endometrial carcinoma: STK15 is frequently overexpressed and amplified in nonendometrioid carcinomas. Cancer Res 63:5697–5702
56. Mutter GL (2001) Pten, a protean tumor suppressor. Am J Pathol 158:1895–1898
57. Mutter GL, Baak JP, Crum CP, Richart RM, Ferenczy A, Faquin WC (2000) Endometrial precancer diagnosis by histopathology, clonal analysis, and computerized morphometry. J Pathol 190:462–469
58. Mutter GL, Lin MC, Fitzgerald JT, Kum JB, Baak JP, Lees JA, Weng LP, Eng C (2000) Altered PTEN expression as a diagnostic marker for the earliest endometrial precancers. J Natl Cancer Inst 92:924–930
59. Nakashima R, Fujita M, Enomoto T, Haba T, Yoshino K, Wada H, Kurachi H, Sasaki M, Wakasa K, Inoue M, Buzard G, Murata Y (1999) Alteration of p16 and p15 genes in human uterine tumours. Br J Cancer 80:458–467
60. Nordstrom B, Strang P, Lindgren A, Bergstrom R, Tribukait B (1996) Endometrial carcinoma: the prognostic impact of papillary serous carcinoma (UPSC) in relation to nuclear grade, DNA ploidy and p53 expression. Anticancer Res 16:899–904
61. Palacios J, Catasus L, Moreno Bueno G, Matias Guiu X, Prat J, Gamallo C (2001) Beta- and gamma-catenin expression in endometrial carcinoma. Relationship with clinicopathological features and microsatellite instability. Virchows Arch 438:464–469
62. Parc YR, Halling KC, Burgart LJ, McDonnell SK, Schaid DJ, Thibodeau SN, Halling AC (2000) Microsatellite instability and hMLH1/hMSH2 expression in young endometrial carcinoma patients: associations with family history and histopathology. Int J Cancer 86:60–66
63. Perucho M (1996) Microsatellite instability: the mutator that mutates the other mutator. Nat Med 2:630–631
64. Potischman N, Hoover RN, Brinton LA, Siiteri P, Dorgan JF, Swanson CA, Berman ML, Mortel R, Twiggs LB, Barrett RJ, Wilbanks GD, Persky V, Lurain JR (1996) Case-control study of endogenous steroid hormones and endometrial cancer. J Natl Cancer Inst 88:1127–1135
65. Riben MW, Malfetano JH, Nazeer T, Muraca PJ, Ambros RA, Ross JS (1997) Identification of HER-2/neu oncogene amplification by fluorescence in situ hybridization in stage I endometrial carcinoma. Mod Pathol 10:823–831
66. Riethdorf L, Begemann C, Riethdorf S, Milde-Langosch K, Loning T (1996) Comparison of benign and malignant endometrial lesions for their p53 state, using immunohisto-

chemistry and temperature-gradient gel electrophoresis. Virchows Arch 428:47–51
67. Risinger JI, Dent GA, Ignar-Trowbridge D, McLachlan JA, Tsao MS, Senterman M, Boyd J (1992) p53 gene mutations in human endometrial carcinoma. Mol Carcinog 5:250–253
68. Risinger JI, Berchuck A, Kohler MF, Watson P, Lynch HT, Boyd J (1993) Genetic instability of microsatellites in endometrial carcinoma. Cancer Res 53:5100–5103
69. Risinger JI, Umar A, Boyd J, Berchuck A, Kunkel TA, Barrett JC (1996) Mutation of MSH3 in endometrial cancer and evidence for its functional role in heteroduplex repair. Nat Genet 14:102–105
70. Risinger JI, Hayes K, Maxwell GL, Carney ME, Dodge RK, Barrett JC, Berchuck A (1998) PTEN mutation in endometrial cancers is associated with favorable clinical and pathologic characteristics. Clin Cancer Res 4:3005–3010
71. Risinger JI, Maxwell GL, Chandramouli GV, Jazaeri A, Aprelikova O, Patterson T, Berchuck A, Barrett JC (2003) Microarray analysis reveals distinct gene expression profiles among different histologic types of endometrial cancer. Cancer Res 63:6–11
72. Rolitsky CD, Theil KS, McGaughy VR, Copeland LJ, Niemann TH (1999) HER-2/neu amplification and overexpression in endometrial carcinoma. Int J Gynecol Pathol 18:138–143
73. Ronnett BM, Burks RT, Cho KR, Hedrick L (1997) DCC genetic alterations and expression in endometrial carcinoma. Mod Pathol 10:38–46
74. Saegusa M, Hashimura M, Yoshida T, Okayasu I (2001) Beta-catenin mutations and aberrant nuclear expression during endometrial tumorigenesis. Br J Cancer 84:209–217
75. Saffari B, Jones LA, el-Naggar A, Felix JC, George J, Press MF (1995) Amplification and overexpression of HER-2/neu (c-erbB2) in endometrial cancers: correlation with overall survival. Cancer Res 55:5693–5698
76. Saito T, Nishimura M, Yamasaki H, Kudo R (2003) Hypermethylation in promoter region of E-cadherin gene is associated with tumor dedifferention and myometrial invasion in endometrial carcinoma. Cancer 97:1002–1009
77. Salvesen HB, Das S, Akslen LA (2000) Loss of nuclear p16 protein expression is not associated with promoter methylation but defines a subgroup of aggressive endometrial carcinomas with poor prognosis. Clin Cancer Res 6:153–159
78. Salvesen HB, MacDonald N, Ryan A, Iversen OE, Jacobs IJ, Akslen LA, Das S (2000) Methylation of hMLH1 in a population-based series of endometrial carcinomas. Clin Cancer Res 6:3607–3613
79. Salvesen HB, MacDonald N, Ryan A, Jacobs IJ, Lynch ED, Akslen LA, Das S (2001) PTEN methylation is associated with advanced stage and microsatellite instability in endometrial carcinoma. Int J Cancer 91:22–26
80. Schlosshauer PW, Ellenson LH, Soslow RA (2002) Beta-catenin and E-cadherin expression patterns in high-grade endometrial carcinoma are associated with histological subtype. Mod Pathol 15:1032–1037
81. Schweizer P, Moisio AL, Kuismanen SA, Truninger K, Vierumaki R, Salovaara R, Arola J, Butzow R, Jiricny J, Peltomaki P, Nystrom-Lahti M (2001) Lack of MSH2 and MSH6 characterizes endometrial but not colon carcinomas in hereditary nonpolyposis colorectal cancer. Cancer Res 61:2813–2815
82. Semczuk A, Schneider-Stock R, Berbec H, Marzec B, Jakowicki JA, Roessner A (2001) K-ras exon 2 point mutations in human endometrial cancer. Cancer Lett 164:207–212
83. Semczuk A, Marzec B, Roessner A, Jakowicki JA, Wojcierowski J, Schneider-Stock R (2002) Loss of heterozygosity of the retinoblastoma gene is correlated with the altered pRb expression in human endometrial cancer. Virchows Arch 441:577–583
84. Sherman ME, Bur ME, Kurman RJ (1995) p53 in endometrial cancer and its putative precursors: evidence for diverse pathways of tumorigenesis. Hum Pathol 26:1268–1274
85. Sherman ME, Sturgeon S, Brinton LA, Potischman N, Kurman RJ, Berman ML, Mortel R, Twiggs LB, Barrett RJ, Wilbanks GD (1997) Risk factors and hormone levels in patients with serous and endometrioid uterine carcinomas. Mod Pathol 10:963–968
86. Shiozawa T, Nikaido T, Shimizu M, Zhai Y, Fujii S (1997) Immunohistochemical analysis of the expression of cdk4 and p16INK4 in human endometrioid-type endometrial carcinoma. Cancer 80:2250–2256
87. Simpkins SB, Bocker T, Swisher EM, Mutch DG, Gersell DJ, Kovatich AJ, Palazzo JP, Fishel R, Goodfellow PJ (1999) MLH1 promoter methylation and gene silencing is the primary cause of microsatellite instability in sporadic endometrial cancers. Hum Mol Genet 8:661–666
88. Sonoda G, du Manoir S, Godwin AK, Bell DW, Liu Z, Hogan M, Yakushiji M, Testa JR (1997) Detection of DNA gains and losses in primary endometrial carcinomas by comparative genomic hybridization. Genes Chromosomes Cancer 18:115–125
89. Soslow RA, Pirog E, Isacson C (2000) Endometrial intraepithelial carcinoma with associated peritoneal carcinomatosis. Am J Surg Pathol 24:726–732
90. Staebler A, Lax SF, Ellenson LH (2000) Altered expression of hMLH1 and hMSH2 protein in endometrial carcinomas with microsatellite instability. Hum Pathol 31:354–358
91. Stefansson I, Akslen LA, MacDonald N, Ryan A, Das S, Jacobs IJ, Salvesen HB (2002) Loss of hMSH2 and hMSH6 expression is frequent in sporadic endometrial carcinomas with microsatellite instability: a population-based study. Clin Cancer Res 8:138–143
92. Stewart RL, Royds JA, Burton JL, Heatley MK, Wells M (1998) Direct sequencing of the p53 gene shows absence of mutations in endometrioid endometrial adenocarcinomas expressing p53 protein. Histopathology 33:440–445
93. Suehiro Y, Umayahara K, Ogata H, Numa F, Yamashita Y, Oga A, Morioka H, Ito T, Kato H, Sasaki K (2000) Genetic aberrations detected by comparative genomic hybridization predict outcome in patients with endometrioid carcinoma. Genes Chromosomes Cancer 29:75–82
94. Sumoi R, Hakala Ala Pietila T, Leminen A, Mecklin JP, Lehtovirta P (1995) Hereditary aspects of endometrial adenocarcinoma. Int J Cancer 62:132–137
95. Sun H, Enomoto T, Shroyer KR, Ozaki K, Fujita M, Ueda Y, Nakashima R, Kuragaki C, Ueda G, Murata Y (2002) Clonal analysis and mutations in the PTEN and the K-ras genes in endometrial hyperplasia. Diagn Mol Pathol 11:204–211
96. Tashiro H, Blazes MS, Wu R, Cho KR, Bose S, Wang SI, Li J, Parsons R, Ellenson LH (1997) Mutations in PTEN are frequent in endometrial carcinoma but rare in other common gynecological malignancies. Cancer Res 57:3935–3940
97. Tashiro H, Isacson C, Levine R, Kurman RJ, Cho KR, Hedrick L (1997) p53 gene mutations are common in uterine serous carcinoma and occur early in their pathogenesis. Am J Pathol 150:177–185
98. Tashiro H, Lax SF, Gaudin PB, Isacson C, Cho KR, Hedrick L (1997) Microsatellite instability is uncommon in uterine serous carcinoma. Am J Pathol 150:75–79
99. Tavassoli FA, Devilee P (eds) (2003) Tumours of the breast and female genital organs. IARC Press, Lyon
100. Tsuda H, Yamamoto K, Inoue T, Uchiyama I, Umesaki N (2000) The role of p16-cyclin d/CDK-pRb pathway in the tumorigenesis of endometrioid-type endometrial carcinoma. Br J Cancer 82:675–682
101. Vasen HF, Watson P, Mecklin JP, Jass JR, Green JS, Nomizu T, Muller H, Lynch HT (1994) The epidemiology of endometrial cancer in hereditary nonpolyposis colorectal cancer. Anticancer Res 14:1675–1678
102. Wada H, Enomoto T, Fujita M, Yoshino K, Nakashima R, Kurachi H, Haba T, Wakasa K, Shroyer KR, Tsujimoto M, Hongyo T, Nomura T, Murata Y (1997) Molecular evidence that most but not all carcinosarcomas of the uterus are combination tumors. Cancer Res 57:5379–5385

103. Watson P, Vasen HF, Mecklin JP, Jarvinen H, Lynch HT (1994) The risk of endometrial cancer in hereditary nonpolyposis colorectal cancer. Am J Med 96:516–520
104. Weiderpass E, Adami HO, Baron JA, Magnusson C, Bergstrom R, Lindgren A, Correia N, Persson I (1999) Risk of endometrial cancer following estrogen replacement with and without progestins. J Natl Cancer Inst 91:1131–1137
105. Wheeler DT, Bell KA, Kurman RJ, Sherman ME (2000) Minimal uterine serous carcinoma: diagnosis and clinicopathologic correlation. Am J Surg Pathol 24:797–806
106. Wijnen JT, Vasen HF, Khan PM, Zwinderman AH, van der Klift H, Mulder A, Tops C, Moller P, Fodde R (1998) Clinical findings with implications for genetic testing in families with clustering of colorectal cancer. N Engl J Med 339:511–518
107. Williams JA Jr, Wang ZR, Parrish RS, Hazlett LJ, Smith ST, Young SR (1999) Fluorescence in situ hybridization analysis of HER-2/neu, c-myc, and p53 in endometrial cancer. Exp Mol Pathol 67:135–143
108. Zhou XP, Kuismanen S, Nystrom-Lahti M, Peltomaki P, Eng C (2002) Distinct PTEN mutational spectra in hereditary nonpolyposis colon cancer syndrome-related endometrial carcinomas compared to sporadic microsatellite unstable tumors. Hum Mol Genet 11:445–450

Virchows Arch (2004) 444:224–230
DOI 10.1007/s00428-003-0968-y

ORIGINAL ARTICLE

J. Pinto-de-Sousa · C. A. Reis · L. David · A. Pimenta · M. Cardoso-de-Oliveira

MUC5B expression in gastric carcinoma: relationship with clinico-pathological parameters and with expression of mucins MUC1, MUC2, MUC5AC and MUC6

Received: 4 September 2003 / Accepted: 8 December 2003 / Published online: 31 January 2004

Abstract Previous studies have shown that mucin expression can be used to evaluate differentiation patterns of gastric carcinoma: MUC5AC expression is associated with diffuse type and early gastric carcinomas, and MUC2 expression is associated with mucinous gastric carcinomas. The role played by MUC5B in the evaluation of differentiation and biological behaviour of gastric carcinoma is largely unknown. Our aim was to characterise the pattern of expression of mucins MUC1, MUC2, MUC5AC, MUC5B and MUC6 in a series of 50 gastric carcinomas to evaluate whether MUC5B expression was associated with the clinico-pathological characteristics of the cases and/or with the co-expression of other mucins. A panel of six monoclonal antibodies (HMFG1, SM3, PMH1, CLH2, EU-MUC5Ba and CLH5) was used to determine the expression of mucins (MUC1, MUC1 underglycosylated form, MUC2, MUC5B, MUC5AC and MUC6, respectively) using immunohistochemistry. Cases were considered positive if more than 5% of the cells expressed immunoreactivity for the several mucins evaluated. Our results showed that: (a) expression of MUC5B was observed in 11 cases (22.0%) and was associated with the "unclassified" histological type of gastric carcinoma according to Laurén (P=0.03) and with the absence of venous invasion (P=0.02); (b) in this series, MUC5B expression had no impact on survival of patients with gastric carcinoma; (c) the expression of MUC5B was associated with the co-expression of MUC5AC (P=0.02) and (d) none of the cases with the so-called complete intestinal phenotype of mucin expression expressed MUC5B.

Keywords MUC5B · MUC5AC · Mucins · Venous invasion · Gastric carcinoma

J. Pinto-de-Sousa · A. Pimenta · M. Cardoso-de-Oliveira
Surgery B,
Hospital S. João, Medical Faculty of the University of Porto and Institute of Molecular Pathology and Immunology of the University of Porto (IPATIMUP),
Porto, Portugal

C. A. Reis
Institute of Molecular Pathology and Immunology of the University of Porto (IPATIMUP),
Porto, Portugal

L. David
Institute of Molecular Pathology and Immunology of the University of Porto (IPATIMUP) and Medical Faculty of the University of Porto,
Porto, Portugal

J. Pinto-de-Sousa (✉)
IPATIMUP, Rua Dr. Roberto Frias s/n, 4200 Porto, Portugal
e-mail: japs@med.up.pt
Tel.: +35-12-25570700
Fax: +35-12-25570799

Introduction

Mucins are high-molecular-weight glycoproteins that are synthesised by secretory epithelial cells as membrane or secreted proteins. Thus far, at least 14 mucin genes have been identified that code for mucin proteins. They are designated MUC1 [19, 27], MUC2 [20], MUC3 [21], MUC4 [38], MUC5AC [1, 22], MUC5B [17], MUC6 [48], MUC7 [7], MUC8 [45], MUC9 [28], MUC11, MUC12, MUC13 [51] and MUC16 [52]. Mucin genes are expressed in a regulated cell- and tissue-specific manner. Numerous studies have demonstrated that mucin expression is altered during the pathogenesis of neoplastic diseases, which suggests that human mucin gene expression is regulated in terms of cell- and tissue-specific expression and that they may play important roles during cell differentiation and carcinogenesis [26].

Human stomach provides a good example of differential expression of mucin genes. In normal stomach, MUC1 is detected in mucous cells of the surface epithelium and neck regions of the gastric antrum, as well as in pyloric glands and oxynthic glands of the body region [23, 24, 41]. MUC5AC is highly expressed in foveolar epithelium of both antrum and body [2, 8, 24, 39], whereas MUC6 protein expression is limited to mucous neck cells of the body and pyloric glands of the antrum [6, 8, 10, 11, 24, 42]. In gastric carcinoma, the

mucin expression is heterogeneous. It includes mucins normally expressed in gastric mucosa (MUC1, MUC5AC and MUC6) and de novo expression of the intestinal mucin MUC2 [5, 11, 23, 24, 40, 42, 44, 49].

The heterogeneous pattern of mucin expression may provide insights into the differentiation pathways of gastric carcinoma. The pattern of mucin expression may also help to understand the biological behaviour of the distinct clinico-pathological entities of gastric carcinoma according to tumour location, proximal versus distal lesions. Previous studies have shown that MUC5AC expression in gastric cancer is associated with diffuse type carcinomas and early gastric carcinomas, and that de novo expression of MUC2 is associated with mucinous carcinomas and with the location in the cardia [37, 39, 40, 42]. The role of the aforementioned mucins expression in the evaluation of prognosis of gastric carcinoma is not yet fully established [30, 37].

Four of the mucin genes, MUC2, MUC5AC, MUC5B and MUC6, have been mapped to 11p15.5 on a single band of 400 kb [35]. MUC5B gene is 39.09 kb in length, contains 49 exons and encodes a 5701-amino-acid polypeptide with a molecular range of approximately 627,000 [12, 13, 15, 50]. The mucin MUC5B is expressed mainly in trachea and bronchus glands and also in submaxillary glands, endocervix, gall bladder and pancreas [3, 4, 14]. Under normal conditions, there is no MUC5B expression in the adult stomach. According to some studies, MUC5B was detected in the period between 8 weeks and 27 weeks gestation in the embryonic stomach, but after that no MUC5B could be consistently detected [8]. Interestingly, MUC5B is expressed de novo in gastric mucosa only in cases of gastric carcinoma [8, 33]. The full coding sequence of the MUC5B gene has recently been obtained, but despite the recent ongoing investigation [12, 13, 15, 33, 50], the role played by MUC5B in the evaluation of differentiation and biological behaviour of gastric carcinoma remains largely unknown.

In this study, we evaluated the role of MUC5B expression in gastric carcinoma using a novel monoclonal antibody EU-MUC5Ba [43]. Our aim was to characterise the pattern of expression of mucins MUC1, MUC2, MUC5AC, MUC5B and MUC6 in a series of gastric carcinomas to evaluate if MUC5B expression was associated with the clinico-pathological characteristics of the cases and/or co-expression of other mucins.

Materials and methods

Tissue samples and histopathological study

Surgical specimens from 50 gastric carcinomas were evaluated retrospectively. The 50 patients were submitted to surgical resection of gastric carcinoma in Serviço Cirurgia B, Hospital S. João, between January 1988 and December 1990. Selected cases were classified as cardia carcinoma, fundus/body and antrum carcinomas according to the tumour location, following the criteria described in a previous study [36]. Mean age and gender were also recorded.

Carcinomas were considered according to Laurén's classification [29]. The growth pattern was classified according to Ming [31]. Orcein-stained sections were used for the detection of venous invasion, which was scored as absent or present. Lymphatic vessels invasion was scored as absent or present. The depth of wall penetration and nodal status were also recorded. The 1997 version of the UICC (International Union Against Cancer) pTNM system was employed to stage the carcinomas [46].

Antibodies and immunohistochemistry

The characterisation of monoclonal antibodies is documented in Table 1. The expression of MUC1, underglycosylated form of MUC1, MUC2, MUC5AC and MUC6 mucins was studied using immunohistochemistry with monoclonal antibodies (HMFG1, SM2, PMH1, CLH2, and CLH5, respectively) according to the methodology described in a former study [37].

The monoclonal antibody EU-MUC5Ba was used to detect MUC5B [43]. Sections from the surgical specimens representative of the carcinomas were immunostained using avidin-biotin-complex staining. The paraffin sections were de-waxed and rehydrated. Sections were treated with 0.3% hydrogen peroxide in methanol for 30 min, to block endogenous peroxidase, followed by incubation with normal non-immune serum for 20 min. Sections were rinsed with Tris-buffered saline (TBS) and incubated with primary antibodies overnight at 4°C. Sections were rinsed and incubated with a biotin-labelled rabbit anti-mouse secondary antibody, diluted 1:200 in TBS for 30 min, then rinsed and incubated with avidin-biotin-peroxidase complex for 1 h. Sections were rinsed and stained for 7 min with 0.05% 3′3diaminobenzidinetetrahydrochloride freshly prepared in 0.05 M Tris/hydroxymethylaminomethane buffer, pH 7.6, containing 0.1% hydrogen peroxide. Sections were counterstained with hematoxylin, dehydrated and mounted. All series included normal human tissues as positive controls (minor salivary glands were used as a positive control for MUC5B). Negative controls were performed using conjugate alone.

Classification of immunohistochemistry

Cases were classified according to the immunostaining for the mucins evaluated (MUC1, MUC2, MUC5AC, MUC5B and MUC6) in two groups: negative (negative or rare/less than 5% of positive cells) and positive (positive in more than 5% of the cells).

Table 1 Characterisation of monoclonal antibodies used to identify the mucins evaluated

Monoclonal antibody	Specificity	Dilution	Reference
HMFG1	MUC1 (tandem repeat)	1:4	(Taylor-Papadimitriou et al. 1981) [47]
SM3	MUC1 (under glycosylated tandem repeat)	Undiluted	(Burchell et al. 1987) [9]
PMH1	MUC2-GalNAc	1:2	Reis et al. 1998 [42]
CLH2[a]	MUC5AC	1:5	Reis et al. 1997 [40]
EU-MUC5Ba	MUC5B	1:2	Rousseau et al. in press [43]
CLH5[b]	MUC6	1:5	Reis et al. 2000 [39]

[a] Code number NCL-MUC-5AC from Novocastra Laboratories Ltd., UK
[b] Code number NCL-MUC-6 from Novocastra Laboratories Ltd., UK

According to the combination of mucins expression, several "phenotypes" of mucin expression in gastric carcinoma cases were considered: gastric "phenotype", if carcinomas expressed MUC5AC and/or MUC6 but not MUC2; complete intestinal "phenotype", if carcinomas expressed MUC2 but neither MUC5AC nor MUC6 mucins; and incomplete intestinal "phenotype", if carcinomas expressed MUC2 and MUC5AC or MUC6 mucins [32].

Survival analysis

Survival data was obtained from the Cancer Registry and from the data of esophagogastric follow-up consultation of Hospital S. João, with a follow-up of 100% of the patients. Cumulative survival was evaluated according to the staining for each of the mucins evaluated.

Statistical analysis

StatView 5.0 and SPSS 11.0 for Windows computer programs were employed in the statistical analysis of data. Distributions were compared using the chi-squared test or by the Fisher's exact test whenever appropriate. Cumulative survival curves were obtained using the Kaplan-Meier limit product [25] and compared using the log rank test. Significance was assumed if P values were less than 0.05.

Results

MUC5B expression was never detected in normal adult human gastric mucosa or in mucosa with intestinal metaplasia in the vicinity of gastric carcinomas.

In the present series, the mucin MUC5B was expressed in 11 of the 50 (22%) surgical specimens of gastric carcinomas analysed using immunohistochemistry (Fig. 1). Of gastric carcinomas in our series, 45 cases (90%) expressed MUC1, 24 (48%) expressed the underglycosylated form of MUC1, defined by SM3 antibody, 16 (32%) expressed MUC2, 25 (50%) expressed MUC5AC and 16 cases (32%) expressed MUC6.

Association between MUC5B expression and clinico-pathological parameters and cumulative survival of gastric carcinoma patients

Significant differences were observed according to MUC5B expression and Laurén's classification of gastric carcinomas (P=0.03). The expression of MUC5B in unclassified gastric carcinomas (57.1%) was higher than in intestinal or diffuse carcinomas (11.1% and 21.4%, respectively) (Table 2).

Significant differences were also observed in the distribution of cases according to the expression of MUC5B and venous invasion (P=0.02). The percentage of carcinoma cases with venous invasion expressing MUC5B (4.8%) was lower than that of cases without venous invasion (34.5%).

Mean age of the whole population was 58.5±13.7 years, and median age was 60 years. Mean age of patients with carcinomas expressing MUC5B (59.0±13.2 years) was not significantly different from that of those not expressing MUC5B (56.7±16.1 years).

No significant differences were observed in the distribution of cases according to the expression of MUC5B and gender of the patients, location of the tumour or Ming's classification (Table 2). No significant differences were observed in the distribution of cases according to the expression of MUC5B and the tumour depth of wall penetration, lymphatic vessels invasion and nodal status (Table 2).

Median follow-up time was 49 months (range 1–159 months). During the study, 31 patients (62%) died. Among these were 25 patients with carcinomas not expressing MUC5B (64.1%) and 6 patients with carcinomas expressing MUC5B (54.5%). For patients with carcinomas not expressing MUC5B (37.7%), 5-year survival was not significantly different than that of those with carcinomas expressing MUC5B (40.0%) (P=0.59). Subdivision of positive cases according to the percentage of positive cells generated groups with a very small number, which did not allow statistical comparisons (data not shown).

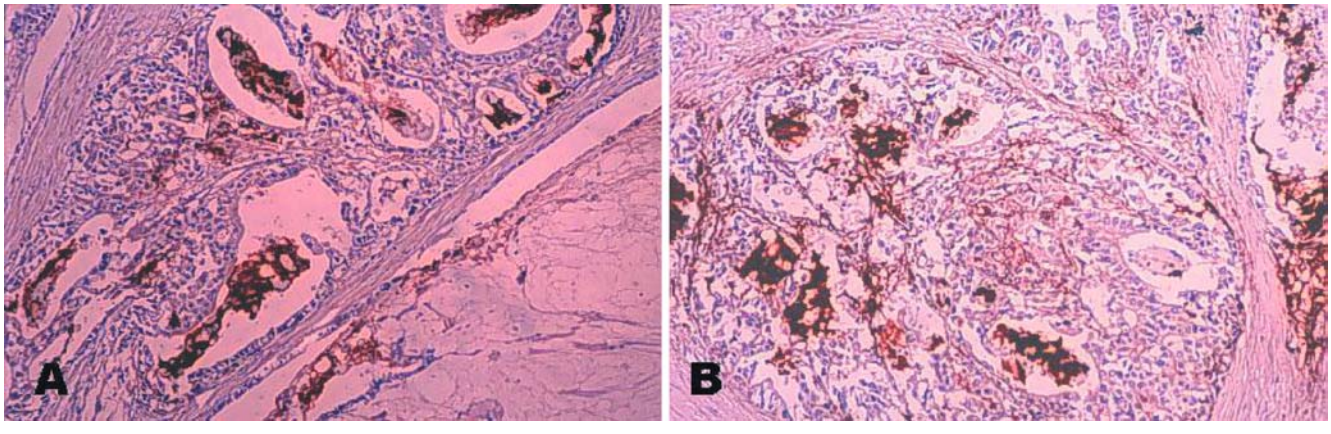

Fig. 1 Immunoreactivity for MUC5B mucin in two cases (**A**, **B**) of gastric carcinoma

Table 2 Summary of MUC5B expression in gastric carcinoma according to clinical and pathological characteristics

Parameters	MUC5B Expression		*P* value
	Negative	Positive	
	n (%)	*n* (%)	
Gender (*n*=50)			0.97
Male	25 (78.1)	7 (21.9)	
Female	14 (77.8)	4 (22.2)	
Tumour site (*n*=50)			0.94
Cardia	9 (75.0)	3 (25.0)	
Fundus/body	10 (76.9)	3 (23.1)	
Antrum	20 (80.0)	5 (20.0)	
Laurén's classification (*n*=50)			0.03
Intestinal	24 (88.9)	3 (11.1)	
Diffuse	11 (78.6)	3 (21.4)	
Unclassified	3 (42.9)	4 (57.1)	
Ming's classification (*n*=48)			0.65
Expansive	12 (80.0)	3 (20.0)	
Infiltrative	25 (75.8)	8 (24.2)	
Venous invasion (*n*=50)			0.02
Absent	19 (65.5)	10 (34.5)	
Present	20 (95.2)	1 (4.8)	
Depth wall penetration (*n*=50)			0.46
T1–2	26 (74.3)	9 (25.7)	
T3–4	13 (86.7)	2 (13.3)	
Lymphatic vessels invasion (*n*=50)			0.69
Absent	5 (55.6)	4 (44.4)	
Present	34 (82.9)	7 (17.1)	
Nodal metastases (*n*=50)			0.66
Absent	13 (72.2)	5 (27.8)	
Present	26 (81.3)	6 (18.7)	

Table 3 Co-expression between MUC5B and mucins MUC1, MUC2, MUC5AC and MUC6

Mucin expression	MUC5B Expression		*P* value
	Negative	Positive	
	n (%)	*n* (%)	
MUC1			
Negative	4 (80.0)	1 (20.0)	0.9
Positive	35 (77.8)	10 (22.2)	
MUC1 underglycosylated			
Negative	20 (76.9)	6 (23.1)	0.85
Positive	19 (79.2)	5 (20.8)	
MUC2			
Negative	27 (79.4)	7 (20.6)	0.73
Positive	12 (75.0)	4 (25.0)	
MUC5AC			
Negative	23 (92.0)	2 (8.0)	0.02
Positive	16 (64.0)	9 (36.0)	
MUC6			
Negative	28 (82.4)	6 (17.6)	0.28
Positive	11 (68.8)	5 (31.2)	

Table 4 Association between mucin "phenotype" and MUC5B expression. *IM* intestinal mucin

Mucin "phenotype"	MUC5B Expression		*P* value
	Negative	Positive	
	n (%)	*n* (%)	
Gastric	17 (77.3)	5 (22.7)	0.18
Complete IM	7 (100.0)	0 (00.0)	
Incomplete IM	5 (55.6)	4 (44.4)	
Negative MUC2, MUC5AC and MUC6	10 (83.3)	2 (16.7)	

Association between expression of MUC5B and expression of mucins MUC1, MUC2, MUC5AC and MUC6

Table 3 documents co-expression of MUC5B and mucins MUC1, MUC2, MUC5AC and MUC6 in gastric carcinomas. A significant association in the expression of MUC5B and MUC5AC in gastric carcinoma cases was observed (*P*=0.02). Of the cases without expression of MUC5AC, 92% also did not express MUC5B. In the group of carcinomas with expression of MUC5AC, nine cases (36%) also expressed MUC5B. No significant association or agreement was observed in the study between the expression of MUC5B and that of MUC1, MUC2 and MUC6 in gastric carcinoma cases (Table 3).

Table 4 documents the association between the mucin "phenotype" and immunoreactivity for MUC5B. No significant association was observed between MUC5B expression and the presence of gastric mucin "phenotype". None of the cases with the so-called complete intestinal "phenotype" (MUC2 immunoreactivity with absent MUC5AC and MUC6 expression) expressed MUC5B. No significant association was observed between MUC5B and the so-called incomplete intestinal "phenotype" (MUC2 and MUC5AC or MUC6 expression), as well as between MUC5B and the absence of MUC2, MUC5AC and MUC6 expression.

Discussion

In this study, we evaluated MUC5B expression in gastric cancer using a novel monoclonal antibody, EU-MUC5Ba. Both the normal mucosa of the stomach and the gastric mucosa with intestinal metaplasia are not immunoreactive for EU-MUC5Ba, and MUC5B was expressed in 22% of gastric carcinoma cases.

In human stomach, MUC5B is expressed only during a brief period of foetal life [8]. MUC5B expression in human stomach is always aberrant, or de novo, and is only observed in cases of gastric carcinoma [8, 33]. These observations suggest that aberrant MUC5B expression might be viewed as an oncofetal marker in the adult and might, therefore, constitute a valuable tool in the diagnosis of gastric carcinoma in the future.

The present study contributed to clarify the role of the expression of MUC5B in the differentiation and in the biological behaviour of gastric carcinoma. Our results showed that MUC5B expression is associated with the differentiation of gastric carcinoma, with absence of venous invasion and with co-expression of the gastric mucin MUC5AC.

In the present series, MUC5B was aberrantly expressed in 22% of the gastric carcinoma cases. This percentage is lower than the 60–66.7% of positive cases reported by other authors, in two small series of five or six cases, respectively [8, 33]. The frequency of MUC5B expression in our study was lower than the frequency of expression of other mucins, whose codifying genes are located in the same chromosome: MUC2 was expressed in 32% of the cases of gastric carcinoma, MUC5AC was expressed in 50% and MUC6 was expressed in 32%.

In our series, MUC5B expression was associated with an absence of venous invasion. Of the gastric carcinoma cases with venous invasion, 95% did not express MUC5B. To the best of our knowledge, this is the first time an association between venous invasion and the expression of MUC5B has been established.

Our results show a lack of association between MUC5B expression and parameters associated to gastric carcinoma prognosis, such as the depth of gastric wall penetration, lymphatic vessels invasion and the presence of lymph-node metastases. To the best of our knowledge, this is the first study addressing the influence of MUC5B expression in the survival of patients with gastric carcinoma. The results of both this series and also of a previous study [37] suggest that, at present, mucin expression in gastric carcinoma should be regarded as an indicator of carcinoma differentiation rather than as a determinant of prognosis. Namely, MUC5AC is associated with diffuse-type gastric carcinoma, MUC2 is associated with mucinous-type gastric carcinoma and MUC5B is associated with unclassified gastric carcinomas.

In our study, an association between the expression of MUC5B and MUC5AC was observed (Table 3). We did not observe an association between the expression of MUC5B and the other mucin genes mapped on the chromosome 11p15 (MUC2 and MUC6). The significant association between MUC5B and MUC5AC expression is in accordance with the speculation that both genes may have evolved from a common ancestral gene [13, 18]. The lack of association between the expression of MUC5B and the co-expression of MUC2 and MUC6 may suggest that these genes, although closely located on the same chromosome, are regulated by different and not-yet understood mechanisms [13, 14, 15, 16, 34].

Our results showed no significant association between MUC5B expression and the "phenotype" of mucin expression (Table 4), although no cases of complete intestinal mucin "phenotype" gastric carcinoma expressed MUC5B. In our series, MUC5B expression was present both in cases with gastric and incomplete intestinal "phenotype". The aforementioned association of MUC5B expression with unclassified type of gastric carcinomas may help to understand the lack of cases with complete intestinal "phenotype" expressing MUC5B.

In summary, this study evaluated the aberrant expression of MUC5B in gastric carcinomas with a novel monoclonal antibody, EU-MUC5Ba. Our results showed that MUC5B expression was associated with gastric carcinoma differentiation and identified for the first time an association with an absence of venous invasion. MUC5B expression was associated with the co-expression of MUC5AC but not with MUC1, MUC2 and MUC6. The observed association between MUC5B and MUC5AC may suggest that both genes share more than their close localisation on the chromosome 11p15.

Acknowledgements This work was supported by Fundação para a Ciência e Tecnologia and Programa Operacional Ciência, Tecnologia, Inovação do Quadro Comunitário de Apoio III (Project POCTI/CBO/39075/2001 and POCTI/CIBO/44598/2002) and European Union Concerted Action Contract BMH4-CT98–3222. We thank Dr. Joy Burchell and Prof. Joyce Taylor-Papdimitriou for providing antibodies HMFG1 and SM3.

References

1. Aubert JP, Porchet N, Crepin M, Duterque-Coquillaud M, Vergnes G, Mazzuca M, Debuire B, Petitprez D, Degand P (1991) Evidence for different human tracheobronchial mucin peptides deduced from nucleotide cDNA sequences. Am J Respir Cell Mol Biol 5:178–185
2. Audie JP, Janin A, Porchet N, Copin MC, Gosselin B, Aubert JP (1993) Expression of human mucin genes in respiratory, digestive, and reproductive tracts ascertained by in situ hybridization. J Histochem Cytochem 41:1479–1485
3. Balague C, Gambus G, Carrato C, Porchet N, Aubert JP, Kim YS, Real FX (1994) Altered expression of MUC2, MUC4, and MUC5 mucin genes in pancreas tissues and cancer cell lines. Gastroenterology 106:1054–1061
4. Balague C, Audie JP, Porchet N, Real FX (1995) In situ hybridization shows distinct patterns of mucin gene expression in normal, benign, and malignant pancreas tissues. Gastroenterology 109:953–964
5. Baldus SE, Zirbes TK, Engel S, Hanisch FG, Moning SP, Lorenzen J, Glossman J, Fromm S, Thiele J, Pichmaier H, Dienes HP (1998) Correlation of the immunohistochemical reactivity of mucin cores MUC1 and MUC2 with histological subtype and prognosis of gastric carcinomas. Int J Cancer 79:133–138
6. Bartman AE, Buisine MP, Aubert JP, Niehans GA, Toribara NW, Kim YS, Kelly EJ, Crabtree JE, Ho SB (1998) The MUC6B secretory mucin gene is expressed in a wide variety of epithelial tissues. J Pathol 186:398–405
7. Bobek LA, Tsai H, Biesbrock AR, Levine MJ (1993) Molecular cloning, sequence, and specificity of expression of the gene encoding the lower molecular weight human salivary mucin (MUC7). J Biol Chem 268:20563–20569
8. Buisine MP, Devisme L, Maunoury V, Deschodt E, Gosselin B, Copin MC, Aubert JP, Porchet N (2000) Developmental mucin gene expression in the gastroduodenal tract and accessory digestive glands. I. Stomach. A relationship to gastric carcinoma. J Histochem Cytochem 48:1657–1666
9. Burchell J, Gendler S, Taylor-Papdimitriou J, Girling A, Millis R, Lamport D (1987) Development and characterization of breast cancer reactive monoclonal antibodies directed to the core protein of the human milk mucin. Cancer Res 47:5476–5482

10. Byrd JC, Yan PS, Sternberg L, Yunker CK, Scheiman JM, Bresalier RS (1997) Aberrant expression of gland-type gastric mucin in the surface epithelium of Helicobacter pylori-infected patients. Gastroenterology 113:455–464
11. De Bolos C, Garrido M, Real FX (1995) MUC6 apomucin shows a distinct normal tissue distribution that correlates with Lewis antigen expression in the human stomach. Gastroenterology 107:723–734
12. Desseyn JL, Aubert JP, Van Seuningen I, Porchet N, Laine A (1997) Genomic organization of the 3′ region of the human mucin gene MUC5B. J Biol Chem 272:16873–16883
13. Desseyn JL, Guyonnet-Duperat V, Porchet N, Aubert JP, Laine A (1997) Human mucin gene MUC5B, the 10.7-kb large central exon encodes various alternate subdomains resulting in a super-repeat. Structural evidence for a 11p15.5 gene family. J Biol Chem 272:3168–3178
14. Desseyn JL, Buisine MP, Porchet N, Aubert JP, Degand P, Laine A (1998) Evolutionary history of the 11p15 human mucin gene family. J Mol Evol 46:102–106
15. Desseyn JL, Buisine MP, Porchet N, Aubert JP, Laine A (1998) Genomic organization of the human mucin gene MUC5B. cDNA and genomic sequences upstream of the large central exon. J Biol Chem 273:30157–30164
16. Desseyn JL, Aubert JP, Porchet N, Laine A (2000) Evolution of the large secreted gel-forming mucins. Mol Biol Evol 17:1175–1184
17. Dufosse J, Porchet N, Audie JP, Guyonnet-Duperat V, Laine A, Van-Seuningen I, Marrakchi S, Degand P, Aubert JP (1993) Degenerate 87-base-pair tandem repeats create hydrophilic/hydrophobic alternating domains in human mucin peptides mapped to 11p15. Biochem J 293:329–337
18. Escande F, Aubert JP, Porchet N, Buisine MP (2001) Human mucin gene MUC5AC: organization of its 5′-region and central repetitive region. Biochem J 358:763–772
19. Gendler SJ, Lancaster CA, Taylor-Papadimitriou J, Duhig J, Peat T, Burchell J (1990) Molecular cloning and expression of human tumor-associated plymorphic epithelial mucin. J Biol Chem 265:15286–15293
20. Gum JR, Byrd JC, Hicks JW, Toribara N, Lamport DT, Kim YS (1989) Molecular cloning and expression of human intestinal mucins cDNAs. J Biol Chem 264:6480–6487
21. Gum JR, Hicks JW, Swallow DM, Lagace RE, Byrd JC, Lamport DT, Siddiki B, Kim YS (1990) Molecular cloning of cDNAs derived form a novel human intestinal mucin gene. Biochem Biophys Res Commun 171:407–415
22. Guyonnet-Duperat V, Audie JP, Debailleul V, Laine A, Buisine MP, Galiegue-Zouitina S, Pigny P, Degand P, Aubert JP, Porchet N (1995) Characterization of the human mucin gene MUC5AC: a consensus cysteine—rich domain for 11p15 mucin genes? Biochem J 305:211–219
23. Ho SB, Niehans GA, Lyftogt C, Yan PS, Cheritz DL, Gumm ET, Dahiya R, Kim YS (1993) Heterogeneity of mucin gene expression in normal, preneoplastic, and neoplastic human gastric epithelium. Cancer Res 53:641–651
24. Ho SB, Shekels LL, Toribara NW, Kim YS, Lyftogt C, Cherwitz DL, Niehans GA (1995) Mucin gene expression in normal, preneoplastic, and neoplastic human gastric epithelium. Cancer Res 55:2681–2690
25. Kaplan E, Meier P (1958) Nonparametric estimation from incomplete observations. J Am Stat Assoc 53:457–481
26. Kim Y, Gum J, Brockhausen I (1996) Mucin glycoproteins in neoplasia. Glycocon J 13:693–707
27. Lan MS, Batra SK, Qi WN, Metzgar RS, Hollingsworth MA (1990) Cloning and sequencing of a human pancreatic tumor mucin. J Biol Chem 265:15294–15299
28. Lapensee L, Paquette Y, Bleau G (1997) Allelic polymorphism and chromosomal localization of a human pancreatic tumor mucin cDNA. J Biol Chem 265:15294–15299
29. Laurén P (1965) The two histological main types of gastric carcinoma: diffuse and the so-called intestinal type carcinoma. Acta Pathol Microbiol Scand 64:31–49
30. Lee H, Lee H, Kim H, Yang H, Kim Y, Kim W (2001) MUC1, MUC2, MUC5AC, and MUC expressions in gastric carcinomas. Their roles as prognostic indicators. Cancer 92:1427–1434
31. Ming SC (1977) Gastric carcinoma: a pathobiological classification. Cancer 39:2475–2485
32. Nogueira AM, Machado JC, Carneiro F, Reis CA, Gott P, Sobrinho-Simões M (1999) Patterns of expression of trefoil peptides and mucins in gastric polyps with and without malignant transformation. J Pathol 187:541–548
33. Perrais M, Pigny P, Buisine MP, Porchet N, Aubert JP, Van Seuningen-Lempire I (2001) Aberrant expression of human mucin gene MUC5B in gastric carcinoma and cancer cells. Identification and regulation of a distal promoter. J Biol Chem 276:15386–15396
34. Perrais M, Pigny P, Copin MC, Aubert JP, Van Seuningen I (2002) Induction of MUC2 and MUC5AC mucins by factors of the epidermal growth factor (EGF) family is mediated by EGF receptor/Ras/Raf/extracellular signal-regulated kinase cascade and Sp1. J Biol Chem 277:32258–32267
35. Pigny P, Van Seuningen I, Desseyn JL, Nollet S, Porchet N, Laine A, Aubert JP (1996) Identification of a 42-kDa nuclear factor (NF1-MUC5B) from HT-29 MTX cells that binds to the 3′ region of human mucin gene MUC5B. Biochem Biophys Res Commun 220:186–191
36. Pinto-de-Sousa J, David L, Seixas M, Pimenta A (2001) Clinicopathologic profiles and prognosis of gastric carcinomas from the cardia, fundus/body and antrum. Dig Surg 18:102–110
37. Pinto-de-Sousa J, David L, Reis CA, Gomes R, Silva L, Pimenta A (2002) Mucins MUC1, MUC2, MUC5AC and MUC6 expression in the evaluation of differentiation and clinico-biological behaviour of gastric carcinoma. Virchows Arch 440:304–310
38. Porchet N, Van Cong N, Dufosse J, Audie JP, Guyonnet-Duperat V, Gross MS, Denis C, Degand P, Bernhein A, Aubert JP (1991) Molecular cloning and chromosomal localization of a novel human tracheo-bronchial mucin cDNA containing tandemly repeated sequences of 48 base pairs. Biochem Biophys Res Commun 175:414–422
39. Reis CA, David L, Nielsen PA, Clausen H, Mirorodskaya M, Roepstorff P, Sobrinho-Simões M (1997) Immunohistochemical study of MUC5AC expression in human gastric carcinomas using a novel monoclonal antibody. Int J Cancer 74:112–121
40. Reis CA, David L, Seixas M, Burschell J, Sobrinho-Simões M (1998) Expression of fully and under-glycosylated forms of MUC1 mucin in gastric carcinoma. Int J Cancer 79:402–410
41. Reis CA, Sorensen T, Mandel U, David L, Mirgorodskaya E, Roepstorff P, Kihlberg J, Hansen JE, Clausen H (1998) Development and characterization of an antibody directed to an alpha-N-acetyl-D-galactosamine glycosylated MUC2 peptide. Glycocon J 15:51–62
42. Reis CA, David L, Carvalho F, Mandel U, Bolós C, Mirorodskaya M, Clausen H, Sobrinho-Simoes M (2000) Immunohistochemical study of the expression of MUC6 mucin and co-expression of other secreted mucins (MUC5AC and MUC2) in human gastric carcinomas. J Histochem Cytochem 48:377–388
43. Rousseau K, Wickstrom C, Whitehouse DB, Carlstedt I, Swallow DM (2004) New monoclonal antibodies to non-glycosylated domains of the secreted MUC5B and MUC7. Hybridoma Hybridomics (in press)
44. Sakamoto H, Yonezawa S, Utsunomiya T, Tanaka S, Kim Y S, Sato E (1997) Mucin antigen expression in gastric carcinomas of young and old adults. Human Pathol 28:1056–1065
45. Shankar V, Pichan P, Eddy RL, Tonk V, Nowak N, Sait SN, Shows TB, Schultz RE, Gotway G, Elkins RC, Gilmore MS, Sachdev GP (1997) Chromosomal localization of a human mucin gene (MUC8) and cloning of the cDNA corresponding to the carboxy terminus. Am J Resp Cell Mol Biol 16:2322–2241
46. Sobin LE, Whitekind CH (eds) (1997) TNM classification of malignant tumours. International Union Against Cancer, 5th edn. John Wiley & Sons, New York

47. Taylor-Papadimitriou J, Peterson JA, Arklie J, Burchell J, Ceriani RL, Bodmer WF (1981) Monoclonal antibodies to epithelium-specific components and reaction of the human milk fat globule membrane: production and reaction with cells in culture. Int J Cancer 28:17–21
48. Toribara NW, Roberton AM, Ho SB, Kuo WL, Gum E, Hicks JW, Gum JR, Byrd JC, Siddiki B (1993) Human gastric mucin. Identification of a unique species by expressing cloning. J Biol Chem 268:4879–5885
49. Utsunomiya T, Yonezawa S, Sakamoto H, Kitamura H, Hokita S, Aiko T, Tanaka S, Irimura T, Kim YS, Sato E (1998) Expression of MUC1 and MUC2 mucins in gastric carcinomas: its relationship with the prognosis of patients. Clin Cancer Res 4:2605–2614
50. Van Seuningen I, Perrais M, Pigny P, Porchet N, Aubert JP (2000) Sequence of the 5′-flanking region and promoter activity of the human mucin gene MUC5B in different phenotypes of colon cancer cells. Biochem J 348:675–686
51. Williams SJ, McGuckin MA, Gotley DC, Eyre HJ, Sutherland GR, Antalis TM (1999) Two novel mucin genes down-regulated in colorectal cancer identified by differential display. Cancer Res 59:4083–4089
52. Yin BWT, Lloyd KO (2001) Molecular cloning of the CA125 ovarian cancer antigen: identification as a new mucin (MUC16). J Biol Chem 276:27371–27375

Virchows Arch (2004) 444:231–234
DOI 10.1007/s00428-003-0965-1

ORIGINAL ARTICLE

Peter J. Barth · Titus Schenck zu Schweinsberg · Annette Ramaswamy · Roland Moll

CD34+ fibrocytes, α-smooth muscle antigen-positive myofibroblasts, and CD117 expression in the stroma of invasive squamous cell carcinomas of the oral cavity, pharynx, and larynx

Received: 22 September 2003 / Accepted: 28 November 2003 / Published online: 31 January 2004

Abstract We investigated tumor-free mucosa and squamous cell carcinomas of the oral cavity, the pharynx, and larynx with respect to the presence of stromal CD34+ fibrocytes and α-smooth muscle antigen (SMA)-positive myofibroblasts. Additionally, stromal expression of CD117 was analyzed. A total of 39 squamous cell carcinomas were assessed immunohistochemically. In all cases investigated, CD34+ fibrocytes were found in the tumor-free stroma, whereas α-SMA-positive myofibroblasts were lacking. Areas of lymphocytic infiltration disclosed a focal reduction of CD34+ fibrocytes. CD117 expression was absent from the tumor-free stroma. Of 39 squamous cell carcinomas, 33 were free of stromal CD34+ fibrocytes, and, in 31 carcinomas, stromal α-SMA-positive myofibroblasts occurred at least focally. CD117-positive stromal spindle cells were found in 25 carcinomas. Compared with tumor-free mucosa, the number of tissue mast cells was significantly increased in carcinomas. We conclude that stromal remodeling induced by invasive carcinomas is characterized by a loss of CD34+ fibrocytes and subsequent gain of α-SMA-positive myofibroblasts. The diagnostic impact of this finding is, however, limited by the fact that chronic inflammation may also be accompanied by a focal loss of CD34+ fibrocytes.

Keywords Fibrocytes · Myofibroblast · Larynx · Pharynx · Invasive squamous cell carcinoma

P. J. Barth (✉) · T. Schenck zu Schweinsberg · A. Ramaswamy · R. Moll
Institute of Pathology,
Philipps-University Marburg,
Baldingerstraße, 35033 Marburg, Germany
e-mail: barthp@med.uni-marburg.de
Tel.: +49-64-212862465
Fax: +49-64-212865640

Introduction

With respect to their cellular composition, tumor-laden and tumor-free stroma are clearly distinct. These differences are widely independent of the anatomical site and histological type of carcinoma and consist of a loss of CD34+ fibrocytes and a subsequent gain of α-smooth muscle antigen (SMA)-positive myofibroblasts [2, 3, 4, 6, 12, 17]. CD34+ fibrocytes appear to be constitutive elements of the connective tissue in a multitude of anatomical sites, such as the skin [12], the breast [3, 6], the gastrointestinal tract [2, 14, 15], and the cervix [4]. In all of the aforementioned locations, the stroma of invasive carcinomas discloses a reduction or complete loss of CD34+ fibrocytes paralleled by the occurrence of α-SMA-positive myofibroblasts [2, 3, 4, 6, 12, 17]. In addition to their function as matrix-producing [5, 8] and antigen-presenting cells [7], CD34+ fibrocytes secrete platelet-derived growth factor (PDGF) [10], the receptor of which, c-kit (CD117), a protein receptor with tyrosine kinase activity, is structurally identical to that of stem cell factor (SCF).

To our knowledge, investigations concerning the occurrence of CD34+ fibrocytes in the upper aero-digestive tract and their behavior in invasive carcinomas of this anatomical site, up to now, have not been published. α-SMA-positive myofibroblasts have recently been reported in squamous cell carcinomas of the larynx [20].

We undertook the present study to analyze the stroma of tumor-free mucosa and squamous cell carcinomas of the oral cavity, the pharynx, and larynx with respect to the presence or absence, respectively, of CD34+ fibrocytes and α-SMA-positive myofibroblasts. We additionally investigated whether stromal cells express the CD117 antigen.

Materials and methods

This study comprises a total of 39 squamous cell carcinomas of the oral cavity (n=16), the oropharynx (n=13), hypopharynx (n=6), and larynx (n=4) obtained from 34 patients. The patients, 28 of which

were males, ranged in age between 44 years and 96 years (arithmetic mean: 61.1 years). The stroma within the border of the invasive carcinoma was defined to be tumor associated, whereas stroma beyond the border of the tumor was regarded as tumor free. In all cases, tumor-free tissue from resection margins was available for comparison. Tissues were fixed in a 10% formalin solution, embedded in paraffin, cut and stained with hematoxylin and eosin (H&E) and periodic acid-Schiff for routine purposes. The Giemsa stain was performed to distinguish tissue mast cells from CD117-positive stromal cells.

Immunohistochemistry

Immunohistochemistry was performed using standard avidin biotin complex-peroxidase method (ABC Elite Kit; Vector, Burlingame, CA) using 3,3′-diaminobenzidine as chromogen. CD34 antigen was detected using a monoclonal antibody (QBEND10, dilution 1:50; Dako, Hamburg, Germany) after microwave pretreatment. CD117 expression was detected accordingly, using a polyclonal rabbit antibody (c-kit, dilution 1:100; Dako, Hamburg, Germany). Microwave pretreatment was performed by heating the deparaffinized and rehydrated sections, immersed in 10 mM sodium citrate buffer (pH 6.0), in a microwave oven at 600 W for 3×5 min. α-SMA was detected using a monoclonal antibody (ASM-1, dilution 1:200; Progen, Heidelberg, Germany) after tissue pretreatment with 0.1% trypsin for 15 min at 37°C.

Quantification of mast cells

In each case, the number of mast cells per HPF (i.e. high power fields at 400× microscopic magnification) was assessed in tumor-free tissue and tumor-associated stroma as the arithmetic mean mast cells in five randomly selected microscopic fields. Comparison of values was performed by means of the student's *t*-test. $P<0.01$ was considered to be statistically significant.

Results

Tumor-free mucosa

$CD34^+$ fibrocytes characterized by an inconspicuous cytoplasm with slender elongated bipolar neurite-like projections and a small nucleus were found in the tumor-free stroma of all specimens investigated. The highest number of $CD34^+$ fibrocytes was observed in the vicinity of vessels, around submucosal glands and adjacent to the covering epithelium (Fig. 1A). In areas with more pronounced lymphocytic infiltration, $CD34^+$ fibrocytes were reduced in number or completely lacking. α-SMA myofibroblasts were absent from the tumor-free stroma, and CD117 expression was also not observed in the tumor-free stroma.

Squamous cell carcinomas

The border of invasive squamous cell carcinomas was characterized by an abrupt loss of $CD34^+$ fibrocytes, which was already visible at low microscopic magnification (Fig. 1B). In 33 cases, the stroma of invasive squamous cell carcinomas was completely devoid of $CD34^+$ fibrocytes; 6 cases disclosed, at least, a focal loss of this cell type. Residual $CD34^+$ fibrocytes showed no local predilection for the center or periphery of the lesion. The tumor-associated stroma was made up of diffusely scattered plump spindle-shaped α-SMA positive myofibroblasts with a characteristic tram-tracking of thick intracytoplasmatic α-SMA-reactive fibers in 12 cases. In 19 cases, these cells were focally distributed throughout the tumor stroma (Fig. 1C). The stroma of 8 carcinomas disclosed no α-SMA-positive myofibroblasts. Cytoplasmic CD117-immunoreactivity of stromal spindle cells was focal in 21 and diffuse in 4 cases; 14 cases showed no CD117 reactivity of stromal spindle cells in the tumor (Fig. 1D; Table 1).

Table 1 Distribution of $CD34^+$ fibrocytes and α-smooth muscle antigen (SMA)-positive myofibroblasts in the tumor-associated stroma together with the expression of CD117 in tumor-associated myofibroblasts. − No positive cells, + focal accumulations of positive cells, ++ diffusely scattered positive cells

	−	+	++
$CD34^+$ fibrocytes	33	6	0
α-SMA-positive myofibroblasts	8	19	12
CD117-positive stromal cells	14	21	4

The tumor stroma contained 23.9±9.5 (arithmetic mean ± standard deviation) mast cells per HPF, a value significantly higher than that observed in the tumor-free stroma (8.1±5.6; $P<0.01$) (Fig. 1E, F).

Discussion

In accordance with previous studies regarding various anatomical sites, the present investigation demonstrates a phenotypical change of the stroma associated with invasive squamous cell carcinomas of the upper aero-digestive tract, consisting of a loss of $CD34^+$ fibrocytes paralleled by a gain of α-SMA-positive myofibroblasts. The mechanisms initiating this process are yet not well understood, but have been thought to be related to a soluble factor secreted by tumor cells [6, 18]. Experimental studies have shown that α-SMA is upregulated in $CD34^+$ fibrocytes exposed to transforming growth factor (TGF)-β [1]. This might be the primary event of stromal remodeling, followed by a complete loss of CD34 expression, resulting in the aforementioned phenotypical alteration of tumor-associated stroma. In squamous cell carcinomas of the upper aero-digestive tract, TGF-β is upregulated [9, 13, 16], and we found tissue mast cells, another important source of TGF-β, to be significantly increased in number in the tumor stroma. The latter finding is not restricted to the upper aero-digestive tracts, since Humphreys and coworkers [11] described elevated numbers of mast cells in the stroma of cutaneous basal cell carcinomas and also suggested that mast cells might play a role in tissue remodeling associated with basal cell carcinoma. Regarding these data, it seems to be reasonable that the phenotypical change of $CD34^+$ fibrocytes toward α-

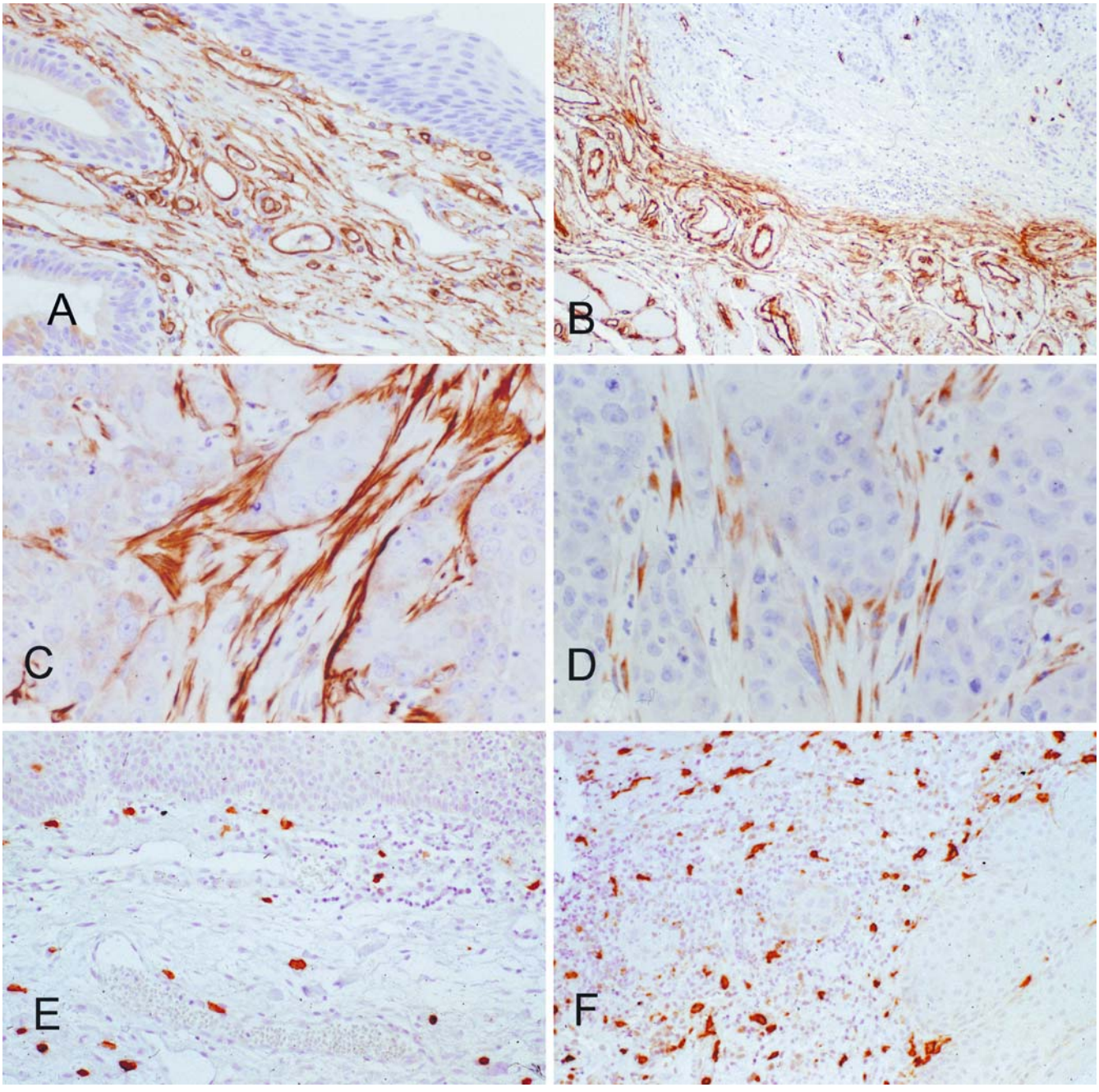

Fig. 1 The stroma of the upper aero-digestive tract harbors diffusely scattered $CD34^+$ fibrocytes, which are more densely packed in the subepithelial stroma (**A**). The stroma of invasive squamous cell carcinoma (to the *upper right*) is devoid of $CD34^+$ fibrocytes (**B**); the infiltrating border of invasive carcinomas shows an abrupt loss of $CD34^+$ fibrocytes. Tumor-associated spindled stromal cells are α-SMA positive (**C**), and 25 cases disclose CD117 positivity (**D**). The number of tissue mast cells in the normal mucosa (**E**, CD117 immunohistochemistry) is significantly lower than tumor-laden stroma (**F**, CD117 immunohistochemistry). In this case, stromal spindle cells were negative for CD117

SMA-positive myofibroblasts is, at least in part, mediated by TGF-β.

In contrast to the tumor-free stroma, tumor-associated myofibroblasts were c-kit (CD117)-positive, indicating that SCF or PDGF or both might play a role in the proliferation of this cell type. Granulocyte-macrophage colony-stimulating factor (GM-CSF) is closely related to macrophage colony-stimulating factor (M-CSF), which is constitutively expressed in $CD34^+$ fibrocytes [8, 10], downregulates CD117 expression in mast cells [19] and, as suggested by our data, in stromal myofibroblasts. In turn, upregulation of CD117 in stromal myofibroblasts in mast cells is likely to be a direct sequel of a reduction of $CD34^+$ fibrocytes.

Phenotypical alterations of the stroma, chiefly the loss of $CD34^+$ fibrocytes, have been considered valuable tools in distinguishing benign from malignant lesions [2, 3, 4, 17]. When applying this criterion, some precautions and recommendations should be regarded. The loss of $CD34^+$ fibrocytes in the breast stroma is, in most cases, due to malignancy, but recent studies also described CD34-negative spindle cell proliferations in areas of previous biopsy [6]. A minority of radial scars of the breast also exhibit stromal areas negative for CD34 and positive for α-SMA [17]. In the present study, a loss of $CD34^+$ fibrocytes was also of reduced value in detecting invasive carcinoma, since areas with lymphocytic infiltration also exhibited a loss of $CD34^+$ fibrocytes. However, α-SMA myofibroblasts were not observed in these areas. Therefore, the diagnosis of malignancy should not solely be based on a loss of $CD34^+$ fibrocytes.

The functional consequences of the loss of CD34+ fibrocytes, along with their value in diagnosing malignancy, remain a matter of speculation requiring further investigation. However, considering that $CD34^+$ fibrocytes are antigen-presenting cells, their reduction or complete elimination enables an invasive tumor to escape immune-surveillance. This might constitute an important step in local tumor infiltration and distant tumor spread.

References

1. Abe R, Donnelly SC, Peng T, Bucala R, Metz CN (2001) Peripheral blood fibrocytes: differentiation pathway and migration to wound sites. J Immunol 166:7556–7562
2. Barth PJ, Ebrahimsade S, Hellinger A, Moll R, Ramaswamy A (2002) $CD34^+$ fibrocytes in neoplastic and inflammatory pancreatic lesions. Virchows Arch 440:128–133
3. Barth PJ, Ebrahimsade S, Ramaswamy A, Moll R (2002) $CD34^+$ fibrocytes in invasive ductal carcinoma, ductal carcinoma in situ, and benign breast lesions. Virchows Arch 440:298–303
4. Barth PJ, Ramaswamy A, Moll R (2002) $CD34^+$ fibrocytes in normal cervical stroma, cervical intraepithelial neoplasia III, and invasive squamous cell carcinoma of the cervix uteri. Virchows Arch 441:564–568
5. Bucala R, Spiegel LA, Chesney J, Hogan M, Cerami A (1994) Circulating fibrocytes define a new leukocyte subpopulation that mediates tissue repair. Mol Med 1:71–81
6. Chauhan H, Abraham A, Phillips JR, Pringle JH, Walker RA, Jones JL (2003) There is more than one kind of myofibroblast: analysis of CD34 expression in benign, in situ, and invasive breast lesions. J Clin Pathol 56:271–276
7. Chesney J, Bacher M, Bender A, Bucala R (1997) The peripheral blood fibrocyte is a potent antigen-presenting cell capable of priming naive T cells in situ. Proc Natl Acad Sci USA 94:6307–6312
8. Chesney J, Metz C, Stavitsky AB, Bacher M, Bucala R (1998) Regulated production of type I collagen and inflammatory cytokines by peripheral blood fibrocytes. J Immunol 160:419–425
9. Hagedorn H, Elbertzhagen A, Ruoss I, Sauer U, Nerlich AG (2001) Immunohistochemical analysis of major TGF-beta isoforms and their receptors in laryngeal carcinomas. Virchows Arch 439:531–539
10. Hartlapp I, Abe R, Saeed RW, Peng T, Voelter W, Bucala R, Metz CN (2001) Fibrocytes induce an angiogenic phenotype in cultured endothelial cells and promote angiogenesis in vivo. FASEB J 15:2215–2224
11. Humphreys TR, Monteiro MR, Murphy GF (2000) Mast cells and dendritic cells in basal cell carcinoma stroma. Dermatol Surg 26:200–203
12. Kirchmann TT, Prieto VG, Smoller BR (1994) CD34 staining pattern distinguishes basal cell carcinoma from trichoepithelioma. Arch Dermatol 130:589–592
13. Koliopanos A, Friess H, di Mola FF, Tang WH, Kubulus D, Brigstock D, Zimmermann A, Buchler MW (2002) Connective tissue growth factor gene expression alters tumor progression in esophageal cancer. World J Surg 26:420–427
14. Nakayama H, Enzan H, Miyazaki E, Kuroda N, Naruse K, Hiroi M (2000) Differential expression of CD34 in normal colorectal tissue, peritumoral inflammatory tissue, and tumour stroma. J Clin Pathol 53:626–629
15. Nakayama H, Enzan H, Miyazaki E, Kuroda N, Naruse K, Kiyoku H, Toi M, Hiroi M (2001) CD34 positive stromal cells in gastric adenocarcinomas. J Clin Pathol 54:846–848
16. Natsugoe S, Xiangming C, Matsumoto M, Okumura H, Nakashima S, Sakita H, Ishigami S, Baba M, Takao S, Aikou T (2002) Smad4 and transforming growth factor beta1 expression in patients with squamous cell carcinoma of the esophagus. Clin Cancer Res 8:1838–1842
17. Ramaswamy A, Moll R, Barth PJ (2003) $CD34^+$ fibrocytes in tubular carcinomas and radial scars of the breast. Virchows Arch 443:536–540
18. Soma L, LiVolsi VA, Baloch ZW (2001) Dendritic interstitial and myofibroblastic cells at the border of salivary gland tumors. Arch Pathol Lab Med 125:232–236
19. Welker P, Grabbe J, Zuberbier T, Grutzkau A, Henz BM (2001) GM-CSF downmodulates c-kit, FcεRIα and GM-CSF receptor expression as well as histamine and tryptase levels in cultured human mast cells. Arch Dermatol Res 293:249–258
20. Zidar N, Gale N, Kambic V, Fischinger J (2002) Proliferation of myofibroblasts in the stroma of epithelial hyperplastic lesions and squamous carcinoma of the larynx. Oncology 62:381–385

Virchows Arch (2004) 444:235–238
DOI 10.1007/s00428-003-0966-0

ORIGINAL ARTICLE

Adriana Handra-Luca · Anne Couvelard · Claude Degott · Jean-François Fléjou

Correlation between patterns of DNA mismatch repair hmlh1 and hmsh2 protein expression and progression of dysplasia in intraductal papillary mucinous neoplasms of the pancreas

Received: 28 July 2003 / Accepted: 9 December 2003 / Published online: 4 February 2004

Abstract Defective DNA mismatch repair results from genetic or epigenetic alterations that most frequently inactivate the genes hMLH1 and hMSH2. This is thought to promote tumourigenesis by accumulation of mutations in oncogenes and tumour suppressor genes. This pathway, first reported in colon cancer, has been recently demonstrated in a subgroup of sporadic pancreatic adenocarcinomas. Intraductal papillary-mucinous neoplasms of the pancreas are a special type of pancreatic tumours, characterised by a spectrum of morphological changes from mild to moderate and to non-invasive, and they may associate with adenocarcinoma. An immunohistochemical study of hmlh1 and hmsh2 protein expression was performed on 26 intraductal papillary-mucinous neoplasms. All tumours showed nuclear expression of hmlh1 and hmsh2 proteins. There were two distinctive patterns of protein expression on the basis of the location of cells expressing these markers: the "normal" pattern, observed mainly in adenoma and rarely in intraductal papillary-mucinous neoplasms with moderate dysplasia and the "dysplastic" pattern, frequently encountered in moderate dysplasia neoplasms, non-invasive and invasive carcinomas. These findings suggest that defective DNA mismatch repair, due to inactivation of hMLH1 and hMSH2, does not play a significant role in the pathogenesis of intraductal papillary-mucinous neoplasms of the pancreas. Two patterns of protein expression were observed and were correlated with the progression of dysplasia in intraductal papillary mucinous neoplasms.

Keywords Pancreas · Immunohistochemistry · Intraductal papillary-mucinous neoplasm · hmlh1 · hmsh2

A. Handra-Luca · A. Couvelard · C. Degott
Department of Pathology,
Hôpital Beaujon, AP-HP,
Paris, France

A. Handra-Luca
Department of Pathology,
Hôpital Pitié-Salpetrière, AP-HP,
Paris, France

J.-F. Fléjou (✉)
Service d'Anatomie Pathologique,
AP-HP, Hôpital Saint-Antoine,
184 rue du Faubourg Saint-Antoine, 75571 Paris Cedex 12, France
e-mail: jean-francois.flejou@sat.ap-hop-paris.fr
Tel.: +33-14-9282170
Fax: +33-14-9282878

Introduction

Intraductal papillary-mucinous neoplasms (IPMNs) of the pancreas represent a clinico-pathological entity. They show a spectrum of morphological changes in the ductal neoplastic epithelium, ranging from benign (adenoma) to malignant (carcinoma), and, in some cases, are associated with invasive adenocarcinoma [8]. Their prognosis is generally better than that of ductal adenocarcinoma.

Defective DNA mismatch repair results from genetic or epigenetic alterations that most frequently inactivate the genes hMLH1 and hMSH2. This is thought to promote tumourigenesis by accumulation of mutations in oncogenes and tumour suppressor genes. Inactivation of hMLH1 and hMSH2 is observed as a loss of these proteins by immunohistochemistry [11]. This pathway, first reported in colon cancer, has been recently demonstrated in a subgroup of sporadic pancreatic adenocarcinomas, sharing the microsatellite instability high (MSI-H) phenotype. This MSI-H phenotype was associated with poor differentiation, but with a good prognosis [20].

We studied, using immunohistochemistry, the expression of mismatch repair proteins in adenocarcinoma associated with pancreatic IPMNs, considered to have a better prognosis than classical ductal adenocarcinoma. We also analysed the patterns of hmlh1 and hmsh2 protein expression in IPMNs with regard to the progression of dysplasia.

Materials and methods

We selected 26 cases of surgically resected IPMNs of the pancreas. These cases were retrieved from the files of the Departments of Pathology of Beaujon Hospital and Saint-Antoine Hospital. The original haematoxylin and eosin slides for each case were reviewed by two observers (AHL and AC), and the IPMNs were classified according to World Health Organization criteria [7, 9]. Four-micron sections were prepared from the selected paraffin blocks, deparaffinised in xylene and rehydrated in pure ethanol. Endogeneous peroxidase was blocked using 3% hydrogen peroxide in methanol for 30 min. The slides were then placed in a microwave oven in citrate buffer (pH 6.0), for antigen retrieval, for 15 min at 750 W and 15 min at 150 W. All slides were processed using an automatic immunostainer (Optimax Plus 1.5, Biogenex, San Ramon, USA) with a supersensitive biotin-streptavidin-peroxidase technique (Supersensitive Detection Kit, Biogenex). Mouse anti-human monoclonal antibodies to hmlh1 (Clone G168–728, dilution 1:70; Pharmigen) and hmsh2 (Clone FE11, dilution 1:100; Calbiochem) were used. The slides were developed with amino-ethyl-carbazol, a red chromogen, and counterstained with Mayer's hemalun. Nuclear staining was interpreted for each antibody. Normal colonic mucosa served as positive control; the nuclei in the crypts showed moderate to strong staining, and the nuclei in the surface epithelium showed no or weak staining (Fig. 1). We considered two distinct patterns of expression in the papillary structures of IPMNs: the "normal" pattern, similar to that observed in the normal colonic mucosa, with a moderate nuclear expression limited to the lower part of the papillae and with weakly positive or negative upper part of the papillae and surface epithelium, and the "dysplastic" pattern, characterised by a random distribution of positive nuclei within the dysplastic epithelium, usually reaching the surface epithelium, and of moderate or strong intensity [2].

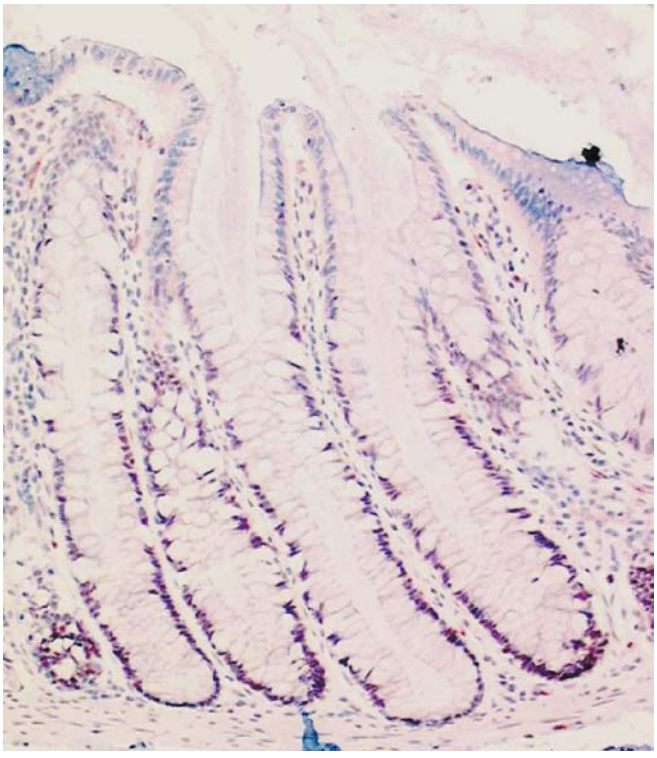

Fig. 1 Normal colonic mucosa showing the "normal pattern" with moderate hmlh1 nuclear expression limited to the lower part of the crypts and with weakly positive or negative upper part of the crypts and surface epithelium

Results

The present series included 14 men and 12 women with a mean of age 61 years (range, 27–81 years). The maximum diameter of the neoplasm ranged from 0.8 cm to 10 cm (mean, 3.3 cm). Histologically, all IPMNs were characterised by a tall, columnar, mucin-containing neoplastic epithelium with papillary proliferations. The intraductal components of the neoplasms were classified as intraductal papillary-mucinous adenoma (IPMA, with mild dysplasia) (eight cases), IPMN with moderate dysplasia (eight cases) and non-invasive intraductal papillary-mucinous carcinoma (IPMC) (ten cases).

We observed that various degrees of dysplasia were associated within the same neoplasm. Thus, we found foci of adenoma in 23 neoplasms, of moderate dysplasia in 16 neoplasms and of non-invasive intraductal papillary mucinous carcinoma in 10 neoplasms. Six of the IPMNs were associated with an invasive ductal type adenocarcinoma. IPMNs were branch duct type (10 neoplasms), main duct type (3 neoplasms) and both main and branch type (12 neoplasms).

All neoplasms showed nuclear expression of hmlh1 and hmsh2. The results are figured in Table 1. The "normal" pattern of hmlh1 protein expression was observed in 13 of 23 IPMAs (56.5%) and in one IPMN with moderate dysplasia (6%), as well as in the normal duodenal mucosa. The "dysplastic" pattern was observed in all types of dysplasia, more frequently in non-invasive IPMC (10/10 cases, 100%) and IPMNs with moderate dysplasia (15/16 cases, 94%) (Fig. 2) than in IPMA (43.5%). This latter pattern was also observed in all cases of invasive adenocarcinoma (6/6 cases, 100%). There were no differences between main duct or branch duct type tumours.

Table 1 Immunohistochemical pattern of hmlh1 and hmsh2 expression in intraductal papillary mucinous neoplasms according to grades of dysplasia. *IPMA* intraductal papillary-mucinous adenoma, *IPMN* intraductal papillary-mucinous neoplasm, *IPMC* intraductal papillary-mucinous carcinoma

	hmlh1		hmsh2	
	"Normal" pattern	"Dyplastic" pattern	"Normal" pattern	"Dysplastic" pattern
IPMA (n=23)	13	10	10	13
IPMN with moderate dysplasia (n=16)	1	15	1	15
Non-invasive IPMC (n=10)	0	10	0	10
Invasive IPMC (n=6)	0	6	0	6

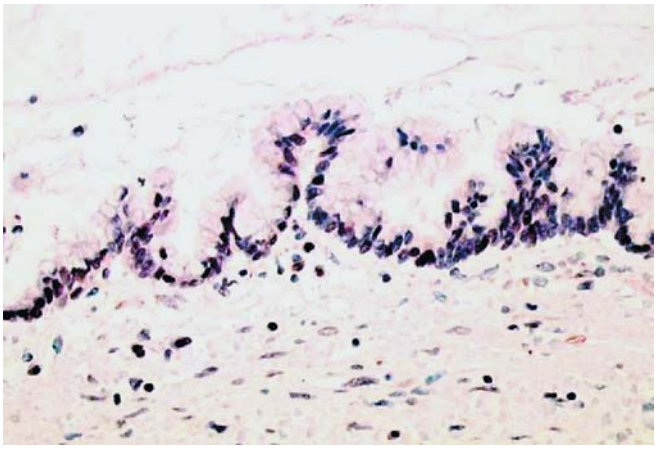

Fig. 2 Intraductal papillary-mucinous neoplasms with moderate dysplasia showing the "dysplastic pattern", characterised by a random distribution of hmlh1 strongly positive nuclei within the dysplastic epithelium, usually reaching the surface epithelium

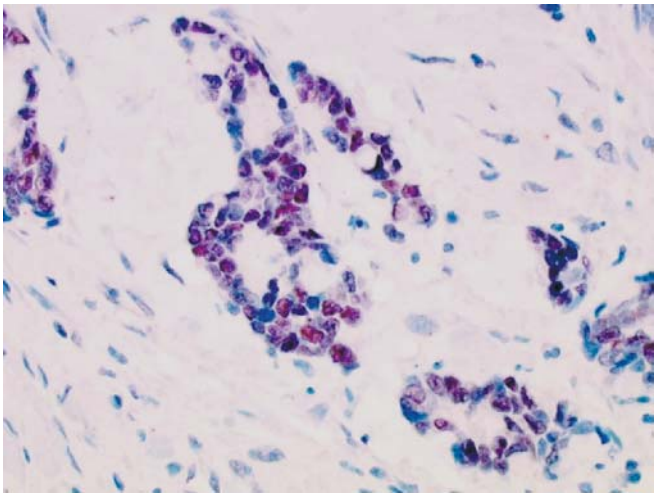

Fig. 3 Invasive adenocarcinoma showing a random distribution of strongly positive nuclei for hmsh2 protein

The "normal" pattern of hmsh2 protein expression was observed in 10 of 23 IPMAs (43.5%) and in 1 IPMN with moderate dysplasia (6%), as well as in the normal duodenal mucosa. The "dysplastic" pattern was observed in all types of dysplasia, more frequently in non-invasive IPMCs (10/10 cases, 100%) and IPMNs with moderate dysplasia (15/16 cases, 94%) than in IPMAs (56.5%). The same pattern was observed in all cases of invasive IPMCs (6/6 cases, 100%) (Fig. 3). There were no differences between main duct or branch duct type tumours.

Among the six invasive adenocarcinomas associated with IPMN, in four tumours, the "dysplastic" pattern was also observed in the adenoma and/or moderate dysplasia-IPMN zones, and, in two tumours, the adenoma and/or moderate dysplasia-IPMN zones showed the "normal pattern" of immunostaining.

Discussion

The DNA mismatch repair inactivation pathway was first described in a subgroup of sporadic and hereditary colorectal cancer [11]. The inactivation of hMLH1, hMSH2 and, less frequently, of hMSH6 genes correlates with MSI-H tumour phenotype and results in loss of nuclear expression of the corresponding protein.

The same pathway is involved in pancreatic adenocarcinoma, both sporadic and as part of the HNPCC syndrome. An MSI-H phenotype has been reported in a small subgroup (13%) of sporadic adenocarcinomas of the pancreas [20]. The proportion of tumours with microsatellite instability in usual ductal adenocarcinomas of the pancreas appears to be similar to that observed in colon cancer [17]. These MSI-H pancreatic adenocarcinomas are considered to form a morphologically distinctive subgroup, showing poor differentiation and a better prognosis [6, 19, 20].

Intraductal papillary mucinous neoplasms of the pancreas represent a clinico-pathological entity, characterised by a spectrum of morphological changes ranging from benign (adenoma) to malignant (carcinoma) [8]. These tumours show genetic heterogeneity [5] with oncogenic pathways that may involve alterations of the K-ras, HER-2/neu, p16, p53, DPC4 and STK11/LKB1 genes [1, 14, 21]. Adenocarcinomas in IPMNs have a better prognosis than ductal adenocarcinomas. Therefore, it seems interesting to study whether the mismatch repair genes are involved in the pathogenesis of these tumours. We show here that in this group of IPMNs associated with pancreatic adenocarcinoma, defective DNA mismatch repair due to inactivation of hMLH1 or hMSH2 genes is not involved. Our results confirm a series composed of IPMNs of various types (low-grade dysplasia, high-grade dysplasia, carcinoma) recently reported by Luttges et al. [12]. As MSI has been mainly observed in tumours within the spectrum of the HNPCC and Muir-Torre syndromes, it is not surprising that this phenomenon is not present in IPMNs, a type of tumour that has not been described in patients with these syndromes. This does not exclude entirely the possibility of involvement of other components of the DNA mismatch repair system, such as hMSH6 and hPMS2 genes, or of other mechanisms, such as the presence of a missense mutation resulting in a nonfunctional immunoreactive protein [11]. However, pathways that do not involve hypermethylation or germinal mutations seem to be more frequently encountered in pancreatic carcinomas [10, 13] than in colorectal carcinomas. This could be explained by the occurrence of tissue-specific mechanisms of inactivation of mismatch repair (MMR) genes and involve target genes/pathways [4] in pancreatic cancer.

The spectrum of dysplasia in IPMNs is similar to the dysplasia sequence of colon adenomas. This similarity concerns not only morphological features, but also the immunoreactivity pattern for hmlh1 and hmsh2 proteins. We observed two distinct patterns of expression for these two proteins, similar to what has been recently reported in

colon adenomas [2]. The first one, the "normal" pattern, is similar to that observed in normal colonic mucosa. The incidence of this pattern decreases with the progression of dysplasia, from IPMA (43.5–56.5% of the cases) to IPMN with moderate dysplasia (6% of the cases) to 0% in non-invasive and invasive IPMC. The second pattern, the "dysplastic" pattern, is characterised by increased protein expression in the dysplastic cells situated at the top of the papillae and in the surface epithelium. The cells at the base of the papillae, such as in normal colonic mucosa, strongly express these proteins. This pattern is present in all grades of dysplasia in IPMNs, similar to what has been reported in colon adenomas [2]. Its incidence increases from IPMA (43.5–56.5% of the cases) to IPMN with moderate dysplasia (94% of the cases) and non-invasive or invasive carcinoma (100% of the cases). Therefore, increased MMR protein expression seems to occur in cells showing an increase of the proliferation rate assessed by Ki67 immunohistochemistry [16], which increases with the progression of dysplasia. This pattern of expression is similar to that observed in colorectal adenomas, with a "top-down" morphogenesis [15].

The MMR system principally corrects nucleotide mismatches that arise during replication [3]. Therefore, the increased MMR protein expression that we observed may reflect a response to an increase of DNA damage with progression of dysplasia, in which the proportion of cells in G1, S, M and G2 phases (demonstrated by Ki67 immunohistochemistry) increases. Moreover, recent data suggest a relationship between MMR proteins and DNA transactions, such as replication and nucleotide excision repair. This relationship is supported by the ability of the proliferating cell nuclear antigen, another marker of proliferation, to bind to MLH1 and MSH2 [18].

In conclusion, immunoreactivity for hmlh1 and hmsh2 proteins in different grades of dysplasia, as well as in invasive adenocarcinoma in IPMNs, indicates that defective DNA mismatch repair in these two genes is unlikely to contribute to the progression of dysplasia and to the gain of invasive features. Two distinctive patterns of expression have been observed and their occurrence is related to the progression of dysplasia.

References

1. Biankin AV, Biankin SA, Kench JG et al (2002) Aberrant p16 and DPC/Smad4 expression in intraductal papillary mucinous tumours of the pancreas is associated with invasive ductal adenocarcinoma. Gut 50:861–868
2. Bonte H, Fléjou JF (2003) Patterns of expression of MMR proteins in serrated adenomas and other polyps of the colorectum. Gut 52:611
3. Brown KD, Rathi A, Kamath R et al (2003) The mismatch repair system is required for S-phase checkpoint activation. Nat Genet 33:80–84
4. Duval A, Hamelin R (2002) Mutation at coding repeat sequences in mismatch repair-deficient human cancers: toward a new concept of target genes for instability. Cancer Res 62:2447–2454
5. Fuji H, Inagaki M, Kasai S et al (1997) Genetic progression and heterogeneity in intraductal papillary mucinous neoplasms of the pancreas. Am J Pathol 151:1447–1454
6. Goggins M, Offerhaus GJ, Hilgers W et al (1998) Pancreatic adenocarcinomas with DNA replication errors (RER+) are associated with wild-type K-ras and characteristic histopathology. Poor differentiation, a syncytial growth pattern, and pushing borders suggest RER+. Am J Pathol 152:1501–1507
7. Hamilton SR, Aaltonen LA (eds) (2000) Pathology and genetics of tumours of the digestive system. IARC Press, Lyon
8. Kloppel G (1998) Clinicopathologic view of intraductal papillary mucinous tumour of the pancreas. Hepatogastroenterology 45:1981–1985
9. Kloppel G, Solcia E, Longnecker DS et al (eds) (1996) Histological typing of tumours of the exocrine pancreas. Springer, Berlin Heidelberg New York
10. Kondo E, Furukawa T, Yoshinaga K et al (2000) Not hMSH2 but hMLH1 is frequently silenced by hypermethylation in endometrial cancer but rarely silenced in pancreatic cancer with microsatellite instability. Int J Oncol 17:535–541
11. Lindor NM, Burgart LJ, Leontovich O et al (2002) Immunohistochemistry versus microsatellite instability testing in phenotyping colorectal tumours. J Clin Oncol 20:1043–1048
12. Luttges J, Beyser K, Pust S et al (2003) Pancreatic mucinous noncystic (colloid) carcinomas and intraductal papillary mucinous carcinomas are usually microsatellite stable. Mod Pathol 16:537–542
13. Nakata B, Yashiro M, Nishioka N et al (2002) Very low incidence of microsatellite instability in intraductal papillary-mucinous neoplasm of the pancreas. Int J Cancer 102:655–659
14. Sato N, Rosty C, Jansen M et al (2001) STK11/LKB1 Peutz-Jeghers gene inactivation in intraductal papillary-mucinous neoplasms of the pancreas. Am J Pathol 59:2017–2022
15. Shih I-M, Wang T-L, Traverso G et al (2001) Top-down morphogenesis of colorectal tumours. Proc Natl Acad Sci U S A 98:2640–2645
16. Terada T, Ohta T, Kitamura Y, Ashida K, Matsunaga Y (1998) Cell proliferative activity in intraductal papillary mucinous neoplasms and invasive ductal adenocarcinomas of the pancreas: an immunohistochemical study. Arch Pathol Lab Med 122:42–46
17. Thibodeau SN, French AJ, Cunningham JM et al (1998) Microsatellite instability in colorectal cancer: different mutator phenotypes and principal involvement of hMLH1. Cancer Res 58:1713–1718
18. Umar A, Buermeyer AB, Simon JA et al (1996) Requirement for PCNA in DNA mismatch repair at a step preceding DNA resynthesis. Cell 87:65–73
19. Wilentz RE, Goggins M, Redston M et al (2000) Genetic, immunohistochemical, and clinical features of medullary carcinoma of the pancreas: a newly described and characterized entity. Am J Pathol 156:1641–1651
20. Yamamoto H, Itoh F, Nakamura H et al (2001) Genetic and clinical features of human pancreatic ductal adenocarcinoma with widespread microsatellite instability. Cancer Res 61:3139–3144
21. Yoshizawa K, Nagai H, Sakurai S et al (2002) Clonality and K-ras mutation analyses of epithelia in intraductal papillary mucinous tumor and mucinous cystic tumor of the pancreas. Virchows Arch 441:437–443

Virchows Arch (2004) 444:239–246
DOI 10.1007/s00428-003-0951-7

ORIGINAL ARTICLE

Wiltrud Coerdt · Jörg-S. Michel · Gerd Rippin · Semen Kletzki · Valentin Gerein · Horst Müntefering · Joachim Arnemann

Quantitative morphometric analysis of the submucous plexus in age-related control groups

Received: 16 July 2002 / Accepted: 26 November 2003 / Published online: 29 January 2004

Abstract An increased number and density of the so-called "giant ganglia" (seven or greater ganglion cells per ganglion) serve as histopathological criteria for a bowel motility disorder called intestinal neuronal dysplasia of the submucous plexus (IND B). However, because these morphological criteria have been defined based upon observations in constipated patients, the diagnostic value of previous studies is open to controversy. Moreover, no age-related reference data from unaffected controls are available. This study reports on data from unaffected controls on the variability of size and distribution of ganglia in the submucous plexus during development. Therefore, for the first time, the normal status has been defined. Four age groups have been defined: (a) premature births, gestational age less than 35 weeks; (b) 1–365 days; (c) 1–14 years and (d) 15 years to greater than 70 years). All of these groups revealed giant ganglia in the submucous plexus. With advancing age, there was a decrease in the number of giant ganglia (from 32.7% in group a to 11.2% in group d) accompanied by an inverse increase in the mean distance between all ganglia (from 0.52 mm in group a to 1.17 mm in group d). The data presented permit the conclusion that the criteria mentioned above are not apt to define IND B as an entity, since they do not allow a sufficient demarcation from the age-correlated normal values presented here.

Keywords Intestinal neuronal dysplasia · Ganglion cells · Giant ganglia · Submucous plexus · Development · Gestation

W. Coerdt (✉) · J.-S. Michel · V. Gerein · H. Müntefering · J. Arnemann
Department of Paediatric Pathology,
Johannes Gutenberg University Hospital,
55101 Mainz, Germany
e-mail: coerdt@kinderpatho.klinik.uni-mainz.de
Tel.: +49-61-31172755
Fax: +49-61-31173546

G. Rippin
Institute of Medical Statistics and Documentation,
Johannes-Gutenberg University Hospital,
Mainz, Germany

S. Kletzki
Department of Paediatric Pathology,
Institute of Pathology, University Hospital,
Minsk, Belo-Russia

J. Arnemann
Institute of Human Genetics,
Johann-Wolfgang-Goethe University Hospital,
Frankfurt/Main, Germany

Introduction

Coping with chronic constipation in young children is a difficult problem for the paediatrician. The clinical features of chronic constipation range from chronic intractable constipation to abdominal distension or to overflow incontinence. Aganglionosis of the distal parts of the colon, commonly known as Hirschsprung's disease (HD) [5] is one of the most frequent causes of these symptoms. It is possible to diagnose this disease histochemically [e.g. from rectal suction biopsies utilising the application of well-established enzymatic tests, for example, for acetylcholinesterase (AchE) assay]. In Hirschsprung's disease, the lack of intramural ganglia leads to an accumulation of the AchE activity on the surface of the parasympathetic intramural mucosal fibres of the distal colon, due to the activity of the extramural parasympathetic innervation. Beyond the eighth week of life, this may serve as a reliable test for the diagnosis of HD in the rectum and lower part of the sigma—except in very rare cases with developmental defects of the extramural parasympathetic nerves [10]. Aganglionosis affects not only the distal part of the colon, but also the descending colon, and, in very rare cases, it may also affect the entire colon, as well as the small intestine. Orally to the lower part of the descending colon, the AchE assay in the mucosa is no longer diagnostic. Here, only the detection of ganglion cells (i.e. using dehydrogenase assays) can serve as a diagnostic tool. As a curative treatment, the aganglionic segments have to be surgically extirpated.

The results of the rectal suction biopsies may confirm the presence of submucous ganglia. However, when clinical symptoms persist, the paediatrician is faced with a problem of a different nature. In order to improve the diagnosis in these cases, Meier-Ruge [11] introduced, as an additional diagnostic tool, the analysis of the density of ganglia and the number of ganglion cells per ganglion within the submucous plexus of the large intestine. His studies on innervation (within a transitional zone between the aganglionic and the normal colon segment) have shown a variability in the size and distribution pattern of ganglia. Ganglia that have a number of seven or more ganglion cells were defined as so-called "giant ganglia". Therefore, an increased number of those ganglia serves as histological proof of a pathological condition.

Observation of giant ganglia (3–5% [13] and 10% [14], respectively) in a number of non-aganglionic, constipated patients led to the introduction of a morphologically defined pathological condition, named intestinal neuronal dysplasia, type B (IND B) [12]. However, the existence of this disease entity is open to controversy [2, 8, 9] because the criteria for this diagnosis have been defined based merely upon observations in patients with bowel motility disturbances. Furthermore, no age-related reference data from unaffected controls are available.

A recent multi-centre study on children with suspected IND showed such a high inter-observer variation with regard to the different morphological features and to the final diagnosis of IND [7] that the validity of IND diagnosis by rectal suction biopsies has become dubious. A further methodical weakness of the IND B diagnosis is that the analysis of the density of ganglia for a given area does not necessarily reflect the developmental status of the patient or his physiological growth.

To date, no systematic studies on unaffected controls of different age groups have been performed, and no reference data have been available on the distribution of ganglia during normal development. The lack of standard values and the unsatisfying outcome of the above-mentioned multi-centre study on children with suspected IND leads to the question: does IND B, in fact, exist as a disease entity?

The hypothesis that IND is an entity came to be because, in some cases of HD, a "dysganglionic" segment, with giant ganglia in the submucous plexus, was observed cranial to the aganglionic segment. The fact that other patients with constipation, but not affected with HD, also rarely showed giant ganglia was enough to suggest the conclusion that IND could exist as an entity and be diagnosed through quantitative analysis of the ganglia [12, 13, 14].

In the case of a disease entity being defined by a quantitative method, a normal collective is necessary for comparison. Until now, ethical and logistical problems hindered these investigations. The presented paper is intended to close this gap.

Materials and methods

Patients and material

With the approval of the ethics authorities, colon segments or colon tissue specimens from 36 control individuals were obtained from different units of general pathology or paediatric pathology (primarily in Austria and Belo-Russia, respectively). We defined our controls as individuals with no clinical history of constipation or other symptoms indicating a disturbed function of the intestine. Samples were immediately removed post-mortem to avoid autolytic processes, and the native specimens that were obtained were frozen on dry ice until further processing.

The resected colon specimens from seven different anatomical localisations within each colon were longitudinally cut perpendicular to the surface and placed upon the cut surface on a cryostat carrier. The native tissue was frozen (at −80°C) and cut (at −20°C) into sections that were 15 μm thick. In order to avoid counting the same anatomical structure more than once every second, stained section was used for morphometric analysis.

Staining with haematoxylin and eosin was used to assess the quality and the morphology of the tissue sections. This study included 32 individuals. Four additional cases that were of substandard quality (artefacts) were excluded.

In total, seven different localisations were investigated within the colon, namely:

Position 1 rectum 5 cm above the anocutaneous line
Position 2 transitional zone between rectum and sigmoid
Position 3 transitional zone between sigmoid and descending colon
Position 4 proximal descending colon
Position 5 middle of transverse colon
Position 6 proximal ascending colon
Position 7 cecum

Enzymatic histochemical staining for AchE, LDH, SDH and NADPH-diaphorase

As part of the routine procedure, the air-dried sections underwent an enzyme–histochemical procedure for an AchE reaction [6], as the marker enzyme for aganglionosis. In accordance with standard methods for histological identification and morphometric measurements, ganglia and nerve cells were selectively stained using reactions for lactic dehydrogenase (LDH) activity [4, 12], succinate-dehydrogenase (SDH) activity [15] and nicotinamide-adenine-dinucleotide-phosphate (NADPH)-diaphorase activity [16].

Morphometric analysis

Morphometric evaluations were performed with a microscope (Zeiss, Axioskop) furnished with an electronic scaling device (μScale, Märzhäuser, Wetzlar). The following parameters were analysed and documented for two different staining patterns (LDH-activity; NADPH-diaphorase activity) in each of seven anatomically defined regions of the colon:

1. Number of ganglion cells per ganglion
2. Distance between ganglia

The distance between two points within a coordinate system can be calculated according to the Pythagorean theorem $a^2+b^2=c^2$ (Fig. 1). The distance between the two points (mm) is equal to the hypotenuse c of a rectangular triangle with the arms a and b. The two points are defined by two different coordinates on the abscissa x and the ordinate y. Point 1 has the coordinates x1, y1; point 2 has the coordinates x2, y2. They correspond with the nonia of the electronic scale device of each ganglion investigated. As a

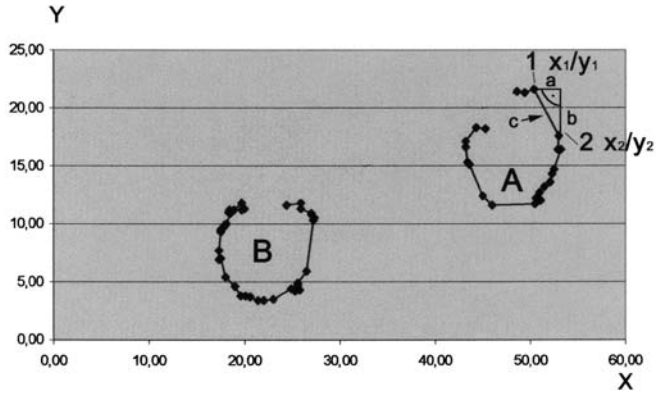

Fig. 1 Symbolic presentation of the submucous plexus: a microscopic slide mounted with two adjacent specimens (*A* and *B*), [scale (mm)]. The distance c between two given ganglia 1 and 2 with the corresponding co-ordinates x_1/y_1 and x_2/y_2 can be calculated according to the Pythagorean theorem: $a^2+b^2=c^2$

representative point of each ganglion, the middle of the ganglion was chosen. According to the following formula:

$$\sqrt{[2](x_1 - x_2)^2 + (y_1 - y_2)^2} = c$$

the distance between the two points can be calculated. The calculation is done automatically by an Excel (Microsoft) database, which contains the registered nonia for each point. The data were collected for 60 ganglia from seven anatomically defined regions of the colon of 32 individuals. A total of 2016 slides were analysed. An example of a representative original slide is given in detail (Fig. 2).

Preparation and format of the available data and information

Efficient statistical evaluation by the SAS program required a numerical coding of all available information. An Excel (Microsoft) database was created, which contained all of the necessary information. Therefore, this set of data could easily be read by the SAS program.

The following parameters were listed in detail, for each analysed ganglion and for each individual sample: sample code of the laboratory; lysis time stated in minutes (i.e. the time from death to sample collection); age of the individual stated in days; gestational age stated in weeks; anatomical localisation of the samples within the colon according to the above-mentioned list; staining [i.e. used for evaluation (1 = LDH; 2 = NADPH diaphorase)]; X-coordinate; Y-coordinate; number of ganglion cells per analysed ganglion and distance to the nearest ganglion (mm). The complete database consisted of 23342 lines (i.e. analysed ganglia).

Statistical evaluation

Our study had two objectives. First, contrary to the previous method, which utilises surface density values, our objective was to create a new procedure using certain anatomical structures as internal reference values. Second, we sought to document the distribution of ganglion size over the patient's lifespan as a means of obtaining age-related reference values.

In order to calculate in advance how many ganglia from a region should be analysed to achieve a mean value of the number of ganglion cells per ganglia, a pilot study was created. A specimen of the colon of optimal size was chosen to analyse all ganglion quantitatively, including confidence intervals and mean values.

As a breadth of the confidence interval of less than two would be sufficient, the mean error calculated was used to find the least number of ganglia fitting the criterion. In addition, the enzymatic reactions were tested for differences of the mean values using the same method.

Significant differences between the various anatomical localisations along the colon of each individual were not found using Fisher's exact test. The age-related cohorts were defined after having tested all values for homogeneity using the same test method.

Results

In order to achieve certainty about the mean values of the size of the ganglia of the submucous plexus, one has to define first how many ganglia must be investigated in each case. A pilot study was done using a specimen of optimal size to permit investigation of 180 ganglia. It revealed the following values:

Number of ganglia analysed 180
Scattering range of the number of ganglion cells per ganglion 2–21
Mean values 5.56
Standard deviation 3.26
Confidence interval 5.08–6.03
Breadth of confidence interval 0.96
Breadth of confidence interval in 60 ganglia 1.37

Defining the postulated confidence interval of less than two, the analysis of 60 ganglia was shown to be sufficient (breadth of confidence interval = 1.37). The above values do not depend on which of the two enzyme–histochemical stainings of the ganglion cells was used. In addition, the seven different anatomical regions of the colon showed no significant differences.

Having established the technical quality of the specimens and having eliminated cases of substandard quality (artefacts), material from 32 individuals could be investigated, representing the following age-related groups:

Group a premature birth, gestational age less than 35th week; 4 individuals
Group b mature birth to 1 year of age; 9 individuals
Group c 1–14 years; 4 individuals
Group d 15 years to greater than 70 years; 15 individuals

The age-related groups were not arbitrarily designed, but were defined according to the mean size of ganglia in each individual. The size of ganglia in all cases ranged between 2 and 25 cells—in preterm newborns even up to 29 cells. Their distribution in percent in the four age-related groups (Fig. 3a, b, c, d) is not normal (as in a Gaussian curve), but unequal. So-called giant ganglia with more than seven ganglion cells are present in all age-related groups. The fraction of very large ganglia with more than 15 ganglion cells is rather low in the group of adolescents and adults, but reaches 10% in the preterm newborns. However, the fraction of small ganglia below seven ganglion cells increases with advancing age.

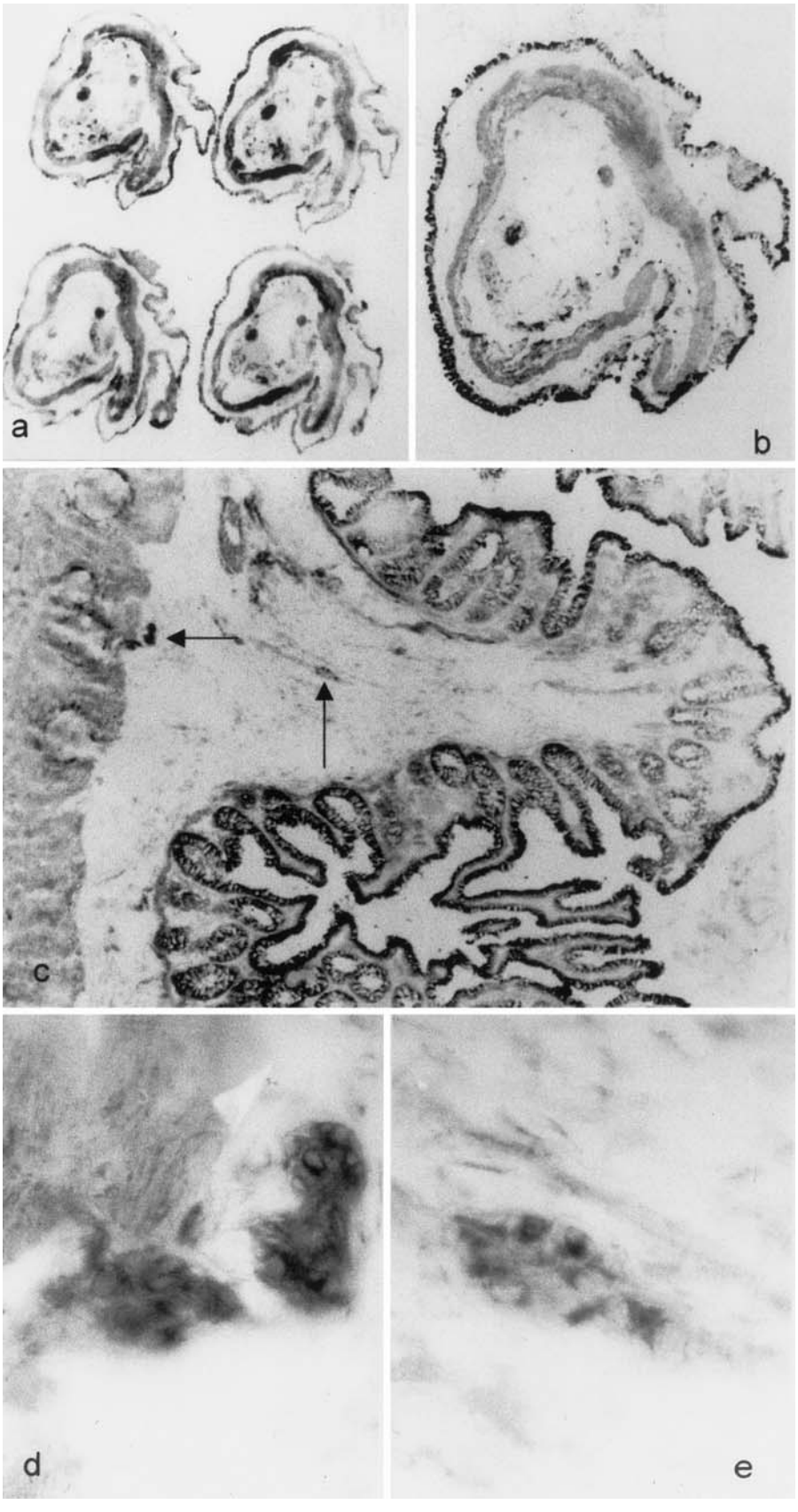

Fig. 2 Enzyme histochemistry of the submucous ganglia. **a** Microscopic slide mounted with four adjacent specimens. Lactic dehydrogenase (LDH) staining, ×2.8. **b** Higher magnification of one specimen—taken from **a**—showing all layers of the colonic wall in more detail. LDH staining, ×3.5. **c** Detail taken from **b**: showing two ganglia; *arrows* in the deep submucous layer and one ganglion *arrow* in the middle of the submucous layer; LDH staining, ×25. **d** Detail: *arrow* taken from **c**: two so-called "giant ganglia" of the submucous plexus with 9 and 13 ganglion cells respectively; LDH staining, ×200. **e** Detail: *arrow* taken from **c**: so-called "giant ganglion" of the submucous plexus with 13 ganglion cells, LDH staining, ×200

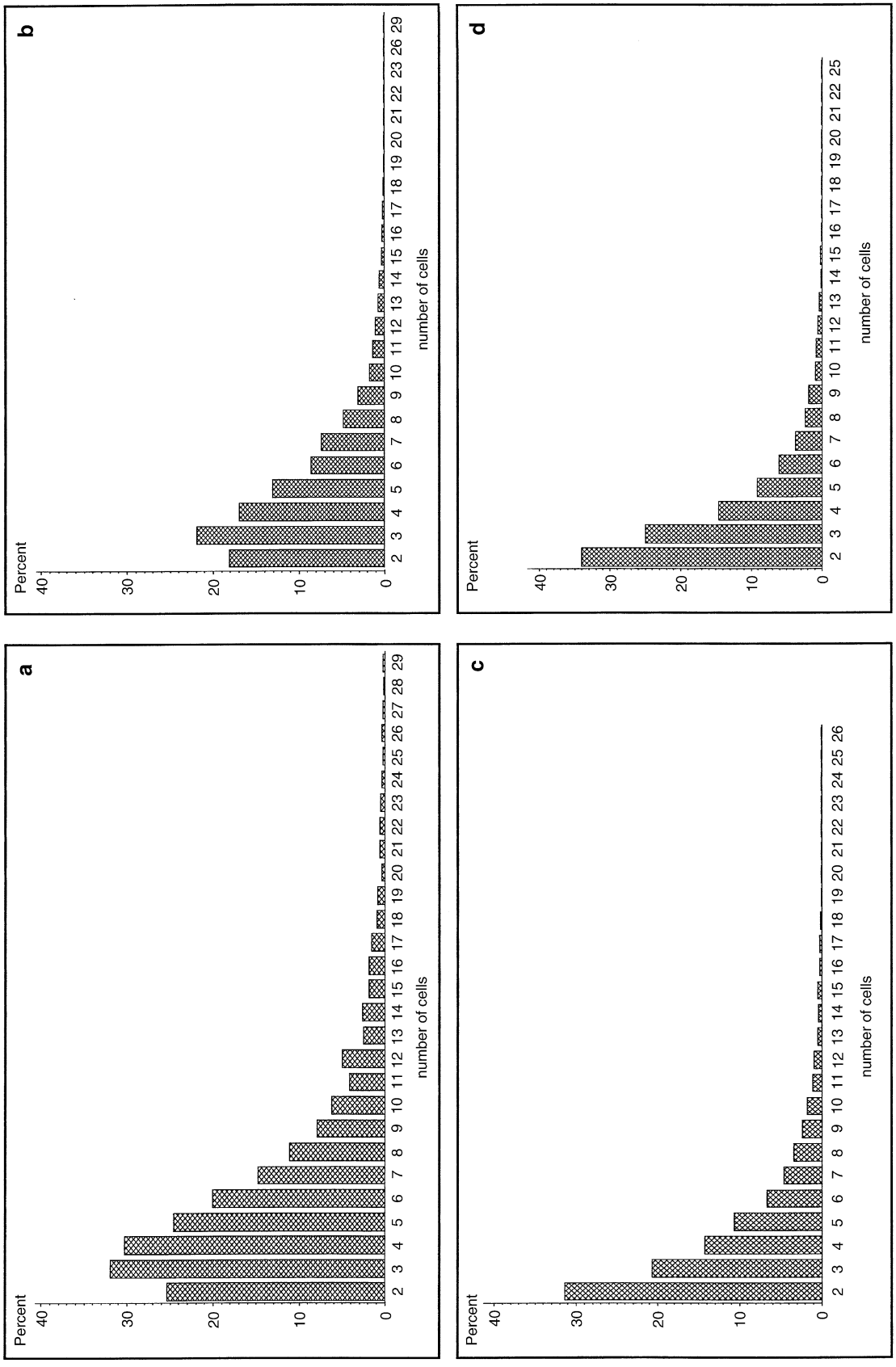

Fig. 3 Frequency distribution (in percent) of ganglia of the submucous plexus correlated to their size (number of ganglion cells per ganglion) in four age-related cohorts **a**, **b**, **c**, **d**. *Ordinate* frequency of ganglia with defined numbers of ganglion cells per ganglion; (height of columns = percent). *Abscissa* number of ganglion cells per ganglion; (width of columns = defined numbers of ganglion cells per ganglion). With increasing age, there is a tendency towards smaller ganglia

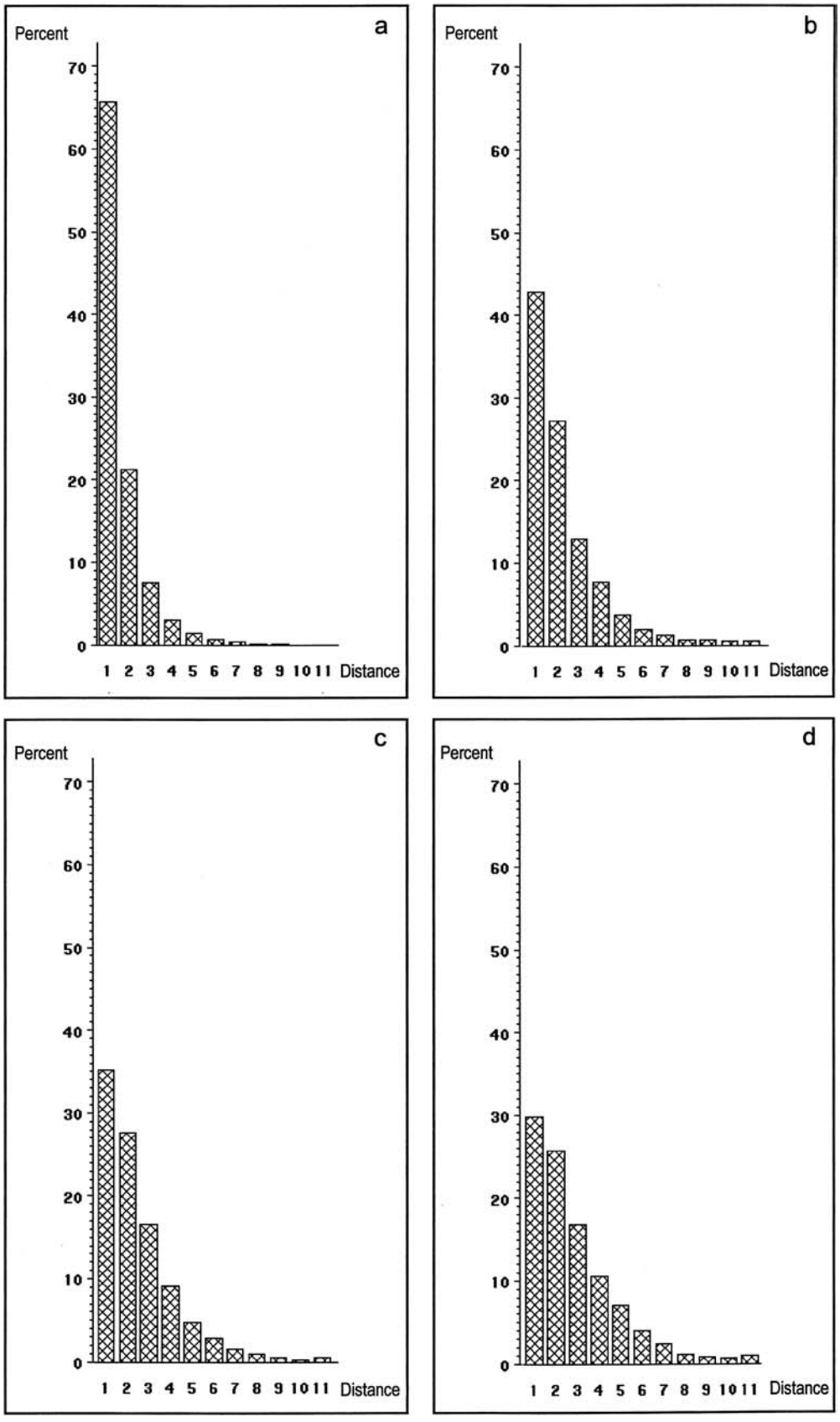

Fig. 4 Frequency distribution (in percent) of distances between ganglia of the submucous plexus in correlation to the length of distances calculated according to the Pythagorean theorem—in steps of 0.5 mm each—given for four age-related cohorts. **a** Group a = premature births, gestation less than 35th week of pregnancy. **b** Group b = mature birth to 1 year of age. **c** Group c = 1–14 years. **d** Group d = 15 years to greater than 70 years. *Ordinate* frequency of calculated distances between ganglia; height of columns = percent. *Abscissa* length of distances between ganglia; width of columns = consecutive steps of 0.5 mm, except the last one (11), which represents all distances above 5 mm. With increasing age, there is a tendency towards greater distances/lower density

Table 1 All values given for four different age-related cohorts (groups a–d)

		Group a	Group b	Group c	Group d
		Gestation less than 35 weeks	1–365 days	1–14 years	15 years to greater than 70 years
A	Mean number of ganglion cells per ganglion	6.10	4.81	4.31	3.84
	Standard deviation	4.16	2.8	2.88	2.32
	Confidence interval	0.14	0.06	0.08	0.06
B	Mean number of ganglion cells per ganglion with greater than seven ganglion cells	10.71	9.088	9.55	9.01
	Percentage of ganglion with greater than seven ganglion cells	32.7%	21.5%	16.3%	11.2%
C	Mean distance (mm) between ganglia	0.52	0.89	0.993	1.176
	Standard deviation	0.512	0.913	0.895	1.047
	Mean number of ganglia per millimetre	1.92	1.12	1.00	0.85

This tendency is seen in the comparison of the mean values of ganglion sizes (Table 1). The mean is 6.1 ganglion cells per ganglion in the group of preterm newborns. In the infant group in the first year of life, the value is 4.81 ganglion cells per ganglion. From age 1 year to 14 years, the mean size is 4.31 ganglion cells per ganglion, and, in the adolescent and adult group, this value is 3.84 ganglion cells per ganglion.

Having assumed a cut point of seven, i.e. calculating only ganglia with seven or more ganglion cells, the mean value decreases during life span. The mean number of giant ganglia is 32.7% in preterm newborns. In the first year of life, this value is 21.5%. In age group 1–14 years, the mean is 16.3%, and, in the group of adolescents and adults, it is 11.2%(Table 1). The latter value would even be pathological according to the criteria of the consensus conference [3].

The distribution of the calculated distances between the ganglia of the submucous plexus in percent shows, in all age-related groups, an unequal distribution (Fig. 4a, b, c, d). The distances increase with advancing age. In preterm newborns, distances of 5 mm are only measured in a very low number, whereas this fraction is up to 2% in the group of adolescent and adults (Fig. 4a, b, c, d).

Different biopsy sizes required for the different age-related groups can be deduced: 3 mm for preterm newborns, 5 mm for infants below 1 year of age, 5–6 mm for children aged 1–14 years, 6–7 mm for infants, adolescents and adults. (The formerly propagated reference value of a constant area can no longer be accepted as relevant.)

Discussion

Diagnosing chronic constipation in young children is a difficult problem for the paediatrician. Often, it is considered to be a dysfunction of the enteric nervous system and—because the symptoms may resemble Hirschsprung's disease—rectal suction biopsies are regularly taken to exclude aganglionosis of the rectum or colon. According to previously defined criteria, in a number of biopsies, the analysis of the submucous layer often leads to the diagnosis of IND B [12]. This condition has been defined as a congenital malformation of the submucous plexus, which presents with the clinical features of constipation. It is defined based upon the increase in the total number of ganglia (hyperganglionosis) and ganglion cells per ganglion (hypercellularity) in the submucous plexus [10]. Intestinal neuronal dysplasia of the submucous plexus is defined as subtype IND B [12].

However, a problem is the lack of any systematic approach to studying the morphometrical and histological features of the colonic submucous plexus during normal development. To close this gap, our study collected and statistically evaluated morphometric base data from a control group comprised of subjects from a gestation age of 30 weeks to an age well above 70 years. As Lumb and Moore [9] pointed out: "obtaining a set of controls presents a challenge, as it would be ethically unsound to put a control child through an unnecessary surgical biopsy." Therefore, our study adhered to their ethical considerations and used cadaveric material, with no history of constipation. The tissue was obtained within 1.5–4 h of death, which significantly reduced any post-mortem artefacts.

In contrast to other authors [1, 17, 18], this study did not analyse density by counting the distribution of ganglia per defined area. Instead, it introduced a new procedure, which is more relevant to the needs of routine daily diagnostics. The indiscriminate analysis of a pre-defined number of ganglia permits data to be more easily compared with other samples. Thus, because it excludes alterations due to advancing age, it serves as internal reference data.

Our data support this approach. There is a clear correlation between age and the distance between the ganglia. With increasing age, the distance between the ganglia increases. This means, that for diagnostic purposes, the ganglion density of diagnostic specimens can only be compared with data of defined controls of similar age. However, to date no sets of age-related control data have been published.

In a second approach, in order to test for inter-individual variations, the pattern and distribution of ganglia were evaluated for seven defined anatomical

localisations within the colon of each individual. In this study, we established a standard for size and distribution of ganglia within the submucous plexus in unaffected controls, which might serve as a reference in future studies on IND B or related disorders with bowel motility disturbances.

Using this method to analyse 60 adjacent ganglia of the submucous plexus for the distribution in the number of ganglion cells per ganglion and the distance between the ganglia, it could be shown that significant changes in the pattern of ganglia take place during the final weeks of pregnancy and in the first year of life. In that time period, the mean number of ganglion cells per ganglion decreases (from 6.10 to 4.81 per ganglion) and the percentage of giant ganglia (with seven or more ganglion cells) decreases from 32.7% to 21.5%, while the distances between the ganglia increase from 0.52 mm to 0.89 mm. Although the absolute values vary slightly between the localisations within an individual, these findings are comparable for all seven localisations that were tested.

Special attention focussed on the so-called giant ganglia, which were arbitrarily defined [11] as ganglia with seven or more ganglion cells. The number and density of these giant ganglia within the submucous plexus have been used [13, 14] as criteria for the histological diagnosis of IND B with defined (but often corrected pathological cut-off) values of 3–5% to 10%, respectively of all ganglia. According to the criteria of the Consensus Conference [3], IND B is defined as a morphological entity, which is characterised by certain quantitative distinctive marks in the submucous plexus, namely the presence of giant ganglia, each containing more than seven ganglion cells, with a frequency of more than 10% of the evaluated ganglia (numerically adjusted to the method presented here). Our data indicate a spectrum of these so-called giant ganglia, falling between 21.5% in the neonatal period and 11.2% in adults. In premature babies, (gestational age less than 35 weeks) the rate of 32.7% is reached. This leads us to conclude that, if the criteria of the Consensus Conference [3] are applied, all the normal cases evaluated here would have to be interpreted as IND B cases. Thus, we agree with the view of Lumb and Moore [8, 9]—that the data on IND B published to date [13, 14] do not show an independent entity, but rather a variation of the normal.

The question of whether other criteria are suitable for defining a morphological entity with a morbidity factor can only be answered after further investigations. The method shown here is suitable for carrying out a morphometrical revisitation of a group of patients and comparing it (the group) with age-correlated normal values. A corresponding re-evaluation of specimens of non-selected patients of our own, where an IND B had previously been diagnosed according to the criteria of the Consensus Conference [3], is in process.

Acknowledgements The authors would like to thank Dr. M. Rossol (Wels, Austria), Prof. Dr. M. Ratschek (Graz, Austria) and Prof. Dr. G. Otto (Mainz) for the very helpful contribution of tissue samples, Mrs. Schilling, Mrs. Heymann and Mrs. Cetin for technical assistance and Mrs. Griesheimer and Mrs. Brucki for their support in the morphometric analysis.

References

1. Ammann K, Stoss F, Meier-Ruge W (1999) Intestinale neuronale Dysplasie des Erwachsenen als Ursache der chronischen Obstipation. Chirurg 70:771–776
2. Berry CL (1993) Intestinal neuronal dysplasia: does it exist or has it been invented? Virchows Arch A Pathol Histopathol 422:183–184
3. Borchard F, Meier-Ruge WA, Wiebecke B, Briner J, Müntefering H, Födisch HJ, Holschneider AM, Schmidt A, Enck P, Stolte M (1991) Innervationsstörungen des Dickdarms: Klassifikation und Diagnostik. Pathologe 12:171–174
4. Hess R, Scarpelli DG, Pearse AGE (1958) The cytochemical localization of oxidative enzymes. II. Pyridine nucleotide-linked dehydrogenase. J Biophys Biochem Cytol 4:753
5. Hirschsprung H (1888) Stuhlträgheit Neugeborener infolge Dilatation und Hypertrophie des Colons. Jahresbericht Kinderheilkunde
6. Karnovsky MJ, Roots L (1964) A direct-coloring thiocholine method for cholinesterase. J Histochem Cytochem 12:219
7. Koletzko S, Jesch I, Faus-Kebetaler T, Briner J, Meier-Ruge W, Müntefering H, Coerdt W, Wessel L, Keller KM, Nützenadel W, Schmittenbecher P, Holschneider A, Sacher P (1999) Rectal biopsies for diagnosis of intestinal neuronal dysplasia in children: a prospective multi-centre study on interobserver variation and clinical outcome. Gut 44:853–861
8. Lumb PD, Moore L (1998) Back to the drawing board. Intestinal neuronal dysplasia type B: not a histological entity yet. Virchows Arch 432:99–102
9. Lumb PD, Moore L (1998) Are giant ganglia a reliable marker of intestinal neuronal dysplasia type B (IND B)? Virchows Arch 432:103–106
10. Meier-Ruge W (1971) Über ein Erscheinungsbild des Kolons mit Hirschsprung-Symptomatik. Verh Dtsch Ges Pathol 55:506–510
11. Meier-Ruge W (1985) Angeborene Dysganglionosen des Colon. Kinderarzt 16:151–164
12. Meier-Ruge W (1990) Das morphologische Erscheinungsbild der neuronalen Dysplasie des Plexus submucosus. Kinderarzt 21:837–844
13. Meier-Ruge W, Brönnimann PB, Gambazzi F, Schmidt PC, Schmidt CP, Stoss F (1995) Histopathological criteria for intestinal neuronal dysplasia of the submucosal plexus (type B). Virchows Arch 426:549–556
14. Meier-Ruge WA, Schmidt CP, Stoss F (1995) Intestinal neuronal dysplasia and its morphometric evidences. Pediatr Surg Int 10:447–453
15. Nachlas M.M, Tsou K-Ch, Souza E, Cheng Ch-S, Seligman AM (1957) Cytochemical demonstration of succinic dehydrogenase by the use of a new p-nitrophenyl substituted ditetrazole. J Histochem Cytochem 5:420
16. Scherer-Singler U, Vincent SR, Kimura H, McGeer EC (1983) Demonstration of a unique population of neurons with NADPH-diaphorase histochemistry. J Neurosi Methods 9:229–234
17. Wester T, O'Briain S, Puri P (1998) Morphometric aspects of the submucous plexus in whole-mount preparations of normal human distal colon. J Pediatr Surg 4:619–622
18. Wester T, O'Briain DS, Puri P (1999) Notable postnatal alterations in the myenteric plexus of normal human bowel. Gut 44:666–674

Virchows Arch (2004) 444:247–256
DOI 10.1007/s00428-003-0963-3

ORIGINAL ARTICLE

José A. Jiménez-Heffernan · Abelardo Aguilera · Luiz S. Aroeira · Enrique Lara-Pezzi · M. Auxiliadora Bajo · Gloria del Peso · Marta Ramírez · Carlos Gamallo · José A. Sánchez-Tomero · Vicente Álvarez · Manuel López-Cabrera · Rafael Selgas

Immunohistochemical characterization of fibroblast subpopulations in normal peritoneal tissue and in peritoneal dialysis-induced fibrosis

Received: 8 September 2003 / Accepted: 23 November 2003 / Published online: 29 January 2004

Abstract Peritoneal fibrosis is one of the most common morphological changes observed in continuous ambulatory peritoneal dialysis (CAPD) patients. Both resident fibroblasts and new fibroblast-like cells derived from the mesothelium by epithelial-to-mesenchymal transition are the main cells involved fibrogenesis. In order to establish markers of peritoneal impairment and pathogenic clues to explain the fibrogenic process, we conducted an immunohistochemical study focused on peritoneal fibroblasts. Parietal peritoneal biopsies were collected from four patient groups: normal controls (n=15), non-CAPD uremic patients (n=17), uremic patients on CAPD (n=27) and non-renal patients with inguinal hernia (n=12). To study myofibroblastic conversion of mesothelial cells, α-smooth muscle actin (SMA), desmin, cytokeratins and E-cadherin were analyzed. The expression of CD34 by fibroblasts was also analyzed. Fibroblasts from controls and non-CAPD uremic patients showed expression of CD34, but no myofibroblastic or mesothelial markers. The opposite pattern was present during CAPD-related fibrosis. Expression of cytokeratins and E-cadherin by fibroblast-like cells and α-SMA by mesothelial and stromal cells supports that mesothelial-to-myofibroblast transition occurs during CAPD. Loss of CD34 expression correlated with the degree of peritoneal fibrosis. The immunophenotype of fibroblasts varies during the progression of fibrosis. Myofibroblasts seem to derive from both activation of resident fibroblasts and local conversion of mesothelial cells.

Keywords Peritoneal dialysis · Myofibroblasts · Fibrosis · Epithelial-to-mesenchymal transition

Manuel López-Cabrera and Rafael Selgas contributed equally to the article.

J. A. Jiménez-Heffernan (✉)
Department of Pathology, University Hospital,
Donantes de sangres s/n, 19002 Guadalajara, Spain
e-mail: jjheffernan@yahoo.com
Tel.: +34-94-9209220

J. A. Jiménez-Heffernan
University of Alcalá de Henares, Madrid, Spain

A. Aguilera · J. A. Sánchez-Tomero · V. Álvarez · R. Selgas
Department of Nephrology,
University Hospital La Princesa, Madrid, Spain

L. S. Aroeira · E. Lara-Pezzi · M. Ramírez · M. López-Cabrera
Department of Molecular Biology,
Hospital La Princesa, Madrid, Spain

M. A. Bajo · G. del Peso
Department of Nephrology,
University Hospital La Paz, Madrid, Spain

C. Gamallo
Department of Pathology,
Hospital La Princesa, Madrid, Spain

J. A. Jiménez-Heffernan · A. Aguilera · L. S. Aroeira · E. Lara-Pezzi · M. A. Bajo · G. del Peso · M. Ramírez · C. Gamallo · J. A. Sánchez-Tomero · V. Álvarez · M. López-Cabrera · R. Selgas
"Grupo de Estudios Peritoneales de Madrid",
Instituto Reina Sofia de Investigaciones Nefrológicas (FRIAT),
Spain

Introduction

Continuous ambulatory peritoneal dialysis (CAPD) is an alternative to hemodialysis for the treatment of end-stage renal disease. Unfortunately, long-term exposure to hyperosmotic, hyperglycemic and acidic dialysis solutions often causes a low-grade chronic inflammation and injury to the peritoneum. Peritoneal fibrosis (or sclerosis) is one of the most common morphological changes observed in patients undergoing CAPD [9, 18, 29]. The degree of peritoneal fibrosis correlates with the time on dialysis and appears to be responsible for the progressive functional decline of the peritoneum, which ultimately may cause ultrafiltration failure. This functional decline of the

peritoneum may be accelerated by recurrent or severe episodes of peritonitis or hemoperitoneum [21]. The pathophysiological processes that lead to peritoneal impairment during long-term CAPD are not well understood. Peritoneal fibroblasts entrapped in the stroma have been classically considered as the main cells involved in peritoneal fibrosis. In contrast, the mesothelial cells have been considered, for long time, as mere victims of the tissue insults induced by CAPD treatments. We have previously demonstrated, in vivo and ex vivo, that mesothelial cells undergo a transition from epithelial to mesenchymal phenotype during CAPD, suggesting a direct and active role for mesothelial cells in the tissue fibrosis and ultrafiltration failure [34]. In addition, a recent report has demonstrated that mesothelial cells treated with transforming growth factor (TGF)-β acquire myofibroblastic properties in vitro, including the upregulation of α-smooth muscle actin (α-SMA) and collagen-I expression [32].

Myofibroblasts, which share biochemical and structural features with smooth muscle cells and fibroblasts, have been described in almost all human pathologies that course with wide-spread tissue fibrosis [19]. The origin of interstitial fibroblasts has been largely overlooked, and their lineage is not fully elucidated. One hypothesis argues that tissue fibroblasts derive from a subpopulation of circulating leukocytes, termed fibrocytes, which express the progenitor marker CD34 [1, 6]. In this context, subpopulations of CD34+ fibroblastic cells have been observed distributed throughout the connective tissue of many organs [25, 26]. Loss of expression of CD34 by tissue fibroblasts has been described in several pathological conditions associated with fibrosis [2, 3, 4, 7, 11, 14, 23]. However, the meaning of this loss of CD34 expression is still unknown and has been used mainly for diagnostic purposes. A second hypothesis propounds that interstitial fibroblasts are formed by local conversion from tissue epithelium by epithelial-to-mesenchymal transition (EMT), which is particularly evident during fibrotic repair following tissue injury [10]. In agreement with this hypothesis, we have demonstrated that peritoneal mesothelial cells undergo EMT in response to inflammatory and mechanical injuries induced by CAPD [34].

Regardless of the organ or tissue where fibrosis takes place, the cellular and molecular mechanisms that lead to fibrosis share many common features. In this study, we conducted immunohistochemical analyses focused on peritoneal fibroblasts to establish the pathogenic clues of the fibrogenic process during CAPD and to identify possible diagnostic markers of peritoneal impairment. More precisely, we evaluated immunohistochemical markers of myofibroblastic differentiation and EMT. In addition, we evaluated the loss of CD34 expression as marker of peritoneal fibrogenesis. In order to assess the specificity of these changes, we also analyzed peritoneal tissue samples with fibrosis unrelated to CAPD or uremia. For this purpose, pathological hernia sac specimens were obtained from patients with inguinal hernia.

Materials and methods

Patients

Biopsies were collected from four patient groups: (1) normal control samples (n=15) of parietal peritoneum obtained from autopsy cases and kidney donors; (2) uremic patients who had never undergone CAPD (n=17); (3) uremic patients on CAPD (n=27) and (4) non-renal patients with inguinal hernia (n=12). In renal patients, surgery was undertaken for renal transplantation, insertion or removal of the CAPD catheter or due to incidental abdominal conditions. Table 1 shows the most relevant clinical features of these patients, including supress episodes of peritonitis, time on CAPD and peritoneal function. Informed consent was obtained from all tissue donors.

Biopsy collection and processing

Except for the samples of visceral peritoneum and hernia sacs, all the remaining samples were obtained from the parietal peritoneum of the anterior abdominal wall. Samples measured 15–25×15–25 mm. In order to avoid mesothelial artifactual detachment, they were carefully manipulated and immediately fixed with neutral-buffered 3.7% formalin (pH 7.3) for 12–24 h. While immersed in formalin, they were gently attached to a flat surface to avoid retraction. Afterward, samples were cut and embedded in paraffin and then cut into 3-μm sections. When preparing the paraffin blocks, special efforts were made to orientate the samples perpendicular to the cutting surface. Sections were stained with hematoxylin-eosin, Masson trichromic and periodic acid-Schiff. For immunohistochemistry, paraffin sections were mounted on precoated slides, routinely deparaffinized and rehydrated and incubated with 3% hydrogen peroxide in methanol to block endogenous peroxidase activity. Antigen retrieval was performed using a citric acid solution (pH 6), which was heated with a microwave. Indirect immunohistochemical studies were performed by means of a dextran-polymer conjugate technique (EnVision+, Dako, Glostrup, Denmark). Table 2 shows the antibodies used in the study. For visualization, diaminobenzidine was used as chromogen. The sections were counterstained with a light hematoxylin stain.

Sample analysis

Histological interpretation was performed using recently published morphological criteria [29]. Morphological data regarding mesothelial status, thickness of submesothelial compact zone, hyalinizing vasculopathy and inflammation were recorded. In addition to the thickness of the submesothelial layer, the presence of dense, sclerotic areas of fibrosis was also evaluated. The density of the mesothelial cells was measured using a semiquantitative scale (grade 3, normal cell density; grade 0, complete denudation) as described by Plum et al. [18]. For this purpose, the whole mesothelial surface of the samples was analyzed. The mesothelial layer was highlighted using anti-cytokeratin antibodies (AE1/AE3). The thickness of the compact zone was measured with a graded (micrometer) ocular. We used the same method as to measure thickness of malignant melanoma. The pattern of α-SMA expression was depicted according to the number of positive fibroblast-like cells, distribution and clustering tendency. The number of positive cells was measured using a semiquantitative scale: (0) absence; (1) isolated positive cells (<15%); (2) frequent positive cells (15–35%) and (3) abundant positive cells (>35%). According to their tissue location, three areas were established: (a) superficial, when fibroblast-like positive cells were present in the mesothelial surface; (b) upper submesothelial level and (c) lower submesothelial area. Finally, the presence of clusters of α-SMA+ cells was recorded. Clusters were defined when a grouping tendency of positive cells was present. These groups were well defined, with high cellular density and showed a variable number of cells usually greater than 30. Clusters were surrounded by areas of α-SMA-

Table 1 Clinical data of the patients on peritoneal dialysis. *MTAC* mass transfer coefficent

Patient	Age (years)/sex	Time on peritoneal dialysis (months)	Episodes of peritonitis	Time since last peritonitis	Previous urea/Cr MTAC (ml/m)
1	55/female	77	6	14	14.2/3.6
2	44/female	8	0	-	16.9/5.5
3	61/female	21	0	-	21.9/7.4
4	71/femal	16	0	-	29/8.7
5	47/male	3	1	6	23.9/12
6	53/male	18	0	-	22/9.1
7	48/female	11	1	6	11.8/7.4
8	74/male	10	0	-	25.8/11.7
9	72/male	22	1	6	26.8/11.5
10	69/male	10	2		27.6/14.5
11	49/female	22	2	17	27.4/14
12	49/female	12	0	-	19/9.5
13	22/female	11	0	-	15.1/3.8
14	23/female	29	0	-	23/9
15	33/female	7	0	-	24.7/6.7
16	48/male	20	1	6	25.5/14
17	46/male	7	0	-	27.8/19.9
18	47/female	4	0	-	18.2/8.7
19	77/male	3	0	-	32.6/13
20	50/male	14	0	-	27.6/15.5
21	46/male	15	0	-	14.1/7.7
22	46/female	44	0	-	22/10.2
23	38/female	86	5	4	16.5/4.3
24	44/female	30	0	0	22.8/9
25	52/female	5	0	-	19.9/11.4
26	54/male	82	1	0.2	22.2/9.4
27	66/male	12	0	-	22.3/9.2

Table 2 Antibodies used in the study. *SMA* smooth muscle actin

Antigen	Clone	Source	Dilution
α-SMA	1A4	Dako	1/50
Muscle actin	HHF35	Dako	1/75
Desmin	D33	Dako	Prediluted
Cytokeratins	AE1/AE3	Immunon	Prediluted
E-cadherin	36	BD Biosciences	1/250
CD34	My10	Becton-Dickinson	1/30
CD34	QBEnd10	Dako	Prediluted
CD31	JC70A	Dako	1/20
Vimentin	V9	Dako	1/50

negative cells. The expression of cytokeratins and E-cadherin by submesothelial fibroblast-like cells was recorded as positive or negative with no further quantification. CD34 expression was measured using a semiquantitative scale: (0) absence; (1) scarce positive cells (<20%); (2) many positive cells with a homogeneous distribution and recognizable network; (3) abundant positive cells (>70%) forming a reticular network. Results of CD34 were compared with those of CD31 to avoid confusion with endothelial cells. To exclude hypocellularity as a reason for CD34 loss of expression, these results were compared with those of vimentin. Histological parameters from hernia sac specimens were not compared with the other specimens due to the different source of the sample, surgical manipulation and the impossibility for a correct orientation of the sample.

In toto experiment

For in toto studies, samples of normal parietal and visceral peritoneum (omentum) were taken from patients with elective abdominal surgical procedures. Patients had no infection, neoplasm or renal disorder. Samples were immediately introduced in a sterile recipient with saline solution. In sterile conditions, they were divided into four pieces, which were carefully extended in a corked petri-dish and fixed with pins. One specimen was fixed with formalin (basal control). The remaining three pieces were flooded with culture medium. One sample was stimulated with TGF-β (1/2000, 0.5 μl/ml), and IL-1 (1/1250, 1.2 μl/ml), during 24 h. A second one received the same stimulus during 48 h. The fourth sample remained in culture medium without treatment during 48 h (control). Samples were kept at 37°C and 5% CO_2. After 24 h or 48 h, the samples were washed with a buffered solution, fixed with formalin and processed routinely.

Statistical analysis

The mean and standard deviation of the semiquantitative scores were calculated for each group of patients. Data were evaluated using the SPSS 9.0 for Windows package. The differences in the scores among the groups were analyzed with the Kruskal-Wallis non-parametric test. Values of $P<0.05$ were considered significant. Differences between groups were ascertained by performing pair-wise comparison with the Mann-Whitney U test, and the level of significance was obtained with the adjusted Bonferroni method.

Results

Histological parameters in uremic non-CAPD and CAPD patients

The mesothelial layer was largely preserved in control and uremic non-CAPD patients (2.53±0.83 and 2.71± 0.47, respectively). As previously described [18, 29], CAPD patients showed a lower density of mesothelial cells (1.25±0.85, $P<0.05$). As shown in Table 3, normal controls and non-CAPD uremic patients showed similar thickness of the submesothelial compact zone (91.33± 46.65 and 111.76±36.91, respectively). In contrast, most

Table 3 Pathological and immunohistochemical findings in peritoneal biopsies. *MF* myofibroblast, *SMA* smooth muscle actin

Patients	Submesothelial thickness (μm)	MF	Superficial α-SMA+ cells	MF clusters	α-SMA+ mesothelial cells	CK+ fibroblasts	E-cadherin+ fibroblasts	CD34
Normal controls (n=15) mean±SD	91.33±46.65	-	-	-	-	-	-	2.47±0.52
Uremic controls (n=17) mean±SD	111.76±36.91	-	-	-	-	-	-	2.41±0.62
Peritoneal dialysis patients (n=27) mean±SD	277.92±155.16	70.4%	57.9%*	47.4%*	26.3%*	48.1%	25.9%	0.83±0.83
Hernia sac patients (n=12) mean±SD	Not present	91.7%	72.7%*	50%*	27.3%*	75%	33.3%	1±0.95

* Of the cases with myofibroblasts

patients on CAPD showed submesothelial fibrosis (277.92±155.16, P<0.05). The existence of CAPD patients with no fibrosis was responsible for wide variations within this group. Although non-CAPD uremic patients showed greater submesothelial thickness than normal controls, these differences were not statistically significant. Two patients on CAPD showed advanced lesions of hyalinizing vasculopathy (grades 3). Both were long-standing CAPD patients and showed submesothelial fibrosis. Another four showed grade 1–2 lesions. Except for two patients who showed a moderate chronic inflammatory infiltrate, no other histological signs of peritonitis were present.

Myofibroblasts are found in peritoneal fibrosis

Results are summarized in Table 3. Neither fibroblasts nor mesothelium from control or non-CAPD uremic patients showed α-SMA, muscle actin or desmin. Smooth muscle cells from the vessel wall were used as a positive internal control. Myofibroblasts were observed in the peritoneal samples of 19 (70.4%) patients on CAPD. In 9 (33.3%), they were a common finding (grades 2 or 3). They showed no relation with time on dialysis or intensity of fibrosis. Myofibroblasts were present in the three patients that were on CAPD treatment for less than 4 months. Of the 19 biopsies showing myofibroblasts, 11 (57.9%) were located exclusively in the upper submesothelial level, near the mesothelial surface (Fig. 1A, B). A remarkable finding was the clustering tendency of myofibroblasts. It was evident in nine cases (47.4%). Clusters were located in the upper submesothelial area and were surrounded by areas of α-SMA-fibroblasts (Fig. 1B). In many of these clusters, myofibroblasts coexisted with cytokeratin+ fibroblastic cells and loss of CD34 expression. Myofibroblasts showed no relation to blood vessels. In five cases (26.3%), there was evidence of α-SMA expression in mesothelial cells (Fig. 1D, E). The location, polygonal morphology and expression of cytokeratins permitted their recognition as mesothelial cells (Fig. 1F). In addition, 11 cases (57.9%) showed α-SMA+ fibroblast-like cells in the mesothelial surface (Fig. 1C). As described in a previous report [34], these cells expressed cytokeratins and corresponded to modified mesothelial cells.

Similar results were observed in the group of peritoneal samples from non-renal patients with inguinal hernia. Myofibroblasts were present in 11 of the 12 (91.7%) samples. In 7 (58.3%), they were a common finding. Of the 11 (72.7%) cases with myofibroblasts, 8 showed expression in superficial fibroblast-like cells. In 3 (27.3%), preserved mesothelial cells showed positive expression. A similar clustering tendency and superficial location of myofibroblasts was observed in this group.

Expression of cytokeratin and E-cadherin in a subset of submesothelial fibroblasts in patients with peritoneal fibrosis

Submesothelial fibroblasts from normal controls and non-CAPD uremic patients showed no expression of cytokeratins or E-cadherin. In both groups, the expression was confined to surface mesothelial cells. However, a subset of peritoneal fibroblasts from CAPD patients and hernia sac specimens showed cytokeratin and E-cadherin expression (Table 3). As in the case of α-SMA, cytokeratin expression was mainly located in the upper submesothelial area (Fig. 2A, B). Positive cells exhibited a spindle morphology and were completely surrounded by extracellular matrix (Fig. 2B, C). Some of these spindle cells also showed E-cadherin expression (Fig. 2D). This expression was located in the cytoplasm rather than in the cytoplasmic membrane, as it is normally seen in mesothelial cells. Both cytokeratin and E-cadherin expression are evidence of EMT of mesothelial cells during CAPD- and hernia-related peritoneal fibrosis. Given that the expression of cytokeratins and E-cadherin is gradually downregulated during the transdifferentiation of the mesothelial cells [34], it can be speculated that the fibroblast-like cells positive for these markers represent only a portion of the whole population of fibroblast that derive from the mesothelium.

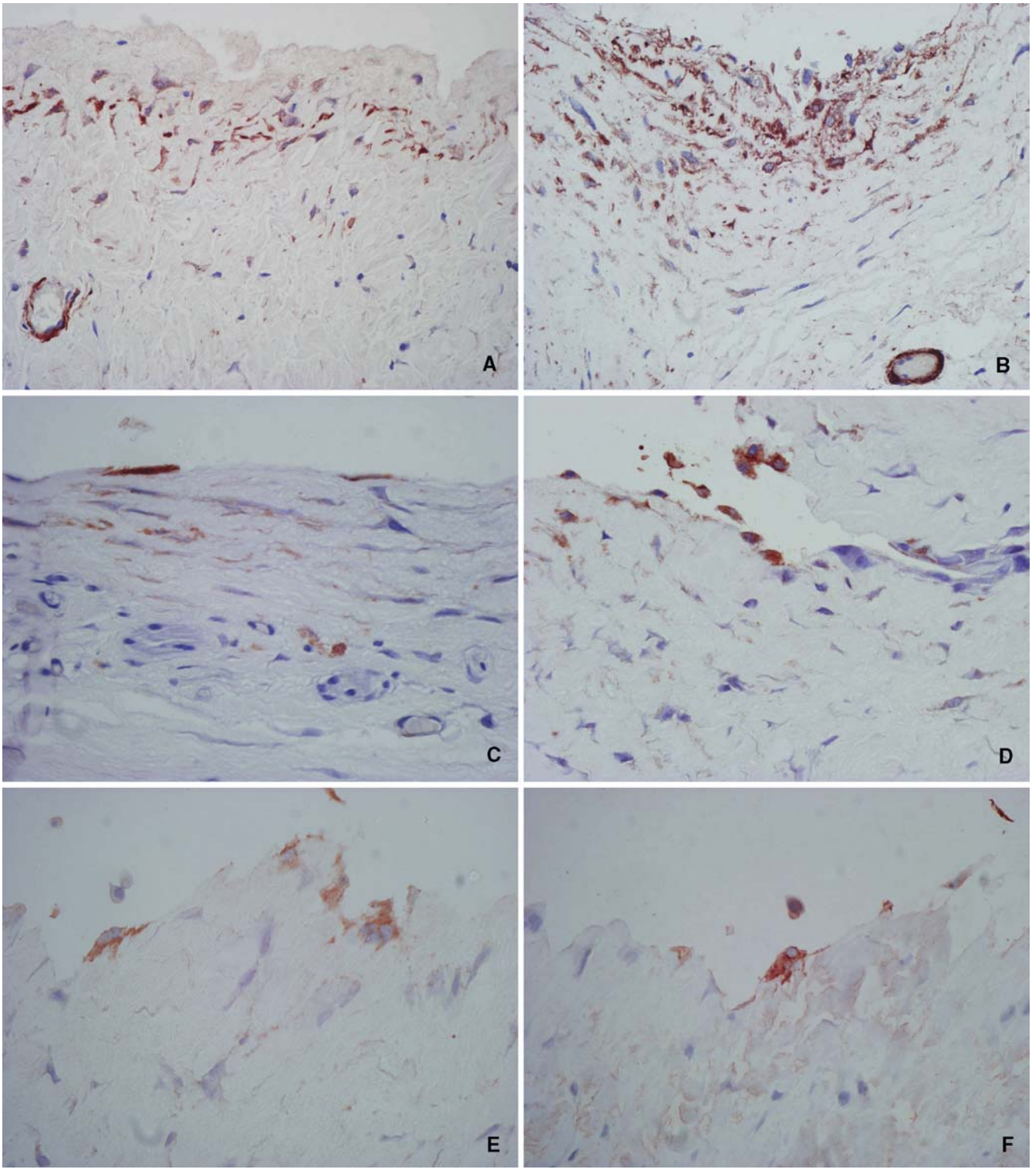

Fig. 1 Expression of α-smooth muscle actin in peritoneal samples from peritoneal dialysis patients. Myofibroblasts were located in the upper submesothelial level (**A**, **B**) and showed a clustering tendency (**B**). In addition to submesothelial cells, superficial cells with fibroblast morphology also showed positive expression (**C**). Immunoexpression was evident in a small subset of mesothelial cells with preserved morphology (**D**, **E**). Mesothelial cells also expressed cytokeratins (**F**, from the same patient as **E**)

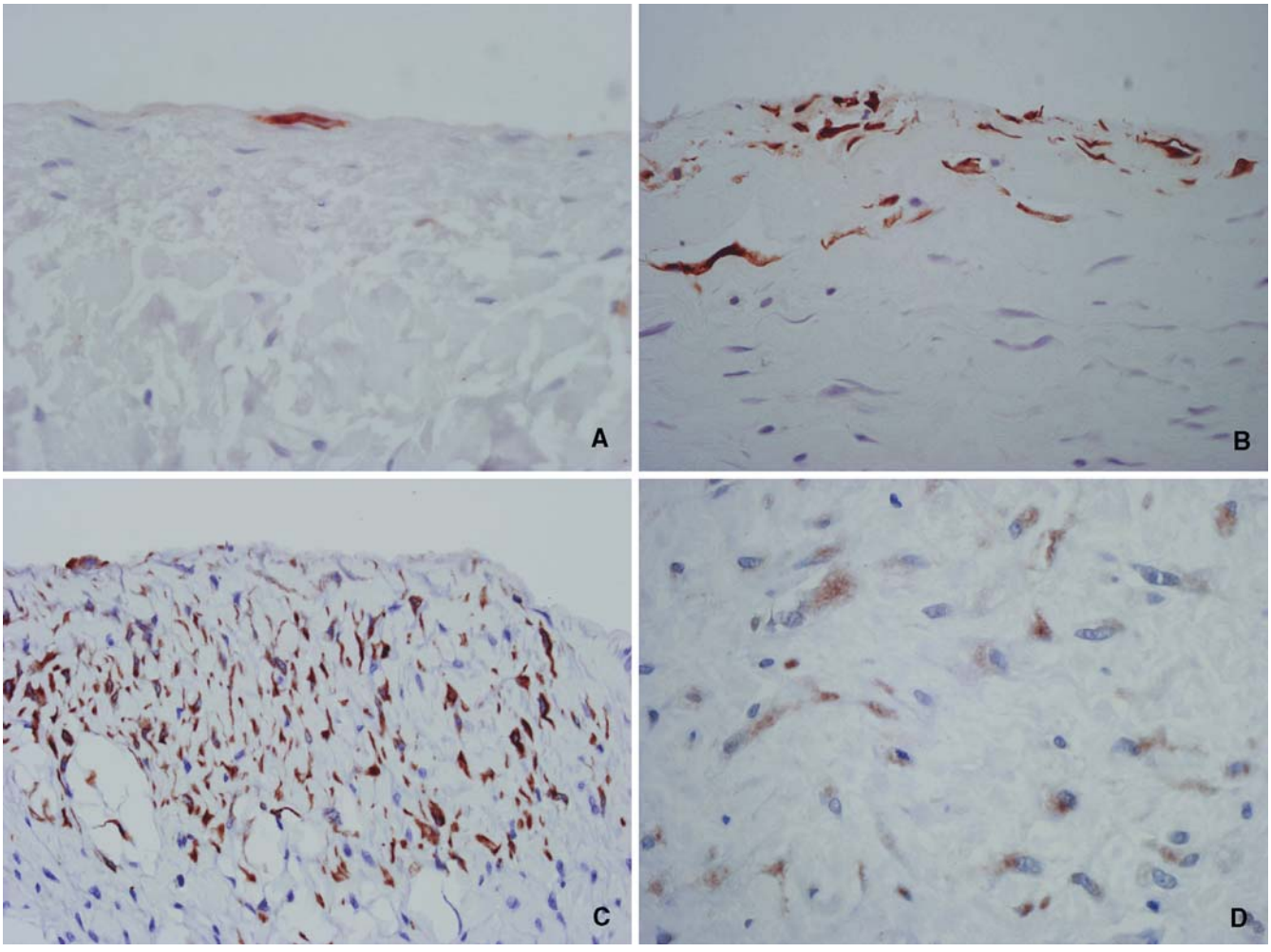

Fig. 2 Immunoexpression of cytokeratins was observed in superficial (**A**) and deeply located (**B**, **C**) cells with fibroblastic morphology. In addition, a subset of submesothelial cells showed cytoplasmic expression of E-cadherin (**D**)

The expression of CD34 on submesothelial resident fibroblasts is lost in patients with peritoneal fibrosis

Expression of CD34 was observed on resident fibroblasts of normal controls and non-CAPD uremic patients, with no differences between these two groups (2.47±0.52 and 2.41±0.62, respectively). The pattern of CD34 expression was a meshwork of slender cellular processes that extended from the immediate submesothelial layer to deeper levels (Fig. 3A, B). Immunoexpression was uniform, with no negative areas. Just below the mesothelial cell layer, the expression was greater, creating the impression of a continuous layer. The pattern of CD34 expression was similar in samples from visceral peritoneum. CD34 expression was evaluated using antibodies raised against different epitopes (My10, QBEnd/10). This suggests a true expression of the CD34 antigen rather than a cross-reaction phenomenon. The majority of patients on CAPD and peritoneal samples of hernia sac showed a partial loss of CD34 immunoexpression when compared with controls (0.83±0.82 and 1±0.95 respectively, $P<0.001$) (Fig. 3C, D, E). This was associated with areas of fibrosis and was greater in the upper submesothelial level (compact zone), with a tendency to show normal expression in the lower levels. Submesothelial thickness correlated inversely with CD34 immunoexpression ($r=-0.724$, $P<0{,}001$). In a few cases, the CD34 expression was variable, with negative and positive areas within the same sample (mixed pattern). They were graded according to the most abundant pattern of expression. Positive areas correlated with normal submesothelial morphology, with loose bands of collagen instead of sclerosis. The normal CD34 expression on endothelial cells was used as a positive internal control. Vimentin expression (Fig. 3F) of fibroblasts demonstrated that hypocellularity was not responsible for CD34 negative results.

TGF-β and IL-1 induce downregulation of CD34 in toto

To verify that the loss of CD34 correlated with resident fibroblasts activation, we performed an in toto experi-

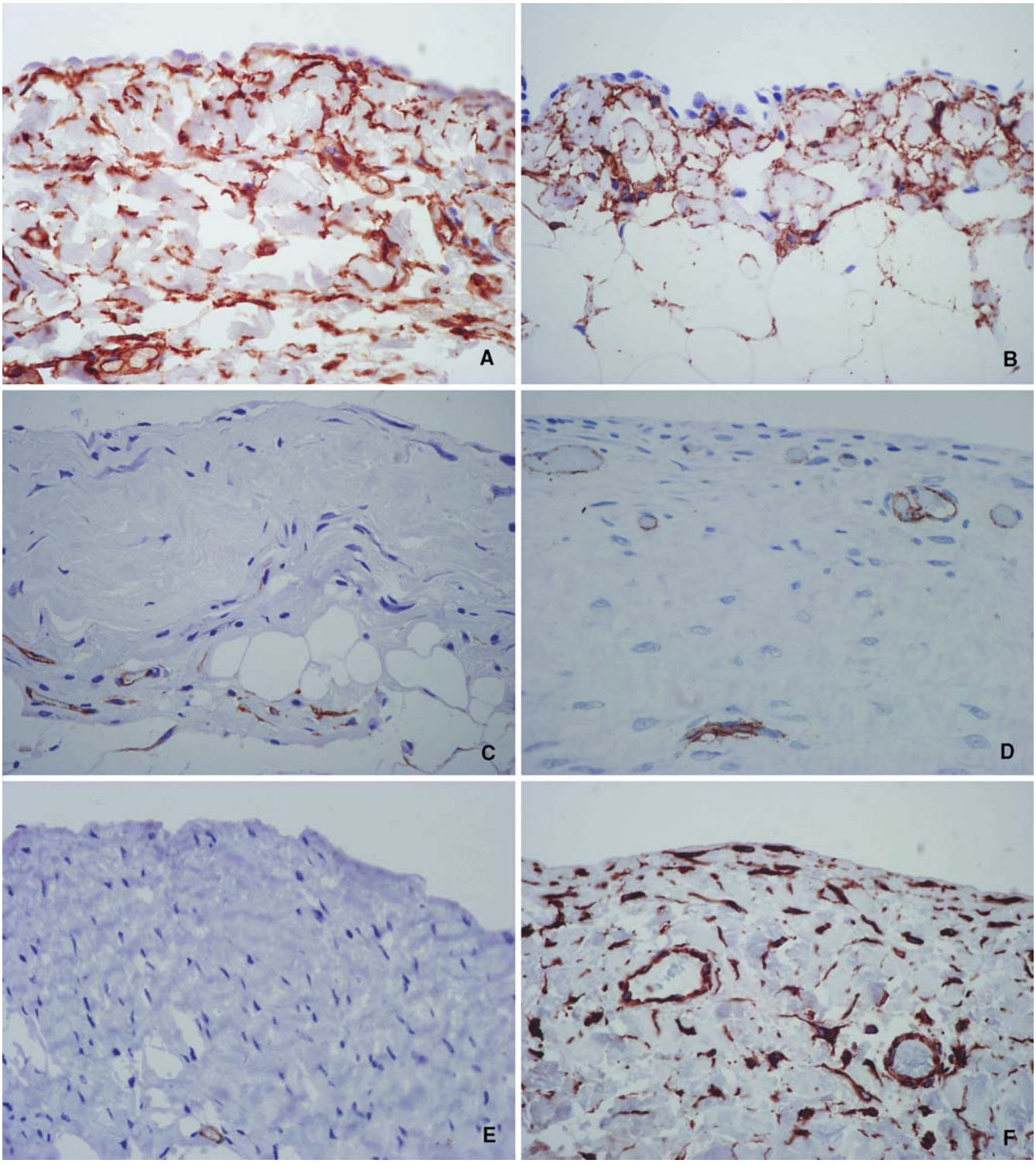

Fig. 3 Parietal (**A**) and visceral (**B**) peritoneum of normal controls showed an intense, submesothelial immunoexpression of CD34. Note the absence of expression in mesothelial cells. Samples with submesothelial fibrosis, either from peritoneal dialysis patients (**C**, **E**) or hernia sac specimens (**D**) showed a marked reduction in the expression of CD34. Its normal expression in endothelial cells (positive internal control) is preserved. The absence of expression is not due to cell loss since numerous negative fibroblasts are clearly visible and express vimentin (**F**)

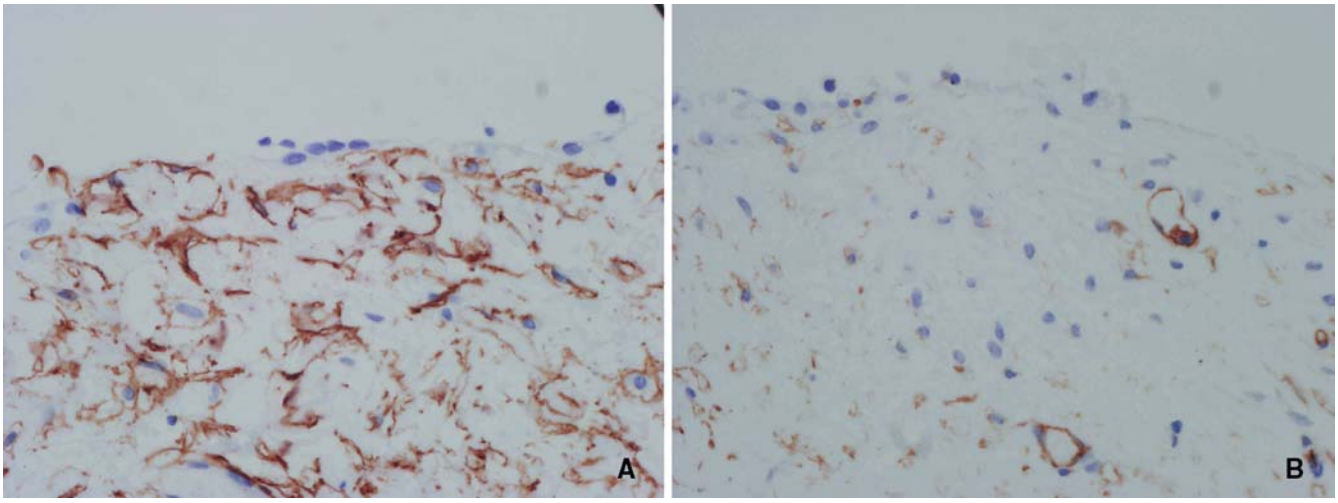

Fig. 4 In toto experiment. When compared with non-stimulated samples (**A**, control at 48 h), those that were treated with transforming growth factor-β and interleukin (IL)-1 for 48 h (**B**) showed a partial loss of CD34 expression

ment, in which samples of omental and parietal peritoneal tissue were split into four pieces, which were either treated or not with TGF-β and IL-1 for 24 h or 48 h. All the samples were processed simultaneously. The two control samples (at 0 h and 48 h, without TGF-β and IL-1) showed a preserved expression of CD34 in submesothelial fibroblasts (Fig. 4A). Similarly, samples incubated with TGF-β and IL-1 for 24 h showed a minimal downregulation of CD34 expression (not shown). However, a significant loss of expression was observed in the sample incubated with TGF-β and IL-1 for 48 h (Fig. 4B). These results indicate that activation of peritoneal fibroblasts induces the downregulation of CD34, as happens in endothelial cells [8].

Discussion

In this report, we show that the immunophenotype of submesothelial fibroblasts varies during the development of peritoneal fibrosis. The molecular markers analyzed show a sharp contrast between fibroblasts of normal and non-CAPD uremic peritoneal samples and those localized in peritoneal fibrotic tissue. Fibroblasts from normal controls and uremic patients show neither myofibroblastic nor mesothelial markers, but they exhibit an intense expression of CD34. The exact opposite immunophenotypical pattern is present under fibrogenic conditions. Our results indicate that myofibroblasts involved in fibrogenesis derive from both activation of resident fibroblasts and local conversion of mesothelial cells. In addition, this information is useful for the differentiation between quiescent and activated fibroblasts.

The simplest definition of myofibroblasts is that of smooth-muscle-like fibroblasts (α-SMA+ fibroblasts) [19, 20]. They show contractile capacity and are major producers of matrix molecules such as collagen, glycosaminoglycans, tenascin and fibronectin. According to the presence of vimentin (V), α-SMA (A) and desmin (D), different types of myofibroblasts have been described. Those identified in our study corresponded to VA-type myofibroblasts. Myofibroblasts have been implicated in almost all the fibrogenic situations that take place in human pathology [19]. Only few reports have mentioned their presence in CAPD patients [13, 15, 22]. The present study demonstrates that myofibroblasts are a common finding during peritoneal fibrosis, but their presence and quantity are not related to time on dialysis, nor to the degree of fibrosis. Similar results were obtained by Mateijsen et al. [13] and Shioshita et al. [22]. Our series included three patients with less than 4 months on dialysis who showed myofibroblasts. These findings demonstrate that myofibroblastic differentiation takes place during the initial phase of treatment and that it precedes the morphological appearance of fibrosis. The constant and periodic exposure to dialysis fluids will maintain the stimuli for myofibroblastic activation, independently of the time on dialysis or fibrosis status. Another remarkable finding of this study was the tendency of myofibroblasts to distribute in clusters, suggesting the existence of a local transforming environment.

Regarding the origin of myofibroblasts, transition from epithelial cells has been described in renal tubular cells under profibrogenic conditions [10, 24, 33]. A recent in vitro report describes a similar conversion of mesothelial cells into myofibroblasts [32]. Our study of the location and distribution of α-SMA+ cells supports such a conversion in vivo. Mesothelial cells and modified mesothelial cells expressing α-SMA were observed. In addition, a gradient in the distribution of myofibroblasts was evident. Most were located in the upper submesothelium, in continuity with the mesothelial surface. Myofibroblastic conversion of mesothelial cells must be regarded as another proof of EMT. Other useful markers that prove such a transition are cytokeratins and E-cadherin. Under normal conditions, both molecules are present in meso-

thelial cells and absent in fibroblasts. This study has shown that, during fibrosis, these markers are expressed in a subset of fibroblast-like cells. The fact that EMT can be induced by advanced glycation end products (AGEs) [17] is very relevant information, since AGEs are thought to play an important pathogenic role in CAPD.

In this study, we have also demonstrated an intense immunoexpression of CD34 in normal submesothelial fibroblasts. Although mentioned in regard to the pleura [5, 28], it has not been evaluated previously in the peritoneum. The pattern is similar to that observed in other tissues [16, 27, 30, 31] and consists of a meshwork of cellular prolongations that extend homogeneously from the immediate submesothelial layer to deeper levels. This pattern is preserved in non-CAPD uremic patients. However, it diminishes and disappears during peritoneal fibrosis. A similar phenomenon of CD34 loss of expression has been described in other types of fibrosis, such as that seen in the skin [2, 3, 11, 23] and in the fibrotic response associated with several types of carcinoma [4, 7, 14]. The role of CD34+ fibroblastic stromal cells in the fibrotic process is not well understood, and the exact meaning of CD34 loss of expression is unknown. As it happened in our study, loss of CD34 expression occurs in cell cultures of endothelial cells. It can be induced by inflammatory mediators, such as interleukin-1β, interferon-γ or tumor necrosis factor-α [8, 12]. These molecules downregulate CD34 and induce upregulation of the adhesion molecule ICAM-1 [12]. A similar phenomenon seems to occur in submesothelial fibroblasts during tissue fibrosis. In addition to CD34 downregulation, we also have observed ICAM-1 expression in submesothelial fibroblasts from CAPD patients [34].

Although, in our samples, the appearance of myofibroblasts was associated with loss of CD34 expression, it is difficult to assess if the two are related. In a few cases, myofibroblasts coexisted with a normal CD34 pattern. However, in the majority of cases, and mainly in those with clusters, an inverse relation was noted. A similar phenomenon of CD34 loss and myofibroblastic transformation has been described for tissue and circulating CD34 fibrocytes [1, 7]. It has been observed under fibrogenic conditions and can be induced by TGF-β [1].

One of the conclusions from this study is that, in contrast to CAPD patients, fibroblasts from non-CAPD uremic patients (predialysis or hemodialysis) showed a normal immunophenotypical pattern. The fact that these patients showed no significant submesothelial thickness when compared with normal controls correlated with the immunohistochemical findings. Another important conclusion is that, except for hyalinizing vasculopathy, the findings described are not specific to CAPD. Similar markers and mechanisms have been observed in fibrotic peritoneal samples (hernia sacs) obtained from non-renal patients with inguinal hernia. It reflects that the mechanisms leading to fibrosis are similar, regardless of the causal agent (chemical or mechanic).

Acknowledgements We would like to thank the surgeons and nephrology nurses involved in the peritoneal biopsy performance and manipulation. We also thank M. Angeles Cuevas and Norma Freire for their technical assistance on immunohistochemical studies. Grants SAF 2001–0305 from Ministerio de Ciencia y Tecnología to M.L-C, FIS 01/0063–02 from Ministerio de Sanidad y Consumo to R.S. We are indebted to Fresenius Medical Care for the provision of an educational grant to L.S.A.

References

1. Abe R, Donnelly SC, Peng T et al (2001) Peripheral blood fibrocytes: differentiation pathway and migration to wound sites. J Immunol 166:7556–7562
2. Aiba S, Tagami H (1997) Inverse correlation between CD34 expression and proline-4-hydroxylase immunoreactivity on spindle cells noted in hypertrophic scars and keloids. J Cutan Pathol 24:65–69
3. Aiba S, Tabata N, Ohtani H et al (1994) CD34+ spindle shaped cells selectively disappear from the skin lesions of scleroderma. Arch Dermatol 130:593–597
4. Barth PJ, Ebrahimsade S, Hellinger A et al (2002) CD34+ fibrocytes in neoplastic and inflammatory pancreatic lesions. Virchows Arch 440:128–133
5. Bongiovanni M, Viberti L, Pecchioni C et al (2002) Steroid hormone receptor in pleural solitary fibrous tumours and CD34+ progenitor stromal cells. J Pathol 198:252–257
6. Bucala R, Spiegel LA, Chesney J et al (1994) Circulating fibrocytes define a new leukocyte subpopulation that mediates tissue repair. Mol Med 1:71–81
7. Chauhan H, Abraham A, Phillips JR et al (2003) There is more than one kind of myofibroblast: analysis of CD34 expression in benign, in situ, and invasive breast lesions. J Clin Pathol 56:271–276
8. Delia D, Lampugnani MG, Resnatti M, Dejana E, Aiello A, Fontanella E, Soligo D, Pierotti MA, Greaves MF (1993) CD34 expression is regulated reciprocally with adhesion molecules in vascular endothelial cells in vitro. Blood 81:1001–1008
9. Dobbie JW (1992) Pathogenesis of peritoneal fibrosing syndromes (sclerosing peritonitis) in peritoneal dialysis. Perit Dial Int 12:14–27
10. Iwano M, Plieth D, Danoff TM et al (2002) Evidence that fibroblasts derive from epithelium during tissue fibrosis. J Clin Invest 110:341–350
11. Kirchmann TT, Prieto VG, Smoller BR (1995) Use of CD34 in assessing the relationship between stroma and tumor in desmoplastic keratinocytic neolasms. J Cutan Pathol 22:422–426
12. Krause DS, Fackler MJ, Civin CI (1996) CD34: structure, biology and clinical utility. Blood 87:1–13
13. Mateijsen MAM, van der Wal AC, Hendriks PMEM et al (1999) Vascular and interstitial changes in the peritoneum of CAPD patients with peritoneal sclerosis. Perit Dial Int 19:517–525
14. Nakayama H, Enzan H, Miyazaki E et al (2000) Differential expression of CD34 in normal colorectal tissue, peritumoral inflammatory tissue, and tumor stroma. J Clin Pathol 53:626–629
15. Nakazato Y, Yamaji Y, Oshima N et al (2002) Calcification and osteopontin localization in the peritoneum of patients on long-term continuous ambulatory peritoneal dialysis therapy. Nephrol Dial Transplant 17:1293–1303
16. Narvaez D, Kanitakis J, Faure M et al (1996) Immunohistochemical study of CD34-positive dendritic cells of human dermis. Am J Dermatopathol 18:283–288
17. Oldfield MD, Bach LA, Forbes JM et al (2001) Advanced glycation end products cause epithelial-myofibroblast transdifferentiation via the receptor for advanced glycation end products (RAGE). J Clin Invest 108:1853–1863

18. Plum J, Hermann S, Fusshöller A et al (2001) Peritoneal sclerosis in peritoneal dialysis patients related to dialysis settings and peritoneal transport properties. Kidney Int 59[Suppl 78]:42–47
19. Powell DW, Mifflin RC, Valentich JD et al (1999) Myofibroblasts. I. Paracrine cells important in health and disease. Am J Physiol 277:C1–C19
20. Schürch W, Seemayer TA, Gabbiani G (1998) The myofibroblast. A quarter century after its discovery. Am J Surg Pathol 22:141–147
21. Selgas R, Fernandez-Reyes MJ, Bosque E et al (1994) Functional longevity of the human peritoneum: how long is continuous peritoneal dialysis possible? Results of a prospective medium–long term study. Am J Kidney Dis 23:64–73
22. Shioshita K, Miyazaki M, Ozono Y et al (2000) Expression of heat shock proteins 47 and 70 in the peritoneum of patients on continuous ambulatory peritoneal dialysis. Kidney Int 57:619–631
23. Skobieranda K, Helm KF (1995) Decreased expression of the human progenitor cell antigen (CD34) in morphea. Am J Dermatopathol 17:471–475
24. Stahl PJ, Felsen D (2001) Transforming growth factor-β, basement membrane, and epithelial-mesenchymal transdifferentiation. Implications for fibrosis in kidney disease. Am J Pathol 159:1187–1192
25. Suster S (2000) Recent advances in the application of immunohistochemical markers for the diagnosis of soft tissue tumors. Semin Diagn Pathol 17:225–235
26. Van de Rijn M, Rouse RV (1994) CD-34. A review. Appl Immunohistochem 2:71–80
27. Vanderwinden JM, Rumessen JJ, De Laet MH, Vanderhaeghen JJ, Schiffmann SN (1999) CD34+ cells in human intestine are fibroblasts adjacent to, but distinct from, interstitial cells of Cajal. Lab Invest 79:59–65
28. Westra WH, Gerald WL, Rosai J (1994) Solitary fibrous tumor. Consistent CD34 immunoreactivity and occurrence in the orbit. Am J Surg Pathol 18:992–998
29. Williams JD, Craig KJ, Topley N et al (2002) Morphologic changes in the peritoneal membrane of patients with renal disease. J Am Soc Nephrol 13:470–479
30. Yamazaki K, Eyden BP (1996) Ultrastructural and immunohistochemical studies of intralobular fibroblasts in human submandibular gland: the recognition of a "CD34 positive reticular network" connected by gap junctions. J Submicrosc Cytol Pathol 28:471–483
31. Yamazaki K, Eyden BP (1997) Interfollicular fibroblasts in the human thyroid gland: recognition of a CD34 positive stromal cell network communicated by gap junctions and terminated by autonomic nerve endings. J Submicrosc Cytol Pathol 29:461–476
32. Yang AH, Chen JY, Lin JK (2003) Myofibroblastic conversion of mesothelial cells. Kidney Int 63:1530–1539
33. Yang J, Liu Y (2001) Dissection of key events in tubular epithelial to myofibroblast transition and its implication in renal interstitial fibrosis. Am J Pathol 159:1465–1475
34. Yañez-Mo M, Lara-Pezzi E, Selgas R et al (2003) Peritoneal dialysis and epithelial-to-mesenchymal transition of mesothelial cells. N Engl J Med 348:403–413

Virchows Arch (2004) 444:257–263
DOI 10.1007/s00428-003-0959-z

ORIGINAL ARTICLE

Katsuyoshi Kanemoto · Joichi Usui · Kosaku Nitta · Shigeru Horita · Atsumi Harada · Akio Koyama · Jan Aten · Michio Nagata

In situ expression of connective tissue growth factor in human crescentic glomerulonephritis

Received: 4 December 2003 / Accepted: 4 December 2003 / Published online: 31 January 2004

Abstract Connective tissue growth factor (CTGF) has recently been recognized as an important profibrotic factor and is up-regulated in various renal diseases with fibrosis. The present study describes the sequential localization of CTGF mRNA and its association with transforming growth factor (TGF)-β1 in human crescentic glomerulonephritis (CRGN). Furthermore, we examined the phenotype of CTGF-expressing cells using serial section analysis. Kidney biopsy specimens from 18 CRGN patients were examined using in situ hybridization and immunohistochemistry. CTGF mRNA was expressed in the podocytes and parietal epithelial cells (PECs) in unaffected glomeruli. In addition, it was strongly expressed in the cellular and fibrocellular crescents, particularly in pseudotubule structures. Serial sections revealed that the majority of CTGF mRNA-positive cells in the crescents co-expressed the epithelial marker cytokeratin, but not a marker for macrophages. Moreover, TGF-β1, its receptor TGF-β receptor-I, and extracellular matrix molecules (collagen type I and fibronectin) were co-localized with CTGF mRNA-positive crescents. Our results suggest that CTGF is involved in extracellular matrix production in PECs and that it is one of the mediators promoting the scarring process in glomerular crescents.

Keywords CTGF · Crescentic glomerulonephritis · Parietal epithelial cell · Macrophage · Scar formation

K. Kanemoto · J. Usui · M. Nagata (✉)
Department of Pathology,
Institute of Basic Medical Sciences, University of Tsukuba,
Tennodai 1-1-1, 305-8575 Tsukuba, Ibaraki, Japan
e-mail: nagatam@md.tsukuba.ac.jp
Tel.: +81-29-8533171
Fax: +81-29-8533171

A. Harada
Department of Nephrology,
Matsuyama Red Cross Hospital,
Matsuyama, Ehime, Japan

K. Nitta · S. Horita
Department of Pathology, Kidney Center,
Tokyo Women's Medical University,
Tokyo, Japan

A. Koyama
Department of Nephrology,
Institute of Clinical Medicine, University of Tsukuba,
Tsukuba, Ibaraki, Japan

J. Aten
Department of Pathology,
Academic Medical Center, University of Amsterdam,
Amsterdam, The Netherlands

Introduction

The scar formation in glomerular crescents is one of the important factors in progressive glomerulosclerosis [17, 22]. However, the pathogenesis of scar formation in the crescents is not clearly understood. Some inflammatory cytokines and profibrotic growth factors, such as platelet-derived growth factor (PDGF) and transforming growth factor (TGF)-β have been implicated in the fibrous progression of crescents [10, 11, 25]. However, the molecules mediating TGF-β and PDGF signaling for glomerular scar formation have not been clearly identified.

Connective tissue growth factor (CTGF/CCN2) was originally isolated from the conditioned media of human umbilical vein endothelial cells and belongs to a new family (CCN family) of cysteine-rich proteins that are induced by TGF-β1 [3, 5, 6]. CTGF has recently received much attention as a possible fibrogenic factor of progressive tissue fibrosis, angiogenesis, and bone formation [2, 6]. Increased expression of CTGF mRNA has been reported in a variety of inflammatory glomerular and tubulointerstitial lesions that are associated with cellular proliferation and matrix deposition, including human crescentic glomerulonephritis (CRGN) [15, 16, 30, 32, 33, 35]. These studies found that CTGF was localized in the cellular crescents, but the cell types synthesizing the CTGF and the sequential expression pattern of CTGF

during the progression of CRGN still remain to be elucidated.

The present study describes the sequential localization of CTGF, the type of cell expressing CTGF mRNA, and the relationship with TGF-β1 during the development of crescents in human CRGN. Our results indicate that CTGF is strongly expressed in the parietal epithelial cells (PECs) of cellular crescents and that expression is enhanced in pseudotubule structures. In addition, our results suggest that CTGF may be involved in the extracellular matrix (ECM) synthesis in crescents in concert with TGF-β1.

Materials and methods

Specimens

Kidney biopsy specimens (n=18) with rapidly progressive glomerulonephritis were selected for this study. Their clinical and pathological features are listed in Table 1. Samples were fixed in 4% buffered formalin and embedded in paraffin. Sections were stained with hematoxylin and eosin, and periodic acid-Schiff (PAS).

In situ hybridization

A 540-bp cDNA fragment of rat CTGF (GenBank gi5070343 496–1037) was amplified by polymerase chain reaction using the following sense and antisense primers: 5′-GCGTGTGCACTGCCAAAGAT-3′ and 5′-TAATACGACTCACTATAGCAGCCAGAAAGCTCAAACTTGA-3′, respectively. The amplicon was cloned in the pCR2.1-TOPO vector (Invitrogen, Breda, Netherlands). In vitro transcription was performed using T7 RNA polymerase and digoxigenin (DIG)-conjugated UTP (Roche, Mannheim, Germany) to produce DIG-labeled antisense riboprobes. Sections were deparaffinized and digested with 10 μg/ml proteinase K (Wako, Osaka, Japan) for 10 min at 37°C. DIG-labeled riboprobes (1 μg/ml) were then added to a hybridization solution containing 50% deionized formamide, 5×sodium saline citrate (SSC), 1% sodium dodecyl sulfate, 50 μg/ml heparin, and 50 μg/ml yeast RNA (Roche). Hybridization was performed for 18 h at 50°C. Subsequently, the slides were washed once with 5×SSC containing 50% formamide and then twice with 2×SSC for 30 min. Sections were then blocked with 0.5% blocking reagent (Roche) and incubated with alkaline phosphatase-conjugated Fab fragments of a sheep anti-DIG antibody (1:1000 dilution; Roche) for 16 h at 4°C. Bound alkaline phosphatase activity was visualized with nitroblue tetrazolium chloride and 5-bromo-4-chloro-3-indolyl phosphate (NBT/BCIP, Roche).

Immunohistochemistry

Immunohistochemistry was performed on serial sections to detect cytokeratin (anti-pan-cytokeratin antibody, 1:200, C-11; Sigma, Tokyo, Japan), synaptopodin (anti-synaptopodin antibody, 1:2, G1D4; Progen, Heidelberg, Germany), macrophages (anti-CD68 antibody, 1:300, PG-M1; Dako, Kyoto, Japan), collagen type I (anti-human collagen type I antibody, 1:100, AB745; Chemicon, Temecula, CA, USA), fibronectin (anti-human fibronectin antibody, 1:200, ICN; Aurora, OH, USA), TGF-β1 (anti-TGF-β1 antibody, 1:100, sc-146; Santa Cruz, CA, USA), and TGF-β receptor type I (anti-TGF-β receptor I antibody, 1:100, sc-399; Santa Cruz). Briefly, after deparaffinization using xylene and a graded alcohol series, sections received an autoclave pretreatment (120°C for 10 min). After blocking of the endogenous peroxidase

Table 1 Clinical and pathological characteristics of cases of crescentic glomerulonephritis (CRGN). *C*, *F–C*, *F* percentage of glomeruli involved by cellular, fibrocellular and fibrous crescents, respectively. *BUN* blood urea nitrogen. *ANCA* antineutrophil cytoplasmic autoantibodies

Number	Sex	Years	From onset to biopsy (months)	Proteinuria (g/day)	Hematuria	BUN (mg/dl)	Cr (mg/dl)	ANCA	% Crescentic glomeruli in total glomeruli (n)	C	F–C	F
											%	
1	Male	26	2	1.2	3+	18.6	1.8	MPO-ANCA	89 (9)	25	50	25
2	Male	40	4	2.4	3+	64.9	5.2	MPO-ANCA	100 (7)	57	29	14
3	Male	40	9	3.4	3+	63.4	2.9	MPO-ANCA	90 (22)	33	61	6
4	Male	57	3	1.8	3+	62.7	4.7	MPO-ANCA	80 (10)	25	50	25
5	Male	66	6	1.8	3+	52.9	5.4	N.D.	75 (20)	67	33	0
6	Male	71	9	3.4	3+	64.5	7.2	MPO-ANCA	73 (11)	13	50	37
7	Male	73	1	4.7	3+	73.4	8.1	N.D.	83 (12)	20	70	10
8	Female	5	6	0.76	3+	12.1	0.5	MPO-ANCA	83 (6)	40	40	20
9	Female	53	4	0.82	2+	45.9	4.5	MPO-ANCA	75 (6)	50	25	25
10	Female	61	3	4	2+	23	1.7	negative	75 (15)	60	20	20
11	Female	61	24	1.8	3+	17.4	1.2	negative	56 (25)	79	14	7
12	Female	62	1	0.9	3+	20.3	0.6	MPO-ANCA	89 (9)	38	50	12
13	Female	63	3	1.95	3+	88.1	5.4	MPO-ANCA	100 (7)	0	0	100
14	Female	66	3	1.6	-	41.8	2.5	MPO-ANCA	88 (8)	29	42	29
15	Female	67	12	2.1	3+	37	4	N.D.	94 (18)	35	41	24
16	Female	67	4	4.9	2+	51	5.8	MPO-ANCA	85 (13)	9	27	64
17	Female	70	2	4	3+	36.3	2.5	MPO-ANCA	63 (8)	60	20	20
18	Female	78	2	1.8	3+	76.9	5.3	N.D.	88 (8)	58	14	28
Mean±SD		57±22.4	5.4±6.1	2.4±1.13		47.2±22.6	3.8±2.4		82.5 (214)	46.7	27.7	25.6

Table 2 Pathological scores for connective tissue growth factor (CTGF) mRNA, CD68, and cytokeratin in crescentic glomerulonephritis. Staining score was graded as follows: 0=negative, 1=mild, 2=moderate, 3=strong, according to intensity in each crescent. Data represent the mean ±SD. *N.S.* not significant

	n	CTGF mRNA score	CD68(macrophage) score	Cytokeratin (epithelial)score
Cellular crescents	83	2.29±0.42	0.30±0.15	2.31±0.32
fibrocellular crescents	49	0.92±0.31	0.22±0.13	1.01±0.28
fibrous crescents	45	0.14±0.04	0.12±0.04	0.21±0.07
*minor glomerular abnormality	*37			

*$P<0.01$

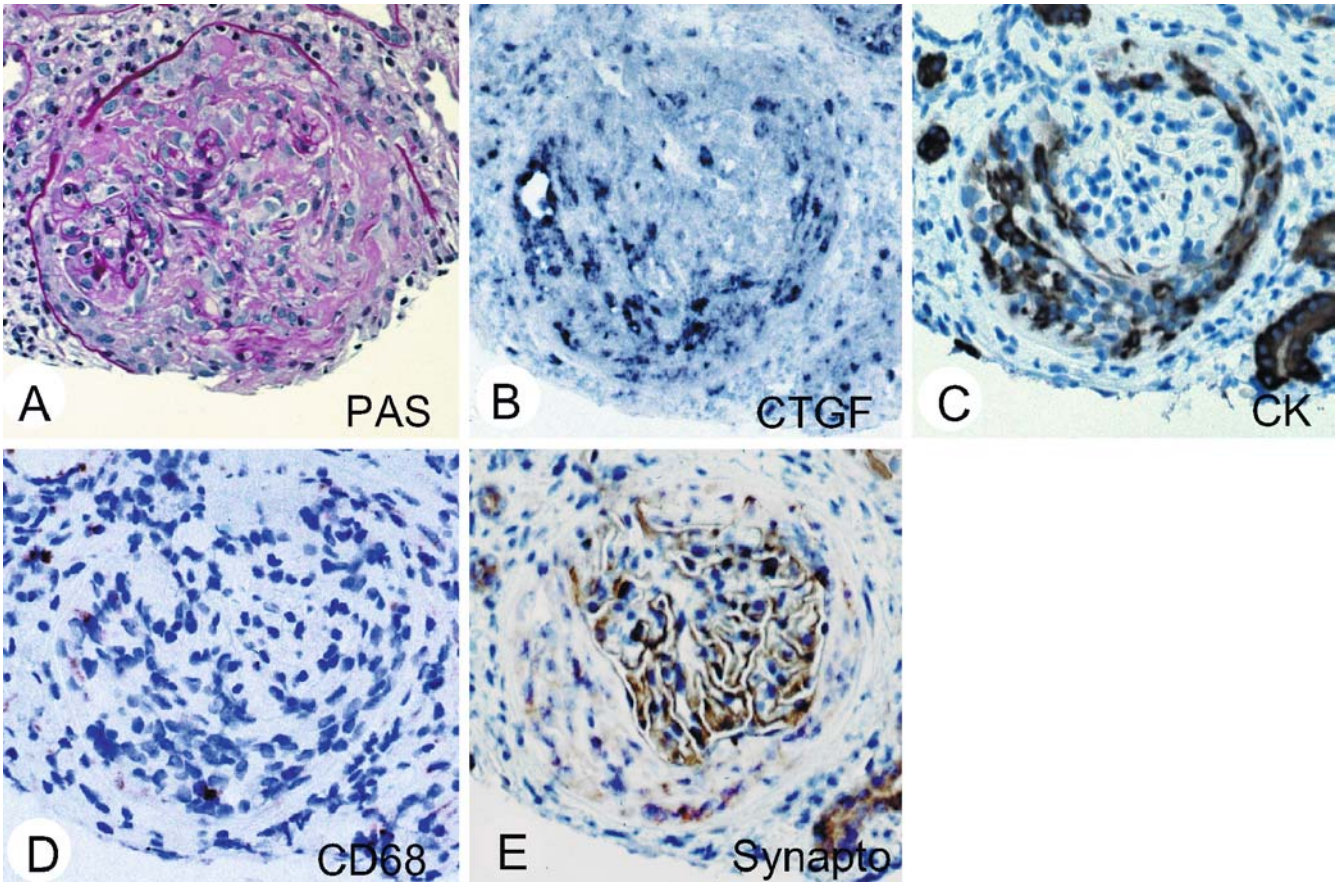

Fig. 1 Serial section analysis of connective tissue growth factor (CTGF) mRNA, cytokeratin, CD68, and synaptopodin (Case no. 5). **A** Periodic acid-Schiff staining. Glomeruli reveal pronounced cellular crescent formation. **B** CTGF mRNA (in situ hybridization). CTGF mRNA is strongly expressed in the cellular crescents. **C** Cytokeratin (immunohistochemistry, IHC). CTGF mRNA-positive cells also strongly express cytokeratin. **D** CD68 (IHC). The macrophage marker CD68 is nearly absent from the crescents. **E** Synaptopodin (IHC). The podocyte marker synaptopodin is virtually absent from the crescents. Magnification ×400

activity with 0.6% H_2O_2, sections were incubated with a primary antibody for 16 h at 4°C. Immunoreaction products were detected using an avidin-biotin-peroxidase complex (MAX-PO multi kit; Nichirei, Tokyo, Japan) and 3′3-diaminobenzidine in phosphate buffered saline with 1% H_2O_2. Counter-staining was performed with hematoxylin.

Pathological examination

The types of crescent identified in PAS-stained glomeruli were classified as follows. Cellular crescents consisted of at least two layers of cells occupying more than a quarter of Bowman's space, without appreciable accumulation of ECM. Fibrous crescents were comprised of abundant ECM, with few, if any, nuclear profiles identified. Fibrocellular crescents were recognized as an intermediate between the cellular and fibrous crescents. For each crescent, the intensity scores of CTGF mRNA, CD68, and cytokeratin were

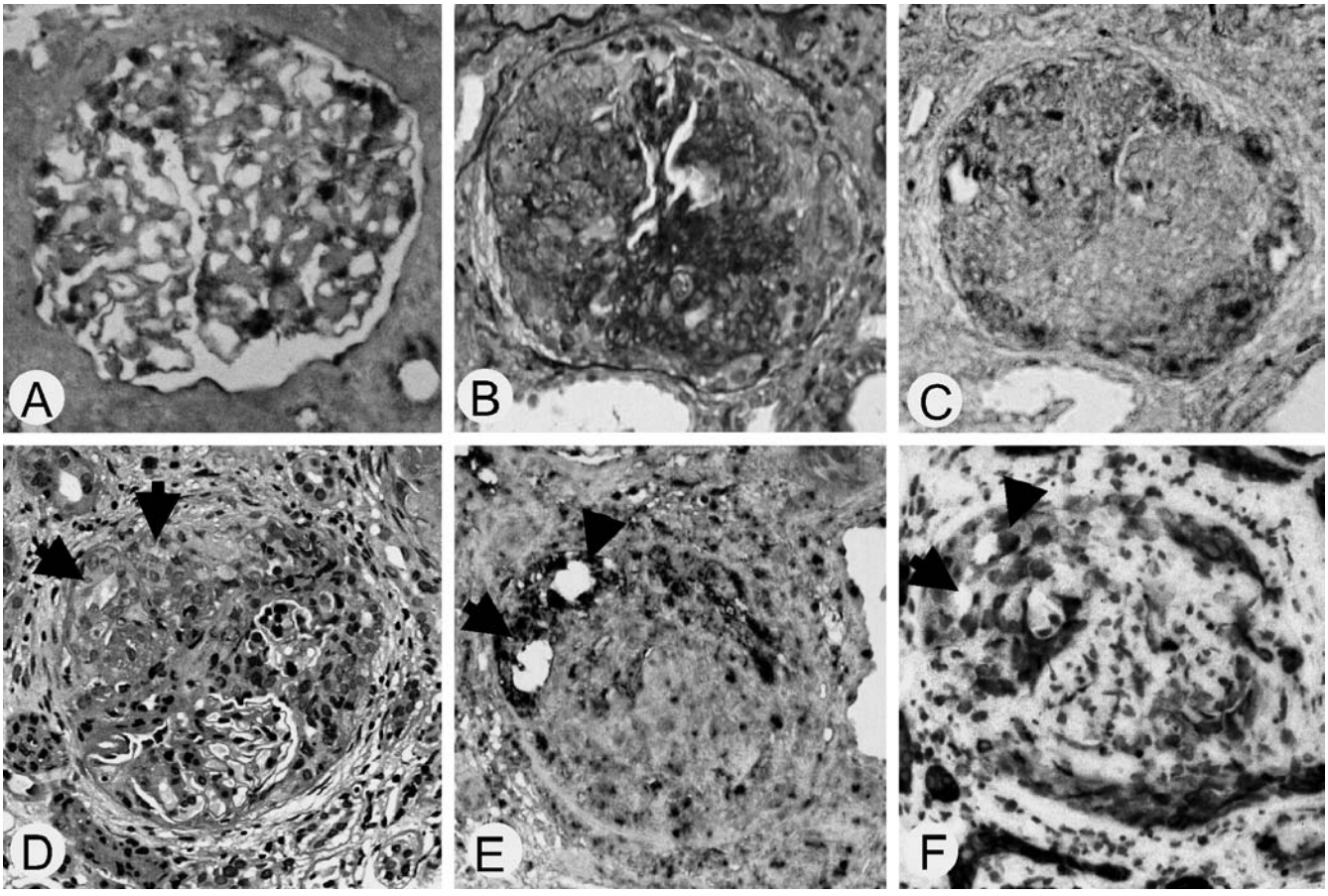

Fig. 2 Connective tissue growth factor (CTGF) mRNA expression in human crescentic glomerulonephritis. **A** Minor glomerular abnormality (case no. 9). CTGF mRNA is expressed in podocytes and parietal epithelial cells. **B** and **C** Cellular crescents (case no. 15, serial sections). CTGF mRNA is strongly expressed in the cellular crescents. **D–F** CTGF mRNA is also expressed in the pseudotubule structures (*arrows*) in the crescents (case no. 5, serial sections). Cytokeratin is also expressed in the pseudotubule structures. **A**, **C**, **E** CTGF mRNA (in situ hybridization). **B**, **D** Periodic acid-Schiff staining. **F** Cytokeratin (IHC). Magnification ×400

estimated according to the following scale: 0 = none; 1 = weak; 2 = moderate; 3 = strong.

Statistical analysis

All values are expressed as the mean±SD. Statistical significance was evaluated using a one-way analysis of variance with the Student's *t*-test using the Statview 5.0 software (Abacus Concepts, Berkeley, CA, USA). $P<0.01$ was considered significant.

Results

PECs expressed CTGF mRNA

In our specimens, the crescents were predominantly composed of PECs, as revealed by the expression scores for cytokeratin and CD68 (Table 2). Synaptopodin-positive cells were absent in the crescents. The cellular and fibrocellular crescents strongly expressed CTGF mRNA, and they also expressed cytokeratin in serial sections. CD68-positive cells were virtually negative for CTGF. The decreases in both the CTGF mRNA and cytokeratin scores were coincident with the fibrotic changes (Fig. 1).

Sequential expression of CTGF mRNA in the crescents

In glomeruli with minor abnormalities, CTGF mRNA was predominantly expressed in podocytes and some PECs (Fig. 2A). Some interstitial cells also exhibited CTGF mRNA. In the crescentic glomeruli, CTGF mRNA was strongly expressed in the cellular crescents (Fig. 2B, C, score = 2.29±0.42, Table 2). In contrast, the expression of

Fig. 3 Serial section analysis of connective tissue growth factor (CTGF) mRNA, transforming growth factor (TGF)-β1, TGF-β receptor-I, and extracellular matrix molecules in crescentic glomerulonephritis. **A–F** Cellular crescents (case no. 3). CTGF mRNA (**B**) is expressed in cellular crescents (**A**) with co-localization of TGF-β1 (**C**) and TGF-β receptor-I (**D**). Cellular crescents also express collagen type I (**E**) and fibronectin (**F**). **G–L** Fibrocellular crescents (case no. 10). CTGF mRNA (**H**) is strongly expressed along the crescentic lesions (**G**) with co-localization of TGF-β1 (**I**) and TGF-β receptor-I (**J**). Fibrocellular crescents appear to show stronger expression of collagen type I (**K**) and fibronectin (**L**) than cellular crescents. Magnification ×400

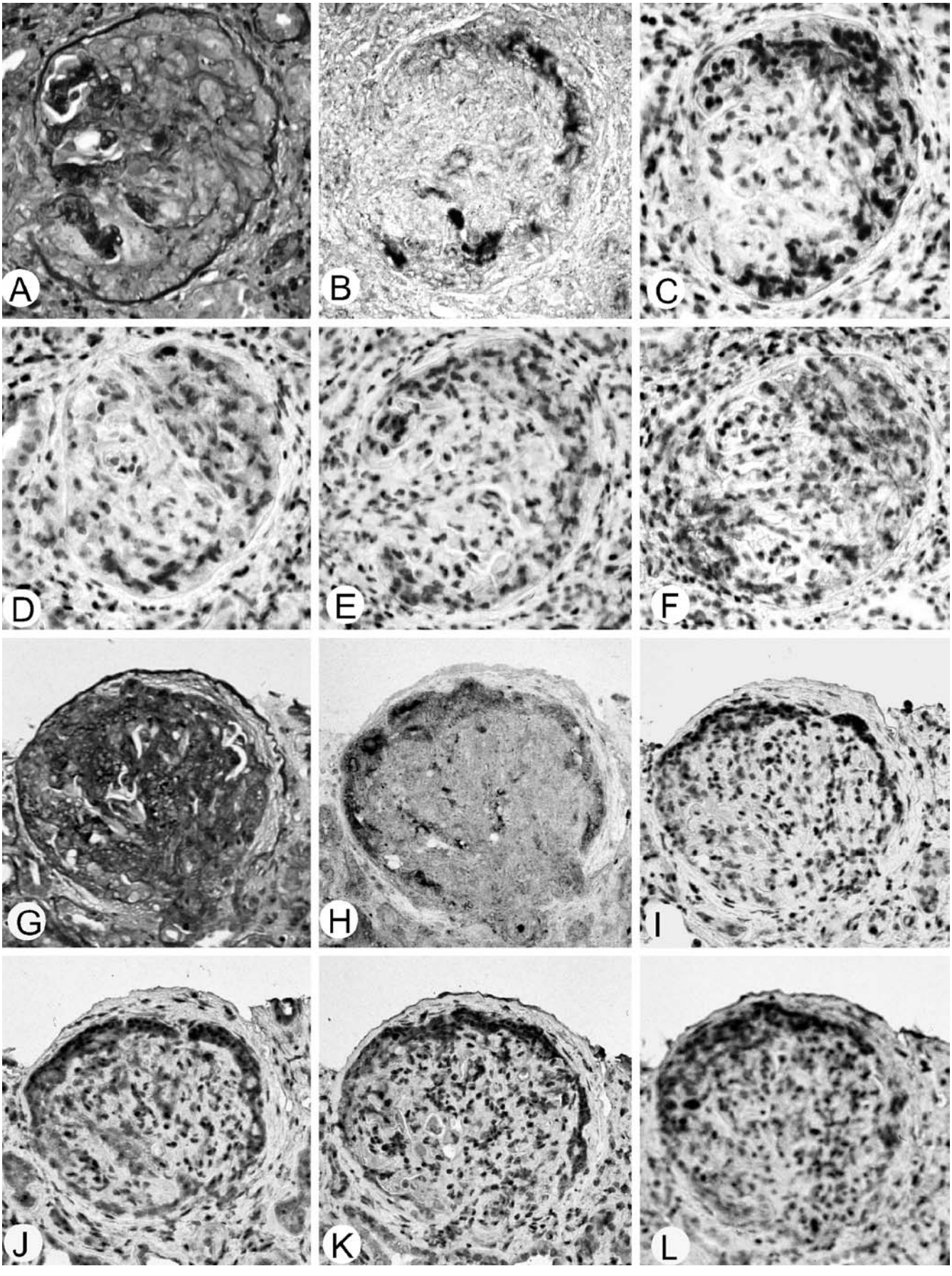
A
B
C
D
E
F
G
H
I
J
K
L

CTGF mRNA was lower in fibrocellular crescents (image not shown, score=0.92±0.31) and almost absent in fibrous crescents (image not shown, score=0.14±0.04). Moreover, CTGF mRNA expression was enhanced in the pseudotubule structures, where cytokeratin was also expressed (Fig. 2D, E, F).

CTGF mRNA is associated with TGF-β1 and ECM production

Since TGF-β1 is known as a potent inducer of CTGF, the expressions of TGF-β1 and its type-I receptor (TβRI) were examined with respect to CTGF mRNA expression using serial sections. TGF-β1 and TβRI were strongly expressed in cellular (Fig. 3C, D) and fibrocellular (Fig. 3I, J) crescents accompanied by CTGF mRNA (Fig. 3B, H). In addition, collagen type I and fibronectin were also both expressed in cellular (Fig. 3E, F) and fibrocellular crescents (Fig. 3K, L). The staining intensities for collagen type I and fibronectin were higher in fibrocellular crescents than in cellular crescents.

Discussion

The role of CTGF in kidney pathology has been investigated in human and animal renal diseases. Studies on mesangial proliferative diseases, such as Thy-1.1 nephritis or diabetic glomerulosclerosis, showed that CTGF enhances ECM synthesis, induces apoptosis in mesangial cells, and may contribute to the remodeling of mesangial regions [16, 30, 31, 32]. Studies on tubulointerstitial fibrosis showed that CTGF induces ECM synthesis and the transformation to myofibroblasts by expression of α-smooth muscle actin in renal fibroblasts [14, 35]. CTGF is expressed in podocytes and parietal epithelial cells, and its expression has also been noted in cellular crescents [15]. The localization of CTGF and its synthesis during the process of scar formation in crescentic glomeruli provide insights into the role of this molecule in CRGN. In this context, we analyzed serial sections for CTGF mRNA and used immunohistochemistry during various stages of human CRGN. Our results clearly demonstrate that the majority of CTGF mRNA-positive cells in the crescents express the epithelial marker cytokeratin, but not CD68, a macrophage marker. Although de-differentiated podocytes in focal segmental glomerulosclerosis with cellular lesions, collapsing glomerulopathy, and murine Denys-Drash syndrome have been reported to express cytokeratin [24, 27, 29], many studies have demonstrated that the major cellular components of glomerular crescents are PECs [4, 18, 20, 26, 28, 34]. Thus, we conclude that proliferating PECs are the main synthesizers of the CTGF in CRGN.

During scar formation in CRGN, cellular crescents frequently reduce cell components associated with excessive matrix deposition, leading to the fibrous changes [17]. The present study demonstrates that CTGF mRNA, which is strongly expressed in the cellular crescents, declined in the fibrocellular crescents in parallel with the matrix deposition and was absent in the fibrous crescents. In addition, we found that TGF-β1 and TβRI were immunohistochemically co-localized with CTGF mRNA in the crescents, which had fibronectin and collagen-type-I depositions. In the kidney, CTGF promoted renal fibrosis under TGF-β1 stimulation in Thy-1.1 nephritis and diabetic nephropathy [16, 23]. In vitro studies showed that TGF-β1 increased CTGF expression in mesangial cells, proximal tubular cells, and renal fibroblasts [1, 8, 12, 31, 33, 35]. Moreover, recombinant CTGF enhances the expression of various ECM proteins, including fibronectin and collagen type I, in cultured mesangial cells [1, 23, 31]. Of note, we found that the upregulation of CTGF was accompanied by TGF-β1- or PDGF-BB-mediated stimulation of ECM synthesis in cultured rat PECs [19]. These results suggest that CTGF induces PECs to stimulate matrix synthesis in the fibrocellular crescents, leading to the scar formation.

Interestingly, we note that CTGF mRNA is strongly expressed in the pseudotubule structures in crescents. The so-called "pseudotubule" or "adenomatoid" structures in crescents have been recognized as a remodeling process that mimics embryological tubulogenesis [14, 21]. Recent reports have indicated that CTGF may contribute to tissue remodeling in the pancreas and urinary bladder following inflammatory tissue damage [7, 9, 13]. Further studies are needed to elucidate CTGF activities other than its fibrogenic properties in the process of glomerular crescent formation.

In summary, CTGF is predominantly localized in the crescents of human CRGN. The high levels of CTGF mRNA expression in the proliferating PECs and the lower expression levels in the macrophages in crescents implicate CTGF in the matrix synthesis by PECs and the subsequent scar formation. In addition, we suggest that CTGF is involved in the matrix synthesis in crescents in concert with TGF-β1, known as a strong inducer of CTGF.

Acknowledgements This work was supported by grants from the University of Tsukuba, Showa University, and Health Sciences Research Grants of Japan (Research on Specific Diseases of the Nephro-urological Study Group).

References

1. Blom IE, Dijk AJ, Wieten L, Duran K, Ito Y, Kleij L, de Nichilo M, Rabelink TJ, Weening JJ, Aten J, Goldschmeding R (2001) In vitro evidence for differential involvement of CTGF, TGFβ, and PDGF-BB in mesangial response to injury. Nephrol Dial Transplant 16:1139–1148
2. Blom IE, Goldschmeding R, Leask A (2002) Gene regulation of connective tissue growth factor: new targets for antifibrotic therapy?
3. Bork P (1993) The molecular architecture of a new family of growth regulators related to connective tissue growth factor. FEBS Lett 327:125–130
4. Boucher A, Droz D, Adafer E, Noel LH (1987) Relationship between the integrity of Bowman's capsule and the composi-

tion of cellular crescents in human crescentic glomerulonephritis. Lab Invest 56:526–533
5. Bradham DM, Igarashi A, Potter RL, Grotendorst GR (1991) Connective tissue growth factor, a cysteine-rich mitogen secreted by human vascular endothelial cells is related to the SRC-induced immediate early gene product CEF-10. J Cell Biol 114:1285–1294
6. Brigstock DR (2003) The CCN family: a new stimulus package. J Endocrinol 178:169–175
7. Chaqour B, Whitbeck C, Han JS, Macarak E, Horan P, Chichester P, Levin R (2002) Cyr61 and CTGF are molecular markers of bladder wall remodeling after outlet obstruction. Am J Physiol Endocrinol Metab 283:E765–E774
8. Chen Y, Blom IE, Sa S, Goldschmeding R, Abraham DJ, Leask A (2002). CTGF expression in mesangial cells: involvement of SMADs, MAP kinase, and PKC. Kidney Int 62:1149–1159
9. di Mola FF, Friess H, Riesle E, Koliopanos A, Buchler P, Zhu Z, Brigstock DR, Korc M, Buchler MW (2002) Connective tissue growth factor is involved in pancreatic repair and tissue remodeling in human and rat acute necrotizing pancreatitis. Ann Surg 235:60–67
10. Fujigaki Y, Sun DF, Fujimoto T, Yonemura K, Morioka T, Yaoita E, Hishida A (2001) Cytokines and cell cycle regulation in the fibrous progression of crescent formation in antiglomerular basement membrane nephritis of WKY rats. Virchows Arch 439:35–45
11. Fujigaki Y, Sun DF, Fujimoto T, Suzuki T, Goto T, Yonemura K, Morioka T, Yaoita E, Hishida A (2002) Mechanisms and kinetics of Bowman's epithelial-myofibroblast transdifferentiation in the formation of glomerular crescents. Nephron 92:203–212
12. Heusinger-Ribeiro J, Eberlein M, Abdel-Wahab N, Goppelt-Struebe M (2001) Expression of connective tissue growth factor in human renal fibroblasts: regulatory roles of Rho A and cAMP. J Am Soc Nephrol 12:1853–1861
13. Hishikawa K, Oemar BS, Nakaki T (2001) Static pressure regulates connective tissue growth factor expression in human mesangial cells. J Biol Chem 276:16797–16803
14. Hughson MD, McManus JFA, Hennigar GR (1978) Studies on "End-stage" kidneys. II. Embryonal hyperplasia of Bowman's capsular epithelium. Am J Pathol 91:71–84
15. Ito Y, Aten J, Bende RJ, Oemer BS, Rabelink TJ, Weening JJ, Goldschmeding R (1998) Expression of connective tissue factor in human renal fibrosis. Kidney Int 53:853–861
16. Ito Y, Goldschmeding R, Bende RJ, Claessen N, Chand MA, Kleij L, Rabelink TJ, Weening JJ, Aten J (2002) Kinetics of connective tissue growth factor expression during experimental proliferative glomerulonephritis. J Am Soc Nephrol 12:472–484
17. Jennette JC (1997) Crescentic glomerulonephritis. In: Jennette JC, Olson JL, Schwartz MM, Silva FG (eds) Heptinstall's pathology of the kidney, 5th edn. Lippincott-Raven, Philadelphia, pp 625–656
18. Jennette JC, Hipp CG (1986) The epithelial antigen phenotype of glomerular crescent cells. Am J Clin Pathol 86:274–280
19. Kanemoto K, Usui J, Tomari S, Yokoi H, Mukoyama M, Aten J, Weening JJ, Nagata M (2003) Connective tissue growth factor participates in scar formation of crescentic glomerulonephritis. Lab Invest 83:1615–1625
20. Magil AB (1985) Histogenesis of glomerular crescents. Am J Pathol 120:222–229
21. McManus JFA, Willman JI (1963) Tubule formation in the crescent of subacute and chronic glomerulonephritis (abstract). Am J Pathol 43:37a
22. Morrin PA, Hinglais N, Nagarra B, Kreis H (1978) Rapidly progressive glomerulonephritis. A clinical and pathologic study. Am J Med 65:446–460
23. Murphy M, Godson C, Cannon S, Kato S, Mackenzie HS, Martin F, Brady HR (1999) Suppression subtractive hybridization identifies high glucose levels as a stimulus for expression of connective tissue growth factor and other genes in human mesangial cells. J Biol Chem 274:5830–5834
24. Nagata M, Hattori M, Hamano Y, Ito K, Saitoh K, Watanabe T (1998) Origin and phenotypic features of hyperplastic epithelial cells in collapsing glomerulopathy. Am J Kidney Dis 32:962–969
25. Ng YY, Fan JM, Mu W, Nikolic-Peterson DJ, Yang WC, Huang TP, Atkins RC, Lan HY (1999) Glomerular epithelial-myofibroblast transdifferentiation in the evolution of glomerular crescent formation. Nephrol Dial Transplant 14:2860–2872
26. Nitta K, Horita S, Honda K, Uchida K, Watanabe T, Nihei H, Nagata M (1999) Glomerular expression of cell-cycle-regulatory proteins in human crescentic glomerulonephritis. Virchows Arch 435:422–427
27. Ohtaka A, Ootaka T, Sato H, Ito S (2002) Phenotypic change of glomerular podocytes in primary focal segmental glomerulosclerosis: developmental paradigm? Nephrol Dial Transplant 17[Suppl 9]:11–15
28. Ophascharoensuk V, Pippen JW, Gordon KL, Shankland SJ, Couser WG, Johnson RJ (1998) Role of intrinsic renal cells versus infiltrating cells in glomerular crescent formation. Kidney Int 54:416–425
29. Patek CE, Fleming S, Miles CG, Bellamy CO, Ladomery M, Spraggon L, Hastie ND, Hooper ML (2003) Murine Denys-Drash syndrome: evidence of podocyte de-differentiation and systemic mediation of glomerulosclerosis. Hum Mol Genet 12:2379–2394
30. Riser BL, Denichilo M, Cortes P, Baker C, Grondin JM, Yee J, Narins RG (2000) Regulation of connective tissue growth factor activity in cultured rat mesangial cells and its expression in experimental diabetic glomerulonephritis. J Am Soc Nephrol 11:25–38
31. Riser BL, Cortes P (2001) Connective tissue growth factor and its regulation: a new element in diabetic glomerulosclerosis. Ren Fail 23:459–470
32. Twigg SM, Cao Z, McLennan SV, Burns WC, Brammar G, Forbes JM, Cooper ME (2002) Renal connective tissue growth factor induction in experimental diabetes is prevented by aminoguanidine. Endocrinology 143:4907–4915
33. Yokoi H, Mukoyama M, Sugawara A, Mori K, Nagae T, Makino H, Suganami T, Yahata K, Fujinaga Y, Tanaka I, Nakao K (2002) Role of connective tissue growth factor in fibronectin expression and tubulointerstitial fibrosis. Am J Physiol Renal Physiol 282:F933–F942
34. Yoshioka K, Takemura T, Akano N, Miyamoto H, Iseki T, Maki S (1987) Cellular and non-cellular compositions of crescents in human glomerulonephritis. Kidney Int 32:284–291
35. Wang S, Denichilo M, Brubaker C, Hirschberg R (2001) Connective tissue growth factor in tubulointerstitial injury of diabetic nephropathy. Kidney Int 60:96–105

Virchows Arch (2004) 444:264–268
DOI 10.1007/s00428-003-0934-8

ORIGINAL ARTICLE

A. Lugli · P. Went · B. Khanlari · Z. Nikolova · S. Dirnhofer

Rare KIT (CD117) expression in multiple myeloma abrogates the usefulness of imatinib mesylate treatment

Received: 3 September 2003 / Accepted: 28 October 2003 / Published online: 16 December 2003

Abstract *Background:* Imatinib mesylate blocks the tyrosine kinase activity of KIT (CD117) and is an effective treatment for gastrointestinal stromal tumors. In multiple myeloma, KIT expression has been detected by flow cytometry in about 33% of specimens, but no previous immunohistochemical assessment has yet been made of the expression pattern of KIT. *Materials and methods:* We performed immunohistochemical analyses of 100 patients, including 72 with multiple myeloma (MM), 8 with lymphoplasmacytic lymphoma (LPL), 10 with monoclonal gammopathy of undetermined significance (MGUS) and 10 with reactive plasmocytosis. One KIT-positive MM was sequenced using polymerase chain reaction analysis. *Results:* In MM, only 2 cases (2.8%) were KIT positive. The great majority of the cases (97, 2%) did not express the KIT receptor tyrosine kinase. No mutation of the c-kit gene was detected. *Conclusions:* KIT expression is a rare event in MM and not detectable in MGUS and LPL. Therefore, treatment with imatinib is unlikely to be effective in these patients.

Keywords KIT (CD117) · Multiple myeloma · Imatinib mesylate

Introduction

Imatinib mesylate (Glivec) is a specific inhibitor of tyrosine kinases, such as Abl, KIT (CD117) and platelet-derived growth factor receptor (PDGF-R). Several studies have shown the effectiveness of imatinib mesylate as a molecular target treatment in chronic myelogenous leukemia [9] via blockade of bcr-abl activity, in gastrointestinal stromal tumors (GIST) [4, 15] via KIT inhibition and in dermatofibrosarcoma protuberans [14] and hypereosinophilic syndrome [3] via interference with PDGF-R activation. This has raised hopes that other malignancies resulting from oncogenic activation of these kinases may benefit from molecular target therapy.

Multiple myeloma (MM) is a malignant plasma cell neoplasia, characterized by osteolytic lesions, marrow plasmocytosis and monoclonal gammopathy [7]. Currently, the therapy for MM includes conventional low-dose chemotherapy or high-dose chemotherapy with autologous or allogeneic stem cell transplantation. Although the tumor burden can be reduced, a complete and sustained remission of disease is rare, and most of the patients suffer from relapsing disease [16]. Therefore, novel therapies are urgently needed. Because flow cytometry has revealed KIT expression in 33% of MM (range 26–43%) [1, 5, 10, 11, 12], aberrant KIT expression in MM could provide the rationale for treatment with imatinib mesylate. However, no immunohistochemical analysis assessing the in situ expression of KIT in MM has been performed prior to the study reported herein.

The aim of our study was to investigate KIT expression by immunohistochemical analysis in a large cohort of bone-marrow biopsies of patients with MM, monoclonal gammopathy of undetermined difference (MGUS), lymphoplasmacytic lymphoma (LPL) and reactive plasmacytosis (RP) to provide the histopathological basis for a putative molecular-targeted therapy with imatinib mesylate.

A. Lugli · P. Went · B. Khanlari · S. Dirnhofer (✉)
Institute of Pathology,
Kantonsspital Basel,
Schönbeinstrasse 40, 4031 Basel, Switzerland
e-mail: sdirnhofer@uhbs.ch
Tel.: +41-61-2652789
Fax: +41-61-2653194

Z. Nikolova
Novartis, Basel, Switzerland

Materials and methods

Patients

We retrospectively reviewed bone marrow biopsies of 100 patients, 90 with monoclonal gammopathies (72 MM, 8 LPL and 10 MGUS) and 10 with RP, retrieved from the archives of the Institute of Pathology, University of Basel.

The diagnoses of MM, LPL, MGUS and RP were established by histomorphology and immunohistochemistry. All specimens were

reviewed and reclassified according to the World Health Organization classification criteria [6].

Immunohistochemistry

Serial sections 4-μm thick of 99 SUSA- and 1 formalin-fixed paraffin-embedded bone-marrow biopsies were used for immunohistochemical studies. The primary antibodies used in this study and types of antigen retrieval performed are summarized in Table 1.

Heat-induced antigen retrieval was performed in a microwave in ethylene diamine tetraacetic acid buffer (pH 8.0). An automated modified streptavidin-biotin system (Ventana Medical Systems, Tucson, AZ) was used for immunohistochemical staining. Mast cells served as internal positive control and a mutation-confirmed GIST as external positive control for CD117. Moreover, to obtain definite specificity control for CD117, the reaction was blocked by pre-incubation of the primary antibody with the specific antigen (10 nmol/ml diluted antibody, Novocastra). Positivity was defined as more than 10% KIT-positive plasma cells, considering only a membranous staining pattern.

Polymerase chain reaction sequence analysis

One MM with moderate CD117 staining was selected for KIT mutation analysis [the MM with weak CD117 staining could not be analyzed by polymerase chain reaction (PCR) due to SUSA fixation of the bone marrow biopsy]. Deparaffinizing the formalin-fixed tissues and DNA extraction was performed using a commercial DNA extraction kit (Qia Amp DNA mini-kit, Cat. #51304, Qiagen GmbH, Hilden, Germany). Exons 2, 8, 9, 11, 13 and 17 were amplified using a semi-nested PCR approach and were sequenced using the Big Dye Terminators Cycle Sequencing Ready Reaction Kit (Applied Biosystems, Foster City, CA). The primers were designed based on a previously published sequence of the human c-kit gene [2]. Sequence products were analyzed on an ABI Prism 310 Genetic Analyzer (Applied Biosystems; Foster City, CA, USA).

Results

Patients

The median age of the various patient populations was: MM (41 males and 31 females) 66 years (range: 31–89 years), LPL (8 males) 70 years (range: 52–81 years), MGUS (3 males and 7 females) 64 years (range: 36–80 years) and RP (5 males and 5 females) 73 years (range: 52–81 years) (Table 2).

Immunohistochemistry

The monotypic immunoglobulin detected in the 72 MM patients was IgG in 53% (21% kappa and 32% lambda) and IgA in 28% (15% kappa and 13% lambda). Monotypic light chains only were observed in 19% (equal distribution of kappa and lambda). In the eight LPL patients, IgM-kappa was found in 75% and IgM-lambda in 25%. In the ten MGUS patients, the M-component was IgG in 60% (kappa in 50% and lambda in 10%), IgA-lambda in 20%, IgM-kappa in 10% and only light chain (lambda) in 10%, respectively. Of the 72 MM cases, two (2.8%) were immunohistochemically KIT positive. One case (IgG-kappa) showed a moderate membranous expression in nearly 100% of the plasma cells (Fig. 1A, B, C), and the other case (IgG-lambda) showed a weak expression in 50% of the plasma cells (Fig. 2). Of MM, 97% (70/72) were KIT negative, and 100% of LPL, MGUS and RP were KIT negative.

Table 1 Primary antibodies and antigen retrieval techniques. *MW* microwave-based antigen retrieval with ethylene diamine tetraacetic acid buffer, pH 8.0

Antibody	Clonality	Antigen retrieval	Dilution	Source	Code number
CD117	Polyclonal	MW; 100°C, 15′	1:40	Dako	A4502
CD138	Monoclonal	MW; 100°C, 15′	1:15	Dako	M7228
IgG	Polyclonal	None	1:5000	Dako	A0423
IgA	Polyclonal	None	1:10,000	Dako	A0262
IgM	Polyclonal	None	1:5000	Dako	A0425
Light chain λ	Polyclonal	None	1:10,000	Dako	A0193
Light chain κ	Polyclonal	None	1:10,000	Dako	A0191

Table 2 Patient characteristics. *LPL* lymphoplasmacytic lymphoma, *MGUS* monoclonal gammopathy of undetermined significance

	Multiple myeloma	LPL	MGUS	Reactive plasmocytosis
General data				
Number of patients	72	8	10	10
Median age, years (range)	66 (31–89)	70 (52–81)	64 (36–80)	73 (52–81)
Gender male	41	8	3	5
M-component				
IgG, kappa	21%		50%	
IgG, lambda	32%		10%	
IgA, kappa	15%		0%	
IgA, lambda	13%		20%	
IgM, kappa	0%	75%	10%	
IgM, lambda	0%	25%	0%	
Lambda, only	9.5%		10%	
Kappa, only	9.5%		0%	

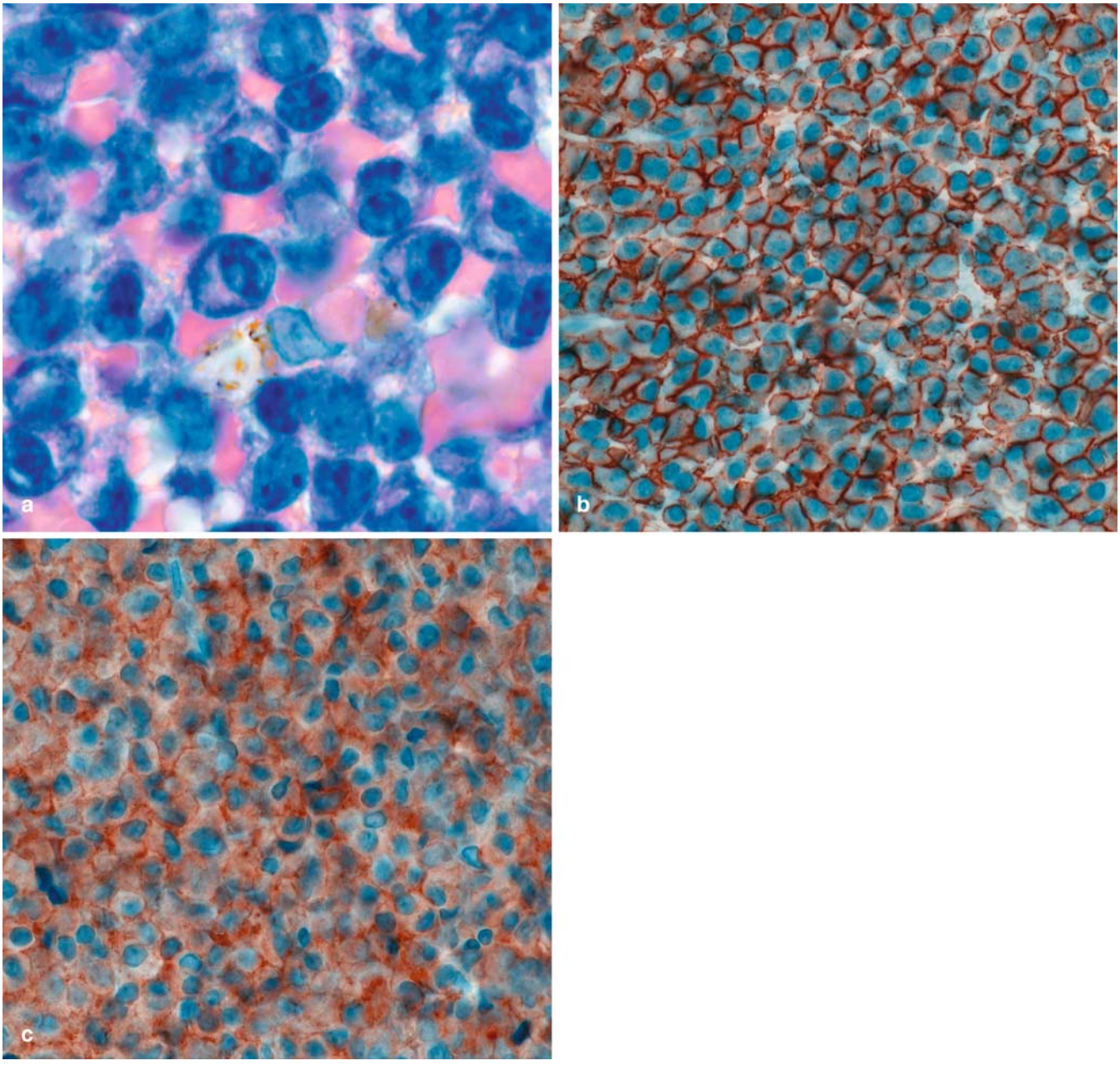

Fig. 1 Bone marrow with diffuse infiltration of atypical plasma cells in multiple myeloma (Giemsa, ×63) (**a**). Immunostaining for CD138 (×40), showing a strong positivity of malignant plasma cells (**b**). Immunostaining for CD117 (×40) with moderate positivity in malignant plasma cells (**c**)

KIT positivity in mast cells serving as internal control was detected in all cases. The definitive specificity control of the two positive MM cases was obtained by pre-incubation of the primary antibody.

PCR

DNA was extracted from the MM case with moderate KIT expression and amplified and sequenced as described. No mutation of the exon 2, 8, 9, 11, 13 and 17 of the c-kit gene was detected.

Discussion

In the present study, we have shown that KIT is rarely expressed in MM. Only 2 of 72 cases (2.8%) demonstrated immunohistochemically detectable expression, and all cases of MGUS, RP and LPL were KIT negative.

To our knowledge, this is the first study to systematically analyze KIT expression in plasma cells on paraffin sections. Yang et al. assessed the immunophenotype of cutaneous and extracutaneous mast cell disease on paraffin sections and included in their study, four cases of MM without finding KIT expression [17]. Natkunam et

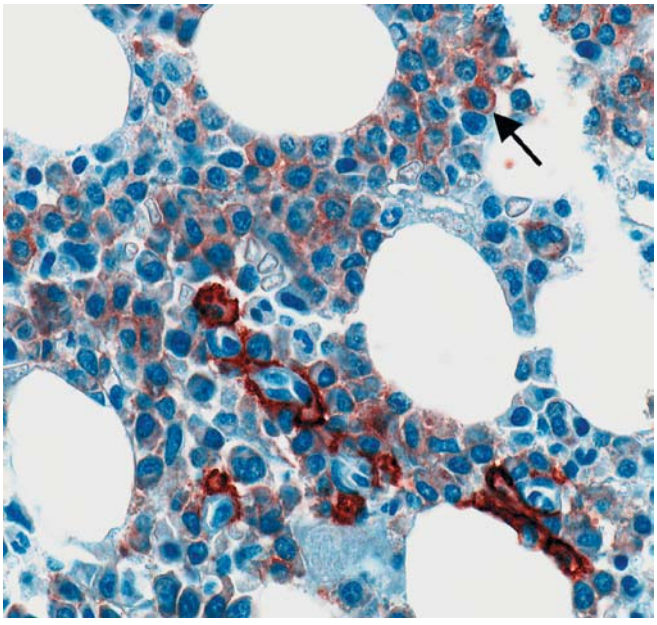

Fig. 2 Immunostaining for CD117 (×40) with weak positive malignant plasma cells (*arrow*) and adjacent strong positive mast cells as internal control

al. analyzed the utility of paraffin section immunohistochemistry for KIT in the differential diagnosis of systemic mast cell disease involving the bone marrow and found no expression of KIT in various B-cell lymphomas or plasma cell tumors [8]. The slight discrepancy in KIT detection between immunohistochemistry and flow cytometry is not unusual and may be related to fixation and processing or to the specificity of the anti-CD117 antibodies employed.

Based on our large series of 72 cases and these few reports from the literature, we conclude that MM is not a candidate disease for treatment with imatinib mesylate, as the majority of cases do not express the KIT target. This conclusion is clearly corroborated by the fact that in the B2225 study, an international multi-center trial assessing the efficacy of imatinib mesylate in advanced/metastatic malignancies, all six patients with MM (some expressing KIT in >50% of plasma cells) showed disease progression while under treatment with imatinib (personal communication with Novartis).

Thus, for the few cases of MM that show KIT expression, demonstration of the imatinib target is not, in itself, sufficient to achieve the expected clinical effects. Obviously, the tyrosine kinase of the involved receptor should be functionally active, such as in most cases of GIST [13]. In general, activating oncogenic mutations of target genes is a prerequisite for a clinical response to imatinib therapy [3, 4, 9, 14, 15].

In agreement with the clinical data from the B2225 study (myeloma patients with disease progression while under treatment), PCR analysis of our MM case with moderate KIT expression revealed a wild-type gene configuration, i.e., no mutations in exons 2, 8, 9, 11, 13 and 17. Another possible pathway of successful treatment of MM patients with imatinib could be targeting PDGFR signaling. We, therefore, tested several anti-PDGFR antibodies, but did not obtain reliable and reproducible results. Continuative mutational analysis was not possible, due to RNA/DNA degradation in SUSA-fixed tissue. However, based on the clinical findings from the B2225 study mentioned above, a pathogenetic and therapeutic role of PDGFR in MM is unlikely.

In summary, most cases of MM are immunohistochemically KIT negative. The very few positive cases probably do not show activating KIT mutations and, therefore, will not respond to imatinib treatment.

References

1. Almeida J, Orfao A, Ocqueteau M, Mateo G, Corral M, Caballero MD, Blade J, Moro MJ, Hernandez J, San Miguel JF (1999) High-sensitive immunophenotyping and DNA ploidy studies for the investigation of minimal residual disease in multiple myeloma. Br J Haematol 107:121–131
2. Andre CHA, Lachaume P, Martin E, Wang XP, Manus V, Hu WX, Galibert F (1997) Sequence analysis of two genomic regions containing the KIT and FMS receptor tyrosine kinase genes. Genomics 39:216–226
3. Cools J, DeAngelo DJ, Gotlib J, Stover EH, Legare RD, Cortes J, Kutok J, Clark J, Galinsky I, Griffin JD, Cross NC, Tefferi A, Malone J, Alam R, Schrier SL, Schmid J, Rose M, Vandenberghe P, Verhoef G, Boogaerts M, Wlodarska I, Kantarjian H, Marynen P, Coutre SE, Stone R, Gilliland DG (2003) A tyrosine kinase created by fusion of the PDGFRA and FIP1L1 genes as a therapeutic target of imatinib in idiopathic hypereosinophilic syndrome. N Engl J Med 348:1201–1214
4. Demetri GD, von Mehren M, Blanke CD, Van den Abbeele AD, Eisenberg B, Roberts PJ, Heinrich MC, Tuveson DA, Singer S, Janicek M, Fletcher JA, Silverman SG, Silberman SL, Capdeville R, Kiese B, Peng B, Dimitrijevic S, Druker BJ, Corless C, Fletcher CD, Joensuu H (2002) Efficacy and safety of imatinib mesylate in advanced gastrointestinal stromal tumors. N Engl J Med 347:472–480
5. Garcia-Sanz R, Orfao A, Gonzalez M, Tabernero MD, Blade J, Moro MJ, Fernandez-Calvo J, Sanz MA, Perez-Simon JA, Rasillo A, Miguel JF (1999) Primary plasma cell leukemia: clinical, immunophenotypic, DNA ploidy, and cytogenetic characteristics. Blood 93:1032–1037
6. Jaffe ES, Jarris NL, Stein H, Vardiman JW (eds) (2001) World Health Organization classification of tumours. Pathology and genetics of tumours of haematopoietic and lymphoid tissues. IARC Press, Lyon
7. Knowles DM (2001) Neoplastic hematopathology, 2nd edn. Lippincott Williams and Wilkins, Philadelphia
8. Natkunam Y, Rouse RV (2000) Utility of paraffin section immunohistochemistry for C-KIT (CD117) in the differential diagnosis of systemic mast cell disease involving the bone marrow. Am J Surg Pathol 24:81–91
9. O'Brien SG, Guilhot F, Larson RA, Gathmann I, Baccarani M, Cervantes F, Cornelissen JJ, Fischer T, Hochhaus A, Hughes T, Lechner K, Nielsen JL, Rousselot P, Reiffers J, Saglio G, Shepherd J, Simonsson B, Gratwohl A, Goldman JM, Kantarjian H, Taylor K, Verhoef G, Bolton AE, Capdeville R, Druker BJ (2003) Imatinib compared with interferon and low-dose cytarabine for newly diagnosed chronic-phase chronic myeloid leukemia. N Engl J Med 348:994–1004
10. Ocqueteau M, Orfao A, Garcia-Sanz R, Almeida J, Gonzalez M, San Miguel JF (1996) Expression of the CD117 antigen (c-Kit) on normal and myelomatous plasma cells. Br J Haematol 95:489–493

11. Ocqueteau M, Orfao A, Almeida J, Blade J, Gonzalez M, Garcia-Sanz R, Lopez-Berges C, Moro MJ, Hernandez J, Escribano L, Caballero D, Rozman M, San Miguel JF (1998) Immunophenotypic characterization of plasma cells from monoclonal gammopathy of undetermined significance patients. Implications for the differential diagnosis between MGUS and multiple myeloma. Am J Pathol 152:1655–1665
12. Rasmussen T, Jensen L, Johnsen HE (2000) The clonal hierarchy in multiple myeloma. Acta Oncol 39:765–770
13. Rubin BP, Singer S, Tsao C, Duensing A, Lux ML, Ruiz R, Hibbard MK, Chen CJ, Xiao S, Tuveson DA, Demetri GD, Fletcher CD, Fletcher JA (2001) KIT activation is a ubiquitous feature of gastrointestinal stromal tumors. Cancer Res 61:8118–8121
14. Rubin BP, Schuetze SM, Eary JF, Norwood TH, Mirza S, Conrad EU, Bruckner JD (2002) Molecular targeting of platelet-derived growth factor B by imatinib mesylate in a patient with metastatic dermatofibrosarcoma protuberans. J Clin Oncol 20:3586–3591
15. van Oosterom AT, Judson I, Verweij J, Stroobants S, Donato di Paola E, Dimitrijevic S, Martens M, Webb A, Sciot R, Van Glabbeke M, Silberman S, Nielsen OS (2001) Safety and efficacy of imatinib (STI571) in metastatic gastrointestinal stromal tumours: a phase I study. Lancet 358:1421–1423
16. Wickramasinghe SN, McCullough J (2003) Blood and bone marrow pathology, 1st edn. Churchill Livingstone, London
17. Yang F, Tran TA, Carlson JA, Hsi ED, Ross CW, Arber DA (2000) Paraffin section immunophenotype of cutaneous and extracutaneous mast cell disease. Am J Surg Pathol 24:703–709

Virchows Arch (2004) 444:269–277
DOI 10.1007/s00428-003-0936-6

ORIGINAL ARTICLE

Claudio Sorio · Patrick S. Moore · Maria Grazia Ennas · Cristina Tecchio · Antonio Bonora · Silvia Sartoris · Piera Balzarini · Piergiovanni Grigolato · Aldo Scarpa

A novel cell line and xenograft model of ampulla of Vater adenocarcinoma

Received: 6 August 2003 / Accepted: 31 October 2003 / Published online: 16 December 2003

Abstract Ampulla of Vater cancers (AVC) are of clinical relevance, as they represent more than one-third of patients undergoing surgery for pancreaticoduodenal malignancies and have a better prognosis than periampullary cancers of pancreaticobiliary origin. The availability of cellular models is crucial to perform cell biology and pharmacological studies and clarify the relationship between AVC and pancreatic and biliary cancers. Numerous cell lines are available for pancreatic and biliary adenocarcinomas, while only two have been reported recently for AVC. These were derived from a poor and a well-differentiated AVC, and both had wild-type K-*ras* and mutated *p53*. We report the establishment of a novel AVC cell line (AVC1) derived from a moderately differentiated cancer, having a mutated K-*ras*, wild-type *p53*, and methylated *p16*. Thus, our cell line adds to the spectrum of available in vitro models representative of the different morphological and molecular presentations of primary AVC. We further characterized AVC1 for the expression of relevant cell surface molecules and sensitivity to chemotherapeutic agents of common clinical use. It expresses MHC-I and CD95/Fas, while HLA-DR, CD40, CD80, CD86, MUC-1, MUC-2, and ICAM-1/CD54 are absent. It has a low to moderate sensitivity to both 5-FU and gemcitabine, at variance with much higher sensitivity displayed by two pancreatic ductal carcinoma cell lines. Lastly, AVC1 can be readily xenografted in immunodeficient mice, making it a suitable model for pre-clinical studies.

Keywords Periampullary cancer · Pancreaticobiliary · Cell line · Ampulla of Vater · Pancreas

C. Sorio · P. S. Moore · C. Tecchio · S. Sartoris · A. Scarpa (✉)
Dipartimento di Patologia,
Università di Verona,
Strada Le Grazie, 37134 Verona, Italy
e-mail: aldo.scarpa@univr.it
Tel.: +39-04-58074822
Fax: +39-04-58027136

M. G. Ennas
Dipartimento di Citomorfologia,
Università di Cagliari, Italy

A. Bonora
Dipartimento di Scienze Chirurgiche e Gastroenterologiche,
Università di Verona, Italy

P. Balzarini · P. Grigolato
Istituto di Anatomia Patologica,
Università di Brescia, Italy

Introduction

Cancers arising from the anatomical structures of the ampulla of Vater (AVC) represent an important clinical entity, as patients affected with AVC account for up to 36% of those undergoing surgery for pancreaticoduodenal malignancies. These patients have a significantly better prognosis compared with patients with ductal pancreatic adenocarcinoma and, in fact, are the only patients among those affected by cancers of biliopancreatic origin who have a chance of up to 50% for a cure by surgery alone [2, 5, 13, 25, 28, 31, 34].

Numerous cell lines derived from pancreatic adenocarcinomas have been established and extensively characterized (see [21, 32] for molecular characterization of the most commonly used lines). In contrast, there is only one report describing the establishment and characterization of two cell lines derived from primary AVC [14]. Particularly true for rare neoplasms, the availability of large amounts of viable, tumor-related material is limited, and substantial progress is achievable only by the exploitation of a cellular model.

In this report, we describe the isolation and characterization of a novel AVC cell line derived from a cancer of unequivocal origin from the ampulla of Vater. This model will be particularly useful in studies aimed at the elucidation of molecular aspects of pancreatic periampullary adenocarcinomas. In addition to extensive molecular characterization, we also demonstrate that this unique cell line has the capability to grow in nude mice.

Materials and methods

Clinicopathololological data

The primary AVC was obtained from a 71-year-old female patient who underwent pancreaticoduodenectomy in March 1997 with curative intent. Informed consent was obtained according to the Helsinki guidelines. Macroscopic examination revealed that the papilla major was obstructed by a villous lesion of 0.8 cm in diameter, which was histologically characterized as a moderately differentiated papilla of Vater adenocarcinoma infiltrating the Oddi muscle and focally extended to the duodenal mucosa (T1, N0, M0). The patient died shortly after surgical intervention, due to complications unrelated to disease.

Culture procedure

One-third of the lesion was removed under sterile conditions, a portion was subjected to cryostat sectioning for pathological analysis, and the remaining portion was transferred in Leibovitz medium (Leibovitz L-15, BioWhittaker, Bergamo, Italy) kept at 4°C until transfer to the cell culture facility. For culture, the tissue was finely minced and transferred into 6-well cell culture dishes (Beckton-Dickinson, Milano, Italy) after re-suspension in RPMI 1640 containing 10% fetal bovine serum (FBS) (Gibco-BRL), 2 mM glutamine, 80 μg/ml gentamycin sulphate, and 2.5 μg/ml amphotericin B (Sigma-Aldrich, Milan, Italy.). The cells were maintained at 37°C in a humidified atmosphere with 5% CO_2, and the medium was changed twice a week. After the cells grew to 80% confluency, we performed a controlled trypsinization to preferentially remove the few contaminating fibroblasts, taking advantage of the differential sensitivity to trypsinization. Additionally, the rapid growth kinetics of this cell line (24 h) allowed for a rapid elimination, within a few passages, of the remaining fibroblast contamination.

Scanning electron microscopy

Glass coverslips were pretreated with carbonate buffer, washed, and incubated with 20 μg/ml fibronectin and vitronectin (1/1) in phosphate-buffered saline (PBS). The slides were rinsed and cells seeded at 1.3×10^4 cells/cm^2 in MEM-0.4% fetal calf serum (FCS) for 24, 48, and 72 h. Cells were then fixed for 1 h in a mixture of 1.5% glutaraldehyde and 1% paraformaldehyde in 0.15 M cacodylate buffer, pH 7.4. The slides were washed, dehydrated, and covered with platinum using the Emitech K575 apparatus (Emitech, England). Analysis was performed using a Hitachi S4000 instrument (Hitachi, Japan) at 15 kV.

Transmission electron microscopy

A cell pellet was fixed in glutaraldehyde 1.25% and paraformaldehyde 1% in 0.15 M cacodylate for 1 h followed by post-fixation in 2% OsO_4 for 1 h and a pre-staining in 0.25% uranyl acetate for 24 h. After one wash in double distilled water, the samples were dehydrated by passage in serial dilutions of acetone (50–70–80–95–100% acetone in water) within 15 min. The cells were then centrifuged, and the pellet was impregnated in EPON 182 (electron microscopy), which was polymerized at 60° for 24 h. Ultra-thin sections (90 nm) were obtained and stained with a saturated solution of uranyl acetate and bismuth nitrate before analysis on a Jeol 100S transmission electron microscope.

Duplication time and colony forming efficiency

The growth curve for the cell line was determined by performing the readings with Alamar blue (Biosource International, Milan, Italy) at 24 h intervals as described below once a linear phase of growth was determined for a given cellular concentration. To assess colony forming efficiency (CFE), aliquots of cells (200, 500, 1000) in 5 ml of culture medium were seeded onto 60-mm plastic dishes and incubated for 7 days. The number of cells that formed colonies was counted by dilution with PBS, and the number of colonies with more than 10 cells then was counted after Giemsa staining. The number of colonies was divided by the number of initially seeded cells, and the percentage ratio was evaluated as the CFE.

DNA ploidy analysis

Exponentially growing cells were collected by trypsinization, centrifuged, and resuspended in PBS. Pellets were incubated for 2 h at 4°C in 1 ml of 0.1% Triton-X containing propidium iodide (50 μg/ml, Sigma, St. Louis, MO, USA) and RNase (1 mg/ml, Sigma, St. Louis, MO, USA). Flow cytometry was performed using a FACScan flow cytometer (Becton Dickinson, Mountain View, CA) equipped with a 15-nm argon laser (488 nm) and a doublet discrimination moduler. Human thymocytes were used to determine the reference peak. The DNA index (DI) was calculated as the ratio of the G_0-G_1 of the two peaks (reference and AVC1). Histograms showing only one cell cycle (normal DNA stemline) were considered to have a DI of one. The DNA histogram was obtained from 10,000 events.

Cytogenetic analysis

The cytogenetic study was performed in G-banded metaphases cells obtained from a 5-day-old culture and was an analysis of a total of 20 cells.

Molecular analysis

All samples were analyzed for mutations in exon 1 of the K-*ras* gene, exons 1 and 2 of *p16*, exons 5–9 of *p53*, and exons 8–11 of *DPC4* by direct sequencing of polymerase chain reaction (PCR)-amplified DNA fragments. Primers for amplification of the *p53* [26] *p16* [37], K-*ras* [27], and *DPC4* genes [8] were as described. Methylation-specific PCR for the 5′ CpG island of the *p16* gene was carried out as described [10].

Immunocytochemical and immunofluorescence analysis

The phenotypic profile of AVC1 was analyzed using the antibodies detailed in Table 1, Table 2, Table 3, and Table 4. For immunocytochemistry, cells were cultured on glass slides, washed with PBS, and fixed in cold acetone. After fixation, slides were rehydrated in PBS and pre-incubated with 10 mM phenylhydrazine in PBS to block endogenous peroxidase activity. Slides were rinsed four times in PBS and incubated with protein blocking agent (UltraTech HRP Kit Immunotech) for 10 min at room temperature. To visualize the presence of specific antigens, the streptavidin-biotin-horseradish peroxidase staining method was used, and antibody localization was visualized with the diaminobenzidine reaction.

For characterization of adhesion molecules by immunofluorescence, four chamber slides (Nunc, Milan, Italy) were cultured as described previously, washed in PBS (0.1 M NaCl, 2 mM KCl, 8 mM Na_2HPO_4, 1 mM KH_2PO_4, pH 7.4), and fixed in methanol at −20°C for 10 min with 4% paraformaldehyde at 37°C for 20 min. After re-hydration, the slides were incubated in a humid chamber and stained with the appropriate antibodies for 1 h at room temperature, washed three times in PBS, and incubated 30 min with biotinylated horse anti-mouse (Vector) 1/200 in PBS-1% horse serum (Sigma, Milan, Italy). After incubation with monoclonal and polyclonal antibodies, slides were sequentially incubated with polyvalent biotinylated secondary antibodies and strepavidin-peroxidase reagent. After three more washes in PBS, the slides were

Table 1 Expression of epithelial/mesenchymal antigens in ampulla of Vater cancer 1. All data were obtained by immunocytochemistry, except those for MUC1 and MUC2 obtained by cytofluorimetry. *CK* cytokeratin. + positive staining graded from one to three plus according to intensity, – negative staining

Antigen	Source/clone	Staining
CK7	Biogenex Laboratories (clone OV-TL 12/30)	+++
CK 8, 18, 19	Biogenex Laboratories (clone 5D3)	+++
AE1–AE3	Dako Corporation	+++
Carcinoembryonic antigen	Dako Corporation	+++
Ber-EP4	Dako Corporation	++
Vimentin	Biogenex Laboratories (clone V9)	++
Chromogranin A	Dako-A3	–
S100	Dako Corporation	–
MUC-1	BD-Pharmingen	–[a]
MUC-2	BD-Pharmingen	–

[a] From – to + after INFγ treatment

Table 2 Adhesion molecules expressed by ampulla of Vater cancer 1. All data were obtained by indirect immunofluorescence, except for CD18, CD29, and CD54, obtained by cytofluorimetry. + positive staining graded from one to three plus according to the intensity, – negative stain

Antigen	Clone	Staining
Integrin α_1	TS 2/7	++
Integrin α_2	HM a2	–
Integrin α_3	P1B5	++
Integrin α_5	P1D6	+
Integrin α_6	GOH3	+
Integrin β_1 (CD29)	BD-Pharmingen	+
Integrin β_2 (CD18)	IB4	–
Integrin β_3	AP3	++[a]
Integrin β_4	3E1	+
Integrin $\alpha_v\beta_3$	LM609	++[a]
ICAM-1 (CD54)	BD-Pharmingen	–

[a] The positivity was localized to adhesion plaques

Table 3 Immunological molecules expressed by ampulla of Vater cancer 1 by cytofluorimetric analysis. + positive staining graded from one to three plus according to the intensity, – negative stain

Antigen	Source/clone	Staining
MHC-I (A, -B, -C)	B9.12.1	+[a]
HLA-DR	D1.12	–[b]
CD80	BD-Pharmingen	–
CD86	BD-Pharmingen	–
CD40	BD-Pharmingen	–
CD95	BD-Pharmingen	+[a]

[a] From + to ++ after INFγ treatment
[b] From – to + after INFγ treatment

Table 4 ID-50 for gemcitabine and 5-fluorouracil

Cell line	Gemcitabine (μM)	5-Fluorouracil (μM)
AVC1	0.26 (n=4)	92 (n=5)
CFPAC1	0.06 (n=2)	227 (n=4)
PACA44	1.44 (n=2)	<2.7 (n=3)
PANC1	N.D.	

incubated in rhodol green 1/600 in PBS for 30 min in the dark, washed in PBS, and mounted in PBS-glycerol.

The antibodies used included the monoclonal antibodies (mAb): AE1-AE3, Ber-EP4, chromogranin A, and p21 (Dako), cytokeratin 7, cytokeratins 8, 18, and 19 (clone 5D3), and vimentin (Biogenex Laboratories), p53 (Oncogene Science, Inc). The antibodies against S100 and carcinoembryonic antigen were polyclonal (Dako).

Expression of integrin chains was analyzed by indirect immunofluorescence using the following mAbs: TS2/7 and TS2/16 (American Type Culture Collection, Bethesda, MD), P1B5, P1D6 (BRL, Milan, Italy), GoH3 (Pierce, Milan, Italy), LM609, 3E1, and Hm a2 (Chemicon, Milan, Italy). Cells were also analyzed by cytofluorimetry on an Epics XL apparatus (Coulter, Hialeah, FL) using the following mAbs: B9.12.1, specific for HLA class I monomorphic determinants [16]; D1.12, specific for HLA-DR monomorphic determinants [1], IB4, anti human CD18 (Dr. S.D. Wright, The Rockefeller University, New York, NY). mAbs specific for human CD29, CD40, CD54, CD80, CD86, CD95, MUC-1, and MUC-2 were purchased from BD-Pharmingen, Milan, Italy. Since all the primary mAbs were mouse IgG, the secondary antibody used was goat anti-mouse IgG, $F(ab')_2$ fluorescein isothiocyanate-IgG conjugate (Instrumentation Laboratory, Milan, Italy).

IFN-γ treatment

IFN-γ treatment to modulate the expression of immunologically relevant molecules in pancreatic cancer [30] was performed by the addition of 1000 units of human recombinant IFN-γ (kindly donated by V. Cantone, Roussel Pharma, Milan, Italy) in RPMI medium supplemented with 10% FCS. After 48 h of incubation, cells were washed and analyzed for expression of cell surface antigens by cytofluorimetric techniques.

Cell adhesion assay

In order to verify that integrin expression is associated with functional receptor complexes, we treated cells in 96-well plates (BD, Milan, Italy) with scalar concentration of bovine fibronectin and vitronectin (Sigma, Milan, Italy) from 100 nM to 6.25 nM in 50 μl PBS for 16 h at 4°C. In the control wells, 100 nM polylysine and 100 nM bovine serum albumin (BSA) (Sigma, Milan, Italy) were added. After 24 h, the wells were rinsed in PBS, and all the wells were further treated with 1 mg/ml BSA for 60 min at 37°C. After three washes, 200 μl of cell suspension (2.5×10^5 cells/ml) in RPMI without serum was seeded and incubated 2 h at 37°C. The wells were washed with PBS and treated with 0.25% trypsin, 2 mM ethylene diamine tetraacetic acid to detach the cells that were counted to evaluate the number of adherent cells under the various experimental conditions.

In vitro sensitivity to chemotherapeutic agents

For chemical agent sensitivity, 10^4 cells were seeded in 96-well plates and cultivated overnight in 100 μl RPMI 1640 containing 10% FBS. In the T_0 reference well, the medium was replaced by 100 μl of the same medium containing 10% Alamar blue, and, after 4 h at 37°C, the absorbance at 570 nm and 600 nm was monitored using a ELX808 microplate reader (BIO-TEK, Winooski, VT, USA). The signal to noise ratio was evaluated according to the manufacturer's instructions. The remaining wells were treated with the various chemotherapeutic agents: fluorouracil (5-FU from TEVA Pharma, Milan, Italy) was added at a concentration varying from 2.7 μM to 704 μM; Gemzar (Lilly, Milan, Italy) was added at a concentration varying from 0.003 μM to 43 μM, incubated for 3 h and removed. The cells were then washed once with PBS, and fresh medium was added. After 96 h, the medium was replaced with Alamar blue solution and evaluated as described above.

Tumorigenicity in nu/nu mice

Subconfluent AVC1 cells were trypsinized, and 1×10^6 cells in 0.2 ml of PBS were injected subcutaneously in the left flank in a total of five 5-week-old *nu/nu* Swiss mice weighing 18–22 g (Charles River, Milan, Italy). Fragments of one of the resulting xenografts were also orthotopically implanted in three additional mice, as previously described [33]. The animal research complied with Italian national legislation and with the Verona University policy on the Care and Use of Animals and with related codes of practice.

Results

A cell line was established from an adenocarcinoma of the papilla of Vater excised from a patient undergoing curative resection without previous chemotherapy. The primary neoplasm was a moderately differentiated intestinal type adenocarcinoma.

This cell line was designed as AVC1. When the original explant was kept in culture, the fibroblast contamination was minimal, and the epithelial component began to grow within a few days. The cells were subcultured until they reached about 80% confluency and were cryopreserved at early passages. During the serial passages, the fibroblast component decreased quickly, as judged by immunophenotyping. The cryopreserved cells could be successfully re-cultured and xenografted (see below).

Morphological and growth features

The morphological characteristics of AVC1, its xenograft, and the primary cancer from which they were derived are shown in Fig. 1. The AVC1 cell line showed an adherent growth pattern and a flattened polygonal morphology in accordance with its epithelial origin. Electron microscopy showed the presence of lamellipodia, filopodia, and a rich secretory compartment. The Golgi apparatus and ribosome-rough endoplasmic reticulum were well developed and the cytoplasm was rich in free ribosomes. The cytoskeleton presented tonofilaments and clear microvilli. The doubling time was 24±1 h (n=3) and the colony forming efficiency was 12.1±4% (n=3).

DNA ploidy, chromosomal, and genetic characterization

The cellular DNA content was diploid with a high G_2M phase index (18.7%), as shown by cytofluorimetric analysis. The cytogenetic analysis of AVC1 is shown in Fig. 2 and can be summarized as follows: 48, XX, +del(1)(p10), +?der(1)t(1;18)(p10;p10), ?der(2)t(2;7)(p10;q10), -5, del(6)(q21), +?der(6)t(6;7)(q21;q11), −7, +9, add(11)(p15), +del(11)(q13), add(12)(p13), add(15)(q26), der(14)t (14;?)(p10;?), −14, −15, +17, −20, +mar. A complex karyotype was revealed with the presence of both numerical and structural chromosomal aberrations. The former included monosomies and trisomies, while the pattern of structural abnormalities was complex. A number of different chromosomes were involved in deletion, translocation, and addition of material of unknown origin, and a marker chromosome was present.

Molecular analysis showed the presence of a mutation in codon 12 of the K-*ras* gene (GGT>GAT), while the *p16* gene had de novo promoter methylation. No mutations in *DPC4* or *p53* were found. These latter observations corresponded with the respective presence of Dpc4 and lack of p53 protein expression, as detected by immunohistochemistry (data not shown). This mutational pattern is in agreement with the molecular features found in primary AVC [22].

Immunophenotyping

Immunophenotypic analysis of AVC1 was performed using a panel of epithelial and mesenchymal markers, as well as adhesion and immunologically relevant molecules. These results are detailed in Table 1, Table 2 and Table 3. This analysis confirmed the epithelial nature of AVC1, as it showed cytoplasmic expression of cytokeratins and Ber-EP4 antigens, associated with the absence of immunoreactivity for chromogranin A, S100, and NSE. Under standard culture conditions, indirect immunofluorescence for cell surface molecules showed that MHC-I and CD95/Fas were expressed, while HLA-DR, CD40, CD80, CD86 (B7–1 and B7–2), MUC-1, MUC-2, and ICAM-1/CD54 were not expressed. The human B lymphoma Raji and T lymphoma Jurkat cell lines were used as positive controls for expression levels of most of the different cell surface molecules considered in the present study.

IFN-γ treatment

Treatment with IFN-γ increased the expression levels of MHC-I and CD95/Fas, while HLA-DR and MUC-1 became apparent.

Cell adhesion assay

In order to verify that integrin expression is associated with functional receptor complexes, we tested the cell

Fig. 1 Morphology of ampulla of Vater cancer (AVC)1 cells, its xenograft, and primary cancer. AVC1 cells display epithelial morphology, adhesion to the surface, and large nucleoli (**a**, phase contrast image ×40), immunocytochemical positivity for cytokeratin 9–19 (**b**), nuclei with marginated chromatin (**c**, ×3.5K) and tonofilaments (**c1**, ×14K) at transmission electron microscopy; filopodia (**d**, ×5K) and a particular of lamellopodia (**d1**, ×20K) are also evident at scanning electron microscopy. The hematoxylin-eosin stains (**e** and **f**, ×10; **g** and **h**, ×40) of formalin-fixed, paraffin-embedded samples show that the xenograft (**e**, **g**) retains the morphological features of the primary cancer from which it was derived (**f**, **h**)

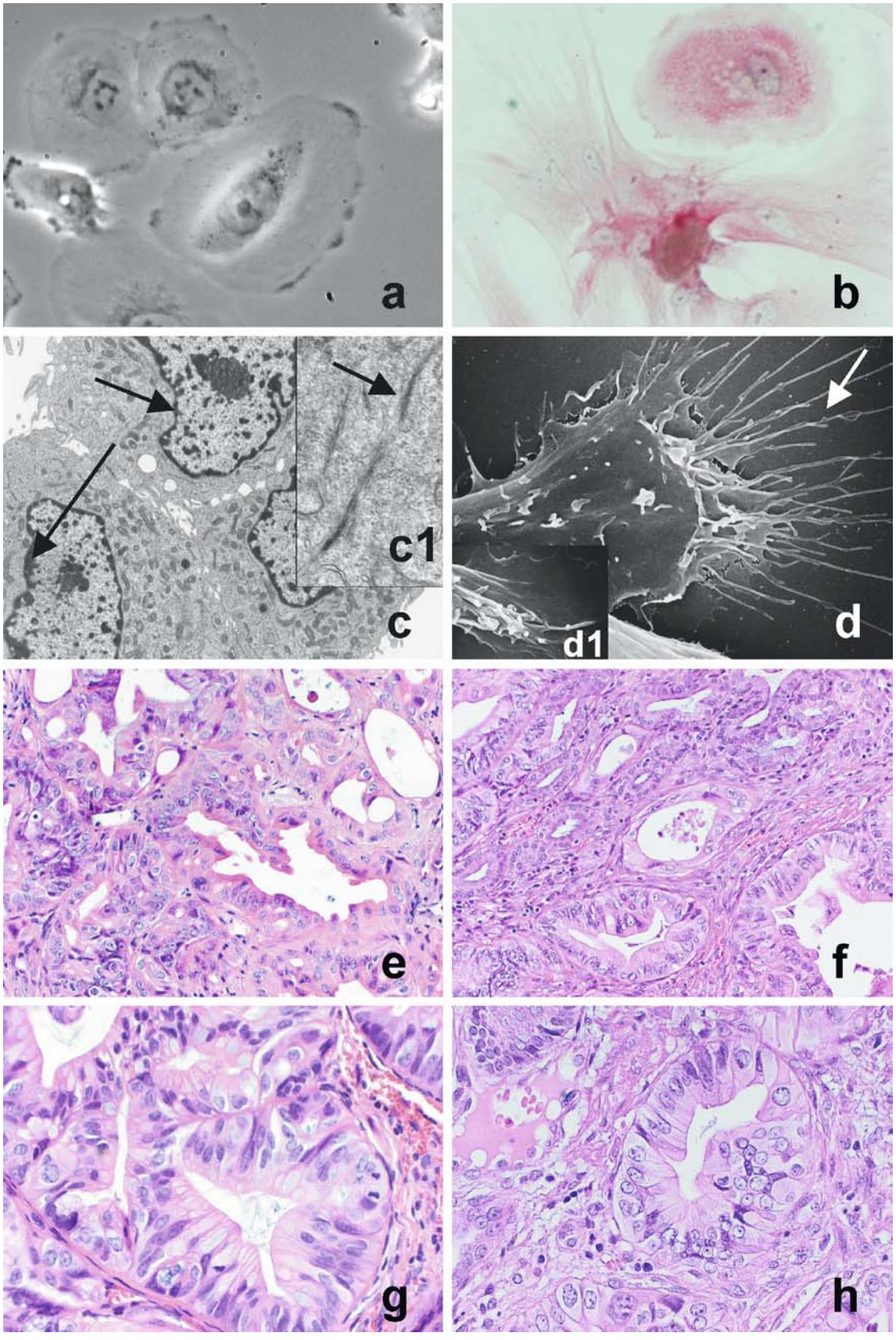
a
b
c1
c
d1
d
e
f
g
h

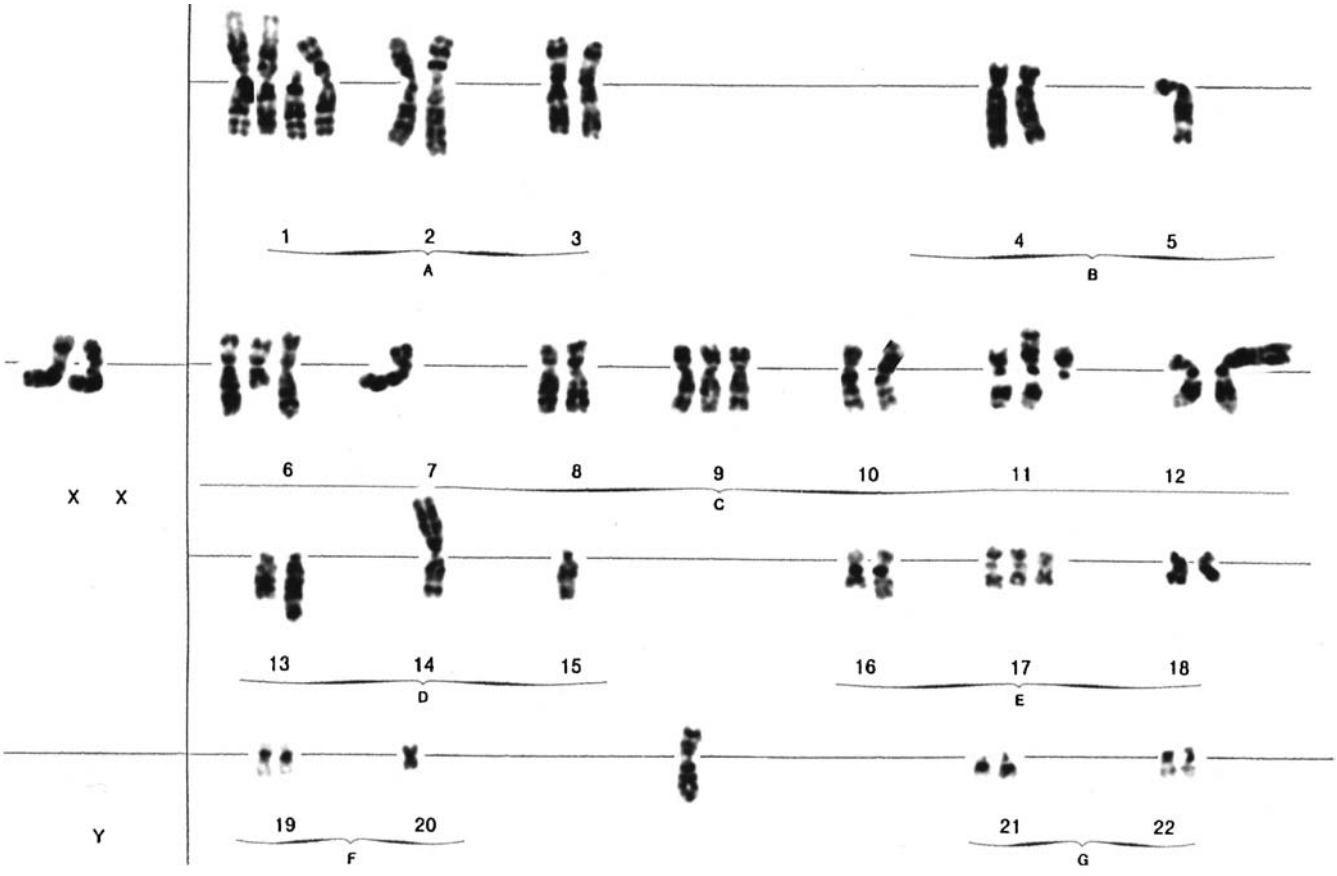

Fig. 2 G-banded karyotype of ampulla of Vater cancer 1

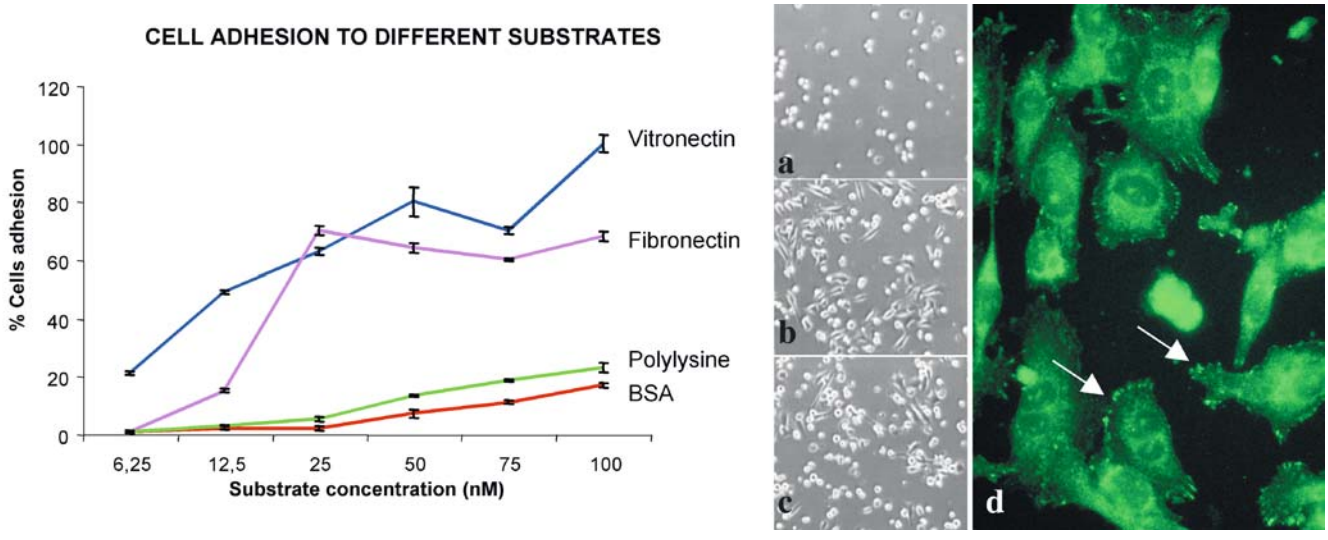

Fig. 3 Ampulla of Vater cancer (AVC)1 cells adhere to extracellular matrix proteins fibronectin and vitronectin. The *left panel* shows the specific binding of AVC1 cells to vitronectin and fibronectin, while no binding was observed with polylysine or bovine serum albumin (*BSA*). The *right panel* shows the adhesion of AVC1 cells to BSA (**a**) with less numerous and rounded shaped cells, to fibronectin (**b**) and vitronectin (**c**) with spread and spindled cells (phase contrast, ×10). Cells adherent to vitronectin (**d**) form adhesion plaques on the cytoplasmic membrane (*arrows*), as shown by indirect immunofluorescence with anti β_3 antibody (×63). Identical results were obtained with anti $\alpha_v\beta_3$ antibody

binding to two purified extracellular matrix proteins, namely, fibronectin and vitronectin. The results of these experiments are shown in Fig. 3 and demonstrated a high affinity of binding to these molecules. No adhesion was observed with either BSA or polylysine. The relatively higher affinity for vitronectin is indicated by the higher percentage of bound cells at a lower substrate concentration. Moreover, this is also substantiated by the formation of adhesion plaques on cell membranes, as shown by indirect immunofluorescence with anti-β_3 and anti-$\alpha_v\beta_3$ antibodies.

Sensitivity to 5-FU and gemcitabine

We evaluated the effect of 5-FU and gemcitabine on AVC1 compared to the ductal adenocarcinoma cell lines PANC-1, CF-PAC1, and PACA 44. The results are detailed in Table 4 and show that AVC1 did not demonstrate any particular sensitivity to these compounds. This is at variance with CFPAC1 and PACA44, which showed higher sensitivity to GMZ or 5-FU, respectively.

AVC1 grows in nu/nu mice

AVC1 cell suspension was injected subcutaneously in five nu/nu mice. Four implants were successful (80% take rate). The histological appearance of the xenografted cancers resembled that of the primary tumor (Fig. 1). Tumor fragments isolated from one of the xenografts were implanted orthotopically in three additional mice and grew in one.

Discussion

AVC are often encompassed within neoplasms arising in other periampullary structures, which include the duodenum, pancreatic head, and extraduodenal bile duct. As such, ampullary cancers are often grouped together with other malignancies. They are classically included by surgeons within the operational entity "periampullary carcinomas" and by clinicians among the extrahepatic bile-duct cancers (International Classification of Diseases for Oncology, ICD-O=156) [23]. This has rendered it extremely difficult to compare the results of different clinicopathological and molecular studies. However, the comparable histopathological characteristics of epithelial tumors arising in this region and the advanced stage at which most cases are diagnosed prevent a precise definition of the structure of origin. The exact site of origin can only be determined in small lesions. Only the study of well-defined series of periampullary tumors will allow for an unraveling of the specific features of their molecular pathogenesis, clinical behavior, and similitude to other cancers arising from the periampullary area.

However, the study of primary cancers is particularly difficult in the case of small lesions. In fact, the amount of tissue is scarcely sufficient for diagnostic purposes, and fresh or frozen material is available only in a very limited number of cases. The availability of cell lines may help to overcome this limitation and also allows one to perform molecular, cell biology, and pharmacological studies. Ideally, cellular models should also be representative of the different histological and molecular subtypes displayed in primary cancers.

A total of 13 cell lines have been established from biliary duct cancers [14], and numerous pancreatic adenocarcinoma cell lines are available. However, only two cell lines have been described from AVC [14]. Our cell line was derived from a moderately differentiated cancer and is characterized by a K-*ras* mutation, wild-type *p53*, and a methylated *p16* gene. The two other existing AVC cell lines were derived from poor and well-differentiated tumors, have wild-type K-*ras*, and also harbor mutations in p53; one of these cell lines had homozygous deletion of *p16*. All three AVC cell lines have wild type *DPC4*. Thus, of the three available AVC cell lines, a different spectrum of molecular mutations and differentiation is present, which is fairly representative of the molecular alterations found in primary AVC.

To date, the most frequent molecular alterations in sporadic ampullary neoplasms include aberrations in the *ras* family and *p16* genes in about 40% and 25% of cases, respectively [12, 22, 28]. The *p53* gene is inactivated in roughly 60% of cases [26, 28]. Similar to other gastrointestinal malignancies, microsatellite instability is present in roughly 10% of AVC and is also associated with favorable prognosis [2, 28].

The karyotype of AVC1 revealed numerous chromosomal rearrangements, in addition to chromosomal loss and duplication. This is a common feature of epithelial cancers, whose genome is highly unstable. It is worth noting the loss of one copy of chromosome 5 in our cell line, a feature that has been previously reported as characteristic in AVC [3]. It has been suggested that among different pancreatic tumor types, only adenocarcinomas arising from the ampulla of Vater have molecular features that are similar to common ductal adenocarcinoma [22]. However, the limited molecular information available for ampullary cancers also suggests that they may show some genetic similarities to gastric cancer [3].

In AVC1, treatment with INFγ resulted in upmodulated expression of HLA I, whereas expression of HLA-DR was observed only after treatment with INFγ. This finding is of interest, as the reduction or complete loss in the expression of MHC class I molecules is common to many tumors of different origin and is frequently accompanied by an increase in the growth rate and metastasizing ability [7, 30].

Adhesion molecules are also involved in several important epithelial cell functions. Indeed, cell proliferation is controlled not only by soluble mitogens, but also by components of the extracellular matrix, such as

fibronectin, to which cells adhere via the integrin family of transmembrane receptors [6]. They may also activate a number of cell signaling cascades that influence a range of biological processes, including cell growth, differentiation, migration, and apoptosis [29]. AVC1 cells express a large repertoire of integrin chains and, in our functional assay, bind to the extracellular matrix proteins fibronectin and vitronectin in a dose-dependent manner. Moreover, it has been recently found that association of active ERK1 with avß3 integrin is necessary for these cells to spread effectively on vitronectin and, thus, may define a mechanism whereby a growth factor-activated signaling pathway can directly influence integrin function [24]. Our results indicate that this pathway is constitutively active in AVC1.

Expression of MUC apomucins, and in particular MUC-1, has been found in various adenocarcinomas of distinct origin, exerting inhibitory effects on the immune response [4]. Expression of MUC-1 apomucin has been reported in ducts and acini of normal pancreas and is constantly expressed during the process of ductal neoplastic transformation, while MUC-2 expression is not observed [35]. The expression of MUC-1 has also been associated with mucinous tumors of the pancreas and, in particular, the invasive components of intraductal papillary mucinous tumors [17, 18, 36]. MUC-2 is ectopically expressed by mucinous carcinomas of the colon, pancreas, breast, and ovary [9]. This marker is, therefore, linked to the mucinous phenotype and, perhaps unsurprisingly, is not expressed in AVC1.

Of clinical interest, while surgery is the treatment of choice for patients with AVC, chemotherapy based on 5-FU is also used [11, 15, 19, 20]. Nonetheless, due to the lack of suitable cellular models, neither the in vitro or in vivo efficacy of the most widely used pharmacological regimens against this tumor entity has been established. In vitro, we detected moderate to low sensitivity to both 5-FU and gemcitabine, at variance with much higher sensitivity displayed by the pancreatic carcinoma cell lines. The demonstration that this cell line can be xenografted also shows that it is a suitable model for pre-clinical studies.

Acknowledgements This study was supported by grants from the Associazione Italiana Ricerca Cancro (AIRC) to A.S., Milan, Italy; Fondazione Cassa di Risparmio di Verona (Bando 2001); Ministero Università e Ricerca (Cofin 2002068231–2001068593), and Ministero Salute, Rome, Italy; European Community Grant QLG1-CT-2002–01196.

References

1. Accolla RS, Gross N, Carrel S, Corte G (1981) Distinct forms of both alpha and beta subunits are present in the human Ia molecular pool. Proc Natl Acad Sci U S A 78:4549–4551
2. Achille A, Biasi MO, Zamboni G, Bogina G, Iacono C, Talamini G, Capella G, Scarpa A (1997) Cancers of the papilla of Vater: mutator phenotype is associated with good prognosis. Clin Cancer Res 3:1841–1847
3. Achille A, Baron A, Zamboni G, Di Pace C, Orlandini S, Scarpa A (1998) Chromosome 5 allelic losses are early events in tumours of the papilla of Vater and occur at sites similar to those of gastric cancer. Br J Cancer 78:1653–1660
4. Agrawal B, Krantz MJ, Reddish MA, Longenecker BM (1998) Cancer-associated MUC1 mucin inhibits human T-cell proliferation, which is reversible by IL-2. Nat Med 4:43–49
5. Allema JH, Reinders ME, van Gulik TM, van Leeuwen DJ, Verbeek PC, de Wit LT, Gouma DJ (1995) Results of pancreaticoduodenectomy for ampullary carcinoma and analysis of prognostic factors for survival. Surgery 117:247–253
6. Danen EH, Yamada KM (2001) Fibronectin, integrins, and growth control. J Cell Physiol 189:1–13
7. Garrido F, Cabrera T, Concha A, Glew S, Ruiz-Cabello F, Stern PL (1993) Natural history of HLA expression during tumour development. Immunol Today 14:491–499
8. Hahn SA, Bartsch D, Schroers A, Galehdari H, Becker M, Ramaswamy A, Schwarte-Waldhoff I, Maschek H, Schmiegel W (1998) Mutations of the DPC4/Smad4 gene in biliary tract carcinoma. Cancer Res 58:1124–1126
9. Hanski C, Hofmeier M, Schmitt-Graff A, Riede E, Hanski ML, Borchard F, Sieber E, Niedobitek F, Foss HD, Stein H, Riecken EO (1997) Overexpression or ectopic expression of MUC2 is the common property of mucinous carcinomas of the colon, pancreas, breast, and ovary. J Pathol 182:385–391
10. Herman JG, Graff JR, Myohanen S, Nelkin BD, Baylin SB (1996) Methylation-specific PCR: a novel PCR assay for methylation status of CpG islands. Proc Natl Acad Sci U S A 93:9821–9826
11. Hoffman JP, Cooper HS, Young NA, Pendurthi TK (1998) Preoperative chemotherapy of chemoradiotherapy for the treatment of adenocarcinoma of the pancreas and ampulla of Vater. J Hepatobiliary Pancreat Surg 5:251–254
12. Howe JR, Klimstra DS, Cordon-Cardo C, Paty PB, Park PY, Brennan MF (1997) K-ras mutation in adenomas and carcinomas of the ampulla of vater. Clin Cancer Res 3:129–133
13. Klempnauer J, Ridder GJ, Pichlmayr R (1995) Prognostic factors after resection of ampullary carcinoma: multivariate survival analysis in comparison with ductal cancer of the pancreatic head. Br J Surg 82:1686–1691
14. Ku JL, Yoon KA, Kim IJ, Kim WH, Jang JY, Suh KS, Kim SW, Park YH, Hwang JH, Yoon YB, Park JG (2002) Establishment and characterisation of six human biliary tract cancer cell lines. Br J Cancer 87:187–193
15. Lee JH, Whittington R, Williams NN, Berry MF, Vaughn DJ, Haller DG, Rosato EF (2000) Outcome of pancreaticoduodenectomy and impact of adjuvant therapy for ampullary carcinomas. Int J Radiat Oncol Biol Phys 47:945–953
16. Lemonnier FA, Rebai N, Le Bouteiller PP, Malissen B, Caillol DH, Kourilsky FM (1982) Epitopic analysis of detergent-solubilized HLA molecules by solid-phase radioimmunoassay. J Immunol Methods 54:9–22
17. Luttges J, Zamboni G, Longnecker D, Kloppel G (2001) The immunohistochemical mucin expression pattern distinguishes different types of intraductal papillary mucinous neoplasms of the pancreas and determines their relationship to mucinous noncystic carcinoma and ductal adenocarcinoma. Am J Surg Pathol 25:942–948
18. Luttges J, Feyerabend B, Buchelt T, Pacena M, Kloppel G (2002) The mucin profile of noninvasive and invasive mucinous cystic neoplasms of the pancreas. Am J Surg Pathol 26:466–471
19. Mehta VK, Fisher GA, Ford JM, Poen JC, Vierra MA, Oberhelman HA, Bastidas AJ (2001) Adjuvant chemoradiotherapy for "unfavorable" carcinoma of the ampulla of Vater: preliminary report. Arch Surg 136:65–69
20. Mehta VK, Poen JC, Ford JM, Oberhelman HA, Vierra MA, Bastidas AJ, Fisher GA (2001) Protracted venous infusion 5-fluorouracil with concomitant radiotherapy compared with bolus 5-fluorouracil for unresectable pancreatic cancer. Am J Clin Oncol 24:155–159

21. Moore P, Sipos B, Orlandini S, Sorio C, Real F, Lemoine N, Gress T, Bassi C, Klöppel G, Kalthoff H, Löhr M, Scarpa A (2001) Genetic profile of 22 pancreatic carcinoma cell lines: analysis of K-ras, p53, p16 and DPC4/Smad4. Virchows Arch 439:798–802
22. Moore PS, Orlandini S, Zamboni G, Capelli P, Rigaud G, Falconi M, Bassi C, Lemoine NR, Scarpa A (2001) Pancreatic tumours: molecular pathways implicated in ductal cancer are involved in ampullary but not in exocrine nonductal or endocrine tumorigenesis. Br J Cancer 84:253–262
23. Percy C, van Holten V, Muir C (eds) (1990) International classification of diseases for oncology (ICD-O), 2nd edn. World Health Organization, Geneva
24. Roberts MS, Woods AJ, Shaw PE, Norman JC (2002) ERK1 associates with alpha vbeta 3 integrin and regulates cell spreading on vitronectin. J Biol Chem 278:1975–1985
25. Roder JD, Schneider PM, Stein HJ, Siewert JR (1995) Number of lymph node metastases is significantly associated with survival in patients with radically resected carcinoma of the ampulla of Vater. Br J Surg 82:1693–1696
26. Scarpa A, Capelli P, Zamboni G, Oda T, Mukai K, Bonetti F, Martignoni G, Iacono C, Serio G, Hirohashi S (1993) Neoplasia of the ampulla of Vater. Ki-ras and p53 mutations. Am J Pathol 142:1163–1172
27. Scarpa A, Zamboni G, Achille A, Capelli P, Bogina G, Iacono C, Serio G, Accolla RS (1994) ras-family gene mutations in neoplasia of the ampulla of Vater. Int J Cancer 59:39–42
28. Scarpa A, Di Pace C, Talamini G, Falconi M, Lemoine NR, Iacono C, Achille A, Baron A, Zamboni G (2000) Cancer of the ampulla of Vater: chromosome 17p allelic loss is associated with poor prognosis. Gut 46:842–848
29. Schwartz MA, Baron V (1999) Interactions between mitogenic stimuli, or, a thousand and one connections. Curr Opin Cell Biol 11:197–202
30. Scupoli MT, Sartoris S, Tosi G, Ennas MG, Nicolis M, Cestari T, Zamboni G, Martignoni G, Lemoine NR, Scarpa A, Accolla RS (1996) Expression of MHC class I and class II antigens in pancreatic adenocarcinomas. Tissue Antigens 48:301–311
31. Shirai Y, Tsukada K, Ohtani T, Koyama S, Muto T, Watanabe H, Hatakeyama K (1995) Carcinoma of the ampulla of Vater: histopathologic analysis of tumor spread in Whipple pancreatoduodenectomy specimens. World J Surg 19:102–106
32. Sipos B, Moser S, Kalthoff H, Torok V, Lohr M, Kloppel G (2003) A comprehensive characterization of pancreatic ductal carcinoma cell lines: towards the establishment of an in vitro research platform. Virchows Arch 442:444–452
33. Sorio C, Bonora A, Orlandini S, Moore PS, Capelli P, Cristofori P, Dal Negro G, Marchiori P, Gaviraghi G, Falconi M, Pederzoli P, Zamboni G, Scarpa A (2001) Successful xenografting of cryopreserved primary pancreatic cancers. Virchows Arch 438:154–158
34. Talamini MA, Moesinger RC, Pitt HA, Sohn TA, Hruban RH, Lillemoe KD, Yeo CJ, Cameron JL (1997) Adenocarcinoma of the ampulla of Vater. A 28-year experience. Ann Surg 225:590–599
35. Terada T, Ohta T, Sasaki M, Nakanuma Y, Kim YS (1996) Expression of MUC apomucins in normal pancreas and pancreatic tumours. J Pathol 180:160–165
36. Yonezawa S, Taira M, Osako M, Kubo M, Tanaka S, Sakoda K, Takao S, Aiko T, Yamamoto M, Irimura T, Kim YS, Sato E (1998) MUC-1 mucin expression in invasive areas of intraductal papillary mucinous tumors of the pancreas. Pathol Int 48:319–322
37. Zhang SY, Klein-Szanto AJ, Sauter ER, Shafarenko M, Mitsunaga S, Nobori T, Carson DA, Ridge JA, Goodrow TL (1994) Higher frequency of alterations in the p16/CDKN2 gene in squamous cell carcinoma cell lines than in primary tumors of the head and neck. Cancer Res 54:5050–5053

Virchows Arch (2004) 444:278–282
DOI 10.1007/s00428-003-0927-7

ORIGINAL ARTICLE

Dirk J. Ruiter · Borghild Roald · James Underwood · Jaime Praton behalf of the UEMS Section of Pathology/European Board of Pathology

Histopathology training in Europe: a lesson for other specialties?

Received: 4 September 2003 / Accepted: 17 October 2003 / Published online: 2 December 2003

Abstract Critical shortages of trained histopathologists limit the capacity of cancer and other clinical services. A survey of histopathology training in 18 European countries conducted by the European Union of Medical Specialists Section of Pathology/European Board of Pathology revealed a considerable shortage of both trained and trainee histopathologists in several of the responding countries. Demographic data indicate a high preponderance of trained histopathologists over 55 years of age and a notable proportion of part-time personnel. Although the training capacity in some countries has been increased, the immediate future of histopathology and the clinical services dependent on the specialty is worrisome. The histopathology workload is growing, and, in some countries, recruitment of trainees is insufficient for future needs. To avert the serious consequences for dependent clinical specialties and their patients, there should be a concerted European action to promote and expand histopathology training.

Keywords Histopathology · Training · Europe

D. J. Ruiter (✉)
Department of Pathology, University Medical Center,
St. Radboud Nijmegen, P.O. Box 9101,
6500 HB Nijmegen, The Netherlands
e-mail: d.ruiter@pathol.umcn.nl
Fax: +31-24-3540520

B. Roald
Department of Pathology,
Ullevål University Hospital, Oslo, Norway

J. Underwood
Department of Pathology,
University of Sheffield Medical School, Sheffield, UK

J. Prat
Department of Pathology,
Hospital de Sant Pau, Barcelona, Spain

Introduction

Histopathology is the medical discipline involved with diagnosis and research of diseases based on the examination of cells and tissues in a clinical context. Histopathology is essential for the diagnosis and treatment of serious common diseases, such as cancer and chronic inflammatory disorders and is fundamental for the education of medical students and postgraduates. The shortage of histopathologists reported in some European countries and the USA [6, 10] is worrisome. As medical specialists who have European Union (EU) nationality enjoy unrestricted movement among EU countries, the histopathology workforce problem also has a European dimension.

The European Union of Medical Specialists (UEMS) is an official organisation representing postgraduate medical training and practice in the EU. It represents the various national authorities of medical specialists from the member and candidate countries and some other European countries, e.g. Norway and Switzerland [5, 12]. The objectives of the UEMS include the promotion of high standards of patient care through the harmonisation and improvement of postgraduate specialist training and continuing medical education. The UEMS sections, including that of pathology, have produced charters on specialist training, inspection of training programs and continuing medical education. With this remit, the section of pathology, which also acts as the European Board of Pathology, examined the magnitude of the shortage of histopathologists by performing a survey among the member nations using a questionnaire.

Materials and methods

Survey

A questionnaire containing 28 questions was sent in early 2002 to the delegates of all 19 member nations, pre-accession states and associated countries. The questionnaire surveyed the number of trained histopathologist (e.g. consultant) positions and vacancies, the number of histopathology trainee positions and vacancies, the future training capacity, the age and sex distribution of histopathol-

ogists and trainees, the ratio of trained staff to trainees, the length of training, exchange of trainees with other institutions, quality assessment of the training programme, opportunities for subspecialisation and research opportunities. Luxembourg, as the smallest country in the EU, was not able to respond, as it has no training programme in histopathology. The response to some issues was incomplete, as recording of histopathology workforce planning and training is not operational in several countries. In order to verify the quality of the responses, they were discussed in detail during the annual meeting of the Section/Board in Ljubljana, Slovenia, May 2002. The final version of the paper was approved by all delegates; their names and member states are listed in the Acknowledgements.

Results

The number of trained histopathologists and trainees per country is given in Table 1. The number of trained histopathologists varies from 14 per million inhabitants (Turkey) to 50 per million inhabitants (Norway). The ratio of trainee positions to trained positions varies from 6% (France) to 67% (Ireland). The length of training in most countries is 5 years, with exceptions in Spain and Turkey (4 years), the UK (5.5 years) and Austria and Germany (6 years). As shown in Table 2, in all of the eight responding countries, vacancies for trained histopathologists exist and are most extreme in Finland, Norway, Sweden, the UK and Turkey. As illustrated in Table 3, a similar pattern is observed for pathology residents in 6 of 11 responding countries. Here, the situation is most serious in Greece, France, Norway, Denmark and Portugal. With the exception of Belgium, where the training capacity has decreased, it is either stable or has increased.

Regarding age distribution, 20% or more of the histopathologists are 55 years or older in all of the eight responding countries, and most are male. With the exception of Finland, Ireland, the Netherlands, Spain and UK, where the number of female trainees equals that of male trainees, in the other countries, an excess of female histopathology trainees is observed (Table 4). In

Table 2 Trained staff vacancies in 2002

<5%: One (Switzerland)
5–10%: Two (Denmark, Netherlands)
>10%: Five (Finland, Norway, Sweden, Turkey, United Kingdom)
Unknown: Ten countries

Table 3 Trainee vacancies in 2002

None: Five (Belgium, Finland, Netherlands, Switzerland, Turkey)
0–10%: One (United Kingdom)
20–30%: Two (Denmark, Portugal)
30–40%: Two (France, Norway)
>40%: One (Greece)
Unknown: Seven countries

Table 4 Demographic data of trained histopathologists and trainees

Age >55 years:
20–30%: Two (Finland, Italy)
30–40%: Four (Denmark, Sweden, Switzerland, Turkey)
40–50%: Two (Germany, Greece)

Gender:
Trained staff: male>female (*n*=5), male<female (*n*=4)
Trainees: male<female (*n*=9), male=female (*n*=5), male>female (*n*=1)

Table 1 Number and proportion of staff pathologists and residents

Country	Trained staff positions (A)	Trainee positions (B)	Duration of training (years)	Ratio B:A (%)	Inhabitants C (millions)	Ratio A:C (per million)
Austria	250	40	6	16	8	31
Belgium	205	55	5	27	10	21
Denmark	170	45	5	26	5	34
France	1650	94	5	6	62	27
Finland	150	30	5	20	5	30
Germany	1300	300	6	23	85	15
Greece	400	90	5	23	10	40
Ireland	90	60	5	67	4	23
Italy	1800	240	5	13	58	31
Norway	148	62	5	42	4	37
Netherlands	300	72	5	24	16	19
Portugal	200	50	5	25	10	20
Slovenia	60	10	5	17	2	30
Spain	1400	160	4	11	40	35
Sweden	190	40	5	21	9	21
Switzerland	180	60	5	33	7	26
Turkey	900	280	4	31	65	14
United Kingdom	1436	436	5.5	30	55	26
Total	10829	2124			455	
Average	605	118	5	25	25	27
Maximum	1800	436	6	67	85	50
Minimum	60	10	4	6	2	14

Table 5 Quality criteria of histopathology training

Criteria	Countries
Mandatory courses only	None
Site visits only	Spain
Exit examination only	Greece, Italy, Portugal, Turkey,
Mandatory courses and site visits	None
Mandatory courses and exit examination	Denmark, France*, Norway, Netherlands, Sweden
Site visits and exit examination	Austria, Belgium, Finland, Greece, Switzerland
All three criteria	Ireland, United Kingdom, Slovenia

* Site visits are optional

all responding countries, the number of trained histopathologists outnumbers that of the trainees.

The quality parameters of histopathology training, i.e. mandatory courses, site visits and exit examinations, are listed in Table 5. In 11 countries, two of the three parameters are used; in 6 countries, only one is used.

Mandatory exchange of trainees with other institutions exists in Switzerland only; it occurs occasionally in other countries, such as Belgium. Most countries have a positive attitude towards international exchange, and some, where there is a considerable shortage of residents, would strongly favour an influx of foreign physicians in their training programme. Some countries are somewhat reluctant, as they fear communication problems due to language incompatibilities.

Formal recognition of subspecialisation was required in Finland until 2002 (i.e. neuropathology and paediatric pathology) and still exists in Switzerland (i.e. neuropathology, cytopathology and molecular pathology) and Turkey (i.e. cytopathology, dermatopathology and neuropathology). In most countries, subspecialisation is optional in the final stage of the training, and it is not formally recognised. Research opportunities are present in most countries, and some (The Netherlands, Norway) have integrated training/research tracks.

Discussion

This survey, distributed among 18 European countries and performed in early 2002, reveals a larger than expected variation in the number of trained pathologists among EU countries. The number of trained pathologists is the net result of various factors, such as the capacity and efficacy of the training programme, the workload-derived parameters to fill vacant trained positions and to establish new ones, the length of the working period, the proportion of part-time workers and the degree of voluntary anticipated retirement. In addition, the registration of the trained staff positions may not be complete, and, in some countries, "anatomical" and "clinical" pathologists are not separately listed.

Although it is difficult to make an unequivocal interpretation, some useful comments can be made. The very low number of trained pathologists observed in one south European country (Turkey) may reflect the underestimated position of the specialty here. Surprisingly, some other countries with long-standing reputations in histopathology (Germany, The Netherlands, Portugal, Sweden and Ireland) have a very low (Germany) or relatively low number of trained staff positions. This may be due to a restrictive workforce planning executed by the professional organisations and/or the government or total lack of workforce planning. The ratio of trainee to trained staff positions is extremely low in one country (France), and very low in two (Spain and Italy), which seems incompatible with adequate workforce planning. The relatively higher proportion of trainees (but below average) in Germany and the Netherlands also are not sufficient for these purposes, due to a very low or low number of trained staff positions. For verification of the data, the number of vacancies was requested from all countries. This revealed a considerable shortage of trained histopathologists in eight of eight responding countries and an even more alarming shortage of histopathology trainees in 6 of 11 responding countries. The data were obtained through the delegates of the national societies or colleges of pathology, which are reliable sources. Unfortunately, the responses were often incomplete, as proper registration of pathology manpower planning and training is not operational in several countries. As this limits the results of our European survey, we strongly advise the countries involved to rectify this administrative deficit. Moreover, a permanent registration of the number of positions and vacancies per country is necessary for proper monitoring of the manpower planning.

How can we explain the current shortage of trained staff histopathologists and histopathology residents in several European countries? The possible explanations are many, the most important being: (a) the restrictive policy of national governments to create new positions for medical specialists and residents in the past decade; (b) the more demanding workload for histopathologists in terms of an increase in number of specimens and their investigation complexity and (c) the increase of part-time histopathologists. The restriction on the creation of new positions for medical specialists has also led to problems in the workforce planning of other specialties, such as anaesthesiology and medical microbiology. As a late reaction to this crisis, several European countries recently have created new trained staff histopathologist positions and those for trainees, with the notable exception of Belgium. As the Belgian government recently even decided to decrease histopathology positions, it should be strongly advised to adopt the policy of the EU nations

in order to prevent irreparable damage to the clinical services and patients relying on expert histopathology.

The laboriousness and complexity of the histopathologist's work have increased based on the new diagnostic and therapeutic options in cancer, leading to more refined and individually tailored clinically relevant questions, mandatory regulations for documentation and registration of case data and material and the increase in cancer patients due to ageing of the population [2, 7]. In addition, strict quality control measures have to be followed in histopathology services to minimise the risk of misdiagnosis and patient harm, further intensifying the professional burden. Finally, the increase of part-time histopathologists associated with the increasing proportion of female colleagues and elderly senior staff will exacerbate the need for trained histopathologists; this strongly supports the policy to expand the training capacity as already initiated in some European countries. As the shortage of histopathologists in Europe is widely distributed, it cannot be solved by influx from those few countries with a surplus. The UEMS Section of Pathology will, therefore, urge all EU nations to expand and intensify their training programmes. This is already underway in England (UK), which has established several histopathology schools to expand training capacity [3].

Other remarkable findings from our survey were the variation in length of training among the EU countries and the differences in the criteria used to evaluate the quality of the training programme. As the goal of the UEMS is to further harmonise specialist training in Europe [2, 12], these points need further discussion. The length of training was reconfirmed as 5 years in the recently revised charter that was accepted unanimously by all delegates. Harmonisation of the length of training could easily be achieved if the national authorities would adhere to it and if the central EU administration would formally establish it. In contrast, harmonisation of training programmes requires an evolutionary approach in recognition of the long-standing historical arrangements (or lack of them) in some countries. Site visits, obligatory courses and exit examinations are all important factors [13]. Therefore, we propose that harmonisation of two of these three would be sufficient to meet the European standards. This would mean that, at present, six European countries are insufficient on this issue, making further action necessary.

The current shortage of trained histopathologists and trainees in several European countries is a serious matter that not only influences the future of the specialty [9], but also will affect the work of other medical specialties with which histopathology closely collaborates and, most importantly, their patients. If this trend persists, histopathology services may even become the capacity-limiting process for many clinical activities: diagnosis and staging of diseases, screening for premalignant disorders and cancer, quality control of clinical management, education at undergraduate and postgraduate levels, research on clinicopathological issues, development of cellular and molecular methods and pathogenesis. As a consequence, patients may face long waits before hearing a final diagnosis, or they will have to endure uncertainty about the diagnosis, as the expertise needed is not available. Therefore, clinical disciplines and other laboratory-oriented disciplines may seek to take over part of the tasks of the histopathologist [11], while not being optimally trained or equipped, which will imperil patient welfare. As this may affect the quality needed for adequate patient care, the UEMS Section of Pathology/European Board of Pathology will urge for a substantial qualitative and quantitative investment in strengthening histopathology and the supply of trainees. This requires reflection on the primary tasks of histopathology, its future professional and technical developments, its relationship with other clinical [8] and laboratory-oriented specialties [1] and its communication with the public [4]. Currently, discussions on these issues are being held in the UK [9] and among surgical pathologists in the USA [1, 7]. They both illustrate the need to reassess the status of histopathology in the EU in order to guarantee sufficient capacity and quality in clinical services to patients.

Acknowledgements The following representatives of the European Union of Medical Specialists Section of Pathology/European Board of Pathology participated in the survey: Dr. Cecilie Alfsen (Norway), Dr. Anne Marie Bak Jylling (Denmark), Dr. Calypso Barbatis (Greece), Dr. Birgitte Bruun Rasmussen (Denmark), Dr. Nesimi Buyukbabani (Turkey), Prof. dr. Claude Cuvelier (Belgium), Prof. dr. Vincenzo Eusebi (Italy), Prof. dr. Dusan Ferluga (Slovenia), Prof. dr. Nina Gale (Slovenia), Dr. Helena Garcia (Portugal), Prof. dr. Claude Genton (Switzerland), Ms. Gisela Kempny (Germany), Dr. Nigel Kirkham (United Kingdom), Prof. dr. Gamze Mocan Kuzey (Turkey), Dr. D. Laedlein Greilshammer (France), Dr. Peter Kelly (Ireland), Prof. dr. Robert Maurer (Switzerland), Prof. dr. Gregor Mikuz (Austria), Dr. Oscar Nappi (Italia), Prof. dr. Jaime Prat, chairman, (Spain), Prof. dr. Borghild Roald (Norway), Prof. dr. Dirk Ruiter, secretary, (The Netherlands), Prof. dr. Eero Saksela (Finland), Dr. Rene Scheiden (Luxemburg), Prof. dr. W. Schlake (Germany), Prof. dr. Christer Sundstrom (Sweden), Prof. dr. Francoise Thivolet Bejui (France), Prof. dr. Jan van den Tweel (The Netherlands), Prof. James Underwood (United Kingdom), Prof. dr. Alain Verhest, Cytopathology (Belgium). The authors wish to thank Prof. dr. sc. Nives Jonjic (Croatia) for useful comments.

References

1. Becich MJ (2000) The role of the pathologist as tissue refiner and data miner: the impact of functional genomics on the modern pathology laboratory and the critical roles of pathology informatics and bioinformatics. Mol Diagnosis 5:287–299
2. Edwards D, Bell J (2000) Cancer registries—future development and uses in Britain. J Public Health Med 22:216–219
3. Gallagher PJ, Dixon MF, Heard S, Moore JK, West KP (2003) An initiative to reform senior house officer training in histopathology. Hosp Med 64:302–305
4. Hamza S, Anderson P, Reddy VVB, Siegal GP (2001) Use of the internet in pathology resident training and education. Adv Anat Pathol 8:290–297
5. Harvey L, Kennedy TE (2000) Editors' foreword. In: UEMS compendium of medical specialists 2000. Kensington Publishers Ltd., London, p 14
6. Kant JA (2001) A tale of two systems: pathology resident recruitment in and out of the National Resident Matching Program. Hum Pathol 32: 677–679

7. Kirkham N (2000) The pathologist in the 21st century-generalist or specialist? J Clin Pathol 53:7–9
8. Murphy WM (2002) The evolution of the anatomic pathologist from medical consultant to information specialist. Editorial. Am J Surg Pathol 26:99–102
9. Pathological Society of Great Britain and Ireland (2001) Pathological Society of Great Britain and Ireland: future of academic pathology. Report of the residential meeting, Beaconsfield, UK
10. Sobonya RE, Weinstein RS (2001) Pathology manpower: a few rays of sunshine. Editorial. Hum Pathol 32:669–670
11. Stein AA (1975) Is pathology a viable discipline? Hum Pathol 6:525–527
12. Twomey C (2000) The UEMS Compendium 2000: introduction. In: UEMS Compendium of Medical Specialists 2000. Kensington Publishers Ltd., London, pp 15–17
13. Yorke RF (2000) Informed evaluation of pathology residency programs. A guide for pathology resident candidates. Arch Pathol Lab Med 124:853–858

Virchows Arch (2004) 444:283–292
DOI 10.1007/s00428-003-0925-9

ORIGINAL ARTICLE

Takeshi Kashimura · Makoto Kodama · Yuko Hotta · Junichi Hosoya · Kaori Yoshida · Takuya Ozawa · Ritsuo Watanabe · Yuji Okura · Kiminori Kato · Haruo Hanawa · Ryozo Kuwano · Yoshifusa Aizawa

Spatiotemporal changes of coxsackievirus and adenovirus receptor in rat hearts during postnatal development and in cultured cardiomyocytes of neonatal rat

Received: 9 July 2003 / Accepted: 7 October 2003 / Published online: 18 November 2003

Abstract Coxsackievirus B is the most common cause of viral myocarditis and is particularly virulent in neonates and children. Adenovirus is also a leading cause of the disease. The determinant of tropism for both viruses is considered to be the expression of coxsackievirus and adenovirus receptor (CAR) in target organs. However, developmental change and physiological localization of CAR in the heart are unknown. We examined expression levels of CAR in rat hearts by quantitative real-time polymerase chain reaction and Western blot analysis and found that CAR decreased gradually during postnatal development, although CAR was detectable, even in adults. Immunohistochemistry revealed CAR on the whole surface of cardiomyocytes in immature rat hearts. In contrast, CAR was detected predominantly on intercalated disks in the adult heart and was accumulated especially at the contact point between the cultured cardiomyocytes, even though they were prepared from the neonatal rat heart. In conclusion, CAR was expressed abundantly on the whole surface of cardiomyocytes in immature rat hearts. Both the expression level and the localization of CAR are possible determinants of the susceptibility to viral myocarditis of neonates and children.

T. Kashimura (✉) · M. Kodama · K. Yoshida · T. Ozawa · R. Watanabe · Y. Okura · K. Kato · H. Hanawa · Y. Aizawa
Division of Cardiology,
Niigata University Graduate School of Medical and Dental Sciences,
1-754 Asahimachi, 951-8510 Niigata, Japan
e-mail: kashi@med.niigata-u.ac.jp
Tel.: +81-25-2272185
Fax: +81-25-2270774

Y. Hotta · J. Hosoya · R. Kuwano
Genome Science Branch,
Center for Bioresource-Based Researches,
Brain Research Institute, Niigata University,
Niigata, Japan

Keywords Coxsackievirus and adenovirus receptor · Myocarditis · Development · Cardiomyocyte · Intercalated disk

Introduction

Acute myocarditis leads to heart failure and sudden death. The chronic type leads to dilated cardiomyopathy, and both remain major causes of morbidity and mortality, particularly in neonates and children [3, 7, 18, 26, 29]. However, the susceptibility to viral myocarditis at early ages has not been elucidated.

Coxsackievirus B [17, 21] and adenovirus [16] are leading causes of viral myocarditis in humans. It is also well known that acute myocarditis can be produced in neonatal and young mice experimentally with coxsackievirus B [12]. The first step of viral infection requires the binding of virus particles to specific cell surface receptors [37]. Interestingly, the two viruses share a common receptor: the coxsackievirus and adenovirus receptor (CAR) [2, 4, 32].

We reported that CAR plays a role in homophilic cell–cell contact[13] and is expressed in the newborn brain and the heart of rodents [13, 14], but the physiological function of CAR has not yet been clarified. However, CAR has been shown to be an important determinant of efficiency of gene transfer using adenovirus vectors: the expression of CAR in target cells or organs enhanced adenoviral gene transfer in both in vitro and in vivo studies [8, 15, 19, 20, 36]. However, the localization, not the expression level, of CAR is considered much more important for infection [6, 9, 25, 33, 34, 35].

Therefore, CAR is currently related to coxsackievirus and adenovirus myocarditis and adenovirus-mediated gene therapy [27]. While cardiac CAR was formerly reported to be unchanged from neonate to adult [19], recent studies suggested a decrease in adult CAR [10, 14], and the localization of CAR in the heart needs to be

Table 1 Primers used for polymerase chain reaction (PCR) and quantitative real-time PCR (qPCR). *CAR* coxsackievirus and adenovirus receptor

	Primer sequence	Number	Product
CAR1 (PCR)	gaacagaggatcgaaaaagctaaag cattcgacttagattaggggcag	AF109644	969 bp
CAR2 (PCR)	gaacagaggatcgaaaaagctaaag ggtaagcgtacttgaact	AF109643	957 bp
CAR1 (qPCR)	catcctcttctgctgtcataaaaa cattcgacttagattaggggcag	AF109644	280 bp
CAR2 (qPCR)	ctgtcatagggacgctgctt gtaagcgtacttgaact	AF109643	306 bp
ANP	atggatttcaagaacctgctagac gctccaatcctgtcaatcctac	E00698	308 bp
α-Cardiac myosin	acaaggttaaaaacctgacagagg tactgttctgctgactgatgtcaa	X15938	360 bp
N-cadherin	gtcaatgaaaatccttattttgcc aagtaaatagatttgcagcgttcc	X06656	318 bp
Connexin43	aagttcaagtacgggattgaagag gcctttgaagaagacgtagaagag	AB017695	306 bp

studied. We reported that neonatal rat hearts exhibited higher immunoreactivity to anti-CAR antibodies than those of adult hearts [14], but did not focus on the precise localization. CAR was re-expressed on the cell surface of myocytes in diseased hearts, such as explanted human hearts from patients with dilated cardiomyopathy [22] and a rat model of myocardial infarction [10]. However, physiological localization and its developmental change have not been examined. In the present study, we reconfirmed the developmental changes of CAR expression, not only mRNA expression, but also protein expression, in rat hearts, and then, spatiotemporal change of CAR was studied in vivo and in vitro. To avoid nonspecific staining of CAR, we used three anti-CAR antibodies.

Materials and methods

Experimental animals

Lewis rats in the late stage of pregnancy were purchased from Charles River, Japan (Yokohama, Kanagawa, Japan). Newborn rats were fed by their own parents and maintained in our animal facilities. The "Principals of laboratory animal care" (NIH publication no. 85–23, revised 1985) were followed.

Reverse-transcription polymerase chain reaction and quantitative real-time polymerase chain reaction

Rats were sacrificed at birth, at the age of 1 week, 1 month, and 3 months (n=4 for each age) under ether anesthesia, and the hearts were removed. Total RNA was extracted from the ventricles using Trizol reagent (Invitrogen), and reverse transcription was performed with 5 μg of RNA from each sample using random primers (Promega) and M-MLV reverse transcriptase (Gibco). To detect the existence of CAR1, CAR2 [9], and splicing variants that were reported in human [31], 35 cycles of polymerase chain reaction (PCR) was performed with cDNA of an adult (3-month-old) rat heart using KOD-Plus (Toyobo). Primers were placed in the V-like domain and in the alternative parts of 3′ terminals of CAR1 and CAR2 (Table 1, Fig. 1A).

Quantitative real-time PCR (qPCR) on LightCycler (Roche) was performed using LightCycler-FirstStart DNA Master SYBR Green I (Roche) as previously described [11]. Primer lists and the scheme of primers for CAR are shown in Table 1 and Fig. 1A. For making standards for quantification, cDNA from the adult rat heart was amplified with each pair of the primers. The products were directly inserted into the pGEM-T vector (Promega) and the recombinant plasmids were isolated after transforming with Escherichia coli JM109 competent cells (Takara) using the MagExtractor plasmid Kit (Toyobo). The plasmids were diluted with DNase free water in a siliconized tube, including 10 ng/ml MS2 RNA (Roche), to prevent adherence to the tube wall, and were used as the standards.

Preparation of antibodies

Polypeptides composing CAR (a: KIYDNYYPDLK in the V-like domain, b: KTQYNQVPSEDFERAPQ in the cytoplasmic domain, and c: PVMIPAQSKDGSIV at C-terminus of CAR1) were chosen to make polyclonal anti-CAR antibodies (Fig. 1A). Anti-CARa antibodies and anti-CARb antibodies were obtained as previously described [13]. Briefly, the polypeptides were synthesized with additional cystein at the C-terminus, conjugated to keyhole limpet hemocyanin (Calbiochem-Novabichem), and used to immunize white rabbits. The resulting antisera were purified by immunoadsorbent affinity chromatography on CNBr-activated Sepharose 4B (Pharmacia) columns coupled with the peptides. Anti-CAR1 C-terminus antibodies (anti-CARc antibodies) were newly prepared to discriminate CAR1 from CAR2. The C terminal polypeptide of CAR1 was conjugated to keyhole limpet hemocyanin (Calbiochem-Novabichem) with glutaraldehyde and used to immunize white rabbits. Purified antibodies were obtained with the same procedures. Monoclonal anti-α smooth muscle actin (αSMA) antibodies (Sigma), monoclonal anti-pan cadherin antibodies (Sigma), and monoclonal anti-connexin43 antibodies (Chemicon International) were purchased.

Sodium dodecyl sulfate-polyacrylamide gel electrophoresis and Western blot analysis

Ventricular tissue of each age group (n=4) was homogenized in cell lysis buffer [20 mmol/l Tris-HCl pH 8.0, 137 mmol/l NaCl, 2 mmol/l ethylene diamine tetraacetic acid (EDTA), 0.3% sodium dodecyl sulfate (SDS), 0.4% sodium deoxycholate, 1 mmol/l phenylmethylsulfonylfluoride (PMSF), and 1% NP-40], rotated at 4°C overnight, and centrifuged at 15,000×g for 30 min. Then, the

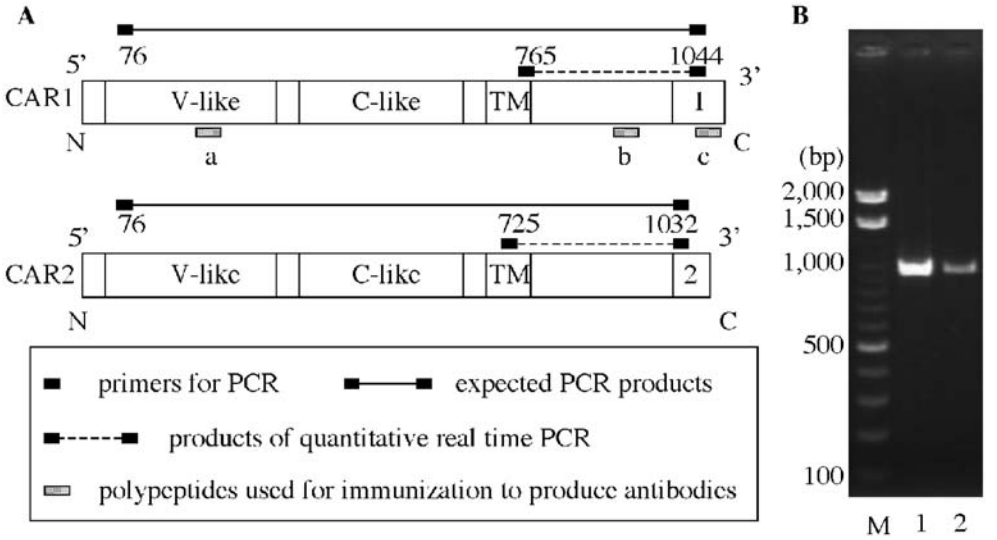

Fig. 1 **A** The design of primers and antibodies. The numbers just beneath or above primers indicate the location in rat coxsackievirus and adenovirus receptor (CAR)1 and CAR2. *V-like* V-like domain. *C-like* C-like domain. *TM* transmembrane domain. *1*, *2* the alternative portions of CAR1 and CAR2. **B** The sizes of polymerase chain reaction products for CAR1 and CAR2 using cDNA from an adult rat heart. A single band was obtained for CAR1 (*1*) and CAR2 (*2*). The sizes were the reasonable and expected ones. *M* size markers

supernatant was stocked at −20°C. After measuring the concentrations of each sample using a DC protein assay kit (Bio-Rad), 10 μg of protein was separated by SDS-polyacrylamide gel electrophoresis (PAGE) (12% acrylamide) and analyzed by immunoblotting with the primary antibodies. Anti-CARa, CARb, and CARc antibodies were diluted to 0.0025 mg/ml, 0.001 mg/ml, and 0.002 mg/ml, respectively. Densitometry was performed for CAR at 46 kDa using computer software (Quantity One, PDI).

Immunohistochemistry and immunofluorescence for tissue samples

The removed hearts of each age group were fixed in Bouin's liquid overnight at 4°C, dehydrated, and embedded in paraffin. Sliced sections (5 micrometers) were prepared on APS coated slides (Matsunami) and deparaffinized. After washing in phosphate-buffered saline (PBS), the slides were heated in 0.01 M citrate buffer (pH 6.0) at 120°C for 20 min in an autoclave, washed three times in PBS, and incubated in methanol containing 0.3% H_2O_2 for neutralizing the endogenous peroxidase. Then, a histofine (R) kit (Nichirei) was diluted with PBS containing 5% skim milk to 1:1 and used for the following procedures. For the detection of CAR, anti-CARc antibodies were chosen based on the results of Western blot analysis to avoid a nonspecific reaction. The antibodies were diluted to 0.002 mg/ml, and normal rabbit immunoglobulin fraction (Dako) was used at the same concentration as the negative control. Visualization was achieved with 3, 3′-diaminobenzidine tetrahydrochloride, and the cell nuclei were counterstained with Mayer's hematoxylin.

Immunofluorescence for CAR was performed using the same methods (without methanol containing 0.3% H_2O_2) until the secondary antibodies, and then, fluorescein isothiocyanate (FITC)-conjugated streptoavidin (Vector, 1/50) was used. Anti-conexin43 antibodies were diluted to 1/500, followed by anti-mouse immunoglobulins labeled with tetramethyl rhodamine isothiocyanate (TRITC) (Dako, 1/50). After the addition of mounting medium (Vector, Vectashield), fluorescent images were obtained using a confocal laser scanning microscope (Fluoview, Olympus).

Primary culture of rat neonatal cardiomyocytes

Cardiomyocytes were prepared from the ventricles of neonatal (3–4 days old) rats by the modified method of Simpson [30]. Briefly, the ventricles were minced and stirred at 37°C in trypsin solution containing 0.1% trypsin (Difco), 0.8% NaCl, 0.04% KCl, 0.1% glucose, and 0.035% $NaHCO_3$. The solution with suspended cells was collected and exchanged every 15 min. The collected solution was added with ice-cold culture medium containing medium199 (Gibco), Ham's F-12 (Gibco), 10% fetal bovine serum (ICN), 0.4% penicillin-streptomycin (Invitrogen), and 0.1 mmol/l 5-bromo-2′-deoxyuridine (Sigma). The suspended cells obtained during the procedures from the second to the seventh cycles were collected by centrifugation at 120×*g*, washed three times with PBS, and resuspended in the culture medium. The cells were cultured for 90 min at 37°C with 5% CO_2 on a flask (Corning), and adherent cells were excluded as fibroblasts. Then, the suspended cells were diluted with the medium at the concentration of 4×10^5 cells/ml and cultured on 6-well cell culture dishes (Iwaki) (1.3×10^3 cells/mm^2) at 37°C with 5% CO_2. The medium was exchanged on day 3.

On days 1, 3, and 7, the wells (n=3) were washed three times with PBS, and only the adherent cells were used as the samples. For preparation of total protein, the wells were agitated with lysis buffer (20 mmol/l Tris-HCl pH 8.0, 137 mmol/l NaCl, 2 mmol/l EDTA, 0.3% SDS, 0.4% sodium deoxycholate, 1 mmol/l PMSF, and 1% NP-40) at room temperature for 10 min and scraped. The contents were rotated at 4°C overnight, and centrifuged at 15,000×*g* for 30 min. Then, the supernatant was stocked at −20°C. For the samples of day 0, the cells suspended prior to starting culturing were used. The cells were washed three times with PBS, and the lysis buffer was added. Total protein was obtained using the same procedures. Then, SDS-PAGE and Western blot analysis were performed as above.

Immunofluorescence for cultured cardiomyocytes

Cardiomyocytes on day 0, prior to starting culturing, were washed three times with PBS, prepared on slides (Matsunami) by Cytospin (Shandon) at 10×*g* for 5 min, and air-dried. For the samples for day 1 and day 2, cardiomyocytes were cultured on collagen I-coated culture slides (Becton Dickinson) at a concentration of 1.1×10^3 cells/mm^2. On day 1 and day 2, the slides were washed three times with PBS, air-dried, and stored at −40°C until the immunofluorescence procedure. The samples were fixed in 4% paraformaldehyde for 20 min, and permeabilized with 0.2% Triton X-100 for 5 min at room temperature. And then, a Histofine (R) kit (Nichirei) was diluted with PBS containing 5% skim milk to 1:1 and used for the following procedures. Anti-CARc antibodies were diluted to 0.002 mg/ml. After washing the secondary antibodies, FITC-conjugated streptoavidin (Vector, 1/50) was used for visualization. Anti-αSMA antibodies, anti-pan cadherin antibodies, and anti-connexin43 antibodies were used at 1/200, 1/500, and 1/500,

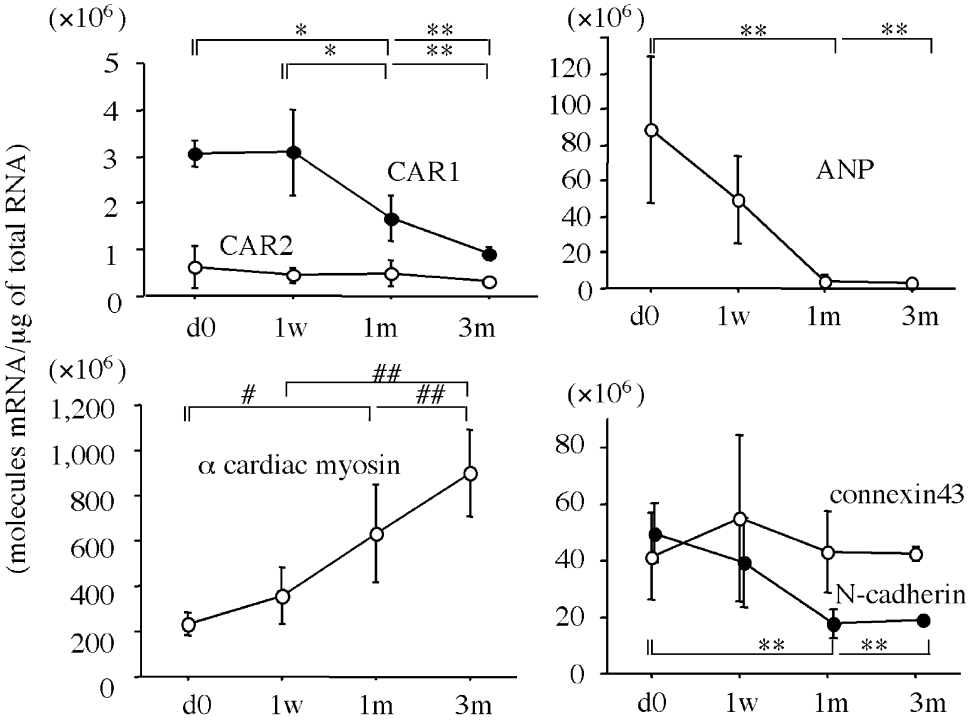

Fig. 2 Expression of cardiac mRNAs during postnatal development. Coxsackievirus and adenovirus receptor (CAR)1 decreased gradually after 1 week, but CAR2 stayed at a lower level. Changes of atrial natriuretic peptide (ANP), α-cardiac myosin, N-cadherin, and conexin43 were also examined as representative mRNAs for fetal phenotypes, adult phenotypes, and intercalated disk molecules. *P<0.05. **P<0.01 by Scheffe test. #P<0.05. ##P<0.01 by the Tukey-Kramer method

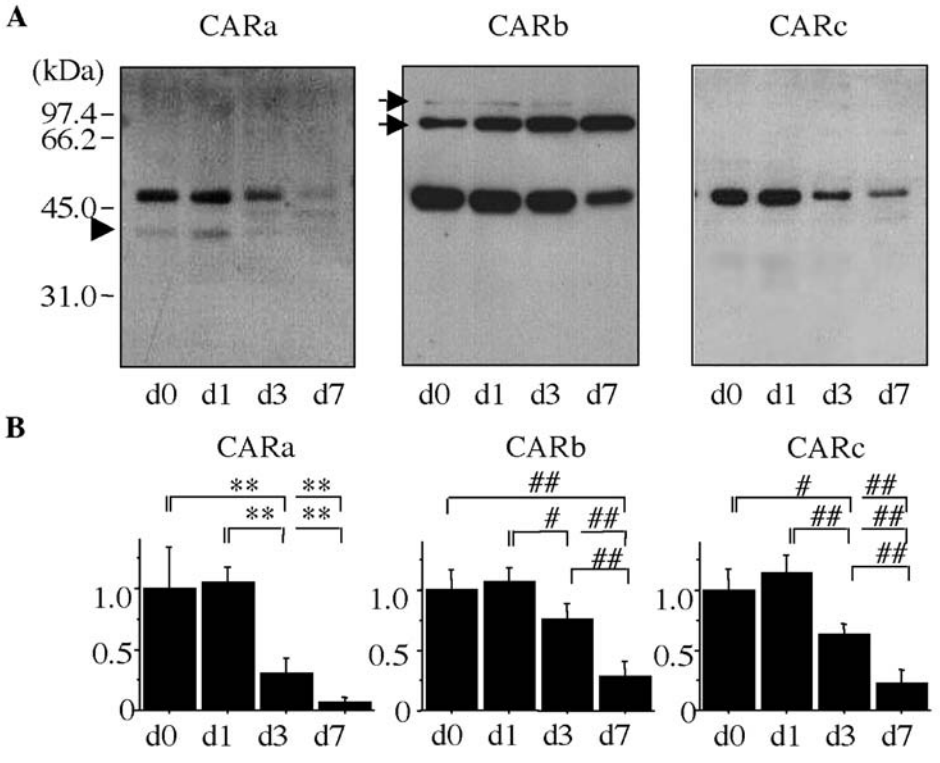

Fig. 3 Expression of coxsackievirus and adenovirus receptor (CAR) and connexin43 proteins during postnatal development. **A** Using three anti-CAR antibodies, CAR was detected at 46 kDa. Anti-CARa and anti-CARb antibodies cross-reacted with other proteins (shown by the *arrowhead* and *arrows*, respectively). Proteins were not identified. Anti-CARc antibodies obviously reacted specifically with CAR. **B** Quantified densitometry. CAR expression relative to day 0 did not change until 1 week after birth. Then, it declined at 1 month and 3 months, and the declines were statistically significant. *P<0.05. **P<0.01 by Scheffe test. #P<0.05. ##P<0.01 by the Tukey-Kramer method

followed by anti-mouse immunoglobulins labeled by TRITC (Dako, 1/50). After the addition of the mounting medium (Vector, VECTASHIELD), fluorescent images were obtained using a confocal laser scanning microscope (Fluoview, Olympus).

Statistical analysis

Values are presented as mean±SD. Statistical analysis was performed by the Tukey-Kramer method, in which SDs of each group were considered equal by the Bartlett test. The Kruskal-Wallis test, followed by the Scheffe test, was used with unequal

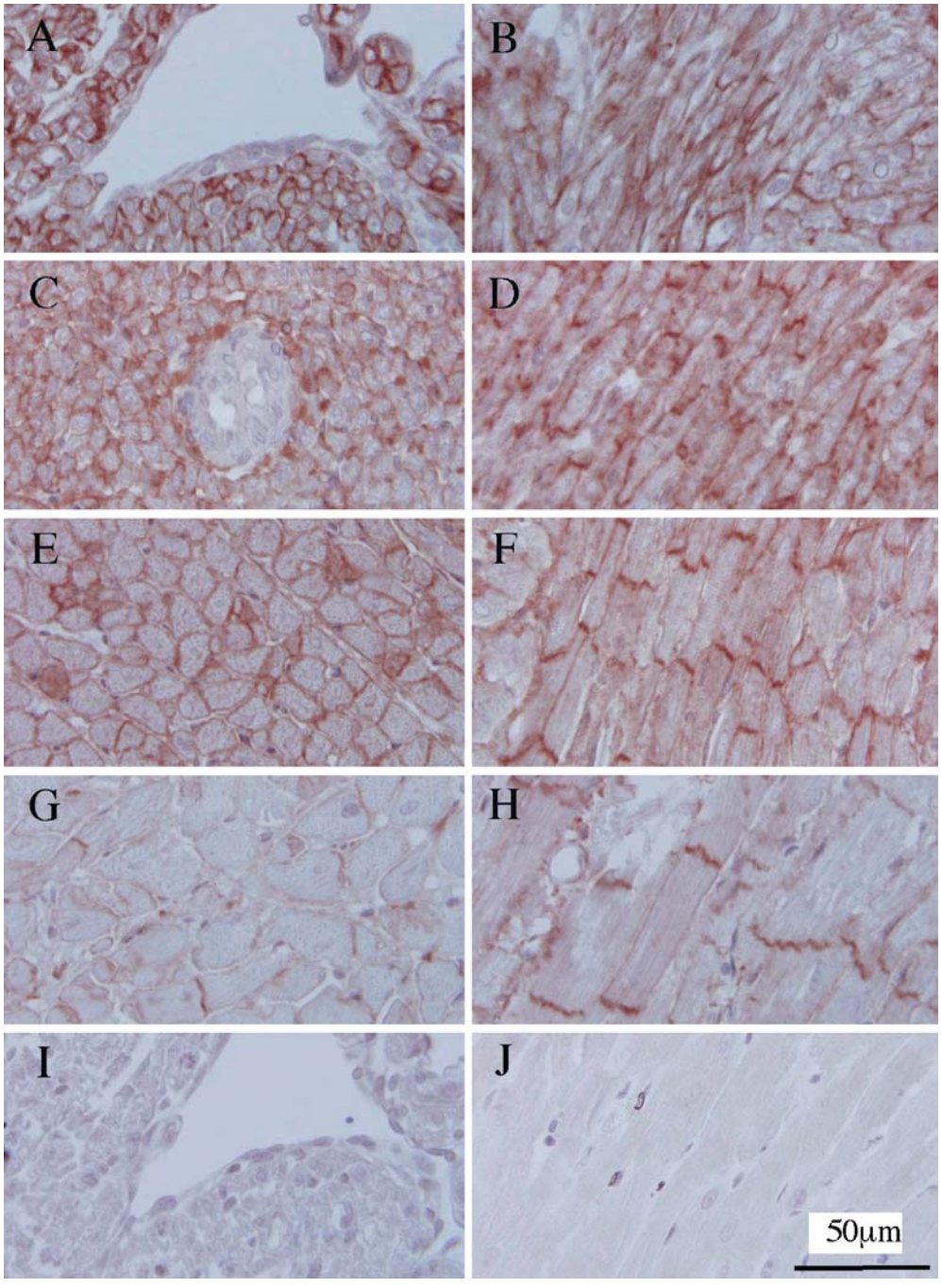

Fig. 4 Imunohistochemistry for coxsackievirus and adenovirus receptor (CAR). The developmental changes in localization of CAR were examined with anti-CARc antibodies. **A**, **B** At birth. **C**, **D** 1 week after birth. **E**, **F** 1 month after birth, **G**, **H** 3 months after birth. **I**, **J** Normal rabbit immunoglobulins were used at the same concentration instead of the anti-CARc antibody as the negative controls for **A** and **H**, respectively. The immunoreactivity of CAR is clearly observed on the whole surface of myocytes at birth. Then, CAR seems to localize predominantly at the intercalated disks. It should be noted that the endocardium (**A**) and the vessel walls (**C**) were free of CAR. Original magnifications, ×600

SDs. The difference was considered statistically significant when the *P* value was less than 0.05.

Results

Expression of mRNA in hearts during postnatal development

The PCR products for CAR1 and CAR2 were detected at expected length, indicating the existence of CAR in adult rat hearts (Fig. 1B). No shorter products, suggesting splicing variants, were detected.

The results of qPCR are shown in Fig. 2. The levels of mRNA of CAR1 were 3.0- to 7.4-fold higher than those of CAR2 throughout the postnatal development. The levels of CAR1 mRNA started to decrease at 1 week after birth. At 1 month of age, the hearts still showed higher levels of CAR1 mRNA ($1.68\pm0.49\times10^6$ molecules mRNA/μg of total RNA) than those at 3 months ($0.91\pm0.14\times10^6$ molecules mRNA/μg of total RNA), although the difference was not statistically significant. However, CAR2 mRNA did not decrease throughout the

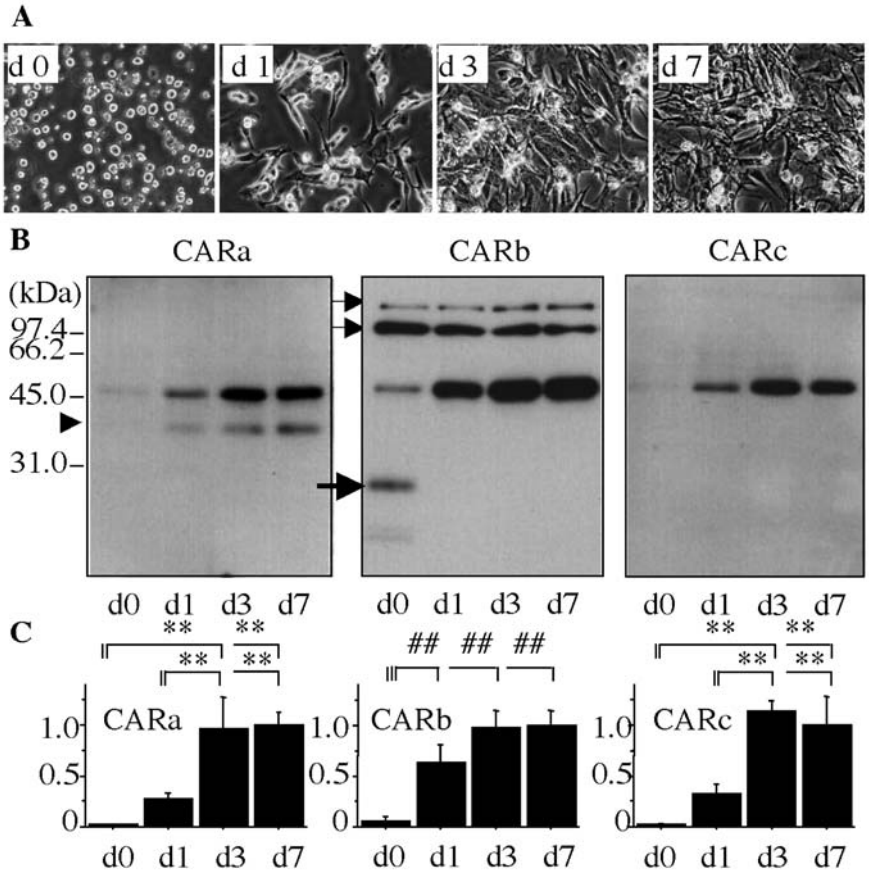

Fig. 5 The culture of cardiomyocytes and expression of coxsackievirus and adenovirus receptor (CAR) protein. **A** Cardiomyocytes were prepared from neonatal rat hearts by trypsin treatment (day 0). Non-adherent cells were removed. From day 0 through day 7, the myocytes grow with increasing intercellular contacts. **B** With three anti-CAR antibodies, CAR was detected at 46 kDa. Anti-CARa antibodies and anti-CARb antibodies cross-reacted with other proteins (*arrowhead* and *thin arrows*, respectively). The smaller band, which detected anti-CARb antibodies (*thick arrow*) was considered to be fragmented CAR. **C** Quantified densitometry. **P*<0.05. ***P*<0.01 by Scheffe test. #*P*<0.05. ##*P*<0.01 by the Tukey-Kramer method

development and stayed at a lower level. CAR1 decreased to 30% at 3 months after birth, and ANP, a typical fetal phenotype, decreased more remarkably to 2.8%. In contrast, α-cardiac myosin, a typical adult phenotype, increased up to 390% at 3 months. N-cadherin, an adhesion molecule, decreased significantly after 1 week of age, similarly to CAR1, but connexin43 did not change during the development.

Expression of CAR protein in hearts during postnatal development

Using three anti-CAR antibodies, bands of CAR were detected at 46 kDa throughout the development, even at 3 months of age (Fig. 3A). Immunoreactivity of each antibody to CAR showed a difference. The anti-CARa antibody showed weaker band expression than other anti-CAR antibodies. Statistical analysis of the results of densitometry revealed significant decreases of CAR from 1 week to 1 month, and 1 month to 3 months (Fig. 3B).

Immunohistochemistry of hearts

In neonatal rat hearts, CAR was stained on almost the whole surface of cardiomyocytes (Fig. 4A, B). The endocardium of the ventricle or the papillary muscles revealed negative staining for CAR (Fig. 4A). Vessel walls were also negative for CAR (Fig. 4C). After birth, polarity of cardiomyocytes began to emerge, and immunoreactivity of CAR became more clear at the sites of intercalated disks as they grew, while immunoreactivity on the non-contacting surface of cardiomyocytes became fainter (1 week: Fig. 4C, D, 1 month: Fig. 4E, F, 3 months: Fig. 4G, H). In the adult heart, CAR was localized predominantly at the intercalated disks (Fig. 4G, H).

Expression of CAR protein in cultured cardiomyocytes

Figure 5A shows the appearances of cultured cells at different stages. The adhesion of cardiomyocytes to the wells was not complete, even after 24 h of culturing, and the density of adhered cardiomyocytes was low. By day 3, most cells adhered to the wells, and the cell density was similar to that of day 7.

Using three anti-CAR antibodies, the bands of CAR were detected at 46 kDa (Fig. 5B). On day 0, cardiomyocytes had lost most of the CAR molecules after treatment in a trypsin solution. The result indicated that most CAR molecules in neonatal rat hearts had existed on the surface of the cells and were digested by trypsin. On day 1, the blot for CAR became apparent, using all three antibodies, although a significant rise was confirmed only

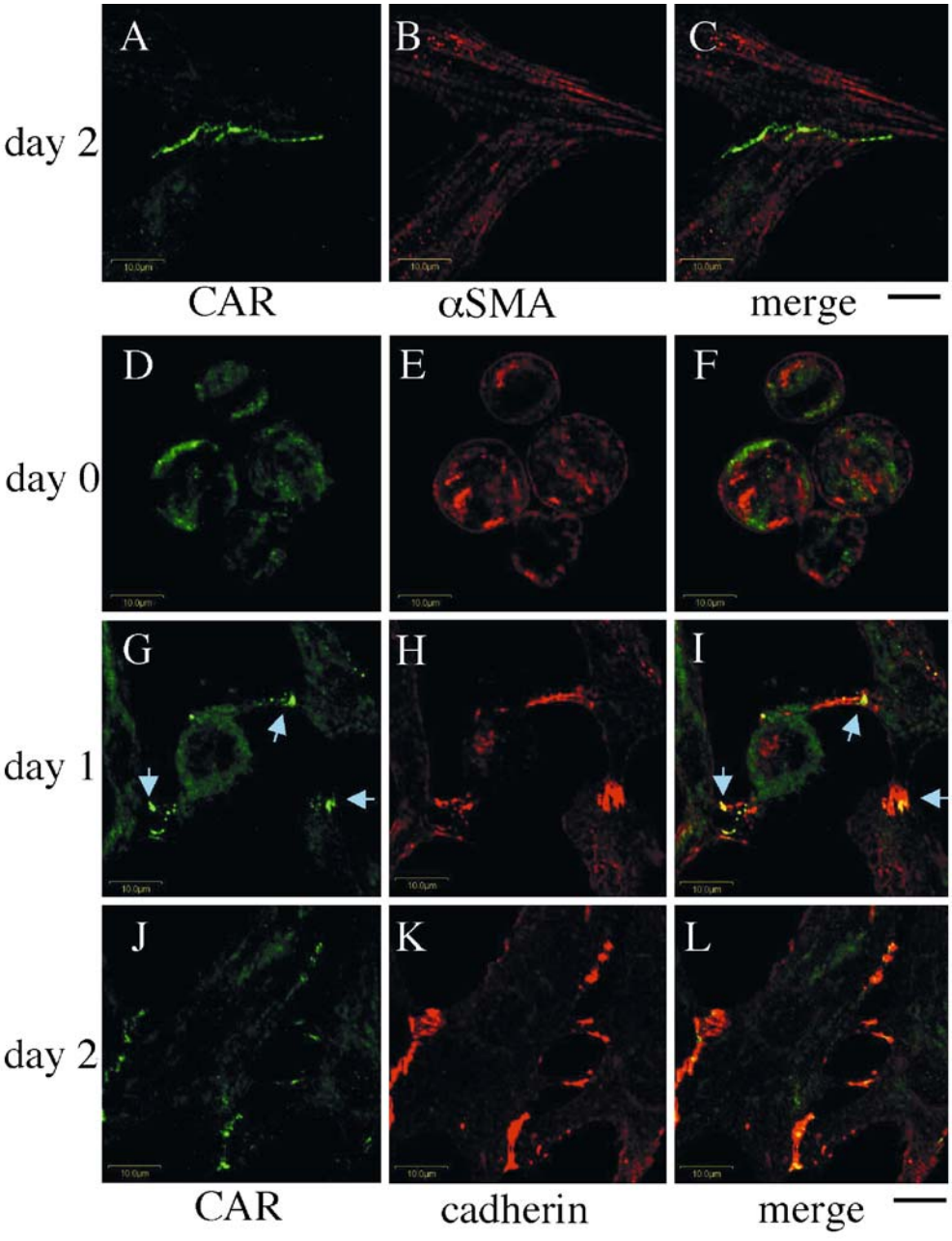

Fig. 6 Immunofluorescence of cultured cardiomyocytes for coxsackievirus and adenovirus receptor (CAR) and cadherin. **A**, **B**, **C** After 2 days of culturing, CAR labeled green with fluorescein isothiocyanate (FITC) localizes along the junction between the two cardiomyocytes, as identified by anti-α smooth muscle actin antibody, labeled red by tetramethyl rhodamine isothiocyanate (TRITC). **D**, **E**, **F**, **G**, **H**, **I**, **J**, **K**, **L** The localization of CAR, labeled green with FITC, was compared with cadherin, labeled red by TRITC. **D**, **E**, **F** The cardiomyocytes on day 0 have lost CAR on the cell surface due to trypsin treatment. Cadherin remains stainable on the cell surface. **G**, **H**, **I** On day 1, CAR starts to localize at the sites of cellular contacts (*arrows*), where cadherin is also stained. **J**, **K**. On day 2, co-localization of CAR and cadherin is obvious along the junctions. Original magnifications, ×600. Scale bars, 10 μm

for CARb (Fig. 5C). The expression of CAR reached a plateau by day 3 and remained stable until day 7.

Immunofluorescence of cultured cardiomyocytes

Neonatal cardiomyocytes were specified by anti-αSMA antibodies. CAR was clearly confined to the sites of intercellular contact of cardiomyocytes (Fig. 6A, B, C). After trypsin treatment on day 0, CAR did not exist on the cell surface and was stained differently than cadherin (Fig. 6D, E, F). Soon after the establishment of cellular contacts on day 1, CAR was localized to the site of intercellular contacts (Fig. 6G, I *arrow*), and cadherin was observed at the same site (Fig. 6H, I). By day 2, CAR was found at the sites of intercellular contact in parallel with cadherin (Fig. 6J, K, L).

Localization of CAR and connexin43 in vivo and in vitro

CAR was shown on the whole surface of cardiomyocytes in vivo at birth. Connexin43 was only sparsely stained, but a polarity was not found (Fig. 7A, B, C). In contrast, at 3 months of age, both CAR and connexin43 showed apparent polarity and were co-localized predominantly at the intercalated disks (Fig. 7D, E, F).

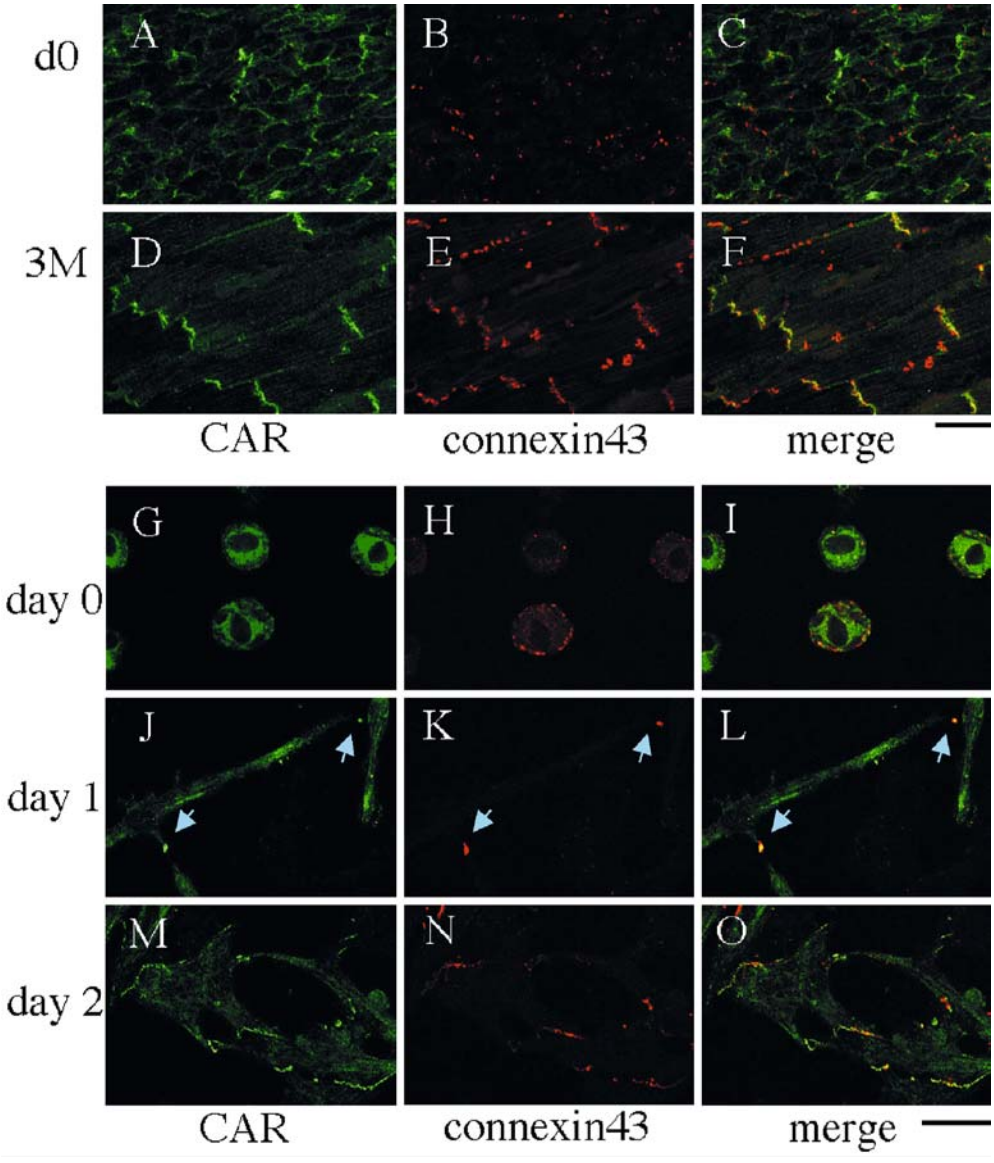

Fig. 7 The localizations of coxsackievirus and adenovirus receptor (CAR) and conexin43 in rat hearts and in cultured cardiomyocytes. **A**, **B**, **C** In newborn rat hearts, CAR, labeled green with fluorescein isothiocyanate (FITC), localizes on almost the whole surface of cardiomyocytes. Connexin43 is only sparsely stained but a polarity is not found. **D**, **E**, **F**. In the adult rat heart, CAR localizes predominantly at the intercalated disks co-localizing with connexin43. **G**, **H**, **I** Trypsin-treated cardiomyocytes have lost CAR from the cell surface, and connexin43 sparsely remains. **J**, **K**, **L** On day 1, CAR and connexin43 are co-localized at the sites of cellular contacts (*arrows*). **M**, **N**, **O** On day 2, CAR and connexin43 are co-localized along the intercellular junctions between the cells. Original magnifications, ×600. Scale bar, 20 μm

In suspended neonatal cardiomyocytes, connexin43 was stained mainly beneath the cell surface, even after trypsin treatment (Fig. 7H, I). On day 1, CAR and connexin43 were shown to coexist at the sites of cell–cell contact (Fig. 7J, K, L *arrow*). By day 2, the sites of intercellular contacts became linear, and CAR and connexin43 existed together as dense lines along the junctions (Fig. 7M, N, O).

Discussion

The localization of CAR was emphasized as the determinant of coxsackievirus and adenovirus infection [6, 9, 25, 33, 34, 35], and this is the first study demonstrating spatiotemporal change of CAR in the heart during postnatal development. The results will explain the susceptibility of neonates and children to viral myocarditis.

In this study, we confirmed the postnatal decrease of cardiac CAR prior to histological examinations. As demonstrated in a previous report [10], the postnatal decrease of CAR mRNA in the heart was confirmed, but in this study, we found that a decline of the mRNA level was associated with a decline of CAR protein. Decreases of CAR expression in adults have already been reported in the skeletal muscle [19], brain [13], and heart [10, 14] of rodents. The decline of cardiac CAR seemed less remarkable and slower than those of skeletal muscle and brain. The presence of a considerable amount of CAR suggested that CAR has some roles in the heart, even in adults. CAR is a molecule belonging to the immunoglobulin superfamily, and we reported its role in homophilic cell–cell contact [13]. It was interesting that the developmental decrease of an adhesion molecule, N-cadherin,

was similar to that of CAR, at least with respect to mRNA, but the developmental change of connexin43, which is a type of channel protein on the intercalated disk, was not. We did not focus on the physiological function of CAR in this study, and the role of CAR in the heart remains to be studied.

Our principal finding was the spatiotemporal change of CAR during postnatal development, and it was determined using anti-CAR antibodies. First, we prepared three anti-CAR antibodies, anti-CARa, anti-CARb, and anti-CARc, to precisely determine the change of localization of CAR and then, tested their specificity. In Western blot analysis, both anti-CARa and CARb antibodies showed additional bands, which were considered to be fragments of CAR or unrelated unknown molecules. Anti-CARc antibody reacted only with CAR1 and showed no additional bands; this is the reason that anti-CARc antibody was used in the histological studies. We also performed immunohistochemistry with anti-CARb antibody to detect both CAR1 and CAR2 and confirmed the same staining pattern in developing hearts (data not shown); at birth, CAR was found diffusely on the surface of myocytes, but was localized predominantly at the site of intercellular contacts in the adult heart.

However, in cultured cardiomyocytes, the cells revealed diffuse immunoreactivity to the anti-CARc antibody, which was strongest on day 0. At that time, Western blot analysis showed almost a negative band at 46 kDa. This would mean that during the preparation of cardiomyocytes, the extracellular domains of CAR must be digested by trypsin, and fragmented CAR in the cytoplasma would be stained or the immunoreactivity might be non-specific. The size of the smaller molecule detected by anti-CARb antibody on day 0 was identical to that of the proteolysed CAR in trypsin-treated HeLa cells [4], and the reason for the absence of the shorter band with anti-CARc antibody was unknown. Nevertheless, CAR was clearly accumulated at the site of the contact once the cultured myocytes established intercellular contact and increased with intercellular contacts.

Interestingly, it was only when cardiomyocytes were in immature hearts that cardiomyocytes expressed CAR and other intercalated disk proteins onto the whole surface without polarity. Reported localizations of intercalated disk proteins, N-cadherin, and connexin43 in vivo [1, 24, 28] and in vitro [23, 28] supported our results and were similar to that of CAR in terms of polarity. The localizations seemed to depend upon the environment, and, thus, there must be factors that lead those molecules, including CAR, to the whole surface of cardiomyocytes without polarity in the immature heart. The spatiotemporal change of CAR was considered to be a part of the dynamic movement of molecules during the maturation of the intercalated disk.

Since CAR acts as a common receptor for both coxsackievirus and adenovirus and the viruses are frequent causes of myocarditis in humans, the up-regulation in the hearts and the change of the intracellular localization of CAR during development may affect the susceptibility to these viruses. Actually, newborn and young children are the most affected. When CAR is localized on the whole cell surface, viral infection occurs more easily, as shown in airway epithelial cells [25, 34]. However, when CAR is exclusively localized at the site of cell–cell contact, the intercalated disks, viruses might be unable to use the receptor to infect the heart, and this can partly explain why viral myocarditis is common in neonates and young children.

In conclusion, CAR was expressed abundantly on the whole surface of cardiomyocytes in immature rat hearts. Not only the expression level, but also the localization of CAR, are the possible determinants of the susceptibility of neonates and children to viral myocarditis. Further studies will be needed to clarify the physiological and pathological role of CAR in the heart and may possibly lead to prevention or treatment of viral myocarditis and dilated cardiomyopathy.

Acknowledgement This study was supported in part by a grant for research on specific diseases from the Ministry of Health, Labor and Welfare.

References

1. Angst BD, Khan LU, Severs NJ, Whitely K, Rothery S, Thompson RP, Magee AI, Gourdie RG (1997) Dissociated spatial patterning of gap junctions and cell adhesion junctions during postnatal differentiation of ventricular myocardium. Circ Res 80:88–94
2. Bergelson JM, Cunningham JA, Droguett G, Kurt-Jones EA, Krithivas A, Hong JS, Horwitz MS, Crowell RL, Finberg RW (1997) Isolation of a common receptor for coxsackie B viruses and adenoviruses 2 and 5. Science 275:1320–1323
3. Bowles NE, Towbin JA (2003) Childhood myocarditis and dilated cardiomyopathy. In: Cooper LT (ed) Myocarditis: from bench to bedside. Humana Press, Totowa, pp 559–587
4. Carson SD (2000) Limited proteolysis of the coxsackievirus and adenovirus receptor (CAR) on HeLa cells exposed to trypsin. FEBS Lett 484:149–152
5. Carson SD, Chapman NN, Tracy SM (1997) Purification of the putative coxsackievirus B receptor from HeLa cells. Biochem Biophys Res Commun 233:325–328
6. Cohen CJ, Shieh JT, Pickles RJ, Okegawa T, Hsieh JT, Bergelson JM (2001) The coxsackievirus and adenovirus receptor is a transmembrane component of the tight junction. Proc Natl Acad Sci U S A 98:15191–15196
7. Dec GW, Fuster V (1994) Idiopathic dilated cardiomyopathy. N Engl J Med 331:1564–1575
8. Douglas JT, Kim M, Sumerel LA, Carey DE, Curiel DT (2001) Efficient oncolysis by a replicating adenovirus (ad) in vivo is critically dependent on tumor expression of primary ad receptors. Cancer Res 61:813–917
9. Fechner H, Haack A, Wang H, Wang X, Eizema K, Pauschinger M, Schoemaker R, Veghel R, Houtsmuller A, Schultheiss HP, Lamers J, Poller W (1999) Expression of coxsackie adenovirus receptor and alpha-integrin does not correlate with adenovector targeting in vivo indicating anatomical vector barriers. Gene Ther 6:1520–1535
10. Fechner H, Noutsias M, Tschoepe C, Hinze K, Wang X, Escher F, Pauschinger M, Dekkers D, Vetter R, Paul M, Lamers J, Schultheiss HP, Poller W (2003) Induction of coxsackievirus-adenovirus-receptor expression during myocardial tissue formation and remodeling: identification of a cell-to-cell contact-dependent regulatory mechanism. Circulation 107:876–882

11. Hanawa H, Abe S, Hayashi M, Yoshida T, Yoshida K, Shiono T, Fuse K, Ito M, Tachikawa H, Kashimura T, Okura Y, Kato K, Kodama M, Maruyama S, Yamamoto T, Aizawa Y (2002) Time course of gene expression in rat experimental autoimmune myocarditis. Clin Sci 103:623–632
12. Hirschman SZ, Hammer GS. Coxsackie virus myopericarditis. A microbiological and clinical review. Am J Cardiol 34:224–232
13. Honda T, Saitoh H, Masuko M, Katagiri-Abe T, Tominaga K, Kozakai I, Kobayashi K, Kumanishi T, Watanabe YG, Odani S, Kuwano R (2000) The coxsackievirus-adenovirus receptor protein as a cell adhesion molecule in the developing mouse brain. Brain Res Mol Brain Res 77:19–28
14. Ito M, Kodama M, Masuko M, Yamaura M, Fuse K, Uesugi Y, Hirono S, Okura Y, Kato K, Hotta Y, Honda T, Kuwano R, Aizawa Y (2000) Expression of coxsackievirus and adenovirus receptor in hearts of rats with experimental autoimmune myocarditis. Circ Res 86:275–280
15. Leon RP, Hedlund T, Meech SJ, Li S, Schaack J, Hunger SP, Duke RC, DeGregori J (1998) Adenoviral-mediated gene transfer in lymphocytes. Proc Natl Acad Sci U S A 95:13159–13164
16. Martin AB, Webber S, Fricker FJ, Jaffe R, Demmler G, Kearney D, Zhang YH, Bodurtha J, Gelb B, Ni J, Bricker TB, Towbin JA (1994) Acute myocarditis. Rapid diagnosis by PCR in children. Circulation 90:330–339
17. Montague TJ, Lopaschuk GD, Davies NJ (1990) Viral heart disease. Chest 98:190–199
18. Nakagawa M, Sato A, Okagawa H, Kondo M, Okuno M, Takamatsu T (1999) Detection and evaluation of asymptomatic myocarditis in schoolchildren: report of four cases. Chest 116:340–345
19. Nalbantoglu J, Pari G, Karpati G, Holland PC (1999) Expression of the primary coxsackie and adenovirus receptor is downregulated during skeletal muscle maturation and limits the efficacy of adenovirus-mediated gene delivery to muscle cells. Hum Gene Ther 10:1009–1019
20. Nalbantoglu J, Larochelle N, Wolf E, Karpati G, Lochmuller H, Holland PC (2001) Muscle-specific overexpression of the adenovirus primary receptor CAR overcomes low efficiency of gene transfer to mature skeletal muscle. J Virol 75:4276-4282
21. Nicholson F, Ajetunmobi JF, Li M, Shackleton EA, Starkey WG, Illavia SJ, Muir P, Banatvala JE (1995) Molecular detection and serotypic analysis of enterovirus RNA in archival specimens from patients with acute myocarditis. Br Heart J 74:522–527
22. Noutsias M, Fechner H, de Jonge H, Wang X, Dekkers D, Houtsmuller AB, Pauschinger M, Bergelson J, Warraich R, Yacoub M, Hetzer R, Lamers J, Schultheiss HP, Poller W (2001) Human coxsackie-adenovirus receptor is colocalized with integrins alpha(v)beta(3) and alpha(v)beta(5) on the cardiomyocyte sarcolemma and upregulated in dilated cardiomyopathy: implications for cardiotropic viral infections. Circulation 104:275–280
23. Oyamada M, Kimura H, Oyamada Y, Miyamoto A, Ohshika H, Mori M (1994) The expression, phosphorylation, and localization of connexin 43 and gap-junctional intercellular communication during the establishment of a synchronized contraction of cultured neonatal rat cardiac myocytes. Exp Cell Res 212:351–358
24. Peters NS, Severs NJ, Rothery SM, Lincoln C, Yacoub MH, Green CR (1994) Spatiotemporal relation between gap junctions and fascia adherens junctions during postnatal development of human ventricular myocardium. Circulation 90:713–725
25. Pickles RJ, Fahrner JA, Petrella JM, Boucher RC, Bergelson JM (2000) Retargeting the coxsackievirus and adenovirus receptor to the apical surface of polarized epithelial cells reveals the glycocalyx as a barrier to adenovirus-mediated gene transfer. J Virol 74:6050–6057
26. Pisani B, Taylor DO, Mason JW (1997) Inflammatory myocardial diseases and cardiomyopathies. Am J Med 102:459–469
27. Poller W, Fechner H, Noutsias M, Tschoepe C, Schultheiss HP (2002) Highly variable expression of virus receptors in the human cardiovascular system Implications for cardiotropic viral infections and gene therapy. Z Kardiol 91:978–991
28. Reinecke H, Zhang M, Bartosek T, Murry CE (1999) Survival, integration, and differentiation of cardiomyocyte grafts: a study in normal and injured rat hearts. Circulation 100:193–202
29. Rosenberg HS, McNamara DG (1964) Acute myocarditis in infancy and childhood. Prog Cardiovasc Dis 7:179–197
30. Simpson P, Savion S (1982) Differentiation of rat myocytes in single cell cultures with and without proliferating nonmyocardial cells. Cross-striations, ultrastructure, and chronotropic response to isoproterenol. Circ Res 50:101–116
31. Thoelen I, Magnusson C, Tagerud S, Polacek C, Lindberg M, Van Ranst M (2001) Identification of alternative splice products encoded by the human coxsackie-adenovirus receptor gene. Biochem Biophys Res Commun 287:216–222
32. Tomko RP, Xu R, Philipson L (1997) HCAR and MCAR: the human and mouse cellular receptors for subgroup C adenoviruses and group B coxsackieviruses. Proc Natl Acad Sci U S A 94:3352–3356
33. Walters RW, Grunst T, Bergelson JM, Finberg RW, Welsh MJ, Zabner J (1999) Basolateral localization of fiber receptors limits adenovirus infection from the apical surface of airway epithelia. J Biol Chem 274:10219–10226
34. Walters RW, van't Hof W, Yi SM, Schroth MK, Zabner J, Crystal RG, Welsh MJ (2001) Apical localization of the coxsackie-adenovirus receptor by glycosyl-phosphatidylinositol modification is sufficient for adenovirus-mediated gene transfer through the apical surface of human airway epithelia. J Virol 75:7703–7711
35. Walters RW, Freimuth P, Moninger TO, Ganske I, Zabner J, Welsh MJ (2002) Adenovirus fiber disrupts CAR-mediated intercellular adhesion allowing virus escape. Cell 110:789–799
36. Wan YY, Leon RP, Marks R, Cham CM, Schaack J, Gajewski TF, DeGregori J (2000) Transgenic expression of the coxsackie/adenovirus receptor enables adenoviral-mediated gene delivery in naive T cells. Proc Natl Acad Sci U S A 97:13784–13789
37. Young JAT (2001) Virus entry and uncoating. In: Kimpe DM, Howley PM (eds) Fieles virology. Lippincott Williams & Wilkins, Philadelphia, pp 87–103

Virchows Arch (2004) 444:293–299
DOI 10.1007/s00428-003-0955-3

CASE REPORT

Stefanie Scheil-Bertram · Erich Hartwig · Silke Brüderlein · Ingo Melzner · Alexandra von Baer · Albert Roessner · Peter Möller · Michael Schulte

Metachronous and multiple aneurysmal bone cysts: a rare variant of primary aneurysmal bone cysts

Received: 5 August 2003 / Accepted: 1 December 2003 / Published online: 20 January 2004

Abstract In 1942, Jaffe and Lichtenstein introduced the term aneurysmal bone cyst (ABC). Primary ABC is characterized by the presence of spongy or multi-cameral cystic tissue filled with blood. The process is benign, but it is locally destructive and has a high propensity for recurrence. In this paper, we present the third case of multiple metachronous primary ABCs as a rare variant of ABC. We describe the 10-year history of a 12-year-old boy with metachronous multiple primary ABCs at five different sites (right proximal humerus, right ulna, bilateral distal radius and right lateral clavicle). Furthermore, our patient suffered from vascular malformations, such as aortic isthmus stenosis, hypoplastic thoracoabdominal aorta and bilateral renal artery stenosis. To date, in contrast to solitary ABC, the multiple lesions have been found more frequently in male individuals. Using interphase cytogenetics, we analyzed three of five of the patient's ABCs and one of these was also analyzed by GTG-banding. No chromosomal abnormalities were found. Significantly, we excluded the missense mutation of codon 201 in guanine nucleotide-binding protein 1 gene consistently found in McCune-Albright syndrome (MAS) and in non-MAS cases of polyostotic fibrous dysplasia of bone with or without secondary ABC.

Keywords Aneurysmal bone cyst · Cytogenetics · CGH · FISH · Review

S. Scheil-Bertram (✉) · S. Brüderlein · I. Melzner · P. Möller
Institute of Pathology,
University of Ulm,
Albert-Einstein-Allee 11, 89081 Ulm, Germany
e-mail: stefanie.scheil@medizin.uni-ulm.de
Tel.: +49-731-50023320
Fax: +49-731-50023884

E. Hartwig · A. von Baer
Department of Trauma, Hand and Reconstructive Surgery,
University of Ulm,
Germany

A. Roessner
Institute of Pathology,
University of Magdeburg,
Germany

M. Schulte
Department of Trauma and Reconstructive Surgery,
Diakoniekrankenhaus,
Rotenburg (Wümme), Germany

Introduction

In 1942, Jaffe and Lichtenstein [11] introduced the term aneurysmal bone cyst (ABC). ABCs are very rare, accounting for approximately 2.5% of all primary bone tumors. They may develop as primary lesions or as secondary lesions superimposed on preexisting conditions, such as benign or malignant bone tumors. Primary ABCs develop without preexisting conditions. The male/female sex ratio is approximately 45:55 [6]. Almost 80% of the lesions occur in skeletally immature patients who are younger than 20 years [8]. ABC may affect every site of the skeleton, but shows evident predilection for the long bones and for the vertebral column. The typical symptoms are pain and swelling, which may vary in duration from weeks to several years. The lesion is lytic, typically involving the metaphysis. Central ABC can be distinguished from subperiosteal lesions. Magnetic resonance imaging demonstrates the expansive nature of the lesion, which is encircled by a thin rim of periosteal bone of low signal intensity. In contrast to simple bone cyst, ABC is characterized by a typical horizontal level of the fluid content in computed tomography and magnetic resonance tomography. The process is benign in nature, but it is locally destructive and has a high propensity for recurrence. Microscopically, ABCs are characterized by the presence of spongy or multilocular cystic tissue filled with blood. Distinguishing them from teleangiectatic osteosarcoma is the most important differential diagnostic problem and may be difficult [1].

To date, seven studies have focused on the cytogenetics of primary solitary intraosseous ABCs, and recurrent breakpoints were located at 16q22 and 17p13 [3, 7, 10, 14, 15, 19, 22]. In this paper, we present the third case of a

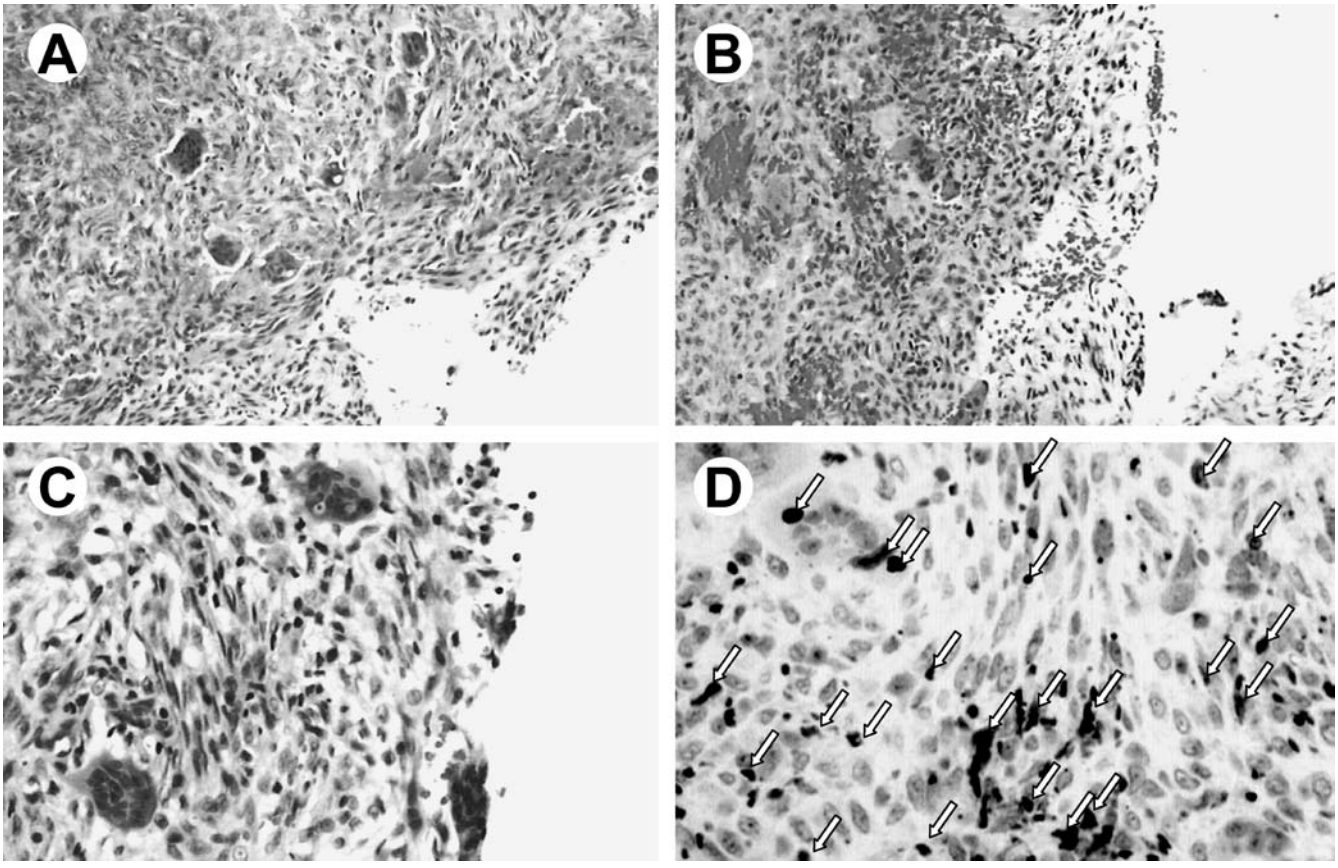

Fig. 1 Morphology of four of five aneurysmal bone cysts (ABCs). The septa and more solid areas are composed of loose, fibrous tissue that has numerous capillary channels, multinucleated giant cells, inflammatory cells and extravasated red blood cells. The cystic spaces do not have any clearly recognizable lining. **A** Right humerus [hematoxylin and eosin (H&E) ×200]. **B** Right clavicle (H&E ×200). **C** Right distal radius (H&E ×400). **D** Right clavicle. Using an anti-p53 antibody, 2% of tumor cell nuclei were immunohistochemically stained. *Arrows* indicate the immunoreactive nuclei (×400)

boy with multiple ABCs, review the literature and discuss the cytogenetics of ABC.

Case report

A 2-year-old boy presented with a pathological fracture of the proximal humerus. Microscopic examination revealed a typical ABC (Fig. 1A). This ABC recurred twice (at the age of 3 years and 7 years; Fig. 2A, B, D) and was treated by a defect reconstruction by a non-vascularized fibula autograft (Fig. 2C). Over a 10-year follow-up period, further lesions became symptomatic. The second lesion occurred at the right lateral clavicle (Fig. 2E), the third at the right distal radius (Fig. 2F) and the fourth at the left distal radius (Fig. 2G). All these ABCs were treated by surgery, due to loss of stability and histological examination of these new ABCs, and re-evaluation of the former lesions excluded malignancy, e.g., teleangiectatic osteosarcoma (Fig. 1B, C, D). Periodic clinical and radiographic follow-up revealed one further ABC at the right ulna (Fig. 2H). Radiographs demonstrated well-defined osteolytic diametaphyseal lesions, which were complicated by a pathological fracture (Fig. 2B, D). The right distal radius had to be reoperated upon at the age of 12 years, due to a pathological fracture. The boy had no history of trauma and was otherwise well. Physical examination revealed arterial hypertension due to bilateral renal artery stenosis. Furthermore, at the age of 9 years, the boy underwent surgery for aortic isthmus stenosis. Angiographically, the whole thoraco-abdominal aorta was hypoplastic. The manuscript was written with the informed consent of the patient's parents.

Materials and methods

Immunohistochemistry

Immunostaining was performed using a routine indirect peroxidase method. The following antibodies were used: CD31 (clone JC/70A, Dako, Glostrup, Denmark), CD68 (clone KP1, Dako), anti-Ki67 (clone MIB-1, Dianova, Hamburg, Germany) and anti-p53 protein (clone DO-7, Dako). The antibodies were used at a final concentration of 1–2 μg/ml.

Cell culture and chromosome preparation

We performed a short-term culture of the third ABC (right distal radius). The primary cells were seeded, cultured and subcultivated as previously described [17].

After short-term culture (2–4 days), metaphase chromosome spreads were prepared from the ABC and from primary blood cell cultures of healthy donors [for comparative genomic hybridization (CGH) experiments] using standard protocols [17]. Cells were karyotyped by conventional GTG-banding techniques according to

Fig. 2 Radiology of five aneurysmal bone cysts (ABCs). Radiographs demonstrated well-defined osteolytic diametaphyseal lesions. **A**–**D** Right humerus. This ABC recurred twice (at the age of 3 years and 7 years). The lesion was treated at least by marginal subperiosteal resection and defect reconstruction by a non-vascularized fibula autograft (**C**). The histology of the recurrence is shown in Fig. 1A. **E** Right clavicle. The second lesion occurred at the right lateral clavicle 1 year later (for histology see Fig. 1B). **F** Right distal radius. Histological examination of this ABC is demonstrated in Fig. 1C, D. **G** Left distal radius. **H** Right proximal ulna (*arrow* indicates the lesion). Periodic clinical and radiographic follow-up revealed further ABCs at the left distal radius and the right ulna

the 1995 International System for Human Cytogenetic Nomenclature.

Comparative genomic hybridization and fluorescence in situ hybridization

The ABCs were available as paraffin-embedded material and as fresh-frozen tissue. Histological evaluation of these samples revealed an estimated tumor cell content of 90% of tissue volume. The DNA from the fresh-frozen tumor tissue and the control-DNA from fresh-frozen material of normal human tonsils were isolated by phenol/chloroform extraction. Nick translation of DNA probes and CGH analysis were carried out according to the protocol previously described in detail [17]. Image acquisition and processing were performed with the image analysis system ISIS (MetaSystems, Altlussheim, Germany).

Fluorescence in situ hybridization (FISH) was performed on imprint cytology slides at the second and third ABC (clavicle and right radius) and on interphase nuclei or metaphase spreads of the last lesion of the third ABC (right radius) as previously described [17]. The following commercially available digoxigenin- or biotin-labeled probes were used with assignment to human chromosomes: 6cen, p53 and the combined probe m-bcr/abl with assignment to 9q34 (*ABL* locus) and 22q11.2 (*BCR* locus) (all probes by Q-Biogene, Illkirch Cedex, France). Additionally, we used the following YAC clones obtained from the CEPH YAC library: 798_G_8 (8p12), 763_A_3 (22q12) and 744_F_6 (22q12) [17]. FISH experiments were performed as dual-color hybridization as previously described [17].

PCR amplification

The polymerase chain reaction (PCR) reactions were carried out in a final volume of 50 µl containing 100 ng DNA, 10 pmol of each primer, 10 mM Tris/HCl pH 8.3, 50 mM KCl, 1.5 mM $MgCl_2$ and 200 mM of each nucleotide in a thermocycler (Primus 96 plus, MWG-Biotech, Germany). In all PCR amplifications, the reverse primer [exon 10 of guanine nucleotide-binding protein 1 (GNAS1) DNA] gnas1b 5′-GCT GCT GGC CAC CAC GAA GAT GAT-3′ was used [13]. A set of forward PCR primers specific for three different point mutations in codon 201 (exon 8) of GNAS1 DNA were selected: gnasCys/R201C, 5′-T CAG GAC CTG CTT CGC TGC T-3′; gnasGly/R201G, 5′-T CAG GAC CTG CTT CGC TGC G-3′ and gnasHIS/R201H, 5′-T CAG GAC CTG CTT CGC TGC CA-3′. Importantly, these primers do not amplify the 372 bp DNA-fragment of the wild type DNA-sequences of GNAS1 in PCR. As the control, we performed PCR with two forward primers to amplify a wild-type specific GNAS1 fragments: WT1, 5′-T CAG GAC CTG CTT CGC TGC C-3′ (gnasWT1; wild-type sequence as control for gnasCys and gnasGly) and WT2, 5′-T CAG GAC CTG CTT CGC TGC CG-3′ (gnasWT2; wild-type sequence as control for gnasHIS). Figure 3 shows the GNAS1 cDNA (Gene bank accession no. NM000516) and the position of the oligonucleotide primer used for PCR amplification.

For all primer sets, hot start PCR was performed with initial denaturation at 95°C for 5 min. This was followed by 30 cycles at 95°C for 1 min, 70°C for 0.5 min and 72°C for 1 min. Final extension was carried out for 10 min at 72°C. One negative control was included for each PCR reaction with DNA of normal human tonsils without GNAS1 mutation. The PCR experiment was reproduced three times. To confirm the GNAS1 cDNA identity of the PCR products, DNA sequencing was performed.

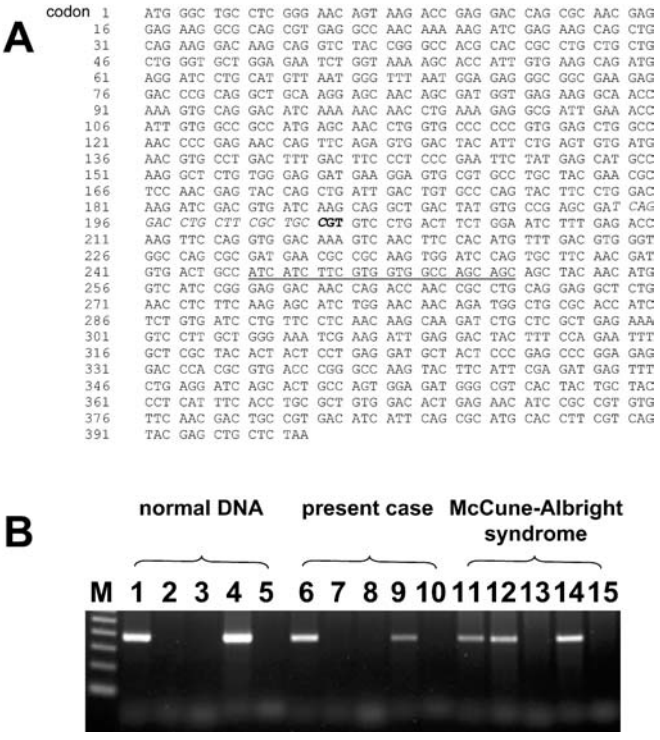

Fig. 3 Guanine nucleotide-binding protein 1 (GNAS1) codon 201 analysis. **A** cDNA sequence of GNAS1. Underlined oligonucleotide sequences demonstrated the previously published reverse primer (gnas1b) [13]. Primer sequences specific for GNAS1 mutations of codon 201 and wild type sequences are given in *italics*. Codon 201 is given in *bold type*. **B** Electrophoresis of polymerase chain reaction (PCR) products on a 1.5% agarose gel. The 372bp-PCR products of DNA are demonstrated in the following order: WT1, R201C, R201G, WT2, R201H. Lanes 1–5 represent PCR products of normal human tonsils DNA. Lanes 6–10 demonstrated PCR products of DNA derived from the fourth aneurysmal bone cyst (left distal radius). Lanes 11–15 showed the positive control, DNA from a biopsy of fibrous dysplasia in McCune-Albright syndrome (heterozygous for the arg201-to-cys, R201C). M = 100 bp ladder

Results

Morphology of the ABC

Microscopically, we examined four of the patient's five ABCs (Fig. 1A, B, C, D). The microscopic features of ABC specimens demonstrated multilocular cystic architecture of the lesion under low-power examination. The septa and more solid areas were composed of loose, fibrous tissue that has numerous capillary channels, multinucleated giant cells, inflammatory cells and extravasated red blood cells. All four specimens demonstrated hemosiderin within the ABC. The cystic spaces did not have any clearly recognizable lining, but rather flattened, endothelial-like, CD31-negative cells. Using an anti-p53 antibody, about 5% of the cell nuclei were immunohistochemically stained. Giant osteoclast-like cells were predominantly located in the area of extravasated red blood cells. Osteoid was frequently deposited in the form of long strands that were partially

mineralized. Sarcomatous cells with atypical mitoses producing tumor osteoid were absent.

Cytogenetics in ABCs (right lateral clavicle, bilateral distal radius)

CGH of total tumor DNA of all three ABCs revealed no chromosomal imbalance. Using interphase FISH, the imprint cytology specimens of the second and third ABC were analyzed with a TP53 locus-specific probe (17p13.1). Dual color FISH analysis of imprint cytology specimens demonstrated two signals per nuclei in 88–99% of nuclei of TP53 locus, whereas the second probe revealed two signals in 85–97% of nuclei (6cen, 8p22, 22q12). Furthermore, using a TP53 locus-specific probe, we screened five metaphases of the short-term cultured cells of the third ABC (right distal radius). TP53 signals were located at the right band (17p13.1) on chromosome 17.

Of 21 metaphase cells of the third ABC (right distal radius), 6 could be analyzed using conventional cytogenetics (passage numbers 1 and 2). Five cells were karyotypically normal (46,XY), one metaphase demonstrated 47,XY,+11. All metaphase cells demonstrated normal chromosomes 16 and 17.

GNAS1 mutation analysis of codon 201

For analysis using PCR, we extracted total DNA of two ABCs (right and left distal radius). Using this technique, we were able to exclude the activating mutations R201G, R201C and R201H in GNAS1 described in polyostotic fibrous dysplasia and McCune-Albright syndrome (MAS) (Fig. 3).

Discussion

A review of the scientific literature shows that cytogenetic studies focusing on ABC are rare. Of 19 cases of intraosseous ABCs, 9 (47%, two were not informative) demonstrated a normal karyotype [3, 7, 10, 14, 15, 19, 22]. Recurrent breakpoints involved 16q22 or 17p13 [7, 10, 14, 19, 22], suggesting that these segments are non-randomly involved in at least some ABCs [10]. Dal Cin and co-workers [7] mentioned that genes in 16p22 or 17p13 can be activated by several alternate mechanisms in ABCs. One group [22] suggested that the putative gene on 17p13 is located between the locus of the tumor suppressor gene TP53 (17p13.1) and the Miller-Dieker syndrome locus (17p13.3). In the present case, we did not find t(16;17)(q22;p13), a structural abnormality of chromosomes 16 or 17, a deletion of the TP53 locus or a split signal of TP53 FISH probe on metaphase spreads. Recently, 22 primary ABCs were screened for TP53 mutations [18]. They did not reveal any mutation of TP53.

An important differential diagnosis in this boy was metastatic disease of teleangiectatic osteosarcoma. In addition to radiological and histological examination, we also used interphase cytogenetics. We did not find any chromosomal imbalances. In contrast, in high-grade osteosarcoma, CGH feature complex genomic imbalances (range 8 to 32 or, on average, 18.5 aberrations/per tumor) [5]. Therefore, CGH might be a helpful tool for differential diagnostics in this specific situation.

According to the literature, only four reports (three male, one female) of multiple ABCs have been found in mammals (Table 1) [2, 20, 21, 23]. Two studies described these multiple ABC in boys [20, 23]. Both showed a history of past trauma. In our case, no trauma was described. The etiology of primary ABC is not quite clear, but initiating trauma was suggested [8]. The remaining

Table 1 Summary of metachronous and multiple aneurysmal bone cysts (ABCs) in humans. Review of the literature and own case

Age	Sex	History	Radiology	Localization	Histology	Follow-up and other symptoms	Reference
18 years	Male	Left elbow: rapidly worsening and painful swelling over a period of 4 months; trauma 4 months previously	Bilateral osteolytic in upper end of ulna and the humerus	Bilateral proximal ulna, humerus/ olecranon	Biopsy from both ulnar lesions: ABC	Follow-up 1.1 year: no other symptoms	[19]
9 years	Male	Left knee: painful for a few months. Previous trauma. 1.25 years later: painful left leg and hip	Osteolytic metadiaphyseal tibial lesion	Tibia with recurrence, pubis	Biopsy from tibia and pubis: ABC	Follow-up 3 years: no further recurrences or new lesions	[17]
2 years	Male	2 year pathological fracture humerus (re-operation at 3 years & 7 years); 9 years: right clavicle; 10 years & 12 years: right radius; 11 years: left radius. No trauma	Expanding central osteolytic metadiaphyseal lesions	Right humerus, right ulna, bilateral radius, right clavicle	Biopsy from humerus, bilateral distal radius, right clavicle: ABC	Follow-up 10 years: aortic isthmus stenosis, hypoplastic thoracoabdomial aorta, bilateral renal artery stenosis	Present case

two previously published cases were reported in animals, one in a male 3.3-year-old llama [2] and the other in a female 5-day-old foal [21]. In this study, we reported the case of a boy who is now 12 years old. In solitary ABC, the male/female sex ratio is approximately 45:55 [6]. In contrast to primary solitary ABC, the multiple lesions were more often observed in male individuals.

Yadav et al. [23] pointed out that, clinically and roentgenologically, their case of multiple ABCs was diagnosed as fibrous dysplasia, but careful histopathological examination did not demonstrate an association of ABC with another lesion. Therefore, another differential diagnosis in this boy was polyostotic fibrous dysplasia with secondary ABCs. Clinically, radiologically (Fig. 2) and histologically (Fig. 1), there was no hint of fibrous dysplasia. In order to confirm our diagnosis, we excluded the missense mutation of codon 201 in GNAS1 gene consistently found in MAS and in non-MAS cases of fibrous dysplasia of bone [16] (Fig. 3).

Furthermore, our patient suffered from bone cysts and complex vascular abnormalities with aortic isthmus stenosis, hypoplastic thoraco-abdominal aorta and bilateral renal artery stenosis. The combination of bone lesions and vascular abnormalities is very rare. In Jaffe-Campanacci syndrome, one 27-year-old woman presented with multiple abnormalities, a combination of multiple left-sided non-ossifying fibromata of the bone and stenosis of the aortic isthmus [12]. In this case, we found no hint for non-ossifying fibromata. In that case, the cytogenetic evaluation of peripheral lymphocytes revealed a normal female karyotype. In chromosome-X-linked genetic disorders, such as Turner's syndrome (46,X0), vascular complications are common. In 15.4% of cases, abnormality of the aortic isthmus is present [9]. This suggests that other chromosomal regions apart from chromosomal band 16q22 and 17p13, especially genes located on chromosome X, might play a pathogenic role in the present case. Using CGH (4/5 ABCs) and GTG-banding (1/5 ABCs) in this case, we failed to detect any chromosomal imbalances or abnormalities, particularly those of chromosome 16 and 17. One reason for this might be that the resolution of CGH is limited to chromosomal imbalances greater than 10–12 Mbp [4]. Another reason might be point mutations, which are, as yet, unknown.

In summary, multiple ABCs do exist in mammals. Worldwide, this is the third boy reported with multiple ABCs. Importantly, we excluded GNAS1-mutation of codon 201, characteristic for MAS. Thus far, unlike solitary ABC, the multiple lesions were more often found in male individuals. We suggest that further chromosomal regions, apart from 16q and 17p13, probably genes located on chromosome X, are of importance in the development of at least this specific subset of ABCs.

Acknowledgements Stefanie Scheil-Bertram was supported by grants from the Medical Faculty of the University of Ulm (Bausteinprogramm, Projects P.641/P.677/P.744) and Rudolf and Clothilde Eberhardt-Stiftung, Germany: D1699. We would like to acknowledge Yvonne Sauter for skillful technical assistance and Caroline Higginson for editorial help.

References

1. Adler CP (1980) Teleangiectatic osteosarcoma of the femur with features of an aggressive aneurysmal bone cyst. Skeletal Radiol 5:56–60
2. Anderson DE, Midla LT, Scrivani PV, Rosario J, Léveillé R, Long JF, Hull BL (1997) Multifocal polyostotic aneurysmal bone cysts in a llama. JAMA 210:808–810
3. Baruffi MR, Neto JB, Barbieri CH, Casartelli C (2001) Aneurysmal bone cyst with chromosomal changes involving 7q and 16p. Cancer Genet Cytogenet 129:177–180
4. Bentz M, Plesch A, Stilgenbauer S, Döhner H, Lichter P (1998) Minimal sizes of deletions detected by comparative genomic hybridization. Genes Chromosomes Cancer 21:172–175
5. Brinkschmidt C, Blasius S, Burger H, Simon R, Diallo R, Battmann A, Winkelmann W, Bocker W, Dockhorn-Dworniczak B (1998) Comparative genomic hybridization (CGH) for detecting heretofore undescribed amplified chromosomal segment in high-grade medullary osteosarcoma. Verh Dtsch Ges Pathol 82:184–188
6. Campanacci M (1990) Bone and soft tissue tumors. Springer, Wien, New York
7. Dal Cin P, Kozakewich HP, Goumnerova L, Mankin HJ, Rosenberg AE, Fletcher JA (2000) Variant translocation involving 16p22 and 17p13 in solid variant and extraosseous forms of aneurysmal bone cyst. Genes Chromosomes Cancer 28:233–234
8. Dorfman HD, Czerniak B (1998) Bone tumors. Mosby, St. Louis, PA
9. Douchin S, Rossignol AM, Klein SK, Siche JP, Baguet JP, Bost M (2000) Heart malformation and vascular complications associated with Turner's syndrome. Prospective study of 26 patients. Arch Mal Coeur Vaiss 93:565–570
10. Herens C, Thiry A, Dresse MF, Born J, Flagothier C, Vanstraelen G, Allington N, Bex V (2001) Translocation (16;17)(q22;p13) is a recurrent anomaly of aneurysmal bone cysts. Cancer Genet Cytogenet 127:83–84
11. Jaffe HL, Lichtenstein L (1942) Solitary unicameral bone cyst, with emphasis on the roentgen picture, the pathologic picture, and the pathogenesis. Arch Surg 46:1004–1025
12. Kotzot D, Stöß H, Wagner H, Ulmer R (1994) Jaffe-Campanacci syndrome: case report and review of literature. Clin Dysmorphol 3:328–334
13. Landis CA, Masters SB, Spada A, Pace AM, Bourne HR, Vallar L (1989) GTPase inhibiting mutations activate the alpha chain of Gs and stimulate adenylyl cyclase in human pituitary tumours. Nature 340:692–696
14. Papanoutsakopoulos G, Pandis N, Kyriazoglou I, Gustafson P, Mertens F, Mandahl N (1999) Recurrent t(16;17)(q22;p13) in aneurysmal bone cysts. Genes Chromosomes Cancer 26:1671–1678
15. Pfeifer FM, Bridge JA, Neff JR, Mouron BJ (1991) Cytogenetic findings in aneurysmal bone cysts. Genes Chromosomes Cancer 3:416–419
16. Riminucci M, Fisher LW, Majolagbe A, Corsi A, Lala R, De Sanctis C, Robey PG, Bianco P (1999) A novel GNAS1 mutation, R201G, in McCune-Albright syndrome. J Bone Miner Res 14:1987–1989
17. Scheil S, Brüderlein S, Liehr T, Starke H, Herms J, Schulte M, Möller P (2001) Genome wide analysis of 16 chordomas by comparative genomic hybridization and cytogenetics of the first human chordoma cell line, U-CH1. Genes Chromosomes Cancer 32:203–211
18. Schneider-Stock R, Hauptmann K, Boltze C, Schulz T, Roessner A (2001) Potential molecular markers of giant cell tumors of bone versus aneurysmatic bone cysts. Pathol Res Pract 197:292

19. Sciot R, Dorfman H, Brys P, Dal Cin P, De Wever I, Fletcher CDM, Jonson K, Mandahl N, Mertens F, Mitelman F, Rosai J, Rydholm A, Samson I, Tallini G, Van den Berghe H, Vanni R, Willén H (2000) Cytogenetics-morphologic correlation in aneurysmal bone cyst, giant cell tumor of bone and combined lesions. A report from the CHAMP study group. Mod Pathol 13:1206–1210
20. Sundaram M, McDonald DJ, Steigman CK, Bocchini T (1997) Metachronous multiple aneurysmal bone cysts. Skeletal Radiol 26:564–567
21. Thomas HL, Liversey MA, Caswell JL (1997) Multiple aneurysmal bone cysts in a foal. Can Vet J 38:570–573
22. Winnepenninckx V, Debiec-Rychter M, Jorisson M, Bogaerts S, Sciot R (2001) Aneurysmal bone cyst of the nose with 17p13 involvement Virchow Arch 439:636–639
23. Yadav SS, Aurora AL, Sharma S, Thamas S, Rajagopal N (1982) Multicentric aneurysmal bone cyst (Report of a case). Indian J Cancer 19:116–119

Virchows Arch (2004) 444:300–303
DOI 10.1007/s00428-003-0938-4

CASE REPORT

Vincent Thomas de Montpréville · Leila Zemoura · Guy Vaksmann · Godeleine Lecourt-Tierny · Claude Planché · Elisabeth Dulmet

Endocardial location of familial myofibromatosis revealed by cerebral embolization: cardiac counterpart of the frequent intravascular growth of the disease?

Received: 3 June 2003 / Accepted: 15 October 2003 / Published online: 9 January 2004

Abstract Myofibromatosis is a rare infantile benign neoplasia, which may involve the heart in the rare and usually fatal generalized form of the disease. Diagnosis of endocardial myofibromas was made on two surgically excised lesions of the mitral valve that were reveled by a cerebral embolization in a 12-month-old female infant. Surprisingly, the patient had no other obvious lesion of myofibromatosis. However, her father had a histologically proven neonatal history of myofibromatosis. This case confirms the likely autosomal dominant mode of inheritance of myofibromatosis. It highlights the embolization risk of the previously unreported endocardial location. We suggest that these clinically isolated non-invasive endocardial myofibromas did not represent a true visceral form of myofibromatosis. They were, rather, similar to the frequent intravascular growth of the disease.

Keywords Myofibromatosis · Heart tumors · Cerebral embolization

V. T. de Montpréville (✉) · L. Zemoura · E. Dulmet
Service d'anatomie pathologique,
Centre chirurgical Marie Lannelongue,
133 Avenue de la Résistance, 92350 Le Plessis Robinson, France
e-mail: de-montpreville@ccml.com
Tel.: +33-14-0942807
Fax: +33-14-0942805

G. Vaksmann · G. Lecourt-Tierny
Department of Pediatric Cardiology,
Cardiologic Hospital,
59037 Lille, France

C. Planché
Department of Pediatric Cardiac Surgery,
Marie Lannelongue Surgical Center,
92350 Le Plessis Robinson, France

Introduction

Solitary myofibromas and myofibromatosis (multicentric myofibromas) mostly involve cutaneous and subcutaneous tissues, muscle or bones [9, 10]. These benign neoplasms carry an excellent prognosis, often with spontaneous regression. However, the rare generalized form of myofibromatosis with visceral involvement, especially of the lungs, heart, gastrointestinal tract and pancreas, is usually fatal [4, 5]. Otherwise, familial occurrences of myofibromas are exceptionally reported, probably due to overlooked small, asymptomatic or regressive lesions in relatives [1]. We herein report revealing endocardial lesions that were treated by surgical resection in a 12-month-old girl whose father had a neonatal history of myofibromatosis. We discuss the significance of these very unusual lesions, which were not associated with other obvious visceral locations of the disease.

Clinical history

At the age of 12.5 months, a female infant in good health and with no personal past history presented with a hemiplegia. Magnetic resonance imaging showed a large ischemic cerebral lesion with no hemorrhage. Echocardiography showed two lesions in the left atrium, one appearing cystic (Fig. 1). These lesions were mobile with the mitral valve. There was no valvular dysfunction. Diagnosis of cerebral embolization from the heart was made. The two lesions were surgically excised from the mitral valve with a leaflet repair 6 weeks later. No other lesions were observed in the heart. Postoperative echocardiography showed only minimal mitral valve insufficiency. Physical examination of the patient showed no obvious skin lesion. Chest and bone radiograms and abdominal echography were normal. The hemiplegia has partly regressed 1 year after its onset, and the patient is able to walk.

In the neonatal period, the 27-year-old father of the child had suffered from severe laryngeal dyspnea, which had required a surgical treatment. At that time, histological diagnosis of congenital fibromatosis had been made by the resection of one of several cutaneous nodules that disappeared in the following months. No pathological report about the laryngeal lesion is available.

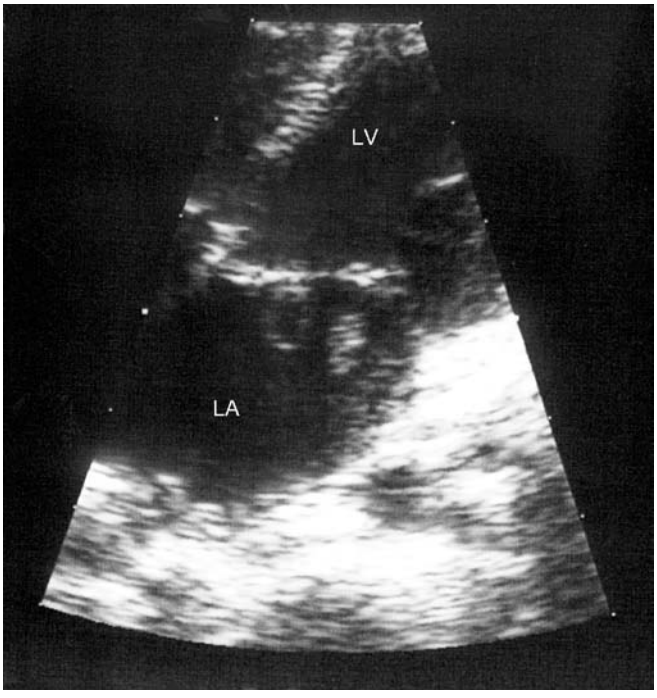

Fig. 1 Echocardiography showing the two lesions in the left atrium (*LA*), close to the mitral valve. The centrally necrotic one appeared cystic. *LV* left ventricle

Materials and methods

The heart lesions were routinely processed, fixed in 10% formalin, embedded in paraffin and stained with hematein and eosin and with Weigert's resorcin-fushin method for elastic fibers. Immunohistochemical study was performed with LSAB2 Kit peroxidase (Dako, Trappes, France). The primary antibodies, directed against the following antigens, were used with the indicated working dilutions: smooth muscle actin (Dako M851, 1/25), desmin (Microm MS376S, Francheville, France, 1/25), CD34 (Immunotech-Beckman 0786, Villepinte, France, 1/25), S100 protein (Dako Z311, 1/50) and ALK1 (Dako M7195, 1/25). Antigen retrieval using microwave was performed for the latter antigen.

Results

The two lesions measured 1×0.8×0.6 cm and 1.5×0.2×0.2 cm, respectively (Fig. 2). Their surface was smooth with no thrombosis. Histological features were characteristic of myofibromas (Fig. 3 and Fig. 4). The lesions were multi-nodular. In the periphery of the nodules, spindle-shaped tumor cells, with an eosinophilic cytoplasm and a vesicular nucleus, were arranged in bundles. In the center of the nodules, tumor cells were smaller and associated with vessels showing a hemangiopericytoma-like pattern. Rare normal mitotic features were present (1/10 high-power field). The lesions also contained fibrous areas. The center of the rounded lesion was necrotic, which explained the echographic cystic appearance. There was no calcification. Fushin resorcin stain showed no elastic fibers in the lesions beyond the

Fig. 2 Macroscopic appearance of the two resected lesions, one rounded and one elongated, with a smooth surface. Millimetric scale

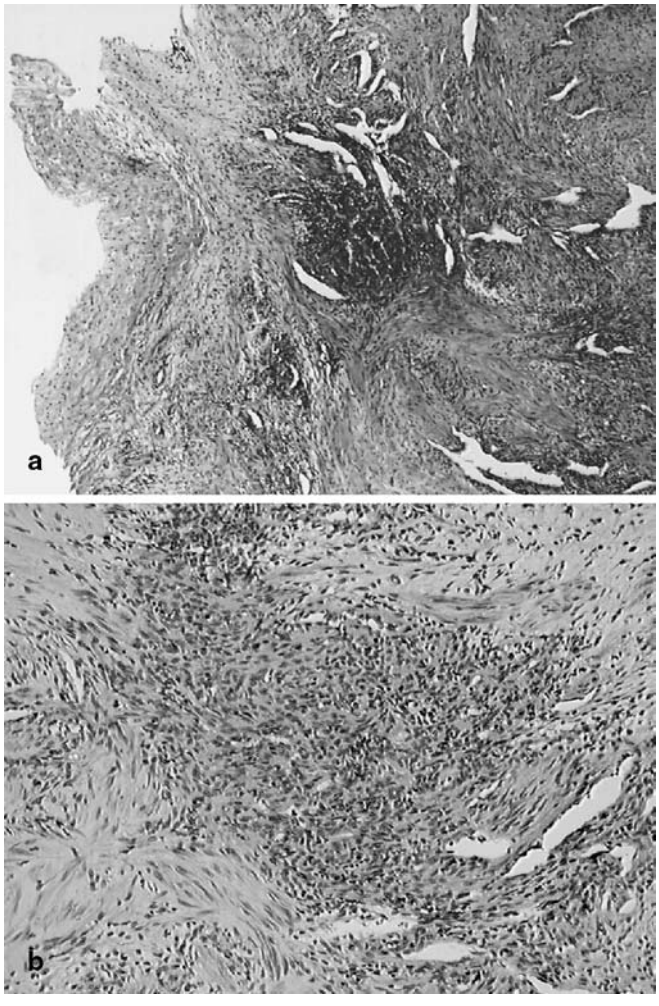

Fig. 3 **A** Low magnification of a lesion with its valvular base (*left*); hematein and eosin, ×20. **B** Cellular nodule with small spindle cells and large vessels, surrounded by bundles of larger elongated cells, characteristic of a myofibroma; hematein and eosin, ×40

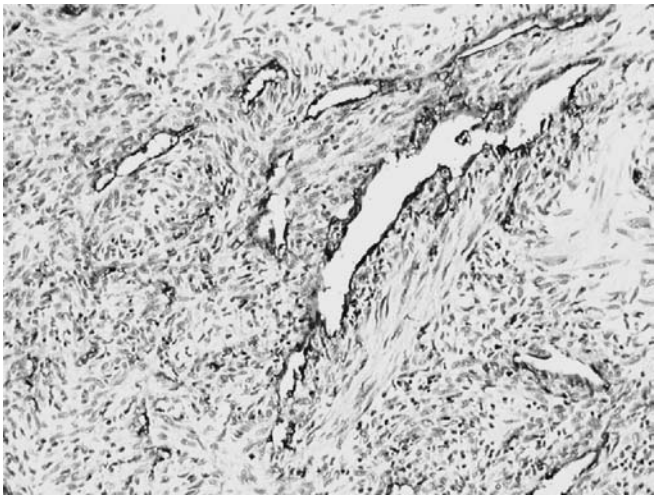

Fig. 4 Immunohistochemistry with anti-CD34 antibody, highlighting the hemangiopericytoma-like appearance of the lesion with CD34-positive endothelial cells of the rich vascular network among CD34-negative tumor spindle cells; ×100

small valvular base. This valvular base was only superficially invaded (Fig. 3).

Tumor cells expressed smooth-muscle actin, especially in the bundles at the periphery of the nodules. These tumor cells were negative for desmin, S100 protein, ALK1 and CD34. CD34 immunostaining of endothelial cells highlighted the hemangiopericytic pattern (Fig. 4). Scattered CD34-positive endothelial cells also were present at the surface of the lesions.

Discussion

In myofibromatosis, heart lesions have only been reported in the rare generalized form, with visceral involvement [4, 5]. This generalized form is characterized by a significant morbidity and mortality, resulting from vital organ obstruction, failure to thrive or infection [10]. Heart involvement has been reported as a frequent finding in autopsy cases with disseminated lesions [4, 5]. Macroscopic appearance of multiple nodules in the left and right ventricular and septal myocardium is illustrated in one case [5]. Otherwise, heart locations are not specifically described, and we have not found any mention of endocardial lesions. Rare visceral myofibromas may be cured by surgery or show spontaneous regression [7]. However, our case, with a cardiac lesion cured by surgery and unassociated with other obvious visceral lesions, is very surprising. Visceral myofibromas are usually not well delineated [10], while the lesions in our case did not invade the underlying cardiac valve. Thus, the clinical setting and the macroscopic feature of our case led us to think that the endocardial lesions did not represent a true visceral involvement. Such endocardial locations are rather similar to the frequent intravascular subendothelial growth frequently observed in myofibromas, regardless of their location [9]. This endovascular growth does not have any prognostic significance [10], but our case illustrates the risk of embolization.

There is no firm conclusion regarding the genetics of myofibromatosis, since only rare familial cases of have been documented [9]. Cases in siblings or with consanguinity suggest an autosomal recessive mode of inheritance, but occurrences in half-sisters or in successive generations, as in our case, make an autosomal dominant hereditary disease more likely [1].

The elongated shape of one endocardial lesion in our case contrasted with the usual nodular shape of a myofibromas. This was possibly related to the constant and rapid movement of the lesion with the mitral valve in the blood flow. However, mechanical phenomena in the heart do not seem to alter histological features of myofibromas, which present no histological particularity related to myocardial or endocardial location.

Our case, occurring on the mitral valve, could have clinically simulated a papillary fibroelastoma, which is the most common primary tumor of heart valves, or a cardiac myxoma, which is the most common primary endocardial tumor. However, pathological features of papillary fibroelastomas and myxomas [2] are totally different from those of myofibromas. Histologically, infantile heart tumors showing the same myofibroblastic differentiation as myofibromas, namely cardiac fibromas and inflammatory myofibroblastic tumors, must be considered in the differential diagnosis [6]. Cardiac fibroma is more frequent. Unlike myofibroma, cardiac fibroma is a unique lesion, which only develops within the myocardium. Furthermore, cardiac fibroma lacks hemangiopericytoma-like features and contains elastic fibers. Single or multiple inflammatory myofibroblastic tumors of the heart have rarely been reported [6]. Inflammatory myofibroblastic tumor differs from myofibroma due to its prominent inflammatory infiltrate, including plasma cells, and its lack of hemangiopericytic areas. ALK1 immunoreactivity in inflammatory myofibroblastic tumor may also be an adjunct to differential diagnosis [3]. Otherwise, infantile hemangiopericytoma and myofibroma are now regarded as a single entity [8].

In conclusion, the present case of myofibromatosis, which occurred in a familial setting, presented with a very unusual endocardial location. We suggest that this isolated cardiac involvement, cured by surgical resection, did not represent a true visceral form of the disease, but was rather a subendothelial lesion without bad neoplastic significance, despite a risk of embolization.

Acknowledgement We thank Pr. B. Gosselin for having enabled us to review the slides of the infantile cutaneous myofibroma of the patient's father.

References

1. Bracko M, Cindro L, Golouh R (1992) Familial occurrence of infantile myofibromatosis. Cancer 69:1294–1299
2. Burke A, Virmani R (eds) (1996) Tumors of the heart and great vessels. Atlas of tumor pathology. AFIP, Washington DC

3. Cessna MH, Zhou H, Sanger WG, Perkins SL, Tripp S, Pickering D, Daines C, Coffin CM (2002) Expression of ALK1 and p80 in inflammatory myofibroblastic tumor and its mesenchymal mimics: a study of 135 cases. Mod Pathol 15:931–938
4. Chung EB, Enzinger FM (1981) Infantile myofibromatosis. Cancer 48:1807–1818
5. Coffin CM, Neilson KA, Ingels S, Frank-Gerszberg R, Dehner LP (1995) Congenital generalized myofibromatosis: a disseminated angiocentric myofibromatosis. Pediatr Pathol Lab Med 15:571–587
6. de Montpréville VT, Serraf A, Aznag H, Nashashibi N, Planché C, Dulmet E (2001) Fibroma and inflammatory myofibroblastic tumor of the heart. Ann Diagn Pathol 5:335–342
7. Hatzidaki E, Korakaki E, Voloudaki A, Daskaloyannaki M, Manoura A, Giannakopoulou C (2001) Infantile myofibromatosis with visceral involvement and complete spontaneous regression. J Dermatol 28:379–382
8. Mentzel T, Calonje E, Nascimento AG, Fletcher CD (1994) Infantile hemangiopericytoma versus infantile myofibromatosis. Study of a series suggesting a continuous spectrum of infantile myofibroblastic lesions. Am J Surg Pathol 18:922–930
9. Rubin BP, Bridge JA (2002) Myofibroma/myofibromatosis. In: Fletcher CDM, Unni KK, Mertens F (eds) WHO classification of tumours. Pathology and genetics of tumours of soft tissue and bone. IARC Press, Lyon, pp 59–61
10. Weiss SW, Goldblum JR (eds) (2001) Enzinger and Weiss's soft tissue tumors, 4th edn. Mosby, St. Louis

Virchows Arch (2004) 444:304–306
DOI 10.1007/s00428-003-0957-1

LETTER TO THE EDITOR

Akihiko Yoshizawa · Hiroyoshi Ota · Nobuki Sakaguchi · Shinichiro Kanai · Jun Nakayama · Kenji Matsuzawa · Shigetoshi Tsuzuki · Reiko Takada · Fujie Miyazawa · Hiroko Kasahara · Tsutomu Katsuyama

Malignant granular cell tumor of the esophagus

Received: 4 February 2003 / Accepted: 28 November 2003 / Published online: 24 January 2004

Sir, We have recently encountered an interesting case of a malignant granular cell tumor of the esophagus. The patient was a 71-year-old man who died of malignant granular cell tumor of the esophagus with pleural effusion and multiple liver metastases.

The patient presented complaining of dysphagia for the past 10 months. A barium swallow showed a filling defect in the lower part of esophagus. Esophagogastroendoscopy showed a submucosal tumor with central ulceration located 35 cm distal from the incisor teeth. The computed tomography scan (CT) of his chest revealed a solid tumor mass measuring 6×4 cm in diameter with obstruction in the mid-esophagus. Biopsies of this area demonstrated a granular cell tumor. The patient subsequently underwent an esophagogastrectomy.

The resected esophagus revealed a submucosal tumor in the mid-esophagus. It was a poorly defined mass, measuring 10×5 cm in length, with circumferential involvement. At the cut surface, the tumor was white, firm and involved beyond the proper muscle layer into the adventitia.

Microscopically, tumor cells mainly grew in the submucosa and infiltrated beyond the proper muscle layer into the adventitia. The surgical margin was free of tumor cells. Pseudoepitheliomatous hyperplasia of the squamous epithelium overlying esophageal tumor was present.

The tumor cells were arranged in small clusters divided by thin fibrous connective tissue septa (Fig. 1). The tumor cells showed oval, polygonal or spindle-shaped cytoplasm with abundant eosinophilic cytoplasmic granules (Fig. 1). Occasional mitotic figures were seen (mitotic index: 0.3%) (Fig. 1). In some areas, the tumor cells showed nuclear pleomorphism with prominent nuclear atypia. Small necrotic foci were present. Oval-shaped tumor cells with small blunt nuclei were noted to proliferate in the lamina propria, just beneath the esophageal epithelium. Lymph-node metastasis was not observed. Immunohistochemically, most tumor cells were positive for S-100 protein (Dako, CA, USA), keratan sulfate (Seikagaku Kogyo, Japan), neuron specific enolase (Dako), CD68 (Dako), and vimentin (Dako), and about one-third of tumor cells were positive for CD57 (Beckton Dickinson, CA, USA). Collagen type IV (Dako) was demonstrated around nests of tumor cells. The tumor cells showed no reactivity for carcinoembryonic antigen (Dako), myelin basic protein (Dako), CD34 (Dako), c-kit (Dako), chromogranin A (Dako), synaptophysin (Dako) and p53 (Dako). The tumor cells showed a higher Ki67 value (8.3%±2.1) than five cases of benign granular cell tumors used as controls (3.3%±2.9). In addition, the tumor cells with small blunt nuclei in the lamina propria, just beneath the esophageal epithelium, showed lower proliferative activity than the tumor cells showing pleo-

A. Yoshizawa · S. Kanai
Department of Laboratory Medicine,
Shinshu University Hospital,
Matsumoto, Japan

H. Ota (✉)
Department of Biomedical Laboratory Sciences,
School of Health Sciences and Department of Laboratory Medicine,
Shinshu University School of Medicine,
3-1-1 Asahi, Matsumoto, 390-8621 Nagano, Japan
e-mail: hohta@gipac.shinshu-u.ac.jp
Tel.: +81-26-3372389
Fax: +81-26-3372389

N. Sakaguchi
First Department of Internal Medicine,
Shinshu University School of Medicine,
Matsumoto, Japan

J. Nakayama
Department of Pathology and Department of Laboratory Medicine,
Shinshu University School of Medicine,
Matsumoto, Japan

K. Matsuzawa · S. Tsuzuki · R. Takada · F. Miyazawa · H. Kasahara
Maruko Chuo General Hospital,
Maruko, Japan

T. Katsuyama
Department of Laboratory Medicine,
Shinshu University School of Medicine,
Matsumoto, Japan

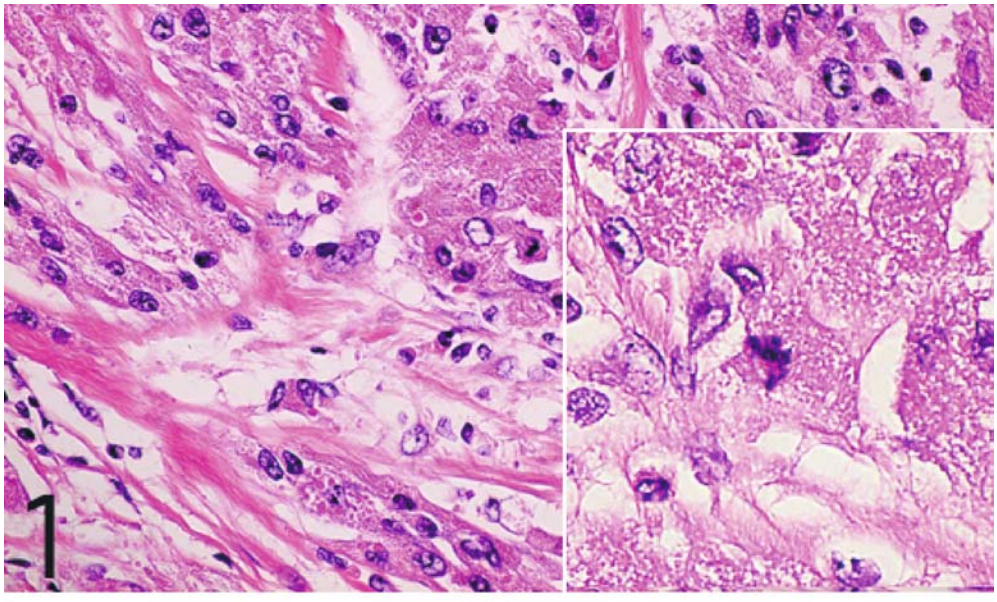

Fig. 1 Tumor cells are arranged in small clusters divided by thin fibrous connective tissue septa. Tumor cells show abundant eosinophilic granular cytoplasm with numerous coarse granules. (Hematoxylin and eosin (H&E) stain, original magnification ×100). Inset: mitotic figure is present. (H&E stain, original magnification ×400)

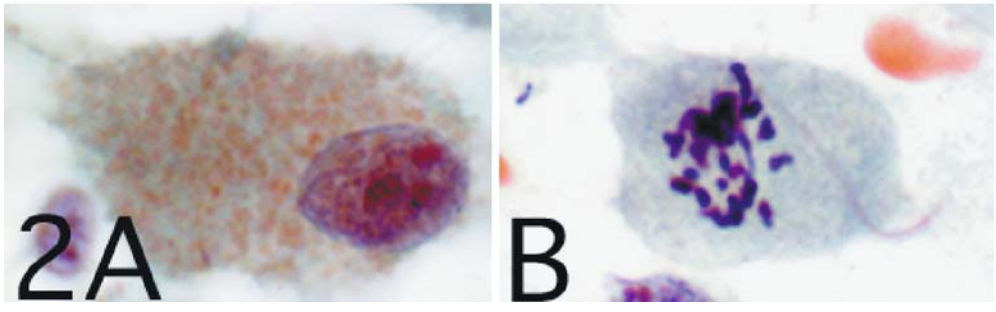

Fig. 2 Tumor cells obtained from the resected tumor showed increased nuclear to cytoplasmic ratio, abundant acidophilic granular cytoplasm with numerous coarse granules, and hyperchromatic coarse nuclei with large nucleoli (**A**). Mitotic figure is present (**B**). (Papanicolaou-stain, original magnification ×1000)

morphism. Electron microscopically, the cytoplasm of the tumor cells was abundant, with numerous lysosomes. On Papanicolaou-stained smears obtained from the resected tumor, tumor cells showed abundant acidophilic granular cytoplasm with a lot of coarse granules positive for diastase-resistant periodic acid-Schiff (PAS) reaction, increased nuclear to cytoplasmic (N/C) ratio, pleomorphic nuclei with hyperchromasia and coarse chromatin, large nucleoli throughout the cytological sample (Fig. 2A) and immunoreactivity for S100 protein. Some multi-nucleate tumor cells and mitotic figures were also seen (Fig. 2B). The patient developed bilateral pleural effusion 4 years after the surgical resection. Aspiration preparations obtained from the pleural effusion revealed tumor cells similar to those seen in smears obtained from the resected tumor, and the tumor cells were immunoreactive for S-100 protein. A CT scan of his abdomen showed multiple nodular lesions in his liver, which had not been seen on the CT scan done before the esophagogastrectomy. The biopsy from the nodular lesions in his liver was not done, and metastasis of the granular cell tumor to the liver was clinically assumed. The patient died of respiratory failure 4 months later. Autopsy was not done.

The present tumor had characteristic morphological and immunohistochemical features, indicating a granular cell tumor. Thus, the tumor cells had abundant acidophilic granular cytoplasm with diastase-resistant PAS-positive lysosomal granules. Immunohistochemically, the tumor cells were positive with markers indicative for granular cell tumors: S-100 protein, keratan sulfate, CD57, vimentin, NSE and CD68 [7]. Negative staining of endocrine markers and myogenic markers was helpful to differentiate this tumor from endocrine tumors or myogenic tumors [7]. This tumor was also different from gastrointestinal stromal tumor on the basis of negative staining for CD34 and c-kit and from peripheral nerve sheath tumor on the basis of positive reaction for keratan sulfate [2, 7].

Granular cell tumor is generally a benign tumor occurring in any part of the body [7]. Malignant granular cell tumor is extremely rare, estimated to be 1–2% of all cases [7]. Four cases of malignant esophageal granular cell tumor have been reported [1, 5, 6, 9]. Crawford and DeBakey reported a case of 31-year-old female patient with infiltration into the trachea and thyroid cartilage [1]. The 23-year-old female patient reported by Obiditsch-Mayer and Salzer-Kuntschik had prominent tracheal and esophageal infiltration, as well as metastases to the cervical lymph nodes, and died 7 months later [5]. Ohmori et al. reported a 70-year-old female patient with malignant granular cell tumor with mitotic figures [6]. Wyatt et al. reported a 78-year-old female patient with malignant granular cell tumor with mitotic figures and vascular invasion [9]. Recently, Fanburg-Smith et al.

proposed histological criteria to define malignant granular cell tumor of the soft part, including necrosis, spindling, vesicular nuclei with lager nucleoli, increased mitotic activity (>2 mitosis/10 high power fields at ×200 magnification) and a high N/C ratio and pleomorphism [3]. They classified the granular cell tumors that satisfy three or more of these criteria as histologically malignant granular cell tumors. More recently, Wieczorek et al. proposed cytological features of malignant granular cell tumor of the soft part, including hyperchromasia, coarse chromatin, increased N/C ratio, nuclear pleomorphism and vesicular nuclei with enlarged nucleoli and spindle cell morphology, which were associated the most closely with malignancy when they were present throughout the cytological sample [8]. They also reported that mitoses were present in malignant granular cell tumors and absent from all benign granular cell tumors [5]. The present case satisfies five of these criteria, including necrosis, spindling, vesicular nuclei with large nucleoli, increased mitotic activity and pleomorphism. In addition, the present case developed pleural dissemination and assumed metastasis to the liver and is, therefore, considered a true malignant form of this generally benign tumor [4]. In the present case, the presence of round to oval shaped tumor cells with small blunt nuclei proliferating in the lamina propria just beneath the esophageal epithelium suggests the possibility of malignant transformation of a preexisting benign granular cell tumor.

Acknowledgements We thank Dr. Kaiyo Takubo, Department of Clinical Pathology, Tokyo Metropolitan Institute of Gerontology, Tokyo, and Professor David Y. Graham, Baylor College of Medicine, Houston, TX, for their helpful comments and encouragement.

References

1. Crawford ES, DeBakey ME (1953) Granular-cell myoblastoma: two unusual cases. Cancer 6:786–789
2. Ehara T, Katsuyama T (1990) Characterization of glycoconjugates found in granular cell tumors, with special reference to keratan sulfate. Virchows Arch 58:221–227
3. Fanburg-Smith JC, Meis-Kindblom JM, Fante R, Kindblom LG (1998) Malignant granular cell tumor of soft tissue: diagnostic criteria and clinicopathologic correlation. Am J Surg Pathol 22:779–794
4. Johnston MJ, Helwig EB (1981) Granular cell tumors of the gastrointestinal tract and perianal region. A study of 74 cases. Dig Dis Sci 26:807–816
5. Obiditsch-Mayer I, Salzer-Kuntschik M (1961) Malignes, "getorntzelliges neurom" sogenanntes, "myoblastenmyom," des oesophagus. Beitr Pathol Anat 125:357–373
6. Ohmori T, Arita N, Uraga N, Tabei R, Tani M, Okamura H (1987) Malignant granular cell tumor of the esophagus. A case report with light and electron microscopic, histochemical, and immunohistochemical study. Acta Pathol Jpn 37:775–783
7. Ordonez NG (1999) Granular cell tumor: a review and update. Adv Anat Pathol 6:186–203
8. Wieczorek TJ, Krane JF, Domanski HA, Akerman M, Carlen B, Misdraji J, Granter SR (2001) Cytologic findings in granular cell tumors, with emphasis on the diagnosis of malignant granular cell tumor by fine-needle aspiration biopsy. Cancer 93:398–408
9. Wyatt MG, O'Donoghue DS, Clarke TJ, Teasdale C (1991) Malignant granular cell tumour of the oesophagus. Eur J Surg Oncol 17:388–391

Virchows Arch (2004) 444:307–308
DOI 10.1007/s00428-004-0983-7

ANNOUNCEMENTS

6–7 April 2004
Non-Operative Breast Pathology Course
Nottingham, UK

This 2-day course will cover aspects of tissue sampling including FNAC and needle core biopsy. Formal lectures and workshops.

For further information contact:
The Blamey Education Centre
Nottingham Breast Institute
City Hospital, Nottingham, NG5 1PB, UK
Tel.: 00 44 (115) 969 1689
E-mail: sbury@ncht.trent.nhs.uk

9–12 May 2004
XIV EUROCELLPATH COURSE: The Impact of Proteomics and Genomics in Pathology
Girona, Spain

The Organising Committee of the next EuroCellPath Course invites you to come to the beautiful city of Girona to enjoy an outstanding program on a very timely topic, addressed by leading authorities in the field, in an inspiring setting. The subjects covered in this course will be the following:

- DNA arrays: Methods and Goals
- Tissue Microarrays: A Tool for Rapid, Efficient Translational Research
- Proteomics: From Genes to Functions
- Tissue Procurement and Handling: Laser Capture Microdissection and Other Techniques
- Bioinformatic Tools for Array Data Mining
- Application of Array Genomics and Proteomics in Pathology
- Molecular Pathology of Genes and Proteins: What to Look For and When.

You may also submit your abstracts on these or other related topics, to be presented either as platform or poster during the Course.

For further information, please contact:
Prof. Josep Lloreta-Trull (local organizer)
Department of Pathology
Hospital del Mar-IMAS-IMIM
Universitat Pumpeu Fabra
Passeig Marítim 25–29, 08003-Barcelona, Spain
Tel.: +34 93 248 30 31, Fax: +34 93 248 31 31
E-mail: jlloreta@imas.imim.es or enter the course website
http://www.tilesa.es/eurocellpath04/

10–14 May 2004
Diagnostic Histopathology of Breast Disease
Hammersmith Hospital (Imperial College), London, UK

A week-long course designed for pathologists at Consultant and Senior Trainee level. The course provides a comprehensive coverage of the Histopathology of Breast Disease, with special emphasis on areas that pose diagnostic difficulties. The participants will be given ample time to study histological preparations, followed by illustrated discussion of the cases. There will be special sessions dealing with the interpretation of core biopsies and fine needle aspirations. There will also be several daily talks dealing with specific topics, given by eminent breast pathologists and followed by discussion. The topics will include reporting breast biopsies, immunohistochemistry, receptor and c-erbB-2 assessment, dealing with the gross specimen, prognostic factors, proliferative lesions/carcinoma in situ, problems in breast pathology, mucinous lesions of the breast, a practical approach to the diagnosis of breast lymphomas and molecular pathology including the morphology of breast cancer associated with BRCA1 & 2 mutation. The faculty will include Ian Ellis, Christopher Elston, Andrew Hanby, Kristin Henry, Stephen Humphreys, Sunil Lakhani, Andrew Lee, Naomi Livni, Sarah Pinder and Sami Shousha.

Further details from:
Wolfson Conference Centre
Hammersmith Hospital
Du Cane Road
London W12 ONN, UK
Tel: (44) 20 8383 3117/3227/3245
Fax: (44) 20 8383 2428
E-mail: wcc@ic.ac.uk

1–11 June 2004
International course on Laboratory Animal Science
Utrecht, The Netherlands

A two week intensive course on laboratory animal science will be organized at the Department of Laboratory Animal Science – Utrecht, The Netherlands in June 2004. This course is organized once a year since 1993.

The objective of this course is to present basic facts and principles that are essential for the humane use and care of animals and for the quality of research.

The contents of the course are in line with recommendations of the Federation of European Laboratory Animal Science Associations (FELASA) regarding the training of the young scientist whose research involves the use of vertebrate animals.

The course may also be of interest for those who intend to set up a similar course at their location. For this purpose, during the course the acquisition of teaching materials can be discussed with the course committee.

For information and application forms please contact:
Prof. L.F.M. van Zutphen, PhD or
Mr. Stephan van Meulebrouck, MA
Department of Laboratory Animal Science
Faculty of Veterinary Medicine
P.O. Box 80.166
3508 TD Utrecht
The Netherlands
Tel.: ++31-30-2532033
Fax: ++31-30-2537997
E-mail: pdk@las.vet.uu.nl
Internet: http://las.vet.uu.nl (click on “Education and Training”)

4–5 June 2004
15th Ljudevit Jurak International Symposium on Comparative Pathology
(http://www.kbsm.hr/Jurak/symposium.htm), will be held in Multimedial center Sestre milosrdnice University Hospital, Vinogradska 29, Zagreb, Croatia.

The main symposium topic is head and neck pathology (including ophthalmopathology). Symposium includes following sections: Pathological Morphology of the Human and Animal Diseases, Iatrogenic, Environmental and Experimental Pathology, Herman Jurak Round Table on Rheumatological Pathology, Telepathology on-line conference, Clinical Forensic Pathology, Slide Seminars *in Histopathology and Cytopathology*, Quiz on Pathology.

For further information please contact:
Davor Tomas, M.D.
Ljudevit Jurak Clinical Department of Pathology
Sestre milosrdnice University Hospital
Vinogradska 29
10000 Zagreb, Croatia
Phone: 385-1-3787-909
Fax: 385-1-3787-244
e-mail: dtomas@kbsm.hr, juraks@kbsm.hr

7–9 June 2004
40th Nottingham Multi-disciplinary Course on breast disease
Nottingham, UK

This non residential course includes one and a half days of multidisciplinary education and one and a half days of seminars specific to each discipline.

For further information contact:
The Blamey Education Centre
Nottingham Breast Institute
City Hospital, Nottingham, NG5 1PB, UK
Tel.: 00 44 (115) 969 1689
E-mail: sbury@ncht.trent.nhs.uk

11–16 July 2004
ULTRAPATH XII: Conference on Diagnostic Electron Microscopy with Surgical, Clinical, and Molecular Pathology Correlations
Barcelona, Spain

The scientific program will cover diagnostic Electron Microscopy as well as Diagnostic Pathology – with immunohistochemical and molecular correlations – and translational research. Renowned experts in the field from both sides of the Atlantic will present updated comprehensive reviews of significant areas of Pathology. In addition, a new section of the meeting will be devoted to a Pathology Review Course. Platform and Poster presentations will also be an important part of the program.

For further information, please contact:
Josep Lloreta-Trull, M.D., Ph.D. (chairman)
Department of Pathology, Hospital del Mar-IMAS-IMIM
Universitat Pompeu Fabra
Passeig Maritim 25–29, 08003-Barcelona, Spain
Tel.: +34 93 248 30 31
Fax: +34 93 248 31 31
E-mail: jlloreta@imas.imim.es.
The Application form and Abstract form can be found on the meeting website, http://www.tilesa.es/ultrapath04/

27–30 July 2004, London
Practical Pulmonary Pathology

This course is designed to provide histopathology and cytopathology trainees and consultants with an opportunity to study diagnostic lung pathology in a comprehensive manner. It comprises lectures and practical microscopy sessions, the latter making up roughly half the time and consisting of individual study of a unique collection of cases.

For further details and application forms please contact:
Professor B Corrin,
Brompton Hospital
London SW3 6NP
Fax: +44 20 7351 8293.
E-mail: b.corrin@ic.ac.uk

9 September 2004
One day course on Advanced Ultrasound of the Breast
Nottingham, UK

For further information contact:
The Blamey Education Centre
Nottingham Breast Institute
City Hospital, Nottingham, NG5 1PB, UK
Tel.: 00 44 (115) 969 1689
E-mail: sbury@ncht.trent.nhs.uk

23–24 September 2004 **(Change of date)**
Thyroid Pathology for the Practicing Pathologist
15 rue de l'Ecole de Médecine, Paris, France

A 2-day course will take place in Paris under the auspices of the French Division of the I.A.P. This course will be given in English by Prof. M. Sobrinho-Simoes (Porto) and Prof. R. Heimann (Brussels).

It will consist of lectures alternating with slide reviews and a slide seminar over a multihead microscope. The cases of this seminar will be sent (on CD) before the meeting. The audience will be limited to 22 participants.

Course fee: 390 euros (320 euros for members of any IAP division). The fees include registration, hand-out, CD of the slide seminar and coffee breaks.

For further information, please contact:
Mrs. M. Fontanière
Administrative Secretary
French Division of the I.A.P. 32 Cours Albert Thomas
69008, Lyon, France
Fax: 33478754311
E-mail: academie.pathologie@wanadoo.fr

11 October 2004
Continuing Medical Education
Nottingham, UK

For further information contact:
The Blamey Education Centre
Nottingham Breast Institute
City Hospital, Nottingham, NG5 1PB, UK
Tel.: 00 44 (115) 969 1689
E-mail: sbury@ncht.trent.nhs.uk

22–24 November 2004
41st Nottingham Multi-disciplinary Course on breast disease
Nottingham, UK

For further information contact:
The Blamey Education Centre
Nottingham Breast Institute
City Hospital, Nottingham, NG5 1PB, UK
Tel.: 00 44 (115) 969 1689
E-mail: sbury@ncht.trent.nhs.uk

Virchows Arch (2004) 444:309–312
DOI 10.1007/s00428-004-0993-5

EDITORIAL

Marco Volante · Francesca Bozzalla-Cassione · Fabio Orlandi · Mauro Papotti

Diagnostic role of galectin-3 in follicular thyroid tumors

Received: 9 October 2003 / Accepted: 27 December 2003 / Published online: 4 March 2004

Background

Galectin-3 is a member of a growing family of beta-galactoside binding animal lectins. It is widely distributed in human tissue and cell types and has a different distribution within the cell, according to cell type and functional status, being either restricted to the nucleus or localized to the cytoplasm and/or the cell surface [1, 13]. Galectin-3 is physiologically produced by macrophages, endothelial cells and several epithelial cells (colon, breast, kidney). Its wide distribution is paralleled by a relatively wide spectrum of actions which have been associated to galectin-3 in both physiological and pathological conditions. In particular, it plays a role in cell–cell and cell–matrix interactions, cell growth, neoplastic transformation, metastatization, cell-cycle regulation and apoptosis, cell damage and repair processes [1, 13]. Since galectin-3 expression is modulated by several oncogenic stimuli, it was shown to be upregulated in different human tumors, including large cell lymphoma, colorectal carcinoma, breast carcinoma, hepatocellular carcinoma, brain tumors, melanoma and finally thyroid carcinoma. In non-medullary thyroid tumors, galectin-3 expression was restricted to malignant follicular-derived tumors. In fact, neither normal nor fetal [17] thyroid cells were found to contain galectin-3 (as opposed to other galectins which can be expressed even in physiological conditions). In addition, hyperplastic lesions and benign thyroid tumors also lacked galectin-3 expression [1, 13], although these latter observations were not confirmed by all authors [9, 11] (see below).

M. Volante · F. Bozzalla-Cassione · M. Papotti (✉)
Department of Biomedical Sciences & Oncology,
University of Turin,
Via Santena 7, 10126 Torino, Italy
e-mail: mauro.papotti@molinette.unito.it
Fax: +39-011-6635267

F. Orlandi
Department of Clinical & Biological Sciences,
University of Turin,
Torino, Italy

F. Orlandi · M. Papotti
S. Luigi Hospital,
Orbassano (Torino), Italy

Surgical and cytological specimens

These findings prompted extensive investigations in the field of follicular-derived thyroid tumors, since the availability of a marker of malignant transformation in follicular tumors would have been of paramount importance in diagnostic pathology in general and in fine-needle aspiration biopsy (FNAB) cytological diagnosis, in particular. The preliminary results obtained in a relatively small series of thyroid tumors and/or FNABs showed a relatively high sensitivity and specificity of the marker galectin-3 in taking follicular adenomas apart from carcinomas [3, 5, 13]. A large multicentric study coordinated in 2001 by Dr A. Bartolazzi (University of Rome) validated the role of galectin-3 in the differential diagnosis of follicular adenomas from follicular/papillary carcinomas, with the specificity and sensitivity being higher than 95% in both surgical and cytological specimens [1]. These results were obtained in six different centers and were based on the use of a purified monoclonal antibody to galectin-3 (produced by Dr A. Bartolazzi) and the use of a strictly biotin-free detection system. Under such strictly controlled technical conditions, it seemed reasonable to suggest that cytological samples of follicular neoplasms found to contain galectin-3 (Fig. 1a) would have probably been malignant tumors to be sent to the surgeon, as opposed to galectin-3-negative follicular nodules, possibly consistent with hyperplastic or adenomatous nodules that could have been kept under clinical follow-up. A special comment is deserved for the rare cases of follicular adenomas immunoreactive for galectin-3, a finding currently poorly understood. These cases may represent true false positives by immunohistochemistry; however, they may also represent lesions having a biologically malignant potential in the absence

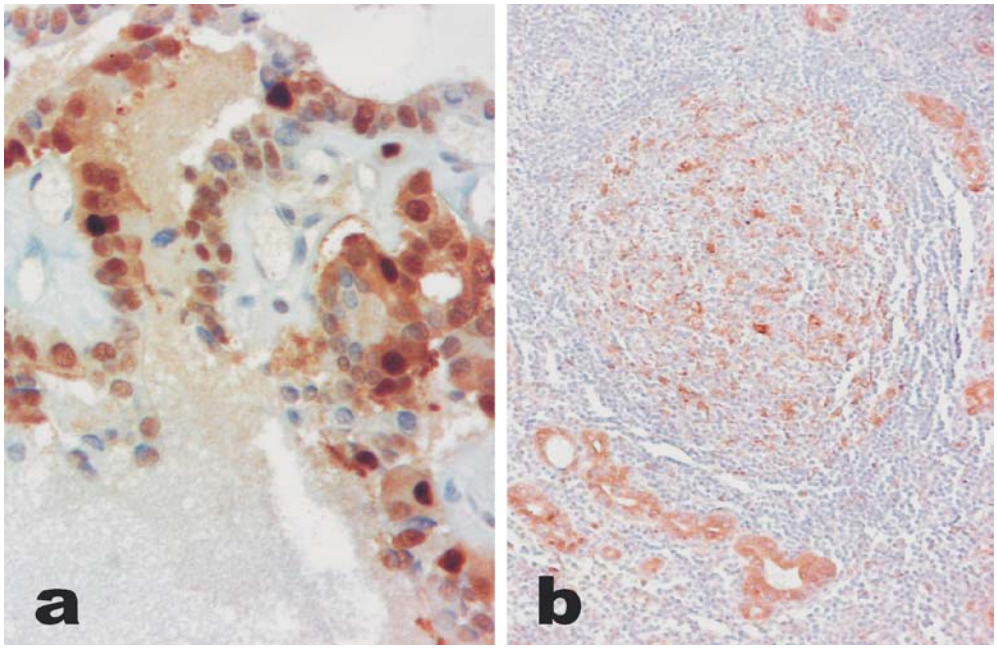

Fig. 1 **a** Galectin-3 immunoreactivity in a "cell block" from a fine-needle aspiration biopsy of a histologically confirmed follicular carcinoma (immunoperoxidase, 400×). **b** Focal galectin-3 positivity in oxyphilic cells of Hashimoto's thyroiditis. Macrophages of the germinal center of a lymphoid follicle are also positive and serve as internal positive control (immunoperoxidase, 200×)

Table 1 Immunohistochemical detection of galectin-3 in oxyphilic cell lesions of the thyroid

Diagnosis	Galectin-3 immunoreactivity
Nodular goiter with oxyphilic changes	0/13 (0%)
Hashimoto's thyroiditis	14*/15 (93%)
Oxyphilic adenomas	6*/45 (13%)
Oxyphilic carcinomas	46/49 (94%)

* Focal immunoreactivity

of morphological signs of invasive growth. As opposed to molecular markers (the PAX8-PPARgamma gene fusion product for example), which possess oncogenic implications and therefore are an early event in malignant transformation, galectin-3 regulation in benign tumors having malignant potential as well as in early malignant lesions is poorly understood. In our experience, the occurrence of galectin-3 immunoreactivity in adenomas is peculiar to oxyphilic tumors. Preliminary data on galectin-3 immunocytochemistry in a large series of oxyphilic cell tumors are summarized in Table 1. In such cases, sensitivity and specificity values were 94% and 87%, respectively. Moreover, we were able to confirm previous findings on the presence of galectin-3 immunoreactivity in single follicular cells in the setting of Hashimoto's thyroiditis (Fig. 1b).

Technical problems

In practical terms, based on some controversial data present in the literature, galectin-3 immunocytochemical procedure still deserves validation and better setting. In fact, a few recent papers suggested that galectin-3 immunodetection is not restricted to malignant tumors, but is also observed in follicular adenomas [9, 10, 11]. The reasons for the reported discrepancies among different authors are multiple. In the thyroid gland, oxyphilic cells are rich in endogenous biotin and galectin-3 immunocytochemistry (as well as many other immunocytochemical stainings) may provide false-positive results in oxyphilic cell lesions due to biotin-based detection systems, especially when heat-induced antigen-retrieval methods, as in the case of galectin-3 immunocytochemistry, are needed. Therefore, as correctly pointed out by the group of Dr LiVolsi [7], galectin-3 immunodetection may be a useful adjunct to distinguish benign from malignant thyroid tumors, only if used in a biotin-free detection system. We would add that, as for any other antibody, the proper working dilutions and technical conditions are to be set in any laboratory, based on the type of primary antibody and the tissue or cell tested (paraffin sections vs smears; formalin vs alcoholic fixation; etc). Moreover, the technical procedure used to reveal galectin-3 is also crucial, because only methods aimed to localize the molecule in the tissue are reliable to interpret the final results. Immunohistochemistry and in situ hybridization are therefore the only acceptable methods in diagnostic pathology or cytology. In fact, polymerase chain reaction-based techniques, although highly sensitive, cannot distinguish the cell population expressing galectin-3 mRNA [11]. Since it is well known that macrophages and endothelial cells produce relatively large amounts of galectin-3 in physiological conditions, such cell types may well be present in the thyroid tumor or nodule submitted to PCR analysis [2]. In addition, although the immunohistochemical expression of galectin-3 was found to correlate with mRNA expression [5], it is not completely understood how mRNA transcription is regulated in benign conditions. That is, could follicular adenoma

lack the protein but express a certain level of galectin-3 mRNA? An answer is currently lacking and preliminary data from our laboratory indicate that in situ hybridization for galectin-3 mRNA using a specific oligonucleotide probe is also positive in some "follicular adenomas" (according to the currently accepted morphological criteria of diagnosis) in the absence of any corresponding immunoreactivity.

Practical applications

In surgical specimens, since the literature reported data on its high sensitivity and specificity (over 95%) [1], galectin-3 is a useful tool to ascertain the malignant nature of a follicular-patterned capsulated nodule, made of cells having clear nuclei suspected for papillary carcinoma, i.e., for the differential diagnosis of follicular adenoma from follicular variant papillary carcinoma. In addition, it is reliable in the distinction of follicular adenoma from minimally invasive follicular carcinoma, in those cases lacking clear-cut morphological criteria [16]. Finally, it may serve in the distinction of malignant thyroid cysts from hemorrhagic cysts in the context of hyperplastic goiter. In FNAB cytological specimens (either smears or cell blocks), the indications to galectin-3 immunostaining are restricted to follicular neoplasms (either conventional or oxyphilic). In this context, galectin-3-producing follicular cells most probably represent a malignant process (follicular carcinoma or follicular variant of papillary carcinoma) which needs further treatment. In addition, galectin-3 immunoreaction has been shown to have a higher sensitivity than cytomorphological examination (89.3% and 75%, respectively) in recognizing malignant cells in a cystic tumor, namely a cystic papillary carcinoma, containing rare epithelial cells in the aspirated fluid [14]. In the case of negative galectin-3 reaction, it has to be kept in mind that a percentage of cases have a focal galectin-3 expression and therefore a negative FNAB result is not a negative case by definition. Conversely, a positive galectin-3 reaction is most probably suggestive of a malignant process, although the possibility of a morphologically benign follicular tumor (adenoma) cannot be excluded, due to the rare galectin-3 expression in adenomas.

Any better marker?

Based on the above observation that galectin-3 is highly sensitive and specific, but still a few cases fail to react in the expected way, the search for alternative or additional markers that can increase the diagnostic accuracy is mandatory. The product of the fusion gene PAX8-PPARgamma was found to be expressed by follicular carcinoma nuclei but not by adenomas [8]. This finding was not confirmed in subsequent reports, and the specificity of this marker is rather low. Conversely, other authors have demonstrated the high sensitivity and specificity of HBME-1, a marker of mesothelial cells and tumors, which is overexpressed also by malignant thyroid tumors (follicular and papillary carcinomas), and of specific isoforms of the thyroid peroxidase enzyme (TPO). The reliability of these makers has also been shown in FNAB specimens [6, 15]. Finally, a role of cytokeratin 19 has been proposed [4] in the recognition of papillary carcinoma (strongly positive for cytokeratin 19) as opposed to benign lesions (which are negative). Since none of the above markers is 100% sensitive and specific, it seems that a panel of markers would probably provide the highest diagnostic accuracy in FNAB cytological diagnosis [15]. Moreover, some authors have demonstrated the presence of two alternative and non-overlapping pathogenetic pathways in follicular carcinoma, being the presence of the PAX8-PPARgamma translocation most frequently associated to a galectin-3 positive/HBME-1 negative immunophenotype and the presence of RAS mutations associated to a galectin-3 negative/HBME-1 positive immunophenotype [12]; these data indirectly indicate that a panel of markers including at least galectin-3 and HMBE-1 would probably increase the sensitivity of an immunohistochemical approach up to nearly 100%. Retrospective and prospective analysis are currently under investigation by our group to validate this approach and to select the ideal markers for the purpose of identifying malignant follicular tumors.

Conclusion

According to the literature data, in surgical pathology, galectin-3 is more than 95% sensitive and specific in diagnosing a follicular carcinoma, and represents a very useful tool especially when the thorough morphological evaluation of tumor capsule and vessels, or of nuclear features if a follicular variant papillary carcinoma is the case, does not present clear-cut signs of malignancy. Other authors use HBME-1 or cytokeratin 19 for the same purposes. The combined use of all these markers will probably improve the diagnostic accuracy, and future studies are needed to define the immunohistochemical panel showing the best sensitivity and specificity. In FNAB cytology, many more variables are encountered (smears versus cell blocks, type of fixation, cellularity, etc.). Galectin-3 is sensitive but less specific (at least when compared with current follicular adenoma diagnostic criteria). As for the surgical specimens, a panel of markers is probably the best solution in FNAB cytology, being HBME-1 and cytokeratin 19 the two major candidates to be associated with galectin-3 in the daily diagnostic practice.

Acknowledgements Supported by grants from the Compagnia di San Paolo (Turin), the Regione Piemonte (Turin) (D.G.R. no.°69–8040, 16.12.2002 and D.D. no. 104, 21.07.2003, research project to F.O.) and the Italian Ministry of Education (Rome, ex-60% to M.P.).

References

1. Bartolazzi A, Gasbarri A, Papotti M, Bussolati G, Lucante T, Khan A, Inohara H, Marandino F, Orlandi F, Nardi F, Vecchione A, Tecce R, Larsson O; Thyroid Cancer Study Group (2001) Application of an immunodiagnostic method for improving preoperative diagnosis of nodular thyroid lesions. Lancet 357:1644–1650
2. Bartolazzi A, Papotti M, Orlandi F (2003) Methodological considerations regarding the use of galectin-3 expression analysis in preoperative evaluation of thyroid nodules. J Clin Endocrinol Metab 88:950
3. Cvejic D, Savin S, Paunovic I, Tatic S, Havelka M, Sinadinovic J (1998) Immunohistochemical localization of galectin-3 in malignant and benign human thyroid tissue. Anticancer Res 18:2637–2641
4. Fonseca E, Nesland JM, Hoie J, Sobrinho-Simoes M (1997) Pattern of expression of intermediate cytokeratin filaments in the thyroid gland: an immunohistochemical study of simple and stratified epithelial-type cytokeratins. Virchows Arch 430:239–245
5. Gasbarri A, Martegani MP, Del Prete F, Lucante T, Natali PG, Bartolazzi A (1999) Galectin-3 and CD44v6 isoforms in the preoperative evaluation of thyroid nodules. J Clin Oncol 17:3494–3502
6. Henry JF, Denizot A, Porcelli A, Villafane M, Zoro P, Garcia S, De Micco C (1994) Thyroperoxidase immunodetection for the diagnosis of malignancy on fine-needle aspiration of thyroid nodules. World J Surg 18:529–534
7. Herrmann ME, LiVolsi VA, Pasha TL, Roberts SA, Wojcik EM, Baloch ZW (2002) Immunohistochemical expression of galectin-3 in benign and malignant thyroid lesions. Arch Pathol Lab Med 126:710–713
8. Kroll TG, Sarraf P, Pecciarini L, Chen CJ, Mueller E, Spiegelman BM, Fletcher JA (2000) PAX8-PPARγ1 fusion oncogene in human thyroid carcinoma. Science 289:1357–1360
9. Martins L, Matsuo SE, Ebina KN, Kulcsar MA, Friguglietti CU, Kimura ET (2002) Galectin-3 messenger ribonucleic acid and protein are expressed in benign thyroid tumors. J Clin Endocrinol Metab 87:4806–4810
10. Nascimento MC, Bisi H, Alves VA, Longatto-Filho A, Kanamura CT, Medeiros-Neto G (2001) Differential reactivity for galectin-3 in Hürthle cell adenomas and carcinomas. Endocr Pathol 12:275–279
11. Niedziela M, Maceluch J, Korman E (2002) Galectin-3 is not an universal marker of malignancy in thyroid nodular disease in children and adolescents. J Clin Endocrinol Metab 87:4411–4415
12. Nikiforova MN, Lynch RA, Biddinger PW, Alexander EK, Dorn GW 2nd, Tallini G, Kroll TG, Nikiforov YE (2003) RAS point mutations and PAX8-PPAR gamma rearrangement in thyroid tumors: evidence for distinct molecular pathways in thyroid follicular carcinoma. J Clin Endocrinol Metab 88:2318–2326
13. Orlandi F, Saggiorato E, Pivano G, Puligheddu B, Termine A, Cappia S, De Giuli P, Angeli A (1998) Galectin-3 is a presurgical marker of human thyroid carcinoma. Cancer Res 58:3015–3020
14. Papotti M, Volante M, Saggiorato E, Deandreis D, Veltri A, Orlandi F (2002) Role of galectin-3 immunodetection in the cytological diagnosis of thyroid cystic papillary carcinoma. Eur J Endocrinol 147:515–521
15. Raphael SJ (2002) The meanings of markers: ancillary techniques in diagnosis of thyroid neoplasia. Endocr Pathol 13:301–311
16. Saggiorato E, Cappia S, De Giuli P, Mussa A, Pancani G, Caraci P, Angeli A, Orlandi F (2001) Galectin-3 as a presurgical immunocytodiagnostic marker of minimally invasive follicular thyroid carcinoma. J Clin Endocrinol Metab 86:5152–5158
17. Savin SB, Cvejic DS, Jankovic MM (2003) Expression of galectin-1 and galectin-3 in human fetal thyroid gland. J Histochem Cytochem 51:479–483

Virchows Arch (2004) 444:313–323
DOI 10.1007/s00428-003-0971-3

REVIEW ARTICLE

Mathewos Tessema · Ulrich Lehmann · Hans Kreipe

Cell cycle and no end

Received: 16 September 2003 / Accepted: 17 December 2003 / Published online: 17 February 2004

Abstract Our knowledge about the molecular circuits regulating the duplication of the genetic material and the subsequent division of a cell into two daughter cells has exploded over the last decade. Aberrations in the regulation of the cell cycle belong to the hallmarks of malignant transformation, leading, in turn, to the development of tumours. After introducing the basics of eukaryotic cell-cycle regulation and describing the four phases of the cell cycle (namely, G1, S, G2 and M) in more detail, alterations of key components of the cell-cycle machinery in human malignancies and their functional consequences are presented. Principally, deregulation of the cell cycle can be caused by unrestricted activity of cell-cycle promoting factors (many oncogenes fall into this class) or by inactivation of inhibitory factors (many tumour suppressor genes belong to this class). Both types of deregulation have been described in human tumours and are discussed in detail. Perspectives concerning the translation of this knowledge into daily routine practice and future applications are discussed at the end. The molecular mechanisms of actual cell division (sister chromatid segregation and cytokinesis) are mentioned only briefly.

Keywords Cancer cell cycle · Cyclin · Cyclin-dependent kinases · CDK-inhibitors · Cell-cycle checkpoints · Cell-cycle deregulation

Introduction

A closer look at the cell cycle was suggested 10 years ago, as the importance of defects in the cell-cycle regulatory machinery accomplishing DNA replication and cell division for the development of malignant neoplasia was just emerging [43]. Until then, deregulation of proliferation-stimulating signals and the molecules transducing these signals from the cell surface to the nucleus were primarily in the spotlight. Since then, our knowledge regarding mechanisms regulating the onset of DNA replication and subsequent cell division has exploded in such a way that comprehensive coverage is no longer possible. Whole books and conferences are now dedicated to a topic not so long ago considered to be a somewhat obscure field, primarily dealing with yeast cells and mutant yeast strains having defects in cell-cycle regulation [63]. In 2001, the Nobel prize for physiology and medicine was jointly awarded to Leland H. Hartwell, R. Timothy Hunt and Paul M. Nurse for their discoveries of "key regulators of the cell cycle", acknowledging the importance of molecular insights into the cell cycle to molecular biology and medicine in general.

The growth in knowledge during the past 10 years is best illustrated by the fact that several key molecules now in the focus of cell-cycle research and also at the heart of molecular cancer research were not yet discovered 10 years ago. To name just a few very prominent examples: the $p15^{INK4b}$ and $p16^{INK4a}$ polypeptides and the corresponding genes were first described in 1993 and 1994, respectively [27, 86]. The $p21^{CIP1}$ gene was also identified in 1993 [28, 107], followed by $p27^{KIP1}$ the next year [69, 99]. The $p57^{KIP2}$ gene was cloned in 1995 [47]. The peculiar structure of the $p14^{ARF}/p16^{INK4a}$ locus was also elucidated during 1995 [54, 70, 96].

The importance of deregulated cell-cycle control in the development and progression of malignant neoplasia became so obvious and the examples of affected genes so numerous that cancer was sometimes called a "cell-cycle disease" [4]. But the scenario is more complex, since a transformed cell has to overcome several built-in control mechanisms, such as apoptosis and immune surveillance and has to be supported by neo-angiogenesis [26]. The ability to evade apoptosis is particularly important, as continuous stimulation of proliferation usually activates the apoptotic program and eliminates

M. Tessema · U. Lehmann · H. Kreipe (✉)
Institute of Pathology,
Medizinische Hochschule Hannover,
Carl-Neuberg-Strasse 1, 30625 Hannover, Germany
e-mail: Kreipe.Hans@MH-Hannover.de
Tel.: +49-05-115324501
Fax: +49-05-115325799

these cells from the body [26]. The mechanisms inducing apoptosis and the pathways regulating cell cycle entry and progression are closely interconnected via key regulatory molecules, such as p53, which are involved in regulating both processes [51, 102].

The cell-cycle regulatory machinery is remarkably conserved during evolution from yeast to humans. This allows the substitution of proteins in yeast by their human counterpart and vice versa in experimental settings. Nevertheless, there exist important species-specific differences in the regulation of the cell-cycle entry and progression. These differences have to be taken into account if results from animal models are to be transferred to human pathology [23].

Overview of the normal cell cycle

"Cell cycle" or "cell division cycle" denotes the orderly sequence of events by which a cell duplicates its genetic material (the chromosomes) and divides into two identical daughter cells. It is divided into four distinct phases: in the S phase ("synthesis phase"), the genetic material is duplicated faithfully once and only once, and, in the M phase ("mitosis phase"), the duplicated chromosomes are distributed equally to the two daughter cells. The phases in between were simply named G1 ("gap-1") and G2 ("gap-2"), G1 preceding the S phase and G2 the M phase. Far from being just "gaps", important regulatory mechanisms act during G1 and G2. When a cell does not reach its homeostatic size, does not get the necessary signal for proliferation and is protected by a specific anti-mitogenic signal or terminally differentiated, then it withdraws from the cycle at the early G1-stage into a non-dividing, quiescent or resting stage termed as G0. Most cells in the body of adults are maintained in this G0 stage [52, 57].

The transition from one cell-cycle phase to the next is executed by different classes of cellular proteins (Fig. 1). Cyclin dependent kinases (CDKs), a family of serine/threonine protein kinases that are activated in a cell-cycle stage-specific manner, are the main engines that drive the cell cycle forward [52, 58, 103]. As indicated by the name, association with a regulatory subunit, called cyclin, is an absolute requirement for the kinase activity of the CDKs [16]. Cyclins form a family of closely related proteins that appear and disappear during the cell-cycle phases in a strictly controlled "cyclic" pattern (from which their name was derived) [89]. In mammals, 16 cyclins and 9 CDKs have been identified thus far, but not all of them have a proven function in cell-cycle regulation [33]. Cyclin C, H, K and T, for example, are all structurally similar to the "bona fide cell-cycle cyclins" A, B, D and E, but function primarily in the regulation of basal transcription as components of the RNA polymerase II holoenzyme [33]. The cyclic appearance and disappearance is mediated by transcriptional activation of the cyclin genes and ubiquitin-mediated degradation of the proteins, respectively. In addition to the availability of a particular cyclin, the activities of the different CDKs are also regulated by binding of CDK-inhibitors (CKI), as well as phosphorylation dephosphorylation events [16]. The functional consequences of phosphorylation depend on the particular residue targeted by the kinase. Phosphorylation of the T-loop threonine (T174 in CDK4, T161 in CDK1, T160 in CDK2) by CDK-activating kinase (CAK) activates the CDKs while dephosphorylation of these amino acids by the CDK-associated protein phosphatase has an inhibitory effect. In contrast, phosphorylation of threonine 14/tyrosine 15 residues by WEE1-like kinases inactivate CDKs while dephosphorylation of these amino acids by CDC25 activates the CDKs [45, 52].

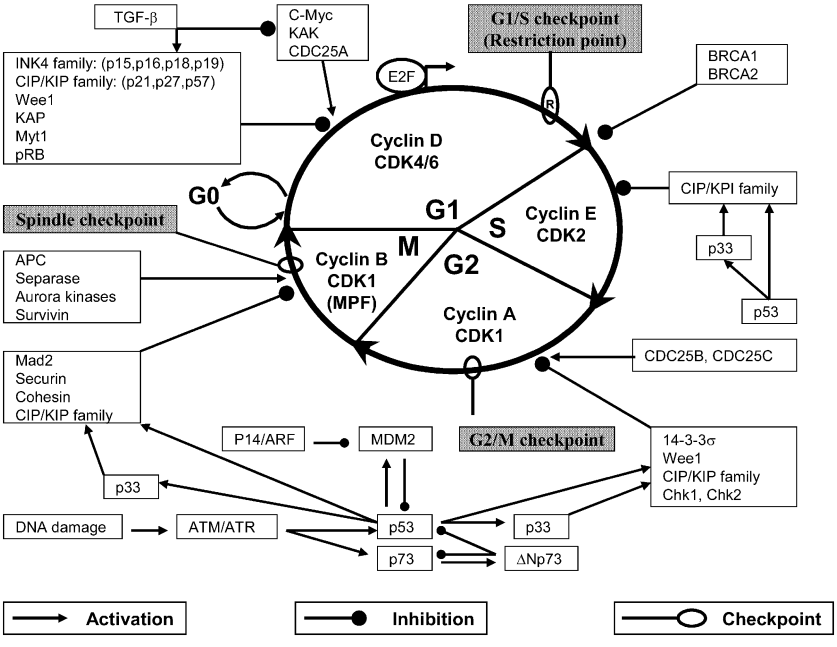

Fig. 1 Negative and positive regulators of the normal cell cycle. Signals promoting and inhibiting the different phases of the cell cycle as well as checkpoints monitoring the proper completion of every phase of the cell cycle are indicated. In the centre of the cycle, the CDK/cyclin complexes driving the respective phase are shown. For details, see the text

In order to strictly control the proper progression of the cell cycle, mammalian cells have also developed a number of regulatory pathways, collectively termed as "cell-cycle checkpoints" (Fig. 1). Checkpoints control the order and timing of cell-cycle transition and ensure that critical events, such as DNA replication and chromosome segregation, are completed accurately. They serve as a brake to pause the cycle in case of DNA damage or errors made in the process [16, 29, 52, 68]. When one cell cycle event has not been successfully completed, checkpoints will delay progression until the step is correctly accomplished, and only then they will relieve the arrest to allow the cell to move to the next phase. In addition to arresting defective cell cycles, checkpoints also mediate repair of DNA damage [64]. Defects in cell-cycle checkpoint pathways result in genomic instability and have been implicated in the transformation of normal cells into cancer cells [16].

Gap-1 phase

Cells respond to extracellular proliferative stimulation only during the G1 phase (and also in G0). Therefore, G1 is the most common target of mitogenic (cell-cycle entry or progression) or anti-proliferative (cell-cycle arrest or exit) signals. Reacting to signals from the extra- or intracellular environment, cells decide either to start a new round of cell division or withdraw from the cell cycle to become quiescent or terminally differentiated [15, 71]. The final commitment to proceed with the cell cycle is made near the end of the G1 phase and is termed the "G1/S transition checkpoint" or "restriction point" (R-point). This represents a "point of no return" because, beyond this checkpoint, cells no longer respond to external signals and proceed with the cycle until completion [90].

In G0 and early G1, the activity of essentially all CDKs (the main cell-cycle engines) is suppressed by the combined action of high CKI activity and low cyclin levels [90]. In the absence of active CDK, the retinoblastoma protein (pRb) stays bound to the E2F, which activates the transcription of genes important for DNA replication only when free from the inhibitory pRb protein [57]. To repeat an already familiar theme: "E2F" is also a family of closely related proteins.

Upon the appropriate extracellular signal stimulating proliferation, D-type cyclins start to accumulate, both due to increased expression as well as reduced proteolysis, indicating a direct link between extracellular stimuli and the cell-cycle machinery [57]. Binding of Cyclin D to CDK4 and CDK6 forms the partially active CDK4/6–Cyclin D complex that later becomes fully active through phosphorylation by CAK [103]. The fully active CDK4/6–Cyclin D holoenzyme phosphorylates pRb and leads to the release of E2F transcription factors, which then, in turn, transcribe many genes that encode proteins required for S-phase entry. Active CDK2/Cyclin E and CDK4/6–Cyclin D holoenzymes together inactivate pRb completely and allow the induction of more E2F-responsive genes that are needed to drive cells through the G1/S transition and to initiate DNA replication [52, 91]. The increase in E2F transcriptional activity further induces more CDK2/Cyclin E as a positive feedback loop. Furthermore, CDK2/Cyclin E facilitates cell-cycle progression through induction of the degradation of inhibitory factors like Hct1 and p27 [57, 90].

In the absence of the appropriate mitogenic signals as well as in the presence of anti-proliferative signals (like transforming growth factor-β) or defective DNA, the G1/S checkpoint is activated and prevents cell-cycle progression. The two families of CKI that serve as effectors of the G1 checkpoint are the INK4 family ($p15^{INK4b}$, $p16^{INK4a}$, $p18^{INK4c}$ and $p19^{INK4d}$) and the CIP/KIP family ($p21^{CIP1}$, $p27^{KIP1}$ and $p57^{KIP2}$). The INK4 family members function only at G1 to inhibit CDK4/6, but the CIP/KIP family serves as CKI in all the four cell-cycle phases [91].

Synthesis phase

S phase is the stage of the cell cycle in which DNA replication and precise duplication of chromosome occurs. It starts when the proteins required for DNA replication reach a sufficient level. Most importantly, during S phase, the cell has to ensure that the chromosomes are replicated once and only once and that restart of DNA replication does not commence before cell division is finished properly. In order to enable replication of the entire genome in a reasonable timeframe, replication in eukaryotes is initiated at multiple (several hundreds to thousands) sites of the chromosomes simultaneously [39]. The re-replication of DNA before proper completion of cell division is prevented by the so-called "replication licensing system". This regulatory system initiates the formation of a pre-replicative complex at every start point of replication. At first, an "origin recognition complex" is established, which is subsequently joined by cdc6/18, cdt1 and the Mcm proteins ("minichromosome maintenance"). Mcm2–7 function as helicases that unwind the DNA ahead of each replication fork. This interaction between Mcm proteins and the origins of replication is a prerequisite for initiation of DNA synthesis, and displacement of the Mcm2–7 during DNA replication prevents re-start of replication [7]. Like in G1, the licensing process and progression during S phase is strictly regulated by CDK activities. Loading of the MCM complex on to chromatin is only allowed when CDK activity is at very low levels, that is, at the end of the M and beginning of the G1 phase [39, 60]. Phosphorylation of components of the DNA replication machinery by CDK2/Cyclin A is important for initiation of DNA replication. Activation of protein kinases is believed to result in changes in the pre-replication complex (pre-RC) that lead to binding of Cdc45 to the Mcm complex and unwinding of the origin of replication [39, 60]. Cyclin A starts to accumulate during S phase and is abruptly destroyed via ubiquitin-mediated proteolysis before meta-

phase [108]. The synthesis of Cyclin A is activated by E2F, but as a negative feedback loop, E2F activity is inhibited by CDK2/Cyclin A via phosphorylation of the E2F heterodimerisation partner DP1 [33]. After complete duplication of all the chromosomes, the cell cycle enters the second gap phase.

Gap-2 phase

Cells at G2 contain replicated chromosomes consisting of two sister chromatids. At this stage of the cell cycle, cells check if all the genetic material and cellular structures, such as centrosomes, are properly duplicated before the actual process of cell division starts. Damage to the DNA and/or incomplete duplication during the synthesis phase triggers checkpoint pathways that initiate cell-cycle arrest in the G2 phase. In case of DNA damage, ATM (ataxia telangiectasia mutated)- and ATR ("ATM and Rad3-related")-dependent signals induce cell-cycle arrest via inhibition of CDK1 (also called CDC2). In response to genotoxic stress caused by ultraviolet light or ionising radiation, the ATR and ATM signalling pathways are activated, which then leads to activating phosphorylation of human checkpoint kinases (Chk1 and Chk2) [12, 76]. Chk1 and Chk2 induce inhibitory phosphorylation of the phosphates CDC25. This phosphorylation event also creates a binding site for a protein called 14–3-3σ, thereby further inhibiting the function. (The name "14–3-3" is derived from the numbering of the fractions in which this protein was originally discovered). This activity of Chk1 and Chk2 keeps CDK1 in an inactive state and prevents entry into mitosis [103].

In addition to the already familiar theme of regulation by phosphorylation/dephosphorylation and synthesis/degradation, the activity of certain molecules is regulated by their intracellular localisation. A prominent example is the CDC25C phosphatase, which normally resides in the nucleus driving the cell cycle forward by dephosphorylation of the inactive CDK1/Cyclin B holoenzyme (as discussed below). Inhibition of CDC25C activity is a key target and occurs in two ways as described above: by phosphorylation and by binding to 14–3-3σ. Formation of the CDC25C/14–3-3σ complex leads to the export of CDC25C into the cytoplasm, where it cannot exert its normal function [1, 20, 95]. Similarly, 14–3-3σ also binds to CDK1/Cyclin B complex and sequesters it in the cytoplasm to maintain a G2 arrest [64].

In addition to its role in G1 arrest, $p21^{CIP1}$ also plays an important role inducing G2 arrest via blocking the interaction between CDC25C and proliferating cell nuclear antigen (PCNA) [1, 38, 95]. *14–3-3σ* and *$p21^{CIP1}$* are direct target genes of transcriptional activation by p53, thereby representing molecular links between the "p53 pathway" (see below) and the cell-cycle machinery [45, 95].

Mitotic phase

The M phase, which combines mitosis (segregation of the cellular components) and cytokinesis (the final division of the cell into two) is the most dynamic phase of the cell cycle. Entry into mitosis is induced by increased activity of CDK1/Cyclin B holoenzyme, also known as MPF ("mitosis promoting factor"). MPF is regulated through inactivating phosphorylation by two other kinases named Myt1 and Wee1. Dephosphorylation of MPF is the rate-limiting step for entry into mitosis and is achieved by at least two phosphatases, CDC25B and CDC25C [45]. Activated MPF phosphorylates numerous substrates, including motor and microtubule-binding proteins that are important for chromosome condensation, nuclear envelop breakdown, spindle assembly and centrosome separation [59].

Sister chromatid separation and exit from mitosis are controlled by anaphase-promoting complex ("APC"), a ubiquitin-protein ligase that targets key proteins for proteolysis [79]. Sister chromatids are bound together at the kinetochore by a protein called "cohesin" and separation occurs only when "separase" (a protease) cleaves the cohesin off. For this to happen, separase must first be liberated from its inhibitor, "securin", which is destined to degradation by active APC [59]. Another checkpoint, the so-called "mitotic checkpoint" or "spindle-assembly checkpoint", prevents entry into anaphase (segregation of sister chromatids) until both kinetochores of every duplicated chromatid pair have attached correctly to spindle microtubules [59, 79]. The presence of even a single unattached kinetochore leads to the activation of Mad2, which binds transiently to loose unattached kinetochores. This binding event activates Mad2 in order to inhibit APC, thereby preventing the transition from metaphase to anaphase [59, 79]. Proper bipolar attachment of the kinetochores leads to dephosphorylation and relocalisation of Mad2, reiterating the theme of "regulation by localisation". Once the inhibition of APC is abolished, mitosis can resume and the cell cycle can be finished [79].

Cell cycle in cancer

Aberrant activation of the cell cycle can be achieved by induction of positive regulators (often encoded by proto-oncogenes) or through inactivation of negative regulators (often encoded by tumour suppressor genes). Induction of positive regulators is caused by overexpression or mutations leading to permanent protein activity. Inactivation of repressors is caused by deletion, mutation or promoter hypermethylation. All mechanisms can be found in human cancer (Fig. 2).

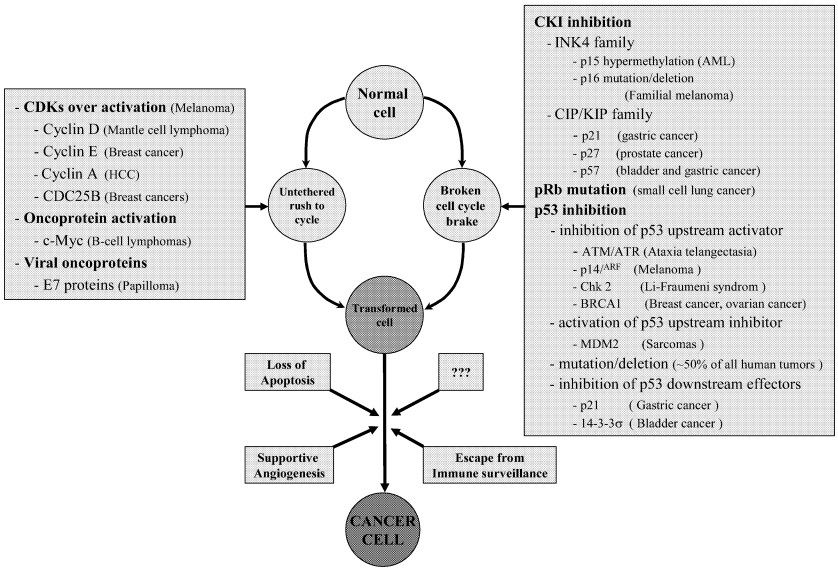

Fig. 2 Deregulation of the cell cycle in cancer. Upregulation of cell-cycle activators and downregulation of cell-cycle inhibitors are both involved in promoting the transformation of a normal cell into a continuously proliferating cell, which is independent of growth-promoting signals and resistant to growth-inhibiting signals. When this transformation is supported by other mechanisms, such as angiogenesis as well as evasion of apoptosis and immune surveillance, it will create the clonogenic malignant cell. For every alteration of cell-cycle regulators, only one example of an associated human malignancy is given. The two-dimensional representation is clearly simplifying the complex interdependence of all participating factors. For further details, see the text and references therein

Activation of cell-cycle promoters

Overexpression of Cyclin D1 caused by gene amplification or aberrant activation of protein synthesis is frequently found in several human tumours. It occurs in more than 90% of mantle cell lymphoma, 60% of breast carcinomas, 40% of squamous cell carcinomas of the head and neck, 40% of colorectal cancers, 20% of prostate cancers and also frequently in lung cancer [24, 67, 94]. Aberrant activation of the *cyclin D1* gene can be induced by chromosomal rearrangement, such as translocation and inversion, which could bring this gene under the influence of a strong promoter or enhancer. t(11;14)(q13;32) and inv(11)(p15;q13), for example, lead to *cyclin D1* activation and are associated with B-cell lymphomas and parathyroid adenomas, respectively [24, 33]. Although not that common, overexpression of Cyclin D2 and D3 has also been reported in some tumours [33]. Deregulation of another G1/S cyclin, Cyclin E, has also been associated with different tumours, and its overexpression is demonstrated to be a powerful predictor of breast cancer outcome [10, 25, 82]. A hyperactive lower molecular weight isoform of Cyclin E that is capable of driving the G1/S transition more efficiently and is overexpressed in breast cancer cells has also been recently identified [32, 46]. Deregulated expression of Cyclin E also induces chromosomal instability, thereby contributing to tumourigenesis [93]. Increased expression of Cyclin A has also been detected in many types of human cancers. In hepatocellular carcinoma, for instance, higher expression of Cyclin A has been found in up to 80% of cases [108]. Despite the strong association between overexpression of several cyclins with the development and progression of tumours, molecular alterations of their binding partners (the CDKs) have been found, thus far, only rarely in cancer. Overexpression of CDK4 and CDK6 as well as constitutively active mutants of these kinases has been reported in some human tumours [46, 95, 104].

c-*Myc* is a potent proto-oncogene that encodes a transcription factor and can promote cell proliferation. It responds to growth-promoting signals in G1 phase by activating the transcription of genes that induce cell-cycle progression, such as *cdc25A*, *cyclin D1*, *D2*, *E*, *A*, *CDK1*, *CDK2*, *CDK4* and *E2F* [32, 45, 46, 103]. Elevated c-Myc expression due to translocation juxtaposing the c-*myc* gene with the immunoglobulin gene enhancer results in B-cell tumours [34]. Overexpression of the c-Myc protein can also be achieved by gene amplification, an alteration frequently seen in breast cancer, which could also serve as a prognostic marker in this malignancy [78].

Overexpression of MDM 2 acts as a positive stimulation of the cell cycle because it antagonises the action of the cell-cycle "brake" p53 (discussed below). Increased expression has been reported in haematological and epithelial malignancies and represents an alternative mechanism to p53 inactivation [103]. Again, this overexpression is mainly caused by an increase in gene copy number.

p73 belongs together with p63 to the family of p53-related proteins, which all are involved in cell-cycle arrest and induction of apoptosis (discussed below). Interest-

ingly, the *p73* gene (first identified in 1997) [35] encodes an N-terminally truncated isoform, called ΔNp73, which acts as a p53 and p73 antagonist. Since the expression of ΔNp73 is induced by p53 and p73, this creates a peculiar negative feedback-loop. Overexpression of ΔNp73 in neuroblastoma turned out to be a new marker for poor prognosis, independent of established prognostic factors, such as tumour stage or N-Myc amplification [56].

The family of CDC25 phosphatases represents another promoter of cell-cycle progression, mainly acting through activation of the CDKs. Overexpression of these phosphatases, particularly of CDC25B, has been observed in 32% of primary breast cancers [103].

Potentially, tumourigenic DNA viruses encode proteins, which also target activation of the cell cycle via pRb hyperphosphorylation [13, 15]. Examples are the adenovirus E1A protein, SV40 T-antigen and HPV protein E7. Although activation of the E2F family of transcription factors is the ultimate target in both normal as well as malignant transformed cells, thus far only circumstantial evidences for molecular alterations of *E2F* genes in human tumours have been described [33].

Inactivation of cell-cycle checkpoints

Similar to the activation of cell-cycle promoters, defects in cell-cycle checkpoints lead to uncontrolled proliferation and could result in malignancy (Fig. 2). In general, two pathways are involved in the negative regulation of the cell cycle: the "Rb pathway" and "p53 pathway" [77]. The "Rb pathway" includes the pRb protein and the two families of CKI (the INK4-family and the CIP/KIP-family). All CKIs inhibit activation of the various CDKs and prevent phosphorylation of *pRb*. The rate of G1/S transition and, therefore, the cell cycle depends on the rate of *pRb* phosphorylation by the CDK4/6–Cyclin D and CDK2/Cyclin E complexes [14, 24]. It is, therefore, not surprising that approximately 90% of human cancers have abnormalities in at least one component of the Rb pathway [24].

Abnormalities in the $p16^{INK4a}$ gene, such as inactivating mutations and deletions, are the second most frequent genetic aberration in human cancers next to defects of the *p53* gene. They occur in a wide range of haematological and epithelial malignancies [14, 45, 87]. The gene encoding the second member of the INK4 family of CKI, namely $p15^{INK4b}$, is located adjacent to the $p16^{INK4a}$ gene at 9p21 and, therefore, a deletion at this region sometimes affects both genes [45, 73]. However, genetic alterations, such as mutations and deletions affecting the $p15^{INK4b}$ gene alone, are rare. Instead, inactivation of $p15^{INK4b}$ occurs mainly through an epigenetic abnormality: promoter hypermethylation has been observed in many haematological malignancies and occurs in up to 75% of acute myeloid leukaemia cases, representing the most frequent abnormality in this malignancy [2, 98, 105]. In acute promyelocytic leukaemia, hypermethylation of the $p15^{INK4b}$ gene has been identified as new prognostic marker for disease-free survival. Also, the $p16^{INK4a}$ gene is epigenetically inactivated in several human tumours [31, 87].

Members of the second CKI family, $p21^{CIP1}$, $p27^{KIP1}$ and $p57^{KIP2}$, share a common N-terminal domain for binding and inhibition of the different CDKs. Therefore, unlike the INK4 family, their effect is not limited to G1/S transition [14]. Downregulation of $p27^{KIP1}$ protein has been observed in human tumours, such as breast, prostate, gastric, lung, skin, colon and ovarian cancers [25, 45], and is also an important marker for cancer progression and poor survival in several malignancies [25, 50]. The $p21^{CIP1}$ gene is a transcriptional target of the p53 protein, with a prominent role in G1/S as well as G2/M arrest in response to DNA damage [45]. Although the critical cell-cycle regulatory role of $p21^{CIP1}$ is not yet strongly supported by a long list of tumour-related abnormalities (as is the case for, e.g. $p16^{INK4a}$ or *cyclin D1*), its key role as a downstream effector of p53 makes it a hot spot of current investigations. As a CKI and as a target gene of p53, $p21^{CIP}$ represents also a direct molecular link between the Rb pathway and the p53 pathway.

Significantly higher survival rate is reported in p53-negative gastric cancer patients with $p21^{CIP1}$ expression than those without $p21^{CIP1}$ [45]. Similarly, a recent study indicated significant correlation between downregulation of $p21^{CIP1}$ with poor prognosis in human gastric cancer [85]. Whether hypermethylation of the $p21^{CIP1}$ gene is a prognostic marker in certain haematological malignancies is still under debate [8, 74, 88].

The above-mentioned transcriptional activation of the $p21^{CIP}$ gene is modulated by $p33^{ING1b}$, which directly interacts with the p53 protein. $p33^{ING1b}$ is encoded by one of several splice-isoforms produced by the *ING1* gene, founding member of the newly discovered "inhibitors of growth" (ING) family. These genes have been implicated in restricting cell growth and proliferation, induction of apoptosis, maintenance of genomic stability and modulation of cell-cycle checkpoints, all classical features of tumour suppressor genes [61].

The third member of the CIP/KIP family of CKIs, $p57^{KIP2}$, is encoded by an imprinted gene that is only expressed from the maternal allele. Decreased expression of $p57^{KIP2}$ has been observed in bladder carcinoma and gastric cancer [45, 65]. Together with the other genes located in the imprinted domain at 11p15.5, *IGF-2* and *H19*, loss of $p57^{KIP2}$ has also been associated with two familial cancer syndromes (Beckwith Wiederman syndrome and Wilms tumor) [33, 45]. In addition to blocking CDK activity, $p21^{CIP1}$ and $p57^{KIP2}$ inhibit proliferation through binding and inactivation of PCNA, which is an auxiliary factor of DNA polymerase [14, 66].

In addition to pRb and its interaction partners, the p53 pathway is of uppermost importance for cell-cycle regulation. It consists of several regulator and effector molecules of the "leading actor", p53. The *p53* gene is mutated in more than 50% of human cancers and is the most frequent genetic alteration associated with malignancy [77]. Furthermore, inactivation of this pathway can

occur via defects in upstream or downstream regulators as seen in several human cancers (Fig. 2). In general, tumours with intact *p53* have a better prognosis and a better response to therapy as compared with those with defective *p53* [77, 103].

The long-sought-after relatives of p53 are p63 and p73 [109]. Despite striking sequence similarities and conserved functional domains, these three proteins exert most probably quite different functions in the cell. The picture is complicated by the fact that p63 and p73 encode several splice-isoforms with partially opposing functions (e.g. ΔNp73, discussed above). Full-length p73 induces cell-cycle arrest and apoptosis, as does p53, but has additional functions in inflammatory response and neurogenesis [56], whereas p63 seems to be most important for proper function of epithelial stem cells [100].

$p14^{ARF}$ is one of the upstream regulators of *p53,* encoded by a gene that shares two common exons with $p16^{INK4a}$ but is translated in an alternative reading frame, creating a completely different protein (therefore the suffix "ARF") [70]. As an upstream activator of *p53* and sharing exons with the $p16^{INK4a}$ gene, the $p14^{ARF}$ gene represents a unique molecular link between the above-mentioned p53 and Rb pathways [87, 90]. It is, therefore, at the centre of intense research activities, and many alterations in human tumours, alone or in concert with $p16^{INK4a}$ or both $p15^{INK4b}$ and $p16^{INK4a}$, have already been described [87].

In addition to its direct activation of genes that drive the cell cycle forward, the already mentioned c-*myc* gene also favours cell-cycle progression indirectly by interfering with the transcription of negative cell-cycle regulators such as *Gadd45*, *Gadd153* or CKIs ($p15^{INK4b}$, $p16^{INK4a}$, $p21^{CIP1}$, and $p27^{KIP1}$) [45, 46, 103].

ATM a protein kinase central to all DNA maintenance responses [1]. Defects in this gene result in the disease ataxia telangiectasia, which is an autosomal recessive disorder characterised by progressive neurological disorders, immunodeficiency and chromosomal instability with a higher predisposition to lymphoid malignancies [92]. Mutation of either *Chk2* or *p53*, both of which act downstream of ATM, results in a genetic disease called Li Fraumeni syndrome, which dramatically predisposes patients to cancer development [5]. The protein product of the breast cancer susceptibility gene *BRCA1* is another substrate of ATM that is involved in cell-cycle checkpoint control and DNA repair [101]. *BRCA1* and its close relative, *BRCA2*, are mutated in approximately half of all familial breast cancer cases [41, 64, 101]. Mutations of these proteins lead to defects in cell-cycle arrest and DNA repair. A reduced expression is also described in sporadic (not inherited) breast cancers [55].

14–3-3σ, one of the seven members of the 14–3-3 family [45], is now considered to represent a new class of CKI. It has been shown to specifically interact with CDK1, CDK2 and CDK4 and can inhibit CDK activities, thereby blocking cell cycle progression [44, 45, 46]. In addition to being a downstream effector of p53, several lines of evidence suggest that loss of 14–3-3σ function correlates with cell transformation. Its expression levels are reduced in several transformed cell lines and primary tumour specimens [44, 45]. Moreover, CpG islands hypermethylation-induced transcriptional silencing of the *14–3-3*σ gene has been reported in breast cancer, gastric cancer and hepatocellular carcinoma [45].

Unequal segregation of chromosomes

Numeric abnormalities in chromosome (aneuploidy) and chromosomal rearrangements are frequently observed in human cancer, and severe karyotypic abnormalities generally are a sign of poor prognosis [30, 43, 75]. Defects in pathways essential for mitotic regulation are likely to be implicated in the cascade of events leading to aneuploidy and neoplasia.

Overexpression of AIM 1 induces defects in cytokinesis and predisposes one to the development of cancer [11]. The Aurora family of serine/threonine kinases is maximally activated in the G2/M phase and comprises key regulators of the mitotic stage of the cell cycle. They are known to be important in centrosome functions, bipolar spindle assembly and chromosomal segregation [36]. All the three members of the mammalian aurora kinase family (Aurora-A, -B, and -C) are reported to be overexpressed in a variety of human cancers. Aurora-A (also known as STK-15, or BTAK) is, for instance, overexpressed in breast, bladder, ovarian, colon and pancreatic cancers and is able to transform cells in culture [6, 36, 59, 84, 97, 110]. The overexpression of Aurora-A correlates with invasiveness and genomic instability in breast cancer and with clinical aggressiveness and aneuploidy in bladder cancer [36]. Centrosome amplification and aneuploidy are also found in cells with ectopic expression of Aurora-A [59]. The chromosomal region in which the Aurora-A gene is located, 20q13.2–13.3, is also often amplified in colon, breast and stomach cancers [83].

Another protein that is expressed in a cell-cycle-dependent manner and could play an important role in chromosomal segregation is survivin. It is a unique member of the inhibitor of apoptosis family, which, in addition to the anti-apoptosis role (as the name implies), also plays a role in the cell cycle. Survivin is specifically expressed at mitosis and forms complexes with various components of the mitotic apparatus, such as centrosomes, microtubules of the metaphase and anaphase spindles and also with the Aurora B [3]. It has also been shown that the kinase activity of Aurora B is stimulated by binding to and phosphorylation of survivin [9]. Dramatic overexpression of survivin has been observed in a wide variety of human tumours, including lung, breast, colon, stomach, oesophagus, pancreas, liver, uterus, ovaries, as well as lymphomas and leukemias [3].

Conclusions and perspectives

The progress in cell-cycle research over the last decade enabled a better understanding of physiological cell-cycle regulation and deregulation in cancer to an extent which only a few could imagine 10 years ago. The cell-cycle field provides a paradigm for the impact of basic research on the development of new diagnostic tests and innovative therapeutic concepts and reagents.

Translation of basic research into the routine practice of histopathological diagnosis has already started. Examples are the demonstration of Cyclin D1 overexpression for the identification of mantle cell lymphoma [19] and the detection of $p16^{INK4a}$ in cervical intraepithelial neoplasia [42]. Both antigens can now readily be detected also in formalin-fixed paraffin-embedded biopsies.

Several proteins with well-defined expression patterns during the cell cycle and well-described molecular function in the cell-cycle machinery are just emerging as new markers for the proliferation status of a given biopsy or even as new prognostic markers. Detection of Cyclin B1 (expressed as a mitotic cyclin only during the G2-M transition) or detection of Mcm2, for instance, seems to be of prognostic significance in squamous cell carcinoma of the oesophagus [37, 62]. Similarly, detection of Cyclin E turned out to be the most important independent predictor of breast cancer outcome, even superior to established proliferation markers [10, 40].

However, the general proliferation marker Ki-67 is still the most widely used and most thoroughly evaluated proliferation marker with proven diagnostic and prognostic power [81]. It labels proliferating cells in all stages of the cell cycle except G0 [22]. Despite the fact that determination of the "proliferation fraction" (percentage of proliferating cells) using this antibody is of uppermost importance for the classification of tumour specimens and prognosis shown in numerous studies, the function of the protein recognised by Ki-67 is not yet well established in molecular terms [17, 80].

Furthermore, immunohistochemical detection of PCNA, an auxiliary protein of DNA polymerase important for DNA synthesis, has been extensively used for quantification of proliferation [18, 49], but its usefulness has been questioned in some studies [81, 106].

As already discussed for some of the cell-cycle regulatory proteins, the cellular localisation as well as phosphorylation status determine biological activity. Therefore, the use of phosphorylation state-specific antibodies will be of great importance in future studies [53].

It should be mentioned that, in the above-cited study of Cyclin E in breast cancer, the occurrence of a low-molecular weight isoform detected by Western blotting was the molecular event with strong predictive power, stressing again that post-transcriptional modifications not detected by many conventional immunohistochemical assays and also not detected by large-scale cDNA microarray screens have to be kept in mind.

Every newly discovered component of the cell-cycle network described above represents a new potential target for therapeutic intervention in case of deregulation. The elucidation of the three-dimensional structure of key components of the cell-cycle regulatory machinery will guide the development of highly specific inhibitors modulating the activity of these molecules. Specific synthetic CDK or proteasome inhibitors represent promising examples [21, 48, 72]. The detailed molecular understanding of the pathways regulating cell-cycle entry and progression will also facilitate the rational design of combination therapies that will maximise therapeutic efficiency and minimise unwanted side effects and development of drug resistance.

Acknowledgements We would like to apologise for any omissions in the reference list due to strict space limitations. The authors would like to thank Nisar P. Malek for advice and Florian Länger for critically reading the manuscript and two anonymous reviewers for critical comments. Research grant support: Deutsche Krebshilfe, 10–1842-Le I. Deutsche Forschungsgemeinschaft, SFB265. Deutsche Forschungsgemeinschaft, DFG Fe 516/1–2.

References

1. Abraham RT (2001) Cell cycle checkpoint signaling through the ATM and ATR kinases. Genes Dev 15:2177–2196
2. Aggerholm A, Guldberg P, Hokland M, Hokland P (1999) Extensive intra- and interindividual heterogeneity of p15INK4B methylation in acute myeloid leukemia. Cancer Res 59:436–441
3. Altieri DC (2003) Validating survivin as a cancer therapeutic target. Nat Rev Cancer 3:46–54
4. Bartek J, Lukas J, Bartkova J (1999) Perspective: defects in cell cycle control and cancer. J Pathol 187:95–99
5. Bell DW, Varley JM, Szydlo TE, Kang DH, Wahrer DC, Shannon KE, Lubratovich M, Verselis SJ, Isselbacher KJ, Fraumeni JF, Birch JM, Li FP, Garber JE, Haber DA (1999) Heterozygous germ line hCHK2 mutations in Li-Fraumeni syndrome. Science 286:2528–2531
6. Bischoff JR, Anderson L, Zhu Y, Mossie K, Ng L, Souza B, Schryver B, Flanagan P, Clairvoyant F, Ginther C, Chan CS, Novotny M, Slamon DJ, Plowman GD (1998) A homologue of Drosophila aurora kinase is oncogenic and amplified in human colorectal cancers. EMBO J 17:3052–3065
7. Blow JJ, Hodgson B (2002) Replication licensing—defining the proliferative state? Trends Cell Biol 12:72–78
8. Boldt DH (2002) p21(CIP1/WAF1/SDI1) hypermethylation: an exciting new lead in ALL biology. Blood 99:2283
9. Bolton MA, Lan W, Powers SE, McCleland ML, Kuang J, Stukenberg PT (2002) Aurora B kinase exists in a complex with survivin and INCENP, and its kinase activity is stimulated by survivin binding and phosphorylation. Mol Biol Cell 13:3064–3077
10. Borg A, Ferno M, Peterson C (2003) Predicting the future of breast cancer. Nat Med 9:16–18
11. Carnero A (2002) Targeting the cell cycle for cancer therapy. Br J Cancer 87:129–133
12. Chaturvedi P, Eng WK, Zhu Y, Mattern MR, Mishra R, Hurle MR, Zhang X, Annan RS, Lu Q, Faucette LF, Scott GF, Li X, Carr SA, Johnson RK, Winkler JD, Zhou BB (1999) Mammalian Chk2 is a downstream effector of the ATM-dependent DNA damage checkpoint pathway. Oncogene 18:4047–4054
13. Classon M, Harlow E (2002) The retinoblastoma tumour suppressor in development and cancer. Nat Rev Cancer 2:910–917
14. Dictor M, Ehinger M, Mertens F, Akervall J, Wennerberg J (1999) Abnormal cell cycle regulation in malignancy. Am J Clin Pathol 112:S40–S52

15. Douglas RM, Haddad GG (2003) Genetic models in applied physiology: invited review: effect of oxygen deprivation on cell cycle activity: a profile of delay and arrest. J Appl Physiol 94:2068–2083
16. Elledge SJ (1996) Cell cycle checkpoints: preventing an identity crisis. Science 274:1664–1672
17. Endl E, Gerdes J (2000) The Ki-67 protein: fascinating forms and an unknown function. Exp Cell Res 257:231–237
18. Faderl S, Keating MJ, Do KA, Liang SY, Kantarjian HM, O'Brien S, Garcia-Manero G, Manshouri T, Albitar M (2002) Expression profile of 11 proteins and their prognostic significance in patients with chronic lymphocytic leukemia (CLL). Leukemia 16:1045–1052
19. Falini B, Mason DY (2002) Proteins encoded by genes involved in chromosomal alterations in lymphoma and leukemia: clinical value of their detection by immunocytochemistry. Blood 99:409–426
20. Furnari B, Rhind N, Russell P (1997) Cdc25 mitotic inducer targeted by chk1 DNA damage checkpoint kinase. Science 277:1495–1497
21. Gali-Muhtasib H, Bakkar N (2002) Modulating cell cycle: current applications and prospects for future drug development. Curr Cancer Drug Targets 2:309–336
22. Gerlach C, Golding M, Larue L, Alison MR, Gerdes J (1997) Ki-67 immunoexpression is a robust marker of proliferative cells in the rat. Lab Invest 77:697–698
23. Hahn WC, Weinberg RA (2002) Modelling the molecular circuitry of cancer. Nat Rev Cancer 2:331–341
24. Hall M, Peters G (1996) Genetic alterations of cyclins, cyclin-dependent kinases, and Cdk inhibitors in human cancer. Adv Cancer Res 68:67–108
25. Han S, Park K, Bae BN, Kim KH, Kim HJ, Kim YD, Kim HY (2003) Prognostic implication of cyclin E expression and its relationship with cyclin D1 and p27Kip1 expression on tissue microarrays of node negative breast cancer. J Surg Oncol 83:241–247
26. Hanahan D, Weinberg RA (2000) The hallmarks of cancer. Cell 100:57–70
27. Hannon GJ, Beach D (1994) p15INK4B is a potential effector of TGF-beta-induced cell cycle arrest. Nature 371:257–261
28. Harper JW, Adami GR, Wei N, Keyomarsi K, Elledge SJ (1993) The p21 Cdk-interacting protein Cip1 is a potent inhibitor of G1 cyclin-dependent kinases. Cell 75:805–816
29. Hartwell LH, Weinert TA (1989) Checkpoints: controls that ensure the order of cell cycle events. Science 246:629–634
30. Heppner GH, Miller FR (1998) The cellular basis of tumor progression. Int Rev Cytol 177:1–56
31. Herman JG, Merlo A, Mao L, Lapidus RG, Issa JP, Davidson NE, Sidransky D, Baylin SB (1995) Inactivation of the CDKN2/p16/MTS1 gene is frequently associated with aberrant DNA methylation in all common human cancers. Cancer Res 55:4525–4530
32. Hermeking H, Rago C, Schuhmacher M, Li Q, Barrett JF, Obaya AJ, O'Connell BC, Mateyak MK, Tam W, Kohlhuber F, Dang CV, Sedivy JM, Eick D, Vogelstein B, Kinzler KW (2000) Identification of CDK4 as a target of c-MYC. Proc Natl Acad Sci U S A 97:2229–2234
33. Johnson DG, Walker CL (1999) Cyclins and cell cycle checkpoints. Annu Rev Pharmacol Toxicol 39:295–312
34. Johnston JM, Carroll WL (1992) c-myc hypermutation in Burkitt's lymphoma. Leuk Lymphoma 8:431–439
35. Kaghad M, Bonnet H, Yang A, Creancier L, Biscan JC, Valent A, Minty A, Chalon P, Lelias JM, Dumont X, Ferrara P, McKeon F, Caput D (1997) Monoallelically expressed gene related to p53 at 1p36, a region frequently deleted in neuroblastoma and other human cancers. Cell 90:809–819
36. Katayama H, Brinkley WR, Sen S (2003) The Aurora kinases: role in cell transformation and tumorigenesis. Cancer Metastasis Rev 22:451–464
37. Kato H, Miyazaki T, Fukai Y, Nakajima M, Sohda M, Takita J, Masuda N, Fukuchi M, Manda R, Ojima H, Tsukada K, Asao T, Kuwano H (2003) A new proliferation marker, minichromosome maintenance protein 2, is associated with tumor aggressiveness in esophageal squamous cell carcinoma. J Surg Oncol 84:24–30
38. Kawabe T, Suganuma M, Ando T, Kimura M, Hori H, Okamoto T (2002) Cdc25C interacts with PCNA at G2/M transition. Oncogene 21:1717–1726
39. Kelly TJ, Brown GW (2000) Regulation of chromosome replication. Annu Rev Biochem 69:829–880
40. Keyomarsi K, Tucker SL, Buchholz TA, Callister M, Ding Y, Hortobagyi GN, Bedrosian I, Knickerbocker C, Toyofuku W, Lowe M, Herliczek TW, Bacus SS (2002) Cyclin E and survival in patients with breast cancer. N Engl J Med 347:1566–1575
41. King MC, Marks JH, Mandell JB (2003) Breast and ovarian cancer risks due to inherited mutations in BRCA1 and BRCA2. Science 302:643–646
42. Klaes R, Benner A, Friedrich T, Ridder R, Herrington S, Jenkins D, Kurman RJ, Schmidt D, Stoler M, von Knebel Doeberitz M (2002) p16INK4a immunohistochemistry improves interobserver agreement in the diagnosis of cervical intraepithelial neoplasia. Am J Surg Pathol 26:1389–1399
43. Kreipe H, Parwaresch R (1993) A closer look at the cell cycle. Virchows Arch 422:341–343
44. Laronga C, Yang HY, Neal C, Lee MH (2000) Association of the cyclin-dependent kinases and 14–3-3 sigma negatively regulates cell cycle progression. J Biol Chem 275:23106–23112
45. Lee MH, Yang HY (2001) Negative regulators of cyclin-dependent kinases and their roles in cancers. Cell Mol Life Sci 58:1907–1922
46. Lee MH, Yang HY (2003) Regulators of G1 cyclin-dependent kinases and cancers. Cancer Metastasis Rev 22:435–449
47. Lee MH, Reynisdottir I, Massague J (1995) Cloning of p57KIP2, a cyclin-dependent kinase inhibitor with unique domain structure and tissue distribution. Genes Dev 9:639–649
48. Lenz HJ (2003) Clinical update: proteasome inhibitors in solid tumors. Cancer Treat Rev 29[Suppl 1]:41–48
49. Lillo C, Velasco A, Jimeno D, Cid E, Lara JM, Aijon J (2002) The glial design of a teleost optic nerve head supporting continuous growth. J Histochem Cytochem 50:1289–1302
50. Lloyd RV, Erickson LA, Jin L, Kulig E, Qian X, Cheville JC, Scheithauer BW (1999) p27kip1: a multifunctional cyclin-dependent kinase inhibitor with prognostic significance in human cancers. Am J Pathol 154:313–323
51. Lundberg AS, Weinberg RA (1999) Control of the cell cycle and apoptosis. Eur J Cancer 35:1886–1894
52. Malumbres M, Barbacid M (2001) To cycle or not to cycle: a critical decision in cancer. Nat Rev Cancer 1:222–231
53. Mandell JW (2003) Phosphorylation state-specific antibodies: applications in investigative and diagnostic pathology. Am J Pathol 163:1687–1698
54. Mao L, Merlo A, Bedi G, Shapiro GI, Edwards CD, Rollins BJ, Sidransky D (1995) A novel p16INK4A transcript. Cancer Res 55:2995–2997
55. McCoy ML, Mueller CR, Roskelley CD (2003) The role of the breast cancer susceptibility gene 1 (BRCA1) in sporadic epithelial ovarian cancer. Reprod Biol Endocrinol 1:72
56. Melino G, De Laurenzi V, Vousden KH (2002) p73: friend or foe in tumorigenesis. Nat Rev Cancer 2:605–615
57. Molinari M (2000) Cell cycle checkpoints and their inactivation in human cancer. Cell Prolif 33:261–274
58. Morgan DO (1997) Cyclin-dependent kinases: engines, clocks, and microprocessors. Annu Rev Cell Dev Biol 13:261–291
59. Nigg EA (2001) Mitotic kinases as regulators of cell division and its checkpoints. Nat Rev Mol Cell Biol 2:21–32
60. Nishitani H, Lygerou Z (2002) Control of DNA replication licensing in a cell cycle. Genes Cells 7:523–534
61. Nouman GS, Anderson JJ, Lunec J, Angus B (2003) The role of the tumour suppressor p33 ING1b in human neoplasia. J Clin Pathol 56:491–496

62. Nozoe T, Korenaga D, Kabashima A, Ohga T, Saeki H, Sugimachi K (2002) Significance of cyclin B1 expression as an independent prognostic indicator of patients with squamous cell carcinoma of the esophagus. Clin Cancer Res 8:817–822
63. Nurse P (2000) A long twentieth century of the cell cycle and beyond. Cell 100:71–78
64. Nyberg KA, Michelson RJ, Putnam CW, Weinert TA (2002) Toward maintaining the genome: DNA damage and replication checkpoints. Annu Rev Genet 36:617–656
65. Oya M, Schulz WA (2000) Decreased expression of p57(KIP2)mRNA in human bladder cancer. Br J Cancer 83:626–631
66. Pan ZQ, Reardon JT, Li L, Flores-Rozas H, Legerski R, Sancar A, Hurwitz J (1995) Inhibition of nucleotide excision repair by the cyclin-dependent kinase inhibitor p21. J Biol Chem 270:22008–22016
67. Park MT, Lee SJ (2003) Cell cycle and cancer. J Biochem Mol Biol 36:60–65
68. Paulovich AG, Toczyski DP, Hartwell LH (1997) When checkpoints fail. Cell 88:315–321
69. Polyak K, Lee MH, Erdjument-Bromage H, Koff A, Roberts JM, Tempst P, Massague J (1994) Cloning of p27Kip1, a cyclin-dependent kinase inhibitor and a potential mediator of extracellular antimitogenic signals. Cell 78:59–66
70. Quelle DE, Ashmun RA, Hannon GJ, Rehberger PA, Trono D, Richter KH, Walker C, Beach D, Sherr CJ, Serrano M (1995) Cloning and characterization of murine p16INK4a and p15INK4b genes. Oncogene 11:635–645
71. Ravitz MJ, Wenner CE (1997) Cyclin-dependent kinase regulation during G1 phase and cell cycle regulation by TGF-beta. Adv Cancer Res 71:165–207
72. Richardson P (2003) Clinical update: proteasome inhibitors in hematologic malignancies. Cancer Treat Rev 29[Suppl 1]:33–39
73. Rocco JW, Sidransky D (2001) p16(MTS-1/CDKN2/INK4a) in cancer progression. Exp Cell Res 264:42–55
74. Roman-Gomez J, Castillejo JA, Jimenez A, Gonzalez MG, Moreno F, Rodriguez Mdel C, Barrios M, Maldonado J, Torres A (2002) 5′ CpG island hypermethylation is associated with transcriptional silencing of the p21(CIP1/WAF1/SDI1) gene and confers poor prognosis in acute lymphoblastic leukemia. Blood 99:2291–2296
75. Ross JS (1996) DNA ploidy and cell cycle analysis in cancer diagnosis and prognosis. Oncology (Huntingt) 10:867–882, 887; discussion 887–890
76. Sanchez Y, Wong C, Thoma RS, Richman R, Wu Z, Piwnica-Worms H, Elledge SJ (1997) Conservation of the Chk1 checkpoint pathway in mammals: linkage of DNA damage to Cdk regulation through Cdc25. Science 277:1497–1501
77. Sandal T (2002) Molecular aspects of the mammalian cell cycle and cancer. Oncologist 7:73–81
78. Schlotter CM, Vogt U, Bosse U, Mersch B, Wassmann K (2003) C-myc, not HER-2/neu, can predict recurrence and mortality of patients with node-negative breast cancer. Breast Cancer Res 5:R30–R36
79. Scholey JM, Brust-Mascher I, Mogilner A (2003) Cell division. Nature 422:746–752
80. Scholzen T, Gerdes J (2000) The Ki-67 protein: from the known and the unknown. J Cell Physiol 182:311–322
81. Scholzen T, Endl E, Wohlenberg C, van der Sar S, Cowell IG, Gerdes J, Singh PB (2002) The Ki-67 protein interacts with members of the heterochromatin protein 1 (HP1) family: a potential role in the regulation of higher-order chromatin structure. J Pathol 196:135–144
82. Schraml P, Bucher C, Bissig H, Nocito A, Haas P, Wilber K, Seelig S, Kononen J, Mihatsch MJ, Dirnhofer S, Sauter G (2003) Cyclin E overexpression and amplification in human tumours. J Pathol 200:375–382
83. Sen S, Zhou H, White RA (1997) A putative serine/threonine kinase encoding gene BTAK on chromosome 20q13 is amplified and overexpressed in human breast cancer cell lines. Oncogene 14:2195–2200
84. Sen S, Zhou H, Zhang RD, Yoon DS, Vakar-Lopez F, Ito S, Jiang F, Johnston D, Grossman HB, Ruifrok AC, Katz RL, Brinkley W, Czerniak B (2002) Amplification/overexpression of a mitotic kinase gene in human bladder cancer. J Natl Cancer Inst 94:1320–1329
85. Seo YH, Joo YE, Choi SK, Rew JS, Park CS, Kim SJ (2003) Prognostic significance of p21 and p53 expression in gastric cancer. Korean J Intern Med 18:98–103
86. Serrano M, Hannon GJ, Beach D (1993) A new regulatory motif in cell-cycle control causing specific inhibition of cyclin D/CDK4. Nature 366:704–707
87. Sharpless E, Chin L (2003) The INK4a/ARF locus and melanoma. Oncogene 22:3092–3098
88. Shen L, Kondo Y, Issa JP, Garcia-Manero G (2002) Lack of p21(CIP1) DNA methylation in acute lymphocytic leukemia. Blood 100:3432–3434
89. Sherr CJ (1996) Cancer cell cycles. Science 274:1672–1677
90. Sherr CJ (2000) The Pezcoller lecture: cancer cell cycles revisited. Cancer Res 60:3689–3695
91. Sherr CJ, Roberts JM (1999) CDK inhibitors: positive and negative regulators of G1-phase progression. Genes Dev 13:1501–1512
92. Shiloh Y (2003) ATM and related protein kinases: safeguarding genome integrity. Nat Rev Cancer 3:155–168
93. Spruck CH, Won KA, Reed SI (1999) Deregulated cyclin E induces chromosome instability. Nature 401:297–300
94. Steeg PS, Zhou Q (1998) Cyclins and breast cancer. Breast Cancer Res Treat 52:17–28
95. Stewart ZA, Westfall MD, Pietenpol JA (2003) Cell-cycle dysregulation and anticancer therapy. Trends Pharmacol Sci 24:139–145
96. Stone S, Jiang P, Dayananth P, Tavtigian SV, Katcher H, Parry D, Peters G, Kamb A (1995) Complex structure and regulation of the P16 (MTS1) locus. Cancer Res 55:2988–2994
97. Tanaka T, Kimura M, Matsunaga K, Fukada D, Mori H, Okano Y (1999) Centrosomal kinase AIK1 is overexpressed in invasive ductal carcinoma of the breast. Cancer Res 59:2041–2044
98. Tessema M, Langer F, Dingemann J, Ganser A, Kreipe H, Lehmann U (2003) Aberrant methylation and impaired expression of the p15(INK4b) cell cycle regulatory gene in chronic myelomonocytic leukemia (CMML). Leukemia 17:910–918
99. Toyoshima H, Hunter T (1994) p27, a novel inhibitor of G1 cyclin–CDK protein kinase activity, is related to p21. Cell 78:67–74
100. van Bokhoven H, McKeon F (2002) Mutations in the p53 homolog p63: allele-specific developmental syndromes in humans. Trends Mol Med 8:133–139
101. Venkitaraman AR (1999) Breast cancer genes and DNA repair. Science 286:1100–1102
102. Vermeulen K, Berneman ZN, Van Bockstaele DR (2003) Cell cycle and apoptosis. Cell Prolif 36:165–175
103. Vermeulen K, Van Bockstaele DR, Berneman ZN (2003) The cell cycle: a review of regulation, deregulation and therapeutic targets in cancer. Cell Prolif 36:131–149
104. Wolfel T, Hauer M, Schneider J, Serrano M, Wolfel C, Klehmann-Hieb E, De Plaen E, Hankeln T, Meyer zum Buschenfelde KH, Beach D (1995) A p16INK4a-insensitive CDK4 mutant targeted by cytolytic T lymphocytes in a human melanoma. Science 269:1281–1284
105. Wong IH, Ng MH, Huang DP, Lee JC (2000) Aberrant p15 promoter methylation in adult and childhood acute leukemias of nearly all morphologic subtypes: potential prognostic implications. Blood 95:1942–1949
106. Wood RD, Shivji MK (1997) Which DNA polymerases are used for DNA-repair in eukaryotes? Carcinogenesis 18:605–610
107. Xiong Y, Hannon GJ, Zhang H, Casso D, Kobayashi R, Beach D (1993) p21 is a universal inhibitor of cyclin kinases. Nature 366:701–704

108. Yam CH, Fung TK, Poon RY (2002) Cyclin A in cell cycle control and cancer. Cell Mol Life Sci 59:1317–1326
109. Yang A, Kaghad M, Caput D, McKeon F (2002) On the shoulders of giants: p63, p73 and the rise of p53. Trends Genet 18:90–95
110. Zhou H, Kuang J, Zhong L, Kuo WL, Gray JW, Sahin A, Brinkley BR, Sen S (1998) Tumour amplified kinase STK15/BTAK induces centrosome amplification, aneuploidy and transformation. Nat Genet 20:189–193

Virchows Arch (2004) 444:324–331
DOI 10.1007/s00428-004-0982-8

ORIGINAL ARTICLE

Reiko Ito · Hirofumi Nakayama · Kazuhiro Yoshida · Shunji Matsumura · Noriko Oda · Wataru Yasui

Expression of Cbl linking with the epidermal growth factor receptor system is associated with tumor progression and poor prognosis of human gastric carcinoma

Received: 16 September 2003 / Accepted: 5 January 2004 / Published online: 26 February 2004

Abstract Cbl proteins play important roles in downregulation of growth factor receptors by acting as ubiquitin ligases and multi-adapter proteins. Ligand-induced desensitization of the epidermal growth factor receptor (EGFR) has been shown to be controlled by Cbl. In the present study, we examined the expression of Cbl in gastric carcinomas and studied the correlation of Cbl expression with clinicopathological characteristics as well as EGFR expression. Cbl protein was expressed in 67% (82/122) of gastric carcinomas, and diffuse expression of Cbl was detected in 29% (35/122) of the cases. The incidence of cases with diffuse expression of Cbl was significantly higher in advanced cases (28/70, 40%) than in early cases (7/52, 14%) (P=0.0010). Diffuse expression of Cbl was significantly associated with metastasis of tumor cells in lymph nodes (P=0.0318). Diffuse expression of EGFR was significantly associated with depth of invasion (P=0.0057), lymph-node metastasis (P=0.0371) and tumor stages (P=0.0278). As the grades of Cbl expression became stronger, the cases with diffuse EGFR expression increased, the positive correlation being significant (P=0.049). All the cases with diffuse expression of Cbl and EGFR were found to show nodal metastasis and to be at an advanced stage. Moreover, the prognosis of the patients with synchronous diffuse expression of Cbl and EGFR was significantly poorer than that of the patients negative for Cbl and focal or negative for EGFR (P=0.0086). The expression of Cbl protein was clearly induced in gastric carcinoma cell lines by transforming growth factor-α treatment. These results suggest that Cbl in connection with the EGFR system may be associated with stomach carcinogenesis, invasion and metastasis. Cbl may serve as a novel molecular marker for aggressive gastric carcinoma.

Keywords Epidermal growth factor receptor · Cbl proteins · Gastric carcinomas

R. Ito · H. Nakayama · S. Matsumura · W. Yasui (✉)
Department of Molecular Pathology,
Hiroshima University Graduate School of Biomedical Sciences,
Hiroshima University, 1-2-3 Kasumi, Minami-ku,
734-8551 Hiroshima, Japan
e-mail: wyasui@hiroshima-u.ac.jp
Fax: +81-82-2575149

K. Yoshida
Department of Surgical Oncology,
Research Institute for Radiation Biology and Medicine,
Hiroshima University, 1-2-3 Kasumi, Minami-ku,
734-8551 Hiroshima, Japan

N. Oda
Department of Human Nutrition, Faculty of Human Sciences,
Hiroshima Bunkyo Women's University,
1-2-1 Kabe-higashi, Asakita-ku, 731-0295 Hiroshima, Japan

Introduction

One of the most important characteristics of a cancer cell is the ability to express multiple growth factors and their receptors, which confer growth autonomy by autocrine mechanisms and contribute to tumor progression, invasion and metastasis. We have previously reported that many gastric carcinomas co-express transforming growth factor (TGF)α and epidermal growth factor (EGF) receptor and that synchronous expression of EGF/TGFα and EGF receptor (EGFR) is tightly associated with biological malignancy and poor prognosis [29, 30]. EGF/TGFα produced by tumor cells acts as a positive autocrine growth factor for gastric carcinoma [33]. The additional members of the EGF family, such as *cripto* and amphiregulin, are also expressed in gastric carcinoma [11, 12].

It is well known that, upon ligand binding, a ligand–receptor complex transduces growth-stimulatory signal through its tyrosine kinase activity and undergoes internalization and downregulation. It has been recently shown that Cbl proteins play important roles in downregulation of growth factor receptors by acting as ubiquitin ligases and multi-adapter proteins [26]. Cbl-mediated ubiquitination of active receptors is essential for receptor degradation and cessation of receptor-induced signal transduction [3, 8, 14, 26, 28]. The tyrosine kinase-binding

module and ring-finger domain of Cbl is able to recruit ubiquitin-conjugation enzymes in the complex with activated receptors [9, 31]. Cbl also recruits the Cbl-interacting protein, 85-kDa (CIN85)-endophilin [4, 19, 20, 21], in complexes with activated receptors, thus controlling receptor endocytosis [8, 14, 18, 22]. Since ligand-induced desensitization of EGFR is controlled by Cbl, EGFR/CIN85-endophilin complex has shed new light on the mechanisms involved in the signal transduction and degradation of EGFR [3, 22, 23].

However, no study has been conducted to elucidate the role of Cbl and its association with EGFR in gastric carcinomas. In the present study, we examined the expression of Cbl in gastric carcinomas using immunohistochemistry and analyzed the correlation of Cbl expression with clinicopathological characteristics, such as tumor stage, tumor invasion, nodal metastasis, patient's prognosis and EGFR expression. We also studied the effect of TGFα on the expression of Cbl in gastric carcinoma cell lines.

Materials and methods

Tissue samples

A total of 122 gastric adenocarcinoma cases were used. The tumor tissues and corresponding non-neoplastic gastric mucosa were obtained from surgeries at Hiroshima University Hospital and its affiliated hospitals. For immunohistochemistry, tissues were fixed in 10% buffered-formalin and embedded in paraffin.

We classified the gastric carcinomas according to the criteria of the Japanese Classification of Gastric Cancer [7]. Histological type was classified as follows: well-differentiated type, wel (papillary adenocarcinoma and well-differentiated tubular adenocarcinoma), moderately differentiated type, mod (moderately differentiated tubular adenocarcinoma) and poorly differentiated type, por (solid- and non-solid-type poorly differentiated adenocarcinoma, signet-ring-cell carcinoma and mucinous adenocarcinoma). Depth of carcinoma invasion was classified as follows: t1, mucosa and submucosa; t2, muscularis propria and subserosa; t3, serosa-exposed (se); t4, serosa-infiltrating (si). The cases with t1 were defined as early cancer, and the cases with t2–t4 were defined as advanced cancer.

Cell line

Two human gastric carcinoma cell lines were used. TMK-1 was established from a poorly differentiated adenocarcinoma in our laboratory [15], and MKN-74, a well-differentiated adenocarcinoma, was kindly provided by Dr. T. Suzuki (Fukushima Medical University, Fukushima, Japan). These cell lines were routinely maintained in RPMI 1640 (Nissui Pharmaceutical Co. Ltd., Tokyo, Japan) containing 10% fetal bovine serum (Whittaker M. A. Bioproducts Inc., Walkersville, MD, USA) under conditions of 5% CO_2 in air at 37°C. EGFR is expressed at a high level in TMK-1 and a low level in MKN-74 [32]. EGF is produced by TMK-1, but not by MKN-74, while TGFα is produced by both cell lines at similar levels [32].

Immunohistochemistry

Consecutive 4-μm tissue sections were prepared from paraffin blocks and immunostained for Cbl. Each section was mounted on a silane-coated glass slide, deparaffinized and soaked for 15 min at room temperature in 3% H_2O_2/methanol to block endogenous peroxidase. Anti-Cbl polyclonal antibody (C-15, Santa Cruz Biotechnology, USA) at a 1:100 dilution was used as primary antibody and was applied for overnight at 4°C. The primary antibody was visualized using the Histofine Simple Stain MAX-PO (MULTI) kit (Nichirei, Tokyo, Japan) according to the instruction manual. The slide was counterstained with hematoxylin. Negative control staining was made using non-specific IgG in the primary reaction. The stained slides were observed without clinicopathological information. Reproducibility of staining was confirmed by repeating immunostaining using the same method in plural number of specimens randomly selected. To decide on the definition for Cbl expression, we counted the number of positive cells among tumor cells in the representative ten microscopic fields and calculated the percentage of positive cells. The definition of staining was as follows: diffuse, over 40% of tumor cells showed immunoreactivity; focal, 5–40% of tumor cells showed immunoreactivity; negative, less than 5% of tumor cells showed immunoreactivity or no tumor cells showed immunoreactivity.

For EGFR immunostaining, anti-EGFR monoclonal antibody (NCL-EGFR, Novocastra Laboratories Ltd., UK) at a 1:200 dilution was used. Definition of staining grade was as follows: diffuse, over 25% of tumor cells showed immunoreactivity; focal or negative, less than 25% of tumor cells showed immunoreactivity or no staining, as described previously [29].

Treatment of TGFα

Gastric carcinoma cell lines TMK-1 and MKN-74 were grown to subconfluence in the regular medium. After 24 h serum starvation, the cells were treated with 1nM TGFα (R&D Systemd, Ltd., USA) for 1, 3, 6, 12 and 24 h.

Western-blot analysis

Whole cell lysates were prepared from the gastric cell lines, and Western blotting was performed as described previously [17]. Protein concentrations were determined by Bradford protein assay (Bio-Rad, Richmond, CA) with bovine serum albumin used as the standard. The lysates (20 μg) were solubilized in Laemmli's sample buffer by boiling and then subjected to 10% sodium dodecyl sulfate-polyacrylamide gel electrophoresis, followed by electrotransfer onto a nitrocellulose filter. Peroxidase conjugated anti-rabbit IgG was used in the secondary reaction. The immune complex was visualized with an enterochromaffin-like Western-blot detection system (Amersham Pharmacia Biotech). The quality and amount of protein samples applied on the gel were confirmed by detection with anti-alpha-tubulin antibody.

Statistical analysis

Statistical analyses were performed with non-parametric test (Spearman rank correlation test) and P values were shown. P values less than 0.05 were regarded as statistically significant. If the P value was less than 0.05, it meant that each parameter had a significant correlation with the level of Cbl expression.

Results

Immunohistochemical detection of Cbl protein in gastric carcinoma tissues and non-neoplastic mucosa

We immunohistochemically examined the expression and localization of Cbl protein in 122 cases of gastric carcinoma and non-neoplastic mucosa. Representative stainings of Cbl are shown in Fig. 1, and the results are

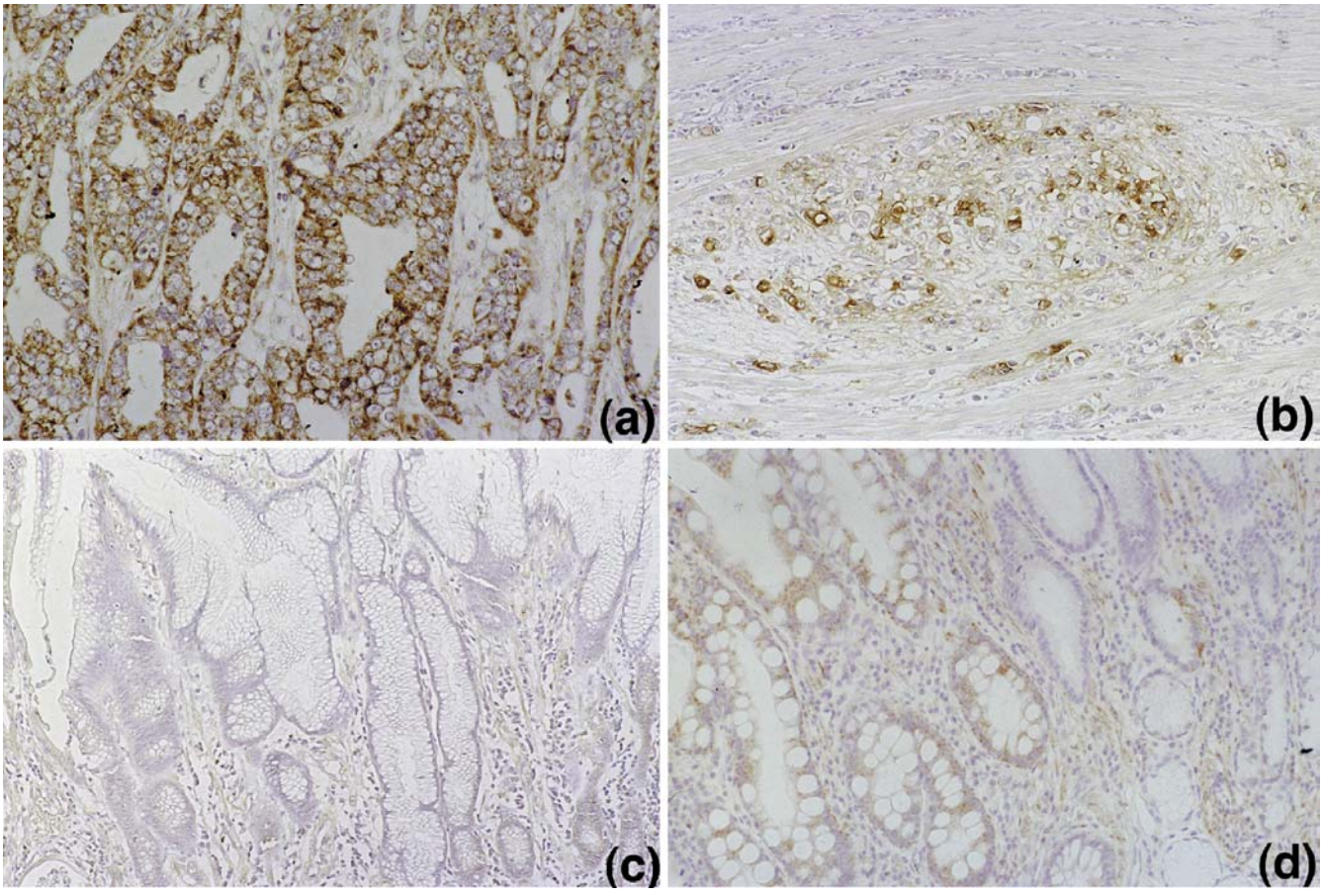

Fig. 1 Expression of Cbl protein in gastric carcinoma tissues and non-neoplastic mucosa. Cbl immunohistochemical staining: **a** well-differentiated tubular adenocarcinoma; **b** solid-type poorly differentiated adenocarcinoma; **c** normal foveolar epithelium; **d** intestinal metaplasia. The Cbl expression was found at various levels in gastric carcinoma tissues, (**a** diffuse; **b** focal). In non-neoplastic mucosa, the expression of Cbl was not recognized in normal foveolar epithelia, while intestinal metaplasia revealed weak expression of Cbl

summarized in Table 1. Cbl protein was expressed in 67% (82/122) of gastric carcinomas at various levels (Fig. 1a, b and Table 1), and diffuse expression of Cbl was detected in 29% (35/122) of the cases. Cbl protein was localized in both cell membrane and cytoplasm. In normal gastric mucosa, Cbl was not detected in epithelial cells, including foveolar epithelia and fundic and pyloric glandular cells (Fig. 1c). Weak expression of Cbl was detected in intestinal metaplasia (Fig. 1d).

Correlation between Cbl expression and clinicopathological characteristics of gastric carcinoma

We then analyzed the relationship between the expression of Cbl protein and clinicopathological parameters of gastric carcinoma. As shown in Table 1, the incidence of cases with diffuse expression of Cbl was significantly higher in advanced cases (28/70, 40%) than in early cases (7/52, 14%) (P=0.0010). Diffuse expression of Cbl was significantly associated with metastasis of tumor cells in lymph nodes (P=0.0318). The incidence of diffuse expression of Cbl tended to be higher in carcinomas of stage III and stage IV than those of stage I and stage II (P=0.0688).

Correlation between EGFR expression and clinicopathological characteristics of gastric carcinoma

We also analyzed the relationship between the expression of EGFR protein and clinicopathological parameters of gastric carcinoma. As shown in Table 2, diffuse expression of EGFR was significantly associated with depth of invasion (P=0.0057), lymph-node metastasis (P=0.0371) and tumor stages (P=0.0278).

Relationship between Cbl and EGFR

We next examined the relationship between Cbl and EGFR expression in gastric carcinomas. Representative

Table 1 Expression of Cbl in gastric carcinomas and its correlation with clinicopathological parameters. Grades of Cbl expression were classified as "diffuse," "focal" and "negative" as described in Materials and methods. Histological type was classified as "wel," "mod" and "por" as described in Materials and methods. Correlation was analyzed by non-parametric test and *P* values were shown; *P* values less than 0.05 were regarded as statistically significant

	Case no.	Cbl expression			*P* value
		Diffuse	Focal	Negative	
Positive cell ratio		(>40%)	(5–40%)	(<5%)	
Gastric carcinomas	122	35 (29%)	47 (38%)	40 (33%)	
Histology					
Wel	36	9 (25%)	16(44%)	11 (31%)	*P*=0.8609
Mod	45	15 (33%)	16 (36%)	14 (31%)	
Por	41	11 (26%)	15 (37%)	15 (37%)	
Depth of invasion*					
Early (t1)	52	7 (14%)	20 (38%)	25 (48%)	*P*=0.0010
Advanced (t2–t4)	70	28 (40%)	27 (39%)	15 (21%)	
Lymph-node metastasis*					
no	59	9 (16%)	25 (42%)	25 (42%)	*P*=0.0318
n1	29	10 (34%)	10 (34%)	9 (32%)	
n2	22	11 (50%)	8 (36%)	3 (14%)	
n3	12	5 (42%)	5 (42%)	2 (16%)	
Stage*					
I and II	80	18(23%)	32 (40%)	30 (37%)	*P*=0.0688
III and IV	42	17(40%)	16(38%)	9 (22%)	

*According to the criteria of the Japanese Classification of Gastric Cancer

Table 2 Expression of epithelial growth factor receptor (EGFR) in gastric carcinomas and its correlation with clinicopathological parameters. Grades of EGFR expression were classified as "diffuse", "focal or negative" as described in Materials and methods. Histological type was classified as "wel," "mod" and "por" as described in Materials and methods. Correlation was analyzed by non-parametric test and *P* values were shown. *P* values less than 0.05 were regarded as statistically significant

	Case no.	EGFR expression		*P* value
		Diffuse	Focal or negative	
Positive cell ratio		(>25%)	(<25%)	
Gastric carcinomas	82	31 (38%)	51 (62%)	
Histology				
Wel	17	8 (47%)	9 (53%)	*P*=0.8846
Mod	27	11 (41%)	16 (59%)	
Por	30	12 (40%)	18 (60%)	
Depth of invasion*				
Early (t1)	18	6 (33%)	12 (67%)	*P*=0.0057
Advanced (t2–t4)	56	25 (45%)	31 (55%)	
Lymph-node metastasis*				
n0	29	9 (31%)	20 (69%)	*P*=0.0371
n1	18	9 (50%)	9 (50%)	
n2	17	8 (47%)	9 (53%)	
n3	10	5 (50%)	5 (50%)	
Stage*				
I and II	35	10 (29%)	25 (71%)	*P*=0.0278
III and IV	39	21 (54%)	18 (46%)	

*According to the criteria of the Japanese Classification of Gastric Cancer

Table 3 Correlation of between Cbl and epithelial growth factor receptor (EGFR) in gastric carcinomas. Grades of EGFR expression were classified as "diffuse" and "focal or negative," as described in Materials and methods. Grades of Cbl expression were classified as "diffuse", "focal" and "negative", as described in Materials and methods. Correlation was analyzed by non-parametric test and *P* values were shown. *P* values less than 0.05 were regarded as statistically significant

	Case no.	EGFR expression		*P* value
		Diffuse	Focal or negative	
Cbl expression				
Diffuse	26	16 (62%)	10 (38%)	*P*=0.0049
Focal	29	10 (34%)	19 (66%)	
Negative	27	5 (19%)	22 (81%)	

Table 4 Clinicopathological character of the 16 cases with simultaneously diffuse expression of Cbl and epithelial growth factor receptor

Histology*	Wel	3	(19%)
	Mod	6	(38%)
	Por	7	(43%)
Depth of invasion*	t1	1	(6%)
	t2	5	(31%)
	t3–t4	10	(62%)
Lymph node metastasis*	n0	0	(0%)
	n1	3	(19%)
	n2	5	(31%)
	n3	8	(50%)
Stage*	I	0	(0%)
	II	2	(13%)
	III–IV	14	(87%)

*According to the criteria of the Japanese Classification of Gastric Cancer

stainings of Cbl and EGFR are shown in Fig. 2, and the results are summarized in Table 3. As the grades of Cbl immunoreactivity became stronger, the cases with strong EGFR immunoreactivity increased, the positive correlation being significant (*P*=0.049). Synchronous expression of Cbl and EGFR was observed in many cases. Most cases with diffuse expression of Cbl and EGFR were found in advanced cases (Fig. 2A, B; Table 4), while both were negative in superficial gastric carcinomas (Fig. 2C, D). Among 16 cases with simultaneous diffuse expression of Cbl and EGFR, 87% (14/16) of cases were in stage III and stage IV with deep invasion and nodal metastasis (Table 4). Moreover, the prognosis of the patients with synchronous diffuse expression of Cbl and EGFR was

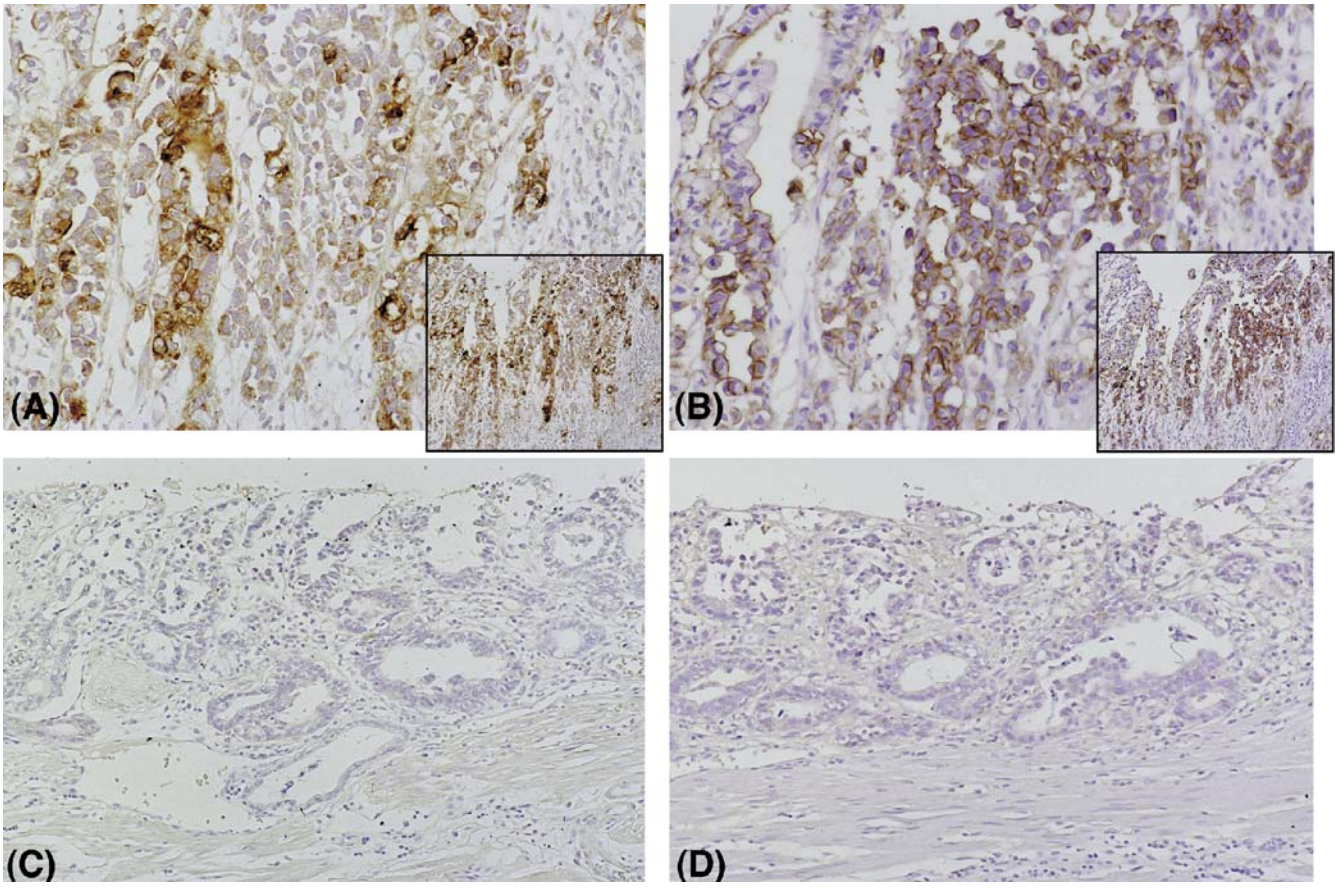

Fig. 2 Relationship of the expression of Cbl and epidermal growth factor receptor (EGFR). An advanced gastric carcinoma (**A**, **B**). An early gastric carcinoma (**C**, **D**). Cbl immunostaining (**A**, **C**). EGFR immunostaining (**B**, **D**). Synchronous expression of Cbl and EGFR was detected in advanced gastric carcinoma, while neither Cbl nor EGFR was found in early gastric carcinoma

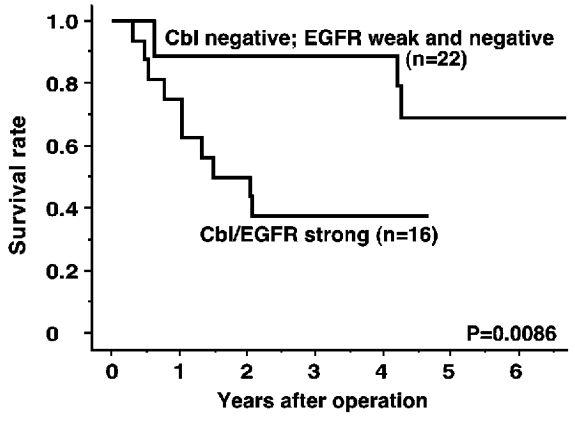

Fig. 3 Comparison of survival rates in patients between Cbl/epidermal growth factor receptor (EGFR)-diffuse cases and Cbl-negative/EGFR-focal or negative cases. The prognosis of the patients with synchronous diffuse expression of Cbl and strong expression of EGFR was significantly poorer than that of the patients negative for Cbl and weak and negative for EGFR

significantly poorer than that of the patients negative for Cbl and focal or negative for EGFR (P=0.0086) (Fig. 3).

In order to determine the influence of Cbl expression on survival, we made a multivariate survival analysis, including clinicopathological parameters (Table 5). The factor that gave the strongest influence was not Cbl expression but tumor stage.

Table 5 Multivariate analysis of factors related to prognosis. *NS* not significant

Factors*	*P* value	Odds ratio (95% confidence interval)
Histology	NS	
Depth of invasion	NS	
Lymph node metastasis	0.0253	3.48 (1.17–4.64)
Stage	0.0062	7.49 (1.79–11.44)
Cbl expression	0.0962	1.01 (0.34–1.21)

*According to the criteria of the Japanese Classification of Gastric Cancer

Effect of TGFα on the expression of Cbl in gastric cancer cells

Finally, we examined whether the treatment of TGFα induces Cbl expression in gastric carcinoma cell lines TMK-1 and MKN-74 using Western-blot analysis. In both cell lines, expression of Cbl protein was clearly induced by TGFα treatment (Fig. 4). Cbl protein expression was

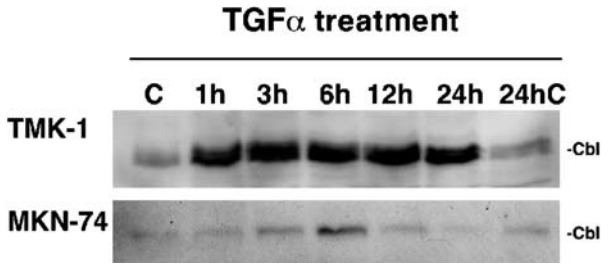

Fig. 4 Induction of Cbl protein in gastric cancer cells by transforming growth factor (TGF)α treatment. Western-blot analysis of Cbl protein expression in gastric carcinoma cell lines TMK-1 and MKN-74, treated with TGFα. The expression of Cbl protein was induced by TGFα treatment in both cell lines

induced at 1 h and preserved for 24 h in TMK-1, while it was induced at 3 h and diminished after 6 h in MKN-74.

Discussion

In the present study, we examined the expression of Cbl in human gastric carcinoma and compared it with clinicopathological parameters and EGFR expression. The expression of Cbl protein was detected in 67% of gastric carcinomas, which was correlated with depth of tumor invasion and nodal metastasis; whereas, Cbl was negative in normal gastric mucosa. The expression of Cbl was significantly associated with the expression of EGFR, and the patients with synchronous expression of Cbl and EGFR showed poor prognosis. However, multivariate survival analysis indicated the strongest influence was not Cbl expression but tumor stage. Therefore, we cannot completely deny a possibility that Cbl expression may be an epiphenomenon during tumor progression. We should certify the biological role of Cbl in stomach carcinogenesis by analyzing more cases and also using a model system.

Binding of growth factors to their receptors promotes receptor dimerization and subsequent activation [13], which enhances autophosphorylation of receptors, phosphorylation of numerous cellular proteins and recruitment of adapter molecules, which initiate signaling cascades [27]. Subsequently, receptors and associated complexes are transferred into multivesicular bodies with characteristic inner vesicles and membrane sorting and are either recycled back to the plasma membrane or directed to lysosomes for destruction [5, 28]. The mechanisms underlying EGFR trafficking are probably the best understood among all growth factor receptors. Ligand-enhanced endocytosis of EGFR requires intrinsic tyrosine kinase activity and endocytic sequence motifs (located in the cytoplasmic domain of the receptor) and also depends on numerous signals in the endosomes that can direct receptors for lysosomal degradation [28]. Polyubiquitination of EGFR mediated by Cbl has been recognized as a critical determinant in controlling EGFR endocytosis.

We have previously demonstrated that no EGF and few EGFR are found in early gastric carcinomas, whereas they are frequently expressed in advanced gastric carcinomas [30]. Similar to the previous data on the expression of EGFR, Cbl expression was detected more frequently in advanced cancer than in early cancer, and there was significant correlation with depth of invasion and nodal metastasis. Synchronous expression of Cbl and EGFR may correspond to the existence of numerous complexes of EGFR and ligands on the cell membrane of gastric carcinoma cells resulting from an activated EGFR system. In these conditions, an endocytic reaction with Cbl might promote turnover of EGFR. Of 122 cases examined, only 7 cases showed diffuse expression of EGFR and were negative for Cbl. While all of the 7 cases were at an advanced stage and 5 of 7 cases were scirrhous type, all the patients survived for more than 5 years, and the prognosis was clearly better than the cases with Cbl/EGFR co-expression.

We have previously confirmed that EGF and TGFα, produced by a gastric carcinoma cell line, TMK-1, act as autocrine growth factors [33]. We have shown that EGF treatment induced not only cell growth, but also the expression of oncogenes and cytokines [6]. In the present study, expression of Cbl was induced after 1 h of TGFα treatment in TMK-1. Because we did not block production of EGF and TGFα by TMK-1, it is possible that there might be EGFR/ligand complexes on the cell membrane before treatment of exogenous TGFα. Rapid elevation of Cbl protein may reflect increased turnover of EGFR, which occurred before the exogenous ligand treatment. However, Cbl induction by TGFα in MKN-74 occurred slowly and at a lower magnitude than TMK-1. This may be explained by a lower level of EGFR in MKN-74 than in TMK-1.

One of the important aspects of human carcinogenesis is the activation of tyrosine phosphorylation of cellular proteins. Activation of c-Src kinase was found frequently in carcinoma of the breast, colorectum and stomach [2, 16, 24]. In various tumor tissues, Cbl was tyrosine phosphorylated in a tumor-specific manner [10], suggesting that Cbl signaling may play an important role in tumorigenesis of various human cancers. It was reported that deregulated tyrosine phosphorylation of Cbl promotes leukemogenesis and that this can be achieved by mutation of Cbl or by an activated form of the tyrosine kinase abl [1]. An oncogenic form of Cbl was identified in the 70Z/3 pre-B-cell lymphoma, which has a deletion of 17 amino acids at the N-terminus of the ring-finger domain [1]. This oncogenic form of Cbl exhibits an enhanced level of tyrosine phosphorylation compared with wild-type Cbl. Differences exist between the rapid stimulatory signal induced by EGF and the prolonged signaling mediated by constitutively active oncogenic Cbl [25]. In the present study, the expression of Cbl was closely associated with tumor progression as well as EGFR expression. Therefore, it is possible that Cbl expression in gastric carcinoma may be an oncogenic form of Cbl with 17 amino acid deletions. However,

because the anti-Cbl antibody used here recognizes the C-terminal portion of Cbl, the antibody reacts with both the wild-type and oncogenic form of Cbl. Moreover, faint differences in molecular weight made it impossible to discriminate oncogenic form from wild type using Western-blot analysis. If the Cbl was oncogenic form, we may be able to restrain the function of EGF receptor system indirectly and put off the carcinoma progression by using obstructive antibody for oncogenic form Cbl. Thus, the inhibitor of oncogenic form Cbl should be a very useful for therapy of the carcinomas that express EGFR system genes at a high level. We should, in the near future, determine whether the Cbl in gastric carcinoma is an oncogenic form.

Nevertheless, our results suggest that Cbl in connection with EGFR system may be associated with stomach carcinogenesis, invasion and metastasis. Cbl may serve as a novel molecular marker for aggressive gastric carcinoma.

Acknowledgements This work was supported, in part, by Grants-in-Aid from the Ministry of Education, Culture, Sports, and Technology of Japan, and the Ministry of Health, Labor, and Welfare of Japan. The authors thank Masayoshi Takatani and Mutsumi Ueda for their skillful technical assistance. The authors are also grateful to Noriko Sagawa for her secretarial assistance.

References

1. Andoniou C, Thien C, Langdon W (1994) Tumour induction by activated abl involves tyrosine phosphorylation of the product of the cbl oncogene. EMBO J 13:4515–4523
2. Bolen JB, Veillette A, Schwarts AM, De Seau V, Rosen N (1997) Activation of pp60c-src protein kinase activity in human colon carcinoma. Proc Natl Acad Sci U S A 84:2251–2255
3. Di Fiore PP, De Camilli P (2001) Endocytosis and signaling. An inseparable partnership. Cell 106:1–4
4. Gad H, Ringstad N, Low P, Kjaerulff O, Gustafsson J, Wenk M, Di Paolo G, Nemoto Y, Crun J, Ellisman MH, De Camilli P, Shupliakov O, Brodin L (2000) Fission and uncoating of synaptic clathrin-coated vesicles are perturbed by disruption of interactions with the SH3 domain of endophilin. Neuron 27:301–312
5. Hopkins C, Gibson A, Shipman M, Miller K (1990) Movement of internalized ligand-receptor complexes along a continuous endosomal reticulum. Nature 346:318–319
6. Ito R, Kitadai Y, Kyo E, Yokozaki H, Yasui W, Yamashita U, Nikai H andTahara E (1993) Interleukin 1 alpha acts as an autocrine growth stimulator for human gastric carcinoma cells. Cancer Res 53:4102–4106
7. Japanese Research Society for Gastric Cancer (1995) Japanese classification of gastric carcinoma. 1st English edn. Kanehara & Co., Ltd., Tokyo, pp 38–65
8. Joazeiro CA, Hunter T (2000) Biochemistry. Ubiquitination—more than two to tango. Science 289:2061–2062
9. Joazeiro CA, Wing SS, Huang H, Leverson JD, Hunter T, Liu YC (1999) The tyrosine kinase negative regulator c-Cbl as a RING-type, E2-dependent ubiquitin-protein ligase. Science 286:309–312
10. Kamei T, Machida K, Nimura Y, Senga T, Yamada I, Yoshii S, Matsuda S, Hamaguchi M (2000) C-Cbl protein in human cancer tissues is frequently tyrosine phosphorylated in a tumor-specific manner. Int J Oncol 17:335–339
11. Kitadai Y, Yasui W, Yokozaki H, Kuniyasu H, Ayhan A, Haruma K, Kajiyama G, Johnson GR, Tahara E (1993) Expression of amphiregulin, a novel gene of the epidermal growth factor family, in human gastric carcinomas. Jpn J Cancer Res 84:879–884
12. Kuniyasu H, Yoshida K, Yokozaki H, Yasui W, Ito H, Toge T, Ciardiello F, Persico MG, Saeki T, Salomon DS, et al (1991) Expression of cripto, a novel gene of the epidermal growth factor family, in human gastrointestinal carcinomas. Jpn J Cancer Res 82:969–973
13. Lemmon MA, Schlessinger J (1998) Transmembrane signaling by receptor oligomerization. Methods Mol Biol 84:49–71
14. Levkowitz G, Waterman H, Ettenberg SA, Katz M, Tsygankov AY, Alroy I, Lavi S, Iwai K, Reiss Y, Ciechanover A, Lipkowitz S, Yarden Y (1999) Ubiquitin ligase activity and tyrosine phosphorylation underlie suppression of growth factor signaling by c-Cbl/Sli-1. Mol Cell 4:1029–1040
15. Ochiai A, Yasui W, Tahara E (1985) Growth-promoting effect of gastrin on human gastric carcinoma cell line TMK-1. Jpn J Cancer Res 76:1064–1071
16. Ottenhoff-Kalff AE, Rijiksen G, van Bewrden EA, Hennipman A, Michels AA, Staal GE (1992) Characterization of protein tyrosine kinases from human breast cancer. Cancer Res 52:4773–4778
17. Oue N, Shigeishi H, Kuniyasu H, Yokozaki H, Kuraoka K, Ito R, Yasui W (2001) Promoter hypermethylation of MGMT is associated with protein loss in gastric carcinoma. Int J Cancer 93:805–809
18. Petrelli A, Gilestro GF, Lanzardo S, Comoglio PM, Migone N, Giordano S (2002) The endophilin-CIN85-Cbl complex mediates ligand-dependent downregulation of c-Met. Nature 416:187–190
19. Ringstad N, Gad H, Low P, Di Paolo G, Brodin L, Shupliakov O, De Camilli P (1999) Endophilin/SH3p4 is required for the transition from early to late stages in clathrin-mediated synaptic vesicle endocytosis. Neuron 24:143–154
20. Schmidt A, Wolde M, Thiele C, Fest W, Kratzin H, Podtelejnikov AV, Witke W, Huttner WB, Soling HD (1999) Endophilin I mediates synaptic vesicle formation by transfer of arachidonate to lysophosphatidic acid. Nature 401:133–141
21. Simpson F, Hussain NK, Qualmann B, Kelly RB, Kay BK, McPherson PS, Schmid SL (1999) SH3-domain-containing proteins function at distinct steps in clathrin-coated vesicle formation. Nat Cell Biol 1:119–124
22. Soubeyran P, Kowanetz K, Szymkiewicz I, Langdon WY, Dikic I (2002) Cbl-CIN85-endophilin complex mediates ligand-induced downregulation of EGF receptors. Nature 416: 183–187
23. Take H, Watanabe S, Takeda K, Yu ZX, Iwata N, Kajigaya S (2000) Cloning and characterization of a novel adaptor protein, CIN85, that interacts with c-Cbl. Biochem Biophys Res Commun 268:321–328
24. Takekura N, Yasui W, Yoshida K, Tsujino T, Nakayama H, Kameda T, Yokozaki H, Nishimura Y, Ito H, Tahara E (1990) pp60c-src protein kinase activity in human gastric carcinomas. Int J Cancer 45:847–851
25. Thien CB, Langdon WY (1997) EGF receptor binding and transformation by v-cbl is ablated by the introduction of a loss-of-function mutation from the Caenorhabditis elegans sli-1 gene. Oncogene 14:2239–2249
26. Thien CB, Langdon WY (2001) Cbl: many adaptations to regulate protein tyrosine kinases. Nat Rev Mol Cell Biol 2:294–307
27. Ullirich A, Schlessinger J (1990) Signal transduction by receptors with tyrosine kinase activity. Cell 61:203–212
28. Waterman H, Yarden Y (2001) Molecular mechanisms underlying endocytosis and sorting of ErbB receptor tyrosine kinases. FEBS Lett 490:142–152
29. Yasui W, Hata J, Yokozaki H, Nakatani H, Ochiai A, Ito H, Tahara E (1988) Interaction between epidermal growth factor and its receptor in progression of human gastric carcinoma. Int J Cancer 41:211–217
30. Yasui W, Sumiyoshi H, Hata J, Kameda T, Ochiai A, Ito H, Tahara E (1988) Expression of epidermal growth factor

receptor in human gastric and colonic carcinomas. Cancer Res 48:137–141
31. Yokouchi M, Kondo T, Houghton A, Bartkiewicz M, Horne WC, Zhang H, Yoshimura A, Baron R (1999) Ligand-induced ubiquitination of the epidermal growth factor receptor involves the interaction of the c-Cbl RING finger and UbcH7. J Biol Chem 274:31707–31712
32. Yokozaki H (2000) Molecular characteristics of eight gastric cancer cell lines established in Japan. Pathol Int 50:767–777
33. Yoshida K, Tsujino T, Yasui W, Kameda T, Sano T, Nakayama H, Toge T, Tahara E (1990) Induction of growth factor-receptor and metalloproteinase genes by epidermal growth factor and/or transforming growth factor-alpha in human gastric carcinoma cell line MKN-28. Jpn J Cancer Res 81:793–798

Virchows Arch (2004) 444:332–339
DOI 10.1007/s00428-003-0969-x

ORIGINAL ARTICLE

Maria P. Foschini · Alessia Gaiba · Roberto Cocchi · Maria G. Pennesi · Maria R. Gatto · Giovanni P. Frezza · Annalisa Pession

Pattern of p63 expression in squamous cell carcinoma of the oral cavity

Received: 30 October 2003 / Accepted: 16 December 2003 / Published online: 2 March 2004

Abstract P63 is a recently discovered gene harbouring different isoforms by alternate splicing. The two main isoforms, TAp63 and ΔNp63, have opposite functions, being responsible for cell-cycle arrest and cell proliferation, respectively. In addition, new isoforms have been described with the same sequence as TAp63 and ΔNp63, but lacking exon 4 (Δ4Tap63 and ΔNp73L). P63 as detected using immunohistochemistry is present in squamous cell carcinomas. To better define the role of p63 in squamous cell carcinomas of the oral cavity (OSCC), 39 patients were investigated using immunohistochemical analysis with a monoclonal antibody recognising all p63 isoforms and an anti-Ki67 antibody. Reverse-transcription polymerase chain reaction (PCR) and nested PCR were also performed using isoform-specific primers to evaluate the p63 mRNA expression pattern. Using immunohistochemistry, p63 was always present in OSCC, and its distribution was similar to that of Ki67. The percentage of positive cells increased from normal to neoplastic mucosa, but there was no relationship between the number of p63 positive cells and prognosis. P63 mRNA was found in all patients. The truncated isoforms Δ4TAp63 and ΔNp73L were more frequently expressed in patients presenting with metastases. ΔNp73L was found in 66.6% of tumours with lymph-node metastases, but in only 33.3% of those devoid of lymph-node metastases at presentation. An impaired expression of the p63 isoforms might favour cell proliferation and indirectly enhance the metastasising capacity of OSCC.

Keywords Squamous cell carcinoma · Oral cavity · p63 · Prognosis

M. P. Foschini · A. Gaiba · A. Pession
Department of Oncological Sciences,
Section of Anatomic Pathology,
University of Bologna at Bellaria Hospital,
Bologna, Italy

R. Cocchi · M. G. Pennesi
Department of Maxillo-Facial Surgery,
Bellaria Hospital, Bologna, Italy

G. P. Frezza
Department of Oncological Sciences, Section of Radiotherapy,
University of Bologna at Bellaria Hospital,
Bologna, Italy

M. R. Gatto
Department of Dental Sciences University of Bologna, Italy

M. P. Foschini (✉)
Anatomia Patologica,
Ospedale Bellaria,
Via Altura 3, 40139 Bologna, Italy
e-mail: Mariapia.foschini@ausl.bologna.it
Tel.: +39-05-16225523
Fax: +39-05-16225759

Introduction

A recently discovered gene, p63, mapped on chromosome 3q27–29 [2, 11, 13, 19] and a member of the p53 gene family [11, 12], is frequently expressed in carcinomas in different sites [4, 5, 7, 8, 10, 15, 16, 17]. The TP63 gene generates protein isoforms based on alternate splicing [6, 7, 8, 13, 14, 18]. The TA p63/p51 group (comprising the α, β and γ isoforms) is the full-length protein and shows p53-like activities, such as inducing cell-cycle arrest and apoptosis. The second group (ΔN p63 in the α, β and γ isoforms) lacks the NH_2 terminal domain and acts as a dominant negative agent, inhibiting the transactivation activity of both TA p63/p51 and p53. As a result, the TA p63/p51 protein favours cell differentiation, while ΔN p63 favours cell proliferation. In addition, Senoo et al. [13] described a new isoform, ΔNp73L, corresponding to ΔN p63, but lacking exon 4. To date, the ΔNp73L variant has been found only in squamous cell carcinomas.

A further isoform, named Δ4TAp63, emerged from a preliminary study in our laboratory (Gaiba et al., unpublished observations). TA p63/p51 expression analysis, performed in squamous cell carcinomas of the oral cavity (OSCC), non-neoplastic oral mucosa and cultured keratinocytes, showed two bands: one corresponding to the TA isoform and a 250-bp shorter band. The amplification

products were sequenced and showed an mRNA that could be translated into a protein, since there is no evidence of frame shift in the sequence. This second variant has the same sequence as TA p63/p51, but lacks exon 4 and was named Δ4TAp63.

A correct function of the p63 gene is important to maintain cell regeneration and differentiation in squamous epithelia and their derivatives. It has been postulated that impaired p63 expression might influence neoplastic cell transformation [5, 7, 9, 15].

P63 expression has been demonstrated in squamous cell carcinomas arising in different organs, like the oral cavity, larynx, lung and uterine cervix, and in transitional cell carcinoma of the urinary bladder. p63, as detected using immunohistochemistry, is always expressed in OSCC, but no relationship with prognosis has been demonstrated [3]. This is probably due to the fact that the antibodies commercially available for immunohistochemical detection of p63 do not distinguish all the different p63 isoforms. In order to better define the possible role of the p63 isoforms in squamous cell carcinomas, 39 cases of OSCC were studied using immunohistochemical analysis with a monoclonal antibody that recognises all p63 isoforms and an anti-Ki67 antibody, recognising proliferating cells, and using reverse-transcription polymerase chain reaction (PCR) and nested PCR using isoform-specific primers to evaluate the p63 mRNA expression pattern.

Materials and methods

Patients

Cases of primary OSSC (n=39) were obtained from the files of the Department of Pathology at Bellaria Hospital, University of Bologna. No previous radio- or chemotherapy had been administered. All the cases had been received fresh, and a sample of neoplastic tissue had been snap frozen in liquid nitrogen and stored at −80°C for molecular studies. Tissue sampling and histological diagnosis were performed according to the guidelines recently published [1]. Haematoxylin–eosin stained sections were reviewed from all the cases to select blocks containing representative areas of invasive carcinoma and, when present, in situ carcinoma. In addition, non-neoplastic mucosa adjacent to the tumour was examined. Clinical charts were reviewed to collect information on the clinical history and follow-up of the patients.

Immunohistochemistry

Immunostaining was performed on 3-μm thick sections, serially cut from the selected blocks. The following antibodies were employed: monoclonal anti-p63 (NeoMarkers, Freemont CA94539, USA, clone 4A4, diluted 1:200) and monoclonal anti-Ki67 (Dako, Denmark, clone MIB-1, diluted 1:200). Sections were deparaffinised and rehydrated, and endogenous peroxidase was blocked in 1% H_2O_2 in methanol. Only sections for Ki67 analysis were submitted to 6 min treatment at high pressure in citrate buffer; then slides were cooled at room temperature. All antibodies were applied at room temperature for 1 h. The processing was performed in an automatic stainer (Autostainer, Dako, Carpintera, CA, USA) using biotinylated coat and anti-polyvalent and streptavidin peroxidase antibodies (LabVision Corporation, Fremont, CA, USA). Dako Liquid DAB–substrate–Chromogen system (Dako, Carpintera, CA, USA) was used to detect the peroxidase activity.

Counting the percentage of positive nuclei in 200 consecutive cells of selected areas representative of the lesion gave a semi-quantitative evaluation of the immunohistochemical results.

RNA extraction and RT-PCR

For each sample, 20 μg of still frozen tissue was put in RNA stabilisation reagent (RNAlater, QIAGEN, Hilden, Germany) and then treated according to the RNeasy Mini Kit protocol (QIAGEN, Hilden, Germany). cDNA synthesis was carried out using 3 μl of total RNA. Retrotranscription was performed at 37°C for 1 h in a total volume of 25 μl in the presence of random examiners (Roche, Manheim, Gemany), 0.5 μM dNTPs (Sigma-Aldrich S.r.l., Italy), 1× buffer, 200 U M-MLV (Promega, Madison, USA) and 40 U RNAguard (Amersham Pharmacia Biotech Inc, USA).

Nested PCR

The first PCR was performed using the following primers: TP63ex3′ (sense 5′ TGCCCAGACTCAATTTAGTG 3′) and TP63ex2 (sense 5′ GTCCCAGAGCACACAGACAA 3′) to identify the ΔNp73L and TAp63 isoforms, respectively, and TP63ex10 (antisense 5′ TGAGGAAGGTACTGCATGAG 3′) and a second antisense called TP63 ex5L (5′ GGATAACAGCTCCCTGAGGA 3′). Next, 200 μm dNTP (Sigma-Aldrich S.r.l., Italy), 1× buffer, 2 mM $MgCl_2$, 0.2 μm each primer, 1 U FastStart *Taq* Polymerase (Roche, Manheim, Gemany) and 2 μl of cDNA were put in a total reaction volume of 50 μl. After a first denaturation step at 95°C for 4 min, the reaction continued for 30 cycles of 95°C for 30 s, 57°C for 30 s and 72°C for 40 s. The final extension was 72°C for 7 min. The second PCR was carried out changing only the antisense primer; the new primers were called TP63ex6 (5′ ACTGGGCATG-GCTGTTCC 3′) and TP ex5S (5′ TTGCAATTTGGCAGTA-GAGTT 3′). The reaction contained 200 μm dNTP (Sigma-Aldrich S.r.l., Italy), 1× buffer, 2 mM $MgCl_2$, 0.2 μm each primer, 1 U FastStart *Taq* Polymerase (Roche, Manheim, Gemany) and 2 μl of the first PCR amplified. The PCR products were run in a 2.2% agarose gel. Some randomly chosen bands were cut off the gel and purified for sequence analysis to prove the authenticity of the resulting band pattern. The PCR for glyceraldehyde-3-phosphate dehydrogenase (GAPDH) analysis was performed using the following primers: GAPDHf (5′CAATGACCCCTTCATTGACC 3′) and GAPDHr (5′TTGATTTTGGAGGGATCTCG 3′). Then, 200 μm dNTP (Sigma-Aldrich S.r.l., Italy), 1× buffer, 2 mM $MgCl_2$, 0.2 μm each primer, 1 U FastStart *Taq* Polymerase (Roche, Manheim, Gemany) and 2 μl of cDNA were put in a total reaction volume of 50 μl. After a first denaturation step at 95°C for 4 min, the reaction continued for 30 cycles of 95°C for 30 s, 57°C for 30 s and 72°C for 40 s. The final extension was 72°C for 7 min.

Band purification and sequence analysis

The bands visualised in the agarose gel were cut off and treated following the protocol of the MinElute Gel Extraction kit (QIAGEN, Hilden, Germany). Preparations of the DNA sequencing reactions were performed in agreement with the CEQ2000 Dye Terminator Cycle Sequencing with Quick Start Kit (Beckman Coulter, Fullerton, CA, USA). After purification with the DyeEx 2.0 spins Kit (QIAGEN, Hilden, Germany), the products were loaded on the CEQ2000 (Beckman Coulter, Fullerton, CA, USA).

Statistical analysis

Chi-square and Fisher's exact test were used for evaluation of statistical significance. Spearman correlation coefficient was used for evaluation of co-graduation between analytical methods.

Results

Results and clinical data are summarised in Table 1.

Histology

All cases were invasive squamous cell carcinoma. All cases were composed of neoplastic nests surrounded by two types of cells. The peripheral part of the nests was mainly composed of oval cells, with scanty basophilic cytoplasm, ovoid and atypical central nucleus, showing frequent mitotic activity. These were identified as "basaloid cells" (BC).

Polygonal cells with eosinophilic cytoplasm and central hyperchromatic nucleus characterised the second cell type. The latter were located at the centre of the neoplastic nests, forming the squamous pearls (Fig. 1A). BC composed less than 30% of the neoplastic population in well-differentiated carcinomas, 30–60% in the moderately differentiated and more than 60% in the poorly differentiated cases. Lymph-node metastases were present in 24 cases at the time of diagnosis. In situ squamous cell carcinoma was present in the mucosa adjacent to the invasive OSCC in 11 cases. Non-neoplastic oral mucosa was examined in all cases and showed features of mild to moderate hyperkeratosis and chronic inflammation.

Immunohistochemistry

Immunohistochemical results are summarised in Table 2.

Table 1 Comparison of the clinico-pathological and molecular results. *T* tumour according to the tumour node metastases staging system (TNM), *N* lymph-node metastases according to the TNM staging system, *G* grade, *FU* follow up (months), *AW* alive and well, *AWD* alive with disease (metastases to lungs and skin), *DOD* died of disease, *W* well differentiated, *Mo* moderately differentiated, *P* poorly differentiated, *ICH %* percentage of neoplastic cells positive with p63 antibody, *MG* mandibular gingiva, *Me* metastasis, *FM* floor of the mouth, *To* tongue, + presence of the isoforms, – absence of the isoform

Case no.	Sex/age (years)	Site	T	N	FU	G	P63 ICH %	P63 isoforms by nested PCR			
								TA p63	Δ4TA p63	ΔNP63	ΔNp73L
1	Female 78	Cheek	2	0	AW 21	W	10	+	+	+	+
2	Female 83	MG	4a	0	AW 22	P	70	+	–	+	–
3	Female 49	MG	2	0	AW 16	Mo	50	+	–	+	–
4	Male 81	MG	4a	0	AW 9	P	80	+	+	+	+
5	Female 77	FM	1	0	AW 10	Mo	60	+	–	+	–
6	Male 59	FM	2	0	AW 10	Mo	60	+	+	+	+
7	Male 78	Palate	4a	0	DOD 3	Mo	60	–	–	+	–
8	Male 44	Palate	1	0	AW 21	Mo	50	+	–	+	–
9	Female 57	Palate	1	0	AW 11	Mo	60	+	–	+	+
10	Female 65	To	1	0	AW 25	W	20	–	+	+	–
11	Female 55	To	2	0	AW 24	P	90	+	–	+	–
12	Male 48	To	1	0	AW 19	P	80	+	–	+	–
13	Female 73	To	1	0	AWD 7	W	25	+	–	+	+
14	Male 87	To	2	0	AW 9	W	20	+	–	+	–
15	Male 65	MG	1	0	AW 9	P	80	+	–	+	–
16	Female 79	To	4a	1	AWD 10	Mo	60	–	+	+	–
17	Female 58	MG	2	1	AWD 11	P	90	+	–	+	+
18	Female 58	FM	3	1	AWD 10	P	90	+	–	+	+
19	Female 64	FM	1	1	AW 18	Mo	60	+	–	+	+
20	Male 78	T	3	1	AWD 15	Mo	60	+	–	+	–
21	Male 74	To	2	1	DOD 9	P	90	–	–	+	–
22	Male 73	To	2	1	AW 24	P	70	+	–	+	–
23	Female 37	To	2	1	AW 28	W	20	+	–	+	+
24	Female 88	MG	4a	1	AW 9	P	70	+	+	+	+
25	Female 66	Cheek	2	1	AW 8	W	20	+	–	–	–
26	Female 63	To	1	1	AW 8	W	20	–	+	+	+
27	Female 62	To	1	1	AW 8	P	90	+	–	+	+
28	Female 76	Cheek	2	2b	AW 10	W	20	+	+	+	+
29	Male 41	MG	2	2b	DOD 7	Mo	40	+	+	+	+
30	Male 66	MG	3	2c	DOD 1	P	80	–	–	+	+
31	Male 55	MG	4a	2a	AW 30	W	30	+	+	+	+
32	Female 65	FM	4a	2b	AW 13	P	90	+	+	+	+
33	Male 79	FM	4a	2b	AWD 7	P	70	+	+	+	+
34	Male 77	To	4a	2c	DOD 6	P	70	–	–	+	–
34Me						P	70	+	+	+	+
35	Male 62	To	2	2b	AW 13	Mo	40	–	–	+	–
36	Male 50	To	2	2b	AW 20	W	20	–	–	+	–
37	Male 52	To	4a	2b	AW 18	W	20	+	+	+	+
38	Male 57	To	3	2c	AWD 12	P	70	+	+	+	+
39	Male 53	To	4a	2a	AW 11	P	80	+	+	+	+

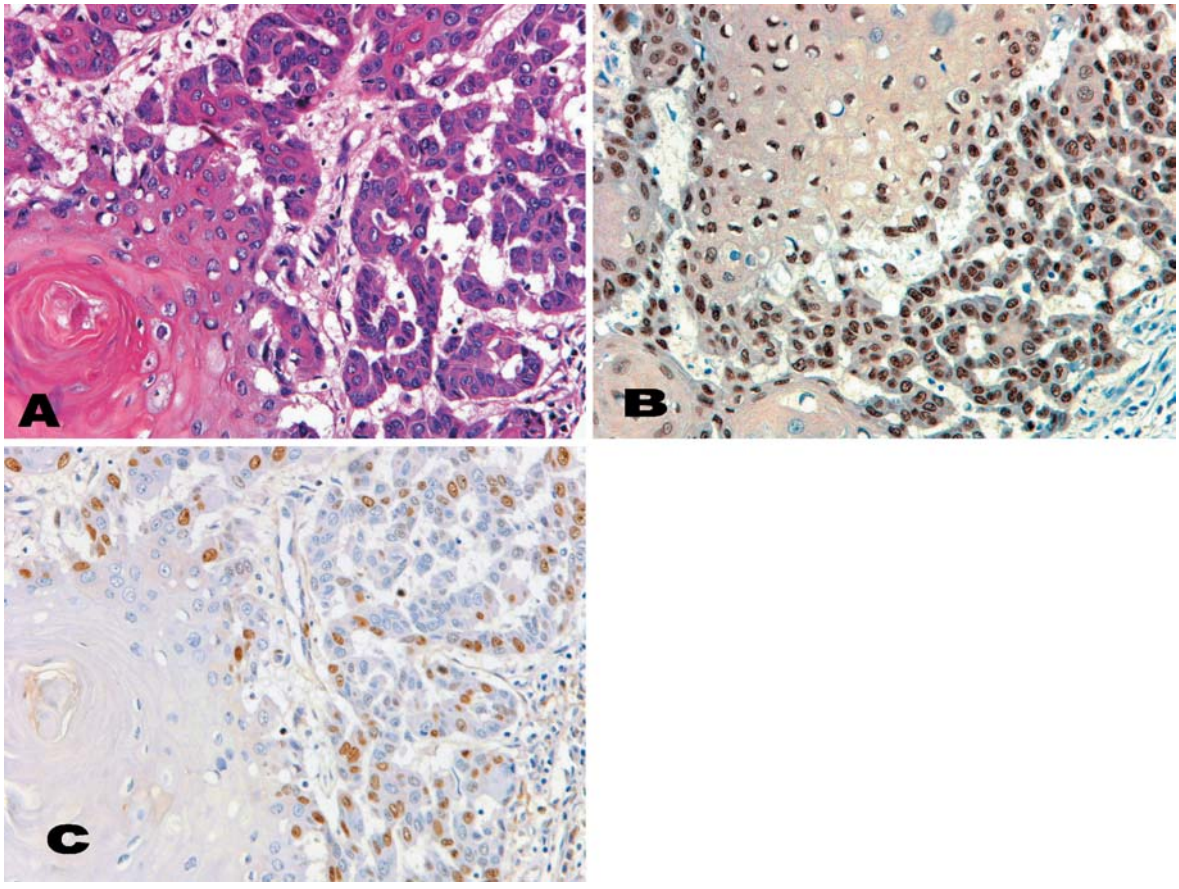

Fig. 1 Invasive squamous cell carcinomas of the oral cavity. **A** The neoplastic nests are composed of basaloid cells (*arrow*) located at the periphery and of eosinophilic cells forming the squamous pearls. Using immunohistochemistry, both p63 (**B**) and Ki67 (**C**) mainly stain the basaloid cells

Table 2 Comparison between immunohistochemical results with P63 and Ki67 antibodies. *N* Number of cases

	N	P63	Ki67
Non-neoplastic mucosa	38	10%*	5–10%**
Chronic inflammation	20	10–20%*	5–15%**
In situ carcinoma	11	30–60%	15–60%
Invasive carcinoma	38	20–90%	20–60%
Well differentiated	9	10–30%	20–30%
Moderately differentiated	10	40–60%	25–50%
Poorly differentiated	20	70–90%	40–60%
Metastases	24	20–90%	20–60%

* Positive cells are located in the basal and suprabasal layers
** Positive cells are located in the basal layer

Neoplastic tissues

P63 positivity was observed in all cases (Fig. 1B, C). P63 stained the nuclei of BC present at the periphery of the neoplastic nests and occasionally only the polygonal eosinophilic cells. Consequently, the percentage of p63-positive cells varied from case to case, being higher in poorly differentiated OSCC. Distribution of Ki67 positivity was similar to that obtained with p63 (P=0.00001), as it was mainly localised in the BC. Immunohistochemical results obtained in the metastatic lesions were almost the same as those of the corresponding invasive OSCC. Specifically, both the p63 and Ki67 antibodies strongly stained 30–60% of the neoplastic nuclei. Positivity was mainly confined to BC.

In the 11 cases of in situ carcinoma (Fig. 2A, B, C), p63 stained 30–60% of the neoplastic intramucosal cells. Ki67 stained 15–30% of the cells in seven cases and more than 30% of the cells in four cases. In all 11 cases of in situ carcinoma, Ki67 positivity was present in both basal and suprabasal cell layers.

Non-neoplastic mucosa

P63 positivity was confined to the basal and immediately suprabasal layers of keratinocytes, with positive cells never exceeding 10% of the keratinocytes (Fig. 3A, B, C, D, E, F). Percentage of p63-positive cells was higher in areas of chronic inflammation, reaching 30% of the keratinocytes and extending to the suprabasal layers. Immunostaining for Ki67 was limited to 5–10% of the normal keratinocytes localised in the basal layer. Like

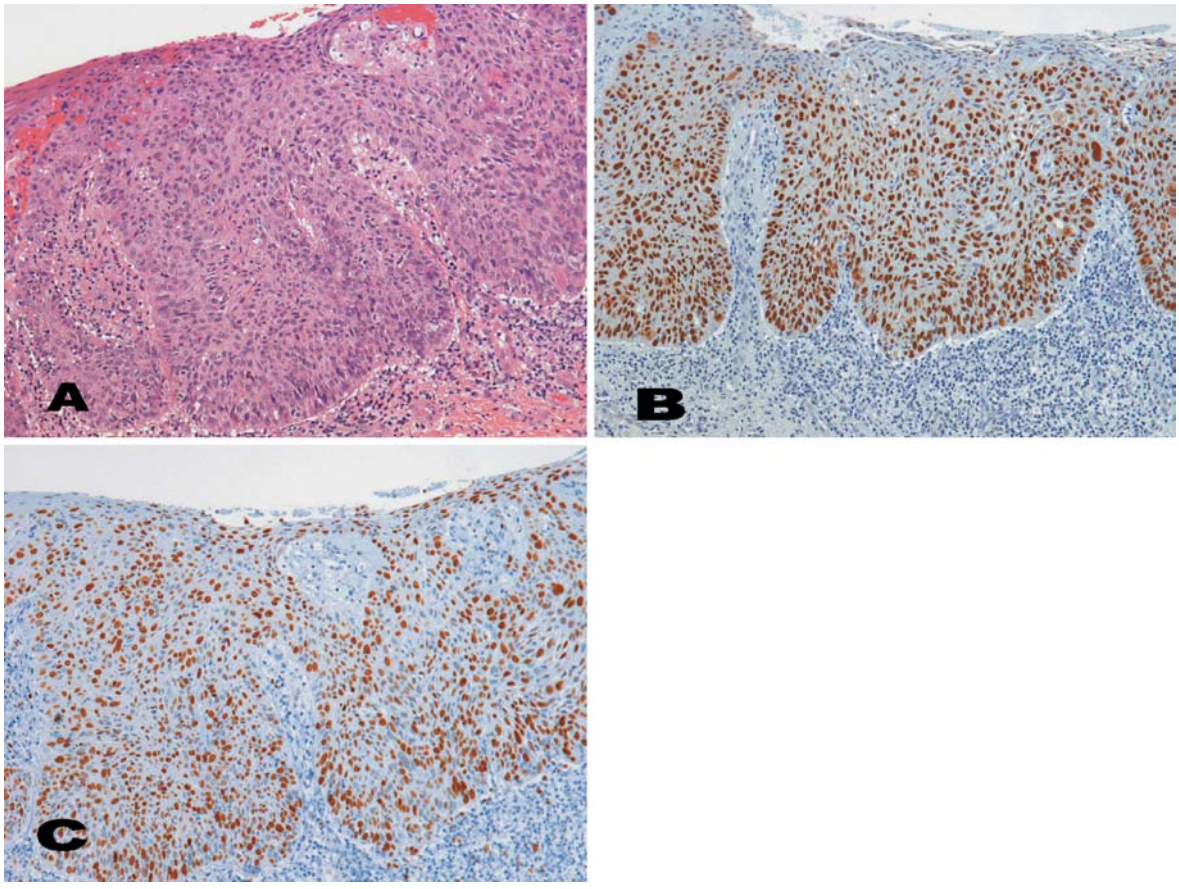

Fig. 2 In situ squamous cell carcinoma (**A**). P63 (**B**) and Ki67 (**C**) stain most of the neoplastic cells

p63, Ki67 positivity was higher in areas of chronic inflammation, reaching 15% of positive keratinocytes.

P63 expression analysis

All the cases presented at least one of the four isoforms. ΔN p63 was the more frequently expressed isoform, being present in 38 of the 39 cases studied (97.4%), while the TAp63 was present in only 30 cases. The truncated variants Δ4TAp63 and ΔNp73L were present in 16 and 22 cases, respectively. The ΔN p73L was always expressed together with ΔNp63, while Δ4TAp63 in three cases was expressed without TA p63. All four isoforms were shown in 11 cases (28.2%). The remaining cases showed variable expression patterns.

Correlation between p63 expression pattern and immunohistochemical results

As shown in Table 1, no correlation was found between the percentage of neoplastic cells stained with the anti-p63 antibody and the expression of the different p63 isoforms. Specifically, the number of cells positive using immunohistochemistry with the anti-p63 antibody was not related to the appearance of the truncated variants ΔN p73L and Δ4TAp63.

Correlation between p63 expression pattern and clinico–pathological features

Comparing the group of patients with lymph-node metastases at the time of surgery with the group of patients without lymph-node metastases at presentation, the truncated variants ΔN p73L and Δ4TAp63 were more frequently expressed by the lymph-node metastasising tumours (Table 3). Specifically, the difference in ΔNp73L expression between the two groups reached statistical significance (P=0.05; Spearman correlation coefficient P=0.00001). It is noteworthy that in case no. 34, the two truncated variants appeared in the metastatic lesion, but not in the primary tumour. In addition, ΔN p73L was present in 6 of 8 (75%) cases presenting in T1 and T2, but showing lymph-node metastases, while it appeared in 4 of 12 (33.3%) T1 and T2 tumours without lymph-node metastases at presentation. One of the latter four cases (case no. 13) developed metastases during the follow-up.

This difference became less evident comparing the group of cases harbouring distant metastases with the

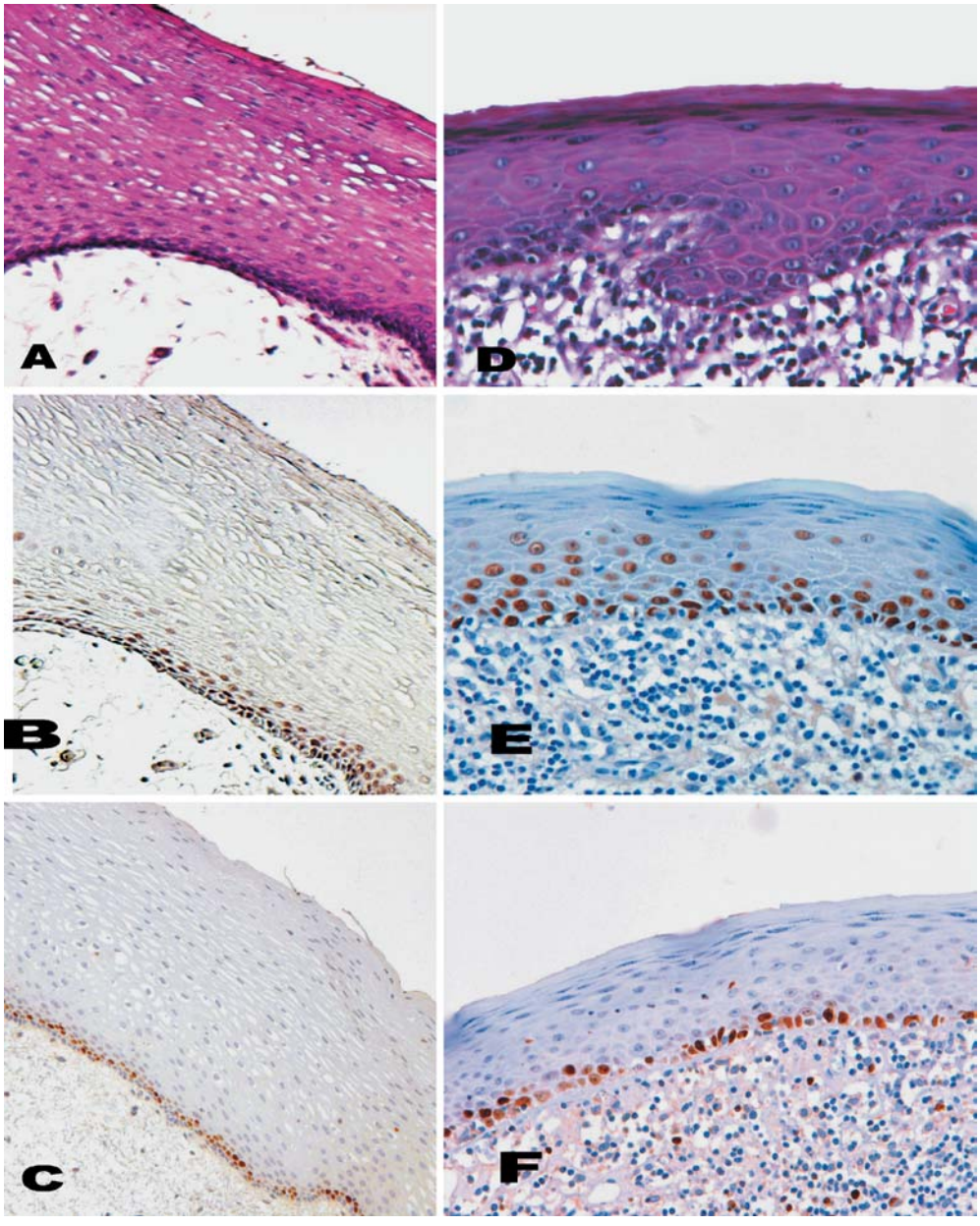

Fig. 3 Non-neoplastic oral mucosa (**A**); p63 (**B**) stains basal and immediately suprabasal keratinocytes, while Ki67 (**C**) is confined to the basal keratinocytes. In areas of chronic inflammation (**D**), positivity for p63 is increased (**E**), while Ki67 is still confined to the basal keratinocytes (**F**)

Table 3 P63 expression pattern and metastases at presentation. *Non-LN Mets* Absence of lymph-node metastases at the time of surgery, *Presence of LN Mets* Presence of lymph-node metastases at the time of surgery

P63 Isoform	Non-LN Mets	Presence of LN Mets
TA p63	13/15 (86.6%)	17/24 (70.8%)
Δ4TAp63	4/15 (26.6%)	11/24 (45.8%)
ΔN p63	15/15 (100%)	23/24 (95.8%)
ΔN p73L	5/15 (33.3%)	16/24 (66.6%)
All four isoforms	3/15 (20%)	8/24 (33.3)

Table 4 P63 expression pattern and clinical behaviour. *AW* alive and well, *AWD* alive with disease, *DOD* died of disease

P63 Isoform	Patients AWD and DOD	Patients AW
TA p63	7/12 (58.3%)	23/27 (85.1%)
Δ4TAp63	4/12 (33.3%)	11/27 (40.7%)
ΔN p63	12/12 (100%)	26/27 (96.2%)
ΔN p73L	7/12 (58.3%)	14/27 (51.8%)
All four isoforms	3/12 (25%)	8/27 (29.6%)

disease-free group of patients (Table 4). The group of patients alive with no evidence of disease more frequently expressed TAp63 (P=0.07). ΔNp63 was the only isoform expressed in five cases; three of these five tumours rapidly displayed distant metastases leading to the death of the patients 3–9 months after surgery. The remaining two cases showed lymph-node metastases, despite the relatively small size (T2) of the primary tumour.

Discussion

The number of p63-positive cells was remarkably higher in squamous neoplastic lesions, either in situ or invasive, compared with non-neoplastic oral mucosa. P63 showed the same distribution as Ki67, being localised in the BC observed at the periphery of the neoplastic nests, but stained more numerous cells. The current immunohistochemical results are consistent with those obtained on OSCC by Choi et al. [4] and in lung squamous cell carcinoma by Wang et al. [16] and Pelosi et al. [8]. All these morphological findings suggest that, in squamous cell carcinomas, p63 is present in a subset of "basaloid/stem" cells [3] and is able to proliferate and differentiate into squamous elements.

On the contrary, none of the published studies disclosed a correlation between p63 immunoreactivity and clinical behaviour of the tumour. Most probably, this is due to the fact that the A4A antibody commonly employed against p63 does not discriminate the different isoforms; thus, RT-PCR and nested-PCR are needed to analyse the expression of Tap63\p51, Δ4TAp63, ΔN p63 and ΔN p73L.

Considering the dual nature of p63 as a proliferative agent with its ΔN isoforms and anti-proliferative agent with its TA isoforms, a transcriptional dysregulation of the p63 gene has been implicated as an oncogene, favouring the proliferative capacity of the neoplastic cell. Several recent reports support this hypothesis. Nylander et al. [7] found an overexpression of ΔN p63a in OSCC, suggesting that it might play an oncogenic role in the oral mucosa. Pruneri et al. [9] reported that a downregulation of the antiproliferative agent TAp63 favours an aggressive behaviour in squamous cell carcinomas of the larynx. Urist et al. [15] found that cell lines from invasive transitional cell carcinoma of the urinary bladder only maintain the expression of the proliferative agent ΔNp63.

In the present series of OSCC, ΔNp63 was the most frequently expressed variant, being present in all but one case. It was the only isoform expressed in five cases, three of which behaved in an extremely aggressive fashion, rapidly giving rise to distant metastases.

Few data are currently available on the truncated variants ΔNp73L and Δ4TAp63. In the present cases, the truncated variants Δ4TAp63 and ΔNp73L were more frequently expressed in those cases showing lymph-node metastases at presentation. In addition, there was no linear relationship between tumour size and ΔN p73L expression. ΔNp73L appeared in 75% of T1 and T2 tumours, showing lymph-node metastases at presentation, compared with only 33.3% of those without lymph-node metastases at presentation. In one further case (case 34), the truncated variant ΔNp73L was not present in the primary tumour, but appeared in the lymph-node metastasis; whereas, one case of T4 without lymph-node metastases (case 2) failed to show ΔNp73L expression. The difference in expression of ΔNp73L between cases with and without lymph-node metastases at presentation was statistically significant (P=0.05). ΔNp73L was described by Senoo et al. [13], who found it only in cell lines derived from squamous cell carcinomas, but not in normal keratinocytes. According to the original data [13], ΔNp73L maintain the dominant–negative activity, inhibiting the function of p53 and TAp63, thus favouring cell proliferation. ΔNp73L was always present in association with ΔNp63, suggesting that the presence of the truncated variant ΔNp73L might strengthen the ability of the neoplastic cell to proliferate.

In contrast, the exact function of Δ4TAp63 remains unknown. Δ4TAp63 is expressed in normal and neoplastic keratinocytes (Gaiba et al., unpublished observations). In the present series, Δ4TAp63, either in combination with the TAp63 isoform or alone, was observed in tumours more likely to develop lymph-node metastases. TAp63 in normal tissue favours epithelial differentiation and inhibits cell proliferation. Loss of TAp63 expression was related to tumour progression in laryngeal and bladder carcinomas [9, 15], and, in the present series, TAp63 appeared in cases with better survival (Table 4). In OSCC, Δ4TAp63 could bind to the same sites as the whole-length isoform TAp63, inhibiting its tumour suppressor role.

In conclusion, impaired p63 expression could be important in neoplastic transformation of the squamous cell, favouring neoplastic proliferation and early metastases. Specifically, the appearance of the truncated variant ΔNp73L is significantly associated with the development of lymph-node metastases.

Acknowledgements Prof. Vincenzo Eusebi is acknowledged for having critically reviewed the paper. Mrs. Luciana Muzzi is acknowledged for technical help and Mrs. Anne Collins for editing the manuscript. The paper was financed with grants from the University of Bologna.

References

1. Association of Directors of Anatomic and Surgical Pathology (2000) Recommendations for reporting of specimens containing oral cavity and oropharynx. Virchows Arch 437:345–347
2. Augustin M, Bamberger C, Paul D, Schmale H (1998) Cloning and chromosomal mapping of the human p53-related KET gene to chromosome 3q27 and its murine homolog Ket to mouse chromosome. Mamm Genom 9:899–902
3. Chilosi M, Zamò A, Brighenti A, Malpelli G, Montagna L, Piccoli P, Pedron S, Lestani M, Inghirami G, Scarpa A, Doglioni M, Menestrina F (2003) Constitutive expression of ΔN-p63α isoform in human thymus and thymic epithelial tumours. Virchows Archiv 443:175–183
4. Choi HR, Batsakis JG, Zhan F, Sturgis E, Luna MA, EP-Naggar AK (2002) Differential expression of p53 gene family members p63 and p73 in head and neck squamous tumorigenesis. Hum Pathol 33:158–164
5. DiComo C, Marshall JU, Babayan I, Drobnyak M, Hedvat CV, Teruya-Feldstein J, Pohar K, Hoos A, Cordon-Cardo C (2002) p63 expression profiles in human normal and tumor tissues. Clin Cancer Res 8:494–501
6. Flores ER, Tsal KY, Crowely D, Sengupta S, Yang A, McKeon F, Jacks T (2002) p63 and p73 are required for p53-dependent apoptosis in response to DNA damage. Nature 416:560–564

7. Nylander K, Coates P, Hall PA (2000) Characterization of the malignant expression pattern of p63α and ΔNp63α in benign and malignant oral epithelial lesions. Int J Cancer 87:368–372
8. Pelosi G, Pasini F, Olsen Stenholm C, Pastorino U, Maisonneuve P, Sonzogni A, Maffini F, Pruneri G, Fraggetta F, Cavallon A, Roz E, Iannucci A, Bresaola E, Viale G (2002) p63 immunoreactivity in lung cancer: yet another player in the development of squamous cell carcinoma? J Pathol 198:100–109
9. Pruneri G, Pignataro L, Manzotti M, Carboni N, Ronchetti D, Neri A, Cesana BM, Viale G (2002) P63 in laryngeal squamous cell carcinoma: evidence for a role of TA-p63 down regulation in tumorigenesis and lack of prognostic implication for p63 immunoreactivity. Lab Invest 82:1327–1334
10. Reis-Filho JS, Simpson PT, Martins A, Preto An Gartner F, Schmitt F (2003) Distribution of p63, cytokeratins 5/6 and cytokeratin 14 in 51 normal and 400 neoplastic human tissue samples using TARP-4 multi-tumor tissue microarray. Virchows Archiv 443:122–132
11. Schmale H, Bamberger C (1997) A novel protein with strong homology to the tumor suppressor p53. Oncogene 15:1363–1367
12. Senoo M, Seki N, Ohira M, Suyano S, Watanabe M, Inuzuka S, Okamoto T, TachibanaM, Tanaka T, Shinkay T, Kato H (1998) A second p53-related protein, p73L, with high homology to p73. Biochem Biophys Res Comun 248:603–607
13. Senoo M, Tsuchiya I, Matsumara Y, Mori T, Saito Y, Kato H, Okamoto T, Habu S (2001) Transcriptional dysregulation of the p73L/p63/p51/p40/KET gene in human squamous cell carcinomas: expression of ΔNp73L, a novel dominant-negative isoform, and loss of expression of the potential tumor suppressor p51. Br J Cancer 84:1235–1241
14. Shimada A, Kato S, Enjo K, Osada M, Ikawa Y, Kohno K, Obinata M, Kanamaru R, Ikawa S, Ishioka C (1999) The transcriptional activities of p53 and its homologue p51/p63: similarities and differences. Canc Res 59:2781–2786
15. Urist MJ, DiComo CJ, Lu ML, Charytonowicz E, Verbel D, Crum CP, Ince TA, McKeon FD, Cordon-Cardo C (2002) Loss of p63 expression in association with tumor progression in bladder cancer. Am J Pathol 161:1199–1206
16. Wang BY, Gil J, Kaufman D, Gan L, Khots DS, Burstain DE (2002) p63 in pulmonary epithelium, pulmonary squamous neoplasm, and other pulmonary tumors. Hum Pathol 33:921–926
17. Wu M, Wang B, Gil J, Sabo E, Miller l, Gan L, Burtein DE (2003). P63 and TTF-1 immunostaining. A useful marker panel for distinguishing small cell carcinoma of the lung from poorly differentiated squamous cell carcinoma of the lung. Am J Clin Pathol 119:696–702
18. Yang A, McKeon F (2000) p63 and p73: p53 mimics, menaces and more. Nat Rev Mol Cell Biol 1:199–207
19. Yang A, Kaghad M, Wang Y, Gillett E, Fleming MD, Dotsch V, Andrews NC, Caput D, McKeon F (1998) p63, a p53 homolog at 3q27–29, encodes multiple products with transactivating, death-inducing, and dominant-negative activities. Mol Cell 2:305–316

Virchows Arch (2004) 444:340–344
DOI 10.1007/s00428-004-0976-6

ORIGINAL ARTICLE

Gary L. Bratthauer · Fattaneh A. Tavassoli

Assessment of lesions coexisting with various grades of ductal intraepithelial neoplasia of the breast

Received: 23 April 2003 / Accepted: 27 December 2003 / Published online: 19 February 2004

Abstract Ductal intraepithelial neoplasia (DIN) is descriptive of in situ breast lesions from usual ductal hyperplasia (UDH) to advanced ductal carcinoma in situ (DCIS). A total of 2628 cases of DIN diagnosed at the Armed Forces Institute of Pathology were separated based on their grade. These were assessed for the presence of invasive carcinoma (ductal or lobular) and lobular intraepithelial neoplasia (LIN) grades 1–3. The frequency of invasive cancer (ductal and lobular) appearing with DIN increased with increasing DIN grade from 2% in low-risk DIN (UDH) to 37% in DIN 2–3 (DCIS grades 2–3). The frequency of these invasive carcinomas, which were either lobular or displayed lobular features, however, decreased with increasing grade of DIN with a peak of 28% in DIN 1-flat type, (flat epithelial atypia) to a low of 2% in DIN 3. Likewise, the frequency of LIN appearing with DIN decreased as the grade of DIN increased, with a peak of 26% in DIN 1-flat type to a low of 9% in DIN 3. Lower-grade LIN 1 comprised 14% of the LIN in low-risk DIN cases, but only 4% of the LIN seen in DIN 3 cases. Conversely, higher-grade LIN 3 comprised only 6% of the LIN seen in low-risk DIN cases, while accounting for 15% of the LIN in DIN 3 cases. The frequency of invasive carcinoma in DIN 1 ranged from 4% in quantitatively limited DIN 1 less than or equal to 2 mm (atypical ductal hyperplasia) to 27% among the more abundant DIN 1 greater than 2 mm (DCIS grade 1). The frequency of LIN associated with DIN 1 less than or equal to 2 mm was 13.4%, and the frequency of LIN associated with DIN 1 greater than 2 mm was 16.6% when there was no DIN 1-flat type present. However, the frequency of the LIN seen in combination with DIN 1-flat type was reduced by 50% as the quantity of DIN exceeded 2 mm. Based on this retrospective analysis of DIN, we noted that: (1) invasive carcinoma is most frequently associated with the higher grades of DIN; (2) the grade of LIN parallels the grade of coexisting DIN; (3) a relationship exists between DIN 1-flat type and the occurrence of LIN and (4) this relationship in association with DIN less than or equal to 2 mm is not maintained in DIN greater than 2 mm.

Keywords Breast · Ductal intraepithelial neoplasia · Flat epithelial atypia · Ductal carcinoma in situ · Lobular intraepithelial neoplasia · Atypical ductal hyperplasia · Invasive ductal carcinoma · Invasive lobular carcinoma

Introduction

Ductal intraepithelial neoplasia (DIN) defines non-invasive breast epithelial proliferations ranging from usual ductal hyperplasias (UDH) to advanced ductal carcinoma in situ (DCIS) [9]. It is well known that the risk of subsequent invasive carcinomas is increased with progressive grade or severity of intraductal disease [5, 8].

In a previous study, we found a correlation between the grade of lobular intraepithelial neoplasia (LIN) and the severity of coexisting disease in pathology specimens [1]. This correlation matched, almost exactly, observations based on numerous follow-up studies [6, 7]. However, the type of invasive carcinoma observed varied with the grade of LIN. LIN grades 1–3 reflect the severity of lobular neoplastic disease. LIN 1 is defined as having increased numbers of lobular cells that do not distend the lobule nor occlude the lumen. LIN 2 refers to neoplastic cells that distend the lobule and/or migrate to the duct. LIN 3 refers to extensive disease where the distended

The opinions or assertions contained herein are the private views of the authors and are not to be construed as official or as reflecting the views of the Department of the Army or Department of Defense.

G. L. Bratthauer (✉) · F. A. Tavassoli
Department of Gynecologic and Breast Pathology,
Armed Forces Institute of Pathology,
Washington, DC 20306-6000, USA
e-mail: Bratthauer@afip.osd.mil
Tel.: +12-02-782-2567
Fax: +12-02-7823939

F. A. Tavassoli
Yale University School of Medicine,
Department of Pathology,
New Haven, CT 06520-8023, USA

Table 1 Relationship between traditional and ductal intraepithelial neoplasia (DIN) classification systems. *UDH* usual ductal hyperplasia, *ADH* atypical ductal hyperplasia, *DCIS* ductal carcinoma in situ

DIN	Traditional
Low-risk DIN	UDH
DIN 1-flat type	Flat epithelial atypia
DIN 1≤2 mm	ADH
DIN 1>2 mm	Grade-1 DCIS
DIN 2	Grade-2 DCIS
DIN 3	Grade-3 DCIS

lobules almost reach confluence and/or the cells become pleomorphic. Patients with LIN 1 from our study were more likely to have invasive ductal carcinoma, whereas those with LIN 3 were more likely to have invasive lobular carcinoma. A directly proportional relationship was also noted between the occurrence of low-grade ductal lesions and that of lower-grade LIN (LIN 1 and LIN 2) in these cases [1].

Having established the DIN classification system (Table 1), it was of interest to conduct a similar analysis of the numerous cases of DIN diagnosed at the Armed Forces Institute of Pathology (AFIP).

Materials and methods

Cases of breast biopsies or mastectomies with intraductal proliferative lesions (low-risk DIN through DIN 3) were obtained from the files of the AFIP. These grades of DIN corresponded to the traditional classification system as follows: usual ductal hyperplasia (UDH)=low-risk DIN, flat epithelial atypia=DIN 1-flat type, atypical ductal hyperplasia (ADH)=DIN 1 less than or equal to 2 mm, DCIS grade 1=DIN 1 greater than 2 mm, DCIS grade 2=DIN 2, DCIS grade 3=DIN 3. A total of 2628 patients diagnosed as having some DIN over a 2-year period at the AFIP comprised the study sample. These included cases of pure DIN and cases of invasive carcinoma containing DIN. Cases were separated according to DIN grade based on the highest grade of DIN present in each case. A DIN 2 case, for example, could contain DIN 1, but a DIN 1 case could not contain any DIN 2. The samples of various grades of DIN type were then assessed for the presence of invasive carcinoma (ductal or lobular) and LIN grades 1–3 (atypical lobular hyperplasia to lobular carcinoma in situ).

Results

The results are listed in Table 2, Table 3 and Table 4 and are graphically illustrated in Fig. 1, Fig. 2, Fig. 3 and Fig. 4. As expected, the frequency of invasive cancer increased as the grade of DIN increased, from 2% in low-risk DIN to 37% and 36% in DIN 2 and 3, respectively, with a plateau at the higher-grade levels (Table 2, Fig. 1). The frequency of LIN appearing simultaneously with DIN was 10% in association with low-risk DIN, reached a peak of 26% in cases of DIN 1-flat type and then decreased to 9% in association with DIN 3 (Table 2, Fig. 1). Given the high frequency of LIN seen along with DIN 1-flat type, all cases of LIN concurrent with the higher grades of DIN were corrected for the presence of DIN 1-flat type when it was also present in the higher-grade lesions. Therefore, the recorded frequency of LIN appearing simultaneously with DIN 2, for example, did not include the LIN appearing with DIN 2 when DIN 1-flat type was also present. While there were only 9 (10%) cases of LIN appearing along with DIN 1-flat type in the DIN 2 and DIN 3 cases combined, there were 31 (27%) such cases among the ADH and grade-1 DCIS forms of DIN 1. When corrected for the influence of DIN 1-flat type in grades DIN 1 (ADH and grade-1 DCIS) to DIN 3, the frequency of LIN decreased more dramatically (Table 2, Fig. 2).

Table 3 Grade of lobular intraepithelial neoplasia (LIN) concurrent with various grades of ductal intraepithelial neoplasia (DIN). *DCIS* ductal carcinoma in situ, *G1* grade 1, *G2* grade 2; *G3* grade 3, *UDH* usual ductal hyperplasia, *ADH* Atypical intraductal hyperplasia

Total LIN	LIN 1	LIN 2	LIN 3
Low-risk DIN (UDH) *n*=43	5 (12%)	36 (84%)	2 (5%)
DIN 1-flat type (Flat epithelial atypia) *n*=257	15 (6%)	219 (85%)	23 (9%)
DIN 1 (ADH/DCIS G1) *n*=116	8 (7%)	101 (87%)	7 (6%)
DIN 2 (DCIS G2) *n*=62	3 (5%)	54 (87%)	5 (8%)
DIN 3 (DCIS G3) *n*=26	1 (4%)	21 (81%)	4 (15%)

Table 2 Frequency of concurrent disease observed with various grades of ductal intraepithelial neoplasia (DIN). *DCIS* ductal carcinoma in situ, *G1* grade 1, *G2* grade 2, *G3* grade 3, *LIN* lobular intraepithelial neoplasia, *UDH* usual ductal hyperplasia, *ADH* atypical intraductal hyperplasia

Grade	Invasive carcinoma	Lobular carcinoma (% of invasive carcinoma)	LIN
Low-risk DIN (UDH) *n*=426	10 (2%)	1 (10%)	43 (10%)
DIN 1-flat type (Flat epithelial atypia) *n*=1000	68 (7%)	19 (28%)	257 (26%)
DIN 1 (ADH/DCIS G1) *n*=538	116 (22%)	11 (9%)	116 (22%) Without DIN 1-flat type=85 (16%)
DIN 2 (DCIS G2) *n*=383	142 (37%)	11 (8%)	62 (16%) Without DIN 1-flat type=57 (15%)
DIN 3 (DCIS G3) *n*=281	102 (36%)	2 (2%)	26 (9%) Without DIN 1-flat type=22 (8%)

Table 4 Frequency of concurrent disease observed with DIN 1 (ADH) and DIN 1 (DCIS grade 1). *DIN* ductal intraepithelial neoplasia, *ADH* atypical intraductal hyperplasia, *DCIS G1* ductal carcinoma in situ grade 1, *LIN* lobular intraepithelial neoplasia

	DIN 1 (ADH) *n*=134	DIN 1 (DCIS G1) *n*=404
Invasive carcinoma	5 (4%)	111 (27%)
LIN total	31 (23%)	85 (21%)
LIN without DIN 1-flat type	18 (13.4%)	67 (16.6%)
LIN with DIN 1-flat type	13 (10%)	18 (4%)
LIN with DIN 1-flat type (as % of total LIN)	42%	21%

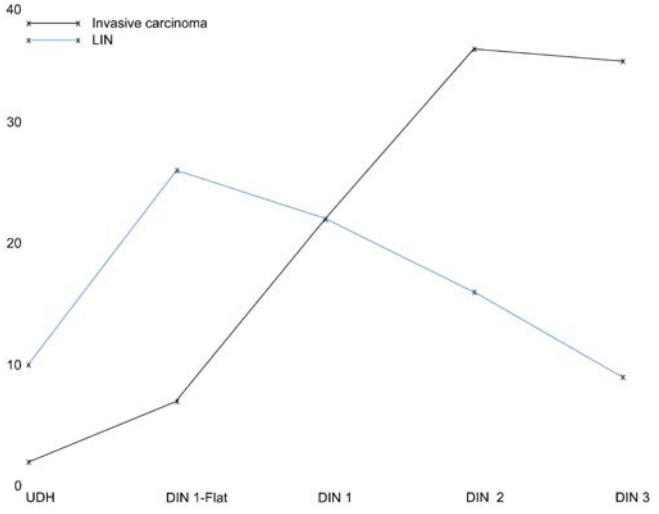

Fig. 1 Depiction of the relationship between lobular intraepithelial neoplasia (LIN) and invasive carcinoma in varying grades of ductal intraepithelial neoplasia (DIN). Note relationship between LIN and DIN 1-flat type

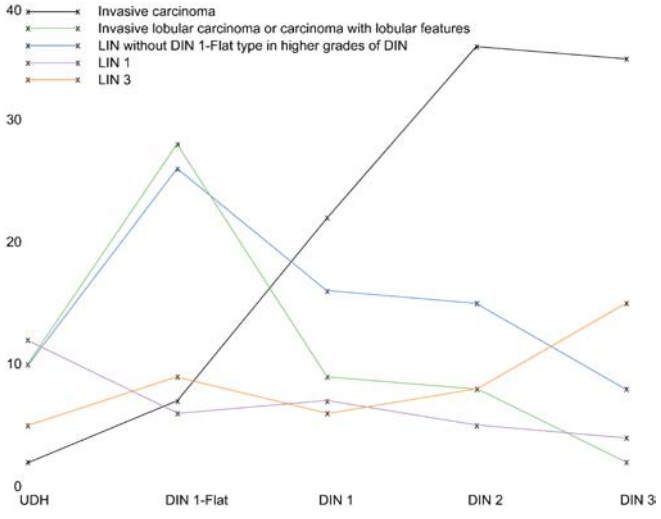

Fig. 3 Depiction of the frequency of lobular intraepithelial neoplasia (LIN), total invasive carcinoma, invasive lobular carcinoma, and different grades of LIN, in varying grades of ductal intraepithelial neoplasia (DIN)

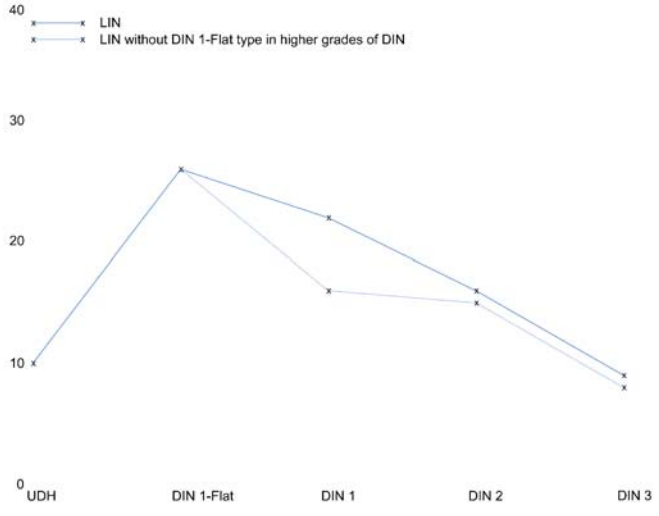

Fig. 2 Depiction of relationship between lobular intraepithelial neoplasia (LIN) and higher grades of ductal intraepithelial neoplasia (DIN), corrected for the presence of DIN 1-flat type in those grades

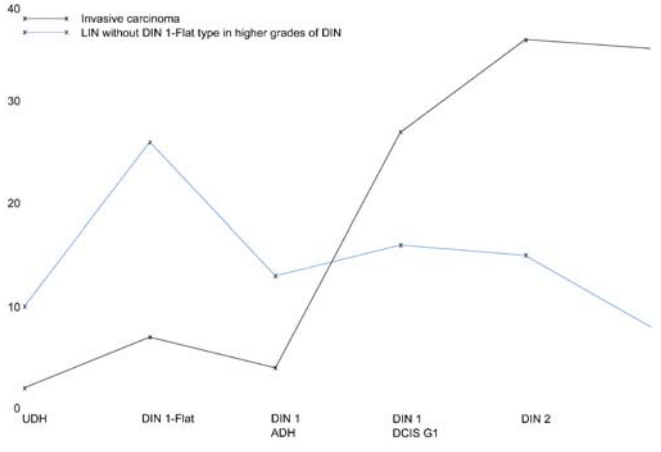

Fig. 4 Depiction of the relationship between lobular intraepithelial neoplasia (LIN) and invasive carcinoma in varying grades of ductal intraepithelial neoplasia (DIN), with DIN 1 cases quantitatively separated into atypical ductal hyperplasia or ductal carcinoma in situ

The grade of LIN also varied with the grade of DIN. The low-grade LIN 1 displayed a negative correlation with the grade of DIN, decreasing in frequency from 12% among low-risk DIN cases containing LIN to only 4% among the DIN 3 cases containing LIN (Table 3, Fig. 3). LIN 3 frequency, conversely, displayed a direct correlation with grade of DIN, increasing from 5% of the low-risk DIN cases containing LIN to 15% of the DIN 3 cases containing LIN. In addition, the fraction of associated

invasive carcinoma that was either lobular or had lobular features went from 10% in the low-risk DIN cases to a peak of 28% in the DIN 1-flat type cases to a low of 2% in the DIN 3 cases (Table 2, Fig. 3).

When the DIN 1 cases were subdivided into ADH or grade-1 DCIS, the frequency of associated invasive carcinoma ranged from 4% among ADH to 27% among grade-1 DCIS lesions (Table 4, Fig. 4). This finding strongly supports the impact of tumor-cell volume on the possibility of invasion. More invasive tumors were seen in cases containing more extensive intraductal disease, possibly because the opportunity for invasion to occur might depend, in part, on cell numbers. Interestingly, when the frequency of LIN was examined in ADH and grade-1 DCIS, there was only a slight difference. Concurrent LIN was observed among 13.4% of ADH and 16.6% of grade-1 DCIS cases. The frequency of DIN 1-flat type dropped from 42% among the ADH cases that contained LIN to 21% among the grade-1 DCIS cases that contained LIN (Table 4).

Discussion

The results observed concurred with and confirmed previously reported features of the various DIN lesions evaluated [8]. The frequencies of 37/36% and 2–7% invasive cancer associated with high- and low-grade ductal lesions, respectively, are consistent with that previously reported [4, 8]. Likewise, the correlation of grade of LIN with the grade of DIN was predictable from our previous study [1].

A recent study comparing the expression of cytokeratins and E-cadherin among non-invasive neoplasms identified a hybrid group distinct from those with clear-cut ductal or lobular immunoprofiles [2]. The presence of morphologically and immunohistochemically hybrid neoplasms raises the possibility of a close relationship between DIN and LIN in some of their earlier developmental stages. Against this background, it was of interest to examine the associated disease in various grades of DIN.

A distinct relationship between DIN 1-flat type and LIN emerged from this study (Fig. 5). The graphic depiction of the data clearly shows a peak for DIN 1-flat-type-associated LIN. Furthermore, among all sizes of DIN 1, 27% of those with LIN also harbored DIN 1-flat type. Removing any influence exerted by DIN 1-flat type from the LIN seen in grade-1 DCIS by discounting those cases containing DIN 1-flat type lowered the frequency of associated LIN in this group to a level similar to that seen in association with DIN 2 (16%). Since DIN 1-flat type was rarely or infrequently present among DIN 2 and DIN 3 cases, the frequency of LIN associated with these grades decreased by only one percentage point when those containing DIN 1-flat type were subtracted.

Among all ductal lesions, less than or equal to 10% are associated with invasive lobular carcinoma or invasive carcinoma with lobular features. Interestingly, of the 68 (7%) DIN 1-flat type cases associated with invasive carcinoma, 19 (28%) were lobular or possessed lobular features; a substantially higher frequency than 10%.

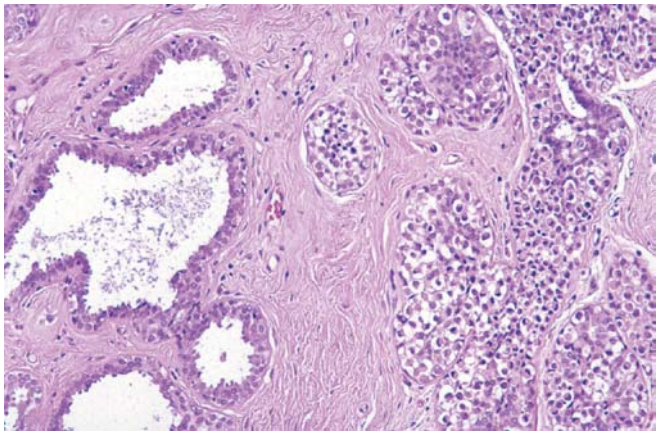

Fig. 5 Hematoxylin and eosin stained section showing lobular intraepithelial neoplasia and ductal intraepithelial neoplasia 1-flat type (×200)

Assessment of the DIN 1 lesions provided particularly interesting data. DIN 1 includes the traditional categories of ADH and grade-1 DCIS; their quantitatively based separation has encountered significant reproducibility problems (Fig. 6) [9]. In this study, the frequency of associated invasive carcinoma and LIN in cases of DIN 1 was in between that found in the higher grades (DIN 2 to 3) and that found in the combined low-risk DIN and DIN 1-flat type cases. However, when separated to reflect ADH and grade-1 DCIS by the traditional system, the DCIS had a seven times higher frequency of concurrent invasive carcinoma than the ADH (Table 4, Fig. 4). This finding underscores the impact of quantity and/or volume of neoplastic cells. What is interesting, however, is the relationship between the quantitatively different DIN 1 and LIN. The overall frequency of LIN observed in association with all DIN 1 changed by only 3% when DIN 1 was separated into ADH and DCIS (Table 4, Fig. 4). Among the low-risk DIN, DIN 1-flat type and DIN 1 less than or equal to 2 mm, the frequency of associated LIN was much higher than that of the concurrent invasive carcinoma, while among the DIN 1 greater than 2 mm, DIN 2 and DIN 3, the frequency of associated invasive carcinoma was much higher than that of concurrent LIN. The crossover point is, not surprisingly, in the middle of the range of DIN 1 (ADH to grade-1 DCIS) lesions (Fig. 4).

While LIN was present in association with 23% of all ADH and 21% of all grade-1 DCIS, 42% of those ADH cases containing LIN also harbored DIN 1-flat type, while DIN 1-flat type was present in only 21% of those LIN containing grade-1 DCIS cases. These findings suggest a relationship between LIN occurring with DIN 1-flat type and ADH that is lost as the DIN 1 less than or equal to 2 mm lesion progresses into a fully developed architecture

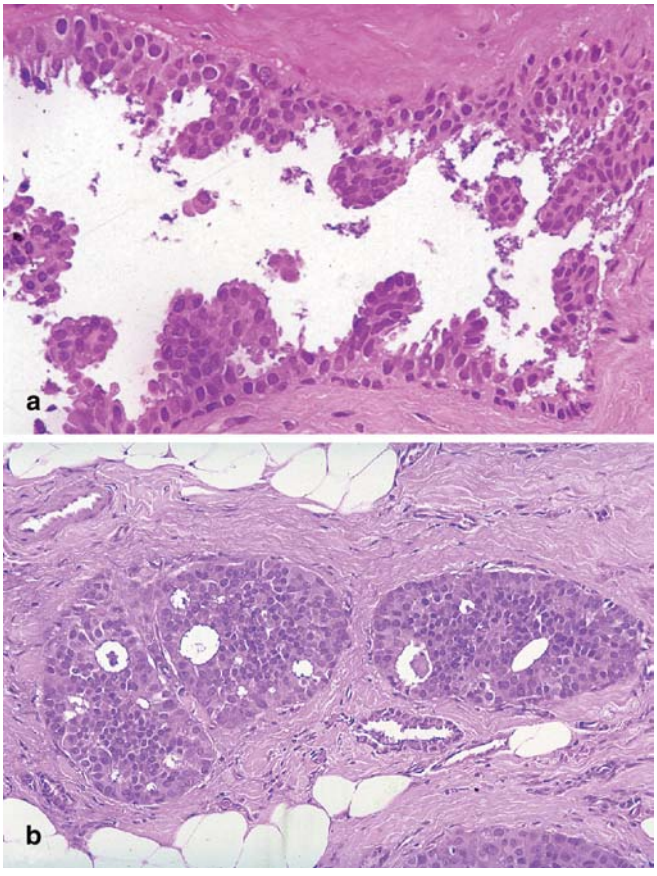

Fig. 6 a Hematoxylin and eosin-stained section showing minimal extent ductal intraepithelial neoplasia 1 (atypical ductal hyperplasia) (×400). **b** Hematoxylin and eosin-stained section showing greater extent ductal intraepithelial neoplasia 1 (ductal carcinoma in situ grade 1) (×200)

with increased quantity of neoplastic cells (grade-1 DCIS).

Of special interest is the substantial increase in the frequency of LIN in the presence of DIN 1-flat type. Also, of all of the various DIN grades, the highest frequency of concurrent invasive lobular carcinoma or invasive carcinomas having lobular features was noted among cases of DIN 1-flat type. Brogi et al. also noted an increased amount of "atypical cystic lobules" (basically comparable with DIN 1-flat type) in patients with lobular neoplasia [3]. These findings all suggest a relationship between LIN and DIN 1-flat type.

Perhaps, up to a certain point, the neoplastic cells retain the capacity to differentiate into either a lobular or ductal morphology. Beyond that point of commitment, one morphology predominates. It is possible that both LIN and DIN 1-flat type are close to the stem cell in their development with their ultimate characteristics still to be determined.

References

1. Bratthauer GL, Tavassoli FA (2002) Lobular intraepithelial neoplasia: previously unexplored aspects assessed in 775 cases and their clinical implications. Virchows Arch 440:134–138
2. Bratthauer GL, Moinfar F, Stamatakos M, Mezzetti TP, Shekitka KM, Man YG, Tavassoli FA (2002) Combined E-cadherin and high molecular weight cytokeratin immunoprofile differentiates lobular, ductal, and hybrid mammary intraepithelial neoplasms. Hum Pathol 33:620–627
3. Brogi E, Oyama T, Koerner FC (2001) Atypical cystic lobules in patients with lobular neoplasia. Int J Surg Pathol 9:201–206
4. Dupont WD, Page DL (1985) Risk factors for breast cancer in women with proliferative breast disease. N Engl J Med 312:146–151
5. Fitzgibbons PL, Page DL, Weaver D, Thor AD, Allred DC, Clark GM, Ruby SG, O'Malley F, Simpson JF, Connolly JL, Hayes DF, Edge SB, Lichter A, Schnitt SJ (2000) Prognostic factors in breast cancer. College of American Pathologists Consensus Statement 1999. Arch Pathol Lab Med 124:966–978
6. Page DL, Kidd TE Jr, Dupont WD, Simpson JF, Rogers LW (1991) Lobular neoplasia of the breast: higher risk for subsequent invasive cancer predicted by more extensive disease. Hum Pathol 22:1232–1239
7. Rosen PP, Kosloff C, Lieberman PH, Adair F, Braun DW Jr (1978) Lobular carcinoma in situ of the breast. Detailed analysis of 99 patients with average follow-up of 24 years. Am J Surg Pathol 2:225–251
8. Tavassoli FA (1999) Pathology of the breast, 2nd edn. Appleton and Lange, Norwalk, CT, pp 205–323
9. Tavassoli FA (2001) Ductal intraepithelial neoplasia of the breast. Virchows Arch 438:221–227

Virchows Arch (2004) 444:345–349
DOI 10.1007/s00428-003-0970-4

ORIGINAL ARTICLE

Mika Sakaki · Tony W. H. Shek · Mitsuyoshi Hirokawa · Kenji Kashima · Tsutomu Daa · Ayako Gamachi · Toshiaki Sano

Melanotic oncocytic metaplasia of the nasopharynx: a report of seven cases and review of the literature

Received: 16 September 2003 / Accepted: 17 December 2003 / Published online: 4 February 2004

Abstract We describe seven cases of melanotic oncocytic metaplasia of the nasopharynx and review five other cases in the literature. It is usually a small, brown to black lesion that occurs around the Eustachian tube opening, where abundant seromucinous glands and lymphoid tissue are present. Multiple or bilateral lesions are sometimes seen. All 12 reported cases are of Asian origin. Melanotic oncocytic metaplasia occurs predominantly in men (male:female=11:1), with a mean age of 68 years. Simple excisional biopsy appears to be curative. Microscopically, melanotic oncocytic metaplasia is a combination of oncocytic metaplasia of the epithelium of the gland and melanin pigmentation in its cytoplasm. Fontana-Masson staining and immunohistochemical staining of S-100 protein revealed numerous melanocytes with conspicuous dendrites in the glands and stroma, which probably transfer melanin to adjacent glands. The exact pathogenesis of melanotic oncocytic metaplasia is unknown, but we postulate that the lesion could be related to the oncocytic metaplasia of the seromucinous glands around the Eustachian tube, which is followed by the local production and/or acquisition of the melanin pigment, under the influence of certain neuropeptides in the vicinity. The recognition of melanotic oncocytic metaplasia is of clinical importance, as it may be misdiagnosed as a malignancy to the unwary.

M. Sakaki (✉) · M. Hirokawa · T. Sano
Department of Pathology,
University of Tokushima School of Medicine,
3-18-15 Kuramoto-cho, 770-8503 Tokushima, Japan
e-mail: smika@basic.med.tokushima-u.ac.jp
Tel.: +81-88-6337064
Fax: +81-88-6339423

T. W. H. Shek
Department of Pathology,
University of Hong Kong,
Queen Mary Hospital, Hong Kong

K. Kashima · T. Daa · A. Gamachi
Department of Pathology,
Oita Medical University,
Oita, Japan

Keywords Melanotic oncocytic metaplasia · Nasopharynx · Excisional biopsy

Introduction

Melanotic oncocytic metaplasia of the nasopharynx is a rare lesion, first described by Shek in 1995 [22]. Macroscopically, it is a small, black-pigmented lesion. Coexistence of melanin pigmentation and oncocytic metaplasia in the same gland characterizes the lesion. There have been only five cases reported thus far in the literature [10, 11, 22, 30]. We report seven additional new cases and review the literature with an attempt to elucidate its possible pathogenesis and histogenesis.

Materials and methods

Case selection

Five cases (cases 1–5) were previously reported in the literature, and seven additional new cases (cases 6–12) were retrieved from the files of the Department of Pathology, University of Tokushima School of Medicine, Tokushima, Department of Pathology, University of Hong Kong, Queen Mary Hospital, Hong Kong, and Department of Pathology, Oita Medical University, Oita. Clinical data were obtained from hospital records for the seven cases (Table 1). Hematoxylin–eosin-stained slides from biopsied material were available for the seven cases.

Special staining and immunohistochemical staining

Sections from paraffin blocks of the lesion were used. No sections except hematoxylin–eosin-stained slides were available for cases 10–12. Fontana-Masson staining, Berlin blue staining and immunohistochemical studies for S-100 protein (Dako, Glostrup, Denmark, dilution; 1:500) and HMB 45 (clone, HMB45; Dako, dilution: 1:50) were performed only for cases 6, 7 and 9. For immunohistochemical studies, the sections were bleached prior to standard labeled streptavidin-biotin method with appropriate use of positive and negative controls. Proteolytic predigestion was performed.

Table 1 Clinical findings of five cases in the literature (cases 1–5) and present seven cases (cases 6–12) of melanotic oncocytic metaplasia. *Eustachian O* Eustachian tube opening

Case	Author (year)	Age (years)/sex	Site	Number	Clinical impression	Associated condition	Smoking history
1	Shek et al. (1995) [22]	67/Male	Eustachian O	1	Carcinoma	Otitis media	Unknown
2	Shek et al. (1995) [22]	63/Male	Eustachian O	1	Carcinoma	Tinnitus	Unknown
3	Kurihara & Nakagawa (1997) [11]	69/Male	Left nasopharynx	3	(Incidental)	–	Unknown
4	Hirakawa et al. (1999) [10]	64/Male	Bilateral Eustachian O/ nasopharynx	Multiple	Malignant tumor	Discomfort of the throat	Unknown
5	Xue & Hui (1999) [30]	70/Male	Bilateral Eustachian O	Multiple	Nevus	Tinnitus	Unknown
6	Present case	80/Male	Right nasal cavity/ pharynx	Multiple	Melanoma	Hoarseness, old Tb	10 per day × 50 years
7	Present case	69/Male	Left Eustachian O	1	Melanoma	Rhinorrhea, old Tb	40 per day × 60 years
8	Present case	74/Male	Left suprapharynx	1	Tumor	Epistaxis	Unknown
9	Present case	74/Female	Right Eustachian O	3	Melanoma	Discomfort of the throat	Unknown
10	Present case	68/Male	Nasopharynx	1	Tumor	Increased EBV-IgA titer	Unknown
11	Present case	56/Male	Right Eustachian O	1	Unknown	Hemoptysis	Unknown
12	Present case	63/Male	Left Eustachian O	1	Melanoma	Epistaxis	Unknown

Results

Clinical findings

Clinical findings of 12 cases were summarized in Table 1. The patients were all of Asian origin, and they were comprised of 11 men and only 1 woman, aged 56–80 years (mean, 68 years). All the lesions were a few millimeters in size, brown to black in color and located in the nasopharynx mucosa. They were found near the Eustachian tube opening in 8 of 12 cases. They occurred in the left in 4 cases, in the right in 3 cases and bilaterally in 2 cases. Multiple lesions were seen in 5 cases. Clinicians' impression of the lesion ranged from a malignant tumor, such as melanoma or carcinoma, to a benign melanocytic nevus. Other associated ear, nose and throat symptoms included otitis media, tinnitus, hoarseness of voice, rhinorrhea, epistaxis, discomfort of the throat and hemoptysis. Cases 7 and 8 had the past history of pulmonary tuberculosis. Case 3 had systemic hypertension and was on angiotensin-converting enzyme inhibitor, but the lesion was otherwise asymptomatic. The information about the smoking history was available only for cases 6 and 7: 10 cigarettes per day for 50 years and 40 cigarettes per day for 60 years, respectively. Smoking history for the other patients was unknown. There has been no recurrence or progression of the lesion reported on all these seven cases after biopsy.

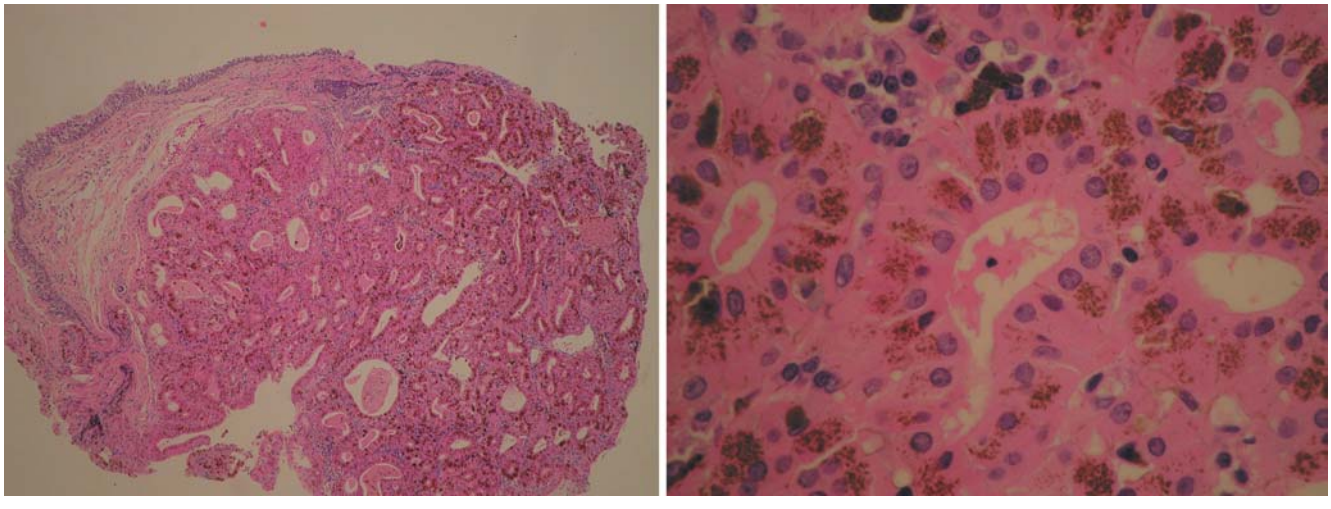

Fig. 1 Beneath overlying respiratory epithelium, a cluster of glands are present (*left*; hematoxylin–eosin, ×15). The epithelium of the glands shows oncocytic metaplasia with melanin pigmentation in its cytoplasm (*right*; hematoxylin–eosin, ×100)

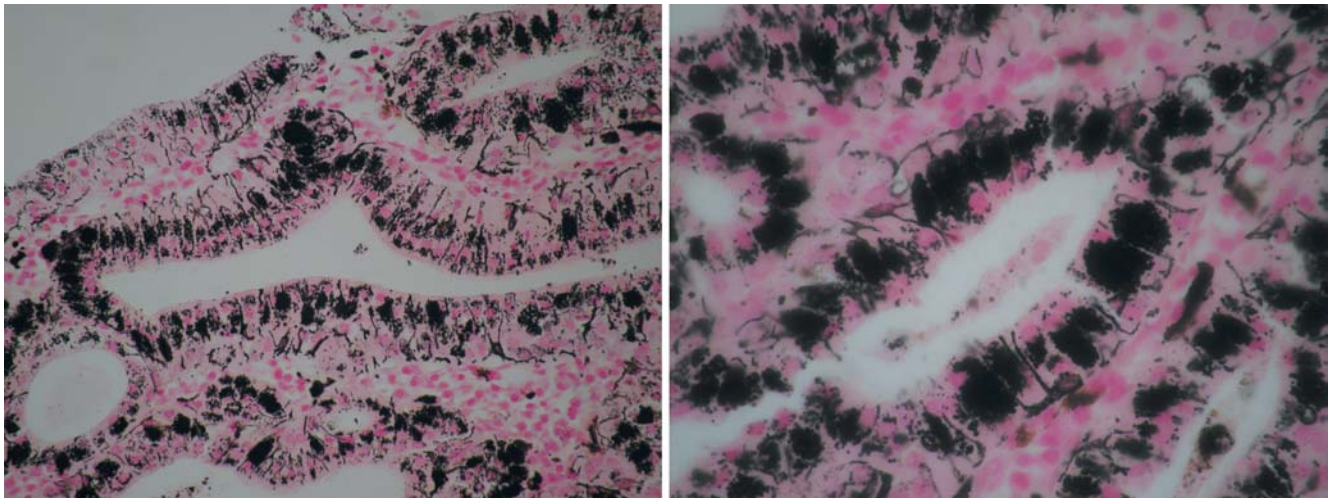

Fig. 2 Fontana-Masson staining reveals numerous melanocytes. Many of them stretch their dendritic processes between the epithelial cells of the glands. (×100, ×200)

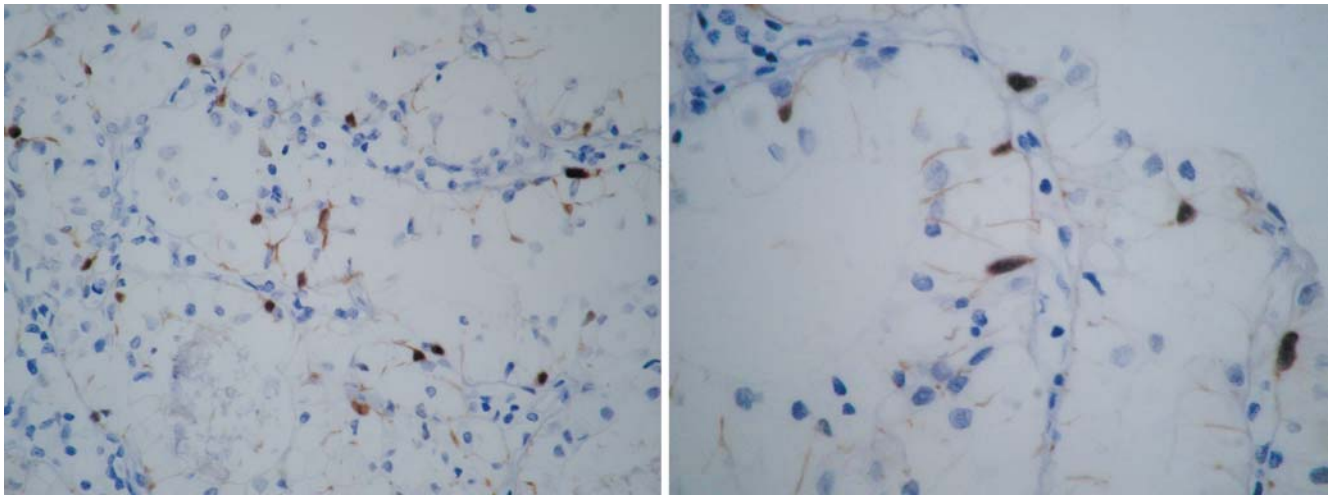

Fig. 3 The location of cells immunoreactive for S-100 protein in the glands corresponds to the one seen in Fontana-Masson staining. (×100, ×200)

Histological findings

Histology of the present seven cases (cases 6–12) was similar. The lesions were well circumscribed, but not encapsulated. Under the overlying respiratory epithelium, which was not present in some cases, there were clusters of seromucinous glands with oncocytic metaplasia and brown pigment in their cytoplasm (Fig. 1). Some glands were dilated and sometimes contained condensed protenacious fluid or melanin granules in the lumina. Pigmentation was also present in the overlying epithelium with or without oncocytic metaplasia. Metaplastic change accompanied the decreased number or absence of mucous cells in the epithelium. No atypia was seen in the epithelial cells of the gland and overlying epithelium. There was scanty amount of stroma between the oncocytic glands, where lymphocytes, plasma cells and some pigmented macrophages were seen. The brown granules stained positive for Fontana-Masson staining and negative for Berlin blue staining, which were indicative of melanin. In Fontana-Masson staining, there were numerous melanocytes with their dendritic processes stretching between the epithelial cells of the glands and abundant melanin granules near them (Fig. 2). Melanocytes were also identified in the surface epithelium and stroma.

Immunohistochemical stainings of HMB 45 and S-100 protein were performed for cases 6, 7 and 9. Dendritic cells were positive for S-100 protein (Fig. 3) and negative for HMB45 in all three cases.

Discussion

The clinical findings on our seven cases and five others in the literature are summarized in Table 1. Melanotic oncocytic metaplasia occurred predominantly in men (1 woman: 11 men) with a mean age of 68 years, and all the patients were Asians. The lesion was usually a few millimeters in size with a slightly elevated surface, and is brown to black in color. Multiple lesions occurred in 5 of 12 (42%) cases and bilateral involvement was sometimes encountered (17%). Most occurred in close vicinity of the Eustachian tube opening (in 8 of 12 cases; 67%). The associated symptoms of tinnitus and otitis media may be caused by compression to the tube [22]. The clinical impression on endoscopic examination is not uncommonly that of a malignant tumor, such as melanoma or nasopharyngeal carcinoma. All the seven present cases pursued a benign clinical course, and no additional treatment is required.

The exact pathogenesis of melanotic oncocytic metaplasia is unknown. Drawing the analogy of the relationship between oral melanin pigmentation and smoking in some races [9, 21, 27], we hypothesize that smoking may be a predisposing factor for melanotic oncocytic metaplasia. The observed male predominance is in keeping with the hypothesis, as there are more male smokers than female smokers among Asians. However, a positive smoking history was only attainable in two patients (cases 6 and 7; Table 1), but was unknown in the other patients. Ethnic background of Asian could be another predisposing factor.

Microscopically, melanotic oncocytic metaplasia is unique in that both oncocytic metaplasia and melanin pigmentation of the epithelium are present simultaneously. Dendritic melanocyte has been reported to exist in the stroma and epithelium of the nasal cavity, paranasal sinus and larynx [7, 25]. In this study, melanocytes were identified in the nasopharynx. Fontana-Masson staining revealed numerous dendritic melanocytes among the epithelial cells of the glands and overlying epithelium and in the stroma in cases 6 and 9 of the present series, and such a finding has been reported in cases 3 and 4 of the previous study [10, 11]. It seems reasonable to postulate that these melanocytes originate in the nasopharynx, since melanocytes are the cells that derived from primordial neural crest and migrate to various sites [1], and that they probably proliferate under the influence of certain trophic substances [22]. The melanin pigment in the oncocytic glands and stroma may be derived from the adjacent melanocytes through their dendrites [10], which is consistent with the observation that ultrastructurally oncocytic cells contained numerous hypertrophied mitochondria, but not premature melanosomes, where melanin is produced [10].

Oncocytic metaplasia of the glandular and ductal epithelium alone is not an uncommon finding, and, in fact, it is considered an age-related phenomenon when seen in the nasopharynx [3, 16], as well as in the salivary gland and larynx [6, 12, 13]. Because it is a more common finding [3, 16] than melanin pigmentation in the nasopharynx, oncocytic metaplasia of the gland probably precedes the melanin pigmentation. The proliferative character of the oncocytes is frequently present in organs with endocrine function or endocrine dependence [8]. In the pharynx and salivary gland, the presence of neuroendocrine peptides has been reported in some species and in humans [2, 4, 14, 17–20, 24, 29, 31]. In addition, it has been shown that some neuropeptidergic nerve fibers located in the tonsil or lymphoid tissue near the tonsil play a regulatory role in the neuro–immuno–endocrine network [5, 23, 26, 28]. Similar lymphoid follicles are also present in the submucosa throughout the nasopharynx, particularly around the Eustachian tube opening, which is sometimes called Gerlach's tonsil [15]. Such neuropeptides might cause the oncocytic metaplasia or melanocyte to proliferate and produce melanin directly or indirectly through the secretion of the oncocytic glands.

In summary, we have described the clinical and histological features of melanotic oncocytic metaplasia. Awareness of melanotic oncocytic metaplasia is of clinical importance, as it may be misdiagnosed as carcinoma or melanoma [10, 22, 30]. Also, because of its histological uniqueness, it is of academic interest and importance to clarify the pathogenesis and histogenesis in further detail.

References

1. Ackermann AB, Chongchitnant N, Sanchez J, Guo Y, Bennin B, Reichel M, Randall MB (1997) Embryonic, histologic, and anatomic aspect. In: Stamathis G (ed) Histologic diagnosis of inflammatory skin disease. Williams & Wilkins, Baltimore, pp 18–21
2. Barka T (1980) Biologically active polypeptides in submandibular glands. J Histochem Cytochem 28:836–859
3. Benke TT, Zitsch RP 3rd, Nashelsky MB (1995) Bilateral oncocytic cysts of thenasopharynx. Otolaryngol Head Neck Surg 112:321–324
4. Bing J, Poulsen K, Hackenthal E, Rix E, Taugner R (1980) Renin in the submaxillary gland: a review. J Histochem Cytochem 28:874–880
5. Bracci-Laudiero L, Aloe L, Stenfors C, Tirassa P, Theodorsson E, Lundberg T (1996) Nerve growth factor stimulates production of neuropeptide Y in human lymphocytes. Neuroreport 7:485–488
6. Gallagher JC, Puzon BQ (1969) Oncocytic lesions of the larynx. Ann Otol Rhinol Laryngol 78:307–318
7. Goldman JL, Lawson W, Zak FG, Roffman JD (1972) The presence of melanocytesin the human larynx. Laryngoscope 82:824–835
8. Hamperl H (1962) Oncocyten und Oncocytome. Virchows Arch 335:452–483
9. Hedin CA, Axell T (1991) Oral melanin pigmentation in 467 Thai and Malaysian people with special emphasis on smoker's melanosis. J Oral Pathol Med 20:8–12
10. Hirakawa E, Miki H, Ohmori M, Kobayashi S, Haba R, Nagai Y (1999) Melanin pigmented oncocytic metaplasia of the nasopharynx. Virchows Arch 434:455–457
11. Kurihara K, Nakagawa K (1997) Pigmented variant of benign oncocytic lesion of the pharynx. Pathol Int 47:315–317
12. Lundgren J, Olofsson J, Hellquist H (1982) Oncocytic lesions of the larynx. Acta Otolaryngol 94:335–344

13. Martinez-Madrigal F, Bosq J, Casiraghi O (1997) Major salivary gland. In: Sternberg SS (ed) Histology for pathologists. Lippincott-Raven, Philadelphia, pp 17–420
14. Mathison R, Davison JS, Befus AD (1994) Neuroendocrine regulation of inflammation and tissue repair by submandibular gland factors. Immunol Today 15:527–532
15. Mills SE, Fechner RE (1997) Larynx and pharynx. In: Sternberg SS (ed) Histology for pathologists. Lippincott-Raven, Philadelphia, pp 391–403
16. Morin GV, Shank EC, Burgess LP, Heffner DK (1991) Oncocytic metaplasia of the pharynx. Otolaryngol Head Neck Surg 105:86–91
17. Murphy RA, Watson AY, Metz J, Forssmann WG (1980) The mouse submandibular gland: an exocrine organ for growth factors. J Histochem Cytochem 28:890–902
18. Pikula DL, Harris EF, Desiderio DM, Fridland GH, Lovelace JL (1992) Methionine enkephalin-like, substance P-like, and beta-endorphin-like immunoreactivity in human parotid saliva. Arch Oral Biol 37:705–709
19. Salata RA, Verbalis JG, Robinson AG (1987) Cold water stimulation of oropharyngeal receptors in man inhibits release of vasopressin. J Clin Endocrinol Metab 65:561–567
20. Salo A, Ylikoski J, Uusitalo H (1993) Distribution of calcitonin gene-related peptide immunoreactive nerve fibers in the human submandibular gland. Neurosci Lett 150:137–140
21. Salonen L, Axell T, Hellden L (1990) Occurrence of oral mucosal lesions, the influence of tobacco habits and an estimate of treatment time in an adult Swedish population. J Oral Pathol Med 19:170–176
22. Shek TW, Luk IS, Nicholls JM, Fok KO (1995) Melanotic oncocytic metaplasia of the nasopharynx. Histopathology 26:273–275
23. Tang SC, Fend F, Muller L, Braunsteiner H, Wiedermann CJ (1993) High-affinity substance P binding sites of neurokinin-1 receptor type autoradiographically associated with vascular sinuses and high endothelial venules of human lymphoid tissues. Lab Invest 69:86–93
24. Uddman R, Ekberg O, Malmberg L, Borgstrom P, Fernstrom G, Ekstrom J, Sundler (1990) Neuropeptide-containing nerve fibers in the pharynx of the rabbit. Dysphagia 4:220–226
25. Uehara T, Matsubara O, Kasuga T (1987) Melanocytes in the nasal cavity and paranasal sinus. Incidence and distribution in Japan. Acta Pathol Jpn 37:1105–1114
26. Ueyama T, Kozuki K, Houtani T, Ikeda M, Kitajiri M, Yamashita T, Kumazawa T, Nagatsu I, Sugimoto T (1990) Immunolocalization of tyrosine hydroxylase and vasoactive intestinal polypeptide in nerve fibers innervating human palatine tonsil and paratonsillar glands. Neurosci Lett 116:70–74
27. Unsal E, Paksoy C, Soykan E, Elhan AH, Sahin M (2001) Oral melanin pigmentation related to smoking in a Turkish population. Community Dent Oral Epidemiol 29:272–277
28. Weihe E, Krekel J (1991) The neuroimmune connection in human tonsils. Brain Behav Immun 5:41–54
29. Whitley BD, Ferguson JW, Harris AJ, Kardos TB (1992) Immunohistochemical localisation of substance P in human parotid gland. Int J Oral Maxillofac Surg 21:54–58
30. Xue WC, Hui YZ (1999) Melanotic oncocytic metaplasia of the nasopharynx. Histopathology 35:481–482
31. Yoshida Y, Tanaka Y, Hirano M, Nakashima T (2000) Sensory innervation of the pharynx and larynx. Am J Med 108[Suppl 4a]:51S–61S

Virchows Arch (2004) 444:350–355
DOI 10.1007/s00428-003-0962-4

ORIGINAL ARTICLE

Mauro Papotti · Andrea D. Manazza · Roberto Chiarle · Gianni Bussolati

Confocal microscope analysis and tridimensional reconstruction of papillary thyroid carcinoma nuclei

Received: 9 October 2003 / Accepted: 2 December 2003 / Published online: 31 January 2004

Abstract Nuclei of papillary thyroid carcinoma (PTC) are characterised by diagnostic morphological features, which include optically clear nuclei, irregular nuclear profile, pseudoinclusions and grooves. In the present study, such nuclear features were analysed by means of confocal microscopy using anti-lamin B antibodies to outline the nuclear membrane. Parallel sections of the nucleus, produced by confocal microscope analysis, showed that the nuclear shape is markedly irregular with profound invaginations, clefts and tunnel-like structures, which correspond to the "grooves" and "holes" detectable using light microscopy, respectively. A tridimensional (3-D) model of the nuclei, obtained by a computer-based reconstruction of confocal microscope images, showed, in the vast majority of PTC cells, nuclei with crateriform areas, clefts and even tunnel-like structures "piercing" the whole nuclear thickness. By rotating these models in space, it became evident that the holes and grooves seen in light microscopy correspond to invaginations and tunnels, depending on the viewpoint. In conclusion, this is the first application of confocal microscopy and tridimensional reconstruction to the study of nuclear morphology of PTC and of tumours in general. The light microscopic appearance of PTC nuclei, so familiar to pathologists, is, therefore, due to profound remodelling of the nuclear shape with invaginations and tunnels, which appear as either grooves or holes, according to the viewpoint.

Keywords Thyroid papillary carcinoma · Confocal microscope · Tridimensional image · Clear nuclei · Lamin B

M. Papotti · R. Chiarle · G. Bussolati (✉)
Department of Biomedical Sciences and Oncology,
University of Turin, Via Santena 7, 10126 Torino, Italy
e-mail: gianni.bussolati@unito.it
Tel.: +39-01-16706505
Fax: +39-01-16635267

A. D. Manazza · R. Chiarle
Center for Experimental Research and Medical Studies (CERMS),
Turin, Italy

Introduction

Papillary thyroid carcinoma (PTC) is characterised by peculiar diagnostic nuclear alterations, which include nuclear clearing due to fine heterochromatin, nuclear grooves, cytoplasmic inclusions and irregular contours [6, 8]. These features are different from those of normal follicular cells and follicular neoplasms, which usually show rigidly spherical nuclei with "smooth" contours. Ret protooncogene rearrangements have been shown to be implicated in the typical nuclear changes of PTC [2].

In diagnostic pathology, the recognition of a PTC is usually an easy task, thanks to the above-described classical nuclear features. This is not always the case in cytological specimens, since material from fine needle aspiration biopsies may contain few cells, and the nuclear features may be easily missed. In addition, some follicular nodules of hyperplastic nature (possibly associated to hyperfunction) may show extensive nuclear clearing, raising the suspicion of a follicular variant of PTC in both surgical and cytological material. Several questions remain to be answered: (1) How specific and ubiquitous are the nuclear changes of PTC? If they are not detected in all cases and in all cells, is this due to their absence or to the technical approach (light microscopy and hematoxylin & eosin staining), which allows detection of the top of an iceberg only? (2) Are nuclear grooves, vacuoles and indentations separate phenomena, or just different aspects of the same alteration?

In order to approach these problems, we planned to use confocal microscopy and a marker for nuclear membranes. Several proteins of the nuclear envelope have been studied using light and confocal microscopy. Recently, a thorough biochemical characterisation of the nuclear membrane components has been reported [3]. In this study, emerin, lamins and other proteins were found to be regularly expressed, even in the nuclear envelopes of PTC cells, thus, indicating that neither downregulation nor abnormal expression of any of these proteins was a common occurrence in PTC, nor were these proteins responsible for any of the changes of PTC nuclei. Among

these proteins, lamin B was found to be intensely expressed by the nuclear membrane, including its infoldings (grooves or "holes") [3]. Experimental studies showed that this protein is also essential for cell replication [7].

The aim of this study was to investigate the nuclear shape and deformities of PTC cells and to identify some peculiar features, which may define PTC nuclei and distinguish them from other conditions associated with nuclear clearing. For this purpose, nuclear membranes of PTC (from cell lines, fine needle aspirates and surgical specimens) and of control follicular tumours were marked with lamin B antibodies and analysed by confocal microscopy. Such images were sequentially arranged to build up a tridimensional (3-D) model, which could be turned and switched along different perspectives, mimicking those occurring in light microscopic examination. Here we show that remarkable nuclear deformities, infolding and "holes" are present only in PTC nuclei, as expected, and that the reported alterations described as "grooves" or "holes" probably represent the same phenomenon of profound nuclear invaginations, according to the viewpoint from which the cell is explored, while the pattern known as "inclusions" appear related to a tunnel-like arrangement of the nuclear shape.

Materials and methods

Tissues and cells

Three cases each of PTC, follicular carcinoma and adenoma were collected from the surgical pathology files of the Department of Biomedical Sciences and Oncology in the year 2003. Two cases of PTC in horses from Eastern Europe were also investigated. A representative block of each case was selected. The tissues were fixed in formalin and embedded in paraffin. In addition, the corresponding fine needle aspiration biopsies of the three papillary carcinomas were studied using the cell block prepared at the time of cytological sampling. Furthermore, in one case of PTC from a 24-year-old man, isolated cells were obtained from either the tumour area or the surrounding normal tissue by fine needle aspiration biopsy. Such cells were collected in fluid and processed according to the Thin-Prep procedure. Two immortalised cell lines derived from human thyroid tumours of follicular origin, i.e. NPA cells originated from a papillary carcinoma and WRO cells from a follicular carcinoma, were generously supplied by Drs. A. Fusco and M. Santoro (University of Naples). Both cell lines were grown directly onto a glass slide in Dulbecco's modified Eagle's medium-F12 medium, supplemented with foetal calf serum 10% and penicillin/streptomycin in a 5% CO_2 humidified atmosphere at 37°C. They were subsequently fixed in methanol and acetone.

Immunofluorescence

Five-micron-thick sections of the paraffin block, serial to those used for conventional histopathological or cytological diagnosis, were obtained from surgical and cytological cases and collected onto poly-L-lysine coated slides. After dehydration in graded alcohols, they were processed for immunofluorescence. Alternatively, isolated cells prepared according to the Thin-Prep procedure or glass slides of cell lines (see above) were stained. An indirect immunofluorescence was performed on tissue sections or cells using a polyclonal goat anti-lamin B antibody (Santa Cruz, CA, USA), diluted 1/5 in phosphate-buffered saline (PBS) containing 5% bovine serum albumin (BSA). The secondary serum was a fluorescein isothiocyanate-conjugated rabbit anti-goat antibody (Sigma Aldrich, Munich, Germany), diluted 1/200 in PBS containing 5% BSA.

Confocal microscopy

Randomly selected fields (n=20) were analysed, and a total number of at least 1200 nuclei were studied for each case. A Leica (Wetzlar, Germany) TCS SP2 confocal microscope was employed. The instrument has standard Acousto Optic Tunable Filters and was used at the following setting conditions: 488 nm wavelength from the Ar/Kr laser; 63× oil planar apochromatic objective with 1.32 Numerical Aperture; wide acquisition window (500–650 nm); airy 1 detection pinhole diameter. Z stacks were collected at each 0.5-μm step and digitally zoomed for the purpose of figure presentation.

Tridimensional reconstruction

Using the serial images obtained by confocal microscope analysis, 3-D models of selected nuclei were obtained by Gaia Bussolati (EDI Effetti Digitali Italiani srl, Milan), employing the original Bistudio Software for 3-D modelling (Bistudio Program, EDI srl, Milan). Briefly, on the base of sequential images of serial nuclear sections, curves were obtained outlining the nuclear profile. Each segment of the curve, matching the steps between sections, was proportional to the size of the nuclei and to the gaps between sections, as measured in confocal microscopy. Using the curves as if they were making up a scaffold, surfaces linking their edges were obtained, as to finally build up the entire nuclear volume. The resulting 3-D images were, therefore, a rough but objective representation of the actual nuclear shape and volume, as observed in confocal microscopy.

Results

Immunofluorescence staining for lamin B showed an intense and diffuse reactivity along the nuclear membrane of all cases (Fig. 1). Most cells were strongly reactive irrespective of the tumour type (papillary carcinoma versus follicular carcinoma or adenoma). In individual nuclei, the staining was continuous along the membrane, including areas in which the membrane had irregular profile or invaginations. Nuclear "holes" typical of PTC were also lined by lamin B immunoreactive nuclear membrane. The type of fixation (formalin versus alcohol) did not appear to affect the immunofluorescence signal.

Papillary carcinoma nuclei

Two different specimens of NPA cells, as well as isolated PTC cells (Thin-Prep preparations) (20 randomly selected

Fig. 1 Confocal microscope analysis of papillary and follicular thyroid carcinoma nuclei using the nuclear membrane marker lamin B, ×630. Calibration bar for **a** and **b**=14 μm, **c**–**g**=8 μm. **a** Cluster of NPA papillary carcinoma cell line showing the irregular nuclear profile outlined by lamin B immunofluorescence staining. **b** In the same cell line, an invagination is evident in the first three and last pictures, which becomes complete in the fourth picture, as if the ▶

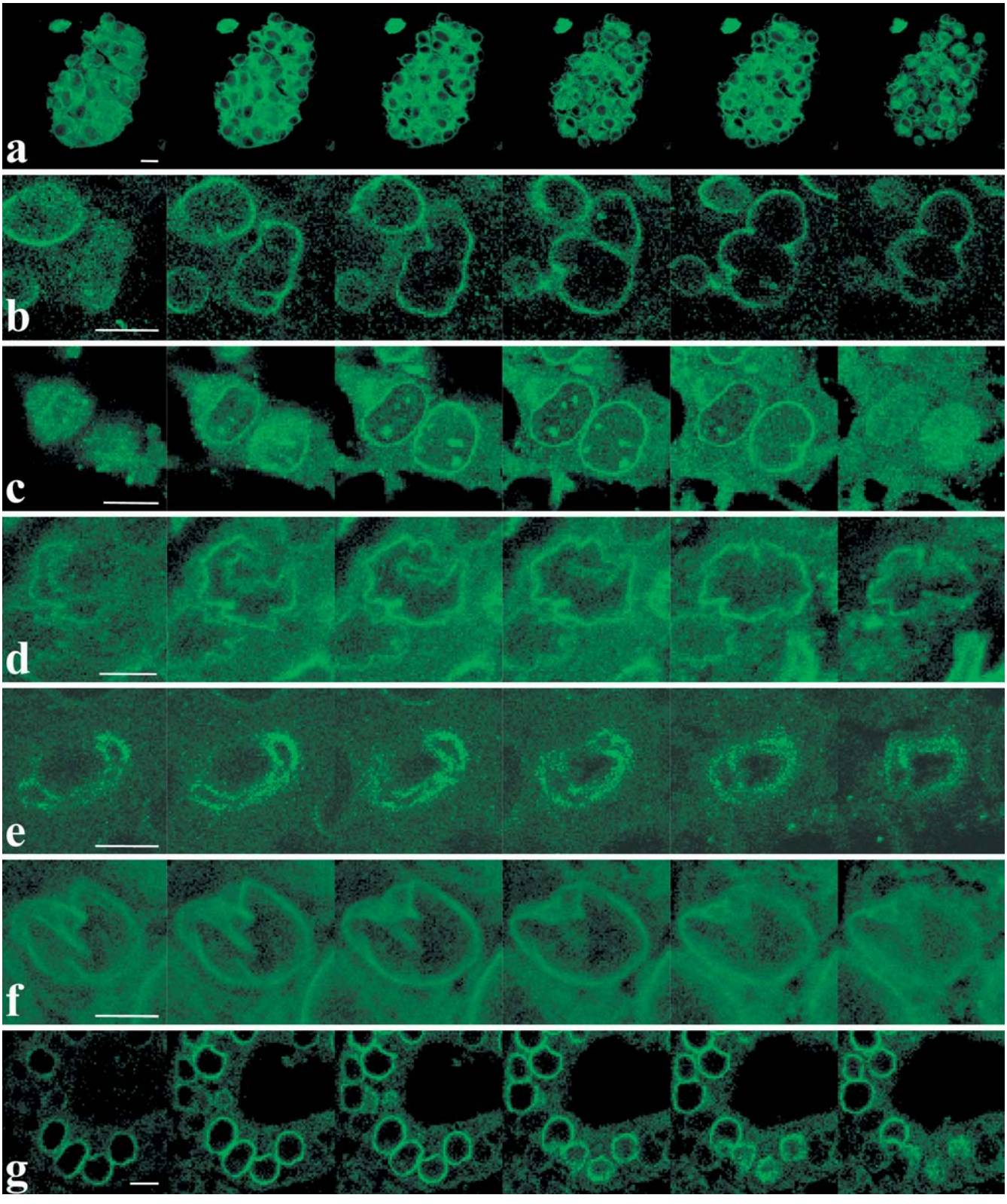

nucleus were cut into two parts. **c** WRO follicular carcinoma cell line. These control nuclei have a round or oval shape and lack profound invaginations. Nucleoli are also prominent. In surgical specimens, papillary thyroid carcinoma nuclei are markedly irregular and have invaginations and cytoplasmic pouches (**d**) or contain a large cytoplasmic pouch, which is initially continuous with the surrounding cytoplasm and then (last image on the right) is apparently isolated, as typically seen in nuclear pseudoinclusions by light microscopy (**e**). **f** This papillary carcinoma nucleus has numerous nuclear membrane invaginations, causing a cup-like appearance (*top left*). In a control case of follicular thyroid carcinoma (**g**), a neoplastic follicle is lined by tumour cells with regular oval or roundish nucleus, completely devoid of invaginations or contour irregularities

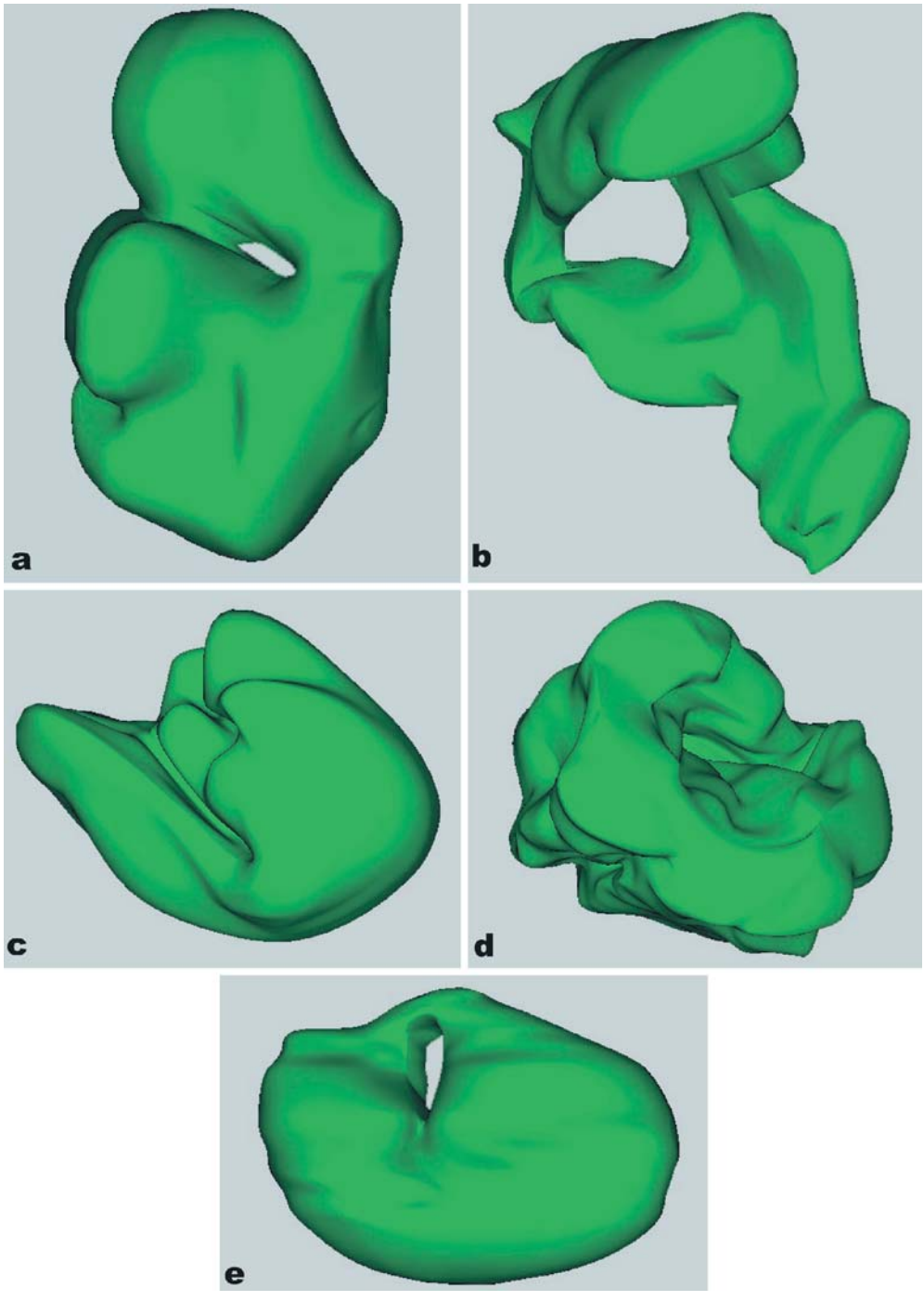

Fig. 2 Tridimensional reconstruction of papillary carcinoma nuclei. The nuclei correspond to those shown in Fig. 1 (respectively, **a=1b**, **b=1e**, **c=1f**, **d=1d**). Marked nuclear profile irregularities are well evident in the tridimensional images, which better outline deep invaginations (**a**, **c**), holes (**c**, **d**) and tunnels (**a**, **b**, **e**) caused by cytoplasmic invaginations into the nucleus. These figures can also be seen in the web site (http://www.oncologiaumana.unito.it/3-D.htm), where a software program allows one to rotate the models in the space, and to appreciate views from different perspectives

fields with 60 nuclei each) were analysed in comparison with three specimens (20 fields, 90 nuclei each) of PTC sections. As expected, papillary carcinoma nuclei from NPA cell line or from human and equine specimens were larger and much more irregular than the corresponding control cases of follicular tumours (see below). They had a mean diameter of 14 μm, as opposed to 8 μm of follicular tumours. In NPA cell line, nuclear grooves and invagination were more prominent than the surgical and cytological specimens, in which several nuclear "holes" (cytoplasmic pseudoinclusions) were evident (Fig. 1a, b). This could be due to the fact that surgical and cell block specimens were thin sections of the tumour, as opposed to the cell line, which was grown directly onto a glass slide. The PTC nuclei had a deeply irregular contour, with numerous indentations and profound invaginations. Following such invaginations with the confocal microscope, in different plans, it was evident that portions of cytoplasm were penetrating deep into the nucleus and even created tunnels, as some nuclei were crossed by the cytoplasm at full thickness (Fig. 1d, e, f). Such cytoplasmic "pouches" or "tunnels" corresponded to the pseu-

doinclusions typical of PTC nuclei and were always connected to the cell cytoplasm at one or more levels of the confocal microscope sections. Rotating the visual angle by 90 degrees, the round cytoplasmic pouches corresponded to a cleft or a groove, suggesting that these contour irregularities were tunnel-like and, therefore, could be seen either as a "hole" or as grooves (Fig. 2).

Control cases of follicular tumours

Two specimens of WRO cells and of isolated normal thyroid cells (Thin Prep preparation) were assessed, as well as three specimens of follicular tumours (20 fields containing 200 and 60 nuclei per field, respectively). Nuclei of WRO cells (follicular carcinoma) (Fig. 1c) and of follicular carcinomas (Fig. 1g) or adenomas were all round and slightly smaller that those of PTC. In addition, a small and generally single nucleolus was always present. The nuclear shape was generally oval or round with a regular and smooth contour. Very short indentations were occasionally present in the WRO cell line nuclei, but never deepened into the nuclear matrix. Confocal microscope images showed that the nuclei had an oval or spherical shape with minimal deformities.

When comparison was made between PTC nuclei (from isolated or cultured cells or from sections) and either normal thyroid cells (Thin-Prep preparation) or follicular tumour nuclei (from WRO cells or follicular tumour sections), it became clear that nuclear surface irregularities of various extents (ranging from minor indentations up to complete tunnelling of the nuclei) were present in the vast majority (approximately 95%) of PTC cells, while absent in control cells.

Tridimensional images

The 3-D nuclear shape reconstruction was performed on both the papillary carcinoma cell line NPA (Fig. 2a) and on papillary carcinomas (Fig. 2b, c, d, e). It showed a markedly deformed and irregular nucleus with indentations and bulging areas of the nuclear surface and, in some nuclei, a more or less deep crater creating a cup-like structure or a profound "hole" in the nucleus. The extreme of such misshaping of the nuclear appearance in the tridimensional models was represented by tunnel-like structures, corresponding to the intranuclear vacuoles or inclusions visible in light microscopy.

Discussion

In the present study, we described the confocal microscope images and a tridimensional reconstruction of papillary thyroid carcinoma nuclei, using an antibody directed to the nuclear membrane protein lamin B. We here showed that the typical features of PTC nuclei, well known at the light microscopy level, namely, cytoplasmic pseudoinclusions and nuclear grooves, are all part of the marked nuclear contour irregularities, which characterise PTC, as opposed to other follicular tumours.

In their recent biochemical study, Fischer and co-workers [3], while demonstrating that none of the nuclear membrane proteins investigated were responsible for the nuclear membrane deformities in PTC cells, also provided nice images of the nuclear "holes" and grooves of PTC, using a confocal microscope and immunofluorescence stainings with lamin and emerin. Since the expression of lamin B was not lost in the PTC nuclear membranes, we investigated some cases of PTC and control follicular tumours using this marker as the trace of the nuclear contour.

We demonstrated that not only minor irregularities of the nuclear profile (spikes or indentations) contained an intact nuclear membrane, but also that deep invaginations and pouches of cytoplasm into the nucleus were lined by intact nuclear membrane. The 3-D models showed that variously profound crateriform invaginations of the cytoplasm into the nuclear matrix could be either viewed as "holes" or as grooves, according to viewpoint. In some cases, the cytoplasmic invaginations penetrated the nucleus at full thickness, determining a tunnel-like shape. As can be observed by rotating the 3-D nuclear models (see web site http://www.oncologiaumana.unito.it/3-D.htm), the nuclear grooving, invaginations and holes, as observed in light microscopy, are only facets of the same phenomenon of irregularities of the nuclear membrane. As a result, different images are featured according to the perspective, so that only occasionally a nucleus, pierced by a tunnel, shows in light microscopy what appears as an intra-nuclear vacuole.

The cause and the significance of these nuclear abnormalities, as well as of the extensive nuclear clearing in PTC, are not fully understood [1]. Early ultrastructural studies [4] described deep and complex cytoplasmic evaginations in PTC, but did not provide any explanation for the "ground glass" appearance using light microscopy, nor for the extremely irregular nuclear profile. More recently, in experimental models, Fischer and co-workers [2] showed that ret/ptc retroviral construct introduction into thyroid cells leads to the appearance of the typical papillary carcinoma nuclear morphology.

Confocal microscopy is useful to better understand the shape and irregularities of PTC nuclei, since a single cell or nucleus can be observed at different planes and a tentative 3-D reconstruction can be obtained. Only one study using confocal microscopy to study the thyroid gland was traced in the literature. This study was, however, devoted to analysing the vascular architecture of tumours, and no mention was made of the structure of PTC nuclei [5]. The results of the present study indicate that confocal microscopy is a valuable tool to analyse thyroid tumour nuclei and that PTC nuclei have remarkable differences from those of control follicular tumours. This is obviously well known in light microscopy. The potential interest of this study is, in fact, not related to the diagnosis of PTC, which is generally an easy task in

routine diagnostic pathology. Rather, a grey area exists in thyroid pathology regarding follicular-patterned lesions characterised by prominent optically clear irregular nuclei, but lacking clear-cut features of PTC. Since it is known that optically clear, irregularly shaped, nuclei can also be found in other conditions, including thyroiditis, hyperplastic lesions (Graves disease) and oxyphilic cell tumours (not to mention post-fine needle aspiration or fixation artefacts) [1], the confocal microscope images and possibly a 3-D reconstruction may help in distinguishing true PTC from the other conditions. Future studies on thyroid tumours having optically clear irregular nuclei, but lacking other features to support a diagnosis of PTC, will help to clarify the role of confocal microscopy in the characterisation of follicular thyroid nodules, with special regard to fine needle aspiration pre-operative specimens. To date, the present findings indicate that, in PTC, the nuclei are markedly irregular, and the nuclear membrane defines profound invaginations and tunnels, which correspond to the holes and grooves well known to all light microscopists.

Acknowledgements Work supported by grants from the Italian Ministry of Education, Rome, MIUR Cofin 40% 2001, and from the Oncology Special Project, Compagnia di San Paolo/FIRMS, Turin. The authors wish to thank Mr. Andrea Grua (University of Turin) for excellent photographic assistance and Mrs. Gaia Bussolati (EDI srl, Effetti Digitali Italiani, Via Legnano 26, Milan, Italy) for the tridimensional model reconstruction.

References

1. Baloch ZW, LiVolsi VA (2002) Etiology and significance of the optically clear nucleus. Endocr Pathol 13:289–299
2. Fischer AH, Bond JA, Taysavang P, Battles OE, Wynford-Thomas D (1998) Papillary thyroid carcinoma oncogene (RET/PTC) alters the nuclear envelope and chromatin structure. Am J Pathol 153:1443–1450
3. Fischer AH, Taysavang P, Weber CJ, Wilson KL (2001) Nuclear envelope organization in papillary thyroid carcinoma. Histol Histopathol 16:1–14
4. Johannessen JV, Gould VE, Jao W (1978) The fine structure of human thyroid cancer. Hum Pathol 9:385–400
5. Katoh R, Hemmi A, Komiyama A, Kawaoi A (1999) Confocal laser scanning microscopic observation of angioarchitectures in human thyroid neoplasms. Hum Pathol 30:1226–1231
6. LiVolsi VA (1990) Surgical pathology of the thyroid. Saunders, Philadelphia
7. Newport JW, Wilson KL, Dunphy WG (1990) A lamin-independent pathway for nuclear envelope assembly. J Cell Biol 111:2247–2259
8. Rosai J, Carcangiu ML, De Lellis RA (1992) Tumors of the thyroid gland. In: Atlas of tumor pathology. Armed Forces Institute of Pathology, Washington

Virchows Arch (2004) 444:356–361
DOI 10.1007/s00428-003-0964-2

ORIGINAL ARTICLE

Stephan Ihrler · Sabine Blasenbreu-Vogt · Andrea Sendelhofert · Matthias Rössle · John D. Harrison · Udo Löhrs

Regeneration in chronic sialadenitis: an analysis of proliferation and apoptosis based on double immunohistochemical labelling

Received: 3 September 2003 / Accepted: 5 December 2003 / Published online: 4 February 2004

Abstract The understanding of regeneration in salivary glands as a finely tuned balance of cellular proliferation, differentiation and apoptosis has been limited by the difficulty of identifying proliferating cells. This has been overcome in the present investigation by double immunohistochemical labelling for the proliferation-associated antigen Ki67 and for different cell-type-specific antigens applied to 8 specimens of normal parotids and 16 specimens of chronic parotid sialadenitis with particular reference to acini and intercalated ducts. In comparison with low baseline rates of proliferation in normal parotids, proliferative indices were significantly increased in chronic sialadenitis in mature acinar cells, intercalated ductal cells and myoepithelial cells without evidence of proliferation by an additional population of cells. In accordance with findings in glands of experimental animals, the present data do not support the previously postulated concept of regeneration of acini and intercalated ducts by a hypothetical population of uncommitted ductal stem cells. The demonstration of a profound capacity for intrinsic glandular regeneration from differentiated cells represents a biological basis for the good results obtained from conservative therapy of chronic sialadenitis and offers hope for novel therapies designed to reconstitute impaired salivary flow.

Keywords Salivary glands · Regeneration · Proliferation · Apoptosis · Glandular atrophy

S. Ihrler (✉) · S. Blasenbreu-Vogt · A. Sendelhofert · M. Rössle · U. Löhrs
Institute of Pathology,
Ludwig-Maximilians-University,
Thalkirchnerstraße 36, 80337 Munich, Germany
e-mail: Stephan.Ihrler@patho.med.uni-muenchen.de
Tel.: +49-89-51604011
Fax: +49-89-51604043

J. D. Harrison
Department of Oral Pathology,
Guy's, King's and St. Thomas' Dental Institute,
London, England

Introduction

Chronic sialadenitis is a common cause of removal of salivary glands, although, recently, interest in conservative procedures has increased due to their excellent results and the morbidity associated with surgery, especially parotidectomy [1, 20]. Preliminary animal studies with gene transfer or transplantation of stem cells are being undertaken with the aim of improving salivary flow rates in severely atrophic glands [3]. However, the understanding of the glandular regeneration that is important for the development of these therapies is limited.

Regeneration of the salivary glands has, for a long time, been predominantly attributed to a putative population of uncommitted stem cells believed to be situated in the ducts [2]. However, investigations on experimental animals have failed to support this concept, and a growing body of evidence indicates the importance of a proliferative capacity of differentiated cells in diverse segments of the salivary duct [7, 8, 10, 29]. The major obstacle for an analysis of the proliferative capacity has been the difficulty of accurately identifying types of proliferating cells in the complex cellular composition of the salivary glands, which is aggravated in sialadenitis by an additional intimate admixture of intensely proliferating inflammatory and stromal cells (Fig. 3a).

The implementation of double immunohistochemical labelling for the proliferation-associated antigen Ki67 and for different cell-type-specific antigens has greatly improved the accurate localisation and quantification of proliferating cells. This technique recently enabled us to demonstrate a quantitatively diverse, but generally low, baseline proliferation in all five types of parenchymal cells of the normal human salivary gland [18]. These findings indicate that acinar cells, intercalated ductal cells and myoepithelial cells regenerate independently, without cellular transition and without the participation of an additional population of cells, while the renewal of luminal columnar cells in striated and excretory ducts is maintained by proliferation and differentiation of basal cells. In conditions of chronic damage, these basal cells

manifest an additional capacity for a pluridirectional morphogenetic differentiation into several types of reactive ductal metaplasias [18, 24]. However, despite this prominent role of basal cells in the striated and excretory ducts, there is no evidence for an active participation of basal cells in the cellular regeneration of the acini and intercalated ducts.

Investigations on the effects of chronic noxious stimuli on the acini and intercalated ducts have shown a limited reaction pattern that is largely confined to atrophy of the acini [11, 12, 13, 15, 21, 23, 25, 26, 27, 28, 29]. The role of cellular proliferation and apoptosis in parenchymal atrophy in chronic sialadenitis is not understood, and it is not clear to what extent cellular regeneration can compensate for the loss of cells in the atrophic glands. The aim of the present investigation is, therefore, to examine proliferation and apoptosis in chronic parotid sialadenitis to provide a biological basis for modern therapies and is focused on the alterations in the acini and intercalated ducts to complement the previous investigation, in which the striated and excretory ducts were examined [18].

Materials and methods

Materials

Surgical specimens (n=24) from human parotids were retrieved from the archives of the Institute of Pathology, Ludwig-Maximilians-University, Munich. They had been fixed in buffered formaldehyde (4%; pH 7), embedded in paraffin wax and cut into 4-µm serial sections. Normal parenchyma lacking inflammation was obtained from 8 of the specimens that had been resected for small Warthin tumours or pleomorphic adenomas (male 5; female 3; ages 36–51 years). Of the specimens, 16 had been diagnosed as chronic sialadenitis with or without sialolithiasis (male 9; female 7; ages 28–58 years) and did not include cases of benign lymphoepithelial lesion.

Methods

The degree of inflammation and parenchymal atrophy in these cases ranged from minor to severe and often demonstrated a variable focal distribution. The 16 cases of chronic sialadenitis were divided into a subgroup of 10 cases with minor acinar atrophy, which varied from mild to moderate and was often focal, and a subgroup of 6 cases with predominantly severe acinar atrophy. An accurate enumeration of cellular proliferation and apoptosis could not be accomplished in the latter subgroup because so few acinar cells were preserved. Previous data on the cellular proliferation of the normal parotids [18] served as a basis for the present investigation.

Quantification of proliferation

The protocols of double immunohistochemical labelling for Ki67–CK7 (labelling intercalated ductal cells) and Ki67–CK18 (labelling acinar cells) are as follows. Deparaffinised slides were subjected to microwave pretreatment (750 Watt) with target retrieval solution (TRS 6; pH 6; 30 min). Endogenous peroxidase was blocked with peroxidase solution (7.5%). An aviditin-biotin peroxidase complex method was applied (ABC-kit; Vector). The slides were incubated with normal horse serum for 20 min. After avidin-biotin blocking, the slides were incubated (room temperature; 60 min) for either monoclonal anti-CK7 (1:500 dilution) or anti-CK18 (1:450 dilution). Biotinylated universal antibody was applied as secondary antibody followed by avidin-biotin complex (Elite; 30 min each). Diaminobenzidine+ (Dako; 3 min) was used as chromogen. For staining with Ki67, the alkaline phosphatase–antialkaline phosphatase (APAAP)-method was used (APAAP-ChemMate; Dako). The monoclonal anti-Ki67 (1:50 dilution) was applied at room temperature for 60 min. Visualisation of the bound anti-Ki67 was obtained with a secondary antibody of mouse immunoglobulin followed by APAAP-immunocomplex (30 min each). Fast red (Sigma) was used as the chromogen (10 min) and Vector haematoxylin (Gill's formula) as the counterstain. For double staining with Ki67 and α-actin (labelling myoepithelial cells), the same procedure was used as outlined above with the following exceptions: a labelled streptavidin biotin kit was applied (LSAB-Kit, Dako) and anti-α-actin was used in a dilution of 1:400. Table 1 summarises the protocols.

The labelling-index was determined by calculating the percentage of Ki67-positive nuclei within a total of 400 acinar cells, intercalated ductal cells and myoepithelial cells, each identified according to cytological criteria and the immunohistochemical staining pattern (Fig. 4) [5, 16, 17, 18, 22]. The mean percentage of cellular proliferation and the standard error of the mean were calculated. For comparison of normal glands with inflamed glands, statistical analysis of the primary data of the three different types of cells was undertaken, using the χ^2 test.

Quantification of apoptosis

Caspase-mediated cleavage of cytoplasmic intermediate filaments is an early event in apoptosis of epithelial cells. The immunohistochemical detection of a specific caspase-cleavage site in CK18 filaments as a neo-epitope (M30) can be applied to formalin-fixed material for the detection of apoptosis in certain types of epithelial cells [9, 19]. Although M30 does not detect apoptosis in myoepithelial cells, due to the absence of CK18 filaments, it is associated with a better morphological result than when other markers of apoptosis are used, and the type of parenchymal cell that is labelled by M30 can be identified morphologically without confusion with the numerous inflammatory and stromal cells in sialadenitis, in which apoptosis is also not detected due to the lack of CK18 filaments. Cytological criteria for apoptosis (especially nuclear condensation and fragmentation) were used as a control for positive M30 labelling. Double labelling for M30 and cell-type specific markers analogous to Ki67 could not be established.

Due to the relatively small number of apoptoses demonstrated by M30, they were counted in 20 microscopical fields (0.25 mm^2

Table 1 Monoclonal mouse antibodies (mAb) used in this study were applied to the antigens listed below. *CK* cytokeratin, *MW* microwave, *TRS 6* target retrieval solution pH 6, *ABC-E* avidin-biotin complex method Elite, *APAAP* alkaline phosphatase anti-alkaline phosphatase method, *LSAB* labelled streptavidin biotin method

Antigen	mAb clone	Source	Pretreatment	Dilution of mAb	Method
CK18[1]	Ks18.04	Progen	MW 30 min TRS 6	1:450	ABC-E[2]
CK7[1]	Ks7.18	Progen	MW 30 min TRS 6	1:500	ABC-E[2]
α-Actin[1]	asm-1	Cymbus Biotec	MW 30 min TRS 6	1:400	LSAB[2]
Ki67[1]	MIB-1	Dako	MW 30 min TRS 6	1:50	APAAP[3]
M30 CytoDeath	M30	Roche Diagn	MW 15 min Citrat	1:60	APAAP[3]

[1] As part of double immunohistochemical labelling (see Methods)
[2] With biotin blocking system
[3] Dako ChemMate

with a 10× eyepiece and 20× objective) separately for acinar cells and intercalated ductal cells. The mean number of cellular apoptoses and the standard error of the mean were calculated.

Results

The striated and excretory ducts contain columnar cells and were easily distinguished from the intercalated ducts, which are smaller and contain cuboidal or flattened lining cells, in normal and moderately atrophic glands. The columnar structure was often maintained in very atrophic glands, but sometimes all the intralobular ducts were very atrophic and lacked columnar cells, although there was a difference in size that enabled the smaller ducts to be interpreted as intercalated ducts.

Double immunohistochemical labelling accurately demonstrated proliferation in the different types of cells of the salivary parenchyma, even with a background of intensely proliferating inflammatory and stromal cells in sialadenitis. The proliferation indices in chronic sialadenitis were increased about twofold in acinar cells, fourfold in intercalated ductal cells and more than tenfold in myoepithelial cells (Fig. 2a, b, c, Fig. 3b, c; Table 2). In the statistical analysis, the proliferation indices were significantly higher in the sialadenitis subgroups, with minor atrophy and severe atrophy compared with normal glands for intercalated ductal cells (both $P<0.001$) and myoepithelial cells ($P<0.02$ and $P<0.01$, respectively). The proliferation indices for intercalated ductal cells and myoepithelial cells were slightly higher in the sialadenitis subgroup with severe atrophy than in the subgroup with minor atrophy, although this was not statistically significant. In contrast to an absence of apoptoses in normal parotids (Fig. 1d), small numbers of apoptoses were seen in acinar and intercalated ductal cells in chronic sialadenitis (Fig. 2d, Fig. 3d; Table 3).

Discussion

A precise identification and quantification of proliferating cells facilitated by double immunohistochemical labelling has recently enabled us to establish a low, yet quantitatively diverse, proliferative capacity in the five types of differentiated parenchymal cells of the human salivary gland that maintain the gland in a steady state [18]. The significant increase of proliferation demonstrated in the present investigation in mature acinar cells, intercalated ductal cells and myoepithelial cells in chronic sialadenitis is consistent with several experimental animal investigations, which indicate a proliferative capacity in differentiated glandular cells [7, 8, 10, 11, 29]. Previous investigations on proliferation in salivary glands have mainly been performed on the animal model of experimental ductal obstruction, followed by removal of obstruction [7, 8, 10, 25, 27, 29] and are of value in helping our understanding of chronic sialadenitis in which ductal obstruction, which is often intermittent, is one of the noxious stimuli [14].

Burgess et al. [7, 8] used a similar immunohistochemical technique to that of the present investigation in rodent glands and found that an increased proliferation predominantly of myoepithelial cells during ductal ligation was followed by an increased proliferation predominantly of acinar cells after removal of the ligation. Thus, the increased proliferation of both of these types of cells in sialadenitis found in the present investigation possibly represents a reaction to intermittent obstruction, in which there is increased proliferation of myoepithelial cells during obstruction in an attempt to overcome the obstruction followed by proliferation of the acini during relief from the obstruction, when the environment is more conducive to secretory activity.

Table 2 Proliferation indices in normal parotids and in glands with chronic sialadenitis (percentage of Ki67-positive cells and standard error of the mean)

	Normal glands	Chronic sialadenitis	
		With minor atrophy	With severe atrophy
	(*n*=8)	(*n*=10)	(*n*=6)
Acinar cells	2.0% (±0.9)[2]	3.6% (±1.2)	-[1]
Intercalated ductal cells	0.8% (±0.3)[2]	3.4% (±0.4)	4.1% (±0.8)
Myoepithelial cells	0.2% (±0.1)[2]	2.3% (±0.3)	3.5% (±1.2)

[1] Too few acinar cells are preserved in severe atrophy for an accurate calculation
[2] Data from Ihrler et al. [18]

Table 3 Apoptotic indices in normal parotids and in glands with chronic sialadenitis [mean of apoptotic cells in 20 high power fields (HPF) and standard error of the mean]; apoptoses are not identifiable in myoepithelial cells in the M30 technique owing to the lack of intermediate filaments of low molecular weight (CK 18)

	Normal glands	Chronic sialadenitis	
		With minor atrophy	With severe atrophy
	(*n*=8)	(*n*=10)	(*n*=6)
Acinar cells	0.0/20 HPF	2.0/20HPF (+/−0.3)	-[1]
Intercalated ductal cells	0.0/20 HPF	1.5/20HPF (+/−0.2)	0.8/20HPF (+/−0.1)

[1] Too few acinar cells are preserved in severe atrophy for an accurate calculation

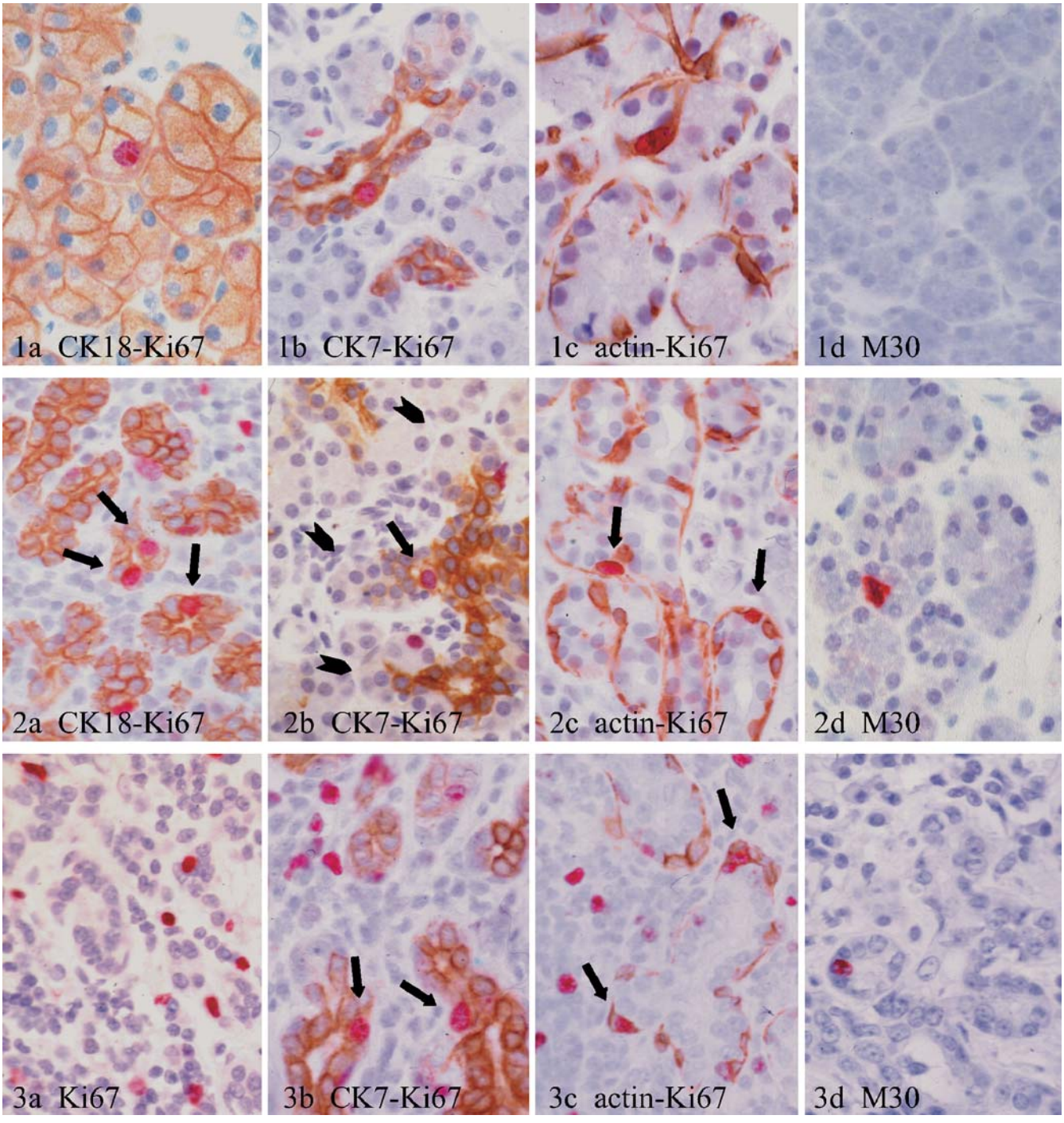

Fig. 1 Cellular proliferation and apoptosis in acini and intercalated ducts illustrated in representative cases of normal parotid. Original magnification: ×160. Double immunohistochemical labelling applied to normal parotids demonstrates proliferation in a CK18-positive acinar cell (**a**), a CK7-positive intercalated ductal cell (**b**) and an α-actin-positive myoepithelial cell (**c**). Apoptoses are absent (**d**; M30)

Fig. 2 Cellular proliferation and apoptosis in acini and intercalated ducts illustrated in representative cases of chronic sialadenitis with minor atrophy. Original magnification: ×160. In chronic sialadenitis with minor atrophy, cellular proliferation is markedly increased. Applying double labelling, increased proliferation can be attributed to CK18-positive acinar cells (**a**; *arrows*), CK7-positive intercalated ductal cells (**b**; *arrow*; remnants of CK7-negative acinar cells are indicated by *arrowheads*) and myoepithelial cells (**c**; *arrows*). One apoptosis is seen and is attributable to an acinar cell (**d**; M30)

Fig. 3 Cellular proliferation and apoptosis in acini and intercalated ducts illustrated in representative cases of chronic sialadenitis with severe atrophy. Original magnification: ×160. In chronic sialadenitis with severe atrophy, **a** illustrates that an accurate demonstration of proliferation is difficult when staining for Ki67 alone, owing to the complex cellular composition. Double labelling demonstrates the increased proliferation in intercalated ductal cells (**b**; *arrows*) and myoepithelial cells (**c**; *arrows*), while recognisable acinar cells are absent. The apoptosis demonstrated by M30 (**d**) is attributable to an intercalated ductal cell

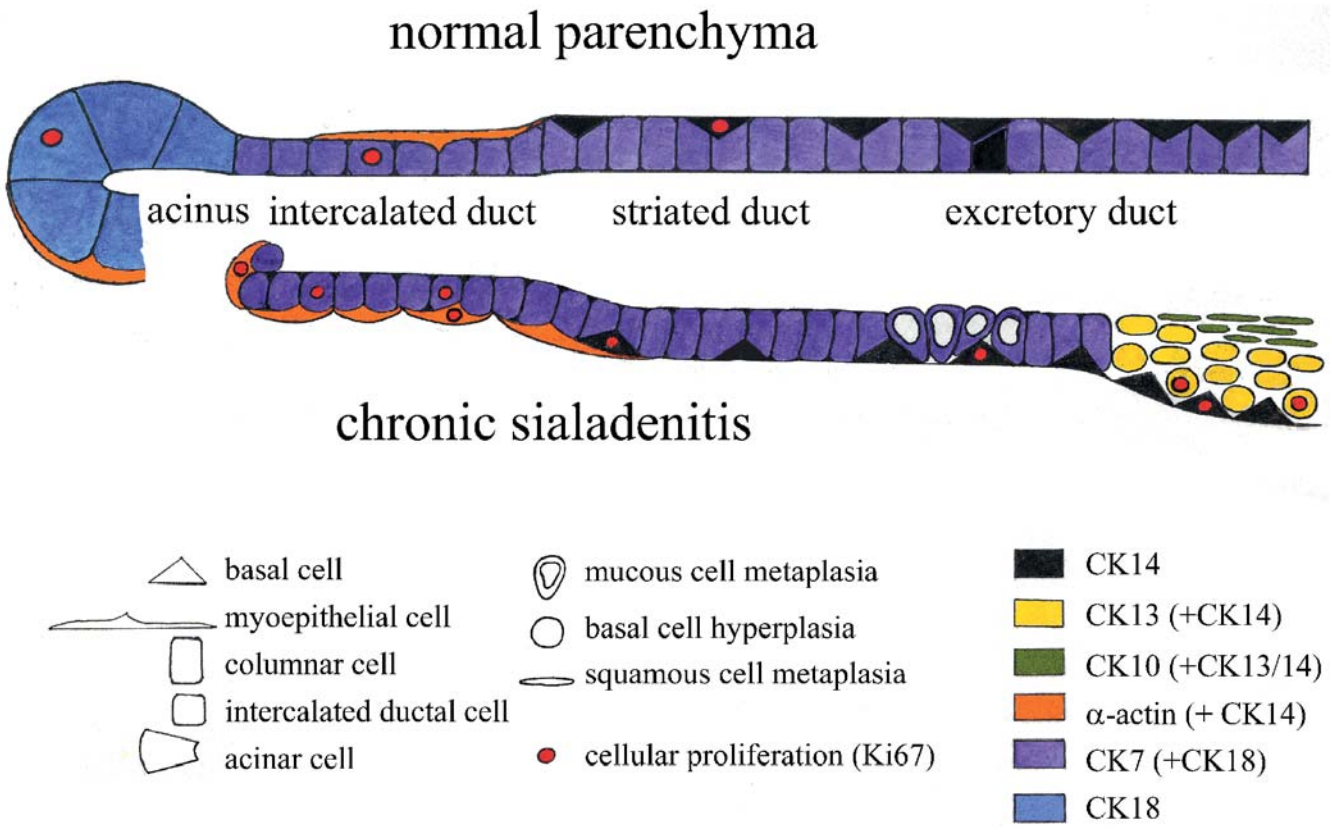

Fig. 4 Schematic illustration of the cellular alterations and proliferation in chronic sialadenitis compared with the normal salivary gland, focusing in the present investigation on acini and intercalated ducts

In addition to increased proliferation, the present investigation demonstrates an increased rate of apoptosis (Fig. 1d, Fig. 2d, Fig. 3d) in acinar and intercalated ductal cells in chronic sialadenitis compared with normal glands, in which apoptosis was not demonstrated. This does not mean that there is no apoptosis of these cells in normal glands, for there is a rapid phagocytic removal of apoptotic cells, which restricts the immunohistochemical demonstration of apoptosis to a much shorter time [19] than the demonstration of cellular proliferation by an antibody to Ki67, which appears to last for about one to several days [6]. Therefore, in contrast to Ki67-based demonstration of proliferation, which includes events that occur during one or more days before removal of the glands, only a relatively small fraction of the apoptoses that occur during this time will be demonstrable. Nevertheless, the presence of M30 labelling indicates that there is an increase in apoptosis in sialadenitis. However, the immunohistological detection of the dynamic processes of cellular proliferation and apoptosis that last for very different lengths of time does not allow a direct quantitative comparison between the proliferation and apoptotic indices. Possibly, the cell loss in chronic sialadenitis is partly compensated by increased cellular proliferation of differentiated cells, which is compatible with partial glandular recovery after removal of experimental ductal ligation [25]. The rates of apoptosis in chronic sialadenitis are much lower than the high rates reported by Walker et al. [29] and Scott et al. [25] in ductal ligation, and this is possibly due to adaptation to a chronic damaging process and to an obstruction that is intermittent and partial in sialadenitis.

Despite the capacity for intrinsic cellular proliferation, chronic sialadenitis eventually leads to progressive glandular atrophy, characterised by a loss of acinar cells with preservation of the intercalated ducts and myoepithelial cells (Fig. 4) [11, 12, 13, 14, 15, 21, 23, 25, 26, 28]. A gradual transformation of acinar cells during severe glandular damage into a less differentiated type of cell, similar to the intercalated ductal cells, has long been postulated. Convincing support for this kind of dedifferentiation of acinar cells is derived from ultrastructural studies [12, 13, 15, 21, 23, 27, 28, 29] and from the gradual gain of CK7 expression, which is seen in atrophic salivary parenchyma of man [18]. This gradual dedifferentiation, together with the increased apoptotic loss of acinar cells, is likely to contribute to the predominant atrophy of acini, which occurs in spite of increased acinar proliferation [25, 29].

The synthesis of data from animal models [7, 8, 10, 25, 29], our previous investigation on reactive metaplasia in human glands [18] and the present investigation of sialadenitis supports the following principles for glandular regeneration: (1) The physiological regeneration of the

acini and intercalated ducts is based on a low baseline proliferation of mature acinar cells, intercalated ductal cells and myoepithelial cells with a capacity for greatly increased proliferation in the presence of noxious stimuli. (2) The basal cells harbour an important role in the central duct segment as reserve cells for the physiological regeneration of luminal columnar cells and for a pluridirectional differentiation into several types of reactive epithelial metaplasia. This function of basal cells, however, obviously is restricted to the striated and excretory ducts. (3) There is a lack of support for the previously prevailing postulate of a predominant role for putative uncommitted stem cells in parenchymal regeneration.

Although the basic principles of cellular proliferation are likely to be universal [4, 6, 18], the complex mechanisms of physiological cellular regeneration, reactive metaplasias and, presumably, also pluriform tumorigenesis of salivary glands are likely to be a consequence of their unique and complex cellular composition. With regard to clinical implications, the low baseline and profound inducible capacity for intrinsic glandular regeneration represents a biological basis for the good functional results from conservative therapies of chronic sialadenitis [1, 3, 20]. This offers hope for novel therapeutic strategies designed to restore impaired salivary function.

Acknowledgements This study was supported by a grant from the "Friedrich-Baur-Stiftung" (Grant no. 0016/2003). The assistance of Mrs. Diane Raabe in reviewing the manuscript is gratefully acknowledged.

References

1. Antoniades D, Harrison JD, Epivatianos A, Papanayotou P (2004) Treatment of chronic sialadenitis by intraductal penicillin or saline. J Oral Maxillofac Surg (in press)
2. Batsakis JG, Regezi JA, Luna MA, El-Naggar A (1989) Histogenesis of salivary gland neoplasms: a postulate with prognostic implications. J Laryngol Otol 103: 939–944
3. Baum B (2000) Prospects for re-engineering salivary glands. Adv Dent Res 14:84–88
4. Bonkoff H, Remberger K (1998) Morphogenetic concepts of normal and abnormal growth in the human prostate. Virchows Arch 433:195–202
5. Born IA, Schwechheimer K, Maier H, Otto HF (1987) Cytokeratin expression in normal salivary glands and in cystadenolymphomas demonstrated by monoclonal antibodies against selective cytokeratin polypeptides. Virchows Arch 411:583–589
6. Brown DC, Gatter KC (1990) Monoclonal antibody Ki-67: its use in histopathology. Histopathology 17:489–503
7. Burgess KL, Dardick I (1998) Cell population changes during atrophy and regeneration of rat parotid gland. Oral Surg Med Oral Pathol Oral Radiol Endod 85:699–706
8. Burgess KL, Dardick I, Cummings MM, Burford-Mason AP, Bassett R, Brown DH (1996) Myoepithelial cells actively proliferate during atrophy of rat parotid gland. Oral Surg Oral Med Oral Pathol 82:674–680
9. Caulin C, Salvesen GS, Oshima RG (1997) Caspase cleavage of keratin 18 and reorganization of intermediate filaments during epithelial cell apoptosis. J Cell Biol 138:1379–1393
10. Dardick I, Byard RW, Carnegie A (1990) A review of the proliferative capacity of major salivary glands and the relationship to current concepts of neoplasia in salivary glands. Oral Surg Oral Med Oral Pathol 69:53–67
11. Donath K, Hirsch-Hoffmann HU, Seifert G (1973) Zur Pathogenese der Parotisatrophie nach experimenteller Gangunterbindung. Ultrastrukturelle Befunde am Drüsenparenchym der Rattenparotis. Virchows Arch 359:31–48
12. Emmelin N, Garrett JR, Ohlin P (1974) Secretory activity and the myoepithelial cells of salivary glands after duct ligation in cats. Arch Oral Biol 19:275–283
13. Harrison JD, Badir MS (1998) Chronic submandibular sialadenitis: ultrastructure and phosphatase histochemistry. Ultrastruct Pathol 22:431–437
14. Harrison JD, Epivatianos A, Bhatia SN (1997) Role of microliths in the aetiology of chronic submandibular sialadenitis: a clinicopathological investigation of 154 cases. Histopathology 31:237–251
15. Harrison JD, Fouad HMA, Garrett JR (2000) The effects of ductal obstruction on the acinar cell of the parotid of cat. Arch Oral Biol 45:945–949
16. Ihrler S, Zietz C, Riederer A, Diebold J, Löhrs U (1996) HIV-related parotid lymphoepithelial cysts. Immunohistochemistry and 3-D reconstruction of surgical and autopsy material with special reference to formal pathogenesis. Virchows Arch 429:139–147
17. Ihrler S, Zietz C, Sendelhofert A, Riederer A, Löhrs U (1999) Lymphoepithelial duct lesions in Sjögren-type sialadenitis. Virchows Arch 434:315–323
18. Ihrler S, Zietz C, Sendelhofert A, Lang S, Blasenbreu-Vogt S, Löhrs U (2002) A morphogenetic concept of salivary duct regeneration and metaplasia. Virchows Arch 440:519–526
19. Leers MPG, Kölgen W, Björklund V, Bergman T, Tribbick G, Persson B, Björklund P, Ramaekers S, Björklund B, Nap M, Jörnvall H, Schutte B (1999) Immunocytochemical detection and mapping of a cytokeratin 18 neo-epitope exposed during early apoptosis. J Pathol 187:567–572
20. Marchal F, Dulguerov P, Becker M, Barki G, Disant F, Lehmann W (2001) Specificity of parotid sialendoscopy. Laryngoscope 111:264–271
21. Matthews TW, Dardick I (1988) Morphological alterations of salivary gland parenchyma in chronic sialadenitis. J Otolaryngol 17:385–394
22. Moll R (1988) Differenzierungsprogramme des Epithels und ihre Änderungen. Verh Dtsch Ges Pathol 72:102–114
23. Palmer RM, Eveson JW (1987) Chronic sialadenitis. An immunohistochemical study in humans. Virchows Arch 412:73–78
24. Pammer J, Horvat R, Weninger W, Ulrich W (1995) Expression of bcl-2 in salivary glands and salivary gland adenomas. A contribution to the reserve cell theory. Pathol Res Pract 191:35–41
25. Scott J, Liu P, Smith PM (1999) Morphological and functional characteristics of acinar atrophy and recovery in the duct-ligated parotid gland of the rat. J Dent Res 78:1711–1719
26. Seifert G, Donath K (1977) Zur Pathogenese des Küttner-Tumors der Submandibularis. Analyse von 349 Fällen mit chronischer Sialadenitis der Submandibularis. HNO 25:81–92
27. Tamarin A (1971) Submaxillary gland recovery from obstruction. II. Electron microscopic alterations of acinar cells. J Ultrastruct Res 34:288–302
28. Tandler B (1977) Ultrastructure of chronically inflamed human submandibular glands. Arch Pathol Lab Med 101:425–431
29. Walker NI, Gobé GC (1987) Cell death and cell proliferation during atrophy of the rat parotid gland induced by duct obstruction. J Pathol 153:333–344

Virchows Arch (2004) 444:362–374
DOI 10.1007/s00428-004-0977-5

ORIGINAL ARTICLE

Tetsuo Goto · Yoshihide Fujigaki · Di Fei Sun · Tatsuo Yamamoto · Akira Hishida

Plasma protein extravasation and vascular endothelial growth factor expression with endothelial nitric oxide synthase induction in gentamicin-induced acute renal failure in rats

Received: 4 September 2003 / Accepted: 15 December 2003 / Published online: 24 February 2004

Abstract Microvascular hyperpermeability to plasma proteins via vascular endothelial growth factor (VEGF) with endothelial nitric oxide synthase (eNOS) induction may contribute to wound healing through matrix remodeling. However, vascular hyperpermeability is not examined in acute renal failure (ARF), a unique form of wound healing. Subcutaneous injection of gentamicin (400 mg/kg per day for 2 days in divided doses every 8 h) in rats increased serum creatinine levels and induced tubular damage, which peaked at day 6, after the last gentamicin injection. Ki67-positive regenerating proximal tubules (PTs) peaked in number at day 6 and almost covered the bare tubular basement membrane (TBM) by day 10. Staining of fibrinogen and plasma fibronectin began to increase in the peritubular regions as early as day 0, steadily increased in TBM and tubular lumen until day 6 and then decreased. Hyperpermeable peritubular capillaries were identified by extravasation of perfused-fluoresceinated dextran (both 70 kDa and 250 kDa) into peritubular regions as early as day 0 and prominently into TBM and tubular lumen at day 6. Electron microscopy further suggested the intraendothelial pathway of dextran. Immunoreactive VEGF increased in the damaged and regenerating PTs. Immunoreactive VEGF receptors-1 and -2 did not change, but immunoreactive eNOS increased in the peritubular capillaries after induction of ARF. Western blotting for VEGF and eNOS supported the immunostaining findings. In addition, we assessed the effects of NOS inhibitor N-nitro-L-arginine methyl ester (L-NAME) on vascular hyperpermeability during the recovery phase of this model. Treatment with L-NAME (s.c. at a dose of 100 mg/kg/day from day 3 to day 6) decreased extravasation of perfused-250-kDa dextran and significantly inhibited the regenerative repair of PTs at day 6 when compared with vehicle-treated rats. In conclusion, plasma protein extravasation occurred, leading to matrix remodeling, such as the process of wound healing during the tubular repair in gentamicin-induced ARF. Since VEGF-induced vascular hyperpermeability may depend on NO production, VEGF/VEGF receptor system with eNOS induction might be responsible for this process.

Keywords Hyperpermeability · VEGF · Gentamicin · Acute renal failure · Nitric oxide · eNOS

T. Goto · Y. Fujigaki (✉) · D. F. Sun · T. Yamamoto · A. Hishida
First Department of Medicine,
Hamamatsu University School of Medicine,
1-20-1 Handayama, 431-3192 Hamamatsu, Japan
e-mail: yf0516@hama-med.ac.jp
Tel.: +81-53-4352261
Fax: +81-53-4349447

Introduction

Microvascular hyperpermeability to plasma proteins (particularly fibrinogen and fibronectin) is a characteristic feature of normal wound healing and may contribute to wound healing through matrix remodeling [9, 12]. Extravasated fibrinogen clots to form a fibrin gel into which other plasma proteins, notably fibronectin, may be incorporated [45]. The interaction of fibronectin with fibrin and its incorporation into fibrin clots are thought to be important for the formation of a provisional matrix that promotes cell adhesion and migration [10, 22]. In this regard, the repair of tubular cells after acute renal failure (ARF) is a unique form of wound healing and a well-ordered response to ischemic or toxic injury characterized by diverse cellular activities, which include inflammation, cell migration and matrix deposition or remodeling [2, 41, 42]. However, plasma protein extravasation in relation to the cellular recovery after ARF is poorly understood.

Since vascular endothelial growth factor (VEGF) is mitogenic, angiogenic and a potent mediator of vascular permeability [8, 14], it is recognized as an important cytokine in wound healing [6, 31]. Nitric oxide (NO) production through NO synthase (NOS) by VEGF is known to play a critical role in VEGF-induced angiogenesis and vascular hyperpermeability [30, 46], and endothelial NOS (eNOS) may play a predominant role in this process [15]. VEGF also acts as a maintenance factor on endothelial cells by stimulating anti-apoptotic actions [16]

and as a chemotactic factor for monocytes. VEGF can function via two specific receptors, VEGF receptor-1 (Flt-1) and VEGF receptor-2 (Flk-1) [14, 39], which are predominantly expressed on endothelial cells [36].

In the kidney, VEGF is expressed in the visceral epithelial cells of glomeruli, proximal and distal convoluted tubules [29] and can induce nephrogenesis and vasculogenesis [43]. VEGF is also essential for endothelial-cell survival and repair during the course of glomerular disease models [26], remnant kidney model [20], obstructive nephropathy [32] and ischemic ARF model [19]. Peritubular capillaries surrounding proximal tubules (PTs) are one of the most fenestrated and permeable capillary networks in the body [33]. In this regard, Breier et al. [3] postulated that VEGF secreted from epithelial cells is involved in the maintenance of fenestrae in the endothelium. Thus, it is possible that an enhanced VEGF/VEGF receptor pathway between PT and peritubular capillary endothelium could enhance the filtering function of the peritubular capillaries by structural modifications of the endothelium under cer-tain pathological conditions. The present study was designed to characterize hyperpermeability of peritubular capillaries to plasma proteins during gentamicin-induced ARF in rats. This model is a well-established toxic ARF model known to induce PT damage followed by recovery mainly in the renal cortex [23]. To better understand the underlying mechanisms responsible for hyperpermeability of peritubular capillaries, we assessed the expression levels of VEGF, VEGF receptors and eNOS as well as structural alterations in peritubular capillary endothelium and localization of infused dextran throughout the disease periods. In addition, we investigated the role of NO on vascular hyperpermeability during the recovery phase of this model by inhibiting NOS.

Materials and methods

Induction of gentamicin-induced ARF

A total of 79 male Wistar rats (200–250 g, SLC, Shizuoka) were used in the present study. Rats (n=44) were injected subcutaneously with 400 mg/kg body weight/day of gentamicin sulfate solution (Sigma-Aldrich Co., St. Louis, MO) for 2 days in divided doses (every 8 h) and were sacrificed before gentamicin administration and 8 h (day 0), day 2, day 6 and day 10 after the end of gentamicin administration. Five rats at each time point and five normal rats as controls were anesthetized with intraperitoneal pentobarbital sodium (30 mg/kg), and a blood sample was collected from the abdominal aorta. Then both kidneys were removed after flushing phosphate-buffered saline (PBS) for immunohistochemistry, immunofluorescence study and Western-blot analysis. Serum creatinine level was measured using the enzymatic method (Mizuho Med., Saga, Japan). For the study of microangiography and electron microscopy, six rats at each time point and six normal rats were used, respectively. As additional controls, eight rats were given a comparable amount of saline subcutaneously instead of gentamicin solution, and two rats at each time point were served for microangiography.

NO inhibition study

To investigate the role of NO on vascular hyperpermeability during the recovery phase of this model, NOS inhibitor N-nitro-L-arginine methyl ester (L-NAME, Sigma-Aldrich Co., St. Louis, MO) (100 mg/kg/day, s.c., n=8) or its vehicle saline (n=8) was administered to rats with gentamicin-induced ARF from day 3 to day 6, the last dose being given 1 h prior to sacrifice at day 6. Kidneys from the L-NAME group (n=5) and the vehicle group (n=5) were served for immunohistochemistry for Ki67 and a blood sample for measurement of serum creatinine level. Rats of L-NAME group (n=3) and vehicle group (n=3) were subjected to microangiography with fluorescein isothiocyanate (FITC)-labeled dextran (250 kDa).

Tissue processing

The harvested kidneys were bisected through the longitudinal axis, and some were cut into smaller pieces. They were fixed with 10% neutral-buffered formalin, 4% paraformaldehyde or methacarn solution and then were embedded in paraffin. Portions of renal cortex were snap frozen in cold N-hexane and stored at −70°C for immunofluorescence studies and Western-blot analysis.

Histochemistry and immunohistochemistry

For histopathological examination, 4-μm-thick paraffin sections were stained with periodic acid-Schiff (PAS). To detect VEGF, VEGF receptors-1 and -2, eNOS, rat endothelial cell antigen (RECA)-1, Ki67 and ED1 paraffin sections were first incubated with normal serum matched to the species for secondary antibodies. After incubation with the primary antibodies listed in Table 1, sections were reacted with biotin-conjugated donkey anti-rabbit IgG (Chemicon International Inc., Temecula, CA) or donkey anti-mouse IgG (Chemicon) for 30 min at room temperature. Then, streptavidin-conjugated peroxidase (Nichirei, Tokyo, Japan) was added for 30 min. After washing in PBS, the reaction products were

Table 1 Antibodies used to detect specific antigens in paraffin-embedded kidney sections. *VEGF* vascular endothelial growth factor, *eNOS* endothelial nitric oxide synthase, *RECA* rat endothelial cell antigen

Primary antibodies	Supplier
Rabbit polyclonal antibody against a peptide corresponding to amino acids 1–140 of VEGF; recognizes the 165, 189 and 121 amino acid splice variants of VEGF (VEGF-147, sc-507)	Santa Cruz Biotechnology, Santa Cruz, CA, USA
Mouse monoclonal antibody against VEGF121 (VEGF Ab-5)	Oncogene, Boston, MA, USA
Rabbit polyclonal antibody against Flt-1 as VEGF receptor-1 (Flt-1 C-17, sc-316)	Santa Cruz Biotechnology, Santa Cruz, CA, USA
Rabbit polyclonal antibody against Flk-1 as VEGF receptor-2 (Flk-1 C-20, sc-315)	Santa Cruz Biotechnology, Santa Cruz, CA, USA
Mouse monoclonal antibody against eNOS	Transduction Laboratories, Lexington, KY, USA
Mouse monoclonal antibody against rat RECA-1 as endothelial cell marker	Serotec, Oxford, UK
Mouse monoclonal antibody against Ki67 as cell proliferation marker	Novocastra Laboratories, Newcastle upon Tyne, UK
Mouse monoclonal antibody against ED1 as rat monocytes/macrophages	Serotec, Oxford, UK

visualized using incubation with a diaminobenzidine detection kit (Nichirei).

Double immunostaining for RECA-1 and Ki67 was performed to evaluate the proliferative activity of peritubular capillary endothelium. After staining with RECA-1, sections were treated with microwave oven heating for 10 min in 0.01 M sodium citrate, pH 6.0, at 800 W and then were incubated with Ki67 as above and with donkey polyclonal biotinylated antibody against mouse IgG. Then $NiCl_2$ reagent (Vector Laboratories, Burlingame, CA) was added to obtain a dark blue staining color.

Histopathological control sections were treated as above except for omitting the primary antibodies or replacing the primary antibodies with normal mouse or rabbit IgG at equivalent concentrations.

Immunofluorescence studies

Immunofluorescence studies were performed on 4-μm-thick cryostat sections fixed in cold acetone. Direct immunofluorescence was performed with FITC-labeled goat polyclonal antibody against human fibrinogen (ICN Pharmaceuticals Inc., Aurora, OH). Indirect immunofluorescence was performed with rabbit polyclonal antibody against rat plasma fibronectin (from rat plasma; Chemicon) and then followed by FITC-labeled donkey anti-rabbit IgG (Chemicon). The staining intensity was determined semi-quantitatively using a grading system of scales: −, +, ++ and +++.

Microangiography

Microangiography was performed using the method of Pillebout et al. [35] with minor modifications. Briefly, 38 rats were anesthetized with ether, and the ventral aspect of both kidneys was exposed through a middle incision of the abdomen. Then rats were subjected to intrajugular injection of FITC-labeled dextran (size, 70 kDa or 250 kDa, Sigma Chemicals Co., St. Louis, MO) (100 μg/g of body weight) in isotonic saline. Next, 60 s after injection, the kidneys were removed and immediately fixed overnight in 4% formalin. We chose the time point of sacrifice 60 s after injection since preliminary examinations showed that fluorescence decreased in renal vessels after 60 s, and only faint fluorescence was left in renal vessels in the cortex after 30 min. Other portions of the kidney were used for electron microscopic examination, while additional portions were paraffin embedded, and 4-μm thick sections were cut, deparaffinized and observed with a fluorescent microscope (B×50, Olympus, Tokyo).

Transmission electron microscopy

Small portions of 4% formalin-fixed renal tissues from FITC-250-kDa dextran-infused rats were further fixed in 2% glutaraldehyde in 0.1 M phosphate buffer (pH 7.4) for 2 h, postfixed in 1% osmium tetroxide resolved in the same buffer for 1 h and then embedded in Epon. Ultra-thin sections were counterstained with uranyl acetate and lead citrate and then examined under an electron microscope (JEM-1220, JEOL, Japan).

Western blot analysis of VEGF and eNOS

Immunoblotting was repeated at least three times with samples from a minimum of four animals for each time point and condition. Frozen kidney cortex was dissolved in radioimmunoprecipitation buffer (25 mM Tris-HCl, pH 7.4; 150 mM NaCl; 0.5% deoxycholic acid; 0.5% Triton-X100 and 0.1% sodium dodecyl sulfate) at 4°C containing 1 mM phenylmethylsulfonyl chloride, 1 μg/ml aprotinin, 1 μg/ml leupeptin and 1 μg/ml pepstatin A. Equal amounts of proteins (40 μg) were loaded for sodium dodecyl sulfate-polyacrylamide gel electrophoresis. After electrophoresis, those proteins were electroblotted onto nitrocellulose membranes. The membranes were subsequently washed three times for 10 min each in Tris-buffered saline (TBS)-T (20 mM Tris-HCl, pH 7.6; 150 mM NaCl; and 0.1% Tween-20), incubated in TBS-T containing 2% skim milk for 1 h at room temperature to block non-specific binding and subsequently incubated with the primary antibody (VEGF-147 or eNOS) overnight at 4°C. After the membranes were washed three times for 10 min each, they were incubated with horseradish peroxidase-conjugated donkey anti-rabbit antibody (OEM concept, Toms Rover, NJ) or sheep anti-mouse antibody (Amersham Life Science, Buckinghamshire, UK), diluted appropriately in TBS-T containing 2% skim milk for 1 h at room temperature. Antibodies bound to membrane-immobilized proteins were visualized using enhanced chemiluminescence (ECLTM, Amersham).

Morphometric analysis of PT cells and immunoreactive cells

To determine the number of PT cells, reflecting a balance of tubular cell death and tubular cell proliferation, we counted the number of nuclei in epithelial cells in cross-sections of the PTs in the cortex using PAS-stained sections and calculated the number of cells per tubular cross-section. The number of Ki67-positive PT cells and interstitial cells in the cortex was counted at ×400 magnification. In addition, the number of ED1-positive cells in the interstitium was counted at ×400 magnification. The number of immunoreactive cells in each rat represented the average number of 40 fields examined and the mean number before and at days 0, 2, 6 and 10, after induction of ARF was displayed in histograms. When double immunostaining of RECA-1 and Ki67 was performed, the total number of Ki67/RECA-1-double-positive cells among RECA-1-positive cells was counted in 40 randomly selected fields of the cortex at ×400 magnification before and at day 2 and day 6 after induction of ARF, and the mean percentage of RECA-1/Ki67-positive cells was calculated at each time point.

Statistical analysis

Data are expressed as mean±SD. Differences between data sets were determined by one-way analysis of variance followed by Fisher's *t*-test. Comparison between values for L-NAME group and vehicle group was performed using paired *t*-test. A P level <0.05 was accepted as statistically significant. All statistical analyses were performed using Statview (Abacus Concept, Inc., Berkeley, CA).

Results

Gentamicin-induced ARF

Serum creatinine increased significantly as early as day 2 after the end of gentamicin administration ($P<0.001$ versus level before induction of ARF) and reached a peak value at day 6 ($P<0.001$ versus level before induction of ARF), then decreased afterward (Fig. 1). Damage of the PTs in the cortex was detected as early as day 0, showing vacuolization, abnormal accumulation of PAS-positive inclusions. Furthermore, frank necrosis of PTs could be found at day 2 and day 6 as reported previously by others [20], and denuded tubular basement membrane (TBM) was most prominent at day 6 (Fig. 2A, B, C). However, regenerating PTs were found at day 6, which were characterized as flat elongated cells with basophilic cytoplasm and dilated lumen (Fig. 2C). These cells almost covered the entire bare TBM by day 10, when PTs became taller with brush-border (Fig. 2D). The density of

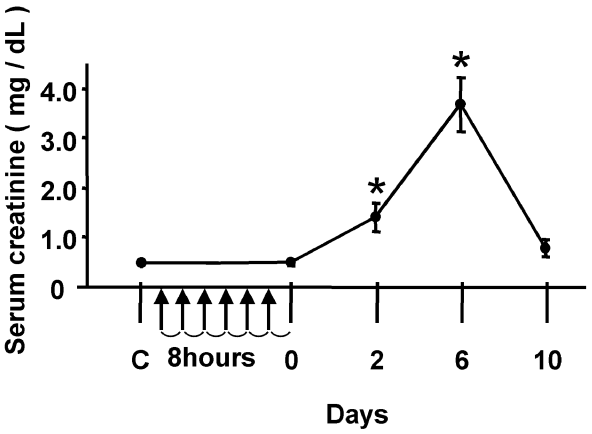

Fig. 1 Serial changes in serum creatinine before and after induction of gentamicin-induced acute renal failure (ARF). Data represent the mean±SD values of five animals. *C* Before induction of ARF. *Asterisk* $P<0.001$ versus before induction of ARF. *Arrows* indicate the time of gentamicin injection

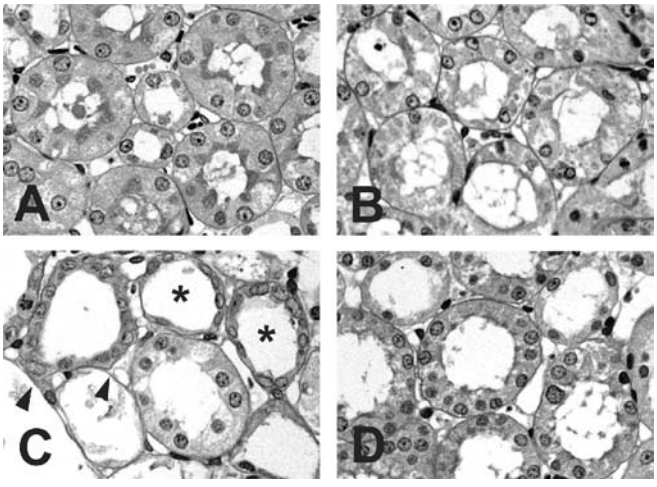

Fig. 2 Photomicrographs of periodic acid-Schiff (PAS)-stained sections in the cortex of a representative normal control rat (**A**) and rats at days 2 (**B**), 6 (**C**) and 10 (**D**) after induction of acute renal failure. At day 2, some proximal tubule (PT) cells showed vacuolization, abnormal accumulation of PAS-positive inclusions and necrosis (**B**). Damaged PTs with denuded tubular basement membrane (TBM) (*arrowheads*) were almost maximally distributed in the cortex at day 6, and regenerating PTs characterized by flat elongated morphology with basophilic cytoplasm and a dilated lumen were also found (*asterisks*) (**C**). The regenerating PTs with brush-border almost covered bared TBM at day 10 (**D**). Original magnification, ×400 (**A**–**D**)

PT cells in the cortex decreased significantly as early as day 0 and progressively decreased by day 6, then increased over the baseline level at day 10 (Fig. 3).

Immunohistochemistry

Immunoreactive VEGF-147 was detected in the cytoplasm of the distal tubules and glomerular epithelial cells

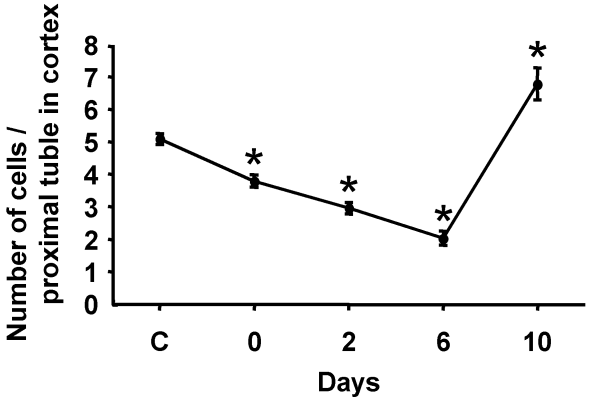

Fig. 3 Serial changes in the number of tubular epithelial cells per cross-section of proximal tubules in the renal cortex. Data represent mean±SD values of five animals. *C* Before induction of acute renal failure (ARF). *Asterisk* $P<0.001$ versus before induction of ARF

and weakly in the cytoplasm and brush-border of PTs in untreated kidneys (Fig. 4A). After induction of ARF, staining of VEGF-147 in PTs was increased as a granular pattern in the cytoplasm as early as day 0 (Fig. 4B, C). In addition to the cytoplasmic staining, staining of VEGF-147 was also found in the apical side of regenerating PTs at day 6 (Fig. 4D). By day 10, staining pattern of VEGF-147 almost returned to the level seen in untreated kidneys (Fig. 4E). VEGF-147 staining along the peritubular capillaries was not seen throughout the experimental period (Fig. 4A, B, C, D, E). Immunoreactive VEGF Ab-5 showed a staining pattern similar to that of VEGF-147 (Fig. 4H, I, J). In untreated kidneys, immunoreactive VEGF receptors-1 (Flt-1) and -2 (Flk-1) were similarly identified in the peritubular capillaries and glomerular endothelium, in the cytoplasm of the distal tubules and in the brush-border of PTs (Fig. 4K, P). The staining intensity of the peritubular capillary endothelium did not change after induction of ARF (Fig. 4L, M, N, O, Q, R, S, T). However, newly expressed VEGF receptors-1 and -2 were found in the regenerating PTs at day 6 (Fig. 4S), and the staining pattern was shifted to the apical side of the PT at day 10 (Fig. 4T).

When primary antibodies were replaced with normal IgGs of the corresponding animals, no significant staining was observed in both normal control (Fig. 4F) and experimental sections (Fig. 4G). Immunoreactive eNOS was found intensely in the glomerular endothelium and slightly in the peritubular capillary endothelium of untreated kidneys (Fig. 5A). After induction of ARF, intense staining for eNOS in the glomerular endothelium was not changed; however, induction of ARF was associated with a marked increase in staining for eNOS in peritubular capillaries as early as day 0 and was persistently high until day 10 (Fig. 5B, C, D, E). However, immunoreactive RECA-1 was identified in peritubular capillaries and glomerular endothelium in untreated kidneys (Fig. 5F). After induction of ARF, the

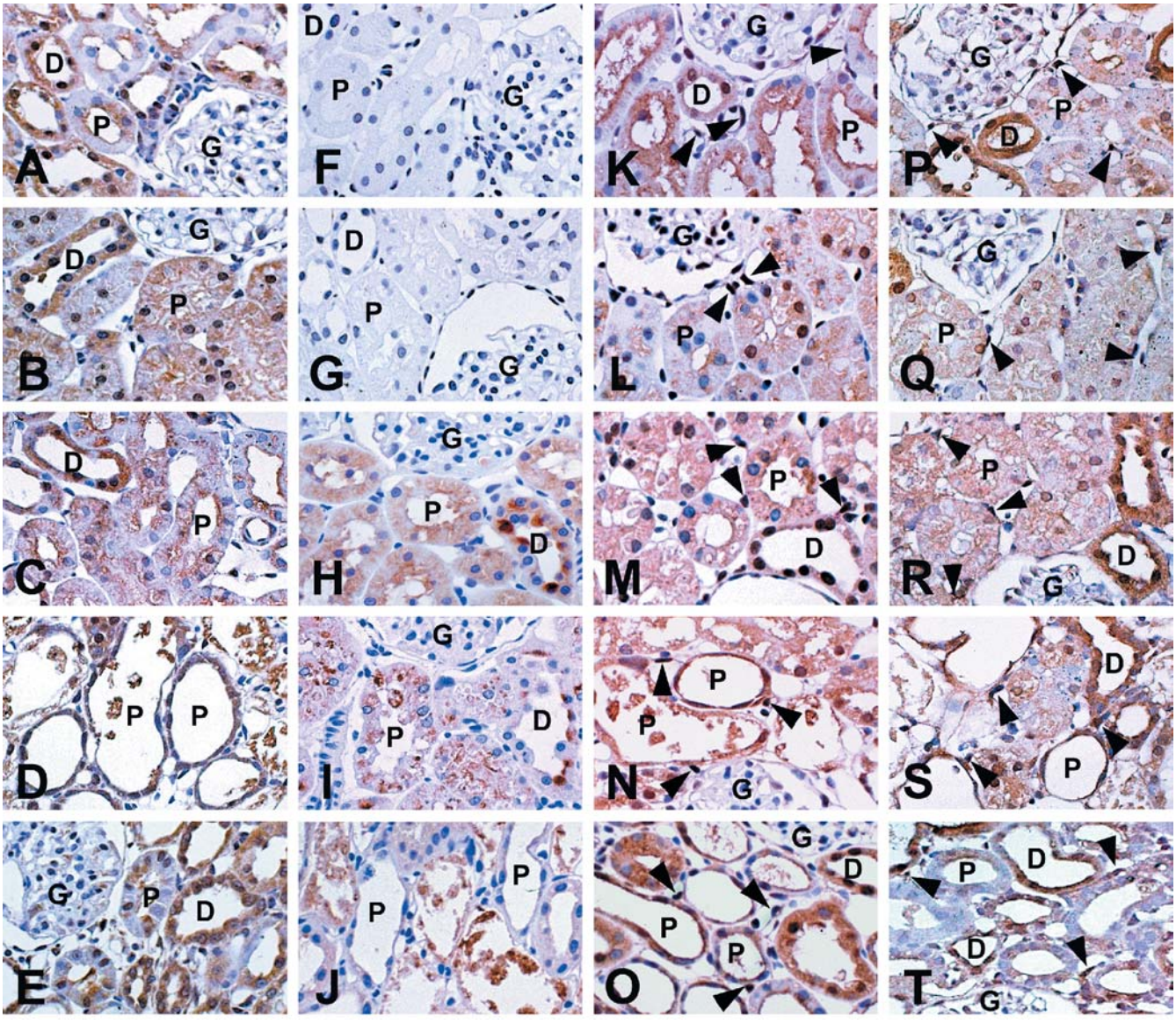

Fig. 4 Representative photomicrographs of immunostaining for vascular endothelial growth factor (VEGF)147 (**A**–**E**), VEGF Ab-5 (**H**–**J**), VEGF receptor-1 (Flt-1) (**K**–**O**) and VEGF receptor-2 (Flk-1) (**P**–**T**) in the renal cortex in rats before induction of acute renal failure (ARF) (**A**, **F**, **H**, **K**, **P**) and at days 0 (**B**, **L**, **Q**), 2 (**C**, **G**, **I**, **M**, **R**), 6 (**D**, **J**, **N**, **S**) and 10 (**E**, **O**, **T**) after induction of ARF. Histopathological control sections in the normal control rat (**F**) and the experimental rat at day 2 (**G**). *Arrowheads* immunoreactive peritubular capillaries, *P* proximal tubules, *D* distal tubules, *G* glomerulus. Original magnification, ×400 (**A**–**O**)

staining was slightly decreased segmentally in some capillary endothelium only at day 6 (Fig. 5G, H, I, J).

The number of Ki67-positive regenerating PT cells was significantly increased at day 6 and then was markedly decreased (Fig. 5K, L and Fig. 6). The number of Ki67-positive interstitial cells was significantly increased at day 2 and reached a peak level at day 6 (Fig. 5K, L and Fig. 6).

Double immunostaining of RECA-1 and Ki67 showed that the majority of RECA-1-positive peritubular capillary endothelial cells were negative for Ki67 (Fig. 5M). The mean percentage of RECA-1/Ki67-double-positive endothelial cells among RECA-1-positive endothelial cells was 0.58% in normal controls, 0.63% at day 2 and 0.98% at day 6, indicating a low proliferative activity of RECA-1-positive peritubular capillary endothelial cells.

ED1-positive monocytes/macrophages were found only occasionally in the interstitium in untreated kidneys (data not shown). The number of ED1-positive cells was significantly increased as early as day 2, reached a peak level at day 6 and then decreased (Fig. 5N, O and Fig. 7) at day 10, although it was still higher than the baseline.

Immunofluorescence findings

Immunoreactive fibrinogen in the normal kidneys was almost confined to small areas in the peritubular capil-

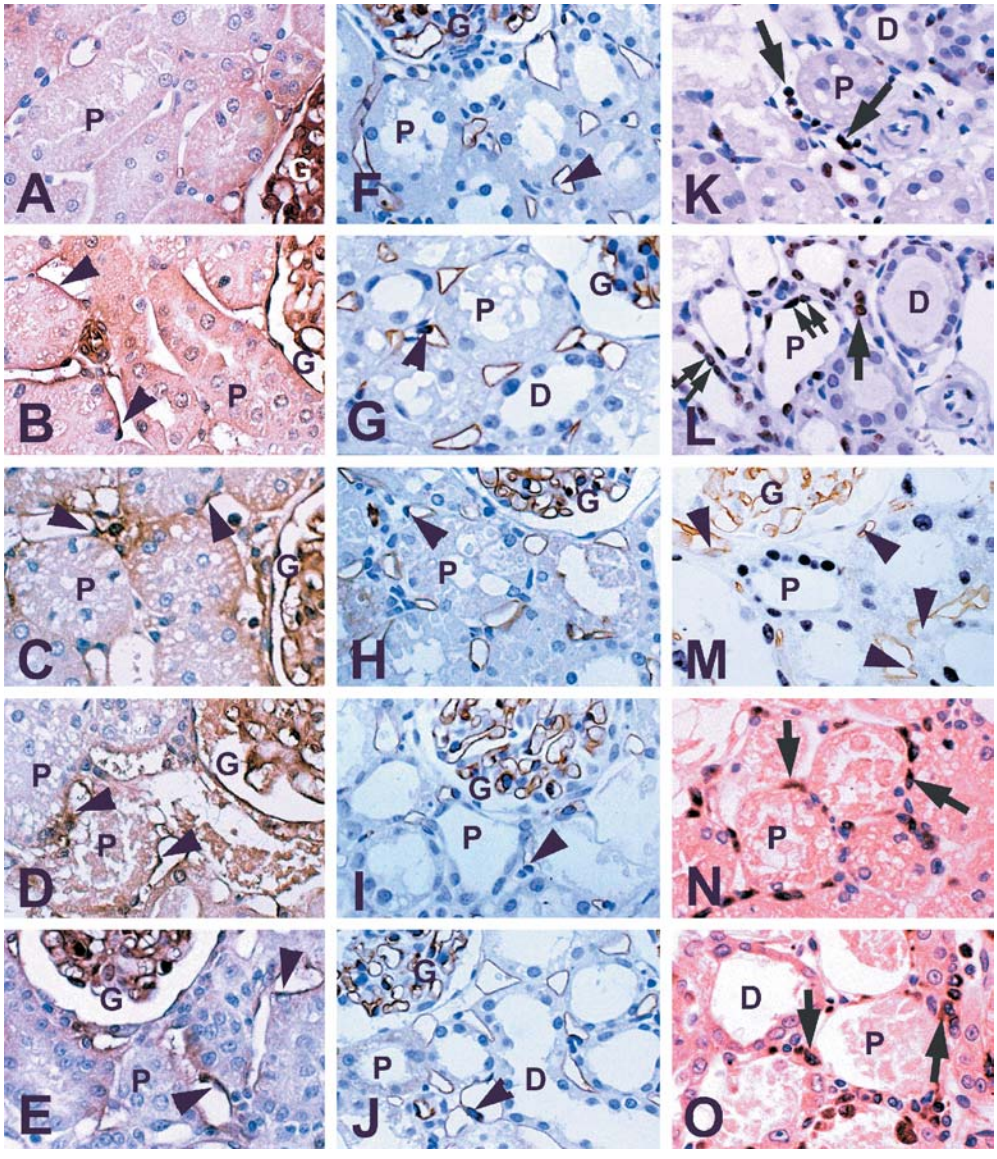

Fig. 5 Photomicrographs of immunostaining for endothelial nitric oxide synthase (**A**–**E**), rat endothelial cell antigen (RECA)-1 (**F**–**J**), Ki67 (**K**, **L**), RECA-1/Ki67 (**M**) and ED1 (**N**, **O**) in the renal cortex in rats before induction of acute renal failure (ARF) (**A**, **F**) and at days 0 (**B**, **G**), 2 (**C**, **H**, **K**, **N**), 6 (**D**, **I**, **L**, **M**, **O**) and 10 (**E**, **J**) after induction of ARF. Ki67-positive interstitial cells (*arrows*) and proximal tubule cells (*double arrows*) at day 2 (**K**) and day 6 (**L**). Double immunostaining of RECA-1 and Ki67 at day 6 (**M**), showing that most RECA-1-positive peritubular capillary endothelial cells (*arrowheads*) were negative for Ki67 (*dark blue nucleus*). ED1-positive monocyte/macrophages (*arrows*) in the interstitium at day 2 and day 6 (**N**, **O**). *Arrowheads* immunoreactive peritubular capillaries, *P* proximal tubules, *D* distal tubules, *G* glomerulus. Original magnification, ×400 (**A**–**O**)

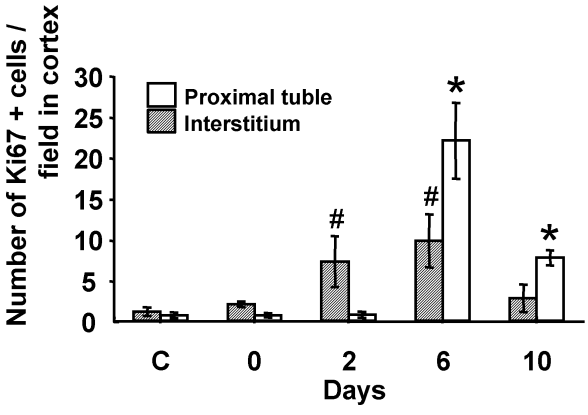

Fig. 6 Density of Ki67-positive cells in proximal tubule and interstitium (number per field in the cortex). Data represents mean±SD values of five rats. *C* Before induction of acute renal failure. *Asterisk* $P<0.001$ versus normal control, *number sign* $P<0.001$ versus normal control

laries in the cortex (Fig. 8A) and increased in the peritubular regions as early as day 0 (Fig. 8B). Deposition of fibrinogen was identified in TBM and the tubular lumen at day 2 (Fig. 8C), reached a peak level at day 6 (Fig. 8D) and then markedly decreased (Fig. 8E). Immunostaining pattern of plasma fibronectin was similar to that of fibrinogen (Fig. 8F, G, H, I, J); however, staining of the TBM was already identified at day 0 (Fig. 8G). Table 2 summarizes the immunofluorescence findings.

Microangiography

In the normal kidneys, we observed fluorescence of infused-FITC-labeled dextran (both 70 kDa and 250 kDa) in peritubular vessels (Fig. 9A, F) and prominently in glomerular capillaries (not shown) in the renal cortex. After induction of ARF, such fluorescence increased in the peritubular regions and TBM as early as day 0

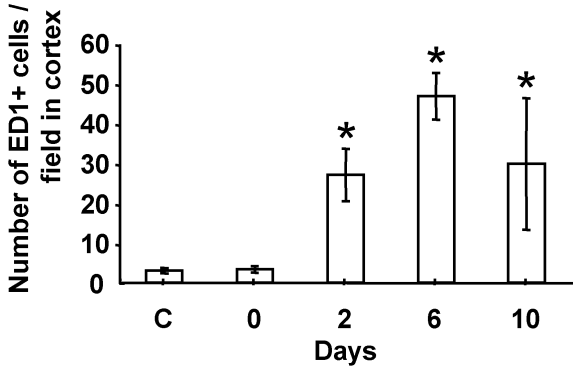

Fig. 7 Morphometric analysis of the number of interstitial ED1-positive monocytes/macrophages in the renal cortex. Data represent mean±SD values of five rats. **C** Before induction of acute renal failure. *Asterisk* $P<0.001$ versus normal control

(Fig. 9B, G) and in the tubular lumen at days 2–6 (Fig. 9C, D, H, I). Extravasation of dextran reached peak levels at day 6 (Fig. 9D, I) and then markedly decreased at day 10 (Fig. 9E, J). Only weak fluorescence was found in some Bowman's spaces in 70-kDa-dextran-infused normal rats, but not in 250-kDa-dextran-infused normal rats; however, there was no evidence for increased fluorescence in Bowman's spaces after induction of ARF (not shown). Extravasation of both sizes of dextran was almost confined to the cortex throughout the course of ARF. The fluorescence findings of infused-FITC-labeled dextran (both 70 kDa and 250 kDa) in peritubular vessels and glomerular capillaries were similar in normal control rats and vehicle saline injected rats at days 0, 2, 6 and 10 (not shown). Table 2 provides a summary of these findings.

Ultrastructural findings of 250-kDa-dextran-infused kidneys

Electron microscopy showed almost intact peritubular capillary endothelial lining without detachment or desquamation during the experimental period (Fig. 10A, B, C, D). Although some parts of endothelial cytoplasm became hypertrophic or swollen as early as day 2, no apparent alteration of fenestrae was evident in the attenuated parts of the endothelium (Fig. 10B, C, D). In normal kidneys, TBM and the basement membrane of the endothelium could be clearly distinguished. However, after induction of ARF, the basement membrane of the endothelium became obscure and somewhat thickened (Fig. 10B, C, D) and could not be clearly separated from TBM (Fig. 10D), suggesting the accumulation of plasma proteins and/or extracellular matrices in the peritubular regions and TBM.

In normal control kidneys, 250-kDa dextran was confined to the capillary lumen (Fig. 10A). At days 2–6, dextran was often found in clusters in the cytoplasm of endothelial cells, in peritubular regions and in TBM (Fig. 10B, C, D), where regenerating PTs could be found (Fig. 10D). At days 2–6, dextran could be also found in the tubular lumen, where PTs were severely damaged or disappeared (Fig. 10C). The amount of extravasated dextran was markedly decreased at day 10 (not shown).

Western-blot analysis

VEGF-147 blots demonstrated that expected VEGF isoforms, VEGF164 and VEGF188, were identified by their molecular weight as ~23 kDa and ~30–31 kDa, respectively (Fig. 11A). After induction of ARF, VEGF levels markedly increased and remained at high levels until day 10 (Fig. 11A). eNOS blots demonstrated that the band of the expected size (~140 kDa) was minimal in normal control kidney and markedly increased after induction of ARF, but transiently reduced at day 2 (Fig. 11B).

NO inhibition study

In L-NAME-treated rats, we observed reduced fluorescence of infused-FITC-labeled dextran (250 kDa) in the peritubular regions and TBM and in the tubular lumen compared with vehicle-treated rats at day 6 (Fig. 12A, B), suggesting that inhibition of NO during the repair phase of this model resulted in decrease in vascular hyperpermeability. In L-NAME-treated rats (n=5), serum creatinine level was significantly increased at day 6 and the number of Ki67-positive regenerating PT cells (Fig. 12C, D) was significantly reduced compared with vehicle-treated rats at day 6 (n=5) (serum creatinine; 3.91± 0.62 mg/dl in vehicle group, 5.39±1.09 mg/dl in

Table 2 Findings of immunofluorescence studies and microangiography. *Control* before induction of acute renal failure (ARF). Staining intensity: – negative, + weak, ++ moderate, +++ strong. *TBM* tubular basement membrane, *FITC* fluorescein isothiocyanate

	Staining pattern	Control	Days after injection of gentamicin			
			0	2	6	10
Fibrinogen	Peritubular	+	++	++	+++	+
	TBM	–	–	+*	++*	–
Plasma fibronectin	Peritubular	+	++	++	+++	+
	TBM	–	+	++*	+++*	–
FITC dextran (70 kDa)	Peritubular	+	++	+++	+++	++
	TBM	–	+	++*	+++*	+
FITC dextran (250 kDa)	Peritubular	+	+	++	+++	++
	TBM	–	+	++*	+++*	–

* In tubular lumen

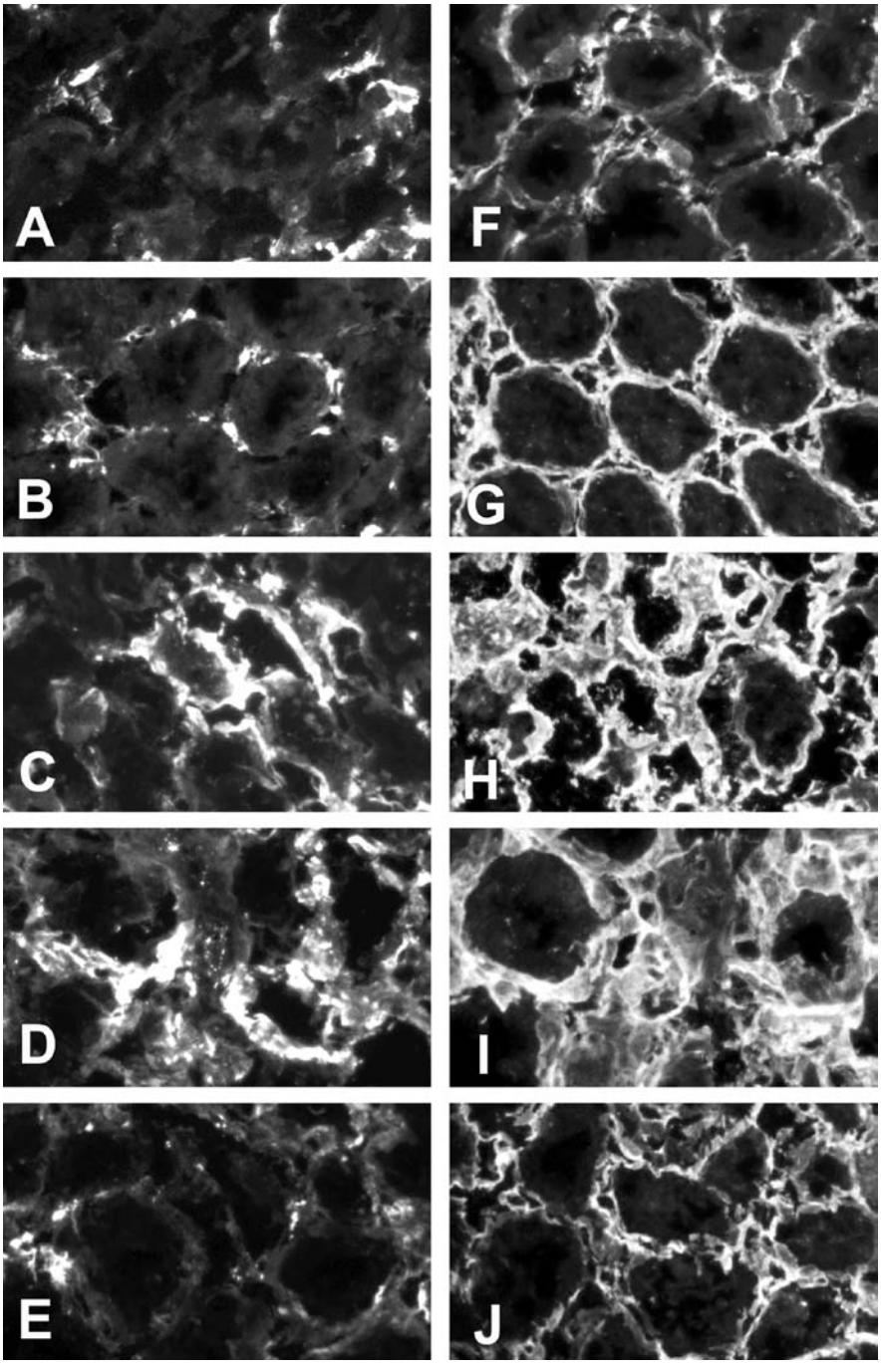

Fig. 8 Photomicrographs of immunofluorescence for fibrinogen (**A**–**E**) and plasma fibronectin (**F**–**J**) in the renal cortex of control rats [before induction of acute renal failure (ARF), **A**, **F**] and at days 0 (**B**, **G**), 2 (**C**, **H**), 6 (**D**, **I**) and 10 (**E**, **J**) after induction of ARF. Immunofluorescence of fibrinogen and plasma fibronectin in the normal kidneys was almost confined to the small areas in the peritubular capillaries in the cortex (**A**, **F**), but increased in the peritubular regions as early as day 0 (**B**, **G**), and found in tubular basement membrane (TBM) and the tubular lumen at days 2–6 (**C**, **D**, **H**, **I**). However, TBM staining pattern of plasma fibronectin was already found at day 0 (**G**). These staining patterns reached peak levels at day 6 (**D**, **I**), then decreased at day 10 (**E**, **J**). Original magnification, ×400 (**A**–**J**)

L-NAME group, $P<0.05$, the number of Ki67-positive regenerating PT cells per field; 22.7±2.7 in vehicle group, 17.6±2.0 in L-NAME group, $P<0.05$), indicating that inhibition of NO is linked to the inhibition of regenerative repair.

Discussion

In the present study, induction of ARF resulted in extravasation and deposition of fibrinogen (molecular weight, 340 kDa) and plasma fibronectin (molecular weight, 220 kDa), which reached peak levels on day 6, coinciding with the peak number of Ki67-positive regenerating PT. The presence of hyperpermeable peritubular capillaries was confirmed by the extravasation of injected FITC-labeled dextran (both 70-kDa and 250-kDa dextran), and the injected dextran was also found in the TBM and tubular lumen mainly at days 2–6, indicating that circulating macromolecules of about 250 kDa molecular weight could leak through the peritubular capillaries into the peritubular regions and modify the TBM, on which PTs actively regenerated. It is also possible that some circulating macromolecules reach the tubular lumen via

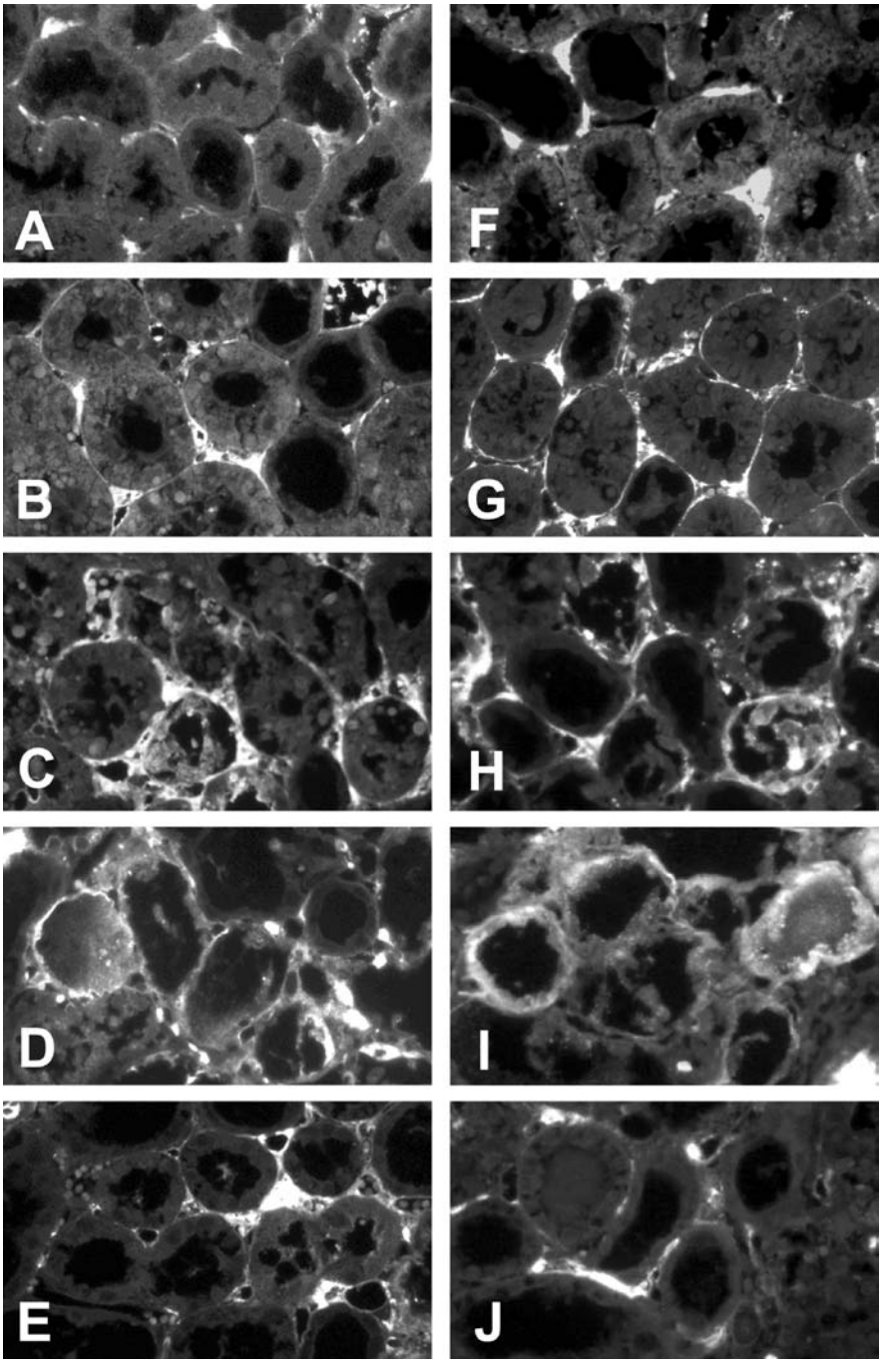

Fig. 9 Fluorescein isothiocyanate-labeled-70 kDa (**A**–**E**) and 250-kDa (**F**–**J**) dextran microangiography of renal cortex in rats before induction of acute renal failure (ARF) (**A**, **F**) and at days 0 (**B**, **G**), 2 (**C**, **H**), 6 (**D**, **I**) and 10 (**E**, **J**) after induction of ARF. In normal rats, fluorescence was found in peritubular vessels (**A**, **F**). After induction of ARF, fluorescence was increasingly found in peritubular regions and tubular basement membrane as early as day 0 (**B**, **G**), and in the tubular lumen at days 2–6 (**C**, **D**, **H**, **I**). Extravasation of both types of dextran reached peak levels at day 6 (**D**, **I**), then markedly decreased at day 10 (**E**, **J**). Original magnification, ×400 (**A**–**J**)

damaged and/or desquamated PTs in our model, as suggested in the post-ischemic rat kidney by Zuk et al. [47].

In wound healing, extravasated fibrinogen clots to form a fibrin gel into which other plasma proteins may be incorporated [45]. Fibrin is thought to be an essential component of the provisional matrix that supports cell–cell and cell–matrix interactions occurring during tissue remodeling and promotes the migration and proliferation of inflammatory cells, endothelial cells and interstitial cells participating in tissue repair [7, 10, 22]. The interaction of fibronectin with fibrin and its incorporation into fibrin clots are also important processes that promote cell adhesion and migration during wound healing [10, 22]. Fibrin(ogen) may provide a reservoir for cytokines and growth factors and has been shown to bind with high affinity to several angiogenic growth factors, including fibroblast growth factor-2 and VEGF [37, 38]. Therefore, it is likely that extravasated plasma fibrinogen and fibronectin acting as the provisional matrix play a role in tubular recovery after gentamicin-induced ARF.

The expression levels of VEGF and its receptor are closely regulated during vasculogenesis and angiogenesis, including wound healing [6, 28]. Capillary hyperperme-

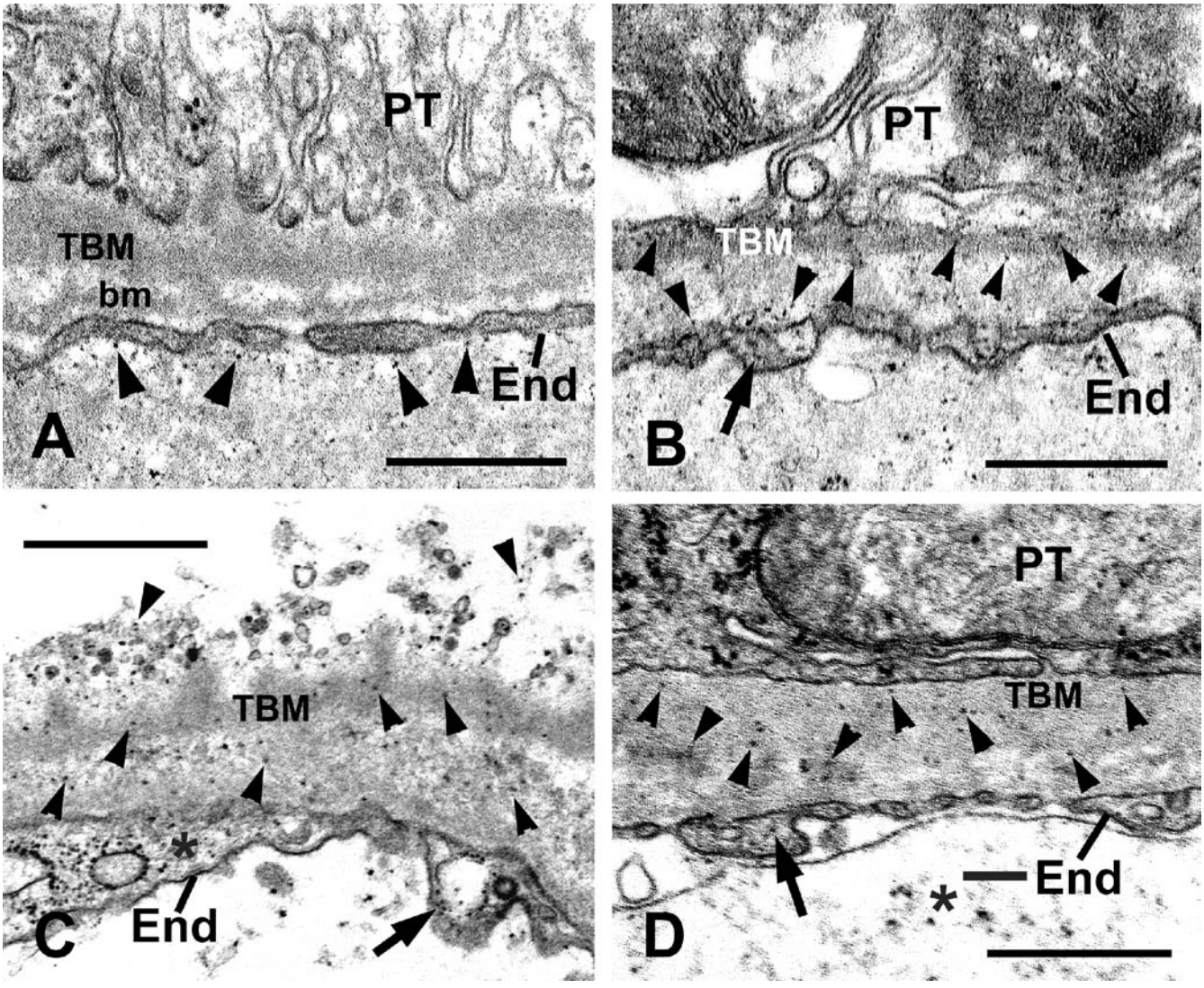

Fig. 10 Electron micrographs of renal cortex after 250-kDa dextran infusion. Localization of dextran particles (*arrowheads*) was confined to the peritubular capillary lumen in the normal control (**A**). At day 2, dextran particles were found in the peritubular regions and tubular basement membrane (TBM) (**B**). At day 6, dextran particles were found in the tubular lumen (**C**) and in the TBM, on which a proximal tubules (PT) cell regenerated (**D**). Note that the basement membrane of the endothelium became obscure at days 2 (**B**) and 7 (**C**, **D**). *End* peritubular capillary endothelium, *bm* basement membrane of the peritubular capillary endothelium, *Asterisk* hypertrophic or swollen endothelium. *Bars* 0.5 μm

ability is also known to occur during wound healing [9, 12], and VEGF appears to be involved, as evidenced by the overexpression of its receptor in the endothelium of regenerating vessels [27, 34]. Our results revealed upregulation of VEGF-147 protein in the cortex and increased immunoreactive VEGF-147 and VEGF Ab-5 in the damaged and regenerating PTs. Although immunoreactive VEGF receptors (Flt-1) and -2 (Flk-1) were not increased in peritubular capillaries, it is possible that increased VEGF released from the PTs can play a role in enhanced permeability via the VEGF/VEGF receptor system in this model. However, active proliferation of peritubular capillary endothelial cells was not found based on the findings of double immunostaining of RECA-1 and Ki67, suggesting vasculogenesis or angiogenesis may not be necessary for cellular recovery after ARF.

We also found that eNOS protein was markedly upregulated in the peritubular endothelium after induction of ARF. VEGF can induce the expression of eNOS and inducible NOS (iNOS) in vascular endothelial cells in vitro [17, 24] and promotes NO production. Murohara et al. [30] reported that NO and prostacyclin were produced by the interaction of VEGF with its VEGF receptor-2 as mediators of VEGF-induced vascular permeability. Furthermore, it is reported that inhibition of in vivo NO production results in reduced angiogenesis and vascular permeability induced by VEGF [30, 46] and that eNOS plays a predominant role in VEGF-induced angiogenesis and vascular permeability [15]. The data presented in this

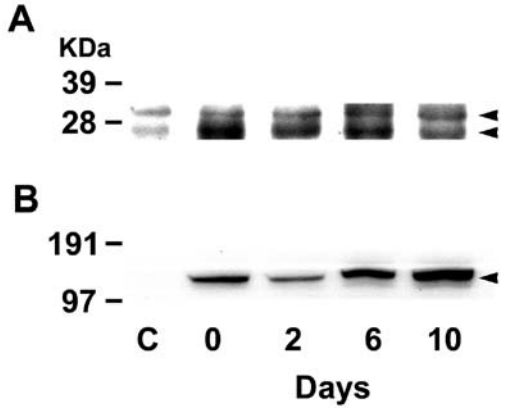

Fig. 11 Western blots of protein from the renal cortex incubated with antibodies for vascular endothelial growth factor (VEGF)-147 (**A**) and endothelial nitric oxide synthase (**B**). VEGF-147 blots (**A**) showed weak bands of ~23 kDa (*lower arrowhead*) and ~30–31 kDa (*upper arrowhead*) in normal control, and the bands became stronger after induction of acute renal failure (ARF) (at days 0, 2, 6 and 10 days). On the other hand, eNOS blots (**B**) showed bands of ~140 kDa (*arrowhead*) only after induction of ARF. **C** Normal control

study demonstrated that the NOS inhibitor L-NAME decreased hyperpermeability of peritubular capillaries during the recovery phase, suggesting that NO is an important mediator of vascular hyperpermeability in this model. However, it is not known whether this is a direct effect of NO on endothelial cells or whether NO merely decreases renal blood flow, although it is unlikely that NO-mediated vascular hyperpermeability is dependent on increase in blood flow. Thus, our findings that upregulation of VEGF in the PTs and of eNOS in the peritubular endothelial cells might suggest that NO, which may be produced through eNOS by VEGF, plays a role in VEGF-induced peritubular hyperpermeability.

eNOS can be positively or negatively regulated by several factors, such as protein–protein interactions and covalent modifications [1]. In this study, immunoreactive eNOS showed intense staining in both the glomerular endothelium and the peritubular capillary endothelium after induction of ARF; however, eNOS blots demonstrated transient reduction of increased eNOS at day 2. It is reported that increased reactive oxygen species (ROS) generation plays a role in the NO-mediated inhibition of eNOS in endothelial cells [4, 5]. Thus, it might be possible that ROS generated by PT cells and mesangial cells during the injury phase of this model could inhibit eNOS production at day 2, as ROS are considered to be important mediators of gentamicin-induced nephrotoxicity [11, 25].

L-NAME treatment in this model inhibited the regenerative repair of PT as judged by Ki67-positive PT cells and aggravated renal dysfunction as judged by serum creatinine level. We postulate that decreased peritubular hyperpermeability affected, at least in part, the morphological and functional recovery from gentamicin-induced ARF. However, L-NAME is a non-selective NOS inhibitor [21]; thus, it is difficult to assess the results because different types of NOS may differently affect cell viability and function [1]. Moreover, it is also possible that inhibition of PT regeneration after L-NAME treatment in this model is secondarily caused by disturbance of NO-dependent regulation of renal hemodynamics and glomerular function as previously reported in gentamicin-induced ARF [44].

Due to the persistent expression of VEGF by epithelial cells adjacent to fenestrated endothelium, it has been

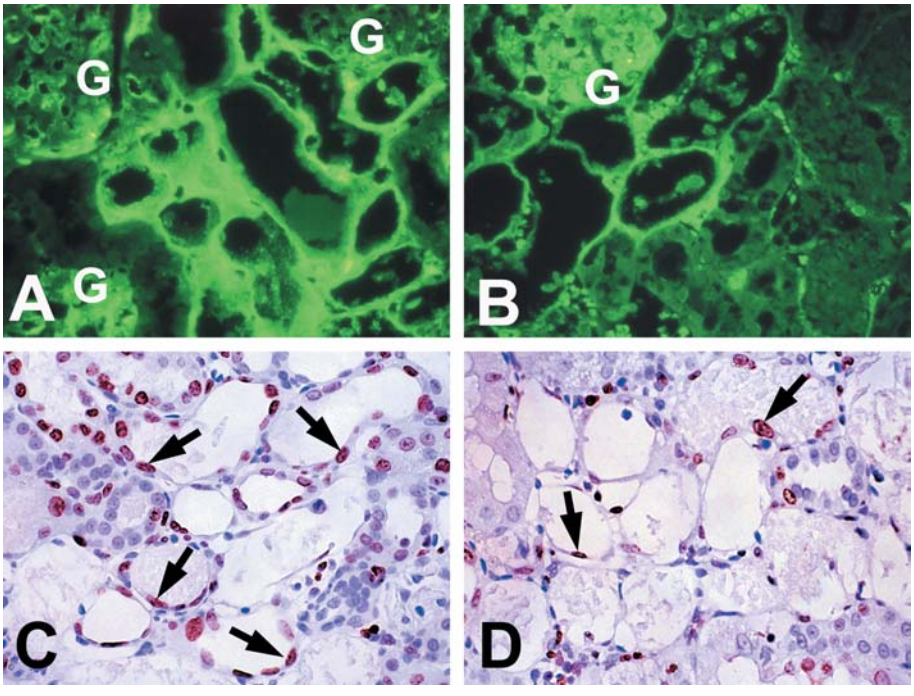

Fig. 12 Fluorescein isothiocyanate-labeled-250-kDa dextran microangiography (**A**, **B**) and photomicrographs of immunostaining for Ki67 (**C**, **D**) in vehicle-treated (**A**, **C**) and L-NAME-treated (**B**, **D**) rats at day 6 after induction of ARF. *G* glomerulus. *Arrows* Ki67-positive proximal tubule cells

hypothesized that VEGF is involved in the maintenance of fenestrae in the endothelium [3]. While the peritubular capillary endothelium is fenestrated in normal kidneys, plasma proteins do not leak freely into the interstitial regions. The relative contribution of pathways of plasma protein extravasation through fenestrated endothelial layer is difficult to assess, since leakage of tracer macromolecules through these fenestrae cannot be excluded, even if other pathways, such as open intercellular junctions and transcellular pores, [3] do exist. In the present study, however, infused 250-kDa dextran could be found in the cytoplasm of peritubular endothelial cells as well as in the abluminal side of the adjacent endothelium after induction of ARF, suggesting the existence of transcellular pathway. However, due to technical limitations of tissue fixation, the resolution was not sufficient to evaluate whether dextran in the cytoplasm was extravasated by the way of vesiculovacuolar organelles [13] in this study. However, our results showed a significant infiltration of ED1-positive macrophages into the peritubular regions from day 2 to day 10. Yet, plasma protein extravasation was found as early as day 0, and the gap formation of peritubular capillary endothelium could not be observed in the cortex.

VEGF is also reported to act as a maintenance factor on endothelial cells through stimulation of anti-apoptotic pathways [16], and this function may be implicated in other renal disease models [18, 40]. Induction of ARF in our experimental model resulted in hypertrophy or swelling of the peritubular capillary endothelium and slight reduction in constitutive molecule of rat endothelium, RECA-1, at day 6, suggestive of sublethal endothelial damage. Therefore, VEGF might also play a protective role for peritubular endothelial cells. The exact role of VEGF in the present model remains to be clarified.

In conclusion, our data suggested that plasma protein extravasation occurred, leading to matrix remodeling, such as the process of wound healing during the tubular repair in gentamicin-induced ARF. VEGF/VEGF receptor system with eNOS induction might be responsible for this process.

References

1. Alderton WK, Cooper CE, Knowles RG (2001) Nitric oxide synthases: structure, function and inhibition. Biochem J 357:593–615
2. Basile DP, Martin DR, Hammerman MR (1998) Extracellular matrix-related genes in kidney after ischemic injury: potential role for TGF-β in repair. Am J Physiol 275:F894–F903
3. Breier G, Albrecht U, Sterrer S, Risau W (1992) Expression of vascular endothelial growth factor during embryonic angiogenesis and endothelial cell differentiation. Development 114:521–532
4. Brennan LA, Wedgwood S, Bekker JM, Black SM (2002) The overexpression of copper-zinc superoxide dismutase protects NOS III from nitric oxide-mediated inhibition. DNA Cell Biol 21:827–838
5. Brennan LA, Wedgwood S, Black SM (2002) The overexpression catalase reduces NO-mediated inhibition of endothelial NO synthase. IUBMB Life 54:261–265
6. Brown LF, Yeo KT, Berse B, Yeo TK, Senger DR, Dvorak HF, van de Water L (1992) Expression of vascular permeability factor (vascular endothelial growth factor) by epidermal keratinocytes during wound healing. J Exp Med 176:1375–1379
7. Brown LF, Lanir N, McDonagh J, Tognazzi K, Dvorak AM, Dvorak HF (1993) Fibroblast migration in fibrin gel matrices. Am J Pathol 142:273–283
8. Carmeliet P, Jain RK (2000) Angiogenesis in cancer and other diseases. Nature 407:249–257
9. Clark RA (1985) Cutaneous tissue repair: basic biologic considerations. I. J Am Acad Dermatol 13:701–725
10. Corbett SA, Wilson CL, Schwarzbauer JE (1996) Changes in cell spreading and cytoskeletal organization are induced by adhesion to a fibronectin-fibrin matrix. Blood 88:158–166
11. Cuzzocrea S, Mazzon E, Dugo L, Serraino I, Di Paola R, Britti D, De Sarro A, Pierpaoli S, Caputi A, Masini E, Salvemini D (2002) A role for superoxide in gentamicin-mediated nephropathy in rats. Eur J Pharmacol 450:67–76
12. Dvorak HF (1986) Tumors: wounds that do not heal. Similarities between tumor stroma generation and wound healing. N Engl J Med 315:1650–1659
13. Feng D, Nagy JA, Hipp J, Dvorak HF, Dvorak AM (1996) Vesiculo-vacuolar organelles and the regulation of venule permeability to macromolecules by vascular permeability factor, histamine, and serotonin. J Exp Med 183:1981–1986
14. Ferrara N, Davis-Smyth T (1997) The biology of vascular endothelial growth factor. Endocr Rev 18:4–25
15. Fukumura D, Gohongi T, Kadambi A, Izumi Y, Ang J, Yun CO, Buerk DG, Huang PL, Jain RK (2001) Predominant role of endothelial nitric oxide synthase in vascular endothelial growth factor-induced angiogenesis and vascular permeability. Proc Natl Acad Sci U S A 98:2604–2609
16. Gerber HP, McMurtrey A, Kowalski J, Yan M, Keyt BA, Dixit V, Ferrara N (1998) Vascular endothelial growth factor regulates endothelial cell survival through the phosphatidylinositol 3′-kinase/Akt signal transduction pathway. Requirement for Flk-1/KDR activation. J Biol Chem 273:30336–30343
17. Hood JD, Meininger CJ, Ziche M, Granger HJ (1998) VEGF upregulates ecNOS message, protein, and NO production in human endothelial cells. Am J Physiol 274:H1054–H1058
18. Kanellis J, Fraser S, Katerelos M, Power DA (2000) Vascular endothelial growth factor is a survival factor for renal tubular epithelial cells. Am J Physiol Renal Physiol 278:F905–F915
19. Kanellis J, Paizis K, Cox AJ, Stacker SA, Gilbert RE, Cooper ME, Power DA (2002) Renal ischemia-reperfusion increases endothelial VEGFR-2 without increasing VEGF or VEGFR-1 expression. Kidney Int 61:1696–1706
20. Kang DH, Hughes J, Mazzali M, Schreiner GF, Johnson RJ (2001) Impaired angiogenesis in the remnant kidney model: II. Vascular endothelial growth factor administration reduces renal fibrosis and stabilizes renal function. J Am Soc Nephrol 12:1448–1457
21. Knowles RG, Moncada S (1994) Nitric oxide synthases in mammals. Biochem J 298:249–258
22. Knox P, Crooks S, Rimmer CS (1986) Role of fibronectin in the migration of fibroblasts into plasma clots. J Cell Biol 102:2318–2323
23. Kosek JC, Mazze RI, Cousins MJ (1974) Nephrotoxicity of gentamicin. Lab Invest 30:48–57
24. Kroll J, Waltenberger J (1998) VEGF-A induces expression of eNOS and iNOS in endothelial cells via VEGF receptor-2 (KDR). Biochem Biophys Res Commun 252:743–746
25. Martinez-Salgado C, Eleno N, Tavares P, Rodriguez-Barbero A, Garcia-Criado J, Bolanos JP, Lopez-Novoa JM (2002) Involvement of reactive oxygen species on gentamicin-induced mesangial cell activation. Kidney Int 62:1682–1692
26. Masuda Y, Shimizu A, Mori T, Ishiwata T, Kitamura H, Ohashi R, Ishizaki M, Asano G, Sugisaki Y, Yamanaka N (2001) Vascular endothelial growth factor enhances glomerular capillary repair and accelerates resolution of experimentally induced glomerulonephritis. Am J Pathol 159:599–608

27. Millauer B, Wizigmann-Voos S, Schnurch H, Martinez R, Moller NP, Risau W, Ullrich A (1993) High affinity VEGF binding and developmental expression suggest Flk-1 as a major regulator of vasculogenesis and angiogenesis. Cell 72:835–846
28. Miller JW, Adamis AP, Shima DT, D'Amore PA, Moulton RS, O'Reilly MS, Folkman J, Dvorak HF, Brown LF, Berse B, Yeo TK, Yeo KT (1994) Vascular endothelial growth factor/vascular permeability factor is temporally and spatially correlated with ocular angiogenesis in a primate model. Am J Pathol 145:574–584
29. Monacci WT, Merrill MJ, Oldfield EH (1993) Expression of vascular permeability factor/vascular endothelial growth factor in normal rat tissues. Am J Physiol 264:C995–C1002
30. Murohara T, Horowitz JR, Silver M, Tsurumi Y, Chen D, Sullivan A, Isner JM (1998) Vascular endothelial growth factor/vascular permeability factor enhances vascular permeability via nitric oxide and prostacyclin. Circulation 97:99–107
31. Nissen NN, Polverini PJ, Koch AE, Volin MV, Gamelli RL, DiPietro LA (1998) Vascular endothelial growth factor mediates angiogenic activity during the proliferative phase of wound healing. Am J Pathol 152:1445–1452
32. Ohashi R, Shimizu A, Masuda Y, Kitamura H, Ishizaki M, Sugisaki Y, Yamanaka N (2002) Peritubular capillary regression during the progression of experimental obstructive nephropathy. J Am Soc Nephrol 13:1795–1805
33. Palade GE, Simionescu M, Simionescu N (1979) Structural aspects of the permeability of the microvascular endothelium. Acta Physiol Scand 463[Suppl]:11–32
34. Peters KG, De Vries C, Williams LT (1993) Vascular endothelial growth factor receptor expression during embryogenesis and tissue repair suggests a role in endothelial differentiation and blood vessel growth. Proc Natl Acad Sci U S A 90:8915–8919
35. Pillebout E, Burtin M, Yuan HT, Briand P, Woolf AS, Friedlander G, Terzi F (2001) Proliferation and remodeling of the peritubular microcirculation after nephron reduction: association with the progression of renal lesions. Am J Pathol 159:547–560
36. Quinn TP, Peters KG, De Vries C, Ferrara N, Williams LT (1993) Fetal liver kinase 1 is a receptor for vascular endothelial growth factor and is selectively expressed in vascular endothelium. Proc Natl Acad Sci U S A 90:7533–7537
37. Sahni A, Francis CW (2000) Vascular endothelial growth factor binds to fibrinogen and fibrin and stimulates endothelial cell proliferation. Blood 96:3772–3778
38. Sahni A, Odrljin T, Francis CW (1998) Binding of basic fibroblast growth factor to fibrinogen and fibrin. J Biol Chem 273:7554–7559
39. Shibuya M (1995) Role of VEGF-flt receptor system in normal and tumor angiogenesis. Adv Cancer Res 67:281–316
40. Suga S, Kim YG, Joly A, Puchacz E, Kang DH, Jefferson JA, Abraham JA, Hughes J, Johnson RJ, Schreiner GF (2001) Vascular endothelial growth factor (VEGF121) protects rats from renal infarction in thrombotic microangiopathy. Kidney Int 60:1297–1308
41. Thadhani R, Pascual M, Bonventre JV (1996) Acute renal failure. N Engl J Med 334:1448–1460
42. Toback FG (1992) Regeneration after acute renal tubular necrosis. Kidney Int 41:226–246
43. Tufro A, Norwood VF, Carey RM, Gomez RA (1999) Vascular endothelial growth factor induces nephrogenesis and vasculogenesis. J Am Soc Nephrol 10:2125–2134
44. Valdivielso JM, Blantz RC (2002) Acute renal failure: is nitric oxide the bad guy? Antioxid Redox Signal 4:925–934
45. Van de Water L, Ffrench-Constant C, Brown L (1992) Fibronectin expression during cutaneous wound healing. In: Adzick NS, Longaker MJ (eds) Fetal wound healing. Elsevier Science Publishing Co., Inc., New York, pp 281–301
46. Ziche M, Morbidelli L, Choudhuri R, Zhang HT, Donnini S, Granger HJ, Bicknell R (1997) Nitric oxide synthase lies downstream from vascular endothelial growth factor-induced but not basic fibroblast growth factor-induced angiogenesis. J Clin Invest 99:2625–2634
47. Zuk A, Bonventre JV, Matlin KS (2001) Expression of fibronectin splice variants in the postischemic rat kidney. Am J Physiol Renal Physiol 280:F1037–F1053

Virchows Arch (2004) 444:375–382
DOI 10.1007/s00428-003-0967-z

ORIGINAL ARTICLE

Ryuichi Wada · Soroku Yagihashi

Nitric oxide generation and poly(ADP ribose) polymerase activation precede beta-cell death in rats with a single high-dose injection of streptozotocin

Received: 4 September 2003 / Accepted: 10 December 2003 / Published online: 4 February 2004

Abstract Streptozotocin (STZ) is widely used for the induction of diabetes in animals by causing destruction of pancreatic beta cells. This experiment was designed to elucidate the sequential process of beta-cell destruction in rats with a single high-dose injection of STZ. At 0, 2, 5, 8 and 24 h after injection, rats were perfused with Krebs-Ringer buffer with dichlorofluorescein diacetate (DCF-DA), a marker for free radicals, and the pancreata were pathologically analyzed. Injection of STZ rapidly elicited an increase in fluorescence of DCF-DA in beta cells at 2 h after the injection. The fluorescence was diminished by carboxy-PTIO, a specific scavenger of nitric oxide (NO), but not by L-NAME, an inhibitor of NO synthase. During this process, an inducible form of NO synthase was not detected. Thereafter, upregulated expression of poly(ADP ribose) polymerase (PARP) and massive beta-cell death were detected at 5–8 h after injection. Migration of macrophages into the islet was conspicuous at 24 h, clearing up the debris of destroyed beta cells. Nicotinamide, a PARP inhibitor, significantly inhibited beta-cell death without apparent suppression of NO generation at 2 h. The current study documented serial processes of STZ-induced beta-cell death, starting with NO generation and PARP activation followed by a clearance with macrophages, where the activation of PARP plays a central role in beta-cell death.

Keywords Beta cell · Streptozotocin · Cell death · Nitric oxide · Poly(ADP ribose) polymerase

R. Wada (✉) · S. Yagihashi
Department of Pathology,
Hirosaki University School of Medicine,
5 Zaifu-cho, 036–8562 Hirosaki, Japan
e-mail: ryuichi@cc.hirosaki-u.ac.jp
Tel.: +81-172-395025
Fax: +81-172-395026

Introduction

Streptozotocin (STZ) is a chemical agent widely used for the induction of diabetes in animals. The agent causes destruction of pancreatic beta cells, the accompanying marked reduction of insulin levels and hyperglycemia. Underlying mechanisms for the STZ-induced beta-cell death are not entirely understood. Nucleic acid alkylation [24, 25] or excessive nitric oxide (NO) production [13] has been proposed to contribute to STZ-induced beta-cell injury. Indeed, the cytotoxic effect of STZ is exerted mainly by alkylation of genomic DNA [24, 25]. During this process, poly(ADP ribose) polymerase (PARP) is activated to play a key role in the destruction of beta cells [5, 14, 25]. However, it has also been shown that STZ generates NO [13], which could damage genomic DNA and may cause beta-cell dysfunction by inhibiting mitochondrial enzymes [12, 19]. Implication of NO in beta-cell death is, however, still controversial, as not all studies confirmed generation of NO after STZ treatment [15]. Temporal changes of rapid beta-cell death and interrelationships of the molecules related to the cell death are largely unknown in vivo. Since rapid destruction of beta cells is encountered in patients with fulminant non-autoimmune type-1 diabetes [8, 9], it would be important to obtain information on the precise changes of beta cells undergoing cell death after STZ injection.

The aim of the current experiment is, therefore, to elucidate the sequential process of rapid beta-cell destruction in rats injected with a single high-dose STZ, with special reference to generation of NO and activation of PARP.

Materials and methods

Experimental rats and injection of STZ

Male 8- to 10-week-old Wistar rats were used for the experiment. The body weights ranged from 280 g to 320 g. STZ (Sigma Chemicals Co, St. Louis, MI, USA) was dissolved in citrate buffer (pH 4.2) and injected into rats from the tail vein at a dose of 40 mg/

kg after overnight fasting. At the time of injection (0) and 2, 5, 8 and 24 h after the STZ injection, glucose levels were measured on the blood from tail tips by glucose oxidase method with plastic strips of To-Echo Super (Eiken, Kyoto, Japan). At each time point, five rats each from STZ-injected rats were deeply anesthetized by pentobarbital (Abbott Laboratories, North Chicago, IL, USA). The whole blood was obtained from the vena cava, and the sera were separated by centrifugation. The serum insulin levels were determined by the enzyme-linked immunosorbent assay kit for rat insulin (Morinaga, Yokohama, Japan). The experiment followed the Guidelines for Animal Experimentation, Hirosaki University (approval number M01012).

In situ detection of free radical

The in vivo free radical generation was detected by the perfusion method adapted from the method described by Suematsu et al. [17]. Under the deep anesthesia with pentobarbital, a 14-G catheter was inserted into the abdominal aorta just above the renal arteries, and the aorta was clumped at the thoracic level. Then, the right cardiac auricle was cut, and the rats were perfused with 20 ml of Krebs-Ringer buffer (KRB) gassed with 95% O_2 and 5% CO_2 to wash out the blood. Then, KRB with 10 μM dichlorofluorescein-diacetate (DCF-DA) (Molecular Probe, Eugene, OR, USA) was perfused by drip infusion from the aorta. The perfusate also contained 100 μM carboxy-2-phenyl-4,4,5,5-tetramethylimidazoline-1-oxyl-3-oxide (carboxy-PTIO, DOJINDO Laboratories, Kumamoto, Japan) or 100 μM L-NAME. After the perfusion, the whole pancreata were dissected out, fixed in 10% formalin and processed to be embedded in paraffin. Sections 5 μm thick were counterstained with propidium iodide (Molecular Probe). The sections were observed under LASER-scan microscopy (LSM-300, Zeiss, Germany). The fluorescence images of the islets were scanned with constant values of brightness and contrast for the comparison of difference of fluorescence intensities between samples. From each experimental rat, images of ten islets were scanned with a 40× objective lens and stored in a magnetico-optical disk.

Immunostaining

Immunostaining was done on 4-μm-thick paraffin sections. After deparaffinization and quenching of endogenous peroxidase, antibodies against insulin, glucagon (raised in the author's laboratory), an inducible form of NO synthase (Pharmingen, San Diego, CA, USA), ED1 (Chemicon, Temecula, CA, USA) and PARP (Santa-Cruz, Santa Cruz, CA, USA) were applied, and the sections were incubated at 4°C overnight. They were processed with biotin-streptavidin peroxidase method using an SAB-PO kit (Nichirei, Tokyo, Japan). The peroxidase activity was visualized with diaminobenzidine and hydrogen peroxide. Normal pancreas and lymph nodes were used as positive control, and specificity was determined in the slides using isotypic primary antibodies.

Terminal dUTP nick end-labeling staining

Terminal dUTP nick end-labeling (TUNEL) staining was done using Apoptag (Oncor, Gaithersburg, MD, USA). The deparaffinized sections were treated with 0.1% trypsin for 30 min at 37°C. The labeling was done with reaction solution containing terminal deoxyribonucleotide transferase and digoxigenin-dUTP. Incorporated digoxigenin-dUTP was detected by peroxidase-labeled anti-digoxigenin antibody, and peroxidase activity was visualized with diaminobenzidine and hydrogen peroxide. For double staining of TUNEL with insulin, the sections were subsequently treated with anti-insulin antibody and then processed with an SAB-ALP kit. The alkaline phosphatase reaction was visualized with naphthol-AS-BI-phosphate (Sigma Chemicals Co) and hexazotized new fuchsin as chromogen. The positive reaction was confirmed in dying lymphocytes in the lymph nodes, and specificity of the reaction was determined in the negative reaction without terminal deoxyribonucleotide transferase.

Nicotinamide treatment

To examine the role of PARP on beta-cell death, nicotinamide (Wako Pure Chemicals Industries, Ltd., Osaka, Japan), a potent PARP inhibitor, was administrated to the rats. Nicotinamide was dissolved in physiological saline and given intraperitoneally at a dose of 350 mg/kg at 10 min before and 3 h after the injection of STZ [23]. Control rats were given physiological saline. STZ was injected to rats from the tail vein at a dose of 40 mg/kg. At 2 h and 5 h after injection, five rats each from nicotinamide-treated and untreated rats injected with STZ were used for the detection of in situ free radicals and for TUNEL staining and expression of PARP same as described above. Serum insulin levels were also determined.

Results

Morphological changes of the beta cells after STZ injection

At 2 h after STZ injection, islets appeared mostly unchanged on hematoxylin and eosin stained sections (Fig. 1A). TUNEL-positive cells were only sparsely detected in the islets (Fig. 1B). At 5 h after injection, most of the islet cells were swollen, and the nuclei were condensed (Fig. 1C). TUNEL stained positively in nearly all the nuclei of the islet cells (Fig. 1D). The cells were completely destroyed by 8 h after the injection. At 24 h, islet areas were filled with numerous macrophages (Fig. 1E), and TUNEL-positive cells were only sparsely found (Fig. 1F, *arrow*).

Double staining of TUNEL and immunostaining with insulin in the islets 5 h after the injection of STZ depicted TUNEL-positive reactions exclusively for beta-cells (Fig. 2A). In contrast to the changes of beta cells, alpha cells positive for glucagon appeared unaffected (Fig. 2B). At this time point, ED1-positive macrophages were found only sparsely in the islets (Fig. 2C). At 24 h, there were numerous ED1-positive macrophages in the islets, occupying the central area of the islets (Fig. 2D).

Changes of blood glucose levels and insulin levels

The changes of blood glucose and serum insulin levels were shown in Table 1. At 2 h after injection, blood glucose levels were increased by 2.5-fold of the basal level, and the insulin levels were slightly decreased. At 5 h, blood glucose levels were close to the basal level, but insulin levels were increased 8.7-fold. Some rats exhibited hypoglycemia below 4.4 mM at 5 h and 8 h. The blood glucose levels were exceeded 30.0 mM, accompanied by a 50% decrease in insulin levels at 24 h.

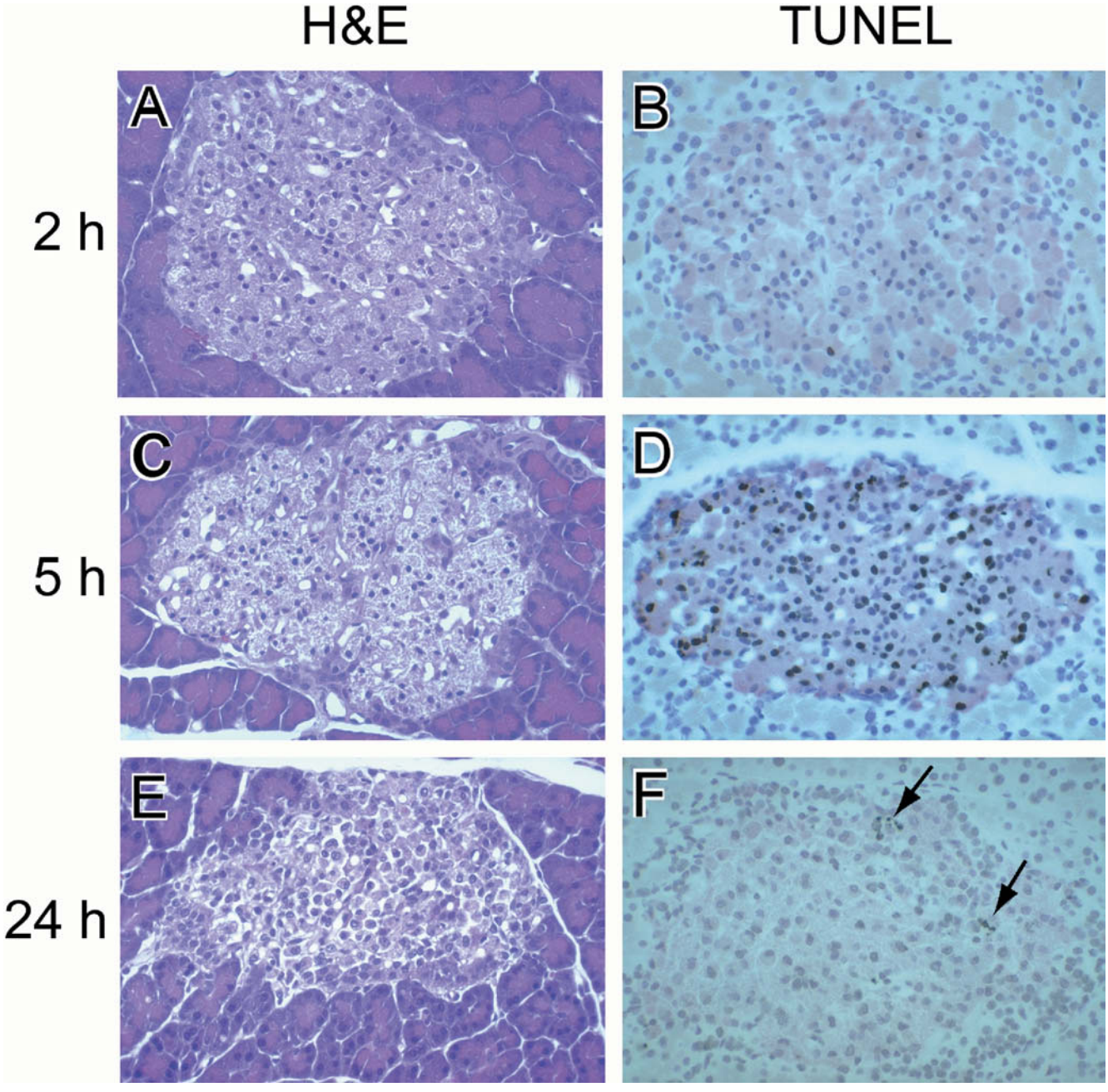

Fig. 1 Time-course change of pancreatic islets. **A**, **B** At 2 h. **C**, **D** At 5 h. **E**, **F** At 24 h. **F** At 24 h, terminal dUTP nick end-labeling (TUNEL)-positive cells were found very sparsely (*arrow*). **A**, **C**, **E** Hematoxylin and eosin. **B**, **D**, **F** Double-stained with TUNEL (*stained black*) and anti-insulin immunostaining (*stained pink*)

Table 1 Temporal change of blood glucose and serum insulin levels

	0	2 h	5 h	8 h	24 h
Blood glucose (mM)	5.9±0.7	14.9±4.1	6.4±1.8	8.0±2.2	31.3±2.6
Serum insulin (pg/ml)	473±126	396±252	4146±2183	2285±280	259±43

Generation of free radicals

Free radical formation in the islets was monitored by fluorescence intensity of DCF-DA under LASER scan microscopy. There was background fluorescence of DCF-DA in acinar cells, and the fluorescence in islet cells was only a trace level (Fig. 3A). At 2 h after the injection, an increase in fluorescence was observed in the islets and acinar cells as well (Fig. 3B). The increase appeared to be more conspicuous in islet cells compared with the

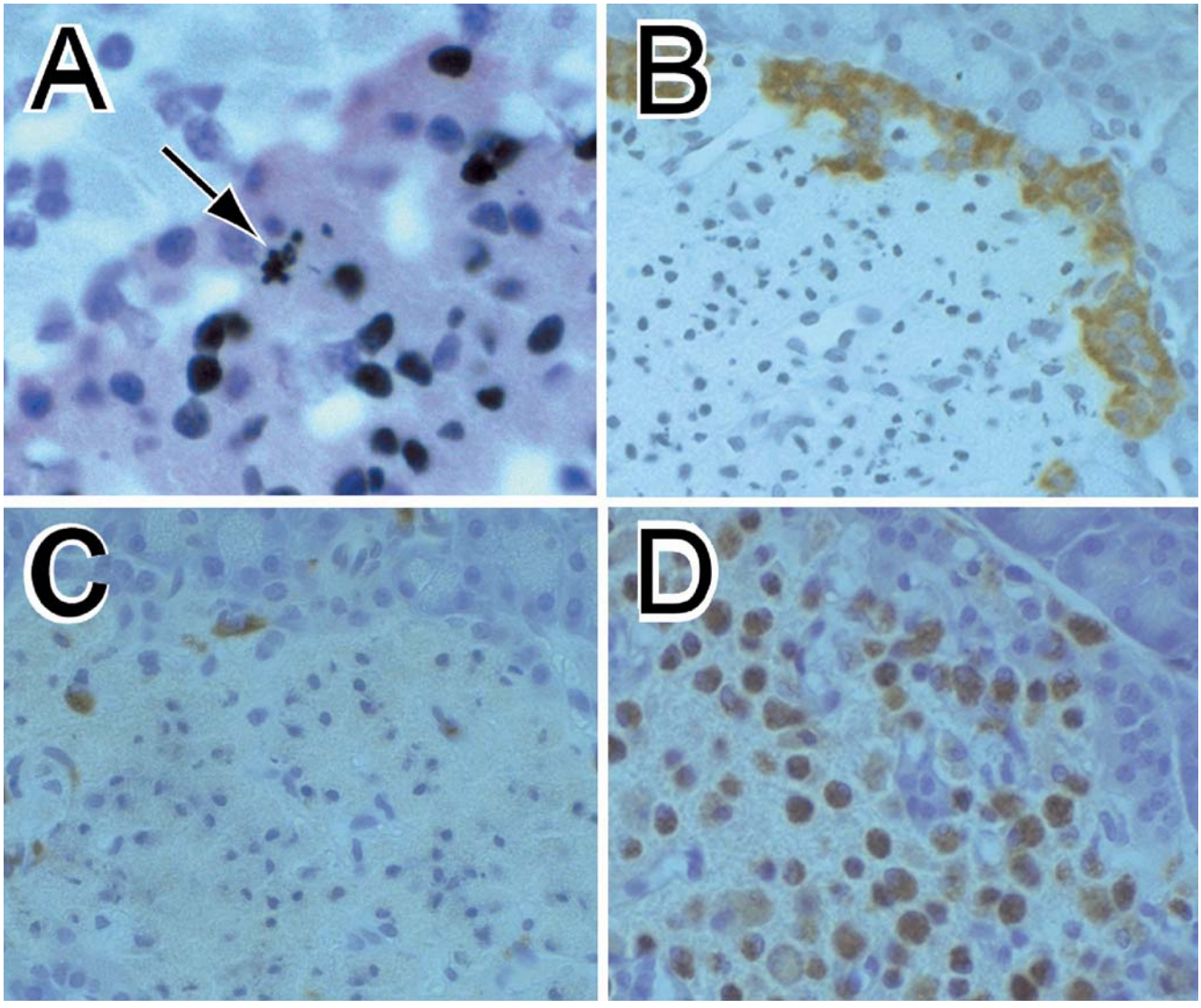

Fig. 2 Detailed changes of pancreatic islets and macrophage infiltration into the islets. **A** Double staining with terminal dUTP nick end-labeling (*stained black*) and immunostaining with insulin (*stained pink*) demonstrated condensed nuclei of beta cells. **B** Pancreatic alpha-cells were unchanged (anti-glucagon immunostaining). **C**, **D** Macrophage infiltration in the islets. **C** At 5 h. **D** At 24 h (anti-ED1 immunostaining)

fluorescence in acinar cells. The fluorescence was detected diffusely in the cytoplasm of beta cells. In contrast, the fluorescence in islets returned to background level at 5 h and 8 h (not shown). At 24 h after injection, strong dot-like fluorescence was detected in the macrophages infiltrating into the islets (Fig. 3C). The fluorescence observed in beta cells at 2 h was reduced when rats were perfused with combination of DCF-DA and carboxy-PTIO (Fig. 3D). The fluorescence intensity was unaffected in rats with combined perfusion with DCF-DA and L-NAME (Fig. 3E). Throughout the observation period, immunostaining did not reveal the expression of inducible nitric oxide synthase (iNOS) in the islets, whereas a weak reactivity was found in vascular endothelial and smooth muscle cells (Fig. 3F). The localization of fluorescence in the islet (Fig. 3G) was identified as the cells positive for insulin (Fig. 3H) using the immunostaining on the same sections used for LASER observations.

PARP activation in beta cells and effects of nicotinamide treatment

Beta cells at time 0 showed only weak positive reactions for PARP (Fig. 4A). When rats were injected with STZ, expression of PARP became intensified at 5 h and 8 h after the injection (Fig. 4B). The upregulated PARP expression was detected in the cytoplasm and also located on the nuclei (Fig. 4C).

Nicotinamide treatment markedly inhibited the destruction of beta cells at 5 h after injection of STZ (Fig. 5A), and TUNEL-positive cells were not detected (data

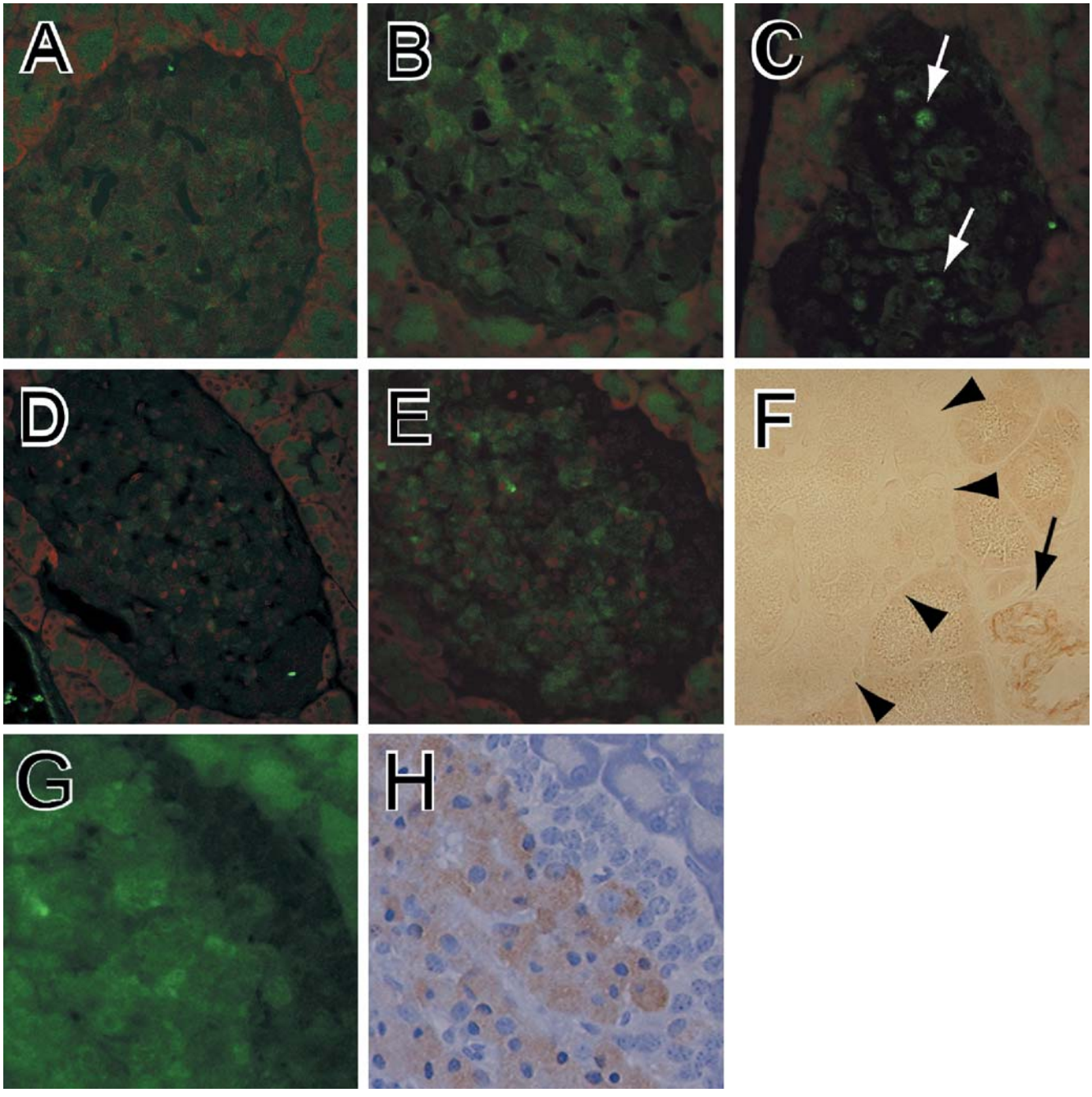

Fig. 3 The change of fluorescence of dichlorofluorescein diacetate (DCF-DA) in the pancreas. **A** At time 0. **B** At 2 h. **C** At 24 h. **D** The fluorescence at 2 h was reduced by carboxy-PTIO. **E** The fluorescence was not apparently changed by L-NAME. **F** Inducible form of NOS was detected in arterial wall (*arrow*) but not in the islet (*arrowheads*). **G** Fluorescence of DCF-DA in islets at 2 h. **H** Anti-insulin immunostaining. The fluorescence of DCF-DA was localized in insulin-positive cells

not shown). The increased fluorescence of DCF-DA in beta cells at 2 h after STZ injection was not much altered by nicotinamide treatment (Fig. 5B) compared with untreated rats (Fig. 3B). Upregulated expression of PARP in beta cells was neither altered by nicotinamide treatment (Fig. 5C).

Serum insulin levels of nicotinamide-treated rats at 2 h were comparable but slightly higher than those in untreated rats at 2 h (462±277 pg/ml versus 396±252 pg/ml in nicotinamide-treated and untreated rats, respectively). At 5 h after injection, the insulin levels were preserved in normal range in nicotinamide-treated rats (714±320 pg/ml versus 4146±2183 pg/ml in nicotinamide-treated and untreated rats, respectively).

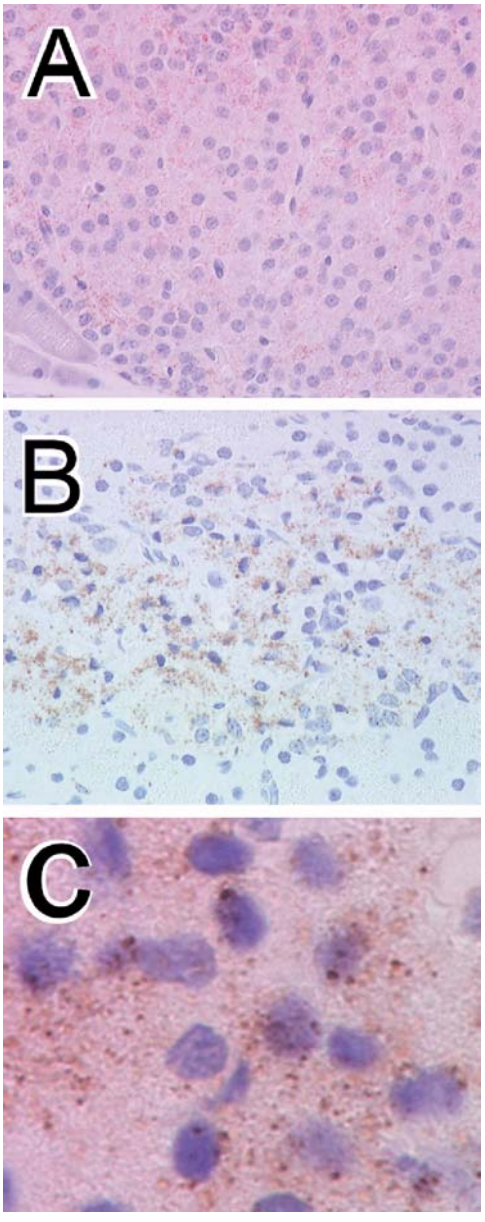

Fig. 4 Poly (ADP ribose) polymerase expression in pancreatic islet. **A** At time 0. **B** At 5 h. **C** Higher magnification of beta cells at 5 h

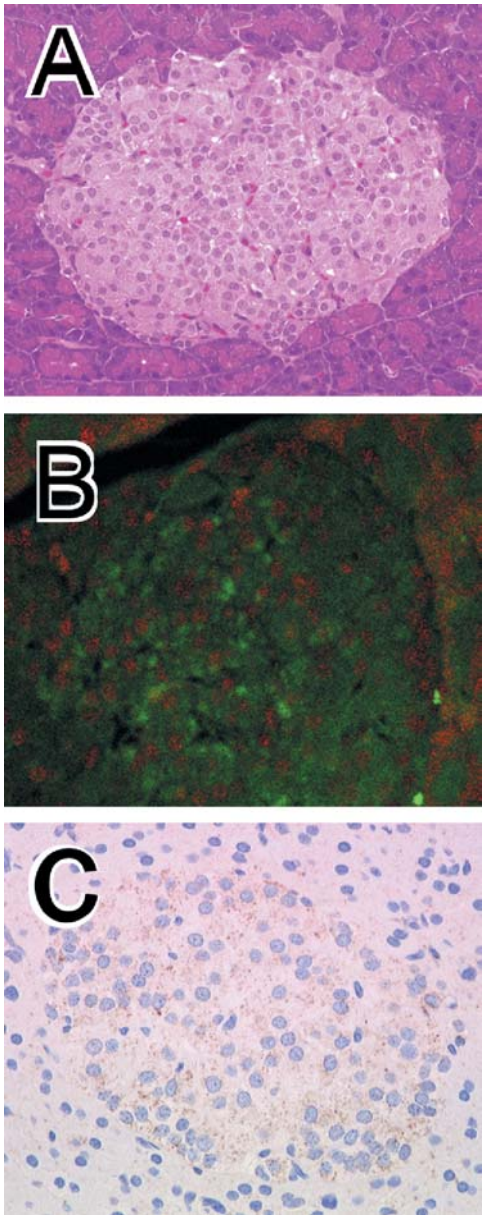

Fig. 5 The change of beta cells in nicotinamide-treated rat. **A** Destruction of beta cells was inhibited in nicotinamide-treated rat at 5 h after streptozotocin injection (hematoxylin and eosin). **B** Fluorescence of dichlorofluorescein diacetate in islets at 2 h after injection. **C** Poly(ADP ribose) polymerase (PARP) expression in the islets of nicotinamide-treated rat at 5 h (anti-PARP immunostaining)

Discussion

The current study documented the time-course changes of molecules related to islet beta-cell destruction in rats injected with a single high-dose STZ. First, at 2 h, NO generation was found in the beta cells, and insulin secretion appeared to be impaired. Then, at 5–8 h, PARP was upregulated and activated, and beta cells were destroyed. Serum insulin levels were markedly increased at 5–8 h, corresponding to the destruction of beta cells. By 24 h, the destroyed beta cells were phagocytosed by macrophages. At this time, the insulin levels were low, and blood glucose levels were markedly elevated. Although rapid destruction of pancreatic beta cells in rats with a single high-dose STZ has been repeatedly reported [4, 10, 18, 22], the current study first added the in vivo evidence on generation of NO and activation of PARP toward the destruction of beta cells.

The generation of free radicals in beta cells was detected as an increase in fluorescence of DCF-DA in the current study. The DCF-DA is a non-specific indicator for free radicals [21]. The fluorescence was reduced in the presence of carboxy-PTIO, a free radical scavenger

specific for NO [1]. Augmented expression of DCF-DA in islets in STZ-injected rats was unchanged by L-NAME, an inhibitor of constitutive form of NOS [3], and expression of iNOS was not induced in beta cells after the injection of STZ. These results were consistent with the previous in vitro studies on the beta-cell destruction, in which STZ committed as an NO donor [11, 12, 13, 19]. In contrast, Papaccio et al. reported that the generation of NO was not detected in the serum at 12 h and 24 h after the injection of a single high-dose STZ [15]. It is likely that the generation of NO is an early event, most evident at 2 h after the injection, as revealed in this study.

In our observation, there was an upregulated expression of PARP in beta cells at 5–8 h after injection of STZ. PARP is involved in the repair of damaged DNA [16]. Injury of DNA is critical to initiate the process of beta-cell death by STZ. DNA damage, in turn, activates PARP and causes reduction of nicotinamide adenine dinucleotide $(NAD)^+$ and adenosine triphosphate levels, resulting in beta-cell death [2, 25]. PARP inhibitors, such as nicotinamide and 3-aminobenzamide, prevent NAD^+ reduction and prevent beta cells from cell death [20, 25]. A trend of preservation of insulin secretion in nicotinamide-treated rats at 2 h may be due to the restoration of insulin secretion by inhibition of NAD^+ reduction, implicating that NAD^+ reduction may also affect insulin secretion [20, 22]. The pivotal role of PARP in beta-cell death was further supported by the targeting studies in which induction of diabetes by STZ was rescued in PARP knock-out mice [5, 14].

It was shown that the injury of DNA of beta cells is exerted mainly by direct alkylating activity of STZ [7]. In our experimental system, we could not address the question of how the alkylation of DNA was related to PARP activation in beta cells, as it was not feasible to examine the alkylating activity of STZ using a histological method. Nevertheless, an early augmented generation of NO followed by PARP activation after STZ injection detected in this study may indicate some interrelationships of these molecules with subsequent death processes. In particular, the implication of NO as a toxic agent for DNA cannot be completely neglected [12, 18]. It was also shown that generated NO can activate guanylate cyclase [19] and inhibit mitochondrial respiratory enzymes in beta cells in vitro [6]. Further studies on the role of NO generated in beta cells is still needed.

Acknowledgements The authors thank Miss Mari Tsujii for her skillful assistance. This work was supported by Grant in-Aid for Scientific Research from Ministry of Education, Science, Sports and Culture of Japan (07770144) to R.W.

References

1. Akaike T, Yoshida M, Miyamoto Y, Sato K, Kohno M, Sasamoto K, Miyazaki K, Ueda S, Maeda H (1993) Antagonistic action of imidazolineoxyl N-oxides against endothelium-derived relaxing factor/NO through a radical reaction. Biochemistry 32:827–832
2. Anderson T, Schein PS, McMenamin MG, Cooney DA (1974) Correlation with extent of depression of pancreatic islet nicotinamide adenine dinucleotide. J Clin Invest 54:672–677
3. Boer R, Ulrich WR, Klein T, Mirau B, Haas S, Baur I (2000) The inhibitory potency and selectivity of arginine substrate site nitric-oxide synthase inhibitors is solely determined by their affinity toward the different isoenzymes. Mol Pharmacol 58:1026–1034
4. Brosky G, Logothetopoulos J (1969) Streptozotocin diabetes in the mouse and guinea pig. Diabetes 18:606–611
5. Burkart V, Wang ZQ, Radons J, Heller B, Herceg Z, Stingl L, Wagner EF, Kolb H (1999) Mice lacking the poly(ADP-ribose) polymerase gene are resistant to pancreatic beta-cell destruction and diabetes development induced by streptozocin. Nat Med 5:314–319
6. Eizirik DL, Sandler S, Sener A, Malaisse WJ (1988) Defective catabolism of D-glucose and L-glutamine in mouse pancreatic islets maintained in culture after streptozotocin exposure. Endocrinology 123:1001–1007
7. Elsner M, Guldbakke B, Tiedge M, Munday R, Lenzen S (2000) Relative importance of transport and alkylation for pancreatic beta-cell toxicity of streptozotocin. Diabetologia 43:1528–1533
8. Imagawa A, Hanafusa T, Miyagawa J, Matsuzawa Y (2000) A novel subtype of type 1 diabetes mellitus characterized by a rapid onset and an absence of diabetes-related antibodies. Osaka IDDM Study Group. N Engl J Med 342:301–307
9. Imagawa A, Hanafusa T, Miyagawa J, Matsuzawa Y (2000) A proposal of three distinct subtypes of type 1 diabetes mellitus based on clinical and pathological evidence. Ann Med 32:539–543
10. Junod A, Lambert AE, Orci L, Pictet R, Gonet AE, Renold AE (1967) Studies of the diabetogenic action of streptozotocin. Proc Soc Exp Biol Med 126:201–205
11. Kaneto H, Fujii J, Seo HG, Suzuki K, Matsuoka T, Nakamura M, Tatsumi H, Yamasaki Y, Kamada T, Taniguchi N (1995) Apoptotic cell death triggered by nitric oxide in pancreatic beta-cells. Diabetes 44:733–738
12. Kroncke KD, Fehsel K, Sommer A, Rodriguez ML, Kolb-Bachofen V (1995) Nitric oxide generation during cellular metabolization of the diabetogenic N-methyl-N-nitroso-urea streptozotozin contributes to islet cell DNA damage. Biol Chem Hoppe Seyler 376:179–185
13. Kwon NS, Lee SH, Choi CS, Kho T, Lee HS (1994) Nitric oxide generation from streptozotocin. FASEB J 8:529–533
14. Masutani M, Suzuki H, Kamada N, Watanabe M, Ueda O, Nozaki T, Jishage K, Watanabe T, Sugimoto T, Nakagama H, Ochiya T, Sugimura T (1999) Poly(ADP-ribose) polymerase gene disruption conferred mice resistant to streptozotocin-induced diabetes. Proc Natl Acad Sci U S A 96:2301–2304
15. Papaccio G, Pisanti FA, Latronico MV, Ammendola E, Galdieri M (2000) Multiple low-dose and single high-dose treatments with streptozotocin do not generate nitric oxide. J Cell Biochem 77:82–91
16. Satoh MS, Lindahl T (1992) Role of poly(ADP-ribose) formation in DNA repair. Nature 356:356–358
17. Suematsu M, Suzuki H, Ishii H, Kato S, Yanagisawa T, Asako H, Suzuki M, Tsuchiya M (1992) Early midzonal oxidative stress preceding cell death in hypoperfused rat liver. Gastroenterology 103:994–1001
18. Szkudelski T (2001) The mechanism of alloxan and streptozotocin action in B cells of the rat pancreas. Physiol Res 50:537–546
19. Turk J, Corbett JA, Ramanadham S, Bohrer A, McDaniel ML (1993) Biochemical evidence for nitric oxide formation from streptozotocin in isolated pancreatic islets. Biochem Biophys Res Commun 197:1458–1464
20. Uchigata Y, Yamamoto H, Nagai H, Okamoto H (1983) Effect of poly(ADP-ribose) synthetase inhibitor administration to rats before and after injection of alloxan and streptozotocin on islet proinsulin synthesis. Diabetes 32:316–318

21. Wang H, Joseph JA (1999) Quantifying cellular oxidative stress by dichlorofluorescein assay using microplate reader. Free Radic Biol Med 27:612–616
22. West E, Simon OR, Morrison EY (1996) Streptozotocin alters pancreatic beta-cell responsiveness to glucose within six hours of injection into rats. West Indian Med J 45:60–62
23. Yamagami T, Miwa A, Takasawa S, Yamamoto H, Okamoto H (1985) Induction of rat pancreatic B-cell tumors by the combined administration of streptozotocin or alloxan and poly(adenosine diphosphate ribose) synthetase inhibitors. Cancer Res 45:1845–1849
24. Yamamoto H, Uchigata Y, Okamoto H (1981) DNA strand breaks in pancreatic islets by in vivo administration of alloxan or streptozotocin. Biochem Biophys Res Commun 103:1014–1020
25. Yamamoto H, Uchigata Y, Okamoto H (1981) Streptozotocin and alloxan induce DNA strand breaks and poly(ADP-ribose) synthetase in pancreatic islets. Nature 294:284–286

Virchows Arch (2004) 444:383–386
DOI 10.1007/s00428-003-0960-6

CASE REPORT

Pao-Hsien Chu · Hung-I. Yeh · Shih-Ming Jung · Li-Ying Chien · Nai-Feng Cheng · Hsueh-Hua Wu · Jaw-Ji Chu · Chuen Hsueh · Ying-Shiung Lee

Irregular connexin43 expressed in a rare cardiac hamartoma containing adipose tissue in the crista terminalis

Received: 26 November 2003 / Accepted: 4 December 2003 / Published online: 27 January 2004

Abstract Cardiac hamartomas are very rare and are demarcated masses of enlarged, hypertrophied, mature myocytes and collagen tissue. Cardiac hamartomas are generally circumscribed in the right ventricle or atrium, but not reported in the crista terminalis (CRT). The CRT is crucial in electrophysiology, is related to arrhythmogenesis, and is targeted by radiofrequency catheter procedures. Previous works only described the benign natures of prominent CRT using non-invasive methods. This study describes an unusual cardiac hamartoma originating from the CRT and extending toward the tricuspid valve. Microscopically, this hamartoma comprised dense collagen and adipose tissue, mixed with hypertrophy, but with disarrayed cardiomyocytes. An irregular gap junction, connexin43, was demonstrated in this cardiac hamartoma.

Keywords Cardiac hamartoma · Crista terminalis · Connexin43

P.-H. Chu (✉) · L.-Y. Chien · H.-H. Wu · Y.-S. Lee
The First Cardiovascular Division,
Department of Internal Medicine,
Chang Gung Memorial Hospital and Chang Gung University,
199 Tun-Hwa North Road, 105 Taipei, Taiwan
e-mail: pchu@adm.cgmh.org.tw
Tel.: +88-63-3281200 ext 8162
Fax: +88-63-3271192

H.-I. Yeh · N.-F. Cheng
Departments of Internal Medicine and Medical Research,
Mackay Memorial Hospital, Taipei Medical University,
Taipei, Taiwan

S.-M. Jung · C. Hsueh
Department of Pathology, Chang Gung Memorial Hospital,
Taipei, Taiwan

J.-J. Chu
Division of Thoracic & Cardiovascular Surgery,
Chang Gung Memorial Hospital, Taipei, Taiwan

Introduction

Cardiac hamartomas are extremely rare [2, 3, 13, 14, 15]. Hamartomas are characterized by demarcated masses of hypertrophied myocytes with variable collagen expression. Cardiac hamartomas generally occur in the right ventricle or atrium and are not reported in the crista terminalis (CRT) [2]. The CRT is a fibromuscular ridge that extends along the postero-lateral aspect of the right atrium and is essential for arrhythmogenesis, such as atrial tachycardia [4]. The CRT marks the embryological division between the portion of the right atrium derived from the sinus venosus and the embryonic atrium. The prominence of the CRT and its associated structures varies markedly. Previous studies described the benign nature of prominent CRT using transesophageal echocardiography [1, 8, 9] and magnetic resonance imaging [6, 7]. However, this study describes a rare protruding hamartoma originating from the CRT, in which the cytoskeletal structure and gap junction were analyzed using immunochemical studies and compared with normal CRT.

Clinical history

A 76-year-old man with mild systolic hypertension, well-controlled by atenolol for 10 years, and catheterization-documented, but insignificant, left arterial artery stenosis, presented with chest tightness on exertion without palpitation lasting 1 week. Electrocardiogram revealed complete right-bundle branch block (Fig. 1). Moreover, transthoracic echocardiography displayed left ventricular hypertrophy, 15 mm, in the interventricular septum (compared with less than 13 mm normally) and a right atrium mass of approximately 6 cm, attached to the free wall and protruding toward the tricuspid valve during the systolic phase (Fig. 2A, B). Surgical exploration, thus, was performed under the impression of cardiac tumor. Specifically, the right atrium was opened longitudinally under general anesthesia. Surgery revealed a tumor originating from the CRT. Two specimens measuring 15×5×5 mm and 10×5×5 mm were resected without any complications of arrhythmia. The tissues of both specimens were formalin fixated using paraffin embedding and sampling of frozen tissue for immunochemical study.

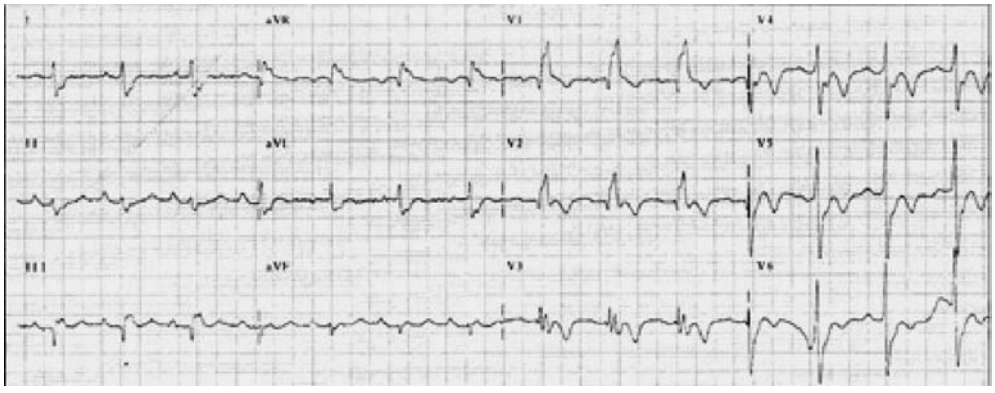

Fig. 1 Electrocardiogram showing the right bundle branch block, without atrial fibrillation or flutter before operation

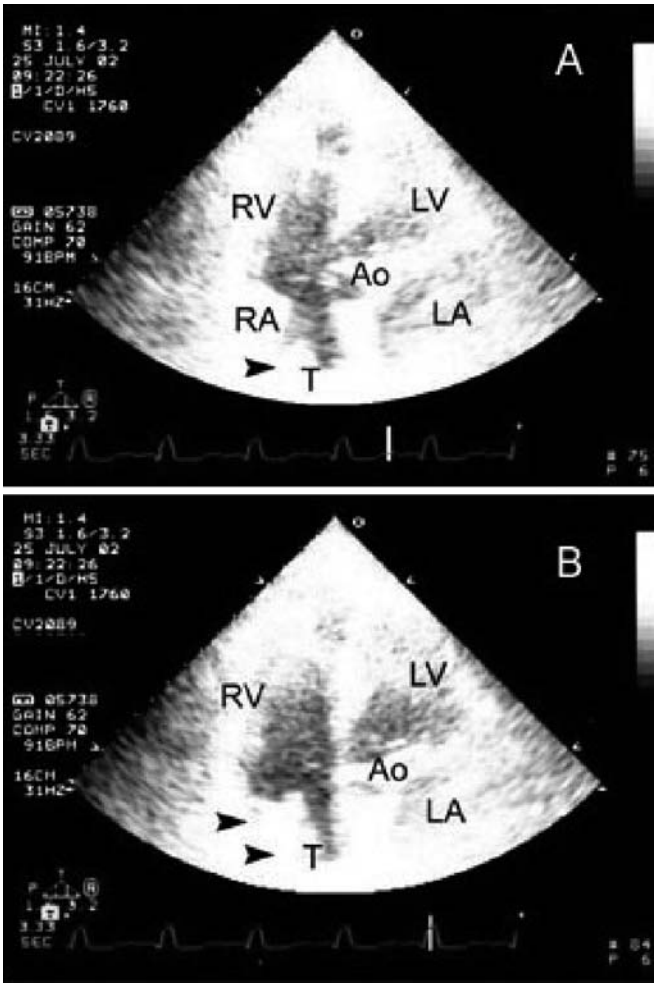

Fig. 2 Transthoracic echocardiography displayed a right atrium mass (*T* and *arrowhead*) of approximately 6 cm, attached to the crista terminalis during the diastolic phase (**A**) and protruding toward the tricuspid valve during the systolic phase (**B**). (*Ao* aorta, *LA* left atrium, *LV* left ventricle, *RA* right atrium, *RV* right ventricle, *T* tumor)

Materials and methods

Hematoxylin-eosin, modified trichome, and immunochemical stains for α-actinin (1:100, Sigma), desmin (1:20, Sigma), and vinculin (1:100, Sigma) were performed following the instructions of the manufacturer. For labeling of connexin43 type (C16, 1:100), cryosections of the samples were blocked in 0.5% bovine serum albumin (15 min) and incubated with anti-Cx43 (1:100, Transduction Laboratory) at 37°C for 2 h as reported previously [16]. The samples were then treated with CY3-conjugated secondary antibody (1:500, room temperature, 1 h). All experiments included a positive control in the form of three CRT sections from the autopsies of a 67-year-old and a 68-year-old male who died of non-cardiovascular causes and had whole-heart weights of 400 g and 420 g, respectively. Meanwhile, omission of primary antibody was used to provide a negative control. Immunostained samples were examined via confocal laser scanning microscopy with a Leica TCS SP.

Results

The histological examination revealed fragments of endomyocardium with foci of significant myocardial hypertrophy, adipose tissue, and moderate interstitial fibrosis (Fig. 3A, B, C). The cytoskeletal structure demonstrated by α-actinin, desmin, and vinculin was well maintained (data not shown), although the gap junction, connexin43, was decreased and irregular (Fig. 4). The patient was in a stable condition and was regularly followed up for over 24 months, with no problems identified other than persisting right bundle branch block.

Discussion

To our knowledge, this is the first detailed immunochemical study of cytoskeletal structures and connexin43 in an unusual cardiac hamartoma located at the CRT. Several conditions can mimic cardiac hamartoma [2] in the right atrium. For example, the prominent CRT may appear as a right atrial mass [4]. Moreover, the large Eustachian valve and the Chiari network [5] also can mimic right atrial masses. In the present case, right atrial myxoma, thrombus, or the prominent CRT should be considered first. Echocardiography is effective for detecting intra-cardiac masses, including neoplasms, thrombi, vegetations, and normal variants of prominent CRT [1, 8, 9]. Magnetic resonance imaging is also helpful in differentiating normal and pathological masses [6, 7]. However, surgical

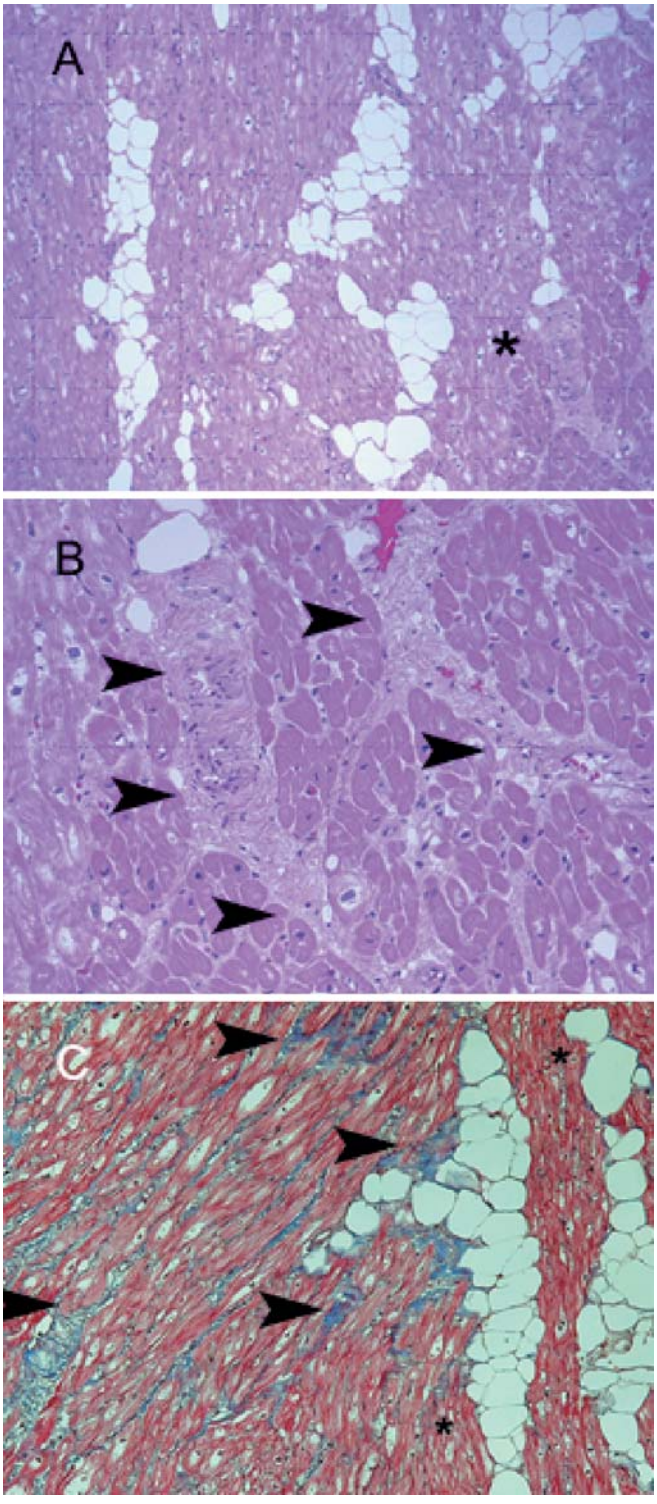

Fig. 3 Biopsy of cardiac hamartoma displayed cardiomyocytes hypertrophy infiltrated by interstitial fibrosis (*arrowheads*) and adipose tissues (*stars*) (**A**, ×100, **B**, ×200, hematoxylin and eosin stain; and **C**, ×200, modified trichome stain)

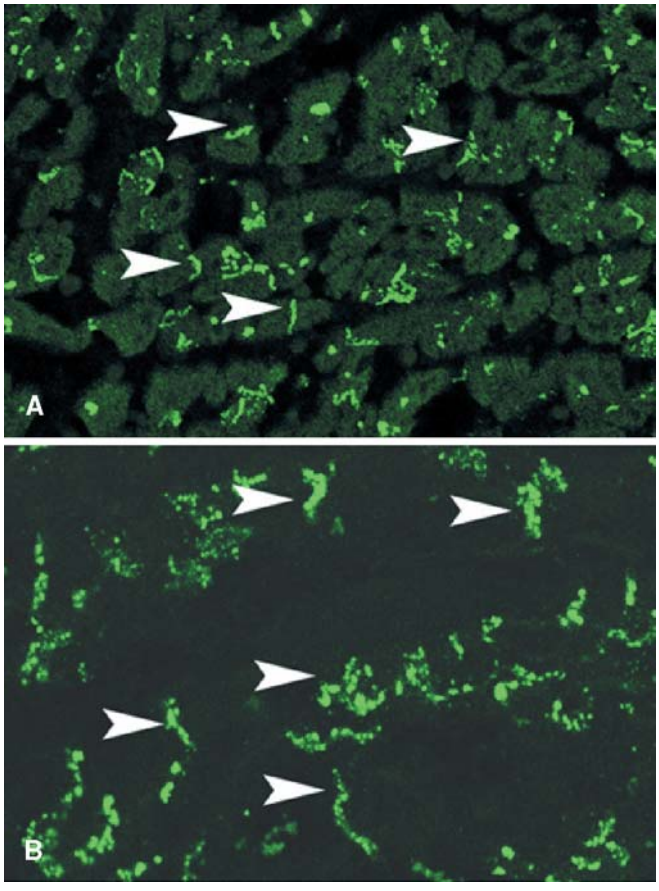

Fig. 4 The cytoskeletal structure of the cardiac hamartoma demonstrated decreased and irregular connexin43 (**B**, *arrowheads*) compared with the control crista terminalis (**A**, *arrowheads*) (×400)

exploration is the only method that can identify the nature of these masses.

This work examined an atrial hamartoma characterized by hypertrophy, cardiomyocytes, fat infiltration, interstitial fibrosis, and disarranged connexin43. First, the adipose tissue is uncommon in the cardiac hamartoma [13], but lipomatus hypertrophy of CRT itself may appear as a right atrial mass [9]. Second, the recent study of the CRT favors non-uniform anisotropic properties, and focal interstitial fibrosis develops with age [10, 11]. Furthermore, irregular connexin43 is first demonstrated in this unusual right atrial hamartoma. Previous ultrastructural analysis demonstrated that CRT myocytes were connected by numerous small gap junctions that occurred in relatively simple, straight intercalated disks. Northern-blot analysis revealed approximately equivalent amounts of mRNAs encoding the gap junction channel proteins connexin43 and connexin45, but around four times more connexin40 mRNA was found in the crista terminalis than in the left ventricle [10, 12, 14]. The presence of disarrayed connexin43 in this tumor confirms that the cardiac hamartoma originated from the CRT and probably retained partial conductivity.

Previous investigations all described the benign natures of prominent CRT using clinical course and noninvasive methods [1, 6, 7, 8, 9]. However, rare cardiac hamartomas still should be considered. The detailed immunochemical methods presented here elucidate this unusual right atrial hamartoma, originating from the CRT, with adipose tissue, but irregular connexin43 expression.

Acknowledgement Dr Chu was supported by grants from the National Health Research Institute in Taiwan.

References

1. Alam M, Sun I, Smith S (1991) Transesophageal echocardiographic evaluation of right atrial mass lesions. J Am Soc Echocardiogr 4:331–337
2. Burkes A, Virmani R (1996) Tumors of the heart and great vessels. In: (eds) AFIP Atlas of Tumor Pathology, AFIP, Washington, pp 63–67
3. Elderkin RA, Radford DJ (2002) Primary cardiac tumours in a paediatric population. J Paediatr Child Health 38:173–177
4. Lukas A, Antzelevitch C (1989) Reflected reentry, delayed conduction, and electrotonic inhibition in segmentally depressed atrial tissues. Can J Physiol Pharmacol 67:757–764
5. McMahon CJ, Nihill MR, Kovalchin JP, Lewin MB (2000) Echocardiographic features of Chiari's network in association with tricuspid atresia. Tex Heart Inst J 27:312–313
6. Meier RA, Hartnell GG (1994) MRI of right atrial pseudomass: is it really a diagnostic problem? J Comput Assist Tomogr 18:398–401
7. Mirowitz SA, Gutierrez FR (1992) Fibromuscluar elements of the right atrium: pseudomass at MR imaging. Radiology 182:231–233
8. Pharr JR, Figueredo VM (2002) Lipomatus hypertrophy of the atrial septum and prominent crista terminalis appearing as a right atrial mass. Eur J Echocardiogr 3:159–161
9. Pharr JR, West MB, Kusumoto FM, Figueredo VM (2002) Prominent crista terminalis appearing as a right atrial mass on transthoracic echocardiogram. J Am Soc Echocardiogr 15:753–755
10. Saffitz JE, Kanter HL, Green KG, Tolley TK, Beyer EC (1994) Tissue-specific determinants of anisotropic conduction velocity in canine atrial and ventricular myocardium. Circ Res 74:1065–1070
11. Sanchez-Quintana D, Anderson RH, Cabrera JA, Climent V, Martin R, Farre J, Ho SY (2002) The terminal crest: morphological features relevant to electrophysiology. Heart 88:406–411
12. Severs NJ, Rothery S, Dupont E, Coppen SR, Yeh HI, Ko YS, Matsushita T, Kaba R, Halliday D (2001) Immunocytochemical analysis of connexin expression in the healthy and diseased cardiovascular system. Microsc Res Tech 52:301–322
13. Sturtz CL, Abt AB, Leuenberger UA, Damiano R (1998) Hamartoma of mature cardiac myocytes: a case report. Mod Pathol 11:496–469
14. ten Velde I, de Jonge B, Verheijck EE, van Kempen MJ, Analbers L, Gros D, Jongsma HJ (1995) Spatial distribution of connexin43, the major cardiac gap junction protein, visualizes the cellular network for impulse propagation from sinoatrial node to atrium. Circ Res 76:802–811
15. Vander Salm TJ (2000) Unusual primary tumors of the heart. Semin Thorac Cardiovasc Surg 12:89–100
16. Yeh HI, Lai YJ, Lee SH, Lee YN, Ko YS, Chen SA, Severs NJ, Tsai CH (2001) Heterogeneity of myocardial sleeve morphology and gap junctions in canine superior vena cava. Circulation 104:3152–3157

Virchows Arch (2004) 444:387–391
DOI 10.1007/s00428-004-0975-7

CASE REPORT

Sabah Boudjemaa · Françoise Boman · Vincent Guigonis · Liliane Boccon-Gibod

Brain involvement in multicentric Epstein–Barr virus-associated smooth muscle tumours in a child after kidney transplantation

Received: 6 January 2004 / Accepted: 6 January 2004 / Published online: 19 February 2004

Abstract Epstein–Barr virus (EBV)-associated smooth muscle tumours (SMT) have been reported in young patients with induced immunosuppression associated with organ transplantation, acquired immunodeficiency syndrome or congenital immunodeficiencies. EBV-associated SMT are frequently multicentric or multifocal and often occur in unusual locations. We are reporting a case of EBV-associated multicentric SMT that occurred after kidney transplantation in a 2-year-old boy with a history of oligomeganephrony. Headaches and left VIth cranial nerve paralysis led to the discovery of a brain tumour 3 years after transplantation. There were multiple pulmonary, hepatic and splenic nodules and enlarged mesenteric lymph nodes. Histological examination revealed multicentric SMT of uncertain malignant potential. Further investigations using in situ hybridisation demonstrated EBV early RNAs in the nucleus of most tumour cells. The immunosuppressive therapy was reduced, and the child was treated with chemotherapy, but died 2 months later, due to neurological complications.

S. Boudjemaa · L. Boccon-Gibod (✉)
Department of Pathology,
University School of Medicine of Paris VI,
Hôpital d'Enfants Armand Trousseau, Assistance Publique-Hôpitaux de Paris,
26 avenue du Docteur Arnold Netter, 75571 Paris Cedex 12, France
e-mail: liliane.boccon-gibod@trs.ap-hop-paris.fr
Tel.: +33(0)1-44-736182
Fax: +33(0)1-44-736282

F. Boman
Department of Pathology,
University School of Medicine, Hospital of Lille,
59037 Lille, France

V. Guigonis
Department of Paediatric Nephrology,
Dialysis and Transplantation,
Hôpital d'Enfants Armand Trousseau,
Assistance Publique-Hôpitaux de Paris,
26 avenue du Docteur Arnold Netter, 75571 Paris Cedex 12, France

Keywords Epstein–Barr virus · Immunosuppression · Organ transplantation · Smooth muscle tumour

Introduction

Leiomyosarcomas are very rare in the paediatric age group [13]. In children with acquired immunodeficiency syndrome (AIDS) or induced immunosuppression following transplantation, the incidence of apparently benign or malignant spindle-cell (usually smooth-muscle) tumours is higher than expected for this age group [3, 9, 20]. Epstein–Barr virus (EBV)-associated smooth muscle tumours (SMT) are uncommon, distinctive mesenchymal tumours found in immunocompromised patients, including children, with AIDS [16], induced immunosuppression following transplantation [15], severe congenital immunodeficiency [12, 17, 28] or ataxia–telangiectasia [22]. The intracranial location of EBV-associated SMT in immunocompromised patients is extremely rare [12].

In this report, we are presenting a case of EBV-associated multicentric SMT that occurred after kidney transplantation in a child. Tumours were located in the brain, lungs, liver, spleen and mesenteric lymph nodes.

Clinical history

At birth, the boy was premature, with bilateral renal hypoplasia related to oligomeganephrony and renal insufficiency necessitating haemodialysis from the age of 15 months. Kidney transplantation was performed at 2 years of age. The recipient was EBV-seronegative and the donor seropositive. EBV primary infection was detected within 6 months of the renal transplant. Post-transplant immunosuppressive therapy included anti-lymphocyte globulin (days 1–10 post-transplantation); methylprednisolone (2 mg/kg per day on days 1–10, then progressively reduced to 0.35 mg/kg per day at 6 months) and cyclosporin (from day 8, 5 mg/kg). Azathioprine was given initially, but the patient was switched to mycophenolate mofetil (600 mg/m^2) at day 5 because of severe leukopenia. Long-term treatment included cyclosporin (7 mg/kg per day), prednisone (0.35 mg/kg per day) and mycophenolate mofetil (400 mg/m^2). The patient was admitted to hospital with headaches and left VIth cranial nerve paralysis 3 years after

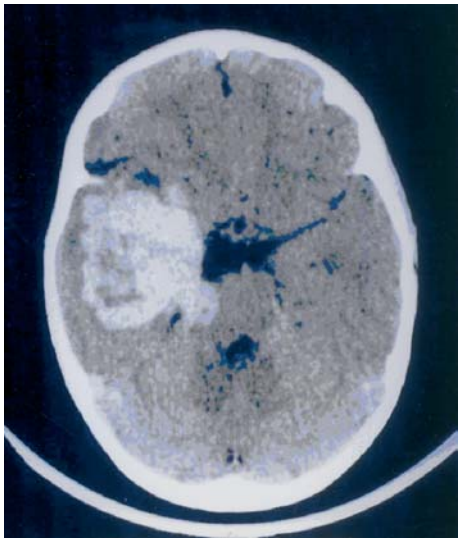

Fig. 1 Cerebral computed tomography scan showing a right temporal mass that was displacing the brain stem

transplantation. Physical examination revealed hepatomegaly and splenomegaly. A cerebral computed tomography (CT) scan demonstrated a right temporal mass, measuring 5 cm, that was displacing the brain stem (Fig. 1). A thoracic–abdominal CT scan revealed multiple pulmonary, hepatic and splenic nodules as well as enlarged mesenteric lymph nodes. Semiquantitative polymerase chain reaction demonstrated a high viral load in the blood (1000–2000 Eqv genome/10^5 cells). A fine-needle biopsy was taken of a hepatic nodule and a splenic nodule (3×2×2 cm) was resected. Following the diagnosis of EBV-associated SMT, the immunosuppressive therapy was reduced to prednisone, and the child was treated with chemotherapy (temozolomide 8 mg/kg per day on 5 days every month). He died after 2 months with seizures and coma. No autopsy was performed.

Materials and methods

Formalin-fixed tissue was sectioned (4 μm) and stained with haematoxylin–eosin–saffron. The immunohistochemical procedure used a panel of antibodies recognising relevant markers, such as vimentin, smooth muscle actin, desmin, CD31, CD34, S100 protein, Ki-67 and EBV latent membrane protein (LMP-1) (Dako, Glostrup, Denmark). Positive staining was visualised using peroxidase conjugates (EnVision+ system, Dako). EBV-encoded early RNAs (EBERs 1 and 2) were detected using in situ hybridisation with biotin-conjugated oligonucleotides (Kreatech, Amsterdam, The Netherlands).

Results

Macroscopically, the splenic nodule was encapsulated, firm and white. Microscopic examinations of biopsies taken from the liver and spleen demonstrated interlacing bundles of spindle cells with moderate cellularity in combination with some loosely textured myxoid areas of low cellularity. Tumour cells displayed eosinophilic cytoplasm and vesicular nuclei. The nuclei were elongated to cigar-shaped and slightly variable in size (Fig. 2). Mitotic figures were very scarce, and there was no haemorrhage or necrosis. Immunohistochemical staining and analysis demonstrated diffuse staining for vimentin and smooth muscle actin. Nuclear staining for Ki-67 was demonstrated in 10% of tumour cells. The results for desmin, CD31, CD34, S100 protein and LMP-1 were negative. The nucleus of most tumour cells expressed EBERs (Fig. 3).

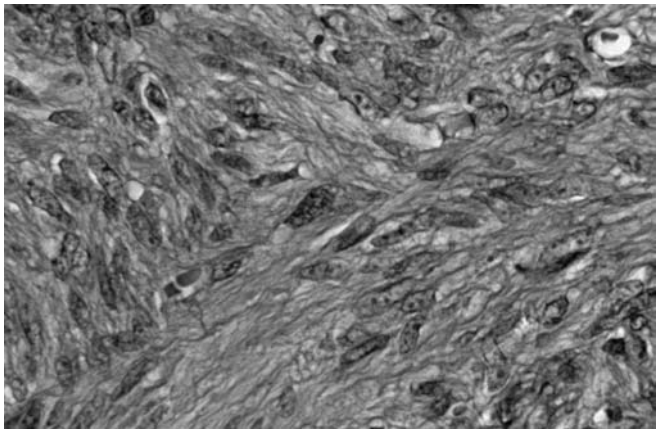

Fig. 2 This micrograph of a splenic nodule demonstrates interlacing bundles of spindle cells with slight nuclear atypia. Haematoxylin–eosin–saffron (original magnification ×600)

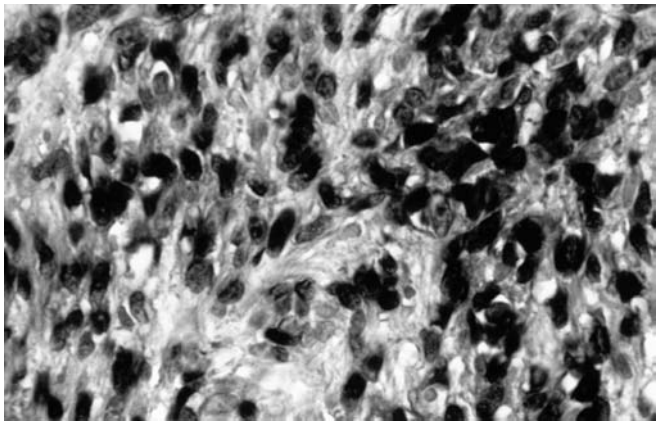

Fig. 3 This microphotograph shows in situ hybridisation in a splenic nodule demonstrating nuclear expression of EBERs by most tumour cells (original magnification ×600)

Discussion

Patients who have undergone organ transplantation require lifelong immunosuppressive therapy. The incidence of various proliferative disorders, including SMT and susceptibility to EBV are increased in immunosuppressed patients. EBV is a DNA herpes virus that is able to immortalise infected cells. It is commonly found in adults, primarily infecting B-lymphocytes and capable of persisting indefinitely in a latent form. Infected B-cells may undergo chromosomal rearrangement and become

Table 1 Clinical and pathological features of Epstein–Barr virus (EBV)-associated smooth muscle tumour (SMT) following organ transplantation. *transpl* transplantation, *UMP* uncertain malignant potential, *LMS* leiomyosarcoma, *m* multifocal, *s* single, *SR* surgical resection of tumor(s), *Red. IT* reduced immunosuppressive therapy, *AVT* antiviral therapy, *CT* chemotherapy

Reference	Sex	Age at transplant	Transplant	Delay transplant—SMT	Location of SMT	Pathology of SMT	Treatment for SMT	Follow-up
[15]	Female	18 months	Liver	3 years	Liver (donor), m	UMP	SR	Alive, no SMT (3 years)
[15]	Female	15 months	Liver	5.5 years	Liver, lungs, heart, stomach, small bowel, colon, m, retroperitoneum (10 cm), s	UMP	Red. IT, AVT, CT	Dead (candidosis), SMT
[15]	Female	20 months	Liver, small bowel	12 months	Colon (recipient), m	UMP	Red. IT, AVT	Dead, SMT (4 m)
[21]	Male	Child	Liver, pancreas, stomach, bowel		Bowel	UMP		Dead (sepsis)
[26]	Male	7 years	Liver	2 years	Liver (donor), s, lungs, m	Poorly differentiated LMS	CT	Dead, SMT (6 months)
[26]	Female	7 years	Liver	5 years	Peritoneum (10 cm) (recipient), s	Well-differentiated LMS	SR	Alive, no SMT (2 years)
[6]	Male	1 year	Heart	4 years	Liver (15 cm), s	UMP	SR, AVT	Alive (10 months)
[11]	Female	2 year	Heart	2 years	Liver, spleen, m	UMP	–	Dead (sepsis, rejection), SMT (1 years)
[14]	Female	49 years	Kidney	4 years	Liver (recipient), spleen, m	Well-differentiated LMS	Red. IT, AT, CT, SR	Dead, SMT (16 months)
[24]	Female	15 years	Kidney	6 years	Liver, m	UMP	–	Dead (cerebral hemorrhage)
[1]	Male	44 years	Heart	4 years	Heart, s	UMP	–	Dead (ruptured aortic aneurysm), SMT
[25]	Male	11 years	Heart, lung	3.5 years	Lung (donor), liver (recipient), m	LMS	Red. IT, AVT	Dead (sepsis) (1 month)
[29]	Male	26 years	Kidney	2 years	Lungs, liver, spleen, lymph nodes, thigh, m	LMS	–	Dead (1 year)
[8]	Male	2 years	Liver	5 years	Mesentery, s	UMP	SR, red. IT	Dead (retranspl.)
[23]	Male	23 years	Heart	3 years	Liver, m, paravertebral, m, vein (ankle), s	Low-grade LMS	SR, red. IT, AVT	Alive, no SMT (3 years)
[27]	Male	34 years	Kidney	4 years	Bones, liver, lungs, m	UMP	Red. IT	Alive, SMT (8 years)
[2]	Female	3 years	Liver	2 years	Liver, lymph nodes, mesentery, m	LMS	Red. IT, CT	Alive, SMT (12 years)
[5]	Female	18 days	Heart	5 years	Epidural intracranial, s, endobronchial, s	SMT	SR	Alive, SMT (3.5 years)
This report	Male	2 years	Kidney	3 years	Brain, s, lungs, liver, spleen, lymph nodes, m	UMP	Red. IT, CT	Dead (brain tumor) (2 months)

hyperproliferative. T-lymphocytes normally constitute the major pool of proliferating cells associated with the host's response to EBV infection [19]. Latent EBV infection is associated with a number of lymphoid, epithelial and mesenchymal tumours. CD21, the B-cell receptor for EBV, is found on the cell surface of SMT in human immunodeficiency virus (HIV)-positive (strong immunostaining) and HIV-negative (weak immunostaining) children [16]. EBERs 1 and 2 are demonstrated using in situ hybridisation in latently infected cells. Large amounts of EBV DNA and RNA have been demonstrated in SMT in immunocompromised patients [15, 16]. Monoclonal or biclonal EBV strains have been identified in SMT found both in patients following organ transplantation [14, 15] and in children with AIDS [10, 16]. Such EBV monoclonality suggests a primary role of the virus in oncogenesis of this tumour [4]. An EBV-associated liver tumour that had occurred after kidney transplantation in a 10-year-old patient presented a phenotypical spectrum, ranging from SMT to inflammatory pseudotumour, with genomic rearrangement of the ALK loci and co-localisation of the viral DNA and the ALK sequences [7]. EBV-

associated SMT following organ transplantation may occur concurrently or sequentially with post-transplant lymphoproliferative disorders (PTLD), which often regress after reduction of immunosuppression. EBV-associated SMT and PTLD occur after similar tumour-free periods post-transplantation, exhibit EBV type-III latency, involve either donor or recipient tissues, are of clonal or multiclonal origin and display a wide spectrum of histological grade and clinical behaviour [19].

EBV-associated SMT following organ transplantation have been reported in 14 children (including the subject of this report) [2, 5, 6, 8, 11, 15, 18, 21, 24, 25, 26, 30] and 5 adults [1, 14, 23, 27, 29]: 10 males, 9 females, aged 18 days to 49 years at transplantation (mean 12.9 years and median 5.1 years). A variety of organs have been transplanted in the subjects of these studies, most often the liver (eight patients), kidney, or heart. The delay between the transplantation and the occurrence of SMT ranged from 1 year to 6 years (mean 3.6 years and median 3.8 years), with a single SMT measuring up to 15 cm [6] or, more often, multifocal or multicentric lesions in multiple organs or tissues. The most common locations of SMT were the liver (12 patients), originating from the donor or recipient, lung (from the donor in one patient), heart and colon (native in one patient) (Table 1). SMT was found in the intracranial, epidural area in a 5-year-old girl following heart transplantation. Immunosuppression was reduced, and the epidural mass was stable 3.5 years after biopsy [5]. The child reported in this study represents the only patient with brain tumour. In 12 of the patients described in the literature, the diagnosis was SMT of uncertain malignant potential. A further seven patients were diagnosed with leiomyosarcoma (well-differentiated in three patients, poorly differentiated in one patient). The malignant potential of these tumours is difficult to assess, and the diagnosis of SMT of uncertain malignant potential might be preferred instead of leiomyosarcoma or leiomyoma. The biological significance of criteria, such as tumour size, cellularity, atypia and mitotic counts probably differs according to the location of such tumours, with some apparently benign tumours proving to be lethal. The tumours did prove to be fatal in most patients, with death most often being a result of sepsis (four patients) or haemorrhage. Five of the seven patients who survived (at a 10-month to 12-year follow-up) have been treated by surgical resection (Table 1). In the case reported here, the brain tumour was lethal, despite the reduction of immunosuppression and the use of chemotherapy with good diffusion through the blood–brain barrier.

Acknowledgement The authors thank Paulo Gomes for his skilful technical help.

References

1. Anguita J, Rico ML, Palomo J, Munoz P, Preciado V, Menarguez J (1998) Myocardial Epstein–Barr virus-associated cardiac smooth-muscle neoplasm arising in a cardiac transplant recipient. Transplantation 66:400–401
2. Brichard B, Smets F, Sokal E, Clapuyt P, Vermylen C, Cornu G, Rahier J, Otte JB (2001) Unusual evolution of an Epstein–Barr virus-associated leiomyosarcoma occurring after liver transplantation. Pediatr Transpl 5:365–369
3. Chadwick EG, Connor EJ, Guerra Hanson C, Joshi VV, Abu-Farsakh H, Yogev R, McSherry G, McClain K, Murphy SB (1990) Tumours of smooth-muscle origin in HIV-infected children. JAMA 263:3182–3184
4. Cheuk W, Li PCK, Chan JKC (2002) Epstein–Barr virus-associated smooth-muscle tumour: a distinctive mesenchymal tumour of immunocompromised individuals. Pathology 34: 245–249
5. Collins MH, Montone KT, Leahey AM, Hodinka RL, Salhany KE, Clark BJ, Duhaime AC, Spray TL, Tomaszewski JE (2001) Metachronous Epstein–Barr virus-related smooth-muscle tumours in a child after heart transplantation: case report and review of the literature. J Pediatr Surg 36:1452–1455
6. Davidoff AM, Hebra A, Clark BJ, Tomaszewski JE, Montone KT, Ruchelli E, Lau HT (1996) Epstein–Barr virus-associated hepatic smooth-muscle neoplasm in a cardiac transplant recipient. Transplantation 61:515–517
7. Debiec-Rychter M, Croes R, De Vos R, Marynen P, Roskams T, Hagemeijer A, Lombaerts R, Sciot R (2003) Complex genomic rearrangement of ALK loci associated with integrated human Epstein–Barr virus in a post-transplant myogenic liver tumor. Am J Pathol 163:913–922
8. Ferlicot S, Bessoud B, Branchereau S, Dubuisson C, Gauthier F, Fabre M (1999) Smooth-muscle mesenteric tumour associated with Epstein–Barr virus (EBV): report of a case in a child with a liver transplant under FK506 regimen (in French). Ann Pathol 19:46–49
9. Ha C, Haller JO, Rollins NK (1993) Smooth muscle tumors in immunocompromised (HIV negative) children. Pediatr Radiol 23:413–414
10. Jenson HB, Leach CT, McClain KL, Joshi VV, Pollock BH, Parmley RT, Chadwick EG, Murphy SB (1997) Benign and malignant smooth-muscle tumours containing Epstein–Barr virus in children with AIDS. Leuk Lymphoma 27:303–314
11. Kingma DW, Shad A, Tsokos M, Fest T, Otsuki T, Frekko K, Werner E, Werner A, Magrath I, Raffeld M, Jaffe ES (1996) Epstein–Barr virus (EBV)-associated smooth-muscle tumour arising in a post-transplant patient treated successfully for two PT-EBV-associated large-cell lymphomas. Am J Surg Pathol 20:1511–1519
12. Kleinschmidt-DeMasters BK, Mierau GW, Sze CI, Breeze RE, Greffe B, Lillehei KO, Stephens JK (1998) Unusual dural and skull-based mesenchymal neoplasms: a report of four cases. Hum Pathol 29:240–245
13. Lack EE (1986) Leiomyosarcomas in childhood: a clinical and pathologic study of 10 cases. Pediatr Pathol 6:181–197
14. Le Bail B, Morel D, Mérel P, Comeau F, Merlio JP, Carles J, Trillaud H, Bioulac-Sage P (1996) Cystic smooth-muscle tumour of the liver and spleen associated with Epstein–Barr virus after renal transplantation. Am J Surg Pathol 20:1418–1425
15. Lee ES, Locker J, Nalesnik M, Reyes J, Jaffe R, Alashari M, Nour B, Tsakis A, Dickman PS (1995) The association of Epstein–Barr virus with smooth-muscle tumours occurring after organ transplantation. N Engl J Med 332:19–25
16. McClain KL, Leach CT, Jenson HB, Joshi VV, Pollock BH, Parmley RT, DiCarlo FJ, Chadwick EG, Murphy SB (1995) Association of Epstein–Barr virus with leiomyosarcomas in young people with AIDS. N Engl J Med 332:12–18
17. Mierau GW, Greffe BS, Weeks DA (1997) Primary leiomyosarcoma of brain in an adolescent with common variable immunodeficiency syndrome. Ultrastruct Pathol 21:301–305
18. Morel D, Merville P, Le Bail B, Berger F, Saric J, Potaux L (1996) Epstein–Barr virus (EBV)-associated hepatic and splenic smooth-muscle tumours after kidney transplantation. Nephrol Dial Transplant 11:1864–1866

19. Nalesnik MA, Makowka L, Starzl TE (1988) The diagnosis and treatment of posttransplant lymphoproliferative disorders. Curr Probl Surg 25:367–472
20. Penn I (1995) Sarcomas in organ allograft recipients. Transplantation 60:1485–1491
21. Pollock AN, Newman B, Putnam PE, Dickman PS, Medina JL (1995) Imaging of post-transplant spindle cell tumours. Pediatr Radiol 25:S118–S121
22. Reyes C, Abuzaitoun O, de Jong A, Hanson C, Langston C (2002) Epstein–Barr virus-associated smooth-muscle tumours in ataxia–telangiectasia: a case report and review. Hum Pathol 33:133–136
23. Rogatsch H, Bonatti H, Menet A, Larcher C, Feichtinger H, Dirnhofer S (2000) Epstein–Barr virus-associated multicentric leiomyosarcoma in an adult patient after heart transplantation. Am J Surg Pathol 24:614–621
24. Sadahira Y, Moriya T, Shirabe T, Matsuno T, Manabe T (1996) Epstein–Barr virus-associated post-transplant primary smooth-muscle tumour of the liver: report of an autopsy case. Pathol Int 46:601–604
25. Somers GR, Tesoriero AA, Hartland E, Robertson CF, Robinson PJ, Venter DJ, Chow CW (1998) Multiple leiomyosarcomas of both donor and recipient origin arising in a heart–lung transplant patient. Am J Surg Pathol 22:1423–1428
26. Timmons CF, Dawson DB, Richards CS, Andrews WS, Katz JA (1995) Epstein–Barr virus-associated leiomyosarcomas in liver transplantation recipients: origin from either donor or recipient tissue. Cancer 76:1481–1489
27. To KF, Lai FMM, Wang AYM, Leung CB, Choi PCL, Szeto CC, Lui SF, Yu AWY, Li PKT (2000) Posttransplant Epstein–Barr virus-associated myogenic tumours involving bone. Cancer 89:467–472
28. Tulbah A, Al-Dayel F, Fawaz I, Rosai J (1999) Epstein–Barr virus-associated leiomyosarcoma of the thyroid in a child with congenital immunodeficiency: a case report. Am J Surg Pathol 23:473–476
29. Uribe-Uribe NO, Aviles-Salas A, Orozco-Estevez H, Alberu J, Angeles-Angeles A (1998) Leiomyosarcoma associated with Epstein–Barr virus in an adult with renal transplant (in Spanish). Rev Invest Clin 50:255–258
30. Wu TT, Swerdlow SH, Locker J, Bahler D, Randhawa P, Yunis EJ, Dickman PS, Nalesnik MA (1996) Recurrent Epstein–Barr virus-associated lesions in organ transplant recipients. Hum Pathol 27:157–164

Virchows Arch (2004) 444:392–394
DOI 10.1007/s00428-003-0875-2

LETTER TO THE EDITOR

Fabio De Giorgio · Vincenzo Arena · Domenico De Mercurio · Vincenzo L. Pascali · Arnaldo Capelli

Right atrial lipoma with "satellite" atrial fibrillation?

Received: 14 February 2003 / Accepted: 6 March 2003 / Published online: 13 August 2003

Sir, We wish to report briefly on a case of cardiac lipoma—the unexpected finding of an autopsy on the body of a 50-year-old woman who suffered from atrial fibrillation. Using morphological findings and close histopathological study, we were able to explain this apparently "functional" symptom as the effect of early autonomous cardiac plexus infiltration.

Cardiac lipoma is a benign neoplasm that occurs at a low rate and is currently well documented in the literature [4, 5, 8]. The original lesion generally develops at the pericardial surface or within the cardiac chambers, in the form of an encapsulated adipose mass that takes the parietal pericardium and occasionally expands over the rest of the heart. The affliction is apparent by non-specific symptoms, but quite often it is not and the diagnosis is instrumental.

In the case under our observation, we were faced with a 50-year-old woman, admitted to the Università Cattolica del Sacro Cuore Internal Medicine department with severe dyspnea and orthopnea symptoms. Suffering from atrial fibrillation since 1999, she had been administered beta-blockers for the last few years. Despite this, her recent electrocardiogram revealed atrial fibrillation at high ventricular frequency. The very night she was hospitalized, the patient passed away suddenly, and it was therefore impossible to carry out echocardiography or any other imaging method that could lead to a clinical diagnosis.

At the necroscopy, a massive pulmonary embolism was identified as the ultimate cause of death. We observed clear-cut cardiac hypertrophy with in-toto dilatation of the heart, more pronounced in the right sector. Here, we found a well-encapsulated, globular, lobulated yellow mass, with a diameter of 5 cm (Fig. 1A). The mass protruded from the lateral wall of the right atrium and the superior vena cava right atrial junction. Microscopic examination of this mass showed proliferation of mature fat cells with large, clear, empty cytoplasm and eccentrically placed nuclei. Myocardial fibers and cells of the sinoatrial (SA) node (Fig. 1B) were interspersed within fat cells. Searching for the presence of nervous tissue, we focused on a careful morphological study of ganglionic structures pertaining to the atrial plexus (Fig. 2). The microscopic evidence of nervous structures trapped in the neoplasm clearly emerged from this study.

In retrospect, this case epitomized for us the challenging situation of a cardiac lipoma with apparently "functional" symptoms that eventually turned out to have a very "organic" cause.

Currently, cardiac lipomas are occasional findings of postmortem heart dissection. Reece et al. described 71 benign cardiac tumors, 3 of which were classified as lipomas [8]. McAllister et al. estimated that lipomas can represent approximately 8.4% of all primary cardiac

Vincenzo Arena and Fabio De Giorgio contributed equally to this work.

F. De Giorgio
Istituto di Medicina Legale,
Università Cattolica del Sacro Cuore,
00168 Rome, Italy

V. Arena
Istituto di Anatomia Patologica,
Università Cattolica del Sacro Cuore,
00168 Rome, Italy

D. De Mercurio
Istituto di Medicina Legale,
Università Cattolica del Sacro Cuore,
00168 Rome, Italy

V. L. Pascali
Istituto di Medicina Legale,
Università Cattolica del Sacro Cuore,
00168 Rome, Italy

A. Capelli (✉)
Istituto di Anatomia Patologica,
Università Cattolica del Sacro Cuore,
Largo F.Vito 1, 00168 Roma
e-mail: acapelli@rm.unicatt.it
Tel.: +39-6-30154270
Fax: +39-6-3051157

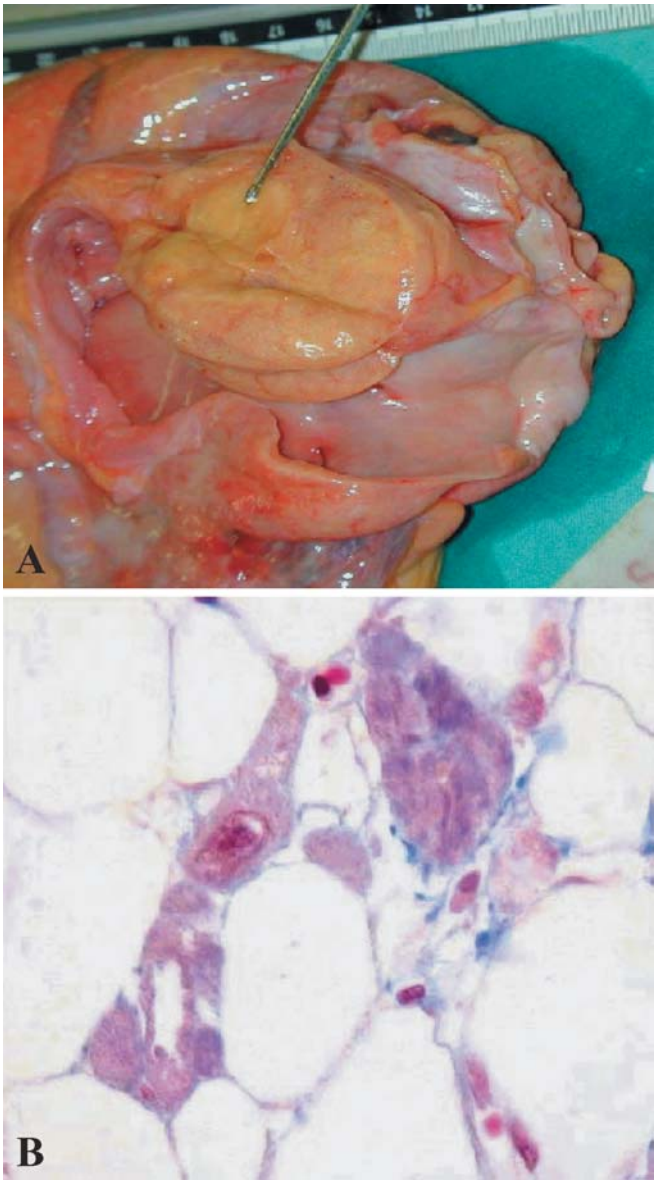

Fig. 1A A heart specimen showing a lobulated yellow mass located in the lateral wall of the right atrium. **B** Light micrograph demonstrating atrial myofibers of conduction system interspersed between mature fat cells.(Hematoxilin and eosin ×400)

tumors [4]. Meng et al. reported figures twice as high: 22 lipomas from 118 heart neoplasies [5]. By morphology and localization, there exist a lipomatous hypertrophy of the interatrial septum (with diffuse fat infiltration of the myocardium) and a so-called "true" lipoma.

In the first case, one is generally faced with a non-encapsulated mass of adipose tissue. The mass occasionally has a pseudoencapsule, supplied by surrounding structures (the fossa ovalis, the atrial wall, the interatrial sulcus, the pericardium of the transverse sinus or the posterior atrioventricular groove) [9]. J.T. Prior identified lipomatous hypertrophy of the interatrial septum as a distinct disease and described five examples [7]. Although the tumor may shape up as a bulge into the right

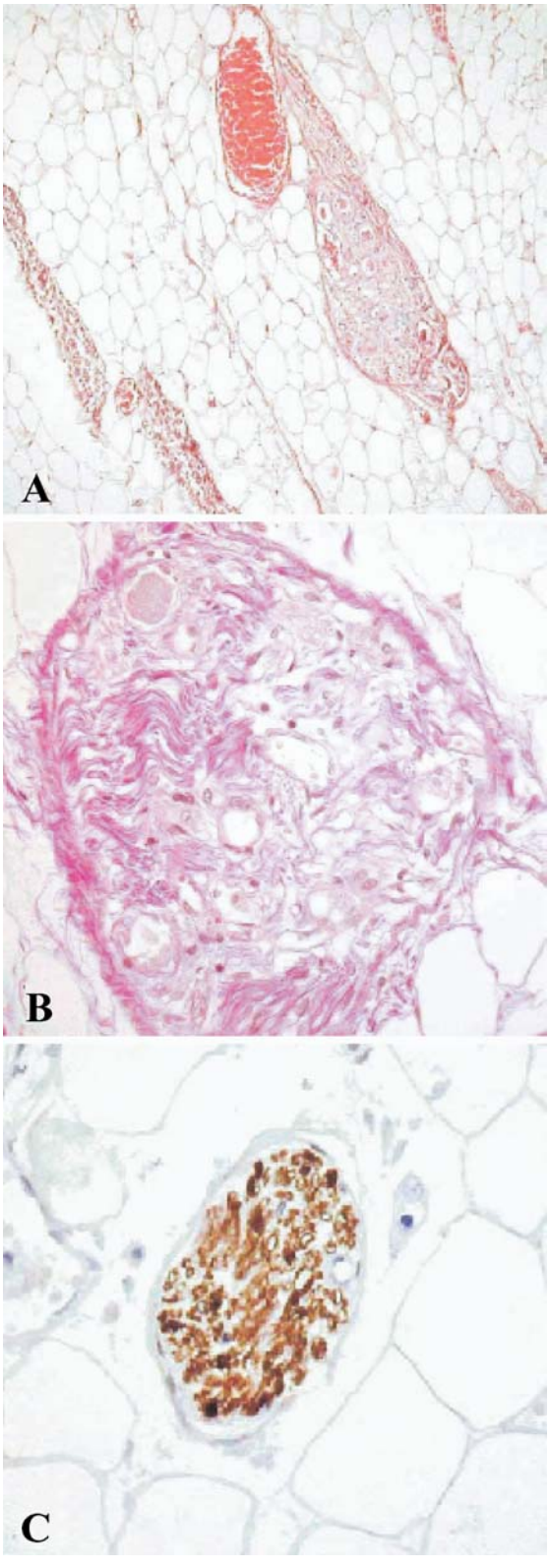

Fig. 2 Autonomous ganglia and nervous structures to be seen in the mass arising from the atrial wall. **A** Hematoxilin and eosin ×100; **B** Van Gieson ×250; **C** Immunostaining for S-100

atrium, its more usual pattern is a wedge-shaped fatty heap, obstructing the fossa ovalis. It may as often create a diffuse thickening of the interatrial septum. Unlike lipomatous hypertrophy, lipomas usually rest on the epicardial surface in virtually any site on the atrial–ventricular surface. Moreover, a lipoma consists of a mature lipocyte population encased into a full-wall or a focally discontinuous or sheared capsule. Of lipomas, 50% are intracavitary and develop under the endocardium. Another 25% are intramyocardial. The remaining 25% are extracavitary, and they can grow to a considerable size [2, 6]. Large subpericardial lipomas resting on cardiac structures may determine angina or impair the heart pump function.

In view of the relevant spatial relationships, atrial lipomas are thought to generate atrial arrhythmia out of a rather generic atrial irritability phenomena. Intramyocardial localization is alleged to involve abnormal electric conduction, then arrhythmia [1]. In fact, the underlying mechanism is seldom well defined. Myocardial atrophy, fibrosis or excessive lipomatous interatrial septum infiltration are the all too generic morpho–histological counterparts of such an ill-defined situation. Patients (particularly the elderly) may as well display cardiomegaly and incur congestive cardiac failure.

Invariably, even once the diagnosis is done, the true relationship between the mass and its symptoms remains elusive [9]. In the case reported here, we were able to find a specific cause for one of the classical cardiac symptoms of atrial lipoma: the atrial arrhythmia.

Our lipoma would arise from the lateral wall of the right atrium and the superior vena cava right atrial junction, at the site of the sinoatrial node. The patient was one with a “satellite” atrial fibrillation.

According to the current anatomy of the affected region, parasympathetic preganglionic fibers (from the dorsal motor nucleus of the vagus and from cells close to the nucleus ambiguous) descend to the cardiac branches of X to synapse with the cardiac plexus and the atrium wall neurons. Ganglia neurons are also present in the atrium walls and the interatrial septum, hidden in the subepicardial connective tissue within the sinoatrial–atrioventricular node context [10]. Ganglions and fibers command a reduction of the cardiac frequency and constriction of the coronary arteries , among other functions.

These structures can be a likely prey of the tumor mass. Accordingly, in our case, we gathered the microscopic evidence of massive infiltration of the nervous and ganglionic structures that would tell us that the SA node and the parasympathetic nervous structures were taken by the process.

Hence, multiple recoiling wave fronts of activation could have been generated and propagated to both atria by an anatomically sheared—then electrically unstable—sinus node and nervous structures. Additionally, atrial dilatation, fibrosis of atrial tissue and increased sympathetic activity could have acted in maintaining the arrhythmia. The whole process was probably perpetuated by prolonged conduction times, up to the final condition of atrial fibrillation [3].

All that undoubtedly qualified as the organic cause of the patient’s arrhythmia.

References

1. Grande M, Minzioni G, Pederzolli C, Rinaldi M, Pederzolli N, Arbustini E, Viganò M (1998) Cardiac lipomas description of 3 cases. J Cardiovasc Surg 39:813–815
2. Lang-Lazdunski L, Oroudjii M, Pansard Y, Vissuzaine C, Hvass V (1994) Successful resection of giant intrapericardial lipoma. Ann Thorac Surg 58:238–241
3. Lip GY, Beevers DG, Singh SP, Watson RD (1995) ABC of atrial fibrillation: aetiology, pathophysiology, and clinical features. BMJ 311:1425–1428
4. McAllister HA, Fenoglio JJ (1978) Tumors of the cardiovascular system. Atlas of tumor Pathology, vol 15, Armed Forces Institute of Pathology, Washington DC
5. Meng Q, Lai H, Lima J, Tong W, Qian Y, Lai S (2002) Echocardiographic and pathologic characteristics of primary cardiac tumors: a study of 149. Int J Cardiol 84:69–75
6. Moulton AL, Jaretzki A, Bowman FO, Silverstein EF, Bregman D (1979) Massive lipoma of the heart. NY State J Med 76:1820–1825
7. Prior JT (1964) Lipomatous hypertrophy of cardiac interatrial septum. A lesion resembling hibernoma, lipoblastomatosis and infiltrating lipoma. Arch Pathol 78:11–15
8. Reece IJ, Cooley DA, Frazier OH, Hallman GL, Powers PL, Montero CG (1984) Cardiac tumors: clinical spectrum and prognosis of lesions other than classical benign myxoma in 20 patients. J Thorac Cardiovasc Surg 88:439–446
9. Reyes CV, Jablokow VR (1979) Lipomatous hypertrophy of the interatrial septum. A report of 38 cases and review of the literature. Am J Clin Pathol 72:785–788
10. Williams PL, Warwick R (1980) Gray’s anatomy, 37th edn. Zanichelli N (ed) Longman Group Ltd., London

Virchows Arch (2004) 444:395–396
DOI 10.1007/s00428-003-0932-x

LETTER TO THE EDITOR

Jean-Louis Dargent · Christiane De Wolf-Peeters

Subcutaneous lymphoid hyperplasia arising at site of ethnic scarifications and mimicking subcutaneous panniculitis-like T-cell lymphoma: a subcuticular T-cell lymphoid dyscrasia

Received: 10 October 2003 / Accepted: 10 October 2003 / Published online: 2 December 2003

Sirs, we have reported in this journal the case of a 40-year-old black man who developed an unusual form of lymphoid hyperplasia primarily involving the subcutis and closely mimicking subcutaneous panniculitis-like T-cell lymphoma (SPTCL) [1]. The lesion, which characteristically arose at the site of tribal scarifications, did not, at first, show any convincing feature of malignancy. It was, therefore, deemed to be a particular variant of subcutaneous lymphoid hyperplasia, perhaps related to the scarification process itself. We wish to report here on this patient's follow-up.

The patient presented with a new swelling involving the same area 3 months after the first recurrence. Complementary clinical investigations and systemic image studies failed to reveal any systemic involvement. Steroid therapy (prednisone) was, therefore, given, with a very good response from the outset of the treatment. However, the lesion consistently relapsed at each cessation of the medication. Thus, local radiation therapy was given. While the disease seemed to be under control with this therapeutic procedure, the patient progressively developed a tumefaction in the left buttock area. A biopsy of this lesion was performed and revealed histological and phenotypic findings similar to those noticed in the two previous samples. The lymphoid infiltrate, however, presently showed slightly increased cytological atypia. A polymerase chain reaction analysis of DNA extracted from this new biopsy did not show any clonal rearrangement of the genes coding for the γ-chain of the T-cell receptor (TCR). Southern blot analysis disclosed clonal rearrangement of the genes coding for the β subunit of the TCR. It is worth noting that the same investigation had also been performed previously on DNA extracted from the first recurrence, and no clonal rearrangement of the genes coding for the β subunit of the TCR could be demonstrated at that time (data not reported in the original description).

Due to disease progression, the patient was treated with chemotherapy. While no improvement could be obtained initially by CHOP (cyclophosphamide, doxorubicin, vincristine, and prednisone) and ProMACE-CytaBOM (mitoxantrone, cyclophosphamide, etoposide, cytarabine, bleomycin, vincristine, and methotrexate), complete remission (CR) was obtained with the ESHAP regimen (etoposide, prednisone, cytarabine, and cisplatin) followed by a BEAM (BCNU, etoposide, cytarabine, and melphalan) intensification procedure and autologous peripheral blood stem cell transplantation. The patient is still in CR, 24 months after the graft.

The clinical and pathological features observed in this patient are bewildering. While the initial findings suggested a benign and reactive disorder, eventually related to the scarification process itself, the subsequent evolution appeared more in keeping with an incipient SPTCL. Hence, the question arises as to whether this disorder represents a peculiar subtype of lymphoid hyperplasia progressing to lymphoma or a true lymphoma from the outset. In an attempt to solve this issue, we wish to refer to a recent article by Magro and colleagues [2]. These authors thoroughly reviewed 32 cases of lymphocytic lobular panniculitis (LLP). On the basis of clinical data, they categorized these cases further as lupus erythematosus profundus, LLP of indeterminate type (ILLP), and SPTCL. In fact, patients with ILLP had no features indicative of lupus erythematosus, and their clinical course was not as aggressive as in SPTCL. In such cases, the infiltrate variably displayed cytological atypia, phenotypic abnormalities, clonal rearrangement of TCR, or some erythrophagocytosis by histiocytes, features that are found to a larger extent in SPTCL. The clinical evolution in ILLP also looked very similar to the waxing and

J.-L. Dargent (✉)
Department of Pathology,
CHU Saint-Pierre/Institut Jules Bordet,
1 rue Héger-Bordet, 1000 Brussels, Belgium
e-mail: jean.dargent@bordet.be
Tel.: +32-25-413124
Fax: +32-25-413281

C. De Wolf-Peeters
Department of Pathology,
Universitaire Ziekenhuizen, KU Leuven,
12 Minderbroedersstraat, 3000 Leuven, Belgium

waning phase of some SPTCL. These findings led Magro and colleagues to consider ILLP possibly as the early phase of SPTCL and to coin the term "subcuticular T-cell lymphoid dyscrasia" (SCTCLD) in order to describe a subset of atypical LLP having some, but not all, of the attributes of SPTCL. In this regard, also, the presence of erythrophagocytosis by histiocytes appeared to be a reliable marker of a supervening SCTCLD.

Similarly, the term "lymphomatoid panniculitis" (LP) was recently introduced to define atypical lesions that histologically resemble SPTCL but in which the clinical behavior is more indolent [3]. However, it is noteworthy that some cases of LP may require the administration of prednisone or even methotrexate to control the disease, which suggests a relatively aggressive behavior, similar to SCTCLD.

In conclusion, the initial findings in our patient likely represent those of a SCTCLD. This is best illustrated by the clinical course, which is comparable with the early phase of SPTCL.

References

1. Dargent JL, Diedhiou A, Lothaire P, Demunter A, Lespagnard L, De Wolf-Peeters C (2001) Subcutaneous lymphoid hyperplasia arising at site of ethnic scarifications and mimicking subcutaneous panniculitis-like T-cell lymphoma. Virchows Arch 438:298–301
2. Magro CM, Crowson AN, Kovatich AJ, Burns F (2001) Lupus profundus, indeterminate lymphocytic lobular panniculitis and subcutaneous T-cell lymphoma: a spectrum of subcuticular T-cell lymphoid dyscrasia. J Cutan Pathol 28:235–247
3. Wood GS (2001) Benign and malignant cutaneous lymphoproliferative disorders including mycosis fungoides. In: Knowles DM (ed) Neoplastic hematopathology, 2nd edn. Lippincott, Williams and Wilkins, Philadelphia, pp 1183–1233

Virchows Arch (2004) 444:397–399
DOI 10.1007/s00428-003-0961-5

LETTER TO THE EDITOR

Susanne Mende · Michael Moschopulos · A. Marx · R. Hubert Laeng

Ectopic micronodular thymoma with lymphoid stroma

Received: 22 September 2003 / Accepted: 21 November 2003 / Published online: 23 January 2004

Sir, Micronodular thymoma (MNT) with lymphoid B-cell hyperplasia, a recently described rare benign neoplasm of thymic epithelium, has been found, thus far, invariably in the anterior mediastinum. We present herein an ectopic MNT incidentally found in the left cervical region related to the parotid gland. Another novel finding is partial myoid differentiation of neoplastic epithelial cells.

A 45-year-old otherwise healthy man appeared in consultation for a feeling of hearing loss when a left cervical tumour was incidentally found. There was neither myasthenia gravis nor any other autoimmune diseases. The tumour, clinically suspicious for cervical lymphadenopathy, was encapsulated and could be completely removed, although minimally adherent with the parotid gland. A follow-up control 1 year after surgery found the patient free of recurrence. At gross examination, the tumour measured 3.5 cm, exhibited a microcystic cut surface and was completely enclosed in a thin fibrous capsule. Histologically, solid micronodules of neoplastic epithelial cells stood out against a lymphoid stromal background in close relationship with the parotid gland (Fig. 1); normal ectopic thymus was not observed. Periodic acid-Schiff and reticulin stains highlighted a delicate envelope of epithelial complexes, but reticulin fibres did not surround individual cells. Using immunohistochemistry, the neoplastic epithelial cells were reactive for cytokeratins (5, 6, 8, 17) and alpha-smooth muscle actin (α-SMA, Fig. 2), but non-reactive for desmin, myoglobin, myogenin, S-100 protein, glial fibrillary acid protein (GFAP) and CD20. In the stromal compartment, reactive lymph follicles displayed hyperplastic germinal centres (Fig. 1 and Fig. 2) and a polyclonal B-cell population, including a minor fraction of immunohistochemically polytypic plasma cells. Polymerase chain reaction for Ig heavy chain gene rearrangement also indicated the presence of polyclonal B cells. There were considerable numbers of CD3+ mature T cells

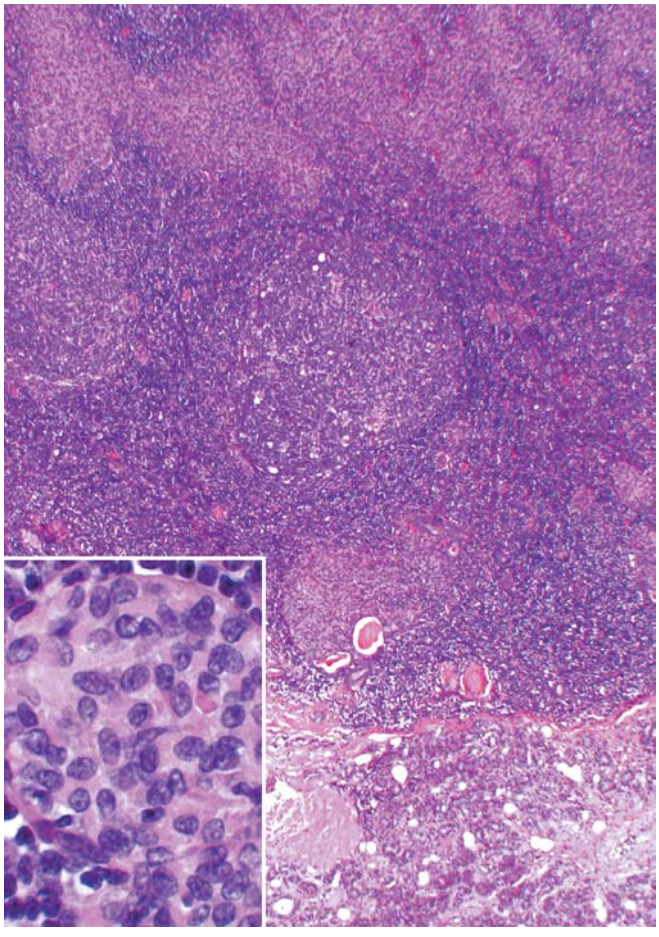

Fig. 1 Low-power view of micronodular thymoma with lymphoid stroma associated with the parotid gland (×88). *Inset* Neoplastic epithelial cells display bland cytomorphology (×380)

S. Mende · M. Moschopulos · R. H. Laeng (✉)
Department of Pathology,
Kantonsspital,
5001 Aarau, Switzerland
e-mail: laeng@ksa.ch
Tel.: +41-62-8386105
Fax: +41-62-8385299

A. Marx
University of Würzburg,
97080 Würzburg, Germany

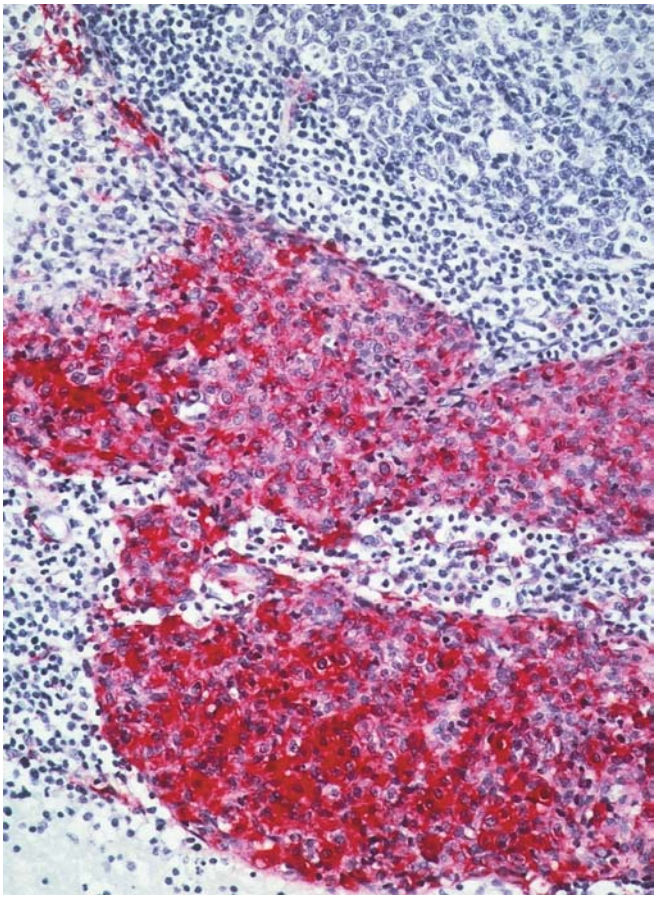

Fig. 2 Cohesive complexes of neoplastic epithelial cells of ectopic micronodular thymoma strongly stain for α-smooth muscle actin; identical results are obtained for cytokeratins (×175)

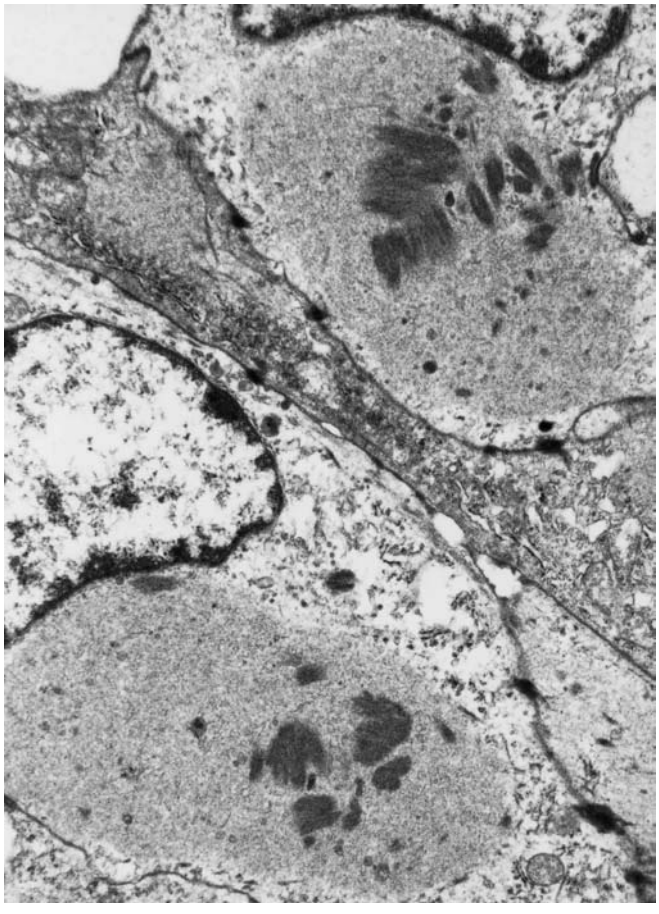

Fig. 3 At the ultrastructural level, neoplastic epithelial cells of this particular example of ectopic micronodular thymoma are equipped with Z band-like structures, while features of striated muscle differentiation typical of thymic myoid cells are absent (×10,400)

among neoplastic epithelia and in the stromal compartment, occupying interfollicular areas and follicular mantle zones. Interdigitating CD1a+ and S-100+ reticulum cells were far more numerous in the epithelial compartment than in the stroma, and CD68+ epithelioid histiocytes were an important stromal component. Immature T cells (CD1a+, CD99+), similar to classical World Health Organization (WHO) type-A thymomas, were an exceptional finding [3]. At the ultrastructural level, osmiophilic Z-band-like structures were found distributed in a disorderly manner in epithelial tumour cells, but further arguments for striational differentiation were lacking (Fig. 3).

MNT with lymphoid B-cell hyperplasia, originally presented in a series of 18 cases by Suster and Moran in 1999, is defined by its distinctive histoarchitecture, cytomorphology and clinical appearance [4]. Meanwhile, only few more examples have come to record [6, 7]. Nevertheless, MNT will be established as a separate but rare entity of organotypical thymoma in the forthcoming WHO blue book. Diagnostic histoarchitectural features include a discretely nodular growth pattern, a multitude of cohesive complexes of neoplastic thymic epithelial cells and a lymphocytic stroma devoid of epithelial cells optionally harbouring a variable number of lymph follicles, usually with prominent germinal centres (Fig. 1). Cytomorphologically, neoplastic epithelia are slender or plump spindle cells with bland-appearing nuclei and inconspicuous nucleoli (Fig. 1, inset); they display either proliferative quiescence or minimal proliferative activity. MNT resemble type-A thymomas, and, therefore, a medullary ancestry has been anticipated [7]. Clinically, MNT are typically asymptomatic and incidental findings; they are usually either encapsulated or minimally invasive, therefore, of low Masaoka stages I or II and curable by local resection. Myasthenia gravis and other autoimmune diseases are absent, unless combined with another type of organotypical thymoma [7]. Organotypical thymomas, thus far, include WHO types A, AB and B; they are conceptually restricted to the thymus, but may be incidentally found on ectopic sites. Immature T cells provide a diagnostic hallmark of organotypical thymomas, although such cells are exceedingly sparse or even lacking in type-A thymomas. Likewise, immature T cells in MNT are rare or absent in the epithelial component, but regularly present in perinodular areas of

the stromal compartment. Therefore, we believe that MNT qualify for organotypical thymomas.

Regarding the morphology of our case, there are two serious differential diagnostic considerations: (i) myoepithelioma of the parotid gland and (ii) metastatic disease in a parotideal lymph node; a third option suggested by the site, (iii) ectopic hamartomatous thymoma comes to mind. While a solid histoarchitecture and spindle-shaped cytomorphology are shared by a majority of salivary gland myoepitheliomas, they display hyaline cytoplasm, mucoid stroma and coexpress S-100 protein, actin and GFAP; none of those features is seen in our case. Furthermore, the coexistence of stromal immature T cells and interepithelial interdigitating reticulum cells is not germane to myoepitheliomas, but is found in MNT and eventually in ectopic hamartomatous thymoma. Ectopic hamartomatous thymoma is a benign non-recurrent tumour composed of a biphasic epithelial component, islands of mature adipose tissue and generally inconspicuous interepithelial lymphocytes. Thus, ectopic hamartomatous thymoma is morphologically distinct from MNT [1]. Finally, there is neither clinical nor morphological evidence of malignancy; regarding metastatic disease, no primary neoplasm is known elsewhere.

The ectopic site in the neck, although infrequently observed in organotypical thymomas, is easily explained by the derivation of the two thymic primordial structures from the third and fourth branchial (pharyngeal) pouches. The supraclavicular and suprasternal region, overlapping with the neck and included in the developmental descent, are also the usual locations of ectopic hamartomatous thymomas [1]. Associated normal ectopic thymus is found only in a minority of ectopic cervical thymomas. Myoid cells are regularly found in the medulla and medullary–cortical junction of the normal human thymus. Myoid differentiation has been reported in single examples of ectopic hamartomatous thymomas and even in other rare non-organotypical thymic epithelial neoplasms (WHO type-C thymic carcinomas) [1, 2, 5]. Myoid cells exhibit striated muscle differentiation and are supposed to derive from thymic epithelium [7]. Unlike thymic neoplasms with myoid components on record, neither immunohistochemistry nor electron microscopy revealed striated muscle differentiation in our case, and a biphasic cytomorphology of neoplastic epithelia as well as pseudosarcomatous stroma were absent [2, 5]. Myoepithelial or partial smooth muscle differentiation of neoplastic cells resembling the findings in our present case, however, is observed in two of five other examples of low-grade metaplastic thymic carcinomas in both the solid and spindle components of this biphasic thymic epithelial tumour, but, thus far, not in MNT [8]. Metaplasia, a common phenomenon in neoplastic disorders, is supposed to be the pathogenic pathway of smooth muscle differentiation in those instances [8]. Our observation of α-SMA immunoreactivity in MNTs nicely illustrates the versatility of neoplastic epithelial cells also in organotypical thymomas and suggests that metaplastic change may be expected in both orthotopic and ectopic thymomas.

Regarding the original term, we believe that the designation "lymphoid B cell hyperplasia" reflects the stromal cellular response in MNT incompletely [4]. In our own and other observers' experience, MNT harbour an important proportion of mature CD3+ CD5+ T cells [6]. A majority displays lymphofollicular hyperplasia with well-developed mantle and marginal zones where T cells play their part in the immune response as elsewhere. Therefore, the term "MNT with lymphoid stroma" has been proposed for the forthcoming WHO blue book.

Acknowledgement A.M. was supported by the EU Grant QLRT-2000–01918.

References

1. Chan JKC (2002) Ectopic hamartomatous thymoma. In: Fletcher CDM, Unni KK, Mertens F (eds) Pathology and genetics of tumours of soft tissue and bone. IARC Press, Lyon, pp 192–193
2. Eimoto T, Kitaoka M, Ogawa H, Niwa H, Murasse T, Tateyama H, Inagaki H, Soji T, Wang HJ (2002) Thymic sarcomatoid carcinoma with skeletal muscle differentiation: report of two cases, one with cytogenetic analysis. Histopathology 40:46–57
3. Rosai J (1999) Histological typing of tumours of the thymus. In: World Health Organisation, International histological classification of tumours. Springer, Berlin
4. Suster S, Moran CA (1999) Micronodular thymoma with lymphoid B-cell hyperplasia. Clinicopathologic and immunohistochemical study of eighteen cases of a distinctive morphologic variant of thymic epithelial neoplasm. Am J Surg Pathol 23:955–963
5. Suster S, Moran CA, Chan JKC (1997) Thymoma with pseudosarcomatous stroma. Report of an unusual histologic variant of thymic epithelial neoplasm that may simulate carcinosarcoma. Am J Surg Pathol 21:1316–1323
6. Tateyama H, Saito Y, Fujii Y, Okumara M, Nakamura K, Tada H, Yasumitsu T, Eimoto T (2001) The spectrum of micronodular thymic epithelial tumours with lymphoid B-cell hyperplasia. Histopathology 38:519–527
7. Thomas de Montpreville V, Zemoura L, Dulmet E (2002) Thymoma with epithelial micronodules and lymphoid hyperplasia: six cases of a rare and equivocal subtype. Ann Pathol 22:177–182
8. Yoneda S, Marx A, Heimann S, Shirakusa T, Kikuchi M, Müller-Hermelink HK (1999) Low-grade metaplastic carcinoma of the thymus. Histopathology 35:19–30

Virchows Arch (2004) 444:400–401
DOI 10.1007/s00428-004-1002-8

ANNOUNCEMENTS

9–12 May 2004
XIV EUROCELLPATH COURSE: The Impact of Proteomics and Genomics in Pathology
Girona, Spain

The Organising Committee of the next EuroCellPath Course invites you to come to the beautiful city of Girona to enjoy an outstanding program on a very timely topic, addressed by leading authorities in the field, in an inspiring setting. The subjects covered in this course will be the following:

- DNA arrays: Methods and Goals
- Tissue Microarrays: A Tool for Rapid, Efficient Translational Research
- Proteomics: From Genes to Functions
- Tissue Procurement and Handling: Laser Capture Microdissection and Other Techniques
- Bioinformatic Tools for Array Data Mining
- Application of Array Genomics and Proteomics in Pathology
- Molecular Pathology of Genes and Proteins: What to Look For and When.

You may also submit your abstracts on these or other related topics, to be presented either as platform or poster during the Course.

For further information, please contact:
Prof. Josep Lloreta-Trull (local organizer)
Department of Pathology
Hospital del Mar-IMAS-IMIM
Universitat Pumpeu Fabra
Passeig Marítim 25–29, 08003-Barcelona, Spain
Tel.: +34 93 248 30 31, Fax: +34 93 248 31 31
E-mail: jlloreta@imas.imim.es or enter the course website
http://www.tilesa.es/eurocellpath04/

10–14 May 2004
Diagnostic Histopathology of Breast Disease
Hammersmith Hospital (Imperial College), London, UK

A week-long course designed for pathologists at Consultant and Senior Trainee level. The course provides a comprehensive coverage of the Histopathology of Breast Disease, with special emphasis on areas that pose diagnostic difficulties. The participants will be given ample time to study histological preparations, followed by illustrated discussion of the cases. There will be special sessions dealing with the interpretation of core biopsies and fine needle aspirations. There will also be several daily talks dealing with specific topics, given by eminent breast pathologists and followed by discussion. The topics will include reporting breast biopsies, immunohistochemistry, receptor and c-erbB-2 assessment, dealing with the gross specimen, prognostic factors, proliferative lesions/carcinoma in situ, problems in breast pathology, mucinous lesions of the breast, a practical approach to the diagnosis of breast lymphomas and molecular pathology including the morphology of breast cancer associated with BRCA1 & 2 mutation. The faculty will include Ian Ellis, Christopher Elston, Andrew Hanby, Kristin Henry, Stephen Humphreys, Sunil Lakhani, Andrew Lee, Naomi Livni, Sarah Pinder and Sami Shousha.

Further details from:
Wolfson Conference Centre
Hammersmith Hospital
Du Cane Road
London W12 ONN, UK
Tel: (44) 20 8383 3117/3227/3245
Fax: (44) 20 8383 2428
E-mail: wcc@ic.ac.uk

1–11 June 2004
International course on Laboratory Animal Science
Utrecht, The Netherlands

A two week intensive course on laboratory animal science will be organized at the Department of Laboratory Animal Science – Utrecht, The Netherlands in June 2004. This course is organized once a year since 1993.

The objective of this course is to present basic facts and principles that are essential for the humane use and care of animals and for the quality of research.

The contents of the course are in line with recommendations of the Federation of European Laboratory Animal Science Associations (FELASA) regarding the training of the young scientist whose research involves the use of vertebrate animals.

The course may also be of interest for those who intend to set up a similar course at their location. For this purpose, during the course the acquisition of teaching materials can be discussed with the course committee.

For information and application forms please contact:
Prof. L.F.M. van Zutphen, PhD or
Mr. Stephan van Meulebrouck, MA
Department of Laboratory Animal Science
Faculty of Veterinary Medicine
P.O. Box 80.166
3508 TD Utrecht
The Netherlands
Tel.: ++31-30-2532033
Fax: ++31-30-2537997
E-mail: pdk@las.vet.uu.nl
Internet: http://las.vet.uu.nl (click on “Education and Training”)

4–5 June 2004
15th Ljudevit Jurak International Symposium on Comparative Pathology
(http://www.kbsm.hr/Jurak/symposium.htm), will be held in Multimedial center Sestre milosrdnice University Hospital, Vinogradska 29, Zagreb, Croatia.

The main symposium topic is head and neck pathology (including ophthalmopathology). Symposium includes following sections: Pathological Morphology of the Human and Animal Diseases, Iatrogenic, Environmental and Experimental Pathology, Herman Jurak Round Table on Rheumatological Pathology, Telepathology on-line conference, Clinical Forensic Pathology, Slide Seminars *in Histopathology and Cytopathology*, Quiz on Pathology.

For further information please contact:
Davor Tomas, M.D.
Ljudevit Jurak Clinical Department of Pathology
Sestre milosrdnice University Hospital
Vinogradska 29
10000 Zagreb, Croatia
Phone: 385-1-3787-909
Fax: 385-1-3787-244
e-mail: dtomas@kbsm.hr, juraks@kbsm.hr

7–9 June 2004
40th Nottingham Multi-disciplinary Course on breast disease
Nottingham, UK

This non residential course includes one and a half days of multi-disciplinary education and one and a half days of seminars specific to each discipline.

For further information contact:
The Blamey Education Centre
Nottingham Breast Institute
City Hospital, Nottingham, NG5 1PB, UK
Tel.: 00 44 (115) 969 1689
E-mail: sbury@ncht.trent.nhs.uk

11–16 July 2004
ULTRAPATH XII: Conference on Diagnostic Electron Microscopy with Surgical, Clinical, and Molecular Pathology Correlations
Barcelona, Spain

The scientific program will cover diagnostic Electron Microscopy as well as Diagnostic Pathology – with immunohistochemical and molecular correlations – and translational research. Renowned experts in the field from both sides of the Atlantic will present updated comprehensive reviews of significant areas of Pathology. In addition, a new section of the meeting will be devoted to a Pathology Review Course. Platform and Poster presentations will also be an important part of the program.

For further information, please contact:
Josep Lloreta-Trull, M.D., Ph.D. (chairman)
Department of Pathology, Hospital del Mar-IMAS-IMIM
Universitat Pompeu Fabra
Passeig Maritim 25–29, 08003-Barcelona, Spain
Tel.: +34 93 248 30 31
Fax: +34 93 248 31 31
E-mail: jlloreta@imas.imim.es.
The Application form and Abstract form can be found on the meeting website, http://www.tilesa.es/ultrapath04/

27–30 July 2004, London
Practical Pulmonary Pathology

This course is designed to provide histopathology and cytopathology trainees and consultants with an opportunity to study diagnostic lung pathology in a comprehensive manner. It comprises lectures and practical microscopy sessions, the latter making up roughly half the time and consisting of individual study of a unique collection of cases.

For further details and application forms please contact:
Professor B Corrin,
Brompton Hospital
London SW3 6NP
Fax: +44 20 7351 8293.
E-mail: b.corrin@ic.ac.uk

9 September 2004
One day course on Advanced Ultrasound of the Breast
Nottingham, UK

For further information contact:
The Blamey Education Centre
Nottingham Breast Institute
City Hospital, Nottingham, NG5 1PB, UK
Tel.: 00 44 (115) 969 1689
E-mail: sbury@ncht.trent.nhs.uk

23–24 September 2004 **(Change of date)**
Thyroid Pathology for the Practicing Pathologist
15 rue de l'Ecole de Médecine, Paris, France

A 2-day course will take place in Paris under the auspices of the French Division of the I.A.P. This course will be given in English by Prof. M. Sobrinho-Simoes (Porto) and Prof. R. Heimann (Brussels).

It will consist of lectures alternating with slide reviews and a slide seminar over a multihead microscope. The cases of this seminar will be sent (on CD) before the meeting. The audience will be limited to 22 participants.

Course fee: 390 euros (320 euros for members of any IAP division). The fees include registration, hand-out, CD of the slide seminar and coffee breaks.

For further information, please contact:
Mrs. M. Fontanière
Administrative Secretary
French Division of the I.A.P. 32 Cours Albert Thomas
69008, Lyon, France
Fax: 33478754311
E-mail: academie.pathologie@wanadoo.fr

11 October 2004
Continuing Medical Education
Nottingham, UK

For further information contact:
The Blamey Education Centre
Nottingham Breast Institute
City Hospital, Nottingham, NG5 1PB, UK
Tel.: 00 44 (115) 969 1689
E-mail: sbury@ncht.trent.nhs.uk

22–24 November 2004
41st Nottingham Multi-disciplinary Course on breast disease
Nottingham, UK

For further information contact:
The Blamey Education Centre
Nottingham Breast Institute
City Hospital, Nottingham, NG5 1PB, UK
Tel.: 00 44 (115) 969 1689
E-mail: sbury@ncht.trent.nhs.uk

Virchows Arch (2004) 444:403–409
DOI 10.1007/s00428-004-0980-x

REVIEW ARTICLE

Kurt Brauchli · Hermann Oberli · Nina Hurwitz · Klaus-Dieter Kunze · Gunter Haroske · Gernot Jundt · Gerhard Stauch · Lech Banach · Mark Wirdnam · Michael Mihatsch · Martin Oberholzer

Diagnostic telepathology: long-term experience of a single institution

Received: 28 October 2003 / Accepted: 15 January 2004 / Published online: 12 March 2004

Abstract *Objectives:* The paper reviews the development of the application of telepathology in a department of surgical pathology between 1991 and 2003. The goal of the efforts during this time was to give up the concept of programming a single application, available only between two fixed workstations with sophisticated devices and special software, and to find the virtual "largest common denominator" for implementing as many different applications as possible with the same basic system. *Methods:* A new telepathology system was designed as a client–server system with a relational database at its centre. The clients interact together by transferring the questions (texts and images) to a record (case) in the database on the server and by transferring the answers to the same record on the database. *Results:* The new "open" telepathology system iPath (http://telepath.patho.unibas.ch) has been very well accepted by many groups around the world. The main application fields are: consultations between pathologists and medical institutions without a pathologist (e.g. for frozen section diagnoses or for surgical diagnoses in hospitals in South Asia or Africa), tumour boards, field studies and distance education (http://teleteach.patho. unibas.ch). *Conclusions:* Having observed that with iPath we have succeeded in satisfying all our telepathology needs, we are inclined to put the emphasis on the nature of the tasks being performed, as opposed to the methods or technical means for performing a given task. The three organisation models proposed by Weinstein et al. (2001) [24] can be reduced to only two models: the model of discussion groups and the model of expert groups (virtual institutes).

Keywords Telepathology · Surgical pathology · Telemedicine

K. Brauchli · N. Hurwitz · G. Jundt · M. Wirdnam · M. Mihatsch · M. Oberholzer (✉)
Department of Pathology of the University, Basel, Switzerland
e-mail: moberholzer@uhbs.ch
Tel.: +41-61-2652525
Fax: +41-61-2653194

H. Oberli
National Referral Hospital,
Honiara, Solomon Islands

K.-D. Kunze
Institute of Pathology, Technical University,
Dresden, Germany

G. Haroske
Institute of Pathology,
Kreiskrankenhaus Dresden-Friedrichsstadt,
Dresden, Germany

G. Stauch
Institute of Pathology,
Aurich, Germany

L. Banach
Institute of Pathology of the University of Transkei,
Umtata, South Africa

Development of telepathology in a department of surgical pathology

The first application of telepathology at the Department of Pathology of the University of Basel in Switzerland was in 1991 [17], implementing a remote diagnosis service on intraoperative frozen sections for the Regional Hospital in Samedan, Oberengadin, Switzerland.

The telepathology system used today (iPath) is an Internet-based system (http://telepath.patho.unibas.ch) and was developed at the Department of Pathology of the University of Basel on the background of over 10 years experience. Current applications include pathology telediagnosis for hospitals, primarily in Asia, and for second-opinion consultations in subspecialities (histopathology, radiology), primarily in Europe. Our experiences have demonstrated that a multi-purpose telemedical system can also comfortably be used for tumour boards, health networks, field studies and even distance learning (http://teleteach.patho.unibas.ch).

The current challenges in telepathology are: (1) the creation of minimal standards allowing the interaction between different systems [4, 11, 25] and (2) the organi-

sation of individual workflow to allow efficient use of telepathology in daily routine (Brauchli et al. unpublished data). Therefore, we would like to achieve the following: (1) to answer the question, "Which are the essential fundaments of a modern, user-friendly telepathology in the future?" and (2) to summarise our observations and own experiences in telepathology and telemedicine.

Essential fundaments for a modern telepathology (telemedicine)

Telepathology is a structured dialogue

Modern computer and network technology offers all the elements for telecollaboration in medicine. For that reason, the development of telemedical systems is currently more focused on how to organise cooperation and how to use the existing technology in a most user-friendly way.

The goal of any kind of telemedicine is to exchange information. Such an exchange of information has to be possible from anywhere at any time, without delay and without additional effort. Basically, any exchange of information in medicine can be considered as a question, part of which often consists of pictures and the answer to that question. We use the terms "expert" and "non-expert" to define the roles of the partners within a real telemedical exchange of information, thus referring to who is asking the question ("non-expert") and who is delivering the answer ("expert").

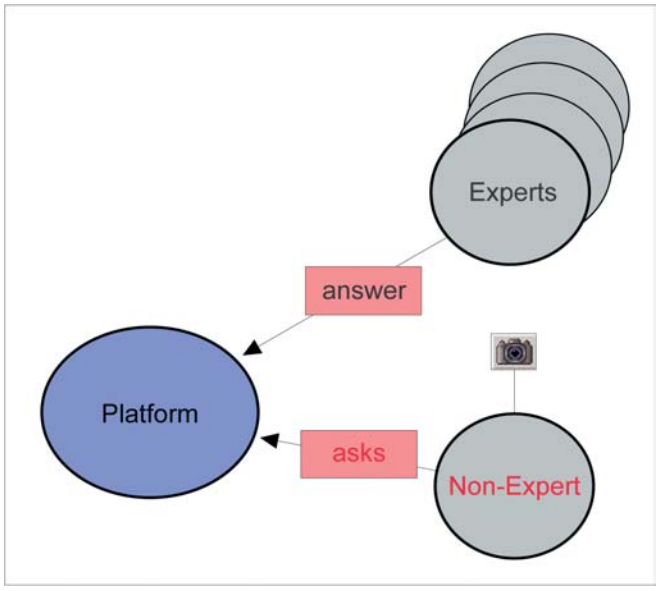

Fig. 1 Telepathology is a structured dialogue. Technically, the non-expert deposits his questions and images on a server (platform). The experts can see what is stored in the database on the server and can add their comments. The non-expert can re-contact the server and see the answers given

Free exchange of information in medicine can be guaranteed by a client–server system

A server (Fig. 1: platform) contains a database connected with a content management system and manages the necessary connections between the clients (experts and non-experts) (Fig. 1). The server is placed within the Internet when connectivity beyond the local network is needed (Fig. 2). The members of the different discussion groups (experts and non-experts) working on the cases (by asking and answering) are all clients. A client application can be a remote microscopy session (synchronous applications) [1, 22] or a standard web-browser or e-mail client for case discussion (asynchronous applications) [1, 22].

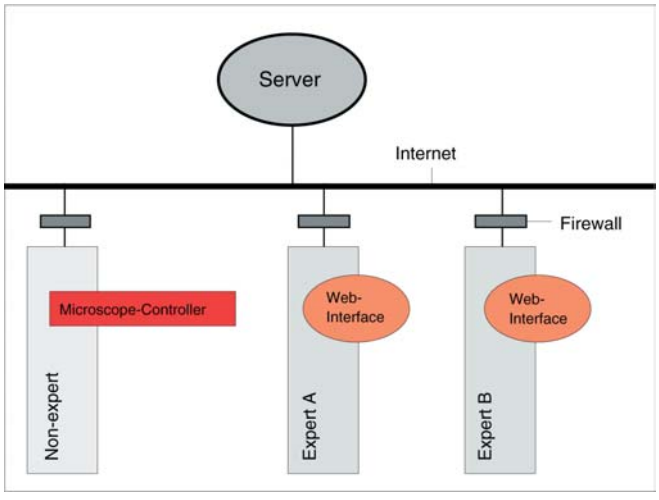

Fig. 2 The location of the server determines the user-friendliness of access to the system. The iPath-Server is in the Internet without access restriction from any firewall. This position guarantees easy access for every authorised user at any time or location

A modern telepathology system should have a modular structure

The experiences in the field of telepathology have demonstrated how important it can be to quickly create a new telepathological (telemedical) connection or to adapt an existing system to new user needs or new technologies. This goal can be achieved through modularisation of single hardware elements and software elements for the different tasks.

The most important module for implementing an efficient telepathology is the Internet. Since Internet browsers and e-mail clients usually exist on all computers, an expert can easily join and participate in a discussion group (even for remote microscopy). The non-expert will only need a digital camera or corresponding appliance connected to his or her computer.

The first application of Internet browser technology for telemicroscopy or dynamic telepathology [1, 8, 16, 24] was demonstrated by the TeleMic project at the Charitée University of Berlin [19, 27]. However, a fundamental problem in using the Internet is firewalls, which are installed in the different institutions, prohibiting a spontaneous and direct connection between computers located within the institution and computers outside of the institution. The most convenient solution for this problem is the use of a server directly located in the Internet and directing all traffic "between two or more computers (clients)" through that server [3, 21] (Fig. 2).

The "conceptional" summary of over 10 years experience in telepathology (telemedicine)

The newly developed telemedical system iPath is the result of broad practical experiences and theoretical analyses in many fields of telemedicine. The first experiences were in remote microscopy [18]. iPath implements characteristics of both a collaboration tool and a content management system. The content that is managed is the questions of the non-experts (texts, images and/or other objects) and the answers of the experts.

The centre of each telepathology system: the database

The relational database allows the collection of all data transferred between the partners. Around this core is the application governing content, an application that currently has a web- and a (standardised) e-mail-interface implemented. The content managed is divided into discussion or expert groups (see above). The importance of a clear database concept as the basis of a telepathology system for routine use is, however, referred to in only a very few publications [18, 21].

Within the groups in the database are the cases (records) (Fig. 3). Finally, each case contains the actual data produced: the questions, the "objects" (images, schemas, forms, other relevant documents or textual information), and the comments (diagnoses, remarks, additional questions). This central storage of data with search facilities serves as an archive of all past collaborations and consultations, if necessary. If the remote microscopy module is used, the session is linked to an open case defined beforehand within a pre-designed group, and the expert can choose to add a selection of the pictures transmitted via the special module from the microscope to the video eye on the server. For real-time conferencing, an online chat function can be used.

Access to the "world of telepathology"

A group on a server is administered automatically. A potential group member must first register an account for the server and then contact the relevant group administrator for a group membership.

An iPath-Server can be installed using freely available open source software tools, such as Apache for the web-interface, and can run on the free operating system, Linux. This approach has been taken by several institutions that want to keep autonomy over their data [West African Doctors Network, Inland Northwest Health Service for the Spokane-district (Washington State, USA), breast carcinoma field studies in Dresden, Germany] (Fig. 4). Among the security measures implemented in our system are automatic interruption of open connections without activity after a predefined time and the possibility to encrypt all traffic to the server.

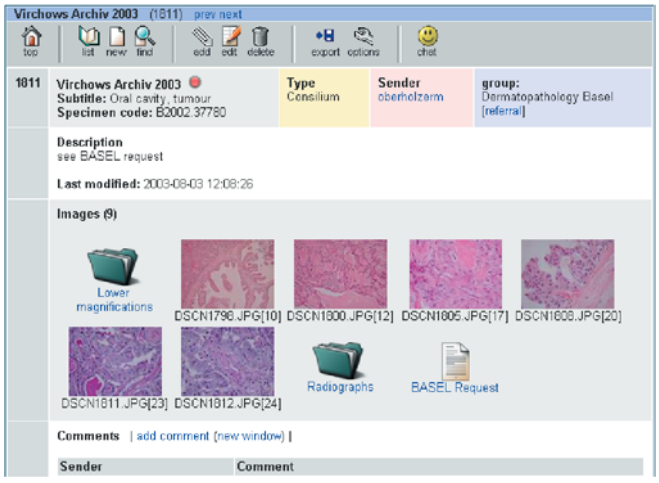

Fig. 3 The database consists of groups and cases (records). A case is stored within a group. Each case is subdivided into four segments: identification, description (free text), images (gallery of documents) and comments

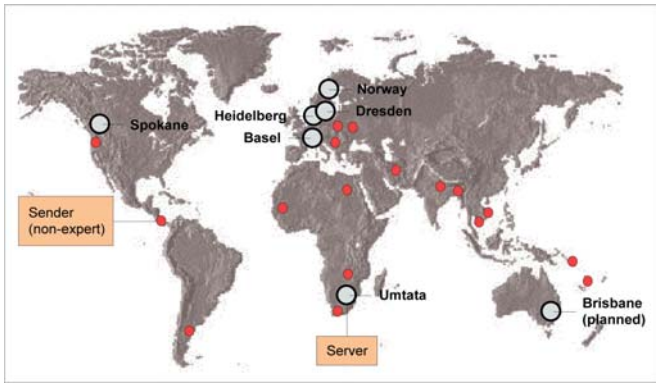

Fig. 4 Use of iPath around the world. iPath runs on six servers around the world. The server in Norway serves a health network in Western Africa. The server in Dresden functions as a centre of a field study about breast carcinoma organised by the German State of Sachsen

Main telemedical tasks

General observations

In September 2001, iPath was released and opened on the main server in Basel, with the intention to empirically observe in which direction the applications of such an open telepathology system would develop. The results are represented as follows.

In contrast to other Internet-based telepathology systems [9, 26], iPath does not impose a predefined workflow or mode of collaboration. It is, rather, a platform on which telemedical consultations and other applications can individually be arranged. The telemedical server in Basel is now used by over 800 users organised in more than 70 discussion or expert groups.

Consultations in pathology

Consultation is one of the main uses for a telemedical application. A recent evaluation showed that 43.8% of all cases on the telemedicine server in Basel were consultations in pathology. Consultations in telehistology and telecytology are desired by: (1) institutions without a pathologist, e.g. the Referral Hospital of Honiara, Solomon Islands (South Pacific); (2) general pathologists who work alone as pathologists in a hospital, e.g. the Department of Pathology of the Dhaka Medical College, Bangladesh or (3) pathologists in a speciality, e.g. at the University Hospital of Teheran, Iran, or the Working Group of Bone Tumours of Austria, Germany and Switzerland.

A very interesting result deduced of our practical experiences in the last 2 years is the Virtual Institute of Pathology (VIRIN). VIRIN represents an organised coworking of many experts distributed over the whole world. These experts work with different institutions. The members of these institutions are non-experts. The experts are members of their own expert group, as well as of the discussion (sender) groups of the non-experts. The non-experts submit their cases in their discussion group. In the VIRIN, one expert of the expert group is always on duty. He monitors the discussion groups (e.g. "South Pacific" for Honiara). He is responsible for a response to cases submitted by Honiara in the "South Pacific" group within 48–60 h. This expert can decide to present a newly submitted case to the other experts in the VIRIN. In the VIRIN, the case can be freely discussed without the non-experts seeing the different comments of the experts on his case. A summary of the discussion of the experts is then added to the original case (in the discussion group) by the expert on duty.

The results of the collaboration with Honiara in the time between 26 September 2001 and 2 May 2003 were analyzed under different aspects. One aspect was that, in the observed period, the percentage of benign diagnoses increased, approaching, in the phase where the VIRIN for Honiara was fully established, an amount as one would expect at a typical Western pathology institution (Fig. 5). This indicates that, after an initial phase of deciding only to discuss cases that mostly were assumed to be malign, Honiara is now comfortable with having an assessment of all the cases a Western hospital would usually submit. The introduction of the VIRIN also improved the percentage of secure diagnoses as opposed to those where doubts remained (Fig. 6).

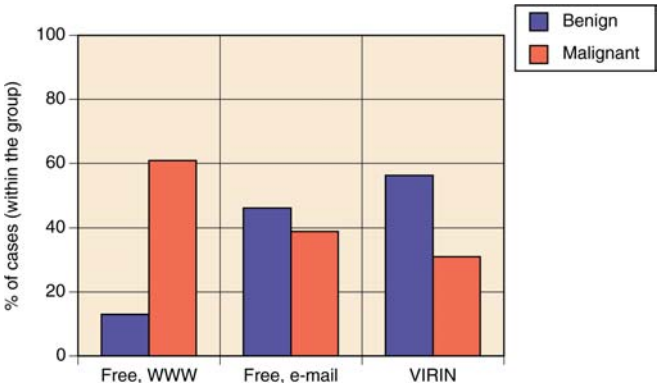

Fig. 5 The percentage of benign and malignant diagnoses. The collective "Free, WWW" consists of 23 cases (Period: 26 September 2001–19 March 2002), the collective "Free, e-mail" of 54 (Period: 20 March 2002–30 Setpember 2002), and the collective "VIRIN" of 71 cases (Period: 1 November 2002–2 May 2003). The submission per e-mail was carried out by a standardised specially developed e-mail procedure. Chi2 value: 10.062, v=2, P<0.01

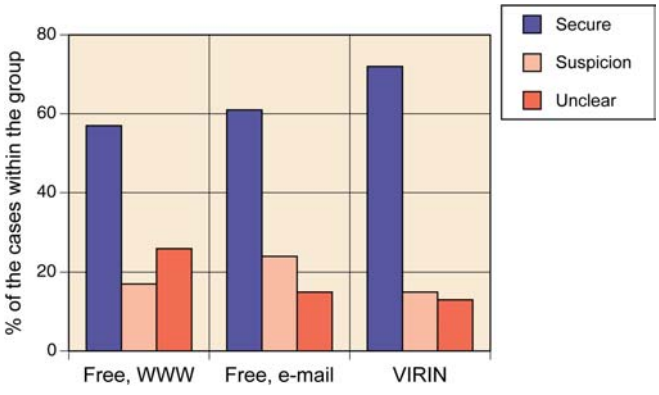

Fig. 6 The percentage of secure, suspicious and unclear diagnoses. Chi2 value: 4.142, v=4, P<0.20)

Interdisciplinary conferences

The tumour board of the Regional Hospital of Lörrach (Germany, near Basel) has been running systematically on iPath for 1.5 years. When preparing the tumour board, the key information from contributing institutions (e.g. pathology or radiology) is added to the cases that are previewed by the specialists before the conference.

Health networks

It could be observed that our telemedical system can simultaneously be used efficiently for both diagnosis and e-learning. This quality led to the idea to use iPath as a nucleus of health networks in the Ukraine (in collaboration with the Swiss Tropical Institute) and in the Eastern Cape province (South-Africa).

Field studies

A surprising result was the application of the actual system for field studies without special adaptations. In such studies, the user needs are the inverse of the original needs in telepathology, where knowledge is provided by a centre to a peripheral institution. The key element allowing this new application is forms. Forms correspond to a media record with empty text fields and can be created individually. The forms are stored as an integral part of the group's record structure. The content of all the forms can be exported as a two-dimensional textfile for further evaluation locally.

Implications after more than 10 years experience from a single institution

In the last years, we and others intensively experimented with an open telemedical system. The most important aspects which crystallised in using telepathology were: (1) working in virtual groups of specialists (experts), (2) a categorisation of telepathology in four main fields, (3) a definition of new (minimal) standards and (4) some hints as to change the general conception of telepathology (paradigm change).

The virtual group model (VIRIN)

The virtual group model was postulated by Weinstein et al. [24]. An open telepathology system allows a successful implementation of this model, of which the objective has become a reality with the Honiara project. Our VIRIN shows the necessity to clearly organise the diagnostic telepathological work and to exactly distinguish the role of all partners. Additionally, virtual working groups can give rise to a new vision of the job of a pathologist: telepathology offers retired professionals the possibility of remaining in their professional activity and allows society to continue to profit from the great experience of retired pathologists.

Categorisations in telepathology

Commenting on subdivisions discussed in previous publications on telepathology [10, 15, 16, 17, 18, 23], we see that the main focus has been on technical aspects of the method. In the early days of telepathology, the main differentiation was made between dynamic–robotic [1, 12, 20] versus static telepathology [5, 6, 20] models, which were mainly applied to point-to-point diagnostic telepathology links. With the advancement of Internet-based telepathology, the workflow process was brought much more into the centre of discussion. Weinstein et al. [24] suggest three categories of workflow organisation, namely the case triage model, subspeciality model and the virtual group practice model.

On the background of our observations and experiences, we propose to discriminate the following four telepathological categories: consultations, tumour boards, field studies/research and educational applications (Table 1). The three workflow models proposed by Weinstein et al. [24] can all be implemented through organising telepathology by discussion groups, optionally linked to an expert group.

Change of paradigm

Modern communication technologies, first and foremost the Internet, have brought telepathology and telemedicine a decisive step forward: a step that anticipates a change of paradigm, a change away from our current constellation of convictions, views and methods [13].

Technically, the field of telemedicine was dominated, until recently, by individual solutions, which could not communicate with each other. With the idea "iPath", we pursued the goal to give non-experts the means of remote dialogue with experts, using as much as possible of the non-experts existing infrastructure. Much of the task was: (1) to intelligently combine the computer resources with a database, (2) to achieve a high degree of organisation in their practical use and (3) to design the whole system as a modular content management system.

We can expect that convictions and methods in pathology will change in relation to the simplicity and spontaneity of telepathology in the future. Because telepathology—especially in rural areas [7, 28, 29, 30]—is increasingly being used by institutions without resident pathologists, the non-pathologist must become more familiar with the evaluation of macroscopy, the sampling of tissue specimens and the selection of microscopic fields.

Standardisation

Any broadly implemented method calls for some basic regulation [2, 14]. The probability of a minimal standardisation grows at the rate with which we succeed in clearly defining the technical elements of the method and precisely structuring the processes. The question of standardisation can be reduced to deciding on a server–client technology, the minimal requirements and structure for the database and the key features of the module's data input and output.

Table 1 The four new main application categories in telepathology. The spontaneous use of iPath has demonstrated that the different applications can be allocated to four main categories: (1) consultations, (2) tumour boards, casuistics/clinical pathological conferences (CPCs), (3) lectures and (4) field studies

Authors	Applications	Model	Activity of the experts in relation to the non-experts	
	(Content)	(Organisation)	At the same time[1]	Time-shifted
[24]	Intraoperative frozen section diagnosis		+	
	Surgical pathology consultation			+
	Expert-to-expert consultations			+
	Distance education			+
		Subspeciality		
		Case triage		
		Virtual group		
Present paper	Consultations	Discussion group	+	
	Active			
	Frozen sections			
	Conventional diagnosis			
	Others			
	Passive	Virtual institute		+
	Tumour boards	Discussion group		+
	Field studies	Discussion groups		+
	Distance education	Discussion groups		+
	Casuistics			
	CPCs			
	e-learning			

[1] iPath offers a chat function, which can be spontaneously used

Telepathology: a modern win–win situation for everyone?

Empirically, we could clearly show that telemedicine as an "open distributed system" based on client–server technology could perform according to the needs of users in a society saturated with information technology, as well as in an environment with minimal communication infrastructure. Open telemedicine allows these environments to be tied together and, thus, generates an added value for all partners.

References

1. Baak JP, van Diest PJ, Meijer GA (2000) Experience with a dynamic inexpensive video-conferencing system for frozen section telepathology. Anal Cell Pathol 21:169–175
2. Belnap CP, Freeman JH, Hudson DA, Person DA (2002) A versatile and economical method of image capture for telepathology. J Telemed Telecare 8:117–120
3. Brauchli K, Christen H, Haroske G, Meyer W, Kunze KD, Oberholzer M (2002) Telemicroscopy by the Internet revisited. J Pathol 196:238–243
4. Brauchli K, Helfrich M, Christen H, Jundt G, Haroske G, Mihatsch M, Oberli H, Oberholzer M (2002) [The future of telepathology. An Internet "distributed system" with "open standards"]. Pathologe 23:198–206
5. Cross SS, Dennis T, Start RD (2002) Telepathology: current status and future prospects in diagnostic histopathology. Histopathology 41:91–109
6. Della Mea V, Cataldi P, Boi S, Finato N, Della Palma P, Beltrami CA (1998) Image selection in static telepathology through the Internet. J Telemed Telecare 4[Suppl 1]:S20–S22
7. Della Mea V, Cortolezzis D, Beltrami CA (2000) The economics of telepathology—a case study. J Telemed Telecare 6[Suppl 1]:S168–S169
8. Demichelis F, Barbareschi M, Boi S, Clemente C, Dalla Palma P, Eccher C, Forti S (2001) Robotic telepathology for intraoperative remote diagnosis using a still-imaging-based system. Am J Clin Pathol 116:744–752
9. Dietel M, Nguyen-Dobinsky TN, Hufnagl P (2000) The UICC Telepathology Consultation Center. International Union Against Cancer. A global approach to improving consultation for pathologists in cancer diagnosis. Cancer 89:187–191
10. Dunn BE, Almagro UA, Choi H, Sheth NK, Arnold JS, Recla DL, Krupinski EA, Graham AR, Weinstein RS (1997) Dynamic-robotic telepathology: Department of Veterans Affairs feasibility study. Hum Pathol 28:8–12
11. Furness PN, Bamford WM (2001) Telepathology. Review. Curr Diagn Pathol 7:281–291
12. Gombas P, Skepper JN, Hegyi L (2002) The image pyramid system—an unbiased, inexpensive and broadly accessible method of telepathology. Pathol Oncol Res 8:68–73
13. Küng H (2002) Erkämpfte Freiheit. Erinnerungen. Pieper Verlag GmbH, München
14. Loane M, Wootton R (2002) A review of guidelines and standards for telemedicine. J Telemed Telecare 8:63–71
15. Nordrum I (1998) Real-time diagnoses in telepathology. Adv Clin Pathol 2:127–131
16. Nordrum I, Eide TJ (1995) Remote frozen section service in Norway. Arch Anat Cytol Pathol 43:253–256
17. Oberholzer M, Fischer HR, Christen H, Gerber S, Bruhlmann M, Mihatsch M, Famos M, Winkler C, Fehr P, Bechthold L (1993) Telepathology with an integrated services digital network—a new tool for image transfer in surgical pathology: a preliminary report. Hum Pathol 24:1078–1085
18. Oberholzer M, Fischer HR, Christen H, Gerber S, Bruhlmann M, Mihatsch MJ, Gahm T, Famos M, Winkler C, Fehr P (1995) Telepathology: frozen section diagnosis at a distance. Virchows Arch 426:3–9
19. Person DA (2000) Pacific Island Health Care Project: early experiences with a Web-based consultation and referral network. Pac Health Dialog 7:29–35
20. Remmelinck M, Lopes MB, Nagy N, Rorive S, Rombaut K, Decaestecker C, Kiss R, Salmon I (2000) How could static telepathology improve diagnosis in neuropathology? Anal Cell Pathol 21:177–182

21. Rogers N, Furness P, Rashbass J (2001) Development of a low-cost telepathology network in the UK National Health Service. J Telemed Telecare 7:121–123
22. Stredney D, Crawfis R, Wiet GJ, Sessanna D, Shareef N, Bryan J (1999) Interactive volume visualizations for synchronous and asynchronous remote collaboration. Stud Health Technol Inform 62:344–350
23. Weinberg DS, Allaert FA, Dusserre P, Drouot F, Retailliau B, Welch WR, Longtine J, Brodsky G, Folkerth R, Doolittle M (1996) Telepathology diagnosis by means of digital still images: an international validation study. Hum Pathol 27: 111–118
24. Weinstein RS, Descour MR, Liang C, Bhattacharyya AK, Graham AR, Davis JR, Scott KM, Richter L, Krupinski EA, Szymus J, Kayser K, Dunn BE (2001) Telepathology overview: from concept to implementation. Hum Pathol 32:1283–1299
25. Wells CA, Sowter C (2000) Telepathology: a diagnostic tool for the millennium? J Pathol 191:1–7
26. Williams BH (1998) The AFIP center for telemedicine application-pathology for the twenty-first century. Telemed Virtual Real 3:64–65
27. Wolf G, Petersen I, Dietel M (1998) Microscope remote control with an Internet browser. Anal Quant Cytol Histol 20:127–132
28. Wootton R (1997) The possible use of telemedicine in developing countries. J Telemed Telecare 3:23–26
29. Wright D (1997) Telemedicine and developing countries: a report of Study Group 2 of the ITU Development Sector. J Telemedicine Telecare 4:1–85
30. Zhao Y, Nakajima I, Juzoji H (2002) On-site investigation of the early phase of Bhutan Health Telematics Project. J Med Syst 26:67–77

Virchows Arch (2004) 444:410–414
DOI 10.1007/s00428-004-0981-9

ORIGINAL ARTICLE

Farid Moinfar · Peter Regitnig · Ali Dastranj Tabrizi · Helmut Denk · Fattaneh A. Tavassoli

Expression of androgen receptors in benign and malignant endometrial stromal neoplasms

Received: 2 December 2003 / Accepted: 9 January 2004 / Published online: 6 March 2004

Abstract Several studies have shown that endometrial stromal neoplasms express estrogen and progesterone receptors (ER, PR). To our knowledge, the presence or absence of androgen receptors (AR) in these rare uterine neoplasms has not been investigated. Tumors (n=20)—3 endometrial stromal nodules, 14 low-grade endometrial stromal sarcomas (ESS, low grade), and 3 high-grade endometrial sarcomas (undifferentiated endometrial sarcoma, UES)—were studied. Immunohistochemical analyses for ER, PR, and AR were performed on formalin-fixed, paraffin-embedded archival material. Positive immunoreactions for ER and PR were observed in 14 (70%) and 17 (85%) cases, respectively. Furthermore, 9 cases (45%) were positive for AR. Among 17 ESS and UES cases, 7 (41%) revealed positivity for AR. Two of three benign stromal nodules were also positive for AR. Moreover, one of the three high-grade sarcomas (undifferentiated endometrial sarcoma) was negative for both ER and PR, but showed positive reaction for AR. In summary, ARs are expressed in 45% of endometrial stromal neoplasms. In addition to determination of ER and PR, the results of immunohistochemical examination of AR in these rare uterine tumors may have some impact on the postoperative management of the patients.

Keywords Endometrial stromal tumors · Androgen receptor · Estrogen receptor · Progesterone receptor · Immunohistochemistry

F. Moinfar (✉) · P. Regitnig · A. D. Tabrizi · H. Denk
Department of Pathology,
Medical University Graz,
8036 Graz, Austria
e-mail: farid.moinfar@uni-graz.at
Fax: +43-31-6384329

F. A. Tavassoli
Department of Pathology,
Yale University School of Medicine,
New Haven, Connecticut, USA

Introduction

Uterine endometrial stromal tumors are among the rarest neoplasms in the female genital tract. Malignant mesenchymal tumors comprise less than 5% of primary uterine cancers, with endometrial stromal neoplasms accounting for less than 10% thereof [1, 11]. Endometrial stromal tumors are composed of cells resembling those of proliferative phase endometrial stroma. These tumors are subdivided into benign and malignant categories based on the type of tumor margin. Uterine endometrial stromal tumors with pushing margins are benign and designated endometrial stromal nodules (ESN). In contrast, endometrial stromal sarcomas (ESS) infiltrate the myometrium; they have been traditionally divided into low and high grades mainly based on mitotic count [16]. However, since high-grade endometrial sarcomas largely lack specific differentiation and hardly display histological resemblance to endometrial stroma, it has been proposed that they should be designated undifferentiated endometrial or uterine sarcomas [5]. Thus, the recent World Health Organization Classification of Tumors of the Breast and Female Genital Organs divides the uterine stromal neoplasms into three groups: (i) benign ESN, (ii) low-grade ESS, and (iii) undifferentiated endometrial sarcoma [27].

While low-grade ESS is a clinically indolent malignant neoplasm, which shows minimal cytological atypia, infrequent mitotic figures, and numerous thin-walled small arteriolar type (plexiform) vessels, the undifferentiated endometrial sarcoma is a highly aggressive tumor that lacks a plexiform vasculature, features severe cytological atypia, and has frequent and often atypical mitotic figures [4, 27].

Several previous biochemical and immunohistochemical studies [13, 21, 22, 29] have shown that uterine stromal neoplasms, particularly low-grade ESS, often express estrogen and progesterone receptors (ER, PR). Studies have also revealed that therapy with progestational agents is an important adjunct to surgical treatment in cases of low-grade ESS [7]. Many of the tumors that

contain PR will, at least partially, respond to hormonal manipulation using progestins [10, 15]. In contrast to ER and PR, the status of androgen receptors (AR) in benign and malignant uterine stromal neoplasms (ESN, ESS) has not yet been investigated. In the present study, we analyzed the immunoexpressions of AR as well as ER and PR in a series of 20 primary endometrial stromal tumors.

Materials and methods

Cases (n=20) comprising 3 benign ESN, 14 low-grade ESS, and 3 undifferentiated endometrial sarcomas were retrieved from the files of the Department of Gynecologic and Breast Pathology, Armed Forces Institute of Pathology, Washington, DC, and the Department of Pathology, Medical University of Graz, Austria. Determination of tumor type and histopathological grade was performed according to the new World Health Organization classification on Tumors of the Breast and Female Genital Organs [27].

Formalin-fixed, paraffin-embedded tissue blocks were cut into 4-μm-thick serial sections, which were mounted on pre-coated slides. The sections were deparaffinized, rehydrated, and rinsed in distilled water. Immunohistochemical assays for AR, ER, and PR were performed on consecutive paraffin sections using standardized automated procedures (Ventana Medical System, Tucson, AZ and Dako, Glostrup, Denmark) (Table 1). Monoclonal mouse antihuman antibody clones 6F11 and 1A6 (Ventana Medical Systems) were used as primary antibodies for ER and PR, respectively. For determination of AR expression, the monoclonal mouse antihuman androgen receptor antibody (clone: AR441; Dako) was used. In brief, antigen retrieval was achieved with microwave treatment (ER, PR) or heating in a water bath (AR) (Table 1). A Ventana ES (Ventana Medical Systems) or Chem-Mate (Dako) autostainer was used in conjunction with an indirect streptavidin-biotin method. After incubation with the primary antibody, incubation with the secondary (link) biotinylated antibody was performed for 30 min. After washing, sections were incubated with streptavidin-peroxidase for 30 min. Finally, the enzyme was visualized with diaminobenzidine. Counterstaining was performed with hematoxylin. In each case, the intensity of immunoreaction (negative, 1+, 2+, 3+) and the percentage of tumor cells with positive nuclear reaction were evaluated. Samples were scored as positive when at least 10% of nuclei were immunoreactive. Internal positive controls included normal endomyometrial tissue surrounding the tumors (Fig. 1A). Negative controls included substitution of the primary antibody with normal sera or phosphate-buffered saline, omission of the secondary antibody, and incubation of the primary antibody solution with lymphoid tissue. All slides were evaluated independently by at least two investigators (F.M. and A.D.T.). The rare cases in which disagreement occurred were reevaluated using a multi-headed microscope; a final agreement was reached in all cases.

Results

Results are summarized in Table 2. Positive immunoreactions for ER and PR in benign and malignant stromal tumors were observed in 14 (70%) and 17 (85%) cases, respectively. Androgen receptor positivity was found in 9

Table 1 Summary of antibodies and methods used in the current study. *DAB* diaminobenzidine

Antigen	Antibody (manufacturer)	Method (autostainer)	Dilution	Incubation time	Antigen retrieval
Androgen receptor	AR441 (Dako)	ChemMate-DAB (Dako ChemMate)	1:100	20 min	Water bath 100°C for 40 min, then cooling in Epitope Retrieval solution (Dako)
Estrogen receptor	6F11 (Ventana)	Biotin-DAB (Ventana ES)	Ready to use	32 min	Microwave at 160 W in sodium-citrate, pH 6.0, for 30 min
Progesteron receptor	1A6 (Ventana)	Biotin-DAB (Ventana ES)	Ready to use	32 min	Microwave at 160 W in sodium-citrate, pH 6.0, for 30 min

Table 2 Expression of androgen receptors, estrogen receptors, and progesterone receptors in benign and malignant endometrial stromal tumors. Less than 10% of tumor cells positive was designated as negative in the results. *ESN* endometrial stromal nodule, *ESS, low* endometrial stroma sarcoma, low grade, *UES* undifferentiated endometrial sarcoma

Case no.	Diagnosis	Androgen receptor		Estrogen receptor		Progesterone receptor	
		Percentage	Intensity	Percentage	Intensity	Percentage	Intensity
1	ESN	<10%	1+	70%	2+	90%	3+
2	ESN	40%	1+	60%	2+	80%	2+
3	ESN	20%	1+	<10%	1+	50%	2+
4	ESS, low	90%	3+	90%	3+	70%	2+
5	ESS, low	40%	1+	20%	1+	80%	2+
6	ESS, low	0	–	50%	1+	0	–
7	ESS, low	20%	1+	60%	2+	80%	3+
8	ESS, low	20%	2+	0	–	90%	3+
9	ESS, low	<10%	1+	<10%	1+	70%	2+
10	ESS, low	0	–	40%	1+	90%	3+
11	ESS, low	0	–	60%	2+	20%	1+
12	ESS, low	90%	3+	60%	2+	90%	3+
13	ESS, low	0	–	30%	1+	70%	2+
14	ESS, low	<10%	1+	80%	3+	20%	1+
15	ESS, low	0	–	60%	2+	70%	3+
16	ESS, low	0	–	30%	2+	30%	2+
17	ESS, low	0	–	0	–	70%	2+
18	UES	40%	2+	0	–	0	–
19	UES	30%	2+	50%	2+	80%	3+
20	UES	0	–	0	–	0	–

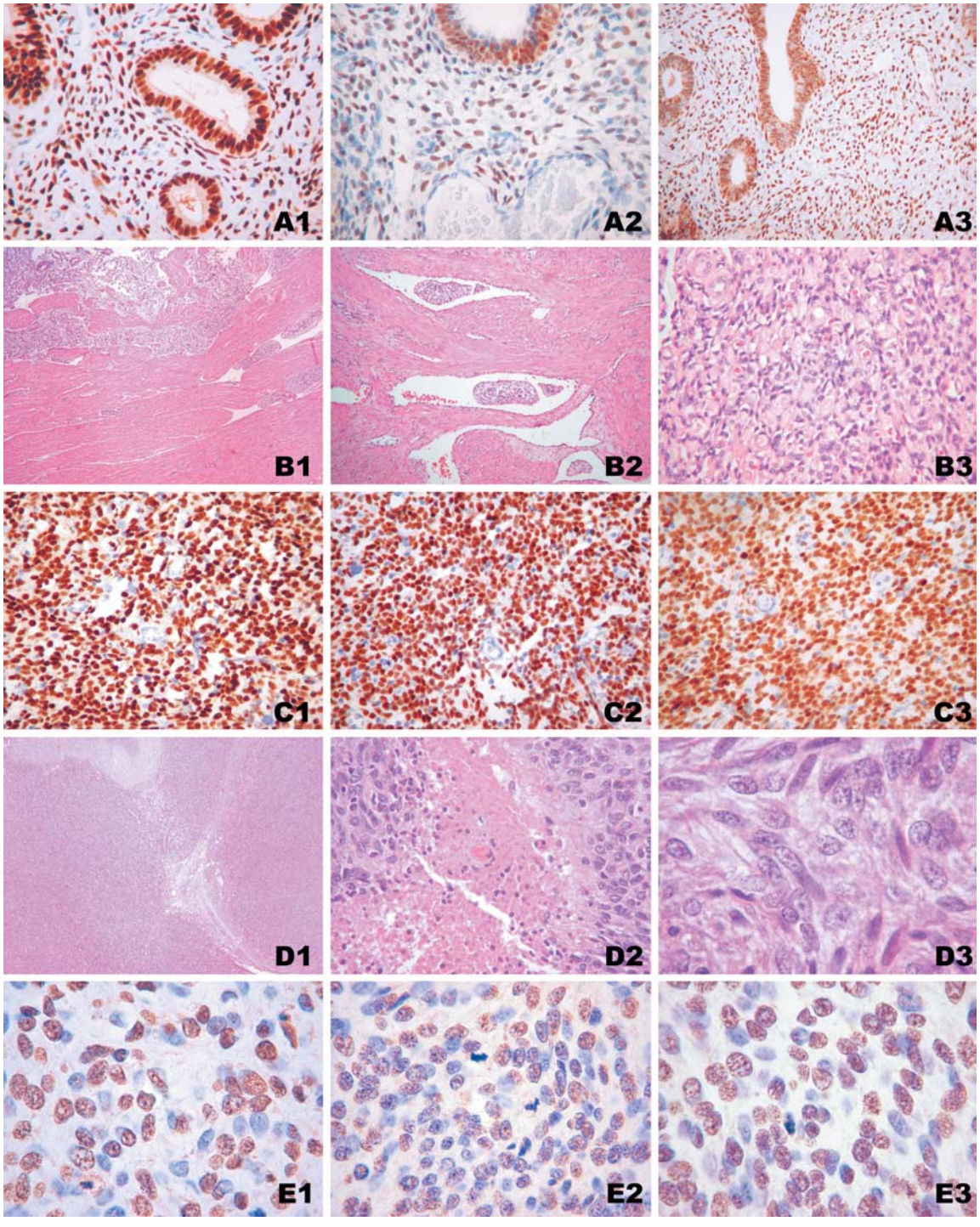

Fig. 1 **A** Expressions of estrogen receptors (ER) (**A1**), progesterone receptors (PR) (**A2**), and androgen receptors (AR) (**A3**) in non-neoplastic, normal endometrium (proliferative phase). **B** A low-grade endometrial stromal sarcoma (ESS) with typical infiltrative margins (**B1**), multiple lymphatic invasions (**B2**), and numerous thin-walled, small blood vessels (**B3**). **C** Expressions of ER (**C1**), PR (**C2**), and AR (**C3**) in a low-grade ESS. **D**, **E** A high-grade endometrial sarcoma (undifferentiated endometrial sarcoma) showing infiltrative pattern (**D1**), tumor cell necrosis (**D2**), and significant nuclear atypia (**D3**). Although the malignant stromal cells were completely negative for ER and PR (data not shown), a positive immunoreaction (1+ to 2+) for AR could be identified in many areas of this high-grade (undifferentiated) sarcoma (**E1**, **E2**, **E3**)

(45%) cases. While all three ESN cases were PR positive, two of them were positive for ER and AR. In 17 sarcomas (14 ESS, low grade and 3 undifferentiated endometrial sarcoma), positive reactions for ER, PR, and AR were observed in 12 (75%), 14 (83%), and 7 (41%) cases, respectively. In low-grade ESS, positive immunoreactions for ER, PR, and AR were found in 11 (79%), 13 (93%), and 5 (36%) cases, respectively (Fig. 1B, C). Although

two of the three undifferentiated endometrial sarcomas were negative for both ER and PR, a positive reaction of highly atypical tumor cells for AR was observed in one of the ER and PR negative cases (Fig. 1D, E) (Table 2).

Discussion

Previous studies demonstrated ER and PR in normal proliferative and secretory phase endometrium, both in endometrial glands and in stromal cells [19, 26]. A previous study also showed high ER and PR content in epithelium and stromal cells of simple and complex hyperplasia [2]. In atypical complex hyperplasia and endometrioid adenocarcinoma, however, the receptor content was significantly lower compared with that of normal proliferative or hyperplastic endometrium [2, 17, 19]. A few studies have demonstrated nuclear staining for AR in normal glands, endometrial stromal cells, and in endometrioid adenocarcinomas [3].

Several previous studies revealed expression of ER and PR in a high percentage of endometrial stromal sarcoma [13, 21, 22, 29]. However, to the best of our knowledge, the issue of AR expression in benign and malignant endometrial stromal neoplasms has not been examined previously.

According to our study, 45% of endometrial stromal neoplasms were AR positive. In sarcomas (low and high grades), a positive immunoreaction for AR was observed in 41% of examined cases. In all cases, the distribution of nuclear positivity for ER, PR, and AR among the tumor cells was quite heterogeneous (Table 2).

At least a partial response of low-grade ESS to hormonal therapy with progestins has been observed [8, 12, 18]. Recurrent or metastatic low-grade ESS have also been reported to be stabilized or suppressed with progestational agents in more than 50% of patients [5, 9, 20]. Tumors with a high level of progesterone receptors are most likely to respond to progestin therapy [20, 23, 28]. Treatment with gonadotropin-releasing hormone agonists has also been used in a few studies [14, 24]. However, although the vast majority of low-grade ESS have been shown to express ER and PR, some of the tumors, even with high ER and PR content, did not respond to adjuvant hormonal treatment [6, 25, 30]. This could be, at least in part, due to the heterogeneity of tumor cells in terms of expression of ER and PR and the presence or absence of other steroid receptors, such as AR. It is possible that the proportional distribution and concentration of each steroid receptor (ER, PR, and AR) among tumor cells influences the response to hormonal treatments. The biological significance of AR (stimulation versus inhibition of the growth of neoplastic endometrial stromal cells) and its interaction(s) with ER and PR in ESS requires further investigation.

In summary, our study shows for the first time that ARs are expressed in 45% of endometrial stromal neoplasms. Thus, in addition to ER and PR, the immunohistochemical examination of AR in endometrial stromal neoplasms, particularly in low-grade ESS, may have impact on the postoperative management of the patients.

Acknowledgement This study was supported by the Lore-Saldow-Reasearch-Fund. The authors thank Mrs. Margit Gogg-Kamerer and Ms. Andrea Sommersacher for their excellent technical assistance.

References

1. Aaro LA, Symmonds RE, Dockerty MB (1966) Sarcoma of the uterus. A clinical and pathologic study of 177 cases. Am J Obstet Gynecol 94:101–109
2. Bergeron C, Ferenczy A, Shyamala G (1988) Distribution of estrogen receptors in various cell types of normal, hyperplastic, and neoplastic human endometrial tissues. Lab Invest 58:338–345
3. Brys M, Semczuk A, Baranowski W, Jakowicki J, Krajewska WM (2002) Androgen receptor (AR) expression in normal and cancerous human endometrial tissues detected by RT-PCR and immunohistochemistry. Anticancer Res 22:1025–1031
4. Chang KL, Crabtree GS, Lim-Tan SK, Kempson RL, Hendrickson MR (1990) Primary uterine endometrial stromal neoplasms. A clinicopathologic study of 117 cases. Am J Surg Pathol 14:415–438
5. Evans HL (1982) Endometrial stromal sarcoma and poorly differentiated endometrial sarcoma. Cancer 50:2170–2182
6. Gadducci A, Sartori E, Landoni F, Zola P, Maggino T, Urgesi A, Lissoni A, Losa G, Fanucchi A (1996) Endometrial stromal sarcoma: analysis of treatment failures and survival. Gynecol Oncol 63:247–253
7. Gloor E, Schnyder P, Cikes M, Hofstetter J, Cordey R, Burnier F, Knobel P (1982) Endolymphatic stromal myosis. Surgical and hormonal treatment of extensive abdominal recurrence 20 years after hysterectomy. Cancer 50:1888–1893
8. Horowitz K, Rutherford T, Schwarz PE (1996) Hormone replacement therapy in women with sarcomas. CME J Gynecol Oncol 1:23–29
9. Katz L, Merino MJ, Sakamoto H, Schwartz PE (1987) Endometrial stromal sarcoma: a clinicopathologic study of 11 cases with determination of estrogen and progestin receptor levels in three tumors. Gynecol Oncol 26:87–97
10. Keen CE, Philip G (1989) Progestogen-induced regression in low-grade endometrial stromal sarcoma. Case report and literature review. Br J Obstet Gynaecol 96:1435–1439
11. Koss LG, Spiro RH, Brunschwig A (1965) Endometrial stromal sarcoma. Surg Gynecol Obstet 121:531–537
12. Krumholz BA, Lobovsky FY, Halitsky V (1973) Endolymphatic stromal myosis with pulmonary metastases. Remission with progestin therapy: report of a case. J Reprod Med 10:85–89
13. Lantta M, Kahanpaa K, Karkkainen J, Lehtovirta P, Wahlstrom T, Widholm O (1984) Estradiol and progesterone receptors in two cases of endometrial stromal sarcoma. Gynecol Oncol 18:233–239
14. Mesia AF, Demopoulos RI (2000) Effects of leuprolide acetate on low-grade endometrial stromal sarcoma. Am J Obstet Gynecol 182:1140–1141
15. Navarro D, Cabrera JJ, Leon L, Chirino R, Fernandez L, Lopez A, Rivero JF, Fernandez P, Falcon O, Jimenez P, et al (1992) Endometrial stromal sarcoma expression of estrogen receptors, progesterone receptors and estrogen-induced srp27 (24 K) suggests hormone responsiveness. J Steroid Biochem Mol Biol 41:589–596
16. Norris HJ, Taylor HB (1966) Mesenchymal tumors of the uterus. I. A clinical and pathological study of 53 endometrial stromal tumors. Cancer 19:755–766
17. Nyholm HC, Nielsen AL, Lyndrup J, Norup P, Thorpe SM (1992) Biochemical and immunohistochemical estrogen and progesterone receptors in adenomatous hyperplasia and endo-

metrial carcinoma: correlations with stage and other clinicopathologic features. Am J Obstet Gynecol 167:1334–1342
18. Pellillo D (1968) Proliferative stromatosis of the uterus with pulmonary metastases. Remission following treatment with a long acting synthetic progestin: a case report. Obstet Gynecol 31:33–39
19. Pickartz H, Beckmann R, Fleige B, Due W, Gerdes J, Stein H (1990) Steroid receptors and proliferative activity in non-neoplastic and neoplastic endometria. Virchows Arch 417:163–171
20. Piver MS, Rutledge FN, Copeland L, Webster K, Blumenson L, Suh O (1984) Uterine endolymphatic stromal myosis: a collaborative study. Obstet Gynecol 64:173–178
21. Reich O, Regauer S, Urdl W, Lahousen M, Winter R (2000) Expression of oestrogen and progesterone receptors in low-grade endometrial stromal sarcomas. Br J Cancer 82:1030–1034
22. Sabini G, Chumas JC, Mann WJ (1992) Steroid hormone receptors in endometrial stromal sarcomas. A biochemical and immunohistochemical study. Am J Clin Pathol 97:381–386
23. Schilder JM, Hurd WW, Roth LM, Sutton GP (1999) Hormonal treatment of an endometrial stromal nodule followed by local excision. Obstet Gynecol 93:805–807
24. Scribner DR Jr, Walker JL (1998) Low-grade endometrial stromal sarcoma preoperative treatment with Depo-Lupron and Megace. Gynecol Oncol 71:458–460
25. Soper JT, McCarty KS Jr, Hinshaw W, Creasman WT, McCarty KS Sr, Clarke-Pearson DL (1984) Cytoplasmic estrogen and progesterone receptor content of uterine sarcomas. Am J Obstet Gynecol 150:342–348
26. Tamaya T, Arabori K, Okada H (1988) Relation between steroid receptor levels and prolactin level in the endometrial stromal cells. Acta Obstet Gynecol Scand 67:265–269
27. Tavassoli FA, Devilee P (2003) World Health Organization classification of tumors: pathology and genetics of tumors of the breast and female genital organs, IARC Press, Lyon
28. Thatcher SS, Woodruff JD (1982) Uterine stromatosis: a report of 33 cases. Obstet Gynecol 59:428–434
29. Tosi P, Sforza V, Santopietro R (1989) Estrogen receptor content, immunohistochemically determined by monoclonal antibodies, in endometrial stromal sarcoma. Obstet Gynecol 73:75–78
30. Wade K, Quinn MA, Hammond I, Williams K, Cauchi M (1990) Uterine sarcoma: steroid receptors and response to hormonal therapy. Gynecol Oncol 39:364–367

Virchows Arch (2004) 444:415–419
DOI 10.1007/s00428-004-0986-4

ORIGINAL ARTICLE

Gonzague de Pinieux · Delphine Colin · Anne Vincent-Salomon · Jérôme Couturier · Delphine Amsellem-Ouazana · Philippe Beuzeboc · Annick Vieillefond

Confrontation of immunohistochemistry and fluorescent in situ hybridization for the assessment of HER-2/*neu* (c-*erb*b-2) status in urothelial carcinoma

Received: 13 March 2003 / Accepted: 20 December 2003 / Published online: 17 March 2004

Abstract Specific treatments targeted toward oncogenes expressed in cancer cells are currently under development. Patients with urothelial carcinomas showing HER-2/*neu* (human epidermal growth factor receptor 2) overexpression are candidates for such a specific treatment (trastuzumab). However, to be effective, this therapeutic approach requires an extremely reliable evaluation of HER-2/*neu* status in tumors. In order to assess the status of expression of this gene and to optimize its assessment, we analyzed a series of 64 primary urothelial carcinomas using immunohistochemistry (IHC) with the CB11 monoclonal antibody coupled with fluorescent in situ hybridization (FISH) in 21 cases. Strong HER-2/*neu* overexpression was detected using IHC in 15 of the 64 (23%) cases analyzed, and this rate rose to 33% for patients with metastases. HER-2/*neu* overexpression, as revealed using IHC, is strongly associated (95%) with gene amplification assessed using FISH. Patients with urothelial carcinomas overexpressing HER-2/*neu* using IHC are potential candidates for targeted chemotherapy.

Keywords HER-2/*neu* status · Immunohistochemistry · FISH · Urothelial carcinomas · HER-2/*neu*-targeted therapies

G. de Pinieux · D. Colin · A. Vieillefond (✉)
Service d'Anatomie Pathologique,
Hôpital Cochin,
27 rue du faubourg Saint Jacques, 75679 Paris Cedex 14, France
e-mail: annick.vieillefond@cch.ap-hop-paris.fr

A. Vincent-Salomon
Department of Pathology,
Institut Curie, Section Médicale,
Paris, France

J. Couturier
Department of Genetics,
Institut Curie, Section Médicale,
Paris, France

D. Amsellem-Ouazana
Department of Urology,
Hôpital Cochin,
Paris, France

P. Beuzeboc
Department of Oncology,
Institut Curie, Section Médicale,
Paris, France

Introduction

Specific treatments targeted to oncogenes expressed in cancer cells are currently under development. The protein HER-2/*neu* (human epidermal growth factor receptor 2), overexpressed in a subset of breast carcinomas, as revealed by amplification of the oncogene HER-2/*neu*, is the therapeutic target of the monoclonal antibody trastuzumab (Herceptin). Urothelial carcinomas, which may also show HER-2/*neu* overexpression, are candidate tumors for such a specific treatment [6, 11, 12, 29]. However, the efficacy of this treatment implies an extremely reliable evaluation of HER-2/*neu* status in tumors. Reported studies of HER-2/*neu* overexpression in urothelial carcinomas have shown varying results. The proportion of cases showing HER-2 overexpression ranged from 12% [16] to 71% [6, 26]. These differences may be explained by the heterogeneity of the techniques used and the population studied. We present a series of 64 urothelial carcinomas using a standardized immunohistochemistry (IHC) procedure, and we confront our results with HER-2/*neu* status as determined by fluorescent in situ hybridization (FISH).

Materials and methods

Patients

Tumor samples were obtained from 64 patients with urothelial carcinomas, all diagnosed and operated on by the Urology Department of Cochin Teaching Hospital. The 64 patients were

56 men and 8 women from 44 years to 82 years of age. Samples were obtained from transurethral resection of bladder (45 cases), cystectomy (15 cases) or nephro-ureterectomy (4 cases). Tumors were graded according to the World Health Organization/International Society of Urological Pathology 98 classification [5]: 12 tumors were classified as grade 2 (moderate differentiation), and 52 tumors were classified as grade 3 (poor differentiation). Staging was done according to the TNM (tumor, node, metastases) classification system of malignant tumors 1997 [25] and included 5 pTa tumors (5 TaN0M0), 9 pT1 tumors (3 T1N0M0, 2 T1N+M0, 3 T1N0M+, 1 T1N+M+), 31 pT2 tumors (15 T2N0M0, 9 T2N+M0, 3 T2N0M+, 4 T2N+M+), 13 pT3 tumors (5 T3N0M0, 4 T3N+M0, 4 T3N+M+) and 6 pT4 tumors (5 T4N0M0, 1 T4N+M+). Of the patients, 31 had metastases: lymph-node metastases, only, for 15 patients and visceral metastases with or without lymph-node metastases for the other 16 patients.

Immunohistochemistry

For each case, the histology of the sample analyzed was verified on hematein eosin safran-stained preparations, and areas showing invasive carcinoma were identified. Tumor material consisted of paraffin-embedded specimens fixed in 10% formalin. Sections were cut at 4 μm, dried for 1 h at 58°C, then 15 h at 37°C. After deparaffinization and rehydration of the sections, antigen retrieval was performed in a solution of citrate 10 mM, pH 6.1. All further steps were performed using an automated system (Techmate 500, Dako). Endogenous peroxidases were inhibited by 5 min incubation in 3% H_2O_2. Then, sections were incubated with the monoclonal HER-2/*neu* antibody CB11 (Novocastra Laboratories, Newcastle-upon-Tyne, UK), for 1 h at 20°C. Immunodetection was achieved using the Vectastain Elite ABC peroxidase mouse IgD kit (Vector Laboratories, Burlingame, CA, USA). Then, sections were incubated with diaminobenzidine for 5 min and counterstained with Mayer's hematoxylin for 1 min.

After several assays of dilution, HER-2/*neu* monoclonal antibody was diluted at 1/800. Under this condition, normal urothelium was not stained, and only tumor cells showed membranous staining. Preparations were analyzed independently by three pathologists (GDP, AV, AVS). Breast carcinomas overexpressing the protein were used as positive control. A three-step classification of the immunostaining was adopted: cases without detectable staining in tumor cells (scored −), cases showing weak or moderate staining (scored +) and cases showing strong membranous staining (scored ++). In each case, the percentage of stained tumor cells was evaluated.

Fluorescent in situ hybridization

FISH and IHC were performed on the same tumor sample, on consecutive slides. FISH experiments used the Kit PathVysion HER-2 probe (Vysis, Downers Grove, IL, USA), following the instructions given by the supplier. Briefly, deparaffinized slides were treated with a protein-digesting enzyme at 37°C for 40 min. Preparations were denatured in 70% formamide/2× standard saline citrate (SSC), pH 7, at 75°C, for 2 min. Then, a solution containing the HER-2/*neu* probe coupled with SpectrumOrange and a specific probe for the centromere of chromosome 17 coupled with SpectrumGreen were applied to the tissue sections at 37°C for 15 h. After hybridization, the unannealed probe was washed in 0.4×SSC/NP40 0.3% at 73°C for 3 min then in 2×SSC/NP40 0.1% at 37°C for 2 min. Nuclei were counterstained using a 4,6-diamidine, 2-phenylindol (DAPI)/antifade solution. A Leica DMRB microscope equipped with appropriate filters for DAPI, SpectrumGreen and SpectrumOrange was used to score the number of signals per nucleus. Images were captured using a Quantics digital camera (Photometrics, Tucson, AZ, USA) and Quips FISH imaging software (Vysis, Downers Grove, IL, USA). The number of fluorescent signals was counted in 25 nuclei of invasive tumor cells in two distant areas of the section for each case. For each tumor, the mean number of signals per nucleus was determined. Amplification was defined by at least a twofold excess of the number of copies of the HER-2/*neu* gene with regard to the number of centromeres of chromosome 17.

Results

Of cases, 15 showed membrane staining scored as ++ in tumor cells, but with substantial heterogeneity in different areas of a given tumor. The percentage of immunolabeled tumor cells was 70–100% in 8 cases, 20–30% in 4 cases and 5–10% in 3 cases (Fig. 1), (Table 1). In 13 cases, a membranous staining was detected, which was scored + (Fig. 2). Staining was not present in 36 cases.

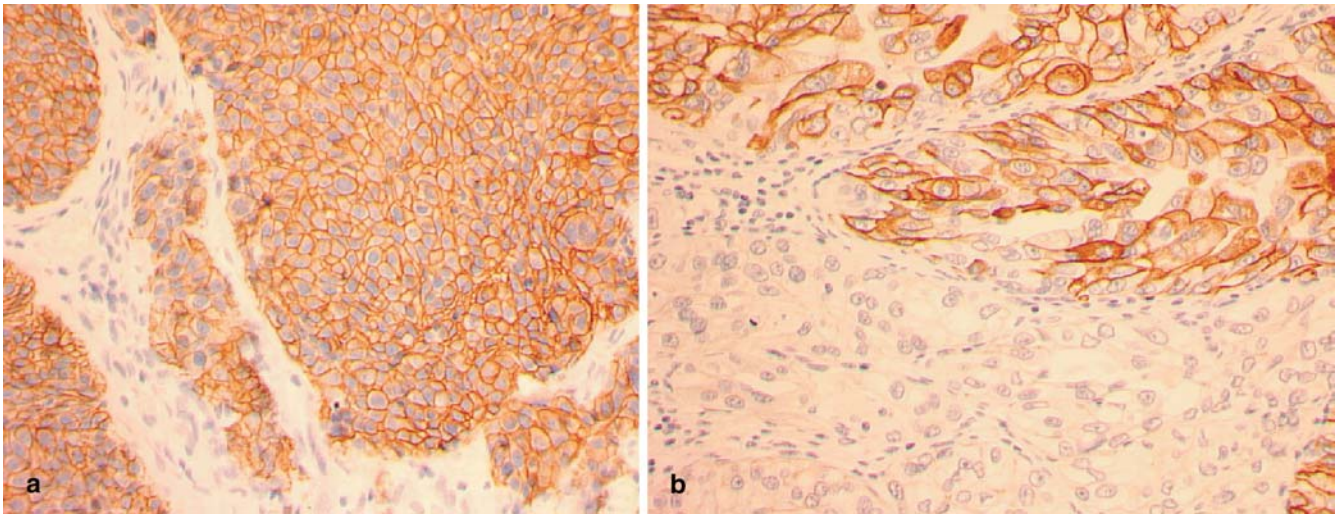

Fig. 1 Immunohistochemistry using the CB11 anti HER-2/*neu* antibody and the aviditin-biotin peroxidase complex technique on a paraffin-embedded tissue section of urothelial carcinoma. Strong membranous expression of the protein scored ++. This overexpression is diffuse (**A**) or focal (**B**)

Table 1 Patients with a positive status HER-2/*neu* (human epidermal growth factor receptor 2). *FISH* fluorescent in situ hybridization, *IHC* immunohistochemistry, *A* amplified, *NA* not amplified,++ strong membranous staining

Patients	Grade	Stade	IHC	FISH
1	G3	TaN0M0	++ 70%	A
2	G3	T2N0M0	++ 100%	A
3	G2	T2N0M0	++ 70%	A
4	G3	TaN0M0	++ 100%	A
5	G3	T2N0M0	++ 100%	A
6	G3	T4N0M0	++ 20%	Not done
7	G3	T1N0M1	++ 70%	Not done
8	G3	T3N+M1	++ 100%	Not done
9	G3	T2N0M1	++ 100%	A
10	G3	T3N0M0	++ 30%	Not done
11	G3	T4N+M1	++ 10%	Not done
12	G3	T4N0M0	++ 20%	Not done
13	G3	T2N+M1	++ 30%	Not done
14	G3	T3N2M1	++ 10%	Not done
15	G3	T2N1M0	++ 5%	NA

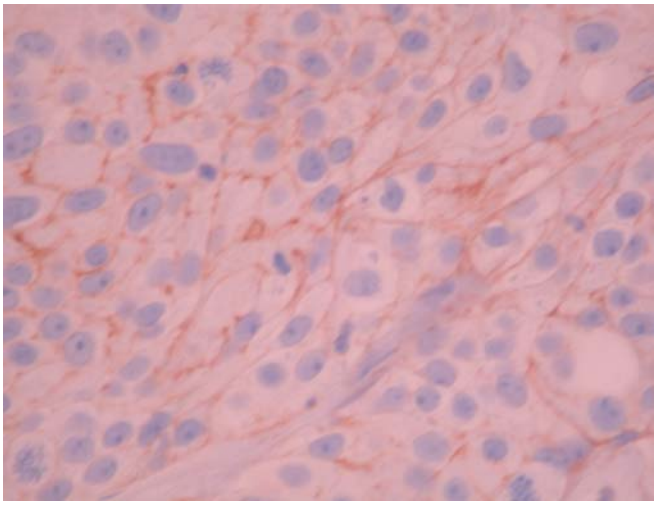

Fig. 2 Immunohistochemistry using the CB11 anti HER-2/*neu* (human epidermal growth factor receptor 2) antibody and the aviditin-biotin peroxidase complex technique on a paraffin-embedded tissue section of urothelial carcinoma. Moderate membranous expression of the protein scored +

FISH was performed on 21 tumors from these 64 patients (Table 2). Of the 15 patients with IHC overexpression of HER-2/*neu* (score ++), 7 were explored using FISH. Six patients showed HER-2/*neu* amplification (more than 20 gene copies per nucleus) (Fig. 3A). One case with strong membrane staining in only 5% of tumor cells showed no evidence of HER-2/*neu* amplification. Of tumors, 11 with score + membranous staining and 3 without any staining showed no HER-2/*neu* amplification (Fig. 3B).

Thus, 15 of 64 (23%) tumors in this series overexpressed HER-2/*neu*. A similarity between HER-2/*neu* expression detected using IHC and gene amplification assessed using FISH was observed in 20 of 21 cases (95%).

Table 2 HER-2/*neu* (human epidermal growth factor receptor 2) status: comparison between amplification determined using fluorescent in situ hybridization (FISH) and overexpression assessed using immunohistochemistry (IHC). *A* amplified, *NA* not amplified, ++ strong membranous staining, + weak to moderate membranous staining

		HER-2/*neu* overexpression (IHC)			
		0	+	++	Total
HER2/*neu* (FISH)	NA	3	11	1	15
	A	0	0	6	6
		3	11	7	21

Discussion

In the literature, about 40 studies have reported the status of HER2/*neu* in urothelial carcinomas. These studies reported a rate of HER-2/*neu* overexpression varying from 12% [16] to 71% [6, 28] and from 15% [2] to 44% [15] in studies using the CB11 antibody. These discordant results are related to the diversity of techniques used and explain why some authors found that HER2/*neu* overexpression is correlated with tumor grade [1, 3, 7, 16, 18, 19, 30, 31] and stage [7, 18, 19, 20, 23, 30, 31], while others found no correlation [8, 9, 10, 14, 17, 21, 26, 27]. Patients with HER-2/*neu* overexpression seem to have a worse prognosis [11], but they also show a better response to chemotherapy [6]. With the emergence of anti-HER2/*neu* treatment, the main interest of investigating HER-2/*neu* status is related to potential therapeutic applications [6, 11, 29]. An extremely reliable IHC technique is necessary in order to identify the patients able to benefit from this new therapeutic. In many studies on breast carcinoma, a comparison was established between overexpression of protein using IHC and number of gene copies observed using FISH. These studies [4, 13, 22] suggested that only strong overexpression of HER-2/*neu* is linked to gene amplification and should be taken into account for the selection of patients for treatment using trastuzumab. A comparison between FISH and IHC in urothelial carcinoma was established in several studies. Sauter et al. [24] compared HER-2/*neu* status assessed using IHC with the polyclonal antibody A485 (Dako, dilution 1/100) and FISH in 141 urothelial carcinomas in an unselected population (36 pTa, 42 pT1, 67 pT2-T3 / 20 G1, 39 G2, 46 G3 and 6 cases of unknown grading and staging). Of these tumors, 43% showed HER-2/*neu* overexpression, while gene amplification was found in only 10 of 141(7%) tumors. All cases with amplification showed HER-2/*neu* overexpression. However, overexpression was present without amplification in 51 tumors. For the authors, this dissociation between amplification and overexpression suggested the existence of several mechanisms leading to protein overexpression (point mutation, translocation or transcriptional upregulation). In this study, only the percentage of positive tumor cells was taken into account, and the grading of intensity was not considered.

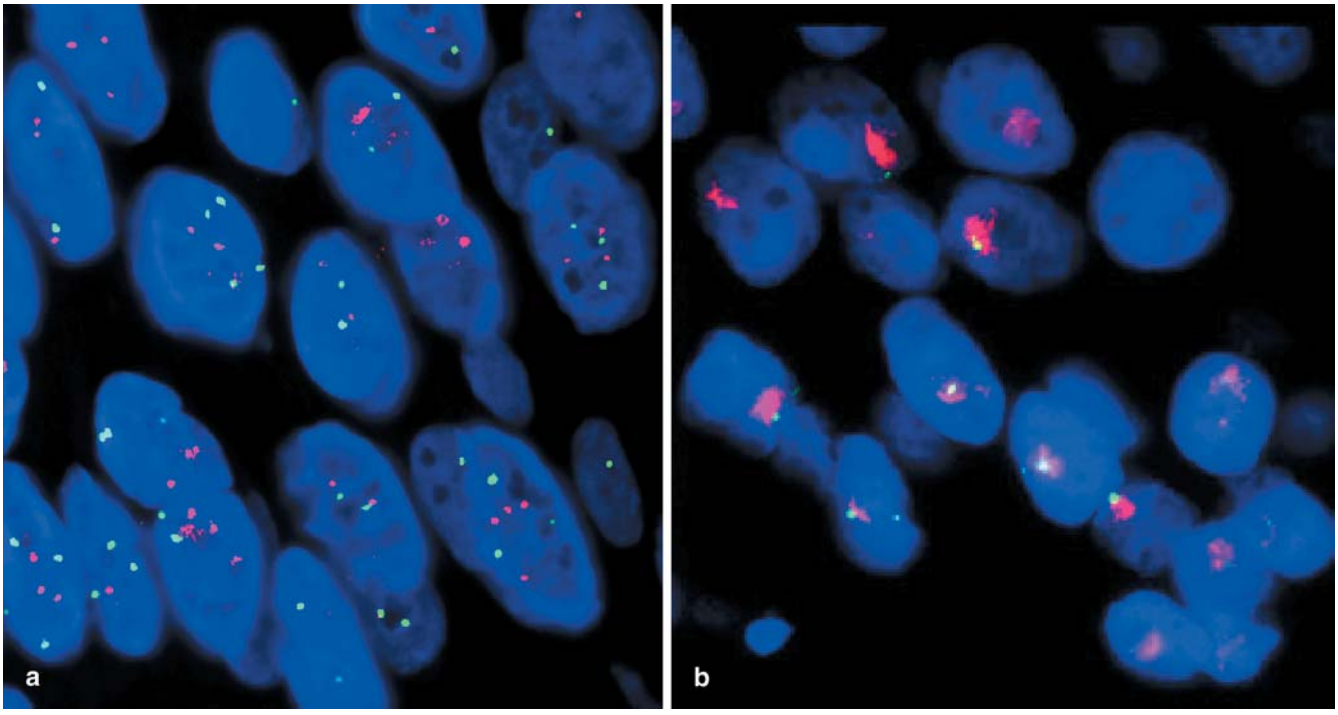

Fig. 3 Fluorescent in situ hybridization of HER-2/*neu* (human epidermal growth factor receptor 2) on paraffin-embedded tissue sections of two cases of urothelial carcinoma (×1000). **A** Tumor without amplification. A mean number of two signals per nucleus was observed. **B** Tumor with a high-level amplification. Presence of numerous signals, arranged in clusters

Kruger et al. [12] observed that in 203 invasive urothelial carcinomas, 37% of tumors overexpressed HER-2/*neu* using IHC, while only 5% of tumors showed gene amplification.

Our study demonstrates that, in a population mainly composed of invasive tumors, 23% of tumors overexpressed HER-2/*neu*. This rate rises to 33% in patients with metastases.

The aim of the present study was to clarify adequate conditions for reliably detecting HER-2/*neu* overexpression in urothelial carcinomas.

For the purpose of standardization and calibration of the IHC technique on FISH, this method was adapted from the technique used in breast carcinomas calibrated on FISH [4].

By considering a three-scale staining score, i.e., strong membrane staining (++), moderate or weak membrane staining (+) and the absence of membrane staining (–), we observed that membrane immunostaining scored as ++ was highly correlated (95%) with gene amplification (>20 copies/nucleus) assessed using FISH. Only one case with strong membrane staining showed no evidence of HER-2/*neu* amplification. However, this discordant case showed strong immunostaining in only 5% of tumor cells. It is likely that these rare positive cells could not be detected using FISH analysis, which, because it requires observation using ×1000 magnification, is unable to detect rare events on wide surfaces. A bias in sampling between slide levels studied could also be involved.

In contrast, tumors scored as + or – using IHC showed no evidence of gene amplification investigated using FISH, but in this preliminary study, we were not able to explore all the cases.

It must be underlined that, in this study, we retain a score of ++ as indicating a very strong and complete IHC membrane staining, which can probably explain the good concordance of IHC and gene amplification using FISH.

In conclusion, in our series, overexpression of HER-2/*neu* was mainly detected in high-grade/high-stage, as well as metastatic, tumors. In contradiction with previous studies, we found that strong overexpression of HER-2/*neu* detected using IHC was associated with gene amplification detected using FISH. Other studies are necessary to obtain better knowledge of the gene amplification status in tumors with weak to moderate overexpression of HER-2/*neu*.

We suggest that selection of patients with urothelial carcinoma who are likely to benefit from HER2/*neu*-targeted therapy would be the same as for breast carcinoma. Such selection relies on strong overexpression of HER-2/*neu* detected using IHC. When this overexpression is difficult to assess using IHC, then a complementary approach using FISH becomes necessary.

References

1. Asamoto M, Hasegawa R, Masuko T, Hashimoto Y, Ueda K, Ohtaguro K, Sasaki S, Washida H, Fukushima S (1990) Immunohistochemical analysis of c-erbB-2 oncogene product

and epidermal growth factor receptor expression in human urinary bladder carcinomas. Acta Pathol Jpn 40:322–326
2. Berner A, Jacobsen AB, Fossa SD, Nesland JM (1993) Expression of c-erbB-2 protein, neuron-specific enolase and DNA flow cytometry in locally advanced transitional cell carcinoma of the urinary bladder. Histopathology 22:327–333
3. Coombs LM, Oliver S, Sweeney E, Knowles M (1993) Immunocytochemical localization of c-erbB-2 protein in transitional cell carcinoma of the urinary bladder. J Pathol 169:35–42
4. Couturier J, Vincent-Salomon A, Nicolas A, Beuzeboc P, Mouret E, Zafrani B, Sastre-Garau X (2000) Strong correlation between results of fluorescent in situ hybridization and immunohistochemistry for the assessment of the ERBB2 (HER2/neu) gene status in breast carcinoma. Mod Pathol 13:1238–1243
5. Epstein JI, Amin MB, Reuter VR, Mostofi FK, The Bladder Consensus Conference Committee (1998) The World Health Organization/International Society of Urological Pathology consensus classification of urothelial (transitional cell) neoplasms of the urinary bladder. Am J Surg Pathol 22:1435–1448
6. Gandour-Edwars R, Lara PN, Folkins AK, LaSalle JM, Beckett L, Li Y, Meyers F, DeVere-White R (2002) Does HER2/neu expression provide prognostic Information in patients with advanced urothelial carcinoma? Cancer 95:1009–1015
7. Gorgoulis VG, Barbatis C, Poulias I, Karameris AM (1995) Molecular and immunohistochemical evaluation of epidermal growth factor receptor and c-erbB-2 gene product in transitional cell carcinomas of the urinary bladder: a study in Greek patients. Mod Pathol 8:758–764
8. Imai T, Kimura M, Takeda M, Tomita Y (1995) Significance of epidermal growth factor receptor and c-erbB-2 protein expression in transitional cell cancer of the upper urinary tract for tumour recurrence at the urinary bladder. Br J Cancer 71:69–72
9. Ioachim E, Charchanti A, Stavropoulos NE, Skopelitou A, Athanassiou ED, Agnantis NJ (2000) Immunohistochemical expression of retinoblastoma gene product (Rb), p53 protein, MDM 2, c-erbB-2, HLA-DR and proliferation indices in human urinary bladder carcinoma. Histol Histopathol 15:721–727
10. Koyuncuoglu M, Kargi A, Cingöz S, Kirkali Z (1998) Investigation of p53, c-erbB-2, PCNA immunoreactivity, DNA content, AgNOR and apoptosis in bladder carcinoma as prognostic parameters. Cancer Lett 126:143–148
11. Krüger S, Weitsch Georg, Büttner H, Matthiensen A, Böhmer T, Marquardt T, Sayk F, Feller AC, Böhle A (2002) HER2 overexpression in muscle-invasive urothelial carcinoma of the bladder: prognostic implication. Int J Cancer 102:514–518
12. Kruger S, Weitsch G, Buttner H, Matthiensen A, Bohmer T, Marquardt T, Sayk F, Feller AC, Bohle A (2002) Overexpression of c-erbB-2 oncoprotein in muscle-invasive bladder carcinoma: relationship with gene amplification, clinicopathological parameters and prognostic outcome. Int J Oncol 21: 981–987
13. Lebeau A, Deimling D, Kaltz C, Sendelhofert A, Iff A, Luthardt B, Untch M, Löhrs U (2001) HER-2/neu analysis in archival tissue samples of human breast cancer: comparison of immunohistochemistry and fluorescence in situ hybridization. J Clin Oncol 19:354–363
14. Lee SE, Chow NH, Chi YC, Tzai TS, Yang WH, Lin SN (1994) Expression of c-erbB-2 protein in normal and neoplastic urothelium: lack of adverse prognostic effect in human urinary bladder cancer. Anticancer Res 14:1317–1324
15. Lipponen PK (1993) Interrelationship between expression of p53, proliferating cell nuclear antigen and C-erbB-2 in bladder cancer. Pathobiology 61:178–182
16. Lipponen P, Eskelinen M, Syrjanen S, Tervahauta A, Syrjanen K (1991) Use of immunohistochemically demonstrated c-erb B-2 oncoprotein expression as a prognostic factor in transitional cell carcinoma of the urinary bladder. Eur Urol 20:238–242
17. Mellon JK, Lunec J, Wright C, Horne W, Kelly P, Neal D (1996) C-erbB-2 in bladder cancer: molecular biology, correlation with epidermal growth factor receptors and prognostic value. J Urol 155:321–326
18. Miyamoto H, Kubota Y, Noguchi S, Takase K, Matsuzaki J, Moriyama M, Takebayashi S, Kitamura H, Hosaka M (2000) C-erbB-2 gene amplification as a prognostic marker in human bladder cancer. Urology 55:679–683
19. Moriyama M, Akiyama T, Yamamoto T, Kawamoto T, Kato T, Sato K, Watanuki T, Hikage T, Katsuta N, Mori S (1991) Expression of c-erbB-2 gene product in urinary bladder cancer. J Urol 145:423–427
20. Onodera T, Hashimoto Y, Yagihashi S (1997) C-myc, c-erbB-1 and c-erbB-2 expressions in urothelial carcinoma. Pathol Int 47:209–216
21. Orlando C, Sestini R, Vona G, Pinzani P, Bianchi S, Giacca M, Pazzagli M, Selli C (1996) Detection of c-erbB-2 amplification in transitional cell bladder carcinoma using competitive PCR technique. J Urol 156:2089–2093
22. Ridolfi RL, Jamehdor MR, Arber JM (2000) HER-2/neu testing in breast carcinoma: a combined immunohistochemical and fluorescence in situ hybridization approach. Mod Pathol 13:866–873
23. Sato K, Moriyama M, Mori S, Saito M, Watanuki T, Terada K, Okuhara E, Akiyama T, Toyoshima K, Yamamoto T, Kato T (1992) An immunohistologic evaluation of c-erbB-2 gene product in patients with urinary bladder carcinoma. Cancer 70:2493–2498
24. Sauter G, Moch H, Moore D, Carroll P, Kerschmann R, Chew K, Mihatsch MJ, Gudat F, Waldman F (1993) Heterogeneity of erbB-2 gene amplification in bladder cancer. Cancer Res 53:2199–2203
25. Sobin LH, Wihekind CH (eds) (1997) TNM classification of malignant tumors, 5th edn. Wiley, New York
26. Swanson PE, Frierson HF Jr, Wick MR (1992) C-erbB-2 (HER-2/neu) oncopeptide immunoreactivity in localized, high-grade transitional cell carcinoma of the bladder. Mod Pathol 5:531–536
27. Underwood M, Bartlett J, Reeves J, Gardiner DS, Scott R, Cooke T (1995) C-erbB-2 gene amplification: a molecular marker in recurrent bladder tumors? Cancer Res 55:2422–2430
28. Wagner U, Sauter G, Moch H, Novotna H, Epper R, Mihatsch MJ, Waldman FM (1995) Patterns of p53, erbB-2, and EGF-r expression in premalignant lesions of the urinary bladder. Hum Pathol 26:970–978
29. Wester K, Sjostrom A, De la Torre M, Carlsson J, Malmstrom PU (2002) HER2 a possible target for therapy of metastastic urinary bladder carcinoma. Acta Oncol 41:282–288
30. Wright C, Mellon K, Neal DE, Johnston P, Corbett IP, Horne CH (1990) Expression of c-erbB-2 protein product in bladder cancer. Br J Cancer 62:764–765
31. Ye DW, Zheng JF, Qian SX, Ma YJ (1993) Correlation between the expression of oncogenes ras and C-erbB-2 and the biological behavior of bladder tumors. Urol Res 21:39–43

Virchows Arch (2004) 444:420–425
DOI 10.1007/s00428-004-1000-x

ORIGINAL ARTICLE

Francisco Miguel Izquierdo-García · Fructuoso García-Díez · Isabel Fernández · Alberto Pérez-Rosado · Anabel Sáez · Dimas Suárez-Vilela · Rafael Guerreiro-González · Manuel Benéitez-Alvarez

Lymphoepithelioma-like carcinoma of the bladder: three cases with clinicopathological and p53 protein expression study

Received: 30 September 2003 / Accepted: 20 February 2004 / Published online: 6 April 2004

Abstract Lymphoepithelioma-like carcinoma of the bladder is an uncommon neoplasm, of which 49 cases have been described in the English literature, none of which has been studied for p53 protein expression. We studied three muscle-infiltrating cases of this tumor using immunohistochemical, in situ hybridization and polymerase chain reaction (PCR) methods. The three cases were positive for epithelial markers and negative for lymphoid antigens in the tumoral syncytial areas. The intensive infiltrate of small cells was negative for epithelial and positive for lymphoid markers. This population was mainly made up of cytotoxic T-lymphocytes, positive for TIA-1. p53 protein was intensely positive in more than 90% of the epithelial component nuclei, being negative in the lymphoid cells. PCR study did not show mutations on p53. Both lymphocytes and epithelium were negative for Epstein–Barr virus markers, such as the latent membrane protein and EBER (Epstein–Barr-encoded RNA). The prognosis was very good after radiotherapy and chemotherapy treatment, preserving the bladder despite the muscle infiltration. The presence of an intense cytotoxic T-lymphocyte population may be related to this good prognosis. Both aspects, p53 protein status and T-lymphoid population, had never been studied before in bladder lymphoepithelioma-like carcinoma.

Keywords Bladder · Lymphoepithelioma-like carcinoma · p53 protein · Immunohistochemistry · Urothelial carcinoma · Epstein–Barr virus

F. M. Izquierdo-García (✉) · D. Suárez-Vilela
Servicio de Anatomía Patológica,
Hospital de León,
Altos de la Nava s/n, 24008 León, Spain
e-mail: pacoizq20@hotmail.com
Tel.: +34-987-237400
Fax: +34-987-233322

F. García-Díez · R. Guerreiro-González · M. Benéitez-Alvarez
Servicio de Urología,
Hospital de León, Spain

I. Fernández · A. Pérez-Rosado · A. Sáez
Programa de Patología Molecular,
Centro Nacional de Investigaciones Oncológicas (CNIO),
Madrid, Spain

A. Sáez
Departamento de Anatomía Patológica,
Facultad de Medicina, Universidad de Granada,
Spain

Introduction

Around 90% of the malignant tumors of the bladder are urothelial carcinomas (UCs). The remaining 10% correspond to other types of carcinomas, sarcomas or other uncommon tumors [37].

Lymphoepithelioma-like carcinoma (LELC) is an infrequent neoplasm, of which only 49 cases have been described in bladder [3, 5, 10, 11, 12, 16, 20, 24, 25, 29, 35, 48, 53, 54]. It is constituted by high nuclear epithelial cells with syncytial growth pattern, widely infiltrated by numerous lymphocytes and plasma cells [13, 54].

This type of tumor was originally described in nasopharynx, where it received the descriptive name of lymphoepithelioma; but it has also been found in other organs, such as salivary gland, thymus, uterine cervix, skin, lung, stomach, oral cavity, breast, vagina, trachea and larynx and, rarely, in other areas of the urinary tract (renal pelvis, ureter, prostate and urethra) [6, 7, 9, 15], where it is called LELC. In the bladder, the prognosis seems to be better than in other invasive carcinomas [3, 12, 20, 21, 29]. It may be treated with cisplatin-based chemotherapy and radiotherapy [3, 54], and it is possible to preserve the bladder.

Although p53 protein expression has been commonly studied in UCs [36], these studies have not been performed in any of the studies about bladder LELC. Here, we studied the status of the p53 gene and its protein expression level in the three cases reported, with muscle

infiltration and conservative treatment (radiotherapy and chemotherapy).

Materials and methods

Histology and immunohistochemistry

The transurethral resection surgical specimens were fixed in formalin and embedded in paraffin blocks. Cut sections, 5 μm in thickness, were stained with hematoxylin and eosin. The immunohistochemical study was performed using the avidin-biotin complex with the Biotek 1000 (Ventana/Biotek, Tucson AZ) automated immunostainer. Heat-induced epitope retrieval in a 5-mM citrate buffer at pH 6, for 2 min, with a pressure-cooking method, was used for all the antibodies: AE1–AE3 anticytokeratin antibody (Signet, dilution 1/500), antileukocytic common antigen antibody (X16/99 clone, Dako, Glostrup, Denmark, dilution 1/50), anti-latent membrane protein of Epstein–Barr virus (EBV) antibody (CS1,2,3,4 clone, Novocastra, Newcastle, England, dilution 1/100), anti-CD8 (C8/144B clone, Dako, dilution 1/25), anti-TIA-1 (2G9 clone, Immunotech, Coulter, Marseille, France, prediluted) and antibody against p53 protein (DO7 antibody, Dako, dilution 1/200).

EBER in situ hybridization

EBV was detected by in situ hybridization with fluorescein-conjugated Epstein–Barr virus (EBER) PNA probe (Dako).

Polymerase chain reaction

Mutations in exons 5–8 of p53 gene were analyzed by direct sequencing of both forward and reverse amplicons for each fragment, using an automated DNA sequencer ABI PRISM 310 genetic analyzer (Applied Biosystems), according to the manufacturer's procedures. The primers and conditions for this sequencing have been previously described [22, 47].

Patients

Case 1

A 74-year-old man came to our hospital in November 1998 presenting with hematuria. He had been a smoker until 1989. At the cystoscopy, a retrotrigonal tumor of 2×2 cm in size was found. It was resected and diagnosed as a solid urothelial carcinoma, grade 3, PT1 stage. No abdominal computed scan or thoracic X-rays showed disseminated disease. He was treated with 82 mg BCG (Connaught) per week for 6 weeks. Urine cytology was normal in February 1999. Cystoscopy revealed a tumor above the left ureteral meatus 3 months later, and the diagnosis was similar in 70% of the tumor, but the resting 30% corresponded to a focal lymphoepithelioma-like carcinoma. The tumor infiltrated the muscular propria. The patient was treated with photons Rx15MV radiotherapy until a total dose of 66 Gy was well tolerated. Currently, after 54 months of follow-up, the patient is alive and without clinically apparent disease.

Case 2

A 77-year-old man came to our hospital presenting with hematuria. He had been a smoker until 4 years prior to our follow-up. On the cystoscopy, a solid tumor was present at the vesical fundus. It was resected and diagnosed as pure lymphoepithelioma-like carcinoma muscle infiltrating. No disseminated disease was found, and treatment with photons Rx15MV radiotherapy until a total dose of 67 Gy was performed. The patient is alive and without clinically apparent disease 39 months later.

Case 3

An 82-year-old woman came to our hospital presenting with hematuria. On the ultrasound, a right lateral vesical mass was found. The computed scan and bone-scan studies were negative for tumoral spreading. A transurethral resection was performed with the diagnosis of predominant (90%) lymphoepithelioma-like bladder carcinoma, infiltrating the muscular propria. She was lost for follow-up 36 months after the initial diagnosis, without evidence of disease.

Results

Pathological, immunohistochemical and in situ hybridization studies

Histologically, in the lymphoepithelioma-like areas, the tumors were constituted by cells that showed large, atypical nuclei with prominent nucleoli and abundant mitotic figures. The cytoplasms were eosinophilic and badly delimited, with a syncytial growth pattern, forming thick cords, and occasional small nests, densely infiltrated by small mature lymphocytes and some plasma cells and separated by stromal tracts, also with an intense lymphoplasmocytoid infiltrate (Fig. 1). In the first case, this lymphoepithelial component represented 30% of the recurrent tumor, but not the primitive one. The second one showed this histological pattern in the whole tumor, while the third case showed it in 90% of the tumoral areas.

On the immunohistochemical study, the large tumoral cells were positive for cytokeratins and negative for leukocytic common antigen. In contrast, the lymphoid component was negative for cytokeratins and positive for leukocytic common antigen. Both components were negative for the latent membrane protein of the EBV and EBER. Between 90% and 95% of the nuclei of the tumoral cells were intensely positive for p53 protein and were negative in the inflammatory cells (Fig. 2). The tumoral cells of the urothelial areas of case 1 and case 3, as well as the first tumor of case 1, were also positive for p53 protein in more than 90% of the nuclei.

Most of the lymphocytes related to the tumor, both in the stroma and permeating the tumoral nests, were CD3-positive T-cells, with a minority of CD20-positive cells. In this T-cell population, there were numerous CD8-positive cells, most of which were also positive for TIA-1, with a granular cytoplasmic distribution (Fig. 3). In some areas, lymphoid follicles were present, staining most of the cells within them intensely for CD20. These B-cell areas were localized in the lamina propria apart from the tumor and not related to it.

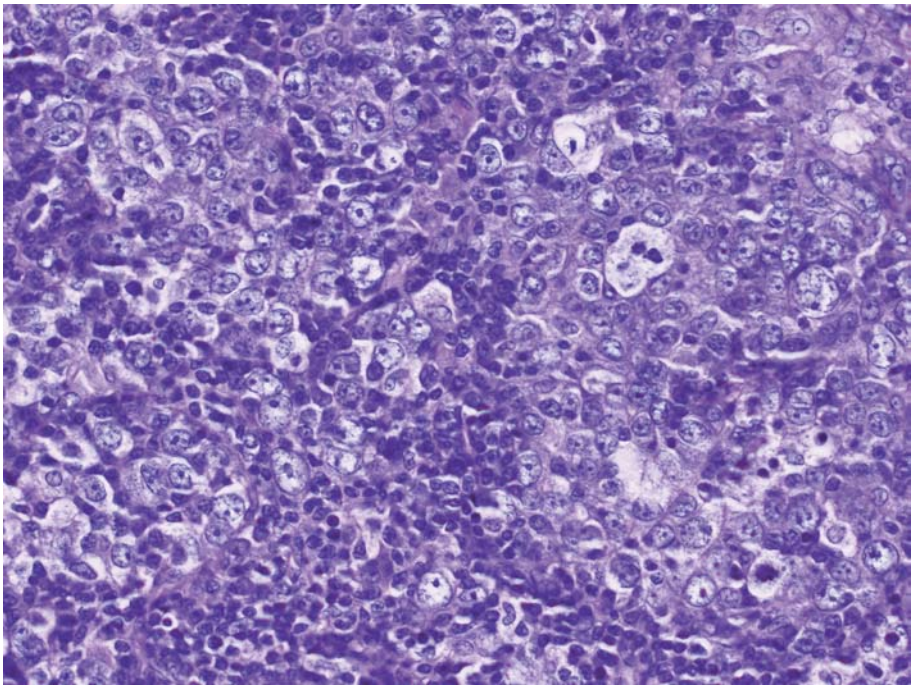

Fig. 1 Tumoral cells with large nuclei, prominent nucleoli and syncytial growth pattern, densely infiltrated by numerous lymphocytes and plasma cells

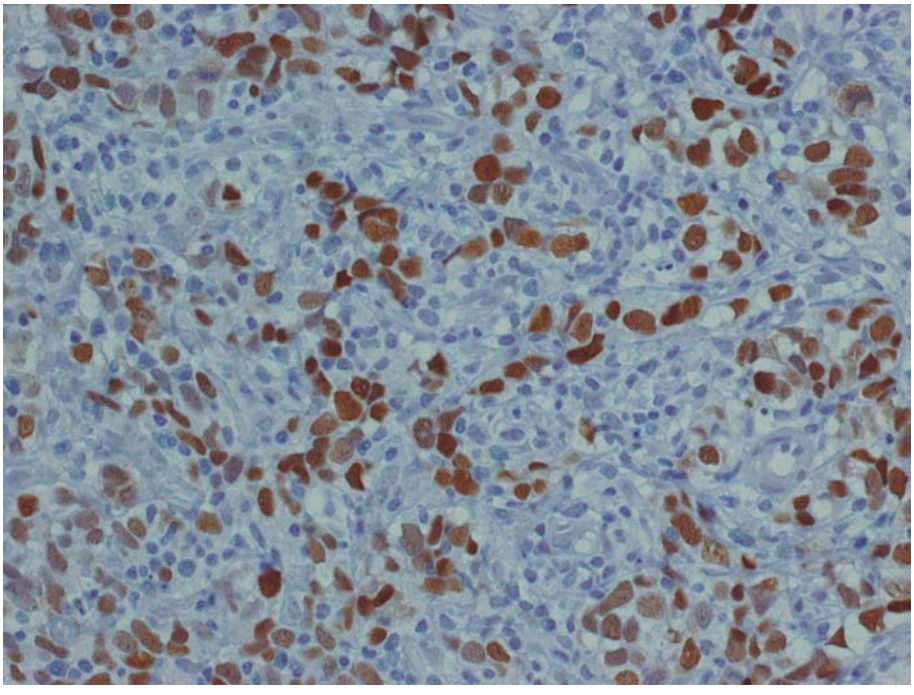

Fig. 2 Almost all the nuclei of the tumoral cells are intensely positive for p53 protein. The inflammatory cells do not show any staining

p53 status

In the three cases, we searched for mutations in exons 5–8 of p53, which have been reported to be the regions where most of the mutations have been found. We did not find any mutations in any of the three cases reported here and in the first tumor of the case 1.

Discussion

Lymphoepithelioma-like carcinoma of the bladder was described by Zuckerberg et al. [54] in a series of carcinomas that mimicked lymphoma. Amin et al. [3] have classified it as pure LELC, predominant (>50%) LELC and focal (<50%) LELC, with concurrent invasive UC in the two latter types. In situ carcinoma is present in 14% of the cases.

They represent between 0.4% and 1.29% of the bladder carcinomas [20, 29], and 49 cases have been pub-

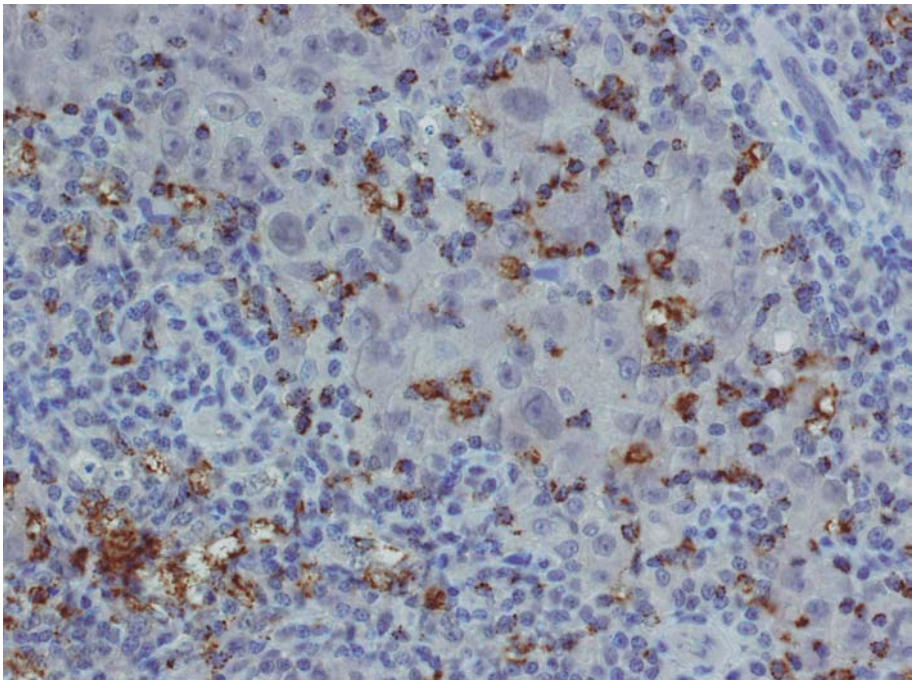

Fig. 3 Numerous lymphoid cells, both in the interstitium and among the tumoral cells, show cytoplasmic granules stained for TIA-1

lished in the English literature [3, 5, 10, 11, 12, 16, 20, 24, 25, 29, 35, 48, 53, 54]. Most of them present a clinical onset with hematuria, as we described in our cases. They are usually small tumors (0.9–5 cm).

Although initially Young and Eble [52] classified it as an undifferentiated and aggressive variant of bladder carcinoma with bad prognosis, only one patient presented as T4 stage neoplasm, and barely 14% of the cases developed metastases along the course of the disease [3, 29], despite the fact that 87.5% of the tumors are invasive at the diagnosis. This favorable prognosis may be due to the intense inflammatory reaction of the host against the tumor, basically formed by T-cells [3, 28], or because the disease is diagnosed earlier than in conventional UC, inasmuch as the symptoms produced by this inflammation may alert the patient to consult the urologist when the tumor is still small [20]. Thus, the diagnosis of this histological type of bladder carcinoma is important because of the better prognosis of this tumor and because it is amenable to conservative treatment of the patient.

Despite the fact that the p53 protein immunohistochemical expression is common in UCs, and it has been widely studied, it has not been performed in the cases of LELC of bladder described in the literature. This positive phenotype is more common in the high-grade and advanced stage UCs [4, 43, 49], and although there is a trend of an independent predictive factor of survival, progression and metastasis, in general there is not a complete agreement, and in numerous series it is not an independent prognostic factor [23, 36, 42]. Our three cases of LELC correspond to high nuclear grade and advanced-stage tumors, and they show an intense reaction in 90–95% of their nuclei. Despite this finding, and despite that they have been treated with conservative therapy and preservation of the bladder, they have followed a good clinical course, without relapses during a follow-up between 36 months and 54 months.

p53 expression, found between 53% and 70% of the cases of UC [2, 14, 45], is usually associated with mutation [4]; but the percentage of tumors in which it is demonstrated is lower (between 33% and 47%) [2, 14, 45]. However, the association between both mutation and immunohistochemical expression is statistically significant [2, 14, 45]. This discordance between mutation and nuclear immunoreaction in some cases may be due to several causes:

1. The dilution of tumoral mutated cells among other normal or not mutated cells. At least 25% of mutated cells are required to demonstrate the mutation using direct sequencing [8].
2. In some cases, the staining may be caused by the storage of wild protein instead of mutated one [26]. In fact, in some types of tumors, it is recognized that p53 expression using immunohistochemistry is not related to mutations [34, 46].
3. It may be also possible that the mutation is out of the portion of DNA studied. Of the mutations, 8% are not in exons 4–9, the most commonly affected and studied [27].
4. Different sensitivity of the technical procedure [2].

However, p53 nuclear staining is frequently positive in LELC of other organs [32, 38, 50] and in more than 50% of nasopharyngeal carcinomas in most series [18, 19, 31, 40]. In this anatomical location, it is frequently associated with EBV [18, 31, 41], with a strong association between p53 overexpression and EBER status [18]. Nevertheless, p53 gene mutation [31, 40] is not demonstrated, and it is supposed that some of the gene products of the EBV may

bind p53, increasing its expression [33, 41]. Szekely et al. [44] have demonstrated that EBNA5 protein binds to p53 protein. Thus, the p53 accumulated is probably wild type instead of mutated. However, LELC of the bladder does not seem to be related to this virus because it has not been found by different methods [17, 24, 28], and we did not find it in our cases. Thus, the p53 protein accumulation must occur in another way.

Several articles studied the lymphoid inflammatory component in LELC of the bladder [3, 20, 29]. It is formed by a mixed population of B-cells and T-cells, with clear predominance of T-cells in some cases [3, 20]; but both the distribution of CD4–CD8 subpopulations and the study of cytotoxic granules were not determined. In our cases, we showed that most of them corresponded to cytotoxic T-lymphocytes (CTLs) with granules positive for TIA-1. CTLs are probably the most important effectors of anti-tumor immunity in vivo, although NK cells and macrophages may also be involved [1]. The activation of CTLs may be triggered specifically by the recognition of tumor-specific antigens on tumor cells associated with the T-cell receptor [51]. The remarkable response of cytotoxic T-lymphocytes may be related to a better survival in some tumors [30, 39, 51], and it may represent an independent prognostic factor [30]. The described better clinical course of LELC of the bladder may be related to the type of CTLs that we have found, as it has been also demonstrated in other organs [30, 39, 51].

In summary, we studied three cases of vesical LELC, which presented an advanced local stage but for which local conservative therapy was enough. We demonstrate that these tumors are intensely and widely positive for p53 protein using immunohistochemistry, which is not related either to p53 mutation or EBV infection or integration. The inflammatory infiltrate is predominantly formed by T-lymphocytes with cytotoxic phenotype that, as in other organs, may be related to the better prognosis usually observed in LELC of the bladder.

References

1. Abbas AK, Lichtman AH, Pober JS (1997) Effector mechanisms of T cell-mediated immune reactions. Immunity to tumors. In Abbas AK, Lichtman AH, Pober JS (eds) Cellular and molecular immunology, 3rd edn. Saunders, Philadelphia, PA, pp 278–405
2. Abdel-Fattah R, Challen C, Griffiths TRL, Robinson MC, Neal DE, Lunec J (1998) Alterations of TP53 in microdissected transitional cell carcinoma of the human urinary bladder: high frequency of TP53 accumulation in the absence of detected mutations is associated with poor prognosis. Br J Cancer 77:2230–2238
3. Amin MB, Ro JY, Lee KM, Ordoñez NG, Dinney CP, Gulley ML, Ayala AG (1994) Lymphoepithelioma-like carcinoma of the urinary bladder. Am J Surg Pathol 18:466–473
4. Bernardini S, Adessi GL, Billerey C, Chezy E, Carbillert JP, Bittard H (1999) Immunohistochemical detection of p53 protein overexpression versus gene sequencing in urinary bladder carcinomas. J Urol 162:1496–1501
5. Bianchini E, Lissato L, Rimondi AP, Pergoraro V (1994) Lymphoepithelioma-like carcinoma of the urinary bladder. J Urol Pathol 5:45–49
6. Bostwick DG, Adalkha K (1994) Lymphoepithelioma-like carcinoma of the prostate. J Urol Pathol 2:319–325
7. Bostwick DG, Lopez-Beltran A (eds) (1999) Bladder biopsy interpretation. United Pathologist Press, New York, pp 149–172
8. Burchill SA, Neal DE, Lunec J (1994) Frequency of H-ras mutations in human bladder cancer detected by direct sequencing. Br J Cancer 73:516–521
9. Cabrero A, Cantu M, García C (1995) Urethral lymphoepithelioma. Report of a case. Rev Med Inst Mexicano Seguro Social 33:567–570
10. Chen KC, Yeh SD, Fang CL, Chiang HS, Chen YK (2003) Lymphoepithelioma-like carcinoma of the urinary bladder. J Formos Med Assoc 102:722–725
11. Constantinides C, Giannopoulos A, Kyriakou G, Androulaki A, Ioannou M, Dimopoulos M, Kyroudi A (2001) Lymphoepithelioma-like carcinoma of the bladder. BJU Int 87:121–122
12. Dinney CPN, Ro JY, Babaian J, Johnson DE (1993) Lymphoepithelioma of the bladder: a clinicopathological study of 3 cases. J Urol 149:840–842
13. Eble JN, Young RH (1997) Carcinoma of the urinary bladder: a review of its diverse morphology. Semin Diagn Pathol 14:98–108
14. Esrig D, Spruck III CH, Nichols PW, Chaiwun B, Steven K, Groshen S, Chen S-C, Skinner DG, Jones PA, Cote RJ (1993) p53 nuclear protein accumulation correlates with mutations in the p53 gene, tumor grade and stage in bladder cancer. Am J Pathol 143:1389–1397
15. Fukunaga M, Ushigome S (1998) Lymphoepithelioma-like carcinoma of the pelvis renal: a case report with immunohistochemical analysis and in situ hybridization for the Epstein–Barr viral genoma. Mod Pathol 11:1252–1256
16. Gastaud O, Demailly M, Guilbert E, Colombat M, Petit J (2002) Prog Urol 12:318–320
17. Gulley ML, Amin MB, Nichols JM, Banks PM, Ayala AG, Srigley JR, Eagan PA, Ro JY (1995) Epstein–Barr virus is detected in undifferentiated nasopharyngeal carcinoma, but not in lymphoepithelioma-like carcinoma of the urinary bladder. Hum Pathol 26:1207–1214
18. Gulley ML, Burton MP, Allred DC, Nicholls JM, Amin MB, Ro JY, Schneider BG (1998) Epstein–Barr virus infection is associated with p53 accumulation in nasopharyngeal carcinoma. Hum Pathol 29:252–259
19. Ho KY, Kuo WR, Chai CY, Tsai SM, Sheu SH, Wu SC, Juan KH (2001) A prospective study of p53 expression and its correlation with clinical response of radiotherapy in nasopharyngeal carcinoma. Laryngoscope 111:131–136
20. Holmäng G, Borghede G, Johansson SL (1998) Bladder carcinoma with lymphoepithelioma-like differentiation: a report of 9 cases. J Urol 159:779–782
21. Iczkowski KA, Shanks JH, Allsbrook WC, Lopez-Beltrán A, Pantazis CG, Collins TR, Wetherington RW, Bostwick DG (1999) Small cell carcinoma of urinary bladder is differentiated from urothelial carcinoma by chromogranin expression, absence of CD44 variant 6 expression, a unique pattern of cytokeratin expression, and more intense γ-enolase expression. Histopathology 35:150–156
22. Kamb A, Gruis NA, Weaver-Feldhaus J, Liu Q, Harshman K, Tavtigian SV, Stockert E, Day RS III, Johnson BE, Skolnick MH (1994) A cell cycle regulator potentially involved in genesis of many tumor types. Science 264:436–440
23. Keegan PE, Lunec J, Neal DE (1998) p53 and p53-regulated genes in bladder cancer. Br J Urol 82:710–720
24. Korabecna M, Ludvikova M, Skalova A (2003) Molecular diagnosis of Epstein–Barr virus in paraffin-embedded tissues of tumors with abundant lymphoid infiltration. Neoplasma 50:8–12
25. Kruslin B, Stanic G, Belicza M, Cupic H, Begic-Fehir J, Muic B, Markoja I (2000) Carcinoma of the urinary bladder resembling lymphoepithelioma. Lijec Vjesn 122:270–272

26. Lane DP (1992) P53, guardian of the genome. Nature 358:15–16
27. Levine AJ, Perry ME, Chang A, Silver A, Dittmer D, Wu M, Welsh D (1994) The 1993 Walter Hebert Lecture: the role of the TP53 tumour-suppressor gene in tumorigenesis. Br J Cancer 69:409–416
28. Lopez-Beltrán A, Morales C, Reymundo C, Toro M (1989) T-zone histiocytes and recurrence of papillary urothelial bladder carcinoma. Urol Int 44:205–209
29. Lopez-Beltrán A, Luque RJ, Vicioso L (2001) Lymphoepithelioma-like carcinoma of the urinary bladder: a clinicopathological study of 13 cases. Virchows Arch 438:552–557
30. Naito Y, Saito K, Shiiba K, Ohuchi A, Saigenji K, Nagura H, Ohtani H (1998) $CD8^+$ T cells infiltrated within cancer cell nests as a prognostic factor in human colorectal cancer. Cancer Res 58:3491–3494
31. Niemhom S, Kitazawa S, Murao S, Kunachak S, Maeda S (2000) Co-expression of p53 and bcl-2 may correlate to the presence of Epstein–Barr virus genome and the expression of proliferating cell nuclear antigen in nasopharyngeal carcinoma. Cancer Lett 160:199–208
32. Ortiz MR, Garijo G, Adrados M, Lopez-Bonet E, Acero D, Bernado L (2000) Epstein–Barr virus-associated cholangiocarcinoma with lymphoepithelioma-like component. Int J Surg Pathol 8:347–351
33. Pagano JS (1999) Epstein–Barr virus: the first human tumor virus and its role in cancer. Proc Assoc Am Physicians 111:573–580
34. Petit B, Leroy K, Kanavaros P, Boulland ML, Druet-Cabanac M, Haioun C, Bordessoule D, Gaulard P (2001) Expression of p53 protein in T- and natural killer-cell lymphomas is associated with some clinicopathologic entities but rarely related to p53 mutations. Hum Pathol 32:196–204
35. Porcaro AB, Gilioli E, Migliorini F, Antoniolli SZ, Iannucci A, Comunale L (2003) Primary lymphoepithelioma-like carcinoma of the urinary bladder: report of one case with review and update of the literature after a pooled analysis of 43 patients. Int Urol Nephrol 35:99–106
36. Rabani F, Cordon-Cardo C (2000) Mutation of cell cycle regulators and their impact on superficial bladder cancer. Urol Clin North Am 27:83–102
37. Reuter VE (1999) Vejiga: Factores de riesgo y pronósticos. Perspectivas del patólogo. In: Bostwick DG (ed) Anatomía patológica en Urología. Ed Clínicas urológicas de norteamérica. McGraw-Hill Interamericana editores, México, pp 509–521
38. Roig JM, Amerigo J, Velasco FJ, Gimenez A, Guerrero E, Soler JL (2001) Lymphoepithelioma-like carcinoma of ureter. Histopathology 39:106–107
39. Saiki Y, Ohtani H, Naito Y, Miyazawa M, Nagura H (1996). Immunophenotypic characterization of Epstein–Barr virus-associated gastric carcinoma: massive infiltration by proliferating CD8+ T-lymphocytes. Lab Invest 75:67–76
40. Sheu L-F, Chen A, Tseng H-H, Leu F-J, Lin JK, Ho K-C, Meng C-L (1995) Assessment of p53 expression in nasopharyngeal carcinoma. Hum Pathol 26:380–386
41. Shi W, Pataki I, MacMillan C, Pintille M, Payne D, O'Sullivan B, Cummings BJ, Warde P, Liu F-F (2002) Molecular pathology parameters in human nasopharyngeal carcinoma. Cancer 94:1997–2006
42. Slaton JW, Benedict WF, Dinney CPN (2001) p53 in bladder cancer: mechanism of action, prognostic value and target for therapy. Urology 57:852–859
43. Soini Y, Turpeenniemi-Hujanen T, Kamel D, Autio Harmainen H, Risteli J, Risteli L, Nuorva V, Paako P, Vahakangas K (1993) p53 immunohistochemistry in transitional cell carcinoma and dysplasia of the urinary bladder correlate with disease progression. Br J Cancer 68:1029–1035
44. Szeleky L, Selivanova G, Magnusson KP, Klein G, Wiman KG (1993) EBNA-5, an Epstein–Barr virus encoded nuclear antigen, binds to the retinoblastoma and p53 proteins. Proc Natl Acad Sci U S A 90:5455–5459
45. Tiguert R, Bianco FJ Jr, Oskanian P, Li Y, Grignon DJ, Wood DP Jr, Pontes JE, Sarkar FH (2001) Structural alteration of p53 protein in patients with muscle invasive bladder transitional cell carcinoma. J Urol 166:2155–2160
46. Villuendas RE, Piris MA, Algara P, Sanchez-Beato M, Sanchez-Verde L, Martinez JC, Orradre JL, Garcia P, Lopez C, Martinez P (1993) The expression of p53 protein in non-Hodgkin's lymphomas is not always dependent on p53 gene mutations. Blood 82:3151–3156
47. Villuendas R, Pezzella F, Gatter K, Algara P, Sáchez-Beato M, Martínez P, Martínez JC, Muñoz K, García P, Sánchez L, Kocialkowsky S, Campo E, Orradre JL, Piris MA (1997) p21 WAF1/CIP1 and MDM 2 expression in non-Hodgkin's lymphoma and their relationship to p53 status: a p53+, MDM 2–, p21– immunophenotype associated with missense p53 mutations. J Pathol 181:51–56
48. Ward JN, Dong WF, Pitts WR (2002) Lymphoepithelioma-like carcinoma of the bladder. J Urol 167:2523–2524
49. Wright C, Thomas D, Mellon K, Neal DE, Horne CH (1995) Expression of retinoblastoma gene product and p53 protein in bladder carcinoma: correlation with Ki 67 index. Br J Urol 75:173–179
50. Wu MS, Shun CT, Wu CC, Hsu TY, Lin MT, Chang MC, Wang HP, Lin JT (2000) Epstein–Barr virus-associated gastric carcinomas: relation to H. pylori infection and genetic alterations. Gastroenterology 118:1031–1038
51. Yakirevich E, Izhak OB, Rennert G, Kovacs ZG, Resnick MB (1999) Cytotoxic phenotype of tumor infiltrating lymphocytes in medullary carcinoma of the breast. Mod Pathol 12:1050–1056
52. Young RH, Eble JN (1991) Unusual forms of carcinoma of the urinary bladder. Human Pathol 22:948–965
53. Young RH, Eble JN (1993) Lymphoepithelioma-like carcinoma of the urinary bladder. J Urol Pathol 1:63–67
54. Zukerberg LR, Harris NL, Young RH (1991) Carcinomas of the urinary bladder simulating malignant lymphomas. Am J Surg Pathol 15:569–576

Virchows Arch (2004) 444:426–435
DOI 10.1007/s00428-004-1003-7

ORIGINAL ARTICLE

Christine Lagorce-Pagès · François Paraf · Dominique Wendum · Antoine Martin · Jean-François Fléjou

Expression of inflammatory secretory phospholipase A2 and cytosolic phospholipase A2 in premalignant and malignant Barrett's oesophagus

Received: 4 September 2003 / Accepted: 1 March 2004 / Published online: 25 March 2004

Abstract *Aims* To establish the prevalence of inflammatory secretory phospholipase A2 (sPLA2) and cytoplasmic phospholipase A2 (cPLA2) expression in a surgical series of Barrett's adenocarcinoma and associated preneoplastic lesions and to correlate this expression with clinicopathological data and prognosis. *Methods:* sPLA2 and cPLA2 were analysed by means of immunohistochemistry in surgical specimens of 67 and 73 cases of Barrett's adenocarcinomas, respectively. Barrett's mucosa was analysed in 31 cases. *Results:* Expression of sPLA2 was detected in 48% of Barrett's mucosa negative for intraepithelial neoplasia and 63% of Barrett's adenocarcinoma. Semi-quantitative analysis revealed a significant increase in sPLA2 expression between Barrett's mucosa negative for intraepithelial neoplasia and adenocarcinoma. cPLA2 expression was detected in 18% of Barrett's adenocarcinoma. An inverse correlation was found between cPLA2 expression and depth of tumour infiltration, neoplastic vascular invasion and neoplastic perineural invasion. Survival analysis showed no significant prognostic value for sPLA2 and cPLA2. *Conclusion:* sPLA2 is frequently expressed in Barrett's oesophagus. The increasing expression of sPLA2 that we observed from Barrett's mucosa to adenocarcinoma suggests that sPLA2 could be involved in Barrett's carcinogenesis. In contrast, cPLA2 expression is less frequently observed in Barrett's oesophagus and is inversely associated with aggressive pathological features of the tumours.

Key words Phospholipase A2 · Cytosolic phospholipase A2 · Inflammatory secretory phospholipase A2 · Barrett's oesophagus · Oesophageal adenocarcinoma

C. Lagorce-Pagès · A. Martin
Service d'Anatomie Pathologique,
Hôpital Avicenne, AP-HP,
Bobigny, France

F. Paraf
Service d'Anatomie Pathologique,
Hôpital Dupuytren,
Limoges, France

D. Wendum · J.-F. Fléjou (✉)
Service d'Anatomie Pathologique A,
Hôpital Saint Antoine, AP-HP,
184 rue du Faubourg Saint-Antoine, 75541 Paris Cedex 12, France
e-mail: jean-francois.flejou@sat.ap-hop-paris.fr
Tel.: +33-1-49283012
Fax: +33-1-49282878

Introduction

Adenocarcinoma of the oesophagus is among the 15 most frequent cancers in the world. The incidence of this cancer throughout the Western world has increased remarkably in the last few decades with a rate of 5–10% per year, greater than that for any other cancer [3, 5]. Barrett's oesophagus is a condition in which the normal squamous epithelium lining the distal oesophagus is replaced by metaplastic intestinalised columnar epithelium and is considered a consequence of severe and prolonged gastrooesophageal reflux disease. Adenocarcinoma of the oesophagus develops in Barrett's oesophagus according to a multistep process in which intestinal metaplastic epithelium progresses to intraepithelial neoplasia (IN) and eventually to carcinoma [14, 38]. This neoplastic progression is associated with several molecular alterations including genomic instability and alterations of the p53 tumour suppressor gene [17]. However, many questions concerning the pathogenesis of Barrett's adenocarcinoma are still unanswered and it may be important to elucidate new molecular events leading to malignant transformation of Barrett's oesophagus in order to detect patients at high risk of cancer.

Phospholipase A2 (PLA2) is a diverse family of lipolytic enzymes that hydrolyse the release of free arachidonic acid from membrane phospholipids and provide it to cyclooxygenase (COX), especially COX-2 and lipooxygenase, which catalyse its conversion into prostaglandins and leukotrienes, respectively. PLA2 is structurally and functionally subdivided into four major classes including secretory PLA2 (sPLA2), cytosolic PLA2 (cPLA2), Ca++-independent PLA2 (iPLA2) and platelet

activating factor acetyl-hydrolase (PAF) [28]. To date, ten sPLA2 isozymes (designated groups IB, IIA, IIC, IID, IIE, IIF, III, V, X and XII) and three cPLA2 isozymes (designated groups IVA, IVB, IVC) have been identified in mammals [34]. Among them, cytoplasmic PLA2 (cPLA2) or group IVA PLA2 is a high molecular weight form of PLA2, which preferentially hydrolyses arachidonic acid at the sn-2 position representing a rate-limiting enzyme in eicosanoid production [6]. In contrast, inflammatory secreted PLA2 or sPLA2-IIa has a low molecular mass and is not specific for phospholipids inducing the release of arachidonic acid involved in prostaglandin formation as well as the production of lysophospholipid [2]. sPLA2-IIa has been implicated in a variety of inflammatory conditions such as rheumatoid arthritis, acute pancreatis and Crohn's disease [28]. sPLA-IIa appears to contribute to the pathogenesis of cardiovascular conditions including atherosclerosis, acute myocardial infarction and neurodegeneration in the ischemic brain [30]. Recent literatures have highlighted the potential implication of PLA2 in the development of human digestive tumours especially in the colon. sPLA2 is frequently overexpressed in colorectal adenomas in familial adenomatous polyposis (FAP) and in colorectal adenocarcinomas [20, 41]. cPLA2 is moderately overexpressed in colorectal cancer [40]. We have previously reported increased COX-2 expression in Barrett's associated oesophageal adenocarcinoma [23]. Recent works raise the possibility that COX-2 selective inhibitors may have chemopreventive potential in Barrett's oesophagus [4, 19]. However, sPLA2 and cPLA2 expression has never been studied in Barrett's adenocarcinoma.

The aim of this study was to evaluate by immunohistochemistry the prevalence of inflammatory secreted PLA2 and cytoplasmic PLA2 expression in a large surgical series of resected Barrett's adenocarcinoma and associated preneoplastic lesions and to correlate this expression with clinicopathological data and prognosis.

Materials and methods

Patients

Seventy-three patients with adenocarcinoma arising in Barrett's oesophagus underwent potentially curative surgical resection at Beaujon hospital between 1976 and 1997. There were 65 men and 8 women with a mean age of 63 years (range 19–84.4 years). None of the patients had received chemo- or radiotherapy before surgery. The medical history of each patient was obtained.

Tumour samples

Surgical specimens were received fresh, fixed in 10% neutral formalin, sampled and embedded in paraffin wax. The tumour was regarded as an adenocarcinoma having developed in Barrett's oesophagus when specialised metaplasia was observed between the tumour and either the squamous oesophageal mucosa or the cardiac line [31]. Specialised metaplasia also called Barrett's metaplasia morphologically corresponds to the incomplete type of intestinal metaplasia (type 2 or 3) [10, 42]. Samples of adenocarcinoma were selected for sPLA2 and cPLA2 immunohistochemical analysis, in 67 and 73 cases, respectively. Seventy three samples of adenocarcinoma were first selected for cPLA2 immunohistochemical analysis. Immunohistochemical analysis for sPLA2 was next performed in 67 cases, as six cases, with tumour areas insufficiently represented on tissue section for a robust evaluation of sPLA2 tumour expression, were excluded. Thirty one samples of Barrett's mucosa adjacent to the tumour were then selected for immunohistochemical analysis including areas of Barrett's mucosa negative for intraepithelial neoplasia (31 cases), areas of Barrett's mucosa with low-grade intraepithelial neoplasia (17 cases) and areas of Barrett's mucosa with high-grade intraepithelial neoplasia (17 cases). Intraepithelial neoplasia was graded using cytological and architectural criteria proposed by the Working Group for Gastroenterological Pathology of the German Society for Pathology in 2001 in Erlangen, Germany, adapted to the proposals of the World Health Organization (WHO) classification of tumours of the digestive system [10, 42]. For each case, the following tumour variables were evaluated: tumour size, tumour differentiation (well, moderate, poor, mucinous and signet-ring cell carcinoma), depth of invasion, evidence of vascular or perineural neoplastic involvement, presence of regional lymph-node metastases, TNM stage according to the International Union Against Cancer (UICC), stage according to the Rosenberg's classification and tumour type following Lauren's criteria [24, 32, 35]. Sections of the tumours, away from the areas of ulceration, were evaluated for the presence of the accompanying inflammation recorded as mild, moderate or severe. Twenty biopsy specimens including five oesophageal biopsy specimens (normal squamous epithelium), five oesophageal squamous cell carcinoma (SCC) and ten gastric biopsy specimens (cardia-type mucosa in five cases and fundic-type mucosa in five cases) were also examined.

The COX-2 expression has been previously assessed by immunohistochemistry in 66 cases of Barrett's adenocarcinomas and 32 cases of Barrett's mucosa of our series [23]. Epithelial expression of COX-2 has been found in 91% (29 of 32) of Barrett's mucosa negative for intraepithelial neoplasia, 94% (16 of 17) of Barrett's mucosa with low-grade and high-grade intraepithelial neoplasia and 97% (64 of 66) of Barrett's adenocarcinoma. COX-2 expression did not significantly differ as the neoplastic process progressed from specialised metaplasia to intraepithelial neoplasia and to adenocarcinoma. COX-2 expression was significantly increased in the well-differentiated tumours when compared with the poorly differentiated ones (P=0.003). There was no significant relationship between COX-2 expression and the other histopathological features of the tumours and survival.

Immunohistochemistry

Immunohistochemistry was performed on formalin-fixed paraffin sections using an avidin-biotin peroxidase complex technique (DAKO LSAB2 System, Peroxydase K675, Dako, Carpinteria, CA). Antibodies used were: sPLA2 (type-II human synovial also called type IIa-sPLA2) rabbit polyclonal antibody (Cayman Chemical, Ann Arbor, USA) at a 1:200 dilution and $cPLA_2$-α mAb (cat. no. sc-454, Santa Cruz Biotechnology, Santa Cruz, CA) a 1:100 dilution. Briefly, 5-μm sections were cut from paraffin-embedded tissue, deparaffinized and rehydrated. After quenching endogenous peroxidase with 0.3% hydrogen peroxide in methanol for 30 min, microwave antigen retrieval was performed for cPLA2 immunostaining by immersing the sections in 0.01 M citrate buffer (citric acid and sodium citrate, pH 6.0). Primary antibodies were applied to tissue sections for 1 h at room temperature. After sequential application of a biotinylated link antibody and a horseradish peroxydase streptavidin complex the colour was developed using 3,3′-diaminobenzidine (Dako, Carpinteria, CA). Sections were then counterstained with haematoxylin, dehydrated and mounted with permount.

For negative controls, non-immune rabbit IgG and non-immune mouse IgG were used as a substitute for sPLA2 and cPLA2 antibodies, respectively. Antibody adsorption studies were performed with its purified protein for sPLA2 or cognate blocking peptide for

cPLA2 as previously described [41]. A section of colon adenocarcinoma, known to express cPLA2 protein assessed by Western blot and immunohistochemistry was used as positive external tissue control for cPLA2 staining (data not shown). Labelled Paneth cells were used as positive internal control for sPLA2 staining.

Evaluation of staining

Slides were assessed using a light microscope in a blinded fashion by two investigators (C.L., J.F.F.) on two separate occasions. Staining intensity was scored as 0 (negative), 1 (weak), 2 (medium), 3 (strong). Grade was scored as 0 (0–4%), 1 (5–29%), 2 (30–59%), 3 (60–100%) according to the percentages of positively stained tumour cells. The final immunoreactive score (range from 0 to 9) was calculated by multiplication of the staining intensity with the grade, as previously described [23]. For each case, the staining pattern for sPLA2 and cPLA2 was noted for both the tumour centre and the tumour invasion front.

Statistical analysis

Qualitative data were compared using the chi square test with Yates correction when appropriate. Quantitative data were expressed as mean±SEM and compared using the non-parametric Mann-Whitney or Kruskal-Wallis tests. Survival rates were calculated by the Kaplan-Meier method using the date of surgery as the starting point and compared using the log-rank test. All deaths were considered. At the time of analysis, the 73 patients had a mean follow-up of 34.1±4.7 months (median 15.6 months; range 0.9–189.4 months). A two-tailed P value <0.05 was considered to indicate statistical significance.

Results

Specificity of sPLA2 and cPLA2 antibodies on immunohistochemistry

The substitution of sPLA2 and cPLA2 antibodies by non-immune rabbit IgG and non-immune mouse IgG, respectively, failed to reveal relevant staining. Antibody preadsorption with its purified protein for sPLA2 or cognate blocking peptide for cPLA2 was associated with no positive staining in epithelial cells and in interstitial cells in Barrett's mucosa and in Barrett's adenocarcinoma (data not shown).

sPLA2 and cPLA2 expression in normal oesophageal epithelium, normal gastric mucosa, and oesophageal squamous cell carcinoma

sPLA2 was not or weakly expressed in the basal and parabasal cell layers of the squamous oesophageal epithelium (Fig. 1A). A moderate to strong sPLA2 staining was observed in the lamina elastica of arteries. No sPLA2 staining was noted in the lamina propria mesenchymal cells including fibroblasts and macrophages. The epithelial cells of the cardia type mucosa did not show any reactivity for sPLA2. In normal fundic type mucosa, sPLA2 staining was confined to the parietal cells with no expression in the normal foveolar epithelia.

Normal oesophageal squamous epithelium was consistently negative for cPLA2 (Fig. 1B). There was no expression of cPLA2 in the epithelial cells of the normal gastric mucosa including cardia type mucosa and fundic type mucosa. 60% (3 of 5) of the squamous cell carcinomas showed intense diffuse granular staining for sPLA2 expression. Of the squamous cell carcinomas, 40% (2 of 5) showed mild to moderate cPLA2 expression. When present, cPLA2 staining in tumour cells was cytoplasmic and granular with a basal intensification.

sPLA2 and cPLA2 expression in Barrett's mucosa

sPLA2 expression was detected in 48% (15 of 31) of Barrett's mucosa negative for intraepithelial neoplasia. Columnar cells showed a cytoplasmic staining pattern. Goblet cells were negative. Staining pattern showed limited or no staining on the surface epithelium and weak staining in the crypt glands (Fig. 1C). Metaplastic Paneth cells consistently exhibited positive granular staining. In Barrett's mucosa with low-grade and high-grade intraepithelial neoplasia, sPLA2 expression was detected in 71% (12 of 17) and 82% (14 of 17) of the cases, respectively. Semi-quantitative analysis showed an enhanced sPLA2 expression in Barrett's mucosa negative for intraepithelial neoplasia and in Barrett's mucosa with intraepithelial neoplasia compared with normal squamous oesophageal epithelium with median immunoreactive scores of 3, 5 and 2, respectively. Barrett's adenocarcinoma revealed a significant increase in sPLA2 expression compared with its respective Barrett's mucosa negative for intraepithelial neoplasia ($P=0.0001$) and Barrett's mucosa with low- and high-grade intraepithelial neoplasia ($P<0.0001$ and $P=0.001$, respectively).

Barrett's mucosa negative for intraepithelial neoplasia showed no detectable expression for cPLA2 (Fig. 1D). In Barrett's mucosa with low- and high-grade intraepithelial neoplasia, cPLA2 expression was present in 12% (2 of 17) and 24% (4 of 17) of the cases, respectively. cPLA2 staining was focal and cytoplasmic with often a basal reinforcement. Semi-quantitative analysis revealed a significant increase in cPLA2 expression between Barrett's mucosa negative for intraepithelial neoplasia and its respective Barrett's adenocarcinoma ($P=0.03$). There was an increase in cPLA2 expression between Barrett's mucosa negative for intraepithelial neoplasia and Barrett's mucosa with low- and high-grade intraepithelial neoplasia with median immunoreactive scores of 0, 2 and 3, respectively; however, this increase did not reach the level of significance.

sPLA2 and cPLA2 expression in Barrett's adenocarcinoma

sPLA2 expression was detected in 63% (42 of 67) of the tumours samples. All positive cases showed cytoplasmic and granular staining of the tumour cells (Fig. 2A–C).

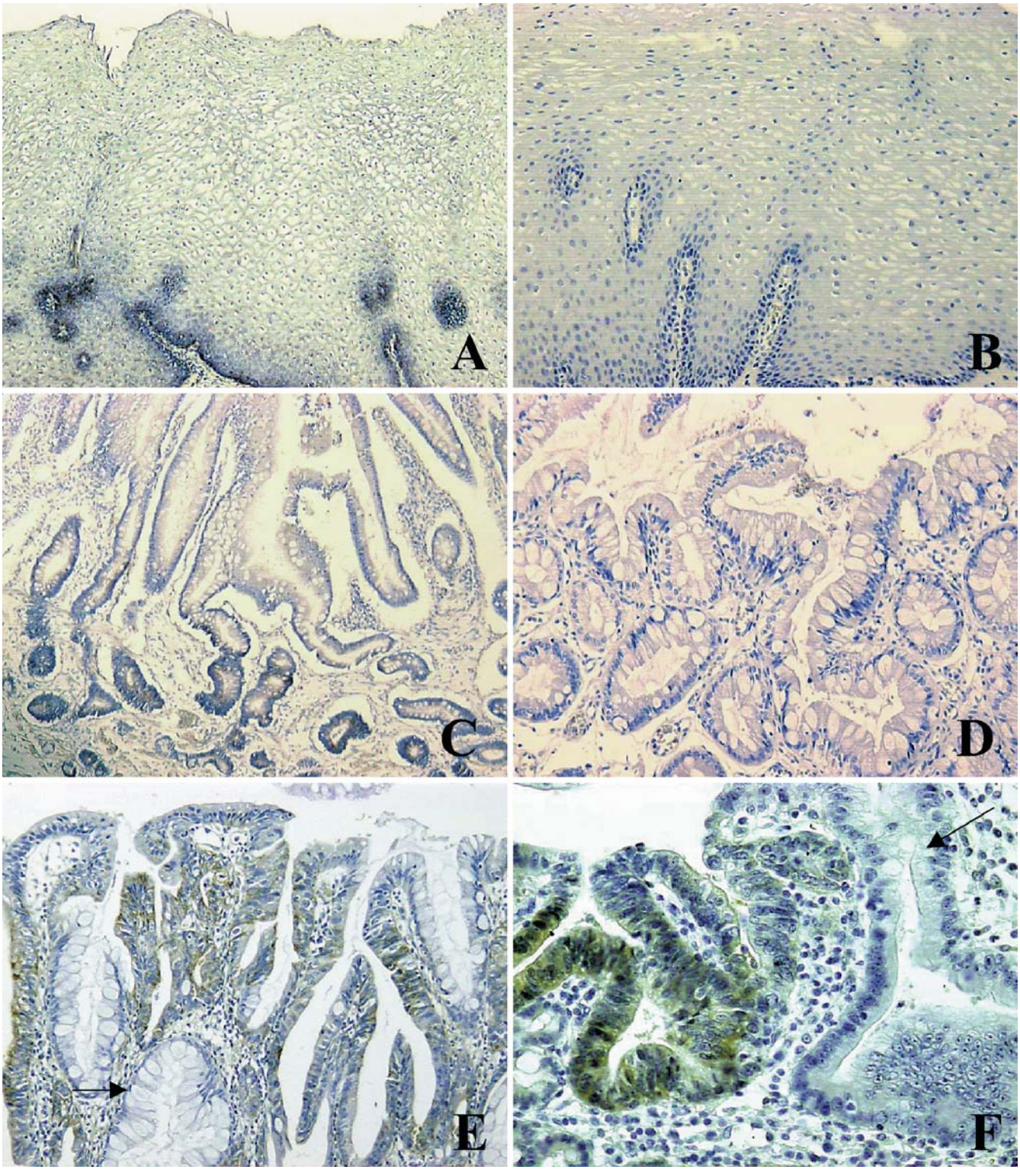

Fig. 1 Secretory phospholipase A2 (sPLA2) and cytoplasmic phospholipase A2 (cPLA2) protein expression in normal squamous epithelium and Barrett's mucosa with and without dysplasia. sPLA2: **A** sPLA2 is weakly expressed in the basal and parabasal cells of the squamous oesophageal epithelium (×100). **C** Barrett's specialised mucosa negative for dysplasia showing a weak to moderate sPLA2 staining limited to the crypt glands (×100). **E** Barrett's mucosa demonstrating moderate sPLA2 staining in areas with high-grade dysplasia and no staining in areas negative for dysplasia (*arrow*) (×200). cPLA2: Normal oesophageal epithelium (**B**) and Barrett's mucosa negative for dysplasia (**D**) showing no detectable staining (×100). **F** Barrett's mucosa showing moderate staining in areas with high-grade dysplasia and no detectable staining in areas negative for dysplasia (*arrow*) (×200). (Immunoperoxidase with nuclear counterstain by Mayer's haematoxylin)

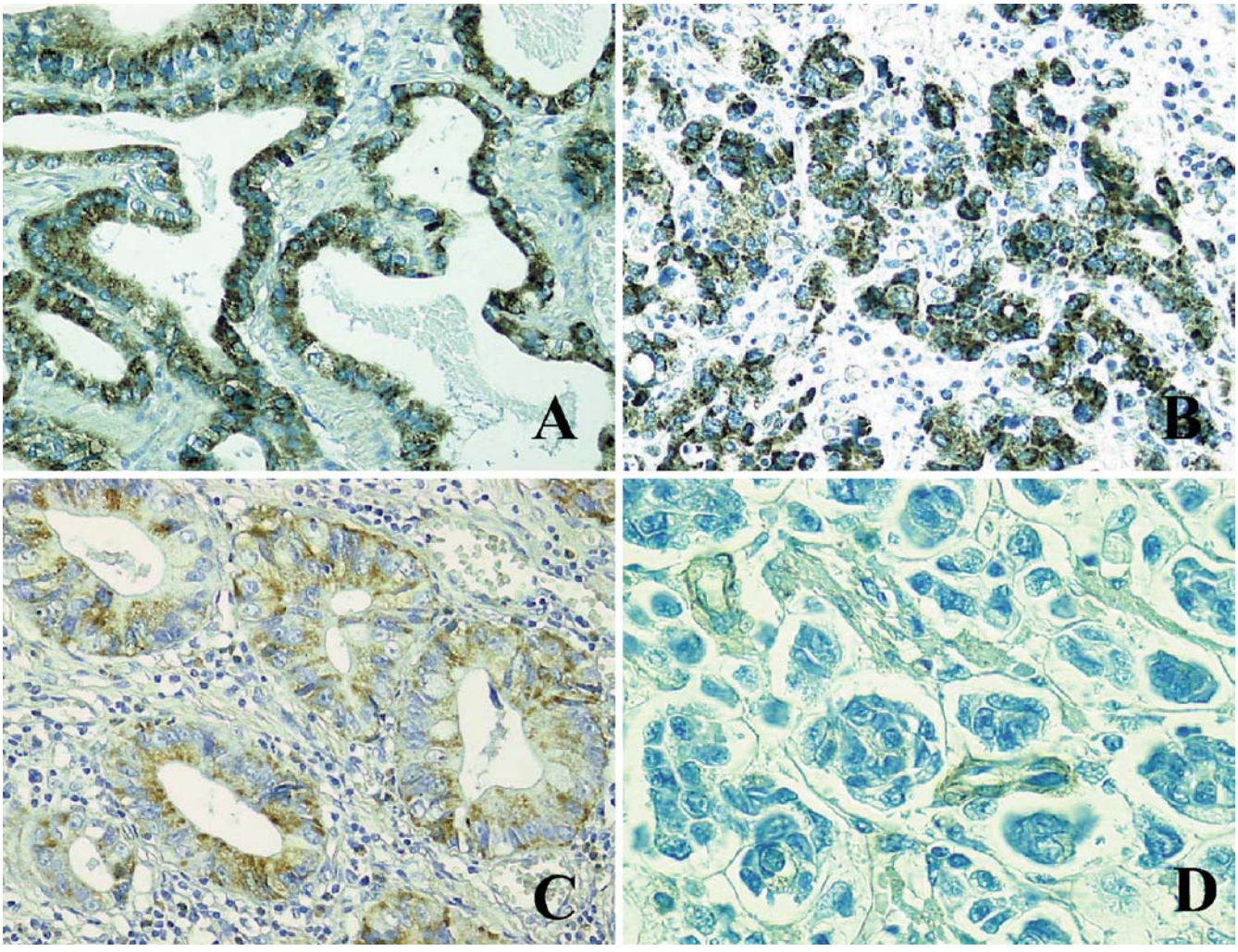

Fig. 2 Immunohistochemical analysis of secretory phospholipase A2 (sPLA2) in Barrett's adenocarcinoma. **A**, **B** Strong and diffuse immunostaining in a well (**A**) and a poorly (**B**) differentiated Barrett's adenocarcinoma. **C** Moderate immunostaining in a well-differentiated Barrett's adenocarcinoma. **D** Signet ring-cell carcinoma showing no staining for sPLA2 (×200) (immunoperoxidase with nuclear counterstain by Mayer's haematoxylin)

Staining intensity was strong in the majority of the cases (83%). There was no difference in the expression pattern of sPLA2 between the tumour centre and the tumour invasion front. The median immunoreactive score was 6 (range 0–9). Based on this analysis, we categorised the 67 patients into two well-balanced groups that were suitable for statistical analysis: 42 high expressers (score greater than 6) and 25 low expressers (score ranging from 0 to 6). The relationship between sPLA2 expression and the pathological features of the tumours is shown in Table 1. A significant relationship was found between sPLA2 expression and tumour differentiation (P=0.01): 78% (21/27) of the well-differentiated Barrett's adenocarcinomas showed a high immunoreactive score compared with 22% (2 of 9) of the mucinous and signet ring-cell carcinoma (Fig. 2D). However, a significant relationship was no longer observed when tumour grade was stratified into two groups, well or moderately differentiated and poorly differentiated. There was a tendency for a relationship between sPLA2 expression and COX-2 expression: 79% of the tumours with a high sPLA2 immunoreactive score showed increased COX-2 expression compared with 21% of the tumours with low sPLA2 immunoreactive score. However, this difference did not reach the level of statistical significance (P=0.06). There was no significant relationship between sPLA2 expression and the other pathological features of the tumours studied, including tumour size, depth of infiltration, degree of the stromal inflammation, lymph-node involvement, pTNM staging and Lauren's classification.

cPLA2 expression was detected in 18% (13 of 73) of the tumour specimens. cPLA2 staining in tumour cells was cytoplasmic with often basal reinforcement (Fig. 3A–B). Staining intensity was moderate in the majority of the cases. Staining pattern for cPLA2 did not differ between the tumour centre and the tumour invasion front. Expression of cPLA2 was categorised according to its observed distribution in order to obtain well-balanced

Table 1 Relationship between secretory phospholipase A2 (sPLA2) expression and pathological features in 67 cases of Barrett's adenocarcinoma

	n	sPLA2 (%)		*P* value
		Low	High	
Tumour differentiation				0.01
Well	27	22	78	
Moderate	23	48	52	
Poor	8	12	88	
Mucinous/signet ring cell	9	78	22	
Stromal inflammation				0.19
Mild	13	54	46	
Moderate	44	36	64	
Strong	10	50	50	
Vascular invasion				0.54
Present	56	36	64	
Absent	11	45	55	
Perineural invasion				0.54
Present	38	34	66	
Absent	29	41	59	
Depth of invasion				0.88
Early	14	36	64	
Advanced	53	38	62	
Nodal involvement				0.23
Present	41	32	68	
Absent	26	46	54	
Distant metastasis				0.99
Present	8	38	62	
Absent	59	37	63	
Rosenberg's classification				0.08
I	2	0	100	
II	18	61	39	
III or IV	47	31	69	
Lauren's classification				0.15
Intestinal type	53	32	68	
Diffuse type	10	50	50	
Indefinite	4	75	25	
COX-2 expression				0.06
Low	41	46	54	
High	19	21	79	

Table 2 Relationship between cytoplasmic phospholipase A2 (cPLA2) expression and pathological features in 73 cases of Barrett's adenocarcinoma

	n	cPLA2+ (%)	cPLA2 (%)	*P* value
Tumour differentiation				0.07
Well	29	31	69	
Moderate	24	8	92	
Poor	10	20	80	
Mucinous/signet ring cell	10	0	100	
Stromal inflammation				0.38
Mild	17	6	94	
Moderate	44	23	77	
Poor	11	18	82	
Vascular invasion				0.003
Present	60	12	88	
Absent	13	46	54	
Perineural invasion				0.04
Present	41	10	90	
Absent	32	28	72	
Depth of invasion				0.02
Early	16	38	62	
Advanced	57	12	88	
Nodal involvement				0.21
Present	45	13	87	
Absent	28	25	75	
Distant metastasis				0.57
Present	9	11	89	
Absent	64	19	81	
Rosenberg's classification				0.21
I	4	25	75	
II	18	33	67	
III or IV	51	11	89	
Lauren's				0.27
Intestinal type	55	22	78	
Diffuse type	14	7	93	
Indefinite	4	0	100	
COX-2 expression				0.72
Low	45	16	84	
High	21	19	81	

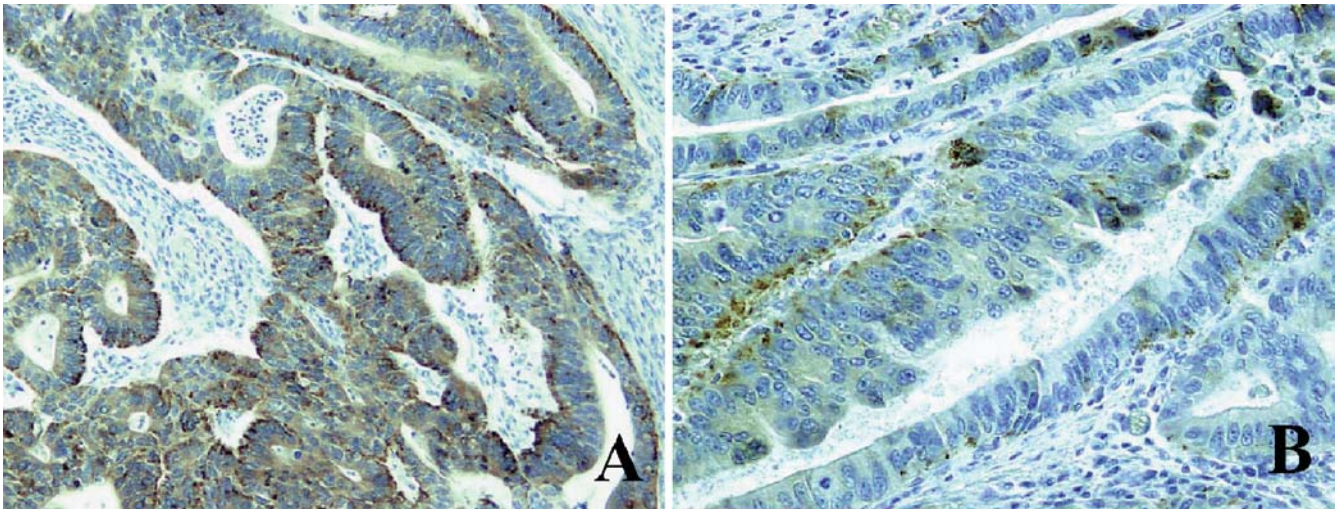

Fig. 3 Immunohistochemical analysis of cytoplasmic phospholipase A2 (cPLA2) in Barrett's adenocarcinoma. **A** Strong immunostaining in a moderately differentiated Barrett's adenocarcinoma. **B** Moderate immunostaining in a well-differentiated Barrett's adenocarcinoma. Staining is cytoplasmic with a basal reinforcement (×200) (immunoperoxidase with nuclear counterstain by Mayer's haematoxylin)

groups that were suitable for statistical analysis. We chose the cut-off value greater than zero to obtain a positive (or high expresser) group containing enough tumours (13 tumours). The relationship between cPLA2 expression and the pathological features of the tumours is shown in Table 2. Superficial carcinomas (confined to the mucosa or the submucosa, pT1) were more frequently positive than the infiltrative cases (38% vs 12%, P=0.02). Tumours without neoplastic vascular or perineural invasion were more frequently positive than those with vascular or perineural invasion (46% vs 12%, P=0.003 and 28% vs 10%, P=0.04, respectively). There was a tendency for a relationship between cPLA2 expression and tumour differentiation: 31% (9 of 29) of the well-differentiated Barrett's adenocarcinomas were positive compared with none (0 of 10) of the mucinous and signet ring cell carcinomas. However, this difference did not reach significance (P=0.07). There was no significant association between cPLA2 expression and the other selected pathological features, including tumour size, depth of infiltration, degree of the stromal inflammation, lymph-node involvement, distant metastasis, pTNM staging and Lauren's classification. There was no significant difference between the cPLA2 positive and negative cases regarding COX-2 expression.

Survival

At the time of analysis, 15 patients of 73 were alive with a mean follow-up of 93.5 months (median 90.7 months; range 41.1–189.4 months) after tumour resection. Five patients who died of diseases other than Barrett's adenocarcinoma were used in this analysis with survival times censored at the time of death. Overall median survival was 18.5 months, and 5-year survival rate was 33%. The survival analysis showed no significant prognostic value for cPLA2 and sPLA2 expression in Barrett's adenocarcinoma (data not shown).

Discussion

The present study demonstrates the increased expression of sPLA2 and, to a lesser extent, of cPLA2 in Barrett's mucosa and Barrett's adenocarcinoma. To our knowledge, this is the first study that focused on sPLA2 and cPLA2 expression in Barrett's oesophagus.

Previous works have shown that carcinogenesis in Barrett's oesophagus is associated with upregulation of COX-2 [23, 27, 33]. COX-2 inhibitors have been reported to reduce the risk of development of oesophageal adenocarcinoma, in animal models [4]. Furthermore, a recent clinical study indicates that COX-2 inhibition may be interesting in chemoprevention of oesophageal cancer by decreasing the cell proliferation in human Barrett's mucosa [19]. According to these reports, it may be supposed that an optimal level of COX metabolites is necessary to support tumour growth in Barrett's oesophagus. The increased expression of sPLA2 and, to a lesser extent, of cPLA2 that we observed in our series of Barrett's oesophagus is in accordance with the eicosanoid production involved in tumour development since overexpression of these enzymes seems to be a contributing substrate to the COX-2 pathway necessary to produce prostaglandins by releasing arachidonic acid from cell membrane phospholipids [1, 28].

The specificity of the two antibodies used in our study was first investigated by performing antibody adsorption studies with its purified protein for sPLA2 and a cognate blocking peptide for cPLA2 which completely blocked sPLA2 and cPLA2 immunoreactivity in Barrett's adenocarcinoma [41]. Expression of sPLA2 in human intestinal tract has been previously analysed by immunohistochemistry and in situ hybridisation with both immunoreactive PLA2-II protein and PLA2-II mRNA detected in Paneth cells and columnar cells of the inflamed intestinal mucosa especially in Crohn's disease and ulcerative colitis [12, 13]. We then analysed sPLA2 and cPLA2 expression in normal oesophageal epithelium and in oesophageal squamous cell carcinoma. Normal oesophageal epithelium showed inconsistent sPLA2 expression and an absence of cPLA2 expression. However, we observed an increased expression of sPLA2 and to a lesser extent of cPLA2 in oesophageal squamous cell carcinoma. These findings suggest that PLA2 is not only associated with Barrett's neoplastic transformation but is probably involved in squamous carcinogenesis of the oesophagus. Additional studies would be necessary to explore the precise role of PLA2 in oesophageal squamous cell carcinogenesis.

Barrett's mucosa negative for intraepithelial neoplasia showed in our series a weak sPLA2 expression with no cPLA2 detectable expression. These results are in accordance with previous data showing an absence or a very weak sPLA2 and cPLA2 expression in the epithelial cells of the normal colonic mucosa [41]. sPLA2 was strongly expressed in Paneth cells, as it has been previously reported [21, 29]. The increasing rate of sPLA2 and to a lesser extent of cPLA2 that we observed during morphological steps of Barrett's carcinogenesis is in agreement with preliminary data demonstrating that COX-2 expression is enhanced in Barrett's mucosa and increases as the neoplastic process progresses to intraepithelial neoplasia and to adenocarcinoma [27, 33]. On the contrary, COX-2 expression was found to be unrelated to the degree of intraepithelial neoplasia, in our series of Barrett's adenocarcinoma [23]. Contradictory results have been obtained for sPLA2 expression in colorectal carcinogenesis. Studies in the Min mouse, a murine model for FAP, have shown that mutations in the sPLA2 gene correlated well with an increased tumour number suggesting a protective effect of sPLA2 expression on colorectal carcinogenesis [7, 26]. In contrast, sPLA2 does not appear to be implicated in the development of phenotypic variation in human FAP as no inactivating mutations in the sPLA2 gene were identified in this disease [8, 39]. In addition, Kennedy et al. described an overexpression of

sPLA2 messenger RNA in colorectal adenomas of FAP [20]. The functional role of cPLA2 in colon tumourigenesis is not elucidated. Recent genetic studies in the APC Min mouse support the notion that cPLA2 may play a role in the expansion of polyps in the small intestine but is not involved in colorectal carcinogenesis as the mutation or deletion of the cPLA2 gene does not affect the number or size of the colonic polyps [16, 40].

sPLA2 was frequently expressed in Barrett's adenocarcinoma. The prevalence of sPLA2 expression in Barrett's adenocarcinoma is comparable with the rate of 66% described in a recently reported series of 48 cases of colorectal adenocarcinomas [41]. Overexpression of sPLA2 has been reported in several types of digestive cancers. There is increased sPLA2 expression in gastric adenocarcinoma, small-bowel adenocarcinoma, hepatocellular carcinoma and pancreatic adenocarcinoma [18, 25, 29, 41, 44]. The upregulation of sPLA2 in our study is also consistent with the frequent enhanced expression of COX-2 reported in Barrett's adenocarcinoma [23, 27, 33]. Moreover, in our series, sPLA2 expression and COX-2 expression showed a tendency to be related to each other; however, this relationship did not reach the level of significance. These results are in accordance with the reported functional coupling of these enzymes that seems to be necessary to produce prostaglandins E2 involved in tumour development [1, 28]. In our study, we found a significant relationship between sPLA2 expression and tumour differentiation. Most mucinous and signet ring cell carcinomas showed no or low expression of sPLA2. These results are in agreement with the expression of this enzyme in gastric carcinoma where the mucinous adenocarcinoma and signet ring cell carcinoma failed to express this protein [29]. However, in our study, sPLA2 expression and tumour type following Lauren's classification were not related to each other. This latter result is probably in part explained by the fact that, in our series, the group of diffuse-type carcinomas according to Lauren's classification is not composed exclusively of tumours classified as signet-ring cell tumours in the WHO classification but also consisted of poorly differentiated adenocarcinomas. In our study, we did not find a significant correlation between sPLA2 expression and any of the usual parameters that are associated with tumour progression, such as tumour depth, vascular invasion, lymph-node involvement and distant metastases. We were unable to demonstrate any prognostic value of sPLA2 expression. Studies dealing with the relationship between sPLA2 expression and tumour progression showed contradictory results. Some studies have suggested a protective effect for sPLA2 against tumour progression. Expression of sPLA2 has been reported to be significantly associated with longer survival and less frequent metastasis in gastric adenocarcinomas [25]. Upregulation of sPLA2 has also been related to longer survival after surgery in pancreatic cancer [18]. In contrast, other studies have suggested that sPLA2 may play a role in tumour development. In gastric cancer, sPLA2 expression was associated with the invasive areas of the tumours [29]. In breast cancer and in prostatic adenocarcinoma, sPLA2 was reported to be associated with aggressive clinicopathological features of the tumours and with poor prognosis [11, 43].

In this study, we have demonstrated by immunohistochemistry an overexpression of cPLA2 in only 18% of Barrett's adenocarcinoma. This result differs from the high prevalence of COX-2 expression (97%), previously reported in our series of Barrett's adenocarcinoma [22]. However, an experimental study by Dong et al. has recently demonstrated an inverse relationship between cPLA2 expression and COX-2 expression during mouse colon carcinogenesis with reduced levels of cPLA2 in colon tumours despite increased expression of COX-2 and prostaglandin E2 (PGE2) [9]. The low expression of cPLA2 found in our series concurs with one of our previous reports showing the absence of Ki-ras mutation in the same series, as cPLA2 has been reported to be a ras-inducible enzyme [15, 22]. cPLA2 expression has been diversely appreciated in digestive cancer. Wendum et al. [41] recently reported a rate of cPLA2 positivity of 35% in a series of colorectal adenocarcinomas, whereas Soydan et al. [37] did not demonstrate any significant difference in the amount of cPLA2 in colorectal cancer compared with the associated normal mucosa. Mean amount and activity of cPLA2 was also reported to be similar in normal gastric mucosa and in gastric adenocarcinoma [36]. In contrast to sPLA2, cPLA2 expression was inversely correlated to aggressive features of the tumour such as depth of infiltration, vascular neoplastic invasion, and perineural neoplastic invasion. Our results suggest that cPLA2 expression may delineate some tumours with less aggressive behaviour. However, we did not demonstrate any prognostic value of cPLA2. The significance of cPLA2 overexpression in digestive carcinomas has been diversely appreciated. Two studies in animal models have suggested that cPLA2 expression promote tumorigenesis in the small intestine with a decrease in intestinal tumorigenesis in the APC mouse deficient for cPLA2 and does not play a role either in the initiation process or in the polyp expansion in the colon [16, 40]. In contrast, a recent study in a mouse model has suggested that downregulation of cPLA2 may decrease TNF-alpha-induced apoptosis during mouse colon carcinogenesis, thus leading to tumour growth [9].

In conclusion, sPLA2 is frequently upregulated in Barrett's oesophagus. The constant increasing rate of sPLA2 expression that we observed from Barrett's metaplasia to adenocarcinoma suggests that sPLA2 may play a role during Barrett's carcinogenesis. cPLA2 is less frequently expressed in Barrett's adenocarcinoma. cPLA2 expression is inversely related with aggressive pathological features of the tumour and may be a marker for delineating a subset of tumours with less aggressive behaviour. Further investigations with functional studies on tumour cells are required to give more information about the functional significance of these enzymes in Barrett's adenocarcinoma and to evaluate the possible association

between sPLA2 and COX-2 in the eicosanoid production in Barrett's carcinogenesis.

Acknowledgements This works was supported in part by grants from Association Charles Debray. We thank K. Aliouat, F. Bouchard, V. Creusot, S. Dufflot, B. Lejeune, M. Pelegrin (Service d'Anatomie Pathologique, Hôpital Avicenne, Bobigny) for their technical assistance.

References

1. Balsinde J, Balboa MA, Dennis EA (1998) Functional coupling between secretory phospholipase A2 and cyclooxygenase-2 and its regulation by cytosolic group IV phospholipase A2. Proc Natl Acad Sci USA 95:7951–7956
2. Balsinde J, Balboa MA, Insel PA, Dennis EA (1999) Regulation and inhibition of phospholipase A2. Annu Rev Pharmacol Toxicol 39:175–189
3. Blot WJ, Devesa SS, Kneller RW, Fraumeni JF Jr (1991) Rising incidence of adenocarcinoma of the esophagus and gastric cardia. JAMA 265:1287–1289
4. Buttar NS, Wang KK, Leontovich O, Westcott JY, Pacifico RJ, Anderson MA, Krishnadath KK, Lutzke LS, Burgart LJ (2002) Chemoprevention of esophageal adenocarcinoma by COX-2 inhibitors in an animal model of Barrett's esophagus. Gastroenterology 122:1101–1112
5. Cameron AJ (2002) Epidemiology of Barrett's esophagus and adenocarcinoma. Dis Esophagus 15:106–108
6. Clark JD, Schievella AR, Nalefski EA, Lin LL (1995) Cytosolic phospholipase A2. J Lipid Mediat Cell Signal 12:83–117
7. Cormier RT, Hong KH, Halberg RB, Hawkins TL, Richardson P, Mulherkar R, Dove WF, Lander ES (1997) Secretory phospholipase Pla2g2a confers resistance to intestinal tumorigenesis. Nat Genet 17:88–91
8. Dobbie Z, Muller H, Scott RJ (1996) Secretory phospholipase A2 does not appear to be associated with phenotypic variation in familial adenomatous polyposis. Hum Genet 98:386–390
9. Dong M, Guda K, Nambiar PR, Rezaie A, Belinsky GS, Lambeau G, Giardina C, Rosenberg DW (2003) Inverse association between phospholipase A2 and COX-2 expression during mouse colon tumorigenesis. Carcinogenesis 24:307–315
10. Faller G, Borchard F, Ell C, Seitz G, Stolte M, Walch A, Ruschoff J, Working Group for Gastroenterological Pathology of the German Society for Pathology (2003) Histopathological diagnosis of Barrett's mucosa and associated neoplasias: results of a consensus conference of the Working Group for Gastroenterological Pathology of the German Society for Pathology on 22 September 2001 in Erlangen. Virchows Arch 443:597–601
11. Graff JR, Konicek BW, Deddens JA, Chedid M, Hurst BM, Colligan B, Neubauer BL, Carter HW, Carter JH (2001) Expression of group IIa secretory phospholipase A2 increases with prostate tumor grade. Clin Cancer Res 7:3857–3861
12. Haapamaki MM, Gronroos JM, Nurmi H, Alanen K, Kallajoki M, Nevalainen TJ (1997) Gene expression of group II phospholipase A2 in intestine in ulcerative colitis. Gut 40:95–101
13. Haapamaki MM, Gronroos JM, Nurmi H, Alanen K, Nevalainen TJ (1999) Gene expression of group II phospholipase A2 in intestine in Crohn's disease. Am J Gastroenterol 94:713–720
14. Hameeteman W, Tytgat GN, Houthoff HJ, van den Tweel JG (1989) Barrett's esophagus: development of dysplasia and adenocarcinoma. Gastroenterology 96:1249–1256
15. Heasley LE, Thaler S, Nicks M, Price B, Skorecki K, Nemenoff RA (1997) Induction of cytosolic phospholipase A2 by oncogenic Ras in human non-small cell lung cancer. J Biol Chem 272:14501–14504
16. Hong KH, Bonventre JC, O'Leary E, Bonventre JV, Lander ES (2001) Deletion of cytosolic phospholipase A(2) suppresses Apc(Min)-induced tumorigenesis. Proc Natl Acad Sci U S A 98:3935–3939
17. Jenkins GJ, Doak SH, Parry JM, D'Souza FR, Griffiths AP, Baxter JN (2002) Genetic pathways involved in the progression of Barrett's metaplasia to adenocarcinoma. Br J Surg 89:824–837
18. Kashiwagi M, Friess H, Uhl W, Berberat P, Abou-Shady M, Martignoni M, Anghelacopoulos SE, Zimmermann A, Buchler MW (1999) Group II and IV phospholipase A(2) are produced in human pancreatic cancer cells and influence prognosis. Gut 45:605–612
19. Kaur BS, Khamnehei N, Iravani M, Namburu SS, Lin O, Triadafilopoulos G (2002) Rofecoxib inhibits cyclooxygenase 2 expression and activity and reduces cell proliferation in Barrett's esophagus. Gastroenterology 123:60–67
20. Kennedy BP, Soravia C, Moffat J, Xia L, Hiruki T, Collins S, Gallinger S, Bapat B (1998) Overexpression of the nonpancreatic secretory group II PLA2 messenger RNA and protein in colorectal adenomas from familial adenomatous polyposis patients. Cancer Res 58:500–503
21. Kiyohara H, Egami H, Shibata Y, Murata K, Ohshima S, Ogawa M (1992) Light microscopic immunohistochemical analysis of the distribution of group II phospholipase A2 in human digestive organs. J Histochem Cytochem 40:1659–1664
22. Lagorce C, Fléjou JF, Muzeau F, Hénin D, Potet F (1995) Absence of c-Ki-ras gene mutation in malignant and premalignant Barrett's oesophagus. J Clin Pathol 48:M198–M199
23. Lagorce C, Paraf F, Vidaud D, Couvelard A, Wendum D, Martin A, Flejou JF (2003) Cyclooxygenase-2 is expressed frequently and early in Barrett's oesophagus and associated adenocarcinoma. Histopathology 42:457–465
24. Laurén P (1965) The two histological main types of gastric carcinoma diffuse and so-called intestinal type carcinoma. An attempt at a histo-clinical classification. Acta Pathol Microbiol Scand 64:31–49
25. Leung SY, Chen X, Chu KM, Yuen ST, Mathy J, Ji J, Chan AS, Li R, Law S, Troyanskaya OG, Tu IP, Wong J, So S, Botstein D, Brown PO (2002) Phospholipase A2 group IIA expression in gastric adenocarcinoma is associated with prolonged survival and less frequent metastasis. Proc Natl Acad Sci U S A 99:16203–16208
26. MacPhee M, Chepenik KP, Liddell RA, Nelson KK, Siracusa LD, Buchberg AM (1995) The secretory phospholipase A2 gene is a candidate for the Mom1 locus, a major modifier of ApcMin-induced intestinal neoplasia. Cell 81:957–966
27. Morris CD, Armstrong GR, Bigley G, Green H, Attwood SE (2001) Cyclooxygenase-2 expression in the Barrett's metaplasia-dysplasia-adenocarcinoma sequence. Am J Gastroenterol 96:990–996
28. Murakami M, Shimbara S, Kambe T, Kuwata H, Winstead MV, Tischfield JA, Kudo I (1998) The functions of five distinct mammalian phospholipase A2S in regulating arachidonic acid release. Type IIa and type V secretory phospholipase A2S are functionally redundant and act in concert with cytosolic phospholipase A2. J Biol Chem 273:14411–14423
29. Murata K, Egami H, Kiyohara H, Oshima S, Kurizaki T, Ogawa M (1993) Expression of group-II phospholipase A2 in malignant and non-malignant human gastric mucosa. Br J Cancer 68:103–111
30. Niessen HW, Krijnen PA, Visser CA, Meijer CJ, Erik Hack C (2002) Type II secretory phospholipase A2 in cardiovascular disease: a mediator in atherosclerosis and ischemic damage to cardiomyocytes? Cardiovasc Res 53:138–146
31. Paraf F, Flejou JF, Pignon JP, Fekete F, Potet F (1995) Surgical pathology of adenocarcinoma arising in Barrett's esophagus. Analysis of 67 cases. Am J Surg Pathol 19:183–191
32. Rosenberg JC, Budev H, Edwards RC, Singal S, Steiger Z, Sundareson AS (1985) Analysis of adenocarcinoma in Barrett's esophagus utilizing a staging system. Cancer 55:1353–1360
33. Shirvani VN, Ouatu-Lascar R, Kaur BS, Omary MB, Triadafilopoulos G (2000) Cyclooxygenase 2 expression in Barrett's esophagus and adenocarcinoma: ex vivo induction by bile salts and acid exposure. Gastroenterology 118:487–496

34. Six DA, Dennis EA (2000) The expanding superfamily of phospholipase A(2) enzymes: classification and characterization. Biochim Biophys Acta 1488:1–19
35. Sobin LH, Wittekind Ch (1997) TNM classification of malignant tumors. Wiley-Liss, Inc, New-York
36. Soydan AS, Gaffen JD, Weech PK, Tremblay NM, Kargman S, O'Neill G, Bennett A, Tavares IA (1997) Cytosolic phospholipase A2, cyclo-oxygenases and arachidonate in human stomach tumours. Eur J Cancer 33:1508–1512
37. Soydan AS, Tavares IA, Weech PK, Temblay NM, Bennett A (1996) High molecular weight phospholipase A2 and fatty acids in human colon tumours and associated normal tissue. Eur J Cancer 32:1781–1787
38. Spechler SJ, Goyal RK (1986) Barrett's esophagus. N Engl J Med 315:362–371
39. Spirio LN, Kutchera W, Winstead MV, Pearson B, Kaplan C, Robertson M, Lawrence E, Burt RW, Tischfield JA, Leppert MF, Prescott SM, White R (1996) Three secretory phospholipase A(2) genes that map to human chromosome 1P35–36 are not mutated in individuals with attenuated adenomatous polyposis coli. Cancer Res 56:955–958
40. Takaku K, Sonoshita M, Sasaki N, Uozumi N, Doi Y, Shimizu T, Taketo MM (2000) Suppression of intestinal polyposis in Apc(delta 716) knockout mice by an additional mutation in the cytosolic phospholipase A(2) gene. J Biol Chem 275:34013–34016
41. Wendum D, Svrcek M, Rigau V, Boelle PY, Sebbagh N, Parc R, Masliah J, Trugnan G, Flejou JF (2003) COX-2, Inflammatory Secreted PLA2, and cytoplasmic PLA2 protein expression in small bowel adenocarcinomas compared with colorectal adenocarcinomas. Mod Pathol 16:130–136
42. World Health Organization Classification of Tumours (2000) Pathology and genetics of tumours of the digestive system. Hamilton SR, Aaltonen LA
43. Yamashita S, Yamashita J, Ogawa M (1994) Overexpression of group II phospholipase A2 in human breast cancer tissues is closely associated with their malignant potency. Br J Cancer 69:1166–1170
44. Ying Z, Tojo H, Komatsubara T, Nakagawa M, Inada M, Kawata S, Matsuzawa Y, Okamoto M (1994) Enhanced expression of group II phospholipase A2 in human hepatocellular carcinoma. Biochim Biophys Acta 1226:201–205

Virchows Arch (2004) 444:436–438
DOI 10.1007/s00428-004-1001-9

ORIGINAL ARTICLE

Manuel Montesinos-Rongen · Razvan Besleaga · Susanne Heinsohn · Reiner Siebert · Hartmut Kabisch · Otmar D. Wiestler · Martina Deckert

Absence of simian virus 40 DNA sequences in primary central nervous system lymphoma in HIV-negative patients

Received: 8 December 2003 / Accepted: 24 February 2004 / Published online: 24 March 2004

Abstract Simian virus 40 (SV40) is known to induce primary brain tumors and lymphomas in animal models. Recently, it was also associated with the pathogenesis of human non-Hodgkin's lymphomas. In the present study, we investigated primary central nervous system lymphomas (PCNSL), a defined subgroup of diffuse large B-cell lymphoma confined to the central nervous system, for the presence of SV40 DNA. Frozen tissue samples of 23 PCNSL derived from human immunodeficiency virus-negative patients were analyzed by two different, fully nested polymerase chain reaction protocols. SV40 DNA sequences could not be detected in any of these samples. Thus, SV40 can be added to the list of viruses that have already been excluded as pathogenetically relevant co-factors in PCNSL.

Keywords PCNSL · SV40

M. Montesinos-Rongen · R. Besleaga · M. Deckert (✉)
Department of Neuropathology,
University of Cologne,
Joseph-Stelzmann Strasse 9, 50931 Cologne, Germany
e-mail: neuropatho@uni-koeln.de
Tel.: +49-221-4785265
Fax: +49-221-4787237

M. Montesinos-Rongen · O. D. Wiestler
Department of Neuropathology,
University of Bonn,
Bonn, Germany

S. Heinsohn · H. Kabisch
Department of Pediatric Hematology and Oncology,
University Hospital Eppendorf,
Hamburg, Germany

R. Siebert
Institute of Human Genetics,
University Hospital Schleswig-Holstein (Campus Kiel),
Kiel, Germany

Introduction

Infection with various viruses, including Epstein–Barr virus (EBV), human herpes virus 8 (HHV-8), and simian virus 40 (SV40), is assumed to play a major role in the pathogenesis of some lymphoma entities, such as Burkitt's lymphoma or primary effusion lymphoma. In primary central nervous system (CNS) lymphomas (PCNSL), EBV infection is regularly observed in acquired immunodeficiency syndrome (AIDS) patients [6]. In contrast, EBV is apparently not involved in the pathogenesis of PCNSL of immunocompetent human immunodeficiency virus (HIV)-negative patients [6]. Interestingly, a characterization of immunoglobulin genes in this subgroup of PCNSL demonstrated that the tumor cells had experienced a germinal center reaction [4, 10]. Moreover, the PCNSL tumor cells or their precursors show patterns of immunoglobulin mutations suggestive of an—at least temporarily—antigen-driven selection for expression of a functional antibody [4]. Thus, it is tempting to speculate that a hitherto unknown antigen in the CNS may trigger proliferation of the malignant B cells or their precursors. In this regard, proteins of neurotropic viruses with the capacity to persist in the CNS are attractive candidate antigens. However, attempts to identify a causative pathogen have failed thus far.

It is known from animal models that SV40 can induce primary brain tumors and lymphomas [2]. These lymphomas were mainly of the diffuse large B-cell type (DLBCL) [2]. Recent studies reported that 42% and 43%, respectively, of systemic non-Hodgkin lymphomas (NHL) harbor SV40 DNA sequences [9, 11]. The incidence was particularly high in DLBCL, reaching 63% and 48%, respectively [9, 11]. These data suggested that SV40 infection was a cofactor in the pathogenesis of these germinal center cell-derived lymphomas. As PCNSL are also derived from germinal center B cells, one may speculate that these lymphomas may also be driven by SV40. Thus, we analyzed a series of 23 PCNSL derived from HIV-negative patients for the presence of SV40 DNA.

Materials and methods

Tumor samples

PCNSL samples from 23 patients were included. All investigations were approved by the ethics committee of the University of Bonn; informed consent was provided according to the Declaration of Helsinki. All patients were HIV negative as tested by serology. There was no evidence of DLBCL manifestation outside the CNS in any patient. Most samples were obtained by stereotactic biopsy. Prior to neurosurgical intervention, all patients were untreated and had received neither corticosteroids nor radiotherapy. Tumor samples were stored at −80°C until used for molecular biological analysis. Cryostat sections 10 µm thick were cut from the blocks to assure that the frozen tissue contained sufficient numbers of tumor cells.

Histopathology

All tumors were histopathologically classified according to the World Health Organization classification [1]. The diagnoses were based on a combination of hematoxylin-eosin and Giemsa stains as well as immunohistochemistry.

The expression of the B-cell-specific antigen CD20, the leukocyte common antigen CD45RB, CD45RO, the T-cell-specific antigen CD3, the macrophage-specific antigen CD68, and the proliferation-associated nuclear antigen Ki-67 (all antibodies from Dako, Hamburg, Germany) was studied using an avidin-biotin-peroxidase complex protocol as described previously [4].

DNA extraction and PCR protocols

DNA was extracted from frozen tissue with the NucleoSpin Tissue Kit (Clontech Laboratories, Heidelberg, Germany). DNA was dissolved in 40 µl TE low buffer (10 mM TRIS, 1 mM EDTA, pH 7.6). Of this DNA stock solution, 500 ng DNA was used in each first round of nested polymerase chain reaction (PCR).

To assess the integrity and quality of the DNA preparations, a 195-, 450-, and 650-bp DNA fragment of the human TP53 gene was amplified out of 100 ng DNA as a control cellular gene according to a single-step PCR protocol described in detail previously [5].

Furthermore, to assure that the DNA extraction protocol is suitable to isolate circular DNA, a nested PCR protocol for 100 ng DNA to amplify sequences of the mitochondrial control region was established. As primers, Mit_CRexF 5′-TCC ACC ATT AGC ACC CAA AG-3′ and Mit_CRexR 5′-TGG CTT TGG AGT TGC AGT TG-3′ were used, amplifying a 280-bp PCR product [according to accession number AF382013, nucleotides (nt) 15976–16256]. Amplification was carried out for one cycle at 95°C for 5 min, 56°C for 30 s, and 72°C for 1 min, followed by 34 cycles at 95°C for 1 min, 56°C for 30 s, and 72°C for 1 min. A final extension step at 72°C for 10 min was added. Of the PCR product, 5 µl was further amplified using the two fully nested primers Mit_CRinF 5′-TGT TCT TTC ATG GGG AAG C-3′ and Mit_CRinR 5′-GAT AGT TGA GGG TTG ATT GC-3′ to yield a 211-bp product (nt 16020–16231). Cycling conditions were identical to the first amplification round.

To detect SV40 DNA sequences in cerebral tissues as well as in two cell lines, SV-80 and COS-7 (kindly provided by Dr. H. Deppert, Heinrich-Pette-Institut, Hamburg, Germany), characterized by 10–30 episomal SV40 DNA copies (SV80) and one integrated SV40 copy (COS-7), respectively, which served as controls, nested PCR with two protocols employing different sets of primers was performed using 500 ng DNA. The first protocol was designed to amplify a DNA fragment encoding the regulatory region. Primers SV_RRexF 5′-GTC CAT TAG CTG CAA AGA TTC CTC-3′ and SV_RRexR 5′-GCG TGA CAG CCG GCG CAG CAC CA-3′ were used, amplifying a 483-bp PCR product (according to accession number J02400, nt 5119–358). Amplification was carried out for one cycle at 95°C for 5 min, 62°C for 30 s, and 72°C for 1 min, followed by 44 cycles at 95°C for 1 min, 62°C for 30 s, and 72°C for 1 min. A final extension step at 72°C for 10 min was added. Of the PCR product, 5 µl was further amplified using the two fully nested primers SV_RRinF 5′-CTA GGC CTC CAA AAA AGC CTC-3′ and SV_RRinR 5′-AAT GTG TGT CAG TTA GGG TGT G-3′ to yield a 322-bp product (nt 5188–266). Cycling conditions were identical to the first amplification round. In addition, a second nested PCR protocol was designed to amplify a DNA fragment of the large T antigen carboxy-terminal region. First, SV_TagexF of 5′-GCA TGA CTC AAA AAA CTT AGC AAT TCT-3′ and SV_TagexR of 5′-CTT TGG AGG CTT CTG GGA TGC AAC T-3′ were used as primers. Amplification was carried out for one cycle at 95°C for 5 min, 56°C for 30 s, and 72°C for 1 min, followed by 44 cycles at 95°C for 1 min, 56°C for 30 s, and 72°C for 1 min. A final extension step at 72°C for 10 min was added. This protocol yielded a 573-bp PCR product (nt 4372–4945). Of the PCR product, 5 µl was added as template in a second round with the same cycling conditions and two fully nested primers—SV_TaginF 5′-GGA AAG TCC TTG GGG TCT TCT ACC-3′ and SV_TaginR 5′-TAG ATT CCA ACC TAT GGA ACT GAT-3′—resulting in a 172-bp PCR product (nt 4402–4574). Each DNA sample was investigated in duplicate, and each PCR was performed in a final volume of 50 µl.

Results

PCR analysis of PCNSL did not detect SV40 DNA sequences in any sample of this series of 23 tumors (Fig 1). All DNA samples proved to be of sufficient quality as evidenced by the effective amplification of a 195-, 450-, and 650-bp DNA fragment of the TP53 gene. In addition, the mitochondrial control region was efficiently amplified, assuming that the DNA extraction protocol had yielded circular DNA in all 23 tumor samples and controls.

In contrast to PCNSL, both the SV-80 as well as the COS-7 cell line gave rise to a SV40-specific DNA fragment of 322 bp and 172 bp of the SV40 regulatory region and the large T antigen region, respectively (Fig 1).

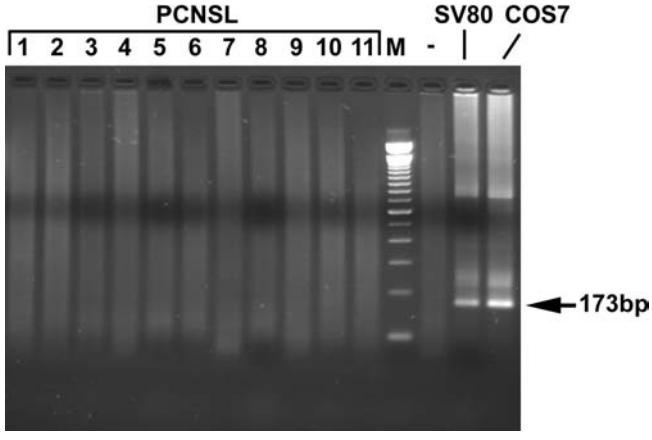

Fig. 1 Polymerase chain reaction (PCR) analysis of SV40 large T antigen sequences in primary central nervous system lymphomas (PCNSL). In contrast to SV80 and COS7, none of the PCNSL harbored SV40 large T antigen sequences as detected in a fully nested PCR protocol. *M* 100 base pair DNA marker; – negative control

Discussion

The present study demonstrates that, while SV40 DNA sequences corresponding to the SV40-specific regulatory region or to the SV40 large T antigen carboxy-terminal region of the SV40 gene were readily detected in the SV-80 and COS-7 cell lines, SV40 DNA sequences were not amplified from any of 23 PCNSL. These data suggest that SV40 does not play a role in the pathogenesis of PCNSL in immunocompetent patients. Therefore, this virus can be added to the list of viruses such as EBV, HHV-6, and HHV-8, which have already been excluded as pathogenetically relevant cofactors in PCNSL [6, 7]. Compared with other lymphoma entities, which have recently been investigated for the presence of SV40 DNA, conflicting results have been obtained. While two studies detected SV40-specific large T antigen DNA in 64 of 154 NHL (42%) and in 29 of 68 NHL (43%), most frequently in DLBCL, follicular lymphoma, and Burkitt's lymphoma, respectively [9, 11], these data were not confirmed by others. For example, SV40 DNA was absent from a comprehensive series of 152 samples derived from various lymphoma entities, including DLBCL, follicular lymphoma, and mantle cell lymphoma [3]. This was also observed by Rizzo et al. [8], who detected SV40 DNA in mesotheliomas, but not in any of 29 NHL.

Taken together, the majority of studies available at present concluded that SV40 is not involved in lymphomagenesis, and the present study adds PCNSL to this group. However, whether other viruses, which have still escaped detection, may play a role in the pathogenesis of PCNSL is still an open question.

Acknowledgements The authors thank Marek Franitza and Alexandra Brüggeman for expert technical assistance. This study was supported by the Deutsche Krebshilfe/Dr. Mildred-Scheel-Stiftung für Krebsforschung (grant no. 10-2153-De 1).

References

1. Gatter KC, Warnke RA (2001) Diffuse large cell lymphoma. In: Jaffe ES, Harris NL, Stein H, Vardiman JW (eds) Pathology and genetics of tumors of haematopoietic and lymphoid tissues. IARC Press, Lyon, pp 171–174
2. Lee JW, Park JH, Kim KS, Lee EJ, Kim MO, Kim SH, Jeong SW, Kim CW, Lee HJ, Kang KS, Chang KT, Hyun BH, Ryoo ZY (2003) Vasopressin-SV40 T antigen expression in transgenic mice induces brain tumor and lymphoma. Biochem Biophys Res Commun 302:785–792
3. MacKenzie J, Wilson KS, Perry J, Gallagher A, Jarrett RF (2003) Association between simian virus 40 DNA and lymphoma in the United Kingdom. J Natl Cancer Inst 95:1001–1003
4. Montesinos-Rongen M, Küppers R, Schlüter D, Spieker T, Van Roost D, Schaller C, Reifenberger G, Wiestler OD, Deckert-Schlüter M (1999) Primary central nervous system lymphomas are derived from germinal-center B cells and show a preferential usage of the V4–34 gene segment. Am J Pathol 155:2077–2086
5. Montesinos-Rongen M, Roers A, Küppers R, Rajewsky K, Hansmann ML (1999) Mutation of the p53 gene is not a typical feature of Hodgkin and Reed–Sternberg cells in Hodgkin's disease. Blood 94:1755–1760
6. Montesinos-Rongen M, Hans VH, Eis-Hübinger AM, Prinz M, Schaller C, Van Roost D, Aguzzi A, Wiestler OD, Deckert M (2001) Human herpes virus-8 is not associated with primary central nervous system lymphoma in HIV-negative patients. Acta Neuropathol 102:489–495
7. Paulus W, Jellinger K, Hallas C, Ott G, Müller-Hermelink HK (1993) Human herpesvirus-6 and Epstein–Barr virus genome in primary cerebral lymphomas. Neurology 43:1591–1593
8. Rizzo P, Carbone M, Fisher SG, Matker C, Swinnen LJ, Powers A, Di Resta I, Alkan S, Pass HI, Fisher RI (1999) Simian virus 40 is present in most United States human mesotheliomas, but it is rarely present in non-Hodgkin's lymphoma. Chest 116:470S–473S
9. Shivapurkar N, Harada K, Reddy J, Scheuermann RH, Xu Y, McKenna RW, Milchgrub S, Kroft SH, Feng Z, Gazdar AF (2002) Presence of simian virus 40 DNA sequences in human lymphomas. Lancet 359:851–852
10. Thompsett AR, Ellison DW, Stevenson FK, Zhu D (1999) V(H) gene sequences from primary central nervous system lymphomas indicate derivation from highly mutated germinal center B cells with ongoing mutational activity. Blood 94: 1738–1746
11. Vilchez RA, Madden CR, Kozinetz CA, Halvorson SJ, White ZS, Jorgensen JL, Finch CJ, Butel JS (2002) Association between simian virus 40 and non-Hodgkin lymphoma. Lancet 359:817–823

Virchows Arch (2004) 444:439–446
DOI 10.1007/s00428-004-0997-1

ORIGINAL ARTICLE

Andrej Cör · Jože Pižem · Nina Gale

Immunohistochemical analysis of pro- and active-caspase 3 in laryngeal squamous cell carcinoma

Received: 28 October 2003 / Accepted: 15 January 2004 / Published online: 25 March 2004

Abstract Active caspase 3 is considered to be the main executioner caspase in apoptotic process. The mechanisms of apoptosis in laryngeal squamous cell carcinoma (LSCC) have been investigated by examining the expression profiles of pro-caspase 3 and active-caspase 3. The correlation between the two forms of caspase 3 and the p53 status was also determined. LSCCs (n=65) were studied using immunohistochemistry with antibodies to pro-caspase 3, active-caspase 3 and p53. The expression of pro-caspase 3 was absent or weak in 16 (24.6%), moderate in 21 (32.3%) and strong in 28 (43.1%) cases. Survival curves for different levels of pro-caspase 3 differed, but the differences were not statistically significant. An apoptotic index (AI) was determined by quantifying the active-caspase 3-positive cells. The AI ranged from 0.2% to 9.4% and did not differ among the different levels of pro-caspase 3 expression. Even in cases in which the expression of pro-caspase 3 was considered negative, caspase 3-positive apoptotic cells were found. The AIs were significantly higher in supraglottic tumours compared with glottic counterparts (P=0.008) and were higher in poorly differentiated tumours compared with well-differentiated and moderately differentiated LSCC (P= 0.06). No correlation between AI and p53 expression was found, although pro-caspase 3 expression trended to be higher in the p53-positive group of LSCC. Our results suggest that the expression of pro-caspase 3, a key executioner caspase in apoptosis, is downregulated in a proportion of LSCC, but this is not associated with decreased apoptotic activity, measured by active-caspase 3 labelling.

Keywords Apoptosis · Caspase · Laryngeal squamous cell carcinoma · p53

A. Cör (✉)
Institute for Histology and Embryology,
Medical Faculty of Ljubljana,
Korytkova 2, 1000 Ljubljana, Slovenia
e-mail: andrej.coer@mf.uni-lj.si
Tel.: +38-60-15437381
Fax: +38-60-15437381

J. Pižem · N. Gale
Institute of Pathology,
Medical Faculty of Ljubljana,
Korytkova 2, 1000 Ljubljana, Slovenia

Introduction

Apoptosis is an essential biological process of active cell death, characterised by morphological alterations, including condensation of the nuclear chromatin, compaction of cytoplasmic organelles, membrane blabbing and cellular fragmentation into apoptotic bodies [16]. It has become clear, 30 years after Kerr and colleagues [16] described apoptosis as a basic biological phenomenon, that altered programmed cell death plays an important role in carcinogenesis. Inappropriate survival and propagation of cells with damaged DNA may contribute to the development of neoplasia and metastases [25]. The apoptotic programme is executed with a cascade of sequential activation of initiator and effector caspases, a family of cysteine-dependent aspartate-specific proteases. Caspases are synthesised as inactive pro-enzymes and must be proteolytically activated to produce mature, catalytically active heterodimers, which specifically cleave target proteins. The caspase family has at least 14 members, which are divided into two groups, based on their function [37]. Caspases 8 and 9 have long prodomains and function in targeting and regulating apoptosis, whereas caspases 3, 6 and 7 have short prodomains and are responsible for the execution of apoptosis. Caspase 3 is among the most studied caspase and is considered the key effector caspase. Proteolytic cleavage at an aspartate residue of the 32-kDa pro-caspase 3 zymogene produces two active fragments of 17–21 kDa and 10–12 kDa, which form an active heterotetrameric structure [19]. During the execution of apoptosis, caspase 3 is responsible, either partly or totally, for the proteolytic cleavage of a large number of proteins and for apoptosis-associated chromatin margination, DNA fragmentation and nuclear

collapse during apoptosis. The detection of activated caspase 3 could, therefore, be a valuable and specific tool for identifying apoptotic cells in tissue sections, even before all the morphological features of apoptosis occur [1].

Only a few studies on the clinical significance of caspase 3 expression in squamous cell carcinoma have been reported [29, 37]. Volm et al. [34] described caspase 3 expression in lung squamous cell carcinoma and Hsia et al. [12] analysed caspase 3 expression in oesophageal squamous cell carcinoma. However, only the inactive proenzyme was analysed in those studies. Whether squamous carcinoma cells contain active-caspase 3 capable of triggering apoptosis, thus, remains to be determined. As far as we know, there is no published immunohistochemical analysis of pro- and active-caspase 3 expression on laryngeal squamous cell carcinoma (LSCC).

In this study, our principal aim was to examine apoptosis in LSCC using immunohistochemistry with antibodies specific for the active and non-active form of caspase 3. We correlated the expression of pro-caspase 3 and active-caspase 3 with tumour histopathological characteristics. We also analysed the correlation between the expression of pro- and active-caspase 3 and p53 status. Furthermore, we determined the prognostic value of both forms of caspase 3.

Materials and methods

The study material was derived from 65 unselected cases of LSCC on which clinical follow-up and biopsy specimens were available for analysis from the 1991–1995 files of the Institute for Pathology, Medical Faculty of Ljubljana, Slovenia. Tumours were classified, according to the World Health Organization classification [27], as well-differentiated, moderately differentiated and poorly differentiated LSCC. The single best tissue block available for each patient was selected for the study. Block selection was based on the largest amount of well-fixed, histologically viable tumour tissue.

Sections (5-μm thick) from archival formalin-fixed paraffin-embedded tissues were placed on poly-L-lysine-coated slides for immunohistochemistry. Sections were dewaxed in xylene, rehydrated in alcohol and blocked for endogenous activity (3% H_2O_2 and normal rabbit serum). Antigen retrieval was carried out by pressure cooking in citrate buffer, pH 6.0. The sections were then incubated overnight at 4°C with primary antibodies. For analysis of pro-caspase 3 expression, we used polyclonal rabbit anti-human caspase 3/CPP32 antibody (Dako, Denmark), diluted 1:100, for active-caspase 3 monoclonal mouse against human cleaved caspase 3 antibody at a dilution of 1:100 (Cell Signaling, MA, USA), and for p53 monoclonal mouse anti human p53 antibody, DO-7 (Dako, Denmark), diluted 1:100, were used. According to the manufacturer, anti-CPP32 antibody recognises the unprocessed pro-caspase 3 molecule. Anti-cleaved caspase 3 antibody specifically recognises the large fragment (17 kDa) of activated, but not full length, caspase 3. Bound antibodies were detected using an aviditin-biotin peroxidase complex (ABC) detection kit (Dako, Denmark) with 3,3′ diaminobenzidine (DAB, Sigma Chemical Co, Germany) for 5 min as chromogen. Slides were then lightly counterstained with haematoxylin. The specificity of the antibodies used was checked with positive or negative control sections. Sections treated without the primary antibodies served as negative controls. For positive controls, tonsil tissue section was processed in the same way as the LSCC slides.

Two pathologists, without knowledge of the tumour response or patient outcome, semi-quantitatively evaluated the pro-caspase 3 slides according to the proportion of positive tumour cells. Tumours were scored as 1+ when none or less than 5% of the tumour cells were slightly positive, 2+ if most of the tumour cells were moderately positive and 3+ if more than 75% of the tumour cells were strongly positive. Scoring differences between observers were resolved by consensus. Immunoreactivity for active-caspase 3 was evaluated quantitatively by counting at least 1000 tumour cells at high-power magnification. Apoptotic bodies, occurring in distinct groups, which were likely to have originated from the same apoptotic cell, were recorded as one apoptotic cell. The number of apoptotic cells, expressed as the apoptotic index (AI) was calculated as the percentage of apoptotic tumour cells. Tumours were considered p53 positive when more than 50% of tumour-cell nuclei were stained.

Statistical analysis was performed using SPSS 10.0 for Windows. The differences in the numerical data of various groups were evaluated using the Mann-Whitney and Kruskal-Wallis tests. The Cox proportional hazard model was used to assess prognostic values of different variables. Overall survival rates were presented by Kaplan-Meier curves.

Results

Included in the study were 65 patients with LSCC. At the time of diagnosis, patients were aged between 37 years and 78 years (mean 59.5 years). Of these patients, 63 were men and 2 were women. Of patients, 41 (63%) had squamous cell carcinoma of the glottic region, with the remaining 24 (37%) patients having tumours of the supraglottis. Of the tumours, 11 (16.9%) were well differentiated, 33 (50.8%) were moderately differentiated and 21 (32.3%) were poorly differentiated.

Malignant epithelium exhibited a heterogeneous pattern of pro-caspase 3 expression. Pro-caspase 3 immunoreactivity in the tumour cells was diffuse and observed mainly in the cytoplasm, though, in some cases, nuclear staining was also found (Fig. 1). In cases exhibiting weak staining, the immunoreactivity was more prominent in the outer part of tumour nests than in the inner part. Some inflammatory cells and stromal cells exhibited strong pro-caspase 3 immunoreactivity and served as an internal positive control. The level of pro-caspase 3 expression was evaluated semi-quantitatively. The degree of pro-caspase 3 expression in different groups of LSCC is summarised in Table 1. In 16 (24.6%) cases, staining was negative or positive in less than 5% of the tumour cells. In 21 (32.3%) cases, the staining was moderate, and in 28 (43.1%) cases, the expression of pro-caspase 3 was strong. In 14 cases, hyperplastic mucosa was found adjacent to carcinoma. In most such cases, the expression of pro-caspase 3 was similar or increased in the carcinoma compared with the epithelium in different types of hyperplastic laryngeal lesions; although, in some cases, the expression of pro-caspase 3 in the carcinoma was clearly weaker than that of the hyperplastic epithelium or even absent (Fig. 2). There was no significant correlation between pro-caspase 3 expression and tumour cell differentiation. However, in 12 (57.1%) of 21 poorly differentiated tumours, the expression of pro-caspase 3 was strong (3+) in comparison with just 2 (19.2%) of well-

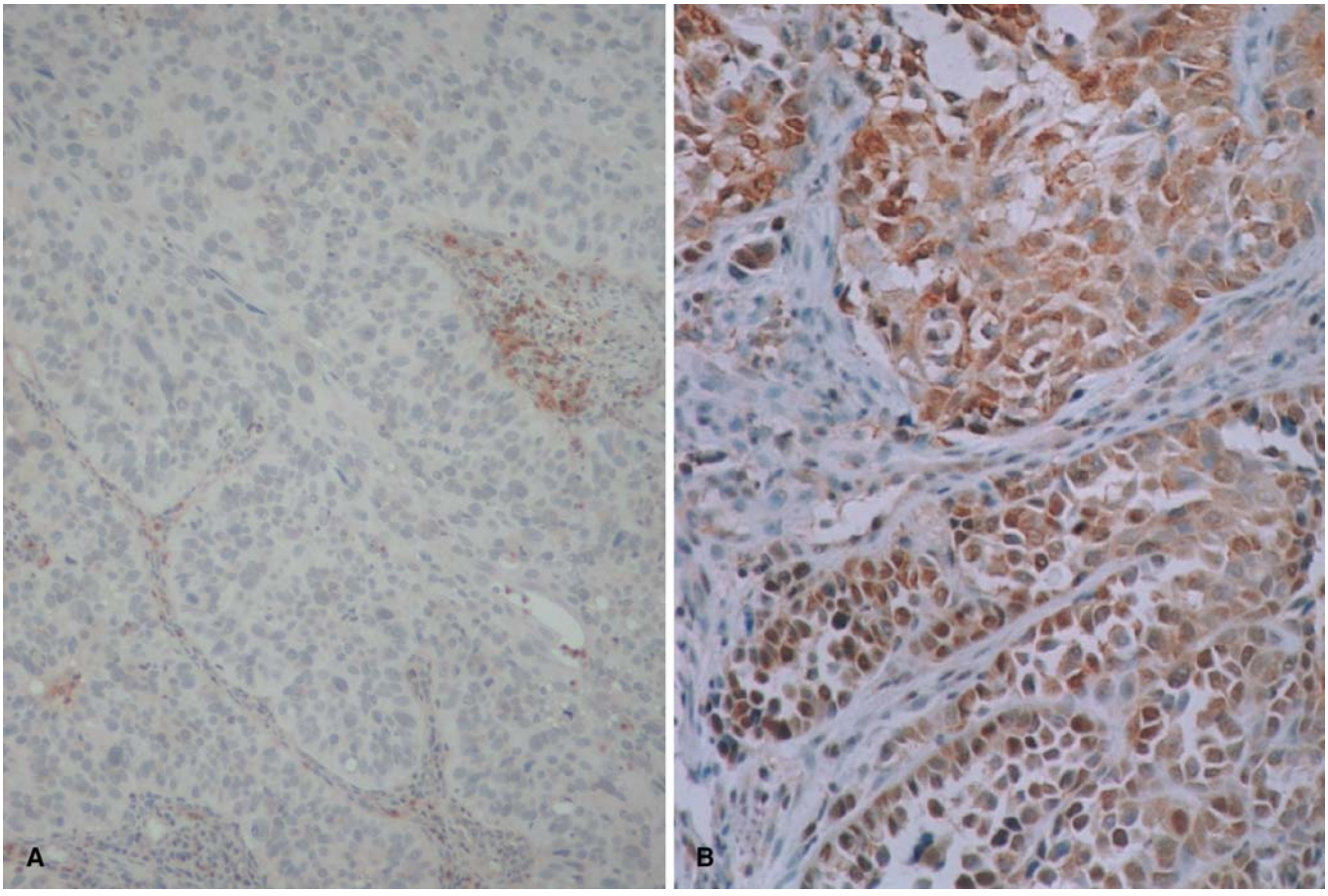

Fig. 1 Immunohistochemical staining for pro-caspase 3 in laryngeal squamous cell carcinoma. **A** Weak reaction (1+) in tumour cells and strong pro-caspase 3-positive lymphocytes. **B** Strong (3+) cytoplasmic and nuclear reaction in tumour cells (immunohistochemistry, ×100)

Table 1 Pro-caspase 3 expression in different groups of laryngeal squamous cell carcinoma

	n (%)	Pro-caspase 3—number of cases (%)			*P* value
		1+	2+	3+	
p53	65				0.112
Negative	43 (66.2)	12 (27.9)	15 (34.8)	16 (37.3)	
Positive	22 (33.8)	3 (13.7)	6 (27.2)	13 (59.1)	
Localisation	65				0.066
Glottis	24 (36.9)	8 (33.3)	10 (41.7)	6 (25.0)	
Supraglottis	41 (63.1)	7 (17.1)	11 (26.8)	23 (56.1)	
Differentiation	65				0.125
Well	11 (16.9)	5 (45.5)	4 (36.3)	2 (19.2)	
Moderate	33 (50.8)	5 (15.2)	13 (39.4)	15 (45.4)	
Poor	21 (32.3)	5 (23.8)	4 (19.1)	12 (57.1)	

differentiated LSCC. The level of pro-caspase 3 expression tended to differ between glottic and supraglottic sites of the tumour. Among the supraglottic tumours, 23 (56.1%) were strongly positive (3+) for pro-caspase 3; only 6 (25%) of the glottic group were strongly positive (Table 1). Kaplan-Meier survival curves for different levels of pro-caspase 3 differed, but the differences were not statistically significant (Fig. 3).

To test whether the level of pro-caspase 3 expression influences apoptotic rate, caspase 3 activation was analysed immunohistochemically, using an antibody that specifically recognises the activated form of caspase 3. The reaction to caspase 3 was strong and was detected in the cytoplasm and nucleus of the apoptotic cells. As a rule, caspase 3-positive cells displayed the morphology of apoptotic cells (condensed and fragmented chromatin, shrunken cytoplasm) (Fig. 4). A few cells with normal cellular morphology were also immunolabelled. The apoptotic index ranged from 0.2% to 9.4% (mean 2.7%). Although a trend was clearly detected towards higher AI with increased grade of tumour, the differences failed to reach statistical significance (Table 2). Even in cases

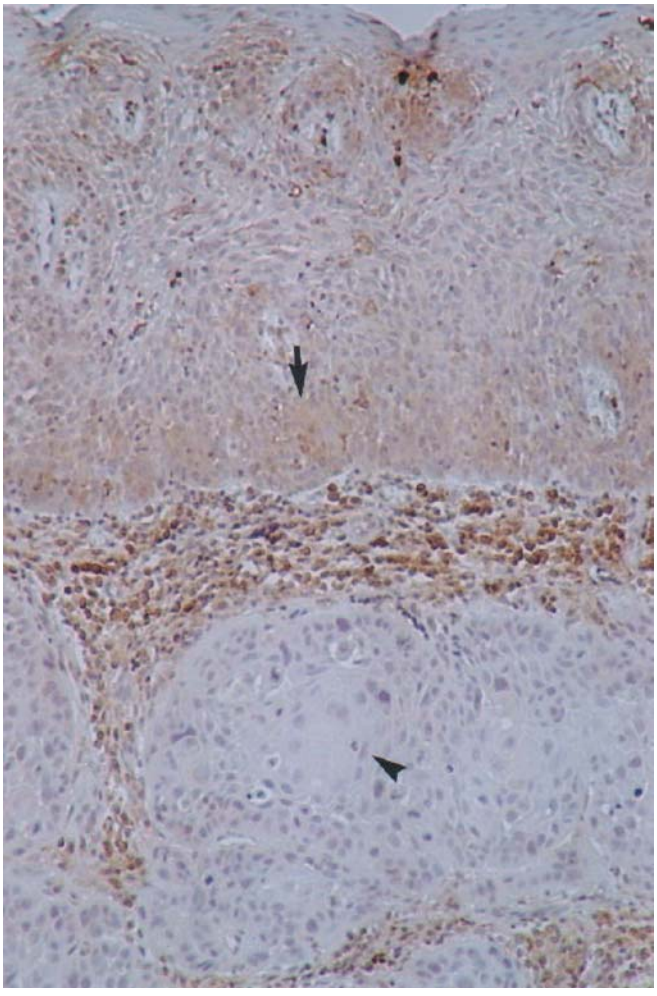

Fig. 2 Expression of pro-caspase 3 in laryngeal squamous cell carcinoma (LSCC) and non-neoplastic epithelium. Immunohistochemical reaction is positive in hyperplastic laryngeal epithelium (especially in basal and parabasal cells) (*arrow*) and stromal inflammatory cells, but is absent in tumour cells of invasive LSCC (*arrowhead*) (immunohistochemistry, ×40)

where the expression of pro-caspase 3 was considered completely negative, caspase 3-positive apoptotic cells were found. The apoptotic index was significantly higher at the supraglottic location.

We found 22 (33.8%) p53-positive LSCC. There was no correlation between pro-caspase 3 and p53 expressions. However, in 13 (59.1%) of the p53-positive tumours, pro-caspase 3 expression was strong (3+) in comparison with just 3 (13.7%) cases where pro-caspase 3 expression was negative or weak (1+). AI was 2.63 in the p53-negative group and just slightly higher, 2.90, in the p53-positive group (Table 2). The proportion of p53-positive LSCC cases was higher ($P<0.05$) in supraglottic tumours (39%) than in glottic tumours (25%).

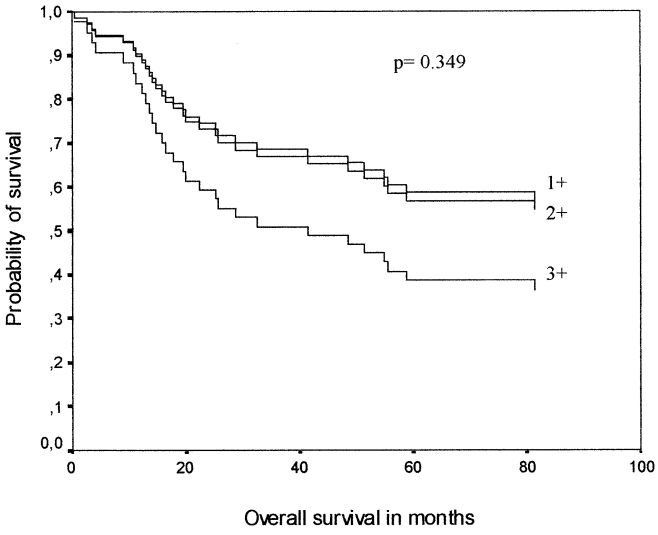

Fig. 3 Kaplan-Meier survival curves for different levels of pro-caspase 3 expression (1+, 2+ and 3+). The differences were not statistically significant ($P=0.349$)

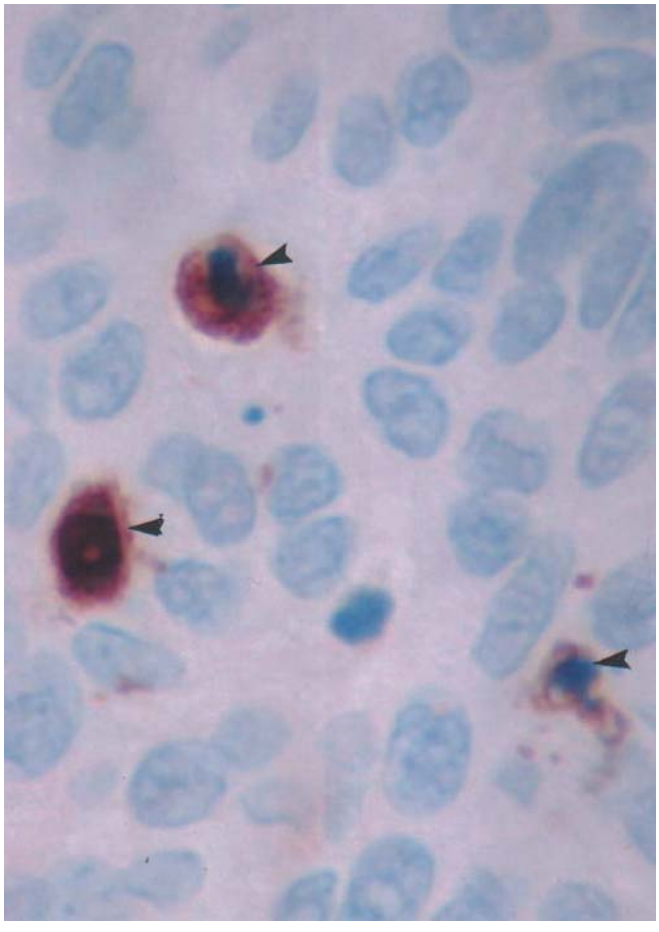

Fig. 4 Active-caspase 3-positive (apoptotic) tumour cells of laryngeal squamous cell carcinoma (*arrowheads*) (immunohistochemistry, ×400)

Table 2 Apoptotic index (% of active-caspase 3-positive cells) in different groups of laryngeal squamous cell carcinoma

	n (%)	Apoptotic index—% of active-caspase 3-positive cells (Mean±SD)	*P* value
Pro-caspase 3	65		0.36
1+	16 (24.6)	2.29±1.96	
2+	21 (32.3)	2.51±1.61	
3+	28 (43.1)	3.16±2.29	
p53	65		0.516
Negative	43 (66.2)	2.63±2.02	
Positive	22 (33.8)	2.90±2.09	
Localisation	65		0.008
Glottis	24 (36.9)	1.91±1.63	
Supraglottis	41 (63.1)	3.19±2.07	
Differentiation	65		0.06
Well	11 (16.9)	2.76±1.50	
Moderate	33 (50.8)	2.19±1.76	
Poor	21 (32.3)	3.55±2.36	

Discussion

Apoptosis is an evolutionary conserved process that regulates development and homeostasis, and defects in these pathways are implicated in tumorigenesis. Two distinct pathways for apoptosis have been characterised, both of which ultimately result in a proteolytic cascade involving caspases [15, 22]. In the present study, the expression of pro- and active-caspase 3, a key caspase implicated in the execution of apoptosis, was analysed using immunohistochemistry in 65 LSCCs. Immunostaining of pro-caspase 3 was predominantly cytoplasmic and mainly diffuse. However, some nuclear staining was also found. This is in line with other studies, in which a cytoplasmic location of pro-caspase 3 was found [7, 28]. Donoghue et al. [4] also described punctuate cytoplasmic staining, and they associated this pattern with mitochondrial localisation of pro-caspase 3. We did not find any punctuate staining pattern in our study. Koomagi and Volm [18] described cytoplasmic and nuclear staining for pro-caspase 3 and demonstrated that pro-caspase 3 may be translocated from the cytoplasm to the nucleus and may be activated in both cellular compartments. Recently, Ramuz et al. [24] showed, using confocal microscopy, a nuclear localisation of pro-caspase 3 in non-apoptotic cells. They described that active-caspase 3 first appeared in cytoplasm and was later observed in the nucleus. Despite all these studies, the localisation of pro- and active-caspase 3 in different cellular compartments remains a controversial issue.

Our data indicate a high degree of variation in the immunostaining and pattern of expression of pro-caspase 3 in tumour cells, which was not correlated with the incidence of apoptosis in situ. Moreover, there was no statistically significant correlation between pro-caspase 3 expression and tumour differentiation and localisation. Our findings are in contrast with a recent report indicating a correlation between pro-caspase 3 expression and elevated apoptotic activity and histological aggression in breast cancer [33]. In stomach cancer, there was a tendency for a positive correlation between pro-caspase 3 expression and the deoxynucleotidyl-transferase (TdT) mediated deoxy uridine triphosphate nick end labelling (TUNEL) labelling index [11]. However, no correlation between pro-caspase 3 expression and apoptosis was found in lung and prostate cancer [28, 29, 31, 37].

In most of our cases, the expression of pro-caspase 3 was similar or increased in the carcinoma in comparison with the adjacent different types of hyperplastic laryngeal lesions [14]. In a few cases, the expression in carcinoma cells was clearly decreased or even absent. Fujikawa et al. [7] reported significant downregulation of pro-caspase 3 expression in hepatocellular carcinoma compared with adjacent non-tumour liver tissue. They did not find any cases in which the expression of the pro-caspase 3 was stronger in tumour compared with non-tumour tissue. The authors assumed that downregulation of pro-caspase 3 could be important, since pro-caspase 3 null cells cannot undergo a rapid and effective apoptotic death programme. However, in our study, we found active-caspase 3-positive cells even in apparently pro-caspase 3-negative cases.

Takata et al. [29] described that enhanced expression of uncleaved, pro-caspase 3 was correlated with poor prognosis in non-small-cell lung cancer. In contrast, Volm et al. [34] reported that patients with non-small-cell lung cancer with positive pro-caspase 3 expression had a significantly better prognosis. They speculated that favourable survival was achieved by accelerated apoptotic cancer cell death when pro-caspase 3 was expressed. Donoghue et al. [4] presented that higher expression of pro-caspase 3 correlated with better prognosis for B-cell diffuse large-cell lymphoma, and they associated the over-expression of pro-caspase 3 with an increased sensitivity to therapy. A recent report indicated that childhood neuroblastomas that can spontaneously regress also had high pro-caspase 3 expression [21]. In our study, Kaplan-Meier survival curves for different levels of pro-caspase 3 expression differed, but the differences did not reach statistical significance.

To test whether the level of pro-caspase 3 expression influences apoptotic rate, we determined the AI by quantifying active-caspase 3-positive cells. The antibody we used to detect apoptotic cells specifically recognises the large fragment (17 kDa) of activated, but not full-length, caspase 3. Hadjiloucas et al. [9] recommended the

method of assessing apoptosis using immunohistochemistry with an antibody against the active-caspase 3 as an accurate and reliable method. This method is sensitive, specific, easy to apply and free of subjective interpretation and, therefore, does not require an experienced observer trained to recognise apoptotic cells in tissue sections. It also does not rely on DNA fragmentation, a late event in the apoptotic process, as detected by the TUNEL method [8]. Duan et al. [5] compared the TUNEL method and the detection of apoptotic cells using an antibody against active-caspase 3. They found good correlation between the two methods, but the latter was much easier and more reliable for detecting and quantifying apoptotic cells. TUNEL assay is prone to certain pitfalls. For instance, the TUNEL assay is associated with a number of technical problems, mostly proteinase digestion, with fixation and processing procedures or with the action of section cutting or various other pre-treatments. The advantage of detecting apoptosis using antibodies against active-caspase 3 as compared with methods such as TUNEL assay and determination of apoptotic bodies on haematoxylin and eosin staining is that it detects apoptotic cells even before the phenotypic changes are clearly recognisable. In our study, only a few cells with normal morphology showed some immunoreactivity, while cells with an apoptotic nuclear and surface morphology displayed strong reactivity in the cytoplasm and nucleus.

Koizumi et al. [17] analysed pro- and active-caspase 3 expression in neuroblastomas. They found some active-caspase 3-positive cells that were not morphologically apoptotic, but few morphologically apoptotic cells were not active-caspase 3 immunohistochemically positive. We found active-caspase 3-positive cells in all tissue samples. Some positive cells did not exhibit the morphological characteristics of apoptotic cells. We assumed that these were cells in which caspase 3 was activated, but morphological changes had not yet occurred. Daverajan et al. [3] described that 75% of evaluated breast tumour samples lacked active-caspase 3 positivity. The AI in the present study ranged from 0.2% to 9.4%. Izawa et al. [13] determined AI using the TUNEL method. AI in their study ranged from 0% to 8.97%. In Hodgkin's lymphoma, Dukers et al. [6] described mainly nuclear staining of active-caspase 3 and the percentage of active-caspase 3-positive cells ranged from 0% to 13%. In their study, 14% of Hodgkin's lymphomas were negative for pro-caspase 3, but in those cases, they did not find any active-caspase 3-positive cells. They presented 33% of cases in which pro-caspase 3 was positive and active-caspase 3 was negative. We found active-caspase 3-positive cells even in cases in which pro-caspase 3 was negative in tumour cells but positive in lymphocytes and hyperplastic epithelium as an internal positive control. The fact that active-caspase 3 was observed even in cases in which pro-caspase 3 was negative implies either that only very small amounts of pro-caspase 3 (below the levels of immunodetectability) are required for activation or that pro-caspase 3 becomes upregulated just prior to apoptosis. Although pro-caspase 3 expression correlates with the differential tendency of cells to undergo apoptosis in some tissue, this is not always true. For example, in the thymus, pro-caspase 3 immunostaining is typically stronger in the medullary than the cortical thymocytes, despite the greater vulnerability of cortical cells to apoptosis induction using irradiation or glucocorticoids [19].

In the treatment of localised LSCC, the site of the primary tumour has particular importance. Supraglottic carcinoma originating above the true vocal cord often presents at a more advanced stage, as voice changes are produced only late in the course of disease. Patients with localised supraglottic LSCC usually have a worse prognosis than their glottic counterparts. Overall survival of patients with cancer of the vocal cord is 80–83%, but for supraglottic carcinoma it approaches 40–45% [26]. In our study, we found strong pro-caspase 3 expression in 22 (56%) supraglottic tumours, but only 6 (26%) in glottic LSCC. The number of active-caspase 3-positive cells in glottic tumours was significantly lower than in supraglottic tumours, which is consistent with the study by Hirvikoski and co-workers [10] in which they report that supraglottic tumours had higher apoptotic and mitotic activities and, thus, a more aggressive nature than glottic tumours. We also found that more supraglottic tumours (39%) were p53-positive than their glottic counterparts (25%).

Alterations in the p53 tumour suppressor gene are the most frequent genetic abnormalities in human cancers. Cancer cells with alterations in this gene have been frequently found to express readily detectable levels of p53 protein. A strong correlation between missense mutation of p53 gene and overexpression of p53 protein has been found. However, p53 overexpression can be seen in tumours that lack apparent gene mutations, and there are a number of p53 mutants that produce a truncated protein that is undetectable using immunohistochemistry [35]. In recent studies, p53 overexpression has been reported in LSCC at a frequency ranging from 38% to 79% of the tumour samples analysed [13, 30, 36]. We found a low frequency (33.8%) of p53 overexpression in patients with LSCC. An extensive body of literature supports the role of p53 in the regulation of apoptosis. In our study, no relationship was found between AI and p53 expression. Izawa and co-workers [13] also found no correlation between AI assessed by the TUNEL method and p53 overexpression. However, in the p53-positive group, we found 59.1% of tumours with strong pro-caspase 3 expression and just 13.7% of tumours with no or weak pro-caspase 3 expression. These results suggest that p53 inactivation might be associated with pro-caspase 3 overexpression in LSCC.

p53 is involved in the regulation of apoptosis in a number of different paradigms. Many apoptosis-related genes that are transcriptionally regulated by p53 have been identified. There is some evidence suggesting that Bax, a proapoptotic member of the bcl-2 family of cell death-regulating genes, may be involved in p53-induced apoptosis. The Bax gene contains p53 consensus sequences within its promoter and has been shown to be

transcriptionally regulated by p53 [20]. Cregan et al. [2] demonstrated that p53-induced cell death involves a Bax-dependent caspase 3 activation. Trask et al. [32] described that 81% of patients with LSCC had an increased level of Bax expression, but they did not find any correlation between Bax expression and p53 status. We did not find any correlation between p53 expression and AI. Other proteins of the bcl-2 family as well as inhibitor apoptotic proteins (IAP) might be involved in regulation of apoptosis in LSCC. We found that the expression of survivin, an IAP member, was significantly higher in the p53-positive group of LSCC [23].

In summary, pro-caspase 3, a key protein involved in the execution of apoptosis, seems to be downregulated in 25% of LSCC. However, the fact that active-caspase 3-positive cells were detected in all, even the apparently pro-caspase 3-negative cases, suggests that complete absence of pro-caspase 3 does not occur during LSCC carcinogenesis. Variations of pro-caspase 3 expression in LSCC seem not to influence apoptotic activity. Understanding the mechanisms of the apoptotic process and the reasons why cell death is bypassed in transformed cells of LSCC is of fundamental importance in cancer research and should have, in the future, great implications in the design of anticancer therapeutics for LSCC treatment.

References

1. Cohen GM (1997) Caspases: the executioners of apoptosis. Biochem J 326:1–6
2. Cregan SP, MacLaurin JG, Craig CG, Robertson GS, Nicholson DW, Park DS, Slack RS (1999) Bax-dependent caspase 3 activation is a key determinant in p53-induced apoptosis in neurons. J Neuroscience 15:7860–7869
3. Deverajan E, Sahin AA, Chen JS, Kristnamurthy RR, Aggarwal N, Sapino AM, Zhang F, Sharma D, Yang XH, Tira AD, Mehta K (2002) Down-regulation of caspase 3 in breast cancer: a possible mechanism for chemoresistence. Oncogene 21:8843–8851
4. Donoghue S, Baden HS, Lauder I, Sobolewski S, Pringle HJ (1999) Immunohistochemical localization of caspase 3 correlates with clinical outcome in B cell diffuse large-cell lymphoma. Cancer Res 59:5386–5391
5. Duan WR, Garner DS, Williams SD, Funckes-Shippy L, Spath IS (2003) Comparison of immunohistochemistry for activated caspase 3 and cleaved cytokeratin 18 with the TUNEL method for quantification of apoptosis in histological sections of PC-3 subcutaneous xenografts. J Pathol 199:221–228
6. Dukers DF, Meijer CJL, Berge L, Vos W, Ossenkoppele GJ, Oudejans JJ (2002) High numbers of active-caspase 3-positive Reed–Sternberg cells in pre-treatment biopsy specimens of patients with Hodgkin disease predict favourable clinical outcome. Blood 100:36–42
7. Fujikawa K, Shiraki K Sugimoto K, Ito T, Yamanaka T, Takase K, Nakano T (2000) Reduced expression of ICE/caspase 1 and CPP32/caspase3 in human hepatocellular carcinoma. Anticancer Res 20:1927–1932
8. Gown AM, Willingham MC (2002) Improved detection of apoptotic cells in archival paraffin sections: immunohistochemistry using antibodies to cleaved caspase 3. J Histochem Cytochem 50:449–454
9. Hadjiloucas I, Gilmore AP, Bundred NJ, Streuli CH (2001) Assessment of apoptosis in human breast tissue using an antibody against the active form of caspase 3: relation to tumour histopathological characteristics. Br J Cancer 85:1522–1526
10. Hirvikoski P, Virtaniemi J, Kumpulainen E, Johansson R, Kosma VM (2002) Supraglottic and glottic carcinomas: clinically and biologically distinct entities? Eur J Cancer 38:1717–1723
11. Hoshi T, Sasano H, Koto K, Yabuki, Ohara S, Konno R, Asaki S, Toyota T, Tateno H, Nagura H (1998) Immunohistochemistry of caspase3/CPP32 in human stomach and its correlation with cell proliferation and apoptosis. Anticancer Res 18:4347–4354
12. Hsia JY, Chen CY, Chen JT, Hsu CP, Shai SE, Yang SS, Chuang CY, Wang PY, Miaw J (2003) Prognostic significance of caspase 3 expression in primary resected esophageal squamous carcinoma. EJSO 29:44–48
13. Izawa H, Yonemitsu N, Shin T, Sugihara H (1999) Histopathological analysis of apoptosis, and expression of p53, bcl-2, bax, and Ki-67 in laryngeal squamous cell carcinomas and dysplasia. Auris Nasus Larynx 26:317–330
14. Kambič V (1997) Epithelial hyperplastic lesions—a challenging topic in laryngology. Acta Otolaryngol 527[Suppl]:7–11
15. Kase S, Osaki M, Honjo S, Adachi H, Tsujitani S, Kaibara N, Ito H (2003) Expression of cyclo-oxygenase-2 is correlated with high intratumoral microvessel density and low apoptotic index in human esophageal squamous cell carcinomas Virchows Arch 442:129–135
16. Kerr JFR, Wyllie AH, Currie AR (1972) Apoptosis: a basic biological phenomenon with wide ranging implications in tissue kinetics. Br J Cancer 26:239–257
17. Koizumi H, Ohkawa I, Tsukahara T, Momoi T, Nakada K, Uchikoshi T (1999) Apoptosis in favourable neuroblastomas is not dependent on Fas (CD95/APO1) expression but on activated caspase 3 (CPP32). J Pathol 189:410–415
18. Koomagi R, Volm M (2000) Relationship between the expression of caspase 3 and the clinical outcome of patients with non-small cell lung cancer. Anticancer Res 20:393–496
19. Krajewska M, Wong H, Krajevski S, Zapata JM, Shabaik A, Goscoyne R, Reed JC (1997) Immunohistochemical analysis of in vivo patterns of expression of CPP32 (caspase 3), a cell death protease. Cancer Res 57:1605–1613
20. Miyashita T, Reed JC (1995) Tumour suppressor p53 is a direct transcriptional activator of the human Bax gene. Cell 80:293–299
21. Nakagawara A, Nakamura Y, Ikead H, Hiwasa T, Kuida K, Su MS, Zhao H, Cnaan A, Sakiyama S (1997) High levels of expression and nuclear localization of inteleukih-1 β converting enzyme (ICE) and CPP32 in favourable human neuroblastomas. Cancer Res 57:4578–4584
22. Nicholson DW (2000) From bench to clinic with apoptosis-based therapeutic agents. Nature 407:810–816
23. Pižem J, Cör A, Gale N (2004) Survivin is a negative prognostic marker in laryngeal squamous cell carcinoma and is associated with p53 accumulation. Histopathology (in press)
24. Ramuz O, Isnardon D, Devilard E, Chorafe-Jauffret E, Hasson-Xeri L (2003) Constitutive nuclear localization and initial cytoplasmic activation of endogeneous caspase 3 evidenced by confocal microscopy. Int Exp Pathol 84:75–81
25. Sarasin A, Stary A (1997) Human cancer and DNA repair-deficient disease. Cancer Detect Prev 21:406–411
26. Sasaki CT, Jassin B (2001) Cancer of the pharynx and larynx. Am J Med 111:118S–123S
27. Shanmugaratnam K (1991) WHO: histological typing of tumours of the upper respiratory tract and ear, 2nd edn. Springer, Berlin Heidelberg New York
28. Sohn JH, Kim DH, Choi NG, Park YE, Ro JY (2000) Caspase 3/CPP32 immunoreactivity and its correlation with frequency of apoptotic bodies in human prostatic carcinomas and benign hyperplasias. Histopathology 37:555–560
29. Takata T, Tanaka F, Yamada T, Yanagihara K, Otake Y, Kawano Y, Nakagawa T, Miyahara R, Oyanagi H, Inui K, Wada H (2001) Clinical significance of caspase 3 expression in

pathologic-stage I, nonsmall-cell lung cancer. Int J Cancer 96:54–60
30. Tan G, Hequing L, Jiangbo C (2002) Apoptosis induced by low-dose paclitaxel is associated with p53 upregulated in nasopharyngeal carcinoma cells. Int J Cancer 97:168–172
31. Törmännen-Näpänkangas U, Soini Y, Kahlos K, Kinnula V, Pääkkö P (2001) Expression of caspase 3, -6 and -8 and their relation to apoptosis in non-small cell lung carcinoma. Int J Cancer 93:192–198
32. Trask DG, Wolf GT, Bradford CR, Fisher SG, Deveney K, Johnson M, Singleton T (2002) Expression of Bcl-2 family proteins in advanced laryngeal squamous cell carcinoma: correlation with response to chemotherapy and organ preservation. Laryngoscope 112:638–644
33. Vakkala M, Pääkkö P, Soini Y (1999) Expression of caspase 3, 6, and 8 is increased in parallel with the apoptosis and histological aggressiveness of the breast lesion. Br J Cancer 81:592–599
34. Volm M, Mattern J, Koomagi R (1999) Inverse correlation between apoptotic (Fas ligand, caspase 3) and angiogenic factors (VGEF, microvessel density) in squamous cell lung carcinoma. Anticancer Res 19:1669–1671
35. Wagata T, Shibagaki I, Immamura M, Shimada Y, Toguchida J, Yandell DW, Ikenaga M, Tobe T, Ishizaki K (1993) Loss of 17p mutation of the p53 gene, and overexpression of p53 protein in esophageal squamous cell carcinomas. Cancer Res 53:846–850
36. Weber A, Bellmann U, Bootz F, Wittekind C, Tannapfel A (2002) Expression of p53 and its homologues in primary and recurrent squamous cell carcinomas of the head and neck. Int J Cancer 99:22–28
37. Winter RN, Kramer A, Borkowski A, Kyprianou N (2001) Loss of caspase 1 and caspase 3 protein expression in human prostate cancer. Cancer Res 61:1227–1232

Virchows Arch (2004) 444:447–453
DOI 10.1007/s00428-004-0984-6

CASE REPORT

Irene Esposito · Andrea Bauer · Jörg D. Hoheisel · Jörg Kleeff · Helmut Friess · Frank Bergmann · Ralf J. Rieker · Herwart F. Otto · Günter Klöppel · Roland Penzel

Microcystic tubulopapillary carcinoma of the pancreas: a new tumor entity?

Received: 9 January 2004 / Accepted: 29 January 2004 / Published online: 11 March 2004

Abstract An unusual pancreatic tumor with microcystic and tubulopapillary features was observed in a 53-year-old woman. The tumor presented as a large, focally cystic mass in the head of the pancreas, which compressed the surrounding structures. The histological and immunohistochemical analysis revealed a neoplasm that could not be assigned to any of the known pancreatic tumor types. At the molecular level, the tumor showed inactivation of the DPC4/SMAD4 gene, deletion of exon 1 of the $p16^{INK4A}$ gene and a point mutation at codon 34 (GGA>AGA) of *β-catenin*. Transcriptional profiling analyses and subsequent correspondence cluster analysis demonstrated that the transcriptional profile of the tumor differed distinctly from that of ductal adenocarcinomas, pancreatic cystic tumors and normal pancreatic tissues. These data suggest that the neoplasm most likely represents a new pancreatic tumor entity, which we would like to refer to as microcystic tubulopapillary tumor.

Keywords Pancreas · Microarray analysis · DPC4/SMAD4 · β-Catenin · $p16^{INK4A}$

I. Esposito (✉) · F. Bergmann · R. J. Rieker · H. F. Otto · R. Penzel
Department of Pathology, University of Heidelberg,
Im Neuenheimer Feld 220, 69120 Heidelberg, Germany
e-mail: irene_esposito@med.uni-heidelberg.de
Tel.: +49-62-21564351
Fax: +49-62-21565251

A. Bauer · J. D. Hoheisel
Department of Functional Genome Analysis,
German Cancer Research Center,
Heidelberg, Germany

J. Kleeff · H. Friess
Department of General Surgery,
University of Heidelberg,
Germany

G. Klöppel
Department of Pathology, University of Kiel,
Germany

Introduction

Pancreatic neoplasms with cystic and papillary features mainly belong to the category of intraductal papillary mucinous cystic tumors. These tumors cause a dilatation of the pancreatic duct and/or of its branches that, especially when focal, may produce a cystic-like gross appearance [26]. Another pancreatic tumor with papillary (or more precisely, pseudopapillary) structures is the solid pseudopapillary neoplasm, a low-grade malignant tumor that occurs predominantly in young women and often displays a cystic gross appearance due to extensive hemorrhage and necrosis [16]. In rare cases, papillary and micropapillary structures can also be found in ductal adenocarcinomas, especially if they are well differentiated [24]. Here, we report the case of an unusual pancreatic tumor with tubulopapillary and microcystic features, which could not be assigned to any of the known pancreatic tumor types. The histological and immunohistochemical data and the results of a molecular analysis, which included the use of the increasingly employed microarray technology [11], all suggest that this tumor represents a new entity, not previously described in the pancreas.

Case report

A 53-year-old woman presented with a short history of discomfort and swelling in the right upper abdomen. Relevant data in her prior history included alcohol intake, interrupted 10 years ago, and episodes of pancreatitis. Moreover, the patient suffered from diabetes mellitus and liver cirrhosis (child A). A computed tomography scan revealed a 10- to 15-cm tumor mass in the pancreatic head; therefore, an exploration and a subsequent pylorus-preserving pancreaticoduodenectomy were performed.

Materials and methods

Formalin-fixed, paraffin-embedded sections obtained from the tumor mass were stained routinely with hematoxylin and eosin and periodic acid-Schiff (PAS). Immunohistochemical analysis was performed on consecutive slides with the streptavidin-biotin meth-

Table 1 Immunohistochemical profile of the reported tumor

Immunohistochemical marker	Result
CK7	+
CK8	+
CK18	+
CK20	+
CEA	–
Vimentin	–
Chromogranin	–
Neuron-specific enolase	–
Synaptophysin	+*
Trypsin	–
Inhibin	–
Thyroglobulin	–
TTF-1	–
Estrogen/progesterone receptors	–
MUC1	–
MUC2	–
MUC6	+
p53	(+)
p16	–
DPC4	–
β-Catenin	+°

* Focal cytoplasmic positivity
° Cytoplasmic and nuclear positivity

od, using diaminobenzidine as the chromogen. A large panel of antibodies (all supplied by Dako, Carpenteria, CA, USA, with the exception of the anti-trypsin antibody, provided by Prof. Klöppel's laboratory) was used (Table 1).

Immunohistochemistry for p16, p53, Dpc4 and β-catenin

The following primary antibodies were used: mouse monoclonal anti-p16 (clone E6H4; mtm laboratories AG-Dako), mouse monoclonal anti-p53 (clone DO7; Dako); mouse monoclonal anti-DPC4/SMAD4 (clone B8; Santa Cruz Biotechnology, Santa Cruz, CA, USA) and mouse monoclonal anti-β-catenin (BD Transduction Laboratories, Lexington, KY, USA). Microwave antigen retrieval in citrate buffer was used with all three antibodies.

Electron microscopy

Small tissue samples were fixed in 3% glutaraldehyde and processed for ultrastructural investigation. Semi-thin sections were stained with 1% toluidine blue and examined using light microscopy to find appropriate areas for ultramicrotomy. Ultra-thin sections were contrasted with lead and examined under an electron microscope (Carl Zeiss, Jena GmbH, Jena, Germany).

DNA isolation

Tumor cells were manually microdissected from formalin-fixed, paraffin-embedded, 5-µm-thick tissue sections. Genomic DNA was isolated using the QIAamp DNA Mini Kit (Qiagen GmbH, Hilden, Germany) according to the manufacturer's protocol.

Deletion analysis of the $p16^{INK4A}$ gene

Tumor DNA and DNA from the corresponding normal tissue were subjected to Duplex polymerase chain reaction (PCR) analysis using *p16* exon 1 (Ex1F: 5′-CTC AGA GCC GTT CCG AGA T-3′; Ex1R: 5′-TTT TCG AGG GCC TTT CCT AC-3′) or exon 2-specific primers (Ex2F: 5′-ACC CTG GCT CTG ACC ATT C-3′; Ex2R: 5′-TGG AAG CTC TCA GGG TAC AAA-3′), each combined with primers for the β-globin gene [22] as a control. Duplex PCRs were carried out as one-tube reactions under the following conditions: initial denaturation at 96°C for 3 min, 35 cycles of denaturation at 96°C for 1 min, annealing at 60°C for 1 min, extension at 72°C for 1 min and final extension at 72°C for 5 min. Duplex PCR products were electrophoretically separated on an ethidium bromide-stained 2% agarose gel and documented by digitalization (Gel documentation system, Herolab GmbH, Wiesloch, Germany).

Sequencing analysis

Exon 1 of the k-ras gene, which contains the codons 12 and 13, was amplified using the primers k-ras 1F (5′-GTG TGA CAT GTT CTA ATA TAG TCA-3′) and k-ras 1R (5′-GAA TGG TCC TGC ACC AGT AA-3′). The primer pairs β-Cat 2F (5′- GGA GTT GGA CAT GGC CAT GG-3′) and β-Cat 2R (5′-CCT GTT CCC ACT CAT ACA GG-3′) were used to amplify exon 3 of the β-catenin gene, which contains four threonine/serine phosphorylation sites essential for APC/GSK-3β-mediated degradation of β-catenin. PCR reactions were performed under standard conditions, and the purified PCR products were sequenced directly in the forward and reverse directions on an ABIPrism 377 DNA sequencer (Applied Biosystems, Foster City, CA, USA), using the BigDye Termination Kit (Applied Biosystems, USA).

DNA microarrays

Human cDNAs representing 3500 different human genes, which had been selected because they are informative with respect to pancreas tumors, were PCR-amplified using amino-modified M13 universal primers. PCR products were purified with PCR multi-screen columns (Millipore GmbH, Schwalbach, Germany), suspended in spotting solution (TeleChem International Inc., Sunnyvale, CA, USA) and arrayed onto slides with an epoxy surface (Epoxy Slides, Quantifoil Micro Tools GmbH, Jena, Germany). DNA spotting was performed with a Micro-Arrayer from Engineering Services Inc. (Virtek's arrayer system, BioRad, Munich, Germany) using SMP3 pins (TeleChem, USA). Each microarray presents 3872 spots divided into 16 blocks, containing each spot in duplicate.

Transcriptional profiling

Total RNA was extracted with guanidine isothiocyanate from snap-frozen pancreatic tissues, including seven normal pancreas samples, five ductal adenocarcinomas and seven cystic tumors (mucinous cystic adenomas, mucinous cystic adenocarcinomas, serous cystic adenomas, intraductal papillary-mucinous tumors). Fluorescence-labeled cDNA samples were prepared from 10 µg total RNA and incorporation of Cy3- or Cy5-labeled dCTP during first-strand synthesis. The labeling reaction was performed at least three times in total. Hybridization was done in SlideHyb-Buffer 1 (Ambion Inc., Austin, TX, USA) under glass coverslips at 62°C overnight. To prevent bias caused by preferential label incorporation into particular sequences, the dyes were swapped between hybridizations. After washing in 0.1× sodium saline citrate for 3 min and drying using nitrogen, fluorescence signals were detected on a confocal ScanArray 5000 scanner (Packard BioChip Technologies, Billerica, MA, USA). Quantification of the signal intensities was performed with the GenePix Pro 4.1 software (Axon Instruments, Inc., Union City, CA, USA).

Data analysis

Data quality assessment, normalization and correspondence cluster analysis were performed with the analysis and data warehouse software package M-CHiPS (Multi-Conditional Hybridization Intensity Processing System), in which more than 5800 hybridization experiments are currently stored (http://www.mchips.org) [8, 9, 10]. Normalization was performed as described in detail by Beissbart et al. [4]. For further analysis, only genes that exhibited significant changes between at least one sample and the control material of the normal pancreas were selected. Data analysis and

also the compilation of experimental and sample-specific annotations met the criteria for MIAME2 compliance [6].

Correspondence analysis [8, 10] is an explorative computational method for the study of associations between variables. Much like principle component analysis, it displays a low-dimensional projection of the data onto a plane. Data are projected simultaneously for two variables, such as genes and patient samples, thus revealing associations between them. The closer the data points are located on the blot, the higher the degree of correspondence, thereby enabling a superior data interpretation.

Results

Morphology

Macroscopic examination of the surgical specimen revealed a 15×9×8-cm tumor with extensive necrotic areas, resulting in a focally cystic appearance. The tumor was surrounded by a thin pseudo-capsule and displayed expansive margins of growth. The duodenum and the distal bile duct were compressed and dislocated, but not infiltrated. Lymph node metastases were not found. Histologically, the tumor was composed of cubic to cylindrical cells, containing elongated, mostly basally located and frequently stratified nuclei, which showed moderate pleomorphism and granular chromatin. The cytoplasm was eosinophilic. The tumor cells formed well-developed tubular and papillary structures, which were often cystically dilated and contained amorphous eosinophilic PAS-positive material (Fig. 1A, B, C). Focally, there were necrotic areas. Extensive sampling failed to reveal solid areas. It was not possible to determine whether the tumor had an intraductal component, since very little pancreatic parenchyma was included in the surgical specimen. Ultrastructurally, the nuclei displayed shallow cytoplasmic invaginations and contained irregular masses of heterochromatin. In the cytoplasm, swollen

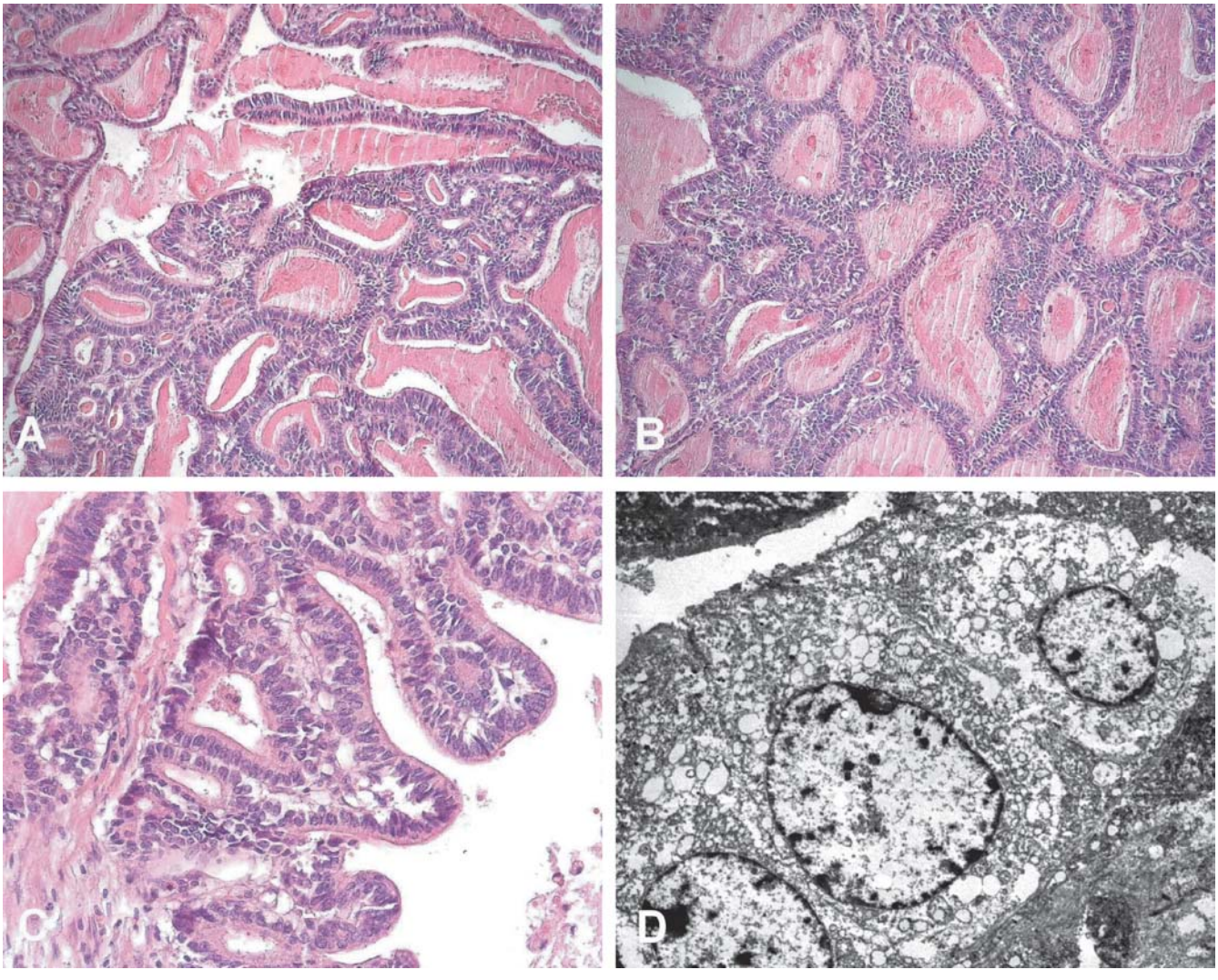

Fig. 1 **A**, **B**, **C** Microscopic appearance of the tumor, consisting of cubic to cylindrical cells with elongated nuclei, arranged to form small glandular or papillary structures, often projecting into cystically dilated lumina (**A**, **B**, ×100; **C**, ×200). **D** Electron microscopy revealed the presence of tight junctions between adjacent cells, which displayed nuclei with shallow invaginations and absence of secretory products in the cytoplasm (×2000)

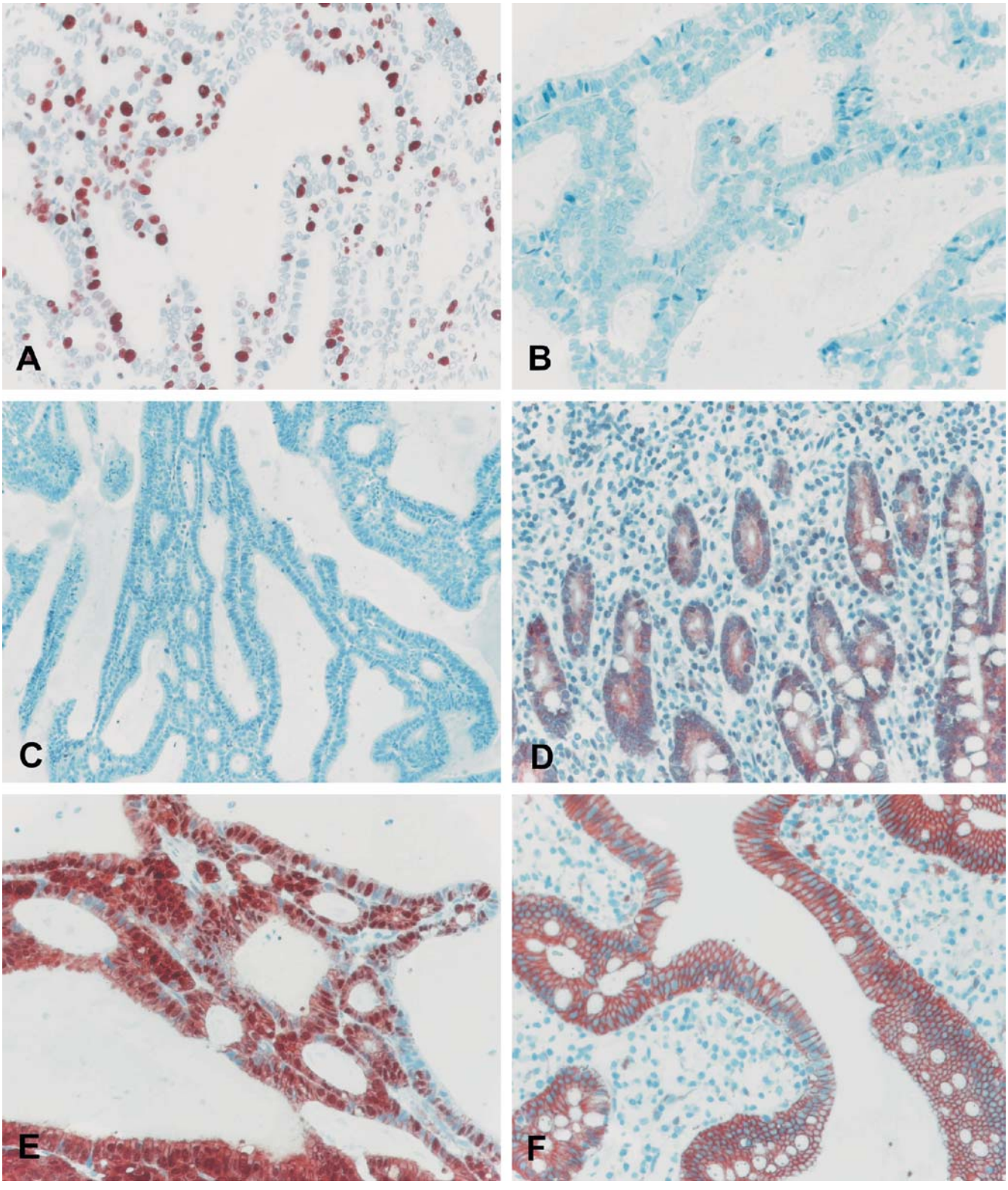

Fig. 2 **A** Immunostaining with MIB1 antibody revealed a proliferation index of about 15% (×200). **B** p53 accumulation was detected only in a small percentage (<2%) of the tumor cells (×200). **C** DPC4/SMAD4 expression was not detectable in the tumor cells (×100). **D** Cytoplasmic and nuclear staining of DPC4/SMAD4 in the surrounding normal duodenal tissue (×200). **E** β-catenin was present at the membranous, cytoplasmic and nuclear levels in the tumor cells (×200). **F** In the normal duodenal tissue, only membranous immunoreactivity of β-catenin was detected (×200)

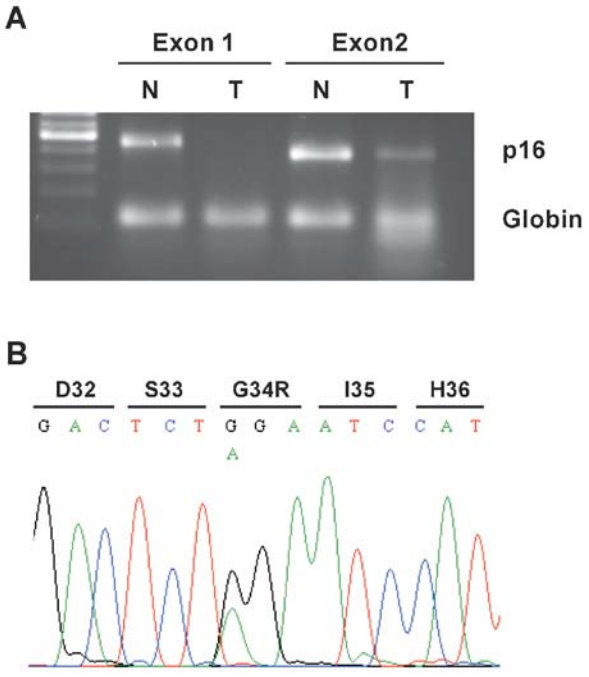

Fig. 3 **A** Deletion analysis of *p16*^{INK4A} using duplex polymerase chain reaction revealed a complete lack of exon 1 in the tumor sample (*T*), whereas the corresponding control (*N*) showed no alteration. Exon 2 was detectable in tumor and control samples. **B** Partial sequence of exon 3 of *β-catenin*, displaying a heterozygous point mutation (GGA>AGA) in codon 34, causing the amino acid substitution glycine to arginine

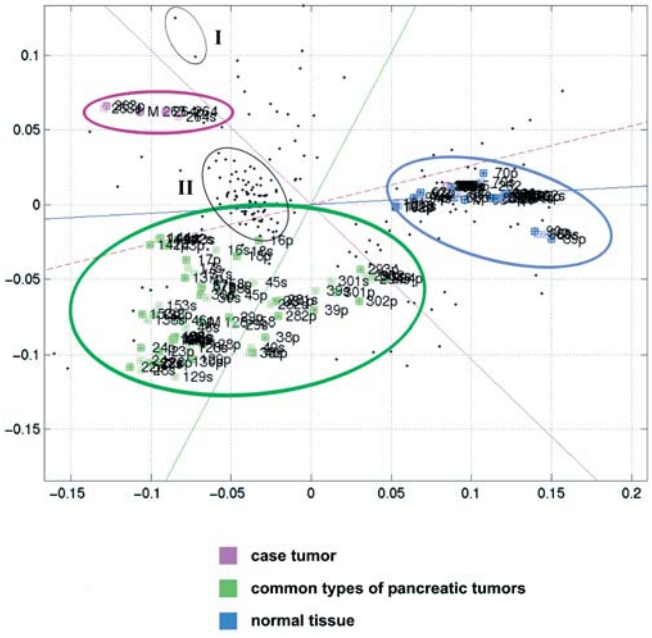

Fig. 4 Correspondence cluster analysis. In the resulting biplot, each hybridization of the RNA from an individual tissue sample is depicted as a *colored square*. Each significantly differentially transcribed gene is shown as a *black dot*. Also, several guiding lines are displayed in the diagram. They correspond to the position of virtual genes, whose transcription profiles would exhibit a signal in one condition only. Genes with insignificant changes would be positioned close to the centroid of these lines, but are not shown in the blot. The samples from the most common types of pancreatic tumors (ductal adenocarcinoma and cystic tumors) and from normal tissues form distinct clusters. The individual case reported here is clearly different from all other analyzed tissues. Two genes (group I) are the most specific ones for discriminating it from the other tumors. Alternatively, group II indicates genes that distinguish tumors from normal tissue, but do not discriminate between the tumor samples

mitochondria, prominent lysosomes and secondary lysosomes were detected. Tight junctions were seen at the border between two adjacent cells (Fig. 1D). The proliferative activity, evaluated using Ki-67 immunostaining, was moderate (15%) (Fig. 2A). Table 1 depicts the results of the immunohistochemical analysis. On the basis of the histological and immunohistochemical data, the descriptive diagnosis of a microcystic tubulopapillary carcinoma was made; however the tumor could not be assigned to any of the known types of pancreatic tumors.

Immunohistochemical and molecular profile

Only a few tumor cells (<1%) displayed positive nuclear staining for p53 (Fig. 2B). p16^{INK4A} and DPC4/SMAD4 were not expressed in the tumor cells, whereas they were normally present in the cytoplasm and nuclei of surrounding non-neoplastic duodenal tissue (Fig. 2C, D). *β*-Catenin was expressed at the membranous and cytoplasmic level in the great majority of the tumor cells; strong *β*-catenin nuclear expression was detected in about 50% of the tumor cells (Fig. 2E). In the epithelial cells of the duodenum, only membranous expression of *β*-catenin was detected (Fig. 2F).

Deletion analysis by duplex PCR revealed a complete lack of exon1 of *p16*^{INK4A} in the tumor sample (Fig. 3A). Sequencing of exon 3 of *β-catenin* showed a point mutation at codon 34 (GGA>AGA), which caused amino acid substitution of glycine with arginine (Fig. 3B). In contrast, no mutations were found in exon 1 of *k-ras*.

Microarray analysis

Transcriptional profiling analyses were performed with material obtained from ductal adenocarcinomas, pancreatic cystic tumors and normal pancreatic tissues. The samples, labeled with either Cy3 or Cy5, were analyzed in competitive hybridizations. Unspecific hybridization to non-homologous sequences did not occur, as could be seen on spots generated with unrelated control DNA fragments. After scanning and quantification of the spot intensities, data were normalized and filtered. In total, 269 PCR fragments contained a sequence that was significantly differentially transcribed in at least one of the samples analyzed. The results were subjected to correspondence cluster analysis [8]. One major advantage of this process is its ability to present the results of cluster analyses on different but corresponding factors in one plot. In Fig. 4, not only the genes (black dots), but also the

results of clustering of the individual hybridizations—and, thus, the individual tissue samples (colored squares)—are shown. Co-localization in the blot of genes and experiments/conditions is indicative of a strong association between them. In addition, virtual transcription profiles were calculated on the basis of the results and projected onto the plot. Classification by correspondence analysis resulted in the formation of two distinct clusters for common types of pancreatic tumors (ductal adenocarcinoma and cystic tumors) and normal tissues (Fig. 4). Profiling the RNA of the tumor described here, however, produced a distinct blot position. All repetitions of the analysis produced the same result, actually forming a cluster of their own in the correspondence analysis. Distances to the other tumor clusters demonstrated that the sample exhibited a significantly different transcriptional profile.

Discussion

In this report, we describe an unusual microcystic tumor of the pancreas, whose histology was characterized by a tubulopapillary architecture. The histological, immunohistochemical and molecular features of this neoplasm were found to differ from all known pancreatic tumors.

The differential diagnosis of this tumor particularly includes other cystic tumors, such as solid-pseudopapillary neoplasm, the cystic variant of acinar cell carcinoma and metastatic tumors.

According to the gross appearance of the tumor (large mass, necrotic–hemorrhagic areas, well-defined demarcation) and its occurrence in a female patient, the possibility of a solid-pseudopapillary tumor had to first be discussed. Points favoring this diagnosis included the immunohistochemical expression of β-catenin, which was found to be accompanied by a point mutation in exon 3 of the β-catenin gene [1]. However, the histological features, in particular the tubulopapillary pattern, the cytology and immunohistochemical data (such as positivity for cytokeratins and negativity for neuron-specific enolase and vimentin) were not in accordance with such a diagnosis [17].

The tubulopapillary and microcystic pattern of the carcinoma partially resembled the cystic variant of acinar cell carcinoma. This rare tumor affects men more frequently than women [14], usually reaches great dimensions and can be encapsulated [15, 25]. It contains macrocysts and microcysts with a cuboidal or cylindrical epithelial cell lining. The tumor cells express pancreatic enzymes, such as trypsin, lipase, chymotrypsin and phospholipase A2, which are useful immunohistochemical markers of acinar cell carcinoma [15]. Moreover, *β-catenin* mutations have also been reported in a small percentage of acinar cell carcinomas [2]. However, the absence of trypsin expression in our case and the absence of secretory granules, as revealed by the ultrastructural analysis, made the diagnosis of acinar cell carcinoma unlikely. In addition, the loss of DPC4/SMAD4 protein expression in the tumor cells is not a common finding in acinar cell carcinomas [2].

Other pancreatic cystic tumors (serous and mucinous tumors) as well as intraductal papillary mucinous tumors were excluded on the basis of the histopathological appearance.

Although unlikely, the possibility of a metastatic tumor was also taken into account. Secondary tumors of the pancreas are a rare event in the absence of widespread disease and can be the consequence of direct infiltration of the organ or, more frequently, of hematogenous metastasis [7]. Colon, gastric and bile duct carcinomas are the most common sources of direct infiltration of the pancreas [7, 19], whereas lung, kidney and breast cancers and melanomas are the most frequent primary tumors in cases of blood-borne metastases to the pancreas [7, 12, 28]. Metastases of renal cell carcinomas often occur as solitary lesions and are subjected to surgical resection [13, 21]. Rarely, symptoms related to the pancreatic metastases, such as jaundice or pancreatitis due to duct obstruction, have been the first clinical manifestations of an otherwise unknown primary tumor [18, 20]. In our case, there was no evidence of a neoplastic disease in the patient's history or in the results of physical, laboratory and imaging tests. Therefore, it was considered very unlikely that the pancreatic tumor mass was a metastasis. However, some additional immunostainings were performed (thyroglobulin, TTF-1, estrogen and progesterone receptors), all with negative results.

The molecular profile of pancreatic adenocarcinomas is characterized by K-*ras* mutations in codon 12. Other frequent alterations include $p16^{INK4A}$ mutations (up to 80% of the cases), p53 mutations (up to 70%) and loss of DPC4/SMAD4 expression (approximately 50%) [3]. The last two alterations lead to abnormal protein expression, so that there is a good correlation between immunohistochemical results and genetic analyses. In particular, the absence of DPC4/SMAD4 immunostaining reflects the inactivation of the corresponding gene [27]; p53 mutations often lead to nuclear accumulation of the protein, which can consequently be visualized using immunohistochemical labeling [5, 23]. The immunohistochemical and molecular analysis of this tumor revealed an unusual pattern, characterized by wild-type K-*ras*, absence of p53 overexpression, loss of DPC4/SMAD4 and deletion of exon 1 of $p16^{INK4A}$.

Transcriptional microarray analysis demonstrated that the tumor had a distinct profile when compared with other pancreatic tumor entities. Although the diagnostic utility of gene profiling techniques has already been emphasized, this is the first report demonstrating the use of microarrays in the field of diagnostic molecular pathology. In addition to the morphological, immunohistochemical and genetic results, the array data helped to define a new type of pancreatic tumor. Larger series are needed to confirm and validate the data presented here.

A last issue that needs to be discussed is the malignant potential of this tumor. The presence of nuclear pleomorphism and atypical mitotic figures, together with the

moderate proliferation index, would indicate malignancy. The extensive areas of necrosis could indicate rapid growth in the absence of suitable vascular supply, although there are no reliable data in the patient's history that could confirm this assumption. However, the expansive growth, the absence of infiltration of surrounding structures and, ultimately, the absence of lymph-node and/or distant metastases would indicate low aggressiveness and a good prognosis.

References

1. Abraham SC, Klimstra DS, Wilentz RE, Yeo CJ, Conlon K, Brennan M, Cameron JL, Wu TT, Hruban RH (2002) Solid-pseudopapillary tumors of the pancreas are genetically distinct from pancreatic ductal adenocarcinomas and almost always harbor beta-catenin mutations. Am J Pathol 160:1361–1369
2. Abraham SC, Wu TT, Hruban RH, Lee JH, Yeo CJ, Conlon K, Brennan M, Cameron JL, Klimstra DS (2002) Genetic and immunohistochemical analysis of pancreatic acinar cell carcinoma: frequent allelic loss on chromosome 11p and alterations in the APC/beta-catenin pathway. Am J Pathol 160:953–962
3. Bardeesy N, DePinho RA (2002) Pancreatic cancer biology and genetics. Nat Rev Cancer 2:897–909
4. Beissbarth T, Fellenberg K, Brors B, Arribas-Prat R, Boer J, Hauser NC, Scheideler M, Hoheisel JD, Schutz G, Poustka A, Vingron M (2000) Processing and quality control of DNA array hybridization data. Bioinformatics 16:1014–1022
5. Bodner SM, Minna JD, Jensen SM, D'Amico D, Carbone D, Mitsudomi T, Fedorko J, Buchhagen DL, Nau MM, Gazdar AF et al (1992) Expression of mutant p53 proteins in lung cancer correlates with the class of p53 gene mutation. Oncogene 7:743–749
6. Brazma A, Hingamp P, Quackenbush J, Sherlock G, Spellman P, Stoeckert C, Aach J, Ansorge W, Ball CA, Causton HC, Gaasterland T, Glenisson P, Holstege FC, Kim IF, Markowitz V, Matese JC, Parkinson H, Robinson A, Sarkans U, Schulze-Kremer S, Stewart J, Taylor R, Vilo J, Vingron M (2001) Minimum information about a microarray experiment (MIAME)-toward standards for microarray data. Nat Genet 29:365–371
7. Cubilla A, Fitzgerald P (1984) Tumors of the exocrine pancreas. Atlas of tumor pathology. Armed Forces Institute of Pathology, Washington DC
8. Fellenberg K, Hauser NC, Brors B, Neutzner A, Hoheisel JD, Vingron M (2001) Correspondence analysis applied to microarray data. Proc Natl Acad Sci U S A 98:10781–10786
9. Fellenberg K, Hauser NC, Brors B, Hoheisel JD, Vingron M (2002) Microarray data warehouse allowing for inclusion of experiment annotations in statistical analysis. Bioinformatics 18:423–433
10. Fellenberg K, Vingron M, Hauser NC, Hoheisel JD (2003) Correspondence analysis with microarray data. In: Appasani K (ed) Perspectives in gene expression. Eaton Publishing, Westborough, pp 307–343
11. Grutzmann R, Foerder M, Alldinger I, Staub E, Brummendorf T, Ropcke S, Li X, Kristiansen G, Jesnowski R, Sipos B, Lohr M, Luttges J, Ockert D, Kloppel G, Saeger HD, Pilarsky C (2003) Gene expression profiles of microdissected pancreatic ductal adenocarcinoma. Virchows Arch 443:508–517
12. Hiotis SP, Klimstra DS, Conlon KC, Brennan MF (2002) Results after pancreatic resection for metastatic lesions. Ann Surg Oncol 9:675–679
13. Hirota T, Tomida T, Iwasa M, Takahashi K, Kaneda M, Tamaki H (1996) Solitary pancreatic metastasis occurring eight years after nephrectomy for renal cell carcinoma. A case report and surgical review. Int J Pancreatol 19:145–153
14. Holen KD, Klimstra DS, Hummer A, Gonen M, Conlon K, Brennan M, Saltz LB (2002) Clinical characteristics and outcomes from an institutional series of acinar cell carcinoma of the pancreas and related tumors. J Clin Oncol 20:4673–4678
15. Hoorens A, Lemoine NR, McLellan E, Morohoshi T, Kamisawa T, Heitz PU, Stamm B, Ruschoff J, Wiedenmann B, Kloppel G (1993) Pancreatic acinar cell carcinoma. An analysis of cell lineage markers, p53 expression, and Ki-ras mutation. Am J Pathol 143:685–698
16. Kloppel G, Kosmahl M (2001) Cystic lesions and neoplasms of the pancreas. The features are becoming clearer. Pancreatology 1:648–655
17. Kosmahl M, Seada LS, Janig U, Harms D, Kloppel G (2000) Solid-pseudopapillary tumor of the pancreas: its origin revisited. Virchows Arch 436:473–480
18. Moazzam N, Mir A, Potti A (2002) Pancreatic metastasis and extrahepatic biliary obstruction in squamous cell lung carcinoma. Med Oncol 19:273–276
19. Nakamura E, Shimizu M, Itoh T, Manabe T (2001) Secondary tumors of the pancreas: clinicopathological study of 103 autopsy cases of Japanese patients. Pathol Int 51:686–690
20. Odzak A, Geliberti F, Farace G, Benitez S, Bistoletti R, Kozima S, Frider B (2001) Pancreatic tumor: an unusual presentation of an occult breast carcinoma (in Spanish). Acta Gastroenterol Latinoam 31:395–398
21. Robbins EG II, Franceschi D, Barkin JS (1996) Solitary metastatic tumors to the pancreas: a case report and review of the literature. Am J Gastroenterol 91:2414–2417
22. Saiki RK, Scharf S, Faloona F, Mullis KB, Horn GT, Erlich HA, Arnheim N (1985) Enzymatic amplification of beta-globin genomic sequences and restriction site analysis for diagnosis of sickle cell anemia. Science 230:1350–1354
23. Scarpa A, Capelli P, Mukai K, Zamboni G, Oda T, Iacono C, Hirohashi S (1993) Pancreatic adenocarcinomas frequently show p53 gene mutations. Am J Pathol 142:1534–1543
24. Solcia E, Capella C, Klöppel G (1997) Tumors of the pancreas. Atlas of Tumor Pathology. Armed Forced Institute of Pathology, Washington, DC
25. Stamm BH (1984) Incidence and diagnostic significance of minor pathologic changes in the adult pancreas at autopsy: a systematic study of 112 autopsies in patients without known pancreatic disease. Hum Pathol 15:677–683
26. Taouli B, Vilgrain V, O'Toole D, Vullierme MP, Terris B, Menu Y (2002) Intraductal papillary mucinous tumors of the pancreas: features with multimodality imaging. J Comput Assist Tomogr 26:223–231
27. Wilentz RE, Su GH, Dai JL, Sparks AB, Argani P, Sohn TA, Yeo CJ, Kern SE, Hruban RH (2000) Immunohistochemical labeling for dpc4 mirrors genetic status in pancreatic adenocarcinomas: a new marker of DPC4 inactivation. Am J Pathol 156:37–43
28. Z'Graggen K, Fernandez-del Castillo C, Rattner DW, Sigala H, Warshaw AL (1998) Metastases to the pancreas and their surgical extirpation. Arch Surg 133:413–417

Virchows Arch (2004) 444:454–458
DOI 10.1007/s00428-004-0985-5

CASE REPORT

Shu Takahashi · Kyoji Okada · Hiroyuki Nagasawa · Yoichi Shimada · Hitoshi Sakamoto · Eiji Itoi

Osteosarcoma occurring in osteogenesis imperfecta

Received: 23 July 2003 / Accepted: 27 December 2003 / Published online: 6 March 2004

Abstract We describe a case history of a 24-year-old male with osteogenesis imperfecta (OI) who developed osteosarcoma of the left thigh. High-dose ifosfamide therapy caused marked tumor regression of multiple lung metastases. Immunohistochemically, the tumor cells were diffusely positive for the p53 protein. Mutation of the p53 gene was not detected by direct genomic sequencing of exons 4–8. The radiographic characteristics, including irregularly distributed osteolytic lesions and cortical discontinuity, should not be confused with hyperplastic callus formation, a benign process. A biopsy is critical to establish the differential diagnosis between osteosarcoma and common hyperplastic callus formation in OI; however, it must be applied with great care.

Keywords Osteosarcoma · Osteogenesis imperfecta · p53 · Mutation · Immunohistochemical staining

Introduction

Osteosarcoma rarely occurs in patients with osteogenesis imperfecta (OI). There are only nine proven cases in the English literature. A delay in the diagnosis of osteosarcoma may be due to the similarity in symptoms between the two conditions and because of the difficulty in differentiating between hyperplastic callus and tumor on conventional radiographs. Recently, there has been an increasing interest in to what extent molecular biological markers are involved in the development of osteoblastic tumors. In conventional, highly malignant osteosarcoma, different alterations in tumor suppressor genes (p53, Rb, p16) have been described and are thought to be involved in tumorigenesis [1, 4, 12, 13, 14]. The p53 gene contains five conserved regions, four of which are hot spots for missense mutations [6].

S. Takahashi (✉) · K. Okada · H. Nagasawa · Y. Shimada · E. Itoi
Department of Orthopedic Surgery,
Section of Neuro and Locomotor Science,
Akita University School of Medicine,
Hondo 1-1-1, 010-8543 Akita, Japan
e-mail: shu@med.akita-u.ac.jp
Tel.: +81-18-8846148
Fax: +81-18-8362617

H. Sakamoto
Department of Orthopedic Surgery,
Taiheiryoikuen Hospital for Disabled Children,
Akita, Japan

Clinical history

A 24-year-old male had been followed-up since his birth with OI. There was no family history of OI. He was diagnosed as having type-III OI and had a typical history of multiple fractures with minimum trauma, short stature and normal sclerae. In April 2000, the patient had pain and tenderness on his distal thigh without any traumatic injury. A micro-fracture of the left femur due to a weakness of the bone was suspected. The region was located distal to the Bailey-Dubow nail placed by correction osteotomy in 1988 (Fig. 1a). The fracture was treated with splint and cast immobilization. However, intra-articular hemorrhage of the left knee continued, and several aspirations were performed. Radiographs in October 2000 showed discontinuities of the anterior cortex and irregularly distributed osteolytic changes of the distal femur and proximal tibia (Fig. 1b). We judged that it was impossible to do any conservative treatments, and a left above-knee amputation was performed in January 2001. Swelling and local heat were observed in the stump 2 months later. Infection was suspected, and curettage was performed. Microscopic examination revealed a proliferation of pleomorphic and polygonal cells with a large amount of cartilage tissue (Fig. 2a). Lace-like osteoid was confirmed among the pleomorphic and polygonal cells (Fig. 2b). There was neither orderly maturation of cartilage and spindle cells into bone, nor reactive bone formation rimmed by palisaded osteoblasts. A diagnosis of osteosarcoma was made. A chest X-ray and computerized tomography (CT) taken 1 month postoperatively revealed metastases. The patient underwent high-dose methotrexate (6 g per square meter of skin), cis-platinum (120 mg per square meter of skin) and adriamycin (20 mg per square meter of skin) chemotherapy. A chest X-ray and CT revealed an increase in the size and number of lung metastases 2 months postoperatively (Fig. 3a). Thus, high-dose ifosfamide (2 g per square meter of skin per day for 4 days) was administrated. After eight cycles of high-dose ifosfamide therapy, we could not detect any lung metastases by CT (Fig. 3b).

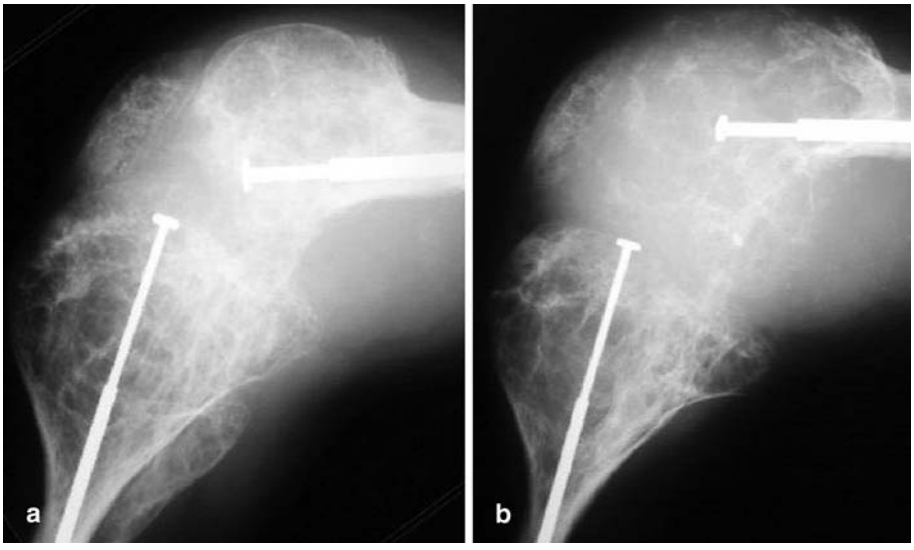

Fig. 1 **a** Lateral view of left knee, April 2000, shows typical osteogenesis imperfecta of femur and tibia treated with intramedullary fixation. **b** Lateral view of left knee, October 2000, shows rarefactions of the anterior cortex and irregularly distributed osteolytic changes of the distal left femur

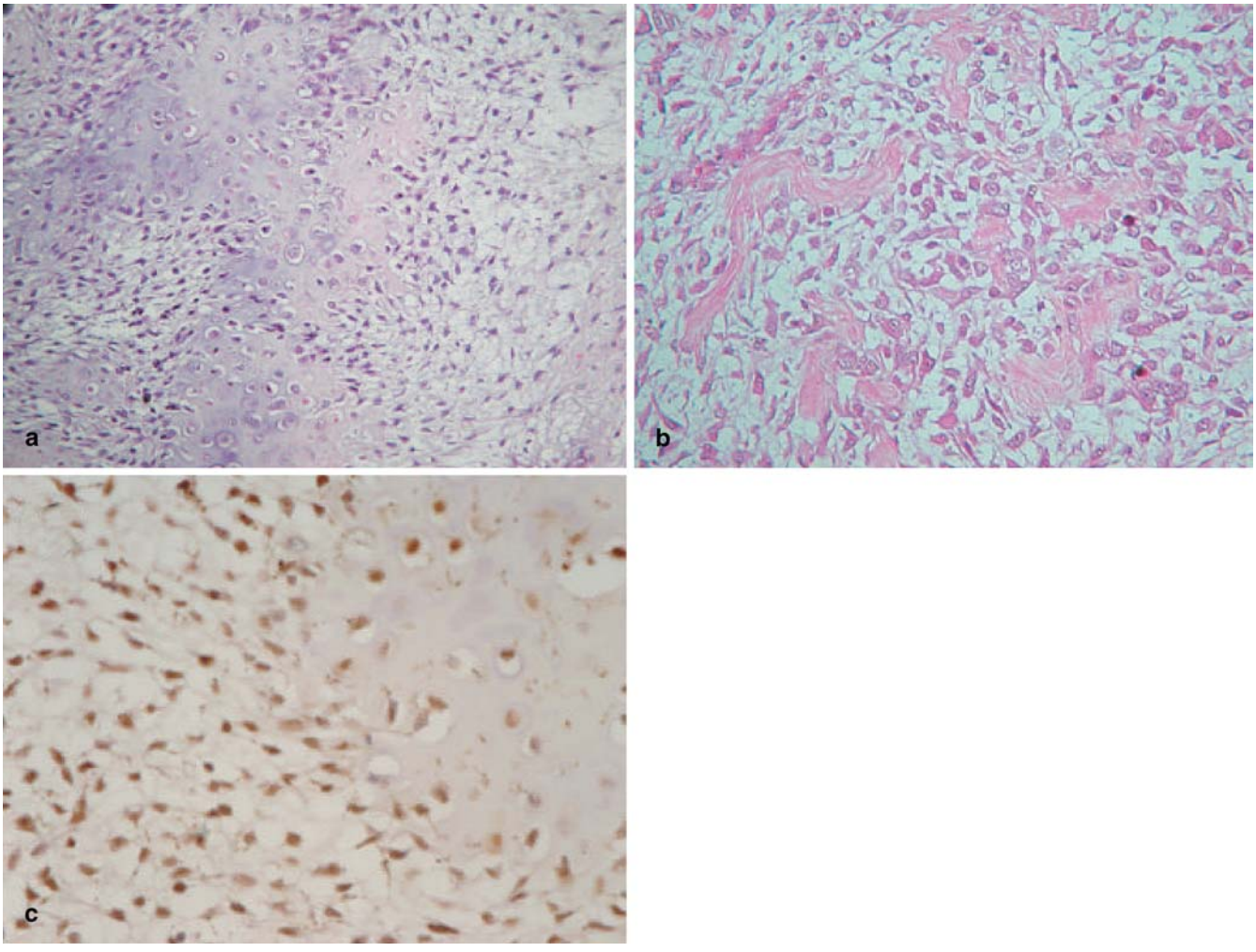

Fig. 2 **a, b** Histological examination revealed a high-grade osteosarcoma comprising pleomorphic, polygonal, discohesive cells, some embedded in osteoid, with hyperchromatic nuclei showing numerous mitotic figures (hematoxylin and eosin, original magnification ×100). **c** Immunohistochemical detection of p53 protein with anti-p53 antibody DO-1. A distinct nuclear reaction is seen in the tumor cells (original magnification ×200)

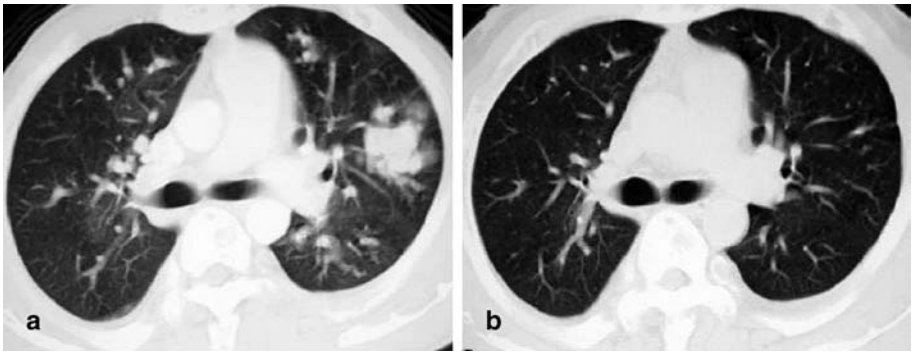

Fig. 3 **a** Computed tomography of chest, March 2001, shows multiple lung metastases. **b** Computed tomography of chest, January 2002, shows dramatic decrease of lung metastasis after eight times high-dose ifosfamide therapy

Materials and methods

Formalin-fixed, paraffin-embedded specimen was processed for routine diagnosis on hematoxylin and eosin (H&E). Immunohistochemical studies were performed on 5-μm-thick formalin-fixed, paraffin-embedded tissue sections. DO1, a murine monoclonal antibody to p53 gene product (Santa Cruz Biotechnology, Inc, Santa Cruz, CA), recognizes residues 21 to 25 in wild-type and mutated forms of p53. Sections were treated in a microwave oven using Antigen Retrieval AR-10 Solution (BioGenex San Ramon, CA) for 5 min. Sections were incubated for 30 min with primary antibody (1:500) at room temperature. The following reactions were performed using mouse ABC Staining System (Santa Cruz Biotechnology, Inc. Santa Cruz, CA) according to the manufacturer's guidelines.

Three tissue sections (5-μm thick) were subjected to DNA preparation using EX-WAX DNA extraction kit (Intergen, Purchase, NY). Each exon (exons 4–8) of the p53 gene was amplified by polymerase chain reaction (PCR). The PCR reaction consisted of 100 ng genomic DNA and 25 pmol of each primer in 50 μl buffer containing 50 μmol/l of dATP, dCTP, dGTP, and dTTP in 20 mmol/l Tris-HCl, 1.5 mmol/l magnesium chloride, and 0.5 U *Taq* polymerase (Takara, Japan). The primers and corresponding annealing temperatures used for amplification were as follows: 4A, 5′-ATCTACAGTCCCCCTTGCCG-3′ and 4B, 5′-GTGCAAGTCACAGACTTGGC-3′ for exon 4 (60°C); 5A, 5′-ATCTGTTCACTTGTGCCCTGACTTTC-3′ and 5B, 5′-ACCCTGGGCAACCAGCCCTGTC-3′ for exon 5 (58°C); 6A, 5′-ACCATGAGCGCTGCTCAGAT-3′ and 6B, 5′-AGTTGCAAACCAGACCTCAG-3′ for exon 6 (60°C); 7A, 5′-CTCCTAGGTTGGCTCTG-3′ and 7B, 5′-GAGGCTGGGGCACAGCAGGCCAGTG-3′ for exon 7 (57°C); 8A, 5′-ACTGCCTCTTGCTTCTCTTT-3′ and 8B 5′-AAGTGAATCTCAGGCATAAC-3′ for exon 8 (58°C). Cycles (n=35) of denaturation (94°C for 60 s), annealing (90 s at 57°C to 60°C) and extension (72°C for 90 s) were performed on an automated thermocycler (PTC-100, MJ Research Inc., South San Francisco, CA). PCR fragments were subjected to direct sequencing using an automated fluorescence sequencer (ABI PRISM 3100 Genetic Analyzer, Applied Biosystems, Foster City, CA).

Results

Immunohistological staining

A distinct nuclear reaction with anti-p53 antibody DO1 was seen in the tumor cells. Approximately 90% of tumor cell nuclei showed positive immunoreaction.

Direct genomic sequencing of exons 4–8

For the analysis of p53 mutations, we amplified five highly conserved regions of the gene corresponding to exons 4–8 using PCR. PCR fragments were sequenced on a fluorescence sequencer. There were no p53 mutations on exons 4–8 in this case.

Discussion

Both OI and osteosarcoma are relatively rare entities. There have been only nine reported cases in the world literature (Table 1) [2, 5, 8, 9, 10, 11, 18, 19], and most authors concluded that osteosarcoma in the setting of OI occurred as a sporadic, rather than a related, event. More important, however, is the fact that osteosarcoma is difficult to diagnose in patients with OI, which was

Table 1 Cases of osteosarcoma with osteogenesis imperfecta

Number	Year	Author	Age of patient (years)	Bone	Type of management	Survival
1	1940	Jewell [7]	49	Pelvis	Amputation	<1 year
2, 3	1967	Klenerman [8]	8	Femur	Palliative	6 months
			13	Femur	Disarticulation	3 years
4	1978	Lasson et al. [9]	13	Femur	Amputation	>6 months
5	1979	B. Reid et al. [18]	14	Femur	Amputation	10 months
6	1979	Rutkowski et al. [19]	15	Femur	Hip disarticulation	8 months
7	1995	Gagliardi et al. [4]	21	Femur	Hemipelvectomy	Not recorded
8	1999	Bedi et al. [2]	37	Scapula	Forequarter amputation	4 months
9	2001	Maiya et al. [10]	6	Femur	Distal femur endoprothesis and total femur later	>6 years
10	2003	Takahashi et al. (unpublished data)	24	Femur	Amputation	>2 years

illustrated in our case. First, there are problems of interpreting old and new changes in radiographs in the OI patient with distorted bony morphology, due to the underlying disease process and recurrent fractures. Second, diagnostic difficulties arise from the similar symptoms between OI and its complications and osteosarcoma. Factors that have been proposed as possible etiological agents in primary bone tumors are radiation, viruses, chemical carcinogens, metal implants, and trauma [17]. Patients with OI have numerous diagnostic radiographs, but the accumulated dosage seemingly required for the development of malignancy is rarely encountered merely by diagnostic procedures and has been more commonly encountered during therapeutic irradiation of a specific site. It is, therefore, possible that radiation played a part in the etiology of these tumors. It is unlikely that metal implantation could be the etiological factor in this patient, because all previously reported cases of similar neoplasms occurred at the site of a metal implant. Finally, previous trauma and fracture have been suggested as a most unlikely factor in the development of osteosarcoma.

Recently, there has been an increasing interest in the extent to which molecular biological markers are involved in the development of osteoblastic tumors. In conventional, highly malignant osteosarcoma, different alterations in tumor suppressor genes (p53, Rb, p16) have been described and are thought to be involved in tumorigenesis [1, 4, 12, 13, 14]. The inactivation of tumor suppressor genes appears to be integral to the development of malignant tumors. Missense mutations in the central core domain of p53 are the most frequent genetic events in diverse tumors. However, the mutational spectrum differs among various types of cancers. In sarcomas, p53 mutations are common but have differed as to the frequency and types of genetic changes. In osteosarcoma, p53 mutations were found in 15–31% [1, 12, 14, 15, 16, 20], and most of them are point mutations in G:C pairs in exon 7 and exon 8 [13]. We used direct sequencing of PCR products from paraffin-embedded samples to screen exons 4–8 for p53 mutations. There were no p53 mutations in this rare osteosarcoma case. However, immunohistochemical detection of the p53 protein in the nucleus was observed. Hall PA et al. reported that the relationship between p53 protein expression and p53 gene mutation is sometimes discrepant [7].

Most investigators conclude that the differential diagnosis between hyperplastic callus formation and osteosarcoma is difficult, because hyperplastic callus and osteosarcoma may show similar clinical, laboratory, radiographic, and histological findings. In our case, retrospective regardful interpretation of radiograph showed discontinuities of the anterior cortex and irregularly distributed osteolytic changes of the distal femur and proximal tibia. Radiographically, hyperplastic callus is seen as a well-circumscribed radiodensity with whirls of new bone formation; however, osteosarcoma tend to expand outward with poorly defined outer margins, due to their aggressive growth [5]. These radiographic findings of cortical bone rarefaction and/or irregularly distributed osteolytic changes warrant a biopsy.

Since both osteosarcoma and exuberant fracture callus of OI histologically exhibit pronounced cellular activity, abundant mitotic figures, and disorganized florid formation of metaplastic cartilage and immature osteoid, a differential diagnosis must be applied with great care. However, partial orderly maturation of cartilage and spindle cell into bone and irregular zones of enchondral ossification of metaplastic cartilage connecting with reactive bone formation rimmed by palisading osteoblasts may suggest the diagnosis of callus of OI [3, 21]. Our diagnosis of osteosarcoma was made from complete lack of maturation and reactive bone formation rimmed by palisaded osteoblasts. Prominent expression of p53 may support the diagnosis of osteosarcoma, although there has been no apparent data on the p53 expression in hyperplastic callus. In addition, progressive extension of osteolytic change within the bones also indicated a neoplastic nature of the current case. Since the differential diagnosis between osteosarcoma and fracture callus of OI has been problematic; therefore, should the existence of this rare lesion be expected, the meticulous inspection of both histological and radiological examinations will become mandatory.

References

1. Andreassen A, Oyjord T, Hovig E, Holm R, Florenes VA (1993) p53 abnormalities in different subtypes of human sarcomas. Cancer Res 53:468–471
2. Bedi HS, Kaufman DV, Choong PF, Slavin JL (1999) Osteosarcoma of the scapula arising in osteogenesis imperfecta. Pathology 31:52–54
3. Dorfman HD, Czerniak B (1998) Reactive and natabolic conditions simulating neoplasm of bone. Bone tumors. Mosby, Missouri, pp 1120–1194
4. Feugeas O, Guriec N, Babin-Boilletot A, Marcellin L, Simon P (1996) Loss of heterozygosity of the RB gene is a poor prognostic factor in patients with osteosarcoma. J Clin Oncol 14:467–472
5. Gagliardi JA, Evans EM, Chandnani VP, Myers JB, Pacheco CM (1995) Osteogenesis imperfecta complicated by osteosarcoma. Skeletal Radiol 24:308–310
6. Greenblatt MS, Bennett WP, Hollstein M, Harris CC (1994) Mutations in the p53 tumor suppressor gene: clues to cancer etiology and molecular pathogenesis. Cancer Res 54:4855–4878
7. Hall PA, Lane DP (1994) p53 in tumour pathology: can we trust immunohistochemistry?—Revisited! J Pathol 172:1–4
8. Jewell FC (1940) Osteogenic sarcoma occurring in fragilitas ossium. Radiology 34:741–743
9. Klenerman L, Ockenden BG, Townsend AC (1967) Osteosarcoma occurring in osteogenesis imperfecta. Report of two cases. J Bone Joint Surg 49:314–323
10. Lasson U, Harms D, Wiedemann HR (1978) Osteogenic sarcoma complicating osteogenesis imperfecta tarda. Eur J Pediatr 129:215–218
11. Maiya S, Grimer RJ, Ramaswamy R, Deshmukh NS (2002) Osteosarcoma occurring in osteogenesis imperfecta tarda. Int Orthop 26:126–128
12. Miller CW, Aslo A, Tsay C, Slamon D, Ishizaki K (1990) Frequency and structure of p53 rearrangements in human osteosarcoma. Cancer Res 50:7950–7954

13. Miller CW, Aslo A, Campbell MJ, Kawamata N, Lampkin BC (1996) Alterations of the p15, p16, and p18 genes in osteosarcoma. Cancer Genet Cytogenet 86:136–142
14. Miller CW, Aslo A, Won A, Tan M, Lampkin B (1996) Alterations of the p53, Rb and MDM 2 genes in osteosarcoma. J Cancer Res Clin Oncol 122:559–565
15. Mousses S, McAuley L, Bell RS, Kandel R, Andrulis IL (1996) Molecular and immunohistochemical identification of p53 alterations in bone and soft tissue sarcomas. Mod Pathol 9:1–6
16. Pompetti F, Rizzo P, Simon RM, Freidlin B, Mew DJ (1996) Oncogene alterations in primary, recurrent, and metastatic human bone tumors. J Cell Biochem 63:37–50
17. Pritchard DJ, Finkel MP, Reilly CA Jr (1975) The etiology of osteosarcoma. A review of current considerations. Clin Orthop 111:14–22
18. Reid BS, Hubbard JD (1979) Osteosarcoma arising in osteogenesis imperfecta. Pediatr Radiol 8:110–112
19. Rutkowski R, Resnick P, McMaster JH (1979) Osteosarcoma occurring in osteogenesis imperfecta. A case report. J Bone Joint Surg Am 61:606–608
20. Toguchida J, Yamaguchi T, Ritchie B, Beauchamp RL, Dayton SH (1992) Mutation spectrum of the p53 gene in bone and soft tissue sarcomas. Cancer Res 52:6194–6199
21. Unni KK (1996) Conditions that commonly simulate primary neoplasm of bone. Dahlin's bone tumors: general aspects and data on 11087 cases, 5th edn. Lippincott-Raven, New York, pp 355–432

Virchows Arch (2004) 444:459–464
DOI 10.1007/s00428-004-0991-7

CASE REPORT

Kumiko Ogawa · Toyohiro Tada · Satoru Takahashi · Naotake Sugiyama · Shingo Inaguma · Seishiro S. Takahashi · Tomoyuki Shirai

Malignant solitary fibrous tumor of the meninges

Received: 20 January 2004 / Accepted: 5 February 2004 / Published online: 10 March 2004

Abstract Increasing numbers of solitary fibrous tumors (SFTs) in the meninges have been reported since this entity was first recognized. While most cases previously reported were considered to be benign, the malignant potential of extrathoracic SFTs has not been excluded. The authors report a rare case of a meningeal SFT with malignant behavior occurring in a Japanese female patient, initially resected when she was 44 years old and recurring in the same place four times during a 26-year follow-up period. A metastatic tumor to the right lung arose 25 years after the resection of the first meningeal tumor and focal invasion into the cerebellum was also observed with her last (5th) meningeal tumor. Immunohistochemical analysis showed all tumors to be diffusely positive for CD34 and negative for EMA, with a so-called "patternless" histological pattern, featuring thin collagen fibers between tumor cells. A focal "staghorn" vascular pattern was also observed. Ki67 (MIB-1) labeling indices and mitosis rates were 3.1±1.2% and less than 1/10 high power fields (HPF) in the first meningeal tumor and 16.1±6.4% and 6/10HPF in the last (5th) one, respectively. Thus, the present case suggests that meningeal SFTs possess malignant potential so that careful long-term follow up is required.

Key words Solitary fibrous tumor · Meninges · Metastasis

K. Ogawa (✉) · S. Takahashi · S. Inaguma · S. S. Takahashi · T. Shirai
Department of Experimental Pathology and Tumor Biology, Nagoya City University Graduate School of Medical Sciences, 1 Kawasumi, Mizuho-cho, Mizuho-ku, 467–8601 Nagoya, Japan
e-mail: kogawa@med.nagoya-cu.ac.jp
Fax: +81-52-8420817

K. Ogawa
Department of Pathology, Nagoya Higashi-Municipal Hospital, Nagoya, Japan

N. Sugiyama
Department of Neurosurgery, Nagoya Higashi-Municipal Hospital, Nagoya, Japan

T. Tada
Department of Pathology, Nagoya City University School of Nursing, Nagoya, Japan

Introduction

The solitary fibrous tumor (SFT) is an uncommon spindle-cell neoplasm, first described as a pleural lesion in 1931 [17]. Extrathoracic SFTs [31] have also been increasingly recognized, including examples in the meninges [1, 2, 4, 5, 7, 8, 10, 15, 20, 21, 22, 23, 24, 25, 26, 27, 28, 29, 30]. Characteristic histological and immunohistochemical features of SFTs in any region are a "patternless" growth pattern, with spindle cells and keloid-like hyalinization, the lesions being intensely and diffusely positive for CD34 antigen and negative for EMA antigen [16]. In the meninges, fibrous meningioma and hemangiopericytoma (HPC) have been recognized as major tumors requiring differential diagnosis from SFTs [5, 10, 24, 29]. Most fibrous meningiomas are positive for EMA antigen, and HPCs are generally only focally and weakly positive for CD34 antigen [24]. The majority of extrathoracic SFTs, including those of meningeal origin, have been described as benign tumors. However, among about forty reported cases of meningeal SFTs, local recurrence was found in six [5, 22, 29, 30], including one case complicated with metastases to the lung and soft tissue [22]. We present here a case of malignant meningeal SFT which progressed after a very long (26 years) and indolent course featuring frequent recurrence and ultimate metastasis to the lung (Table 1). To our knowledge, this is only the second case in the English or Japanese literatures of a meningeal SFT which developed distant metastasis.

Materials and methods

All surgically resected tissues were routinely fixed in 10% formalin, embedded in paraffin and prepared for histological observation. Immunohistochemical analyses were performed by the

Table 1 Sequential changes of the histology and proliferation potential

Year, month	Age	Region (size, ∅ cm)	p53 (%)	Necrosis	Cellularity (/cm^2)	Ki67 (%)	Mitosis (/10 HFP)
1976, June	44	Meninges (3[a])	2.1±0.4	–	94.9±24.0	3.1±1.2	<1
1984, Nov	52	Meninges (1.5[a])	1.1±0.3	+	122.2±5.7	8.0±0.3	5
1995, April	63	Meninges (3)	7.1±1.9	–	93.5±6.3	5.3±1.4	<1
1999, Sept	67	Meninges (3)	13.6±2.4	–	114.0±9.5	8.4±2.1	2
2001, Jan	69	Right upper lung (1.8)	1.3±0.3	+	90.8±12.2	9.8±2.3	5
2002, Aug	70	Meninges (3)	13.2±3.2	–	84.0±18.3	16.1±6.4	6

[a] Tumor size was retrospectively estimated from the pathological specimen

avidin-biotin-peroxidase complex technique using a Vectastain ABC Elite Kit (Vector Laboratories Inc., Burlingame, CA) and diaminobenzidine for visualization of binding. The following antibodies were employed: anti-keratin (AE1/AE3, DakoCytomataion, Glostrup, Denmark, 1:50, with heat-pretreatment), anti-EMA (Zymed Laboratories Inc., South San Francisco, CA, 1:1), anti-vimentin (Ventana Medical Systems, Tucson, AZ, 1:1, with protease-pretreatment), anti-CD34 (Nichirei, Tokyo, Japan, 1:50), anti-Leu-7 (CD57, Ventana, 1:1, with heat-pretreatment), anti-S-100 protein (Dako, 1:400, with trypsin-pretreatment), anti-CD99 (12E7, Dako, 1:100), anti-CD99 (O-13, Santa Cruz Biotechnology Inc., Sant Cruz, CA, 1:40), anti-p53 (CM1, Novocastra Laboratories Ltd., Newcastle upon Tyne, UK, 1:100) and anti-Ki67 (MIB-1, Novocastra, 1:3000, with heat-pretreatment). Labeling indices for p53 and Ki67 and cellularity were generated from counts under a light-microscope in three randomly selected areas (with scale on the ocular, 0.25^2 mm×3 sights, which covered totally 1500~2000 cells) of each tumor, then expressed as mean values with standard deviation.

Case Report

This 70-year-old Japanese woman has been followed up as suffering from repeated local recurrence of atypical meningiomas in her left tentorial area and treated by repeated excision since 1976, when she was 44 years old (Table 1). To date, she has undergone six surgical resections of tumors, including five operations in the left tentoreal area (1976, 1984, 1995, 1999, 2002) and one in the lung (2001) (Fig. 1). Specimens from the last excision of the recurrent meningeal tumor showed histological and immunohistochemical characteristics of SFT, and, therefore, all of the previous slides of meningeal and pulmonary tumors were reviewed histologically and immunohistochemically. The immunohistochemical analyses demonstrated the lesions to be CD34 positive and EMA negative, suggesting a SFT rather than a meningioma. Histologically, a so-called patternless pattern was recognized, with focal staghorn-like vascular channels and no whirl formation, in line with the diagnosis as SFT. The pulmonary lesion was diagnosed as a metastatic tumor.

Clinical history

In 1976, when the patient was 44 years old, she first visited a hospital with the complaint of headache persisting from 2 years previously. At that time, she walked with a shift to her right side and demonstrated an elevation of intra-cranial pressure (over 200 mmH_2O), congestion of the retinal papilla and hemorrhage in her eyeground. A solid tumor, estimated to be 3 cm in diameter, was evident in her left tentorium on computed tomography (CT) scanning. Total resection of the tumor was performed and then histopathological diagnosis of a meningioma with immature features was given. The second meningeal tumor in the same region was noted 7.5 years later when she was 52 years old and again was totally resected. With continuous follow-up and magnetic resonance imagine (MRI) examination, the third (Fig. 1a) and fourth (Fig. 1b) local recurrent tumors were found when she was 63 years and 67 years old, respectively, and resected when they became 3 cm in diameter. She expressed only slight headaches before the operations. When she was 69 years old, a fifth tumor was apparent as a round and well-bordered abnormal shadow in the upper lobe of her right lung on chest X-rays, and CT and MRI confirmed the presence of a 1.8-cm diameter lesion (Fig. 1c). With histological observation of frequent mitosis and atypia indicative of malignancy in frozen sections, the right upper lobe was removed. The sixth tumor in her left sub-occipital region was resected 20 months later, when she was 70 years old (Fig. 1d).

Pathological findings

As shown above and in Fig. 2 and Fig. 3, all six tumors showed basically the same histological character, consisting of moderately hypercellular spindle cells with a "patternless" growth pattern, without apparent whirled cell arrangement or psammoma bodies. The tumors had thick collagen bundles with a hyaline appearance and intercellular collagen (Fig. 2a) and a reticulin network recognized with silver staining. Staghorn-like vascular channels were focally evident (Fig. 2b). Immunohistological analysis (Fig. 2c and d) showed the tumor cells to be completely negative for keratin and EMA and diffusely positive for vimentin and CD34. S-100 protein was negative and Leu-7 was positive. The staining results with anti-CD99 antibodies were contradictory, being positive with the 12E7 clone but negative with the O-13 clone. The lung tumor also had similar histological features with more apparent necrosis, with no attachment to the pleura.

Sequential changes in malignant and/or proliferative features are summarized in Table 1. Focal cysts and/or necroses were more or less observed in all the tumors. The second meningeal tumor and the lung metastatic tumor had larger areas of necrosis (Fig. 3c). All tumors were well demarcated but the last meningeal tumor slightly invaded into the cerebellum (Fig. 3e). Cellularity was mildly high from the first tumor but the Ki67 index and mitosis index were low in the first and third tumors and higher in the later lesions (Table 1 and Fig. 3b, d, f). Labeling indices for p53 protein varied considerably.

Discussion

We have presented here a case of meningeal malignant SFT, which locally relapsed four times, metastasized to the lung and invaded in the cerebellum over a period of

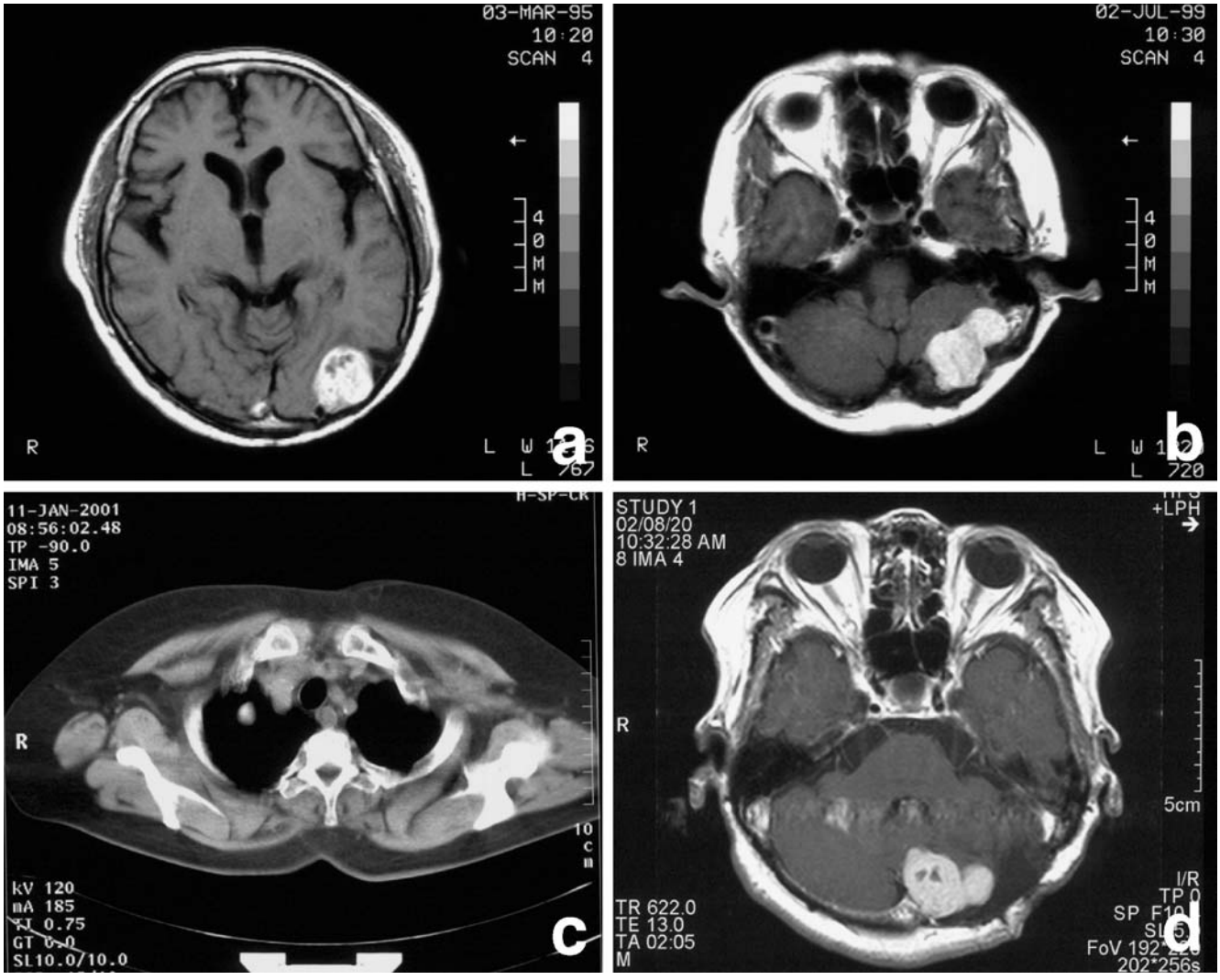

Fig. 1 Magnetic resonance imaging (MRI) observation of the meningeal and lung tumors. **a** Third meningeal tumor found in left tentorium area in 1995. **b** Fourth meningeal tumor found in the same area in1999. **c** Lung metastatic tumor in the right upper lobe in 2001. **d** Fifth meningeal tumor of the left suboccipital region in 2002

26 years. The histopathological and immunohistochemial features of the tumors fit those for SFTs described in previous literature [31], including examples originating in the meninges [5, 24]. Since the first report by Carnerio and co-workers in 1996 [5], retrospective reviews of pathology files of meningioma and/or HPC of the meninges revealed that approximately 30 cases should be reclassified as SFT [5, 29, 30], and overall more than 40 cases have now been reported [1, 2, 4, 5, 6, 7, 8, 10, 20, 21, 22, 23, 24, 25, 26, 27, 28, 29, 30]. Of these, only one case showed metastasis to other organs (lung and soft tissue) [22]. In terms of the biological behavior of SFT, the pathological criteria for determining malignant potential are of obvious clinicopathological interest for pathologists.

Histological features associated with local or distant recurrence of intrathoracic SFTs are reported to include high cellularity, mitotic activity (>4/10 HPF), nuclear pleomorphism, and necrosis [13, 31, 33]. In extrathoracic SFTs, such as those occurring in the abdomen/pelvis, retroperitoneum, groin, trunk, and upper arm, these factors are associated with, but are not by themselves predictive of, aggressive clinical behavior [31]. It seems that there is no strict correlation between morphology and biology [14, 15, 19, 31]. The results of a recent karyotyping study showing tetrasomy 8 to be associated with malignant behavior in the SFT of the pleura [11] might provide a new solution to this issue. In the present case, the first tumor showed hypercellularity and some mitoses. Therefore, according to the histological criteria mentioned above, the tumors had an aggressive nature and malignant potential from the beginning. Of importance is the very long duration between surgical removal of the first tumor and the second tumor occurrence, and between the first tumor and lung metastasis (7.5 years and 25 years, respectively). The mitotic index and the Ki67 labeling

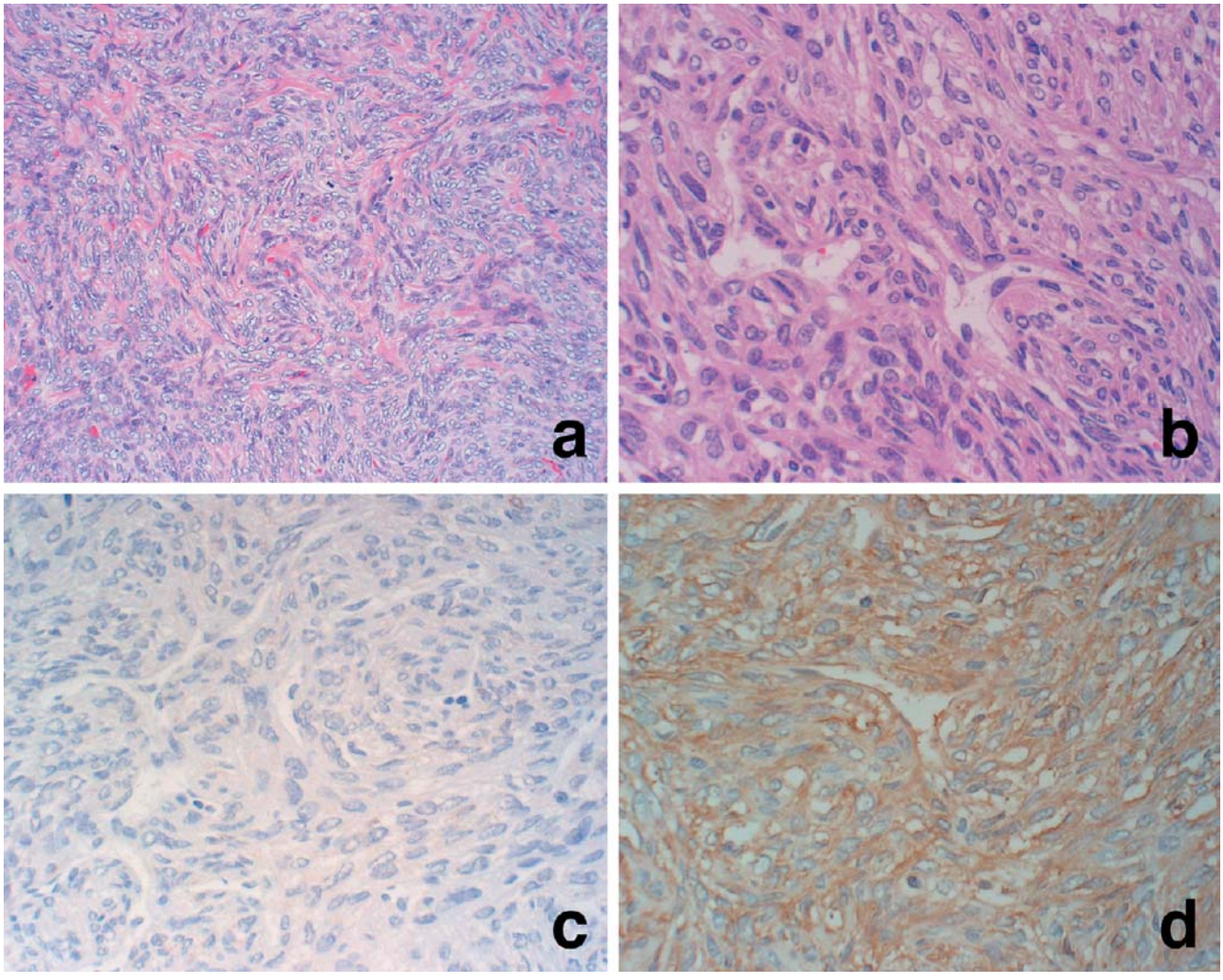

Fig. 2 Histopathological and immunohistochemical findings for the fifth meningeal tumor. **a** Collagen bundles with a hyaline appearance are evident. **b** Staghorn-like vascular channels are focally present. **c** Tumor cells are negative for EMA. **d** Tumor cells are diffusely positive for CD34

index were medium in the first tumor and tended to gradually increase with shortening of the interval before recurrence. However, the patient is now (2003, 2 years after surgical excision of the metastatic tumor in the lung) clinically free from distant metastasis. This might mean that the biological nature of meningeal SFT is very indolent, even when atypical histological features are evident. However, meningeal SFT cases with malignant features are very low in number, and the follow-up duration has not been sufficiently long in most cases. Therefore, further clinicopathological analyses are required for clarification.

The confusion surrounding the relationship between the SFT and the HPC may be particularly due to the fact that both show "staghorn" sinusoidal vessels and CD34 positive immunoreactivity, even though HPCs react less strongly and diffusely for CD34 than do SFTs [24]. The tissue patterns of the two lesions appear to coexist in occasional cases, and the border between them is blurred [14]. It is the present consensus that small foci of HPC-like tissue can be accepted in SFT, but the histological overlap is not yet clear. Moreover, while not observed in the present case, not only intrathoracic but also extrathoracic HPC [3, 9] as well as SFT [12] may be sources of hypoglycemia due to the production of an insulin-like growth factor. Intracranial HPCs are reported to have a relatively high rate of recurrence (60–83%) and metastasis (23–28%) [18, 30] and it is difficult to predict malignant potential from cell proliferation indices such as Ki67 or PCNA [32]. Further comparative analysis of links between the presence of HPC-like tissue in a meningeal SFT and malignant behavior is necessary. Another tumor to be differentiated from meningeal SFT is fibrous meningioma but this can generally be achieved on the basis of its positivity for EMA and only weak or negative CD34 staining.

In conclusion, we have experienced a case of SFT derived from the meninges with malignant potential. In

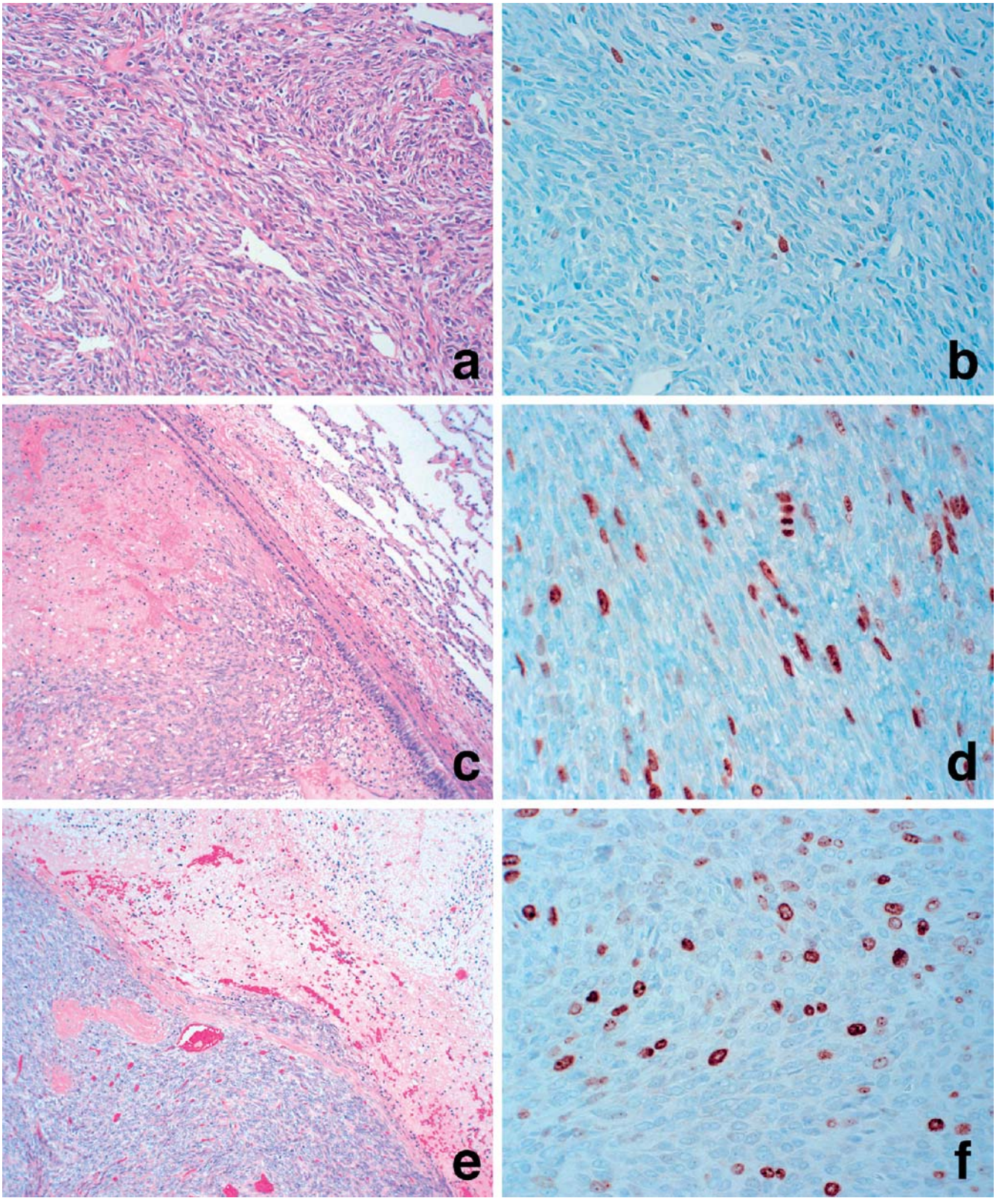

Fig. 3 Histological findings of the sequentially resected tumors (**a**, **c**, **e**; HE staining and **b**, **d**, **f**; anti-Ki67 immunohistochemical staining). **a**, **b** The primary meningeal tumor resected in 1976. Note the hypercellular fibrous nature with a "pattern-less" pattern and a few Ki67 positive cells. **c**, **d** The metastatic tumor found in left lung in 2001. The lesion demonstrates necrosis and pressure on the surrounding lung tissue with many Ki67 positive cells. **e**, **f** The fifth meningeal tumor resected in 2002. Partial invasion into the cerebellum and many Ki67 positive cells are apparent

such lesions, even mitotic and Ki67 indices are quite low, caution and careful follow-up are therefore needed. Regarding meningeal SFTs in the previous literature, so far one case having both recurrence and metastasis to the soft tissues and lungs [22] and five cases having local recurrence [5, 29, 30] have been reported. Considering that the first recurrence was observed 7 years after resection of the primary tumor in the present case, it is conceivable that follow-up in some of the previous cases may not have been long enough to allow the conclusion that they did not recur.

Acknowledgements We appreciate the valuable comments of Dr. Christopher D.M. Fletcher, Brigham and Women's Hospital, Harvard Medical School. This work was supported in part by a grant from the Society for Promotion of Toxicological Pathology of Nagoya, Japan.

References

1. Ahn JY, Shim JY, Yang WI, Kim TS (2001) Meningeal solitary fibrous tumor as an unusual cause of exophthalmos: case report and review of the literature. Neurosurgery 48:1362–1366
2. Barron J, Lownie SP, Lee DH, Hammond RR (2001) June 2001: 61 year old woman with confusion and obtundation. Brain Pathol 11:485–487
3. Bommer G, Altenähr E, Kühnau J, Jr., Klöppel G (1976) Ultrastructure of hemangiopericytoma associated with paraneoplastic hypoglycemia. Z Krebsforsch 85:231–241
4. Brunori A, Cerasoli S, Donati R, Giangaspero F, Chiappetta F (1999) Solitary fibrous tumor of the meninges: two new cases and review of the literature. Surg Neurol 51:636–640
5. Carneiro SS, Scheithauer BW, Nascimento AG, Hirose T, Davis DH (1996) Solitary fibrous tumor of the meninges: a lesion distinct from fibrous meningioma. A clinicopathologic and immunohistochemical study. Am J Clin Pathol 106:217–224
6. Cassarino DS, Auerbach A, Rushing EJ (2003) Widely invasive solitary fibrous tumor of the sphenoid sinus, cavernous sinus, and pituitary fossa. Ann Diagn Pathol 7:169–173
7. Castilla EA, Prayson RA, Stevens GH, Barnett GH (2002) Brain-invasive solitary fibrous tumor of the meninges: report of a case. Int J Surg Pathol 10:217–221
8. Challa VR, Kilpatrick SE, Ricci P, Wilson JA, Kelly DLJ (1998) Solitary fibrous tumor of the meninges. Clin Neuropathol 17:73–78
9. Cotterill AM, Holly JM, Davies SC, Coulson VJ, Price PA, Wass JA (1991) The insulin-like growth factors and their binding proteins in a case of non-islet-cell tumour-associated hypoglycaemia. J Endocrinol 131:303–311
10. Cummings TJ, Burchette JL, McLendon RE (2001) CD34 and dural fibroblasts: the relationship to solitary fibrous tumor and meningioma. Acta Neuropathol 102:349–354
11. de Leval L, Defraigne J-O, Hermans G, Dôme F, Boniver J, Herens C (2003) Malignant solitary fibrous tumor of the pleura: report of a case with cytogenetic analysis. Virchows Arch 442:388–392
12. Dotan ZA, Mor Y, Olchovsky D, Aviel-Ronen S, Engelberg S, Pinthus J, Shefi S, Leibovitch I, Ramon J (1999) Solitary fibrous tumor presenting as perirenal mass associated with hypoglycemia. J Urol 162:2087–2088
13. England DM, Hochholzer L, McCarthy MJ (1989) Localized benign and malignant fibrous tumors of the pleura. A clinicopathologic review of 223 cases. Am J Surg Pathol 13:640–658
14. Guillou L, Fletcher JA, Fletcher CDM, Mandahl N (2002) Extrapleural solitary fibrous tumor and hemangiopericytoma. In: CDM Fletcher, KK Unni, F Mertens (eds) World Health Organization Classification of Tumors Pathology and Genetics of Tumors of Soft Tissue and Bone. IARC Press, Lyon, pp 86–90
15. Hasegawa T, Matsuno Y, Shimoda T, Hasegawa F, Sano T, Hirohashi S (1999) Extrathoracic solitary fibrous tumors: their histological variability and potentially aggressive behavior. Hum Pathol 30:146–173
16. Kempson RL, Fletcher CDM, Evans HL, Hendrickson MR, Sibley RK (2001) Solitary fibrous tumor of the soft tissues. In: J Rosai (ed) Tumors of the soft tissue. A.F.I.P., Washington, D.C., pp 52–55
17. Klemperer P, Rabin CB (1931) Primary neoplasms of the pleura: a report of five cases. Arch Pathol 11:385–412
18. Mena H, Ribas JL, Pezeshkpour GH, Cowan DN, Parisi JE (1991) Hemangiopericytoma of the central nervous system: a review of 94 cases. Hum Pathol 22:84–91
19. Morimitsu Y, Nakajima M, Hisaoka M, Hashimoto H (2000) Extrapleural solitary fibrous tumor: clinicopathologic study of 17 cases and molecular analysis of the p53 pathway. APMIS 108:617–625
20. Nawashiro H (2000) Intracranial solitary fibrous tumor of the meninges. Hum Pathol 31:1536
21. Nawashiro H, Nagakawa S, Osada H, Katoh H, Ohnuki A, Tsuzuki N, Miyazawa T, Shima K, Ogata S, Aida S (2000) Solitary fibrous tumor of the meninges in the posterior cranial fossa: magnetic resonance imaging and histological correlation—case report. Neurol Med Chir 40:432–434
22. Ng HK, Choi PCL, Wong CW, To KF, Poon WS (2000) Metastatic solitary fibrous tumor of the meninges. Case report. J Neurosurg 93:490–493
23. Nikas DC, De Girolami U, Folkerth RD, Bello L, Zamani AA, Black PM (1999) Parasagittal solitary fibrous tumor of the meninges. Case report and review of the literature. Acta Neurochir 141:307–313
24. Perry A, Scheithauer BW, Nascimento AG (1997) The immunophenotypic spectrum of meningeal hemangiopericytoma: a comparison with fibrous meningioma and solitary fibrous tumor of meninges. Am J Surg Pathol 21:1354–1360
25. Prayson RA, McMahon JT, Barnett GH (1997) Solitary fibrous tumor of the meninges. Case report and review of the literature. J Neurosurg 86:1049–1052
26. Rodriguez L, Lopez J, Marin A, Cardozo D, Molina O, Cardozo J (2000) Solitary fibrous tumor of the meninges. Clin Neuropathol 19:45–48
27. Sanno N, Shimura T, Maeda S, Teramoto A (2001) A case of solitary fibrous tumor of the meninges. Brain Tumor Pathol 18:43–47
28. Slavik T, Bentley RC, Gray L, Fuchs HE, McLendon RE (1998) Solitary fibrous tumor of the meninges occurring after irradiation of a mixed germ cell tumor of the pineal gland. Clin Neuropathol 17:55–60
29. Suzuki SO, Fukui M, Nishio S, Iwaki T (2000) Clinicopathological features of solitary fibrous tumor of the meninges: an immunohistochemical reappraisal of cases previously diagnosed to be fibrous meningioma or hemangiopericytoma. Pathol Int 50:808–817
30. Tihan T, Viglione M, Rosenblum MK, Olivi A, Burger PC (2003) Solitary fibrous tumors in the central nervous system. A clinicopathologic review of 18 cases and comparison to meningeal hemangiopericytomas. Arch Pathol Lab Med 127:432–439
31. Vallat-Decouvelaere A-V, Dry SM, Fletcher CDM (1998) Atypical and malignant solitary fibrous tumors in extrathoratic locations. Evidence of their comparability to intra-thoracic tumors. Am J Surg Pathol 22:1501–1511
32. Vuorinen V, Sallinen P, Haapasalo H, Visakorpi T, Kallio M, Jaaskelainen J (1996) Outcome of 31 intracranial haemangiopericytomas: poor predictive value of cell proliferation indices. Acta Neurochir (Wien) 138:1399–1408
33. Witkin GB, Rosai J (1989) Solitary fibrous tumor of the mediastinum: a report of 14 cases. Am J Surg Pathol 13:547–557

Virchows Arch (2004) 444:465
DOI 10.1007/s00428-004-0973-9

LETTER TO THE EDITOR

Edwin N. Beckman

Tumor with features of renal cell carcinoma and of transitional cell carcinoma

Received: 28 November 2003 / Accepted: 10 December 2003 / Published online: 18 March 2004

Sir, There is a precedent for the tumor with features of renal cell carcinoma and of transitional cell carcinoma reported by Terada and associates [2]. The previous report would be hard to discover with a literature search because of the title, "Atypical carcinoma of kidney possibly originating from collecting duct epithelium [1]." The renal medullary neoplasm reported by Chromie, Davis, and DeTure had features both of conventional renal cell carcinoma of the clear cell type and of transitional cell carcinoma, arising from the renal pelvis. Both components were periodic acid-Schiff positive. The authors foresaw the additional methodologies needed to study the lesion. Based upon current standards, the neoplasm would not be classified as a carcinoma of collection duct origin. Their report was, however, a seminal event in the development of the concept of collection duct carcinomas, as it suggested the possible origin of neoplasms from collection ducts.

References

1. Chromie WJ, Davis CJ, DeTure FA (1979) Atypical carcinoma of kidney possibly originating from collecting duct epithelium. Urology 13:315–317
2. Terada T, Inatsuchi H, Yasuda M, Osamura Y (2003) A kidney carcinoma with features of clear cell renal carcinoma and transitional cell carcinoma: a combined renal cell and transitional cell carcinoma? Virchows Arch 443:583–585

A reply to this letter is available at http://dx.doi.org/10.1007/s00428-004-0972-x

E. N. Beckman (✉)
Pathology Department,
Ochsner Clinic Foundation,
New Orleans, Louisiana, 70121 USA
e-mail: ebeckman@ochsner.org
Tel.: +1-504-8423330
Fax: +1-504-8423884

Virchows Arch (2004) 444:466
DOI 10.1007/s00428-004-0972-x

LETTER TO THE EDITOR

Tadashi Terada

Reply to the letter by Dr. E.N. Beckman

Received: 10 December 2003 / Accepted: 10 December 2003 / Published online: 18 March 2004

Sir, I am very grateful to Dr. Beckmann for informing me of a precedent case [1] similar to our previous report [3]. I had not been able to detect the case by computer-aided reference search [3]. Chromie, Davis, and Deture [1] reported in 1979 an atypical kidney tumor with cellular elements of renal cell carcinoma (RCC) and transitional cell carcinoma (TCC). The kidney carcinoma consisted of a mixture of renal clear cell carcinoma-like cells and TCC-like cells [1]. The latter involved the renal pelvis and showed occasional papillary configurations. Both malignant cells were positive with periodic acid-Schiff and negative for epithelial mucin. No definite features were obtained using an electron microscope. They suggested three hypotheses [1]. The first was that the atypical carcinoma was RCC, which strikingly mimicked papillary TCC, projecting the pelvis. The second was that the carcinoma was TCC with tubular features. The third was that the carcinoma originated from the collecting duct epithelium. They preferred the third hypothesis. Our case [3] is very similar to theirs [1]. I admit that their report is a precedent for our case. However, our case is different from collecting duct carcinoma (Bellini duct carcinoma), which shows features of tubular and papillary proliferations of carcinoma cells resembling collecting duct epithelium [2]. In addition, we could not demonstrate that our tumor originated from collecting duct epithelium. In any event, further studies using new methods are required to reveal the histogenesis of such atypical kidney carcinomas with RCC and TCC components.

References

1. Chromie WJ, Davis CJ, Deture FA (1979) Atypical carcinoma of the kidney possibly originating from collecting duct epithelium. Urology 13:315–317
2. Murphy WM, Beckwith JB, Farrow GM (1994) Atlas of tumor pathology. Tumor of the kidney, bladder, and related urinary structures. Third series, Fascicle 11. Armed Forces Institute of Pathology, Washington, DC
3. Terada T, Inatsuchi H, Yasuda M, Osamura Y (2003) A kidney carcinoma with features of clear cell renal carcinoma and transitional cell carcinoma: a combined renal cell and transitional cell carcinoma? Virchows Archiv 443:583–585

This reply refers to the letter to the editor which can be found at http://dx.doi.org/10.1007/s00428-004-0973-9

T. Terada (✉)
Department of Pathology,
Shizuoka Municipal Shimizu Hospital,
Shizuoka, Japan
Fax: +81-54-3361315

Virchows Arch (2004) 444:467–469
DOI 10.1007/s00428-004-0988-2

LETTER TO THE EDITOR

Tomotaka Akatsu · Michiie Sakamoto · Motohide Shimazu · Masaki Kitajima

Pedunculated angiomyolipoma of the liver with a predominant pelioid pattern

Received: 8 October 2003 / Accepted: 5 January 2004 / Published online: 26 March 2004

Sir,

Angiomyolipomas (AMLs) are mesenchymal tumors often described in the kidney and rarely in the liver. Nonomura et al. summarized 52 reported cases of hepatic AML in 1994 [3]. Tsui et al. reported 30 cases of hepatic AML and delineated unusual morphological variants in 1999 [4]. Increasing familiarity with radiological and histological features of this tumor facilitates its diagnosis, and, recently, more cases have been reported. AML can have a variety of imaging and pathological appearances, which are dependent on the proportion of each of the three components. Pedunculated AML of the liver, in which the pedicle arises from the hepatic lobe, has been never described. In this paper, we report the first case of a pedunculated hepatic AML with a predominant pelioid pattern.

A 44-year-old woman was admitted to a local hospital with a chief complaint of dull epigastric pain. Ultrasonography demonstrated a 10-cm well-demarcated tumor with a mosaic pattern in the left lobe of the liver. Contrast-enhanced computed tomography confirmed the low-density tumor with mild heterogeneous enhancement. The patient was referred to our institution for further examination. On physical examination, a firm mass was palpable in the upper middle abdomen. There was mild upper abdominal tenderness. The patient had no prior history of hepato–biliary disease or tuberous sclerosis. Pertinent laboratory data on admission were all normal. Serological tests for hepatitis B and C were negative. Tumor markers, including alpha-fetoprotein, carcinoembryonic antigen, and carbohydrate antigen 19–9 were all within normal limits. Hepatic angiogram disclosed a huge hypervascular tumor and dilated tortuous vessels. T1-weighted gradient-echo magnetic resonance imaging revealed a small fatty component of the tumor. Surgery was performed under the preoperative diagnosis of hepatic AML. However, hepatocellular carcinoma with fatty change could not be completely ruled out. Interestingly, surgical exploration showed a huge, whitish-yellow tumor that protruded from the left lobe of the liver, which was markedly atrophic. Many reddish-purple areas were observed on the tumor surface. On intraoperative frozen section histology, polygonal or rounded cells with clear cytoplasm were arranged in the trabeculae (Fig. 1). The patient underwent a left hepatectomy. Grossly, the resected tumor was connected to the liver by a short pedicle. Bloody areas of various sizes were observed within the tumor (Fig. 2). Histologically, the predominant distribution of pelioid spaces was identified. Pelioid spaces were filled with eosinophilic serous fluid

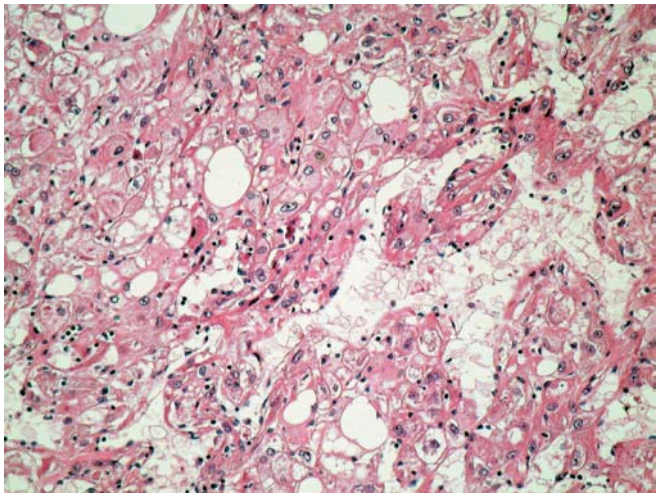

Fig. 1 Microscopic appearance of intraoperative frozen section of the tumor. Polygonal or rounded cells with clear cytoplasm are arranged in the trabeculae (hematoxylin and eosin staining, ×200)

T. Akatsu · M. Shimazu · M. Kitajima
Department of Surgery,
Keio University School of Medicine,
Tokyo, Japan

M. Sakamoto (✉)
Department of Pathology,
Keio University School of Medicine,
35 Shinanomachi, Shinjyuku-ku, 160-8582 Tokyo, Japan
e-mail: msakamot@sc.itc.keio.ac.jp
Tel.: +81-3-33531211
Fax: +81-3-33533290

Fig. 2 Macroscopic feature of the resected tumor. The tumor is connected to the liver by a short pedicle. Bloody areas of various sizes are observed within the tumor

and many red blood cells without distinct endothelial lining (Fig. 3A). An admixture of sheets of epithelioid myoid cells, thick-walled abnormal blood vessels, and islands of mature adipocytes were identified (Fig. 3B). The epithelioid myoid cells had a spider-web cell morphology with clear cytoplasm. Extramedullary hematopoiesis was absent. The underlying liver was normal. Immunohistochemically, the epithelioid and spindle myoid cells were positive for HMB-45 (Fig. 3C) and negative for cytokeratin (CAM5.2). Although the epithelioid myoid cells strongly stained with HMB-45, the spindle myoid cells were weakly reactive. The staining of actin, desmin, and vimentin was strong in spindle myoid cells and weaker in epithelioid myoid cells. The postoperative course was uneventful. The patient survived for 4 years without evidence of recurrence.

Pedunculated AML is a gross anatomical variant of AML. We have reported the first case of pedunculated hepatic AML. Macroscopically, the tumor was closely attached to the neighboring liver by a short pedicle, and the left lobe was remarkably atrophic. Thus, the tumor preoperatively appeared as an intrahepatic tumor in the left lobe of the liver. Although only one malignant case of hepatic AML has been reported to date [2], most AMLs can be managed conservatively because of their low potential for malignant transformation. However, pedunculated hepatic AMLs grow to massive sizes and may rupture spontaneously. In addition, torsion of the pedicle is possible. Thus, we believe that surgical intervention should be undertaken if a diagnosis of pedunculated hepatic AML can be made.

On the intraoperative frozen section histology, the samples incidentally included many areas that showed a trabecular pattern; thus, the tumor was very difficult to differentiate from hepatocellular carcinoma. However, a careful survey of the entire specimen demonstrated a typical pattern that was characterized by an admixture of sheets of epithelioid myoid cells, thick-walled abnormal blood vessels, and islands of mature adipocytes.

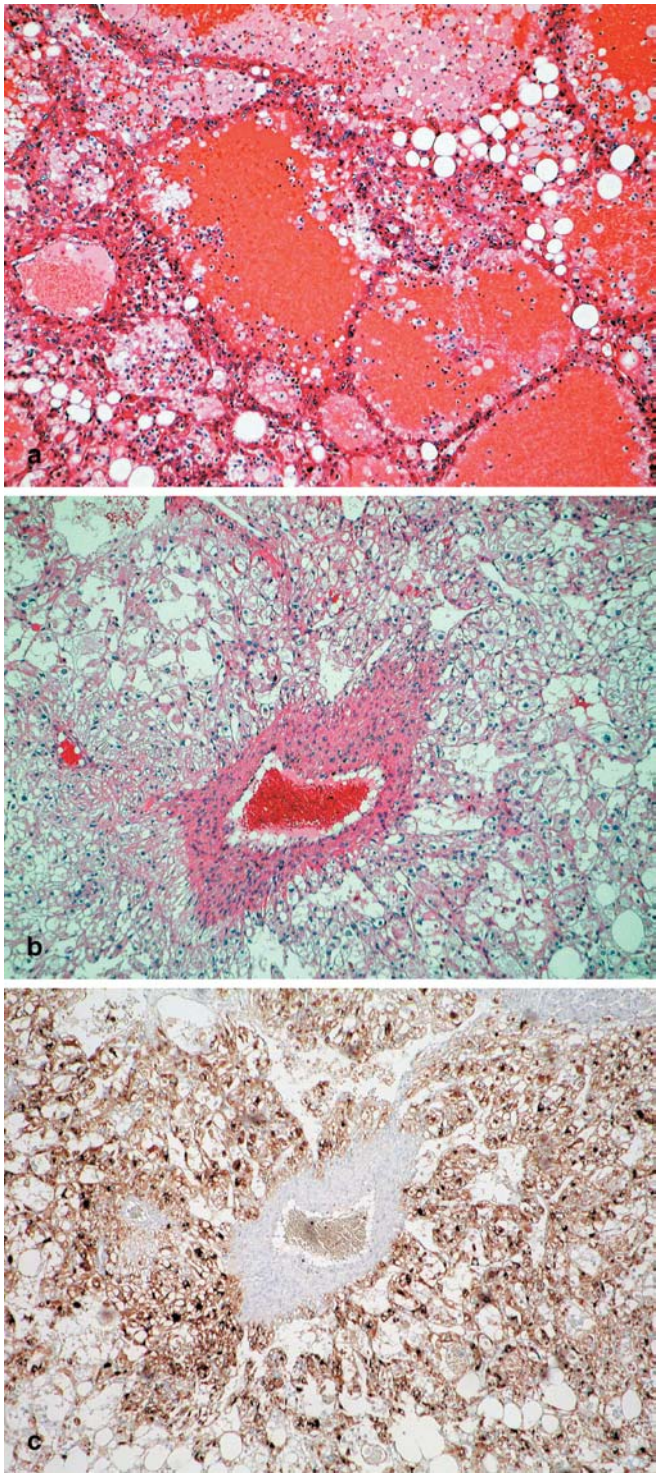

Fig. 3 Microscopic and immunohistochemical appearances of the tumor. **A** Pelioid spaces without distinct endothelial lining are filled with eosinophilic serous fluid and many red blood cells (hematoxylin and eosin staining, ×40). **B** An admixture of sheets of epithelioid and spindle myoid cells, thick-walled abnormal blood vessels, and islands of mature adipocytes. The blood vessels are surrounded by mantles of epithelioid myoid cells and lack an elastic lamina (hematoxylin and eosin staining, ×100). **C** The epithelioid myoid cells strongly stain with HMB-45 (×100)

Uniquely, the tumor predominantly (almost 60% of the maximal cross section of the tumor) showed a peliotic pattern [4]. AML can create various histological appearances within an individual tumor and sometimes poses a diagnostic challenge histologically. An unusual case of AML, as in this case, is the most difficult to diagnose. Recently, fine-needle aspiration biopsy has been reported to be useful in the preoperative diagnosis of this tumor [1]. However, more attention should be paid to its protean morphological appearances when minute samples are interpreted.

References

1. Blasco A, Vargas J, Agusti P, Lopez-Carreira M (1995) Solitary angiomyolipoma of the liver: report of a case with diagnosis by fine needle aspiration biopsy. Acta Cytol 39:813–816
2. Dalle I, Sciot R, de Vos R, Aerts R, van Damme B, Desmet V, Roskams T (2000) Malignant angiomyolipoma of the liver: a hitherto unreported variant. Histopathology 36:443–450
3. Nonomura A, Mizukami Y, Kadoya M (1994) Angiomyolipoma of the liver: a collective review. J Gastroenterol 29:95–105
4. Tsui WMS, Colombari R, Portmann BC, Bonetti F, Thung SN, Ferrell LD, Nakanura Y, Snover D (1999) Hepatic angiomyolipoma: a clinicopathologic study of 30 cases and delineation of unusual morphologic variants. Am J Surg Pathol 23:34–48

Virchows Arch (2004) 444:470–472
DOI 10.1007/s00428-004-0989-1

LETTER TO THE EDITOR

Makoto Sano · Kentaro Kikuchi · Chen Zhao · Michiyo Kobayashi · Yoko Nakanishi · Norimichi Nemoto

Osteoclastogenesis in human breast carcinoma

Received: 15 September 2003 / Accepted: 15 January 2004 / Published online: 11 March 2004

Dear Sir, We herein report the involvement of vascular endothelial growth factor (VEGF) expression and osteoclast-like giant cell (OGC) formation in human breast carcinoma. We believe that OGCs are osteoclasts derived from peripheral blood macrophages, while overexpression of VEGF in the carcinoma cells may play a pivotal role in the osteoclastogenesis.

A 46-year-old Japanese woman had a 30-mm palpable mass at the upper outer quadrant of her left breast. She underwent ultrasonography and mammography. Mammography showed a high-density mass in her left upper outer quadrant, but neither spiculation nor microcalcification were observed. Moreover, an oval-shaped hypoechoic mass with a well-demarcated margin was detected by ultrasonography. These imaging findings suggested that the tumor mass was a benign lesion, and the patient was suspected of having a fibroadenoma. She underwent fine-needle aspiration from the breast lesion, from which the cytological diagnosis was a suspected carcinoma with OGCs. The patient underwent conservative surgery of the left breast with dissection of the tumor and lymph nodes.

Gross macroscopic analysis of the resected surface of the 25×25×20-mm nodule showed a yellowish solid appearance with a well-circumscribed margin, but a part of the peripheral margin of the tumor appeared dark brownish. Microscopically, the major histological pattern of the tumor was invasive ductal carcinoma, papillotubular carcinoma, with OGCs being frequently observed in the fibroblastic or hemorrhagic vascular stroma as well as in abutted carcinoma nests or the glandular lumen (Fig. 1a). Moreover, severe hemorrhage and infiltration of hemosiderin-laden macrophages were observed in the dark-brownish and yellow-brownish lesions. Lymph-node metastasis was microscopically seen in one-fourteenth of excised lymph nodes, while carcinoma metastasis was accompanied by an OGC component.

To determine the characteristics of the carcinoma and OGCs, we performed immunohistochemical analysis (Table 1). OGCs were immunoreactive for anti-CD68 (monoclonal, 1:80; Dako Japan) (Fig. 1b), but not for antibodies to epithelial markers, such as cytokeratin (monoclonal, 1:50; Dako Japan) and epithelial membrane antigen (EMA, monoclonal, 1:50; Dako Japan). These results suggest that OGCs are derived from macrophages. Progesterone receptor (monoclonal, 1:50; Dako Japan) was detected in the nuclei of carcinoma cells, whereas estrogen receptor (monoclonal, 1:50; Dako Japan) p53 (monoclonal, 1:100; Dako Japan) and c-erbB2 (monoclonal, 1:100; Nichirei Co.) were under the detectable level. Of the carcinoma nuclei, 22% were positive for a proliferation marker Ki-67 (monoclonal, 1:25; Dako Japan). These bodies of evidence indicated that the carcinoma cells were at a biologically low grade of malignancy compared with other subtypes of breast carcinomas.

To elucidate the hypervascular stroma and OGC formation in breast carcinoma, we determined the expression of VEGF and VEGF receptors. An antibody to endoglin (CD105, monoclonal, 1:100; Dako, catalyzed signal amplification system) revealed dense angiogenesis in the stroma (Fig. 1c). Prominent VEGF (polyclonal, 1:100; Santa Cruz Biotechnology) was detected in the carcinoma cells and OGCs, but mononuclear macrophages were negative (Fig. 1d). Flt-1 (VEGFR-1, polyclonal, 1:100; Santa Cruz Biotechnology) was detected in the carcinoma cells and the round OGCs located at the carcinoma lumen, but not detected in the elongated OGCs seen adjacent to the periphery of carcinoma nest (Fig. 1e).

M. Sano (✉) · K. Kikuchi · M. Kobayashi · Y. Nakanishi · N. Nemoto
Department of Pathology,
Nihon University School of Medicine,
30-1 Ohyaguchi-kamimachi, Itabashi-ku, 173-8610 Tokyo, Japan
e-mail: msano@med.nihon-u.ac.jp

N. Nemoto
Pathology Laboratory,
Nihon University Itabashi Hospital,
30-1 Ohyaguchi-kamimachi, Itabashi-ku, 173-8610 Tokyo, Japan

C. Zhao
Department of Microbiology,
Keio University School of Medicine,
35 Shinanomachi, Shinjuku-ku, 160-8582 Tokyo, Japan

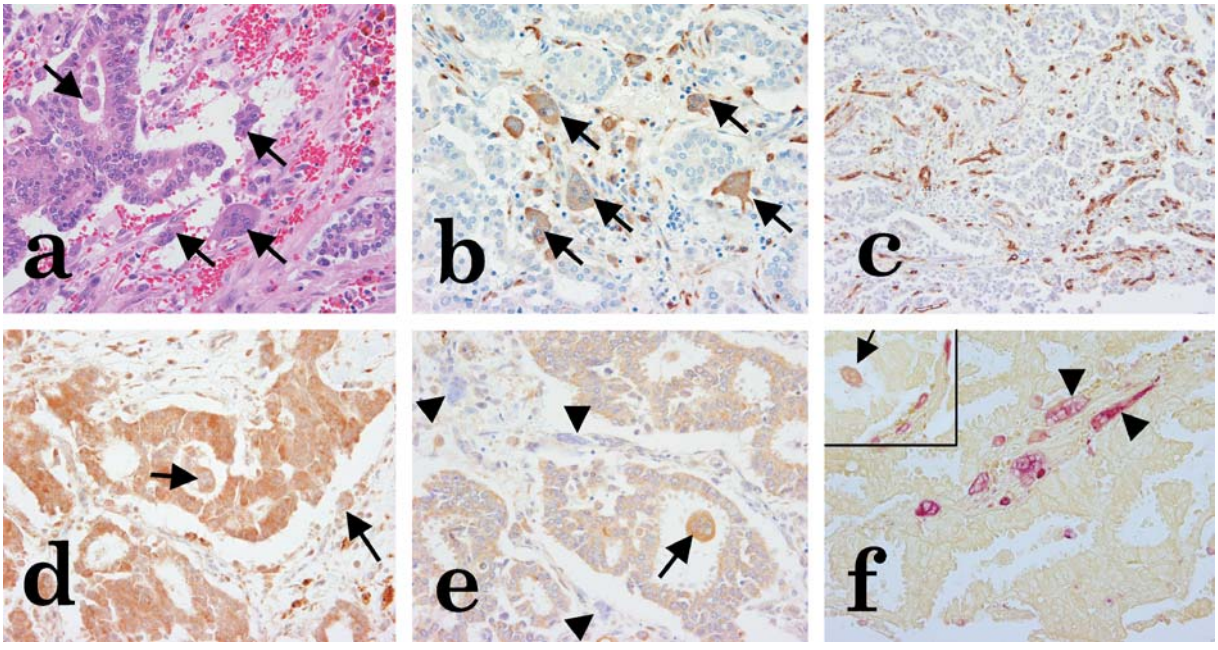

Fig. 1 The breast tumor shows invasive ductal carcinoma, papillotubular carcinoma with osteoclast-like giant cells (OGCs) (**a**, HE stain, *arrows*). OGCs (*arrows*) and mononuclear cells are positive for CD68 (**b**). Low-power magnification shows hypervascular stroma with CD105 (**c**). Vascular endothelial growth factor is expressed in the OGCs (*arrows*) as well as carcinoma cells (**d**). Flt-1 is present in the carcinoma cells and the round OGCs that have located at the carcinoma lumen (*arrow*), but elongated OGCs are negative (**e**, *arrowheads*). Tartrate-resistant acid phosphatase activities are detected in the elongated OGCs (*arrowheads*) and focal mononuclear cells (**f**), while the round OGCs in the lumen are weakly positive (*arrow*, *separate column*)

Table 1 Immunohistochemical analysis of breast carcinoma with osteoclast-like giant cells (OGCs). *EMA* epithelial membrane antigen, *ER* estrogen receptor, *PR* progesterone receptor, *VEGF* vascular endothelial growth factor, *TRAP* Tartrate-resistant acid phosphatase

Cell types	CD68	EMA	Keratin	ER	PR	Ki-67	p53	c-erbB2	VEGF	Flt-1	TRAP
Carcinoma cells	−	+	+	−	+	+	−	−	+	+	−
Macrophages	+	−	−	−	−	−	−	−	−	+	+/−
OGCs (round cells)	+	−	−	−	−	−	−	−	+	+	±
OGCs (elongated cells)	+	−	−	−	−	−	−	−	+	−	+

Meanwhile, KDR/Flk-1 (VEGFR-2, monoclonal, 1:100; Santa Cruz Biotechnology) was not observed in the carcinoma cells, OGCs, or macrophages. Tartrate-resistant acid phosphatase (TRAP, Sigma diagnostic Inc.), an osteoclast marker, was strongly present in the elongated OGCs and occasional mononuclear cells (Fig. 1f). The round OGCs in the carcinoma lumen were weakly positive for TRAP.

To determine the detailed expression level of VEGF and Flt-1, we performed reverse-transcription polymerase chain reaction (RT-PCR) analysis after microdissection (LS-337; Cell Robotics International Inc.). The primers used were 5′-ATGCGGATCAAACCTCACC-3′ and 5′-ATCTGGTTCCCGAAACCCTG-3′ for VEGF, 5′-GGCCTCTGATGGTGATTGTT-3′ and 5′-TTGGTTTCTTGCCTTGTTCC-3′ for Flt-1 and 5′-AAACTGGAACGGTGAAGGTG-3′ and 5′-GTGGCTTTTAGGATGGCAAG-3′ for β-actin. Each PCR regime involved a 95°C, 5-min initial denaturation step, followed by 50 cycles at 54°C for 1 min (VEGF) or at 60°C for 1 min (Flt-1 and β-actin), and then at 72°C for 1 min on a Gene Amp PCR system 2100 (Perkin Elmer). In RT-PCR analysis, the isoform 121 of VEGF was predominantly detected in the carcinoma cells and OGCs, but other isoforms were not detected (Fig. 2). Flt-1 was detected in carcinoma cells, but not in OGCs. These RT-PCR analysis results were essentially compatible with the immunohistochemical investigations.

Peripheral blood monocytes/macrophages have recently been reported to differentiate into osteoclasts and promote bone resorption in the presence of several cytokines or growth factors. The CD14-positive monocytes differentiate into TRAP-positive osteoclasts through a combination of macrophage colony-stimulation factor (M-CSF) and interleukin-4 [1]. Moreover, the addition of granulocyte-macrophage colony-stimulating factor stimulates the terminal differentiation of monocytes/macrophages into osteoclasts that co-expressed CD-68, the osteoclast marker vitronectin receptor and TRAP [2]. Meanwhile, recombinant VEGF induces osteoclast formation in osteopetrotic mice that are deficient in M-CSF [4]. Cultured osteoclasts derived from bone marrow

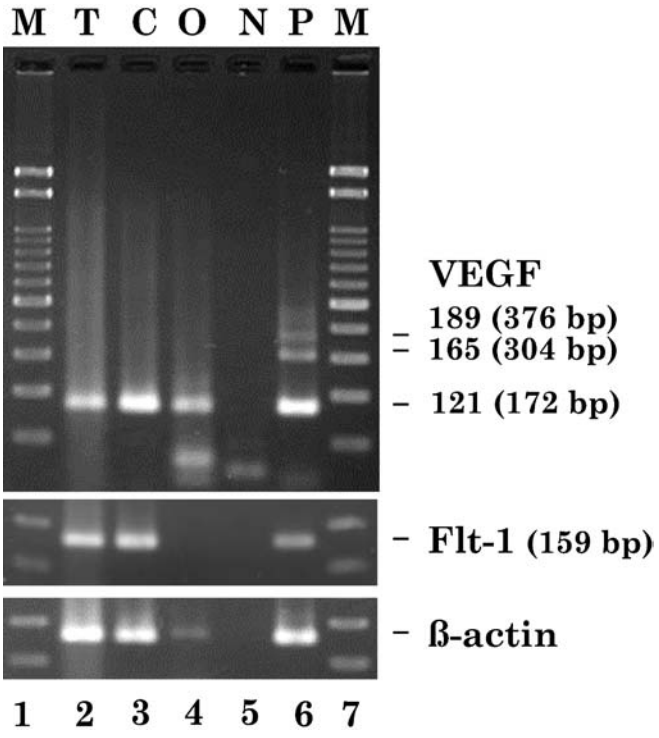

Fig. 2 Total sample (*T*), carcinoma component (*C*) and osteoclast-like giant cells (*O*) were collected with the laser microdissection system. The transcripts of vascular endothelial growth factor isoforms: 121, 165, and 189 (*upper column*) and Flt-1 (*middle column*) were detected by reverse-transcription polymerase chain reaction amplification. The presence of β-actin served as a loading control (*lower column*). Negative (no template) and positive controls (KATO III gastric carcinoma cell line) are indicated as *N* and *P*, respectively. Molecular weight markers (*M*, 100 base pairs ladders) are shown in *lane 1* and *lane 7*

promote bone resorption by the dose-dependent addition of VEGF [3]. Moreover, under VEGF, cultured osteoclasts demonstrate partially delayed cell death.

In this paper, we hypothesized that VEGF is associated with OGC formation in breast carcinomas. The excess VEGF, which is secreted from the carcinoma cells, promotes tumor angiogenesis and migration of macrophages, which are double positive for Flt-1 and CD68. These macrophages accumulate and fuse with each other, and they differentiate into TRAP-positive OGCs in the presence of VEGF. TRAP activities are upregulated during the macrophage differentiation into osteoclasts, whereas Flt-1 is reduced through the process of differentiation.

In conclusion, OGCs in breast carcinoma are osteoclasts that are terminally differentiated from macrophages, and the study also shows that high expression of VEGF in carcinoma cells is, at least, possibly essential for osteoclastogenesis.

Acknowledgments We obtained KATO III gastric carcinoma cell line from Cell Resource Center for Biomedical Research, Tohoku University. This work was supported by a grant from the Kanagawa Academy of Science and Technology Research Grants Ministry of Education to M.S. and by Nihon University Research Grant for Assistants and Young Researchers to M.S.

References

1. Akagawa KS, Takasuka N, Nozaki Y, Komuro I, Azuma M, Ueda M, Naito M, Takahashi K (1996) Generation of CD1+RelB+ dendritic cells and tartrate-resistant acid phosphatase-positive osteoclast-like multinucleated giant cells from human monocytes. Blood 88:4029–4039
2. Heinemann DE, Siggelkow H, Ponce LM, Viereck V, Wiese KG, Peters JH (2000) Alkaline phosphatase expression during monocyte differentiation. Overlapping markers as a link between monocytic cells, dendritic cells, osteoclasts and osteoblasts. Immunobiology 202:68–81
3. Nakagawa M, Kaneda T, Arakawa T, Morita S, Sato T, Yomada T, Hanada K, Kumegawa M, Hakeda Y (2000) Vascular endothelial growth factor (VEGF) directly enhances osteoclastic bone resorption and survival of mature osteoclasts. FEBS Lett 473:161–164
4. Niida S, Kaku M, Amano H, Yoshida H, Kataoka H, Nishikawa S, Tanne K, Maeda N, Kodama H (1999) Vascular endothelial growth factor can substitute for macrophage colony-stimulating factor in the support of osteoclastic bone resorption. J Exp Med 190:293–298

Virchows Arch (2004) 444:473–476
DOI 10.1007/s00428-004-0990-8

LETTER TO THE EDITOR

Juan B. Laforga

Salivary duct carcinoma with neuroendocrine features

Received: 1 September 2003 / Accepted: 21 December 2003 / Published online: 11 March 2004

Sir, Salivary duct carcinoma (SDC) is a highly aggressive salivary gland neoplasm affecting older, male patients and arising in the major salivary glands. The most frequent location is the parotid gland, followed by submandibular glands or minor salivary-gland sites [10]. Clinically, these tumors are characterized by aggressive behavior with early distant metastasis, local recurrence, and high mortality. Some studies, including three large series [1, 2, 6], characterized the clinical pathological features as a distinct entity. We describe a SDC with oncocytic-like appearance and morphological and immunohistochemical features of endocrine differentiation, studied by means of fine-needle aspiration (FNA) and immunohistochemistry.

A 75-year-old man presented with a rapidly enlarging tumor mass in his right parotid gland. There was no clinical evidence of hormonal secretion. A FNA disclosed three-dimensional groups of epithelial cells with discohesion. The individual cells were large and polyhedrical, with abundant granular cytoplasms and atypical nuclei (Fig. 1). A diagnosis of malignancy, consistent with a high-grade carcinoma was made. The patient suffered a right facial palsy and, thereafter, a radical parotidectomy with regional lymph-node dissection, followed by the administration of local radiotherapy (50 Gy). The postoperative course was uneventful, and the patient is alive and well 5 years after surgery. Grossly, the parotid gland was replaced by a multicentric tumor mass measuring 5×3×2 cm, whitish and with hard consistency. Microscopically, the tumor exhibited a mixture of patterns such as solid with few foci of comedonecrosis, cribiform, trabecular and a striking organoid pattern of growth (Fig. 2). The cells were of large size, containing round and central nuclei and with abundant eosinophilic and granular cytoplasm (Fig. 3), which reacted positively with Grimelius stain. The phosphotungstic acid hematoxylin (PTAH) was negative. The mitotic count was 12/10 HPF with atypical mitoses. Frequent lymphatic perineural invasion was observed. The radical right neck dissection contained 12 lymph-node metastases. Immunohistochemical study showed strong positivity to pancytokeratin (AE1/AE3), cytokeratin 7, GCDFP-15 (Fig. 4) and C-erbB-2 (3+). Chromogranin-A and synaptophysin stains disclosed a diffuse cytoplasmatic granular positivity (Fig. 5). Mib-1 and topoisomerase II alpha was positive in more than 20% of nuclei. The nuclei overexpressed p53 in more than 20% of the cells. Androgen receptors (ARs) were positive, while estrogen and progesterone receptors were both negative. Cytokeratin 20, S-100 protein and antimitochondrial antigen were uniformly negative.

Cytological features of SDC include loose clusters of cribiform and gland-like aggregates, with monomorphic polygonal cells containing round nuclei with abundant, finely granular cytoplasm, indistinct nucleoli and a background of necrosis.

We draw attention to an oncocytic-like appearance in SDC. Interestingly, 4 of 21 cases in one series exhibited ill-defined eosinophilic cytoplasm and scant or absence of necrosis, as in our case [4]. Actually, the monomorphism of the individual cells with large and eosinophilic granular cytoplasm led us to consider an oncocytic carcinoma (OC) in the differential diagnosis. Separation of SDC from OC lies in the demonstration in the later tumor, the presence of cytoplasmatic granules composed of a large number of mitochondria, which can be highlighted by PTAH, antimitochondrial antigen stain or electron microscopy. Distinction between SDC and large cell-type undifferentiated carcinoma may be difficult and is based on the lack of glandular pattern, and negativity for GCDFP-15 and AR expression.

The immunohistochemical profile of SDC shows positivity for cytokeratins, GCDFP-15 [3, 6, 9] and ARs. Between 70% and 90% of SDCs exhibit AR positivity, indicating hormonal influences, which may have therapeutic benefits. Similarly, in apocrine carcinoma of the breast, ARs are positive in 22% of tumors analyzed, while both estrogen and progesterone receptor expression is negative. Our case also showed intense

J. B. Laforga (✉)
Department of Pathology,
Hospital Marina Alta,
Ptda Plana Est 4, 03700 Denia Alicante, Spain
e-mail: laforga_jua@gva.es

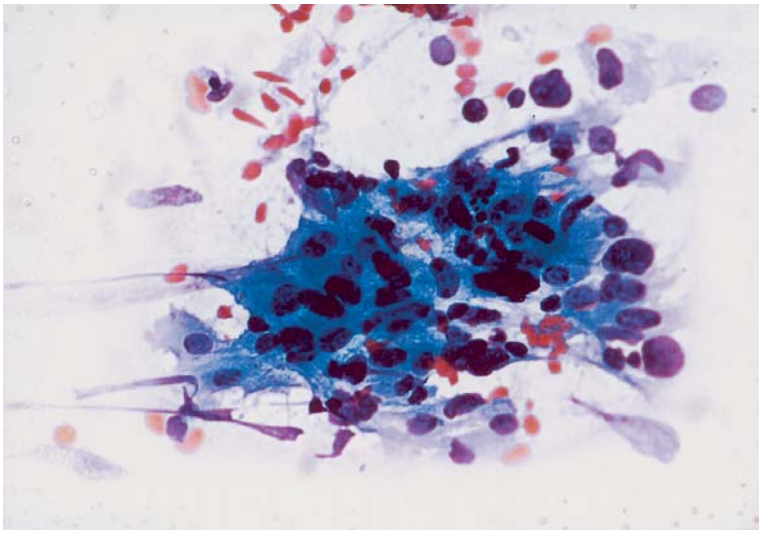

Fig. 1 Fine-needle aspiration showing loose aggregates of atypical epithelial cells containing round to oval nuclei and granular cytoplasm (original magnification, Papanicolaou stain ×250)

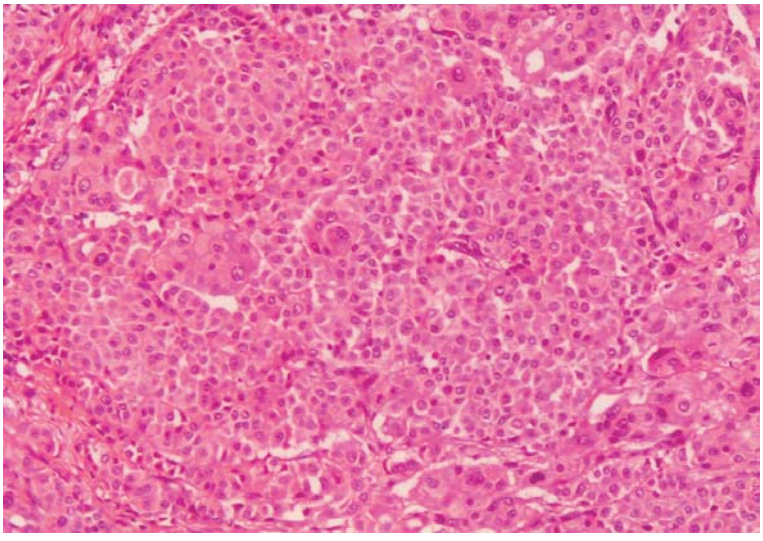

Fig. 2 The tumor showed an organoid pattern with striking granular and glassy cytoplasm (original magnification, HE ×250)

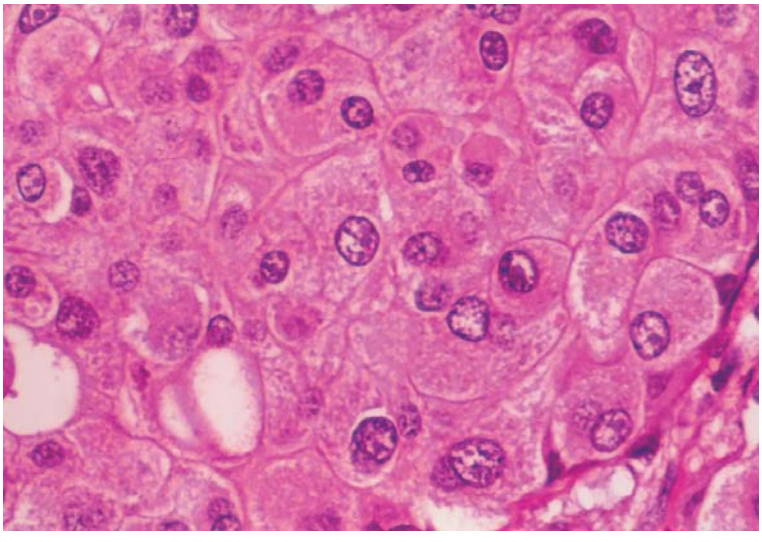

Fig. 3 The tumor cells were large and pleomorphic with eosinophilic cytoplasm (original magnification, HE ×400)

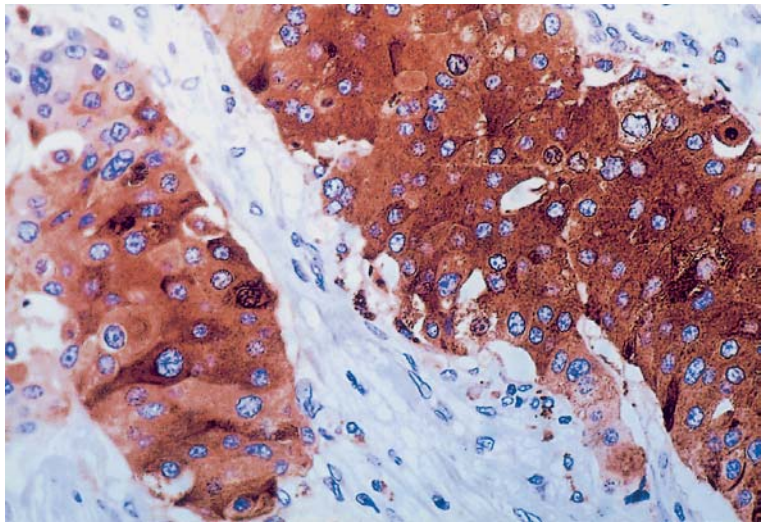

Fig. 4 The cells showed intense and diffuse cytoplasmic positivity for GCDFP-15 stain (original magnification, GCDFP-15 ×250)

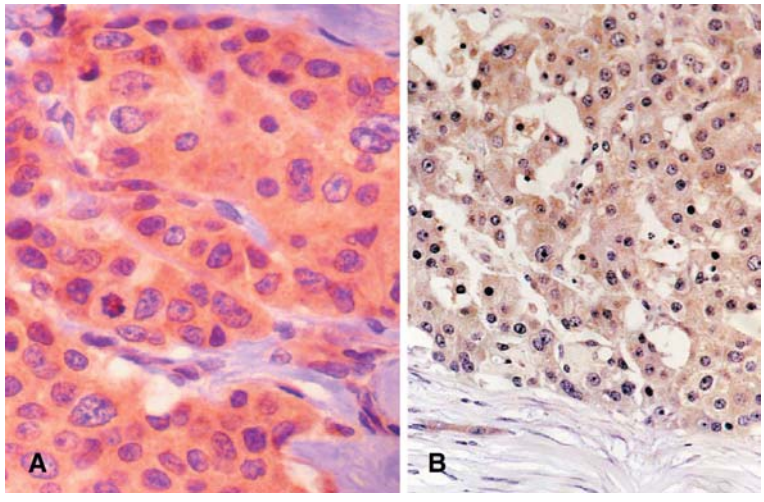

Fig. 5 Immunostaining is positive for chromogranin-A (**A**), and synaptophysin (**B**) (original magnification, chromogranin-A and synaptophysin stain ×250)

positivity for CK 7, which fulfills the phenotype CK 7+/CK 20– of salivary-gland tumors. This fact may be useful in the differential diagnosis with other head and neck tumors. The expression of GCDFP-15 is also shared with apocrine ductal infiltrating carcinoma of the breast and its variants. Morphologically, both tumors bear also a striking morphological resemblance with large cells containing granular or "glassy" eosinophilic cytoplasm. Because of the striking similarity with ductal infiltrating carcinoma of the breast, it is not surprising that SDC may disclose endocrine differentiation. In female mammary gland, the incidence of endocrine features varies from 3% to 25%. The hallmark of these tumors consists of dense core granules documented ultrastructurally and argyrophilic cytoplasmatic granules highlighted with histochemical techniques, such as Grimelius stain, or demonstrating chromogranin and synaptophysin expression. Cytologically, the cells are monomorphic with granular cytoplasm rich in neuroendocrine (NE) granules and round and uniform nuclei, in addition to occasional fine vessels [5]. According to Sapino et al. more than 50% of cells must be positive for at least one NE marker (chromogranin A or B and synaptophysin) to define a breast tumor as NE [7]. They classified their series of 47 cases into five types (solid cohesive, alveolar, small cell, solid papillary and cellular mucinous). The comparison of our case with NE breast carcinomas may show some resemblance with the "alveolar type" characterized by solid alveolar-like structures, separated by scanty dense stroma with an infiltrative growth pattern. The cells are large, with a faintly granular cytoplasm. The mitotic count is high. The cells contained chromogranin and/or synaptophysin. In our case, the presence of diffuse positivity for chromogranin and synaptophysin may contribute to explaining the granular eosinophilic appearance of the cells. To the best of our knowledge, the presence of endocrine differentiation in SDC was not investigated in the series recorded in the English literature. In our case, C-erbB-2, topo II and Mib-1 expression were positive, correlating with the aggressive clinical outcome (extra glandular extension and high proliferative activity), and resistance to chemotherapeutic drugs.

Regarding the ominous prognosis in SDC, Simpson et al. reported a series in which up to 70% of patients died of disease within 3 years of diagnosis with widespread metastases. Interestingly 1 of 7 patients was a long-term survivor, although the tumor measured 3 cm and had invasive edges, and the excision was incomplete, it was distinguished by the absence of any necrosis [8]. Similarly, this case here described had a better behavior than the conventional SDC. We suspect that the presence of scanty necrotic areas and the NE differentiation may be relevant for prognosis. Perhaps this is a point for further investigation in future studies.

References

1. Delgado R, Vuitch F, Albores-Saavedra J (1993) Salivary duct carcinoma. Cancer 72:1503–1512
2. Hui KK, Batsakis JG, Luna MA, Mackay B, Byers RM (1986) Salivary duct adenocarcinoma: a high grade malignancy. J Laryngol Otol 100:105–114
3. Kapadia SB, Barnes L (1998) Expression of androgen receptor, gross cystic disease fluid protein, and CD44 in salivary duct carcinoma. Mod Pathol 11:1033–1038
4. Klijanienko J, Vielh P (1998) Cytologic characteristics and histomorphologic correlations of 21 salivary duct carcinomas. Diagn Cytopathol 19:333–337
5. Laforga JBM, López JI (1998) Breast carcinoma with endocrine features. Report of a case with cytologic and immunohistochemical studies. Acta Cytol 42:1017–1021
6. Lewis JE, McKinney BC, Weiland LH, Ferreiro JA, Olsen KD (1996) Salivary duct carcinoma. Clinicopathologic and immunohistochemical review of 26 cases. Cancer 77:223–230
7. Sapino A, Righi L, Cassoni P, Papotti M, Pietribiasi F, Bussolati G (2000). Expression of the neuroendocrine phenotype in carcinomas of the breast. Semin Diagn Pathol 17:127–137
8. Simpson RHW, Clarke TJ, Sarsfield PTL, Babajews AV (1991) Salivary duct carcinoma. Histopathology 18:229–235
9. Wick MR, Ockner DM, Mills SE, Ritter JH, Swanson PE (1998) Homologous carcinomas of the breasts, skin, and salivary glands. A histological and immunohistochemical comparison of ductal mammary carcinoma, ductal sweat gland carcinoma, and salivary duct carcinoma. Am J Clin Pathol 109:75–84
10. Zohar Y, Shem-Tov Y, Gal R (1988) Salivary duct carcinoma in major and minor salivary glands. J Craniomaxillofac Surg 16:320–323

Virchows Arch (2004) 444:477–479
DOI 10.1007/s00428-004-0994-4

LETTER TO THE EDITOR

Triantafyllia Koletsa · Vassiliki Kotoula · Prodromos Hytiroglou · Panayiotis Spanos · Constantine S. Papadimitriou

Synovial sarcoma of the heart

Received: 16 December 2003 / Accepted: 16 February 2004 / Published online: 11 March 2004

Sir,

Synovial sarcoma (SS) is the fourth most common type of soft-tissue sarcoma, and usually occurs in the paraarticular regions of the extremities [10]. Despite its name, this tumor is uncommon in joint cavities, while it may be encountered in areas with no apparent relationship to synovial structures, such as the parapharyngeal region, abdominal wall, pleura and heart. In a search of the literature, we identified only nine cases of primary SS of the heart [1, 2, 3, 4, 6, 7, 8, 9], four of which arose in the right atrium and formed polypoid masses [1, 4, 8, 9].

SSs are composed of two distinct types of cells: epithelial cells, resembling those of carcinoma, and spindle cells, similar to those of fibrosarcoma [10]. Depending on the relative prominence of the two cellular elements and the degree of differentiation, SSs are classified into four categories: biphasic, monophasic fibrous, monophasic epithelial, and poorly differentiated. Whereas the biphasic type is readily recognizable by the coexistence of the two cell types, the diagnosis of the other three types of SS often requires the input of immunohistochemical and molecular methods. SS is characterized by a specific chromosomal translocation, t(X;18)(p11.2;q11.2), involving the SYT gene on chromosome 18 and one of the SSX genes (SSX1, SSX2 or SSX4) on the X chromosome.

We report a case of monophasic fibrous SS of the right atrium. The patient was a 28-year-old man who presented with facial edema, distention of neck veins and systemic hypertension (170/120 mmHg). His past medical history was unremarkable. Magnetic resonance imaging of the chest revealed a polypoid mass in the apex of the right atrium, which on echocardiogram measured 2.9 cm in greatest dimension. Transesophageal echocardiogram confirmed the presence of an atrial tumor extending to the superior vena cava. Work-up of the patient was negative for metastases. A sternotomy was performed; the tumor was excised in pieces and sent for histological examination.

On gross examination, the tumor fragments were polypoid, white-pink and soft. The cut surfaces had myxoid or elastic consistency. Frozen section examination revealed a high-grade spindle-cell sarcoma. On permanent sections, the tumor had myxoid areas of moderate cellularity alternating with densely cellular areas. The neoplastic cells were arranged in sheets and interlacing fascicles (Fig. 1A). They contained moderately pleomorphic, hyperchromatic nuclei and a small amount of cytoplasm. Mitotic activity was high; three to six mitotic figures per high power field were found in many areas (Fig. 1B). There were multiple small foci in which the tumor cells had ovoid or roundish shape and appeared more cohesive than the surrounding spindle cells, forming clusters. The neoplastic cells infiltrated the wall of the right atrium.

Immunohistochemical stains were performed on paraffin sections with a standard streptavidin-biotin peroxidase method. The tumor cells were diffusely positive for vimentin. The majority of tumor cells were also positive for bcl-2 oncoprotein. The cells in the cohesive clusters were additionally positive for epithelial markers, including cytokeratin cam5.2, cytokeratin AE-1/AE-3 (Fig. 1C) and epithelial membrane antigen (Fig. 1D). Some spindle cells showed mild positivity for smooth muscle actin. Stains for desmin, myoglobin, S-100 protein, CD34 antigen, factor VIII-related antigen, CD99 antigen and CD117 antigen were negative.

The presence of SYT-SSX fusion transcripts was assessed using a reverse-transcription polymerase chain reaction (RT-PCR) method [5] on RNA extracted from paraffin-embedded tumor tissue. RNA extracted from a case of biphasic synovial sarcoma of the thigh was used as

T. Koletsa · V. Kotoula · P. Hytiroglou · C. S. Papadimitriou (✉)
Department of Pathology, Aristotle University Medical School,
540 06 Thessaloniki, Greece
e-mail: kpapadim@med.auth.gr
Tel.: +30-2310-999204
Fax: +30-2310-999229

P. Spanos
Department of Cardiothoracic Surgery,
Aristotle University Medical School,
Thessaloniki, Greece

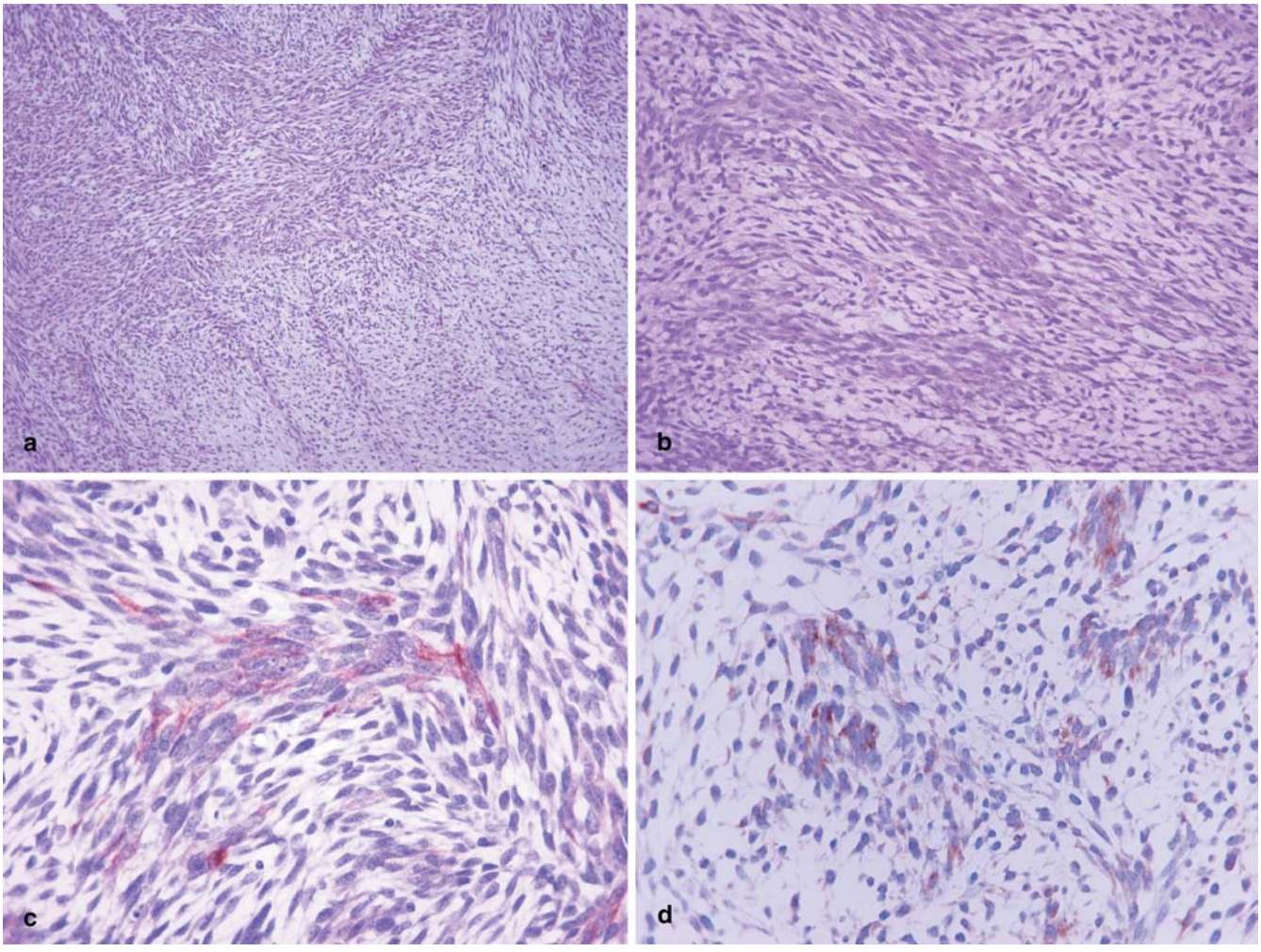

Fig. 1 Histological and immunohistochemical findings. **A** Low-power magnification of a representative area of the tumor showing interlacing fascicles of neoplastic cells. Dense cellularity is present in the *upper left* part of the field, whereas moderate cellularity and a myxoid stroma are seen in the *lower right* part. **B** On high-power magnification, the neoplastic cells demonstrate moderate nuclear pleomorphism and high mitotic activity. In addition, they exhibit a tendency to form cohesive clusters. **C**, **D** The tumor cells in the cohesive clusters show positive immunostaining for cytokeratins AE-1/AE-3 (**C**) and for epithelial membrane antigen (**D**). (**A** H&E, ×40; **B** H&E, ×200; **C**, **D** streptavidin-biotin, ×400)

positive control, RNA from a healthy donor peripheral blood sample as negative control, and PCR grade water as internal negative control for the reaction. The adequacy of cDNA quality was evaluated by RT-PCR for a glyceraldehyde-3-phosphate dehydrogenase gene (GAPDH) transcript. All cDNA samples were run in three dilutions (1:1, 1:10, 1:100). For the assessment of SYT-SSX, the following primer pair was used: forward, 5′-cagcagaggccttatggatatga-3′, and reverse, 5′-ttgtgggccagatgcttc-3′. The reverse primer spans a region common in the SSX1 and SSX2 genes, enabling the identification of SYT-SSX1 and SYT-SSX2 transcripts, which are the most commonly found SYT-SSX fusion products in SSs, without allowing distinction between them. PCR was performed in 50-μl reactions with 2 mM $MgCl_2$, 400 nM of each primer, and 2 U of platinum *Taq* polymerase (Invitrogen, Paisley, United Kingdom), under the following conditions: 95°C for 3 min; then 40 cycles of 95°C (15 s), 60°C (5 s), 72°C (40 s); and finally 72°C for 7 min. The reaction products were electrophoresed in 2.5% agarose gels. All samples were positive for the GAPDH transcript at all dilutions. The 96-bp product of the SYT-SSX transcript was detected at all dilutions of the present case, as well as in the positive control sample (Fig. 2).

Surgical resection of the tumor was followed by radiation therapy. Four months following surgery, the patient developed multiple lung and neck nodules. Two of the lesions were excised. On histological examination, they consisted of metastatic sarcoma displaying slightly increased cellularity and pleomorphism, relative to the primary tumor. Subsequently, the patient was referred to the Medical Oncology Department for chemotherapy.

In the present case, the diagnosis of monophasic fibrous SS was established with the assistance of immunohistochemical and molecular methods. This is the first time that a SYT-SSX fusion transcript was detected in a

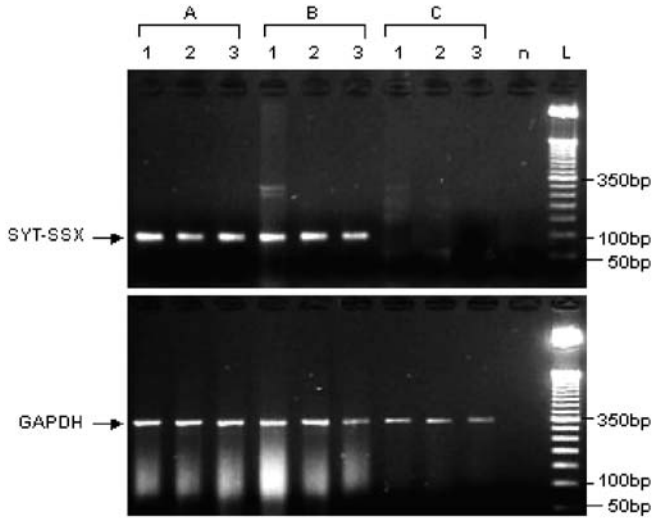

Fig. 2 Reverse-transcription polymerase chain reaction results for the SYT-SSX fusion transcript (*upper panel*) and the glyceraldehyde-3-phosphate dehydrogenase control transcript (*lower panel*). *A* present case; *B* positive control (case of synovial sarcoma of thigh); *C* negative control (peripheral blood from a healthy donor); *n* PCR negative control (H_2O), *L* 50-bp DNA ladder. *1*, *2*, *3* 1:1, 1:10, and 1:100 cDNA dilutions, respectively, in each case

SS of the heart using RT-PCR. This method is very useful in confirming the diagnosis of SS in unusual locations, especially in cases lacking the typical biphasic pattern, as the one we report. In two other cases of SS of the heart, t(X;18) was detected by conventional cytogenetic analysis [6, 7]. Both cases were of the monophasic fibrous type. In seven additional cases reported in the literature (five of the biphasic type, and two of the monophasic fibrous type), cytogenetic or molecular studies were not performed [1, 2, 3, 4, 8, 9]. In those cases, diagnosis was based on the findings of the histological, immunohistochemical and/or ultrastructural examination.

Primary sarcomas of the heart are rare tumors. In a series of 75 sarcomas, only two cases of SS were found [2]. In that series, angiosarcoma was the most frequent sarcoma type (26 cases), followed by undifferentiated sarcoma (18 cases), osteosarcoma (6 cases), malignant fibrous histiocytoma (6 cases), leiomyosarcoma (4 cases) and myxofibrosarcoma (3 cases). It would be of interest to assess undifferentiated sarcomas for presence of SYT-SSX fusion transcripts.

The question then arises what the line of differentiation of cardiac SS is. One previously reported case was considered to have arisen from a mesothelioma of the atrioventricular node [9]; however, no similar cases have appeared in the literature in the 16 years following that publication. Until the line of differentiation of this tumor is elucidated, we may consider SS of the heart a "carcinosarcoma", as has been suggested for this tumor in more common locations [10].

References

1. Bittira B, Tsang J, Huynh T, Morin JF, Hüttner I (2000) Primary right atrial synovial sarcoma manifesting as transient ischemic attacks. Ann Thorac Surg 69:1949–1951
2. Burke A, Cowan D, Virmani R (1992) Primary sarcomas of the heart. Cancer 69:387–395
3. Casselman F, Gillinov M, Kasirajan V, Ratliff N, Cosgrove D (1999) Primary synovial sarcoma of the left heart. Ann Thorac Surg 68:2329–2331
4. Donsbeck AV, Ranchere D, Coinde JM, Le Gall F, Cordier JF and Loire R (1999) Primary cardiac sarcomas: an immunohistochemical and grading study with long-term follow-up of 24 cases. Histopathology 34:295–304
5. Hostein I, Menard A, Bui BN, Lussan C, Wafflart J, Delattre O, Peter M, Benhattar J, Guillou L, Coindre JM (2002) Molecular detection of the synovial sarcoma translocation t(X;18) by real-time polymerase chain reaction in paraffin-embedded material. Diagn Mol Pathol 11:16–21
6. Iyengar V, Lineberger A, Kerman S, Burton N (1995) Synovial sarcoma of the heart—correlation with cytogenetic findings. Arch Pathol Lab Med 119:1080–1082
7. Karn C, Socinski M, Fletcher J, Corson J, Craighead J (1994) Cardiac synovial sarcoma with translocation (X;18) associated with asbestos exposure. Cancer 73:74–78
8. Nicholson AG, Rigby M, Lincoln C, Fisher C (1997) Synovial sarcoma of the heart. Histopathology 30:349–352
9. Sheffield EA, Corrin B, Addis BJ, Gelder C (1988) Synovial sarcoma of the heart arising from a so-called mesothelioma of the atrioventricular node. Histopathology 12:191–202
10. Weiss SW, Goldblum JR (2001) Enzinger and Weiss's soft tissue tumors, 4th edn. Mosby, St. Louis, pp 1483–1509

Virchows Arch (2004) 444:480–481
DOI 10.1007/s00428-004-0995-3

LETTER TO THE EDITOR

Takahiro Kawakami · Keisei Okamoto · Hiroyuki Sugihara · Takanori Hattori · Anthony E. Reeve · Osamu Ogawa · Yusaku Okada

The MET proto-oncogene is not a major target for the gain of chromosome 7 in testicular germ-cell tumors of adolescents

Received: 16 December 2003 / Accepted: 13 February 2004 / Published online: 6 March 2004

Sir, Testicular germ-cell tumors (TGCTs) are the most common malignancy of young men, with a peak incidence between 20 years and 40 years of age. The incidence of TGCTs has risen dramatically over the last century [1]. The potential for loss of productive years at young ages indicates that TGCT medically and economically is an important disease. However, the molecular pathogenesis of the TGCT still remains poorly understood.

Cytogenetic findings have revealed specific gains and losses from several chromosomal regions in TGCTs [5]. In particular, a gain of chromosome arm 12p, often through the presence of isochromosome 12p, is the most common genetic aberration in TGCTs. One of the candidate genes on 12p has been the KRAS2 gene. However, the incidence of KRAS2 mutations in TGCTs is low [3]. So far, a common mutation of oncogenes contributing to the development of TGCTs has not been identified. Other than i(12p), a gain of chromosome 7 is frequently observed in TGCTs [2]. The MET proto-oncogene at chromosome 7q31 encodes the tyrosine-kinase receptor for hepatocyte growth factor (HGF), which controls genetic programs leading to cell growth, invasiveness, and protection from apoptosis. Recently, trisomy of chromosome 7 and constitutively activating mutations of the MET gene have been identified in both hereditary and sporadic forms of papillary renal carcinoma (PRC) [6, 7]. All of these point mutations were missense mutations that localized to the tyrosine kinase domain of the MET receptor [6].

Based on these lines of evidence, we have tested for the presence of c-Met mutations in TGCT samples. Here, we performed polymerase chain reaction (PCR)-based single-strand conformation polymorphism (SSCP) and sequence analysis of the tyrosine kinase domain of the Met gene (exon 15–19) in four TGCT-derived cell lines (Tcam-2, JKT-1, ITO-II and NEC8) and 35 surgically resected TGCT tissues: Tcam-2 is a seminoma-derived cell line obtained from Dr. Isao Hara at the University of Kobe School of Medicine (Kobe, Japan); JKT-1 is a seminoma-derived cell line obtained from Dr. Hiroyoshi Tanaka at the Kawasaki Medical School (Kurashiki, Japan); ITO-II is an embryonal cell carcinoma-derived cell line; and NEC8 is a mixed-type germ-cell tumor-derived cell line (embryonal carcinoma and yolk-sac tumor). ITO-II and NEC8 were both purchased from the Japanese Collection of Research Bioresources. Thirty-five tumor specimens (21 seminomas and 14 non-seminomatous TGCT tissues) were obtained from 35 patients with TGCTs who were treated at Shiga University of Medical Science and other affiliated hospitals. All human tissue samples were obtained after receiving fully informed consent.

All five exons of the Met gene were examined with the previously described primer pairs [4]. For SSCP analysis, the GenePhor system (Amersham Pharmacia Biotech, San Francisco, CA) was used. SSCP bands were visualized using a commercially available silver-staining kit (Amersham Pharmacia Biotech) as recommended by the manufacturer.

Samples with band shifts were analyzed further by cloning into plasmids and sequencing the cloned DNA; to sequence the PCR products containing the DNA inser-

T. Kawakami · K. Okamoto (✉) · Y. Okada
Department of Urology,
Shiga University of Medical Science,
Otsu, 520–2192 Shiga, Japan
e-mail: keisei@belle.shiga-med.ac.jp
Tel.: +81-77-5482273
Fax: +81-77-5482400

H. Sugihara · T. Hattori
Department of Pathology,
Shiga University of Medical Science,
Otsu, Shiga, Japan

A. E. Reeve
Cancer Genetics Laboratory, Department of Biochemistry,
University of Otago,
Dunedin, New Zealand

O. Ogawa
Department of Urology,
Graduate School of Medicine, Kyoto University,
Kyoto, Japan

Table 1 A single nucleotide polymorphism of *c-MET* found in this study

Location	DNA alteration	Restriction enzyme	Product size (bp)		Genotype frequency (%)		
			Wild type (A)	Variant (B)	AA	AB	BB
Intron 17	T→C 75 bp upstream of exon 18	*SspI*	215, 75	290	22.9	37.1	40.0

tions, the fragments were cloned using TOPO TA cloning kit according to the manufacturer's protocol (Invitrogen). We sequenced the cloned DNA using internal gene-specific primers in both directions.

DNA sequencing was performed using an automated ABI PRISM 310 DNA Sequencer (Perkin Elmer, Norwalk, CT). Sequencing reactions were performed as recommended by the manufacturer.

The PCR–SSCP analysis showed three different band-shift patterns using primer pairs encompassing exon 18. These alterations turned out to be a polymorphism at intron 17 (Table 1), which has not been previously reported. However, no missense or nonsense mutations were revealed in the TGCT-derived cell lines and TGCT tissues. In conclusion, the MET proto-oncogene is not a candidate target gene of the gain of chromosome 7 in TGCTs.

Identification of target oncogenes involved in TGCT tumorigenesis awaits further investigation.

Acknowledgments This work was supported in part by Grants-in-Aid for Scientific Research from the Ministry of Education (13470332, 15591680, 15591682).

References

1. Bergstrom R, Adami HO, Mohner M, Zatonski W, Storm H, Ekbom A, Tretli S, Teppo L, Akre O, Hakulinen T (1996) Increase in testicular cancer incidence in six European countries: a birth cohort phenomenon. J Natl Cancer Inst 88:727–733
2. Mostert MM, van de Pol M, Olde Weghuis D, Suijkerbuijk RF, Geurts van Kessel A, van Echten J, Oosterhuis JW, Looijenga LH (1996) Comparative genomic hybridization of germ cell tumors of the adult testis: confirmation of karyotypic findings and identification of a 12p-amplicon. Cancer Genet Cytogenet 89:146–152
3. Olie RA, Looijenga LH, Boerrigter L, Top B, Rodenhuis S, Langeveld A, Mulder MP, Oosterhuis JW (1995) N- and KRAS mutations in primary testicular germ cell tumors: incidence and possible biological implications. Genes Chromosomes Cancer 12:110–116
4. Park WS, Dong SM, Kim SY, Na EY, Shin MS, Pi JH, Kim BJ, Bae JH, Hong YK, Lee KS, Lee SH, Yoo NJ, Jang JJ, Pack S, Zhuang Z, Schmidt L, Zbar B, Lee JY (1999) Somatic mutations in the kinase domain of the Met/hepatocyte growth factor receptor gene in childhood hepatocellular carcinomas. Cancer Res 59:307–310
5. Sandberg AA, Meloni AM, Suijkerbuijk RF (1996) Reviews of chromosome studies in urological tumors. III. Cytogenetics and genes in testicular tumors. J Urol 155:1531–1556
6. Schmidt L, Duh FM, Chen F, Kishida T, Glenn G, Choyke P, Scherer SW, Zhuang Z, Lubensky I, Dean M, Allikmets R, Chidambaram A, Bergerheim UR, Feltis JT, Casadevall C, Zamarron A, Bernues M, Richard S, Lips CJM, Walther MM, Tsui LC, Geil L, Orcutt ML, Stackhouse T, Lipan J, Slife L, Brauch H, Decker J, Niehans G, Hughson MD, Moch H, Storkel S, Lerman MI, Linehan WM, Zbar B (1997) Germline and somatic mutations in the tyrosine kinase domain of the MET proto-oncogene in papillary renal carcinomas. Nat Genet 16:68–73
7. Zhuang Z, Park WS, Pack S, Schmidt L, Vortmeyer AO, Pak E, Pham T, Weil RJ, Candidus S, Lubensky IA, Linehan WM, Zbar B, Welrich G (1998) Trisomy 7-harbouring non-random duplication of the mutant MET allele in hereditary papillary renal carcinomas. Nat Genet 20:66–69

Virchows Arch (2004) 444:482–484
DOI 10.1007/s00428-004-0999-z

LETTER TO THE EDITOR

A. Brunner · R. Ladurner · M. Kosmahl · G. Mikuz · A. Tzankov

Mucinous non-neoplastic cyst of the pancreas accompanied by non-parasitic asymptomatic liver cysts

Received: 27 November 2003 / Accepted: 20 February 2004 / Published online: 25 March 2004

Sir,

Cystic tumors of the pancreas are rare. Most common are intraductal papillary mucinous neoplasms, serous cystic neoplasms, mucinous cystic neoplasms and solid pseudopapillary neoplasms [5]. Recently, a novel mucinous cystic lesion of the pancreas, so-called mucinous non-neoplastic cyst (MNC), was described [6]. MNCs are mainly located in the pancreatic head and have no obvious sex predilection. They are either detected incidentally or may present with abdominal discomfort or, rarely, obstructive jaundice. On gross examination, most lesions are macrocystic and well circumscribed, filled with blood or fluid and lack communication with the pancreatic duct system; microscopically, the cysts appear to be flat and lined by cuboidal epithelium without any signs of cellular atypia [6]. In contrast to mucinous cystic neoplasms of the pancreas, the most important cystic tumor in the differential diagnosis, MNCs do not seem to recur or undergo neoplastic transformation [6]. In view of all these features, these cystic pancreatic lesions are considered "non-neoplastic" [6].

A 58-year-old man was referred to the outpatient clinic of our hospital in December 2002 with symptoms of acute pancreatitis. Laboratory findings included slightly elevated serum amylase levels, consistent with the clinical diagnosis. Sonography revealed an enlarged head of the pancreas with multiple small calcifications and several liver cysts, the largest approximately 2.7 cm in greatest diameter. To exclude a pancreatic carcinoma, computerized imaging was performed (Fig. 1A). It revealed a multicystic lesion in the uncinate process. The lesion was about 3 cm in diameter and composed of small hypodense lesions, partially forming cysts without storage of the contrast medium. The lesion was well circumscribed, except for the dorsal part, where it was not clearly demarcated. The bile and pancreatic duct systems and the peripancreatic fat tissue were inconspicuous. Multiple smooth-walled hypodense lesions were also found in the liver and were interpreted as being consistent with non-parasitic cysts. No renal cysts were observed. A pancreatoduodenectomy was performed. The patient was released from the hospital 11 days after the operation. Seven months later he is well without recurrence.

On gross examination, the pancreatoduodenectomy specimen showed a pancreatic lesion of 3 cm in diameter and composed of multiple cysts subdivided by thin septa and filled with small amounts of fluid. The surrounding tissue was focally fibrotic, but otherwise inconspicuous. Light microscopy revealed that the cysts were mainly lined by flattened mucinous epithelium (Fig. 1B). The epithelial cells showed no evidence of atypia or mitotic activity. The cysts were surrounded by a dense fibrous stroma containing a few scattered lymphocytes and small areas of calcification adjacent to the pancreatic ducts and acini. The apical portions of the epithelial cells stained positively for periodic acid-Schiff and alcian blue. They were focally positive for MUC5AC, CK7, carcinoembryonic antigen (CEA) and CA 19–9 (Fig. 1C, D), but negative for MUC1, MUC2, CK20, p53, α-inhibin, calretinin and the neuroendocrine markers synaptophysin and chromogranin. The proliferation index, assessed with Ki-67, was less than 1%.

Mucinous cystic neoplasms of the pancreas play an important role in the differential diagnosis of MNCs. Mucinous cystic neoplasms are usually located in the pancreatic body and tail (93%) and show a strong female predominance, while MNCs lack these features [6, 8].

A. Brunner (✉) · G. Mikuz · A. Tzankov
Institute of Pathology,
Medical University of Innsbruck,
Muellerstrasse 44, 6020 Innsbruck, Austria
e-mail: andrea.brunner@uibk.ac.at
Tel.: +43-512-5073654
Fax: +43-512-582088

R. Ladurner
Department of Surgery,
Medical University of Innsbruck,
Austria

M. Kosmahl
Department of Pathology,
University of Kiel,
Germany

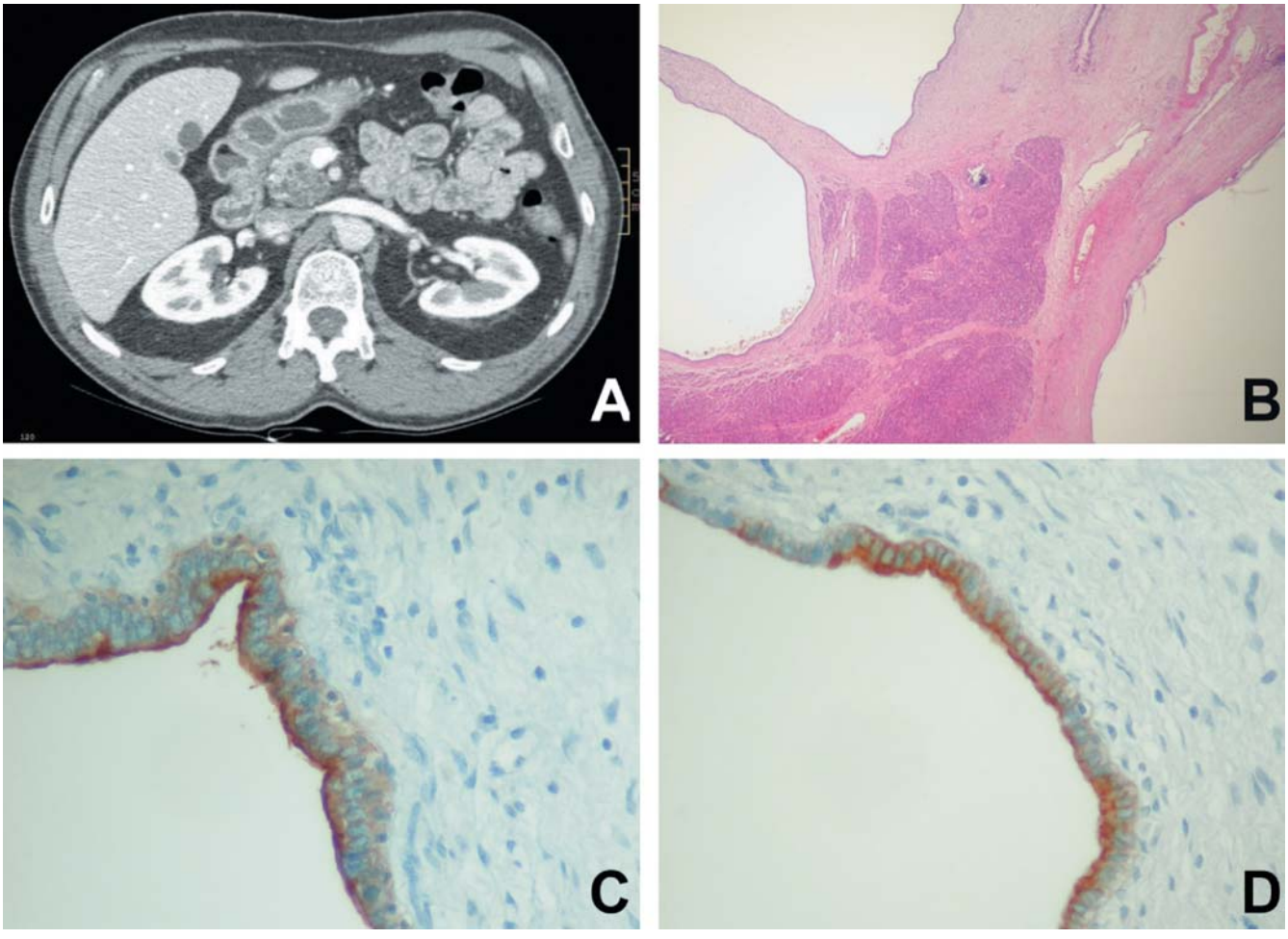

Fig. 1 Contrast medium computerized imaging venous phase with the mesenteric and splenic vein showing smooth-walled liver cysts and a multicystic lesion in the head of the pancreas (**A**). Low-power view of the pancreatic cysts mainly showing flattened epithelial lining, hematoxylin and eosin ×10 (**B**) and immunostaining for CA19–9 (**C**) and carcinoembryonic antigen (**D**)

These entities also seem to differ in their prognosis, because mucinous cystic neoplasms tend to recur and have a malignant potential if not fully resected, while, to the best of our knowledge within the reported mean follow-up of 2 years, the five documented cases of MNC did not [5, 6]. Histologically, the two entities are clearly distinct. The cysts of mucinous cystic neoplasms do not communicate with the pancreatic duct system and are surrounded by an ovarian-like stroma composed of densely-packed spindle cells with elongated nuclei. They are lined by a mucinous epithelium that sometimes even lacks cytological atypia [8]. The stroma supporting the MNCs is composed of dense fibrous tissue, sometimes containing lymphocytes, macrophages or, occasionally, areas of calcification or even metaplastic bone formation [6]. The epithelial lining of the cysts does not show pleomorphism or mitotic activity [6]. However, MNCs and mucinous cystic neoplasms also have some features in common. Both are alcian blue and periodic acid-Schiff positive and express cytokeratins 7, 8, 9 and 19, CA 19–9 and MUC5AC [6]. It has been suggested that these findings indicate a similar epithelial phenotype in MNCs and mucinous cystic neoplasms [6].

In our case, the mucinous epithelium also expressed CEA predominantly in the apical portion of the cells, but a small percentage of the cells stained in their cytoplasms. CEA labeling in normal pancreatic tissue should be limited to the apical membrane; cytoplasmic staining is observed only in pancreatic neoplasms [1, 4]. Expression of CEA has not been reported so far in MNCs, but is characteristic of mucinous cystic neoplasms and may further support a common origin of the epithelial component of MNCs and mucinous cystic neoplasms [4, 6]. The pathogenesis of MNCs, speculating a developmental defect (see discussion below), and their "non-neoplastic" nature appear to be arguable, since they are determined only using morphological and clinical evidence [6]. Considering the observed staining pattern of CEA in our case, one may speculate that MNCs might have at least a staining pattern signature of a pancreatic neoplasm. Molecular studies on large collectives should clarify this intriguing question.

Compared with the MNCs reported by Kosmahl and co-authors, the cysts in our case were rather small, since MNCs usually have a diameter of more than 3 cm [6]. Therefore, if lesions of this size are encountered, retention cysts should be included in the differential diagnosis. They usually measure approximately 0.5–1 cm in diameter and result from an obstruction of the pancreatic ducts due to severe chronic pancreatitis or pancreatic neoplasms [6]. None of these conditions was detected in the present case.

In addition to the cystic lesion in the pancreas, several liver cysts were detected in our patient. Non-parasitic liver cysts are a frequent incidental finding, with up to 5% of the population having one or more cysts, and do not require treatment unless they become symptomatic or if complications such as rupture, torsion, infection or hemorrhage occur [2, 7]. The differential diagnosis includes non-parasitic benign cysts, polycystic disease, cystic neoplasms and hydatid cysts, the vast majority being non-parasitic liver cysts [2, 7]. Non-parasitic liver cysts are thought to arise as a congenital aberration of bile duct development [3]. MNCs may arise due to the duplication of gastrointestinal tissue, forming an enterogenic cyst. It has also been suggested that they are the result of a developmental defect of the pancreas with cystic transformation of the duct system [6]. This raises the question of whether the coincidence of the two maldevelopmental lesions in our patient could indicate an event occurring concomitantly in the liver and the pancreas during embryogenesis. However, given the frequency of non-parasitic liver cysts, the presence of asymptomatic liver cysts in a patient with MNC of the pancreas is most likely accidental [7].

References

1. Adsay NV, Merati K, Nassar H, Shia J, Sarkar F, Pierson CR, Cheng JD, Visscher DW, Hruban RH, Klimstra DS (2003) Pathogenesis of colloid (pure mucinous) carcinoma of exocrine organs: coupling of gel-forming mucin (MUC2) production with altered cell polarity and abnormal cell-stroma interaction may be the key factor in the morphogenesis and indolent behavior of colloid carcinoma in the breast and pancreas. Am J Surg Pathol 27:571–578
2. Ammori BJ, Jenkins BL, Lim PCM, Prasad KR, Pollard SG, Lodge JPA (2002) Surgical strategy for cystic diseases of the liver in a Western hepatobiliary center. World J Surg 26:462–469
3. Arai H, Nagamine T, Suzuki H, Shimoda R, Abe T, Yamada T, Takagi H, Mori M (2002) Simple liver cyst with spontaneous regression. J Gastroenterol 37:755–757
4. Helpap B, Vogel J (1989) Immunohistochemical studies on cystic pancreatic neoplasms. Pathol Res Pract 184:39–45
5. Klöppel G, Kosmahl M (2001) Cystic lesions and neoplasms of the pancreas. The features becoming clearer. Pancreatology 1:648–655
6. Kosmahl M, Egawa N, Schröder S, Carneiro F, Lüttges J, Klöppel G (2002) Mucinous nonneoplastic cyst of the pancreas: a novel nonneoplastic cystic change? Mod Pathol 15:154–158
7. Martin IJ, McKinley AJ, Currie EJ, Holmes P, Garden OJ (1998) Tailoring the management of nonparasitic liver cysts. Ann Surg 228:167–172
8. Zamboni G, Scarpa A, Bogina G, Iacono C, Bassi C, Talamini G, Sessa F, Capella C, Solcia E, Rickaert F, Mariuzzi GM, Klöppel G (1999) Mucinous cystic tumors of the pancreas: clinicopathological features, prognosis and relationship to other mucinous cystic tumors. Am J Surg Pathol 23:410–422

Virchows Arch (2004) 444:485–486
DOI 10.1007/s00428-004-1025-1

ANNOUNCEMENTS

1–11 June 2004
International course on Laboratory Animal Science
Utrecht, The Netherlands

A two week intensive course on laboratory animal science will be organized at the Department of Laboratory Animal Science – Utrecht, The Netherlands in June 2004. This course is organized once a year since 1993.

The objective of this course is to present basic facts and principles that are essential for the humane use and care of animals and for the quality of research.

The contents of the course are in line with recommendations of the Federation of European Laboratory Animal Science Associations (FELASA) regarding the training of the young scientist whose research involves the use of vertebrate animals.

The course may also be of interest for those who intend to set up a similar course at their location. For this purpose, during the course the acquisition of teaching materials can be discussed with the course committee.

For information and application forms please contact:
Prof. L.F.M. van Zutphen, PhD or
Mr. Stephan van Meulebrouck, MA
Department of Laboratory Animal Science
Faculty of Veterinary Medicine
P.O. Box 80.166
3508 TD Utrecht
The Netherlands
Tel.: ++31-30-2532033
Fax: ++31-30-2537997
E-mail: pdk@las.vet.uu.nl
Internet: http://las.vet.uu.nl (click on "Education and Training")

4–5 June 2004
15th Ljudevit Jurak International Symposium on Comparative Pathology
(http://www.kbsm.hr/Jurak/symposium.htm), will be held in Multimedial center Sestre milosrdnice University Hospital, Vinogradska 29, Zagreb, Croatia.

The main symposium topic is head and neck pathology (including ophthalmopathology). Symposium includes following sections: Pathological Morphology of the Human and Animal Diseases, Iatrogenic, Environmental and Experimental Pathology, Herman Jurak Round Table on Rheumatological Pathology, Telepathology on-line conference, Clinical Forensic Pathology, Slide Seminars *in Histopathology and Cytopathology*, Quiz on Pathology.

For further information please contact:
Davor Tomas, M.D.
Ljudevit Jurak Clinical Department of Pathology
Sestre milosrdnice University Hospital
Vinogradska 29
10000 Zagreb, Croatia
Phone: 385-1-3787-909
Fax: 385-1-3787-244
e-mail: dtomas@kbsm.hr, juraks@kbsm.hr

7–9 June 2004
40th Nottingham Multi-disciplinary Course on breast disease
Nottingham, UK

This non residential course includes one and a half days of multidisciplinary education and one and a half days of seminars specific to each discipline.

For further information contact:
The Blamey Education Centre
Nottingham Breast Institute
City Hospital, Nottingham, NG5 1PB, UK
Tel.: 00 44 (115) 969 1689
E-mail: sbury@ncht.trent.nhs.uk

11–16 July 2004
ULTRAPATH XII: Conference on Diagnostic Electron Microscopy with Surgical, Clinical, and Molecular Pathology Correlations
Barcelona, Spain

The scientific program will cover diagnostic Electron Microscopy as well as Diagnostic Pathology – with immunohistochemical and molecular correlations – and translational research. Renowned experts in the field from both sides of the Atlantic will present updated comprehensive reviews of significant areas of Pathology. In addition, a new section of the meeting will be devoted to a Pathology Review Course. Platform and Poster presentations will also be an important part of the program.

For further information, please contact:
Josep Lloreta-Trull, M.D., Ph.D. (chairman)
Department of Pathology, Hospital del Mar-IMAS-IMIM
Universitat Pompeu Fabra
Passeig Maritim 25–29, 08003-Barcelona, Spain
Tel.: +34 93 248 30 31
Fax: +34 93 248 31 31
E-mail: jlloreta@imas.imim.es.
The Application form and Abstract form can be found on the meeting website, http://www.tilesa.es/ultrapath04/

27–30 July 2004, London
Practical Pulmonary Pathology

This course is designed to provide histopathology and cytopathology trainees and consultants with an opportunity to study diagnostic lung pathology in a comprehensive manner. It comprises lectures and practical microscopy sessions, the latter making up roughly half the time and consisting of individual study of a unique collection of cases.

For further details and application forms please contact:
Professor B Corrin,
Brompton Hospital
London SW3 6NP
Fax: +44 20 7351 8293.
E-mail: b.corrin@ic.ac.uk

9 September 2004
One day course on Advanced Ultrasound of the Breast
Nottingham, UK

For further information contact:
The Blamey Education Centre
Nottingham Breast Institute
City Hospital, Nottingham, NG5 1PB, UK
Tel.: 00 44 (115) 969 1689
E-mail: sbury@ncht.trent.nhs.uk

23–24 September 2004 **(Change of date)**
Thyroid Pathology for the Practicing Pathologist
15 rue de l'Ecole de Médecine, Paris, France

A 2-day course will take place in Paris under the auspices of the French Division of the I.A.P. This course will be given in English by Prof. M. Sobrinho-Simoes (Porto) and Prof. R. Heimann (Brussels).

It will consist of lectures alternating with slide reviews and a slide seminar over a multihead microscope. The cases of this seminar will be sent (on CD) before the meeting. The audience will be limited to 22 participants.

Course fee: 390 euros (320 euros for members of any IAP division). The fees include registration, hand-out, CD of the slide seminar and coffee breaks.

For further information, please contact:
Mrs. M. Fontanière
Administrative Secretary
French Division of the I.A.P. 32 Cours Albert Thomas
69008, Lyon, France
Fax: 33478754311
E-mail: academie.pathologie@wanadoo.fr

11 October 2004
Continuing Medical Education
Nottingham, UK

For further information contact:
The Blamey Education Centre
Nottingham Breast Institute
City Hospital, Nottingham, NG5 1PB, UK
Tel.: 00 44 (115) 969 1689
E-mail: sbury@ncht.trent.nhs.uk

22–24 November 2004
41st Nottingham Multi-disciplinary Course on breast disease
Nottingham, UK

For further information contact:
The Blamey Education Centre
Nottingham Breast Institute
City Hospital, Nottingham, NG5 1PB, UK
Tel.: 00 44 (115) 969 1689
E-mail: sbury@ncht.trent.nhs.uk

Virchows Arch (2004) 444:487–501
DOI 10.1007/s00428-004-1012-6

EUROPATH NEWS 1/2004

Newsletter of the European Society of Pathology

European Society
of
Pathology

Dear Colleagues,

We are very pleased to present the first 2004 issue of our ESP Newsletter. This issue begins with the Presidential Address of Prof. Antonio Cardesa and continues with the Minutes from the Extraordinary General Assembly meeting of the European Society of Pathology in Paris by Prof. Roderick Simpson and the presentation of the Executive Committee of ESP (2003–2005), followed by the farewell address of the past Treasurer, Prof. Urbain van Haelst. Also included are announcements of forthcoming conferences, seminars, and tutorial courses, as well as information about the working groups formed. Please do not hesitate to provide us with material on activities in your department and share your problems with us, through *Europath News*. Last but not least, remember that we must increase the number of ESP members, a vital matter for the continuity of our Society. You can easily influence the young staff in your department and ask them to use the application form for membership or the new website included in each issue of the *Europath News*.

With warmest thanks and regards,

Prof. Niki J. Agnantis
Chief Editor

Dr. Bjørn Risberg
Assistant Editor

Editors
Prof. Niki J. Agnantis
University Department of Pathology
Medical School of Ioannina
GR-45110 Ioannina, Greece
Tel.: +302-651-097795
Fax: +302-651-097858
e-mail: nagnanti@cc.uoi.gr

Dr. Bjørn Risberg
Department of Pathology
The Norwegian Radium Hospital
0310 Oslo, Norway
Tel.: +47-22934174
Fax: +47-22508554
e-mail: brisberg@labmed.uio.no

The newsletter of the European Society of Pathology, EUROPATH NEWS, is sponsored by Leica Microsystems Nussloch GmbH

Farewell Address from Niki J. Agnantis

I would like to express, from the bottom of my heart, my sincere thanks to all of you for your support and for offering me the privilege to be your President Elect for the period 2005–2007. I promise to make every effort to meet your expectations for the benefit of our ESP. This is my last contribution to *Europath News*, which I have been working on since 1997. I am very pleased to announce my successor, Dr. Grete Krag Jacobsen, who will take on this difficult task, together with Dr. Bjorn Risberg. Because of this *transition period* the next issue will appear in October 2004.

Address by the President of the European Society of Pathology, Antonio Cardesa

Presidential Address II

Dear ESP Members:

I am happy to be able to report that our Society is overcoming quite satisfactorily the recent electoral problems we had. These problems and the procedures proposed to solve them were commented upon in my first address, written in November 2003 and published in *Virchows Archiv* in the February edition.

We welcome our new President-elect, Prof. Niki J. Agnantis from Ioannina, Greece, who was overwhelmingly elected in the recent election by over 70% of the votes cast. The Executive Committee and the Extraordinary General Assembly of 7 February 2004 unanimously accepted the results and accordingly confirmed her election. In the preparation and evaluation of the ballot Michael Wells, Antonio Llombart-Bosch, Fatima Carneiro, Roderick Simpson, and Teresa Ribalta were of great help.

Roderick H.W. Simpson from Exeter, United Kingdom, is the newly appointed Secretary. His candidacy was also unanimously approved by the Executive Committee and by the General Assembly. He will continue in office until the next Congress in Paris 2005, replacing Jahn M. Nesland whose resignation we regret.

The adaptation of our Statutes to Belgian law was also approved by the Paris Extraordinary General Assembly. This was an important step forward to make sure that our Society conforms to current legal requirements, a task made possible by the dedicated work of. Mia Marichal, Roderick Simpson, and Urbain van Haelst. As a result of this approval, a new adaptation of the by-laws will be required and will be presented for approval at the next General Assembly during the Paris Congress of September 2005. It will also include new regulations for the election of officers and other members of the Executive Committee, as proposed by a constitutional subcommittee.

Another gratifying piece of information is that the elaboration, by Pierre Bedossa and his team, of the scientific and social programs of the Paris Congress 2005 is well advanced. The Congress promises to be of the highest standard.

Finally, I shall conclude by expressing my optimistic view that the tradition of harmony and the cordial atmosphere characterizing our Society are still present.. Let all of us, the whole membership, continue working together in this rewarding way, discussing and reaching agreement as colleagues and friends for the sake of the European Society of Pathology. My thanks to all of you all for your remarkable efforts in this endeavor!

Yours sincerely,

Antonio Cardesa
President
Barcelona, February 2004

European Society of Pathology (ESP)

Extraordinary General Assembly

A. Date: Saturday, 7 February 2004
Place: Palais des Congrès, Porte Maillot 75016, Paris, France
Time: 15.30 hours

As the total number of members attending was only 21, the meeting was declared non-quorate. A second meeting was therefore called for 30 min later.

B. Date: Saturday, 7 February 2004
Place: Palais des Congrès, Porte Maillot 75016, Paris, France
Time: 16.00 hours

1. Welcome

The chairman, the President of the Society, Professor Antonio Cardesa, welcomed 25 members of the Society to the extraordinary general assembly.

2. Approval of the Agenda

This was approved unanimously.

3. Approval of the Minutes of the previous General Assembly in Ljubljana, Slovenia on 10 September 2003

These minutes were accepted as a true and accurate record of the meeting.

Matters Arising. It was announced that as Prof. Jahn Nesland had resigned as Secretary and that Dr. Roderick H.W. Simpson had acted as temporary secretary. The members agreed that Dr. Simpson should complete the term of Prof. Nesland.

4. Report of the President

The President reported that the Executive Committee had met that morning and discussed the issues to be presented to the General Assembly.

5. Statutes and By-Laws

The statutes as they stand are out of date and do not comply with the Belgian Law on non-profit societies. Therefore, Profs. Cardesa, Marichal, and van Haelst and Dr. Simpson had looked at these in attempt to eliminate some of the ambiguities. Dr. Simpson presented the amended statutes. The proposed changes were approved by the meeting and will be published on the ESP website, *www.europathology.org*.

6. Announcement of the Results of the Election for President Elect 2003–2005

The election was held in Barcelona in December 2003. The question on the ballot was: "The recommendation of the Executive Committee (2001–2003) for the post of President-elect was N.J. AGNANTIS (Ioannina, Greece). Please indicate your approval of this recommendation by placing an X in the appropriate box."

Results

The total number of votes cast was as follows:

Approved:	367	(70.31%)
Not Approved:	142	(27.20%)
Abstentions:	2	(0.38%)
Spoiled papers:	11	(2.11%)
Total:	522	(100%)

The meeting therefore decided unanimously that Prof. Niki Agnantis was elected as President-Elect of the European Society of Pathology with immediate effect until September 2005, whereupon she will succeed to the Presidency.

7. Report of the Chairman of the Organizing Committee of the 20 ESP Congress, Paris 2005

Prof. Pierre Bedossa had earlier presented the outline scientific program to the Advisory and Executive Committees. The program is well advanced. The first announcement has already been issued, and the second announcement is due for publication in September 2004, together with the registration and abstract submission forms. The budgetary aspects will be discussed by the Executive Committee at their next meeting at Iguaçu Falls, Brazil, in June 2004.

8. Any Other Business

a) Updating the By-Laws Will Be Performed by a Constitutional Sub-Committee.
b) Proposed Rules for Elections

Prof. Wells presented proposals to the Executive Committee and it is expected that they will form part the By-Laws.

9. Date and Place of Next General Assembly

The next General Assembly will take place during the 20th European Congress of Pathology in Paris, in September 2005.

Signed:
Professor Antonio Cardesa, President of the ESP
Dr. Roderick HW Simpson, Secretary of the ESP
28 February 2004

Presentation of the Executive Committee of the European Society of Pathology, 2003–2005

President

Prof. Antonio Cardesa, Spain

Past President

Prof. G. Bussolati, Italy

President elect

Prof. N.J. Agnantis, Greece

Treasurer

Prof. H. van Krieken, Netherlands

Secretary General

Prof. R.H.W. Simpson, UK

Members

Prof. M. Wells, UK

Dr. G. Krag Jacobsen, Denmark

Prof. R. Golouh, Slovenia

Prof. F. Carneiro, Portugal

Dr. V-p. Lehto, Finland

Dr. D. Yilmazbayhan, Turkey

Members also include Dr. F. Capron, France, and Prof. Ch. de Wolf-Peeters, Belgium.

Farewell of the Treasurer

General Assembly –
19th ECP Ljubljana –
10 September 2003

Dear President, Dear Colleagues,

Appointed since the eleventh congress in Prague in 1987 and standing down this year in Ljubljana marks for me a period of 16 years of treasurership for the ESP.
Looking back upon this period, I hope I have fulfilled the wishes and met in part the needs of a society with great and growing prospects. As such, I should feel delighted and in a sense proud of having rendered service to an international society of pathology.

However, having just said these first reflections, I am only telling you a half truth! From the very beginning until the last minute I have to be openly most grateful to my wife, Christine. She was not my right hand, but instead my right arm. Although we did a lot of financial and membership matters together, she taught me to be concerned, to assign priorities, to work meticulously, and to work in time and on time. When worrying, I could console her with the idea that worry is like a rocking chair. It gives you something to do, but it doesn't get you anywhere.

On the occasion of my retirement from the Department of Pathology of the Academic Medical Center in Nijmegen (March 1998), our friend Günter Klöppel said in his address that with a savings book, a computer and Christine, I built up my empire and established, systematized, and urbanized the financial basis of the ESP, making many things and activities possible. I can agree with this, but again this is a half truth. Besides urbanization, we have also introduced christi(a)nization.

During the past 16 years and with the skillful leadership of successively eight presidents and the members of the respective executive committees, the conviction became stronger that we were and are still standing up for a just and valuable cause for our profession within and outside Europe. I experienced each meeting as friendly, with open discussions in favor of efficient decision making and, fortunately, never devoid of humorous remarks. (A few pictures of the past-presidents taken on different occasions were shown just to refresh our minds.)

Time and the agenda of this General Assembly do not permit me to elaborate on the ESP activities and its program in the past. Nevertheless, I would like to compliment the workers and members who, from the very beginning, readeach of the four introductions written by our presidents and published in the fourth edition of the Members' Handbook; this should impress both friend and foe. At this moment, I would like to unburden my heart by expressing a personal regret that the total number of ESP members has remained far below expectations. We have not made a spectacular improvement on the membership in the last 15 years! I am fully aware of the meaning of the proverb "nothing ventured, nothing gained." Having said this, it is not easy to know when and how to seed productivity. Until now, I have not been able to find a good reason or argument why a European pathologist, besides his or her membership of a national society, should not also belong to a European coordinating association of pathologists with great advantages. By the same token, this gesture promotes mutual communication with national societies. The latter was a wish expressed by the president of this congress, Prof. Ferluga, in his report to the general assembly in 1983. I will continue to be at your service to find and implement new and appropriate ways of bringing in more members in the future.

Now that I am almost at the end of this address, Christine and I would like to express our gratitude to everybody ranking from the president to the ordinary member we have met on countless business meetings and social occasions. I am sure that our memory will always serve us well in this matter.

I extend words of encouragement to my successor, Prof. J.H.J.M van Krieken, and wish him a very successful term.

Finally, I would like to quote the wise words put in perspective by an author unknown to me, but whose words appeal to me:

Sometimes when you're feeling important,
Sometimes, when your ego's in bloom,
Sometimes, when you take it for granted
You're the best qualified in the room.
Sometimes, when you feel that your going
Would leave an unfillable hole,
Just follow this simple instruction
And see how it humbles your soul.
Take a bucket and fill it with water,
Put your hand in it, up to the wrist,
Pull it out, and the hole that's remaining,
Is the measure of how you'll be missed.
You may splash all you please when you enter,
You can stir up the water galore,
But stop, and you'll find in a minute,
That it looks quite the same as before.
The moral in this quaint example,
Is to do the best you can,
Be proud of yourself, but remember,
There is no indispensable man.

Dear President, Dear Members,

On behalf of both Christine and myself, I again extend our special thanks for making us honorary members of the ESP, and we heartily appreciate all the friendship over the years and your attention today.

Urbain van Haelst
Past-treasurer

Montebello Conferences

Scientific Conferences with Clinical and Basic Research Aspects in the Montebello Centre, close to Lillehammer. The conferences give you an excellent opportunity to combine science and pleasure. The limited number of participants stimulates interaction between speakers and audience.

Malignant serosal tumors – diagnostic and experimental aspects

19–22 June 2004

with world-famous Lecturers: *Elise Kohn, NIH – Israel Vlodavsky, Jerusalem – Carlos Bedrossian, Chicago – Fernando Schmitt,Porto – Reuven Reich, Jerusalem – Ben Davidson Oslo – Ole Didrik Lærum, Bergen*

We are planning a "Norway in a nutshell" tour 17–19 June – if enough participants are interested.

www.montebelloconf.org

EUROPEAN SOCIETY OF PATHOLOGY
ACADEMY OF MEDICAL SCIENCES OF CROATIA
INSTITUTE FOR CLINICAL MEDICAL RESEARCH OF
SESTRE MILOSRDNICE UNIVERSITY HOSPITAL ZAGREB
VETERINARY FACULTY ZAGREB

15TH LJUDEVIT JURAK INTERNATIONAL SYMPOSIUM ON COMPARATIVE PATHOLOGY

MAIN TOPIC
HEAD & NECK PATHOLOGY
INCLUDING OPHTALMOPATHOLOGY

SECOND ANNOUNCEMENT AND CALL FOR PAPERS

JUNE 4-5, 2004
ZAGREB, CROATIA

http://www.kbsm.hr/Jurak/symposium.htm

First Announcement

XIV EuroCellPath Course

THE IMPACT OF PROTEOMICS AND GENOMICS IN PATHOLOGY

May 9-12, 2004 - Girona, Spain

PRELIMINARY PROGRAM

- DNA arrays: Methods and Goals
- Tissue Microarrays: A Tool for Rapid, Efficient Translational Research
- Proteomics: From Genes to Functions
- Tissue Procurement and Handling: Laser Capture Microdissection and Other Techniques
- Bioinformatic Tools for Array Data Mining
- Application of Array Genomics and Proteomics in Pathology
- Molecular Pathology of Genes and Proteins: What to Look For and When

Local Organiser:

Prof. Josep Lloreta-Trull
Department of Pathology,
Hospital del Mar-IMAS-IMIM
Universitat Pompeu Fabra
Passeig Marítim 25-29
08003-Barcelona, Spain
jlloreta@imas.imim.es
Phone +3493 248 30 31
Fax +3493 248 31 31

1996-2004

IOANNINA UNIVERSITY COURSES IN PATHOLOGY (IUCP)

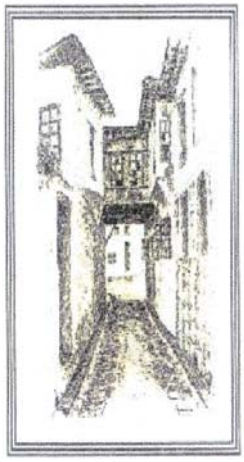

Under the auspices of the ESP within the frame of the European Institute for Continuing Medical Education (EICME) and the collaboration of the European School of Oncology (ESO).

Ioannina University Courses in Pathology (IUCP)

Part one:	Vagina, Vulva & Cervix Pathology-Oncology 25–26 May, 2004	M. Paschopoulos (Gr) K. Pavlaki (Gr) E. Sivridis (Gr)
Faculty:	M. Arbyn (B) I. Arvaniti (Gr) E, Bairaktari (Gr) E. Karaiossifidi (Gr) V. Malamou-Mitsi (Gr) L. Pappa (Gr) E. Paraskevaidis (Gr) G. Pentheroudakis (Gr) B. Risberg (N) J. Varakis (Gr) M. Wells (UK)	Ch. Tolis (Gr) J. Varakis (Gr) M. Wells (UK)
Part two:	Endometrium, Ovaries & Accessories Pathology -Oncology 27-28 May, 2004	**Director-Coordinator: Prof. Niki J Agnantis**
Faculty:	E. Bairaktari (Gr) Em. Diacomanolis (Gr) S. Kalantaridou (Gr) M. Kalpaktsidou-Vakiani (Gr) E. Karaiossifidi (Gr) G. Makrydimas (Gr) V. Papacostas (Gr)	*Registration fees for each part:* EUROS 400 (200 for residents) Accommodation (double room, shared) and full board are included Account number in EUROS: 400-002101-298097 ALPHA Bank, Ioannina, Greece
		Correspondence: Prof. Niki J. Agnantis, M.D., Institute of Pathology, University of Ioannina, Medical School, University Campus

Pathology of the Uterus

Prof. J. Prat, Barcelona

Pathology of the Bladder & Prostate

Prof. F. Algaba, Barcelona

2004 courses

September 23-29 Turin, Italy

AIM

Post-graduate residential course for young European pathologists based on workshops, slide seminars and few lectures to update and standardise participants' diagnostic ability.

FEE

Registration is 300 Euro. Full board accomodation (to be paid upon departure) is 75 Euro/ day/person.
A limited number of EScoP scholarship (for ESP Members) is also available upon request.

DATES

Uterus Pathology Sept. 23-25, 2004
Bladder & Prostate Pathology Sept. 27-29, 2004

PLACE & ORGANIZATION

Institute for Scientific Interchange (ISI)
Villa Gualino, Viale S. Severo 65, 10133 Torino, Italy
Phone Office: +39 0116603090
Phone Residence: +39 0116603555
E-mail: isi@isi36a.isi.it

PAST COURSES

1991 Liver & GI path (non neopl) - Ovarian pathology & Breast pathology
1992 Pulmonary pathology & Endocrine pathology
1993 Hematopathology
1994 Hematopathology -Uterine pathology & Breast pathology
1995 Quantitative pathology - Neuropathology & Head & Neckpathology
1996 Uropathology & Dermatopathology (neopl)
1997 Tumors of liver & pancreas - Tumors of GI tract
1998 Soft tissue tumors & Breast pathology
1999 Lungpathology & Cytopathology
2000 Ovarian pathology GI pathology
2001 Haemato pathology
2002 Head & Neck Pathology Thyroid & Parathyroid Pathology
2003 Pathology of the Pancreas - Pathology of the Liver & Biliary Tract

APPLY before April 30 to

European School of Pathology
c/o Dept of Pathology, Univ. Turin, Via Santena 7
I-10126 Torino, Italy
Fax: +39 011 6635267
E-mail: antonella.davello@unito.it
Note: by end June a note will confirm or reject the application. Do not send money now, please.

To EScoP RE: Preliminary application

Surname …….…… Name ……..…… Sex ……..
Date & place of birth …….…….. Citizenship ……
Full address ……..……
……
……
Phone …… Fax …… E-mail ……..

☐ Application for 2 Courses ☐ Application for 1 course ☐ Sept. 23-25 ☐ Sept. 27-29
☐ I apply for: ☐ EScoP scholarship ☐ EU grant, if available
☐ Member of ESP ☐ Non member (I apply for 2004 ESP Membership)
☐ I enclose a brief curriculum vitae stating my experience in pathology

Date……. Signature ……

Array Technology in the Digestive Tract
A Meeting of the ESP Working Group for Pathology of the Digestive Tract

On Sunday, 15 February, the ESP Working Group for Pathology of the Digestive Tract held a meeting. This meeting was organized as a satellite symposium of the 2nd Multidisciplinary Colorectal Cancer Congress in Noordwijk, The Netherlands. The meeting was well attended (65 participants) and included presentations on a variety of new developments, mainly focused on array technology and the application in the pathology of colorectal cancer and gastric cancer.

The first presentation was by N. Maughan, from the group of P. Quirke. She presented a study on 77 Dukes-B patients, 52 of whom were long-term disease-free survivors. The methodology and its pitfalls were extensively described. One of the remarkable findings was that the expression profiles from Leeds patients were different than those from Sheffield, indicating the importance of standardized workup, even at the level of tissue sampling.

L. Goethals from Leuven, Belgium, presented a study using tissue microarray and pointed to potential pitfalls in its use. She studied pretreatment biopsies and post-treatment resection specimens of colorectal cancer patients and showed that increased expression of CaIX after preoperative chemoradiotherapy was related to better disease-free survival.

After the genome wide-array technology and the large numbers of cases in TMA, the focus was shifted to a very specific protein, EpCAM. M. Gosens, Nijmegen, The Netherlands, showed that this protein is less expressed at the invasive front of colorectal cancer, that its loss is associated with local and distance recurrence, and she gave data to support the hypothesis that the loss of expression is due to cleavage of the protein.

The next topic was matrix-CGH (or array-CGH). B. Radlwinner from P. Lichter's group in Heidelberg gave an in-depth overview of the technology, focusing on the applicability for gene finding, tumor classification, and prognostification. An interesting finding was a single clone loss in normal tissue of one patient. A point of attention was the importance of DNA quality obtained from paraffin tissue.

The value of large patient series and standardized quality-controlled pathology was illustrated by I. Nagtegaal, Nijmegen, The Netherlands. She proposed a new staging system for rectal cancer, including only two factors: lymph-node status and circumferential margin involvement. She showed that this relatively simple and objective method provides more superior information on prognosis than the TNM system.

Assessment of the lymph-nodes status can be improved and automated according to a study by M. Mesker, Leiden, The Netherlands. She had used a automated system with a slide feeder that enables detection of immunostained cells. These cells are depicted on a computer screen for visual control. Between 5 and 10% more positive nodes were detected by this method.

C. Peeters, Nijmegen, The Netherlands, presented her work on vascularization in liver metastasis in colorectal cancer patients. She was able to demonstrate that removal of the primary tumor influenced vascularization in the metastasis. These findings were supported by PET scanning.

In the afternoon, the meeting was started by a presentation by T. Bradletz, Erlangen, Germany. His hypothesis was that instead of the linear model for cancer development there are transient intermediate steps. This was confirmed by his data on beta-catenin staining. At the invasive front there is increased nuclear accumulation of the protein (accompanied by low numbers of Ki67-positivity), but in metastasis there is again normal expression. The involved molecular pathways were described and had partially been analyzed. An important factor might be the laminin 5 gamma 2 protein fragment (one of the many beta-catenin target genes) that plays a role in migration of cells in the extracellular matrix.

A. Ensari from Ankara, Turkey, presented her laborious study into the relevance of beta-catenin, P- and E-cadherin expression in colorectal adenomas using tissue microarrays. She demonstrated that increased dysplasia in the adenomas was associated with beta-catenin expression, but that P- and E-cadherin expression was not.

An important methodological study for the use of expression arrays was presented by S. van der Pas, Leiden, The Netherlands. She demonstrated that two rounds of amplification after laser microdissection affected the expression profiles such that clustering of the results led to separation of double-amplified cases from single amplification. This stresses the importance of many controls and suggests that macrodissection is the more sensible approach.

The importance of vascular invasion for prognostification in colorectal cancer was stressed by A. Sternberg, Hadera, Israel. He showed that increased sampling, awareness, and elastin staining are all relevant. Tangentially taken blocks near the outer border of the tumor especially enhance the identification of this feature.

The pathology of colorectal cancer was the topic of G. Meijer, Amsterdam, The Netherlands, who gave a large amount of data on both CGH and the expression array of gastric cancers. He showed both the feasibility and the other crucial factors needed to obtain high-quality data.

The final presentation was from X. Sun, Linkoeping, Sweden. She showed that the PINCH protein is an independent prognostic factor in colorectal cancer patients.

The meeting was a success not only because of the quality of the data presented, but also thanks to the many questions raised by the participants and the ensuing discussion.

A next meeting of the digestive tract working group is foreseen for 11–12 September in Ankara, Turkey, hosted by A.. Ensari. Further information will be forwarded mainly by e-mail. Those who are not yet on the mailing list, please send your e-mail address to *J.vankrieken@pathol.umcn.nl*

Han van Krieken
Nijmegen, the Netherlands

homepage:http://www.uni-graz.at/
patwww/umweltpat/umweltpat.html

Helmut H. Popper, M.D., Prof. of Pathology
Laboratories for Molecular Genetics,
Environmental and Respiratory Pathology, Institute of Pathology
University of Graz
Auenbruggerplatz 25
Graz, A-8036, Austria
Tel.: +43-316-3804405
Fax: +43-316-384329
popper@uni-graz.at

Working Group on Molecular Pathology

Foundation meeting: Baveno, Monday, 20 May, 2002

For further information use the following e-mail addresses:

For Prof. Dr. Heinz Höfler
renate.hartmann@lrz.tu-muenchen.de
(his secretary's e-mail address)

and Prof. Generoso Bevilacqua:
g.bevilacqua@med.unipi.it

For information concerning ESP activities, please contact

ESP web-site: http://www.Europathology.org

Working Group on Head and Neck Pathology
by Antonio Cardesa

Information address:
Prof. Antonio Cardesa,
Dept. Anatomic Pathology,
Hospital Clinic, Villarroel 170,
08036 Barcelona, Spain
(Tel: +34 93 227 5450,
Fax: +34 93 227 5717,
e-mail: acardesa@clinic.ub.es)

New address:
Prof. Henrik B. Hellquist, Chairman,
Department of Laboratory Medicine
and Pathology, Hamad Hospital,
P.O. Box 3050, Doha, Qatar

Working Group on Endocrine Pathology
by Gianni Bussolati

E.C.E.P
The European Club of Endocrine Pathology

The European Club of Endocrine Patholgoy
Via Santena 7, Torino 10126, Italy
Tel.: +39-11-6706505, Fax: +39-11-6635267
e-mail: fassina@uxl.unipd.it

Working Group of Uropathology
by Gregor Mikuz

Addresses for information:
Gregor Mikuz M.D.,
FRCPath (Chairman),
Institute of Pathology University
Innsbruck, Muellerstrasse 44,
6020 Innsbruck, Austria
(gregor.mikuz@uibk.ac.at)

Ferran Algaba M.D.,(Vice-chairman),
Fundacion Puigvert,
C/Cartagena 340 –350,
08025 Barcelona, Spain
(19612itp@comb.es)

Antonio Lopez-Beltran M.D.,
(Secretary),
Unit of Anatomical Pathology,
Faculty of Medicine,
14004 Cordoba, Spain
(Em1lobea@uco.es)

Margaret Constance Parkinson BSc,
M.D. (Secretary),
(HP) Fourth Floor Rockefeller Building,
University Street, London WC1E6JJ,
UK (Rmkdhmp@ucl.ac.uk)

Rodolfo Montironi M.D.,
FRCPath (Treasurer),
Institute of Pathology,
University of Ancona,
60020 Torrette / Ancona, Italy
(r.montironi@popcsi.unian.it)

Michael J Mihatsch MD
(Nephropathology),
Institute of Pathology,
University Basel,
4003 Basel, Switzerland
(Mihatschmj@uhbs.ch)

Important message to all ESP members who want to send material for publication in the *Europath News,* which will appear four times a year (February, May, August, November) incorporated in *Virchows Archiv:* the material should be sent to one of the editors 2 months ahead of time by e-mail:

grfa@gentoftehosp.kbhant.dk brisberg@labmed.uio.no

Slide seminar in the Internet

Diagnostic histopathology cases presented at the European School of Pathology courses in Turin are going to be shown via Internet.

You are kindly invited to visit the site at http://www.isi.it/pathology/index.htm.

A message from the Editors to the Chairpersons of the formulated ESP Working Groups

Dear Colleagues,
If you are interested in presenting your activities to the EUROPATH NEWS, please send your material by e-mail 2 months ahead of publication.

PLEASE NOTE:
Due to the restricted number of pages in each issue, texts will appear on a "first come, first served" basis.

Working Group of Cytopathology
by Fernando Schmitt

Address for information:
Prof Fernando Schmitt, IPATIMUP,
Rua Roberto Frias S/N,
4200 Porto, Portugal
(e-mail: fernando.schmitt@ipatimup.pt,
Fax: +351–225570799)

Working Group of Gynaecology
by Manfred Dietel

Addresses for information:
e-mail: manfred.dietel@charite.de

Working Group on Molecular Pathology

Foundation meeting:
Baveno Monday, 20 May 2002

For further information use the following e-mail addresses:

For Prof. Dr. Heinz Hofler:
renate.hartmann@lrz.tu-muenchen.de
(his secretary's e-mail address)

For Prof. Generoso Bevilacqua:
g.bevilacqua@med.unipi.it

Electron Microscopy Working Group:

Address for information:
Dr. Brian Eyden (PhD), Head of
Diagnostic Electron Microscopy,
Christie Hospital NHS Trust,
Manchester M20 4BX,
United Kingdom
Tel.: +44 161 446 3292
Fax: +44 161 446 3300
e-mail:
Brian.Eyden@christie-tr.nwest.nhs.uk

The European Society of Pathology

Dear Colleague,

It will surely not have escaped your attention that *Virchows Archiv* is now the Official Journal of the European Society of Pathology.

But did you realise what benefits membership in the society offer you?

- A subscription to the journal *Virchows Archiv* at no extra charge – this is automatically sent to every member every month.
- Access to the journal online (take a look at http://link.springer.de). If you are already a member of ESP but have not yet registered for your free electronic access, you will find the necessary form to complete online here too.
- A discount of 20% on most titles published by Springer. To take advantage of this, simply send your order directly to the publisher, with details of your membership.
- Attendance at the Society's conferences at a reduced fee.

If you have not yet joined the European Society of Pathology, why not do so now?
Simply complete and return the form enclosed. If you are already a member, please wait for our renewal letter for 2004.

We look forward to welcoming you as a member in 2004

Yours sincerely

A. Cardesa
President
European Society of Pathology

H. van Krieken
Treasurer
European Society of Pathology

H. Höfler
Managing Editor
Virchows Archiv

Application for Membership of the EUROPEAN SOCIETY OF PATHOLOGY

For formatting of old application, please follow old application (old Newsletter, p. 238)

This application can also be downloaded from our website:
http://www.Europathology.org

Please complete the following form (block capitals please) and return it to the Office of the Treasurer

FAMILY NAME: .....

First Name(s): .....

Male ❑ Female ❑

Place and date of birth: .....

Title/Present Position: Prof. ❑ Dr. ❑ Resident ❑

Other: .....

Please clearly indicate which one of the following addresses should be used for subsequent correspondence, mailings, and listing in the Members Handbook:

❑ PRIVATE ADDRESS:

Name: .....
Street: .....
Postcode .....
City: .....
Country: .....

❑ INSTITUTE / OFFICE ADDRESS:

Name Institute: .....
Department: .....
Street: .....
Postcode: .....
City: .....
Country: .....
Telephone: .....
Telefax: .....
E-mail: .....

FIELDS OF INTEREST: .....

Date: ..... Signature of Applicant: .....

Please mail or fax the completed application form to:

ESP – OFFICE OF THE TREASURER,
Prof. Dr. H. VAN KRIEKEN,
University Medical Center Nijmegen
Dept. of Pathology / 437 PA
P.O.Box 9101
6500 HB NIJMEGEN, The Netherlands

Tel.: +31-24-3614352
Fax: +31-24-3540520
e-mail: j.vankrieken@pathol.umcn.nl

Your acceptance as a member of E.S.P. will be confirmed in due course.

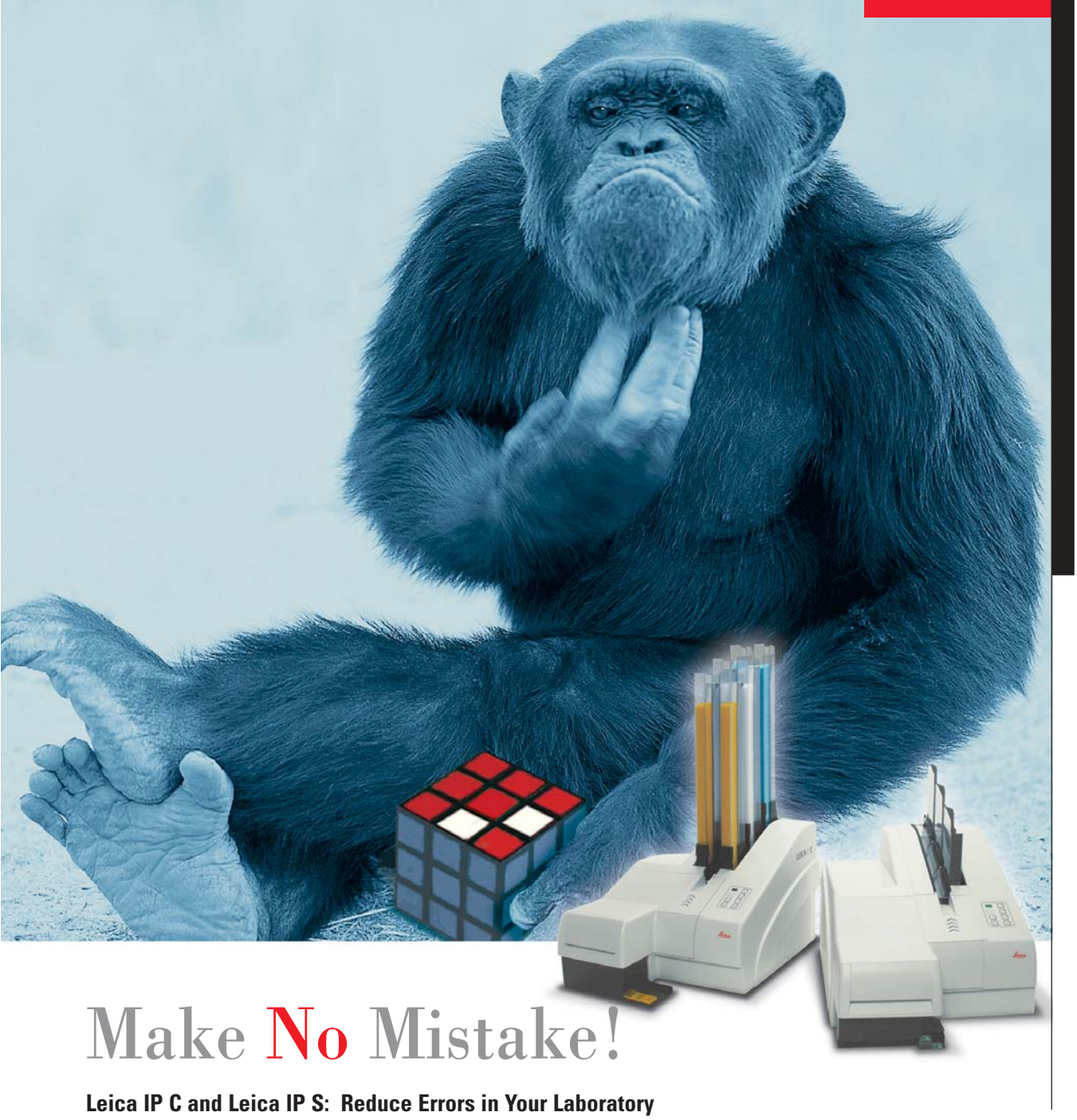

Make No Mistake!

Leica IP C and Leica IP S: Reduce Errors in Your Laboratory

With the new printing systems Leica IP C and Leica IP S for histology cassettes and slides you can easily minimize common marking problems such as illegible writing or incorrect labeling. Costly mistakes can also be avoided with:

- Durability: the chemically and mechanically resistant ink remains legible under adverse conditions
- Flexibility: the Leica IP C and Leica IP S can print bar and data-matrix codes, logos, alphanumeric characters and photos
- Versatility: most commonly used slides and cassettes, even those with lids, can be handled
- Simplicity: data entry is customized to the specific requirements of your laboratory

Make no mistake(s), call for more information today!
Leica Microsystems. Different to the Rest.

Leica Microsystems Nussloch GmbH
Heidelberger Strasse 17-19
D-69226 Nussloch

Phone: (6224) 143-0
Fax: (6224) 143-200
e-mail: histo_info@leica-microsystems.com
www.leica-microsystems.com

Leica
MICROSYSTEMS

Virchows Arch (2004) 444:503–508
DOI 10.1007/s00428-004-0996-2

REVIEW ARTICLE

Rodolfo Montironi · Marina Scarpelli · Antonio López Beltran

Carcinoma of the prostate: inherited susceptibility, somatic gene defects and androgen receptors

Received: 17 February 2004 / Accepted: 17 February 2004 / Published online: 26 March 2004

Abstract Multiple factors contribute to the development of prostate carcinoma (PCa) and to its progression to an androgen-independent state. In addition to the expected role of androgens and their receptors in facilitating the development of PCa, mutations in a growing number of candidate hereditary prostate cancer loci and genes, such as RNASEL and MSR1, have been detected, suggesting that defects in critical pathways involving DNA damage response, apoptosis and innate immunity may have a particularly important role in the initiation of PCa. Many somatic mutations, gene deletions, gene amplifications, chromosomal rearrangements, and changes in DNA methylation are detectable in PCa cells at the time of diagnosis. The identification of key molecular alteration cells implicates carcinogen defenses, including GSTP1, growth factor signaling pathways (such as PTEN and p27) and androgens as critical determinants of the phenotype of PCa.

Keywords Prostate carcinoma · Somatic gene defects · Susceptibility genes · Androgen receptors

Introduction

In developed countries, prostate carcinoma is the most commonly diagnosed non-skin malignancy in males [28]. It is estimated that one in six males will be diagnosed with PCa during their lifetime—the risk of death due to metastatic PCa being 1 in 30 [32]. Multiple factors contribute to the development of PCa as well as to its progression to an androgen-independent state [32]: dietary factors, inherited susceptibility factors, gene defects and androgens and their receptors [7, 14, 49].

In this contribution, several recent findings related to inherited and somatic gene defects as well as to androgen receptor changes in PCa are reviewed.

R. Montironi (✉) · M. Scarpelli
Institute of Pathological Anatomy and Histopathology,
Polytechnic University of the Marche Region (Ancona),
School of Medicine,
Azienda Ospedaliera Umberto I, 60020 Torrette, Ancona, Italy
e-mail: r.montironi@univpm.it
Fax: +39-071-889985

A. López Beltran
Unit of Anatomic Pathology,
Cordoba University Medical School,
Cordoba, Spain

Inherited susceptibility

Currently, the evidence for a strong genetic basis in PCa is compelling: about 9% of all cases of PCa are thought to have a genetic basis, which is about twice the percentage of familial tumors seen in breast cancer. Strengthening the genetic evidence is a high frequency for PCa in monozygotic as compared with dizygotic twins in a large study of twins from Sweden, Denmark and Finland [24] and the higher risk of developing PCa for a man having other family members affected [45].

The identification of highly penetrant PCa genes, i.e., genes that markedly increase the risk of cancer, has been particularly difficult for two main reasons. First, due to the advanced age of onset (median 60 years), the availability of more than two generations to perform molecular studies on is limited. Second, given the high frequency of PCa, it is likely that cases considered to be hereditary during segregation studies actually represent phenocopies, i.e., sporadic cases in families with high rates of PCa. In addition, hereditary prostate cancer (HPC) does not occur in any of the known cancer syndromes and does not have any clinical (other than a somewhat early age of onset at times) or pathological characteristics to allow researchers to distinguish it from sporadic PCa [29].

Hereditary PCa is characterized by Mendelian autosomal dominant or X-linked mode of inheritance and an early onset of the disease. Based on the family clustering of PCa, a number of groups have worked to identify the genes involved. Generally, they have used linkage analysis of large families affected by PCa. Work over the past

decade using genome-wide scans in PCa families has identified high-risk loci [32].

Susceptibility loci

There are at least seven susceptibility loci for PCa identified on different chromosomes [49]. Chromosome 1 is of particular interest, with three proposed loci. The chromosomal region 1q24–25, designated the locus of the hereditary prostate cancer (HPC1) gene, has been the most thoroughly investigated. Some analyses have confirmed a link between HPC1 and PCa, but others have failed to detect an association. The other two proposed susceptibility loci are 1q42.2-q43 (i.e., predisposing for PCa or PCaP) and 1p36 (i.e., cancer, prostate and brain or CAPB). Additional loci have been identified on chromosome 16 (16q23.2), chromosome 17 (17p11, or HPC2, i.e., hereditary prostate cancer 2, also called ELAC2), chromosome 20 (20q13 or HPC20) and chromosome X (Xq27–28 or HPCX). The candidate HPC genes in these regions have rarely been identified, although potential predisposing genes for HCP1 and HCP2 regions have now been cloned [32].

Candidate HPC genes

Mutations in a growing number of candidate HPC loci and genes have been detected, suggesting that defects in critical pathways involving DNA damage response, apoptosis and innate immunity may have a particularly important role in the initiation of PCa. The types of alterations associated with such genes are basically represented by base substitutions, deletions and insertions [32]. The following highly penetrant genes probably account for 10% or less of hereditary PCa cases [7]: *RNASEL* (a candidate tumor suppressor gene within the HPC1 locus located on 1q24–25) [8, 35], *MSR1* (located on 8p22, encodes subunits of class A macrophage-scavenger receptor 1) [55], *CYP17* (located on 10q24.3, encodes cytochrome P_{450}c17α, an enzyme that catalyzes key reactions in sex-steroid biosynthesis) [51], *HPC2/ELAC2* (located on 17p11 and is considered a tumor suppressor gene) [41], *BRCA2* (located on chromosome 13q) [41] and *CHEK2* (encodes an upstream regulator of p53 in the DNA damage signaling pathway) [40]. A number of germline variants and mutations of these genes have been associated with increased risk of PCa.

An increased risk of PCa has been associated with sexually transmitted infections, regardless of the pathogen, suggesting that inflammation, rather than infection, initiates prostatic carcinogenesis. Inflammatory cells elaborate numerous microbiological oxidants that might cause cellular or genomic damage in the prostate [7]. Two of the candidate PCa susceptibility genes identified thus far, RNASEL and MRS1, encode proteins with critical functions in host response to infections. Mutations in these genes might reduce the ability to eradicate infectious agents, thus resulting in chronic inflammation. RNASEL is believed to regulate cellular proliferation and apoptosis through the interferon-inducible 2′,5′-oligoadenylate-dependent RNA decay pathway. At least two mutations inactivating RNASEL have been identified that are potentially responsible for PCa cases in families showing linkage to HPC1 [8, 35]. Germline MSR1 mutations have been linked to PCa in some families with early-onset hereditary PCa [55].

BRCA2, located on chromosome 13q, is a gene that has been implicated as a prostate cancer susceptibility locus, primarily due to its analysis in breast cancer families. Studies of families with breast cancer suggest that male carriers of BRCA2 mutations are at increased risk for PCa, particularly at an early age. Inactivating mutations in BRCA2 have been reported in approximately 2% of men with early onset PCa, confirming the relevance of this gene to PCa susceptibility [41].

Genetic polymorphisms

Perhaps even more important in terms of inherited susceptibility for PCa are common polymorphisms in a number of low-penetrance alleles of other genes—the so-called genetic modifier alleles. The major pathways currently under examination include those involved in androgen action, DNA repair, carcinogen metabolism and inflammation pathways [3, 32]. It is widely assumed that the specific combinations of these variants, in the proper environmental setting, can profoundly affect the risk of developing PCa.

The androgen receptor (AR) gene, a member of the steroid and thyroid hormone receptor gene superfamily, is a transcription factor that mediates the action of androgen in prostate cells. It is located on Xq11–12. The amino-terminal domain encoded by exon 1 contains a variable number of trinucleotide repeats [53]. Decreased transactivation activity and binding affinity for androgen is associated with an increased number of trinucleotide repeats. Shorter CAG repeat lengths have been associated with a greater risk of developing PCa [12, 13, 39, 46].

Additional examples of genetic polymorphisms are related to SRD5A2—a gene located on 2p23 that encodes a polypeptide that catalyzes the conversion of testosterone to dihydrotestosterone—and to vitamin D receptor (VDR). Polymorphisms in the former have been reported to confer an increased risk of PCa, particularly in African Americans and Hispanics [31]. The contribution of the VDR gene polymorphisms to PCa susceptibility remains controversial [33].

Somatic gene alterations and DNA methylation

Many somatic mutations, gene deletions, gene amplifications, chromosomal rearrangements and changes in DNA methylation are detectable in PCa cells at the time of diagnosis. These alterations probably accumulate over

a period of several decades, and the number of changes increases with the stage of the disease. Telomerase activity is frequently upregulated in PCa. This may contribute to genetic instability and promote neoplastic transformation [1, 2, 43]. Although multiple alterations that appear to contribute to disease progression have been suggested, no single key change has been detected [21, 27].

Gene alterations

Table 1 summarizes the most common somatic gene alterations in PCa. The role of PTEN (phosphatase and tensin homologue), CDKN1B (cyclin-dependent kinase inhibitor) and AMACR (alpha-methylacyl-CoA racemase) [20] has been investigated in several recent publications.

PTEN is a tumor-suppressor gene encoding a phosphatase active against both protein and lipid substrates. PTEN induces G1 cell-cycle arrest via negative regulation of the phosphatidylinositol 3′-kinase/protein kinase B (PI3/Akt) signaling pathway, which is essential for cell-cycle progression and cell survival. By inhibiting PI3 K/Akt, PTEN can increase the levels of CDKN1B messenger RNA and p27 protein (see below). PTEN is frequently mutated or deleted in PCa cell lines and tumors. PTEN alterations are more common in metastatic deposits than in primary carcinomas. Using immunohistochemistry, PTEN is present in normal epithelial cells and prostatic intraepithelial neoplasia (PIN). The level of PTEN is frequently reduced in PCa of high grade or stage. Somatic allelic losses (i.e., haploinsufficiency) in both PTEN and NKX3.1 appear to be common in prostate carcinoma and may promote an abnormal proliferation of prostate cells [23, 44, 56].

CDKN1B encodes $p27^{kip1}$, a cyclin-dependent kinase inhibitor. The $p27^{kip1}$ protein regulates cell-cycle progression from G1 phase to S phase by its inhibitory interaction with the cyclin E/cdk2 complex. In PCa, $p27^{kip1}$ expression progressively decreases with increasing tumor grade and stage. Low levels of $p27^{kip1}$ may be as much a result of CDKN1B alterations as of the PTEN loss, whose function is mediated by the PI3K-Akt signaling pathway [6, 16, 52]. A recent paper by Dreher et al. dealt with a combined analysis of PTEN and $p27^{kip1}$ expression in PCa and greatly contributed to the knowledge that activated Akt blocks $p27^{kip1}$ entry into the nucleus by phosphorylating a residue within the nuclear localization signal of $p27^{kip1}$ [9].

AMACR encodes an enzyme that plays an important role in the β-oxidation of branched-chain fatty acids and serves as a "caretaker" gene. It has been found consistently upregulated in PCa and in high-grade PIN, a direct precursor of PCa [10, 19, 26, 29, 38].

DNA methylation

Epigenetic events that can affect gene expression without altering the actual sequence of DNA include phenomena such as DNA methylation, chromatin remodeling, histone modification and RNA interference [32]. Many gene promoters are associated with GC-rich regions of the DNA known as CpG islands. Abnormal methylation of CpG islands located within gene promoters is associated with decreased transcriptional activity, and it occurs in many types of cancers. Abnormal methylation of genes, such as those involved with control of cellular growth or detoxification, is believed to have a critical role in early stages of PCa progression [7]. A certain number of genes, such as GSTP1 (pi-class of glutathione S-transferase) and E-cadherin, are commonly methylated in human PCa.

GSTP1, located on 11q13, probably serves as a caretaker gene. It defends prostate cells against genomic damage mediated by carcinogens or various oxidants. GSTP1 demonstrates hypermethylation in more than in 90% of prostate carcinomas, thus, preventing expression of this protective gene [22, 25, 29, 57].

E-cadherin, located on 16q22.1, encodes a Ca^{2+}-dependent cell-adhesion molecule that is important in normal cell growth and development and is considered a suppressor of neoplastic invasion. E-cadherin is methylated in approximately 50% of cases [14]. Decreased ex-

Table 1 Somatic gene alterations in prostate carcinoma

Gene	Location	Alterations	References
AMACR (Alpha-methylacyl-CoA racemase)	5p13.2	Increased expression	[10, 19, 20, 26, 29, 38]
EZH2 (Enhancer of zeste homolog 2)	7q35	Increased expression	[48]
NKX3.1 (NK3 transcription factor homolog A)	8p21	Decreased expression	[4, 17, 18, 50]
KLF-6 (Kruppel-like factor 6)	10p15	Decreased expression	[30]
PTEN (Phosphatase and tensin homolog)	10q23.3	Decreased expression	[21, 23, 44, 56]
KAI1	11p11.2	Decreased expression	[11]
CDKN1B (Cyclin-dependent kinase inhibitor)	12p12	Decreased expression	[6, 9, 16, 52]
RB (Retinoblastoma susceptibility gene)	13q	Decreased expression	[54]
Hepsin	19q11–13.2	Increased expression	[5]

pression of E-cadherin has been detected in several primary and metastatic prostate carcinomas [36, 47].

Androgen receptors

Many somatic alterations of AR have been detected in those PCa cases that progress despite hormonal treatment [53]. At the same time, prostate tumor cells appear to have several possible mechanisms by which they could become androgen refractory [15, 34].

Mutations in the AR hormone-binding domain or amplification of the AR gene could increase tumor cell sensitivity to androgens. In fact, the increased levels of AR DNA are associated with an increase in AR messenger RNA. Increased levels of AR protein associated with AR gene amplification have been implicated in the ability of cells to more effectively use the low levels of androgens that are produced by the adrenal glands and that are still available during androgen deprivation therapy [48].

Mutations of the AR could allow it to respond to other steroids or even anti-androgens. In particular, mutations in the ligand-binding domain of AR could not only increase sensitivity to normal ligands, such as adrenal androgens, which are present at low levels, but also may cause the AR to be responsive to other molecules, such as anti-androgens, which are not normal ligands [12].

Alterations of the interactions between the AR and some of its co-activators could allow unmutated and mutated ARs to become activated by adrenal androgens, other steroids or anti-androgens. There are several possible ways by which co-activators may be involved in the progression of androgen-sensitive PCa to androgen-refractory PCa. First, overexpression of certain co-activators may cause activation of AR by non-androgenic steroids. Second, overexpression of other co-activators may cause activation of the AR by anti-androgens. Third, AR mutations may result in conformational changes of the AR that, in combination with certain co-activators, can result in activation of the AR. These three mechanisms, alone or in combination, may provide a means for PCa cells to overcome their initial dependence on androgens [53].

Alterations in the expression or function of genes in regulatory pathways involving peptide growth factors or cytokines could cause inappropriate activation of the AR. For instance, growth factors serve as ligands for receptor tyrosine kinases and activate downstream intracellular kinase cascades. Receptor tyrosine kinases may also be involved in the progression to androgen-refractory PCa through an interaction with the AR. The receptor tyrosine kinase Her2/Neu (also known as erbB2) is expressed at low levels in normal epithelial cells. Several studies have demonstrated Her2/Neu protein overexpression and/or gene amplification in a subset of PCa patients. Overexpression of Her2/Neu not only stimulates proliferation of LNCaP cells, but also enhances AR-transactivating activity both in the absence of androgens and in the presence of androgens, in which case activation is synergistic. Moreover, Her2/Neu induces prostate-specific antigen expression, and this induction can be partially inhibited by blocking the multiple antigen peptide (MAP) kinase pathway. Thus, MAP kinase may mediate the activation of the AR by Her2/Neu [42].

The AR could be bypassed entirely, possibly as a result of constitutive activation of regulatory molecules downstream of the AR. For instance, PTEN inactivation, p53 mutations, bcl-2 pathway alterations, neuroendocrine factors and alternative growth-factor regulation and utilization could bypass the need for activation of the AR [37].

Conclusions

Recent molecular studies have confirmed altered expression of some known genes and, more importantly, identified novel genes involved in PCa development and progression [7, 14, 24, 32, 49]. Mutations in a growing number of candidate HPC loci and genes have been detected, suggesting that defects in critical pathways involving DNA damage response, apoptosis and innate immunity may have a particular important role in the initiation of PCa. The possibility that infections might lead to PCa has been raised with the identification of RNASEL and MSR1 as familial PCa genes, an insight that will profoundly affect future studies and may ultimately lead to new approaches to the prevention of PCa. Many somatic mutations, gene deletions, gene amplifications, chromosomal rearrangements and changes in DNA methylation are detectable in PCa cells at the time of diagnosis [29]. The AR gene has been implicated in both risk of PCa development and progression. Many somatic alterations of AR have been detected in those carcinomas that progress despite hormonal treatment [53]. Knowledge of genetic alterations in PCa is rapidly expanding as new powerful techniques are applied. The goals are to find links between genetic and environmental factors and to define specific targets for detection, diagnosis and treatment of PCa.

Acknowledgement This contribution has been supported by a grant from the Italian Ministry of University and Scientific Research (RM) (MIUR 2003).

References

1. Artandi SE, Chang S, Lee SL, Alson S, Gottlieb GJ, Chin L, DePinho RA (2000) Telomere dysfunction promotes non-reciprocal translocations and epithelial cancers in mice. Nature 406:641–645
2. Blasco MA, Lee HW, Hande MP, Samper E, Lansdorp PM, DePinho RA, Greider CW (1997) Telomere shortening and tumor formation by mouse cells lacking telomerase RNA. Cell 91:25–34
3. Bova GS, Partin AW, Isaacs SD, Carter BS, Beaty TL, Isaacs WB, Walsh PC (1998) Biological aggressiveness of hereditary

prostate cancer: long-term evaluation following radical prostatectomy. J Urol 160:660–663
4. Bowen C, Bubendorf L, Voeller HJ, Slack R, Willi N, Sauter G, Gasser TC, Koivisto P, Lack EE, Kononen J, Kallioniemi OP, Gelmann EP (2000) Loss of NKX3.1 expression in human prostate cancers correlates with tumor progression. Cancer Res 60:6111–6115
5. Chen Z, Fan Z, McNeal JE, Nolley R, Caldwell MC, Mahadevappa M, Zhang Z, Warrington JA, Stamey TA (2003) Hepsin and maspin are inversely expressed in laser capture microdissectioned prostate cancer. J Urol 169:1316–1319
6. Cordon-Cardo C, Koff A, Drobnjak M, Capodieci P, Osman I, Millard SS, Gaudin PB, Fazzari M, Zhang ZF, Massague J, Scher HI (1998) Distinct altered patterns of $p27^{kip1}$ gene expression in benign prostatic hyperplasia and prostatic carcinoma. J Natl Cancer Inst 90:1284–1291
7. Crawford ED (2003) Epidemiology of prostate cancer. Urology 62[Suppl 1]:3–12
8. Cunningham JM, McDonnell SK, Marks A, Hebbring S, Anderson SA, Peterson BJ, Slager S, French A, Blute ML, Schaid DJ, Thibodeau SN (2003) Genome linkage screen for prostate cancer susceptibility loci: results from the Mayo Clinic Familial Prostate Cancer Study. Prostate 57:335–346
9. Dreher T, Zentgraf H, Abel U, Kappeler A, Michel MM, Bleyl U, Grobholz R (2004) Reduction of PTEN and $p27^{kip1}$ expression correlates with tumor grade in prostate cancer. Virchows Arch DOI 10.1007/s00428-004-1004-6
10. Ferdinandusse S, Denis S, Ijlst L, Dacremont G, Waterham HR, Wanders RJ (2000) Subcellular localization and physiological role of alpha-methylacyl-CoA racemase. J Lipid Res 41:1890–1896
11. Gao AC, Lou W, Dong JT, Barrett JC, Danielpour D, Isaacs JT (2003) Defining regulatory elements in the human KAI1 (CD 82) metastasis suppressor gene. Prostate 57:256–260
12. Gelmann EP (2002) Molecular biology of the androgen receptor. J Clin Oncol 20:3001–3015
13. Giovannucci E, Stampfer MJ, Krithivas K, Brown M, Dahl D, Brufsky A, Talcott J, Hennekens CH, Kantoff PW (1997) The CAG repeat within the androgen receptor gene and its relationship to prostate cancer. Proc Natl Acad Sci U S A 94:3320–3323
14. Gonzalgo ML, Isaacs WB (2003) Molecular pathways to prostate cancer. J Urol 170:2444–2452
15. Grossmann ME, Huang H, Tindall DJ (2001) Androgen receptor signaling in androgen-refractory prostate cancer. J Natl Cancer Inst 93:1687–1697
16. Guo Y, Sklar GN, Borkowski A, Kyprianou N (1997) Loss of the cyclin-dependent kinase inhibitor p27(Kip1) protein in human prostate cancer correlates with tumor grade. Clin Cancer Res 3:2269–2274
17. He WW, Sciavolino PJ, Wing J, Augustus M, Hudson P, Meissner PS, Curtis RT, Shell BK, Bostwick DG, Tindall DJ, Gelmann EP, Abate-Shen C, Carter KC (1997) A novel human prostate-specific, androgen-regulated homeobox gene (NKX3.1) that maps to 8p21, a region frequently deleted in prostate cancer. Genomics 43:69–77
18. Kim MJ, Bhatia-Gaur R, Banach-Petrosky WA, Desai N, Wang Y, Hayward SW, Cunha GR, Cardiff RD, Shen MM, Abate-Shen C (2002) NKX3.1 mutant mice recapitulate early stages of prostate carcinogenesis. Cancer Res 62:2999–3004
19. Kotti TJ, Savolainen K, Helander HM, Yagi A, Novikov DK, Kalkkinen N, Conzelmann E, Hiltunen JK, Schmitz W (2000) In mouse alpha-methylacyl-CoA racemase, the same gene product is simultaneously located in mitochondria and peroxisomes. J Biol Chem 275:20887–20895
20. Jiang Z, Woda BA, Rock KL, Xu Y, Savas L, Khan A, Pihan G, Cai F, Babcook JS, Rathanaswami P, Reed SG, Xu J, Fanger GR (2001) P504S: a new molecular marker for the detection of prostate carcinoma. Am J Surg Pathol 25:1397–1404
21. Latil A, Lidereau R (1998) Genetic aspects of prostate cancer. Virchows Arch 432:389–406
22. Lee WH, Morton RA, Epstein JI, Brooks JD, Campbell PA, Bova GS, Hsieh WS, Isaacs WB, Nelson WG (1994) Cytidine methylation of regulatory sequences near the pi-class glutathione S-transferase gene accompanies human prostatic carcinogenesis. Proc Natl Acad Sci U S A 91:11733–11737
23. Li J, Yen C, Liaw D, Podsypanina K, Bose S, Wang SI, Puc J, Miliaresis C, Rodgers L, McCombie R, Bigner SH, Giovanella BC, Ittmann M, Tycko B, Hibshoosh H, Wigler MH, Parsons R (1997) PTEN, a putative protein tyrosine phosphatase gene mutated in human brain, breast, and prostate cancer. Science 275:1943–1947
24. Lichtenstein P, Holm NV, Verkasalo PK, Iliadou A, Kaprio J, Koskenvuo M, Pukkala E, Skytthe A, Hemminki K (2000) Environmental and heritable factors in the causation of cancer—analyses of cohorts of twins from Sweden, Denmark, and Finland. N Engl J Med 343:78–85
25. Lin X, Tascilar M, Lee WH, Vles WJ, Lee BH, Veeraswamy R, Asgari K, Freije D, van Rees B, Gage WR, Bova GS, Isaacs WB, Brooks JD, DeWeese TL, De Marzo AM, Nelson WG (2001) GSTP1 CpG island hypermethylation is responsible for the absence of GSTP1 expression in human prostate cancer cells. Am J Pathol 159:1815–1826
26. Luo J, Zha S, Gage WR, Dunn TA, Hicks JL, Bennett CJ, Ewing CM, Platz EA, Ferdinandusse S, Wanders RJ, Trent JM, Isaacs WB, De Marzo AM (2002) Alpha-methylacyl-CoA racemase: a new molecular marker for prostate cancer. Cancer Res 62:2220–2226
27. Meeker AK, Hicks JL, Platz EA, March GE, Bennet CJ, De Marzo A (2002) Telomere shortening is an early somatic DNA alteration in human prostate tumorigenesis. Cancer Res 62:6405–6409
28. Montironi R (2001) Prognostic factors in prostate cancer. Br Med J 322:378–379
29. Montironi R, Mazzucchelli R, Scarpelli M (2003) Molecular techniques and prostate cancer diagnostic. Eur Urol 44:390–400
30. Muhlbauer KR, Grone HJ, Ernst T, Grone E, Tschada R, Hergenhahn M, Hollstein M (2003) Analysis of human prostate cancers and cell lines for mutations in the TP53 and KLF6 tumour suppressor genes. Br J Cancer 89:687–690
31. Nam RK, Zhang WW, Trachtenberg J, Jewett MA, Emami M, Vesprini D, Chu W, Ho M, Sweet J, Evans A, Toi A, Pollak M, Narod SA (2003) Comprehensive assessment of candidate genes and serological markers for the detection of prostate cancer. Cancer Epidemiol Biomarkers Prev 12:1429–1437
32. Nelson WG, De Marzo AM, Isaacs WB (2003) Prostate cancer. N Engl J Med 349:366–381
33. Ntais C, Polycarpou A, Ioannidis JP (2003) Vitamin D receptor gene polymorphisms and risk of prostate cancer: a meta-analysis. Cancer Epidemiol Biomarkers Prev 12:1395–1402
34. Nupponen NN, Kakkola L, Koivisto P, Visakorpi T (1998) Genetic alterations in hormone-refractory recurrent prostate carcinomas. Am J Pathol 153:141–148
35. Nupponen NN, Wallen MJ, Ponciano D, Robbins CM, Tammela TL, Vessella RL, Carpten JD, Visakorpi T (2004) Mutational analysis of susceptibility genes RNASEL/HPC1, ELAC2/HPC2, and MSR1 in sporadic prostate cancer. Genes Chromosomes Cancer 39:119–125
36. Otto T, Rembrink K, Goepel M, Meyer-Schwickerath M, Rubben H (1993) E-cadherin: a marker for differentiation and invasiveness in prostatic carcinoma. Urol Res 21:359–362
37. Ross RK, Pike MC, Coetzee GA, Reichardt JK, Yu MC, Feigelson H, Stanczyk FZ, Kolonel LN, Henderson BE (1998) Androgen metabolism and prostate cancer: establishing a model of genetic susceptibility. Cancer Res 58:4497–4504
38. Rubin MA, Zhou M, Dhanasekaran SM, Varambally S, Barrette TR, Sanda MG, Pienta KJ, Ghosh D, Chinnaiyan AM (2002) Alpha-Methylacyl coenzyme A racemase as a tissue biomarker for prostate cancer. JAMA 287:1662–1670
39. Schoenberg MP, Hakimi JM, Wang S, Bova GS, Epstein JI, Fischbeck KH, Isaacs WB, Walsh PC, Barrack ER (1994) Microsatellite mutation (CAG24→18) in the androgen receptor

gene in human prostate cancer. Biochem Biophys Res Commun 198:74–80
40. Seppala EH, Ikonen T, Mononen N, Autio V, Rokman A, Matikainen MP, Tammela TL, Schleutker J (2003) CHEK2 variants associate with hereditary prostate cancer Br J Cancer 89:1966–1970
41. Simard J, Dumont M, Labuda D, Sinnett D, Meloche C, El-Alfy M, Berger L, Lees E, Labrie F, Tavtigian SV (2003) Prostate cancer susceptibility genes: lessons learned and challenges posed. Endocr Relat Cancer 10:225–259
42. Skacel M, Ormsby AH, Pettay JD, Tsiftsakis EK, Liou LS, Klein EA, Levin HS, Zippe CD, Tubbs RR (2001) Aneusomy of chromosomes 7, 8 and 17 and amplification of HER-2/neu and epidermal growth factor receptor in Gleason score 7 prostate carcinoma: a differential fluorescent in situ hybridization study of Gleason pattern 3 and 4 using tissue microarray. Hum Pathol 32:1392–1397
43. Sommerfeld HJ, Meeker AK, Piatyszek MA, Bova GS, Shay JW, Coffey DS (1996) Telomerase activity: a prevalent marker of malignant human prostate tissue. Cancer Res 56:218–222
44. Steck PA, Pershouse MA, Jasser SA, Yung WK, Lin H, Ligon AH, Langford LA, Baumgard ML, Hattier T, Davis T, Frye C, Hu R, Swedlund B, Teng DH, Tavtigian SV (1997) Identification of a candidate tumour suppressor gene, MMAC1, at chromosome 10q23.3 that is mutated in multiple advanced cancers. Nat Genet 15:356–362
45. Tavtigian SV, Simard J, Teng DH, Abtin V, Baumgard M, Beck A, Camp NJ, Carillo AR, Chen Y, Dayananth P, Desrochers M, Dumont M, Farnham JM, Frank D, Frye C, Ghaffari S, Gupte JS, Hu R, Iliev D, Janecki T, Kort EN, Laity KE, Leavitt A, Leblanc G, McArthur-Morrison J, Pederson A, Penn B, Peterson KT, Reid JE, Richards S, Schroeder M, Smith R, Snyder SC, Swedlund B, Swensen J, Thomas A, Tranchant M, Woodland AM, Labrie F, Skolnick MH, Neuhausen S, Rommens J, Cannon-Albright LA (2001) A candidate prostate cancer susceptibility gene at chromosome 17p. Nat Genet 27:172–180
46. Trapman J, Cleutjens KB (1997) Androgen-regulated gene expression in prostate cancer. Semin Cancer Biol 8:29–36
47. Umbas R, Schalken JA, Aalders TW, Carter BS, Karthaus HF, Schaafsma HE, Debruyne FM, Isaacs WB (1992) Expression of the cellular adhesion molecule E-cadherin is reduced or absent in high-grade prostate cancer. Cancer Res 52:5104–5109
48. Varambally S, Dhanasekaran SM, Zhou M, Barrette TR, Kumar-Sinha C, Sanda MG, Ghosh D, Pienta KJ, Sewalt RG, Otte AP, Rubin MA, Chinnaiyan AM (2002) The polycomb group protein EZH2 is involved in progression of prostate cancer. Nature 419:572–573
49. Visakorpi T (2003) The molecular genetics of prostate cancer. Urology 62[Suppl 1]:3–10
50. Voeller HJ, Augustus M, Madike V, Bova GS, Carter KC, Gelmann EP (1997) Coding region of NKX3.1, a prostate-specific homeobox gene on 8p21, is not mutated in human prostate cancers. Cancer Res 57:4455–4459
51. Xu J, Zheng SL, Komiya A, Mychaleckyj JC, Isaacs SD, Hu JJ, Sterling D, Lange EM, Hawkins GA, Turner A, Ewing CM, Faith DA, Johnson JR, Suzuki H, Bujnovszky P, Wiley KE, DeMarzo AM, Bova GS, Chang B, Hall MC, McCullough DL, Partin AW, Kassabian VS, Carpten JD, Bailey-Wilson JE, Trent JM, Ohar J, Bleecker ER, Walsh PC, Isaacs WB, Meyers DA (2002) Germline mutations and sequence variants of the macrophage scavenger receptor 1 gene are associated with prostate cancer risk. Nat Genet 32:321–325
52. Yang RM, Naitoh J, Murphy M, Wang HJ, Phillipson J, deKernion JB, Loda M, Reiter RE (1998) Low p27 expression predicts poor disease-free survival in patients with prostate cancer. J Urol 159:941–945
53. Yong EL, Lim J, Qi W, Ong V, Mifsud A (2000) Molecular basis of androgen receptor diseases. Ann Med 32:15–22
54. Wang Y, Hayward SW, Donjacour AA, Young P, Jacks T, Sage J, Dahiya R, Cardiff RD, Day ML, Cunha GR (2000) Sex hormone-induced carcinogenesis in Rb-deficient prostate tissue. Cancer Res 60:6008–6017
55. Wiklund F, Jonsson BA, Goransson I, Bergh A, Gronberg H (2003) Linkage analysis of prostate cancer susceptibility: confirmation of linkage at 8p22–23. Hum Genet 112:414–418
56. Wu X, Senechal K, Neshat MS, Whang YE, Sawyers CL (1998) The PTEN/MMAC1 tumor suppressor phosphatase functions as a negative regulator of the phosphoinositide 3-kinase/Akt pathway. Proc Natl Acad Sci U S A 95:15587–15591
57. Zitzelsberger H, EngertD, Walch A, Kulka U, Aubele M, Hofler H, Bauchinger M, Werner M (2001) Chromosomal changes during development and progression of prostate adenocarcinoma. Br J Cancer 84:202–208

Virchows Arch (2004) 444:509–517
DOI 10.1007/s00428-004-1004-6

ORIGINAL ARTICLE

Tina Dreher · Hanswalter Zentgraf · Ulrich Abel · Alexandra Kappeler · Maurice S. Michel · Uwe Bleyl · Rainer Grobholz

Reduction of PTEN and p27^{kip1} expression correlates with tumor grade in prostate cancer. Analysis in radical prostatectomy specimens and needle biopsies

Received: 27 November 2003 / Accepted: 1 March 2004 / Published online: 29 April 2004

Abstract The extreme variability of prostate cancer implies latent disease with missing clinical symptoms in some cases. Tumor suppressors PTEN (phosphatase and tensin homolog deleted on chromosome ten) and p27^{kip1} are frequently mutated in various human cancers. PTEN negatively influences cell growth and induces apoptosis, while p27^{kip1} binds to cyclin-E-Cdk2 and counteracts mitosis. This study investigated the expression of PTEN and p27^{kip1} in prostatectomies and needle biopsies in order to determine whether protein localization or expression levels are correlated with tumor grade and whether PTEN and p27^{kip1} expression in biopsies are valuable predictive tumor markers. Analysis of PTEN demonstrated that weak expression levels were significantly more prevalent in high-grade tumors. Analysis of p27^{kip1} revealed that high-grade tumors had a higher percentage of cytoplasmic localization of the protein than low-grade tumors, where nuclear localization was more frequent. Furthermore, this study indicated a positive association between PTEN and p27^{kip1} levels. An increase of high-grade tumors corresponded to a progressive loss of both tumor suppressors in needle biopsies and prostatectomies. p27^{kip1} and PTEN did not show a higher predictive accuracy of the tumor grade in the surgical specimen than the Gleason score. However, p27^{kip1} had the same predictive value as the Gleason score in needle biopsies.

Keywords PTEN/MMAC1 · p27^{kip1} · Immunohistochemistry · Prostatic carcinoma · Needle biopsy

R. Grobholz (✉)
Pathologisches Institut,
Universitätsklinikum Mannheim,
Theodor-Kutzer-Ufer 1–3, 68167 Mannheim, Germany
e-mail: rainer.grobholz@path.ma.uni-heidelberg.de
Tel.: +49-621-3832781
Fax: +49-621-3832005

T. Dreher · A. Kappeler · U. Bleyl
Pathologisches Institut,
Universitätsklinikum Mannheim,
Theodor-Kutzer-Ufer 1–3, 68167 Mannheim, Germany

M. S. Michel
Urologische Klinik,
Universitätsklinikum Mannheim,
Theodor-Kutzer-Ufer 1–3, 68167 Mannheim, Germany

U. Abel
Tumorzentrum Heidelberg/Mannheim,
Abt. Medizinische Biometrie und Statistik, Universität Heidelberg,
INF 305, 69120 Heidelberg, Germany

H. Zentgraf
ATV, Deutsches Krebsforschungszentrum,
INF 282, 69120 Heidelberg, Germany

Introduction

The search for prognostic markers to estimate a tumor's aggressiveness is essential for the selection of an optimal therapeutic treatment for individual cancer patients. As some tumor types show similar histological characteristics, it is important to reveal aspects that give the pathologist hints about the protein status or even genetic information that underlies the tumor's clinical behavior. Prostate cancer is number one of the estimated new cancer cases (30%) and the second most frequent cause of cancer-related death (11%) among men [9]. Mutation or downregulation of tumor suppressor genes are frequent incidents in cancer development. To find a reliable indicator of tumor aggressiveness and progressive disease, we studied the expression of the tumor suppressors PTEN (phosphatase and tensin homolog deleted on chromosome ten, also known as MMAC1 or TEP1) and p27^{kip1}.

PTEN and p27^{kip1} are part of a variety of genes that control the cell cycle. PTEN is located on chromosome 10q23 [12]. Mutations of the PTEN gene have been described in several types of tumors in different frequencies. Somatic mutations have been found in various human cancer-cell lines and primary tumors of the endometrium, brain, breast, kidney and prostate [12, 24, 25]. Further-

more, germline mutations in PTEN are associated with three human autosomal-dominantly inherited tumor syndromes: Cowden syndrome, Bannayan–Zonana syndrome and Lhermitte-Duclos disease [3, 17]. PTEN, a 403-amino acid protein, is a dual-specificity protein phosphatase and lipid phosphatase, and it has been implicated in regulating cell survival through the phosphatidylinositol 3-kinase (PI3K)/Akt pathway. Via this and PI3K/Akt-independent pathways, PTEN signaling leads to G1 cell-cycle arrest and/or apoptosis. PTEN cleaves a phosphate residue on position 3 of phosphatidylinositol 3,4,5-triphosphate (PIP3), the product of PI3K, which is an activator of Akt, so that mutations of PTEN result, consequently, in constitutive activation of the PI3K/Akt-signaling pathway. Activation of this pathway induces growth, survival and proliferation of cells [3, 19]. In a previous investigation, we did, in fact, show that Akt is increased in prostatic carcinoma [14].

lt has been shown that $PTEN^{+/-}$ knockout mice develop various types of tumors, including prostatic carcinomas [3]. A loss of PTEN protein expression was found to be a useful marker for early precancerous lesions in human endometrial carcinomas [16]. Reduced PTEN expression, therefore, seems to support the identification of early and possibly aggressive tumors. The first studies of protein expression in prostate cancer found a reduced PTEN expression, which was associated with advanced stage of disease [15]. $p27^{kip1}$, located on chromosome 12p13, is a member of a family of cyclin-dependent kinase inhibitors that bind to cyclin/cyclin-dependent kinase (CDK) complexes and arrest mitosis [22]. lt appears to play a critical role in the pathogenesis of several human malignancies, and its reduced expression has been shown to be associated with poor prognosis in cancer patients. There is a connection between PTEN and $p27^{kip1}$, as $p27^{kip1}$ plays a role in PTEN-mediated growth inhibition. Activated Akt blocks $p27^{kip1}$ entry into the nucleus by phosphorylating a residue within the nuclear localization signal of $p27^{kip1}$ [13, 23, 29].

In this study, we determined that PTEN is underexpressed, and $p27^{kip1}$ is mislocalized in human prostatic tumors. Both protein expressions correlated with tumor grade, and low PTEN expression correlated with mislocalized $p27^{kip1}$ expression. In addition, we compared expression patterns in biopsies and corresponding prostatectomies. This study suggests that parallels in protein expression in bioptical tissue and operation specimens may be of predictive value for prostate needle biopsies.

Materials and methods

Patients and tissue samples

Radical prostatectomy specimens of 130 consecutive patients who underwent surgery at the Department of Urology, Universitätsklinikum Mannheim, Germany, were retrieved from the files of the Department of Pathology. Informed consent was acquired from all patients prior to all investigations. Patients were excluded from the study if they had received preoperative androgen-deprivation therapy or radiation therapy. The study population included men between the ages of 47 years and 79 years (63.1±6.3 years) by the time of radical prostatectomy.

The 6th edition of the tumor-node-metastasis (TNM) staging system (2002) was used to classify tumor stage. Tumors were graded using the Gleason grading system [7]. Tumors with Gleason scores of six and lower were considered as low grade, Gleason scores of seven and higher were considered as high grade. This study included 64 of 130 (49.2%) low-grade tumors and 66 of 130 (50.8%) high-grade tumors. Mean value of the preoperative prostate-specific antigen values in low-grade tumors was 10.5±9.4 ng/ml and in high-grade tumors was 15.0±14.3 ng/ml. Tumor stages were classified as organ confined (pT2a-c) in 70 of 130 cases (53.8%) and advanced (pT3a,b and pT4) in 60 of 130 cases (46.2%). All tumors included in this study had no regional lymph-node metastasis. Microscopic residual tumor was classified in 49 of 130 prostatectomies, while all other specimens had no residual tumor.

Tumor-suspicious areas were resected and snap frozen in liquid nitrogen and stored at −80°C until use. The remaining material was fixed in 4% buffered formaldehyde for 24 h and sectioned following standard protocols [26]. The frozen sections of the native material identified tumor and tumor-free areas and were included in the diagnostic process.

For a subgroup of 86 of 130 patients, fresh tumor and tumor-free material was available, and PTEN expression could be investigated using Western-blot analysis. Immunohistochemistry was performed in 118 of 130 cases using a monoclonal PTEN antibody and in 125 of 130 cases using a monoclonal $p27^{kip1}$ antibody. For a subset of 116 of 130 patients, immunohistochemical data of both PTEN and $p27^{kip1}$ expression was available.

Needle biopsies were available from a subset of 32 patients. The time interval between the biopsy and open surgical procedures was 52.44±37 days. The proportion of tumor cells within the needle biopsy ranged from less than 25% to greater than 75%. Of 32 biopsies, 9 contained less than or equal to 25%, 16 of 32 biopsies contained 26–50%, 5 of 32 biopsies contained 51–75% and 2 of 32 biopsies contained greater than 75% tumor cells. Gleason score was determined for all biopsies independently by two observers (T.D., R.G.). Cases included 18 of 32 (56.3%) low-grade tumors and 14 of 32 (43.7%) high-grade tumors.

Immunohistochemistry

The original hematoxylin and eosin (HE)-stained slides were examined to identify the tumor and tumor-free tissue areas. Serial 3-μm sections were cut on a SM200R microtome (Leica, Bensheim, Germany), mounted on silane-coated glass slides and dried overnight at 37°C. All sections were deparaffinized with xylene and rehydrated in a series of graded alcohols. Antigen retrieval was performed by placing the slides in a microwave oven for 3×5 min with 10 mM sodium citrate buffer (pH 6.0) at 600 W. The slides were then incubated with 3% bovine serum albumin (BSA) for 10 min. For detection of $p27^{kip1}$, the slides were incubated with a monoclonal mouse-anti-human antibody (Dako clone SX53G8, Hamburg, Germany), diluted at 1:50 in Tris buffered saline (TBS) (pH 7.6) at 4°C overnight. Visualization of antigenic sites was performed using EnVision-Kit (Dako, Hamburg, Germany) according to the manufacturer's instructions. Sections were counterstained with hematoxylin and mounted in Kaiser's Glycerol Gelatine (Merck, Darmstadt, Germany).

For detection of PTEN, a self-generated monoclonal mouse-anti-human antibody (PTEN5) was used. PTEN5 was raised essentially according to the method of Kohler and Milstein [10], following standard protocols, with the use of recombinant His_6-tagged PTEN for immunization. The sections were incubated with PTEN5 diluted at 1:50 in TBS (pH 7.6) at 4°C overnight. Subsequently, a secondary biotinylated goat-anti-mouse antibody (Jackson Immuno Research, Pennsylvania, USA) was applied and incubated at room temperature (RT) for 30 min. Slides were then incubated with alkaline phosphastase-conjugated streptavidin

(Jackson Immuno Research, Pennsylvania, USA). Fast Red, containing levamisole (Roche Diagnostics, Mannheim, Germany), was added as chromogen. Sections were counterstained with hematoxylin and mounted in Kaiser's Glycerol Gelatine (Merck, Darmstadt, Germany).

Analysis of immunohistochemical stainings

The expression rate of PTEN in tumor tissue was determined using evaluation of intensity and quantity. Intensity was considered as weak (1) or strong (2). Quantity was evaluated using the method of McMenamin et al. [15]. The cases were divided into three groups: (a) positive (the entire tumor showed staining, score 2); (b) mixed (both positive and negative cells/glands were present, score 1) and (c) negative (no staining was seen in the represented tumor, score 0). The final score was calculated by multiplying intensity and quantity of the expression. Final score was grouped into absent or weak expression (scores 0 and 1) and moderate to strong expression (scores 2 and 4).

The expression rate for $p27^{kip1}$ was scored for localization and quantity of the protein following Liang et al. [13]. Expression patterns showed either exclusive cytoplasmic (c) or exclusive nuclear (n) staining or a mixture of both (c+n). Furthermore, quantity was considered as high ($\geq$50%) or low (<50%) levels of positive tumor cells. The following groups were formed: (1) c<50%, (2) c+n<50%, (3) n<50%, (4) c$\geq$50%, (5) c+n$\geq$50%, (6) n$\geq$50%. Statistical analyses were performed for cytoplasmic staining versus additional or total nuclear staining.

Protein extraction; Western blotting

Western-blot analysis was performed as described previously [28]. Briefly, tumor and tumor-free tissue were snap frozen in liquid nitrogen. The original HE-stained 6-μm frozen tissue slides were examined to identify the tumor and tumor-free tissue areas. Serial 20-μm sections were then cut on a CM1900 cryostat (Leica, Bensheim, Germany) from each frozen block. The last section of the series was again stained with HE to ensure the presence or absence of tumor throughout all sections. Tumor and tumor-free tissue were manually microdissected, and proteins were subsequently extracted in lysis buffer [NaCl 150 mM, ethylenediaminetetraacetic acid 1.5 mM, glycerol 3%, BSA 1 mg/ml, IGEPAL CA-630 (Sigma-Aldrich Chemie, Steinheim, Germany) in aqua destillata] for 1 h on ice. Protein concentration in lysates were determined photometrically (595 nm) using a Bradford dye-binding assay (Bio-Rad, Munich, Germany), following the manufacturer's instructions before adding proteinase inhibitors leupeptin (Amersham Pharmacia Biotech, Freiburg, Germany) 1 μg/ml, aprotinin (Roth, Karlsruhe, Germany) 5 μg/ml, pepstatin A (Amersham Pharmacia Biotech, Freiburg, Germany) 2 μg/ml and pefabloc (Roche Diagnostics, Mannheim, Germany) 0.5 mM. Proteins were separated on 12% sodium dodecyl sulfate-polyacrylamide gel electrophoresis and transferred to nitrocellulose membranes (Hybond-C; Amersham Pharmacia Biotech, Freiburg, Germany). Protein transfer was controlled by staining the membrane with Ponceau-S. After blocking, membranes were incubated with primary PTEN5 antibody diluted at 1:2 in phosphate buffered saline (PBS) at RT for 1 h. Secondary alkaline phosphatase-conjugated goat anti-mouse antibody (Dako, Hamburg, Germany, diluted at 1:1000 in PBS) was added for 1 h at RT and visualized using 5-bromo-4-chloro-3-indolyl phosphate/nitroblue tetrazolium (BCIP/NBT) (Roche Diagnostics, Mannheim, Germany) in AP-buffer (Tris 100 mM, NaCl 100 mM, $MgCl_2$ 0.05 M). Loading buffer served as negative control for PTEN antibody. Recombinant unglycosylated PTEN served as positive control for PTEN antibody. Expression rate was evaluated using semiquantitative densitometry (AIDA Image Analyzer, Straubenhardt, Germany). Rates for tumor tissue density were divided by rates for tumor-free tissue density, comparing only samples that were taken from the same patient. These ratios were taken for statistical analysis.

Statistics

Arithmetic means, medians and standard deviations were calculated as descriptive parameters. Values are given as mean±standard deviation. Data were analyzed for normal distribution using Shapiro–Wilk test. Normal distribution was determined for the variables age and PTEN expression in Western-blot analysis.

χ^2-test was used to assess the association between binary variables. Comparison of two independent samples of ordered variables was done using the Wilcoxon rank sum test. P values <0.05 were considered to be statistically significant. The association between PTEN expression in biopsies and Gleason score of the operation specimen could not be analyzed because there was no low-grade biopsy having an absent or weak PTEN expression. The validity of the combination of the parameters $p27^{kip1}$ and the Gleason score (binary variables) in biopsies as a predictive test for the Gleason score of the surgical specimen was analyzed both for the "believe-the-positive (BTP)" and "believe-the-negative (BTN)" interpretation rule. The validity was assessed by means of the predictive accuracy, i.e., the total proportion of correct predictions, along with exact 95% confidence intervals. All statistical analyses were performed using the SAS software package.

Results

PTEN immunoblotting

PTEN antibody detected a band of 65 kDa in human prostate tissue and a band of 47 kDa representing recombinant unglycosylated PTEN, which was used as positive control (Fig. 1). PTEN protein was detectable in 85 of 86 tumor tissue samples and in all tumor-free tissue samples. The density of the obtained bands was evaluated, and a ratio of the density of tumor tissue (T) divided by the density of tumor-free tissue (TF) was calculated using pairs from the same patient (T/TF). Of 86 tumors, 76 (88.4%) showed a lower PTEN expression compared with tumor-free tissue (ratio T/TF<1) and 10 of 86 (11.6%) tumors showed a higher PTEN expression than tumor-free tissue (ratio T/TF>1). PTEN expression levels were significantly higher in tumor-free tissue than tumor tissue (0.68±0.15 versus 0.32±0.14; P<0.0001). PTEN protein levels in carcinoma never exceeded the mean or median PTEN level of the surrounding tumor-free prostatic tissue.

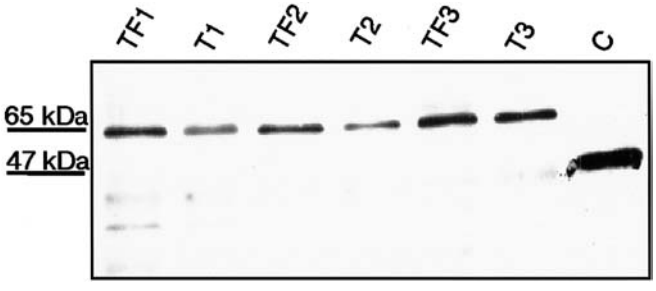

Fig. 1 Representative Western blot of fresh frozen prostate tissue homogenates. Protein bands of PTEN from tumor-free (TF) and tumor (T) tissue were detected by the self-generated monoclonal antibody PTEN5. Each lane contains 10 μg of total protein extract. The lane with purified recombinant unglycosylated PTEN (C) contains 10 ng. Note the weak bands of tumor tissue compared with tumor-free tissue

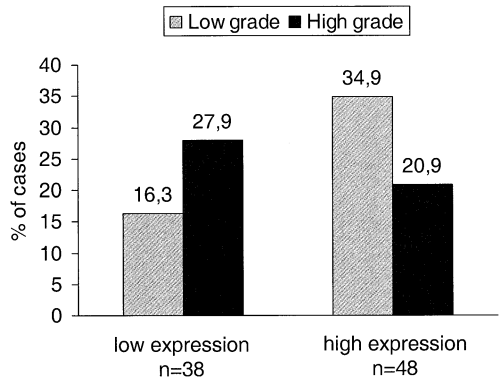

Fig. 2 Association of PTEN expression in Western blot with tumor grade in prostatic carcinoma (n=86). Tumors with Gleason scores less than or equal to six were considered as low grade, Gleason scores greater than or equal to seven as high-grade tumors. High-grade tumors (*black bars*) were significantly more prevalent in cases with low PTEN expression (score$\leq$0.5), while low-grade tumors (*hatched bars*) were more prevalent in cases with high PTEN expression (score>0.5). χ^2-test revealed 5.59, P=0.018

The cut-off point (T/TF=0.5), which was close to the median (0.53), was chosen to define low and high PTEN expression, respectively. PTEN expression in tumors with a ratio $\leq$0.5 (38/86, 44.2%) was compared with PTEN expression in tumors with a ratio >0.5 (48/86, 55.8%). Significantly more high-grade tumors were found in the group with a ratio $\leq$0.5 (24/38, 63.2%) than in the group with a ratio >0.5 (18/48, 37.5%), while significantly more low-grade tumors were found in the group with a ratio >0.5 (30/48, 62.5%) than in the group with a ratio $\leq$0.5 (14/38, 36.8%; P=0.0181, Fig. 2). No statistical association was found between PTEN expression in Western blot and pathological tumor stage.

PTEN immunohistochemistry

Paraffin-embedded sections showed a positive cytoplasmic staining in secretory cells of tumor-free tissue. No expression was found in basal cells and stroma cells (Fig. 3). A weak PTEN expression in tumor tissue was found in 112 of 118 (94.9%) cases, while a strong expression, as in tumor-free tissue, was found in 6 of 118 (5.1%) cases. A mixture of stained and unstained tumor cells was found in 44 of 118 (37.3%) cases, while a ubiquitous positive staining of tumor cells was found in 74 of 118 (62.7%) cases. Absent or weak PTEN expression in tumor tissue with a score $\leq$1 (39/118, 33.1.%) was compared with moderate to strong PTEN expression with a score $\geq$2 (79/118, 66.9%). High-grade tumors were significantly more prevalent in the group with a score $\leq$1 (28/39, 71.8%) than in the group with a score $\geq$2 (34/79, 43%), while low-grade tumors were significantly more prevalent in the group with a score $\geq$2 (45/79, 47%) than in the group with a score $\leq$1 (11/39, 28.2%; P=0.0033, Fig. 4). In contrast to tumor grade, protein expression was not significantly associated with tumor stage (organ-confined versus advanced).

$p27^{kip1}$ Immunohistochemistry

A positive nuclear staining could be seen in secretory cells of tumor-free tissue, while no expression was found in basal cells and stroma cells (Fig. 5a). Tumor tissue, however, showed either cytoplasmic expression only (21/125, 16.8%), nuclear and cytoplasmic expression (95/125, 76%) or nuclear expression (9/125, 7.2%) in tumor cells (Fig. 5b, c, d). A positive staining (either cytoplasmic or nuclear) in more than 50% of the tumor cells was found in 71 of 125 (56.8%) cases. A positive staining in less than 50% of the tumor cells was found in 54 of 125 (43.2%) cases. Nuclear and additional cytoplasmic expression (104/125, 83.2%) was compared with entirely cytoplasmic expression (21/125, 16.8%). High-grade tumors were significantly more prevalent in cases with an exclusive cytoplasmic expression of $p27^{kip1}$ (17/21, 81%), indicating a non-functional protein, while low-grade tumors were significantly more prevalent in cases with an additional or exclusive nuclear expression (57/104, 54.8%; P=0.0028, Fig. 6). No significant association was found between the localization of the expression of $p27^{kip1}$ and pathological tumor stage (organ-confined versus advanced).

PTEN and $p27^{kip1}$ immunohistochemistry

Tumor tissue that expressed moderate to strong levels of PTEN protein showed significantly more prevalent cases with nuclear staining for $p27^{kip1}$ (70/78, 89.7%) than exclusive cytoplasmic staining (8/78, 10.3%). Tumor tissue with absent or low levels of PTEN showed a higher percentage of exclusive cytoplasmic staining for $p27^{kip1}$ than the previous group (12/38, 31.6%) (P=0.0077).

Cases were separated into three groups to look more closely at the simultaneous PTEN and $p27^{kip1}$ expression: (1) tumors with a nuclear $p27^{kip1}$ expression and a moderate to strong PTEN expression; (2) tumors with either cytoplasmic $p27^{kip1}$ expression only and a moderate to strong PTEN expression or a nuclear $p27^{kip1}$ expression and an absent or weak PTEN expression; (3) tumors with a cytoplasmic $p27^{kip1}$ expression only and an absent or weak PTEN expression. Cases in which both tumor suppressors were moderate to strong (PTEN) and not mislocalized ($p27^{kip1}$) (group 1) included 43 of 70 (61.4%) low-grade tumors and 27 of 70 (38.6%) high-grade tumors. Cases in which one of the tumor suppressors was either downregulated (PTEN) or mislocalized ($p27^{kip1}$) (group 2) included 9 of 34 (26.5%) low-grade tumors and 25 of 34 (73.5%) high-grade tumors. Cases in which both tumor suppressors were downregulated (PTEN) or mislocalized ($p27^{kip1}$) (group 3) included 2 of 12 (16.7%) low-grade tumors and 10 of 12 (83.3%) high-grade tu-

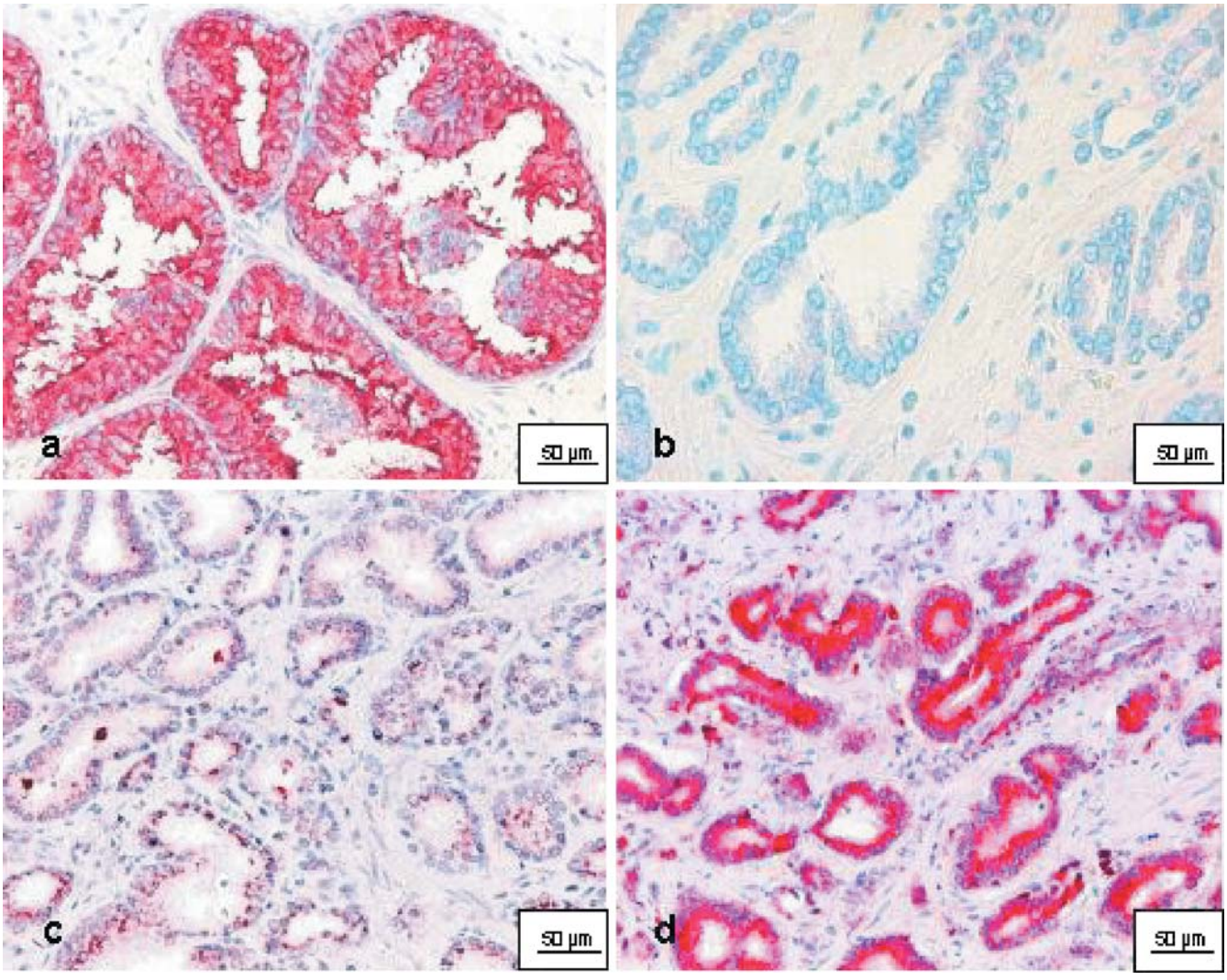

Fig. 3 Immunohistochemical analysis of PTEN. The expression rate was scored for both intensity and quantity of tumor cells stained. The score was evaluated by multiplication of intensity and quantity. Representative pictures show: tumor-free tissue (**a**), tumor tissue with no staining (**b**), mixed staining (**c**), ubiquitous staining (**d**)

mors. Because of the rather small size of the third group, statistical analysis could not be performed (Fig. 7).

PTEN and $p27^{kip1}$ expression in needle biopsies

Gleason grade in biopsies and surgical specimens was unchanged in 25 of 32 (78.1%) cases while grading changed in 7 of 32 (21.9%) cases. An absent or weak PTEN expression was found in one high-grade biopsy, while a moderate to strong PTEN expression was found in 18 of 32 biopsies with low-grade tumors and in 13 of 32 biopsies with high-grade tumors. Because the group of absent or weak PTEN expression included only one case, no reasonable analysis of the association between PTEN expression and Gleason score in biopsies was possible. In 20 of 32 (62.5%) cases, the PTEN expression pattern in the biopsy and operation specimen was the same, while in 12 of 32 (37.5%) cases, expression patterns changed.

Cytoplasmic $p27^{kip1}$ expression was found in one biopsy with low-grade tumors and 7 of 32 biopsies with high-grade tumors, while an additional or total nuclear expression was found in 17 of 32 biopsies with low-grade and 7 of 32 biopsies with high-grade tumors. High-grade tumors were significantly more prevalent in cases with cytoplasmic $p27^{kip1}$ expression (7/8, 87.5%), while low-grade tumors were more prevalent in cases with an additional or total nuclear expression (17/24, 70.8%; P= 0.0103). In 23 of 32 (71.9%) cases, the $p27^{kip1}$ expression in the biopsy was nuclear and or cytoplasmic, as in the prostatectomy, while in 9 of 32 (28.1%) cases, the localization changed.

Analysis of the simultaneous expression of both tumor suppressors in biopsies showed similar results compared with prostatectomies. Group 1 [both tumor suppressors were moderate to strong (PTEN) and not mislocalized ($p27^{kip1}$)] included 16 of 24 (66.7%) low-grade and 8 of 24 (33.3%) high-grade tumors. Group 2 [one of the tumor

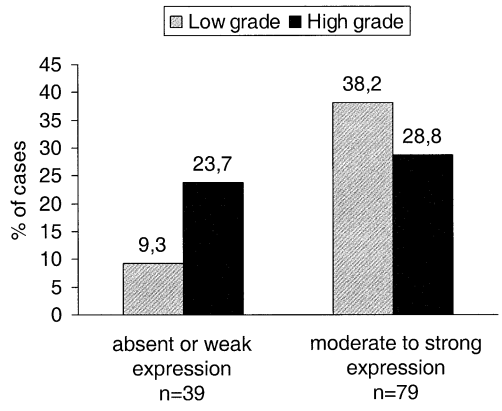

Fig. 4 Association of PTEN expression in immunohistochemistry with tumor grade in prostatic carcinoma (n=118). Tumors with Gleason scores less than or equal to six were considered as low-grade tumors, Gleason scores greater than or equal to seven as high-grade tumors. High-grade tumors (*black bars*) were significantly more prevalent in cases with absent or weak PTEN expression (score$\leq$1), while low-grade tumors (*hatched bars*) were more prevalent in cases with moderate to strong PTEN expression (score$\geq$2). χ^2-test revealed 8.66, P=0.003

suppressors was either downregulated (PTEN) or mislocalized ($p27^{kip1}$)] included 2 of 7 (28.6%) low-grade and 5 of 7 (71.4%) high-grade tumors, while group 3 [both tumor suppressors were downregulated (PTEN) or mislocalized ($p27^{kip1}$), respectively] included one high-grade tumor. For statistical analysis, a larger number of biopsies in group 3 would be needed.

PTEN expression pattern in the biopsies could correctly predict the tumor grade in the surgical specimen in 19 of 32 cases (absent or weak expression identified high-grade tumors while moderate to strong expression identified low-grade tumors). $p27^{kip1}$ expression pattern in the biopsies could correctly predict the tumor grade in the surgical specimen in 24 of 32 cases (cytoplasmatic expression identified high-grade tumors while additional or exclusive nuclear expression identified low-grade tumors). The Gleason grading matched in 25 of 32 cases in biopsies and prostatectomies. While the combination using the BTP rule yielded almost identical accuracy as the Gleason score alone (26/32 versus 25/32), the BTN rule was clearly inferior, with an accuracy of 18 of 32. The combination of the Gleason score and $p27^{kip1}$ expression in biopsies as predictor for the Gleason grade of the surgical sample was, therefore, as reliable as the Gleason score alone.

Discussion

Early-stage prostate cancer is curable, and since a reliable preventive care is not available, an early diagnosis is of eminent significance. The clinical course of the disease is of extreme variability and cases of asymptomatic progressive disease are frequent.

According to this, promising expectations focus on research concerning the molecular biology of prostate cancer. To gain insight into the molecular mechanisms of carcinogenesis and tumor markers to predict a definitive prognosis and to find cellular functions suitable for therapeutic interference is the focus of many current investigations.

It has been shown that $PTEN^{+/-}$- and $p27^{kip1-/-}$-knockout mice develop a variety of tumor types and, in all cases, prostate cancer. However, mice that were lacking only one PTEN allele and possessed intact $p27^{kip1}$ on both chromosomes showed tumor development in the prostate in only 50% of all cases. In the remaining tumor-free prostatic tissue, Di Cristofano et al. observed a two-times higher proliferation rate in prostate tumors of $PTEN^{+/-}$- and $p27^{kip1-/-}$-knockout mice compared with tumor-free prostatic tissue in mice that were lacking either one PTEN allele or both $p27^{kip1}$ alleles [4]. PTEN and $p27^{kip1}$ cooperate in tumor suppression, and loss of both is a key event in the pathogenesis of epithelial cancers. It needs to be demonstrated whether the critical relevance of these two tumor suppressors for prostate cancer pathogenesis in a mouse model parallels the human disease. PTEN can be inactivated through a variety of mechanisms, such as somatic mutations, promoter methylation, decreased translation and/or transcription, increased protein degradation or subcellular compartmentalization [2, 27]. Loss of heterozygosity has been shown to occur in a range of 19% to 65%, according to different studies [18]. As reduced PTEN expression in immunohistochemistry appeared to be a useful marker for early precancerous lesions in endometrial carcinomas, there is good reason to believe that this could be of similar value in prostate cancer [16]. Our results showed a high rate of PTEN protein downregulation in prostate tumors. High-grade tumors were significantly more prevalent in cases with absent or weak PTEN expression, and low-grade tumors were more prevalent in cases with moderate to strong PTEN expression using immunohistochemistry and Western-blot analysis. The association between reduced PTEN expression and increased Gleason grade finds support in a previous study on prostate cancer [15].

$p27^{kip1}$ expression can be regulated using transcription, control of mRNA translation or protein degradation [5, 8]. Even though there are number of tumors in which total $p27^{kip1}$ protein levels are not significantly downregulated [1], which has also been reported for prostate cancer [6, 11], some studies still observe associations between $p27^{kip1}$ levels and tumor grade [30]. To inhibit cyclinE/Cdk2 complex, $p27^{kip1}$ needs to be imported into the nucleus [20]. As cells progress along the cell cycle, $p27^{kip1}$ shuttles between nucleus and cytoplasm. In response to mitogenic stimulation, a characteristic of malignancies, $p27^{kip1}$ is phosphorylated through Akt and translocated to the cytoplasm [21]. Cytoplasmic $p27^{kip1}$, therefore, is inactive and cannot induce apoptosis. Immunohistochemical results of $p27^{kip1}$ showed a significant correlation between the localization of the tumor cells stained and tumor grade. Cases with nuclear staining or additional cytoplasmic staining showed more low-grade tumors, while high-grade tumors were found more often

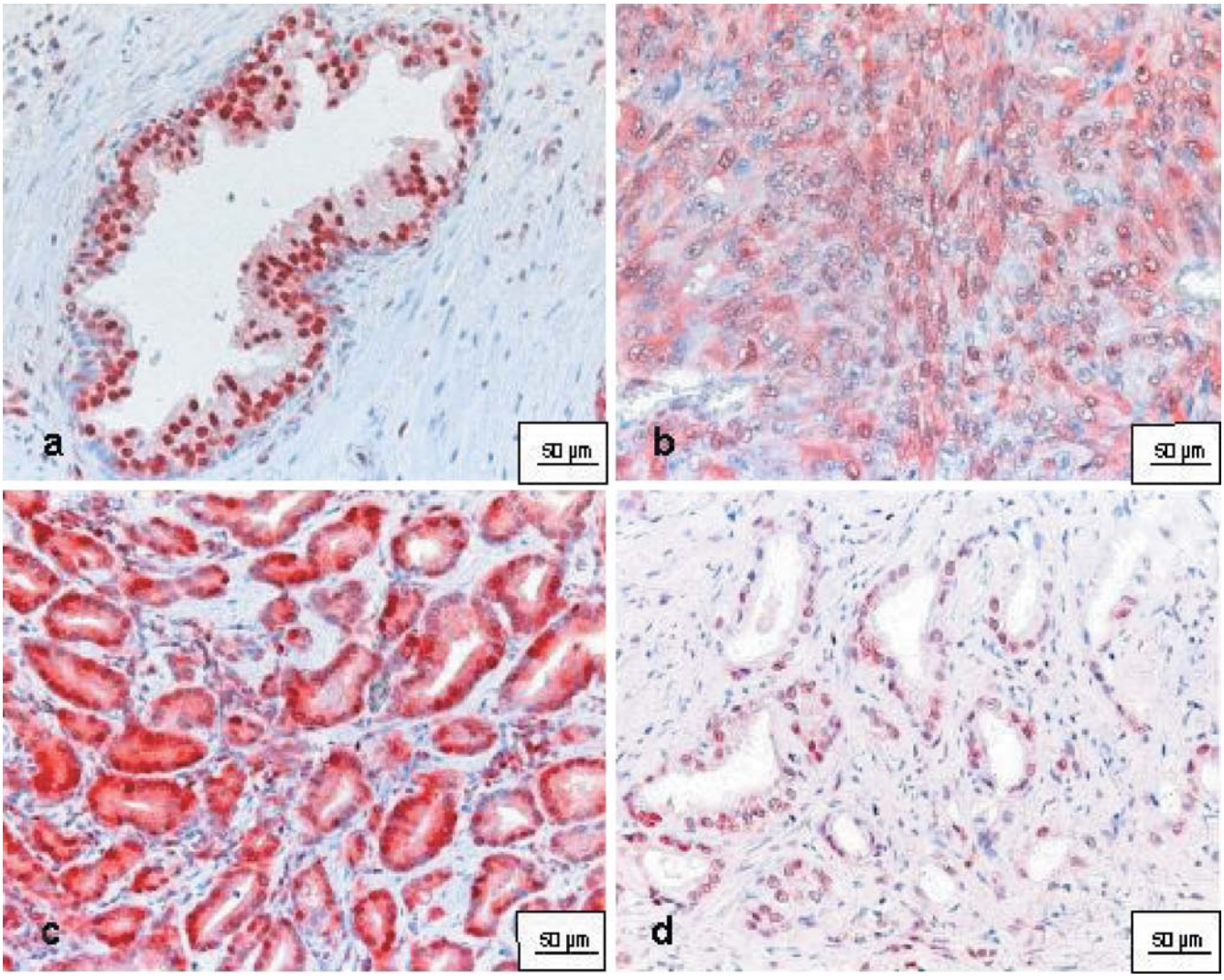

Fig. 5 Immunohistochemical analysis of $p27^{kip1}$. The expression rate was scored for both localization and quantity of tumor cells stained. Representative pictures show tumor-free tissue (**a**), tumor tissue with cytoplasmic (**b**), cytoplasmic and nuclear (**c**), nuclear staining of tumor cells (**d**)

in cases with exclusive cytoplasmic staining. This holds true in breast cancer, where cytoplasmic localization was linked to both differentiation state of tumors and patient survival [13].

The observation that tumor tissue expressing high levels of PTEN had also a significantly high expression rate of nuclear $p27^{kip1}$ confirmed previous studies, where PTEN influenced $p27^{kip1}$ positively through negative implication of the Akt-pathway [29, 31]. Accordingly, tumor tissue with low levels of PTEN expressed $p27^{kip1}$ more often only in the cytoplasm. In other words, missing PTEN leads to higher Akt levels, which result in dissociation of the $p27^{kip1}$/cyclinE/Cdk2-complex, phosphorylation of $p27^{kip1}$ and transport from the nucleus into the cytoplasm. In a previous investigation, we could, in fact, show that Akt is increased in prostatic carcinoma [14]. Akt perturbation, therefore, seems to play an important role in the initiation and progression of prostate cancer.

The observation that reduced PTEN or $p27^{kip1}$ expression or a reduced expression of both promotes an aggressive tumor phenotype, as demonstrated in this study, follows the concept of tumorigenesis in the prostate by missing or deleted tumor suppressors.

The results obtained from a relatively small number of needle biopsies indicate that expression patterns of PTEN and $p27^{kip1}$ are very similar in biopsies and corresponding prostatectomies. In 62.5%, PTEN showed the same expression pattern (absent or weak versus moderate to strong) in needle biopsies and prostatectomies, while in 71.9%, $p27^{kip1}$ expression showed the same localization (cytoplasmic expression versus additional or total nuclear expression) in needle biopsies and prostatectomies.

Differences between the expression patterns in the needle biopsy and the surgical specimen may be due to the fact that biopsies do not always contain representative tumor tissue, which is also reflected in the cases in which grading changed between the biopsy and the prostatec-

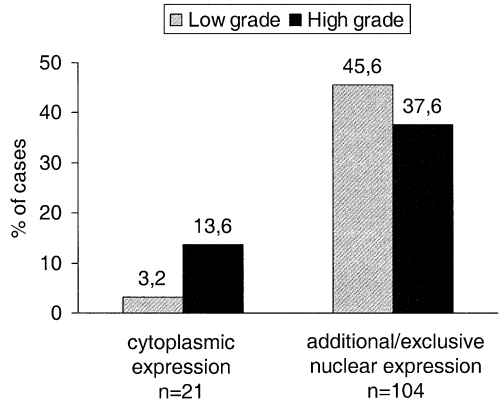

Fig. 6 Association of $p27^{kip1}$ expression with tumor grade in prostatic carcinoma (n=125). Tumors with Gleason scores less than or equal to six were considered as low-grade, Gleason scores greater than seven as high-grade tumors. High-grade tumors (*black bars*) were significantly more prevalent in cases with an exclusive cytoplasmic expression of $p27^{kip1}$ (scores=1; 4) while low-grade tumors (*hatched bars*) were more prevalent in cases with an additional or exclusive nuclear staining (scores=2; 3; 5; 6). χ^2-test revealed 8.94, P=0.003

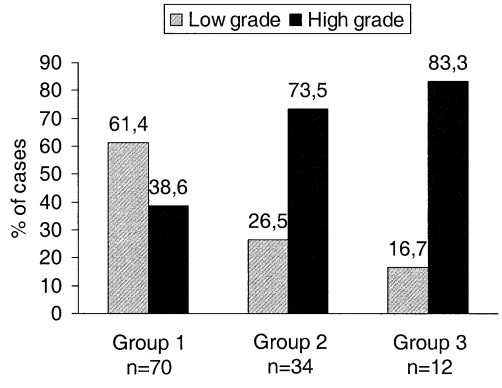

Fig. 7 Association of PTEN and $p27^{kip1}$ expression with tumor grade in prostatic carcinoma (n=118). Tumors with Gleason scores less than or equal to six were considered as low-grade (*hatched bars*), Gleason scores greater than or equal to seven as high-grade tumors (*black bars*). Cases with moderate to strong levels of PTEN and functional $p27^{kip1}$ showed only 38.6% high-grade tumors (group 1), while cases with one downregulated/mislocalized tumor suppressor showed 73.5% high-grade tumors (group 2) and cases with absent or weak PTEN levels and non-functional $p27^{kip1}$ showed 83.3% high-grade tumors (group 3)

tomy. It may occur that the main growth or expression pattern of the tumor tissue is not present in the needle biopsy, which is a general problem. It is more likely, that representative tumor areas are missing in the biopsy rather than a progress or change of growth pattern. Prediction of tumor grade is important, since grading has an impact on the decision of therapeutic approaches. The interpretation of an expression pattern instead of a growth pattern in needle biopsies has the advantage that small tumor samples can also be evaluated.

In this study, $p27^{kip1}$ and PTEN, or their combination with the Gleason score in biopsies, did not show a higher predictive accuracy of the tumor grade in the surgical specimen than the Gleason score alone. However, the immunohistochemical profile of $p27^{kip1}$ has the same predictive value as the Gleason score alone in needle biopsies.

Acknowledgement This work was supported by Tumorzentrum HD/MA grant 781012.

References

1. Catzavelos C, Bhattacharya N, Ung YC, Wilson JA, Roncari L, Sandhu C, Shaw P, Yeger H, Morava-Protzner I, Kapusta L (1997) Decreased levels of the cell-cycle inhibitor $p27^{kip1}$ protein: prognostic implications in primary breast cancer. Nat Med 3:227–230
2. Dahia PL, Aguiar RC, Alberta J, Kum JB, Caron S, Sill H, Marsh DJ, Ritz J, Freedman A, Stiles C (1999) PTEN is inversely correlated with the cell survival factor Akt/PKB and is inactivated via multiple mechanisms in haematological malignancies. Hum Mol Genet 8:185–193
3. Di Cristofano A, Pandolfi PP (2000) The multiple roles of PTEN in tumor suppression. Cell 100:387–390
4. Di Cristofano A, De Acetis M, Koff A, Cordon-Cardo C, Pandolfi PP (2001) PTEN and $p27^{kip1}$ cooperate in prostate cancer tumor suppression in the mouse. Nat Genet 27:222–224
5. Dijkers PF, Medema RH, Pals C, Banerji L, Thomas NS, Lam EW, Burgering BM, Raaijmakers JA, Lammers JW, Koenderman L (2000) Forkhead transcription factor FKHR-L1 modulates cytokine-dependent transcriptional regulation of $p27^{kip1}$. Mol Cell Biol 20:9138–9148
6. Freedland SJ, deGregorio F, Sacoolidge JC, Elshimali YI, Csathy GS, Dorey F, Reiter RE, Aronson WJ (2003) Preoperative $p27^{kip1}$ status is an independent predictor of prostate specific antigen failure following radical prostatectomy. J Urol 169:1325–1330
7. Gleason DF (1992) Histologic grading of prostate cancer: a perspective. Hum Pathol 23:273–279
8. Hengst L, Reed SI (1996) Translational control of $p27^{kip1}$ accumulation during the cell cycle. Science 271:1861–1864
9. Jemal A, Momas A, Murray T, Thun M (2002) Cancer statistics, 2002. CA Cancer J Clin 52:23–47
10. Kohler G, Milstein C (1975) Continuous cultures of fused cells secreting antibody of predefined specificity. Nature 256:495–497
11. Kuczyk M, Machtens S (1999) Predictive value of decreased $p27^{kip1}$ protein expression for the recurrence-free and long-term survival of prostate cancer patients. Br J Cancer 81:1052–1058
12. Li J, Yen C, Liaw D, Podsypanina K, Bose S, Wang SI, Puc J, Miliaresis C, Rodgers L, McCombie R (1997) PTEN, a putative protein tyrosine phosphatase gene mutated in human brain, breast, and prostate cancer. Science 275:1943–1947
13. Liang J, Zubovitz J, Petrocelli T, Kotchetkov R, Connor MK, Han K, Lee JH, Ciarallo S, Catzavelos C, Beniston R (2002) PKB/Akt phosphorylates p27, impairs nuclear import of p27 and opposes p27-mediated G1 arrest. Nat Med 8:1153–1160
14. Liao Y, Grobholz R, Abel U, Trojan L, Michel MS, Angel P, Mayer D (2003) Increase of AKT/PKB expression correlates with Gleason pattern in human prostate cancer. Int J Cancer 107:676–680
15. McMenamin ME, Soung P, Perera S, Kaplan I, Loda M, Sellers WR (1999) Loss of PTEN expression in paraffin-embedded primary prostate cancer correlates with high Gleason score and advanced stage. Cancer Res 59:4291–4296
16. Mutter GL, Lin MC, Fitzgerald JT, Kum JB, Baak JP, Lees JA, Weng LP, Eng C (2000) Altered PTEN expression as a diagnostic marker for the earliest endometrial precancers. J Natl Cancer Inst 92:924–930
17. Nelen MR, van Staveren WC, Peeters EA, Hassel MB, Gorlin RJ, Hamm H, Lindboe CF, Fryns JP, Sijmons RH, Woods DG

(1997) Germline mutations in the PTEN/MMAC1 gene in patients with Cowden disease. Hum Mol Genet 6:1383–1387
18. Ramaswarny S, Sellers WR (2000) PTEN: a prostate cancer tumor-suppressor gene. Prostate J 2:55–61
19. Ramaswamy S, Nakamura N, Vazquez F, Batt DB, Perera S, Roberts TM, Sellers WR (1999) Regulation of G1 progression by the PTEN tumor suppressor protein is linked to inhibition of the phosphatidylinositol 3-kinase/Akt pathway. Proc Natl Acad Sci U S A 96:2110–2115
20. Reynisdottir I, Massague J (1997) The subcellular locations of p15(Ink4b) and p27(Kip1) coordinate their inhibitory interactions with cdk4 and cdk2. Genes Dev 11:492–503
21. Rodier G, Montagnoli A, Di Marcotullio L, Coulombe P, Draetta GF, Pagano M, Meloche S (2001) p27 cytoplasmic localization is regulated by phosphorylation on Ser10 and is not a prerequisite for its proteolysis. EMBO J 20:6672–6682
22. Sherr CJ (1996) Cancer cell cycles. Science 274:1672–1677
23. Shin I, Yakes FM, Rojo F, Shin NY, Bakin AV, Baselga J, Arteaga CL (2002) PKB/Akt mediates cell-cycle progression by phosphorylation of p27(Kip1) at threonine 157 and modulation of its cellular localization. Nat Med 8:1145–1152
24. Steck PA, Pershouse MA, Jasser SA, Yung WK, Lin H, Ligon AH, Langford LA, Baumgard ML, Hattier T, Davis T (1997) Identification of a candidate tumour suppressor gene, MMAC1, at chromosome 10q23.3 that is mutated in multiple advanced cancers. Nat Genet 15:356–362
25. Teng DH, Hu R, Lin H, Davis T, Iliev D, Frye C, Swedlund B, Hansen KL, Vinson VL, Gumpper KL (1997) MMAC1/PTEN mutations in primary tumor specimens and tumor cell lines. Cancer Res 57:5221–5225
26. True LD (1994) Surgical pathology examination of the prostate gland. Practice survey by American Society of Clinical Pathologists. Am J Clin Pathol 102:572–579
27. Vazquez F, Grossman SR, Takahashi Y, Rokas MV, Nakamura N, Sellers WR (2001) Phosphorylation of the PTEN tail acts as an inhibitory switch by preventing its recruitment into a protein complex. J Biol Chem 276:48627–48630
28. Verbeke CS, Wenthe U, Grobholz R, Zentgraf H (2001) Fas ligand expression in Hodgkin lymphoma. Am J Surg Pathol 25:388–394
29. Viglietto G, Motti ML, Bruni P, Melillo RM, D'Alessio A, Califano D, Vinci F, Chiappetta G, Tsichlis P, Bellacosa A (2002) Cytoplasmic relocalization and inhibition of the cyclin-dependent kinase inhibitor p27(Kip1) by PKB/Akt-mediated phosphorylation in breast cancer. Nat Med 8:1136–1144
30. Vis AN, Noordzij MA, Fitoz K, Wildhagen MF, Schroder FH, van der Kwast TH (2000) Prognostic value of cell cycle proteins p27(kip1) and MIB-1, and the cell adhesion protein CD44s in surgically treated patients with prostate cancer. J Urol 164:2156–2161
31. Wu X, Senechal K, Neshat MS, Whang YE, Sawyers CL (1998) The PTEN/MMAC1 tumor suppressor phosphatase functions as a negative regulator of the phosphoinositide 3-kinase/Akt pathway. Proc Natl Acad Sci U S A 95:15587–15591

Virchows Arch (2004) 444:518–526
DOI 10.1007/s00428-004-1016-2

ORIGINAL ARTICLE

Christian G. Sauer · Alexandra Kappeler · Monika Späth · Jens J. Kaden · Maurice S. Michel · Doris Mayer · Uwe Bleyl · Rainer Grobholz

Expression and activity of matrix metalloproteinases-2 and -9 in serum, core needle biopsies and tissue specimens of prostate cancer patients

Received: 2 February 2004 / Accepted: 17 March 2004 / Published online: 16 April 2004

Abstract Prostate cancer is the most common cancer in men and second in the cancer-related frequency of mortality. Matrix metalloproteinases (MMPs) are involved in tumor invasion and metastasis in various malignancies. MMP-2 and MMP-9 are capable of digesting collagen type IV. Numerous studies have demonstrated an association between increased MMP-2 and -9 expression and tumor progression in various tumors. In this study, the expression and activities of MMP-2 and -9 were assessed in serum probes and tumor tissue from core needle biopsies and radical prostatectomies of 97 patients. MMP-2 and -9 serum expression was analyzed in a subgroup of 31 patients. MMP-9 serum expression was significantly increased in tumor patients and correlated with tumor grade. In contrast, the MMP-9 tissue expression and activity revealed no significant correlations to tumor stage or grade. The MMP-2 activity, however, showed a positive correlation for MMP-2 with tumor stage. Increased activity was predominantly detected in advanced tumor stages. Immunohistochemical analysis of MMP-2 expression demonstrated a positive association with tumor grade in prostatectomy specimens. The relative expression rates in biopsies matched in 65% with those of the prostatectomies. Detection of MMP-2 in core needle biopsies seems not to be a helpful marker for diagnostic purposes.

Keywords Matrix metalloproteinases · Prostatic carcinoma · Gelatin zymography · Western blot · Immunohistochemistry

C. G. Sauer · A. Kappeler · U. Bleyl · R. Grobholz (✉)
University Hospital Mannheim,
Department of Pathology,
Mannheim, Germany
e-mail: rainer.grobholz@path.ma.uni-heidelberg.de
Tel.: +49-621-383-2781
Fax: +49-621-383-2005

M. Späth · M. S. Michel
University Hospital Mannheim,
Department of Urology,
Mannheim, Germany

J. J. Kaden
University Hospital Mannheim,
I. Department of Medicine,
Mannheim, Germany

D. Mayer
Research Group Hormones and Signal Transduction,
German Cancer Research Center (DKFZ),
Heidelberg, Germany

Pathologisches Institut,
Universitätsklinikum Mannheim,
Theodor-Kutzer-Ufer 1-3, 68167 Mannheim, Germany

Introduction

Prostate cancer has evolved as a major health problem in males in Western countries. The introduction of new diagnostic tools, such as the prostate-specific antigen, rapidly increased the number of newly diagnosed cases over the last two decades. Prostatic carcinoma (PCa) is now the most frequent malignancy and the second leading cause of cancer-related death among men [11].

Although a large proportion of PCa appears as clinically indolent localized disease, some PCas develop to life-threatening tumors with a high metastatic potential. Currently, the tumor progression is assessed particularly by clinical and pathological parameters, such as staging and histopathological grading [7, 28]. The variable aggressive behavior of the tumor makes prediction of individual patient outcome very difficult. Identification of novel prognostic factors is, therefore, an important issue in prostate cancer research.

Matrix metalloproteinases (MMPs) constitute a large family of zinc-dependant endopeptidases involved in the degradation of the extracellular matrix and the basement membrane [24, 34]. The 24 currently known members of this protein family have been shown to be involved in physiological processes, such as tissue remodeling or wound healing, but also play a crucial role in pathological conditions, including tumor invasion and metastasis [3, 22]. Two important members of the MMP-family are

MMP-2 and MMP-9, also known as gelatinases-A and -B, respectively. They specifically cleave type-IV collagen, the major structural component of basement membranes. Increased expression of MMP-2 and MMP-9 has been associated with malignant progression in various cancer types, such as breast, lung or colorectal cancers [4, 6, 15, 19, 25, 35]. Studies on MMP-2 and MMP-9 expression and activity in human PCa have been focused on cell culture systems or blood specimens of cancer patients [5, 8, 14, 21, 33], although only sparse data is available for prostatic tissue directly [2, 9, 26, 29, 30]. While the majority of these studies found a positive correlation between MMP expression and tumor aggression, others could not demonstrate such associations [13].

n this study, we examined MMP-2 and MMP-9 expression and activity in radical prostatectomies, core needle biopsies and serum probes to gain comprehensive insight into the role of MMP-2 and -9 as markers in PCa. Using gelatin zymography, we determined MMP-2 and -9 activity in radical prostatectomies. The expression of MMP-2 was evaluated using immunohistochemistry in surgical specimens and core needle biopsies. MMP-9 expression in tissue specimens was assessed using Western-blot analyses. In addition, the serum levels of MMP-2 and -9 were analyzed using enzyme-linked immunosorbent assay (ELISA). These molecular parameters were then correlated with established clinical markers, such as tumor grade and stage.

Materials and methods

Patients and tissue samples

This study included 97 consecutive patients diagnosed with PCa who had undergone radical prostatectomy at the University Hospital Mannheim. Informed consent was acquired from all patients prior to the investigations. In all cases, native and paraffin-embedded tumor tissue was available. All patients were untreated before surgery. Patient age ranged from 43 years to 79 years (mean 63.0±0.7 years). For all patients, surgical specimens were sectioned according to standard protocols [31]. For pathological evaluation and immunohistochemistry, the biopsies and tissue blocks were fixed in 4% buffered formaldehyde for 24 h and were paraffin embedded. Fresh prostate tissue samples were snap frozen in liquid nitrogen and stored at −80°C until use.

Histomorphological grading was performed according to the Gleason system [7] and staging according to the tumor, nodal and metastasis classification [28]. For statistical evaluations, tumors with Gleason scores of seven and higher were considered as high grade and tumors with Gleason scores of six and lower were considered as low grade. Tumor stages were classified as organ confined (pT2) or advanced (pT3 and pT4). The pathological grades and stages in this study included 49 high-grade and 48 low-grade, 56 organ-confined and 41 advanced tumors.

Core needle biopsies were available from a subset of 23 patients. The mean proportion of tumor cells within the biopsies was 25% (range 1% to 75%). For all biopsies, the Gleason score was determined. The biopsies included 7 high-grade and 16 low-grade tumors.

Gelatin zymography

Gelatin zymography for MMP-2 and MMP-9 activity was performed on 97 specimens of frozen tumor and tumor-free prostate tissue. For localization of tumor and tumor-free tissue, sections of 6 µm were stained with hematoxylin/eosin, respectively. Unstained sections of 20 µm were then used for microscopically controlled manual microdissection of morphologically characterized tumor or tumor-free tissue areas. The tissues were homogenized in ice-cold lysis buffer (50 mM Tris-HCl (pH 7.5), 10 mM $CaCl_2$, 0.05% Brij 35, 0.1% sodium dodecyl sulfate (SDS), 1% Triton X-100, 1 M urea and 1 mM phenylmethylsulfonyl fluoride), and the cellular debris was precipitated. The MMP-containing supernatant was transferred into a fresh tube, and total protein concentrations were determined by a dye-binding assay (Bio-Rad, Munich, Germany) at 450 nm according to Bradford. Of total protein from tumor and tumor-free tissue, 10 µg were separated under non-reducing conditions on a 12% SDS gel containing 1 mg/ml gelatin. Next, 10 ng purified human MMP-2 and MMP-9 (Chemicon International Inc., Temecula, USA) were loaded as controls, respectively. After electrophoresis, the gels were soaked twice for 15 min in 2.5% (w/v) Triton-X 100, 50 mM Tris-HCl (pH 7.5) with gentle shaking at room temperature. The gels were rinsed and incubated overnight at 37°C in calcium buffer (50 mM Tris-HCl pH 7.5, 10 mM $CaCl_2$, 0.3% Brij-35).

After incubation, the gels were stained in 0.2% Coomassie blue R250 in 25% (v/v) isopropyl alcohol and 10% (v/v) acetic acid followed by washout of excessive dye by a mixture of 25% (v/v) isopropyl alcohol and 10% (v/v) acetic acid. The dried gels were digitally scanned, and lysis bands of the latent and active forms of MMP-2 and -9 were separately analyzed using densitometry (AIDA Software, Raytest Isotopenmeßgeräte GmbH, Straubenhardt, Germany). The tumor/tumor-free (T/TF) ratios were calculated for the latent and active MMP forms individually for each case.

MMP-9 protein expression

MMP-9 immunohistochemistry was performed using two different commercially available monoclonal antibodies (clone IA5; Oncogene, Boston, USA; clone 4H3; R&D Systems, Minneapolis, USA). Using various unmasking procedures and visualization techniques, no satisfactory staining results could be obtained. The expression of MMP-9 was, therefore, analyzed by Western blotting of manually microdissected tissue. In brief, samples of frozen tumor and tumor-free tissue were isolated as described above. The tissues were homogenized in lysis buffer [150 mM NaCl, 105 mM ethylenediaminetetraacetate (EDTA), 3% glycerol, 1 mg/ml bovine serum albumin, 1% IGEPAL CA-630 (Sigma-Aldrich Chemie, Steinheim, Germany)]. After determining the protein concentration using a Bradford-assay, a cocktail of proteinase inhibitors [1 µg/ml leupeptin (Amersham Pharmacia Biotech, Freiburg, Germany), 5 µg/ml aprotinin (Roth, Karlsruhe, Germany), 2 µg/ml pepstatin A (Amersham Pharmacia Biotech, Freiburg, Germany) and 0.5 mM pefabloc (Roche Diagnostics, Mannheim, Germany)] was added. From each sample, 10 µg of total protein were separated on 18% SDS-polyacrylamide gel electrophoresis (PAGE) and transferred to PVDF membranes. The membranes were blocked with 5% skim milk (Slimfast, Wiesbaden, Germany) and incubated overnight at 4°C with a monoclonal anti–human MMP-9 antibody (clone 4H3; R&D Systems, Minneapolis, USA) at a dilution of 1:500. After thorough washing, a biotin-SP-conjugated goat-anti mouse antibody (Jackson Immuno Research, Pennsylvania, USA) was applied at a 1:1000 dilution for 90 min at room temperature. Subsequently, the membranes were washed as above and incubated with streptavidin conjugated alkaline phosphatase (Jackson Immuno Research, Pennsylvania, USA) diluted to 1:250 at room temperature for 60 min. Bands were visualized using 5-bromo-4-chloro-3-indolyl phosphate/nitroblue tetrazolium (BCIP/NBT) (Roche Diagnostics, Mannheim, Germany) in AP-buffer (100 mM Tris-HCl pH 8.0, 100 mM NaCl, 50 mM $MgCl_2$). On each blot, 10 ng of purified human MMP-9 protein (Chemicon International Inc., Temecula,

USA) served as control. The expression rate of MMP-9 was calculated as tumor/tumor-free ratios after densitometrical analyses (AIDA Software, Raytest Isotopenmeßgeräte GmbH, Straubenhardt, Germany).

Immunohistochemistry

Immunohistochemistry was performed using a mouse monoclonal antibody to human MMP-2 (clone MAB13431, Chemicon International Inc., Temecula, USA). This antibody recognizes both the pro and active form of human MMP-2 and does not cross react with pro and active forms of other MMPs.

Sections of 3 μm were obtained from formaldehyde-fixed and paraffin-embedded biopsies and radical-prostatectomy specimens. The tissue was deparaffinized and rehydrated through a series of graded alcohols. For antigen retrieval, the slides were placed in 10 mM citrate buffer (pH 6.0) and boiled using microwave heating at 600 W for 3×5 min. Non-specific sites were blocked with 3% bovine serum albumin (Sigma, Munich, Germany). Sections were incubated with the MMP-2 antibody at a 1:1.500 dilution at 4°C overnight. Immunoreactive sites were detected using incubation with a 1:1.000 dilution of biotin-SP-conjugated goat-anti mouse IgG/IgM (Jackson Immuno Research, Pennsylvania, USA) for 30 min at room temperature and subsequent incubation with streptavidin-conjugated alkaline phosphatase (Jackson Immuno Research, Pennsylvania, USA) diluted to 1:250 at room temperature for 30 min. Immunoreactive sites were developed using Fast Red substrate containing levamisole (Roche Diagnostics, Mannheim, Germany). Sections were counterstained with hematoxylin and mounted in Kaiser's glycerol gelatin (Merck, Darmstadt, Germany).

Stained slides were examined to identify the cellular localization of MMP-2 immunoreactivity and scored for both intensity (–/+, ++, +++) and proportion (0–5%, 6–25%, 26–50%, 50–75%, >75%) of tumor cells stained. Stromal staining was scored for intensity (–/+, ++, +++). Integer values were assigned to the scores of intensity (1–3), proportion of tumor cells stained (1–5) and stromal staining (1–3). These values were multiplied to provide a single score for each case.

Enzyme-linked immunosorbent assay

Preoperative serum samples were available from a subset of 31 patients. Those included 20 high-grade and 11 low-grade, 19 organ-confined and 12 advanced tumors. The serum levels of MMP-2 and MMP-9 in these samples were determined using commercially available ELISAs for MMP-2 and MMP-9 (BIOTRAK, Amersham Biosciences, Freiburg, Germany). The assays were performed according to the manufacturer's instructions. The serum probes were diluted at 1:50 for the MMP-2 assay and at 1:20 for the MMP-9 assay. A group of five and eight patients with benign prostate hyperplasia (BPH) was used as controls, respectively.

Statistical analysis

Data is presented as mean value±standard error of mean. Statistical analyses were performed using chi-square (χ^2)-test for correlation between molecular and histopathological parameters. Normal distribution of data was analyzed using Kolmogorov-Smirnov test. Comparison between non-paired data of ELISA was made using the Mann-Whitney test. P values of <0.05 are considered statistically significant. Statistical calculations were done using Microsoft Excel data analysis software (Microsoft, Richmond, USA) and PC-Statistik 2.05 software package (TopSoft, Hannover, Germany).

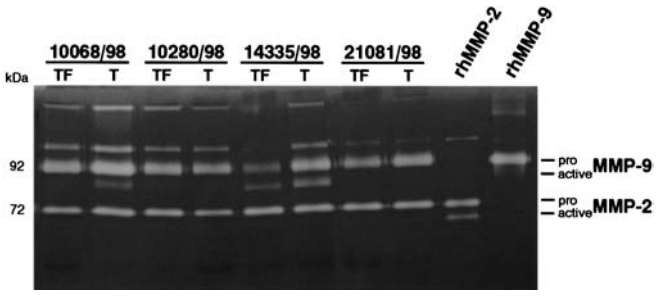

Fig. 1 Representative gelatin zymography of prostate tissue homogenates. Gelatinolytic activities of matrix metalloproteinase (MMP)-2 and MMP-9 from tumor-free (*TF*) and tumor (*T*) prostate tissue are visible as clear bands against the stained background. Each lane contains 10 μg of total protein extract. Lanes with purified recombinant human MMPs (rhMMPs) contain 10 ng each

Results

MMP-2 and MMP-9 activity

The activities of MMP-2 and MMP-9 were evaluated in tumor and tumor-free tissue of 97 radical prostatectomies using gelatin zymography. Two distinct bands of gelatinolytic activity were detected in all analyzed samples at approximately 90 kDa and 70 kDa (Fig. 1). Additional weaker lysis bands below the main bands were detected in 88 of 97 (90.7%) of the analyzed samples. Gelatinolytic activity could be completely inhibited by incubating the zymograms in 10 mM EDTA, an unselective MMP inhibitor, identifying the observed enzymes as gelatinases. The lysis bands were further characterized as pro-MMP-9 (92 kDa), pro-MMP-2 (72 kDa), active MMP-2 (90 kDa) and active MMP-9 (70 kDa) by comparison with purified human MMP-2 and MMP-9 protein (Fig. 1).

The mean value of all tumor/tumor-free ratios was 0.96±0.08 for pro-MMP-2 and 1.84±0.17 for active MMP-2. An increased MMP-2 activity, which was defined by a cutoff point of 1 for the ratios of tumor versus tumor-free tissue was found in 33 of 97 (34.0%) of the patients for pro-MMP-2 and in 49 of 88 (55.7%) of the patients for the active form of MMP-2. A raised MMP-2 activity was generally found in advanced tumor stages (pT3 and pT4), while decreased activity was associated with organ-confined tumors (pT2) (P=0.046, pro-MMP2; P=0.014, active MMP-2) (Fig. 2). A significant correlation between MMP-2 activity and tumor grade could not be detected.

The mean values for all calculated ratios were 2.70±0.76 for the pro-form and 2.48±0.33 for the active form of MMP-9. An increased tumor/tumor-free ratio (cutoff=1) was found in 57 of 97 (58.8%) samples of pro-MMP-9 and 45 of 88 (51.1%) of active MMP-9. Association analysis between activity of pro and active forms of MMP-9 and tumor stage or grade yielded no significant correlations.

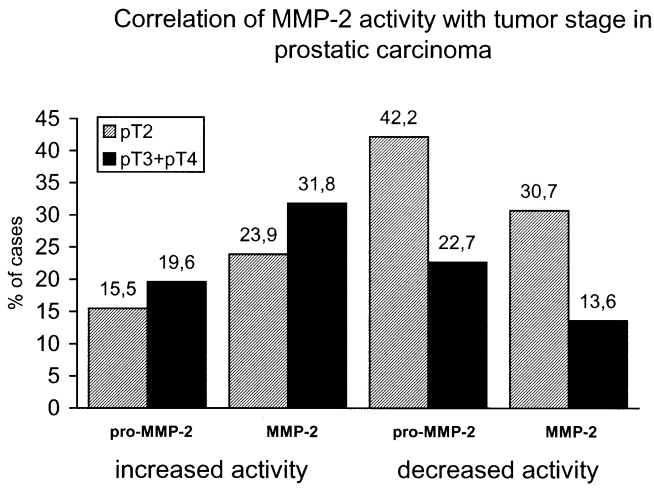

Fig. 2 Increased matrix metalloproteinase (MMP)-2 activity is associated with advanced (pT3, pT4) tumor stages, while organ-confined (pT2) tumors showed a decreased MMP-2 activity. A similar association was found for the pro (P=0.046) and active form (P=0.014) or MMP-2. A cut-off point of 1 for tumor/tumor-free ratio was chosen to discriminate between increased and decreased activity. Advanced tumor stages are represented by a *solid bar*, while the group of organ-confined tumors is show as a *hatched bar*

MMP-2 and MMP-9 tissue expression

The staining in tumor cells with MMP-2 was cytoplasmic and variable regarding intensity and proportion. An additional non-uniform reactivity at a generally lower level was observed in benign cells. Immunoreactivity of MMP-2 was scored as product of the intensity and proportion of stained tumor cells and intensity of stained stromal cells in prostatic tumor tissue of surgical specimens (Fig. 3a, b, c, d) and core needle biopsies (Fig. 3e). The mean values of all determined expression scores were 4.1±0.3 for 96 prostatectomies and 3.1±0.7 for 23 biopsies. The thereby deduced cutoff values for prostatectomies of four and biopsies of three gave 50 specimens and 16 biopsies a weak and 46 specimens and 7 biopsies a strong expression score. Statistical analyses revealed a positive correlation between expression score and tumor grade in surgical specimens (Fig. 4). High expression levels were predominantly found in high-grade tumors (Gleason score $\geq$7), while low expression scores were associated with low-grade tumors (Gleason score <7) (P=0.024).

The expression pattern of MMP-2 in biopsies was similar compared with prostatectomies. In 15 of 23 (65.2%) of the biopsies, the relative expression levels were identical to those found in the surgical specimens of the same patients. In five of the remaining seven biopsies, the relative expression levels were decreased, while they were increased in the respective prostatectomies. Two patients, however, showed an increased expression in biopsy and a decreased expression in the surgical specimen. A significant correlation between MMP-2 expression score and tumor grade or stage, as observed in prostatectomies, could not be found in the biopsies.

The expression of MMP-9 was analyzed using immunoblotting (Fig. 5). MMP-9 was detectable in all 94 prostatic tissue samples available. The mean value of all calculated tumor/tumor-free ratios was 1.62±0.28. An increased MMP-9 expression, defined by a tumor versus tumor-free ratio $\geq$1 was found in 36 of 94 (38.3%) specimens. MMP-9 expression showed no significant correlation with tumor stage or grade.

MMP activity and protein expression

The expression rates of MMP-2 and MMP-9 determined using immunohistochemistry and Western blotting were correlated with the activity data of the pro and active forms. The expression of MMP-2 as well as MMP-9 showed no significant correlation to the activity of the respective pro-MMP. However, a significant inverse correlation was found for the activity of the active form of MMP-2 and MMP-2 expression (P=0.04, Table 1). More patients with an increased MMP-2 activity had a weak MMP-2 expression (33.3% versus 21.8%), while more patients with a decreased MMP-2 activity had a strong MMP-2 expression (27.6% versus 17.2%). For MMP-9, a similar correlation between the active form and the protein expression was not present (Table 1).

MMP-2 and MMP-9 serum expression

Serum levels of MMP-2 and MMP-9 were determined in a subgroup of 31 PCa patients and five or eight BPH controls, respectively (Table 2). No significant differences were found in serum levels of MMP-2 between BPH controls (1246.45±87.28 ng/ml) and PCa patients (1121.43±25.51 ng/ml) or between groups of different tumor stages and grades (Table 2). The relative serum levels found in 16 of 31 (51.6%) PCa patients matched with those found in the corresponding surgical specimens. In 10 of the 15 remaining PCa patients, the relative expression levels were increased in the serum probes, while they were decreased in the prostatectomies, respectively.

The serum concentration of MMP-9 was significantly increased in PCa patients (383.58±31.87 ng/ml) compared with the control group (250.92±22.43 ng/ml) (P=0.008) (Table 2). A significant correlation was found for the expression of MMP-9 in PCa patients and Gleason score, based on a cutoff value of 307.03 ng/ml representing the median of all evaluated MMP-9 serum concentrations in PCa patients (P=0.044) (Table 2, Fig. 6).

MMP-2 expression in biopsies, prostatectomies and serum

In six cases, probes were available for all three analyses of MMP-2 expression in prostatectomies, biopsies and serum (Table 3). In three of those (27780/99, 37736/99 and 29701/99), consistent relative expression rates could be

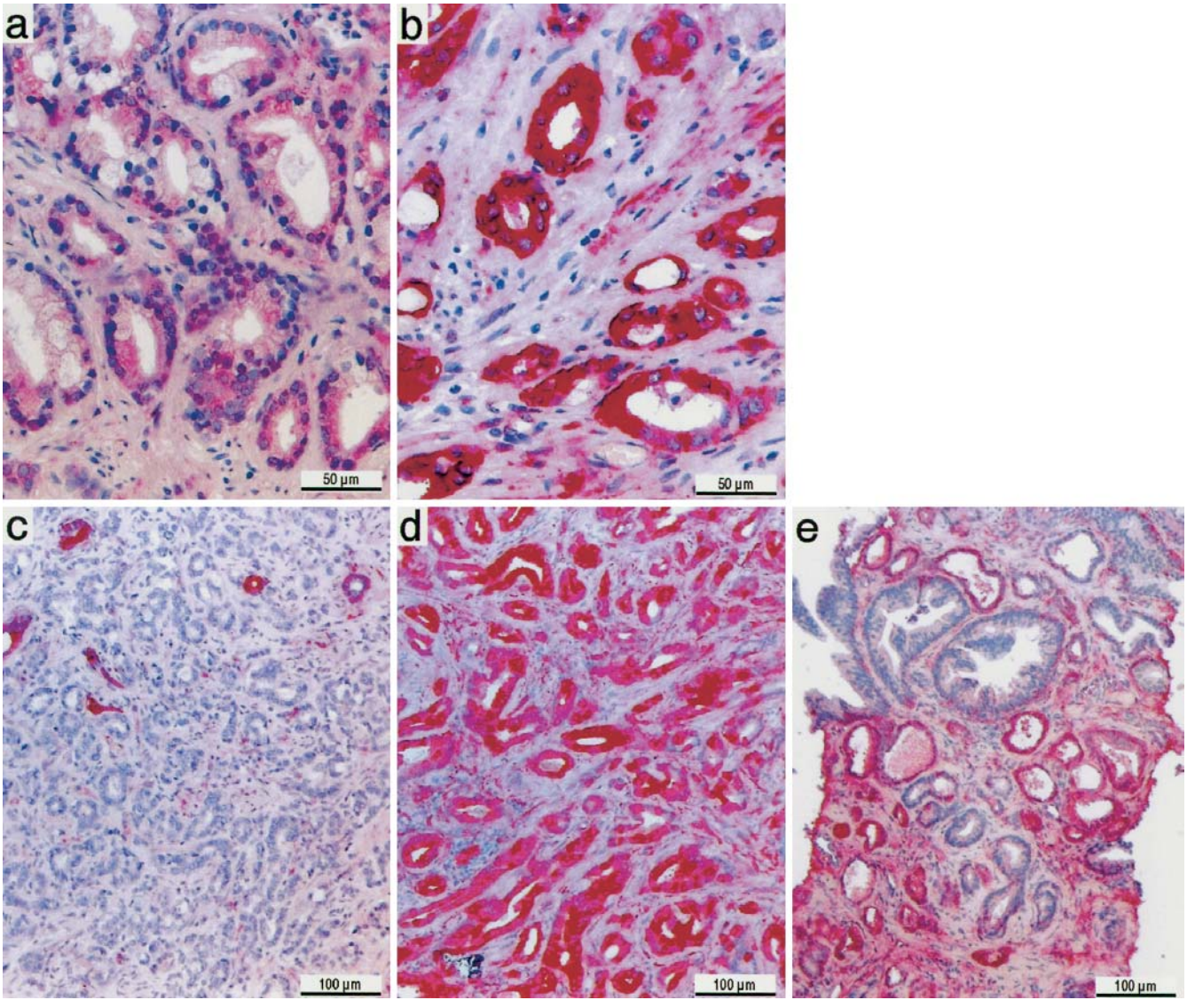

Fig. 3 Immunohistochemical analysis of matrix metalloproteinase (MMP)-2. The expression rate was scored as the product of intensity (I, range 1 to 3) and proportion (P, range 1 to 5) of stained tumor cells. Representative pictures show weak (**a**) (I1), strong (**b**) (I3), occasional (**c**) (P1) and ubiquitous (**d**) (P5) staining of tumor cells, respectively. **e** Representative staining of core needle biopsy with heterogeneous staining pattern

found by all three analyses. Two (27780/99 and 37736/99) showed an overall increased expression while the other (29791/99) had a generally reduced expression. In four of six (66.7%), the relative expression levels detected by preoperative samples (serum and biopsy) were identical.

Discussion

PCa has an enormous impact on the health services of the Western countries, as it is one of the major causes for cancer-related death in men. The prediction of an individual patient's outcome is quite difficult, due to the variably aggressive nature of the disease. Investigations on potential new prognostic markers are, therefore, an important prerequisite for the development of optimized therapy strategies. MMP-2 and MMP-9 have been reported to be associated with tumor progression in various types of cancer, and several studies have reported their role in PCa [4, 5, 6, 15, 19, 21, 25, 35]. This is the first report in which the expression and activity of MMP-2 and MMP-9 has been investigated in prostatic tumor tissue from core needle biopsies and radical prostatectomies, as well as serum probes of the same patient group. Together with the applied analytical techniques, zymography, immunohistochemistry, Western blotting and ELISA, we tried to gain a comprehensive insight into the role of gelatinases in PCa on the protein level.

Gelatin zymography revealed gelatinolytic activity in all 97 analyzed tumor and tumor-free tissue samples. The major activity was identified as the latent forms of both gelatinases. MMP-2 and MMP-9 are both secreted as

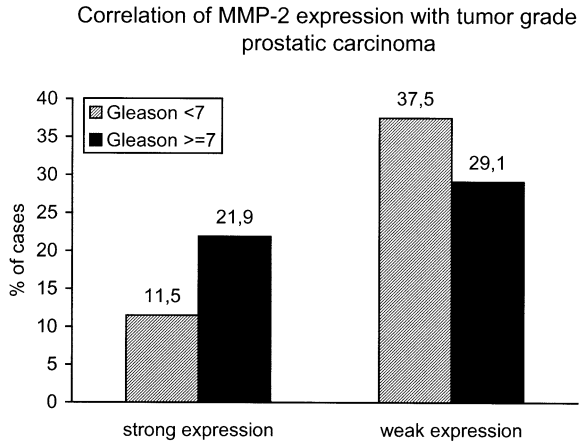

Fig. 4 A strong matrix metalloproteinase (MMP)-2 expression correlates with high-grade (Gleason≥7) tumors. Low-grade (Gleason<7) tumors are associated with weak expression (P=0.024). A cut-off point of 4 reflects the mean value (4.1±0.3) of all expression scores. The group of high-grade tumors is shown as a *solid bar*, while the low-grade tumors are represented by a *hatched bar*

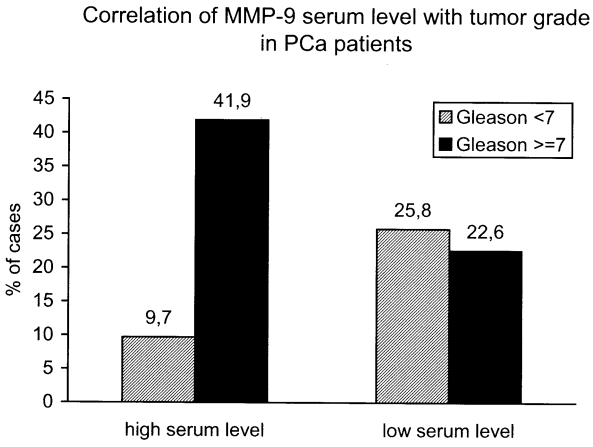

Fig. 6 The matrix metalloproteinase (MMP)-9 serum levels are increased in patients with high-grade tumors. Patients with low-grade tumors have lower MMP-9 serum levels (P=0.044). The median of all serum concentrations was chosen as cut-off point. The group of patients with high-grade tumors is shown as a *solid bar*, while patients with low-grade tumors are represented by a *hatched bar*

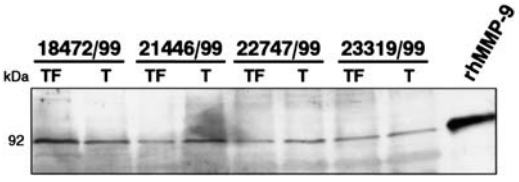

Fig. 5 Representative Western-blot analysis of matrix metalloproteinase (MMP)-9 in prostate tissue homogenates. Protein bands of MMP-9 in tumor-free (*TF*) and tumor (*T*) prostate tissue were detected by a monoclonal anti-human MMP-9 antibody. Each lane contains 10 μg of total protein extract. The lane with purified recombinant human MMP-9 (rhMMP-9) contains 10 ng

zymogens, which need further activation. The active enzymes, however, can easily form complexes with their natural inhibitors, the tissue inhibitors of metalloproteinases (TIMP) [1]. Pro-MMP-2 is activated by interaction with membrane type-1-matrix metalloproteinase (MT1-MMP) on the cell surface [18, 27]. Both gelatinases may also be activated by MMP-13, which in turn is activated by MT1-MMP and active MMP-2 [16, 17]. A direct comparison of MMP activity in tumor and tumor-free tissue using densitometry demonstrated that 55.7% of the analyzed tumor probes had an increased MMP-2 activity, while 51.1% had an elevated MMP-9 activity. A recent study by Lichtinghagen et al. [20] in 17 patients found no significant difference for the overall activity of MMP-2 in malignant and benign prostate tissue, while the MMP-9 activity level was increased in cancerous parts of the prostate. They also found an association of tumor stage and grade with the expression of MMP-2; but only 2 of 17 tumors had a Gleason score less than or equal to seven. In our study of 97 patients, we found a positive association (P<0.05) between MMP-2 activity and the tumor stage of the PCa patients. An increased tumoral activity of MMP-2 was predominantly found in patients with advanced tumor stages (pT3, pT4), while a reduced MMP-2 activity in the tumor tissue was mainly observed in organ-confined stages (pT2).

Immunohistochemical data showed an increased MMP-2 expression in prostatic carcinoma. The staining pattern of MMP-2 was variable concerning intensity and localization of positive tumor cells, which had been observed previously [23, 32]. A semi-quantitative scoring system was used to categorize MMP-2 expression as increased or decreased. The applied cutoff score of 4 reflects the mean value of all analyzed immunostainings. Reactivity of normal secretory epithelial and basal cells

Table 1 Protein expression versus protein activity of active forms of matrix metalloproteinases (MMPs) in prostatic carcinoma. χ^2-test for MMP-2 revealed 4.15 (P=0.04), for MMP-9 0.15 (P=0.69)

	MMP-2 (n=87)		MMP-9 (n=84)	
	Strong expression#	Weak expression#	Increased expression§	Decreased expression§
Increased activity*	19 (21.8%)	29 (33.3%)	15 (17.9%)	28 (33.3%)
Decreased activity*	24 (27.6%)	15 (17.2%)	16 (19.0%)	25 (29.8%)

* Determined using zymography
\# Determined using immunohistochemistry
§ Determined using Western blot

Table 2 Serum concentration (mean±SEM) of matrix metalloproteinase (MMP)-2 and MMP-9 in benign prostatic hyperplasia (BPH) controls and prostatic carcinoma (PCa) patients

	Controls (BPH)	PCa patients				
		Total	Low-grade tumors	High-grade tumors	pT2	pT3+4
		(*n*=31)	(*n*=11)	(*n*=20)	(*n*=19)	(*n*=12)
MMP-2 (ng/ml)	1246.45±87.28 (*n*=5)	1121.43±25.51	1148.27±26.79	1106.67±36.77	1105.01±35.67	1147.43±34.45
MMP-9 (ng/ml)	250.92±22.43 (*n*=8)	383.58±31.87*	305.17±44.03	426.71±40.61#	367.30±36.86	409.35±59.47

*$P<0.01$ versus BPH controls
#$P<0.05$ versus low-grade tumors

Table 3 Relative matrix metalloproteinase (MMP)-2 expression in serum, core needle biopsies and prostatectomies. An increased relative expression level is indicated by a plus (+), while a decreased expression is represented by a minus (–)

Patient ID	Serum	Core needle biopsy	Surgical specimen
27780/99	+	+	+
37736/99	+	+	+
40473/99	+	+	–
4570/00	+	–	+
29507/01	+	–	–
29701/01	–	–	–

might represent pro-MMP-2 levels in these tissues, as the used MMP-2 antibody detects both pro- and active MMP-2. Also, it should be noted that the staining of benign elements was only partial compared with carcinoma cells. Confirming previous reports, we found a significant correlation between MMP-2 expression and tumor grade [23, 29]. Patients with high-grade tumors (Gleason score $\geq$7) had an increased MMP-2 expression, while a reduced expression was predominantly present in the patient group with low-grade tumors (Gleason score <7). The observed association between MMP-2 expression in prostatectomies and tumor grade, however, could not be confirmed in core needle biopsies. The relative expression scores in biopsies and surgical specimens corresponded in 16 of 23 analyzed patients, and the mean expression scores (4.1±0.3 versus 3.1±0.7) were similar for both specimen groups. This indicates that investigation of MMP-2 expression in biopsies facilitates conclusions on the state of MMP-2 expression in the surgical specimen. An important issue for the observed differences between biopsies and prostatectomy specimens might be the discrepancy in Gleason scoring. Actually, the investigated 23 biopsies included 7 high-grade and 16 low-grade tumors, based on the Gleason scores determined in biopsies. The same group of patients included 15 high-grade and 8 low-grade tumors when the Gleason scores were determined in prostatectomies. This sampling error could be explained by high Gleason patterns being present in the radical prostatectomies that were not sampled in the biopsies.

MMP-2 expression and activity showed an inverse correlation, indicating that the protein expression does not necessarily reflect the activity status of the enzyme (Table 1).

In support of previous studies, our results on MMP-2 activity and expression, as assessed using zymography and immunohistochemistry, indicated an important role for MMP-2 on tumor progression [2, 9, 26, 29].

MMP-2 serum levels were not significantly different in 31 PCa patients and 5 BPH controls (Table 2). The MMP-2 concentrations in serum from PCa patients tended to be even lower than in BPH controls. Previous studies on MMP-2 serum concentrations in PCa patients displayed controversial results. Some groups demonstrated that the serum levels of MMP-2 were significantly increased in samples from PCa patients compared with normal controls and BPH patients [8, 14]. Others, however, found no differences between MMP-2 concentrations in plasma probes of PCa patients and a control group [13]. Investigations from the same authors showed no differences in MMP-2 expression from serum and plasma [12]. Only 16 of the 31 relative expression levels determined using ELISA matched with those obtained using immunohistochemistry of radical prostatectomies. This confirms that MMP-2 serum analyses play only a minor role in indicating MMP-2 expression in PCa.

In contrast to MMP-2, we found significantly increased serum levels of MMP-9 in PCa patients compared with BPH controls (Table 2). Furthermore, MMP-9 serum levels revealed a significant correlation to tumor grade. However, these results have to be considered very carefully, since additional MMP-9 might be released during the degranulation of neutrophil blood cells [36]. However, the conditions of serum preparations were the same for both groups, PCa patients and BPH controls. Since the probes were collected preoperatively on a routine basis, only serum probes were available.

A recent study by Ishimaru et al. demonstrated a positive MMP-9 immunostaining in 27 of 41 (65.9%) specimens [10]. A significantly larger number of high-grade tumors expressed MMP-9, while more low-grade tumors did not express MMP-9 at all. Since MMP-9 immunohistochemistry using the antibodies tested was not satisfactory, protein expression was determined in manually microdissected tumor and tumor-free tissues using immunoblotting. In our study, MMP-9 protein expression could be detected in all tumor and tumor-free tissues of

the 94 tissue specimens in contrast with the aforementioned study. This may be due to different antibody specificity and sensitivity. An increased expression compared with tumor-free tissue was found only in 38% of the tumors, and no correlation to tumor stage or grade could be detected. To clarify the role of MMP-9 as a marker in prostatic carcinoma, further investigations with a larger number or other type of specimens (e.g., plasma) will be necessary.

The different results in MMP-2 expression in prostatectomies, biopsies and serum probes might be caused by the relatively low numbers examined in the latter two groups. In only six cases, tissue and serum samples were available for all investigations.

In summary, this study showed that although the MMP-9 activity was increased in the majority of analyzed tumor samples, we could not find an association to histopathological parameters, such as tumor stage or grade. MMP-9 protein overexpression was present only in a minority of the cases. The observed correlation between MMP-9 expression in serum and tumor grade has to be addressed very carefully and needs further examination.

We could demonstrate an association between MMP-2 expression and activity to tumor grade and stage. Increased MMP-2 activity is associated with advanced tumor stages, while an elevated expression is correlated with high-grade tumors. In addition, as our immunohistochemical analyses demonstrated, the relative expression levels assessed in core needle biopsies match in about 65% of the patients with those of the surgical specimens. This indicates that detection of MMP-2 in core needle biopsies seems not to be a helpful marker. Further follow-up studies are needed on a large number of biopsies to clarify the role of MMPs for prognostic purposes.

Acknowledgements We thank Tina Dreher for kindly providing protein lysates for Western-blot analyses. This work was supported by Tumorzentrum HD/MA grant 781010.

References

1. Birkedal-Hansen H (1995) Proteolytic remodeling of extracellular matrix. Curr Opin Cell Biol 7:728–735
2. Boag AH, Young ID (1993) Immunohistochemical analysis of type IV collagenase expression in prostatic hyperplasia and adenocarcinoma. Mod Pathol 6:65–68
3. Curran S, Murray GI (1999) Matrix metalloproteinases in tumour invasion and metastasis. J Pathol 189:300–308
4. Davies B, Miles DW, Happerfield LC, Naylor MS, Bobrow LG, Rubens RD, Balkwill FR (1993) Activity of type IV collagenases in benign and malignant breast disease. Br J Cancer 67:1126–1131
5. Festuccia C, Bologna M, Vicentini C, Tacconelli A, Miano R, Violini S, Mackay AR (1996) Increased matrix metalloproteinase-9 secretion in short-term tissue cultures of prostatic tumor cells. Int J Cancer 69:386–393
6. Giannelli G, Fransvea E, Marinosci F, Bergamini C, Daniele A, Colucci S, Paradiso A, Quaranta M, Antonaci S (2002) Gelatinase levels in male and female breast cancer. Biochem Biophys Res Commun 292:161–166
7. Gleason DF (1992) Histologic grading of prostate cancer: a perspective. Hum Pathol 23:273–279
8. Gohji K, Fujimoto N, Hara I, Fujii A, Gotoh A, Okada H, Arakawa S, Kitazawa S, Miyake H, Kamidono S (1998) Serum matrix metalloproteinase-2 and its density in men with prostate cancer as a new predictor of disease extension. Int J Cancer 79:96–101
9. Hamdy FC, Fadlon EJ, Cottam D, Lawry J, Thurrell W, Silcocks PB, Anderson JB, Williams JL, Rees RC (1994) Matrix metalloproteinase 9 expression in primary human prostatic adenocarcinoma and benign prostatic hyperplasia. Br J Cancer 69:177–182
10. Ishimaru H, Kageyama Y, Hayashi T, Nemoto T, Eishi Y, Kihara K (2002) Expression of matrix metalloproteinase-9 and bombesin/gastrin-releasing peptide in human prostate cancers and their lymph node metastases. Acta Oncol 41:289–296
11. Jemal A, Thomas A, Murray T, Thun M (2002) Cancer statistics, 2002. CA Cancer J Clin 52:23–47
12. Jung K, Laube C, Lein M, Lichtinghagen R, Tschesche H, Schnorr D, Loening SA (1998) Kind of sample as preanalytical determinant of matrix metalloproteinase 2 and 9 and tissue inhibitor of metalloproteinase 2 in blood. Clin Chem 44:1060–1062
13. Jung K, Laube C, Lein M, Turk I, Lichtinghagen R, Rudolph B, Schnorr D, Loening SA (1998) Matrix metalloproteinase-2 in blood does not indicate the progression of prostate cancer. Int J Cancer 78:392–393
14. Kanoh Y, Akahoshi T, Ohara T, Ohtani N, Mashiko T, Ohtani S, Egawa S, Baba S (2002) Expression of matrix metalloproteinase-2 and prostate-specific antigen in localized and metastatic prostate cancer. Anticancer Res 22:1813–1817
15. Kawano N, Osawa H, Ito T, Nagashima Y, Hirahara F, Inayama Y, Nakatani Y, Kimura S, Kitajima H, Koshikawa N (1997) Expression of gelatinase A, tissue inhibitor of metalloproteinases-2, matrilysin, and trypsin(ogen) in lung neoplasms: an immunohistochemical study. Hum Pathol 28:613–622
16. Knauper V, Will H, Lopez-Otin C, Smith B, Atkinson SJ, Stanton H, Hembry RM, Murphy G (1996) Cellular mechanisms for human procollagenase-3 (MMP-13) activation. Evidence that MT1-MMP (MMP-14) and gelatinase a (MMP-2) are able to generate active enzyme. J Biol Chem 271:17124–17131
17. Knauper V, Smith B, Lopez-Otin C, Murphy G (1997) Activation of progelatinase B (proMMP-9) by active collagenase-3 (MMP-13). Eur J Biochem 248:369–373
18. Lehti K, Lohi J, Valtanen H, Keski-Oja J (1998) Proteolytic processing of membrane-type-1 matrix metalloproteinase is associated with gelatinase A activation at the cell surface. Biochem J 334:345–353
19. Liabakk NB, Talbot I, Smith RA, Wilkinson K, Balkwill F (1996) Matrix metalloprotease 2 (MMP-2) and matrix metalloprotease 9 (MMP-9) type IV collagenases in colorectal cancer. Cancer Res 56:190–196
20. Lichtinghagen R, Musholt P, Lein M, Romer A, Rudolph B, Kristiansen G, Hauptmann S, Schnorr D, Loening S, Jung K (2002) Different mRNA and protein expression of matrix metalloproteinases 2 and 9 and tissue inhibitor of metalloproteinases 1 in benign and malignant prostate tissue. Eur Urol 42:398–406
21. Lokeshwar BL, Selzer MG, Block NL, Gunja-Smith Z (1993) Secretion of matrix metalloproteinases and their inhibitors (tissue inhibitor of metalloproteinases) by human prostate in explant cultures: reduced tissue inhibitor of metalloproteinase secretion by malignant tissues. Cancer Res 53:4493–4498
22. Matrisian LM (1990) Metalloproteinases and their inhibitors in matrix remodeling. Trends Genet 6:121–125
23. Montironi R, Lucarini G, Castaldini C, Galluzzi CM, Biagini G, Fabris G (1996) Immunohistochemical evaluation of type IV collagenase (72-kd metalloproteinase) in prostatic intraepithelial neoplasia. Anticancer Res 16:2057–2062
24. Nagase H, Woessner JF Jr (1999) Matrix metalloproteinases. J Biol Chem 274:21491–21494
25. Nawrocki B, Polette M, Marchand V, Monteau M, Gillery P, Tournier JM, Birembaut P (1997) Expression of matrix met-

alloproteinases and their inhibitors in human bronchopulmonary carcinomas: quantificative and morphological analyses. Int J Cancer 72:556–564
26. Ross JS, Kaur P, Sheehan CE, Fisher HA, Kaufman RA Jr, Kallakury BV (2003) Prognostic significance of matrix metalloproteinase 2 and tissue inhibitor of metalloproteinase 2 expression in prostate cancer. Mod Pathol 16:198–205
27. Sato H, Takino T, Okada Y, Cao J, Shinagawa A, Yamamoto E, Seiki M (1994) A matrix metalloproteinase expressed on the surface of invasive tumour cells. Nature 370:61–65
28. Sobin LH, Wittekind CH (eds) (1997) TNM classification of malignant tumours, 5th edn. Wiley-Liss Inc., New York
29. Stearns M, Stearns ME (1996) Evidence for increased activated metalloproteinase 2 (MMP-2a) expression associated with human prostate cancer progression. Oncol Res 8:69–75
30. Trudel D, Fradet Y, Meyer F, Harel F, Tetu B (2003) Significance of MMP-2 expression in prostate cancer: an immunohistochemical study. Cancer Res 63:8511–8515
31. True LD (1994) Surgical pathology examination of the prostate gland. Practice survey by American society of clinical pathologists. Am J Clin Pathol 102:572–579
32. Upadhyay J, Shekarriz B, Nemeth JA, Dong Z, Cummings GD, Fridman R, Sakr W, Grignon DJ, Cher ML (1999) Membrane type 1-matrix metalloproteinase (MT1-MMP) and MMP-2 immunolocalization in human prostate: change in cellular localization associated with high-grade prostatic intraepithelial neoplasia. Clin Cancer Res 5:4105–4110
33. Varani J, Hattori Y, Dame MK, Schmidt T, Murphy HS, Johnson KJ, Wojno KJ (2001) Matrix metalloproteinases (MMPs) in fresh human prostate tumour tissue and organ-cultured prostate tissue: levels of collagenolytic and gelatinolytic MMPs are low, variable and different in fresh tissue versus organ-cultured tissue. Br J Cancer 84:1076–1083
34. Woessner JF Jr (1991) Matrix metalloproteinases and their inhibitors in connective tissue remodeling. FASEB J 5:2145–2154
35. Yamagata S, Yoshii Y, Suh JG, Tanaka R, Shimizu S (1991) Occurrence of an active form of gelatinase in human gastric and colorectal carcinoma tissues. Cancer Lett 59:51–55
36. Zucker S, Hymowitz M, Conner C, Zarrabi HM, Hurewitz AN, Matrisian L, Boyd D, Nicolson G, Montana S (1999) Measurement of matrix metalloproteinases and tissue inhibitors of metalloproteinases in blood and tissues. Clinical and experimental applications. Ann N Y Acad Sci 878:212–227

Virchows Arch (2004) 444:527–535
DOI 10.1007/s00428-004-0987-3

ORIGINAL ARTICLE

N. Volkan Adsay · Aleodor Andea · Olca Basturk · Nihal Kilinc · Hind Nassar · Jeanette D. Cheng

Secondary tumors of the pancreas: an analysis of a surgical and autopsy database and review of the literature

Received: 3 December 2003 / Accepted: 3 February 2004 / Published online: 1 April 2004

Abstract The vast majority of pancreatic carcinomas are primary, and, among these, more than 90% are of ductal origin. However, a variety of extrapancreatic tumors may involve the pancreas secondarily and may manifest different clinicopathological characteristics and outcomes. In this study, pathology material from 973 surgical specimens and 4955 adult autopsy cases was reviewed to identify the tumors metastatic to or secondarily involving the pancreas. Biliary and periampullary neoplasms and tumors confined to peripancreatic soft tissue were excluded. In the autopsy series, the pancreas was involved by tumor in 190 cases, and 81 of these were secondary tumors. These were predominantly of epithelial origin, most commonly from lung (34), followed by GI tract (20), kidney (4), breast (3), liver (2), ovary (1), and urinary bladder (1). In addition, there were six tumors of hematopoietic origin, two melanomas, two sarcomas, and two mesotheliomas. Among the 973 surgical specimens, 38 cases contained metastatic tumors to the pancreas. Of these, 11 were lymphomas, and the others were carcinomas of stomach (7), kidney (6), lung (2), liver, prostate, ovary, uterus (1 case of each), and a Merkel cell carcinoma. In addition, there were three malignant gastrointestinal stromal tumors and one retroperitoneal leiomyosarcoma. In conclusion, lung cancer is the most common source of metastasis to pancreas, followed by gastrointestinal carcinomas and lymphomas. These tumors are usually seen in patients with disseminated disease and are detected mainly in autopsies. Secondary tumors constitute about 4% of pancreatic specimens in the authors' surgical database. Approximately one-third of them are clinically mistaken as primary tumors of the pancreas. These are predominantly hematopoietic malignancies or carcinomas of renal or gastric origin. Secondary tumors should be entertained in both the clinical and pathological differential diagnosis of pancreatic neoplasia.

Keywords Pancreas · Metastasis · Secondary tumors · Neoplasms · Cancer

N. V. Adsay (✉) · A. Andea · O. Basturk · N. Kilinc · H. Nassar · J. D. Cheng
Department of Pathology,
The Karmanos Cancer Institute and Wayne State University,
Harper Hospital,
3990 John R. Street, Detroit, MI 48201, USA
e-mail: adsayv@med.wayne.edu
Tel.: +1-313-9932965
Fax: +1-313-7459299

Introduction

While the majority of the tumors involving the pancreas are either of pancreatic, biliary, or periampullary origin, there are a variety of tumors involving this organ secondarily, which have different clinicopathological presentations and outcomes [10, 11, 20, 26, 32, 39, 45, 46, 53, 63, 66, 67, 75, 77, 96]. Most of the studies reported in the literature focus on the radiological and ultrasonographic characteristics of secondary tumors and their differential diagnosis from primary pancreatic carcinomas [10, 11, 20, 26, 39, 66, 67, 77, 96].

In this study, we undertook a review of secondary pancreatic tumors in the autopsy and surgical files of The Karmanos Cancer Institute, Detroit Medical Center and Wayne State University to determine the types and relative frequency of secondary pancreatic tumors and their potential clinicopathological significance. The findings were compared with the previous experience reported in the literature.

Materials and methods

Pathology materials from autopsies and surgical pancreatic specimens obtained in the authors' institution during a 20-year (1977–1997) period have been reviewed to identify the tumors secondarily involving the pancreas. In autopsy files, among 4955 adult autopsies performed for various reasons, 190 had tumors in the pancreas. In surgical files, 973 surgical specimens were identified as having tumors in the pancreas [466 resections and 507 open (incisional) or large core needle biopsies].

Tumors that are metastatic to the pancreas from a remote site, those that secondarily invade the pancreas from the neighboring

organs (other than the biliary, ampullary, or duodenal ones), and lymphomas were regarded as "secondary" tumors and were included in this study. Tumors that were confined to the peripancreatic soft tissue or lymph nodes, without pancreatic involvement, were excluded.

The slides, pathology reports, and, where needed, hospital charts of the patients were reviewed. For surgical cases, in order to determine if any diagnostic difficulty was encountered, the reports were analyzed for frozen section diagnoses, microscopic notes, and additional work-up utilized. Accordingly, further analysis was performed—in some cases with additional immunostains, in others with clinical follow-up, and yet with others by careful scrutiny of hematoxylin-eosin slides. For all melanoma cases, an immunohistochemical panel composed of S-100, HMB-45, and cytokeratin was performed. For lymphoma cases, a common panel of cytokeratin, LCA, as well as B-cell and T-cell markers, including at least, but not limited to CD20 and CD3, was performed.

Results

Autopsies

Of the 190 autopsy cases with pancreatic tumors, 43% were secondary tumors (81 cases). These were 50 men and 31 women with a mean age of 59 years. A variety of tumors were found to metastasize to the pancreas. These were predominantly of epithelial origin, most commonly from lung (34 cases, 42%) and gastrointestinal tract (20 cases, 24.7%), followed by kidney (4 cases, 5%), breast (3 cases, 3.7%), liver (2 cases, 2.5%), ovary (1 case, 1.2%), and urinary bladder (1 case, 1.2%) (Table 1). Among the pulmonary tumors, 10 were small cell carcinomas, and 24 were non-small cell carcinomas (10 adenocarcinomas, 9 large cell carcinomas, and 5 adenosquamous/squamous cell carcinomas) (Fig. 1). The metastatic renal cell carcinomas were composed of one clear cell, one papillary, and two sarcomatoid carcinomas. Four metastases (5%) were classified as unknown primary and did not appear to be originating in the pancreas. Among the six tumors of hematopoietic origin (7.4%), four were non-Hodgkin's lymphoma, (two diffuse large B-cell, one B-cell chronic lymphocytic leukemia/small lymphocytic lymphoma, and one peripheral T-cell) one was Hodgkin, and one case of multiple myeloma was noted. In addition, we found two cases (2.5%) of each metastatic melanoma, mesothelioma, and sarcoma.

All tumors in the autopsy series presented as disseminated disease, with the exception of two gastric adenocarcinomas that had extension limited to the pancreas. In 20 cases (25%), the metastatic tumors were confined to the head (13 cases), body (1 case), or tail (6 cases) of the pancreas. In the remaining majority of 61 cases (75%), the tumors involved multiple segments of the organ. In 20 cases (25%), the metastases within the pancreas were only detected at the microscopic level, whereas in 47 cases

Table 1 Site of primary tumor in the autopsy series

Location of primary tumor	No. of cases (%) *n*=81
Lung	34 (42%)
GI tract	20 (24.7%)
Esophagus	4 (4.9%)
Stomach	10 (12.3%)
Colon	5 (6.2%)
Rectum	1 (1.2%)
Kidney	4 (5%)
Breast	3 (3.7%)
Liver	2 (2.5%)
Ovary	1 (1.2%)
Urinary bladder	1 (1.2%)
Hematopoietic tumors	6 (7.4%)
Non-Hodgkin's lymphoma	4 (4.9%)
Hodgkin's lymphoma	1 (1.2%)
Multiple myeloma	1 (1.2%)
Melanoma	2 (2.5%)
Sarcomas	2 (2.5%)
Mesothelioma	2 (2.5%)
Carcinomas of undetermined origin	4 (5%)

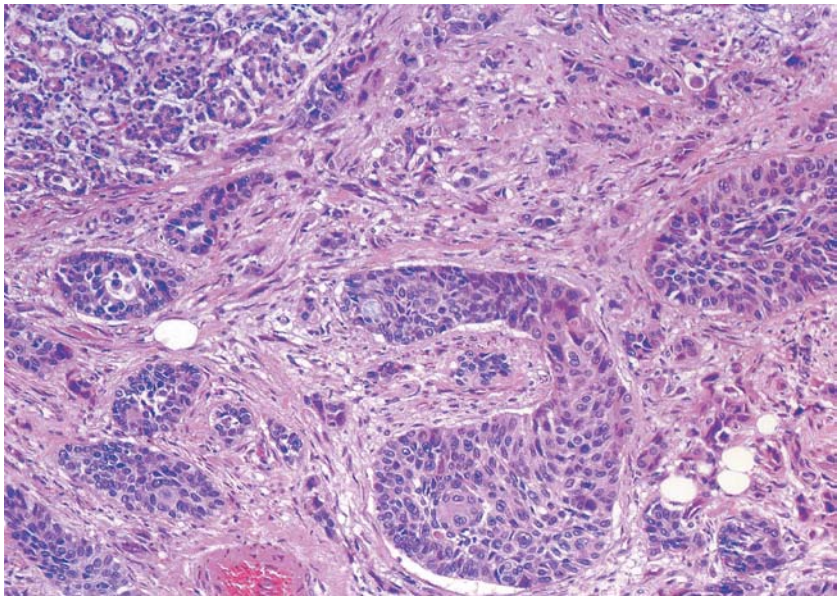

Fig. 1 Metastatic adenosquamous carcinoma from the lung. Glandular structures are admixed the squamous nests

Table 2 Site of primary tumor in the surgical series. *GIST* gastrointestinal stromal tumor

Location of primary tumor	No. of cases (%) *n*=38
Non-Hodgkin's lymphomas	11 (29%)
Stomach	7 (18.4%)
Kidney	6 (15.7%)
Lung	2 (5.3%)
Liver	1 (2.6%)
Prostate	1 (2.6%)
Ovary	1 (2.6%)
Uterus	1 (2.6%)
Merkel cell carcinoma	1 (2.6%)
Malignant GIST	3 (7.9%)
Stomach	1 (2.6%)
Intestine	2 (5.3)
Leiomyosarcoma	1 (2.6%)
Carcinomas of undetermined origin	3 (7.9%)

(58%), they were seen grossly as single or multiple tumors or were reported as diffuse involvement of the pancreas.

Seven cases were suspected to be of primary origin (8.5%) before the autopsy was performed. Two of these were melanoma; the rest were originating from lung, kidney, liver, and breast. One case was of unknown origin.

Surgical specimens

Of 973 cases, 38 (3.9%) showed secondary tumors diagnosed in 17 resections and 21 large-core needle biopsies, taken from 27 men and 11 women with a mean age of 59 years. Of these, most were lymphomas (11 cases, 29%)—all of non-Hodgkin's type (7 diffuse large B-cell lymphoma, 1 precursor B-lymphoblastic lymphoma, 1 follicular center cell lymphoma, 1 marginal zone B-cell lymphoma, 1 peripheral T-cell lymphoma)—carcinomas of the stomach (7 cases, 18.4%), and renal cell carcinomas (6 cases, 15.7%)—all of clear cell type. In addition, there were 2 cases of lung carcinoma (5.3%) and 1 case (2.6%) each of prostate, liver, ovary, uterus, and Merkel cell carcinoma. Four metastatic sarcomas were identified; among them were three (7.9%) malignant gastrointestinal stromal tumors tumors and one (2.6%) leiomyosarcoma of retroperitoneal origin (Table 2). Three cases were diagnosed as metastatic carcinoma of unknown origin.

Fig. 2 Gross photograph of metastatic renal cell carcinoma forming two polypoid masses in the duodenum. The lower one involves the ampulla of Vater

Clinically, in 13 patients (34%), the preoperative diagnosis of pancreatic adenocarcinoma was rendered; 6 were lymphoma on histology, 4 were renal cell carcinoma, and the rest were single examples of metastasis from stomach, liver, and ovary. An interesting observation was that all cases of metastatic renal cell carcinoma in our

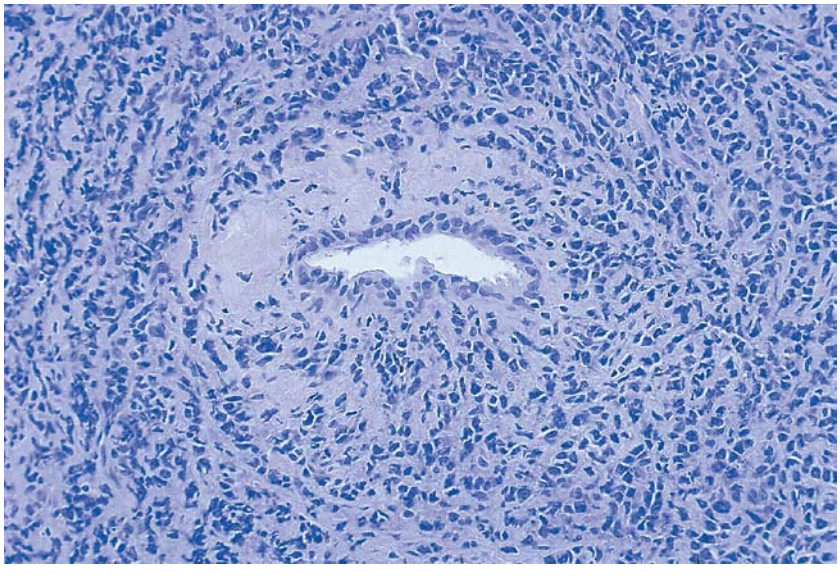

Fig. 3 High-power view of lymphoma, showing lymphocytes with atypical nuclei. Distinguishing anaplastic pancreatic carcinomas from this tumor could be difficult

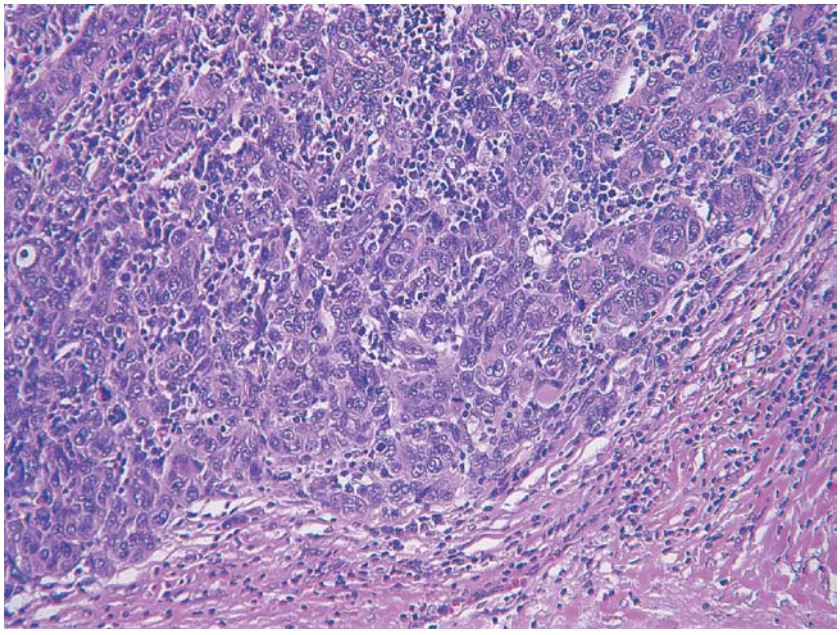

Fig. 4 Malignant melanoma. Syncytial growth pattern and sprinkling of lymphocytes is similar to medullary carcinoma of the pancreas

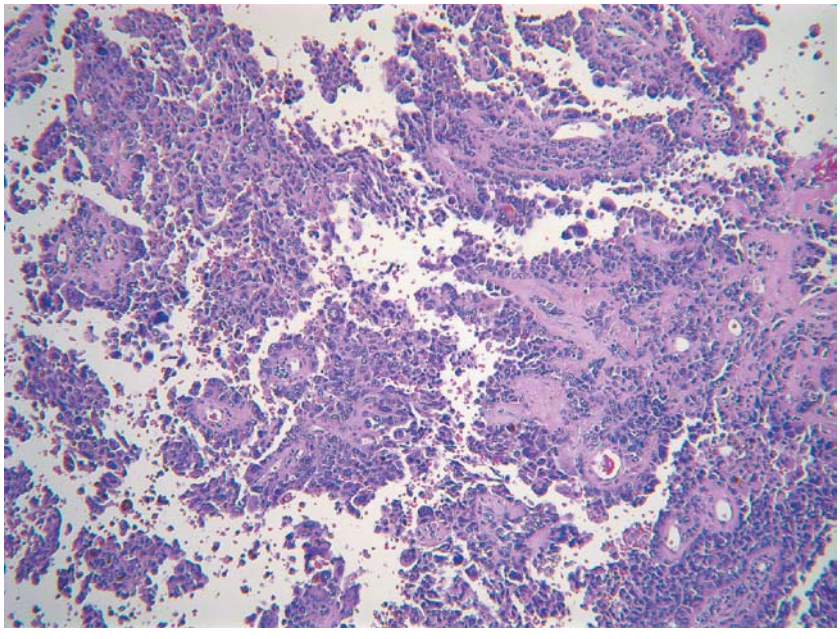

Fig. 5 This malignant melanoma has a pseudopapillary pattern due to dyscohesiveness of the neoplastic cells away from the fibrovascular cores

series presented clinically with signs of gastrointestinal bleeding; some had a polypoid growth pattern (Fig. 2).

Review of the reports and slides

The review of microscopic reports and histological sections showed that lymphomas, melanomas, and sarcomas were difficult to distinguish from anaplastic pancreatic carcinomas (Fig. 3, Fig. 4). A case of melanoma had an artificial pseudopapillary pattern in a young female patient, raising the differential of solid-pseudopapillary tumor (Fig. 5). Colorectal, gastric, and mammary adenocarcinomas were often mistaken for conventional ductal adenocarcinomas. Gastric carcinomas were especially noted to form dense desmoplastic stroma in the pancreas, characteristic of ductal adenocarcinoma (Fig. 6). A case of Merkel cell carcinoma was originally mistaken for a primary endocrine carcinoma of the pancreas (Fig. 7), and one example of clear cell ovarian carcinoma was misinterpreted as serous cystadenocarcinoma (Fig. 8). Colonization of the ductal epithelium by metastatic tumor cells was noted in some cases.

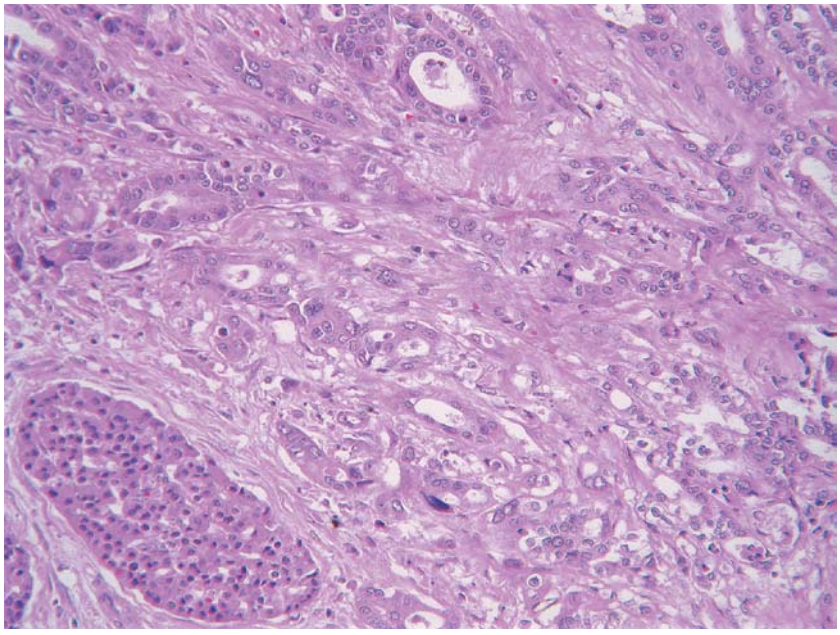

Fig. 6 Metastatic gastric carcinoma with stromal desmoplasia simulates a primary pancreatic ductal adenocarcinoma. Adjacent normal islets are seen on the *left*

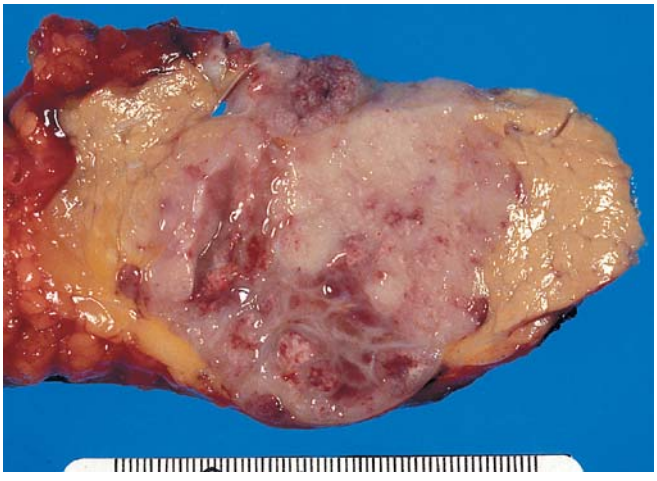

Fig. 7 Merkel cell carcinoma in the tail of the pancreas. The cut surface of this relatively well-circumscribed mass contains multiple hemorrhagic foci and cysts of various size

Discussion

Primary pancreatic carcinomas of ductal origin constitute the vast majority of pancreatic tumors, to an extent that "pancreas cancer" is used synonymously with pancreatic ductal adenocarcinoma. As a consequence, other tumor types that occur in this organ are often misdiagnosed as "pancreas cancer," both clinically and pathologically. Although uncommon, secondary tumors (those that metastasize to the pancreas from remote sites, arise in the adjacent organs and directly invade to pancreas, or arise from tissue types that are not normally present in the pancreas, such as lymphoid) constitute a small but an important category that fall into the differential diagnosis of pancreatic masses, often presenting a diagnostic challenge [10, 11, 20, 26, 32, 39, 45, 46, 53, 63, 66, 67, 75, 77, 96].

Previous autopsy studies investigating the dissemination patterns of carcinomas from various organs have noted that the pancreas and peripancreatic lymph nodes may be involved in 3–12% of patients with widely metastatic disease [45, 74, 97].

This current study was undertaken to determine the types and relative frequency of secondary tumors involving the pancreas and their potential implications in the pathological and clinical differential diagnosis of pancreatic neoplasia by studying the autopsy and surgical files of Harper Hospital, Detroit Medical Center, The Karmanos Cancer Institute, and Wayne State University.

Among 4955 adult autopsies performed for various reasons (neoplastic and non-neoplastic) in the authors' institution, 190 exhibited tumors involving the pancreas, and 81 of these (43%) were secondary tumors. This figure was slightly less than the 65% reported from the files of Memorial Sloan-Kettering Cancer Center [17] and may be attributable to the differences in the patient population. With the exception of two gastric adenocarcinomas that had direct extension to the pancreas, most were seen as a part of widely disseminated carcinoma. As expected, the patients were predominantly elderly (mean age, 59 years), which is similar to the occurrence age of primary carcinomas. The vast majority of tumors were of epithelial origin, most commonly from lung, followed by gastrointestinal tract and kidney. These findings are in accordance with the previous literature. In most studies, lung carcinomas or renal cell carcinomas are reported to be the most common [32, 39, 46, 75], although one study from Japan indicated stomach as the main source, suggesting population-based differences [63]. Cubilla et al. [17] and Klöppel et al. [40] reported, in an autopsy series, carcinomas of the breast, lung, and skin melanomas as the

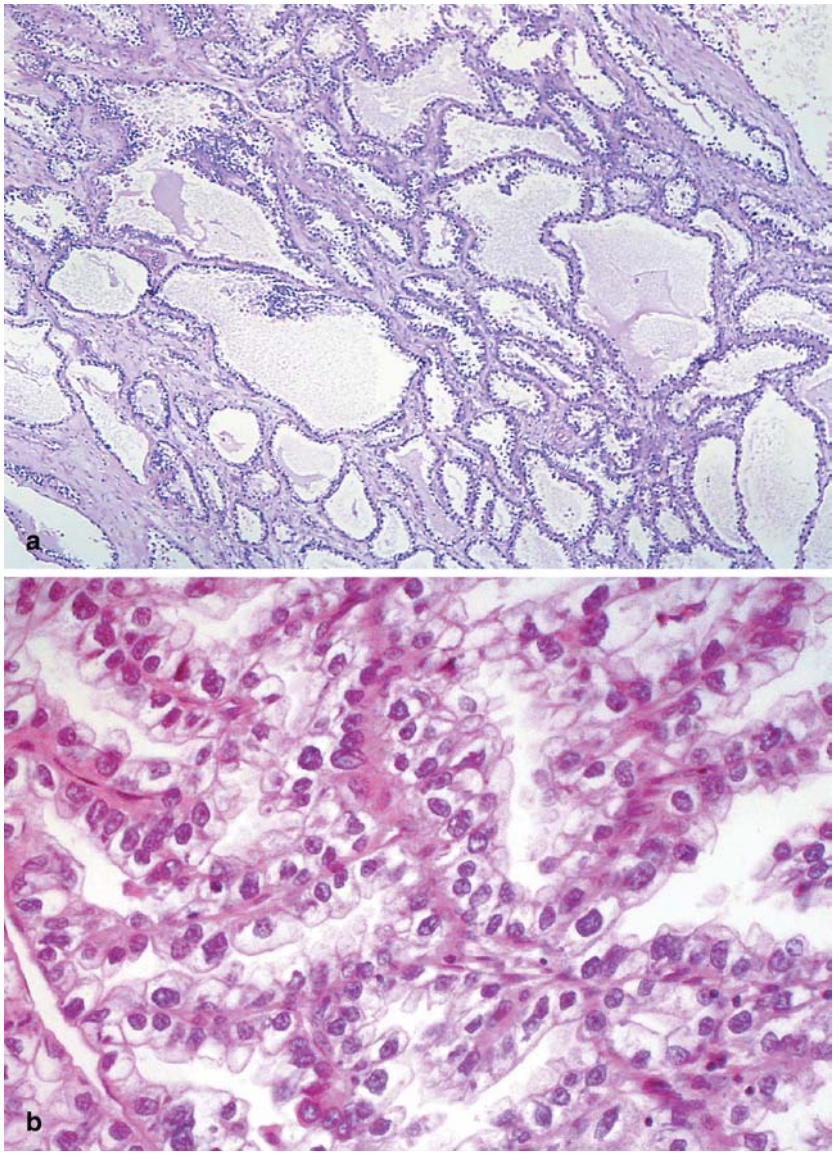

Fig. 8a, b Ovarian clear cell carcinoma that was misinterpreted as serous cystadenocarcinoma

principal source of metastasis to the pancreas. In contrast, in our autopsy series, metastasis from breast and melanomas did not comprise a significant percentage (3.7% and 2.5%, respectively).

Other tumors noted among our autopsy cases, in decreasing order, were lymphoma, breast carcinoma, melanoma, mesothelioma, myeloma, sarcoma, and hepatic and ovarian malignancies. Such examples were also noted in the literature [5, 12, 25, 36, 44, 55, 60, 67, 68, 81, 93, 98]. In fact, individual or a small number of cases exemplifying almost every tumor type have been reported, including thyroid [35, 87], testis [59], cervix [94], meningioma [88], Merkel cell carcinoma [6, 78], transitional cell carcinoma [32, 79], myeloma [9, 33], solitary fibrous tumor [50], malignant fibrous histiocytoma [82], leiomyosarcoma [41], liposarcoma [2], osteosarcoma [27, 76], chondrosarcoma [58, 67], Ewing sarcoma [61], schwannoma [47], and even medulloblastoma [43].

In more than half of our autopsy cases, the tumor was visible during autopsy dissection (and was, therefore, potentially detectable radiologically), and, also, in about a quarter of our autopsy cases, the metastatic tumor was confined to one segment of the organ [head (13 cases), body (1 case) or tail (6 cases)]. Most patients did not have any signs or symptoms attributable to pancreatic involvement, which is in accordance with what has been reported in the literature [15, 31, 38, 51, 52, 95]. However, in seven patients (8.5%), the tumor in the pancreas was suspected to be a primary neoplasm before the autopsy was performed; two of these were melanomas, and the others originated from lung, kidney, liver, breast, and an undetermined site. It may be interesting to note here that ovarian tumors, which are notorious for forming intraabdominal carcinomatosis, only rarely involved the pancreas.

The autopsy series provides a better estimate of the relative frequency of the types of tumors that metastasize

to the pancreas. However, the surgical series is biased toward clinically manifest tumors, in which the possibility of a primary pancreatic cancer was entertained preoperatively. Whereas, in the autopsy series, the most frequent tumor metastatic to the pancreas was lung carcinoma, among the surgical cases, it was lymphoma. In the authors' institutional files, 3.9% of the biopsies and resections were performed for secondary tumors (knowingly or unknowingly), which is in accordance with what was reported from the Mayo Clinic files as 2% [75]. A substantial proportion of the patients in our files (34%) had the clinical suspicion of a primary pancreatic neoplasm. Lymphomas and renal cell carcinomas were especially prone to being mistaken for a primary carcinoma clinically (six and four examples, respectively). In fact, half the lymphomas were misdiagnosed as a primary carcinoma. This is attributable to the fact that both lymphomas and renal cell carcinomas often formed solitary masses in the pancreas [1, 3, 7, 8, 18, 19, 24, 57, 70, 71, 92], with no obvious evidence of metastasis in other organs. Pancreatic metastases from colorectal carcinomas were also previously noted to mimic primary neoplasms, although this was not the case in our experience. Charnsangavej et al. [16] reported that in 7 of their 12 patients with colorectal carcinoma metastatic to the pancreas, clinical features and computed tomography findings were indistinguishable from primary pancreas cancer, and, in 4 patients, the diagnosis at referral was pancreas cancer. Renal cell carcinoma is more notorious for being problematic in this regard. In a review of 752 renal cell carcinomas over a span of 38 years, it was found that 0.9% developed solitary pancreatic metastasis [65]. In many instances, the interval after the diagnosis to the development of metastasis was several years, sometimes even decades [1, 3, 4, 15, 18, 21, 23, 26, 28, 30, 31, 34, 65, 66, 71, 74, 83, 86, 87, 89, 93, 94, 98]. In our patients, the mean interval was 2.6 years; however, in two patients, the metastasis appeared after 5 years.

However, lymphomas [8, 42] and renal cell carcinomas [91, 99] are also among the tumor types that may benefit from resections, even in secondary sites. It may be interesting to note here that most of the lymphoma and renal cell patients in our experience survived longer than a year after the resection of their pancreatic lesion, which is still an uncommon occurrence for pancreatic ductal adenocarcinoma. Therefore, we support the approach others have taken—that an attempt to resect secondary tumors can be made whenever possible, particularly for renal cell carcinoma, but also for others [13, 22, 32, 46, 85, 91, 99].

Analogous to primary neoplasms, the symptoms of secondary tumors of the pancreas, if present, were also often subtle and non-specific [20]. In our series, similar to other studies, non-specific abdominal pain appeared to be the most common symptom [75]. Pancreatitis [29, 40, 48, 49, 54, 59] and obstructive jaundice may also be seen [9, 37, 75, 100]. It is speculated that pancreatitis is attributable not only to the destructive effect of the mass, but also to release of other factors [73]. Interestingly, metastatic renal cell carcinomas often present with gastrointestinal hemorrhage [14, 51, 56, 89] (as did all six cases in our surgical series), possibly due both to their hypervascular nature as well as the fact that they often also involve the ampulla of Vater. More interestingly, all patients with lymphoma in our series had hyperglycemia.

Secondary tumors of the pancreas may create a diagnostic challenge, not only clinically, but also histopathologically. Review of the surgical pathology reports in our data indicated that lymphomas, melanomas, and sarcomas were difficult to distinguish from anaplastic pancreatic carcinomas. A case of melanoma had an artificial pseudopapillary pattern in a young female patient, raising the differential of solid pseudopapillary tumor. Carcinomas of colorectal, mammary, and especially gastric origin were often mistaken for a primary conventional ductal adenocarcinoma of the pancreas, due to formation of tubular elements and desmoplastic stroma. A case of Merkel cell carcinoma was originally mistaken for a primary endocrine carcinoma of the pancreas, and one example of clear cell ovarian carcinoma was misinterpreted as serous cystadenocarcinoma. We also observed colonization of the ductal epithelium by metastatic tumor cells in some of our cases. Both intraductal growth and pagetoid spread to the ducts have been reported in the literature as well [53]. Fat necrosis and other signs of pancreatic injury may be seen [63]. Secondary dilatation of the ducts has also been observed [62].

In summary, this study confirms that the most common tumors that involve pancreas secondarily are carcinomas of pulmonary and gastrointestinal origin, followed by lymphomas, kidney tumors, and others. Secondary tumors are responsible for almost half of the pancreatic masses detected at autopsy. However, these are usually seen as a part of widely disseminated disease and seldom cause symptoms or signs that come to clinical attention. The tumors that seem to cause the most difficulty in the differential diagnosis with primary pancreas cancer (and, hence, leading to surgical resections) are lymphomas, renal cell carcinomas, melanomas, and, reportedly, also colorectal carcinomas. These tend to be misdiagnosed because they often form solitary lesions in the pancreas, often in the absence of any detectable masses elsewhere. Secondary tumors of the pancreas ought to be considered in both the clinical, radiological, and pathological differential diagnosis of pancreatic lesions.

References

1. Abbas MA, Collins JM, Mulligan DC (2001) Renal cell carcinoma metastatic to pancreas. Am J Surg 182:183–184
2. Alcala Pedrajas JN, Jimenez Murillo L, Clemente Millan MJ (1996) Retroperitoneal liposarcoma with lung, skin and pancreatic metastases. Arch Bronconeumol 32:313–315
3. Audisio RA, La Monica G (1985) Solitary pancreatic metastasis occurring 20 years after nephrectomy for carcinoma of the kidney. Tumori 71:197–200
4. Avisse C, Flament JB, Deville J et al (1994) Late and multiple endocrine metastases of an adenocarcinoma of the kidney. Chirurgie 120:50–53

5. Azzarelli A, Clemente C, Quagliuolo V et al (1982) A case of pancreatoduodenectomy as resolutive treatment for a solitary metastasis of breast cancer. Tumori 68:331–335
6. Bachmeyer C, Alovor G, Chatelain D et al (2002) Cystic metastasis of the pancreas indicating relapse of Merkel cell carcinoma. Pancreas 24:103–105
7. Barras JP, Baer H, Stenzl A et al (1996) Isolated late metastasis of a renal cell cancer treated by radical distal pancreatectomy. HPB Surg 10:51–54
8. Behrns KE, Sarr MG, Strickler JG (1994) Pancreatic lymphoma: is it a surgical disease? Pancreas 9:662–667
9. Bell HG, David R, Shamsuddin AM (1982) Extrahepatic biliary obstruction and liver failure secondary to myeloma of the pancreas. Hum Pathol 13:940–942
10. Biset JM, Laurent F, de Verbizier G et al (1991) Ultrasound and computed tomographic findings in pancreatic metastases. Eur J Radiol 12:41–44
11. Boudghene FP, Deslandes PM, LeBlanche AF et al (1994) US and CT imaging features of intrapancreatic metastases. J Comput Assist Tomogr 18:905–910
12. Brodish RJ, McFadden DW (1993) The pancreas as the solitary site of metastasis from melanoma. Pancreas 8:276–278
13. Butturini G, Bassi C, Falconi M et al (1998) Surgical treatment of pancreatic metastases from renal cell carcinomas. Dig Surg 15:241–246
14. Calmes JM, Meyer A (1993) Pancreatic hypernephroma manifested by a duodenal hemorrhage. Rev Med Suisse Romande 113:629–631
15. Carini M, Selli C, Barbanti G et al (1988) Pancreatic late recurrence of bilateral renal cell carcinoma after conservative surgery. Eur Urol 14:258–260
16. Charnsangavej C, Whitley NO (1993) Metastases to the pancreas and peripancreatic lymph nodes from carcinoma of the right side of the colon: CT findings in 12 patients. Am J Roentgenol 160:49–52
17. Cubilla LA, Fitzgerald PJ (1984) Tumors of the exocrine pancreas, 19th volume, 2nd edn. Armed Forces Institute Pathology, Washington, DC
18. Derias NW, Chong WH (1993) Fine needle aspiration diagnosis of a late solitary pancreatic metastasis of renal adenocarcinoma. Cytopathology 4:369–372
19. Diaz Dominguez J, Rodriguez Alvarez de la Marina J, Galindo Garcia A et al (1993) Solitary metachronous pancreatic metastasis of renal adenocarcinoma. Rev Esp Enferm Dig 83: 467–469
20. Diederich S, Wernecke K, Lohnert J et al (1993) Pancreatic metastases: sonographic and computed tomographic findings. Rofo Fortschr Geb Rontgenstr Neuen Bildgeb Verfahr 158: 325–331
21. Dousset B, Andant C, Guimbaud R et al (1995) Late pancreatic metastasis from renal cell carcinoma diagnosed by endoscopic ultrasonography. Surgery 117:591–594
22. Fabre JM, Rouanet P, Dagues F et al (1995) Various features and surgical approach of solitary pancreatic metastasis from renal cell carcinoma. Eur J Surg Oncol 21:683–686
23. Franciosi RA, Russo JF (1969) Renal cell carcinoma metastatic to the pancreas thirteen years following nephrectomy. Mil Med 134:200–203
24. Fritscher-Ravens A, Sriram PV, Krause C et al (2001) Detection of pancreatic metastases by EUS-guided fine-needle aspiration. Gastrointest Endosc 53:65–70
25. Germain M, Strich M, Chaput JC et al (1976) Obstructive jaundice caused by pancreatic metastasis from an ocular nevocarcinoma operated on 30 years previously. Arch Fr Mal App Dig 65:307–311
26. Ghavamian R, Klein KA, Stephens DH et al (2000) Renal cell carcinoma metastatic to the pancreas: clinical and radiological features. Mayo Clin Proc 75:581–585
27. Glass RJ, Eftekhari F, Kleinerman ES et al (1996) Osteosarcoma metastatic to the pancreas in young patients. Clin Radiol 51:293–294
28. Gohji K, Matsumoto O, Kamidono S (1990) Solitary pancreatic metastasis from renal cell carcinoma. Hinyokika Kiyo—Acta Urol Jpn 36:677–681
29. Gutman M, Inbar M, Klausner JM (1993) Metastases-induced acute pancreatitis: a rare presentation of cancer. Eur J Surg Oncol 19:302–304
30. Guttman FM, Ross M, Lachance C (1972) Pancreatic metastasis of renal cell carcinoma treated by total pancreatectomy. Archiv Surg 105:782–784
31. Hermanutz KD, Sonnenberg GE (1977) Late metastasis of a hypernephroid kidney carcinoma to the pancreas with tumor invasion to the duodenum. ROFO Fortschr Geb Rontgenstr Nuklearmed 127:595–597
32. Hiotis SP, Klimstra DS, Conlon KC et al (2002) Results after pancreatic resection for metastatic lesions. Ann Surg Oncol 9:675–679
33. Hirata S, Yamaguchi K, Bandai S et al (2002) secondary extramedullary plasmacytoma involving the pancreas. J Hepatobiliary Pancreat Surg 9:111–115
34. Jenssen E (1952) A metastatic hypernephroma to the pancreas. Acta Chir Scand 104:177–180
35. Jobran R, Baloch ZW, Aviles V et al (2000) Tall cell papillary carcinoma of the thyroid: metastatic to the pancreas. Thyroid 10:185–187
36. Johansson H, Krause U, Olding L (1970) pancreatic metastases from a malignant melanoma. Scand J Gastroenterol 5:573–575
37. Johnson DH, Hainsworth JD, Greco FA (1985) Extrahepatic biliary obstruction caused by small-cell lung cancer. Ann Int Med 102:487–490
38. Kishimoto H, Nimura Y, Okamoto K et al (1985) A case of resected renal cell carcinoma with massive pancreatic metastases. Gan No Rinsho—Jpn J Cancer Clin 31:91–96
39. Klein KA, Stephens DH, Welch TJ (1998) CT characteristics of metastatic disease of the pancreas. Radiographics 18:369–378
40. Klöppel G, Heitz PU (1984) Pancreatic pathology. Churchill Livingstone, Edinburgh, p 108
41. Komoda H, Nishida T, Yumiba T et al (2002) Primary leiomyosarcoma of the pancreas—a case report and case review. Virchows Arch 440:334–337
42. Koniaris LG, Lillemoe KD, Yeo CJ et al (2000) Is there a role for surgical resection in the treatment of early-stage pancreatic lymphoma? J Am Coll Surg 190:319–330
43. Krouwer HG, Vollmerhausen J, White J et al (1991) Desmoplastic medulloblastoma metastatic to the pancreas: case report. Neurosurgery 29:612–616
44. Ladouch A, Fabre M, Vieillefond A et al (1975) Malignant melanoma occurring on a dermoid cyst of the ovary. Pancreatic metastasis. Arch Anat Pathol 23:217–220
45. Lankisch PG, Lohr A, Kunze E (1987) Acute metastasis-induced pancreatitis in bronchial carcinoma. Dtsch Med Wochenschr 112:1335–1337
46. Le Borgne J, Partensky C, Glemain P et al (2000) Pancreaticoduodenectomy for metastatic ampullary and pancreatic tumors. Hepatogastroenterology 47:540–544
47. Lee JS, Kim HS, Jung JJ et al (2001) Ancient schwannoma of the pancreas mimicking a cystic tumor. Virchows Arch 439:697–699
48. Leger L, Bondel P, Charpentier Y et al (1974) Secondary cancer of the pancreas of cystic form. J Chir (Paris) 108:195–202
49. Levine M, Danovitch SH (1973) Metastatic carcinoma to the pancreas. Another cause for acute pancreatitis. Am J Gastroenterol 60:290–294
50. Lüttges J, Mentzel T, Hubner G et al (1999) Solitary fibrous tumour of the pancreas: a new member of the small group of mesenchymal pancreatic tumours. Virchows Arch 435:37–42
51. Marcote Valdivieso E, Arlandis Felix F, Baltasar A et al (1993) Synchronous pancreatic metastasis of renal carcinoma. Rev Esp Enferm Dig 83:471–473

52. Marquand J, Giraud B, Maliakas S (1971) Pancreatic metastasis revealing a kidney neoplasm. J Urol Nephrol 77:595–601
53. Matsukuma S, Suda K, Abe H et al (1997) Metastatic cancer involving pancreatic duct epithelium and its mimicry of primary pancreatic cancer. Histopathology 30:208–213
54. McLatchie GR, Imrie CW (1981) Acute pancreatitis associated with tumour metastases in the pancreas. Digestion 21:13–17
55. Mehta SA, Jagannath P, Krishnamurthy SC et al (1991) Isolated pancreatic metastasis from locally controlled breast cancer: a case report. Indian J Cancer 28:48–50
56. Melo CR, Melo IS, Monteiro AZ et al (1992) Pancreatic metastasis from renal cell carcinoma. Arq Gastroenterol 29:110–112
57. Merkle EM, Bender GN, Brambs HJ (2000) Imaging findings in pancreatic lymphoma: differential aspects. AJR Am J Roentgenol 174:671–675
58. Mikhail MG, Lim KB (1989) Dedifferentiated chondrosarcoma metastasizing to the pancreas in pregnancy. Acta Obstet Gynecol Scand 68:467–468
59. Mossner J, Wagner T, Wunsch PH et al (1982) Differential diagnosis of pancreatitis: metastasis to the pancreas. Leber Magen Darm 12:165–170
60. Mountney J, Maury AC, Jackson AM et al (1997) Pancreatic metastases from breast cancer: an unusual cause of biliary obstruction. Eur J Surg Oncol 23:574–576
61. Mulligan ME, Fellows DW, Mullen SE (1997) Pancreatic metastasis from Ewing's sarcoma. Clin Imaging 21:23–26
62. Muranaka T, Teshima K, Honda H et al (1989) Computed tomography and histologic appearance of pancreatic metastases from distant sources. Acta Radiol 30:615–619
63. Nakamura E, Shimizu M, Itoh T et al (2001) Secondary tumors of the pancreas: clinicopathological study of 103 autopsy cases of Japanese patients. Pathol Int 51:686–690
64. Nishida O, Matsunaga Y, Dekigai H et al (1991) Three elderly cases of renal cell carcinoma with pancreatic metastasis. Nippon Ronen Igakki Zasshi—Jpn J Geriatr 28:392–396
65. Onishi T, Ohishi Y, Iizuka N et al (1995) Clinical characteristics of 7 renal cell carcinoma patients developing a solitary pancreatic metastasis after nephrectomy. Nippon Hinyokika Gakkai Zasshi—Jpn J Urol 86:1538–1542
66. Opocher E, Galeotti F, Spina GP et al (1982) Diagnosis of secondary tumors of the pancreas. Analysis of 13 cases. Minerva Medica 73:577–581
67. Palazzo L, Borotto E, Cellier C et al (1996) Endosonographic features of pancreatic metastases. Gastrointest Endosc 44:433–436
68. Pappo I, Feigin E, Uziely B et al (1991) Biliary and pancreatic metastases of breast carcinoma: is surgical palliation indicated? J Surg Oncol 46:211–214
69. Paz A, Koren R, Gal R et al (1996) Late solitary pancreatic metastasis from renal cell carcinoma. Isr J Med Sci 32:1319–1321
70. Piccinini EE, Ugolini G, Rosati G et al (1996) Solitary pancreatic metastasis of renal cell cancer treated by pancreaticoduodenectomy: a case report. Cancer Control 3:466–468
71. Pietsch JB, Shankar S, Ford C et al (2001) Obstructive jaundice secondary to lymphoma in childhood. J Pediatr Surg 36:1792–1795
72. Reale D, Squillaci S, Guarino M et al (1993) Late pancreatic metastasis of renal carcinoma. Description of 2 cases and review of the literature. Minerva Urol Nefrol 45:183–186
73. Reinhard H, Hill K (1977) Tryptic pancreatitis in small-cell bronchial carcinoma (Author's Translation). Dtsch Med Wochensch 102:797–799
74. Robbins EG II, Franceschi D, Barkin JS (1996) Solitary metastatic tumors to the pancreas: a case report and review of the literature. Am J Gastroenterol 91:2414–2417
75. Roland CF, van Heerden JA (1989) Nonpancreatic primary tumors with metastasis to the pancreas. Surg Gynecol Obstet 168:345–347
76. Rubin E, Dunham WK, Stanley RJ (1985) Pancreatic metastases in bone sarcomas: CT demonstration. J Comput Assist Tomogr 9:886–888
77. Rumancik WM, Megibow AJ, Bosniak MA et al (1984) Metastatic disease to the pancreas: evaluation by computed tomography. J Comput Assist Tomogr 8:829–834
78. Safadi R, Pappo O, Okon E et al (1996) Merkel cell tumor in a woman with chronic lymphocytic leukemia. Leuk Lymphoma 20:509–511
79. Saitoh H, Hida M, Wakabayashi T et al (1982) Metastasis of urothelial tumors of the bladder: correlation between sites and number of organs involved. Tokai J Exp Clin Med 7:517–526
80. Sauvanet A, Barthes T, Levy P et al (1993) Late pancreatic metastasis from renal cell carcinoma [Letter]. Pancreas 8:742–744
81. Schumacher A (1993) Delayed diagnosis of ovarian cancer with metastasis to the pancreas. Zentralbl Gynakol 115:568–569
82. Shinagawa Y, Suzuki T, Hamanaka Y et al (1992) Solitary pancreatic metastasis of malignant fibrous histiocytoma treated by distal pancreatectomy. Pancreas 7:726–730
83. Simpson NS, Mulholland CK, Lioe TF et al (1989) Late, solitary metastatic renal carcinoma in the pancreas. Ulster Med J 58:198–199
84. Skaarup P, Jorgensen T, Larsen S (1984) Asynchronous metastasizing renal cell carcinoma associated with progressive immune complex glomerulonephritis and proteinuria. Scand J Urol Nephrol 18:351–356
85. Sohn TA, Yeo CJ, Cameron JL et al (2001) Renal cell carcinoma metastatic to the pancreas: results of surgical management. J Gastrointest Surg 5:346–351
86. Stankard CE, Karl RC (1992) The treatment of isolated pancreatic metastases from renal cell carcinoma: a surgical review. Am J Gastroenterol 87:1658–1660
87. Sugimura H, Tamura S, Kodama T et al (1991) Metastatic pancreas cancer from the thyroid: clinical imaging mimicking non-functioning islet cell tumor. Radiat Med 9:167–169
88. Tanabe S, Soeda S, Mukai T et al (1984) A case report of pancreatic metastasis of an intracranial angioblastic meningioma (hemangiopericytoma) and a review of metastatic tumor to the pancreas. J Surg Oncol 26:63–68
89. Taziaux P, Dallemagne B, Delforge M et al (1994) An unusual case of clear-cell carcinoma of the pancreas. J Chir 131:86–89
90. Temellini F, Bavosi M, Lamarra M et al (1989) Pancreatic metastasis 25 years after nephrectomy for renal cancer. Tumori 75:503–504
91. Thompson LD, Heffess CS (2000) Renal cell carcinoma to the pancreas in surgical pathology material. Cancer 89:1076–1088
92. Ueda K, Nagayama Y, Narita K et al (2000) Pancreatic involvement by non-Hodgkin's lymphoma. J Hepatobiliary Pancreat Surg 7:610–613
93. Viliavin GD, Sarkisov DS, Daurova TT (1965) Metastasis from an ovarian cilioepithelial cyst to the pancreas (a case). Vopr Onkol 11:88–89
94. Wastell C (1966) A solitary secondary deposit in the pancreas from a carcinoma of the cervix. Postgrad Med J 42:59–61
95. Weerdenburg JP, Jurgens PJ (1984) Late metastases of a hypernephroma to the thyroid and the pancreas. Diagn Imaging Clin Med 53:269–272
96. Wernecke K, Peters PE, Galanski M (1986) Pancreatic metastases: US evaluation. Radiology 160:399–402
97. Willis RA (1973) The spread of tumors in the human body, 3rd edn. Butterworths, London, pp 216–217
98. Wolfson P, Rybak BJ, Kim U (1978) Cystosarcoma phyllodes metastatic to the pancreas. Am J Gastroenterol 70:184–187
99. Z'Graggen K, Fernandez-del Castillo C, Rattner DW et al (1998) Metastases to the pancreas and their surgical extirpation. Arch Surg 133:413–419
100. Zhao B, Kimura W, Futakawa N et al (1997) Renal cell carcinoma of the spindle cell type with metastasis to the pancreas: a case report. Jpn J Clin Oncol 27:58–61

Virchows Arch (2004) 444:536–541
DOI 10.1007/s00428-004-1008-2

ORIGINAL ARTICLE

Yesim Gürbüz · Günter Klöppel

Differentiation pathways in duodenal and ampullary carcinomas: a comparative study on mucin and trefoil peptide expression, including gastric and colon carcinomas

Received: 31 October 2003 / Accepted: 4 February 2004 / Published online: 8 April 2004

Abstract Duodenal carcinomas, such as ampullary tumors, may be a heterogeneous group of neoplasms that share differentiation features with gastric or colorectal carcinomas. Because of the cell- and tissue-specific expression patterns of mucins and trefoil peptides, these markers were used to investigate the differentiation status of duodenal and ampullary carcinomas in comparison with gastric and colorectal carcinomas. Adenocarcinomas (14 duodenal, 10 gastric, 11 ampullary and 10 colorectal) were examined immunohistochemically for the mucin gene products MUC1, MUC2, MUC5AC, MUC6 and the trefoil peptides TFF1 and TFF2. The tumors' expression profile for MUC5AC, MUC6 and TFF1 was used to distinguish between gastric- and intestinal-directed differentiation. The mucins that were most often expressed in the individual tumor types were MUC1 (duodenal and ampullary carcinomas), MUC2 (colorectal carcinomas) and MUC5AC (gastric carcinomas). Further classification focusing on the expression profile for MUC5AC, MUC6 and TFF1 revealed that 21% of the duodenal and 45% of the ampullary carcinomas demonstrated mainly gastric differentiation (positivity for all three markers or only two of them). The remaining duodenal and ampullary carcinomas showed nongastric, i.e., intestinal differentiation (all three markers negative or only one marker positive). The gastric differentiation pattern characterized 60% of gastric carcinomas. Colorectal carcinomas showed intestinal differentiation in 100% of cases. Duodenal carcinomas have a heterogeneous mucin expression pattern that is mainly related to either gastric differentiation or intestinal differentiation. This also holds for ampullary carcinomas. Among the markers used, MUC5AC, MUC6 and TFF1 are most useful for revealing differentiation pathways in duodenal and ampullary carcinoma.

Keywords Duodenal carcinomas · Ampullary carcinomas · MUC expression · MUC1 · MUC2 · MUC5AC · MUC6 · Trefoil peptides

Y. Gürbüz
Department of Pathology,
University of Kocaeli,
Turkey

G. Klöppel (✉)
Department of Pathology,
University of Kiel,
Michaelisstrasse 11, 24105 Kiel, Germany
e-mail: gkloeppel@path.uni-kiel.de
Tel.: +49-431-5973401
Fax: +49-431-5973462

Introduction

Adenocarcinomas of the small intestine are remarkably rare, accounting for only 2% of all intestinal carcinomas [11]. Their epidemiological features, however, are comparable with those of colorectal carcinomas. Duodenal carcinomas reach their peak incidence in patients between the ages of 60 years and 70 years and show an almost equal gender distribution. Risk factors include diets rich in fat, cigarette smoking, alcohol intake, cholecystectomy, peptic ulcer disease, Crohn's disease and familial adenomatous polyposis [19]. The 5-year survival rate is 30.5%. Histopathologically, most duodenal cancers are mucin-producing adenocarcinomas, 34% of which are poorly differentiated [11, 22]. They occur most commonly in the proximal duodenum and particularly in the periampullary region [4, 18, 26]. Like their counterparts in the colorectum, they can originate from adenomas using the adenomatous polyposis coli (APC) mutation pathway [1].

Although the duodenum is part of the intestine, its embryological origin from the foregut, the existence of Brunner's glands and the gastric metaplasia potential of the mucosa may cause differences in the immunophenotypical profile. The ampulla of Vater also has a special anatomical localization, representing a crossroads between pancreaticobiliary and intestinal differentiation [5]. It would, therefore, be interesting to analyze whether different types of duodenal carcinomas may be distinguished on the basis of their phenotypical features and how duodenal carcinomas compare with ampullary car-

cinomas. To this purpose, we investigated the expression of two groups of distinct phenotypical markers, mucin gene products (MUCs) and trefoil peptides (TFFs).

Mucins are glycoproteins characterized by high molecular mass, high carbohydrate content and marked heterogeneity involving both the apoprotein and the oligosaccaride side chains [8, 9]. Mucin (MUC) genes are expressed in a regulated cell-and tissue-specific manner. In the gut, MUC5AC and MUC6 are expressed in the gastric mucosa and MUC2 is expressed in goblet cells of the intestinal mucosa [28]. TFFs constitute a group of small secretory peptides bearing one or more trefoil structural motifs (P-domains) [16]. TFF1 (pS2) co-localizes with MUC5AC in the superficial epithelium of antral and oxyntic glands, and TFF2 (hSP) is expressed together with MUC6 in the mucous neck cells of the oxyntic mucosa, in the pyloric glands of the antrum and in the pancreatic ductal epithelium [13, 29, 30].

In this study, we compared the MUC2, MUC5AC, MUC6, TFF1 and TFF2 expression profiles in primary duodenal carcinomas with those in ampullary, gastric and colorectal carcinomas. Since MUC5AC, MUC 6 and TFF1 were strongly expressed in the non-neoplastic stomach, we interpreted the positivity for all three markers or only two of them as a sign of gastric differentiation. Negativity for the markers was regarded as nongastric, i.e., intestinal differentiation [28, 30].

Materials and methods

The tumors reviewed in this series were retrieved from the surgical pathology files and the consultation files of the Department of Pathology of the University of Kiel. Clinical information was obtained from the patients' records. The review spanned the period from 1978 to 2001. We examined 14 primary duodenal adenocarcinomas, 11 ampullary adenocarcinomas, 10 colorectal adenocarcinomas (2 from the caecum, 1 from the ascendant colon, 1 from the transverse colon, 2 from the descendent colon, 3 from the sigmoid colon and 1 from the rectum) and 10 gastric adenocarcinomas (5 of the intestinal type and 5 of the diffuse type according to Lauren's classification). The tumors were classified according to the World Health Organization classification (WHO classification pathology and genetics tumors of the digestive system 2000). One appropriate tissue block was selected from each tumor for the immunohistochemical evaluation.

From each paraffin-embedded tissue block, 4-µm sections were cut. The sections were deparaffinized, washed with tap water and boiled in citrate-buffered saline for 3.5 min for antigen retrieval. This was followed by staining with antibodies to MUC1 (Ma695 Novocastra, Newcastle, UK), MUC2 (Ccp58 Novocastra), MUC5AC (CLH2 Chemicon, Temecula, CA, USA), MUC6 (CLH5 Novocastra) and TFF1 and TFF2 (pS2 and hSP, kindly provided by G. Elia). Monoclonal antibodies were used for MUC1, MUC2, MUC5AC, MUC6 and TFF1, and a polyclonal antibody was used for TFF2. To improve the staining sensitivity, a 3,3′-diaminobenzidine-enhanced detection kit (Ventana Medical Systems, Tucson, AZ, USA) and an amplification kit (Ventana) were used. Antibody detection was performed by adding biotinylated secondary antibodies, avidin-biotin complex and 3,3′-diaminobenzidine. Negative controls were run with non-immune serum and positive controls with the appropriate tissue.

Following the suggestion of Nougeira et al. [20], we used the expression of MUC5AC and TFF1 as criterion for gastric differentiation. As a third marker, MUC6 was added. Tumors that expressed all three markers, or two of them, were classified as showing gastric-type differentiation. Cases that lacked MUC5AC, MUC6 and TFF1 expression or were positive for only one marker were classified as non-gastric, i.e., intestinal-type differentiation. An immunoreaction in more than 5% of the tumor cells was considered as positive.

The various immunostaining data were compared using the chi square test (using SPSS 11.0 for Windows). *P* values less than 0.05 were considered significant.

Results

The 14 patients with duodenal adenocarcinomas included 11 females and 3 males with an average age of 60.7 years (range between 40 years and 78 years). All were localized in the vicinity of the papilla of Vater, without involving it. Four were well differentiated, eight moderately and two poorly differentiated. An intestinal type of adenocarcinoma was recognized in eight tumors; six tumors, all moderately and poorly differentiated, showed an unspecific pattern, and one of these latter tumors displayed focal basaloid and squamous differentiation. Two intestinal-type carcinomas were associated with tubulovillous adenomas.

Ampullary carcinomas (n=11) were examined. Seven occurred in female and four in male patients with an average age of 71 years (range between 51 years and 80 years). They involved the ampulla or both the ampulla and the periampullary mucosa. Two were well differentiated, seven moderately differentiated and two poorly differentiated. Five corresponded to the intestinal type of adenocarcinoma (three with remnants of adenomas), and four corresponded to the pancreatobiliary type; one was a mixed type, and another one was a mucinous carcinoma with a signet-ring cell component [5].

Table 1 Mucin gene product (MUC) and trefoil peptide (TFF) expression and percentages (%) in adenocarcinomas of the duodenum, ampulla of Vater, stomach and colorectum. *P* values were calculated by comparing the various MUC and TFF data in the four tumor groups using the chi square test

	MUC1	MUC2	MUC5AC	MUC6	TFF1	TFF2
Duodenal carcinoma	11/14 (78.6)	10/14 (71.4)	5/14 (35.7)	5/14 (35.7)	5/14 (35.7)	1/14 (7.1)
Ampullary carcinoma	8/11 (72.7)	3/11 (27.3)	6/11 (54.5)	5/11 (45.5)	1/11 (9)	1/11 (9)
Gastric carcinoma	7/10 (70)	6/10 (60)	8/10 (80)	2/10 (20)	6/10 (60)	3 /10 (30)
Colorectal carcinoma	4/10 (40)	10/10 (100)	2/10 (20)	0/10 (0)	0/10 (0)	0/10 (0)
P<	0.236	0.006	0.041	0.092	0.107	0.001

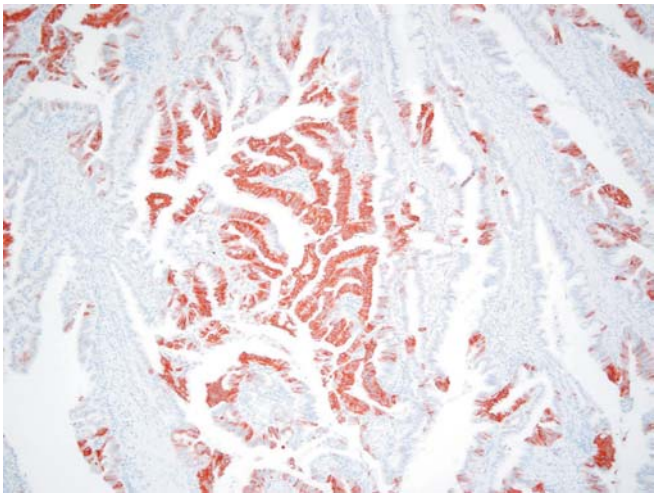

Fig. 1 MUC5AC expression in a duodenal adenocarcinoma. (MUC5AC immunostaining ×50)

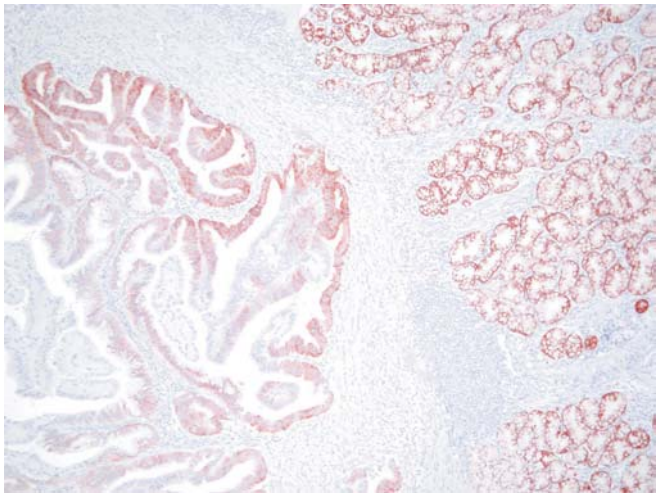

Fig. 3 MUC6 expression in a duodenal carcinoma and MUC6 immunoreactivity of Brunner's glands in the adjacent mucosa (MUC6 immunostaining ×50)

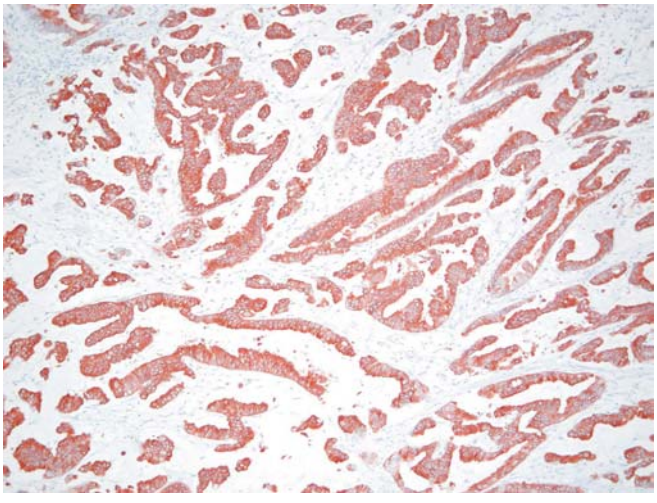

Fig. 2 MUC5AC expression in an ampullary adenocarcinoma (MUC5AC immunostaining ×50)

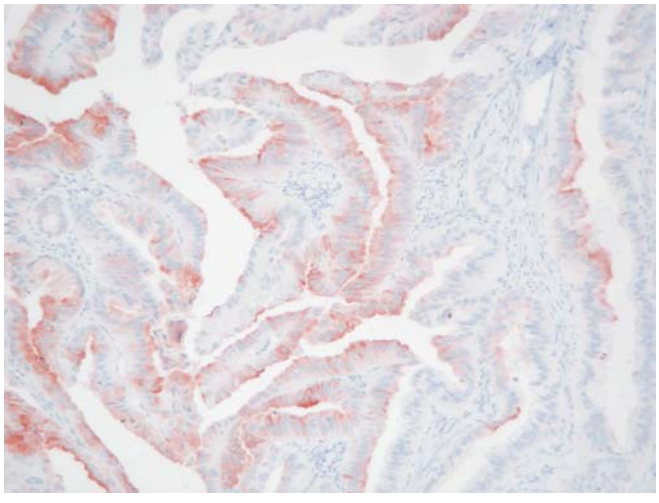

Fig. 4 Focal and faint intracytoplasmic and apical trefoil peptide 1 expression in a duodenal carcinoma

Table 1 summarizes the detailed results of the MUC and TFF staining in the various tumors. MUC1 positivity was most common in duodenal and ampullary carcinomas. Of the tumor cells, 20–90% showed either intracytoplasmic and/or luminal staining. MUC2 expression was most frequent in colorectal carcinomas (100%), followed by duodenal, gastric and ampullary carcinomas. MUC2 was expressed in the cytoplasm of most cells of the colorectal carcinomas, while in the other tumors, the proportion of stained cells ranged between 30% and 70%. MUC5AC was positive in most gastric carcinomas (80%) and in a significant number of ampullary (54.5%) and duodenal (35.7%) carcinomas, but rare in colorectal carcinomas (20%) (Fig. 1 and Fig. 2). MUC6 expression was completely lacking in colorectal carcinomas, but was seen in ampullary, duodenal and gastric carcinomas, where it was generally focal and faint (Fig. 3). TFF1 immunoreactivity was also lacking in colorectal carcinomas, but was found in duodenal and gastric carcinomas (Fig. 4). The single ampullary carcinoma that was positive for TFF1 showed mucinous differentiation. TFF1 expression was intracytoplasmic, with an apical concentration in some cases. TFF2 was rarely observed and only seen in single duodenal, gastric and ampullary carcinomas, where it was focally and faintly expressed. When we compared the results of MUC and TFF expression in duodenal, ampullary, gastric and colorectal tumors, the differences between the data on MUC2 ($P>0.006$), MUC5AC ($P>0.041$) and TFF2 ($P>0.001$) expression were statistically significant (Table 1).

Table 2 summarizes the data on the combined expression of MUC5AC, MUC6 and TFF1. A gastric pattern (positivity for three markers or two of them) was found in 60% of gastric carcinomas and in 45% of ampullary

Table 2 Gastric and nongastric (i.e., intestinal) differentiation of duodenal, ampullary, gastric and colorectal carcinomas according to their MUC5AC, MUC6 and trefoil peptide 1 (TFF1) expression. *GD* gastric differentiation. *NGD* nongastric differentiation

MUC5AC, MUC6 and TFF1	GD* (%)#	NGD**(%)
Duodenal carcinoma	3/14 (21.4)	11/14 (78.6)
Ampullary carcinoma	5/11 (45.4)	6/11 (54.6)
Gastric carcinoma	6/10 (60)	4/10 (40)
Colorectal carcinoma	0/10 (0)	10/10 (100)

* Positivity for MUC5AC, MUC6 and TFF1, or two of the three markers

** Positivity for one of the three markers or negativity for all markers

Comparison of the gastric differentiation of the tumor groups (chi square test) revealed statistical significance ($P<0.018$)

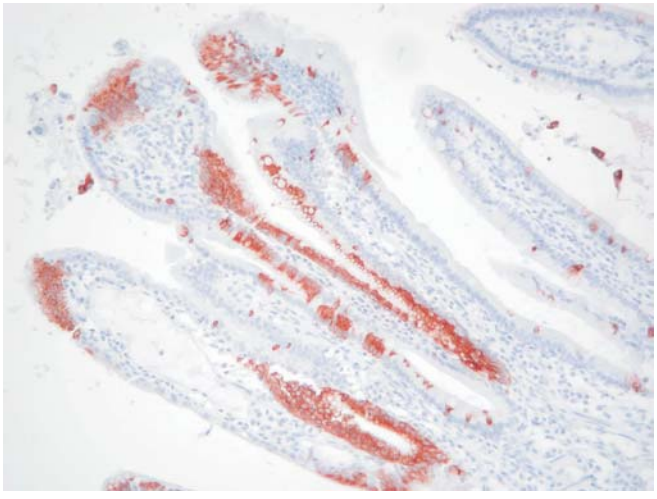

Fig. 5 MUC5AC immunostaining of a focus of gastric metaplasia

carcinomas, followed by duodenal carcinomas (21%). Three of the five ampullary carcinomas were histologically classified as pancreatobiliary type, one as mixed type and another one as mucinous type. The three duodenal carcinomas represented adenocarcinomas without typical intestinal features.

A nongastric, i.e., intestinal pattern, characterized all colorectal carcinomas (100%), but was also seen in 40% of the gastric carcinomas, 55% of the ampullary carcinomas and 79% of the duodenal carcinomas (Table 2). Three of the four gastric carcinomas displayed positivity for at least one marker. Five ampullary carcinomas showed the histological features of the intestinal type, and one showed features of the pancreatobiliary type [5]. Most (9 of 11) duodenal carcinomas were classified as intestinal-type carcinomas; two were adenocarcinomas with an uncharacteristic pattern.

Non-neoplastic duodenal mucosa was observed adjacent to tumors in 21 cases. The goblet cells stained for MUC2 and MUC5AC and Brunner's glands for MUC6 and TFF2 (Fig. 3). Occasionally, a few superficial mucosa cells were labeled by MUC6 and TFF2. In 7 of 21 cases, the duodenal mucosa contained foci of gastric metaplasia, which stained brightly for MUC5AC and TFF1 (Fig. 5).

In 14 cases, the non-tumorous tissue also contained pancreatic parenchyma, which included portions of the bile duct and pancreatic duct. In 11 cases, the pancreatic duct showed hyperplastic lesions, which stained for MUC5AC and, in 6 cases, also for MUC2. TFF1 expression was found in the normal duct epithelium and hyperplastic mucosa of 9 cases and TFF2 expression in the ductal epithelium of all cases except one.

Non-neoplastic gastric mucosa was observed in all cases. MUC1, MUC2, MUC5AC, MUC6, TFF1 and TFF2 expression was observed in their known locations. MUC2 stained intestinal metaplastic foci.

Non-neoplastic colonic mucosa was observed in eight cases. Focal MUC5AC immunoreactivity was detected in half of the cases in both goblet cells and mucous cells, while there was no MUC1, MUC6, TFF1 and TFF2 expression.

Discussion

In this study, we found that the MUC5AC, MUC6 and TFF1 expression patterns of duodenal carcinomas allow them to be separated into two groups that are more closely related to either gastric differentiation or intestinal differentiation. A similar tendency is seen in ampullary carcinomas.

A number of studies have revealed that gastric carcinomas are characterized either by the expression of MUC1, if they belong to the intestinal type according to Lauren's classification, or by MUC2 and MUC5AC, if they are classified as diffuse type [10, 16, 23, 24]. Colorectal carcinomas were found to express MUC2 in almost all cases and, to a lesser degree, also MUC1 and MUC5AC [6, 12, 15, 17, 27]. Our study confirms these data and, in addition, shows that duodenal carcinomas and ampullary carcinomas also express MUC1, MUC2 and MUC5AC in many cases. This indicates that they may share differentiation features with gastric or colorectal carcinomas and, therefore, may have their roots in both the gastric and the intestinal differentiation pathway, an idea that has also emerged from recent studies on the molecular genetics of duodenal and ampullary carcinomas [3].

To find out whether a further breakdown of the expression data for MUCs and TFFs can identify subtypes of duodenal and ampullary carcinomas, we followed the suggestion of Nogueira [20] and used the combination of MUC5AC and TFF1 as a criterion for gastric differentiation. As a further marker, we added MUC6 because of its consistent expression in the mucous cells of the neck of oxyntic mucosa crypts and in antral glands [20, 30]. Using this set of markers, we separated duodenal and ampullary carcinomas that were positive for MUC5AC, MUC6 and TFF1 or either two of the three markers from those that were MUC5AC, MUC6 and TFF1 negative. The group of duodenal and ampullary carcinomas that stained for MUC5AC, MUC6 and TFF1 or two of them were regarded as tumors that were related to mainly gastric dif-

ferentiation, since 60% of the gastric carcinomas but none of the colorectal carcinomas revealed the same marker set. Duodenal and ampullary carcinomas that were negative for all or two of the three markers corresponded to colorectal carcinomas and were hence classified as tumors of the intestinal type.

Almost 80% of the duodenal and 55% of the ampullary carcinomas failed to stain for MUC5AC, MUC6 and TFF1 or two of these three markers and were, therefore, classified as intestinal-type tumors. Histopathologically, the majority (85%) of these tumors resembled the usual colorectal carcinomas, and five of them were also associated with tubulovillous adenomas. The remaining duodenal and ampullary carcinomas, which were positive for MUC5AC, MUC6 and TFF1 (or two of these markers) and were regarded as gastric-type tumors, showed a histological pattern that was either unspecific (duodenal carcinomas) or of the pancreatobiliary type (ampullary carcinomas) [5], indicating that there is a rough correlation between the histopathological and immunophenotypical features of the carcinomas.

As to the origin of duodenal carcinomas with mainly gastric differentiation, it is interesting to note that the foci of gastric metaplasia that were encountered in the vicinity of the tumor in one-third of the cases expressed MUC5AC and TFF1. Moreover, a recent study located the metaplastic foci to the neck of the Brunner's gland ducts, which stain for MUC6 [14]. It is, therefore, tempting to speculate that the gastric-type duodenal carcinomas may develop from these special metaplastic areas of the duodenal mucosa, where cells expressing MUC5AC, MUC6 and TFF1 occur. It is of interest in this context that MUC5AC and TFF1 expression also seems to be a marker of altered/metaplastic non-neoplastic mucosa of the small and large intestine [7, 21, 31].

The normal enterocytes of the duodenal mucosa are, with occasional exceptions, negative for the markers MUC5AC, MUC6 and TFF1, and only the goblet cells express MUC2 and MUC5AC. As about 80% of the duodenal and 50% of the ampullary carcinomas are also negative for these markers, these tumors may arise from reserve cells that may follow the enterocyte differentiation pathway. Further support for this notion comes from the fact that tubulovillous adenomas of the duodenum, which may also arise from reserve cells and are known to precede carcinomas, were observed in association with two of the intestinal-type carcinomas.

Recent studies on the genetic profile of duodenal carcinomas revealed two different patterns of changes [3]. The first group of tumors was characterized by K-ras and p53 alterations as well as allelic losses at chromosomes 3p, 5q, 17p and 18q—changes that are similar to those observed in colorectal carcinomas. The second group was distinguished by high levels of microsatellite instability and mutations in the TGF-βRII gene—changes characteristic of the so-called mutator-phenotype pathway [3]. Although correlative studies combining the molecular data with MUC- and TFF-expression patterns are thus far lacking, it may be speculated that the duodenal carcinomas with gastric differentiation features are associated with the mutator phenotype, whereas the intestinal-type duodenal carcinomas follow the molecular pathway of carcinogenesis for colorectal carcinomas.

In ampullary carcinomas, it has been found that there is a group of tumors that share common molecular pathways (mutations and/or deletions of K-ras, p16, p53 and DPC4) with ductal adenocarcinomas of the pancreas and may have a poor prognosis in the case of an allelic loss at chromosome 17p [25]. Apart from these tumors, there are other ampullary carcinomas that show mutations in the APC gene [1] or high levels of microsatellite instability [2]. As in duodenal carcinomas, these data suggest that there could be an association between the molecular data and the differentiation status of ampullary carcinomas.

In summary, we found that duodenal carcinomas differ in their MUC- and TFF-expression patterns and may be separated into two groups, one with mainly gastric differentiation and another with mainly intestinal differentiation. This also seems to be the case for ampullary carcinomas. These data, combined with the results of molecular studies, support the hypothesis that at least two types of duodenal and ampullary carcinomas exist. Since, in a number of cases, the distinction between gastric and intestinal differentiation was not clear-cut, the possibility must also be considered that some of the duodenal and ampullary tumors have a dual differentiation.

Acknowledgements Yesim Gürbüz was a fellow of the Alexander von Humboldt-Stiftung, Bonn, Germany. The authors would like to thank Maike Pacena and Anja Paulus for their excellent technical assistance and Katherine Dege for editing the manuscript.

References

1. Achille A, Scupoli MT, Magalini AR, Zamboni G, Romanelli MG, Orlandini S, Biasi MO, Lemoine NR, Accolla RS, Scarpa A (1996) APC gene mutations and allelic losses in sporadic ampullary tumours: evidence of genetic difference from tumours associated with familial adenomatous polyposis. Int J Cancer 68:305–312
2. Achille A, Biasi MO, Zamboni G, Bogina G, Iacono C, Talamini G, Capella G, Scarpa A (1997) Cancers of the papilla of vater: mutator phenotype is associated with good prognosis. Clin Cancer Res 3:1841–1847
3. Achille A, Baron A, Zamboni G, Orlandini S, Bogina G, Bassi C, Iacono C, Scarpa A (1998) Molecular pathogenesis of sporadic duodenal cancer. Br J Cancer 77:760–765
4. Adedeji OA, Trescoli-Serrano C, Garcia-Zarco M (1995) Primary duodenal carcinoma. Postgrad Med J 71:354–358
5. Albores-Saavedra J, Murakata L, Krueger JE, Henson DE (2000) Noninvasive and minimally invasive papillary carcinomas of the extrahepatic bile ducts. Cancer 89:508–515
6. Biemer-Hüttmann AE, Walsh MD, McGuckin MA, Simms LA, Young J, Leggett BA, Jass JR (2000) Mucin core protein expression in colorectal cancers with high levels of microsatellite instability indicates a novel pathway of morphogenesis. Clin Cancer Res 6:1909–1916
7. Buisine MP, Desreumaux P, Leteurtre E, Copin MC, Colombel JF, Porchet N, Aubert JP (2001) Mucin gene expression in intestinal epithelial cells in Crohn's disease. Gut 49:544–551
8. Carvalho F, David L, Aubert JP, Lopez-Ferrer A, De Bolos C, Reis CA, Gartner F, Peioxoto A, Alves P, Sobrinho-Simoes M (1999) Mucins and mucin-associated carbohydrate antigens

expression in gastric carcinoma cell lines. Virchows Arch 435:479–485
9. Gendler SJ, Spicer AP (1995) Epithelial mucin genes. Annu Rev Physiol 57:607–634
10. Gürbüz Y, Kahlke V, Klöppel G (2002) How do gastric carcinoma classification systems relate to mucin expression patterns? An immunohistochemical analysis in a series of advanced gastric carcinomas. Virchows Arch 440:505-511
11. Howe JR, Karnell LH, Menck HR, Scott-Conner C (1999) The American College of Surgeons Commission on Cancer and the American Cancer Society. Adenocarcinoma of the small bowel: review of the National Cancer Data Base, 1985–1995. Cancer 86:2693–2706
12. Jang KT, Chae SW, Sohn JH, Park HR, Shin HS (2002) Coexpression of MUC1 with p53 or MUC2 correlates with lymph node metastasis in colorectal carcinomas. J Korean Med Sci 17:29–33
13. Katoh M (2003) Trefoil factors and human gastric cancer (Review). Int J Mol Med 12:3–9
14. Kushima R, Manabe R, Hattori T, Borchard F (1999) Histogenesis of gastric foveolar metaplasia following duodenal ulcer: a definite reparative lineage of Brunner's gland. Histopathology 35:38–43
15. Lee MJ, Lee HS, Kim WH, Choi Y, Yang M (2003) Expression of mucins and cytokeratins in primary carcinomas of the digestive system. Mod Pathol 16:403–410
16. Machado JC, Nogueira AM, Carneiro F, Reis CA, Sobrinho-Simoes M (2000) Gastric carcinoma exhibits distinct types of cell differentiation: an immunohistochemical study of trefoil peptides (TFF1 and TFF2) and mucins (MUC1, MUC2, MUC5AC, and MUC6). J Pathol 190:437–443
17. Manne U, Weiss HL, Grizzle WE (2000) Racial differences in the prognostic usefulness of MUC1 and MUC2 in colorectal adenocarcinomas. Clin Cancer Res 6:4017–4025
18. Moss WM, McCart PM, Juler G, Miller DR (1974) Primary adenocarcinoma of the duodenum. Arch Surg 108:805–807
19. Neugut AI, Jacobson JS, Suh S, Mukherjee R, Arber N (1998) The epidemiology of cancer of the small bowel. Cancer Epidemiol Biomarkers Prev 7:243–251
20. Nogueira AM, Machado JC, Carneiro F, Reis CA, Gott P, Sobrinho-Simoes M (1999) Patterns of expression of trefoil peptides and mucins in gastric polyps with and without malignant transformation. J Pathol 187:541–548
21. Nollet S, Forgue-Lafitte ME, Kirkham P, Bara J (2002) Mapping of two new epitopes on the apomucin encoded by MUC5AC gene: expression in normal GI tract and colon tumors. Int J Cancer 99:336–343
22. O'Riordan BG, Vilor M, Herrera L (1996) Small bowel tumors: an overview. Dig Dis 14:245–257
23. Pinto-De Sousa J, David L, Seixas M, Pimenta A (2001) Clinicopathologic profiles and prognosis of gastric carcinomas from the cardia, fundus/body and antrum. Dig Surg 18:102–110
24. Reis CA, David L, Carvalho F, Mandel U, De Bolos C, Mirgorodskaya E, Clausen H, Sobrinho-Simoes M (2000) Immunohistochemical study of the expression of MUC6 mucin and co-expression of other secreted mucins (MUC5AC and MUC2) in human gastric carcinomas. J Histochem Cytochem 48:377–388
25. Scarpa A, Di Pace C, Talamini G, Falconi M, Lemoine NR, Iacono C, Achille A, Baron A, Zamboni G (2000) Cancer of the ampulla of Vater: chromosome 17p allelic loss is associated with poor prognosis. Gut 46:842–848
26. Spira IA, Ghazi A, Wolff WI (1977) Primary adenocarcinoma of the duodenum. Cancer 39:1721–1726
27. Sylvester PA, Myerscough N, Warren BF, Carlstedt I, Corfield AP, Durdey P, Thomas MG (2001) Differential expression of the chromosome 11 mucin genes in colorectal cancer. J Pathol 195:327–335
28. Taylor KL, Mall AS, Barnard RA, Ho SB, Cruse JP (1998) Immunohistochemical detection of gastric mucin in normal and disease states. Oncol Res 10:465–473
29. Van De Bovenkamp JH, Korteland-Van Male AM, Warson C, Buller HA, Einerhand AW, Ectors NL, Dekker J (2003) Gastric-type mucin and TFF-peptide expression in Barrett's oesophagus is disturbed during increased expression of MUC2. Histopathology 42:555–565
30. Wong WM, Poulsom R, Wright NA (1999) Trefoil peptides. Gut 44:890–895
31. Wright NA, Poulsom R, Stamp G, van Noorden S, Sarraf C, Elia G, Ahnen D, Jeffery R, Longcroft J, Pike C (1993) Trefoil peptide gene expression in gastrointestinal epithelial cells in inflammatory bowel disease. Gastroenterology 104:12–20

Virchows Arch (2004) 444:542–553
DOI 10.1007/s00428-004-1014-4

ORIGINAL ARTICLE

Kazuto Yamazaki

Electron microscopy and immunohistochemistry studies of pulmonary carcinosarcomas expressing the transcription factor MEF-2 and showing significant cell-to-cell, cell-to-matrix, and epithelial–mesenchymal interactions

Received: 15 January 2004 / Accepted: 17 March 2004 / Published online: 9 April 2004

Abstract Pulmonary carcinosarcomas are typified by the rare histological combination of mixed epithelial and mesenchymal malignant tumor cells. The author has experienced three cases of pulmonary carcinosarcomas with large mass formation. Case 1 was the combination of adenocarcinoma with focal squamous cell differentiation and chondrosarcoma. In case 2, adenocarcinoma was combined with rhabdomyosarcoma. Case 3 demonstrated a large cell neuroendocrine carcinoma and rhabdomyosarcoma. The immunohistochemical findings showed that many of the carcinoma cells in case 3 and some carcinoma cells in case 2 demonstrated neuroendocrine cell differentiation. The nuclei in all sarcoma cells stained definitively positive for the transcription factor MEF-2. Many of the lineage-specific transcription factors for lung development were not distributed in the tumor tissue. Ultrastructurally, in all three cases, cell-to-cell (forming cellular junctions), cell-to-matrix, and epithelial-mesenchymal interactions were seen. In the interface or boundary between the carcinoma cell nests and the matrix-embedded sarcoma cells, well-developed basal lamina and fibroblastic spindle cells were frequently seen, with an appearance similar to primitive fibroblastic or mesenchymal cells, extending thin cytoplasmic process around the carcinoma cell nests. In summary, carcinosarcoma cells interacted with each other and with their extracellular matrix, revealed MEF-2 in the sarcoma cells, and showed unique histological findings associated with a variety of phenotypic differentiation patterns very different from normal lung development.

K. Yamazaki (✉)
Department of Pathology,
Saiseikai Central Hospital,
l-4-17 Mita, Minatoku, 108-0073 Tokyo, Japan
e-mail: KazutoYamazaki@aol.com
Tel.: +81-3-34518211
Fax: +81-3-34516102

Keywords MEF-2 · Pulmonary carcinosarcoma · Electron microscopy · Rhabdomyosarcoma · Chondrosarcoma

Introduction

Among the entire repertoire of lung tumors, pulmonary carcinosarcomas alone show the very rare histological pattern in which mixed epithelial and mesenchymal malignant tumor cells are combined [3, 6, 11, 16]. The pulmonary blastoma, although related to the pulmonary carcinosarcoma, and demonstrating a well-known and unique histological entity, differs greatly from it. Whereas the former mimics the branching stage of the histology of normal lung development with an organized combination of epithelial glands and immature mesenchymal components [3, 6, 11, 16, 21, 22], the latter demonstrates a much more heterogeneous (heterologous or homologous) development, which is distorted or greatly deviates from normal lung development, with the combination of well-differentiated or poorly differentiated epithelial malignancy and heterogeneous malignant mesenchymal components[3, 6, 11, 16, 21, 22]. The author has experienced three cases of very rare pulmonary carcinosarcoma, and this study evaluated in detail their immunohistochemical and ultrastructural features.

Recently in molecular embryology of the lung or other tissues and organs, great progress has been made in significant molecular determinants of the growth and development process [9, 18, 19]. In normal lung epithelial development, through the possible interaction with their mesenchymal components, TTF-1, GATA-6, Gli-1, HNF-3 alpha, and HNF-3 beta were assumed to play the key roles and regulate the expression of surfactant proteins and some lineage-specific marker proteins for airway epithelial cell differentiation [18, 19]. The expression of these factors in lung diseases and tumors, however, remains to be clarified, although it has begun to be reported in some lung epithelial tumor pathology [21]. As for

mesenchymal differentiation, MEF-2 has become recognized as one of the well-known examples of the key transcription factors for myogenic differentiation, in addition to MyoD1 and chondrogenic differentiation for Sox9 [7, 9, 15, 20]. In contrast to the skeletal muscle specificity of myogenic basic helix-loop-helix transcription factors (MyoD family), MEF-2 factors are reportedly expressed not only in skeletal, cardiac, and smooth muscle cells but also in neurons and at lower levels in several other cell types in the physiological developmental process [9, 17]. The expression of MEF-2 may be used as a sensitive marker of for the diagnosis of their malignant or neoplastic counterparts, and their distribution should be clarified. Part of the information was provided by the previous reports [10, 22]. The importance of MEF-2 to characterize the tumors should be emphasized in more detail.

Using immunohistochemical techniques, the author attempted to demonstrate the distribution of significant phenotypic molecules including the transcription factors, which are significant in the lung or other tissue morphogenesis and cell differentiation, and to clarify the differentiation status of tumor cells comparing them with the normal developmental process to realize their histogenesis. Furthermore, the implications of the frequent ultrastructural features, correlated with light microscopic immunohistochemistry in the tumor tissue, were pursued. The correlative mesenchymo–epithelial interactions in pulmonary carcinosarcoma to tumor cell differentiation were analyzed.

Materials and methods

Patients

As shown in Table 1, three cases were filed in the archives of the Department of Pathology. Two were females on whom excisional surgery had been performed, and one was a male who had undergone postmortem autopsy. All tumors had been over approximately 5 cm in diameter. The autopsy case and one surgical case had metastatic foci. In the two surgical cases, no recurrent or metastatic foci were found during the post-excisional surgery follow-up for over 5 months until this description. The autopsy case died of generalized metastasis of the tumor.

Tissue samples

Tumors tissue specimens from three patients were fixed in 15% neutral formalin, embedded in paraffin, and were allocated to conventional light microscopy and immunohistochemistry. For transmission electron microscopy, part of the tumor tissues were fixed in phosphate buttered 2.5% glutaraldehyde [10, 21, 22].

Light microscopy and immunohistochemistry

Tissue specimens were processed according to conventional histological techniques for subsequent sectioning and staining in hematoxylin and eosin (H&E), PAS (periodic acid Schiff), and Alcian blue. For immunohistochemistry, the primary antibodies listed in Table 2 were applied in this study so as to clarify and add value to the origin and nature of the neoplastic cells. Immunostaining was done with and without antigen-retrieval techniques [10, 21, 22].

Electron microscopy

Samples of the tumor tissue were fixed in phosphate-buffered 2.5% glutaraldehyde, then osmium tetroxide, and embedded in epoxy resin following conventional procedures. Ultrathin sections were stained with uranyl acetate and lead citrate and examined under a JEOL 1200EXII electron microscope [10, 21, 22].

Results

Light microscopy

Histological examination of the tissue specimens in all three cases confirmed the diagnosis of pulmonary carcinosarcoma. The dominant histological pattern of case 1 was adenocarcinoma with focal squamous cell differentiation plus chondrosarcoma (Fig. 1A). In case 2, adenocarcinoma was identified plus rhabdomyosarcoma (Fig. 1B). The tumor in case 3 was identified as large cell

Table 1 Patients, clinical features, and methods of determination of the pulmonary carcinosarcomas

Case no.	Age (years)/sex at surgery or autopsy	Number and size of the primary tumor	Metastatic site	Clinical features	Dominant histological pattern	Method of determination
1	72/Female	Single, 5×5×4 cm, rounded mass	Right, S2 (none)	Rapidly growing lung mass, surviving after excisional surgery of the right lung (p-T2N0M0). Surgical case	Adenocarcinoma with focal squamous cell differentiation plus chondrosarcoma	TEM, IHC
2	60/Female	Single, 6.5×6×6.5 cm, rounded mass	Right, S1–2 hilar lymph node	Lung tumor with hemosputum, surviving after excisional surgery of the right lung (p-T2N2M0). Surgical case	Adenocarcinoma plus rhabdomyosarcoma	TEM, IHC
3	62/Male	Single, 9×7×9 cm, rounded mass, extensively invading the lung and pleura	Left, S6 (generalized)	Died of generalized metastasis of lung tumor. Autopsy case	Large-cell neuroendocrine cell carcinoma plus rhabdomyosarcoma	TEM, IHC

Table 2 The results of the immunostaining for epithelial and mesenchymal components of three pulmonary carcinosarcomas

Antibodies: categories or rationale of use (commercial sources)		Case 1		Case 2		Case 3	
		Epithelial component	Mesenchymal component	Epithelial component	Mesenchymal component	Epithelial component	Mesenchymal component
		Adeno-carcinoma adenosqua-mous carcinoma	Chondro-sarcoma	Adeno-carcinoma	Rhabdomyo-sarcoma	Large cell neuro-endocrine carcinoma	Rhabdomyo-sarcoma
Organella	Mitochondria (CHEMICON, Temecula, CA)	Negative (–)	Negative (–)	Negative (–)	Positive (+++)	Negative (–)	Positive (++)
Myogenic differentia-tion	Myoglobin (Dako, Glostrup, Denmark)	Negative (–)	Negative (–)	Negative (–)	Positive (+++)	Negative (–)	Positive (+++)
	a-SMA (Dako)	Negative (–)	Negative (–)	Negative (–)	Negative (–)	Negative (–)	Negative (–)
	HHF-35 (Enzo, New York, USA)	Negative (–)	Negative (–)	Negative (–)	Positive (+++)	Negative (–)	Positive (++)
	Desmin (Dako)	Negative (–)	Focally posi-tive (+)	Negative (–)	Positive (++)	Negative (–)	Positive (++)
Mesenchymal cytoskeleton	Vimentin (Dako)	Negative (–)	Positive (++)	Negative (–)	Positive (+++)	Negative (–)	Positive (++)
Neurogenic differentia-tion	Neuron specific enolase (NSE, Dako)	Negative (–)	Negative (–)	Negative (–)	Negative (–)	Negative (–)	Negative (–)
	S-100 (Dako)	Mostly negative (–)	Positive (++)	Negative (–)	Occasionally positive (+)	Negative (–)	Occasionally positive (+)
Membrane-bound receptor	c-kit (CALBIOCHEM)	Negative (–)	Negative (–)	Negative (–)	Negative (–)	Negative (–)	Negative (–)
Pulmonary epithelial differentia-tion	APA (surfactant apoprotein A, Dako)	Negative (–)	Negative (–)	Negative (–)	Negative (–)	Negative (–)	Negative (–)
	SPB (surfactant pro-tein B, Calbiochem)	Focally positive (+)	Negative (–)	Negative (–)	Negative (–)	Negative (–)	Negative (–)
	proSPC (prosurfactant protein C, Research Diagnostics, Flanders, NJ)	Negative (–)	Negative (–)	Negative (–)	Negative (–)	Negative (–)	Negative (–)
Common epithelial differentia-tion	CEA (Mochida, Tokyo, Japan)	Positive (++)	Negative (–)	Positive (++)	Negative (–)	Positive (+)	Negative (–)
	EMA (epithelial membrane antigen, Dako)	Positive (++)	Negative (–)	Positive (++)	Negative (–)	Positive (++)	Negative (–)
Keratins	PK (pankeratin, AE1-AE3, Dako)	Positive (++)	Negative (–)	Positive (++)	Positive (+++)	Positive (++)	Negative (–)
	34bE12 (high molecu-lar weight cytokeratin, Enzo)	Focally positive (++)	Negative (–)	Mostly negative (–)	Negative (–)	Mostly negative (–)	Negative (–)
	Cam 5.2 (low-molecu-lar weight cytokeratin, Becton Dickinson, San Jose, CA)	Positive (+++)	Negative (–)	Positive (++)	Negative (–)	Positive (++)	Negative (–)
	CK7 (cytokeratin 7, Dako)	Positive (++)	Negative (–)	Focally positive (+)	Negative (–)	Focally positive (+)	Negative (–)
	CK20 (cytokeratin 20, Dako)	Negative (–)	Negative (–)	Negative (–)	Negative (–)	Negative (–)	Negative (–)
Neuroendo-crine differ-entiation	Chromogranin	Negative (–)	Negative (–)	Negative (–)	Negative (–)	Positive (++)	Negative (–)
	Synaptophysin (Dako)	Negative (–)	Negative (–)	Focally posi-tive (+)	Negative (–)	Positive (++)	Negative (–)
Glial inter-mediate fiber	GFAP (Dako)	Negative (–)	Negative (–)	Negative (–)	Negative (–)	Negative (–)	Negative (–)

neuroendocrine carcinoma with small tubular gland formation plus rhabdomyosarcoma with occasional definitive cross striations in the tumor cells (Fig. 1C, D). In the metastatic foci, either sarcoma, carcinoma, or carcinosarcomatous histology could be seen. In all three cases, pure carcinoma areas were seen at the periphery or rim of the tumor and accounted for approximately 5–30% of the total area of the main tumor.

PAS and Alcian blue stain revealed distribution of mucin in most of the adenocarcinoma cells in case 1 and case 2. A small number of cells in case 3 with tubular structure formation stained positive for mucin in the same

Table 2 (continued)

Antibodies: categories or rationale of use (commercial sources)		Case 1		Case 2		Case 3	
		Epithelial component	Mesenchymal component	Epithelial component	Mesenchymal component	Epithelial component	Mesenchymal component
		Adeno-carcinoma adenosqua-mous carcinoma	Chondro-sarcoma	Adeno-carcinoma	Rhabdomyo-sarcoma	Large cell neuro-endocrine carcinoma	Rhabdomyo-sarcoma
Lineage-specific transcription factors	GATA-6 (Santa Cruz Biotechnology, Santa Cruz, CA)	Negative (–)	Negative (–)	Negative (–)	Negative (–)	Negative (–)	Negative (–)
	TTF-1	Negative (–)	Negative (–)	Negative (–)	Negative (–)	Negative (–)	Negative (–)
	Gli-1 (Santa Cruz Biotechnology)	Negative (–)	Negative (–)	Negative (–)	Negative (–)	Negative (–)	Negative (–)
	MEF-2 (Santa Cruz Biotechnology)	Negative (–)	Positive (++)	Negative (–)	Positive (+++)	Negative (–)	Positive (++)
	MyoD1 (Dako)	Negative (–)	Negative (–)	Negative (–)	Focally Positive (+)	Negative (–)	Focally Positive (+)
	Sox9 (Santa Cruz Biotechnology)	Negative (–)	Negative (–)	Negative (–)	Negative (–)	Negative (–)	Negative (–)
Cluster of differentia-tion(CD) markers	CD10 (Novocastra, Newcastle upon Tyne, UK)	Focally positive (+)	Positive (++)	Negative (–)	Positive (+)	Negative (–)	Positive (+)
	CD34 (Dako)	Negative (–)	Negative (–)	Negative (–)	Negative (–)	Negative (–)	Negative (–)
	CD56 (Novocastra)	Negative (–)	Positive (++)	Negative (–)	Positive (+)	Negative (–)	Positive (++)
	CD57 (Leu7, Becton Dickinson)	Negative (–)	Mostly negative (–)	Negative (–)	Mostly negative (–)	Negative (–)	Mostly negative (–)
Hormone receptors	ER (Estrogen receptor, Dako)	Negative (–)	Negative (–)	Negative (–)	Negative (–)	Negative (–)	Negative (–)
	PGR (Progesterone receptor, Dako)	Negative (–)	Negative (–)	Negative (–)	Negative (–)	Negative (–)	Negative (–)
Extracellular matrix(ECM)	Type-II collagen (LSL Co. LTD, Tokyo, Japan)	Negative (–)	Focally positive (+) in ECM	Negative (–)	Negative (–)	Negative (–)	Negative (–)
	Type-IV collagen (Dako)	Positive (+) in ECM	Positive (+) in ECM	Positive (+) in ECM	Positive (+) in ECM	Positive (+) in ECM	Positive (+) in ECM
	Laminin (Dako)	Positive (+) in ECM	Positive (+) in ECM	Positive (+) in ECM	Positive (+) in ECM	Positive (+) in ECM	Positive (+) in ECM
Cardiomyo-genic-specific transcription factors	Nkx2.5 (Santa Cruz Biotechnology)	Negative (–)	Negative (–)	Negative (–)	Negative (–)	Negative (–)	Negative (–)
	GATA4 (Santa Cruz Biotechnology)	Negative (–)	Negative (–)	Negative (–)	Negative (–)	Negative (–)	Negative (–)
	eHAND (Santa Cruz Biotechnology)	Negative (–)	Negative (–)	Negative (–)	Negative (–)	Negative (–)	Negative (–)
Others	Parathyroid hormone-related polypeptide (PTHrP, Biogenesis, Poole, UK)	Negative (–)	Negative (–)	Negative (–)	Negative (–)	Negative (–)	Negative (–)

manner. In case 1, a loose stromal matrix in the chondrosarcomatous areas was demonstrated with Alcian blue stain.

Immunohistochemistry

The result of the immunohistochemical study was summarized in Table 2. The sarcoma cells in case 1 stained positively for the antigens or antibodies of vimentin, MEF-2, CD10, and CD56 (Fig. 1F, G). Some sarcoma cells in case 1 stained weakly or occasionally positively for NSE, S-100 (Fig. 1E), and rarely for desmin. A small number of sarcoma cells in case 1 stained positively for CD57 (Leu7) and NSE, whereas the sarcoma cells in case 1 stained negatively for the other antibodies examined. In the rhabdomyosarcomatous tissue in cases 2 and 3, sarcoma cells stained strongly positive for myoglobin, vimentin, HHF-35, desmin, CD10, and CD56 (Fig. 1J, K). Some rhabdomyosarcoma cells showed positive staining for S-100, NSE, CD57, and were very faintly positive for MyoD1 (Fig. 1I). In particular, the nuclei of all sarcoma cells studied in this study stained definitively positive for the transcription factor MEF-2 (Fig. 1G, H), whereas rhabdomyosarcoma cells from cases 2 and 3 stained negatively for other antibodies examined. Particularly noteworthy was that the sarcoma cells from all three cases failed to stain positively for Nkx2.5, GATA4,

eHAND, Sox9, and parathyroid hormone related polypeptide (PTHrP). In the stromal tissue of these three cases, type-IV collagen and laminin were variously distributed in the stromal matrix. Type-II collagen was also positive in the loose stromal matrix in the chondrosarcomatous areas of case 1.

Carcinoma cells from all three cases showed positive staining for the conventional epithelial markers CEA, Cam 5.2, CK7, EMA, and PK, but all stained negatively for the markers of mitochondria, myoglobin, vimentin, S-100, c-kit, CK20, GFAP, HHF-35, MEF-2, MyoD1, CD34, CD56, ER, and PGR. In the case of airway epithelial differentiation markers (APA, SPB, and proSPC), carcinoma cells revealed no positive stains. Many of the carcinoma cells in case 3 and some carcinoma cells in case 2, both of which had a rhabdomyosarcomatous component in the tumor tissue, revealed strongly positive staining for the neuroendocrine cell markers of chromogranin and synaptophysin (Fig. 1L). Lineage-specific transcription factors for airway epithelial differentiation (TTF-1, GATA-6, Gli-1) were all negative in cancer cells from case 1 through case 3. Some carcinoma cells in case 1 showed positive staining for CD10, while other carcinoma cells failed to reveal any positive staining. Some carcinoma cells in case 1 with squamous differentiation showed positive stains for 34bE12, while other carcinoma cells revealed no positive stain. Positive staining for type-II collagen was not conspicuous in the stroma of any of the carcinoma area. The basement membrane consisted of molecules of type-IV collagen, and laminin was distributed on the interface of the epithelial carcinoma and surrounding stroma in the sarcomas. Transcription factors Nkx2.5, GATA4, and eHAND, which are believed to be specific for cardiomyocyte differentiation, were not seen in the cancer cells. Parathyroid hormone related polypeptide(PTHrP) was not distributed in the cancer cells. CD57(Leu7) and NSE were positive in a small number of carcinoma cells from all three cases.

Electron microscopy

In case 1 (adenocarcinoma with squamous differentiation plus chondrosarcoma), adenocarcinoma cells formed cellular nests or irregular tubular glands. Primitive sarcoma cells with spindle or satellite shaped cells proliferated in the surrounding loose extracellular matrix containing fibrous collagen fibers and an abundant extracellular matrix (Fig. 2A). In adenocarcinoma cells forming small lumina, apico-lateral junctional complexes and short apical microvillus-like cytoplasmic processes were well-developed (Fig. 2A, B, D). In the cytoplasm of carcinoma cells, mitochondria, free ribosomes, rough endoplasmic reticulum (rER), and medium-sized secretory or lysosomal granules with contents of medium electron density were scattered in the cytoplasm (Fig. 2A, B, C, E). In case 1 sarcoma cells, mitochondria-rER complexes were frequently observed (Fig. 2C, F, G), in which close associations of mitochondria with loops of the rER were seen. The adjacent sarcoma cells frequently formed primitive cellular junctions with opposing cytoplasmic membranes having submembranous electron densities (Fig. 2F, H).

In case 2 (adenocarcinoma plus rhabdomyosarcoma), adenocarcinoma cells formed irregular cellular nests or tubular glands with lumina (Fig. 3A). Cancer cells proliferated in a pseudostratified fashion with ill-developed short apical microvillus-like cytoplasmic processes and a well-developed apico-lateral junctional complex (Fig. 3A, B). In their apical cytoplasm large mucin-filled secretory granules and subnuclear small granules were observed, which were consistent with the occasional positive findings in the light microscopic immunohistochemistry of the glandular and/or neurosecretory differentiation—hybrid or amphicrine nature of carcinoma cells (Fig. 3B). In sarcoma cells, proliferated tumor cells were seen with an opaque swollen cytoplasm and an irregular nucleus, with intracytoplasmic aggregation of myofilament with electron dense z-band-like structures (Fig. 3C, D). In case 3, similar findings to case 2 of carcinoma plus rhabdomyosarcoma were seen, whereas in case 3, carcinoma cells appeared more primitive with neurosecretory differentiation compared with in the carcinoma cells in case 2 (Fig. 3E).

In all three cases, at the interface or boundary between carcinoma and sarcoma cells, cell-to-matrices, and epithelial–mesenchymal interactions were revealed by electron microscopy. At the interfaces between or boundaries separating the nest of carcinoma cells and matrix-embedded sarcoma cells, fibroblastic spindle cells were frequently seen (Fig. 2A, B, C). They showed a primitive fibroblastic or mesenchymal cell appearance, extending thin cytoplasmic process and intimately associated with the basal lamina of the carcinoma cell nest (Fig. 2A, B, C). Sometimes, at the boundary of carcinoma cell nests, well-developed basal lamina were directly associated with abundant fibrous collagen and amorphous extracellular matrix in the sarcomatous area (Fig. 2B, C, B, E).

Fig. 1 Light micrographs of the tumor cells of pulmonary carcinosarcoma. **A** Case 1. Hematoxylin and eosin stain (H&E), ×95. **B** Case 2. H&E stain, ×95. **C** Case 3. H&E stain, ×95. **D** Case 3. Sarcoma cells with definitive cross striations and rhabdomyeloblastic differentiation. H&E stain, ×950. **E** Case 1. Immunohistochemical stain for S-100 protein (S100). The staining results for S100 are specific taking into account the nuclear positivity. ×95. **F** Case 1. Immunohistochemical stain for CD56. The membrane or cytoplasm of sarcoma cells stains positively. ×190. **G** Case 1. Immunohistochemical stain for MEF-2. The staining results for MEF-2 are specific taking into account the nuclear positivity. ×190. **H** Case 2. Immunohistochemical stain for MEF-2. Sarcoma cells reveal nuclear positivity. ×190. **I** Case 2. Immunohistochemical stain for MyoD1. Some sarcoma cells stains faintly positive both in their nuclei and cytoplasm. ×190. **J** Case 2. Immunohistochemical stain for desmin (DSM). Sarcoma cells stain positive in their cytoplasm. ×190. **K** Case 2. Immunohistochemical stain for CD10. Some sarcoma or mesenchymal cells stain positive in their membrane or peripheral cytoplasm. ×190. **L** Case 3. Immunohistochemical stain for chromogranin A (CGA). Carcinoma cells stain positive in their cytoplasm. ×190

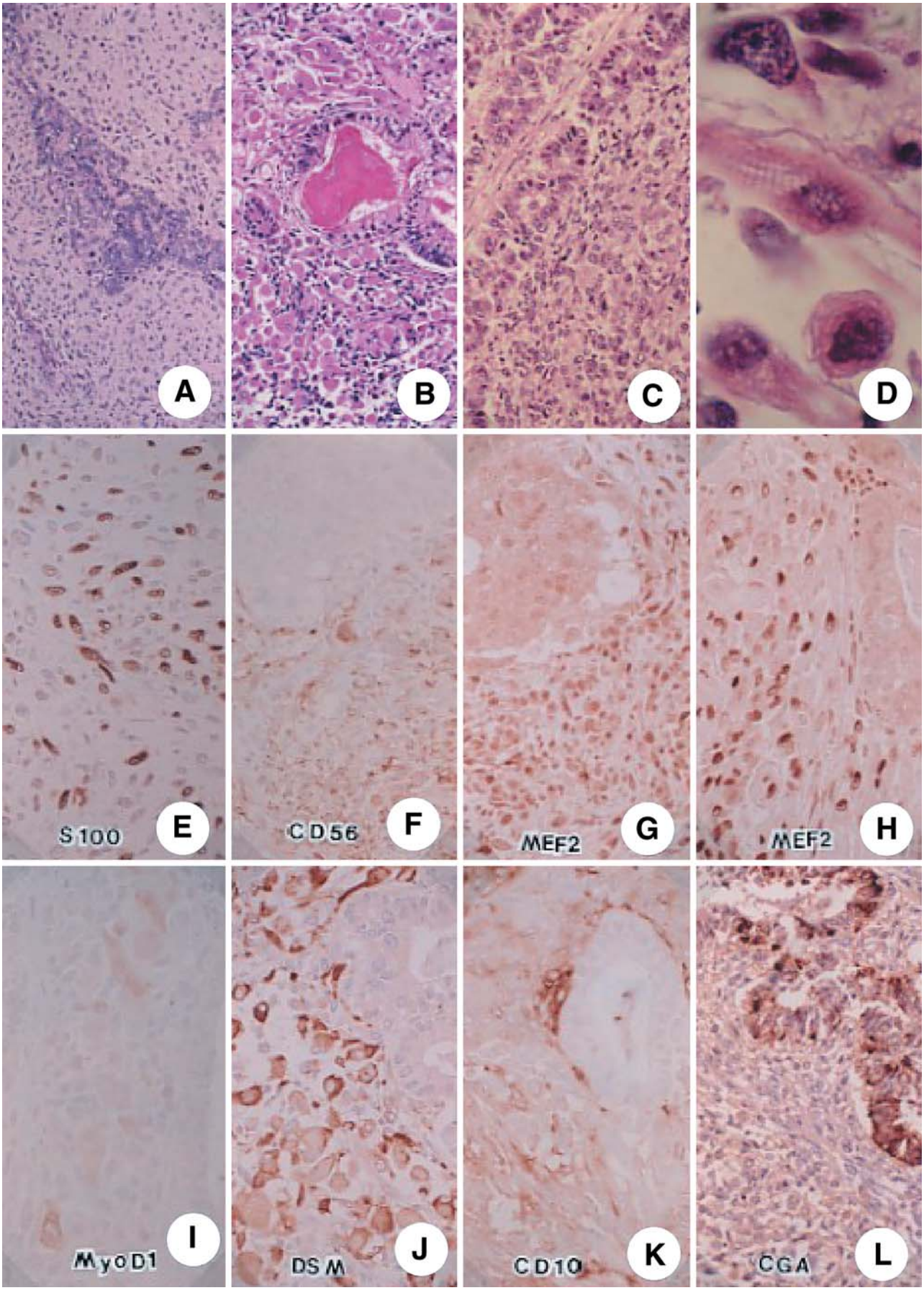
A
B
C
D
S100
E
CD56
F
MEF2
G
MEF2
H
MyoD1
I
DSM
J
CD10
K
CGA
L

Discussion

In this series of cases, the histopathological diagnosis of pulmonary carcinosarcoma was verified by the fact of definitive primary lung tumors with the uniquely combined histology of mixed epithelial and mesenchymal malignant tumor cells [3, 6, 11, 16]. The distinction from pulmonary blastoma with heterogeneous stromal elements is important, well recognized in the literature, and finely illustrated by the World Health Organization Histological Typing of Lung and Pleural Tumors (1999) [16]. Although pulmonary blastoma could have occasionally foci of osteosarcoma, chondrosarcoma, or rhabdomyosarcoma, the epithelial component has a distinctive primitive appearance, often resembling well-differentiated fetal adenocarcinoma [3, 6, 11, 16]. The latter finding is absolutely inconspicuous in this series of pulmonary carcinosarcomas [3, 6, 11, 16].The sarcomatous component of case 1 was assumed to be chondrogenic, since type-II collagen and acid mucopolysaccharide (Alcian blue positive) were distributed in the rich and loose extracellular matrix. Sometimes the presence of S-100 in the nuclei of sarcoma cells is interpreted as chondrogenic differentiation [4]. However, the sarcomatous components of case 2 and case 3 were definitively myogenic, since occasional cross striations, vimentin, myoglobin, desmin and HHF35 are commonly used as sensitive markers of myogenic differentiation, especially of rhabdomyosarcoma [4].

All the tumors in the present study were large, with approximate diameters of more than 5 cm. When they were identified, they were in the advanced stage of tumor proliferation. The autopsy case and one of the surgical cases had metastatic foci. The large tumor size at the examination may reflect the chance of the occurrence of frequent genetic changes and their accumulation during tumor cell proliferation in the primary site of the lung [5]. The existence of a peripherally positioned pure carcinoma component without any mixed mesenchymal component may suggest the generation of carcinosarcomatous histology from the conventional pre-existent carcinomatous histology [5].

In the ultrastructure of sarcoma cells in case 1, frequent mitochondrial associations could be observed [8]. When rERs are located near a supply of substrate, mitochondrial ATP generation is required. Their intimate associations sometimes form the mitochondria-rER complex, in which close associations of mitochondria with loops of rough endoplasmic reticulum were seen. Profiles of rER wrapping around mitochondria are not as rare, particularly in cells engaged in active protein synthesis (for example, the pancreas), and juxtaposition of this organelle to a site of energy utilities has been reported to occur [8]. It could be speculated that the proliferation of this tumor cell was very active. In the active growing state of the tumor, genetic mutations might have been accumulated to reach the advanced level seen in the production of the unique histology of the carcinosarcoma [5].

In sarcoma cells of the present study, the distribution of CD56, CD10, and MEF-2 was shown using immunohistochemistry. Very faint staining for MyoD1 was observed in some sarcoma cells of case 2 and case 3. MyoD1 is reported to be strictly localized to the cellular nuclei; hence background cytoplasm labeling should be ignored as a spurious pattern of staining [4]. As for the regulatory gene expression by lineage-specific transcription factors, the recently introduced Sox9, which has begun to be used for the diagnosis of chondrosarcoma, [7, 9, 20] was not present in the sarcoma cells of case 1. N-CAM (CD56), which was present in the sarcoma cells of case 1, is reported to be critical for chondrogenic differentiation [9, 12, 13]. During the normal process of the differentiation of myoblasts to into muscle cells, several cadherins and CAMs mediate the cell alignment process required for differentiation [9]. In the rhabdomyosarcomatous tissue of case 2 and case 3, the distribution of CD56 was absolutely confirmed [12, 13]. In the uterine body, occurrence of the heterologous or homologous type of carcinosarcoma is well known. The histological similarity of the more common uterine carcinosarcoma to pulmonary carcinosarcoma in the present study might be interesting. Case 1 sarcoma cells expressed CD10. Recently, the utility of CD10 in distinguishing between endometrial stromal sarcoma and uterine smooth muscle tumor was recognized [1, 2, 14].

It may well say that the staining results in the different sarcomatous features of the three tumors only proves the specificity of the antibody and should not be used as a reference to illustrate the lineage of the tumor. Characteristically, the nuclei of all sarcoma cells stained definitively positive for the transcription factor MEF-2 [10, 15, 22], and immunostaining for MEF-2 was intensely positive in all cases, irrespective of the histological characteristics. Sarcoma cells showed strong immunoreactivity for MEF-2, thus suggesting that sarcoma cells might present a different type of myogenic differentiation from skeletal or smooth muscle cells. Although the exact mechanism should be clarified in the future, some intrathoracic sarcoma would stain positive for MEF-2 [10, 15, 22]. In contrast to the skeletal muscle specificity of MyoD, MEF-2 factors are reportedly expressed not only in skeletal, cardiac and smooth muscle cells, but also in neurons and at lower levels in several other cell types in the physiological developmental process [9, 17]. From the previous studies, the expression of MEF-2 may be used as a sensitive marker of for the diagnosis of certain tumors. Part of the information was provided by the previous reports [10, 22]. It should be stressed that the positive reaction of MEF-2 is so important in the regulation of cellular differentiation of sarcomatous cells. The importance of MEF-2 to characterize the tumors should be emphasized in more detail in future studies. Transcription factors of Nkx2.5, GATA4, and eHAND, which are believed to be specific for cardiomyocytes (a kind of striated muscle cell), were not seen in the differentiated lineages in the rhabdomyosarcoma cells of the present study [9, 10]. In the histological analysis of the present sarcomatous component, certain transcription factors might be useful to detect the lineage of differentiation.

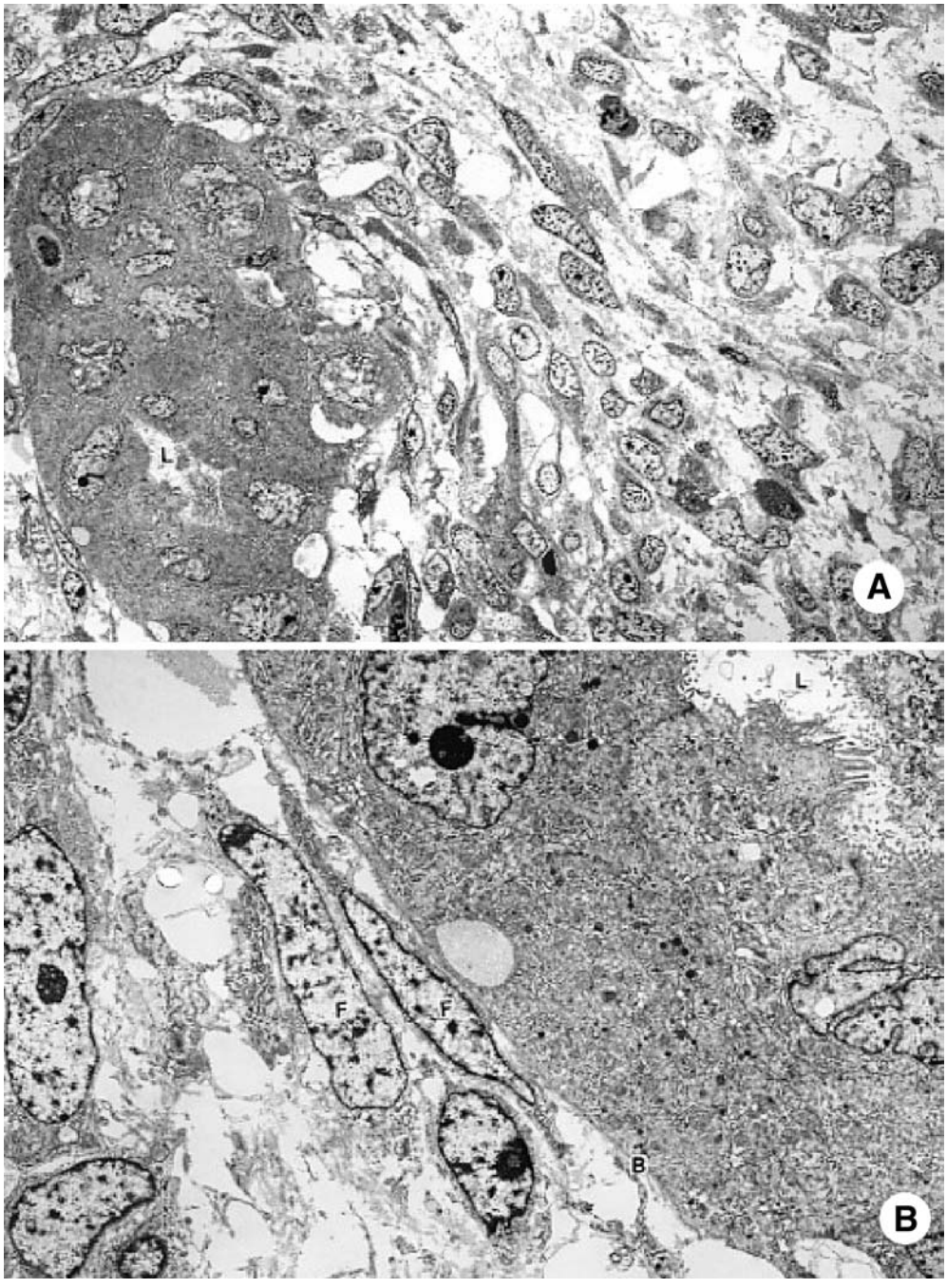

Fig. 2 Transmission electron photomicrographs of the pulmonary carcinosarcoma tumor cells from case 1. **A** Low-power view of carcinosarcoma tissue. A carcinoma cell nest with a glandular lumen (*L*) with apical microvilli. ×1200. **B** Interface or boundary between carcinoma and sarcoma. *B* basal lamina. Fibroblastic cells (*F*) at the boundary. Carcinoma cells formed a lumen. ×4800. **C** Interface or boundary between carcinoma and sarcoma. A mitochondria-rER complex in a sarcoma cell (*arrowheads*). These organelles may look like lysosomes, but they have definitive cristae in the inner structures to characterize the mitochondria. ×9500. **D** Apical differentiation of carcinoma cells with well-developed apical cellular junctions and microvilli. ×24,000. **E** Apical differentiation of carcinoma cells with secretory granules in the cytoplasm. ×48,000. **F** Sarcoma cells with primitive cellular junctions (*arrow*) and a mitochondria-rER complex (*arrowheads*).The organella (*arrowheads*) may look like lysosomes, but they have definitive cristae in the inner structures to characterize the mitochondria. ×9500. **G** A high-power view of the mitochondria-rER complex in the a sarcoma cell in **F**. Cristae to differentiate the mitochondria from lysosomes and myelin-like figure in the internal structure of the organella. ×24,000. **H** A high-power view of primitive cellular junctions between adjacent sarcoma cells. ×24,000

In normal lung development, mesenchymal signals induce a specific lung epithelial phenotype [18, 19]. Of high possible interest in this immunohistochemical study was the fact that many of the carcinoma cells in case 3 and some carcinoma cells in case 2, both of which formed a rhabdomyosarcomatous component in the tumor tissue, revealed strong positive staining for the neuroendocrine cell markers of chromogranin and synaptophysin. When these findings are compared with previous reports of pulmonary carcinosarcoma, neuroendocrine cell differentiation in the carcinoma component of the present case 2 and case 3 is rather unique [3, 6, 11, 16]. However, no carcinoma cells in the present study revealed the expression of airway epithelial cell differentiation-specific transcription factors, TTF-1, GATA6, HNF3 alpha, and HNF3 beta, nor any surfactant proteins (SPA, SPB, and SPC) [18, 19, 20]. Pulmonary neuroendocrine cells are among the first cells to differentiate in the primitive lung epithelium [19]. In the interfaces of carcino-stromal and carcino-sarcomatous area, amorphous matrices with immunohistochemical distribution of laminin and type-IV collagen were seen. As for how mesenchymal–epithelial interaction was achieved, some of the significant cell-to-cell, cell-to-matrix, and epithelial–mesenchymal interactions were revealed in this study by the electron microscopy and immunohistochemistry findings [8, 9, 18, 19].

Fig. 2 (continued)

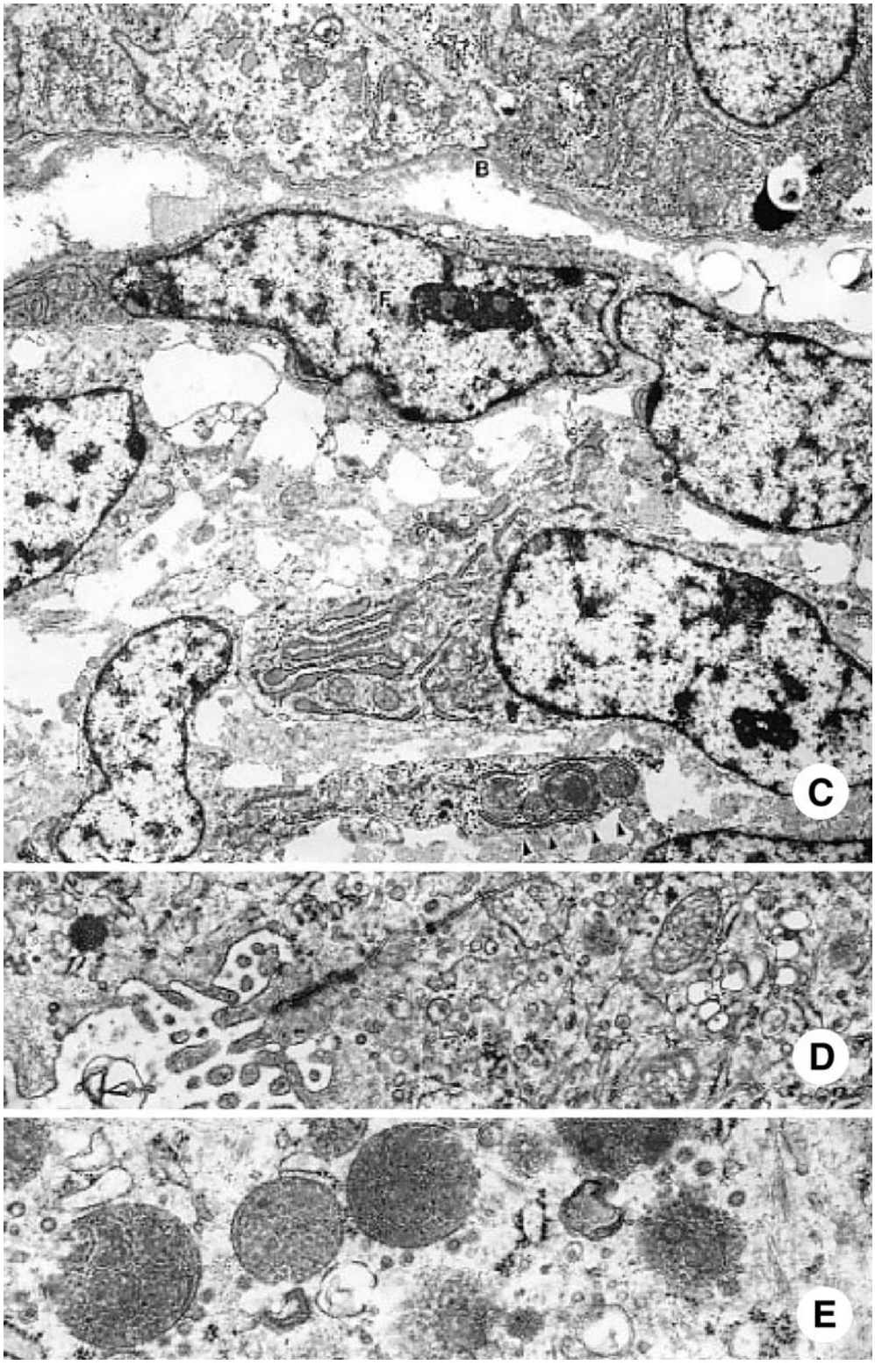

In the interface or boundary between the nest of carcinoma cells and matrix-embedded sarcoma cells, well-developed basal lamina and fibroblastic spindle cells were frequently seen. They showed a primitive fibroblastic or mesenchymal cell appearance, extending thin cytoplasmic processes and being intimately associated with the basal lamina of the carcinoma cell nests [8, 9]. Primitive cellular junctions between adjacent sarcoma cells and well-developed cellular junctional complexes between adjacent cancer cells are assumed to be the definitive evidence of cell-to-cell interactions between these cell types [8, 9]. Present ultrastructural studies revealed where the cell

Fig. 2 (continued)

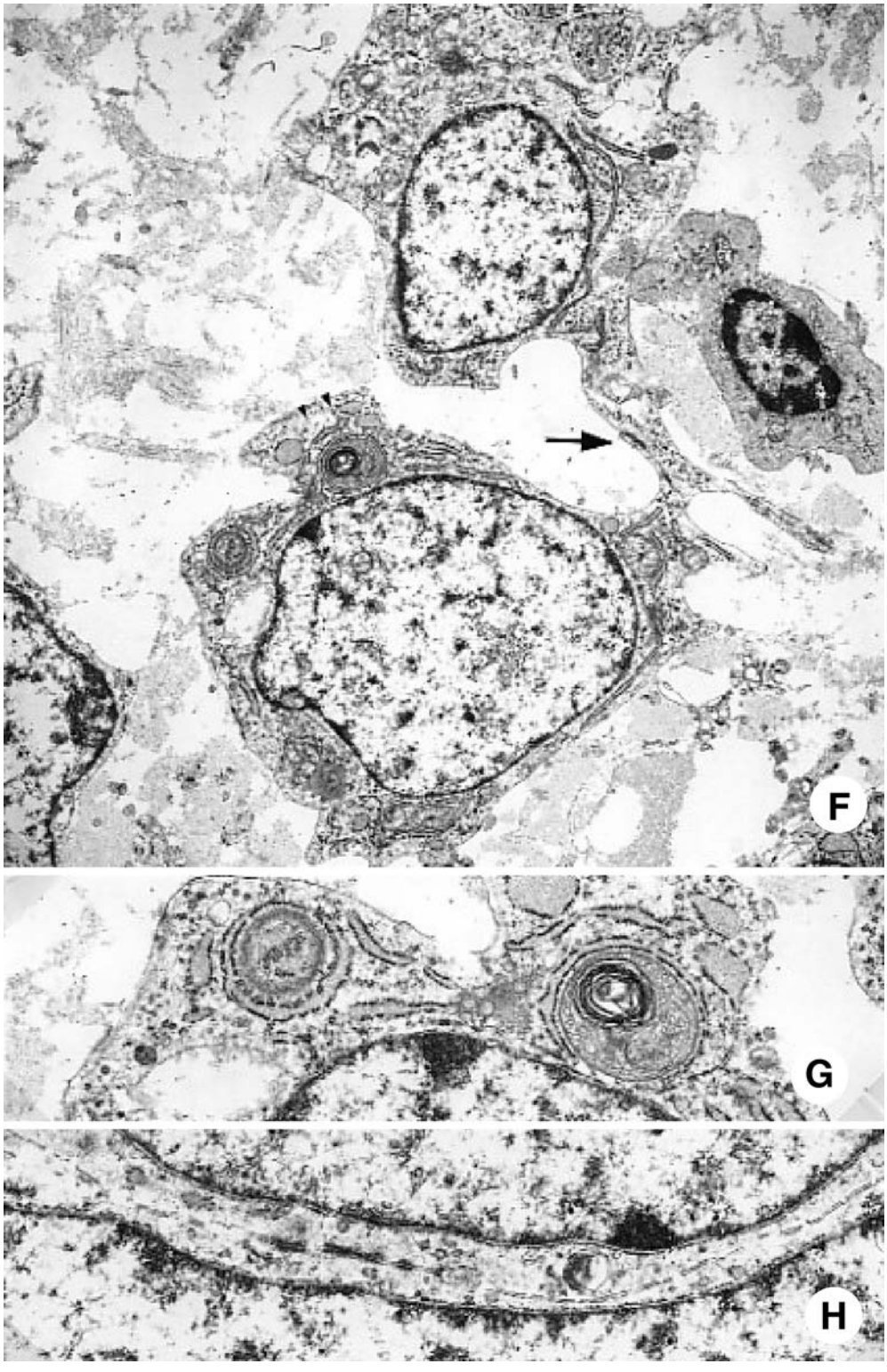

junctions were seen. Not only frequent desmosomes between squamous tumor cells could be seen, but also primitive cellular junctions in sarcoma cells. Some cancer cells formed a well-developed apico-lateral junctional complex. Although the roles of cell junctions, missing of cell junctions as well as the role of prominent cell junctions and cell matrix interactions should be discussed in more detail, it ought to be said that the cell junctions and cell matrix interactions play an important role for migration and development of tumor cells [8, 9]. Well-developed basal lamina connecting with the collagenous or amorphous extracellular matrix which surrounded the sarcoma cells could be assumed to be the evidence of cell-to-matrix and epithelial–mesenchymal interactions in the

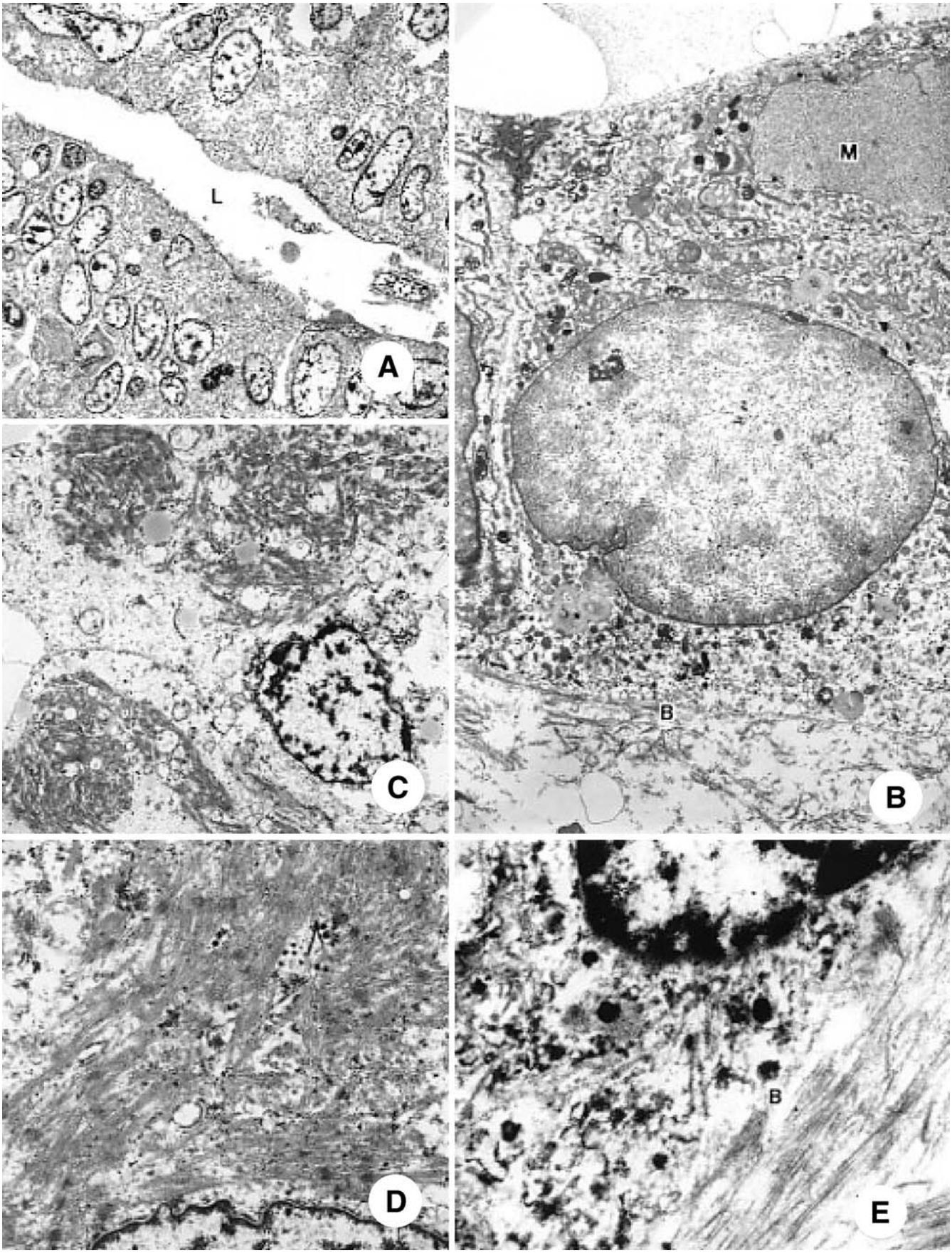
L
A
M
B
B
C
D
B
E

Fig. 3 Transmission electron photomicrographs of the pulmonary carcinosarcoma tumor cells from case 2 (**A**–**D**) and case 3 (**E**). **A** Low-power view of carcinoma tissue. *L* a lumen among carcinoma cells. ×1050. **B** Carcinoma cells with neuroendocrine cell differentiation. In the subnuclear basal cytoplasm of the cell, many small electron-dense granules of the neuroendocrine type seen. *M* mucin-filled granule, *B* basal lamina. ×7000. **C** Sarcoma cells with abundant aggregation of myofilament with z-band-like dense patches. ×5250. **D** High-power view of an aggregation of myofilament with z-band-like dense patches. ×17,500. **E** Although there are autolytic changes and poor preservation in the ultrastructure of post-mortem specimen, possibly undifferentiated carcinoma cells with small electron-dense granules of neuroendocrine cell differentiation is suspected. Neurosecretory granules are not clearly visible owing to the poor preservation or sub-optimum fixation. ×17,500

present carcinosarcoma tissue [8, 9]. The importance of the basement membrane in controlling cells had already been reported in the previous literature with details. Briefly, basement membrane, similar to other extracellular matrix, plays a role in assembling the extracellular matrix, promoting cell adhesion and growth, changing cell shape, and permitting cell migration [8, 9]. The possible effect of cellular interactions in pulmonary carcinosarcoma on tumor cell differentiation was speculated on in this histopathological, ultrastructural, and immunohistochemical study [9, 18, 19].

To interpret the histogenesis of a certain tumor type with a unique histology, exact comparison with the normal lineage-specific differentiation seems to be helpful, and not just the use of simple markers for that certain tumor, so that some reason could be advanced for the immunohistochemical distribution or expression of certain molecules. In conclusion, in the pulmonary carcinosarcoma tissues in the present study, tumor cells interacted with each other and with their extracellular matrix, expressing the transcription factor MEF-2 and other functionally significant molecules for their differentiation. Subsequently they showed a unique histology and phenotypic tumor cell differentiation completely different from normal lung development and even pulmonary blastoma with heterogeneous stromal elements [3, 6, 9, 11, 16, 18, 19, 21].

Acknowledgements The author would like to acknowledge T. Nagai and K. Fujita for technical assistance with the electron microscopy; M. Furihata, T. Kohno, K. Nagawatari, A. Furusawa, T. Oyama, and M. Sasahara for assistance with the light microscopic histology and immunohistochemistry and also the valuable discussion and help offered by Drs. H. Orikasa, H. Kayano, J. Shiraishi, M. Mori, H. Nomori, I. Ootuka, A. Ebihara, and T. Aoki.

References

1. Chu P, Arber DA (2000) Paraffin-section detection of CD10 in 505 nonhematopoietic neoplasms. Frequent expression in renal cell carcinoma and endometrial stromal sarcoma. Am J Clin Pathol 113:374–382
2. Chu P, Arber DA, Weiss LM, et al (2001) Utility of CD10 in distinguishing between endometrial stromal sarcoma and uterine smooth muscle tumors: an immunohistochemical comparison of 34 cases. Mod Pathol 14:465–471
3. Colby T, Koss MN, Travis WD (1995) Atlas of tumor pathology. 21 Tumors of the lower respiratory tract. Armed Forces Institute of Pathology, Washington, D.C.
4. Dabbs D (2002) Diagnostic immunohistochemistry. Churchill Livingstone, New York
5. Dacic S, Finkelstein SD, Sasatomi E, et al (2002) Molecular pathogenesis of pulmonary carcinosarcoma as determined by microdissection-based allelotyping. Am J Surg Pathol 26:510–516
6. Dail D (ed) (1993) 33 Uncommon tumors. In: Pulmonary pathology, Springer-Verlag, Berlin, Heidelberg, New York, pp 1279–1461
7. de Crombrugghe B, Lefebre V, Behringer RR, et al (2000) Transcriptional mechanism of chondrocyte differentiation. Matrix Biol 19:389–394
8. Ghadially F (1997) Ultrastructural pathology of the cell and matrix. Butterworth-Heinemann, Boston
9. Gilbert S (2000) Developmental Biology. Sinauer Associates Inc, Sunderland
10. Kodama H, Hirotani T, Suzuki Y, et al (2002) Cardiomyogenic differentiation in cardiac myxoma expressing lineage-specific transcription factors. Am J Pathol 161:381–389
11. Koss M, Hochholzer L, Frommelt RA (1999) Carcinosarcomas of the lung: a clinicopathologic study of 66 patients. Am J Surg Pathol 23:1514–1526
12. Mechersheim G, Staudter M, Moller P(1991) Expression of the natural killer cell-associated antigens CD56 and CD57 in human neural and striated muscle cells and in their tumors. Cancer Res 51:1300–1307
13. Miettinen M, Cupo W (1993) Neural cell adhesion molecule distribution in soft tissue tumors. Hum Pathol 24:62–66
14. Mikami Y, Hata S, Kiyokawa T, et al (2002) Expression of CD10 in malignant Mullerian mixed tumors and adenosarcomas: an immunohistochemical study. Mod Pathol 15:923–930
15. Puri P, Wu Z, Zhang P, et al (2000) Induction of terminal differentiation by constitutive activation of p38 Map kinase in human rhabdomyosarcoma cells. Genes Dev 14:574–584
16. Travis W, Colby TV, Corrin B, Shimosato Y, Brambilla E (1999) Histological typing of lung and pleural tumors. World health organization international classification of tumors. Springer, Berlin, Heidelberg, New York
17. Wang D-Z, Valdez MR, McAnally et al (2001) The Mef2c gene is a direct transcriptional target of myogenic bHLH and MEF2 proteins during skeletal muscle development. Development 128:4623–4633
18. Warburton D, Wuenschell C, Flores-Delado G, et al (1998) Commitment and differentiation of lung cell lineage. Biochem Cell Biol 76:971–995
19. Warburton D, Zhao J, Berberich MA, et al (1999) Molecular embryology of the lung, now, and in the future. Am J Physiol 276:L697–L704
20. Wehri B, Huang W, De Crombrugghe B, et al (2003) Sox9, a master regulator of chondrogenesis, distinguishes mesenchymal chondrosarcoma from other small blue round cell tumors. Hum Pathol 34:263–269
21. Yamazaki K(2003) Pulmonary well-differentiated fetal adenocarcinoma expressing lineage-specific transcription factors (TTF-1 and GATA-6) to respiratory epithelial differentiation: an immunohistochemical and ultrastructural study. Virchows Archiv 442:393–399
22. Yamazaki K (2003) An ultrastructural, immunohistochemical, and cytogenetical study of monophasic synovial sarcoma: Implications of the frequent ultrastructure of oligocilia and concentric membranous bodies with positive immunostaining for VS38c and MEF-2. Ultrastruct Pathol 27:235–241

Virchows Arch (2004) 444:554–560
DOI 10.1007/s00428-004-0998-0

ORIGINAL ARTICLE

Michele Barone · Eugenio Maiorano · Roberta Ladisa · Antonia Pece · Pasquale Berloco · Mario Strazzabosco · Maria Lucia Caruso · Anna Maria Valentini · Enzo Ierardi · Alfredo Di Leo · Antonio Francavilla

Ursodeoxycholate further increases bile-duct cell proliferative response induced by partial bile-duct ligation in rats

Received: 25 June 2003 / Accepted: 16 February 2004 / Published online: 8 April 2004

Abstract *Background:* Bile salts (BSs) stimulate cholangiocyte proliferation in vitro and in vivo in normal rats. In this study, we evaluated the effects of BS-enriched diets on cholangiocyte proliferative activity already triggered by partial bile-duct ligation (pBDL), a surgical model that induces mild cholestatic conditions, focusing our attention on ursodeoxycholate (UDC). *Methods:* Animals (n=45) were fed either a standard diet, or a 0.2% deoxycholate- or 0.2% UDC-enriched diet for 4 weeks. Then, in each group, ten animals underwent pBDL and five underwent sham operation. Serum and biliary BS levels, serum cholestasis and cytolysis indexes, as well as liver conventional histology, apoptosis and proliferative activity were evaluated 48 h after the operation. *Results:* Animals that underwent pBDL showed sustained proliferative response compared with sham-operated rats. BS-enriched diets did not influence cholangiocyte proliferation in sham-operated rats. However, significantly increased proliferation was observed in pBDL rats fed a UDC-enriched diet. The evaluation of humoral and histological parameters excluded the possibility that the increased proliferation induced by UDC-enriched diet could be related to concomitant liver cell damage. *Conclusion:* A UDC-enriched diet is able to amplify the magnitude of the cholangiocyte hyperplastic process, which occurs by a stimulatory mechanism after partial bile-duct ligation.

Keywords Bile salts · Cholangiocyte proliferation · Cholestasis · Partial bile-duct ligation

M. Barone · R. Ladisa · A. Di Leo · A. Francavilla
Section of Gastroenterology,
D.E.T.O., University of Bari, Italy

E. Maiorano · A. Pece
Department of Pathological Anatomy and Genetics,
University of Bari, Italy

P. Berloco
Laboratory of Biochemistry,
IRCSS "S. De Bellis, " Castellana Grotte,
Bari, Italy

M. Strazzabosco
Department of Internal Medicine,
University of Padua, Italy

M. Strazzabosco
Division of Gastroenterology,
Ospedali Riuniti di Bergamo, Italy

M. L. Caruso · A. M. Valentini
Department of Pathology,
IRCSS "S. De Bellis, " Castellana Grotte,
Bari, Italy

E. Ierardi
Department of Gastroenterology,
University of Foggia, Italy

A. Francavilla (✉)
Sezione di Gastroenterologia,
D.E.T.O., Università di Bari, Ospedale Policlinico,
Piazza G. Cesare, 11, 70124 Bari, Italia
e-mail: a.francavilla@gastro.uniba.it
Tel.: +39-080-5592577
Fax: +39-080-5593251

Introduction

Bile-duct epithelial cells (cholangiocytes) are able to intensely proliferate under several pathophysiological conditions. In humans, their proliferative activity is particularly stimulated in chronic cholestatic disorders [17, 28]. In animals, in addition to spontaneously occurring pathological conditions, such as infectious diseases [15, 21, 25], cholangiocyte proliferation can be experimentally induced using toxic agents [23, 32, 35], partial hepatectomy [13] and total bile-duct ligation (tBDL) [33].

The development of the partial bile-duct ligation (pBDL) model, i.e., the obstruction of lobar ducts draining 60% of the hepatic mass, demonstrated that this condition triggers cholangiocyte proliferation both in obstructed and freely draining lobes, suggesting that bile-duct cell proliferation is under the control of humoral

factors [27]. The demonstration that different hormones, cytokines and growth factors stimulate proliferation of cultured rat cholangiocytes and cholangiocyte-derived cell lines further supports this hypothesis [5, 34].

The possible involvement of bile salts (BSs) in the control of cell proliferation was first suggested by the demonstration of their stimulatory effects on hepatocyte replicative activity [7, 8, 9]. Subsequently, Alpini and coworkers [1, 2] demonstrated both in vitro, in primary cultures and in vivo (in intact animals fed BS-enriched diets) that BSs are able to stimulate the proliferation of bile-duct cells.

Finally, rats undergoing common bile-duct ligation demonstrated reduced cholangiocyte damage and proliferation following the administration of ursodeoxycholate (UDC) [3, 19], a result that apparently is in contrast with what is observed in UDC-fed mice [18].

The current study was aimed at evaluating, for the first time, the ability of a UDC-supplemented (0.2% wt/wt) diet to modulate rat cholangiocyte proliferative response induced by pBDL, an animal model that determines moderate cholestasis, thus making it an ideal condition to test substances with potential stimulatory or inhibitory effects. The expected results could be relevant to establish whether the improvement observed in UDC-treated patients could derive not only from the reduction of liver damage, but also from delaying the ductopenic end stage by stimulating cell proliferation.

Preliminary data obtained using the tBDL model led us to conclude that this model is unsuitable to evaluate the effects of putative cholangiocyte growth factors, since it induces a maximal proliferative response and, therefore, is hardly, if not at all, susceptible to further amplification (unpublished data). Paradoxically, it is known that some growth factors can show inhibitory effects once utilized in the presence of maximal proliferative stimuli [24].

In the current experimental setting, the use of unconjugated UDC- and deoxycholate (DC)-enriched diets was justified by the following observations:

a. Similar UDC- and DC-enriched diets determined the maximal increase of proliferation in rat hepatocytes, submaximally stimulated by 40% partial hepatectomy [9]
b. The widespread therapeutic use of UDC makes it interesting to investigate whether this BS is able to exert stimulatory effects on cholangiocyte proliferation

To adequately investigate the effects of BS-enriched diets on cell proliferation induced by pBDL, the latter procedure followed a 4-week period of BS-enriched diet in the animals. This made it possible to obtain consistent BS pool modifications at the moment when the surgical model triggers proliferation.

Materials and methods

Animals

Fischer (F-344) rats (n=45), weighing 100–125 g, were obtained from Charles River, Calco (CO), Italy. They were kept in a temperature- and light-controlled room (light on from 0700 hours to 1900 hours) for at least 1 week prior to being used and received food and water ad libitum. All animals received human care in compliance with the Italian National Research Council criteria.

Chemicals

DC, UDC and cholylglycine hydrolase from Clostridium Perfringens and 4-Bromo-methyl-7-methoxy-coumarin were purchased from Sigma Chemical Company, St. Louis, MO (USA). Glycoursodeoxycholic acid and 7α,12α-dihydroxy-5β-cholanic acid were purchased by Calbiochem Corporation, USA.

Dietary treatment and study design

All diets used in this study were purchased from Mucedola srl, Settimo Milanese (MI), Italy. Rats were divided into three groups of 15 animals each and received standard, 0.2% DC- and 0.2% UDC-enriched diets, respectively, for 4 weeks before the operation and for the following 2 days. Ten animals for each of the three groups underwent pBDL as previously described [27], and five underwent sham operation.

All surgical procedures were performed under metaphane anesthesia between 0830 hours and 0930 hours. The absence of ductal cross-communication between obstructed and non-obstructed lobes was proved with methylene blue injections in rats who underwent pBDL as described elsewhere [27]. At the time of the maximal proliferative response of cholangiocytes after pBDL [27], i.e., 48 h after the operation, the common bile duct was cannulated, and the bile was drawn for 10 min. Subsequently, blood was collected for biochemical determinations, and the liver specimens were taken off and fixed in 10% neutral buffered formalin for 12–24 h for histological and immunohistochemical evaluations.

Histological and immunohistochemical procedures

Following paraffin embedding, 2- to 4-μm-thick sections were cut and stained with hematoxylin/eosin (H&E), periodic acid Schiff and Gomori's reticulin stain. Consecutive sections, collected on silane-coated slides, were employed for the terminal deoxynucleotidyl transferase-mediated dUTP nick end labelling (TUNEL) and immunohistochemical procedures.

The extent of the histological damage of the biliary tree was independently evaluated by two observers (E.M. and A.P.) by taking into account inflammatory infiltration, degenerative changes and necrosis of both the hepatocellular and cholangiocellular compartments, according to the scheme proposed by Attili et al. [6], with appropriate modifications for our specific animal model. Each of the above-mentioned features was scored in a 0–3 scale according to the severity of damage (absent-low-moderate-severe). Subsequently, the single scores of individual features were added to express the extent of bile duct and/or lobular damage (absent=0; 0<weak$\leq$3; 3<moderate$\leq$6; 6<severe$\leq$9).

Evaluation of apoptosis

DNA fragments of apoptotic cells were visualized using an enzymatic reaction that involves a TUNEL procedure, based on the specific binding of terminal deoxynucleotidyl transferase to 3′-OH ends of DNA breaks, as previously described [11].

Cholangiocyte and hepatocyte apoptotic indexes (AI) were calculated as the number of TUNEL-positive cells over 100 cells

and the number of TUNEL-positive cells/cm^2, respectively, using a ×25 magnification.

PCNA immunolabeling

After rehydration, the silane-coated slides were treated with 0.3% H_2O_2 in methyl alcohol for 15 min and then briefly washed in phosphate buffer saline. They were then pre-incubated with 1.5% normal horse serum for 20 min and subsequently incubated overnight, at room temperature, with a 1:50 dilution of anti-proliferating-cell nuclear antigen (PCNA) monoclonal antibody (Dako Italia Spa, Milan, Italy) and sequentially incubated with biotinylated rabbit-anti-mouse IgG, avidin DH-peroxidase and amino-ethyl-carbazole for 30 min at 37°C. Finally, the sections were counterstained with Meyer's hematoxylin and coverslipped. All reagents were purchased from Vector, Burlingame, CA, USA.

PCNA labeling index

PCNA immunolabeling of cholangiocytes was semi-quantitatively evaluated by counting at least 500 bile-duct cells in 20 randomly selected high-power fields (×40) and by determining the percentages of PCNA-reactive cells. Only bile-duct cells that exhibited strong nuclear immunostaining were considered for PCNA-reactive cell counting.

Biochemical determinations

Bilirubin, γ-glutamyl transpeptidase (γ-GT) and alanine aminotransferase (ALT) serum levels were determined using standard laboratory methods.

BS determination

Total BS and UDC levels in the serum were evaluated using a modification of the chromatographic method described by Kamada et al. [22], as described elsewhere [9]. Total BSs in the bile were assayed enzymatically, using a fluorimetric enzymatic Kit (Sterognost 3-Flu; Nycomed AS, Oslo, Norway). UDC biliary levels were analyzed using a modification of Scalia's chromatographic method [31]. Briefly, bile samples were thoroughly mixed, and their pH was adjusted to 9.0 by NaOH 0.1 mol/l. An aliquot was passed through a Sep-Pak C_{18}, and BSs were eluted with methanol. Aliquots of this eluate were analyzed for individual BSs (specifically UDC) using reverse-phase high-performance liquid chromotography, using as a mobile phase an acidic isocratic methanol/KH_2PO_4 0.05 mol/l/acetonitrile solution (60/30/10). BS detection was made using ultraviolet absorption at 205 nm.

Statistical analysis

The statistical evaluation of the results was performed using *t*-tests or analysis of variance (ANOVA). When the single-factor ANOVA rejected the hypothesis of the mean equality among the groups, the Tukey test was applied for comparing the mean values in the different groups. In the latter case, only a value of $P<0.05$ was considered statistically significant.

Results

The results reported in Table 1 indicate that pBDL determined a two- to threefold increase of total BS serum levels compared with sham-operated animals. Moreover, in UDC-fed rats, UDC represented about 23% of total BS concentration.

Table 1 Total bile salt (BS) and ursodeoxycholate (UDC) concentrations in the serum of rats fed either a normal, deoxycholate (DC)- or UDC-enriched diet, 48 h after sham operation or partial bile-duct ligation (pBDL). *n.m.* not measurable

	Sham operated		pBDL	
Diet	Total BSs*	UDC	Total BSs*	UDC
Standard	3.1±2.2	n.m.	9.3±15.3	n.m.
DC	11.7±9.1	n.m.	18.9±16.3	n.m.
UDC	2.8±0.9	0.9±0.2	14.9±10.5	3.4±1.1
Analysis of variance	[a]$P<0.01$	-	[a]$P<0.05$	-

* The values reported, obtained from five sham-operated animals and at least ten pBDL animals, represent the mean±SD of unconjugated and conjugated bile salt levels, expressed as μmol/l
[a] Standard=UDC≠DC using Tukey test

Table 2 Total bile salt (BS) and ursodeoxycholate (UDC) concentrations in the bile of rats fed either a normal, deoxycholate (DC)- or UDC-enriched diet, 48 h after sham operation or partial bile-duct ligation (pBDL). *n.m.* not measurable

	Sham-operated		pBDL	
Diet	Total BSs*	UDC	Total BSs*	UDC
Standard	13.1±2.0	n.m.	12.5±2.3	n.m.
DC	12.0±3.5	n.m.	12.0±2.5	n.m.
UDC	13.4±3.3	3.5±1.2	13.2±3.3	3.4±0.9

* The values reported, obtained from five sham-operated animals and at least ten pBDL animals, represent the mean±SD of unconjugated and conjugated bile salt levels, expressed as mmol/l

As shown in Table 2, biliary total BS concentration was not significantly influenced by pBDL or by the administration of BS-enriched diets. Interestingly, UDC levels paralleled the modifications observed in the serum and were significantly increased when compared with standard-diet-fed rats.

Figure 1 illustrates bilirubin, γ–GT and ALT serum levels in sham-operated rats (A) and in animals with pBDL (B), receiving standard, DC- and UDC-enriched diets. As illustrated, all the above parameters were slightly increased in rats undergoing pBDL in comparison with sham-operated animals, but they were much lower (about 1/10) than those observed in rats undergoing tBDL (unpublished data). In all cases, DC dietary treatment induced a significant increase of ALT in comparison with standard or UDC-enriched diet ($P<0.05$). According to these results, the evaluation of the extent of histological damage demonstrated that pBDL caused significant biliary tree damage in all groups compared with sham-operated animals (Table 3). In most cases, the damage was more evident in ligated lobes than in freely draining lobes. As for hepatocellular damage, there was no increased damage after pBDL both in ligated and freely draining lobes. However, DC dietary treatment was invariably associated with hepatocellular damage in comparison with standard and UDC groups.

Also, all examined liver samples, both from sham-operated and pBDL rats, showed mild peri-ductular col-

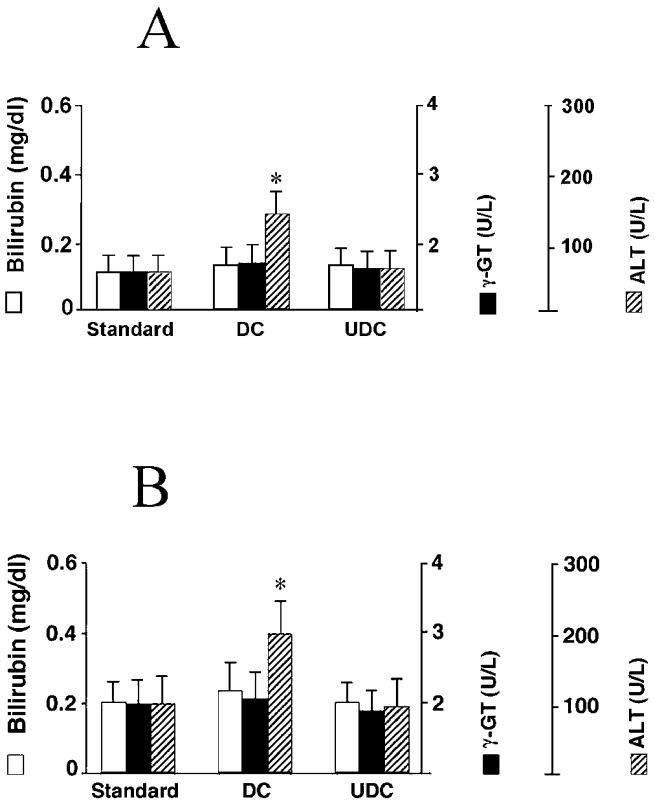

Fig. 1 Bilirubin, γ-glutamyl transpeptidase and alanine aminotransferase serum levels in sham-operated (**A**) and partial bile-duct ligation (**B**) rats fed a standard or bile-salt-enriched diet. The values reported represent mean±SD obtained from at least five animals in each group. **P*<0.05 using analysis of variance, (DC ≠Stan-UDC, using Tukey test)

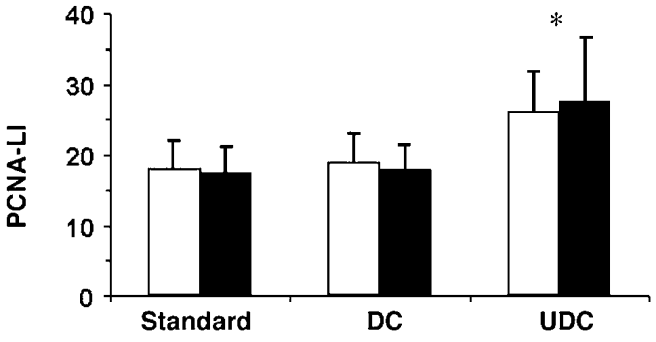

Fig. 2 Proliferating-cell nuclear antigen labeling index (PCNA-LI) of cholangiocytes in livers from partial bile-duct ligation rats treated with a standard or bile-salt-enriched diet. *Open square* ligated lobes. *Closed square* freely draining lobes. In sham-operated rats receiving a standard diet, PCNA-LI was 0.2±0.1 and was not influenced by dietary treatment. The values reported represent mean±SD obtained from all animals in each group. **P*<0.01 using analysis of variance, (Standard=DC≠UDC, using Tukey test)

lagen accumulation. Nevertheless, this feature was common to all tissue samples and, therefore, was interpreted as non-specific.

The evaluation of PCNA immunostaining in rats fed a standard diet (Fig. 2) and that underwent pBDL demonstrated consistent cholangiocyte proliferative response compared with sham-operated animals [PCNA labeling index (PCNA-LI) 0.2±0.1]. BS-enriched-diet-fed animals that underwent sham operation did not show relevant modifications of cholangiocyte proliferative activity, as detected by PCNA immunolabeling.

In rats that underwent pBDL, UDC dietary treatment determined a further significant increase of cholangiocyte proliferation, both in freely draining and ligated lobes compared with animals fed a standard or a DC-enriched diet (Fig. 2). In all instances, the evaluation of PCNA-positive cells was essentially carried out on the cholangiocytes lining intra-hepatic bile ducts larger than 15 μm—essentially interlobular and septal bile ducts (Fig. 3).

As for the evaluation of cholangiocyte-programmed cell death using the TUNEL procedure, apoptotic cells were only exceptionally seen in the epithelium of intra-hepatic bile ducts from ligated or freely draining lobes, and the number of these cells was similar in all groups with pBDL (AI=0.2±0.1% in standard, 0.1±0.1% in DC and 0.2±0.1% in UDC groups) or sham operation (AI= 0.1±0.1% in standard, 0.1±0.2% in DC and 0.1±0.1% in UDC groups). Interestingly, hepatocyte AI showed a trend toward reduction in the UDC group compared with the DC and standard groups undergoing pBDL (AI=

Table 3 Histological evaluation of liver damage expressed as damage score in rats fed with standard (ST), deoxycholate (DC)- and ursodeoxycholate (UDC)-enriched diets, 48 h after partial bile-duct ligation (pBDL). The extent of histological damage was calculated as reported in "Material and Methods" section. The values reported were obtained examining five sham-operated animals and at least ten pBDL animals. *ANOVA* analysis of variance

	Biliary-tree damage			ANOVA	Hepatic-lobule damage			ANOVA
	ST	DC	UDC		ST	DC	UDC	
Sham-operated	0.6±0.7	2.6±0.9	0.4±0.5	[d]*P*<0.005	0.4±0.5	3.3±1.7	0.6±0.6	[d]*P*<0.01
pBDL ligated lobe	3.6±1.5	3.3±0.7	3.3±1.2	-	1.3±1.8	2.1±1.3	0.8±1.6	-
pBDL freely draining lobe	2.6±1.1	4.2±1.6	1.3±1.0	[e]*P*<0.01	0.7±0.5	2.5±1.5	0.2±0.6	[d]*P*<0.05
ANOVA	[a]*P*<0.01	[b]*P*<0.05	[c]*P*<0.01		-	-	-	

Evaluation by Tukey test:
[a] Sham-operated≠pBDL/ligated lobe=pBDL/freely draining lobe
[b] pBDL/freely draining lobe≠sham-operated=pBDL/ligated lobe
[c] Sham-operated≠pBDL/freely draining lobe≠pBDL/ligated lobe
[d] Standard=UDC≠DC
[e] Standard≠UDC≠DC

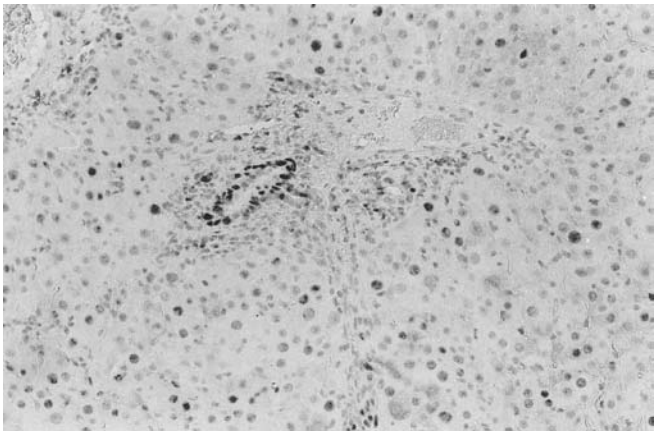

Fig. 3 Proliferating-cell nuclear antigen labeling index immunolabeling pattern in liver bile ducts. High-power field (×400)

3.5±4.5% in standard, 3.6±5.6% in DC and 1.3±2.4% in UDC group). However, in sham-operated animals, AI was 0.6±0.5% in standard, 0.5±0.6% in DC and 0.4±0.5% in UDC groups.

Discussion

Over the last decade, our interest has been focused on the effects of BSs on cell proliferation and the possible mechanism(s) mediating this biological effect [7, 8, 9, 10, 11, 12, 14, 26, 27]. The main goal of the current study was to evaluate the effects of UDC on cholangiocyte proliferative activity already triggered by pBDL. This experimental model was used since it induces mild cholestatic damage, mimicking the conditions that spontaneously occur in cholestatic liver diseases in humans. In addition, we also tested the effects of DC to establish if the possible stimulatory effects related to UDC administration are specific for this BS or are commonly shared by other BSs.

Total BSs as well as DC and UDC concentrations were measured in the serum and bile of both operated and sham-operated animals. In addition, cholangiocyte proliferative activity, as well as salient histopathological features indicative of both cholangiocyte and hepatocellular damage and apoptotic activity, were evaluated. The latter was also considered because it is known that BSs can modulate apoptosis in cells naturally exposed to BS enterohepatic circulation [20, 30].

As shown in Table 1 and Table 2, rats undergoing pBDL developed very mild cholestasis compared with sham-operated animals. In fact, total BS concentrations became only threefold higher in the serum and remained unchanged in the bile (Table 1 and Table 2). The latter was an expected result, since a 100-fold increase in total serum BS concentration is associated with only a three- to fourfold increase of total BS biliary concentration following tBDL (serum contains micromolar concentrations while bile contains millimolar concentrations of BSs).

Independently from the diet, in all animals, pBDL induced an increase in cholangiocyte proliferative response that appeared similar both in ligated and freely draining lobes compared with sham-operated rats (Fig. 3). However, in pBDL rats receiving UDC, a further elevation of the proliferative response was detected in comparison with controls, as demonstrated by the PCNA-LI ($P<0.01$). In contrast, the administration of DC had no influence on cholangiocyte proliferative activity compared with controls. We have previously demonstrated that UDC-enriched diets do not stimulate hepatocyte proliferation in intact animals, but are able to amplify the regenerative response already triggered by partial hepatectomy, acting as an "augmenter" [8]. As expected, since pBDL does not induce hepatocyte proliferation [27], in the present study, a UDC-enriched diet did not influence hepatocyte proliferative activity. The evaluation of liver damage by conventional histology (H&E) (Table 3), humoral parameters (Fig. 1) such as bilirubin, γ-GT and ALT and apoptosis demonstrated that the increase of PCNA-LI observed in UDC-treated animals was not damage related. In fact, all the above parameters were similar in UDC-treated animals and in rats fed a standard diet. Interestingly, according to the data reported by Rodrigues et al. in isolated hepatocytes and normal rat liver [30], our data demonstrated a trend toward a protective effect of UDC on programmed cell death in parenchymal liver cells. In fact, hepatocyte AI decreased in the UDC group compared with rats fed a standard diet, almost reaching statistical significance ($P<0.1$), a datum that could possibly become significant using a larger cohort of animals. The current data, excluding a direct damage of UDC treatment on rat biliary tree, are in agreement with those reported by others [3, 19]. However, Fickert et al. [18] have demonstrated that a 0.5% UDC-enriched diet is able to increase the cholestatic damage induced by total or partial bile-duct ligation in mice. In the latter study, however, the same authors explain these differences, hypothesizing that, in rats, a UDC-enriched diet probably has reduced choleretic effects in comparison with what is demonstrated in mice.

In our experimental conditions, both UDC- and DC-enriched diets induced comparable modifications of BS levels in the enterohepatic circulation (Table 1 and Table 2), but only the former diet further enhanced cholangiocyte proliferation, suggesting the possibility that UDC, per se, could have an additive stimulatory effect on cholangiocyte proliferation.

The apparent discrepancy between our results in UDC-treated animals and those (reduced cholangiocyte proliferation) observed by others in rats with tBDL receiving a UDC-enriched diet [3] was not surprising. In fact, at 4 weeks after tBDL using a 0.2% UDC-enriched diet, we also found no increase of cholangiocyte proliferation in comparison with controls [10]. The explanation for these findings may derive from the consideration that pBDL and tBDL models are profoundly different. In fact, tBDL is associated with maximal cholestasis-induced proliferative response and is not suitable for the evaluation

of further stimuli of cholangiocyte proliferation. Some growth factors may show inhibitory effects once utilized in presence of maximal proliferative stimuli [24]. In the tBDL model, the proliferative response was assessed 1 week after operation [3], when it already had declined, and not 48 h after surgery, when cholangiocyte proliferation is maximal [27, 33]. Finally, our animals were fed a UDC-enriched diet for 4 weeks before undergoing pBDL, while tBDL rats received UDC after surgery [3]. In our experience, after operation, animals refuse food for at least 24 h, especially if it contains very bitter substances, such as 1% BSs.

In a previous study [27], we hypothesized that pBDL could trigger cholangiocyte proliferation by modulating the activity of specific growth factors. This hypothesis was based on the fact that cholangiocyte proliferative response was simultaneous and of the same magnitude both in freely draining and ligated lobes. However, Alpini et al. [2] suggested that the increase of total BS concentration in the bile could be the major pathophysiological stimulus for cholangiocyte proliferation. Based on the current findings, we certainly attribute a pivotal role in the induction of cholangiocyte proliferation to the modifications of BS concentrations. However, our results suggest that the increase of biliary total BS concentrations is not the only driving force for cholangiocyte proliferation; otherwise, we are not able to explain the dramatic difference of proliferative activity observed in sham-operated and pBDL animals in the presence of similar a biliary BS concentration.

As far as the possible mechanism mediating UDC-stimulatory activity, in the literature, there are studies on hepatocytes, human cholangiocarcinoma cell lines and colonocytes that suggest the involvement of protein kinases, epidermal growth factor receptor [14, 29, 36], a type of receptor present in normal cholangiocyte [16], as well as cyclooxygenase-2 [36] and Raf-1/MEK/ERK [29]. Finally, data obtained in vitro in cholangiocytes isolated from rats with biliary obstruction suggest that activation of the PI3-K pathway is responsible for BS stimulatory activity on cholangiocytes [4].

In conclusion, the present article, for the first time, describes the ability of UDC to augment cholangiocyte proliferative response following partial obstruction of the extra hepatic biliary tree. This demonstration further supports the use of UDC for the therapy of cholestatic chronic liver disease in which this bile salt would not only reduce damage and apoptosis, but also delay the ductopenic stage by stimulating proliferation.

References

1. Alpini G, Glaser S, Robertson W, Phinizy JL, Rodgers RE, Caligiuri A, Le Sage G (1997) Bile acids stimulate proliferative and secretory events in large but not small cholangiocytes. Am J Physiol 273:G518–G529
2. Alpini G, Glaser SS, Ueno Y, Rodgers R, Phinizy JL, Francis H, Baiocchi L, Holcomb LA, Caligiuri A, LeSage GD (1999) Bile acid feeding induces cholangiocyte proliferation and secretion: evidence for bile acid-regulated ductal secretion. Gastroenterology 116:179–186
3. Alpini G, Baiocchi L, Glaser S, Ueno Y, Marzioni M, Francis H, Phinizy JL, Angelico M, LeSage G (2002) Ursodeoxycholate and tauroursodeoxycholate inhibit cholangiocyte growth and secretion of BDL rats through activation of PKC alpha. Hepatology 35:1041–1052
4. Alpini G, Glaser S, Alvaro D, Ueno Y, Marzioni M, Francis H, Baiocchi L, Stati T, Barbaro B, Phinizy JL, Mauldin J, LeSage G (2002) Bile acid depletion and repletion regulate cholangiocyte growth and secretion by a phosphatidylinositol 3-kinase-dependent pathway in rats. Gastroenterology 123:1226–1237
5. Alvaro D, Alpini G, Onori P, Perego L, Svegliata Baroni G, Franchitto A, Baiocchi L, Glaser SS, Le Sage G, Folli F, Gaudio E (2000) Estrogens stimulate proliferation of intrahepatic biliary epithelium in rats. Gastroenterology 119:1681–1691
6. Attili AF, Rusticali A, Varriale M, Carli L, Repice AM, Callea F (1994) The effect of ursodeoxycholic acid on serum enzymes and liver histology in patients with chronic active hepatitis. A 12-month double-blind, placebo-controlled trial. J Hepatol 20:315–320
7. Barone M, Angelini A, Romanelli D, Montanari A, Francavilla A (1992) Screening of bile salts (BSs) for the evaluation of their effect on hepatocyte proliferation. Ital J Gastroenterol 24:259
8. Barone M, Panella C, Angelini A, Romanelli D, Francavilla A (1993) Studies in vitro on the influence of ursodeoxycholate sodium salt (UDC) on hepatocyte proliferation. J Surg Oncol 3[Suppl]:8–13
9. Barone M, Francavilla A, Polimeno L, Ierardi E, Romanelli D, Berloco P, Di Leo A, Panella C (1996) Modulation of rat hepatocyte proliferation by bile salts: in vitro and in vivo studies. Hepatology 23:1159–1166
10. Barone M, Maiorano E, Panella C, Ladisa R, Carrino C, Pece A, Berloco P, Cavallini A, Francavilla A (1998) Evidence of bile salt (BS) involvement in the modulation of bile duct cell proliferation. Ital J Gastroenterol Hepatol 30:A127
11. Barone M, Berloco P, Ladisa R, Ierardi E, Caruso ML, Valentini AM, Notarnicola M, Di Leo A, Francavilla A (2002) Demonstration of a direct stimulatory effect of bile salts on rat colonic epithelial cell proliferation. Scand J Gastroenterol 37:88–94
12. Barone M, Maiorano E, Ladisa R, Cuomo R, Pece A, Berloco P, Caruso ML, Valentini AM, Iolascon A, Francavilla A, Di Leo A, Ierardi E (2003) Influence of ursodeoxycholate-enriched diet on liver tumor growth in HBV transgenic mice. Hepatology 37:880–886
13. Bucher NLR, Malt RA (1971) Morphological and biological aspects. In: Ingelfinger FJ (ed) Regeneration of liver and kidney. Little, Brown and Company, Boston, pp 23–54
14. Capuano F, Barone M, D'Eri N, Russo E, Varone D, Francavilla A, Papa S (1997) Ursodeoxycholate promotes protein phosphorylation in the cytosol of rat hepatocytes. Biochem Mol Biol Int 41:329–337
15. Da Silva LC, Alves VA, Abrantes CP, Lima DM, Christo CH, De Brito T (1985) Effects of chemotherapy on mice submitted to multiple Schistosoma mansoni infections. A controlled randomized prospective study. Trop Med Parasitol 36:150–154
16. De Groen PC, Vroman B, Laakso K, LaRusso NF (1998) Characterization and growth regulation of a rat intrahepatic bile duct epithelial cell line under hormonally defined, serum-free conditions. In Vitro Cell Dev Biol Anim 34:704–710
17. Desmet VJ (1986) Current problems in diagnosis of biliary disease and cholestasis. Semin Liver Dis 6:233–245
18. Fickert P, Zollner G, Fuchsbichler A, Stumptner C, Weiglein AH, Lammert F, Marschall HU, Tsybrovskyy O, Zatloukal K, Denk H, Trauner M (2002) Ursodeoxycholic acid aggravates bile infarcts in bile duct-ligated and Mdr2 knockout mice via disruption of cholangioles. Gastroenterology 123:1238–1251

19. Frezza EE, Gerunda GE, Plebani M, Galligioni A, Giacomini A, Neri D, Faccioli AM, Tiribelli C (1993) Effect of ursodeoxycholic acid administration on bile duct proliferation and cholestasis in bile duct ligated rat. Dig Dis Sci 38:1291–1296
20. Garewal H, Bernstein H, Bernstein C, Sampliner R, Payne C (1996) Reduced bile acid-induced apoptosis in "normal" colorectal mucosa: a potential biological marker for cancer risk. Cancer Res 56:1480–1483
21. Isseroff H, Sawma JT, Reino D (1977) Fascioliasis: role of proline in bile duct hyperplasia. Science 198:1157–1159
22. Kamada S, Maeda M, Tsuji A (1983) Fluorescence high-performance liquid chromatographic determination of free and conjugated bile acids in serum and bile using 1-bromoacetylpyrene as a pre-labeling reagent. J Chromatogr 272:29–41
23. Kossor DC, Goldstein RS, Ngo W, DeNicola DB, Leonard TB, Dulik DM, Meunier PC (1995) Biliary epithelial cell proliferation following alpha-naphthylisocyanate (ANIT) treatment: relationship to bile duct obstruction. Fundam Appl Toxicol 26:51–62
24. LaBrecque DR, Wilson M, Fogerty S (1984) Stimulation of HTC hepatoma cell growth in vitro by hepatic stimulator substance (HSS). Interactions with serum, insulin, glucagon, epidermal growth factor and platelet derived growth factor. Exp Cell Res 150:419–429
25. Lichtman SN, Sartor RB, Keku J, Schwab JH (1990) Hepatic inflammation in rats with experimental small bowel bacterial overgrowth. Gastroenterology 98:414–423
26. Panella C, Ierardi E, De Marco MF, Barone M, Guglielmi FW, Polimeno L, Francavilla A (1995) Does tauroursodeoxycholic acid (TUDC) treatment increase hepatocyte proliferation in patients affected by chronic liver disease? Ital J Gastroenterol 27:256–258
27. Polimeno L, Azzarone A, Zeng QH, Panella C, Subbotin V, Carr B, Bouzahzah B, Francavilla A, Starzl TE (1995) Cell proliferation and oncogene expression after bile duct ligation in the rat: evidence of a specific growth effect on bile duct cells. Hepatology 21:1070–1078
28. Popper H (1986) General pathology of the liver: light microscopic aspect serving diagnosis and interpretation. Semin Liver Dis 6:175–184
29. Rao YP, Studer EJ, Stravitz RT, Gupta S, Qiao L, Dent P, Hylemon PB (2002) Activation of the Raf-1/MEK/ERK cascade by bile acids occurs via the epidermal growth factor receptor in primary rat hepatocytes. Hepatology 35:307–314
30. Rodrigues CM, Fan G, Ma X, Kren BT, Steer CJ (1998) A novel role for ursodeoxycholic acid in inhibiting apoptosis by modulating mitochondrial membrane. J Clin Invest 101:2790–2799
31. Scalia S (1988) Simultaneous determination of free and conjugated bile acids in human gastric juice by high-performance liquid chromatography. J Chromatogr 431:259–269
32. Sirica AE (1996) Biliary proliferation and adaptation in furan-induced rat liver injury and carcinogenesis. Toxicol Pathol 24:90–99
33. Slott PA, Liu MH, Tavoloni N (1990) Origin, pattern, and mechanism of bile duct proliferation following biliary obstruction in the rat. Gastroenterology 99:466–477
34. Yokomuro S, Tsuji H, Lunz JG III, Sakamoto T, Ezure T, Murase N, Demetris AJ (2000) Growth control of human biliary epithelial cells by interleukin 6, hepatocyte growth factor, transforming growth factor beta1, and activin A: comparison of a cholangiocarcinoma cell line with primary cultures of non-neoplastic biliary epithelial cells. Hepatology 32:26–35
35. Yokoyama S, Satoh M, Lombardi B (1986) Bile ductular cells and the phenotypic heterogeneity of the population of the hepatic non parenchymal epithelial cells induced in rats by chemical carcinogenesis. Carcinogenesis 7:1215–1219
36. Yoon JH, Higuchi H, Werneburg NW, Kaufmann SH, Gores GJ (2002) Bile acids induce cyclooxygenase-2 expression via the epidermal growth factor receptor in a human cholangiocarcinoma cell line. Gastroenterology 122:985–993

Virchows Arch (2004) 444:561–566
DOI 10.1007/s00428-004-1006-4

ORIGINAL ARTICLE

Camilla Birch Nielsen · Søren Krag · Ruth Østerby · Allan Flyvbjerg · Jens Nyengaard · Axel Forman · Lise Wogensen

Transforming growth factor β1-induced glomerulopathy is prevented by 17β-estradiol supplementation

Received: 20 October 2003 / Accepted: 2 March 2004 / Published online: 24 April 2004

Abstract Transforming growth factor β1 (TGF-β1) affects extracellular matrix (ECM) accumulation. It plays a role in the thickening of the peripheral basement membrane (PBM) and expansion of the mesangium in several renal diseases. The beneficial influence of female gender on the progression of chronic renal diseases may be explained by a favorable effect of estrogen on ECM homeostasis. Interactions between TGF-β1 and estrogen have been investigated in mesangial cell cultures. However, it is unknown if TGF-β1-induced glomerulopathy in vivo is influenced by exogenous estrogen. Thus, the aim of the present experiment was to explore whether estrogen prevents the development of TGF-β1-induced glomerular disease in transgenic mice expressing active TGF-β1 under control of the Ren-1^c promoter. Mice were treated from 3 weeks to 6 weeks of age with 17β-estradiol release pellets (5–10 μg/kg body weight per day). At the age of 6 weeks, all investigated animals were sacrificed for estimation of PBM thickness, the mesangium per glomerulus [Vv(mes/glom)], the mesangial matrix per glomerulus [Vv(matrix/glom)] and the PBM per glomerulus [Vv(PBM/glom)] using electron microscopy and stereological methods. Furthermore, the total collagen content was determined. We found that TGF-β1-induced alterations in Vv(mes/glom), Vv(matrix/glom) and Vv(PBM/glom) were prevented in mice exposed to exogenous 17β-estradiol. In addition, the interstitial fibrosis that develops in TGF-β1 transgenic mice was attenuated by administration of 17β-estradiol. In conclusion, estrogen may oppress TGF-β1-mediated kidney diseases and, thereby, contribute to the protracted development of end-stage renal disease in pre-menopausal women.

Keywords Kidney · TGF-β1 · Estrogen · Glomerulopathy · End-stage renal disease

C. Birch Nielsen · S. Krag · L. Wogensen (✉)
The Research Laboratory for Biochemical Pathology,
The Institute of Experimental Clinical Research,
Aarhus University, Aarhus Kommunehospital,
44-Noerrebrogade, 8000 Aarhus C Aarhus, Denmark
e-mail: lwb@biobase.dk
Tel.: +45-89-492167
Fax: +45-89-492150

C. Birch Nielsen · A. Forman
The Department of Gynecology,
Skejby Sygehus,
Aarhus, Denmark

R. Østerby · J. Nyengaard
Electron Microscopy and Stereological Research Laboratory,
Aarhus University,
Aarhus, Denmark

A. Flyvbjerg
Medical Research Laboratories,
The Institute for Experimental Clinical Research,
Aarhus University,
Aarhus, Denmark

Introduction

In man as well as in a variety of animal species, there is a gender difference in the progression of chronic renal diseases [29]. Among patients suffering from kidney diseases, such as nephrotic syndrome, polycystic kidney disease, chronic glomerulonephritis or IgA-nephropathy, men show a more rapid decline in renal function than women [23]. The accelerated progression of kidney failure in males is also evident in experimental models, e.g., after renal ablation, the development of proteinuria, segmental glomerulosclerosis and procollagen synthesis progresses faster in male rats than in female rats [20, 29]. It is not fully elucidated whether the presence of testosterone or the absence of estrogen is the determining factor. The accumulation of extracellular matrix (ECM) in glomerulosclerosis is a product of an imbalance between ECM synthesis and degradation. The beneficial influence of female gender, at least before the onset of menopause, on the progression of chronic renal disease may partly be explained by the favorable influence of estrogen on ECM homeostasis [22, 29]. Estrogen inhibits the proliferation of mesangial cells in vitro, suppresses the synthesis of collagen type I and type IV and increases the production

of matrixmetallo-proteinases-2 and -9 (MMP-2 and MMP-9) [11, 17, 18, 25, 30]. The biological effects of estrogen on the mesangial cells are mediated by the two estrogen receptor (ER) subtypes, ERα and ERβ, which appear in the developing cortex from embryonic day E14.5 [19, 25].

Transforming growth factor β1 (TGF-β1) affects cellular differentiation and the homeostasis of the ECM. It may play a role in the thickening of the peripheral basement membrane (PBM), abnormal deposition of ECM therein and expansion of the mesangium in several renal diseases [2, 3, 4, 7, 9, 27, 28]. Several experiments were conducted to investigate a possible interaction between TGF-β1 and estrogen on mesangial cells in vitro [18, 21, 30, 34]. However, it is unknown whether TGF-β1-induced glomerulopathy in vivo is susceptible to exogenous estrogen.

We have established a transgenic (Tg) model with overproduction of active TGF-β1 from the juxta-glomerular apparatus (JGA) [32]. The mice exhibit mesangial expansion, increased basement membrane thickness (BMT), decreased filtration surface and proteinuria [16]. The aim of the present experiment was to investigate whether estrogen prevents the development of TGF-β1-induced glomerular disease and interstitial fibrosis.

Materials and methods

Animals

TGF-β1 Tg mice, expressing active, porcine TGF-β1 under control of the Ren-1^c promoter on the genetic background of the Balb/cA strain, were used in all experiments [32]. The mice were housed at the animal facility at the University of Aarhus and handled according to the guidelines and procedures recommended by the Animal Experiments Inspectorate, Denmark. They were kept at 21°C with a 12 h day/night cycle and were given free access to water and food. The mice were fed a special synthetic estrogen-free diet while breeding and nursing their pups (Altromin C-1000, GmbH, Lage, Germany) [17.3% protein, 3500 Kcal/kg (14.6 Mj/kg)]. At 3 weeks of age, the genotype of the pups was determined by polymerase chain reaction with primers against the terminator sequence in the transgene [32], and the pups were divided into the following groups: non-transgenic (WT) males (n=6), WT females (n=6), Tg males (n=18) and Tg females (n=19). The animals in the two Tg groups were randomized to treatment for 3 weeks with pharmacological doses of 17β-estradiol (+E_2): Tg+E_2 males (n=9) and Tg+E_2 females (n=9). During the treatment period [from 3–6 weeks of age (~21 days)], the pups were given the same estrogen-free diet as above. The food intake was less in mice offered the low-phytoestrogen diet compared with mice on normal chow [3.8±0.03 g/day per mouse (n=6) versus 7.1±0.43 g/day per mouse (n=5)]. However, this had no impact on body weight or kidney weight in adult mice. At 6 weeks of age, at least 50 μl of blood was taken from the tail vein for measurement of the plasma concentration of 17β-estradiol (see below). Then the mice were sacrificed by cervical dislocation. The kidneys were removed, decapsulated and immersed in optimum cutting temperature medium (OCT) or fixative (formaldehyde 3%, glutaraldehyde 1% in modified Tyrode buffer). The blocks were dehydrated and embedded into epon. The project was approved by the Animal Experiments Inspectorate, Denmark (#1999/561–218) and the Danish Working Environment Service (#BK 1994–1531–164).

17β-estradiol treatment and enzyme-linked immunosorbent assay

Two groups of Tg mice, Tg+E_2 males (n=9) and Tg+E_2 females (n=9), received subdermal implants containing 17β-estradiol (5 mg/pellet) with a release period of 21 days (Innovate Research of America, Sarasota, FL, USA). These release 5–10 μg/kg body weight per day. On the day of sacrifice, the plasma levels of estradiol were determined by a commercial available enzyme-linked immunosorbent assay method (DRG Instruments GmbH, Germany). According to the supplier's instructions, the plasma samples were extracted with ether before the analysis. The lowest detectable level of estradiol was 4.6 ng/l and the intra- and interassay variations were 5% and 6%, respectively, as reported by the supplier.

Sectioning for light and electron microscopy

After 6–7 days fixation, the kidney was cut into slaps of 0.5 mm thickness with a set of fixed razorblades. Tissue blocks were punched out of the cortical part of the slaps, thus providing a sample with an uniform distribution from the kidney cortex. The blocks were systematically sectioned with 1-µm-thick sections for the determination of glomerular volume and for the identification of glomeruli for electron microscopy (see below). The volume of individual glomeruli [V(glom)] appearing in the tissue blocks as the sectioning proceeded was estimated with Cavalieri's method for glomeruli [24]. The area of glomerular profiles with 5-µm intervals were measured by point counting in a light microscope, transmitting the visual fields to a computer screen at a magnification of ×1500. Volume of individual glomeruli is then $V(glom)=t\times\Sigma A$, where t is distance between the levels and A is the area of profiles. The true distance between levels was measured as previously described in detail [24]. On average, 12 glomeruli were measured per animal (range 10–14).

Electron microscopy

Thin sections were prepared from three glomeruli in each animal, representing at least two different blocks of tissue. Beforehand, it was decided that the first- and second-appearing glomeruli in the first block and the first-appearing glomerulus in the second block would be used for electron microscopy. Furthermore, the thin sections were always cut 30 μm from the top of the glomerulus. The thin glomerular profile sections (60 nm) were photographed at different magnifications. The total area of glomeruli was covered at low magnification (×6,680). At a higher magnification (×26,000), a subsample of the area was photographed using systematic uniformly random sampling. The images from the electron microscope were digitalized and transferred to the computer screen for measurements. Point counting was used to estimate the different volume fractions (%). At low magnification, the majority of the glomerular profile was measured and used for estimates of the mesangium per glomerulus [Vv(mes/glom)], the mesangial matrix per glomerulus [Vv(mat/glom)] and the PBM per glomerulus [Vv(PBM/glom)]. The higher magnification was used to measure the fractions of mesangium and mesangial matrix and to measure the BMT, which was estimated with the orthogonal intercept method [12]. Combining low- and high-magnification electron microscopy, we calculated the Vv(mes/glom), Vv(mat/glom) and Vv(PBM/glom).

Hydroxyproline assay

The renal collagen content was estimated using the determination of the quantity of hydroxyproline [8]. In short, available kidneys stored in OCT were thawed, defatted and dried. Pulverized tissue (2–8 mg) was hydrolyzed for 12 h in 200 μl 6 M HCl at 118°C, followed by neutralization with 10 N NaOH. After centrifugation, the content of hydroxyproline in the supernatant (1:100) was determined in the presence of chloramin-T, perchloric acid and Er-

Table 1 Basement membrane thickness (BMT) and volume fractions (%) of mesangium [Vv(mes/glom)], mesangial matrix [Vv(mat/glom)] and the peripheral basement membrane per glomerulus [Vv(PBM/glom)] in 6-week-old transgenic (Tg) and non-transgenic (WT) male (♂) and female (♀) mice offered phyto-estrogen-low diet. Transgenic male and female mice were supplemented with 17β-estradiol from 3–6 weeks of age (Tg+17β-estradiol). Results are given as mean±standard error of mean

	WT ♂	Tg ♂	Tg ♂+17β-estradiol	WT ♀	Tg ♀	Tg ♀+17β-estradiol
Number of mice	6	9	9	6	10	9
Vv(mes/glom) (%)	30±2.4	47±3.2**	34±2.7## NS	29±3.4	44±3.7*	34±2.7 (P=0.07) NS
Vv(mat/glom) (%)	9.2±0.6	16.6±2.0 (P=0.1)	10.1±1.1# NS	8.5±1.8	17.2±2.2*	9.9±0.9# NS
Vv(PBM/glom) (%)	6.3±0.4	3.0±0.5**	5.5±0.7## NS	6.3±0.5	4.4±0.6*	5.9±0.3 (P=0.08) NS
BMT (nm)	113±7	120±6 ns	118±3 NS	111±4	141±11 ns	129±11 NS

* $P\leq0.05$, **$P\leq0.01$, ns: non-significant: Tg versus WT
# $P\leq0.05$, ##$P\leq0.01$: Tg+17β-estradiol versus Tg. For marginally altered data, the P values are given in brackets
NS: non-significant: Tg+17β-estradiol versus WT

lich's reagent. The standard curve gapped from 0.2 μg/ml to 3.2 μg/ml. The collagen content was extrapolated from the hydroxyproline determination by multiplication with 7.5.

Statistical methods

All data are presented as mean±standard error of mean. Statistical analysis between more than two groups was performed by one-way analysis of variance (ANOVA) after exclusion of variance in-homogeneity as determined by the Bartlett test. The ANOVA was followed by the Student's t-test and corrected a.m. Bonferoni. In the case of variance in-homogeneity, the Kruskall-Wallis test was used, followed by the Mann-Whitney rank sum test, which was corrected for the number of comparisons. Data were tested for the presence of outliners. Differences were considered statistically significant at a level of $P\leq0.05$.

Results

In animals supplemented with 17β-estradiol, the mean circulating levels of estradiol at time of sacrifice was 2.96±0.552 ng/ml. This is similar to values seen during pregnancy [1]. All values in the mice without treatment were below the detection limit of the assay.

Both male and female Tg mice exhibited a rise in Vv(mes/glom) versus sex-matched WT mice (both $P\leq0.01$) (Table 1). Female Tg mice showed a statistically significant rise in Vv(mat/glom) compared with that in sex-matched WT animals ($P\leq0.01$), whereas the increase in Vv(mat/glom) in male Tg animals versus sex-matched WT mice was statistically insignificant (P=0.10) (Table 1). Both male and female Tg mice showed a decline in Vv(PBM/glom) versus sex-matched WT animals ($P\leq0.01$ and $P\leq0.05$, respectively) (Table 1). Although the thickness of the basement membrane was elevated in Tg animals of both genders, it was statistically insignificant from that in sex-matched WT mice (Table 1).

Male Tg mice supplemented with 17β-estradiol exhibited a decline in Vv(mes/glom) and Vv(mat/glom) versus sex-matched Tg animals ($P\leq0.01$ and $P\leq0.05$, respectively); whereas, 17β-estradiol treatment led to an increase in Vv(PBM/glom) compared with sex-matched Tg mice without 17β-estradiol supplementation ($P\leq0.01$) (Table 1). Female Tg mice supplemented with 17β-estradiol (Tg+E_2) exhibited a reduction in Vv(mat/glom) ($P\leq0.05$), a minor decline in Vv(mes/glom) (P=0.07) and a marginal rise in Vv(PBM/glom) (P=0.08) versus Tg animals without 17β-estradiol supplementation (Table 1). The volume fractions in female and male Tg mice treated with 17β-estradiol (Tg+E_2) were similar to that in sex-matched WT animals (Table 1). Since the BMT, Vv(mat/glom), Vv(mes/glom) and Vv(PBM/glom) were similar in male and female mice within each of the three investigated groups (WT, Tg, Tg+E_2) (all P values >0.05), we pooled the data from both genders within each of the classes to perform a final statistical evaluation of the effect of exogenous 17β-estradiol. We found that the Vv(mes/glom) and Vv(mat/glom) were elevated in the Tg group versus the group of WT animals (both $P\leq0.01$) as well as versus the Tg+E_2 group (both $P\leq0.01$). Furthermore, the Vv(PBM/glom) was reduced in the Tg mice compared with that in normal mice ($P\leq0.01$) as well as versus the Tg+E_2 group ($P\leq0.01$). There were no differences between the group of Tg mice treated with 17β-estradiol (Tg+E_2) and the WT animals. The BMT was similar among the three groups of animals. Figure 1 demonstrates the ultramorphological structure of a representative glomerulus from each of the three groups of animals.

The V(glom) varied between the three groups of male mice ($P\leq0.05$) (Fig. 2). This was due to a reduced V(glom) in the Tg+E_2 group versus the WT animals ($P\leq0.05$) (Fig. 2). The V(glom) in the two groups of Tg mice (Tg and Tg+E_2) was similar. The V(glom) was comparable among the three groups of female mice (P=0.14) (Fig. 2). Male and female mice within the three groups of tested mice exhibited similar V(glom).

The renal collagen content was increased in male and female Tg mice versus sex-matched WT mice (both $P\leq0.01$) (Fig. 3). Both male and female Tg mice supplemented with 17β-estradiol (Tg+E_2) exhibited a tendency to a decline in the collagen content compared with that of sex-matched Tg animals (Fig. 3). However, this was not statistically significant (P=0.14 and P=0.12, respectively). In addition, the collagen content in male and female Tg mice given exogenous E_2 was still raised compared with that in sex-matched WT animals (both $P\leq0.01$). The collagen content was similar in male and female mice within each of the three investigated groups (WT, Tg, Tg+E_2) (all P values>0.05); therefore, we pooled the data from both genders within each of the

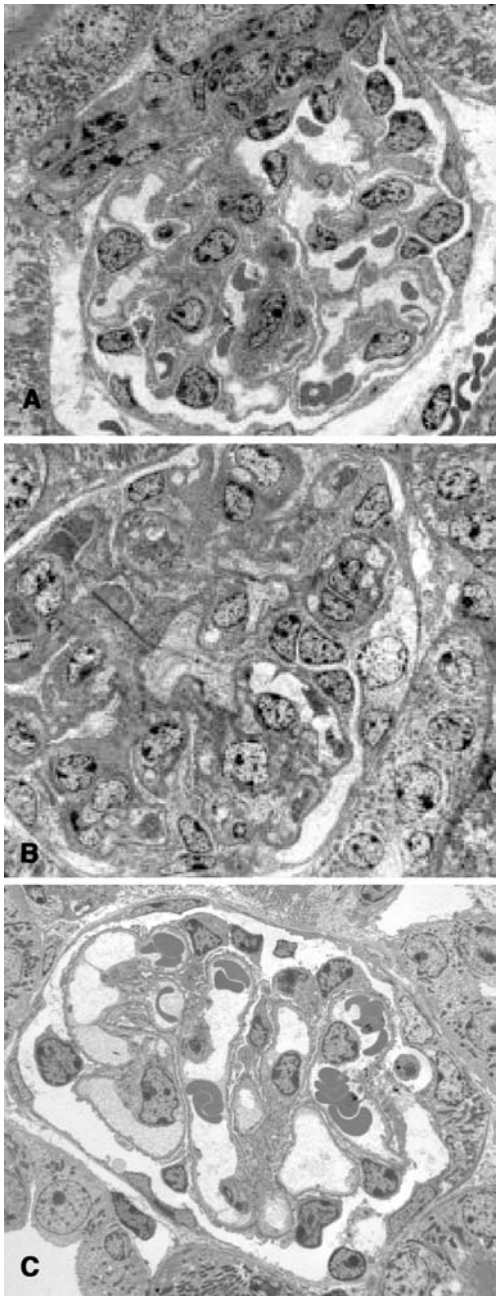

Fig. 1 Electron microscopy demonstrates the appearance of a representative glomerulus from a non-transgenic (WT) female mouse (**A**), a transgenic (Tg) female mouse (**B**) and a Tg female mouse treated with 17β-estradiol (**C**). All mice were served a low-phyto-estrogen diet. Original magnifications ×6,680

classes to perform a final statistical evaluation of the effect of 17β-estradiol. We found that the collagen content was raised in the Tg group versus the group of WT animals ($P \leq 0.01$) as well as versus the Tg+E_2 group ($P \leq 0.05$). Finally, the collagen content was elevated in the Tg+E_2 group compared with that in WT animals ($P \leq 0.01$).

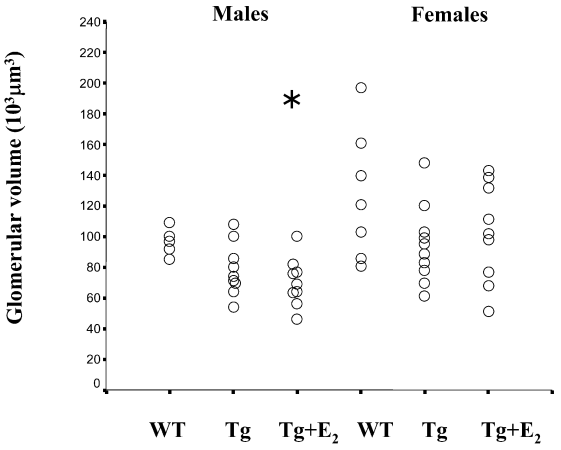

Fig. 2 The glomerular volume in 6-week-old non-transgenic (WT) and transgenic (Tg) mice, and Tg animals receiving 17β-estradiol. All mice received a low-phyto-estrogen diet. Data from both male and female mice are shown. *$P \leq 0.05$ when compared with WT mice

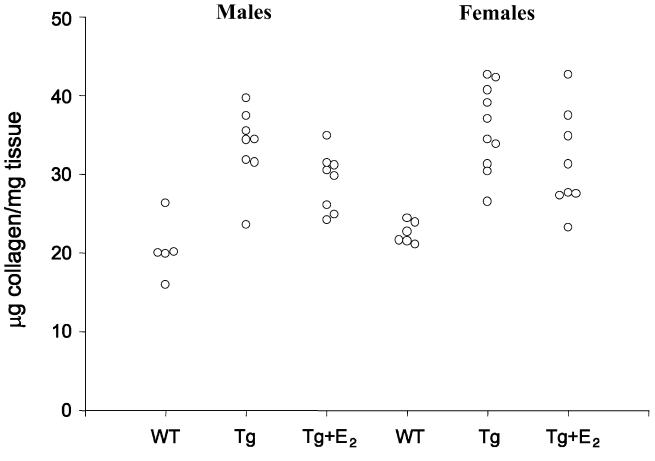

Fig. 3 The renal content of collagen as estimated by the amount of hydroxyproline present in the kidney in 6-week-old non-transgenic (WT) and transgenic (Tg) mice and Tg animals receiving 17β-estradiol. All mice received a low-phyto-estrogen diet. Data from both male and female mice are shown

Discussion

TGF-β1 affects the homeostasis of the ECM. It plays a role in the thickening of the PBM, the abnormal deposition of ECM therein and the expansion of the mesangial matrix in several renal diseases characterized by glomerulosclerosis. Bioactive TGF-β1 in the glomerulus may derive from the circulation, the JGA or from the glomerular cells themselves [3, 13]. We have previously demonstrated that local expression of TGF-β1 leads to glomerulopathy [16, 32]. Several kidney diseases exhibit a more aggravated course in males versus pre-menopausal females, and they are responsive to exogenous estrogen [22]. Thus, the present experiment was undertaken to investigate whether TGF-β1-induced glomerulopathy was

susceptible to pharmacological treatment with 17β-estradiol. To avoid unwanted effects of phyto-estradiols in the normal chow, the mice were offered an estrogen-free diet prior to conceiving and during nursing. The progeny continued on this diet until sacrifice. At 6 weeks of age, the transgenic mice exhibited increased Vv(mes/glom) and Vv(mat/glom) and decreased filtration surface Vv(PBM/glom). This is similar to previous observations [16], although the increase in Vv(mat/glom) did not reach statistical significance in the male transgenic mice in the present investigation. This may be due to the sample size, since there certainly was a trend toward an elavation (P=0.1). Our data indicate that both cellular components and the ECM contribute to the changes in the 6-week-old transgenic mice on the expense of the filtration surface. It is apparent that statistically significant changes in the BMT seem to appear later than alterations in the mesangium. This is in line with previous investigations, in which we demonstrate that expansion of the basement membrane is not apparent until 8 weeks of age [16]. However, it is impossible to state whether an increased BMT is a consequence of the enlarged Vv(mes/glom) and Vv(mat/glom) or appears independently. It should be emphasized that we found no impact of gender on TGF-β1-induced changes in Vv(mes/glom), Vv(mat/glom) and Vv(PBM/glom) during conditions of an estrogen-free diet. However, this does not exclude the possibility that sex-related differences in TGF-β1-induced glomerulopathy may develop in older (>6 weeks), sexually mature mice.

Treatment with pharmacological doses of 17β-estradiol prevented the TGF-β1-induced glomerulopathy in both genders. Whether estradiol also affects Vv(mes/glom), Vv(mat/glom) and Vv(PBM/glom) in WT is unknown. However, since Vv(mes/glom) and Vv(mat/glom) were similar in 6-week-old WT females and WT males served a low phytoestrogen diet, this appears unlikely (Table 1). Supplementation with 17β-estradiol did not fully prevent the deposition of collagen in the interstitial space in Tg mice, an observation that may imply that the processes leading to excessive deposition of collagen in the interstitial space may differ from those in the glomeruli or may be less sensitive to 17β-estradiol. A recent study compares the preventive effect of estriol and estradiol on glomerulopathy and interstitial fibrosis in uninephrectomized spontaneous hypertensive rats [10]. Although it was found that estriol was more effective in preventing glomerular injuries versus estradiol, tubulointerstitial damage was not attenuated by estradiol. This is similar to the observation reported herein.

We have previously shown that collagen type IV(α1), fibronectin and specific laminin isotypes contribute to the enhanced Vv(matrix/glom) [6]. The murine collagen type IV α1 (COL4A1) and α2 (COL4A2) genes have no estrogen response elements, but contain binding sites for the transcription factor Sp1 [5]. Using murine mesangial cells, it has been shown that estradiol-induced suppression of collagen type IV gene expression is mediated by interactions with Sp1 [30, 31]. Furthermore, it is known that TGF-β1 interacts with Sp1-containing complexes to activate COL1A1, COL1A2 and COL4A1 transcription [14, 15, 31]. It was recently demonstrated that estradiol reverses TGF-β1-induced collagen type IV expression by binding of estrogen-receptor complexes to Sp1 [31, 34]. Thus, an inhibition of TGF-β1-induced ECM production is a likely explanation of the beneficial effects of 17β-estradiol in our transgenic mice. A second explanation is that estradiol may stimulate the expression and/or activity of MMP-2 and MMP-9, which accelerates ECM degradation [11, 25]. Third, decreased synthesis of nitric oxide (NO) by damaged or dysfunctional glomerular endothelial cells is associated with glomerulosclerosis due to hampered microcirculation [26]. Estradiol has stimulatory effects on NO synthesis [33]; therefore, recovery of the NO production from the glomerular endothelial cells is likely to normalize the glomerular microcirculation, thereby contributing to normalization of the glomerular morphology. Finally, estradiol inhibits mesangial cell proliferation [17, 33]. However, we have no evidence of increased proliferation in the glomeruli of 6-week-old TGF-β1 transgenic mice (unpublished data).

The glomerular volume was reduced in Tg males treated with estradiol versus WT males. This outcome was not obvious in female mice, which showed similar glomerular volumes between the three groups. We have previously found a marginally increased glomerular volume in 8-week-old mice [16]. The food intake was less in mice offered the low-phytoestrogen diet compared with mice on normal chow. This had no impact on body weight or kidney weight in adult mice, but could influence the glomerular maturation in offspring. Whether the presence of relatively small glomeruli and the unexpected changes in the glomerular volumes are due to lack of phyto-estrogens in the diet, reduced protein consumption or reduced intake of calories or combinations hereof is unknown.

In conclusion, TGF-β1-induced glomerulopathy is prevented by pharmacological doses of 17β-estradiol. A suppressive effect of estrogen on TGF-β1-mediated kidney diseases may contribute to the protracted progression of end-stage renal disease in pre-menopausal women. However, during post-menopause estrogen deficiency, lack of estrogen-mediated inhibition of the TGF-β1 pathway leads to a progression of end-stage renal disease comparable with men.

Acknowledgements We are indebted to Anita Morell, Ulla Hovgaard, Lone Lysgaard, and Kirsten Nyborg for their excellent technical assistance. We are obliged to the staff at the animal facility, The Bartholin Building, Aarhus University, Denmark. Camilla Nielsen was the recipient of a fellowship from Aarhus University. The project was supported by the Danish Diabetes Association, the Danish Medical Research Council [grants no #9601759, #9802621 and #9600822 (Aarhus University—Novo Nordisk Center for Research in Growth and Regeneration)], the Novo Nordisk Foundation, Aarhus University, The Fougner Hartmanns Foundation and The Institute of Experimental Clinical Research, Aarhus University, Aarhus.

References

1. Bebo BF Jr, Fyfe-Johnson A, Adlard K, Beam AG, Vandenbark AA, Offner H (2001) Low-dose estrogen therapy ameliorates experimental autoimmune encephalomyelitis in two different inbred mouse strains. J Immunol 166:2080–2089
2. Border WA, Noble NA (1997) TGF-beta in kidney fibrosis: a target for gene therapy. Kidney Int 51:1388–1396
3. Border WA, Yamamoto T, Noble NA (1996) Transforming growth factor beta in diabetic nephropathy. Diabetes Metab Rev 12:309–339
4. Bruijn JA, Roos A, de Geus B, de Heer E (1994) Transforming growth factor-beta and the glomerular extracellular matrix in renal pathology. J Lab Clin Med 123:34–47
5. Burbelo PD, Martin GR, Yamada Y (1988) Alpha 1(IV) and alpha 2(IV) collagen genes are regulated by a bidirectional promoter and a shared enhancer. Proc Natl Acad Sci U S A 85:9679–9682
6. Chai Q, Krag S, Miner JH, Nyengaard JR, Chai S, Wogensen L (2003) TGF-beta1 induces aberrant laminin chain and collagen type IV isotype expression in the glomerular basement membrane. Nephron Exp Nephrol 94:e123–e136
7. Cosgrove D, Rodgers KD, Meehan DT, Miller CC, Bovard K, Gilroy A, Gardner H, Koteliansky V, Gotwals P, Amatucci A, Kalluri R (2000) Integrin $\alpha1\beta1$ and transforming growth factor-$\beta1$ play distinct roles in Alport glomerular pathogenesis and serve dual targets for metabolic therapy. Am J Pathol 157:1649–1659
8. Danielsen CC, Andreassen TT (1988) Mechanical properties of rat tail tendon in relation to proximal-distal sampling position and age. J Biomech 21:207–212
9. Fine LG, Orphanides C, Norman JT (1998) Progressive renal disease: the chronic hypoxia hypothesis. Kidney Int 65[Suppl]: S74–S78
10. Gross ML, Adamczak M, Rabe T, Harbi NA, Krtil J, Koch A, Hamar P, Amann K, Ritz E (2004) Beneficial effects of estrogens on indices of renal damage in uninephrectomized SHRSP rats. J Am Soc Nephrol 15:348–358
11. Guccione M, Silbiger S, Lei J, Neugarten J (2002) Estradiol upregulates mesangial cell MMP-2 activity via the transcription factor AP-2. Am J Physiol Renal Physiol 282:F164–F169
12. Hirose K, Osterby R, Nozawa M, Gundersen HJ (1982) Development of glomerular lesions in experimental long-term diabetes in the rat. Kidney Int 21:889–895
13. Hong SW, Isono M, Chen S, Iglesias D, Han DC, Ziyadeh FN (2001) Increased glomerular and tubular expression of transforming growth factor-beta1, its type II receptor, and activation of the Smad signaling pathway in the db/db mouse. Am J Pathol 158:1653–1663
14. Inagaki Y, Truter S, Ramirez F (1994) Transforming growth factor-beta stimulates alpha 2(I) collagen gene expression through a cis-acting element that contains an Sp1-binding site. J Biol Chem 269:14828–14834
15. Jimenez SA, Varga J, Olsen A, Li L, Diaz A, Herhal J, Koch J (1994) Functional analysis of human alpha 1(I) procollagen gene promoter. Differential activity in collagen-producing and -nonproducing cells and response to transforming growth factor beta 1. J Biol Chem 269:12684–12691
16. Krag S, Østerby R, Chai Q, Nielsen B, Hermans C, Wogensen L (2000) TGF-$\beta1$-induced glomerular disorder is associated with impaired concentrating ability mimicking primary glomerular disease with renal failure in man. Lab Invest 80:1855–1868
17. Kwan G, Neugarten J, Sherman M, Ding Q, Fotadar U, Lei J, Silbiger S (1996) Effects of sex hormones on mesangial cell proliferation and collagen synthesis. Kidney Int 50:1173–1179
18. Lei J, Silbiger S, Ziyadeh FN, Neugarten J (1998) Serum-stimulated alpha 1 type IV collagen gene transcription is mediated by TGF-beta and inhibited by estradiol. Am J Physiol 274:F252–F258
19. Lemmen JG, Broekhof JL, Kuiper GG, Gustafsson JA, van der Saag PT, van der BB (1999) Expression of estrogen receptor alpha and beta during mouse embryogenesis. Mech Dev 81: 163–167
20. Mulroney SE, Woda C, Johnson M, Pesce C (1999) Gender differences in renal growth and function after uninephrectomy in adult rats. Kidney Int 56:944–953
21. Negulescu O, Bognar I, Lei J, Devarajan P, Silbiger S, Neugarten J (2002) Estradiol reverses TGF-beta1-induced mesangial cell apoptosis by a casein kinase 2-dependent mechanism. Kidney Int 62:1989–1998
22. Neugarten J, Gallo G, Silbiger S, Kasiske B (1999) Glomerulosclerosis in aging humans is not influenced by gender. Am J Kidney Dis 34:884–888
23. Neugarten J, Acharya A, Silbiger SR (2000) Effect of gender on the progression of nondiabetic renal disease: a meta-analysis. J Am Soc Nephrol 11:319–329
24. Østerby R, Asplund J, Bangstad HJ, Nyberg G, Rudberg S, Viberti G, Walker JD (1997) Glomerular volume and the glomerular vascular pole area in patients with insulin-dependent diabetes mellitus. Virchows Arch 431:351–357
25. Potier M, Elliot SJ, Tack I, Lenz O, Striker GE, Striker LJ, Karl M (2001) Expression and regulation of estrogen receptors in mesangial cells: influence on matrix metalloproteinase-9. J Am Soc Nephrol 12:241–251
26. Raij L, Baylis C (1995) Glomerular actions of nitric oxide. Kidney Int 48:20–32
27. Sayers R, Kalluri R, Rodgers KD, Shield CF, Meehan DT, Cosgrove D (1999) Role for transforming growth factor-beta1 in alport renal disease progression. Kidney Int 56:1662–1673
28. Sharma K, Ziyadeh FN (1994) The emerging role of transforming growth factor-beta in kidney diseases (editorial). Am J Physiol 266:F829–F842
29. Silbiger SR, Neugarten J (1995) The impact of gender on the progression of chronic renal disease. Am J Kidney Dis 25:515–533
30. Silbiger S, Lei J, Ziyadeh FN, Neugarten J (1998) Estradiol reverses TGF-beta1-stimulated type IV collagen gene transcription in murine mesangial cells. Am J Physiol 274:F1113–F1118
31. Silbiger S, Lei J, Neugarten J (1999) Estradiol suppresses type I collagen synthesis in mesangial cells via activation of activator protein-1. Kidney Int 55:1268–1276
32. Wogensen L, Nielsen CB, Hjorth P, Rasmussen LM, Høj Nielsen A, Gross K, Sarvetnick N, Ledet T (1999) Under control of the renin-1c promoter, locally produced transforming growth factor-$\beta1$ induces accumulation of glomerular extracellular matrix in transgenic mice. Diabetes 48:182–192
33. Xiao S, Gillespie DG, Baylis C, Jackson EK, Dubey RK (2001) Effects of estradiol and its metabolites on glomerular endothelial nitric oxide synthesis and mesangial cell growth. Hypertension 37:645–650
34. Zdunek M, Silbiger S, Lei J, Neugarten J (2001) Protein kinase CK2 mediates TGF-beta1-stimulated type IV collagen gene transcription and its reversal by estradiol. Kidney Int 60:2097–2108

Virchows Arch (2004) 444:567–571
DOI 10.1007/s00428-004-1017-1

ORIGINAL ARTICLE

Eva Compérat · Fréderique Tissier · Karine Boyé · Gonzague de Pinieux · Annick Vieillefond

Non-Leydig sex-cord tumors of the testis. The place of immunohistochemistry in diagnosis and prognosis. A study of twenty cases

Received: 4 December 2003 / Accepted: 17 March 2004 / Published online: 16 April 2004

Abstract In 20 sex-cord tumors of the testes, we investigated immunohistochemistry as a possible method for histopathological diagnosis and evaluation of prognosis. We examined the following molecules: inhibin, CD99, cytokeratin, vimentin, MIB-1, estrogen receptors and progesterone receptors. These tumors of the testes comprised 18 Sertoli cell tumors (ScT) and two undifferentiated sex-cord tumors (USCT). Four tumors have been considered as malignant, because of metastatic spread. Inhibin was expressed by the tumor cells in 80% of sex cord tumors, without any correlation to the degree of differentiation and only in 25% of the malignant cases. Inhibin is a specific marker for sex-cord tumors of the testis and is particularly useful for the diagnosis of USCT. CD99, vimentin, keratin, progesterone and estrogen receptors were expressed in, respectively, 60%, 75%, 35%, 65% and 20% of cases; 95% expressed one of the three following markers: inhibin, CD99 or vimentin. Proliferation index MIB-1 was equal to or higher than 30% in the four malignant cases versus less than 20% in other cases. Lack of inhibin expression and a proliferation index (MIB-1) greater than 30% should be considered as a criterion in favor of malignancy.

Keywords Testicular sex-cord tumors · Sertoli cell tumors · Inhibin · MIB-1 · CD99

Introduction

Sex cord-stromal tumors of the testis are very rare tumors representing between 3% and 6% of testicular neoplasms. About 50% correspond to well-characterised Leydig cell tumors. The other 50% represent a histological heterogeneous group, the non-Leydig sex-cord testicular tumors constituted by different histological types [13].

Sertoli cell tumors (ScT) are separated into several groups. The most frequent group, however, are ScT(NOS)—not otherwise specified—which are either well differentiated or poorly differentiated [16]. Other tumors are rare, such as the large cell calcifying ScT and the sclerosing ScT [10].

Some sex-cord tumors are sometimes very difficult to recognize. They are either undifferentiated sex cord tumors (USCT), with only a minor sex-cord component or granulosa-like pattern [15]. Most of these tumors are benign, but about 15% show malignant progression with metastasis up to 10 years after orchidectomy [3]. There is a lack of reliable histopathological criteria to predict the clinical outcome. Size, mitotic activity and vascular invasion have a pejorative predictive value, but the only criterion of malignancy is metastasis.

The aim of our study was to try to define an antigen profile that might be useful to establish the diagnosis of sex-cord stromal tumors and to appreciate their prognosis.

E. Compérat · F. Tissier · K. Boyé · G. de Pinieux · A. Vieillefond (✉)
Service Central d'Anatomie et Cytologie Pathologiques,
Groupe hospitalier Cochin—Saint Vincent de Paul,
27 rue du Faubourg Saint Jaques, 75679 Paris, Cedex 14, France
e-mail: annick.vieillefond@cch.ap-hop-paris.fr
Tel.: +33-1-58411465
Fax: +33-1-58411480

Materials and methods

We studied 20 non-Leydig sex-cord tumors of the testis analyzed in our department of Pathology between 1995 and 2002, most of them being consultation cases. These 20 cases comprised 18 ScT (6 ScT NOS well differentiated, 11 ScT NOS poorly differentiated and 1 large cell calcifying) and 2 undifferentiated sex cord tumors.

Of the 20 patients, 4 had malignant tumors due to the presence of retroperitoneal para-aortic nodal metastasis either at the time of orchidectomy for 2 cases, or during the follow-up in 2 other patients. The resected surgical specimens were fixed in a solution of 10% neutral buffered formalin. Small tumors were examined in totality; larger tumors were sampled every centimeter. Routine 3-µm thick sections were prepared from paraffin-embedded tissue and stained with hematoxylin-eosin.

For all tumors, mitotic count on 10 HPF (high power fields) was performed. Immunohistochemistry was performed using the modified streptavidin-biotin-peroxidase method and diaminobenzidine as chromogen. The panel of antibodies included anti-cytokeratin (monoclonal, clone KL-1; Immunotech SA, Marseille, France; 1/50), anti-inhibin (monoclonal, α-subunit, clone R1; Serotec, Kid-

Table 1 Antibodies used in this study

CK	Monoclonal, clone KL-1; Immunotech SA, Marseille, France; 1:30
Vimentin	Monoclonal, clone Vim3B4; Dako Corporation, Glostrup, Denmark; 1/20
CD99	Monoclonal, clone 12E7; Dako, 1/40
Inhibin	Monoclonal, clone α-subunit, clone R1; Serotec, Kidlington, Oxford
Estrogen receptor	Monoclonal, clone 1D5; Dako, 1/50
Progesterone receptor	Monoclonal, clone PgR 636; Dako, 1/30
MIB-1	Monoclonal, clone MIB-1; Dako, 1/100

Table 2 Anatomo-clinical data concerning the 20 cases and comparison of mitotic activity, tumor size and MIB-1 expression. *n* total number of cases, *NLSCT* non-Leydig sex-cord tumors, *USCT* undifferentiated sex-cord tumors

Cases	Well-differentiated NLSCT	Poorly differentiated NLSCT and USCT	Malignant NLSCT
	n=6	*n*=10	*n*=4
Age (years)	28–76	15–52	36–70
Predominant architecture	Tubules and trabeculae	Sheets and cords, rarely compact	Tubules trabeculae
Predominant type of cells	Polygonal	Oval, fusiform	Oval, fusiform (3 cases), polygonal (1 case)
Stroma	Abundant	Few stroma	Abundant (3 cases) Few stroma (1 case)
Size (cm)	1.5–3.1	0.7–3.5	3–11
Mitosis	0–4	0–12	10–20
Metastasis	No	No	Yes
MIB-1 expression	0–15%	0–20%	30–60%

lington, Oxford; 1:30), antivimentin (monoclonal, clone Vim3B4; Dako Corporation, Glostrup, Denmark; 1/20), anti-estrogen receptor (ER) (monoclonal, clone 1D5; Dako, 1/50), anti-progesterone receptor (PR) (monoclonal, clone PgR 636; Dako, 1/30), CD99 (monoclonal, clone 12E7; Dako, 1/40), and MIB-1 (monoclonal, clone MIB-1; Dako, 1/100). Positive and negative controls were performed for each antibody (Table 1).

Cytokeratin and vimentin were considered positive if cytoplasmic staining was seen in more than 20% of tumor cells. CD99 staining was considered positive if membranous and/or cytoplasmic staining was seen in more than 10% of tumor cells. Inhibin staining was considered positive if more than 10% of cells were stained. Staining had to be cytoplasmic; even weak staining was considered. Anti-ER and anti-PR stainings were considered positive if more than 10% of tumor cells were stained. MIB-1 displayed nuclear staining; we evaluated the percentage of positive cells on 500 cells.

Results

Clinical findings

The age of the patients ranged from 15 years to 76 years (median age 42 years). All the patients presented painless palpable testicular masses without hormonal manifestations. The 20 sex-cord tumors were compact, well-delimited masses realizing whitish nodules in the testes. Tumor size varied from 0.7 cm to 11 cm in diameter. Three small tumors (<1.1 cm) were surgically treated by tumor resection. The other 17 tumors (>1.1 cm) were treated by orchidectomy. The follow-up period was 47.8 months (range 7–122 months).In two cases, there was lymph-node metastasis at the time of diagnosis. In one case, the patient died 1 year after diagnosis with lymph-node and pulmonary metastasis. Another patient displayed para-aortic lymph-node metastasis 10 years after orchidectomy.

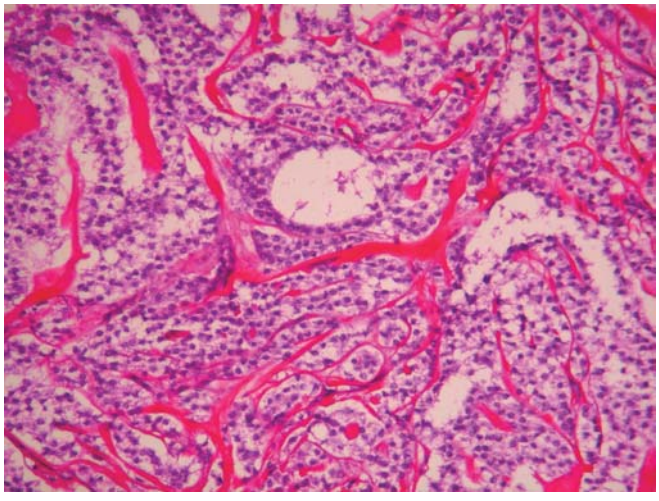

Fig. 1 Well-differentiated Sertoli cell tumors (ScT) constituted of polygonal large cells arranged in sheets, trabeculae or tubules, separated by an abundant fibrous stroma; hematoxylin and eosin staining ×100

Histological findings

Eighteen tumors were diagnosed as ScT: 1 large cell calcifying ScT and 17 ScT NOS. In 6 cases, the diagnosis of well-differentiated ScT was easy to establish on cytological and architectural criteria (Table 2). The tumors were almost exclusively constituted of polygonal large eosinophilic cells arranged in sheets, trabeculae or tubules, separated by an abundant fibrous stroma (Fig. 1). In 11 cases, the diagnosis of ScT NOS was not easy to establish. These tumors were considered as poorly differentiated ScT NOS. The most important part of the tumors consisted of ovoid or fusiform cells with diffuse growth, and only in a few areas could some tubules with polyg-

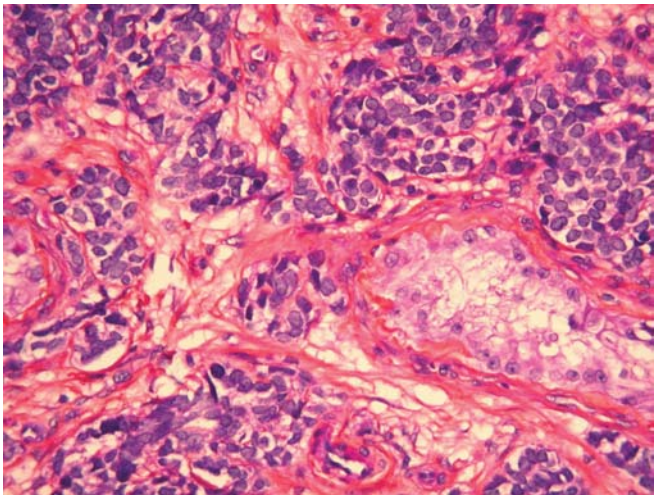

Fig. 2 Undifferentiated sex-cord tumors (USCT); absence of any recognizable pattern of Sertoli cell tumors (ScT); hematoxylin and eosin staining ×200

onal cells be seen resembling the remaining Sertoli tubules. In one well-differentiated ScT NOS and in 2 poorly differentiated ScT NOS, granulosa-like areas were observed. In one well-differentiated and 4 poorly differentiated cases, small nests of large eosinophilic cells resembling Leydig cells could be recognized. Two cases were diagnosed as USCT due to the absence of any recognizable pattern of Sertoli cell tumor (Fig. 2).

The four patients presenting malignant ScT defined by nodal metastatic progression, comprised one well-differentiated ScT NOS and three poorly differentiated ScT NOS. Metastasis was the most important criterion for malignancy, as vascular invasion is difficult to recognize and is not always observed, and tumor size and mitotic figures are not sufficient to determine malignancy. The remaining 16 cases were considered as tumors with unproven malignant potential, comprising 5 well-differentiated ScT NOS, 8 poorly differentiated ScT NOS, 1 large cell calcifying ScT and 2 USCT.

The size of the 16 tumors regarded as tumors with unproven malignant potential ranged from 0.7 cm to 3.5 cm in diameter, while the malignant types ranged from 3 cm to 11 cm (Table 2). The mitotic rate ranged from 0 to 12 mitotic figures per HPF in tumors with unproven malignant potential, while it varied from 10 to 20 in malignant cases (Table 2). Vascular invasion was detected in 3 of the 4 malignant cases, but in none of the cases with a benign course. Among the 16 patients with a non-malignant course, three cases presented a tumor size of respectively 3 cm, 3.5 cm and more than 3 cm. Additional criteria could be interesting for predicting a better or a worse evolution.

Immunohistochemistry

Immunohistochemical findings are summarized in Table 3. Staining against alpha-feto-protein had been performed before selection, to exclude Yolk-sac-tumor differentiation (data not shown).

Cytokeratin staining was positive in only 7 of 20 of the ScT and USCT (35%). One well-differentiated ScT NOS, 5 poorly differentiated ScT NOS, and 1 large cell calcifying ScT expressed cytokeratin. A diffuse cytoplasmic staining for vimentin was observed in 15 of 20 of the cases (75%). Five ScT NOS well-differentiated, 9 ScT NOS poorly differentiated, and 1 large cell calcifying ScT showed vimentin expression. Two malignant tumors displayed positive staining. It was interesting to see that all ScT NOS tumors with unproven malignant potential with a diameter of more than 3 cm expressed vimentin (as well as inhibin). Vimentin expression was not linked to a specific histological pattern.

CD99 a transmembrane glycoprotein coded by the MYC-2 gene, which stains normal Sertoli cells, showed cytoplasmic staining in 12 of 20 of the cases (60%). The staining was diffuse or focal, and there was no correlation with the histological pattern. Only 2 of the 4 malignant tumors expressed CD99. In our study, CD99 co-expression was associated with inhibin expression in 2 well-differentiated ScT, in 6 poorly differentiated ScT, in one USCT and in the large cell calcifying ScT.

In 16 tumors, the proliferation index (MIB-1) corresponded less than 20% to the tumors with an non-malignant course. The four tumors with a malignant course showed a MIB-1 expression between 30% and 60%. Thus, the expression of MIB-1 appeared to be a good marker to distinguish benign and malignant non-Leydig sex-cord tumors.

Table 3 Results of immunohistochemistry. *n* total number of cases, *NLSCT* non-Leydig sex-cord tumors, *USCT* undifferentiated sex-cord tumors, *ER* estrogen receptor, *PR* progesterone receptor

Positive antibody expression	Well-differentiated NLSCT (*)	Poorly differentiated NLSCT and USCT	Malignant NLSCT (†)
	n=6	*n*=10	*n*=4
CK	2/6	3/10	2/4
Vimentin	5/6	7/10	3/4
CD99	3/6	7/10	2/4
Inhibin	5/6	10/10	1/4
ER	1/6	1/10	2/4
PR	3/6	8/10	2/4
MIB-1	0–15%	0–20%	30–60%

* The large cell calcifying Sertoli cell tumors was counted in the group of well-differentiated NLSCT
† In one malignant case, ER and PR staining only on metastatic tissue

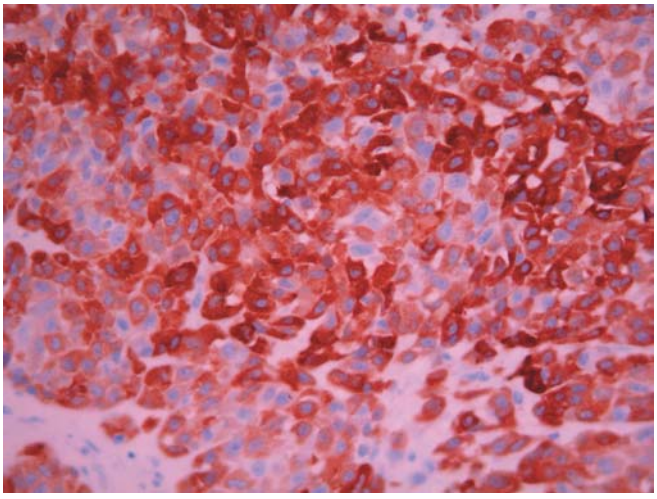

Fig. 3 Inhibin immunostaining, strong cytoplasmic expression ×400

Concerning the ER, only 4 of 20 (20%) cases showed nuclear staining. By contrast, 13 of 20 (65%) displayed nuclear positivity for the PR. No relationship with special histological features could be observed. However, malignant tumors always expressed ER/PR in a concordant way.

Inhibin, a gonadal polypeptide hormone that inhibits follicle-stimulating hormone secretion by the anterior pituitary gland, was expressed by tumor cells in 16 of 20 tumors (80%). In 14 cases, the cytoplasmic expression was strongly positive—either diffuse (Fig. 3) or focal. In 2 cases the expression was focal, with 10% of tumor cells labeled. Staining was usually strong in well-differentiated ScT NOS, and in poorly differentiated ScT NOS with fusiform cells. Four tumors were negative for inhibin (Table 3). Of the 4 malignant cases (ScT NOS poorly differentiated), 1 stained focally positive for inhibin; the three others were negative (Table 3).

Of the sex cord tumors of the testis, 95% expressed 1 of the 3 following markers: inhibin, CD99 or vimentin, with 10 cases co-expressing CD99 and inhibin, 15 cases displaying vimentin and inhibin expression and 8 cases were positive for vimentin and CD99.

Discussion

Leydig cell tumors have a characteristic well-defined histological and immunohistochemical profile. However, immunohistochemistry is generally not required for their diagnosis. By contrast, non-Leydig sex-cord tumors show various histological appearances and their immunohistochemical profile is not well established [5, 11]. In the present study, we tried to demonstrate an immunophenotypic profile of these tumors, which might contribute to their diagnosis and help to predict their clinical behavior.

Inhibin seems to be one of the most important molecules to detect. It is expressed in normal Sertoli and Leydig cells, and treatment in hypogonadotrophic men with gonadotrophin-releasing hormone shows increase of inhibin concentrations in the blood [8, 14]. All the Leydig cell tumors are inhibin positive [8]. Yet, inhibin expression in ScT varies from 30% to 91% according to the reported series [7, 8, 13]. Cytoplasmic expression of inhibin has been observed in 80% of our cases. Sometimes inhibin expression was only focal and weak, but usually it was diffuse and strong. There was no correlation in ScT NOS between inhibin expression and the degree of differentiation of the tumor cells. The same applied to the four inhibin-negative ScT NOS cases; two were ScT NOS poorly differentiated, while two others were ScT NOS well differentiated. The two USCT expressed cytoplasmic inhibin. Correlation with the clinical course was difficult to evaluate due to the small number of cases of malignant ScT, but only one of the malignant cases was positive for inhibin. Expression of inhibin in our series was a good criterion for the diagnosis of ScT, particularly in poorly differentiated ScT NOS or in USCT. However, negative staining does not allow excluding the diagnosis of ScT. In cases with malignant evolution, absence of staining was perhaps due to the modifications of some epitopes of inhibin, related to the malignant growth, as this can be seen in other malignancies [2]. More cases should be studied before interpreting the absence of inhibin expression as an argument for a malignant course.

It was interesting to see that cases with low mitotic activity, except one case generally showed inhibin expression and low MIB-1 expression. In our four cases negative for inhibin expression, MIB-1 staining was respectively 15%, 30%, 40% and 60%, which was much higher than the rest of the population.

There also seems to be a direct correlation between size, mitotic activity and MIB-1 expression. Tumors of more than 3 cm in diameter, independently of their histological differentiation, displayed between 4 and 12 mitosis per 10 HPF and MIB-1 expression was between 10% and 60%. Tumors of less than 3 cm in diameter showed less than 4 mitosis per 10 HPF, their MIB-expression varied between 0% and 10%. Therefore, we think that 3 cm might be a threshold value from which mitotic activity and MIB-1 expression increases.

CD99 is expressed by 100% of normal Sertoli and Leydig cell, but also by granulosa cells [5]. Kommoss et al. [9] reported positive staining in 29% of non-Leydig cell tumors. CD99 seems to be especially interesting together with inhibin in the differential diagnosis between ovary sex-cord stromal tumors and endometrioid carcinomas resembling sex-cord stromal tumors [11]. Nevertheless, CD99 seems to be less useful than inhibin. In our series, CD99 was positive in 60% of the cases and in 50% of malignant tumors. CD99 expression was associated with inhibin expression, but no particular histological differentiation could be observed. Consequently, co-expression of these two antibodies does not always help to resolve differential diagnostic problems.

Vimentin stained 75% of the ScT as in different other studies [12, 13]. In only one series [1] were 90% of ScT

found to express vimentin. In our series, only 35% of the cases expressed cytoplasmic cytokeratin. We have no explanation for the discordant results between our study and the findings of Amin et al. [1] showing cytokeratin expression in 80% or more of their ScT. We used KL-1 antibody, whereas authors in other studies used CAM 5.2 or AE1/AE3 antibodies, which might explain the difference. Henley et al. [6] demonstrated cytokeratin expression in 50% of malignant ScT, which joins our results as we also find positivity of 50% in our malignant cases. We did not find any significant difference between benign or malignant cases.

PRs and ERs are not detected in normal Sertoli and in Leydig cells. They can be detected in sex-cord tumors [4]. We found more frequent nuclear expression with PRs (65%) than ERs (20%). No correlation with the expression of other markers, histological differentiation or malignant behavior could be found. In malignant ScT, we always observed expression of ER/PR in a concordant way. As our study comprises only four malignant ScTs, the value of these results it is difficult to interpret.

The expression of MIB-1 in our series allows discriminating cases of tumors with unproven malignant potential and malignant course. In cases with metastasis, about 30–60% of the tumor cells showed a nuclear positivity while, in non-metastatic tumors, the number of positive nuclei was always inferior to 20%. One case showed 20% MIB expression, but was considered as a tumor with unproven malignant potential. It should be pointed out that the large size of the tumor (3 cm) and high MIB-1 expression (>30%) should be regarded as criteria for possible malignant course. Our cases displaying these features are actually considered as tumors with unproven malignant potential, but, as our study has shown, some of these tumors present metastases 10 years after orchidectomy. Maybe these cases should benefit from longer and more important clinical controls.

For the diagnosis, inhibin expression seems to be indeed the most discriminatory antibody, but its expression was not correlated to histological aspects or degree of differentiation. These results permitted us to confirm diagnosis in difficult cases, such as poorly or undifferentiated ScT. Although CD99 is not specific, positivity represents a good argument in favor of ScT diagnosis, especially in cases without immunoreactivity for inhibin. Of ScTs, 95% displayed at least one of the antibodies: inhibin, vimentin and/or CD99. Cases with low mitotic activity generally displayed low MIB-1 expression and inhibin staining. In cases with lots of inhibin expression, MIB-1 staining varied between 15% and 60%, and mitotic activity increased.

It is difficult to predict the clinical course for all patients in this series, because metastases may occur many years later. However, the four patients with metastatic disease presented grossly and microscopic findings usually seen in malignant tumors, such as tumor size equal or higher than 3 cm, vascular invasion and high mitotic activity. Our study permitted us to retain two additional criteria of malignancy which are the MIB-1 expression over 30% and perhaps the loss of inhibin antibody expression. We think it is important to survey particularly those patients with a tumor size over 3 cm, a high mitotic activity and/or a MIB-1 expression over 20%.

References

1. Amin MB, Young RH, Scully RE (1998) Immunohistochemical profile of Sertoli cell tumors of the testis. Mod Pathol 11:76A
2. Arora DS, Cooke IE, Ganesan TS, Ramsdale J, Manek S, Charnock FM, Groome NP, Wells M (1997) Immunohistochemical expression of inhibin/activin subunits in epithelial and granulosa cell tumors of the ovary. J Pathol 181:413–418
3. Compérat E, Tissier F, Vieillefond A (2004) Métastase ganglionnaire 10 ans après orchidectomie. Ann Pathol 24 (in press)
4. Düe W, Dieckmann, K-P, Niedobitek G, Bornhoft G, Loy V, Stein H (1990) Testicular sex cord stromal tumor granulosa cell differentiation: detection of steroid hormone receptors as a possible basis for tumor development and therapeutic management. J Clin Pathol 43:732–737
5. Gordon MD, Corless C, Renshaw AA, Beckstead J (1998) CD99, keratin, and vimentin staining of sex cord-stromal tumors, normal ovary and testis. Mod Pathol 11:769–773
6. Henley JD, Young RH, Ulbright TM (2002) Malignant Sertoli cell tumors of the testis. A study of 13 examples of a neoplasm frequently misinterpreted as seminoma. Am J Surg Pathol 26:541–550
7. Iczkowski KA, Bostwick DG, Roche PC, Cheville JC (1998) Inhibin A is a sensitive and specific marker for testicular sex cord-stromal tumors. Mod Pathol 11:774–779
8. Kinniburgh D, Anderson RA (2001) Differential patterns of inhibin secretion in response to gonadotrophin stimulation in normal men. Int J Androl 24:95–101
9. Kommoss F, Oliva E, Bittinger F, Kirkpatrick CJ, Amin MB, Bhan AK, Young RH, Scully RE (2000) Inhibin-alpha, CD99, HEA 125, PLAP, and chromogranin immunoreactivity in testicular neoplasms and the androgen insensitivity syndrome. Hum Pathol 31:1055–1061
10. Kratzer SS, Ulbright TM, Talerman A, Srigley JR, Roth LM, Whale G, Moussa M, Stephens JK, Millos A, Young RH (1997) Large cell calcifying Sertoli cell tumor of the testis. Contrasting features of six malignant and six benign tumors and a review of the literature. Am J Surg Pathol 21:1271–1280
11. Matias-Guiu X, Pons C, Prat J (1998) Mullerian inhibiting substance, alpha-inhibin, and CD99 expression in sex cord-stromal tumors and endometroid ovarian carcinomas ressembling sex cord-stromal tumors. Hum Pathol 29:840–845
12. McCluggage WG, Shanks JH, Whiteside C, Maxwell P, Banerjee SS, Biggart JD (1998) Immunohistochemical study of testicular sex cord-stromal tumors, including staining with anti-inhibin antibody. Am Surg Pathol 22:615–619
13. Mostofi FK, Price EB Jr (1973) Tumors of the male genital system. In: Firminger HI (ed) Atlas of Tumor Pathology. Fascicle 8, Series 2. Armed Forces Institute of Pathology, Washington, DC, pp 85–114
14. Nachtigall LB, Boepple PA, Seminara SB, Khoury RH, Sluss PM, Lecain AE, Crowley WF Jr (1996) Inhibin B secretion in males with gonadotropin-releasing hormone (GnRH) deficiency before and during long-term GnRH replacement: relationship to spontaneous puberty, testicular volume, and prior treatment—a clinical research center study. J Clin Endocrinol Metab 81:3520–3525
15. Ulbright TM, Srigley JR, Reuter VE, Wojno K, Roth LM, Young RH (2000) Sex cord stromal tumors of the testis with entrapped germ cells. A lesion mimicking unclassified mixed germ cell sex cord stromal tumors. Am J Surg Pathol 24:535–542
16. Young RH, Koelliker DD, Scully RE (1998) Sertoli cell tumors of the testis, not otherwise specified. A clinicopathologic analysis of 60 cases. Am J Surg Pathol 22:709–721

Virchows Arch (2004) 444:572–576
DOI 10.1007/s00428-004-1018-0

ORIGINAL ARTICLE

Paula Soares · Vítor Trovisco · Ana Sofia Rocha · Tália Feijão · Ana Paula Rebocho · Elsa Fonseca · Inês Vieira de Castro · José Cameselle-Teijeiro · Manuel Cardoso-Oliveira · Manuel Sobrinho-Simões

BRAF mutations typical of papillary thyroid carcinoma are more frequently detected in undifferentiated than in insular and insular-like poorly differentiated carcinomas

Received: 4 February 2004 / Accepted: 19 March 2004 / Published online: 17 April 2004

Abstract Somatic mutations of the *BRAF* gene ($BRAF^{V599E}$ and $BRAF^{K600E}$) were found to be closely associated with different histotypes of papillary thyroid carcinoma (PTC). The V599E mutation is highly prevalent in PTC with a papillary or mixed papillary follicular growth pattern, and the K600E mutation is apparently restricted to the follicular variant of PTC. It is usually accepted that thyroid malignancies may follow a progression path from well-differentiated to poorly differentiated (PDC) and undifferentiated (UC) carcinomas. One would expect that at least some of the less differentiated carcinomas would harbour the genetic alterations of pre-existing well-differentiated tumours. In order to find the prevalence of *BRAF* mutations in PDC and UC, we screened a series of 19 PDCs and 17 UCs, as well as 3 UC-derived cell lines, for both mutation types. The group of PDCs was restricted to the so-called insular and insular-like PDCs, thus excluding PTCs with solid, insular or trabecular foci of growth and PDCs displaying typical PTC nuclei. No *BRAF* mutations were detected in any of the 19 cases of PDC, whereas 6 of the UCs (35%) and one UC-derived cell line presented the $BRAF^{V599E}$ mutation. The $BRAF^{K600E}$ mutation was not detected in any case. We conclude that UC may progress from $BRAF^{V599E}$-mutated PTC. The absence of *BRAF* mutations in our series of PDC supports the assumption that pure insular and insular-like PDCs are more closely related to follicular carcinoma than to PTC.

Keywords *BRAF* · Oncogene · Mutation · Papillary thyroid carcinoma · Undifferentiated thyroid carcinoma · Poorly differentiated thyroid carcinoma

Paula Soares and Vítor Trovisco contributed equally to this work.

P. Soares · V. Trovisco · A. S. Rocha · T. Feijão · A. P. Rebocho · M. Sobrinho-Simões (✉)
IPATIMUP (Institute of Molecular Pathology and Immunology of the University of Porto),
R. Roberto Frias s/n,
4200 Porto, Portugal
e-mail: ssimoes@ipatimup.pt
Tel.: +351-22-5570799
Fax: +351-22-5570700

P. Soares · M. Sobrinho-Simões
Department of Pathology,
Medical Faculty, University of Porto,
Porto, Portugal

E. Fonseca · M. Sobrinho-Simões
Department of Pathology,
Hospital São João,
Porto, Portugal

I. Vieira de Castro
Department of Pathology,
Medical Faculty, University of São Paulo,
Brazil

J. Cameselle-Teijeiro
Department of Pathology,
Hospital Clínico Universitario,
University of Santiago de Compostela,
Santiago de Compostela, Spain

M. Cardoso-Oliveira
Department of Surgery B,
Hospital São João,
Porto, Portugal

Introduction

The thyroid gland presents a wide spectrum of tumours derived from follicular cells that range from well-differentiated papillary and follicular carcinomas (PTC and FTC, respectively), usually carrying a good prognosis, to the clinically aggressive, poorly differentiated (PDC) and undifferentiated (UC) carcinomas [17].

It is usually accepted that PDC and UC occur either de novo or progress from pre-existing well-differentiated carcinomas through a multi-step process of mutations and clonal expansion [17, 23, 26].

Recently, our group and others reported a very high prevalence of a particular missense mutation in the *BRAF* gene ($BRAF^{V599E}$) in PTC—46%—as well as in PTC-derived cell lines [4, 8, 22]. We have also shown that such a mutation occurs in a high proportion of PTCs with a papillary or mixed papillary follicular pattern of growth (53%) in contrast with its absence in the follicular variant of PTC [25]; in the latter, we detected another missense *BRAF* mutation ($BRAF^{K600E}$) in about 9% of the cases [25]. This genetic alteration, like the V599E, corresponds with the activation segment of the *BRAF* gene (exon 15); it had been previously detected in a few cases of melanoma and colorectal carcinoma [2, 15] and, by our group, in a follicular adenoma of the thyroid [22].

Genetic alterations in PDC and UC are far from being totally clarified. Assuming that PDC and UC may derive from well-differentiated thyroid carcinomas, it is expected that some PDCs and UCs would harbour genetic alterations that are typical of PTC (*RET/PTC* rearrangements and *BRAF* mutations) and FTC (*Ras* mutations and PAX8-PPAR gamma rearrangements) [9, 12].

Regarding the prevalence of *BRAF* mutations in PDC and UC, there is very little (and contradictory) evidence on record. The $BRAF^{V599E}$ mutation has been screened in PDC by Nikiforova and colleagues [13], who found the mutation in 2 of 16 cases (13%); the two positive cases had a PTC component in which the $BRAF^{V599E}$ was also detected. In UC, the results are contradictory: Namba and colleagues [11] detected $BRAF^{V599E}$ in 2 of 6 cases (33%) and Nikiforova and colleagues [13] found $BRAF^{V599E}$ in 3 of 29 UC cases (10%), while Fukushima and colleagues [5] did not detect any $BRAF^{V599E}$ mutations in 7 UC cases.

Since part of the aforementioned controversy may be due to the small size of the samples, we decided to search for *BRAF* mutations in a series of 19 PDCs and 17 UCs, as well as in 3 UC-derived cell lines. Taking into consideration our finding of different *BRAF* mutations in conventional PTCs and follicular variants of PTC ($BRAF^{V599E}$ and $BRAF^{K600E}$, respectively) [25], we have specifically looked for both types of *BRAF* mutations in our series of PDC and UC in an attempt to find out whether any of them may be associated with the neoplastic progression of PTC.

Materials and methods

Materials

Material from 36 patients with thyroid tumours was collected from four institutions in three countries: Hospital de S. João/Medical Faculty of Porto, Portugal; IPATIMUP, Porto, Portugal; University Hospital of the State University of São Paulo, Brasil; Hospital Clínico Universitario, Santiago de Compostela, Spain. This study was approved by the ethics committees of the four institutions, and informed consent was obtained from all patients. We also studied three UC-derived cell lines, kindly provided by Prof. J.E. Dumont and Prof. Marc Mareel: 8505c; Hth74; c643.

The tumours were classified according to the criteria of Hedinger and colleagues [7], LiVolsi [10] and Rosai and colleagues [17]. The cases were screened for thyroglobulin, calcitonin, carcinoembryonic antigen (CEA) and cytokeratins. All the carcinomas displaying extensive immunoreactivity for calcitonin and/or CEA (medullary carcinoma) were not included in the series. From the group of PDCs, we also did not include PTCs with foci of a solid growth pattern [18], PTCs with an insular component [1] and trabecular and/or solid thyroid carcinomas with nuclei with the typical features of PTC nuclei [7, 10, 17]. Whenever there was disagreement in the diagnosis, the sections were reviewed by the authors in an attempt to reach a consensus. The few cases in which such consensus was not achieved were also not included in the series.

The material was retrieved from paraffin blocks after careful microdissection performed by an experienced pathologist. DNA extraction was performed using the Puregene DNA Isolation Kit (GENTRA Systems, Minneapolis, USA) following the manufacturers instructions. Cases in which there were doubts on the quality of the DNA preservation have not been included in the study.

BRAF mutation analysis

To screen for *BRAF* mutations, we analysed DNA from tumour tissue. We studied the regions (activation segment—exon 15) of the *BRAF* gene where mutations had been previously identified in PTC. The PCR conditions were described elsewhere [22]. The amplicons were then subjected to single-stranded conformation polymorphism (SSCP) analysis: PCR reaction products of *BRAF* exon 15 were diluted 1:1 with loading buffer (95% formamide, 0.05% bromophenol blue and 0.05% xylene cyanol), denatured at 96°C for 10 min and cooled on ice for 5 min; electrophoresis of the denatured PCR products was carried out in non-denaturing 0.8× mutation detection enhancement (MDE) gels (BMA, Rockland, ME USA) at 180 V and 8°C for 15 h; PCR/SSCP products were visualised by standard DNA silver staining of the gels.

BRAF sequencing analysis

Whenever a case presented aberrant bands in the SSCP analysis the remaining PCR sample was subjected to a purifying treatment using Exonuclease I (New England Biolabs, Inc., Beverly, USA) and Shrimp Alkaline Phosphatase (Amersham Biosciences, Piscataway, NJ) and subjected to automatic sequencing, using ABI Prism dGTP BigDye Terminator Ready Reaction Kit (Perkin-Elmer, Foster City, California) and an ABI prism 3100 Genetic Analyser (Perkin-Elmer). Sequencing was performed on both strands using the aforementioned primers.

Results

We did not detect *BRAF* mutations (V599E or K600E) in any of the 19 PDCs (Fig. 1) despite the existence in several cases of nuclei that superficially resembled those of papillary carcinoma (Fig. 1D).

The $BRAF^{V599E}$ mutation was detected in 6 of the 17 UCs (35%) (Fig. 2). The 6 BRAF-positive UCs were predominantly composed of spindle cells (n=3), epithelioid cells (n=2) and giant cells (n=1). The histotype distribution of *BRAF*-positive cases is not significantly different from that of UC without *BRAF* mutation. No $BRAF^{K600E}$ mutations were detected in any UC.

One of the three cell lines (8505c) displayed only the $BRAF^{V599E}$ allele (Fig. 3). No $BRAF^{K600E}$ mutations were detected in any of the cell lines.

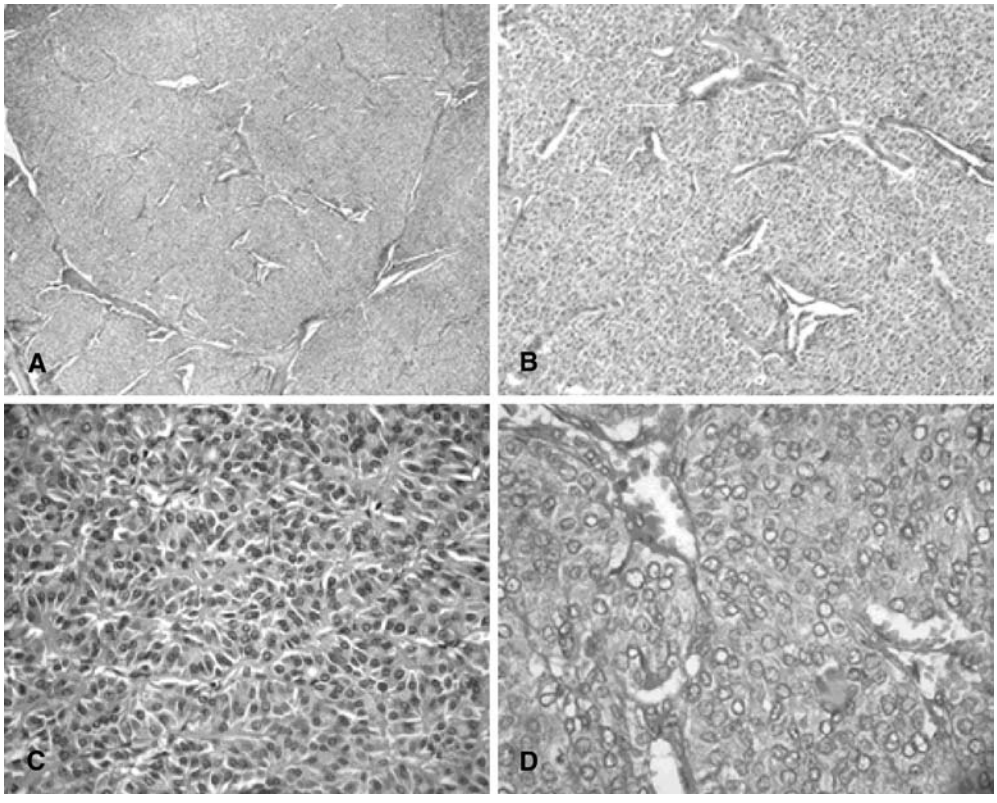

Fig. 1 **A** Poorly differentiated carcinoma (PDC) of the insular-type with wild-type *BRAF* (4×). **B** Higher magnification of the insular-type PDC depicted in **A** (10×). **C** Higher magnification of the case depicted in **A** and **B** (40×). **D** High magnification of a PDC of the insular-type displaying nuclei superficially resembling those of papillary thyroid carcinoma, with wild-type *BRAF* (40×)

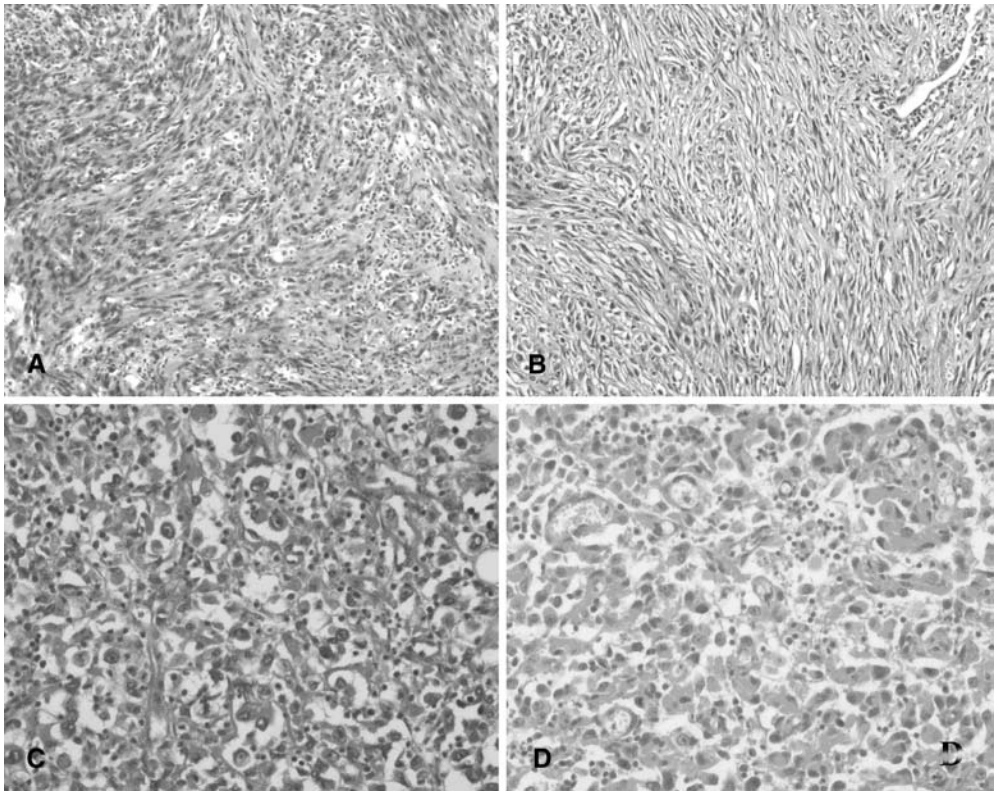

Fig. 2 Undifferentiated carcinoma (UC) with and without $BRAF^{V599E}$ mutation with similar histotypes. **A** UC predominantly composed of spindle cells harbouring the $BRAF^{V599E}$ mutation (10×). **B** UC predominantly composed of spindle cells with the wild-type *BRAF* (10×). **C** UC predominantly composed of polygonal cells harbouring the $BRAF^{V599E}$ mutation (20×). **D** UC predominantly composed of polygonal cells with wild-type *BRAF* (20×)

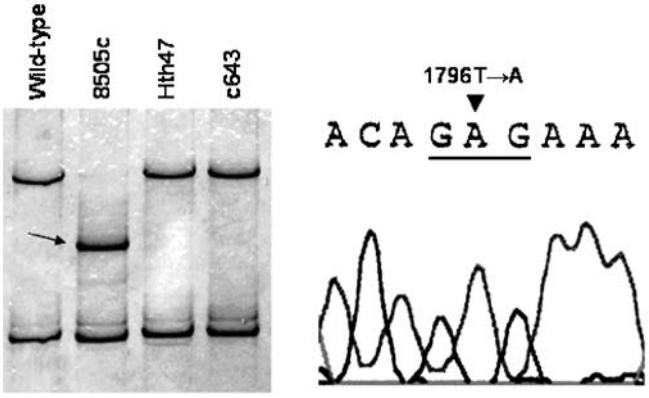

Fig. 3 Single-stranded conformation polymorphism analysis for the *BRAF* exon 15 in the undifferentiated carcinoma cell lines. *Arrow* indicates the shifted band that corresponds to the sequence. There is a total nucleotide substitution at the 1796 position (V599E) identified by the *arrowhead*

Discussion

Genetic alterations in PDC and UC are still poorly known. It is usually accepted that less-differentiated thyroid carcinomas may progress from well-differentiated carcinomas. Since PTC is far more frequent than FTC, one would expect that at least some PDCs and UCs would harbour typical genetic alterations of PTC, namely RET/PTC rearrangements and/or *BRAF* mutations.

We have detected the $BRAF^{V599E}$ mutation in about 35% of the cases of UC and in one of the three UC-derived cell lines. Our result fits with the finding of Namba and colleagues (2 of 6 cases—33%—displayed the V599E mutation) [11] and contrasts with the absence of *BRAF* mutations reported by Fukushima and colleagues in his small series of 7 UC cases [5] and the low prevalence reported by Nikiforova and colleagues (10% of the UC had the mutation) [13].

The frequency of $BRAF^{V599E}$ mutation in PTC varies from 29% to 69% in different series [4, 8, 22, 27], depending mainly on the prevalence of PTC histotypes which are known to be more associated with $BRAF^{V599E}$ (namely papillary and mixed follicular/papillary forms of PTC) [25].

The detection of the $BRAF^{V599E}$ mutation in about one-third of UC of our series supports the assumption that PTCs harbouring such a mutation may progress to UC. So far, we have detected the presence of the $BRAF^{V599E}$ mutation in both components of an UC displaying an independent focus of PTC (data not shown). The search for $BRAF^{V599E}$ mutations in both components of cases of mixed PTC/UC and the analysis of the outcome of patients with *BRAF*-positive PTCs followed-up for long periods will hopefully clarify whether or not *BRAF* mutations are associated with a more frequent progression of PTC towards UC.

We did not detect the $BRAF^{K600E}$ mutation in any UCs; but, given the small prevalence of the mutation in the follicular variant of PTC, it is difficult to evaluate the meaning of this negative result (i.e. we cannot conclude that PTCs harbouring this mutation do not progress towards undifferentiated tumours). At variance with UC, we did not detect *BRAF* mutations (V599E or K600E) in any of the 19 PDCs.

The method we used for the selection of the cases that constitute our series of PDC—namely the exclusion of PTC with foci of solid growth pattern [18], PTC with an insular component [1], and trabecular and/or solid carcinomas with nuclei of the PTC type [7, 10, 17]—contributed to reducing the heterogeneity of tumours classified as PDC [23] and may explain the absence of *BRAF* mutations in any of the 19 cases. This possibility is indirectly confirmed by the results of Nikiforova and colleagues [13], who have only detected the $BRAF^{V599E}$ mutation in the two PDCs displaying foci of typical PTC in which the mutation was also detected.

The quite different percentages of RET/PTC rearrangement and *β-catenin* mutations reported in different series of PDC [6, 16, 19, 20, 21, 24] probably reflect also the heterogeneity of tumours that are often included under the umbrella category of PDC [23]. In contrast to the aforementioned heterogeneity, our series is only constituted by cases that fit the original description of insular carcinoma [3], and by insular-like carcinomas (solid and trabecular carcinomas without PTC nuclei) [14].

The absence of *BRAF* mutations in our series of 19 PDCs supports the assumption that the PDCs we analysed are more closely related to FTC than to PTC. Our findings thus confirm the data previously obtained by electron microscopy, morphometry and lectin histochemistry in a group of PDCs selected according to the same criteria used in the present study [23].

We did not study PTC with morphological signs of poor differentiation (solid, insular and trabecular foci) and therefore we ignore the prevalence of the two types of *BRAF* mutations in such PTC-derived poorly differentiated tumours. Additional studies including these and other morphological subtypes of PDC will help to clarify the role played by *BRAF* mutations in the progression towards different histotypes of less-differentiated thyroid carcinomas.

Acknowledgements This study was supported by Fundação para a Ciência e Tecnologia POCTI/FEDER (POCTI/NSE/48171/2002). We are grateful to FCT for grant support to Vítor Trovisco (FSRH/BD/13055/2003) and Ana Sofia Rocha (FSRH/BD/21775/99). We would also like to thank Prof. J.E. Dumont and Prof. Marc Mareel for providing the cell lines included in this study.

References

1. Ashfaq R, Vuitch F, Delgado R, Albores-Saavedra J (1994) Papillary and follicular thyroid carcinomas with an insular component. Cancer 73:416–423
2. Brose MS, Volpe P, Feldman M, Kumar M, Rishi I, Gerrero R, Einhorn E, Herlyn M, Minna J, Nicholson A, Roth JA, Albelda SM, Davies H, Cox C, Brignell G, Stephens P, Futreal PA, Wooster R, Stratton MR, Weber BL (2002) BRAF and RAS

mutations in human lung cancer and melanoma. Cancer Res 62:6997–7000
3. Carcangiu ML, Zampi G, Rosai J (1984) Poorly differentiated ("insular") thyroid carcinoma. A reinterpretation of Langhans' "wuchernde Struma". Am J Surg Pathol 8:655–668
4. Cohen Y, Xing M, Mambo E, Guo Z, Wu G, Trink B, Beller U, Westra WH, Ladenson PW, Sidransky D (2003) BRAF mutation in papillary thyroid carcinoma. J Natl Cancer Inst 95:625–627
5. Fukushima T, Suzuki S, Mashiko M, Ohtake T, Endo Y, Takebayashi Y, Sekikawa K, Hagiwara K, Takenoshita S (2003) BRAF mutations in papillary carcinomas of the thyroid. Oncogene 22:6455–6457
6. Garcia-Rostan G, Camp RL, Herrero A, Carcangiu ML, Rimm DL, Tallini G (2001) Beta-catenin dysregulation in thyroid neoplasms: down-regulation, aberrant nuclear expression, and CTNNB1 exon 3 mutations are markers for aggressive tumour phenotypes and poor prognosis. Am J Pathol 158:987–996
7. Hedinger C, Williams ED, Sobin LH (1988) World Health Organization international histological classification of tumours. Springer, Berlin Heidelberg New York
8. Kimura ET, Nikiforova MN, Zhu Z, Knauf JA, Nikiforov YE, Fagin JA (2003) High prevalence of BRAF mutations in thyroid cancer: genetic evidence for constitutive activation of the RET/PTC-RAS-BRAF signalling pathway in papillary thyroid carcinoma. Cancer Res 63:1454–1457
9. Kroll TG, Sarraf P, Pecciarini L, Chen CJ, Mueller E, Spiegelman BM, Fletcher JA (2000) PAX8-PPARgamma1 fusion oncogene in human thyroid carcinoma. Science 289:1357–1360
10. LiVolsi V (1990) Surgical pathology of the thyroid. WB Saunders, Philadelphia
11. Namba H, Nakashima M, Hayashi T, Hayashida N, Maeda S, Rogounovitch TI, Ohtsuru A, Saenko VA, Kanematsu T, Yamashita S (2003) Clinical implication of hot spot BRAF mutation, V599E, in papillary thyroid cancers. J Clin Endocrinol Metab 88:4393–4397
12. Nikiforova MN, Lynch RA, Biddinger PW, Alexander EK, Dorn GW 2nd, Tallini G, Kroll TG, Nikiforov YE (2003) RAS point mutations and PAX8-PPAR gamma rearrangement in thyroid tumours: evidence for distinct molecular pathways in thyroid follicular carcinoma. J Clin Endocrinol Metab 88:2318–2326
13. Nikiforova MN, Kimura ET, Gandhi M, Biddinger PW, Knauf JA, Basolo F, Zhu Z, Giannini R, Salvatore G, Fusco A, Santoro M, Fagin JA, Nikiforov YE (2003) BRAF mutations in thyroid tumours are restricted to papillary carcinomas and anaplastic or poorly differentiated carcinomas arising from papillary carcinomas. J Clin Endocrinol Metab 88:5399–5404
14. Papotti M, Botto Micca F, Favero A, Palestini N, Bussolati G (1993) Poorly differentiated thyroid carcinomas with primordial cell component. A group of aggressive lesions sharing insular, trabecular, and solid patterns. Am J Surg Pathol 17:291–301
15. Rajagopalan H, Bardelli A, Lengauer C, Kinzler KW, Vogelstein B, Velculescu VE (2002) RAF/RAS oncogenes and mismatch-repair status. Nature 418:934
16. Rocha AS, Soares P, Fonseca E, Cameselle-Teijeiro J, Oliveira MC, Sobrinho-Simoes M (2003) E-cadherin loss rather than beta-catenin alterations is a common feature of poorly differentiated thyroid carcinomas. Histopathology 42:580–587
17. Rosai J, Carcangiu ML, DeLellis RA (1992) Tumours of the thyroid gland. Armed Force Institute of Pathology, Washington, DC
18. Sakamoto A, Kasai N, Sugano H (1983) Poorly differentiated carcinoma of the thyroid. A clinicopathologic entity for a high-risk group of papillary and follicular carcinomas. Cancer 52:1849–1855
19. Santoro M, Carlomagno F, Hay ID, Herrmann MA, Grieco M, Melillo R, Pierotti MA, Bongarzone I, Della Porta G, Berger N et al (1992) Ret oncogene activation in human thyroid neoplasms is restricted to the papillary cancer subtype. J Clin Invest 89:1517–1522
20. Santoro M, Papotti M, Chiappetta G, Garcia-Rostan G, Volante M, Johnson C, Camp RL, Pentimalli F, Monaco C, Herrero A, Carcangiu ML, Fusco A, Tallini G (2002) RET activation and clinicopathologic features in poorly differentiated thyroid tumours. J Clin Endocrinol Metab 87:370–379
21. Shiels OM, O'Leary JJ, Sweeney EC (2000) Assessment of ret/PTC-1 rearrangements in neoplastic thyroid tissue using TaqMan RT-PCR. J Pathol 192:32–36
22. Soares P, Trovisco V, Rocha AS, Lima J, Castro P, Preto A, Maximo V, Botelho T, Seruca R, Sobrinho-Simoes M (2003) BRAF mutations and RET/PTC rearrangements are alternative events in the etiopathogenesis of PTC. Oncogene 22:4578–4580
23. Sobrinho-Simões M, Sambade C, Fonseca E, Soares P (2002) Poorly-differentiated carcinomas of the thyroid gland. Int J Surg Pathol 10:123–131
24. Tallini G, Santoro M, Helie M, Carlomagno F, Salvatore G, Chiappetta G, Carcangiu ML, Fusco A (1998) RET/PTC oncogene activation defines a subset of papillary thyroid carcinomas lacking evidence of progression to poorly differentiated or undifferentiated tumor phenotypes. Clin Cancer Res 4:287–294
25. Trovisco V, Castro IV, Soares P, Máximo V, Silva P, Magalhães J, Abrosimov A, Guiu XM, Sobrinho-Simões M (2004) BRAF mutations are associated with some histological types of papillary thyroid carcinoma. J Pathol 202:247–251
26. Wynford-Thomas D (1997) Origin and progression of thyroid epithelial tumours: cellular and molecular mechanisms. Hormone Res 47:145–157
27. Xu X, Quiros RM, Gattuso P, Ain KB, Prinz RA (2003) High prevalence of BRAF gene mutation in papillary thyroid carcinomas and thyroid tumor cell lines. Cancer Res 63:4561–4567

Virchows Arch (2004) 444:577–586
DOI 10.1007/s00428-004-1020-6

ORIGINAL ARTICLE

Ikuo Kudawara · Nobuhito Araki · Akira Myoui · Yoichi Kato · Atsumasa Uchida · Hideki Yoshikawa

New cell lines with chondrocytic phenotypes from human chondrosarcoma

Received: 7 October 2003 / Accepted: 22 March 2004 / Published online: 29 April 2004

Abstract In the present study, we investigated chondrocytic characterization for newly established human chondrosarcoma cell lines. A chondrosarcoma cell line, HCS-TG, was established by the implantation of grade-2 human chondrosarcoma into athymic mice. Cloning of HCS-TG cells from passage 17 was performed. After cell cloning, two clonal-cell lines (HCS-TG C3 and E2) with good proliferative activities were obtained. These cell lines in monolayer culture retained a polygonal morphology. Their doubling times were 68 h and 45 h, respectively. mRNA expressions of type-I, -II, -X, and -XI collagens and aggrecan core protein were detected on reverse-transcription polymerase chain reaction. Protein expression of type-II collagen was confirmed in each cell line using Western blotting. However, there was no expression of type-I collagen. Moreover, gelatin zymography revealed that both cell lines produced extracellular matrices with matrix metalloproteinases 2 and 9. The parental HCS-TG cells had tumorigenicity in athymic mice; however, C3 and E2 were not tumorigenic. New clonal-cell lines HCS-TG C3 and E2 derived from human chondrosarcoma are morphologically chondrocytic in serial monolayer cultures and express chondrocytic phenotypes.

Keywords Chondrosarcoma · Cell line · Type-II collagen · Proteoglycan · Matrix metalloproteinase

No benefits in any form have been received or will be received from a commercial party related directly or indirectly to the subject of this article. This work was partly supported by the grants from the Japanese Ministry of Education, Science and Culture.

I. Kudawara (✉)
Department of Orthopaedic Surgery,
Osaka National Hospital,
Osaka 2-1-14 Hoenzaka, Chuo-ku, 540-0006 Osaka, Japan
e-mail: kudawara@onh.go.jp
Tel.: +81-6-69421331
Fax: +81-6-69436467

N. Araki
Department of Orthopaedic Surgery,
Osaka Medical Center for Cancer and Cardiovascular Diseases,
Osaka 1-3-3 Nakamichi, Higashinari-ku, 537-8511 Osaka, Japan

A. Myoui · H. Yoshikawa
Department of Orthopaedics,
Osaka University Graduate School of Medicine,
Suita 2-2 Yamadaoka, 565-0871 Suita, Japan

Y. Kato
Clinical Development Department Asahi Kasei
Pharma Corporation,
9-1 Kanda Mitoyo-cho, Chiyoda-ku, 101-8481 Tokyo, Japan

A. Uchida
Department of Orthopaedic Surgery,
Faculty of Medicine, Mie University,
Tsu, 2-74 Edobashi, 514-0001 Tsu, Japan

Introduction

Chondrosarcoma (CS) is the second most frequent primary malignant bone tumor after osteosarcoma and is characterized by basic neoplastic histology with cartilaginous stroma. The most frequent locations are the femur, pelvis and humerus, and approximately 62% of patients are in the fourth, fifth and sixth decades of life [3, 20, 31, 48]. Histological gradings of CS are described as grades 1–3 and dedifferentiated CS. Approximately 70% of CS cases are designated as grade 1 or 2 [14, 20]. These grades correlate with the prognosis, that is, low- or intermediate-grade CS tends to grow slowly and metastasize late. This is in contrast to dedifferentiated CS, which develops early metastases [20, 42]. The current clinical study indicates that independent poor prognostic factors are local recurrence, pelvic location and a high grade [25]. Though the prognosis of CS is better than other high-grade sarcomas, such as osteosarcoma and Ewing tumor, there are significant clinical difficulties concerning the treatment of CS. It is well known that CS has little sensitivity to chemotherapy or radiotherapy, therefore, surgical excision is an essential treatment for this tumor. However, the rates of local failure were reported as 24% [25] and 28% [42], and, in pelvic or in high-grade cases,

the local recurrence rate is higher than at other locations or in low-grade cases [25]. Moreover, high-grade CS develops metastasis frequently, despite complete local tumor ablation. Therefore, a new treatment modality for CS is required.

There are few experimental models, and applicable treatment procedures from experimental results have not been described. It is, therefore, important to establish a model of CS with a chondrosarcomatous phenotype for clinical investigation. Until now, there have been some reported cell lines of CS; however, those with chondrocytic phenotypes were limited [4, 10, 11, 24, 45]. In this study, new cell lines with chondrocytic phenotypes were established from a pelvic chondrosarcoma, and the morphological and molecular analyses were performed.

Materials and methods

Materials

A 36-year-old Japanese man with a grade-2 chondrosarcoma that arose in the ilium was treated with surgery. The patient provided written informed consent. Tumor tissue from a surgical specimen was implanted subcutaneously (s.c.) into 6-week-old athymic mice ICR nu/nu (Oriental Kobo, Japan), which were housed in sterile cages. The tumor was maintained in the mice using the s.c. trocar implantation of 3-mm tumor fragments. A tumor from a fifth generation source was minced with scissors aseptically 1 mm and digested in 0.1% collagenase (Sigma) and 0.6% dispase in phosphate-buffered saline (PBS) for 40 min at 37°C. The cell suspension was passed through a nylon mesh and washed twice using medium.

Cell culture

The cells were placed in 35-mm culture dishes (Falcon) and maintained at 37°C in 95% air/5% CO_2. The medium used was minimum essential medium alpha modification (α-MEM) medium (Gibco) supplement with 20% fetal bovine serum (FBS) (Hyclone) or 20% fetal calf serum (FCS) (Gibco), 5000 IU/ml penicillin and 5000 μmg/ml streptomycin. The culture medium was changed three times per week, treated with 0.25% trypsin (Gibco) and split 1:3 at confluence. When the cultures were well established, the medium was switched to α-MEM supplement with 10% FCS and 10% calf serum (CS) (Gibco). The cell was named HCS-TG (human chondrosarcoma T.G.).

Chromosomal analysis

The cytogenetic analysis of HCS-TG cells was carried out using the G-band method. After the cloning of cell lines, each cell line was also examined using the same method.

Cloning of HCS-TG

HCS-TG cells from passage 17 were inoculated to eight dishes at a density of 100 cells per 100-mm culture dish (Corning). Colonies (n=39) were obtained 5 weeks or 6 weeks after inoculation. After a 3-min treatment with 0.25% trypsin, each colony was picked up with a pipetter, and the cell suspension with medium was transferred to a 35-mm dish.

Tumorigenicity in athymic mice

Suspensions of 1×10^7 HCS-TG cells were injected s.c. into the right and left flanks of 6-week-old athymic mice ICR nu/nu, obtained from Oriental Kobo (Japan). When tumor sizes reached approximately 3 cm at the maximum diameter, transplantation was performed. Tumor samples were fixed with 20% formaldehyde and examined histologically after staining with alcian blue, toluidine blue and safranin-O. HCS-TG C3 and E2 cells, 1×10^7, were homogenized with 0.1-ml Matrigel (Becton Dickinson Labware) and injected s.c. into the right flank of 4- or 5-week-old athymic mice. The mice were examined for tumor growth every week for 4 months.

Immunohistochemistry on xenograft

Xenografts were fixed with 20% neutral formaldehyde and embedded in paraffin wax. S-100 protein (polyclonal rabbit anti-S-100, Dako Cytomation, Glostrup, Denmark; 1/2000 dilution) staining was performed on an automated immunostainer (Ventana NX system, Ventana Medical Systems, Inc.) using the avidin-biotin-peroxidase technique (DAB universal kit, Ventana Medical Systems, Inc., Tucson, AZ, USA). Ki-67 (monoclonal mouse anti-human Ki-67 antigen clone Mib1, Dako Cytomation, Glostrup, Denmark; 1/50 dilution) was incubated for 40 min at 95°C in 0.01 M citrate buffer (pH 6.0), using the streptavidin-biotin technique (Histofine DAB kit, Nichirei, Tokyo, Japan).

Chondrocytic characterization of clonal HCS-TG C3 and E2 alcian blue staining

Each cell line was plated on a 24-well culture plate at 5×10^3 cells/well. The cells were cultured in α-MEM supplemented with 20% FCS or 10% FCS+10% CS, and the medium was changed two times per week. After 12 days culture, the cells were fixed with 95% methanol and stained with 1% alcian blue solution (pH 1.0) for 1 h at room temperature. After observation of the staining pattern, a semi-quantitative analysis of the plate was carried out. The stain was extracted from the air-overnight-dried plate using 500 μl/well of 4-M guanidium chloride. The extracts were transferred to 96-well micro-titer plates and measured at 650 nm of absorbance using a Micro Plate Reader (M-Emax; Molecular Device).

DMMB method

The cells, 5×10^4, were plated on each well of a 24-well culture plate and cultured in the same medium as above. After 3 days or 7 days culture, the cell layer was digested using incubating at 60°C for 3 h in 250 μl or 500 μl of papain solution. Dissolved acidic sugar chains were quantified using the dimethylmethylene blue (DMMB) staining method, according to the previous report [9].

Immunohistochemistry on C3 and E2 cells

Immunohistochemistry was performed using the avidin-biotin-peroxidase technique using antibodies to S-100 protein (Dako Cytomation, Glostrup, Denmark) and Mib1 (Dako Cytomation, Glostrup, Denmark). As negative controls, S-100 and Ki-1 were replaced by universal rabbit negative control (Dako, Glostrup, Denmark) and mouse IgG1 negative control (Dako, Glostrup, Denmark), respectively.

RNA isolation and RT-PCR

All clonal cells were cultured to confluency in 70 ml of Flasco (Falcon), and mRNA was extracted using FastTrack 2.0 Kit (Invitrogen, CA, USA) according to the manufacturer's instructions. Of

the mRNA, 1 μg was reverse-transcribed (RT) using M-MLV reverse transcriptase and oligo dT (Gibco BRL, Rockville, MD, USA). Polymerase chain reaction (PCR) analyses for specific primer sets are described as follows: type-I collagen=5′-AAGAACCCCAAGGACAAGAGG-3′ for sense and 5′-GGAGGGAGTTTACAGGAAGCA-3′ for antisense; type-II collagen=5′-CCCTGAGTGGAAGAGTGGAG-3′ for sense and 5′-ATTGGAGCCCCTGGATGAGCA-3′ for antisense; type-IX collagen=5′-GGGCCCAGAACACATAGTCCTA-3′ for sense and 5′-CTCCTCTCCACGCCAATCAT-3′ for antisense; type-X collagen=5′-CTGGGACCCCTCTTGTTAGT-3′ for sense and 5′-GTTTTTACGTTGCTGCTCAC-3′ for antisense; type-XI collagen (α1)= 5′-CGTAACAACCCTCGCATTGACC-3′ for sense and 5′-TTCTCCACGCTGATTGCTACCC-3′ for antisense; type-XI collagen (α2) =CAAAACCAACAGCCTCAGAG for sense and CCCCTCCACGAGCATACCAG for antisense. PCR amplification was carried out in a programmable thermal cycler system (GeneAmp PCR System, PE Applied Biosystems, Foster City, CA).

Denaturation for 35 cycles at 94°C for 30 s, annealing at 55°C for 30 s, and extension at 72°C for 40 s was routinely performed after initial denaturation for 1 min. The final cycle was incubation for 7 min and extension at 72°C. To confirm the reverse-transcribed cDNA of each sample, amplification was also carried out with two G3PDH primers (Clontech, CA, USA).

All clonal cells were cultured to confluence on a 100-mm culture dish. Total RNA was isolated from the confluent dish using ISOGEN (Nippon gene) according to the manufacturer's instructions. Isogen (1 ml) was used for each dish. cDNA was synthesized by oligo dT priming using Super Script Preamplification System (Gibco BRL) from 3 μg of total RNA in a 20-μl reaction mixture according to manufacturer's instruction. The cDNA, 0.5–2%, was amplified using TaKaRa PCR Thermal Cycler MP (TaKaRa) in a 20-μl reaction mixture containing 1×PCR buffer (TaKaRa), 1.5 mM $MgCl_2$, 200 μM dNTP mixture, 5 pmol of sense and antisense primer, and 0.5 U of *Taq* DNA polymerase (TaKaRa). Amplification was performed for 25 cycles following the reaction profile: 94°C for 1 min, 64°C for 1 min and 72°C for 2 min. The following primer set was used as aggrecan core protein cDNA: 5′-CCCAAGAATCAAGTGGAGCCGTGT-3′ for sense and 5′-AAAGACCTCACCCTCCATCTCCTC-3′ for anti-sense. Each initial cDNA amount was normalized against the result of β-actin PCR using the same protocol as above. The following primer set was used with 58°C annealing and 15 cycles of amplification for the β-actin cDNA: 5′-TTGAGACCTTCAACACCCCAG-3′ and 5′-ACTTGCGCTCAGGAGGAGCAA -3′.

Protein expression of type-I and type-II collagen (Western blotting)

Cells, 5×10^4, were plated on each well of a 24-well culture plate. After 7 days culture, the cells were washed with PBS and lysed directly by the addition of 200 μl of reduced sodium dodecyl sulfate polyacrylamide gel electrophoresis sample buffer to each well. Aliquot lysates were heated to 95°C for 5 min, loaded on to a 7.5–15% gradient gel and transferred to nitrocellulose membranes following electrophoresis. The membranes were blocked with 5% bovine serum albumin (BSA) in Tris-buffered saline (TBS) buffer (50 mM Tris-HCl, 150 mM NaCl, pH 7.2) overnight at 4°C. Anti-type-I collagen antibody (Calbiochem) diluted 1:40 or anti-human type-II collagen antibody (Fuji-yakuhinkogyo) diluted 1:100 each in TBS buffer containing 1% BSA were used as the primary antibodies. After a 2 h reaction at room temperature with the primary antibody, the membranes were washed four times with TBS-T, and a secondary antibody reaction was carried out. As the secondary antibody, peroxidase-conjugated affinity purified F(ab') fragment goat anti mouse IgG (H+L) (Jackson Immuno Research Lab, Inc.) was used at a 1:2000 dilution in TBS buffer containing 2% skimmed milk. Signals were detected on an enterochromaffin-like Western blotting detection system (Amersham) as described by the manufacturer.

Determination of MMP activity and expression (gelatin zymography and Western blotting)

HCS-TG C3, 1×10^5 cells, and HCS-TG E2, 5×10^4 cells, were plated on respective wells of two 24-well culture plates. After 4 days culture, both cell lines became confluent. Then the medium was changed to fresh medium containing various concentrations of cytokines: recombinant human IL-1 β (Genzyme, Cambridge, MA, USA) (25, 50 or 100 U/ml), recombinant human tumor necrosis factor (TNF) (Asahi Kasei Co., Japan) (25, 50 or 100 U/ml) or lipopolysaccharide (LPS) IL-1 (25, 50 or 100 μg/ml) or nothing. After 48 h additional culture, these culture media were harvested, and gelatin zymography analyses were carried out according to a previous report [40]. Cell lysates were also prepared for Western blot analysis of matrix metalloproteinase (MMP)-3. The procedure used was as listed above for type-I or type-II collagen. Anti-human-MMP-3 antibody (Fuji-yakuhinkogyo) was used as the primary antibody in this case.

Results

Morphological, cytochemical and biological characterization of HCS-TG cells

HCS-TG cells were polygonal or spindle shaped in monolayer culture and formed nodules 2 weeks after inoculation and were grown to confluence (Fig. 1A). Toluidine blue (TB) staining (pH 4.1) demonstrated metachromasia in the nodule, and alcian blue (AB) staining (pH 2.3) demonstrated blue stain (Fig. 1B), suggesting the presence of proteoglycan. When 1×10^5 cells were inoculated on 16-mm diameter wells, the formation of whitish membranes was seen 4 weeks after inoculation. The membranes were fixed with 20% formaldehyde and embedded in paraffin. Extracellular matrices in the cross-sections of membranes showed cartilaginous features in TB and AB stains (Fig. 1C).

Clonal-cell line, HCS-TG C3 and E2

The cells of 39 clonal-cell lines were polygonal or spindle shaped and showed various growth characteristics. Two cell lines with good growth activity were selected for further characterization and were designated C3 and E2 (Fig. 1D, E). The doubling times in the exponential growth phase of C3 and E2 in the media with 20% FBS were 68 h and 48 h, respectively (Fig. 2). In the medium containing 10% FCS+10% CS, cell proliferation was also good. However, cell growth was poor in the media with 20% FCS. The shape and proliferation of cells were stable up to passage 45. Immunohistochemically, both clonal cells were focally positive for S-100 (Fig. 1F, G) and Ki67 (Mib1) (Fig. 1H).

Chromosomal analysis

Chromosomal analysis on HCS-TG indicated that the cells had a modal number of 79. A total of 20 cells from each cell line were analyzed for their modal number. The

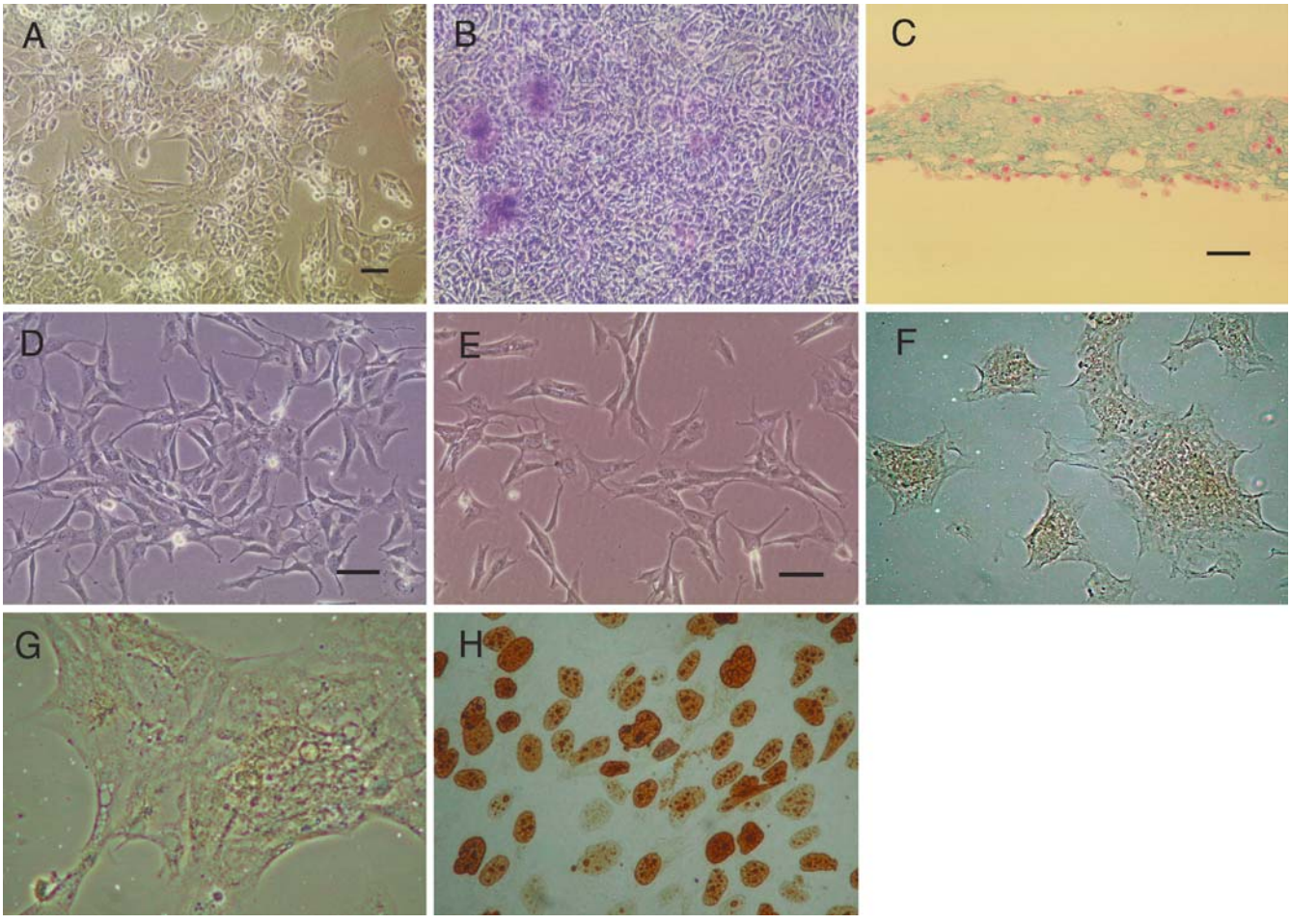

Fig. 1 Phase-contrast photomicrograph of HCS-TG cells (passage 11) shows polygonal shape 10 days after inoculation in monolayer culture (**A**). *Scale bars*. 100 μm. HCS-TG cells demonstrate several nodules at confluency, which show metachromasia with toluidine blue staining (**B**). Cross-section of the membrane by HCS-TG cells 4 weeks after inoculation. Abundant extracellular matrix shows *light blue* in alcian blue staining. *Scale bar*. 50 μm (**C**). Phase-contrast photomicrograph of HCS-TG C3 (**D**) and E2 (**E**) cells (passage15 each) shows *polygonal shape* 5 days after inoculation in monolayer culture. *Scale bars*. 100 μm. Immunohistochemical staining of HCS-TG E2 cells showing S-100 protein. Magnification ×10 (**F**) and ×40 (**G**). HCS-TG C3 cells were positive for Mib1(Ki-67) ×40 (**H**)

modal numbers ranged from 67 to 71 in C3 and from 62 to 73 in E2. The karyotype analysis on C3 indicated that 69,XX,-Y, +add(1)(p36),+add(1)(q11) ×2, add(2)(q37), +i(3)(p10), del(3)(q26), -4, add(5)(p15)×2, add(5)(p15),-6,del(6)(p23), del(7)(q22), add(9)(q34), add(9)(q22), +10, +add(11)(q13), del(11)(q?22)×2, +add(12)(q13), +del(12)(q24), +add(13)(p11), -14, -15×2, -16,add(16)(p13), -17, add(17)(p11), add(18)(q23), add(18)(q23), del(20)(q13) ×2, +21,+22×3, +15mar.

The karyotype analysis on E2 indicated that 67, XX, add(1)(p11), +3, +add(5)(p11), +add(5)(p11)×2, del(6)(p23), add(6)(q11), +add(7)(q22)×2, add(8)(q11), add(8)(q24), add(9)(q34), der(9)add(9)(p22)add(9)(q34), +add(11)(p11), add(11)(p11), add(11)(q13), add(12)(p11), add(13)(q32), add(13)(p32), -15, -15, add(16)(p13), add(16)(q24), add(17)(p11), add(17)(p13), add(18)(q23), add(18)(q23), add(20)(p13), del(20)(q13), +21, add(21)(p11)×2, +del(22)(q13), +13mar.

Tumorigenicity in athymic mice

In four of five mice, tumors developed following the inoculation of HCS-TG cells. Tumors were observed 1 week after inoculation and grew to a size of 5 cm in diameter 3 months later (Fig. 3A). Histological examinations of the xenografts showed abundant homogeneous matrix, which was stained deep pink-red with safranin O and showed metachromasia with toluidine blue. Chondrocyte-like tumor cells demonstrated nuclear atypism compatible with grade-2 CS (Fig. 3B). Immunohistochemically, the tumor cells were positive for S-100 protein and Ki-67 (Mib1) (Fig. 3C, D). However, when HCS-TG C3 and E2 cells were inoculated, no tumors developed. Therefore, HCS-TG C3 and E2 are non-tumorigenic, whereas HCS-TG has tumorigenicity.

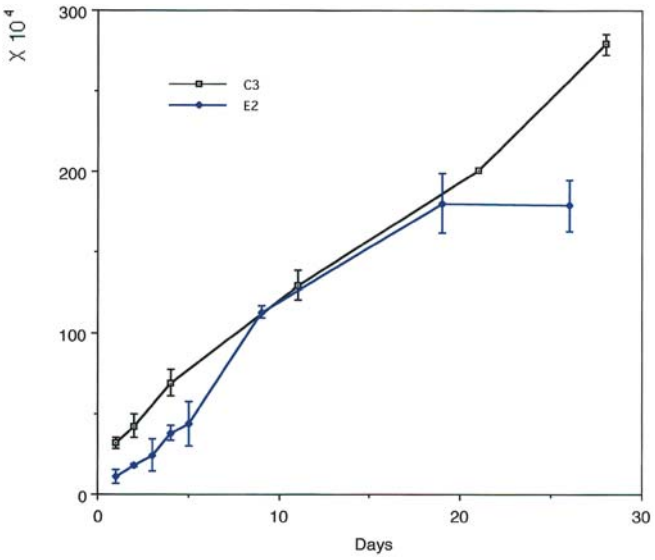

Fig. 2 Growth curves of HCS-TG C3 and E2. Each point represents the mean value (±SD) of triplicate determinations

Proteoglycan synthesis on HCS-TG C3 and E2

C3 and E2 cells showed blue in alcian blue staining, and semi-quantitative analysis revealed that both cell lines have high intensity staining. C3 cells in the medium with 10% FCS+10% CS showed higher intensity than with 20% FCS (Fig. 4A). Quantitative analysis using the DMMB method indicated that both cell lines produced proteoglycan in each medium (Fig. 4B).

Expression of m RNA of type-I, -II, -IX, -XI collagen and aggrecan core protein (RT-PCR)

The expected nucleotide length of the amplified products for type-I, -II, -IX, -X, -XI (α1), -XI (α2) and aggrecan core proteins were 461, 384, 685, 622, 465, 348, and 560 bp, respectively. Each type of collagen and aggrecan core protein-specific RT-PCR products except type-IX collagen were identified in both C3 and E2 cell lines (Fig. 5, Fig. 6A).

Protein expression of type-I and -II collagens (Western blotting)

The protein expression of type-II collagen in C3 and E2 cells was identified. The expression of type-I collagen was not detected in either cell line (Fig. 6B).

Determination of MMP activity and expression

Matrix degradation by MMP-2 and -9 with/without cytokines (IL-9, TNF and LPS) stimulation were found in C3 and E2 cells in gelatin zymography. Amplification of MMP-3 was detected only in C3 when treated with TNF (Fig. 7). This result was also achieved in Western blotting (Fig. 8).

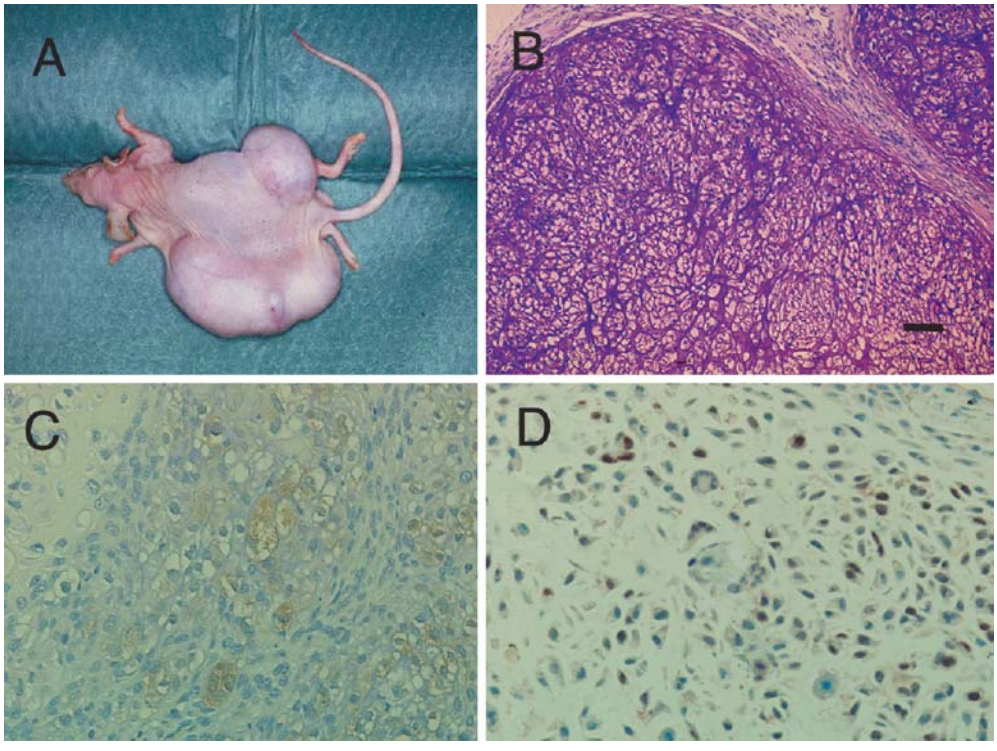

Fig. 3 Huge tumor (xenograft) on bilateral flank of nude mouse 3 months after inoculation of HCS-TG (cells) (**A**). Photomicrograph of xenograft shows abundant homogeneous matrix, which stains metachromasia with toluidine blue. Chondrocyte-like tumor cells demonstrated nuclear atypism. *Scale bar*. 100 μm (**B**). Immunohistochemical staining was positive for S-100 protein (**C**) and Mib 1(Ki-67) (**D**) on xenograft. Mib1 index was 20%

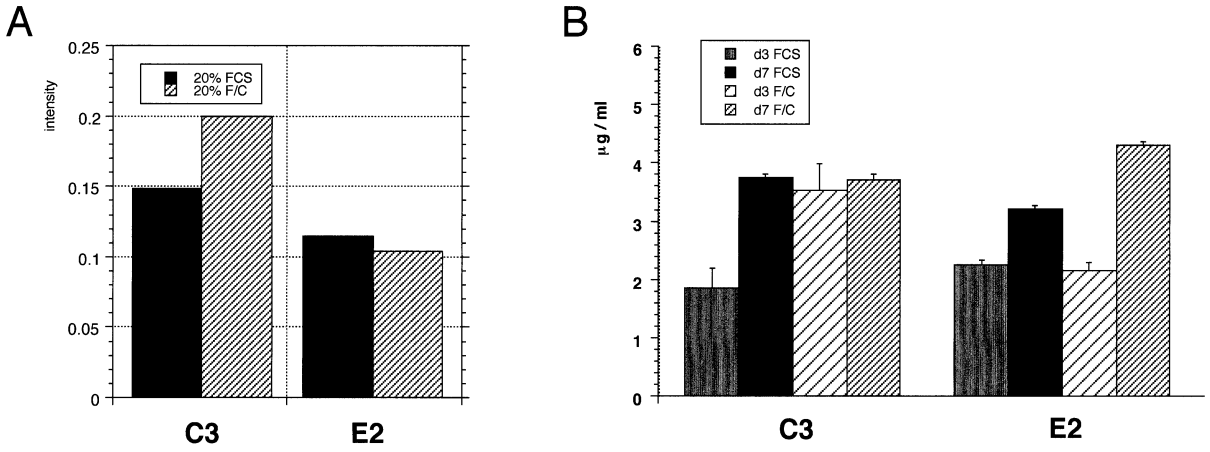

Fig. 4 Semi-quantitative analysis of the extracted dye in alcian blue staining revealed that staining intensity in C3 and E2 are high. C3 cells in the medium with 10% fetal calf serum+10% calf serum (F/C) showed higher intensity than with 20% fetal calf serum (**A**). Quantitative analysis using dimethylmethylene blue method revealed that glycosaminoglycan production in both C3 and E2 from early phase in monolayer culture. F/C: 10% fetal calf serum+10% calf serum (**B**)

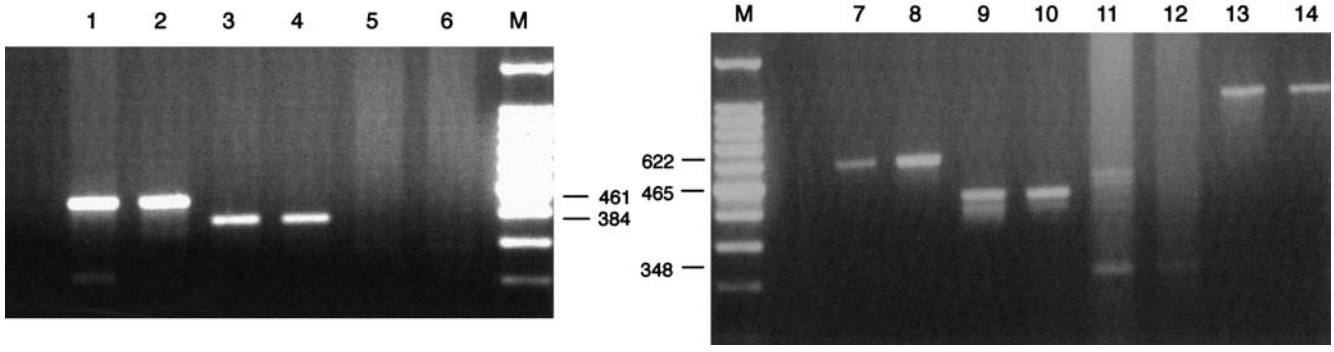

Fig. 5 Reverse-transcription polymerase chain reaction analysis of type-I, -II, -IX, -X, -XI (α1), -XI (α2) collagens in HCS-TG C3 and E2. *Lane M*, 1 kilobase DNA; *lane 1*, type-I collagen (C3); *lane 2*, type-I collagen (E2); *lane 3*, type-II collagen (C3); *lane 4*, type-II collagen (E2); *lane 5*, type-IX collagen (C3); *lane 6*, type-IX collagen (E2), *lane 7*, type-X collagen (C3), *lane 8*, type-X collagen (E2); *lane 9*, type-IX (α1) collagen (C3); *lane 10*, type-IX (α1) collagen (E2); *lane 11*, type-IX (α2) collagen (C3); *lane 12*, type-IX (α2) collagen (E2); *lane 13*, G3PDH (C3); *lane 14*, G3PDH (E2)

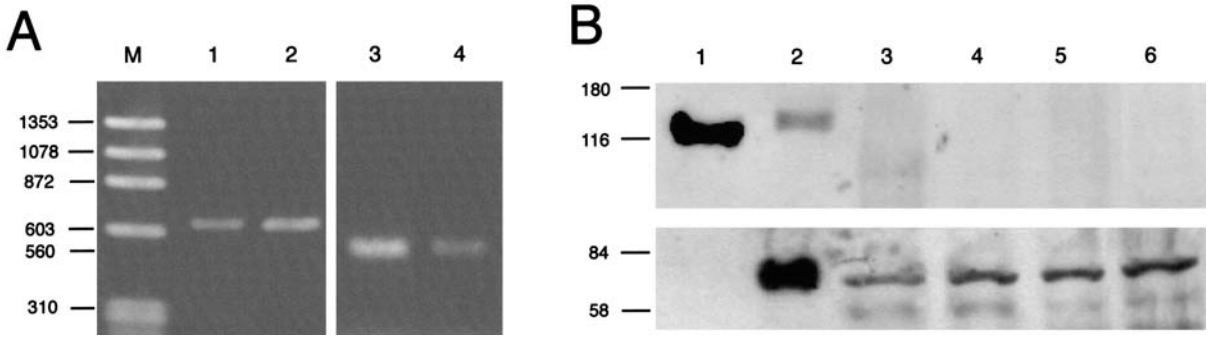

Fig. 6 Reverse-transcription polymerase chain reaction analysis of aggrecan core protein in HCS-TG C3 and E2. *Lane 1*, β actin (C3); *lane 2*, β actin (E2); *lane 3*, aggrecan core protein (C3); *lane 4*, aggrecan core protein (E2) (**A**). Western blotting of type-I and -II collagens in HCS-TG C3 and E2. Expression of type-II collagen was detected in both C3 and E2, but not type-I collagen. *Lane 1*, type-I collagen standard (STD) (positive control); *lane 2*, type-II collagen STD (positive control); *lane 3*, C3 cultured with fetal calf serum (FCS); *lane 4*, E2 cultured with FCS; *lane 5*, C3 cultured with FCS and calf serum (CS); *lane 6*, E2 cultured with FCS and CS (**B**)

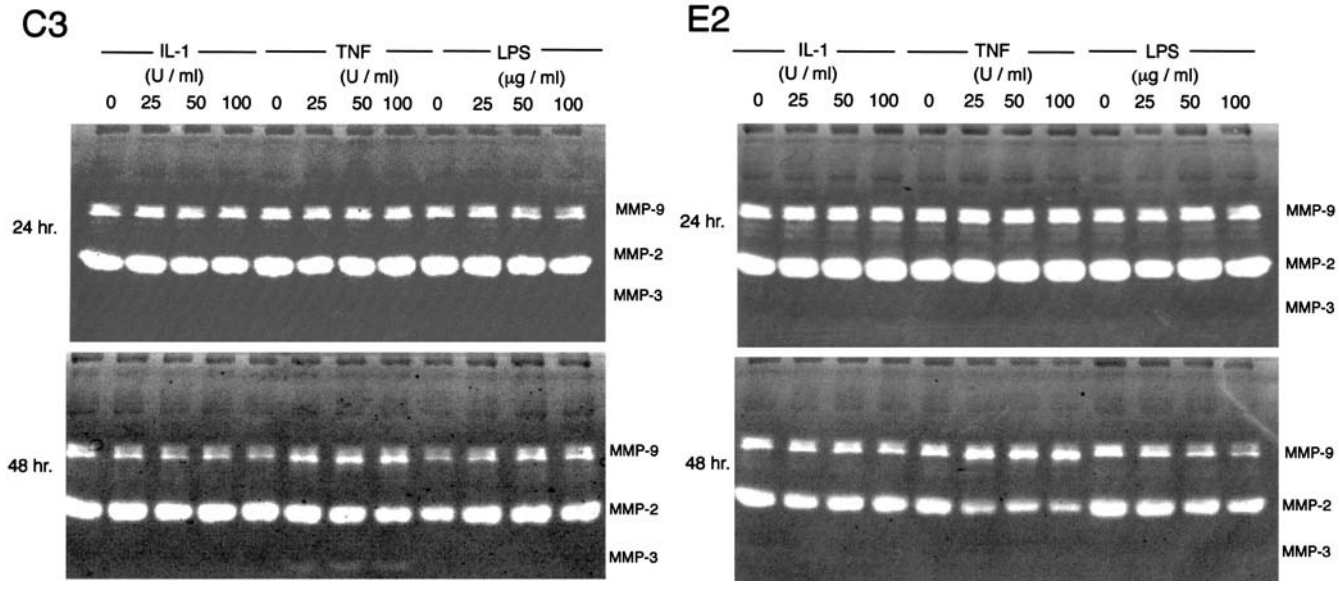

Fig. 7 Gelatin zymography of matrix metalloproteinase (MMP)-2, -3 and -9 with IL-1, tumor necrosis factor (TNF) and lipopolysaccharide on C3 and E2. Matrix degradation in MMP-2 and -9 with/without cytokines treatment in C3 and E2 cells were found. Amplification of MMP-3 was detected only in C3 with TNF treatment

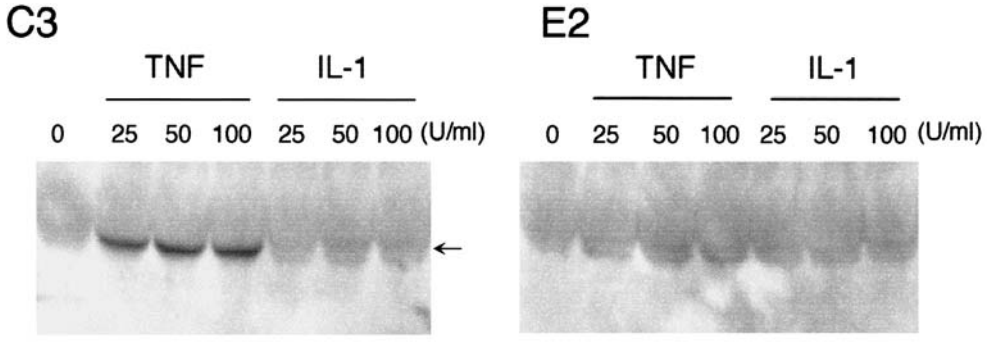

Fig. 8 Western blotting of matrix metalloproteinase (MMP-3) in C3 and E2 cells. Amplification of MMP-3 was detected only in C3 with tumor necrosis factor treatment

Discussion

Human cartilaginous matrix includes type-II, -IX, -X [8, 30], -XI [7, 32] collagens, and cartilage proteoglycan includes core protein, chondroitin sulfates, hyaluronic acid and keratan sulfate [21, 29, 33, 34]. These are generally found in various normal cartilages. The types of collagens in the matrix of CS are similar to normal cartilage and have been detected in in vitro studies, that is, type-II [10, 24, 45], -IX [11], -X [10], -XI [11] collagens. However, type-I collagen has been detected in two human CS cell lines [10, 24]. In immunohistological studies, type-I collagen has also been demonstrated in grade-1 and grade-2 CS. Immunoreactivities to type-II collagen were detected in all grades; however, they were relatively weak in grade-3 CS [47]. Type-II and -IX collagens are widely detected immunohistochemically in enchondroma and CS [22]. HCS-TG C3 and E2 expressed many cartilage-specific collagen mRNAs, including type-II, -X and -XI. Moreover, mRNA of type-I collagen was found in each cell line, although its protein expression was not detected on Western blotting. This is probably because of low expression of type-I collagen in these tumor cells. Expression of type-I collagen increases, while that of type-II collagen decreases upon subculturing in cultured chondrocytes [13, 35]. In the same manner, type-I collagen increases with loss of cartilaginous phenotype in CS [2]. We believe that CS cell, which expresses type-I collagen at mRNA level, has potency to lose cartilaginous phenotype and obtain more malignant characteristics. Previous authors have reported that several cell lines with chondrocytic phenotypes have different types of collagens as follows: HCS 2/8 [45] expressed type-II collagen and not type-I collagen; CS-OKB [10] expressed type-I, -II, -III, -IV and -X collagens; OUMS-27 [24] expressed type-I,-II and -III collagens; Ch-1 [11] expressed type-IX and -XI collagens and ch-2879 [16] expressed type-II collagen. Thus, each CS cell line has expressed various types of collagens, including non-cartilaginous collagens, and their phenotypes were distinctive from each other. CS cells probably have different cartilage differentiation from

normal cartilage, and they often have undifferentiated mesenchymal characteristics.

Analysis of proteoglycan in the matrix of CS showed that keratan sulfate and chondroitin sulfate were dominant [5, 18, 28, 33, 44, 46] and that there were no significant differences between the grades and distribution of glycosaminoglycans (chondroitin 4-, chondroitin 6- and keratan sulfates) [27]. However, the results for hyaluronic acid are variable [18, 44]. Herwing [18] indicated that an increase in the proportion of keratan sulfate was associated with CS grade. Aggrecan [10, 11] biglycan and decorin [11] were demonstrated in two cell lines. Though a detailed analysis of the distribution of proteoglycan was not carried out in this study, the extracellular matrices of HCS-TG cells in high-density culture and those of C3 and E2 cells in monolayer culture were shown to have produced proteoglycan from the results of alcian blue and toluidine blue staining. In clonal-cell line C3 and E2, the high intensity of alcian blue staining and the results of quantitative analysis (DMMB method) proved the existence of proteoglycan synthesis. Moreover, the expression of mRNA of aggrecan core protein was detected in both cell lines.

It is well known that S-100 protein also expresses in various cartilaginous tumors [1, 36, 38, 50]. Several authors reported expression of S-100 protein in cultured CS cells [10, 16]. In this study, immunohistochemical staining was positive for S-100 protein on both clonal cells and xenograft.

Thus, HCS-TG C3 and E2 have chondrocytic phenotypes, including many types of collagen and proteoglycan that are characteristic of cartilage. These characteristics are unique compared with the cell lines with cartilaginous phenotypes reported previously [4, 10, 11, 24, 45].

The identification of consistent chromosomal translocations associated with tumors is one of the recent advances in the molecular study of mesenchymal tumors. These translocations result in recombined fusion genes. In extraskeletal myxoid CS, the gene fusion is EWS-CHN, due to the t(9:22)(q22;q11). However, in conventional CS, neither specific chromosomal aberrations nor fusion genes are known; whereas, some karyotype analyses of CS have revealed many numerical and structural chromosomal aberrations, including chromosomal rearrangements and deletions of entire chromosomes [6, 12, 15, 19, 26]. In this study, both C3 and E2 cells exhibited represent complex chromosomal aberrations, however break-points concerning tumor genetics were unknown.

Further characterization of HCS-TG C3 and E2 indicated the expression of MMP-2 and -9. MMP-3 was detected only in C3 with TNF treatment; it was not detected without cytokines in either cell line. MMP-1, -2, -3, -9 and -13 play a role in the degradation of normal cartilage, including the resolution of proteoglycans and collagens. Several studies of human cartilage chondrocytes have demonstrated that IL-1 stimulates proteogylcanase (MMP-3) [17] and that recombinant human IL-1α or TNF α causes increased production of latent MMPs (collagenase and caseinase) [43] or MMP-3 [37]. From the results of previous reports, the MMPs and the reactions of the cytokines of HCS-TG C3 and E2 have different characteristics to normal or degenerated chondrocytes. However, many human tumors express various MMPs, the expression of which may play a role in the proliferation and metastasis of tumor cells [39]. A study by Kawashima suggested that the increased expression of MMP-1 and -9 and the decrease in MMP-3 expression are associated with malignant cartilaginous tumors [23]. Berend described that a high ratio of MMP-1 to tissue inhibitor of MMP-1 in CS may be indicative of a more invasive and aggressive tumor and of a worse prognosis [3]. Another study indicated that MMP-2 or the tissue inhibitor of MMP-2 demonstrates a significant correlation with CS grade [41]. Furthermore, the expression of MMP-13 is found in CS immunohistochemically in contrast to its absence in chondromas [49]. According to these results, the expression of MMP-2 and -9 in HCS-TG C3 and E2 seems likely to be one of their malignant manifestations.

In conclusion, new clonal-cell lines HCS-TG C3 and E2 derived from human chondrosarcoma have been established. These cells are morphologically chondrocytic in serial monolayer cultures and express chondrocytic phenotypes, including type-II, -X, -XI collagens and proteoglycans. To our knowledge, there have been few human CS cells that express the majority of cartilage collagens. We believe that these cell lines will be very useful in the investigation of new modalities for CS treatment and for research into cartilage metabolism.

Acknowledgements We are grateful to Noriyuki Tsumaki, M.D. Ph.D., Takanobu Nakase, M.D. Ph.D., and Tetsuya Tomita, M.D. Ph.D., for provision of primers of collagens and to Akihiko Matsumine, M.D. Ph.D., and Yukihiro Isogai, Ph.D., for technical assistance.

References

1. Aigner T, Dertinger S, Vornehm SI, Dudhia J, von der Mark K, Kirchner T (1997) Phenotypic diversity of neoplastic chondrocytes and extracellular matrix gene expression in cartilaginous neoplasm. Am J Pathol 150:2133–2141
2. Aigner T, Müller S, Neureiter D, lllstrup DM, Kirchner T, Björnson J (2002) Prognostic relevance of cell biologic and biochemical features in conventional chondrosarcomas. Cancer 94:2273–2281
3. Berend KR, Toth AP, Harrelson JM, Layfield LJ, Hey LA, Scully SP (1998) Association between ratio of matrix metalloproteinase-1 to tissue inhibitor of metalloproteinase-1 and local recurrence, metastasis, and survival in human chondrosarcoma. J Bone Joint Surg Am 80:11–17
4. Block JA, Inerot S, Gitelis S, Kimura JH (1991) Synthesis of chondrocytic keratan sulphate-containing proteoglycans by human chondrosarcoma cells in long-term cell culture. J Bone Joint Surg Am 73:647–658
5. Boström H, Friberg U, Larsson KS, Nilsonne U (1968) In vitro incorporation of S^{35}-sulfate in chondrosarcomatous tissue. Acta Orthop Scandinav 39:58–72
6. Bridge JA, Bhatia PS, Anderson JR, Neff JR (1993) Biologic and clinical significance of cytogenetic and molecular cytogenetic abnormalities in benign and malignant cartilaginous lesions. Cancer Genet Cytogenet 69:79–90

7. Burgeson R (1998) New collagens, new concepts. Ann Rev Cell Biol 4:551–577
8. Burgeson RE, Hollister DW (1979) Collagen heterogeneity in human cartilage: identification of several new collagen chains. Biochem Biopys Res Commun 87:1124–1131
9. Chandrasekhar S, Esterman M, Hoffman HA (1987) Microdetermination of proteoglycans and glycosaminoglycans in the presence of guanidine hydrochloride. Anal Biochem 161:103–108
10. Chano T, Okabe H, Saeki Y, Ishizawa M, Matsumoto K, Hukuda S (1998) Characterization of a newly established human chondrosarcoma cell line, CS-OKB. Virchows Arch 432: 529–534
11. Chansky H, Robbins JR, Cha S, Raskind WH, Conrad EU, Sandell LJ (1998) Expression of cartilage extracellular matrix and potential regulatory genes in a new human chondrosarcoma cell line. J Ortop Res 16:521–530
12. Dijkhuizen T, Berg E, Molenaar WM, Oosterhuis JW, Dam A, Wiersema J, Koops H, de Jong B (1994) Cytogenetics as a tool in the histologic subclassification of chondrosarcoma. Cancer Genet Cytogenet 76:100–105
13. Elima K, Vuorio E (1989) Expression of mRNAs for collagens and other matrix components in dedifferentiating and redifferentiating human chondrocytes in culture. FEBS Lett 258:195–198
14. Evans HL, Ayala AG, Romsdahl MM (1977) Prognostic factors in chondrosarcoma of bone. A clinicopathologic analysis with emphasis on histologic grading. Cancer 40:818–831
15. Fletcher JA, Lipinski KK, Weidner N, Morton CC (1989) Complex cytogenetic aberrations in a well-differentiated chondrosarcoma. Cancer Genet Cytogenet 41:115–121
16. Gil-Benso R, Lopez-Gines C, López-Guerrero JA, Carda C, Callaghan RC, Navarro S, Ferrer J, Pellín A, Llombart-Bosch A (2003) Establishment and characterization of a continuous human chondrosarcoma cell line, ch-2879: comparative histologic and genetic studies with its tumor of origin. Lab Invest 83:877–887
17. Gowen M, Wood DD, Ihrie EJ, Meats JE, Russell RGG (1984) Stimulation by human interleukin 1 of cartilage breakdown and production of collagenase and proteoglycanase by human chondrocytes but not by human osteoblasts in vitro. Biochim Biophys Acta 797:186–193
18. Herwig J, Roessner A, Buddecke E (1986) Isolation and characterization of proteoglycans and glycosaminoglycans from human chondrosarcoma. Exp Mol Pathol 45:118–127
19. Hirabayashi Y, Yoshida MA, Ikeuchi T, Ishida T, Kojima T, Higaki S, Machinami R, Tonomura A (1992) Chromosomal rearrangements at 12q13 in two cases of chondrosarcomas. Cancer Genet Cytogenet 60:35–40
20. Huvos AG (1991) Chondrosarcoma including spindle-cell (dedifferentiated) and myxoid chondrosarcoma; mesenchymal chondrosarcoma. In: Huvos AG (ed) Bone tumors. W.B. Saunders Company, Philadelphia, pp 343–381
21. Kaplan D, Meyer K (1959) Ageing of human cartilage. Nature (London) 183:1267–1268
22. Kawashima A, Ueda Y, Tsuchiya H, Tomita K, Nagai Y, Nakanishi I (1993) Immunohistochemical localization of collagenous proteins in cartilaginous tumors: characteristic distribution of type IX collagen. J Cancer Res Clin Oncol 120:35–40
23. Kawashima A, Okada Y, Nakanishi I, Ueda Y, Iwata K, Roessner A (1997) Immunolocalization of matrix metalloproteinases and tissue inhibitors of metalloproteinases in human chondrosarcomas. Gen Diagn Pathol 142:129–137
24. Kunisada T, Miyazaki M, Mihara K, Gao C, Kawai A, Inoue H, Namba M (1998) A new human chondrosarcoma cell line (OUMS-27) that maintains chondrocytic differentiation. Int J Cancer 77:854–859
25. Lee FY, Mankin HJ, Fondren G, Gebhardt MC, Springfield DS, Rosenberg, AE, Jennigs, LC (1999) Chondrosarcoma of bone: an assessment of outcome. J Bone Joint Surg Am 81:326–337
26. Mandahl N, Heim S, Arheden K, Rydholm A, Willén H, Mitelman F (1990) Chromosomal rearrangements in chondromatous tumors. Cancer 65:242–248
27. Mankin HJ, Cantley KP, Lippiello L, Schiller AL, Campbell CJ (1980) The biology of human chondrosarcoma. I. Description of the cases, grading, and biochemical analyses. J Bone Joint Surg Am 62:160–175
28. Mankin HJ, Cantley KP, Schiller AL, Lippiello L (1980) The biology of human chondrosarcoma. II. Variation in chemical composition among types and subtypes of benign and malignant cartilage tumors. J Bone Joint Surg Am 62:176–188
29. Mathews MB, Glacov S (1966) Acid mucopolysaccharide patterns in aging human cartilage. J Clin Invest 45:1103–1111
30. Miller E, Gay S (1987) The collagens: an overview and update. In: Colowick SP and Kaplan NO (eds) Methods in enzymology. 144 Academic Press, Inc., London, pp 3–41
31. Mirra JM, Eckardt JJ (1989) Enchondroma versus chondrosarcoma. In: Mirra JM (ed) Bone tumors. Lea & Febiger, Philadelphia, pp 476–535
32. Morris NP, Bächinger HP (1987) Type XI collagen is a heterotrimer with the composition (1 alpha, 2 alpha, 3 alpha) retaining non-triple-helical domains. J Biol Chem 262:11345–11350
33. Mourão PAS, Rozenfeld S, Laredo J, Dietrich CP (1976) The distribution of chondroitin sulfates in articular and growth cartilage of human bones. Biochem Biophys Acta 428:19–26
34. Mourão PAS, Michelacci YM, Toledo OMS (1979) Glycosaminoglycans and proteoglycans of normal and tumoral cartilages of humans and rats. Cancer Res 39:2802–2806
35. Müller PK, Lemmen C, Gay S, Gauss V, Kühn K (1977) Immunochemical and biochemical study of collagen synthesis by chondrocytes in culture. Exp Cell Res 108:47–55
36. Nakamura Y, Becker LE, Marks A (1983) S-100 protein in tumors of cartilage and bone. 52:1820–1824
37. Okada Y, Shinmei M, Tanaka O, Naka K, Kimura A, Nakanishi I, Bayliss MT, Iwata K, Nagase H (1992) Localization of matrix metalloproteinase3 (stromelysin) in osteoarthritic cartilage and synovium. Lab Invest 66:680–690
38. Okajima K, Honda I, Kitagawa T (1988) Immunohistochemical distribution of S-100 protein in tumors and tumor-like lesions of bone and cartilage. Cancer 61:792–799
39. Powell WC, Matrisian LM (1996) Complex roles of matrix metalloproteinases in tumor progression. In: Günthert U, Birchmeier W (eds) Attempts to understand metastasis formation I. Springer Verlag, Berlin Heidelberg New York, pp 1–21
40. Saito S, Katoh M, Matsumoto M, Matsumoto S, Masuho Y (1997) Collagen degradation induced by the combination of IL-1 alpha and plasminogen in rabbit articular cartilage explant culture. J Biochem 122:49–54
41. Sakamoto A, Oda Y, Iwamoto Y, Tsuneyoshi M (1999) Expression of membrane type 1 matrix metalloproteinase, matrix metalloproteinase 2 and tissue inhibitor of metalloproteinase 2 in human cartilaginous tumors with special emphasis on mesenchymal and dedifferentiated chondrosarcoma. J Cancer Res Clin Oncol 125:541–548
42. Sheth DS, Yasko AW, Johnson ME, Alaya AG, Murray JA, Romsdahl MM (1996) Chondrosarcoma of the pelvis. Prognostic factors for 67 patients treated with definitive surgery. Cancer 15:745–750
43. Shinmei M, Masuda K, Kikuchi T, Shimomura Y (1989) The role of cytokines in chondrocyte mediated cartilage degradation. J Rheumatol 16[Suppl]:32–34
44. Sweet MBE, Thonar EJAL, Immelman AR (1976) Glycosaminoglycans and proteoglycans of human chondrosarcoma. Biochem Biophys Acta 437:71–86
45. Takigawa M, Tajima K, Pan HO, Enomoto M, Kinoshita A, Suzuki F, Takano Y, Mori Y (1989) Establishment of a clonal human chondrosarcoma cell line with cartilage phenotypes. Cancer Res 49:3996–4002
46. Thonar EJA, Sweet MBE, Immelman AR, Lyons G (1979) Structural studies on proteoglycan from human chondrosarcoma. Arch Biochem Biophys 194:179–189

47. Ueda Y, Oda Y, Tsuchiya H, Tomita K, Nakanishi I (1990) Immunohistological study on collagenous proteins of benign and malignant human cartilaginous tumours of bone. Virchows Archiv 417:291–297
48. Unni KK (1996) Chondrosarcoma. In: Unni KK (ed) Dahlin's bone tumors. Lippincott-Raven, Philadelphia, pp 71–108
49. Uría JA, Balbín M, López JM, Alvares J, Vizoso F, Takigawa M, López-Otín C (1998) Collagenase-3 (MMP-13) expression in chondrosarcoma cells and its regulation by basic fibroblast growth factor. Am J Pathol 153:91–101
50. Weiss APC, Dorfman HD (1986) S-100 protein in human cartilage lesions. J Bone Joint Surg Am 68:521–526

Virchows Arch (2004) 444:587–589
DOI 10.1007/s00428-004-1010-8

CASE REPORT

F. Garavan · R. Grainger · M. Jeffers

Endometrioid carcinoma of the urinary bladder complicating vesical Mullerianosis: a case report and review of the literature

Received: 27 November 2003 / Accepted: 3 March 2004 / Published online: 23 April 2004

Abstract Endometriosis of the urinary bladder is uncommon, and malignant transformation within vesical endometriosis is extremely rare. Vesical endometriosis and Mullerianosis can cause problems in differential diagnosis with vesical neoplasm, and, conversely, primary vesical neoplasm arising in endometriosis can be difficult to distinguish from secondary vesical involvement. Mullerianosis has rarely been described in the urinary bladder. A case of endometrioid adenocarcinoma of the urinary bladder is reported, which illustrates the difficulties in diagnosis and the importance of morphology and ancillary studies in establishing the correct diagnosis.

Keywords Endometriosis · Mullerianosis · Bladder · Endometrioid · CD10

Introduction

Endometriosis is defined as the presence of endometrial tissue outside the uterus [7]. The most common sites affected are the ovaries, uterine ligaments, recto- and vesicovaginal septae, pelvic peritoneum, cervix, labia and vagina. Less commonly, it can involve the urinary bladder, ureters, intestines, skin and laparotomy scars. The urinary bladder is involved in less than 1% of cases [1, 8, 10, 11]. Malignant transformation of endometriosis is well documented, with endometrioid and clear-cell carcinomas being the most common malignancies described. Malignant transformation of Mullerian-derived epithelium in extra-gonadal sites is exceeding rare. Epithelial structures of Mullerian origin other than endometriosis, including endocervical and tubal-type epithelium, have been described in extra-uterine sites, and the term "Mullerianosis" has been proposed for lesions containing admixtures of endosalpingiosis, endometriosis and endocervicosis at any site [14]. Only five cases of benign proliferation of Mullerian glandular epithelium, other than endometriosis, within the urinary bladder have been reported [5, 6, 14]. We report a case of endometrioid carcinoma arising within endometriosis of the urinary bladder.

F. Garavan · M. Jeffers (✉)
Department of Cellular Pathology,
The Adelaide and Meath Hospital,
Tallaght, Dublin 24, Ireland
e-mail: michael.jeffers@amnch.ie
Tel.: +353-1-4143929
Fax: +353-1-4143980

R. Grainger
Department of Urology,
The Adelaide and Meath Hospital,
Tallaght, Dublin 24, Ireland

Case report

A 53-year-old female, 2 years postmenopausal, was referred for investigation of intermittent painful gross haematuria over a 6-week period. She was otherwise well and was not taking hormone replacement therapy.

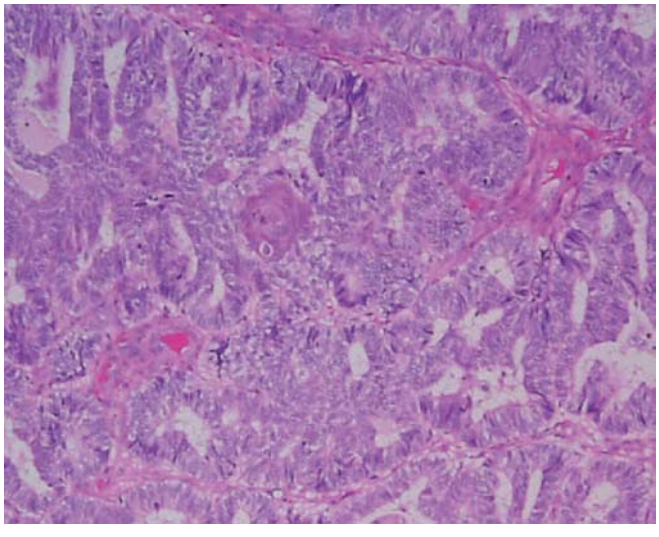

Fig. 1 Adenocarcinoma of endometrioid type infiltrating bladder wall (haematoxylin and eosin ×100)

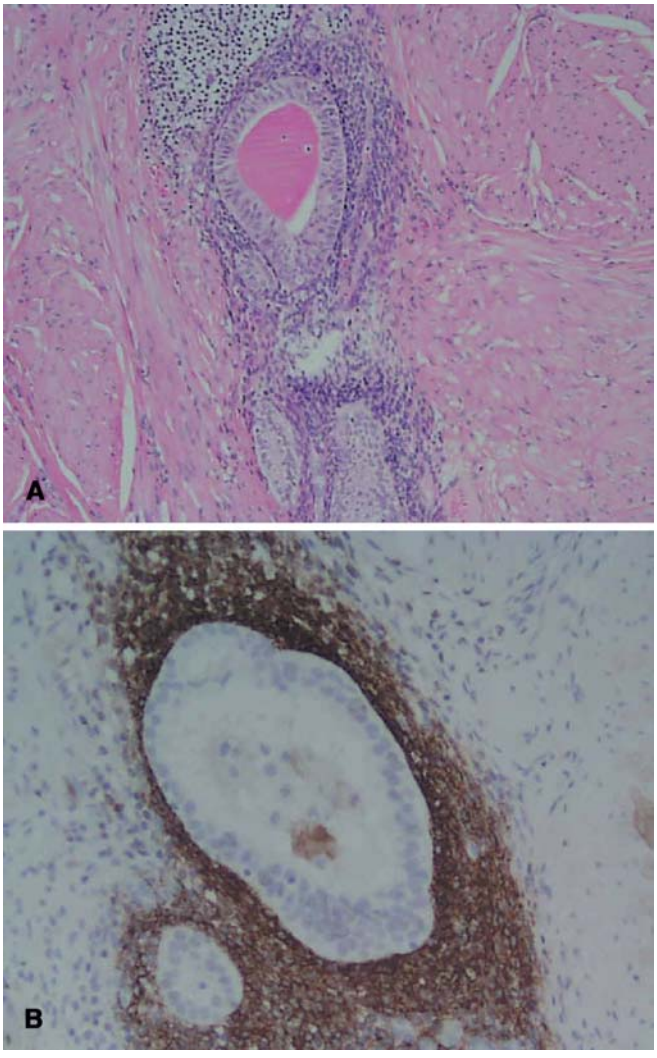

Fig. 2 a Endometriosis within the bladder wall (haematoxylin and eosin ×200). **b** Endometriosis within the bladder wall: CD 10 immunohistochemistry demonstrates endometrial type stroma (CD10 ×200)

Intra-venous pyelogram suggested a filling defect in the bladder. Cystoscopy confirmed a tumour in the posterior wall of the bladder, 1 cm in diameter. The tumour was resected transurethrally.

Bladder tumour chippings at presentation contained fragments of bladder wall infiltrated by adenocarcinoma with typical morphology of endometrioid type (Fig. 1), including areas of squamous differentiation. Tumour infiltrated within the lamina propria underneath intact urothelium, and invasion of muscularis propria was present. Multiple foci of benign Mullerian tissue, including foci of endometriosis (Fig. 2a) and glands of endocervical and tubal type were present within the bladder wall. Atypical hyperplastic changes were present within endometriotic foci (Fig. 3). Immunohistochemical staining for CD10 demonstrated endometrial stroma surrounding glands in foci of benign and atypical endometriosis (Fig. 2b).

Subsequent transurethral resection contained foci of residual endometriosis and some foci of endocervicosis. Pelvic computed tomography scan demonstrated adhesions between the uterus and bladder and raised the possibility of a primary endometrial neoplasm with secondary involvement of the bladder. The patient subsequently underwent hysterectomy with resection of the posterior wall of the bladder, which was adherent to the uterus. A single microscopic focus of endometrioid-type adenocarcinoma was present on the serosal aspect of the anterior wall of the uterus, but there was no evidence of a primary endometrial carcinoma. Multiple foci of endometriosis were present within the posterior wall of the bladder, and ovarian endometriosis was also present.

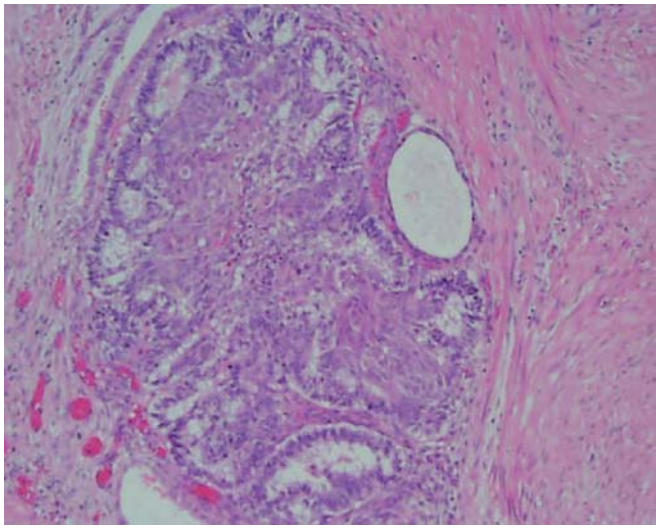

Fig. 3 Atypical hyperplasia in endometriosis (haematoxylin and eosin ×200)

Discussion

Neoplastic transformation is a rare complication of endometriosis, documented in 0.3–0.8% of cases of ovarian endometriosis [7]. Of neoplasms, 75% complicating endometriosis arise in the ovary, and the majority (almost 70%) of these are of endometrioid type. The most common extra-ovarian site of neoplastic transformation in endometriosis is the rectovaginal septum, and at least 90% of cases of carcinoma arising in extra-ovarian endometriosis are of endometrioid type [7]. Clear-cell carcinoma is the second most common malignancy arising in endometriosis, and a small number of cases of a variety of other tumour types have been described.

The urinary bladder is believed to be involved in endometriosis in approximately 1% of all cases, and, until recently, only endometrioid-type proliferation was described. More recently, however, Mullerianosis of the urinary bladder has been reported [5, 6, 14]. Endometriosis and Mullerianosis of the urinary bladder can be difficult to distinguish, both clinically and radiologically, from vesical neoplasm.

Malignant transformation of endometriosis within the urinary bladder is a rare phenomenon, with only six cases to date reported in the literature [2, 3, 4, 13]. Of these cases, five were adenocarcinomas and one was adenosarcoma.

Criteria for establishing endometriosis as a precursor lesion of carcinoma in foci of extra-gonadal endometriosis were originally proposed as: (i) there must be

clear evidence of endometriosis present in close proximity to the tumour; (ii) no other primary tumour can be found, (iii) the histological appearance must be such that its origin from endometriosis is possible. Demonstration of a dysplastic phase between the benign endometriosis and the carcinoma may be the most convincing feature. Endometriosis within the bladder wall must also be distinguished from urachal glandular remnants, and vesical endometrioid adenocarcinoma arising in endometriosis must be distinguished from primary vesical adenocarcinoma, including adenocarcinoma arising in urachal remnants. Demonstration of endometrial-type stroma is crucial in this regard. Expression of CD10 by endometrial stromal cells is a sensitive and specific marker of endometriosis [9, 12] in extra-gonadal sites. In the case reported here, strong CD10 expression was demonstrated in many foci of endometriosis in the bladder wall, confirming endometriosis and supporting the diagnosis of endometrioid carcinoma ex endometriosis. Interestingly, CD10 was negative in foci of endocerviciosis.

Vesical Mullerianosis is uncommon, and neoplastic transformation of vesical Mullerianosis is even less common. Close attention to morphology, particularly the presence of atypical hyperplasia within foci of endometriosis/Mullerianosis, is central to correct diagnosis. Demonstration of CD10 expression by endometrial stromal cells in foci of endometriosis is a useful adjunct in the diagnosis of endometrioid carcinoma arising in endometriosis in extra-gonadal sites.

References

1. Arap Neto W, Lopes RN, Cury M, Montelatto NI, Arap S (1984) Vesical endometriosis. Urology 24:271–274
2. Balat O, Kudelka AP, Edwards CL, Silva E, Kavanagh JJ (1996) Malignant transformation in endometriosis of the urinary bladder: case report of clear cell adenocarcinoma. Eur J Gynaecol Oncol 17:13–16
3. Bruson G (1988) Malignant extraovarian endometriosis: two case reports and review of the literature. Gynaecol Oncol 30:123–130
4. Chor PJ, Gaum LD, Young RH (1993) Clear cell adenocarcinoma of the urinary bladder: report of a case of probable Mullerian origin. Mod Pathol 6:225–228
5. Clement PB, Young RH (1992) Endocervicosis of the urinary bladder. Am J Surg Pathol 16:533–542
6. Donne C, Vidal M, Buttin X, Becerra P, Carvia R, Zuluaga A, Nogales FF (1998) Mullerianosis of the urinary bladder: clinical and immunohistochemical findings. Histopathology 33:290–292
7. Kurman RJ (ed) (1994) Blaustein, 4th edn. Pathology of the female genital tract. Chapter 17, Springer, Berlin Heidelberg New York
8. Lichteneld FR (1961) Endometriosis involving the urinary tract, a collective review. Obstet Gynaecol 17:763–768
9. McCluggage WG, Sumathi VP, Maxwell P (2001) CD10 is a sensitive and diagnostically useful immunohistochemical marker of normal endometrial stroma and of endometrial stromal neoplasms. Histopathology 39:273–278
10. O'Conor V (1945) Endometriosis of the bladder and ureter. Surg Gynaecol Obstet 80:113–119
11. Skor AB, Warren MM, Mueller EO Jr (1977) Endometriosis of the urinary bladder. Urology 9:689–692
12. Sumathi VP, McCluggage WG (2002) CD10 is useful in demonstrating endometrial stroma at ectopic sites and in confirming a diagnosis of endometriosis. J Clin Pathol 55:391–392
13. Vara AR, Ruzics EP, Moussabeck O, Martin DC (1990) Endometrioid adenosarcoma of the bladder arising from endometriosis. J Urol 143:813–815
14. Young RH, Clement PB (1996) Mullerianosis of the urinary bladder. Mod Pathol 9:731–737

Virchows Arch (2004) 444:590–593
DOI 10.1007/s00428-004-1013-5

CASE REPORT

Susanne van Eeden · G. Johan A. Offerhaus · Folkert H. Morsink · Bastiaan P. van Rees · Olivier R. C. Busch · Carel J. M. van Noesel

Pyogenic granuloma: an unrecognized cause of gastrointestinal bleeding

Received: 23 January 2004 / Accepted: 17 March 2004 / Published online: 15 April 2004

Abstract Pyogenic granuloma is a lobular capillary hemangioma that mostly occurs on the skin, but it is also encountered on the mucosal surface of the oral cavity. Only a few cases in other parts of the digestive tract have been reported in Japanese patients. In this report, two Caucasian patients are described, who presented with gastrointestinal bleeding due to the presence of a pyogenic granuloma. One was located in the distal esophagus and could be treated with local excision and laser-photocoagulation therapy. The other one was located in the small intestine and was removed by surgical resection. Although extremely rare, pyogenic granuloma as a cause of gastrointestinal bleeding needs consideration. The lesion is benign, presumably reactive and can be adequately treated by excision or laser photocoagulation. Immunohistochemistry and/or polymerase chain reaction for herpesvirus 8 can reliably distinguish pyogenic granuloma from Kaposi's sarcoma, an important differential diagnosis.

Keywords Pyogenic granuloma · Esophagus · Small intestine · Gastrointestinal bleeding · HHV-8

Introduction

Pyogenic granuloma is a lobular capillary hemangioma that presents as a polypoid red mass with a size of several millimeters to a few centimeters. It is friable, bleeds easily and resembles exuberant granulation tissue. The overlying epithelial lining is flattened and mostly ulcerated [5]. The lesion is found on the skin, particularly the lips, face and fingers and, furthermore, on the mucosal surface of the oral cavity and tongue [2]. Sexes are affected equally, and the disease is evenly distributed over all ages. It is a benign tumor thought to be reactive—e.g., due to minor trauma—and excision is, in general, curative.

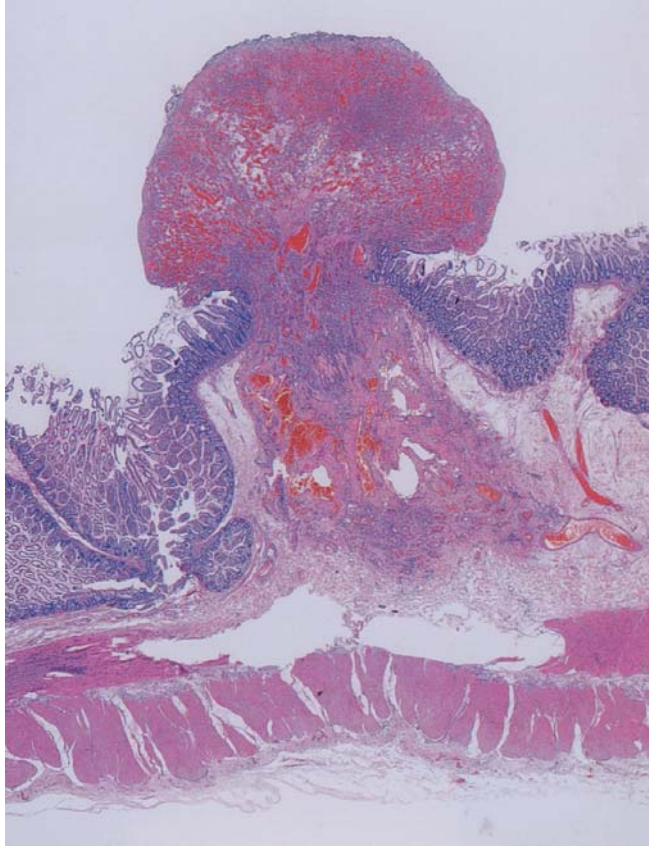

Fig. 1 Low-power view of the pyogenic granuloma in the ileum. The lesion protrudes into the lumen and extends into the submucosa

S. van Eeden (✉) · G. J. A. Offerhaus · F. H. Morsink · B. P. van Rees · C. J. M. van Noesel
Department of Pathology,
Academic Medical Center,
PB 22660, 1100DD Amsterdam, The Netherlands
e-mail: s.vaneeden@amc.uva.nl
Tel.: +31-20-5665638
Fax: +31-20-6960389

O. R. C. Busch
Department of Surgery,
Academic Medical Center,
Amsterdam, The Netherlands

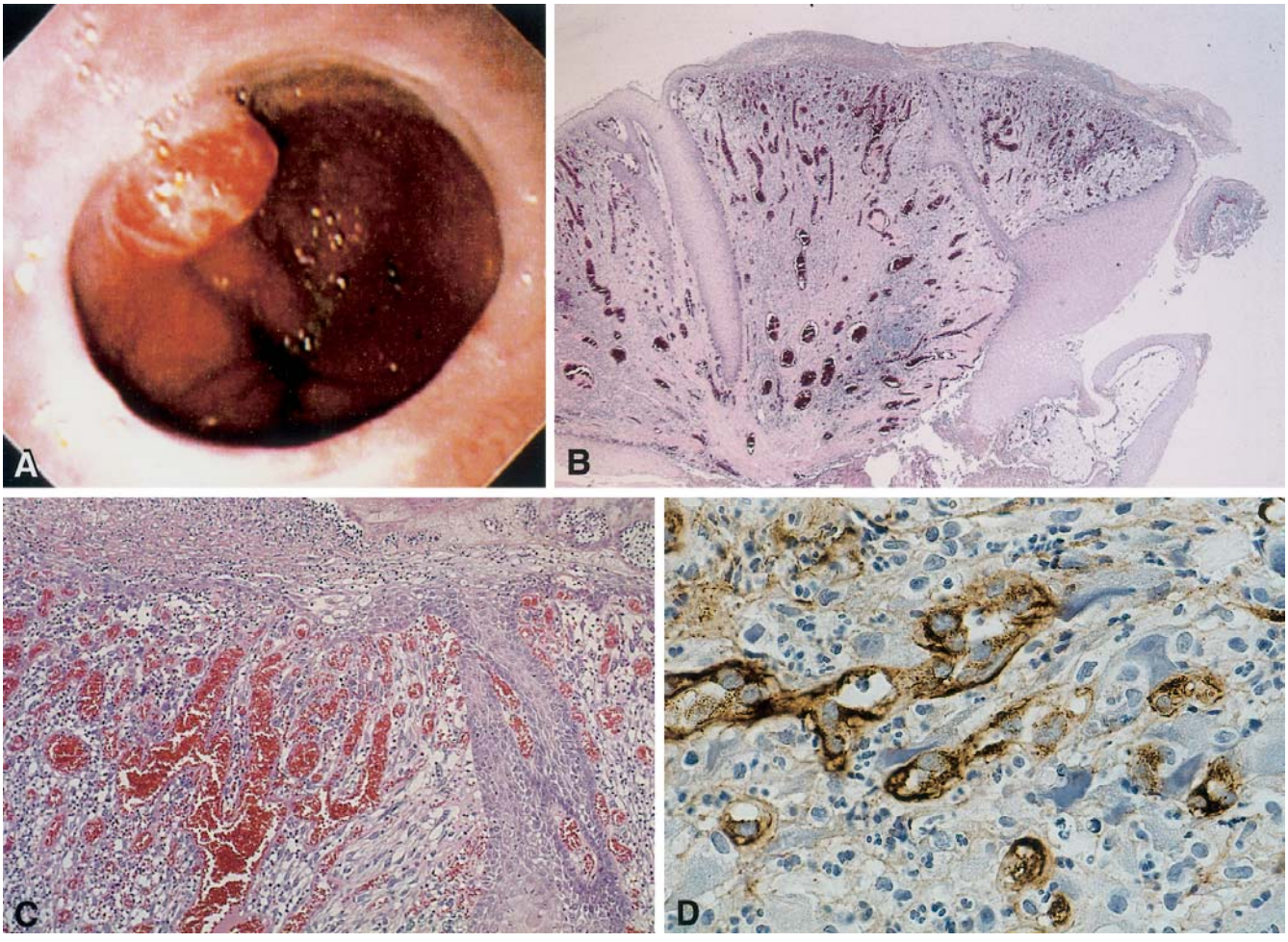

Fig. 2 **A** Endoscopic picture of the pyogenic granuloma of the esophagus. **B** The microscopic picture shows a mucosal vascular nodule protruding into the lumen. **C** At higher power, the capillary arrangement with edematous inflamed stroma in between is recognized. **D** Factor-VIII immunoperoxidase shows positive staining of endothelial cells

To our knowledge, only very few cases of pyogenic granuloma occurring in other parts of the gastrointestinal tract than the oral cavity have been reported, and these patients all came from Japan [6]. In a Dutch patient, a case of multiple angiomatous proliferations reminiscent of pyogenic granuloma has been described in an ileal stoma following Campylobacter enteritis. However, the lesions did not show an obvious lobular architecture, and the endothelial cells were not as bland as usual in a pyogenic granuloma [4]. We have recently seen two patients referred to our institution for gastrointestinal blood loss caused by a pyogenic granuloma of the distal esophagus and of the ileum, respectively. The occurrence of these lesions with their clinicopathological features and differential diagnosis were evaluated and are described in this report.

Clinical history

Case 1

A 55-year-old female suffered from repeated melena and had anemia. At colonoscopy, it was felt that the bleeding might be due to angiodysplasia, but no obvious and specific abnormality could be seen. The patient underwent an ileocecal resection. Grossly, a polypoid lesion in the ileum 8 cm from the ileocecal valve was visible in the resected specimen. It measured 9 mm in diameter and protruded into the lumen (Fig. 1). The surface was eroded.

Case 2

A 55-year-old female presented with hematemesis and dysphagia. At endoscopy, a small lobulated mass was seen in the distal esophagus (Fig. 2) with ulceration at the surface. The polypoid lesion measured 11 mm in largest diameter. A polypectomy with laser photocoagulation therapy was performed.

Materials and methods

Surgical and biopsy specimens were all fixed in 10% buffered formalin, embedded in paraffin and cut in 4-μm sections. Hema-

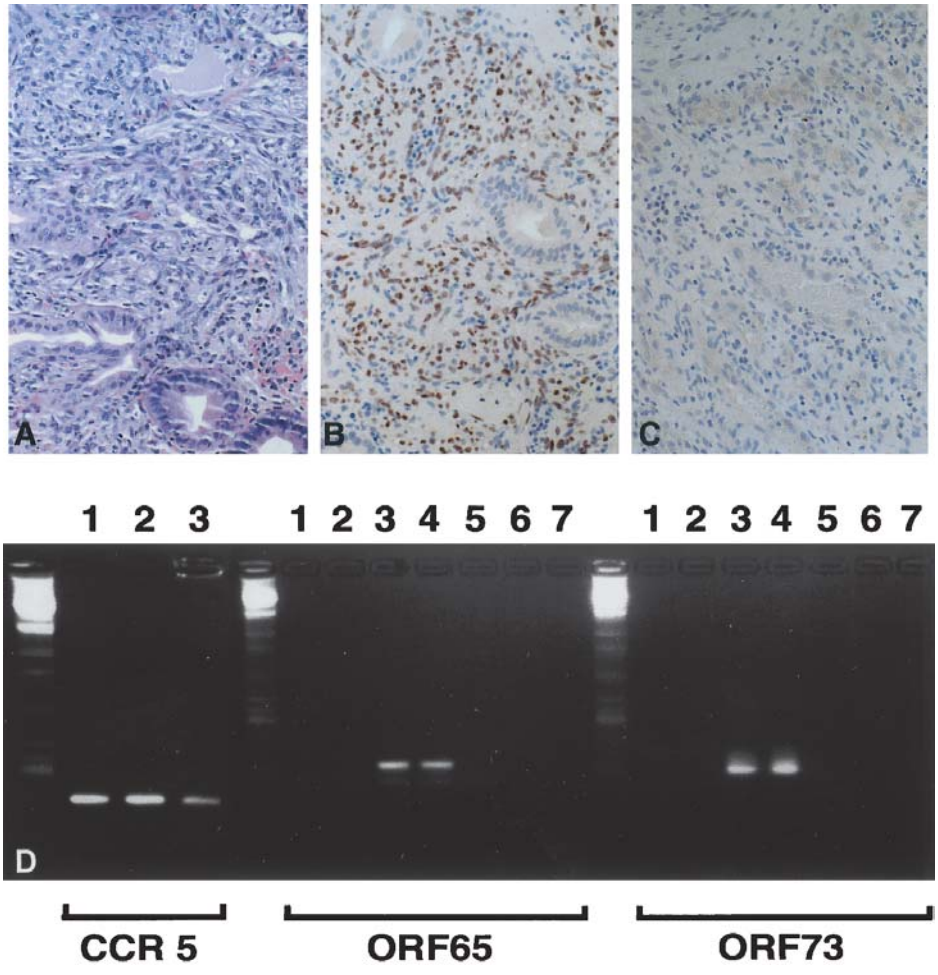

Fig. 3 Microscopy (hematoxylin and eosin) of the intestinal Kaposi's sarcoma (**A**), with the positive immunohistochemistry for herpesvirus 8 (HHV-8) (**B**); whereas, the HHV-8 immunohistochemistry in the pyogenic granuloma (**C**) is negative. The agarose gel of the polymerase chain reaction (PCR) products (**D**) shows positive bands for the household gene in the *first three lanes* of the *left panel* (CCR 5) as a control for proper DNA isolation. The *middle and the right panel* provide the nested PCR products of ORF65 and ORF73 of HHV-8 respectively. *Lanes 1 and 2* are the pyogenic granulomas of cases 1 and 2. *Lane 3* is the intestinal Kaposi's sarcoma in an acquired immunodeficiency syndrome patient. *Lane 4* is the positive control. *Lane 5* is a negative control, *lane 6* is a paraffin block without tissue and *lane 7* is H_2O, the latter two to exclude contamination

toxylin and eosin-stained section slides were prepared for histological evaluation, and the clinical history was reviewed.

Immunohistochemical stains were performed using the Power Vision poly-horseradish peroxidase methodology with primary antibodies against Factor VIII-related antigen, smooth muscle antigen (SMA), CD34 and human herpesvirus 8 (HHV-8). The HHV-8 antibody is a rat monoclonal antibody against ORF-73 of the virus (ABI, Columbia, MD, USA) that causes Kaposi's sarcoma [1].

For the polymerase chain reaction (PCR) of HHV-8, two 4-μm tissue sections were deparaffinated using, subsequently, xylene and ethanol. After centrifugation, the tissue was digested overnight at 60°C using 50 μl of a 50 mM TRIS/HCl buffer (pH 8.5) with 0.2% Tween, 1 mM EDTA and proteinase K at a final concentration of 1 mg/ml. After proteinase K inactivation, for 5 min at 95°C, the ORF65 and ORF73 regions of HHV-8 were amplified out of 1-μl DNA solution using a nested PCR protocol as previously described [3]. As a DNA control, a non-nested CCR5-specific PCR, with the oligonucleotides 5′-GATAGGTACCTGGCTGTCGTCCAT and 5′-ACCAGCCCCAAGATGACTATCT as sense and antisense primers, respectively, was performed concurrently with the first round of the ORF65 and ORF73 PCRs. The amplified fragments were identified using 1.5% agarose gel electrophoresis.

A well-established intestinal Kaposi's sarcoma in an acquired immunodeficiency syndrome (AIDS) patient was included as positive control for the immunohistochemistry and PCR for HHV-8.

Results

The microscopic appearance of both lesions was similar. The ileal lesion involved the mucosa and extended into the submucosa. The surrounding mucosa was unremarkable, and the cecum was also normal. The lesion in the esophagus only involved the mucosa. Both lesions were ulcerated on their mucosal surface. The lesions had a lobular architecture and consisted of clusters of small capillary vessels lined by a single layer of bland endothelial cells. The edematous stroma contained variable amounts of inflammatory cells, including neutrophils.

Immunohistochemistry showed positivity for CD34 and factor VIII in the endothelial cells and SMA-positivity in surrounding pericytes. Immunohistochemistry and PCR for HHV-8 were negative in the two lesions, whereas it was clearly positive in the control Kaposi's sarcoma (Fig. 3).

Discussion

The macroscopic and microscopic features described above are those of a pyogenic granuloma. To our knowledge, only five cases of pyogenic granuloma in the gastrointestinal tract have been reported, and these were all

Japanese patients [6]. One case occurred in the stomach, two in the jejunum, one in the ileum and one in the sigmoid colon. This report describes the first case, which was in the esophagus. Blood loss and anemia were the main clinical symptoms. The patient with the esophageal pyogenic granuloma described in this report also had dysphagia.

Endoscopy and radiological imaging techniques, such as angiography and radioactive-labeled red-blood-cell scintigraphy can be used to detect the lesion [6]. Local excision with or without photocoagulation or segmental resection is the treatment of choice. The lesion needs to be differentiated from Kaposi's sarcoma. Kaposi's sarcoma is typically encountered in patients with AIDS, who frequently have lesions at other locations as well. Grossly, Kaposi's sarcoma has a darker, more bluish color than pyogenic granuloma, and it is mostly covered by a moistly glistening intact mucosa. Microscopically, Kaposi's sarcoma has slit-like vascular channels lined by atypical endothelial cells, and it shows extravasation of red blood cells, features not encountered in pyogenic granuloma. Compared with pyogenic granuloma, Kaposi's sarcoma is less well circumscribed. Kaposi's sarcoma is usually positive for HHV-8, whereas pyogenic granuloma is negative.

Pyogenic granuloma is a benign lesion that is considered reactive, e.g., as the result of minor trauma. However, the precise etiology is unknown. On the skin satellite lesions have been described, which argues against trauma as the sole cause. On the skin and in the mouth, the lesions are found more frequently during pregnancy, and, therefore, hormonal influences may also play a role. All the gastrointestinal pyogenic granulomas reported thus far occurred in elderly patients; however, they occurred in both males and females.

In summary, gastrointestinal pyogenic granuloma apparently is a rare cause of hemorrhage in the digestive tract. Awareness of this infrequent benign lesion makes it easy to diagnose and treat it properly.

References

1. Boshoff C (2003) Kaposi virus scores cancer coup. Nat Med 9:261–262
2. Enzinger FM, Weiss SW (2001) Benign tumors and tumor-like lesions of blood vessels. In: Soft tissue tumors, 4th edn. CV Mosby Company, St. Louis, pp 864–865
3. Goudsmit J, Renwick N, Dukers NHTM, et al (2000) Human herpesvirus 8 infections in the Amsterdam Cohort Studies (1984–1997): analysis of the seroconversions to ORF65 and ORF73. PNAS 97:4838–4843
4. Meuwissen SGM, Willig AP, Hausman R, et al (1986) Multiple angiomatous proliferations of ileal stoma following campylobacter enteritis. Effect of laser photocoagulation. Dig Dis Sci 31:327–332
5. Rosai J (1995) Pyogenic granuloma and related lesions. In: Ackerman's surgical pathology, 8th edn. CV Mosby Company, St. Louis, pp 182–188
6. Yao T, Nagai E, Utsunomiya T, Tsuneyoshi M (1995) An intestinal counterpart of pyogenic granuloma of the skin. A newly proposed entity. Am J Surg Pathol 19:1054–1060

Virchows Arch (2004) 444:594–596
DOI 10.1007/s00428-004-1009-1

LETTER TO THE EDITOR

Mário Rodrigues Montemor Neto · Tiago Noguchi Machuca · Renato Valmassoni Pinho · Lucas Dan Yuasa · Luiz Fernando Bleggi-Torres

Gastrointestinal stromal tumor: report of two unusual cases

Received: 20 October 2003 / Accepted: 2 March 2004 / Published online: 30 April 2004

Sir, Gastrointestinal stromal tumor (GIST) is a neoplasm with recently established diagnostic criteria (immunoreactivity to CD117). The most common anatomical site of GIST occurrence is the stomach, followed by small bowel and colon [1]. Despite the term gastrointestinal, they have also been reported in extraintestinal sites, such as the omentum, retroperitoneum and mesentery. We present two cases of tumors arising from unusual sites, one from the retroperitoneum and one from the pancreas, with the latter representing the first report in the literature of a GIST in such a topography.

The first case concerns a 48-year-old female patient who had a mass on her left hypochondrium detected on a routine evaluation. Radiological follow-up revealed progressive growth, and a laparotomy was performed. At operation, the tumor was located between the stomach and spleen. Adhesions with these organs were present, more pronounced in the spleen. The mass was resected *en bloc* with the spleen and a gastric margin.

Gross evaluation revealed a 19×17.5×6-cm whitish granular tumor. Histological sections stained with hematoxylin-eosin revealed a neoplasm composed of fusiform cells arranged in bundles. Mild atypia and nuclear palisading areas were also present (Fig. 1A). A rich hyaline matrix and calcifications were observed. Mitotic count was 6/50 high-power field (HPF). Tumor infiltration was not present in the spleen or in the gastric margin. Immunohistochemical assessment displayed positivity to CD117 and CD34. Desmin and synaptophysin yielded negative results.

In the second case, a 67-year-old female patient presented with epigastric pain and gastric bloating associated with weight loss. Radiological examination revealed a cystic tumor in the body of the pancreas. Since there was no history of pancreatitis and due to the tumor location, a primary neoplasm was suspected, and surgery was proposed. At exploration, a cystic mass was present in the transition of the body to the tail of the pancreas. A biopsy was performed, and frozen section examination was consistent with malignancy. A distal pancreatectomy with splenectomy was undertaken.

On gross evaluation, the pancreatic surface was deformed by a 20×19×12-cm mass with both solid and cystic areas. Histological section revealed a tumor with both epithelioid and fusiform cells arranged to form nodules and bundles (Fig. 1B). Atypia was prominent, as was necrotic foci and vesicular chromatin. Mitotic count was unusual: 120/50 HPF (Fig. 1C). Immunohistochemical examination was positive to CD-117 (Fig. 1D) and CD34. Results for CK7, CK20, desmin and synaptophysin were negative.

The patient presented with weight loss and abdominal pain in the first month after surgery. Investigation displayed recurrence of the disease, with findings of peritoneal spread and retroperitoneal nodal enlargement. The patient is currently enrolled in a STI-571 protocol.

Despite being the most common non-epithelial neoplasm of the stomach and small bowel, GIST occurs infrequently [2]. In a population-based study, this tumor accounted for 2.2% of gastric cancers, 13.9% of small bowel cancers and 0.1% of colorectal cancers [10].

In addition to the GI tract, GIST has also been reported in the omentum, retroperitoneum, mesentery and, more rarely, in the bladder and gallbladder [3, 4, 6, 7]. These

M. R. M. Neto · T. N. Machuca · L. F. Bleggi-Torres
Department of Pathology,
Hospital Nossa Senhora das Graças,
Curitiba, Brazil

R. V. Pinho
Department of General Surgery,
Hospital Nossa Senhora das Graças,
Curitiba, Brazil

L. D. Yuasa
Department of Oncological Surgery,
Hospital Nossa Senhora das Graças,
Curitiba, Brazil

L. F. Bleggi-Torres (✉)
Serviço de Anatomia Patológica,
Hospital de Clínicas/UFPR,
Rua General Carneiro 181, 80060-900 Curitiba, Paraná, Brasil
e-mail: lfbt@terra.com.br

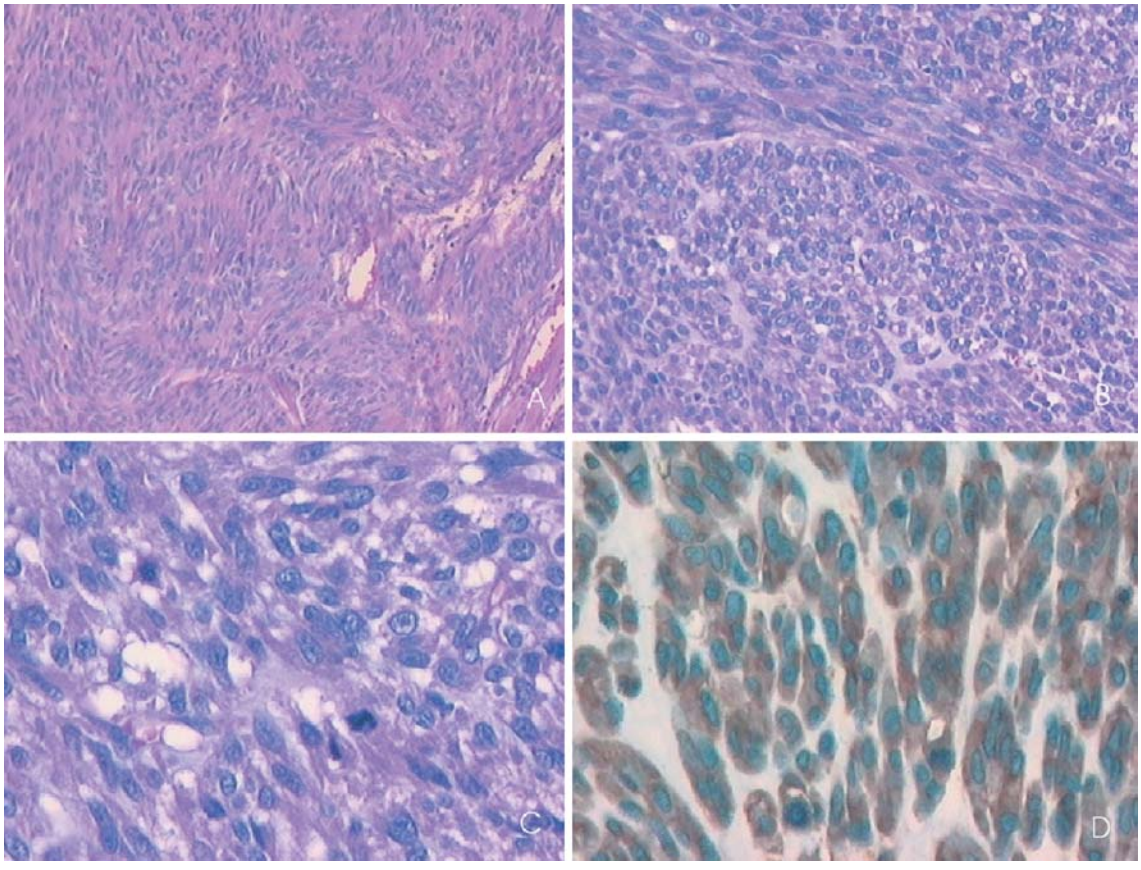

Fig. 1 **A** Case 1, photomicrography showing bundles of fusiform cells and nuclear palisading [hematoxylin-eosin (HE) 100×]. **B** Case 2, photomicrography displaying both fusiform and epithelioid cells (HE 200×). **C** Case 2, photomicrography of a pancreatic gastrointestinal stromal tumor with enhanced mitotic activity (HE 400×). **D** Case 2, photomicrography displaying marked intracytoplasmic positivity for CD117 (400×)

unusual locations account for 5% of primary sites harboring GISTs [1]. To the best of our knowledge, this is the first description of a pancreatic GIST.

Clinical presentation of tumors outside the GI tract tends to be different from their GI counterpart. Due to lack of mucosal connection and the deeper location, omental and retroperitoneal lesions are usually asymptomatic or present as vague abdominal pain and may achieve large dimensions when detected, frequently larger than 10 cm [3, 7]. In the cases reported herein, unspecific abdominal pain and bulking tumors (19 cm and 20 cm in greater dimensions) were present.

The diagnosis of GIST is based on histological and immunohistochemical features. The most valuable immunohistochemical marker for the diagnosis of GIST is CD-117 [9]. According to experts' consensus, it is the gold-standard diagnostic criterion and should be routinely performed [1]. However, CD-117 positivity should be always interpreted based on histological findings. Immunohistochemical profile of GISTs also includes positivity for CD34 in 60–70% [1]. Markers such as desmin/smooth-muscle actin, S100, glial fibrillary acidic protein and chromogranin/synaptophysin are helpful when evaluating mesenchymal tumors with possible myogenic, schwannian, glial or neuronal differentiation, respectively [8].

On an individual-case basis, only mitotic count and tumor size have gained acceptance as predictors of outcome [5]. According to a consensus, tumors larger than 5 cm with more than 5 mitoses per 50 HPFs as well as tumors larger than 10 cm, regardless of mitotic count, should be considered lesions with high risk for aggressive behavior. The two GISTs of this report presented as high risk for aggressive behavior, with the pancreatic one displaying an explosive mitotic count. This latter finding was corroborated by the early recurrence despite complete surgical resection.

References

1. Fletcher CDM, Berman JJ, Corless C, Gorstein F, Lasota J, Longley BJ, Miettinen M, O'Leary TJ, Remotti H, Rubin BP, Shmookler B, Sobin LH, Weiss SW (2002) Diagnosis of gastrointestinal stromal tumors: a consensus approach. Hum Pathol 33:459–465
2. Kindblom LG, Remotti HE, Aldenborg F, Meis-Kindblom JM (1998) Gastrointestinal pacemaker cell tumor (GIPACT): gastrointestinal stromal tumor show phenotypic characteristics of the interstitial cells of Cajal. Am J Pathol 152:1259–1269
3. Lasota J, Carlson JA, Miettinen M (2000) Spindle cell tumor of urinary bladder serosa with genotypic and phenotypic fea-

tures of gastrointestinal stromal tumor. Arch Pathol Lab Med 124:894–897
4. Miettinen M, Monihan JM, Sarlomo-Rikala M, Kovatich AJ, Carr NJ, Emory TS, Sobin LH (1999) Gastrointestinal stromal tumors/smooth-muscle tumors (GISTs) primary in the omentum and mesentery: clinicopathologic and immunohistochemical study of 26 cases. Am J Surg Pathol 23:1109–1118
5. Miettinen M, El-Rifai WM, Sobin LH, Lasota J (2002) Evaluation of malignancy and prognosis of gastrointestinal stromal tumors: a review. Hum Pathol 33:478–483
6. Ortiz-Hidalgo C, Bojorge BL, Albores-Saavedra J (2000) Stromal tumors in the gallbladder with phenotype of interstitial cells of Cajal. A previously unrecognized neoplasm. Am J Surg Pathol 24:1420–1423
7. Reith JD, Goldblum JR, Lytes RH, Weiss SW (2000) Extragastrointestinal (soft tissue) stromal tumors: an analysis of 48 cases with emphasis on histologic predictors of outcome. Mod Pathol 13:577–585
8. Rudolph P, Chiaravalli AM, Pauser U, Oschlies I, Hillemanns M, Gobbo M, Marichal M, Eusebi V, Hofler H, Capella C, Kloppel G (2001) Gastrointestinal mesenchymal tumors—immunophenotypic classification and survival analysis. Virchows Arch 441:238–248
9. Sarlomo-Rikala M, Kovatich AJ, Barusevicius A, Miettinem M (1998) CD117: a sensitive marker for gastrointestinal stromal tumors that is more specific than CD34. Mod Pathol 11:728–734
10. Thomas RM, Sobin LH (1995) Gastrointestinal cancer incidence and prognosis by histologic type, SEER population-based data 1973–1987. Cancer 75:154–170

Virchows Arch (2004) 444:597
DOI 10.1007/s00428-004-1045-x

ANNOUNCEMENTS

11–16 July 2004
ULTRAPATH XII: Conference on Diagnostic Electron Microscopy with Surgical, Clinical, and Molecular Pathology Correlations
Barcelona, Spain

The scientific program will cover diagnostic Electron Microscopy as well as Diagnostic Pathology – with immunohistochemical and molecular correlations – and translational research. Renowned experts in the field from both sides of the Atlantic will present updated comprehensive reviews of significant areas of Pathology. In addition, a new section of the meeting will be devoted to a Pathology Review Course. Platform and Poster presentations will also be an important part of the program.

For further information, please contact:
Josep Lloreta-Trull, M.D., Ph.D. (chairman)
Department of Pathology, Hospital del Mar-IMAS-IMIM
Universitat Pompeu Fabra
Passeig Maritim 25–29, 08003-Barcelona, Spain
Tel.: +34 93 248 30 31
Fax: +34 93 248 31 31
E-mail: jlloreta@imas.imim.es.
The Application form and Abstract form can be found on the meeting website, http://www.tilesa.es/ultrapath04/

27–30 July 2004, London
Practical Pulmonary Pathology

This course is designed to provide histopathology and cytopathology trainees and consultants with an opportunity to study diagnostic lung pathology in a comprehensive manner. It comprises lectures and practical microscopy sessions, the latter making up roughly half the time and consisting of individual study of a unique collection of cases.

For further details and application forms please contact:
Professor B Corrin,
Brompton Hospital
London SW3 6NP
Fax: +44 20 7351 8293.
E-mail: b.corrin@ic.ac.uk

9 September 2004
One day course on Advanced Ultrasound of the Breast
Nottingham, UK

For further information contact:
The Blamey Education Centre
Nottingham Breast Institute
City Hospital, Nottingham, NG5 1PB, UK
Tel.: 00 44 (115) 969 1689
E-mail: sbury@ncht.trent.nhs.uk

23–24 September 2004 **(Change of date)**
Thyroid Pathology for the Practicing Pathologist
15 rue de l'Ecole de Médecine, Paris, France

A 2-day course will take place in Paris under the auspices of the French Division of the I.A.P. This course will be given in English by Prof. M. Sobrinho-Simoes (Porto) and Prof. R. Heimann (Brussels).

It will consist of lectures alternating with slide reviews and a slide seminar over a multihead microscope. The cases of this seminar will be sent (on CD) before the meeting. The audience will be limited to 22 participants.

Course fee: 390 euros (320 euros for members of any IAP division). The fees include registration, hand-out, CD of the slide seminar and coffee breaks.

For further information, please contact:
Mrs. M. Fontanière
Administrative Secretary
French Division of the I.A.P. 32 Cours Albert Thomas
69008, Lyon, France
Fax: 33478754311
E-mail: academie.pathologie@wanadoo.fr

11 October 2004
Continuing Medical Education
Nottingham, UK

For further information contact:
The Blamey Education Centre
Nottingham Breast Institute
City Hospital, Nottingham, NG5 1PB, UK
Tel.: 00 44 (115) 969 1689
E-mail: sbury@ncht.trent.nhs.uk

22–24 November 2004
41st Nottingham Multi-disciplinary Course on breast disease
Nottingham, UK

For further information contact:
The Blamey Education Centre
Nottingham Breast Institute
City Hospital, Nottingham, NG5 1PB, UK
Tel.: 00 44 (115) 969 1689
E-mail: sbury@ncht.trent.nhs.uk